Calendar of forthcoming meetings

11–15 May 2009
Frankfurt am Main, Germany
Achema 2009: 29th International Exhibition-Congress on Chemical Engineering, Environmental Protection and Biotechnology. URL: http://www.achema.de

30 May – 2 June 2010
Portoroz, Slovenia
Monoliths 2010: 4th Summer School of Monolith Technology for Biochromatography, Bioconversion, and Solid Phase Synthesis. URL: www.monolith-events.com

21–25 June 2009
Denver, CO, USA
Transducers 2009: 15th International Conference on Solid-State Sensors, Actuators and Microsystems. URL: www.transducers09.org

6–10 September 2009
Innsbruck, Austria
Euroanalysis 2009. Contact: Euroanalysis 2009 Symposium Office, PCO Tyrol Congress, c/o Ina Kaehler, Rennweg 3, 6020 Innsbruck, Austria. Tel. (+43-512) 575-600; Fax: (+43-512) 575-607; E-mail: euroanalysis09@come-innsbruck.at; URL: www.euroanalysis2009.at

9–12 September 2009
Milan, Italy
RDPA 2009: 13th International Meeting on Recent Developments in Pharmaceutical Analysis. URL: www.rdpa2009.com

14–18 September 2009
Toronto, ON, Canada
SIMS XVII: 17th International Conference on Secondary Ion Mass Spectrometry. E-mail: email@simsxvii.org; URL: www.simsxvii.org/

14–18 September 2009
Pollensa, Mallorca, Spain
Flow Analysis XI. URL: http://www.uib.es/depart/dqu/dquiweb/grupo_e.html

30 September – 3 October 2009
Caparica, Portugal
5th Congress of the Portuguese Proteomics Network – ProCura: 1st International Congress on Analytical Proteomics (ICAP). URL: http://www.cqfb.fct.unl.pt/Procura_ICAP

4–7 October 2009
Rapid City, SD, USA
ExTech 2009. URL: http://www.extech.sdstate.edu

4–8 October 2009
Athens, Greece
IMA 2009: 6th International Conference on Instrumental Methods of Analysis – Modern Trends and Applications. URL: www.chem.uoa.gr/ima2009

11–14 October 2009
Orlando, FL, USA
PBA 2009: 21st International Symposium on Pharmaceutical and Biomedical Analysis. URL: www.pba2009usa.com

4–6 November 2009
Prague, Czech Republic
Food Analysis 2009: 4th International Symposium on Recent Advances in Food Analysis. URL: www.rafa2009.eu

26–28 May 2010
Glasgow, UK
Biosensors 2010: The Eleventh World Congress on Biosensors. URL: http://www.biosensors-congress.elsevier.com

20–23 September 2010
Antwerp, Belgium
Drug Analysis. URL: www.druganalysis.org

8–10 December 2010
Nagoya, Japan
International Conference on Polymer Analysis and Characterization & 15th Symposium on Polymer Analysis in Japan. Contact: ohtani.hajime@nitech.ac.jp

doi:10.1016/S0039-9140(09)00287-2

Talanta

The International Journal of Pure and Applied Analytical Chemistry

Aims & Scope

Talanta provides a forum for the publication of original research papers, preliminary communications, and reviews in all branches of pure and applied analytical chemistry. Analytical data should be submitted only if they are clearly related to new analytical measurements. Original research papers on fundamental studies and novel sensor and instrumentation development are especially encouraged. Novel or improved applications in areas such as clinical chemistry, environmental analysis, geochemistry, and materials science and engineering are welcome. Methods should be validated by comparison with a standard method or analysis of a certified reference material, and relevant literature should be cited. Since classical spectrophotometric measurements and applications, solvent extraction, titrimetry, chemometrics, etc. are well established, studies in such areas should demonstrate a unique and substantial advantage over presently known systems. New reagents or systems should demonstrate clear advantage, and their presentation should be comprehensive rather than generating a series of similar papers for several analytes. Modifications of reagents should demonstrate significant improvements. Solvent extraction methods in particular, but others as well, should focus on the use of non-hazardous material substitutes and the minimization of waste generation. But obvious application of known chemistries or methods to established techniques are discouraged. Application of classical analytical approaches to relatively sample matrices having no major interferences, such as pharmaceutical preparations or reconstituted samples, are discouraged unless considerable improvements over other methods in the literature are demonstrated. Papers dealing with analytical data such as stability constants, pK_a values, etc. should be published in more specific journals, unless novel analytical methodology is demonstrated, or important analytical data are provided which could be useful in the development of analytical procedures.

Talanta 78 (2009) 1422–1428

Contents lists available at ScienceDirect

Talanta

journal homepage: www.elsevier.com/locate/talanta

Determination of ethanol and specific gravity in gasoline by distillation curves and multivariate analysis

Helga G. Aleme[a], Letícia M. Costa[b], Paulo J.S. Barbeira[a,*]

[a] Laboratório de Ensaios de Combustíveis, Departamento de Química, ICEx, UFMG, Av. Antônio Carlos 6627, 31270-901 Belo Horizonte, Minas Gerais, Brazil
[b] Grupo de Espectrometria Atômica e Preparo de Amostras, Departamento de Química, ICEx, UFMG, Av. Antônio Carlos 6627, 31270-901 Belo Horizonte, Minas Gerais, Brazil

ARTICLE INFO

Article history:
Received 25 November 2008
Received in revised form 17 February 2009
Accepted 18 February 2009
Available online 4 March 2009

Keywords:
Ethanol
Gasoline
Partial least-squares regression
Distillation curve
Specific gravity

ABSTRACT

The partial least-squares regression method (PLS) was employed to predict the amount of ethanol and specific gravity in automotive gasoline using distillation curves (ASTM-D86). Additionally, a comparison was made between regression coefficients of all the algorithms, after selecting the number of latent variables. The low values obtained for RMSEC and RMSEP, associated with high accuracy when compared to the standard methodologies (NBR-13992, ASTM-D4052 and D1298) showed that PLS was efficient to determine the ethanol content and specific gravity in gasoline, since the model contains samples of different gasoline compositions, thus reflecting the variety of fuel in the Brazilian market. In addition, the proposed method is low cost, time reducing and easy to implement, as it utilizes the results of a routine assay carried out to evaluate the quality of automotive fuel.

1. Introduction

With the increase in energy demands throughout the latest centuries, fossil fuels are becoming limited. As a result, there is a major interest in developing alternative energy resources. Brazil was the first country in the world to change tetra-ethyl lead for ethanol as an antiknocking additive in automotive gasoline. This occurred after the introduction of Programa Nacional do Álcool (PROALCOOL) in 1975, which was created to stimulate the production and consumption of alcohol in the domestic and external markets. The addition of alcohol to gasoline has had some benefits such as the reduction of harmful emissions and the lessening of dependence on petroleum [1].

Since 1979 different amounts of ethanol, varying from 19 to 27% (v/v), have been added to Brazilian gasoline and, nowadays, this percentage is approximately 24–26% (v/v) of anhydrous ethanol [2]. According to ANP (Brazilian regulatory authority), around 23 billion liters of ethanol–gasoline mixture were commercialized [3] in 2008, and about 30% of these samples violated Brazilian legislation [4]. In Brazil, the determination of ethanol content in gasoline is carried out according to NBR 13992 [5], based on an extraction with solvent, whereby an aqueous NaCl solution is added to the sample. The alcoholic content, % (v/v), in the sample is determined by the difference between final and initial volumes of water, after phase separation.

The specific gravity of gasolines commercialized in gas stations has no limits defined by ANP [2], with the exception of the gasolines used for the first filling and motor homologation, but it is an important parameter to evaluate in order to guarantee the good functioning of the engine. This assay can be performed by standardized methods such as American Society for Testing and Materials (ASTM) D1298 and D4052. ASTM-D1298 [6] describes the use of glass hydrometers, while ASTM-D4052 [7] explains the digital density meter. In the latter, a small volume of liquid sample is introduced into an oscillating U-tube, excited into oscillation by a Piezo element, and the oscillating frequency of the U-tube is directly related to the specific gravity of the filled sample.

The addition of ethanol to gasoline causes some changes in its volatility, vapor pressure and enthalpy of vaporization. In general, the increase of ethanol concentration causes a reduction of the vapor pressure and an increase in the enthalpy of vaporization [8].

Multivariate calibration associated to infrared and gas chromatography techniques has been used to predict several automotive fuel properties as specific gravity [9–11], viscosity [9,11–13], distillation fractions [9,11,13,14], octane number [14,15], cetane number [9,11,14–16], sulfur content [17,18], oxygen (MTBE) [15,19], aromatics [12,15,20], flash point [12,13], benzene [15], motor octane number (MON) [10,21] and research octane number (RON) [21].

Eight parameters (flash point, aromatics, freezing point, viscosity and distillation—initial, 10% (v/v), 90% (v/v) and final boiling

* Corresponding author. Tel.: +55 3134095767; fax: +55 3134096650.
E-mail address: barbeira@ufmg.br (P.J.S. Barbeira).

0039-9140/$ – see front matter © 2009 Elsevier B.V. All rights reserved.
doi:10.1016/j.talanta.2009.02.042

point) of kerosene were predicted by Gómez-Carracedo et al. [13] applying vapor-phase generation, Fourier transform mid-infrared (FT-MIR) spectra and partial least-squares regression (PLS). The corrected average prediction errors are low and the joint test for the slope and intercept ensures that no bias is being introduced. Further, the precision values (repeatability and reproducibility) are lower than those from the corresponding official methods, the unique relevant exception being viscosity.

Oliveira et al. [10] evaluated MON and specific gravity for gasoline and alcoholic content, and specific gravity for hydrated ethanol by PLS and FT-NIR (Fourier transform near infrared). In the determination of alcoholic content and specific gravity, the method proposed herein – compared to the correlation spectra method for choosing the adequate spectral region – leads to PLS models with lower root mean square error of prediction (RMSEP) values. For specific gravity, the RMSEP values obtained were 0.0026 and 0.00019, for gasoline and hydrated ethanol respectively, and 0.0399 for alcoholic content.

Santos et al. [11] carried out a comparative study using infrared spectroscopy techniques (FTIR, FT-NIR and FT-Raman) associated with PLS and artificial neural network (ANN) along with diesel oil samples, for the determination of specific gravity, distillation temperatures at 50 and 85% (v/v) volume evaporated, viscosity and total sulfur content. In the specific gravity determination, considering the entire spectra region, the RMSEP values obtained in the range of 0.00071 and 0.0029 for other types of techniques led us to conclude that the best technique was Fourier transform infrared spectroscopy with conventional attenuated total reflectance (FTIR-ART1), since it provides a larger spectral range, better signal-to-noise ratios and lower RMSEP values.

Balabin et al. [22] used infrared (NIR) spectroscopy data and compared the performances of linear (MLR – multiple linear regression, PCR – principal component regression and PLS) and non-linear calibration techniques (polynomial and spline PLS, ANN) to predict six important gasoline properties: specific gravity and the temperatures of initial boiling point (IBP), final boiling point (FBP), and 10, 50 and 90% (v/v) volume evaporated points. The results showed that the non-linear methods proved their superiority over the linear ones, and neural networks turned out to be the most suitable methods for building a calibration model, providing low root mean square error of calibration with cross validation (RMSECV) values.

In order to simplify and speed up the analytical process for gasoline during inspection or production procedures, this research proposes to quantify the ethanol content in gasoline samples – which is the main nonconformity detected with the ANP regulations in Brazil – and the specific gravity, employing distillation curves (ASTM-D86), a routine assay that is done to evaluate the quality of gasoline associated with multivariate calibration, based on the PLS method.

ASTM-D86 [23] describes the method for distillation at atmospheric pressure of several petroleum products in order to determine volatility features, another critical problem of nonconformities in Brazil. This is carried out by checking if the light and heavy proportions of the fuel produced are appropriate to enable good performance during combustion, and to detect adulterations with other products. For Brazilian automotive gasoline, the ANP establishes maximum temperature values for 10, 50 and 90% of the volume recovered, beyond final boiling point and residue volume [2].

2. Experimental

2.1. Samples

2.1.1. Alcoholic content prediction

Two different sets of samples were used to build calibration and validation PLS models. In the first group, named ethanol doped gasoline (EDG), different amounts of anhydrous ethanol were used to dope a gasoline in a final proportion of 15–30% (v/v). The second group was composed by samples collected in fuel stations by the ANP's Fuel Quality Control Program (FQCP-ANP), with different amounts of ethanol. As these samples have different origins, which directly affect the properties of the fuel [24–26], a representative set of samples from different refineries was selected and named Monitoring Program Group (MPG).

The gasoline, without ethanol, used to prepare the EDG samples was supplied by REGAP (Gabriel Passos Refinery) and doped with anhydrous ethanol (BR Distribuidora). The calibration matrix was constructed with 34 samples, whereas validation matrix with 14 samples.

The MPG group was built with a total of 135 samples of regular gasolines, collected in the east of Minas Gerais, Brazil. In this group, the addition of 19–31% (v/v) of ethanol has been a routine procedure performed by fuel distributors. For these sets of monitoring samples, 100 samples were used as calibration matrix and 35 samples were used as the validation matrix.

2.1.2. Specific gravity prediction

Another set of 135 samples was used in the determination of specific gravity. In this set, 35 samples were used for validation, aiming at determining the specific gravity of the gasoline, and the values were later compared with those obtained using the digital density meter (ASTM-D4052). The samples of this set came from five different refineries, all of them belong to FQCP-ANP, and have different quantities of ethanol, varying from 19 to 31% (v/v) and specific gravities in the range of 0.740–0.768 g mL^{-1}.

The gasoline samples were stored in appropriate polyethylene flasks, sealed and kept in cold storage (8–15 °C) until distillation analysis in order to avoid loss of volatile components [23].

2.2. Equipment and materials

Gasoline samples were distilled in a Herzog HDA 627 Automatic Distillation Analyzer, according to ASTM-D86 assay [23].

In the ethanol addition procedure, a graduated cylinder of 100 mL with 1 mL resolution, calibrated and covered according to NBR-13992 [5] was used. The 10% (w/v) NaCl solution was prepared by dissolving the salt (Reagen) in distilled water.

The specific gravity was determined by using an Anton Paar DMA 4500 digital density meter, according to ASTM-D4052 assay [7].

2.3. Experimental procedure

2.3.1. Distillation

For the distillation procedure, 100 mL of gasoline were transferred to a specific distillation flask equipped with a thermocouple sensor, and heated to keep the distillation ratio between 4 and 5 mL min^{-1}. The distilled and condensed steam was collected in a cooled test-tube (13–18 °C) and the recovered volume was measured with a digital volume sensor. Distillation curves (distillation temperature according to the recovered volume) were obtained after correcting temperature readings to atmospheric pressure of 101.3 kPa, and volume loss after measuring residue volume, according to ASTM-D86 [23].

2.3.2. Ethanol content

In the ethanol addition procedure, 50 mL of gasoline were added to a clean and dry graduated cylinder of 100 mL. Volume was completed with a 10% (w/v) NaCl solution, followed by a non-vigorous agitation and allowed to rest for 15 min, as described in NBR-13992 [5]. The final volume of the aqueous phase was read after this time and expressed in milliliters. The ethanol content is calculated

according to the equation below:

$$\text{ethanol content (v/v\%)} = [(A - 50) \times 2] + 1 \quad (1)$$

in which A is the final volume of the liquid phase given in milliliters. The addition of 1% (v/v) to the final result is necessary to compensate the volume contraction resulting from the water–ethanol mixture. When the difference $(A - 50)$ is less than 0.5 mL, the result must be written as ≤1% (v/v) [5].

2.3.3. Specific gravity

In this assay, approximately 0.7 mL of the gasoline previously cooled down to 10 °C is introduced, with a dry and clean syringe, into an oscillating sample tube, and the change in oscillation frequency caused by the change in the mass of the tube is used in conjunction with calibration data to determine the specific gravity of the sample [7]. After temperature stabilization of the measurement cell at 20 °C the specific gravity is noted.

2.3.4. Calibration multivariate tool

The aim of PLS is to find a small number of relevant factors that are predictive for Y and utilize X efficiently. The method effectively achieves a canonical decomposition of X in a set of orthogonal factors which are used for fitting Y [27]. In this method, each latent variable of the X matrix is modified for its covariance and the vector of matrix Y was maximized. In PLS, matrixes X and Y were decomposed in lesser matrixes according to the equations below:

$$X = TP^T + E \quad (2)$$

$$y = UQ^T + F \quad (3)$$

where X and Y are matrixes that will be decomposed, T and U are score matrixes with perpendicular rows (T and U are n-rows and d-columns matrixes, respectively), P is the matrix of d-rows and p-columns of loading matrix X, and E is the error (residue). Q is the matrix of d-rows and m-columns of the loading matrix of Y, F is the error (residue) for the Y matrix [28].

All calculations were performed with Minitab Release software (version 14 for Windows).

2.3.5. Evaluation of repeatability and reproducibility

The evaluation of repeatability and reproducibility of the methods were carried out according to ISO-5725-2 [29]. Therefore, 10 samples of gasoline were used and, for each sample, assays were done by three different analysts with seven replicates for each one [30], producing a total of 21 results.

3. Results and discussion

In order for the distillation to occur within a rate of 4–5 mL min^{-1} [23], the resistance needs to be significantly heated. Initially, this can lead to a vigorous ebullition – causing oscillation in temperature values – which raises from the initial point to approximately 4% (v/v) and produces low reproducible measurements. Another issue that should be emphasized on is that not all the distillation curves have equivalent temperatures in 94–98% (v/v) range due the pyrolysis phenomenon, in which the larger molecules are broken causing the decrease of boiling temperature [23]. Therefore, the interval 4–93% (v/v) (T4 to T93) was used to construct the PLS models.

The addition of ethanol leads to an essential change in the shape of the distillation curve: a plateau appears at about 70–77 °C. Fig. 1 shows that the distillation curves from the mixtures of gasoline–ethanol – up to a concentration of 40% (v/v) of ethanol – have lower boiling temperatures than the distillation curves of the gasoline without the addition of ethanol. This occurs due to the formation of an azeotropic mixture of hydrocarbons–ethanol

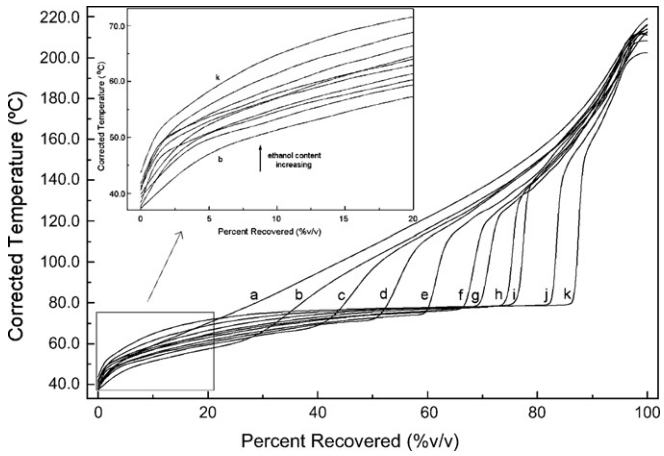

Fig. 1. Distillation curves (ASTM-D86) obtained for a gasoline doped with different ethanol contents. (a) 0% (v/v); (b) 5% (v/v); (c) 10% (v/v); (d) 15% (v/v); (e) 20% (v/v); (f) 25% (v/v); (g) 30% (v/v); (h) 35% (v/v); (i) 40% (v/v); (j) 50% (v/v); (k) 60% (v/v).

that have lower boiling temperatures than the original hydrocarbons [31], since mixtures of ethanol with hydrocarbons exhibit large deviations from ideal mixing. Consequently, Raoult's law cannot be used. It has also been observed that, the more ethanol added, the higher the plateau formed in the distillation curve. As from the concentration of 50% (v/v) of ethanol the plateaus become closer to each other and the initial temperatures rise. Fig. 1 also shows that at the beginning of the distillation process the influence of the azeotropic mixture is stronger that at the end, because the amount of ethanol in the system is higher at the beginning. Most of the ethanol boiled in the 75–80 °C range and did not form an azeotropic mixture at the end of the distillation process [32]. Another fact to be considered is the dispersed structure of ethanol–gasoline mixture, demonstrated by Balabin et al. [33] using the method of correlation spectroscopy of scattered light. The results showed that the colloidal structures are microspheres, whose size depends on the concentration of ethanol.

Due to the fact that the samples are from different refineries, and therefore have different chemical composition, some normalizations were used in an attempt to minimize the differences in behavior of the distillation curves, and to improve the RMSEC values. For this, each distillation point was divided by the temperature reading at different evaporated volumes, from 5% (v/v) (T5) to the final boiling point (FBP), out of a total of 19 normalizations.

The PLS data pre-processing was carried out in two different ways, as reported by Geladi and Kowalsky [34]: autoscaling and centering. In the first one, each data was subtracted from the average of its column and divided by the standard deviation. In the latter, each data was subtracted from the average value of its corresponding column. The cross validation was carried out using the leave-one-out method.

3.1. Alcoholic content prediction

The PLS model was built from calibration data. The alcoholic content of the prediction sample set was obtained using the best number of factors. The selection of components in PLS is very important to reach a good prediction [34,35]. With numerous and correlated X-variables there is a substantial risk of "over-fitting", thus creating a well fitting model with little or no predictive power. Hence, a strict test of the predictive significance of each PLS component is necessary, stopping when components start to be non-significant [36].

The number of latent variables with higher Q^2 values (coefficient of linearity for prediction using cross validation) were chosen

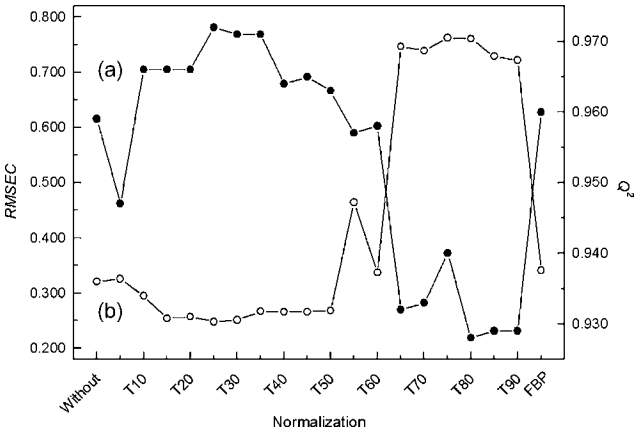

Fig. 2. RMSEC and Q^2 values obtained for models with different normalizations for the determination of alcoholic content in gasoline with the MPG set. (a) Q^2; (b) RMSEC.

to build the PLS model [37], and it was calculated by PRESS values, according to Wakeling and Morris [38]. For the EDG set, it was observed that only three variables were used to build the model, and for the MPG set, 4–10 latent variables were used, depending on the type of normalization applied. Fig. 2 (curve a) shows that the higher values were obtained for the normalization with temperature reading at 25% evaporated volume (T25).

The weight graphs of sets EDG and MPG showed a different behavior of the variables in the distillation curve. This difference may be related to the fact that the EDG set is composed of samples of only one gasoline doped with different concentrations of ethanol, unlike the MPG set composed of samples from various refineries. In the EDG set, three latent variables were responsible for 81.9% of the total variance explained by the model (Table 1), out of which 76.4% were from the first latent variable.

Analysis of Fig. 3A shows that three areas of distilled volume, % (v/v), were formed in the EDG set. The first area (I) is related to the initial part of the distillation curve, between 4 and 55% (v/v). The second area (II) is related to the interval between 56 and 63% (v/v), and a third area (III) between 64 and 93% (v/v). It was also observed that these areas have similar weights in latent variable 1. In the MPG set without normalization (Fig. 3B), three latent variables explained 80.8% of the model variance, 31.1% corresponds to the first latent variable and 45.6% to the second latent variable. The three areas have different weights for the two first latent variables, and show a distinct behavior from the EDG set. This behavior is due to the different origin of the samples, thus indicating that gasoline composition has a significant impact on the weight of variables. A

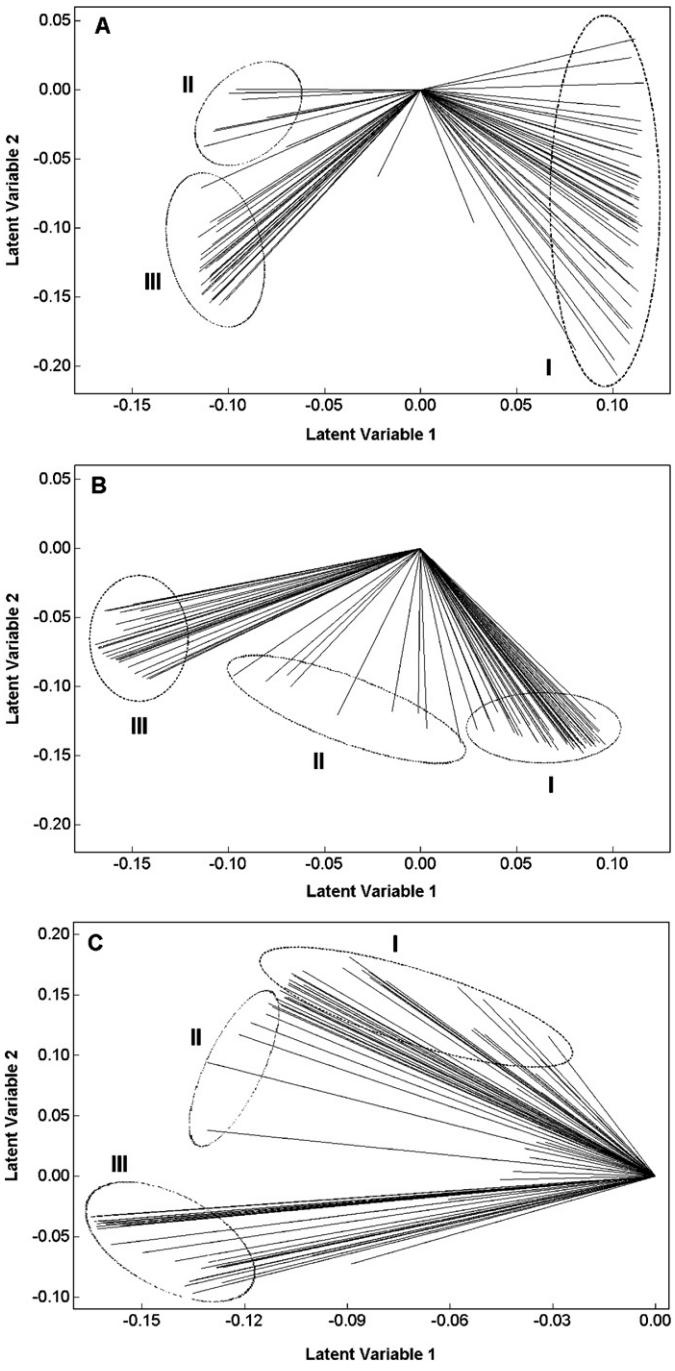

Fig. 3. Weight graphics obtained for the determination of alcoholic content in gasoline with EDG (A), MPG (B) and MPG25 (C) sets, highlighting three different areas of the distillation curves: (I) 4–55% (v/v); (II) 56–63% (v/v); (III) 64–93% (v/v).

Table 1
RMSEC, RMSEP and Q^2 values, among other parameters, obtained for several models built with different sets (EDG and MPG), in the determination of alcoholic content in gasoline as from the distillation curves.

Parameter	EDG	MPG without normalization	MPG normalized by 25% (v/v) point
Q^2	0.992	0.959	0.972
Number of latent variables	3	9	10
Explained variance LV1 (%)	76.4	31.1	42.9
Explained variance LV2 (%)	3.6	45.6	21.7
Explained variance LV3 (%)	1.9	4.1	11.7
RMSEC	0.227	0.321	0.248
RMSEP	0.304	0.691	0.538
RMSEP autoscaled	0.437	0.665	0.652
RMSEP mean centered	0.422	0.641	0.534
Test t (t_{calc})	1.0	1.7	1.8
Test t (t_{tab})	2.1	2.0	2.0

previous study [26] confirmed that the initial part of the distillation curve, between 34 and 45% (v/v), had greater weight in the model for prediction of gasoline origin with distillation curves.

For the MPG set normalized by the temperature reading at 25% volume evaporated, MPG25 (Fig. 3C) three latent variables explained just 76.3% of the model variance, with 42.9% for the first one. The use of this normalization provided a weight increase of the first latent variable in area C, which corresponds to the distillation of ethanol. Thus, the variables of area C have greater weight in the explanation of the model, mainly in the 77–93% (v/v) range, since the first latent variable is the most important in determining the alcoholic content.

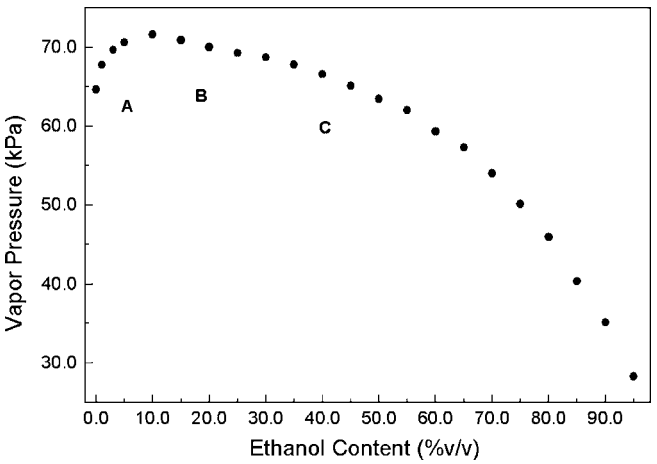

Fig. 4. Behavior of vapor pressure according to the volume of ethanol added to gasoline. Figure adapted from Brand et al. [39].

After building the calibration models, it was observed that the samples of sets EDG and MPG had separated according to the different alcoholic content in the two first latent variables. In the EDG set, the data set was separated into two groups with alcoholic content ranging from 15 to 23 and 24 to 30% (v/v), whereas for the MPG set the separations ranged from 19 to 24 and 25 to 31% (v/v), with or without normalizations. This separation is not only related to the formation of azeotropes mentioned above, but also to the vapor pressure variance in ethanol–gasoline mixtures, an important characteristic which is indicative of the behavior of fuel in different operating conditions in spark-ignition engines, and is also directly related to its volatility.

Fuels with high vapor pressure present a high rate of emission of volatile compounds [8], and the addition of different concentrations of ethanol causes alterations in vapor pressure, since the pressure of gasoline is approximately three times higher than that of ethanol, as shown in research done by Brand et al. [39]. In this research, vapor pressure measurements were carried out in several ethanol–gasoline mixtures, demonstrating that the vapor pressure of the gasoline was initially raised by the addition of up to 4% (v/v) of ethanol, but at an ethanol concentration of 15% (v/v) the vapor pressure dropped, as can be observed in Fig. 4 (reproduced from Brand et al. [39] results). Vapor pressure reduced approximately 0.159 kPa $^{\circ}C^{-1}$ in the range of 15 and 25% (v/v) of ethanol, whereas in the range of 25 and 30% (v/v) it decreased slightly less at a rate of 0.110 kPa $^{\circ}C^{-1}$. These first two ranges coincide, to an extent, with the ranges observed in the separation of sets EDG and MPG, demonstrating a close relationship between vapor pressure and the separation of alcoholic content.

RMSEC values were calculated from the calibration models for each set of samples (Table 1), and showed that the EDG set presented the lowest value for the model whose data had neither been normalized nor preprocessed. The same did not occur with the MPG set, which presented the lowest RMSEC for the data normalized by the temperature reading at 25% volume evaporated. The EDG model was built with only one type of gasoline and, therefore, it presented lower RMSEC values than the MPG set. Test *F* [40] was carried out to determine the existence of a significant statistical difference between the RMSEC values obtained for the different normalizations. Using this test, it was determined with a confidence level of 95% that in the MPG set there was a significant difference between the models normalized by the temperature reading at 25% volume evaporated and those with no normalization. This demonstrates that this normalization was the most appropriate to determine the alcoholic content in automotive gasoline. In addition, for the EDG set the *F* test showed that all the RMSEC values are statistically equivalent; indicating that in this instance there is no need to use normalizations.

The accuracy of each of the models may be verified by calculating the RMSEP [16]. According to Table 1, for the EDG set, the lowest RMSEP values were obtained for the models whose data had not been preprocessed nor normalized, and this value was lower than those for the MPG set. This is due to the higher linearity, that is, a higher Q^2 value of the analytical curves of set EDG over those of the MPG set.

The application of test *F* to the obtained RMSEP values demonstrated with a confidence level of 95% that, in general, preprocessing did not provide a significant improvement of the values in any of the sets studied. However, for the MPG set, the normalization by the temperature reading at 25% volume evaporated provided a significant decrease in the values found, and showed it is the best option.

An evaluation of the accuracy of the proposed method was done by comparing its results with those obtained through a different method such as NBR-13992, using test *t* (Eq. (4)) and analyzing the calculated *t* value (t_{calc}) [40]:

$$t_{calc} = \frac{\bar{d}}{\sqrt{\sum (d_i - \bar{d})^2 / n - 1}} \sqrt{n} \quad (4)$$

where $\bar{d}$ is the average difference between methods, d_i the difference between methods for each sample, and n the number of data pairs.

The t values in the tables (t_{tab}) for the EDG and MPG sets of samples were lower than the calculated values (t_{calc}), with a confidence level of 95%, showing that there was no significant difference between the PLS models based on distillation curves and those of the NBR-13992 method. This demonstrates the accuracy of the proposed method.

To evaluate the repeatability and reproducibility of the method, the model chosen was one whose data was normalized by the temperature reading at 25% volume evaporated with the MPG set. The repeatability and reproducibility values obtained for NBR-13992 were 0.37 and 0.44% (v/v), respectively, whereas for the proposed method, the values were 0.54 and 0.57% (v/v), respectively. Test *F*, applied to these values, showed with a confidence level of 95% that the repeatability and reproducibility of both methods are equivalent and lower than the maximum limit established by NBR 13992 [5], 1 and 2% (v/v), respectively, thus demonstrating the effectiveness of the proposed method.

In addition to supplying the same results as the normalized method, the proposed method provides more decimal digits, i.e., it is more accurate, as the results obtained by NBR-13992 have no decimal digits due to the inexactness of the graduated cylinder. When the values obtained by the proposed method have no decimal digits, the repeatability and reproducibility values drop slightly (0.60 and 0.68, respectively), although they are still significantly equivalent to NBR-13992.

3.2. Prediction of specific gravity

The same normalizations and preprocesses mentioned above were applied to determine specific gravity, using distillation curves associated to multivariate calibration as well as cross validation (leave-one-out), in a set of samples from different refineries containing 100 samples for the calibration set and 35 for validation.

Several latent variables were used in this work, depending on the type of normalization used. Nine latent variables were employed to build the calibration curve in the non-normalized data, whereas 7–10 latent variables were used to build the calibration of data, depending on the type of normalization applied. As opposed to the

Table 2
RMSEC, RMSEP and Q^2 values, among other parameters, obtained in the determination of specific gravity in gasoline as from the distillation curves.

Parameter	Values
Q^2	0.841
Number of latent variables	9
Explained variance LV1 (%)	72.1
Explained variance LV2 (%)	5.3
Explained variance LV3 (%)	3.5
RMSEC	0.00063
RMSEP	0.00088
RMSEP autoscaled	0.00136
RMSEP mean centered	0.00088
Test t (t_{calc})	0.33
Test t (t_{tab})	2.0

determination of alcohol content, normalizations produced higher RMSEC values, as shown in Table 2 and Fig. 5. Test F, applied to these values showed, with a confidence level of 95%, that all the normalizations provided higher RMSEC values as well as statistically different, thus indicating that the calibration model should be built taking into consideration non-normalized data.

Compared to the values presented in other studies, the RMSEC value for this model (0.0006) was lower than the RMSECV value obtained by Balabin et al. [22] (0.0028) using PLS and FT-NIR. This comparison of values was feasible because the calibration model was built with the best amount of latent variables (associated to the highest Q^2 value), which was calculated using a cross-validation method, i.e., in this case the RMSEC value can be considered similar to the RMSECV value.

In the weight graph of non-normalized data, the first latent variable provided 72.1% of the model variance, whereas the second one presented 5.3%. Fig. 6 shows that the 8–53% (v/v) interval of the distillation curve presented the highest weight of the first latent variable, indicating that this variable is the most relevant to build the PLS model.

In the graph analysis of the three first latent variables, the same separation of samples was observed – according to the specific gravity – in two groups in the 0.740–0.750 and 0.751–0.768 g mL^{-1} intervals. Although the addition of anhydrous alcohol to gasoline causes significant alterations in the distillation curve, the specific gravity of the mixture increases linearly in the 10 and 70% (v/v) interval.

For each sample, the estimate of RMSEP values was carried out using different preprocesses, and indicated (with a confidence level of 95% according to test F) that the lowest value is also associated with the model containing non-preprocessed or self-scaled data.

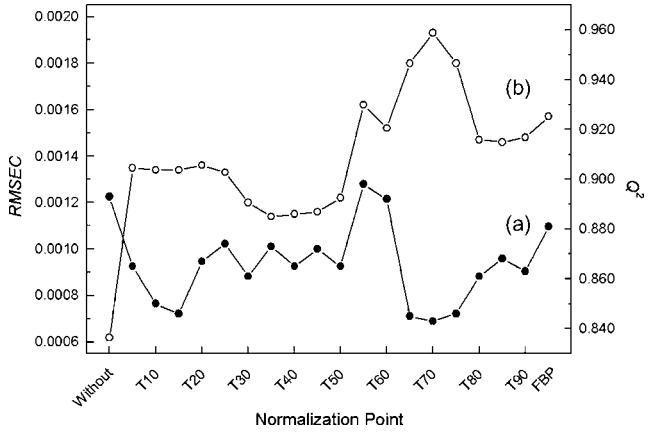

Fig. 5. RMSEC and Q^2 values obtained for models with different normalizations for the determination of specific gravity in gasoline. (a) Q^2; (b) RMSEC.

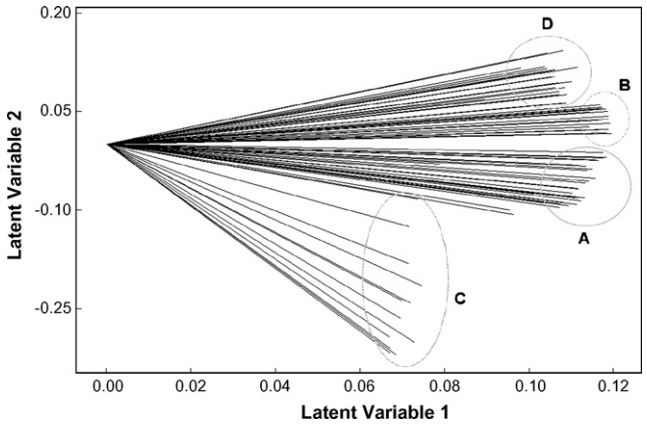

Fig. 6. Weight graphics obtained for the determination of specific gravity in gasoline, highlighting four different areas of the distillation curves: (A) 8–33% (v/v); (B) 34–53% (v/v); (C) 55–66% (v/v); (D) 70–93% (v/v).

Test t was also performed to check the accuracy of the proposed method compared to the ASTM-D4052 method. This test proved that the t_{calc} value was lower than the t_{tab} value, i.e., the accuracy of the proposed method is statistically similar to the accuracy of the ATSM-D4052 method. The analyses of the Q^2 values of the calibration models, as well as the results of tests t and F, indicated that the best method to determine specific gravity is the method with non-normalized distillation curves, unlike the result obtained in the determination of alcohol content.

Compared to the values presented in other studies, the RMSEP value for this model (0.0009) was lower than those obtained by Oliveira et al. [10] (0.0026 and 0.0050) using PLS and FT-NIR, thereby showing the great accuracy of the proposed method.

To evaluate the repeatability and reproducibility of the method, the model chosen included non-normalized and non-preprocessed data. The values obtained for repeatability and reproducibility for ASTM-D4052 were 0.00012 and 0.00020 g mL^{-1}, for ASTM-D1298 values were 0.00034 and 0.00040 g mL^{-1}, and for the method proposed in this work, values were 0.00065 and 0.00076 g mL^{-1}, respectively.

4. Conclusions

The distillation curves obtained by ASTM-D86, together with the PLS multivariate calibration method, managed to predict the alcoholic content in the 19–31% (v/v) range, with gasoline specific gravity in the 0.74–0.76 mg L^{-1} range, regardless the refineries from which they came from, with low RMSEC and RMSEP values.

The weight graphs presented different behaviors of the distillation curve, of the EDG and MPG sets in the determination of the alcoholic content, and of the set of samples used in the determination of specific gravity.

For the determination of alcoholic content it was found that it is best to use a non-preprocessed, normalized by the temperature reading at 25% volume evaporated model with different origins and ethanol concentrations (as the MPG set). The repeatability and reproducibility values in the determination of the alcoholic content using the distillation curves and PLS were equivalent to those of the NBR-13992 method.

In the determination of specific gravity the best model was the one whose data had no preprocess nor normalization, with lower RMSEP values than those found in the literature. In addition to accuracy, the proposed method provides higher repeatability and reproducibility values and it is statistically different from the ASTM-D1298 and D4052 methods.

The use of distillation curves associated with chemometric techniques leads to high accuracy, demonstrating that it can be easily implemented in routine analyses, providing different parameters in only one assay.

Acknowledgements

The authors would like to thank CTPetro-FINEP and ANP for their financial support.

References

[1] J.P.A. Magalhães, N. Kuperman, R.C. Machado, Proalcool: Uma Avaliação Global, 1st ed., Publ. ASTEL, Rio de Janeiro, 1991.
[2] Agência Nacional do Petróleo e Biocombustíveis, Portaria no. 309, 27/12/2001, http://www.anp.gov.br.
[3] Agência Nacional do Petróleo, Gás Natural e Biocombustíveis, Anuário Estatístico, 2007, http://www.anp.gov.br.
[4] Agência Nacional do Petróleo, Gás Natural e Biocombustíveis, Boletim da Qualidade, Não-Conformidades no Brasil, December 2008, http://www.anp.gov.br.
[5] Gasolina Automotiva-Determinação do Teor de Álcool Etílico Anidro Combustível (AEAC), NBR-13992, Associação Brasileira de Normas Técnicas, 1997.
[6] Standard Test Method for Density, Relative Density (Specific Gravity), or API Gravity of Crude Petroleum and Liquid Petroleum Products by Hydrometer Method, ASTM-D1298, American Society for Testing and Materials, 2005.
[7] Standard Test for Density and Relative Density of Liquids by Digital Density Meter, ASTM-D4052, American Society for Testing and Materials, 2002.
[8] R. Cataluña, R. Silva, Quim. Nova 29 (2006) 580.
[9] G.E. Fodor, R.A. Mason, S.A. Hutzler, Appl. Spectrosc. 53 (1999) 1292.
[10] F.C.C. Oliveira, A.T.P.C. de Souza, J.A. Dias, S.C.L. Dias, J.C. Rubim, Quim. Nova 27 (2004) 218.
[11] V.O. Santos Jr., F.C.C. Oliveira, D.G. Lima, A.C. Petry, E. Garcia, P.A.Z. Suarez, J.C. Rubim, Anal. Chim. Acta 547 (2005) 188.
[12] V.K. Seinsche, Fuel Energy Abstr. 38 (1997) 11.
[13] M.P. Gómez-Carracedo, J.M. Andrade, M. Calviño, E. Fernández, D. Prada, S. Muniategui, Fuel 82 (2003) 1211.
[14] D.L. Flumignan, F.O. Ferreira, A.G. Tininis, J.E. de Oliveira, Abstracts of Papers, 234th ACS National Meeting, Boston, MA, United States, August 19–23, 2007, FUEL-011.
[15] B. Janis, Society of Automotive Engineers [Special Publication] SP-1461 (1999) 95.
[16] J.J. Kelly, C.H. Barlow, T.M. Jinguji, J.B. Callis, Anal. Chem. 61 (1989) 313.
[17] M.C. Breitkreitz, I.M. Raimundo Jr., J.J.R. Rohwedder, C. Pasquini, H.A. Dantas Filho, G.E. Jose, M.C.U. Araujo, Analyst 128 (2003) 1204.
[18] K.J. Johnson, R.E. Morris, S.L. Rose-Pehrsson, Energy Fuels 20 (2006) 727.
[19] J.B. Cooper, K.L. Wise, W.T. Welch, R.R. Bledsoe, M.B. Sumner, Appl. Spectrosc. 50 (1996) 917.
[20] J.B. Cooper, K.L. Wise, W.T. Welch, M.B. Sumner, B.K. Wilt, R.R. Bledsoe, Appl. Spectrosc. 51 (1997) 1613.
[21] J.B. Cooper, K.L. Wise, J. Groves, W.T. Welch, Anal. Chem. 67 (1995) 4096.
[22] R.M. Balabin, R.Z. Safieva, E.A. Lomakina, Chem. Intell. Lab. Syst. 88 (2007) 183.
[23] Standard Test for Distillation of Petroleum Products at Atmospheric Pressure, ASTM-D86, American Society for Testing and Materials, 2007.
[24] P.J.S. Barbeira, R.C.C. Pereira, C.N.C. Corgozinho, Energy Fuels 21 (2007) 2212.
[25] R.M. Balabin, R.Z. Safieva, Fuel 87 (2008) 1096.
[26] P.J.S. Barbeira, H.G. Aleme, L.M. Costa, Fuel 87 (2008) 3664.
[27] D.L. Massart, B.G.M. Vandeginste, L.M.C. Buydens, S. Jong, P.J. Lewi, J. Smeyers-Verbeke, Handbook of Chemometrics and Qualimetrics. Part B, 1st ed., Elsevier Publ., Amsterdam, Lausanne, New York, Oxford, Shannon, Singapore, Tokyo, 1998.
[28] M. Otto, Chemometrics: Statistics and Computer Application in Analytical Chemistry, 1st ed., Wiley-VCH Publ., Weinheim, New York, Chichester, Brisbane, Toronto, 1999.
[29] ISO/IEC 5725-2, Accuracy (Trueness and Precision) of Measurement Methods and Results. Part 2. Basic Method for the Determination of Repeatability and Reproducibility of a Standard Measurement Method, 2002.
[30] INMETRO DOQ-CGCRE-008, Orientação sobre Validação de Métodos de Ensaios Químicos, 2007.
[31] R.M. Balabin, R.Z. Syunyaev, S.A. Karpov, Energy Fuels 21 (2007) 2460.
[32] R. French, P. Malone, Fluid Phase Equilib. 228–229 (2005) 27.
[33] R.M. Balabin, R.Z. Syunyaev, S.A. Karpov, Fuel 86 (2007) 323.
[34] P. Geladi, B.R. Kowalsky, Anal. Chim. Acta 185 (1986) 1.
[35] B. Hemmateenejad, A. Abbaspour, H. Maghamia, R. Miri, M.R. Panjehshahin, Anal. Chim. Acta 575 (2006) 290.
[36] S. Wold, M. Sjöström, L. Eriksson, Chemometr. Intell. Lab. Syst. 58 (2001) 109.
[37] Minitab-14, Statistical Software for Windows, Minitab Inc., State College, PA, 2003.
[38] I.N. Wakeling, J.J. Morris, J. Chemometr. 7 (1993) 291.
[39] J.I. Brand, J.A. Pumphrey, W.A. Scheller, Fuel 79 (2000) 1405.
[40] D.C. Harris, Análise Química Quantitativa, 5th ed., LTC Editora, Rio de Janeiro, 2001.

Talanta 78 (2009) 1446–1451

Contents lists available at ScienceDirect

Talanta

journal homepage: www.elsevier.com/locate/talanta

Use of multiple sequential injections of equal volumes to determine the apparent binding constant for antibody-antigen complexes by capillary electrophoresis

Sara Almeda[a], Eloy Salinas[b], Cristina Arce[c], Angela Moreno[c], Lourdes Arce[a], Miguel Valcárcel[a,*]

[a] Department of Analytical Chemistry, University of Córdoba, Campus of Rabanales, E-14071 Córdoba, Spain
[b] Department of Biochemistry and Biological Sciences, National University of San Luis, Chacabuco and Pedernera, 5700 San Luis, Argentina
[c] Mixed Research Unit on Molecular Genetic Markers, University of Córdoba, Building C-5, Campus of Rabanales, E-14071 Córdoba, Spain

ARTICLE INFO

Article history:
Received 24 September 2008
Received in revised form 12 February 2009
Accepted 20 February 2009
Available online 5 March 2009

Keywords:
Antibody
Antigen
Binding constant
Capillary electrophoresis
ELISA
Flow-through partial-filling technique

ABSTRACT

A new modified version of the well-known flow-through partial-filling technique [*viz.* multiple sequential injection of equal volumes (MSI-EV) of neutral marker, antigen (Ag) and antibody (Ab)] was used to calculate the apparent binding constant (K_a) of monoclonal Ab (mAb) and polyclonal Ab (pAb) to their specific antigens (Ags). Such a constant is very important in immunoassays. The procedure involves the sequential injection of small, identical volumes of a neutral marker (dimethyl sulfoxide, DMSO), an Ag and an Ab into a capillary column for electrophoresing. The apparent K_a values thus obtained from a Scatchard plot were $0.76 \pm 0.15\ mg^{-1}$ mL for the complex of anti-canine Immunoglobulin G (IgG) as mAb and canine IgG as Ag, and $0.79 \pm 0.14\ mg^{-1}$ mL for that between anti-human IgG as pAb and human IgG as Ag. These values are of the same order to those provided by indirect competition enzyme-linked immunosorbent assay (ELISA) (*viz.* $0.42 \pm 0.28\ mg^{-1}$ mL for the mAb–Ag complex and $0.81 \pm 0.09\ mg^{-1}$ mL for the pAb–Ag complex). The high sensitivity of the MSI-EV–CE technique affords the detection of very low concentrations of Ab.

1. Introduction

Characterizing receptor–ligand interactions, which are essential with a view to understanding some essential biological processes, requires the use of effective methods to examine biomolecular interactions. The idea of using capillary electrophoresis (CE) to examine binding interactions was conceived in the 1990s and has been developed in several subsequent studies [1–13]. The CE technique not only provides the advantages derived from the small dimensions of a capillary [*e.g.* high mass sensitivity, reduced consumption of expensive reagents such as antigens (Ags) and antibodies (Abs), short analysis times, automatability, operational flexibility], but also affords efficient separation and reproducible quantitation by on-line detection of unlabeled components in the bulk solution rather than at the liquid–solid interface. Moreover, CE is a unique choice for directly examining interactions between molecules under near-physiological conditions without the need to previously immobilize the reactants in a solid phase [14].

CE variants including the Hummel–Dreyer (HD) [15], vacancy peak (VP), frontal analysis (FA) [16], affinity capillary electrophoresis (ACE) [17,18] and vacancy affinity capillary electrophoresis (VACE) methods have been used to estimate binding constants (K_a) [19]. Based on existing literature, ACE has to date been the most frequently used CE method for this purpose.

In ACE, the mobility of a ligand (*e.g.* an antigen (Ag) is altered by the presence of a receptor (*e.g.* an additive such as antibody (Ab)) in the electrophoretic solution. The ability to easily monitor mobility changes via shifts in migration time of the ligand allows the presence of interacting substances to be readily detected. ACE is therefore a convenient tool for identifying interacting substances [14]. However, the accuracy of the K_a values it provides can be compromised by some shortcomings of this technique. Thus, changes in viscosity with increase in concentration of the buffer additive can alter electrophoretic and electroosmotic mobilities [20,21]; also, accurately determining K_a with traditional ACE methods may be impossible unless the procedure is appropriately modified if the amount of ligand or receptor available is inadequate. The use of partial-filling modes in CE has proved an effective method for measuring some types of interaction [22]. Thus, receptor–ligand interactions can be studied by using three modified versions of the parent partial-filling technique, namely: partial-filling affinity CE (PFACE) [22,23], flow-through PFACE [24,25], and multiple-step ligand injection affinity CE [26,27].

The aim of this work was to develop a new electrophoretic method to determine apparent K_a for two different Abs [*viz.* monoclonal Ab (mAb) and polyclonal Ab (pAb)] with their specific Ags. To this end, we developed a new version of flow-through PFACE called "multiple sequential injection of equal volumes" (MSI-EV). The pro-

* Corresponding author.
E-mail address: qa1meobj@uco.es (M. Valcárcel).

0039-9140/$ – see front matter © 2009 Elsevier B.V. All rights reserved.
doi:10.1016/j.talanta.2009.02.049

posed technique uses only a few nanoliters of receptor and ligand to calculate apparent K_a with a high sensitivity. For this purpose, small, identical volumes of a neutral marker, receptor and ligand are sequentially injected into a capillary in order to extract qualitative and quantitative information about their molecular interactions. Appropriate mathematical treatment of the relationship between the mobility change in the complex formed inside the capillary and the Ab concentration allows one to establish a simplified equation that affords calculation of K_a from a conventional Scatchard plot [14]. The main differences between the proposed, MSI-EV–CE method and flow-through PFACE are that Ab is not dissolved in the separation electrophoresis buffer used to fill the capillary and that our method uses identical volumes of Ag and Ab. Also, no electroosmotic flow (EOF) marker need be injected together with Ag or Ab in order to avoid contaminating such valuable substances and facilitate their reuse.

The apparent K_a value obtained with MSI-EV–CE was compared with that provided by ELISA. Classical ELISA [28] measures the amount of Abs interacting with Ags coated on a microtiter plate to obtain a relative dissociation constant. By contrast, the proposed MSI-EV–CE method calculates apparent K_a in solution without the need to immobilize Ag or Ab.

2. Experimental

2.1. Reagents

Anti-human immunoglobulin G (IgG) developed in goat (whole molecule), IgG from human serum, anti-goat IgG (whole molecule)-peroxidase developed in rabbit, anti-mouse polyvalent immunoglobulins (IgG, IgA, IgM)-peroxidase, phosphate buffer saline (PBS) in tablets, sodium borate, sodium carbonate, sodium azide, dimethyl sulfoxide (DMSO), dimethyl formamide (DMF) and Met–Arg–Phe–Ala synthetic peptide were obtained from Sigma (St. Louis, MO). Boric acid, Tween 20, sodium hydroxide and methanol were purchased from Panreac (Barcelona, Spain). Anti-canine IgG mAb and canine IgG were produced by the Mixed Research Unit on Molecular Genetic Markers of the University of Córdoba (Spain) [29]. Working solutions were prepared on a daily basis by diluting the stock solutions to an appropriate extent with electrophoretic buffer. All water used was purified by passage through a Milli-Q system from Millipore (Bedford, MA). Ag and Ab solutions were stored at −20 °C and allowed to reach room temperature prior to use. Also, the separation buffer and NaOH solution were passed through a microporous nylon filter of 0.45 μm pore size and 25 mm diameter purchased from Macherey–Nagel (Easton, PA).

2.2. Apparatus and procedure

CE was performed on a P/ACE MDQ System from Beckman Coulter (Palo Alto, CA) equipped with a diode array detector (DAD). Neutral marker, Ag and Ab, all dissolved in buffer solution, were each injected hydrodynamically at 0.5 psi for 5 s, which was equivalent to *ca.* 25 nL as calculated from the Hagen–Poiseuille equation. Separation was done by applying 10 kV voltage at 25 °C for 10 min and monitoring at 214 nm. An uncoated narrow bore silica capillary (Beckman Coulter) with an inner diameter of 75 μm, a total length of 60.2 cm and an effective separation length of 50 cm was used for this purpose. The P/ACE MDQ System software was used for data acquisition and OriginPro 7.0 for data processing. An uncoated, narrow bore fused-silica capillary was used in the tests since the intrinsically negatively charged wall at pH 8 reduced adsorption of the anionic Ab–Ag complex.

Prior to first use, the capillary was conditioned by rinsing with 1 M HCl for 5 min, H_2O for 1 min, 0.1 M NaOH for 10 min, H_2O for 1 min and separation buffer for 10 min. The capillary was prepared for daily use by rinsing with 0.1 M NaOH for 10 min, H_2O for 5 min and separation buffer for 5 min. Before each analysis, the capillary was flushed with H_2O for 1 min, 0.1 M NaOH for 4 min, H_2O for 1 min and separation buffer for 2 min prior to injection. The separation buffer was prepared by freshly mixing 65 mM boric acid and 15 mM sodium borate [28,30], and adjusting to pH 8 with 0.1 M NaOH.

2.3. Sample preparation

Anti-canine IgG mAb (CA3B8) recognizing antigenic determinants on canine IgG heavy and light chains was previously produced and characterized by Arce et al. [29]. Anti-canine IgG mAb was obtained at a final concentration of 3.57 mg mL^{-1} and dissolved in PBS for subsequent dilution in electrophoretic buffer.

Serum samples were collected from adult dogs at the Veterinary Clinic Hospital of the University of Córdoba. The serum was separated from cells by centrifugation and stored frozen at −20 °C until use. Immunoglobulin was isolated from a normal pool serum, using affinity chromatography with protein A as affinity ligand. The total protein content was determined with the commercial Bio-Rad kit (Munich, Germany). Finally, the purity of the canine IgG was checked by sodium dodecyl sulphate–polyacrylamide gel electrophoresis (SDS-PAGE). Canine IgG was obtained at a final concentration of 5.95 mg mL^{-1}, which was estimated from its UV absorbance at 280 nm as measured in a cell of 1 cm path length, $A_{280\ nm}$ being unity for a 0.685 mg mL^{-1} concentration of IgG. Subsequent dilutions were also made in electrophoretic buffer. The samples were split into aliquots and stored frozen until use in the binding tests. Commercial anti-human IgG pAb at a concentration of 0.3 mg mL^{-1} and human IgG at 15.23 mg mL^{-1} were also diluted in electrophoretic buffer. These samples were also split into aliquots and stored frozen until use in the binding tests.

2.4. Data analysis

The methodology used in this work relies on measuring differences in electrophoretic mobility ($\Delta\mu$) between the Ab–Ag complex and uncomplexed Ag at variable Ab concentrations:

$$\Delta\mu = \mu_{Ag-Ab} - \mu_{Ag} \quad (1)$$

where μ_{Ag-Ab} is the mobility of the Ab–Ag complex and μ_{Ag} that of Ag. The electrophoretic mobility of the analytes was calculated from the observed migration time, using the following equation:

$$\Delta\mu = \frac{L_w L_t}{V[(1/t_{Ag} - 1/t_{EOFAg}) - (1/t_{free} - 1/t_{EOF})]} \quad (2)$$

where L_w and L_t are the effective and total capillary length, respectively; t_{Ag} is the migration time of Ag in the presence of Ab; t_{free} is the migration time of Ag in the absence of Ab; t_{EOFAg} and t_{EOF} are the migration times for the neutral marker in the presence and absence of Ab, respectively; and V is the applied voltage [31].

We used the following linear equation to estimate K_a for a 1:1 Ag–Ab complex from a Scatchard plot:

$$\frac{\Delta\mu}{Ab} = -K_a\Delta\mu + K_a\Delta\mu_{max} \quad (3)$$

where $\Delta\mu$ is the change in electrophoretic mobility of the complex in the presence of variable concentrations of Ab and $\Delta\mu_{max}$ the mobility of Ag upon saturation with Ab. A plot of $\Delta\mu$/Ab against $\Delta\mu$ provided a straight line of slope $-K_a$ and intercept $K_a\ \Delta\mu_{max}$.

The Scatchard analysis of the data was done by using OriginPro 7.0. K_a values were expressed in mg^{-1} mL and all concentrations in mg mL^{-1}.

In all calculations, the equilibrium free Ab concentration used was approximated to the total concentration of Ab (i.e.,

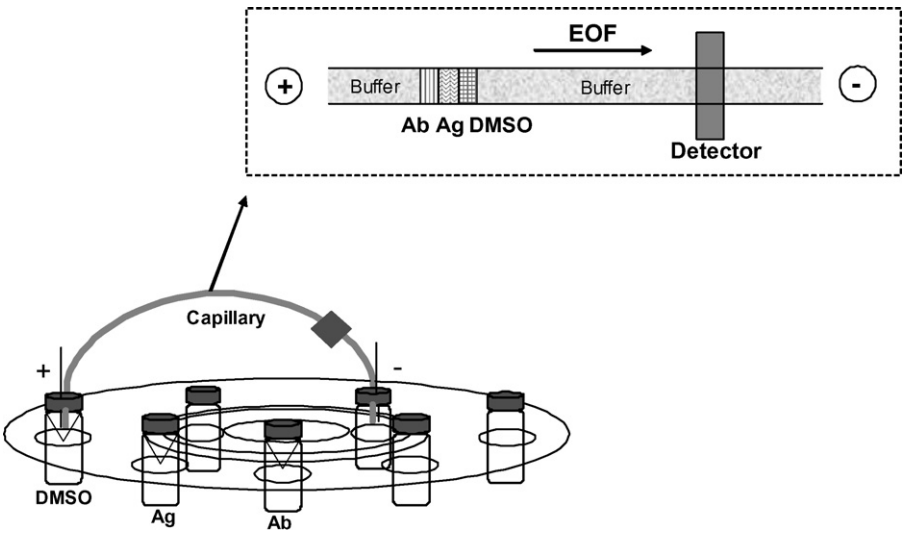

Fig. 1. Scheme of a multiple sequential injection-capillary electrophoresis run. DMSO = Dimethyl sulfoxide; Ag = antigen; Ab = antibody; EOF = electroosmotic flow.

$Ab_{free} = Ab_{total}$). This provides a reasonably good estimate when the total ligand concentration is much greater than the total solute concentration [32,33].

2.5. Determination of binding constants by indirect ELISA

Variable concentrations of Ag from 0.15 to 0.9 mg mL^{-1} were mixed with a fixed amount of Ab (0.004 mg mL^{-1}) in buffer solution (65 mM boric acid, 15 mM sodium tetraborate, pH 8). Note that the concentrations of Ag and Ab used for monoclonal and polyclonal complexes were identical. After 12 h of incubation at 22 °C, a volume of 250 μL of each mixture was transferred to wells of a Nunc-Immuno microtitration plate and incubated for 1 h at 37 °C; the plate was previously coated with Ag (1 μg mL^{-1}) in sodium carbonate buffer (50 mM, pH 9.6) containing sodium azide (0.02% m/v) overnight at 4 °C (100 μL/well). Following washing with PBS containing 0.05% v/v Tween 20, bound immunoglobulins were detected by addition of anti-mouse polyvalent immunoglobulins (IgG, IgA, IgM) for the monoclonal complex and anti-goat IgG for the polyclonal complex, both conjugated with peroxidase, and the peroxidase activity retained in each well was determined according to Friguet et al. [34].

The dissociation constant in solution was determined by using an equation derived elsewhere [34] from a Scatchard plot obtained in the presence of excess Ag, namely: $\frac{1}{\nu} = 1 + Kd\frac{1}{a_o}$ where ν is the fraction of bound Ab, a_o the total concentration of Ag and K_d the dissociation constant at equilibrium. ν *denotes* $\frac{A_o - A}{A_o}$, where A is the absorbance at a given concentration as measured by ELISA, and A_o that of Ab as measured in the absence of Ag. The dissociation constant, K_d, was calculated from the equation of the best-fit straight line where the slope equalled K_d and $K_a = 1/K_d$.

3. Results and discussion

3.1. Electrophoretic medium for determining apparent binding constants by CE

We considered various factors in optimizing the electrophoretic buffer with a view to determining mAb–Ag complexes. Thus, the anti-canine IgG mAb employed contain a single, homogeneous population of Ab molecules specific to a well-defined epitope on Ag and should exhibit a single, homogeneous peak in the electropherogram [12,28,35]. However, the anti-canine IgG mAb was also a glycoprotein and thus likely to exhibit multiple peaks in the electropherogram [28,36] because of its microheterogeneity in two charged *N*-linked branched oligosaccharide chains bound to the CH_2 domains [28,37]; this might hinder estimation of the migration time for the target analyte. Based on the foregoing, the first step of the process involved examining and optimizing the CE conditions with a view to ensuring homogeneity and good recoveries of mAb in the electropherogram. Once the electrophoretic medium was optimized to identify the mAb–Ag complex, it was also used to calculate apparent K_a for the pAb–Ag complex.

The most suitable electrophoretic separation medium compatible with the physiological conditions allowing the molecules to interact was then identified. In most situations, phosphate buffer has proved the best running background buffer for this purpose [14,15,17,38–42]. In our case, however, it resulted in multiple peaks throughout the studied pH range, probably as the result of a twofold effect (a reduced EOF and an increased difference in charge between glycoforms).

Using a solution containing 65 mM boric acid and 15 mM sodium borate at pH 7.0 as the running buffer [28,30] resulted in multiple peaks for the mAb–Ag complex, which can be ascribed to microheterogeneity in the sugar chains of mAb [28,43]. At pH 8.0–8.5, where EOF was faster, Abs was eluted as a single peak and no separation of glycoforms was observed [28]. This can be ascribed to the IgG molecule existing as a negative species at pH 8, and the interaction between solutes and the negatively charged capillary wall being minimized as a result of a charge repulsion effect. We therefore assumed that protein adsorption has little effect on affinity shift measurements and posed no problem in the tests as a result. For this reason, we chose to use borate at pH 8.0 as running background buffer, which resulted in a single peak for the complex and in good repeatability. Also, we used the same electrophoretic buffer to calculate apparent K_a for the pAb–Ag complex as it also led to a single peak in the electropherogram.

The EOF marker was used to monitor EOF and determine the reproducibility of the migration time for the complex. The markers studied included Met–Arg–Phe–Ala synthetic peptide [28], DMSO [40], dimethyl formamide [17,41] and methanol, the best among which was DMSO, with good repeatability.

3.2. In-line complex formation

MSI-EV from one end of the capillary was used to obtain the Ag–Ab complex in-line. The first parameter to be optimized was

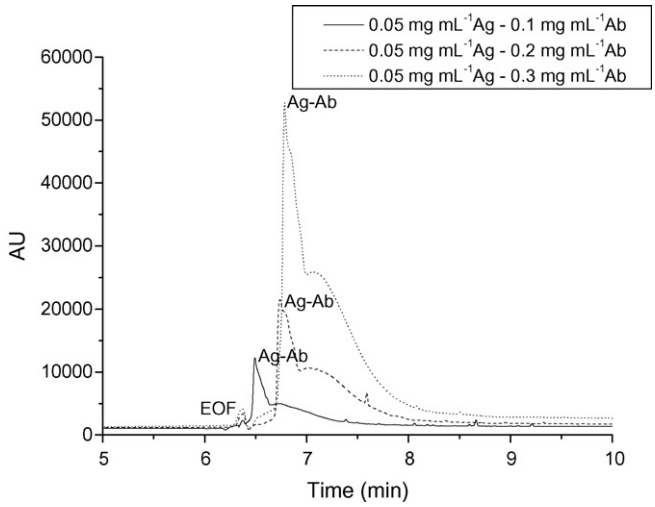

Fig. 2. Evaluation of antigen binding to monoclonal antibody by multiple sequential injection-capillary electrophoresis. Concentrations of 0.01% DMSO, 0.05 mg mL^{-1} antigen and 0.1–0.3 mg mL^{-1} antibody were sequentially injected into the capillary at 0.5 psi for 5 s each; analyzed by CE using a 65 mM boric acid—15 mM sodium borate buffer (pH 8) at a separation voltage of 10 kV and a capillary temperature of 25 °C; and detected at 214 nm.

the reaction temperature inside the capillary. Concentrations of 0.01% v/v DMSO, 0.05 mg mL^{-1} Ag and 0.3 mg mL^{-1} mAb in buffer were used for this purpose. A volume of 20 μL of each solution was placed in electrophoresis minivials (see Fig. 1). Samples were kept at ambient temperature in the autosampler and injected by pressure at 0.5 psi for 5 s. Injected Ag and Ab reacted inside the capillary (Fig. 1) to form the Ag–Ab complex, which was completely separated from the neutral marker within 10 min. The complex was obtained at three different temperatures (25, 37 and 47 °C) and separation was done at 10 kV. Each test series was performed in triplicate. The increased temperature inside the capillary boosted formation of the complex and caused its peak area to increase with increasing temperature. Although the higher temperatures (37 and 47 °C) resulted in increased sensitivity, they detracted from repeatability. A temperature of 25 °C was thus chosen for subsequent tests.

Once the reaction temperature inside the capillary was optimized, the influence of the separation voltage was studied over the range of 7–25 kV. Too high voltages resulted in poor separation and low repeatability in the capillary current as the likely result of an excessive Joule effect. A voltage of 10 kV was therefore adopted as optimal. Fig. 2 illustrates the influence of the Ab concentration on the migration time of the complex under the optimum CE conditions for in-line formation of the complex.

Although the formation kinetics of the complex was not studied in depth here, we can confirm that Abs of moderate affinity such as CA3B8 mAb bind to Ags in a short time. Thus, Arce et al. [29] characterized this Ab and found the Ab–Ag binding reaction to complete within a few minutes. Also, the moderate-affinity Ab used in this work complexed the Ag in less than 8 min (see the electropherogram of Fig. 2). The complex exhibited no dissociation during this time, which is consistent with applicable theory and confirms that the dissociation half-time for a moderate-affinity Ab is 30 min or longer, whereas that for a low-affinity Ab can be a few minutes or even less [44].

3.3. Analytical features

The applicability of the proposed CE system was assessed from its within-day and between-day repeatability as determined with standard solutions of the analytes. The within-day repeatability in the migration time for the mAb–Ag complex was studied in 3 different analyses involving the injection of 0.05 mg mL^{-1} Ag and 0.3 mg mL^{-1} Ab; the average relative standard deviation (RSD) thus obtained was 0.4%. The between-day repeatability in the migration time, also expressed as RSD, was evaluated by measuring standard solutions containing 0.05 mg mL^{-1} Ag and 0.3 mg mL^{-1} Ab over 9 runs performed on 3 different days; the resulting RSD was 2.6%. Similar tests were performed for the pAb–Ag complex that provided a within-day repeatability of 0.7% and a between-day repeatability of 2.9%.

Table 1
Calibration curves and analytical figures of merit of the Ab–Ag complex as obtained by using multiple sequential injections of equal volumes in capillary electrophoresis.

Analyte	$y = a + bx$	R^2	LOD mg mL^{-1}
Monoclonal Ab–Ag	$a = 175{,}042 \pm 661$ $b = 6351 \pm 404$	0.99398	0.05
Polyclonal Ab–Ag	$a = -65{,}277 \pm 84{,}538$ $b = 467{,}859 \pm 25{,}635$	0.99111	0.08

x = concentration (mg mL^{-1}); y = absorbance; a = intercept; b = slope; R^2 = correlation coefficient; LOD = limit of detection.

We used the above-described optimum experimental conditions to obtain calibration curves (see Table 1) as plots of peak area for the monoclonal and polyclonal Ab–Ag complexes against the Ab concentration; R^2 was 0.994 and 0.991, respectively. Plots were constructed by using a constant Ag concentration (0.05 mg mL^{-1}) and increasing Ab concentrations over the range 0.1–0.3 mg mL^{-1}. Each point in the calibration graph was the average of three independent measurements. Limits of detection (LODs) were determined by using variable concentrations of Ab and a constant concentration of Ag. The LOD for the complexes as obtained with the in-line MSI-EV method were 0.05 mg mL^{-1} for the monoclonal complex and 0.08 mg mL^{-1} for the polyclonal complex.

3.4. Determination of apparent binding constants

The apparent K_a for the monoclonal and polyclonal Ab–Ag complexes were calculated by using multiple sequential injections of 5 s at 0.5 psi each of 0.01% v/v DMSO, 0.05 mg mL^{-1} Ag and variable concentrations of Ab over the range of 0.1–0.3 mg mL^{-1}. No mAbs concentrations in other ranges could be studied owing to the low initial concentration (3.57 mg mL^{-1}) and volume (2 mL) of mAbs available. Commercial anti-human IgG pAb was also obtained at quite a low concentration (0.3 mg mL^{-1}).

The migration times for the complexes formed at variable Ab concentrations were substituted into equation (2) in order to calculate the electrophoretic mobility of the analytes (μ). Plotting such mobility against the $\Delta\mu/|\mathrm{Ab}|$ ratio provided a straight line of slope $-K_a$ throughout the studied concentration range. Based on the results, the proposed system is suitable for calculating apparent K_a in both monoclonal and polyclonal Abs.

Applying the Scatchard equation required assuming the following as regards molecular interactions: (*a*) the binding interaction was univalent; (*b*) bound and unbound species were in equilibrium; (*c*) interactions of Ag and Ab with the capillary wall had no significant effect on their mutual binding interactions; and (*d*) the electric field had no influence on K_a [45,46]. The Scatchard method is only valid for binding systems exhibiting moderate to strong affinity. In strongly bound complexes, the interacting compounds and the complex have unique migration mobilities. In weakly bound complexes, the complex dissociates gradually during the run, so only the interacting compounds—not the final complex—can be detected [46].

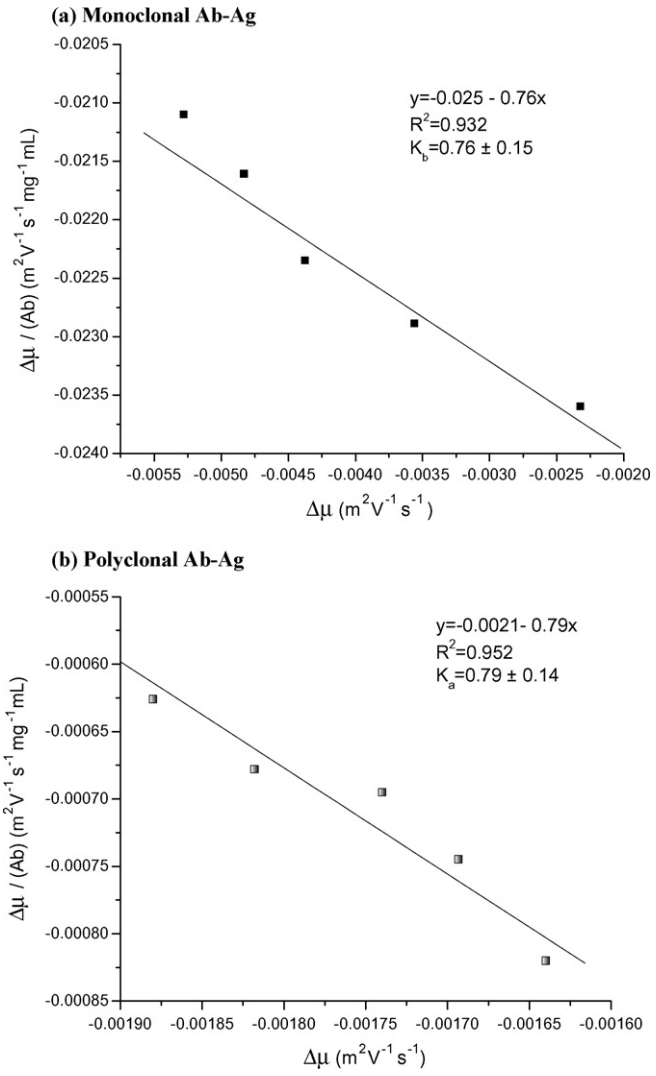

Fig. 3. Scatchard plot of antigen to monoclonal and polyclonal antibody binding obtained by using multiple sequential injection-capillary electrophoresis in combination with Eq. (2).

Fig. 3 shows the Scatchard plots used to determine apparent K_a. The correlation coefficients for the monoclonal and polyclonal Ab–Ag complexes were greater than 0.932 and 0.952, respectively. The two apparent K_a values obtained were similar ($0.76 \pm 0.15\,mg^{-1}$ mL and $0.79 \pm 0.14\,mg^{-1}$ mL for the monoclonal and polyclonal complex, respectively). Based on them, the Ab has a moderate affinity for the Ag. Also, the results testify to the high quantifying potential of the proposed method. It should be noted that the K_a value obtained was an average value characterizing binding interactions in two "mixtures" of closely related proteins (Ag and Ab) since interactions were measured between two protein mixtures rather than two specific molecules.

The results obtained with this new MSI–CE method were validated by comparison with those provided by ELISA. A number of ELISA and radioimmunoassay methods have lately been used to quantify Ag–Ab interactions. However, only those based on indirect competition ELISA afford accurate quantitation of the actual thermodynamic affinity of Abs for their Ags [28,47]; this led us to use an indirect competition method based on ELISA [28,38] to determine the true K_a for the complex and enable a legitimate comparison with our MSI–CE method. The experimental K_a values thus obtained by linear regression were $0.42 \pm 0.28\,mg^{-1}$ mL for the monoclonal Ab–Ag complex and $0.81 \pm 0.09\,mg^{-1}$ mL for the polyclonal complex. As can been seen, the K_a value provided by the MSI–CE method compares favorably with that calculated by ELISA.

4. Conclusions

The proposed method affords the calculation of statistically reliable binding parameters for the complexes of mAb with canine IgG and pAb with human IgG. Based on its simplicity, wide applicability and adaptability to high-throughput systems, the proposed MSI-EV–CE method, based on analyte mobility changes, is an effective alternative to existing K_a calculation methods. Under specific conditions, our method can be useful for studying the moderate to high affinity of specific Abs for any type of Ag. In addition, it has the great advantage that it requires no labeling of the Ag or Ab, which affords application to unmodified molecules.

Acknowledgement

This work was supported by DGI, Spain's Ministry of Science and Technology, within the framework of Project CTQ2007-60426.

References

[1] J.L. Carpenter, P. Camilleri, D. Dhanak, D. Goodall, J. Chem. Soc. Chem. Commun. (1992) 804.
[2] Y.-H. Chu, G.M. Whitesides, Org. Chem. 57 (1992) 3524.
[3] Y.-H. Chu, L.Z. Avila, H.A. Biebuyck, G.M. Whitesides, J. Med. Chem. 35 (1992) 2915.
[4] M. Gayton-Ely, T. Pappas, L. Holland, Anal. Bioanal. Chem. 382 (2005) 570.
[5] A. Guttman, N. Cooke, Anal. Chem. 63 (1991) 2038.
[6] N.H.H. Heegaard, F.A. Robey, Anal. Chem. 64 (1992) 2479.
[7] N.H.H. Heegaard, M.H. Nissen, D.D.Y. Chen, Electrophoresis 23 (2002) 815.
[8] S. Honda, S. Suzuki, A. Nose, K. Yamamoto, K. Kakehi, Carbohydr. Res. 275 (1991) 193.
[9] H. Kajiwara, H. Hirano, K. Oono, J. Biochem. Biophys. Methods 22 (1991) 263.
[10] H. Kajiwara, J. Chromatogr. 559 (1991) 345.
[11] J.C. Kraak, S. Busch, H. Poppe, J. Chromatogr. 608 (1992) 257.
[12] R.G. Nielsen, E.C. Rickard, P.F. Santa, D.A. Sharknas, G.S. Sittaampalam, J. Chromatogr. 559 (1991) 177.
[13] C. Schou, N.H.H. Heegaard, Electrophoresis 27 (2006) 44.
[14] S. Honda, A. Taga, Methods Enzymol. 362 (2003) 434.
[15] A.V. Rudnev, S.S. Aleksenko, O. Semenova, C.G. Hartinger, A.R. Timerbaev, B.K. Keppler, J. Sep. Sci. 28 (2005) 121.
[16] T. Le Saux, H. Hisamoto, S. Terabe, J. Chromatogr. A 1104 (2006) 358.
[17] A. El-Shafey, H. Zhong, G. Jones, I.S. Krull, Electrophoresis 23 (2002) 945.
[18] F. Progent, M. Taverna, I. Le Potier, F. Gopée, D. Ferrier, Electrophoresis 23 (2002) 938.
[19] F.B. Erim, J.C. Kraak, J. Chromatogr. B 710 (1998) 205.
[20] V.L. Lamache, M. Taverna, D. Wouessidjewe, D. Duchene, D. Ferrier, J. Chromatogr. A 735 (1996) 321.
[21] Y. Tanaka, S. Terabe, J. Chromatogr. B 768 (2002) 81.
[22] J. Heintz, M. Hernandez, F.A. Gomez, J. Chromatogr. A 840 (1999) 261.
[23] A. Brown, I. Silva, D. Chinchilla, L. Hernandez, F.A. Gomez, LC_GC Europe (2004) 2.
[24] J. Kaddis, E. Mito, J. Heintz, A. Plazas, F.A. Gomez, Electrophoresis 24 (2003) 1105.
[25] E. Mito, F.A. Gomez, Chromatographia 50 (1999) 689.
[26] J. Zavaleta, D. Chinchilla, K. Martinez, F.A. Gomez, J. Chromatogr. A 1105 (2006) 59.
[27] Y. Zhang, F.A. Gomez, J. Chromatogr. A 897 (2000) 339.
[28] S. Lin, I.-Y. Hsiao, S.-M. Hsu, Anal. Biochem. 254 (1997) 9.
[29] C. Arce, A. Moreno, Y. Millán, J. Martín de las Mulas, D. Llanes, Vet. Immunol. Immunopathol. 88 (2002) 31.
[30] S. Lin, J.-C. Tsai, S.-M. Hsu, Anal. Biochem. 284 (2000) 422.
[31] F.A. Gomez, L.Z. Avila, Y. Chu, G.M. Whitesides, Anal. Chem. 66 (1994) 1785.
[32] K.A. Connors, Bingind Costants—The Measurement of Molecular Complex Stability, John Wiley & Sons, New York, 1987.
[33] K.L. Rundlett, D.W. Armstrong, J. Chromatogr. A 721 (1996) 173.
[34] B. Friguet, A.F. Chaffotte, L. Djavadi-Ohaniance, M.E. Goldberg, J. Immunol. 77 (1985) 305.
[35] F.T.A. Chen, J. Chromatogr. 680 (1994) 419.
[36] H. Schwartz, T. Pritchett, Separation of Proteins and Peptides by Capillary Elestrophoresis: Application to Analytical Biotechnology, Beckman Instruments, Fullerton, CA, 1994, p. 2.
[37] G.M. Edelman, P.J. Speck, B. Syred, J. Immunol. 96 (1969) 822.
[38] M.H.A. Busch, L.B. Carels, H.F.M. Boelens, J.C. Kraak, H. Pope, J. Chromatogr. A 777 (1997) 311.

[39] Y. Ding, B. Lin, C.W. Huie, Electrophoresis 22 (2001) 2210.
[40] S. Kiessig, F. Thunecke, J. Chromatogr. A 982 (2002) 275.
[41] G.D. Li, X.J. Zhou, Y.H. Wang, A. El-Shafey, N.H.L. Chiu, I.S. Krull, J. Chromatogr. A 1053 (2004) 253.
[42] A. Liang, X. He, Y. Du, K. Wang, Y. Fung, B. Lin, Electrophoresis 25 (2004) 870.
[43] A. Tran, S. Park, P.J. Lisi, J. Chromatogr. 542 (1991) 459.
[44] Ed. Harlow, D. Lane, Antibodies. A Laboratory Manual, Cold Spring Harbor Laboratory, New York, 1988.
[45] Y.H. Chu, L.Z. Avila, J. Gao, G.M. Whitesides, Acc. Chem. Res. 28 (1995) 461.
[46] X. He, H. Xiao, X. Liang, B. Lin, J. Sep. Sci. 25 (2002) 711.
[47] M.E. Goldberg, L. Djavadi-Ohaniance, Curr. Opin. Immunol. 5 (1993) 278.

Talanta 78 (2009) 1315–1320

Contents lists available at ScienceDirect

Talanta

journal homepage: www.elsevier.com/locate/talanta

Automated headspace solid-phase microextraction versus headspace for the analysis of furan in foods by gas chromatography–mass spectrometry

M.S. Altaki, F.J. Santos*, M.T. Galceran

Departament de Química Analítica, Universitat de Barcelona, Diagonal 647, 08028 Barcelona, Spain

ARTICLE INFO

Article history:
Received 4 August 2008
Received in revised form 26 January 2009
Accepted 2 February 2009
Available online 10 February 2009

Keywords:
Food analysis
Furan
Headspace solid-phase microextraction
Headspace
GC–MS
Automation

ABSTRACT

A simple, fast and fully automated method based on headspace solid-phase microextraction coupled on-line with gas chromatography–ion trap mass spectrometry (HS-SPME–GC–ITMS) is proposed for furan determination in foods. The performance of the proposed method was compared to the automated headspace-GC–MS method, proposed by the US Food and Drugs Administration (US FDA), in terms of repeatability, limits of the detection and quantification. Both methods gave similar results for furan determination in selected food samples, although slightly worse precision (RSD%, 9–12%) and higher limits of detection (from 5 to 20 times higher) were obtained by the headspace method. In addition, higher sample throughput in routine furan analysis was obtained using the proposed HS-SPME–GC–ITMS method with isotope dilution than using the US FDA method, which recommends standard addition for quantification. The proposed method provides good precision (RSD% <10%) and low limits of detection, ranging from 0.02 to 0.12 ng g^{-1} depending on the sample. The developed HS-SPME–GC–MS method was used to analyse furan in several Spanish food commodities and concentrations ranging from 0.1 ng g^{-1} to 1.1 μg g^{-1} were found.

1. Introduction

Furan (C_4H_4O) is a volatile heterocyclic compound which is formed during the heat treatment of foods and drinks as one of the Maillard reaction products [1]. Furan occurs in a wide variety of foods, such as coffee, canned and jarred foods containing meat, and various vegetables [2,3], at concentration levels up to 174 ng g^{-1}. The common presence of furan suggests that there are probably multiple routes of formation rather than a single mechanism [4]. Nowadays, it is accepted that its generation is mainly related to the thermal degradation of carbohydrates, the oxidation of polyunsaturated fatty acids and the decomposition of ascorbic acid or its derivatives [5–11]. The occurrence of furan in food and drink is a cause for concern because it is both carcinogenic and cytotoxic in rats and mice [12–14]. It has been classified as possibly carcinogenic to humans (Group 2B) by the International Agency for Research on Cancer (IARC) [15], and has been included by the US Department of Health and Human Service in the human pathogen list [16]. Since furan has become a potential food safety issue, several international food organizations such as the US Food and Drugs Administration (FDA) and the EFSA have launched monitoring programs to survey the furan content of selected foods and beverages and to collect more information about furan formation, human exposure and toxicity [4,17]. Recently, the EFSA issued a call for more information on the occurrence of furan in foods [18]. Therefore, there is great interest in finding rapid, selective and sensitive analytical methods for obtaining reliable data to assess the risk to human health [19,20].

Due to its high volatility (B.P. 31.4 °C), furan is currently being analysed by headspace (HS) combined with gas chromatography–mass spectrometry (HS-GC–MS) [21,22]. This method, first proposed by the FDA in 2004, is relatively simple and well-established: a food sample in liquid or slurry form is heated at 80 °C for 30 min and the headspace is sampled and analysed by GC–MS. Furan is quantified by standard addition using furan-d_4 as internal standard. A similar method was used by the Swiss Federal Office of Public Health (SFOPH) for collecting data from a great number of foods likely to contain furan [3,23]. Since furan is formed during the analysis by sample heating [10,24–26], the FDA method was updated in 2006 by decreasing the headspace temperature from 80 to 60 °C [27]. This new FDA method provides limits of detection of 2–5 ng g^{-1} for most food matrices. To date, the method has only been validated in-house [24] and a limited number of proficiency tests have been performed [21]. Recently, the Health Canada modified this headspace method [28], achieving limits of detection in foods between 0.8 and 4.85 ng g^{-1}. Nevertheless, the use of standard addition for quantification increases the analysis time and reduces the applicability of the method in a high-throughput routine laboratory operation.

* Corresponding author. Tel.: +34 934034874; fax: +34 934021233.
E-mail address: javier.santos@ub.edu (F.J. Santos).

0039-9140/$ – see front matter © 2009 Elsevier B.V. All rights reserved.
doi:10.1016/j.talanta.2009.02.003

Headspace solid-phase microextraction (HS-SPME) has also been used for furan determination. HS-SPME coupled with GC–MS has proved to be an excellent alternative to headspace for the analysis of volatile compounds at low concentration levels in food samples [29,30], since it provides enough sensitivity with minimum interferences of matrix compounds. HS-SPME has been used for the analysis of furan in coffee [31], orange juice [9] and foods in general [32–34]. Most of these methods are based on manual HS-SPME providing limits of detection in the low pg g^{-1} range. In a previous paper, we proposed a manual HS-SPME method combined with isotope dilution and GC–IT–MS for the analysis of furan in foods [34]. This HS-SPME approach provided high selectivity and limits of detection between 8 and 70 pg g^{-1}. Although this method is rapid and effective for furan analysis, it is labour-intensive when a lot of samples are analysed. Therefore, full automation of HS-SPME could shorten total analysis time, thus improving productivity.

The aim of the present paper was to develop a fully automated HS-SPME method coupled on-line with GC–MS for routine analysis of furan in food commodities. The method was evaluated by comparing its performance to that of the US FDA method based on headspace, the usual reference procedure for furan analysis. Quality parameters of the two methods were established and compared using several food samples. Finally, the fully automated HS-SPME–GC–MS method was applied to the determination of furan in several food commodities.

2. Experimental

2.1. Chemicals and standards

Furan and [$^2H_4$] furan (furan-d_4) were purchased from Sigma–Aldrich (Munich, Germany) at purity higher than 99%. Individual stock standard solutions of furan and furan-d_4 at a concentration of 9 mg g^{-1} in methanol were prepared by transferring 15 μl of each pure compound to a 2 ml amber sealed vial previously filled with methanol. Intermediate individual standard solutions of furan and furan-d_4 were prepared at a concentration of 45 μg g^{-1} from the stock standard solutions by appropriate dilution with methanol. All these solutions were stored at 0 °C and prepared weekly. For HS-SPME analysis, individual water working standard solutions of furan and furan-d_4 at a concentration of 30 ng g^{-1} were prepared daily by spiking 20 ml of water with appropriate volumes of the intermediate standard solutions. For furan determination by the isotope dilution method, eight-calibration standard solutions at concentrations ranging from 0.01 to 10 ng g^{-1} were prepared by adding in weight, through the septum, an appropriate amount of the furan water working standard solution (30 ng g^{-1}) into a 20 ml sealed vial containing a 10 mm × 5 mm PTFE-coated stir bar, 2 g of sodium chloride and water (up to 8 ml). In addition, 70 μl of the furan-d_4 water working solution (30 ng g^{-1}) was added to each calibration solution, to achieve a concentration of 0.2 ng g^{-1}. For headspace analysis, individual water working standard solutions of furan and furan-d_4 at a concentration of 500 ng g^{-1} were prepared daily from intermediate standard solutions and were used for the furan quantification by standard addition method. Water of organic trace grade, methanol of gas chromatography grade and sodium chloride of analytical grade were all obtained from Merck (Darmstadt, Germany).

2.2. Food sample preparation

A total of twenty-four food samples purchased from a local supermarket in Barcelona (Spain) were analysed for furan. Packaged food samples were stored at 4 °C to prevent possible losses of furan. Liquid samples (juices, honeys and broths) were homogenized in their own container for 1 min by manual shaking, while semi-solid samples (baby foods and sauces) were homogenized for 1 min at 4 °C by immersing the pot in an ice/water bath (15 min) and using a mixer and an Ultra-Turrax T25 basic disperser (IKA-Werke, Staufen, Germany). Cooked pulse samples (lentils, white kidney beans and chickpeas) were prepared in the same way as semi-solid samples by adding an appropriate amount of cold water (1:1, w/w) to facilitate the homogenization processes. For ground coffee, nine grams of solid coffee were used to obtain approximately 60 ml of brewed coffee, using both an automatic espresso coffee machine and a home coffee pot-brewer. After preparation, the brewed coffee was placed in a 40 ml screw-cap glass vial, which was stored at 4 °C before analysis. Furan in instant coffee was determined in both brewed coffee and powdered material. The brewed instant coffee was prepared according to the recommendations of the manufacturer, mixing 2 g of powder with 60 g of boiling water. To determine the content of furan in powdered instant coffee, 0.5 g of powder was mixed with 40 ml of cold water (4 °C) in a 40 ml closed glass vial. Soup samples (dehydrated material) were prepared in line with the manufacturer's indications. Approximately 50 g of solid soup was mixed first with 100 g of warm water until complete dissolution and then with 200 g of water. The mixture was heated for 15 min with manual shaking. After preparation and the homogenization process, all samples were immediately kept in a closed vial without headspace to minimize the possible loss of furan.

2.3. GC–MS conditions

All GC–MS analyses were performed on a CP-3800 gas chromatograph coupled with a Saturn-2200 ion trap mass spectrometer (Varian, Mississauga, Canada). A BPX-volatile (cyanopropylphenyl polysilphenylene-siloxane), 60 m × 0.25 mm I.D., fused-silica capillary column (SGE Europe, Villebon, France) of 1.4 μm film thickness was used for chromatographic separation. The oven temperature program was 35 °C (held for 2 min) to 230 °C at 20 °C min^{-1} (held for 5 min). Helium was used as carrier gas at a constant flow-rate of 1.7 ml min^{-1} held by electronic flow control (EFC). The injector temperature was maintained at 275 °C and the splitless injection mode (3 min) was used for HS-SPME experiments, while for headspace (US FDA method) the injector was operated in split injection mode at 2:1 split ratio. An SPME glass inlet liner (I.D., 0.75 mm, SGE Europe) and a 23-gauge Merlin Micro-seal septum (Supelco, Bellefonte, PA, USA) were used for SPME analysis, while for headspace a split inlet liner (I.D., 3 mm, SGE Europe) was used. The ion trap MS was operated in electron ionization (EI) mode with 70 eV of electron energy and 30 μA of emission current, using automatic gain control (AGC). The instrument was tuned using perfluorotributylamine (FC-43) according to the manufacturer's recommendations to achieve the best sensitivity. Manifold, ion source trap and transfer line temperatures were set at 80, 200 and 280 °C, respectively. The electron multiplier voltage and the axial modulation amplitude were set to 1350 V (10^5 gain) and 4.0 V, respectively. In addition, a maximum ionization time of 25,000 μs, a pre-scan ionization time of 100 μs with a background mass of 45 *m/z* and an RF dump value of 650 *m/z*, were set for all experiments. For data acquisition, EI full-scan mode was used over the mass range *m/z* 35–100 at 0.75 s/scan (7 μscan per scan). Varian MS Workstation software (version 6.42) was used for control, general operating and data acquisition. For quantification and confirmation, *m/z* 68 $[M]^{+\cdot}$ and *m/z* 39 $[M\text{-}CHO]^+$ for furan and *m/z* 72 and *m/z* 42 $[M\text{-}C^2HO]^+$ for furan-d_4 were monitored.

2.4. Automatic HS-SPME method

The HS-SPME experiments were carried out with a 75-μm Carboxen-polydimethylsiloxane fibre (CAR/PDMS) (Supelco, Bellefonte, PA, USA) on a CTC Combi-Pal autosampler (CTC Analytics

AG, Zwingen, Switzerland), which was equipped with a sample tray for 32 vials of 20 ml, an SPME fibre conditioning station, and a temperature-controlled single magnet mixer tray (SMM tray) (Chromtech, Idstein, Germany). CTC Combi-Pal autosampler was controlled and programmed with the Cycle composer software version 1.5.3. Before use, the CAR/PDMS fibre was conditioned at 300 °C under helium flow for 1 h in accordance with the manufacturer's recommendations. Fibre blanks were run daily to ensure the absence of contaminants or carry-over.

After optimization, the automatic HS-SPME procedure used for furan determination in the selected food samples was as follows: 3 g of the prepared and homogenized sample (for baby food, brewed coffee, soup and broth, 1–2 g were used) was quickly transferred to a 20 ml headspace vial containing a PTFE-coated stir bar, 2 g of sodium chloride and an adequate amount of water (up to 8 ml). During preparation, the sample vial was immersed in an ice/water bath (4 °C) to prevent possible losses of the analyte. The vial was then spiked with 70 μl of furan-d_4 water working solution (30 ng g^{-1}) by weight through the septum of the vial and was vortexed for 3 min before analysis. Then the sample and calibration solutions were placed in the sample tray of the autosampler and were analysed by means of the automatic HS-SPME procedure. Before HS-SPME analysis, the vials were conditioned in the SMM tray for 5 min at a temperature of 30 °C and under a magnetic agitation rate of 750 rpm. At the end of this time period, the CAR/PDMS fibre was cleaned for 1 min at 275 °C using the SPME fibre conditioning station, and the sample was extracted from the headspace at 30 °C for 20 min with a constant magnetic agitation rate of 750 rpm. Thermal desorption of the analyte was accomplished by exposing the fibre in the GC injector port at 275 °C for 2 min. To reduce the analysis time and to obtain a high sample throughput, a new HS-SPME experiment was performed while the GC was being run.

2.5. Headspace method

Headspace analysis of furan in food was performed following the proposed US FDA method [27] but using a BPX-volatiles as GC column and a CTC Combi-Pal autosampler for headspace analysis. This autosampler was equipped with a 1 ml gas-tight headspace syringe (1001N CTC, Hamilton Company, Bonaduz, Switzerland), a syringe heater and plunger holder (CTC Analytics), was used. For conditioning and cleaning the headspace syringe, the CTC syringe heater was set to 150 °C for 2 min with helium flushing. Furan was determined by standard addition method with internal standard, as proposed in the FDA method. For this purpose, replicate analyses ($n = 3$) of the food sample were carried out by transferring an adequate amount of the homogenized sample (5 g for solid and semi-solid samples and 10 g for liquid samples) to a 20 ml headspace vial containing a PTFE-coated stir bar and an appropriate amount of water saturated with NaCl (up to 10 ml). Then the sample was spiked with adequate amounts of a furan aqueous working standard solution (500 ng g^{-1}) at 0% ($n = 3$), 25% ($n = 2$), 50% ($n = 2$), 100% ($n = 1$), 150% ($n = 1$) and 200% ($n = 1$) of the estimated concentration of furan in sample. Finally, furan-d_4 was added to each sample vial to obtain a concentration of 200% of the estimated furan content. Automated headspace sampling conditions were as follows: the sample vial was conditioned for 30 min at an incubation temperature of 60 °C stirring at 750 rpm using the temperature-controlled single magnet mixer tray (Chromtech, Idstein, Germany). The temperature of the syringe heater was set to 100 °C and the syringe was flushed with helium before and after each extraction. Headspace (1 ml) was sampled at 100 μl s^{-1} and injected into the GC port at 275 °C and with an injection speed of 250 μl s^{-1}. GC–MS conditions for furan determination using the headspace method were the same as those used for SPME experiments (Section 2.3).

Table 1
Effect of the extraction temperature, extraction time, headspace/aqueous volume ratio and stirring rate on the response of furan using automated HS-SPME (optimum conditions are indicated in bold).

Temperature		Time		Volume ratio		Stirring rate	
°C	RR*	min	RR	V_h/V_w	RR	rpm	RR
30	**100%**	5	42%	5.7	75%	0	62%
35	78%	10	65%	3	87%	250	80%
40	43%	**20**	**100%**	**1.5**	**100%**	500	91%
		30	100%			**750**	**100%**

* Relative response ($n = 3$).

3. Results and discussion

3.1. Automated HS-SPME method

The optimum key parameters affecting HS-SPME efficiency for furan determination in food were previously reported for manual HS-SPME [34]. Nevertheless, to automate this method some SPME conditions such as extraction time and temperature, sampling stirring speed and headspace/aqueous volume ration were optimized because of certain characteristics of the Combi-Pal autosampler (vial size up to 20 ml, stirring speed ≤750 rpm and extraction temperature ≥30 °C) may affect SPME efficiency. Initially, the effect of sampling temperature on the furan extraction yield was examined from 30 to 40 °C using CAR/PDMS fiber and maintaining constant the other extraction (extraction time 30 min, stirring speed 750 rpm and 20% (w/w) of NaCl) and desorption conditions (275 °C for 2 min). Table 1 shows the relative response of furan obtained at the different conditions studied using an aqueous standard solution of furan at 0.08 ng g^{-1}. As can be seen, the response of furan decreased when temperature increased. So, 30 °C was chosen for subsequent experiments because the temperature-controlled mixer stay (SMM tray) does not permit work at lower temperatures. In addition, the highest extraction efficiency of furan was obtained at the maximum stirring speed allowed by the autosampler (750 rpm) and it was chosen as optimal value. The effect of the headspace/aqueous volume ratio (V_h/V_w) on furan extraction was also studied using 20 ml glass vials and maintaining constant the other parameters. The best results were obtained using an aqueous volume of 8 ml (12 ml of headspace). Aqueous volumes higher than 8 ml ($V_h < 12$ ml) were not studied because a minimum volume of 12 ml of headspace is required for the complete spreading of fibre. Finally, extraction time, from 5 to 30 min, was evaluated and 20 min was enough to reach equilibrium. Other HS-SPME parameters, such as ionic strength and desorption temperature and time, were set according to those previously optimized by manual SPME [34].

Quality parameters of the HS-SPME method such as linearity, instrumental limit of detection and quantification and repeatability were established. Good linearity, between 0.01 and 10 ng g^{-1}, with correlation coefficients (r^2) higher than 0.999 was obtained. Instrumental limit of detection (iLOD) and quantification (iLOQ) based on a signal-to-noise ratio (S/N) of 3:1 and 10:1, were determined using water standard solutions and were 1.4 and 5 pg ml^{-1}, respectively. The precision of the automated HS-SPME method was determined analysing five water standard solutions spiked at two concentration levels, 0.05 and 1 ng ml^{-1}. Relative standard deviations (RSD %) lower than 3% were obtained for the two levels.

In addition, the variability of the method associated with the SPME manufacturing process, when different SPME fibres were used, was also examined. For this, fifteen aqueous standard solutions spiked with furan at 0.1 ng g^{-1} were analysed under the optimal HS-SPME conditions, using three previously conditioned 75 μm CAR/PDMS fibres obtained from different lots. After five

Table 2
Analysis of furan in selected foods by automated HS-SPME and HS methods.

Food sample	Description	Concentration (ng g^{-1})[a]								
		Automated HS-SPME				HS (US FDA method)				Significance level (P-value)[b]
		Mean ± S.D.	RSD (%)	LOD (ng g^{-1})	LOQ (ng g^{-1})	Mean ± S.D.	RSD (%)	LOD (ng g^{-1})	LOQ (ng g^{-1})	
Apple juice	Concentrated base	1.10 ± 0.08	7	0.02	0.05	1.25 ± 0.13	10	0.42	1.39	0.1716
Honey	Multi-floral	4.8 ± 0.2	5	0.03	0.10	5.2 ± 0.45	9	0.58	1.93	0.2122
Baby food	Chicken with rice	15.7 ± 1.3	8	0.06	0.20	17.1 ± 2.1	12	0.80	2.86	0.3766
Coffee	Brewed instant coffee	35.0 ± 2.0	6	0.12	0.40	31.1 ± 3.7	12	0.62	2.06	0.1802
Pulses	Cooked chickpeas	0.24 ± 0.02	8	0.05	0.17	n.d.	–	0.50	1.67	–

n.d.: not detected.
[a] $n = 3$.
[b] Significant differences between methods for P-value < 0.05 (at 95% confidence level).

independent analyses with each fibre, the results obtained showed no significant differences between the fibres, with relative standard deviations lower than 10%. The durability of the fibre was also examined for any changes in the sensitivity of the fibre during its lifetime. The durability of the 75 μm CAR/PDMS fibre was estimated through a control standard solution and no significant differences on the extraction yield of furan were found after 150 analyses and only a 15% decrease was observed after 200 analyses. The stability of furan in sample vial before analysis was also investigated using several food samples: an apple juice, a baby food and a brewed coffee. For this purpose, four sample vials of each food matrix were prepared and analysed after 0, 1, 6 and 15 h. During this time, the sample vials were placed in the sample tray of autosampler at laboratory temperature (21 ± 2 °C). For all food samples and standing times, good agreement (RSD < 12%) in the results was obtained demonstrating the stability of furan in sample vials.

3.2. Comparison of HS-SPME and HS methods for the analysis of furan

To date, no comparative study between headspace extraction, the most commonly used method proposed by the US FDA, and HS-SPME for the analysis of furan in foods has been performed. In this paper, several food samples, such as apple juice (liquid sample), honey and coffee (rich flavours sample), chicken pap baby food (semi-solid sample) and cooked chickpeas (solid sample), were analysed in triplicate by automated headspace (HS) and HS-SPME, both coupled to GC–MS under the optimal conditions described in Section 2. Quantification with automated HS-SPME was performed by isotope dilution using furan-d_4. For HS, the standard addition method with the internal standard proposed by the US FDA for furan quantification was employed [27]. The results obtained in the analysis of furan by the two methods in selected food samples are summarized in Table 2. As can be seen, furan was detected in all selected food samples by using automated HS-SPME at concentrations ranging from 0.24 ng g^{-1} for cooked chickpeas to 35.0 ng g^{-1} for brewed instant coffee. In order to assure that the matrix did not affect the reliability of the results obtained by isotope dilution, the standard addition method was also applied for the analysis of these samples using HS-SPME and no significant differences were observed between both quantification methods. In addition, these results were consistent with those obtained with the HS method. To compare the results of the two methods, a statistical treatment of the data was performed

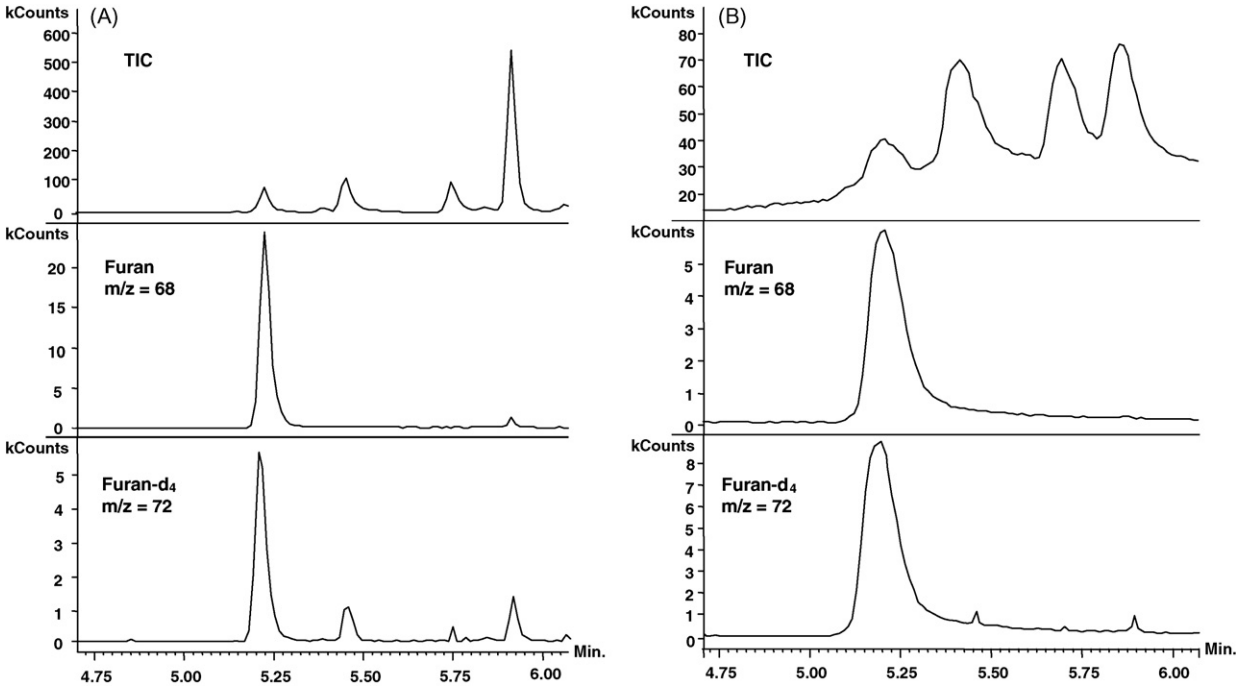

Fig. 1. GC–MS chromatograms of the total-ion-current (TIC) and the reconstructed ion current m/z 68 for furan and m/z 72 for furan-d_4, obtained by (A) automated HS-SPME method and (B) HS method proposed by the FDA.

Table 3
Analysis of furan in food by HS-SPME–GC–IT–MS.

Food sample	Description	Concentration[a] ($ng\,g^{-1}$)		Published data ($ng\,g^{-1}$) [ref.]
		Mean	RSD (%)	
Juice	Apple	1.7	3	1–4 [2,3]
	Orange	0.7	4	2.5 [32]
	Multi-fruit	2.0	3	6 [23]
	Tropicana	2.3	3	6 [23]
Honey	Multi-floral (brand 1)	3.6	7	3–10 [4]
	Multi-floral (brand 2)	6.5	5	3–10 [4]
Soup and broth	15 vegetable soup	0.5	10	19–49 [23,28]
	Fish and shellfish with rice and pea soup	39.0	3	–
	Chicken with vermicelli soup	5.0	5	–
	Beef with vegetable broth	2.0	5	–
	Vegetable broth	0.3	10	–
Sauce	Fried tomato with olive oil (brand 1)	0.6	8	–
	Fried tomato with olive oil (brand 2)	1.0	5	–
	Ketchup with 6 vitamins	0.9	7	–
	Mayonnaise	0.1	10	–
	Cocktail sauce	0.1	10	–
Pulses	Cooked lentils	1.0	8	3 [23]
	Cooked white kidney beans	1.2	8	–
Baby food	Multi-fruit pop	0.5	7	1–16 [23,28]
	Mixed vegetable pop	1.0	9	35–150 [2,23,28,33]
	Beef with spaghetti pop	40	10	42–100 [23,28]
Coffee	Brewed natural coffee (automatic espresso machine)	70	4	46–146 [21,23]
	Brewed natural filter coffee (filter-home pot brewer)	20	7	9–40 [21,23]
	Brewed natural instant coffee	35	5	36.9–51.3 [23]
	Brewed decaffeinated instant coffee	28	5	8–31 [21]
	Powdered natural instant coffee	1100	3	44–2200 [21,23]
	Powdered decaffeinated instant coffee	820	5	309–2800 [21,23]

[a] $n = 3$ replicates.

using the Student's *t*-test for equal or/and unequal variances and the results (*P*-value) are shown in Table 2. As can be seen, no significant differences were observed between the results with the two methods ($P > 0.05$), although the precision achieved by automated HS-SPME (RSD, 5–8%) was better than that found for the HS method (RSD, 9–12%). Limits of detection and quantification were also determined in food samples for the two methods. Since no blank food samples were found, samples spiked with furan-d_4 at very low concentration levels were used to estimate LODs and LOQs. The results given in Table 2 show that automated HS-SPME provided LOD values between 0.02 $ng\,g^{-1}$ (apple juice) and 0.12 $ng\,g^{-1}$ (brewed instant coffee), while for the HS method LODs were between 0.42 $ng\,g^{-1}$ (apple juice) and 0.80 $ng\,g^{-1}$ (chicken baby food). These results show that the automated HS-SPME method provided LODs from 5- to 20-fold lower than those obtained with the HS method, which is mainly because the HS-SPME technique has a higher preconcentration capacity than HS and because the HS-SPME method used the splitless injection mode instead of split injection. In addition, the HS method applied in this study provided LOD, LOQ and RSD values very close to those reported by FDA method [24], demonstrating that it can be used for comparative purposes. Fig. 1 shows as an example the GC–MS total ion current (TIC) chromatograms of a brewed instant coffee sample and the single ion chromatograms of *m/z* 68 (furan) and *m/z* 72 (furan-d_4) obtained by the two methods. As can be seen, higher sensitivity and better peak shape were achieved with the HS-SPME method mainly due to the use of a narrow SPME inlet liner (I.D., 0.75 mm). Moreover, no interfering compounds from matrix components were found in any of the analysed samples when comparing spectra of standards and samples. In addition, a higher sample throughput in routine furan analysis was obtained using HS-SPME–GC–MS with isotope dilution than HS with standard addition.

3.3. Analysis of furan in food commodities

To examine the feasibility of the automated HS-SPME method, several selected food commodities (27 different samples) were analysed. Furan was determined in triplicate by isotopic dilution, using the optimized method. The results obtained for the samples analysed are summarized in Table 3. Furan was detected and quantified in all samples at concentration levels ranging from 0.1 $ng\,g^{-1}$ for mayonnaise and cocktail sauces to 1.1 $\mu g\,g^{-1}$ for powdered natural instant coffee, with a precision better than 11%. These results are consistent with data published in the literature for similar food samples (Table 3). For instance, concentrations of furan in apple, orange and multi-fruit juices ranging from 1 to 6 $ng\,g^{-1}$ have been reported [2,3,23,32], which corroborates the figures determined using the proposed method for fruit juices (0.7–2.3 $ng\,g^{-1}$). In addition, furan levels found by EFSA in honey samples (3–10 $ng\,g^{-1}$) [4] were similar to those obtained in this study (3.6–6.5 $ng\,g^{-1}$). For soup and broth samples, a wide range of furan concentrations have been reported in the literature (3–125 $ng\,g^{-1}$) [2–4] due to the different ingredients and cooking procedure. In this case, furan was found at low concentration levels, with the lowest value (0.3 and 0.5 $ng\,g^{-1}$) being those found for vegetable soup and broth samples. This could be attributed to the low presence of furan in vegetables often below the detection limits [23]. Furan in sauces was also determined at low concentration levels, between 0.1 and 1 $ng\,g^{-1}$.

In baby food samples, furan concentrations ranging from 1 to 150 $ng\,g^{-1}$ have been reported depending on the food matrix. In this study, furan was found in multi-fruit and mixed vegetable samples at low concentration levels (0.5–1 $ng\,g^{-1}$), while for beef with spaghetti baby food a higher level of furan (40 $ng\,g^{-1}$) was found. Finally, the brewed natural coffee sample obtained from an automatic espresso machine gave a higher furan concentration level (70 $ng.g^{-1}$) than the filter-home pot brewer sample (20 $ng.g^{-1}$),

which confirmed previous data published by Zoller et al. [23], who indicate that the highest furan values are found in coffee prepared with an automatic espresso machine.

4. Conclusions

The automated headspace-SPME technique combined with GC–ion trap–MS has shown to be fast, sensitive and suitable for the analysis of furan in food commodities at low ng g^{-1} levels using isotope dilution. The proposed method provided low limits of detection, between 0.02 ng g^{-1} for apple juice and 0.12 ng g^{-1} for brewed instant coffee, which were from 5- to 20-fold lower than those obtained with the HS-GC–MS method. In addition, both methods gave similar results for furan determination in selected food samples, although a relatively worse precision with HS method was obtained. In addition, HS-SPME–GC–MS is able to provide accurate and precise results (RSD% <11%) for the analysis of foods containing a broad range of furan levels with enough selectivity and sensitivity. Therefore, the HS-SPME–GC–MS method can be proposed as an alternative to the FDA method for routine analysis of furan in foods.

Acknowledgments

This study was supported by the European Union, Priority 5 on Food Quality and Safety (Contract No. FOOD-CT-2003-506820 Specific Targeted Project, "Heat-generated food toxicants-identification, characterization and risk minimization"). This publication reflects the authors' views and does not necessarily those of the EU. The information in this document is provided as seen and no guarantee or warranty is given that the information is fit for any particular purpose. The user thereof uses the information at his sole risk and liability. M. Soubhi Altaki thanks the Ministry of Foreign Affairs and Cooperation of Spain (MEAC) and the Spanish Agency for International Cooperation (AECI) for a Ph.D. grant.

References

[1] J.A. Maga, CRC Crit. Rev. Food Sci. Nutr. 11 (1979) 355.
[2] Exploratory data on furan in food, US Food and Drug Administration (FDA), Washington, DC, 2004; http://www.cfsan.fda.gov/~dms/furandat.html.
[3] Furan in food: detailed list of results. Swiss Federal Office of Public Health (SFOPH), Bern, 2004; http://www.bag.admin.ch/themen/ernaehrung/%2000171/00460/01328/index.html?lang=de.
[4] Report of the Scientific Panel on Contaminants in the Food Chain on provisional findings on furan in food, European Food Safety Authority (EFSA), The EFSA Journal 137 (2004) 1–20, Brussels, Belgium; http://www.efsa.eu.int/science/contam/contam_documents/760_en.html.
[5] H.Z. Senyuva, V. Gökmen, Food Addit. Contam. 24 (2007) 136.
[6] A. Becalski, S. Seaman, J. AOAC Int. 88 (2005) 102.
[7] J. Mark, P. Pollien, C. Lindinger, I. Blank, T. Mark, J. Agric. Food Chem. 54 (2006) 2786.
[8] V.A. Yaylayan, J. Verbr. Lebensm. 1 (2006) 5.
[9] X. Fan, K. Mastovska, J. Agric. Food Chem. 54 (2006) 8266.
[10] S. Hasnip, C. Crews, L. Castle, Food Addit. Contam. 23 (2006) 219.
[11] A. Limacher, J. Kerler, B. Conde-Peti, I. Blank, Food Addit. Contam. 24 (2007) 122.
[12] H. Glatt, H. Schneider, Y. Liu, Mutat. Res. 580 (2005) 41.
[13] L.A. Peterson, M.E. Cummings, J.Y. Chan, C.C. Vu, B.A. Matter, Chem. Res. Toxicol. 19 (2006) 1138.
[14] L.J.K. Durling, K. Svensson, L. Abramsson-Zetterberg, Toxicol. Lett. 169 (2007) 43.
[15] Dry cleaning some chlorinated solvents and other industrial chemicals, Monographs on the Evaluation of Carcinogenic Risks to Humans, International Agency for Research on Cancer (IARC), Lyon, France, 1995, vol. 63, pp. 393.
[16] 11th Report on Carcinogens, US Department of Health and Human Service, Public Health Service, National Toxicology Program, Research triangle park, NC, 2005; ntp.niehs.nih.gov/ntp/roc/eleventh/profiles/s090fura.pdf.
[17] Furan in foods-Thermal treatment, US Food and Drug Administration (FDA), Washington, DC, 2004; http://www.cfsan.fda.gov/~lrd/fr040510.html.
[18] Invitation to submit data on furan in food and beverages, European Food Safety Authority (EFSA) (2006 and 2007), Brussels, Belgium; http://www.efsa.europa.eu/de/science/data_collection/furan.html.
[19] D. Roberts, C. Crews, H. Grundy, C. Mills, W. Matthews, Food Addit. Contam. 25 (2008) 25.
[20] C.W. Heppner, J.R. Schlatter, Food Addit. Contam. 24 (2007) 114.
[21] C. Crews, L. Castle, Trends Food Sci. Technol. 18 (2007) 365.
[22] C. Crews, L. Castle, LC-GC Eur. 20 (2007) 498.
[23] O. Zoller, F. Sager, H. Reinhard, Food Addit. Contam. 24 (2007) 91.
[24] P.J. Nyman, K.M. Morehouse, T.P. McNeal, G.A. Perfetti, G.W. Diachenko, J. AOAC Int. 89 (2006) 1417.
[25] H.Z. Senyuva, V. Goekmen, Food Addit. Contam. 22 (2005) 1198.
[26] C. Crews, S. Hasnip, D.P.T. Roberts, L. Castle, Food Addit. Contam. 24 (2007) 108.
[27] Determination of furan in foods, US Food and Drug Administration (FDA), Center for food safety and applied nutrition, Washington, DC, October 27, 2006; www.cfsan.fda.gov/~dms/furan.html.
[28] A. Becalski, D. Forsyth, V. Casey, B.P.-Y. Lau, K. Pepper, S. Seaman, Food Addit. Contam. 22 (2005) 535.
[29] W. Wardencki, M. Michulec, J. Curylo, Int. J. Food Sci. Technol. 39 (2004) 703.
[30] H. Kataoka, L.H. Lord, J. Powliszyn, J. Chromatogr. A 880 (2000) 35.
[31] I.-P. Ho, S.-J. Yoo, S. Tefera, J. AOAC Int. 88 (2005) 574.
[32] T. Goldmann, A. Perisset, F. Scanlan, R.H. Stadler, Analyst 130 (2005) 878.
[33] F. Bianchi, M. Careri, A. Mangia, M. Musci, J. Chromatogr. A 1102 (2006) 268.
[34] M.S. Altaki, F.J. Santos, M.T. Galceran, J. Chromatogr. A 1146 (2007) 103.

Talanta 78 (2009) 1414–1421

Contents lists available at ScienceDirect

Talanta

journal homepage: www.elsevier.com/locate/talanta

Direct electrochemistry of catalase at multiwalled carbon nanotubes-nafion in presence of needle shaped DDAB for H_2O_2 sensor

Periasamy Arun Prakash, Umasankar Yogeswaran, Shen-Ming Chen*

Department of Chemical Engineering and Biotechnology, National Taipei University of Technology, No. 1, Section 3, Chung-Hsiao East Road, Taipei 106, Taiwan, ROC

ARTICLE INFO

Article history:
Received 15 January 2009
Received in revised form 16 February 2009
Accepted 17 February 2009
Available online 24 February 2009

Keywords:
Direct electrochemistry
Catalase
Multiwalled carbon nanotubes
Didodecyldimethylammonium bromide
Electrocatalysis
Hydrogen peroxide

ABSTRACT

The direct electrochemistry of catalase (CAT) at didodecyldimethylammonium bromide (DDAB) present on nafion dispersed multiwalled carbon nanotubes (MWCNTs-NF) modified glassy carbon electrode (GCE) has been reported. The presence of DDAB in MWCNTs-NF-CAT film enhances the surface coverage concentration of CAT ($Fe^{III/II}$) to 48%. Similarly, in presence of DDAB, there is a 57% enhancement in electron transfer rate (k_s) with 66% increase in CAT stability. ($Fe^{III/II}$) redox couple exhibits linear dependence with the pH variation ($-51\,mV\,pH^{-1}$). The UV–vis absorption spectroscopy study reveals the entrapped CAT in DDAB film retains its native structure at MWCNTs-NF modified electrodes. Similarly, electrochemical impedance spectroscopy results confirm the co-existence of CAT and DDAB in the modified film. Further, scanning electron microscopy results reveal the structural morphological difference between various components in MWCNTs-NF-(DDAB/CAT) film. The cyclic voltammetry (CV) and amperometry (i–t curve) have been used for the measurement of electroanalytical properties of H_2O_2 by means of various film modified GCEs. The sensitivity values of MWCNTs-NF-(DDAB/CAT) film for H_2O_2 using CV ($35.62\,\mu A\,mM^{-1}\,cm^2$) are higher than the values which are obtained for MWCNTs-NF-CAT film ($2.74\,\mu A\,mM^{-1}\,cm^2$). Similarly, the sensitivity values using i–t curve are $101.74\,\mu A\,mM^{-1}\,cm^2$ for MWCNTs-NF-(DDAB/CAT) and $74.69\,\mu A\,mM^{-1}\,cm^2$ for MWCNTs-NF-CAT film. Finally, the diffusion coefficient of H_2O_2 at MWCNTs-NF-(DDAB/CAT) film ($3.4 \times 10^{-10}\,cm^2\,s^{-1}$) has been calculated using rotating disc electrode studies.

1. Introduction

Perpetually, the direct electrochemistry of redox enzymes shows significant interest since they catalyzes variety of biological process like photosynthesis, metabolism and respiration pathways [1–3]. As a result, many comprehensive studies associated with direct electrochemistry of redox enzymes have been exclusively studied in the past [4–8]. All these findings clearly illustrate that, it is impossible to achieve direct electron transfer between enzyme and bare electrodes. Where prosthetic group of the enzyme gets deeply buried inside the polypeptide chain which leads to the passivity of the electrode [9–13]. Among enzymes, oxidoreductase enzymes represent an important group which plays a major role in the metabolism of living cells [14]. In this oxidoreductase, catalase (CAT) is an active enzyme, which catalyzes the disproportionation process of H_2O_2. This catalytic ability of CAT has been applied in the development of enzyme based H_2O_2 sensors. However, the rapid response of such CAT based sensors relies on the rate of electron transfer between CAT and the electrode. Earlier, few attempts were made to achieve direct electron transfer between CAT and glassy carbon and graphite electrodes using electrode modification methods [15–17]. The different matrices used for electrode modification are chitosan [18], polyacrylammide hydrogel [19], methyl cellulose [20], agarose hydrogel [21], collagen [22], and silica sol–gel [23]. The long time stability of CAT in the immobilized matrix is much needed, and recently good stability has been reported with CAT encapsulated dendrimer films [24–26]. Though CAT immobilized on the above matrices illustrate their unique advantage, the matrix composition, fabrication and enzyme immobilization procedure remains rather complicated and time consuming one. Thus suitable matrix material and simple immobilizing techniques relies on the ease of fabrication of an enzyme sensor.

In recent years, multiwalled carbon nanotubes (MWCNTs) have fascinated much attention due to their exceptional stability, good electrical conductivity and high mechanical strength [27–33]. Moreover, the antifouling property of MWCNTs has made them extremely suitable for enzyme immobilization and thus for the fabrication of enzyme based amperometric sensors [34]. Earlier studies reveal that, several redox enzymes, proteins, DNA and antigen/antibody were successfully immobilized on MWCNTs modified surfaces [35–45]. Further development has been made by using

* Corresponding author. Tel.: +886 2270 17147; fax: +886 2270 25238.
E-mail address: smchen78@ms15.hinet.net (S.-M. Chen).

0039-9140/$ – see front matter © 2009 Elsevier B.V. All rights reserved.
doi:10.1016/j.talanta.2009.02.033

functionalized MWCNTs produced by covalent and non-covalent approaches for electrode modification [46–53]. Though this kind of functionalizing approaches leads to significant advances, they often result in the shortening of nanotubes and may cause minimal damage to the sidewalls of MWCNTs [54,55]. These shortcomings are overcome by Wang et al. approach of wrapping MWCNTs with hydrophobic polymer chains of nafion (NF) [56]. In their results, NF association leads to stable dispersion of MWCNTs. This stable MWCNTs-NF has been widely used in the fabrication of many oxidase enzyme based sensors, such as: Rivas et al. immobilized oxidase enzymes on MWCNTs-NF by layer-by-layer technique. Recently, bienzyme sensors with oxidase enzyme have been developed using MWCNTs-NF [57,58]. However, this kind of direct approach cannot be extended to enzymes like CAT which possesses huge structure, where direct electron transfer occurs only in the presence of suitable matrix. To challenge this, we made an attempt to immobilize CAT on MWCNTs-NF layer coated glassy carbon electrode (GCE). Fortunately, we noticed direct electron transfer between CAT and MWCNTs-NF. However the stability and electron transfer rate of the resulting MWCNTs-NF-CAT film is poor. In contrast, Rusling and coworkers reported 1000-fold increase in electron transfer for myoglobin entrapped didodecyldimethylammonium bromide (DDAB) surfactant films [59]. Similarly, Huang et al. noticed a dramatic enhancement in electron transfer at heme proteins, NF and DDAB incorporated pyrolytic graphite electrodes, which has been observed to be several folds greater than bare and NF coated electrodes [60]. Similar supporting results have also been found in literature [61–65]. These studies greatly emphasis that DDAB can promote the electron transfer rate to large extent even for huge structured proteins. Thorough view of literature shows, no one has attempted to immobilize CAT along with DDAB at MWCNTs-NF film. In the present study, we report DDAB/CAT immobilized at MWCNTs-NF film for H_2O_2 reduction. Eventually, this MWCNTs-NF-(DDAB/CAT) modified GCE shows rapid response with good stability towards the catalytic reduction of H_2O_2 at physiological pH.

2. Experimental details

2.1. Apparatus

Cyclic voltammetry (CV) study was performed with a conventional three electrode system using CHI 405 electrochemical work station. GCE with an electrode surface area of 0.079 cm^2 was modified either with CAT, DDAB, DDAB/CAT, MWCNTs-NF, MWCNTs-NF-CAT or MWCNTs-NF-(DDAB/CAT) films. These modified GCEs were used as working electrodes. A thin Pt wire (diameter of 0.5 mm) was used as counter electrode. The potential mentioned in all experimental results were measured with respect to standard Ag/AgCl reference electrode. UV–vis absorption spectroscopy measurements were carried out using Hitachi U-3300 spectrophotometer. Electrochemical impedance spectroscopy (EIS) measurements were performed using IM6ex ZAHNER (Kroanch, Germany). Surface morphology study of the films was carried out using Hitachi S-3000 H scanning electron microscope (SEM). Rotating disc electrode (RDE) and amperometric (*i–t* curve) measurements were performed using CHI 750 potentiostat with analytical rotator AFMSRX (PINE Instruments, USA).

2.2. Reagents

CAT from bovine liver (4540 units mg^{-1}) was purchased from Sigma and DDAB (98%) was purchased from Aldrich were used without further purification. MWCNTs with O.D. 10–15 nm, I.D. 2–6 nm, length 0.1–10 μm was obtained from Sigma–Aldrich, and 5 wt% NF perfluorinated ion exchange resin was obtained from Aldrich were used as received. 0.05 M phosphate buffer solution (PBS) was prepared by mixing 0.05 M Na_2HPO_4 and 0.05 M NaH_2PO_4 and then, pH of the buffer was adjusted to 6.5 using 0.05 M H_2SO_4. All other chemicals used were of analytical grade. All reagents were prepared with twice distilled deionised water. In prior to each experiment, buffer solutions were deaerated by continuous bubbling of prepurified N_2 gas for 10 min. During the experiments, N_2 was continuously passed over the solution in order to maintain inert atmosphere.

2.3. Preparation of MWCNTs-NF dispersion and DDAB/CAT mixture

MWCNTs-NF dispersion was prepared according to the procedure reported in the literature [66]. Previous studies show that stable dispersion of MWCNTs-NF association does not affect the catalytic properties of MWCNTs [56]. Similarly, Zhou et al. have recently reported specific interactions between the sidewalls of MWCNTs and the hydrophobic domains of NF, which leads to the stable dispersion of MWCNTs than in other solvents [67]. Briefly, 10 mg of MWCNTs was added to 0.5 wt% NF solution and the whole mixture was ultrasonicated for 6 h until a homogeneous and well-distributed black suspension was obtained. This black suspension has been sealed well to avoid evaporation of lower aliphatic alcohol present in 5 wt% NF solution. DDAB/CAT mixture was prepared by the following procedure. About 0.5 mg of DDAB was added into 10 ml of PBS followed by continuous stirring for 30 min. After 30 min, a uniform colorless DDAB solution (0.1 mM) has been obtained. Similarly, bovine liver CAT solution (10 mg ml^{-1}) has been prepared (pale yellow). Equal volumes of the above prepared DDAB and CAT solutions were mixed and stirred continuously for 1 h. This results in deep straw colored DDAB/CAT (1:1) solution. For comparative studies, DDAB and CAT mixtures of different ratios (1:2, 1:3, 1:4 and 1:5) were prepared (eight experiments). All the above prepared solutions were stored at 4 °C when not in use.

2.4. Fabrication of MWCNTs-NF-(DDAB/CAT)/GCE

In prior to modification, GCE surface was polished to a mirror finish using 0.05 μm alumina slurry and Buehler polishing cloth. Then, the GCE was washed and ultrasonicated in twice distilled deionised water for 10 min to remove the loosely adsorbed Al_2O_3 particles. About 0.13 ml cm^{-2} of MWCNTs-NF was spread evenly on the GCE surface and dried at 35 °C. Then, 0.13 ml cm^{-2} of DDAB/CAT mixture was dropped carefully over the MWCNTs-NF film and dried at 25 °C. The above said composite film was also modified over pre-cleaned gold and indium tin oxide (ITO) electrode surfaces to experience a comparative study. All the prepared GC, gold and ITO film modified electrodes were stored in PBS at 4 °C when not in use.

3. Results and discussions

3.1. Direct electrochemistry of CAT

The direct electrochemical behavior of CAT has been investigated with different film modified GCEs in PBS using CV as shown in Fig. 1(a). Similar investigations have been done with gold and ITO film modified electrodes (figures not shown). In prior to each experiments, N_2 was purged into PBS for 10 min. CVs were recorded in the potential range of −0.1 to −0.7 V. To obtain well-defined reversible redox peak for CAT, MWCNTs-NF volume has been optimized to 0.13 ml cm^{-2} (figures not shown). Similarly, DDAB and CAT ratio was optimized using different ratios of DDAB and CAT mixtures (1:1, 1:2, 1:3, 1:4, 1:5, total eight experiments). The inset in Fig. 1(a) shows the dependence of peak currents with DDAB and CAT ratio recorded at MWCNTs-NF-(DDAB/CAT) on GCE. This above result shows the

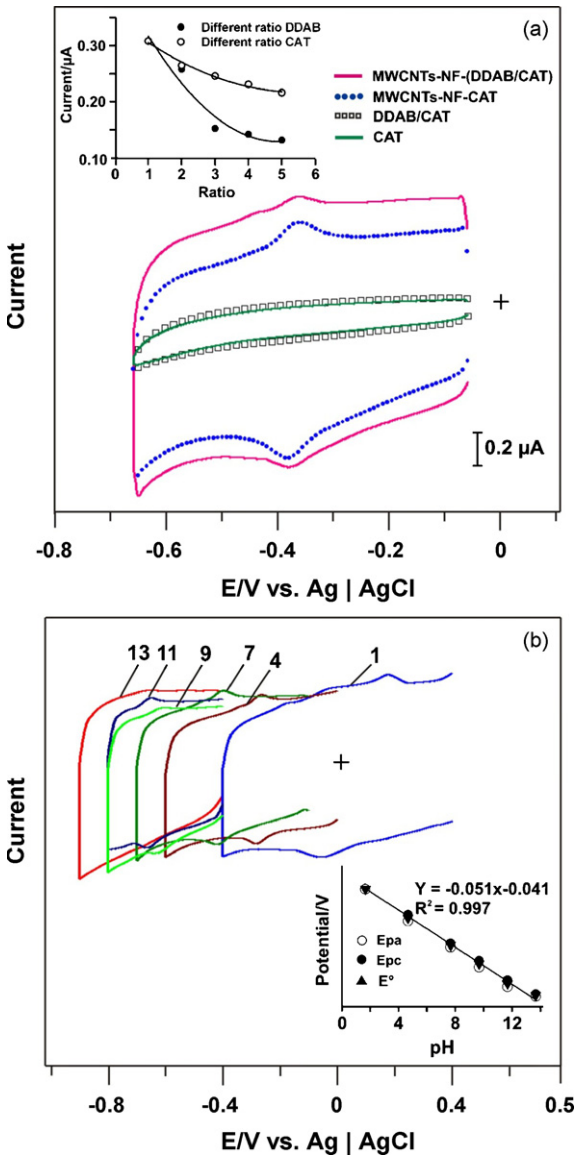

Fig. 1. (a) CVs of CAT, DDAB/CAT, MWCNTs-NF-CAT and MWCNTs-NF-(DDAB/CAT) modified GCE in N_2 saturated PBS at 20 mV s^{-1}. Inset in (a) shows the plot of different ratios of DDAB and CAT present in the mixture vs. cathodic peak current. (b) CVs of MWCNTs-NF-(DDAB/CAT) modified GCE in N_2 saturated PBS at 20 mV s^{-1} in different pH solutions. Inset in (b) shows the influence of pH on E_{pa}, E_{pc} and $E^{0'}$ of MWCNTs-NF-(DDAB/CAT) film.

maximum peak current attained with DDAB and CAT (1:1) mixture. Thus, this optimized ratio has been used in all the following experiments. From Fig. 1(a), a pair of well defined redox peak has been observed at formal potential ($E^{0'}$) = −0.38 V vs. Ag/AgCl reference electrode for MWCNTs-NF-(DDAB/CAT) and MWCNTs-NF-CAT films. However, no peaks at MWCNTs-NF, MWCNTs-NF-DDAB (figure not shown), CAT and DDAB/CAT films. Similar results have been observed at ITO and gold electrodes (figure not shown). Moreover, Wu et al. reported nearly reversible redox peaks for CAT immobilized silk fibroin films at $E^{0'}$ = −0.37 V vs. SCE in pH 7 [68]. Thus, the redox peak observed at $E^{0'}$ = −0.38 V in the present study belongs to $Fe^{III/II}$ redox reaction of the CAT heme group [21–23]. These above results show that, CAT exhibits reversible redox peaks only in the presence of MWCNTs-NF at various electrodes. The surface coverage (Γ) values for CAT at different modified electrodes have been calculated and given in Table 1. The Γ value has been calculated

Table 1
Comparison of Γ values of immobilized CAT at various electrodes in presence and absence of DDAB.

Type of film	Electrode type	Γ (pmol cm^{-2})
MWCNTs-NF-CAT	GC[a]	49.4
	Gold[a]	22.6
	ITO[a]	9.48
MWCNTs-NF-(DDAB/CAT)	GC[a]	73.0
	Gold[a]	27.0
	ITO[a]	21.2

[a] CV studies were done using PBS at 20 mV s^{-1} scan rate.

using the following equation:

$$\Gamma = \frac{Q}{nFA} \quad (1)$$

where Q is the charge, n is the number of electrons involved, F, Faraday current and A, electrode area. Where the number of electrons transferred is 1 for $Fe^{III/II}$ redox reaction of CAT. Generally, Table 1 reveals that, maximum concentration of CAT is immobilized and active at GC rather than gold and ITO electrodes. Also the Γ values show that, in the absence of MWCNTs-NF no significant redox peak obtained for CAT. In addition, Γ of CAT further gets significantly amplified in the presence of both MWCNTs-NF and DDAB. Thus maximum Γ of CAT is present in MWCNTs-NF-(DDAB/CAT) film on GCE and is observed to be 27% higher than Au and 21% higher than ITO modified electrodes. Further, MWCNTs-NF-(DDAB/CAT) film on GCE possess 48% higher Γ than MWCNTs-NF-CAT film on GCE.

The peak to peak separation (ΔE) for MWCNTs-NF-(DDAB/CAT) is 0.0119 V s^{-1} at 20 mV s^{-1} scan rate, which is lower than MWCNTs-NF-CAT film (ΔE = 0.0169 V s^{-1}). This shows that, CAT undergoes more facile reversible redox process at the former, which is also

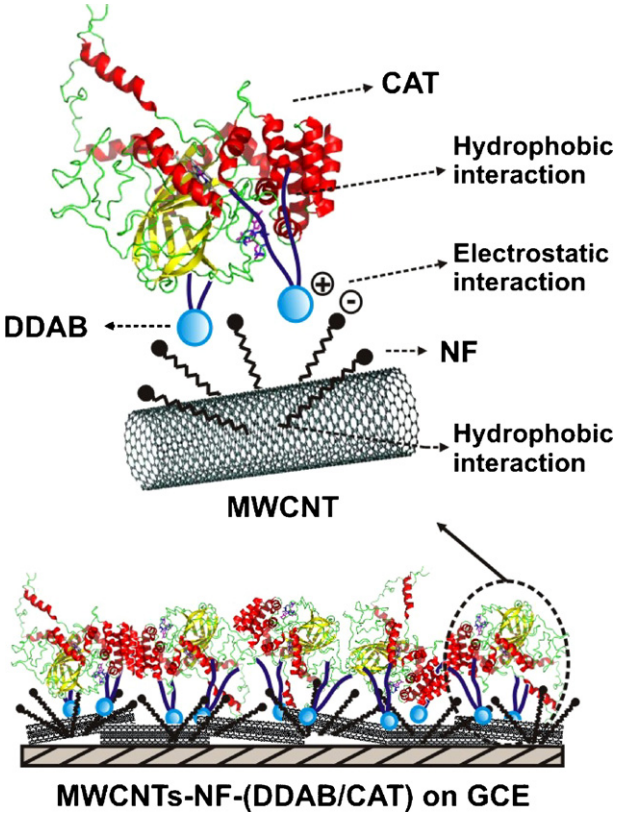

Scheme 1. Schematic representation of possible interaction between MWCNTs, NF, DDAB and CAT in the formation of MWCNTs-NF-(DDAB/CAT) film modified electrodes.

understandable from the maximum redox peak current (Fig. 1(a)). The reason for this enhanced redox peak current could be due to two reasons: (i) in the presence of DDAB, electron transfer process between heme group of CAT and the MWCNTs-NF layer becomes more facile, which is similar to that noticed by Chen et al. [62]. (ii) MWCNTs with good functional properties act as nanowires and facilitate the electron transfer between DDAB/CAT and GCE surface. Moreover, MWCNTs-NF provides stable biocompatible environment for the immobilization of large number of biomolecules and oxidase enzymes [69,70], which in turn leads to the enhanced electron transfer rate at MWCNTs-NF-(DDAB/CAT), and it has been revealed in the following sections. Possible interactions between MWCNTs-NF, DDAB and CAT at MWCNTs-NF-(DDAB/CAT) film on GCE has been given in Scheme 1. Where NF is negatively charged polyelectrolyte which possess hydrophobic fluoro carbon chains and hydrophilic perflurosulphonate groups ($-SO_3^-$) in its backbone [60]. These fluoro carbon chains of NF undergo hydrophobic interactions with the side walls of MWCNTs. Whereas, the negatively charged $-SO^{3-}$ group of NF undergoes electrostatic interactions with the positively charged head group of DDAB [71,72]. This results in the strong binding of DDAB head group and MWCNTs-NF which adds more stability to the film. Similarly, the long tail of DDAB undergoes hydrophobic interactions with CAT. Recently, Xu et al. have reported such hydrophobic interactions between the alkane chains of surfactant molecules and hydrophobic regions of hemoglobin, which improves the electron transfer rate [73].

3.2. Influence of pH

Fig. 1(b) represents the influence of pH on the voltammetric behavior of CAT at MWCNTs-NF-(DDAB/CAT) film in the pH range of 1–13. CAT molecule exhibits reversible redox peak in the pH range from 1 to 11. However, there is no redox peak associated with $Fe^{III/II}$ couple of CAT at pH 13. The reason for the loss of CAT redox behavior at pH 13 may be attributed to the denaturation of the enzyme at higher pH. Thus, CAT incorporated into DDAB mixture is stable in the wide pH range of 1–11 (Fig. 1(b)). Inset in Fig. 1(b) shows the linear dependence of anodic peak potential (E_{pa}), cathodic peak potential (E_{pc}) and $E^{0'}$ on pH. Both E_{pa} and E_{pc} of $Fe^{III/II}$ redox couple of CAT shows negative shift with increase in pH. The slope value of $E^{0'}$ vs. pH is $-51\,mV\,pH^{-1}$, which is close to the theoretical value of Nernstian equation for equal number of proton and electron transfer process.

3.3. Different scan rate studies

The different scan rate studies for MWCNTs-NF-(DDAB/CAT) and MWCNTs-NF-CAT films have been investigated by CV in the potential range of -0.1 to -0.7 in N_2 saturated PBS (CVs not shown). Fig. 2(a) shows the linear dependence of peak currents on different scan rate from 20 to $760\,mV\,s^{-1}$. This result shows that electrode process is a surface confined process for both films. However, Fig. 2(b) represents the dependence of peak currents on the square root of scan rate which shows, the rate of current increase is less than the rate of scan rate until $400\,mV\,s^{-1}$. This result reveals that the MWCNTs-NF-(DDAB/CAT) film possess surface confined process up to $400\,mV\,s^{-1}$. Whereas, above $400\,mV\,s^{-1}$ it possess diffusion controlled process. From the slope values of ΔE vs. log scan rate (figure not shown), by assuming the value of $\alpha \approx 0.5$, and the number of electrons involved as one, the electron transfer rate constants (k_s) have been calculated using Laviron theory [74]. The k_s values are 11 and $7\,s^{-1}$ for MWCNTs-NF-(DDAB/CAT) and MWCNTs-NF-CAT modified GCEs, respectively. The reason for higher k_s value at MWCNTs-NF-(DDAB/CAT) film is due to the presence of DDAB. It has been observed that $126\,ng\,cm^{-2}$ of DDAB present in MWCNTs-NF-(DDAB/CAT) film increases 57% of k_s. Further, the k_s value of MWCNTs-NF-(DDAB/CAT) film is higher than the values obtained for previous reported CAT films [21,23].

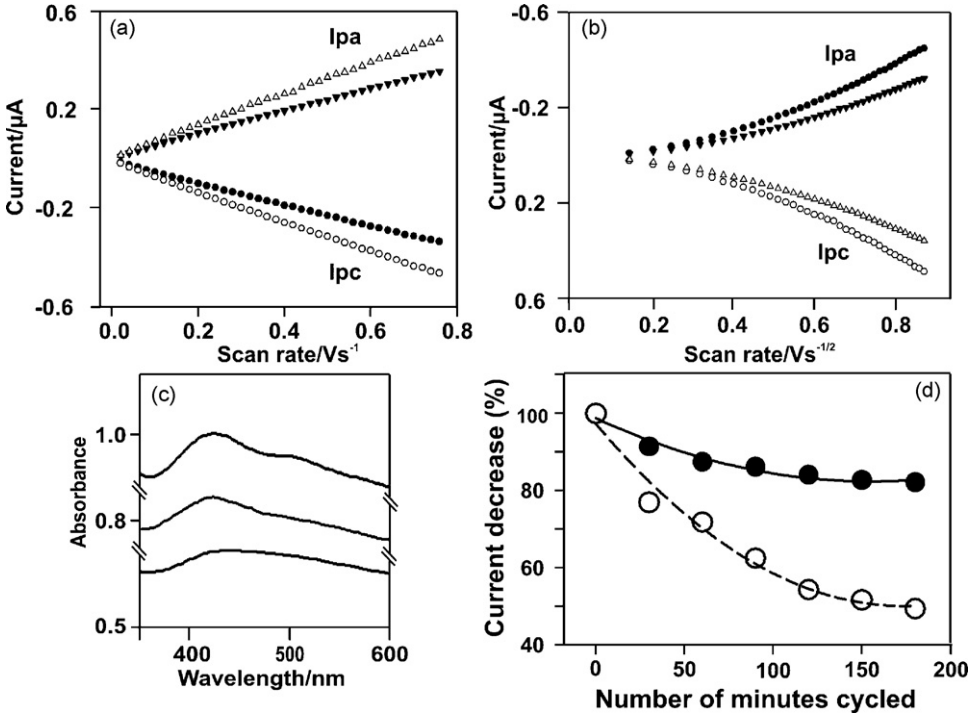

Fig. 2. Plot of anodic (I_{pa}) and cathodic peak (I_{pc}) currents vs. (a) scan rates (0.02–0.076 V s^{-1}) and (b) square root of scan rate. (c) UV–vis absorption spectra of CAT (Top = a'), DDAB/CAT (middle = b'), MWCNTs-NF-(DDAB/CAT) (bottom = c') modified ITO. (d) Shows the plot of current decrease in (%) vs. number of minutes cycled. Where continuous line represents MWCNTs-NF-(DDAB/CAT) film on GCE and dashed lines represents MWCNTs-NF-CAT film on GCE. Scan rate: $20\,mV\,s^{-1}$.

3.4. Investigation of immobilized CAT and its stability

UV–vis absorption spectroscopy has been used as an effective tool to probe the presence of heme group in CAT. Fig. 2(c) shows the UV–vis absorption spectra recorded for CAT, DDAB-CAT and MWCNTs-NF-(DDAB/CAT) coated ITO electrodes. A soret band has been observed at 406 nm for CAT film modified ITO (Top = a') [50]. Similar absorption peaks have been observed at 406 nm for DDAB/CAT and MWCNTs-NF-(DDAB/CAT) films without any shift in wavelength (middle = b') and (bottom = c'), respectively. These results reveal that, CAT molecule retains its native structure in both DDAB/CAT and MWCNTs-NF-(DDAB/CAT) films. Further, the stability of MWCNTs-NF-(DDAB/CAT) and MWCNTs-NF-CAT films have been investigated by 30 min continuous cycling in the potential range of −0.1 to −0.7 V in N_2 saturated PBS at 20 mV s^{-1} scan rate (Fig. 2(d)). At the end of each 30 cycles, the decrease in peak current (E_{pc}) was observed and plotted against time. The stability results clearly show that MWCNTs-NF-(DDAB/CAT) film exhibits a steady response after 90 cycles. However, for MWCNTs-NF-CAT film, the peak current keeps on decreasing even after 90 cycles. Further calculation shows that, stability of CAT on MWCNTs-NF-(DDAB/CAT) film enhanced about 66% when comparing CAT on MWCNTs-NF-CAT film. These stability results clearly illustrate that CAT molecule remains more stable in the presence of DDAB at MWCNTs-NF modified GCE.

3.5. EIS studies of different films

The interfacial changes originating from the biorecognition events at the electrode surfaces can be analyzed through impedance spectroscopy [75]. Biological materials such as enzymes immobilized on conducting or semiconductor surfaces change the double layer capacitance and interfacial electron transfer resistance of those corresponding electrodes. The knowledge about these equivalent circuit components thus specify the presence of biomaterials and surfactants immobilized on the electrode surface. Fig. 3(a) shows the impedance spectra represented as Nyquist plots (Z_{im} vs. Z_{re}) for bare, CAT, DDAB and DDAB/CAT films on GCE using 5 mM $Fe(CN)_6^{3-/4-}$ in PBS. The semicircle appeared in the Nyquist plot indicates the parallel combination of R_{et} and C_{dl} resulting from electrode impedance [76]. All the above said films exhibit semicircles with variable diameters in the frequency range 0.1 Hz to 100 kHz. The semicircles obtained at lower frequency correspond to a diffusion limited electron transfer process and those at higher frequency represent a charge transfer limited process. Comparing the films in presence and absence of DDAB, the film containing DDAB reduces the electron transfer resistance, which in turn reduces the semicircle diameter. This may be more likely due to the ordered bi-layered structure formed by DDAB on the electrode surface [77]. Similarly, the presence of CAT increases the electron transfer resistance. Thus, above result reveals the co-existence of DDAB and CAT film on GCE. Inset in Fig. 3(a) and (b) shows the Randles equivalence circuit model used to fit the experimental data. Where R_s represents the electrolyte resistance, R_{et} charge transfer resistance, C_{dl} double layer capacitance and Z_w Warburg impedance. The R_{et} and C_{dl} values for different films are given in Table 2. Fig. 3(b) represents the Nyquist plots of MWCNTs-NF, MWCNTs-NF-CAT and MWCNTs-NF-(DDAB/CAT) films on GCE using 5 mM $Fe(CN)_6^{3-/4-}$ in PBS. Where MWCNTs-NF-CAT film shows larger semicircle which indicates the presence of CAT film on GCE. As discussed in Fig. 3(a), the R_{et} value has been increased in the presence of CAT and decreased in the presence of DDAB. Thus, the results from Fig. 3 and Table 2 reveal the presence of DDAB and CAT in MWCNTs-NF-(DDAB/CAT) film modified GCE.

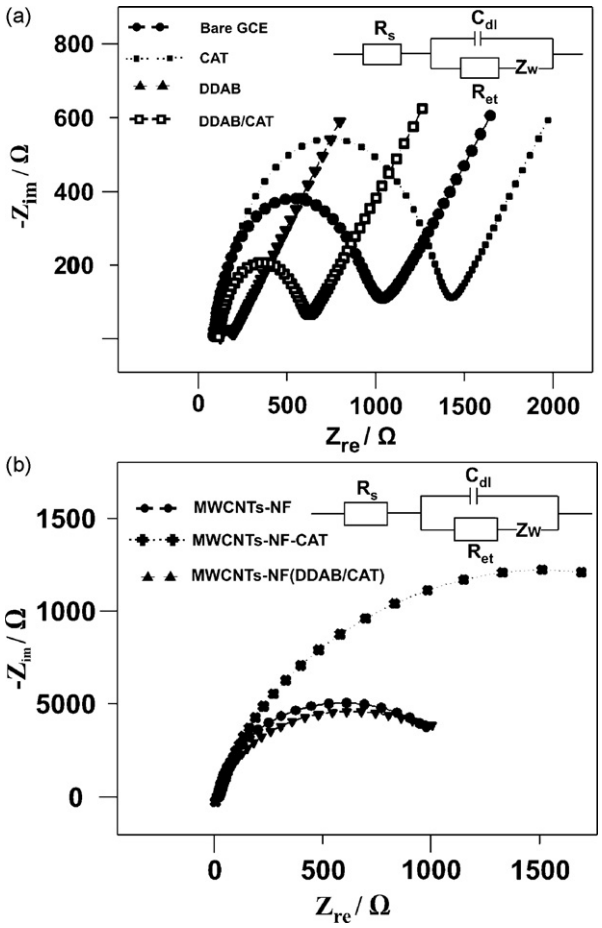

Fig. 3. (a) EIS of bare, CAT, DDAB and DDAB/CAT modified GCE in 5 mM $Fe(CN)_6^{3-}/Fe(CN)_6^{4-}$ in PBS solution. Applied AC voltage: 5 mV, frequency: 0.1 Hz to 100 kHz. (b) EIS of MWCNTs-NF, MWCNTs-NF-CAT and MWCNTs-NF-(DDAB-CAT) modified GCE at similar conditions. Insets in (a) and (b) shows the Randles circuit for above modified GCEs.

Table 2
R_{et} and C_{dl} values obtained from EIS studies for different film modified GCEs.

Film type	Electron transfer resistance, R_{et} (Ω)	Double layer capacitance, C_{dl} (μF)
Bare	850.6	0.399
CAT	1.193	0.293
DDAB	62.71	0.343
DDAB/CAT	456.7	0.313
MWCNTs-NF	4023	30.06
MWCNTs-NF-CAT	8427	37.26
MWCNTs-NF-(DDAB/CAT)	3556	29.76

3.6. Surface morphological characterizations using SEM

Fig. 4 represents the top view SEM images of different films coated on ITO surfaces taken at a resolution of 5k×. In prior to modification, ITO surfaces were cleaned and ultrasonicated in acetone–water mixture for 15 min and then dried. The obtained ITOs where drop casted with various composition of MWCNTs-NF, CAT, DDAB or DDAB/CAT solutions and dried at 25 °C. Fig. 4(a') shows the bare ITO surface; (a) MWCNTs-NF film, which shows well-dispersed MWCNTs in NF casted on ITO. (b') Shows the bud like structure of CAT. Whereas, (b) shows the needle shaped DDAB coated on the ITO. The arrow in (b) indicates a needle shaped structure of DDAB. This reveals the discriminate structure morphology that exists between DDAB and CAT films. (c') and (c) Shows DDAB/CAT, MWCNTs-NF-(DDAB/CAT) films where the bud like structures of CAT incorporate with needle shaped structures of

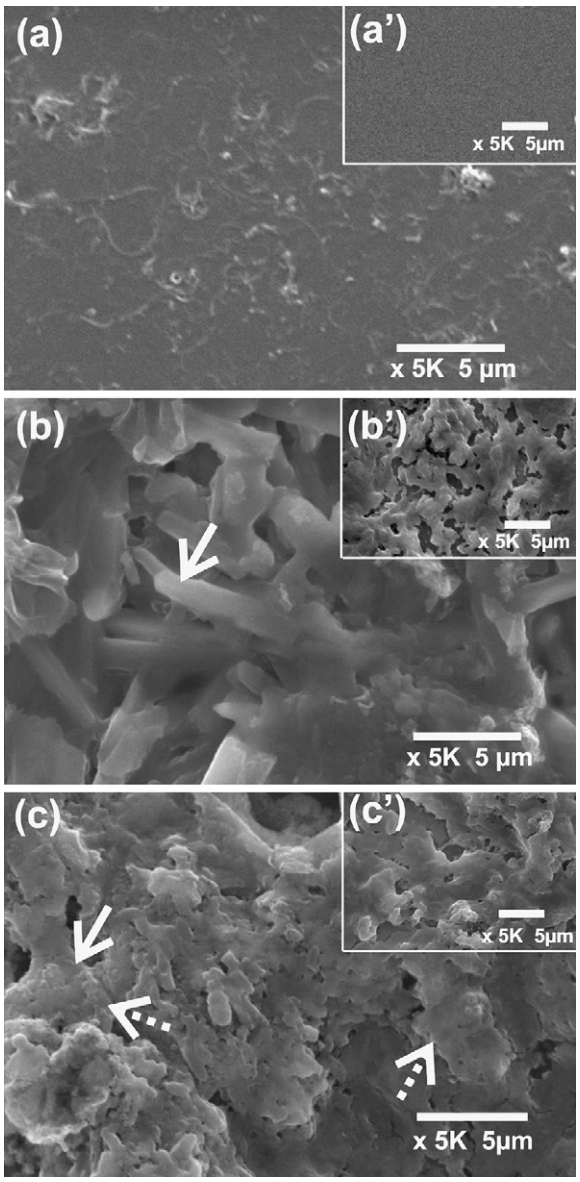

Fig. 4. SEM images of (a') bare, (a) MWCNTs-NF, (b') CAT, (b) DDAB, (c') DDAB/CAT and (c) MWCNTs-NF-(DDAB/CAT) modified ITO.

DDAB. In (c), the continuous and discontinuous arrows shows only DDAB and CAT incorporated DDAB, which covers the MWCNTs-NF. The above SEM results show that MWCNTs-NF-(DDAB/CAT) film has been formed on ITO surface.

3.7. Electrocatalytic response of MWCNTs-NF-CAT and MWCNTs-NF-(DDAB/CAT) film towards H_2O_2 reduction

Fig. 5 shows the CVs of different films modified GCEs in presence of minimum (0.05 mM) and maximum concentration (1.2 mM) of

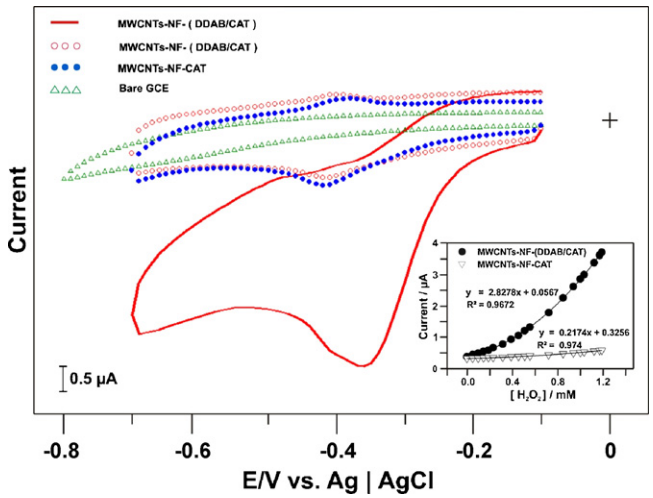

Fig. 5. Electrocatalytic response of bare GCE, MWCNTs-NF-CAT at the highest concentration of H_2O_2, and MWCNTs-NF-(DDAB/CAT) at the lowest and highest concentration of H_2O_2, present in N_2 saturated PBS at 20 mV s^{-1}. Inset is the plot of cathodic peak current vs. [H_2O_2] from 0.05 (lowest) to 1.2 mM (highest).

H_2O_2 in PBS. CVs have been recorded in the potential range −0.2 to −0.8 V vs. Ag/AgCl reference electrode. In Fig. 5, bare GCE shows no response even in the presence of 1.2 mM H_2O_2. Whereas, significant increase in catalytic reduction peak (−0.36 V) is observed at MWCNTs-NF-(DDAB/CAT) film even for the minimum addition of H_2O_2 (0.05 mM). The reduction peak current of H_2O_2 increased (as shown in inset) for successive addition of H_2O_2 at both MWCNTs-NF-CAT and MWCNTs-NF-(DDAB/CAT) films, whereas the anodic peak current decreased. In Fig. 5 for 1.2 mM H_2O_2, MWCNTs-NF-(DDAB/CAT) film shows much higher cathodic peak current than at MWCNTs-NF-CAT film. Similarly, the reduction peak potential (−0.36 V) of H_2O_2 at MWCNTs-NF-(DDAB/CAT) film is 60 mV lower than MWCNTs-NF-CAT (−0.42 V) film. This shows that, catalytic ability of MWCNTs-NF-(DDAB/CAT) film is higher than MWCNTs-NF-CAT film for H_2O_2. Where both the increase in peak current and decrease in over potential are considered as electrocatalysis [78]. The inset in Fig. 5 shows the linear dependence of cathodic peak currents of MWCNTs-NF-CAT and MWCNTs-NF-(DDAB/CAT) films with H_2O_2. With MWCNTs-NF-(DDAB/CAT) film the linear range is between 0.5 and 1.2 mM H_2O_2. In addition, the calculated E_{pc}, sensitivity and detection limit values are given in Table 3. These results in Table 3 show that, maximum catalytic activity with higher sensitivity could be achieved at MWCNTs-NF-(DDAB/CAT) film than at MWCNTs-NF-CAT film.

3.8. RDE studies for MWCNTs-NF-(DDAB-CAT) film

RDE is a hydrodynamic electrochemical technique which involves the convective mass transport of reactants and products at the electrode surface, when the electrode is rotated at a moderate speed [79]. RDE technique is used in the present study to investigate the catalytic reduction reaction of H_2O_2 associated with CAT at MWCNTs-NF-(DDAB/CAT) film on a rotating GCE present in PBS

Table 3
Comparison of electroanalytical values of various CAT modified electrodes for H_2O_2 reduction using different techniques.

Electroanalytical values	E_{pc} (mV)		Sensitivity (µA mM^{-1} cm^2) [correlation coefficient]		Detection limit (mM)	
	CV	*i–t*	CV	*i–t*	CV	*i–t*
MWCNTs-NF-CAT	−420	−420	2.74 [0.974]	74.69 [0.762]	0.19	1.3
MWCNTs-NF-(DDAB/CAT)	−360	−360	35.62 [0.9672]	101.74 [0.9983]	0.15	0.9
Nanocrystalline diamond/CAT [82]	−400	–	0.7	–	0.3	–
NiO/CAT [83]	−450	−300	24.17	15.9×10^{-6}	0.01	0.6×10^{-3}

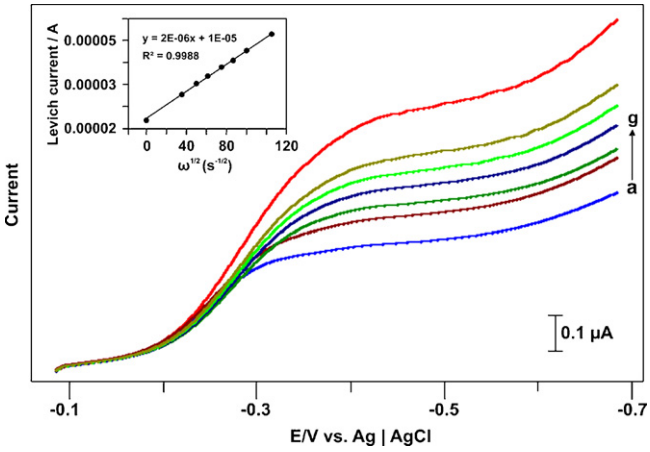

Fig. 6. RDE voltammogramms of MWCNTs-NF-(DDAB/CAT) modified rotating disc GCE in 0.21 mM H_2O_2 in PBS. Rotating speed: (a) 200 RPM, (b) 400 RPM, (c) 600 RPM, (d) 900 RPM, (e) 1200 RPM, (f) 1600 RPM and (g) 2500 RPM. Scan rate = 10 mV s^{-1}. Inset is a plot of Levich current vs. rotation rate.

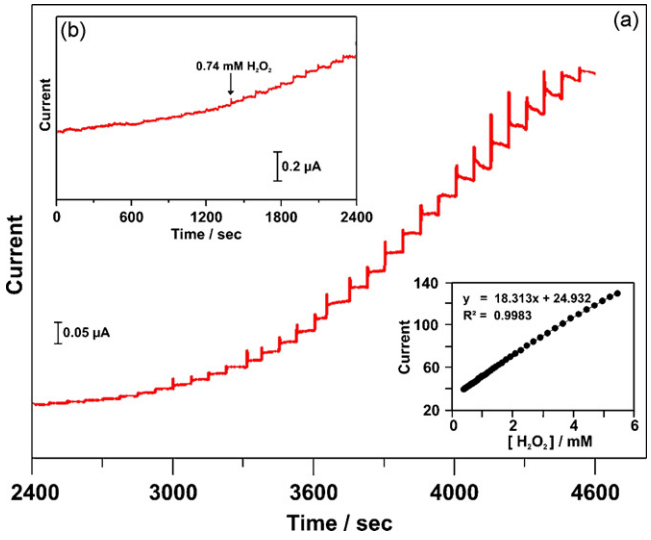

Fig. 7. (a) Amperometric *i–t* curve of MWCNTs-NF-(DDAB/CAT) modified rotating disc GCE at an applied potential of −0.36 V for the addition of 0.36–5.42 mM H_2O_2 in N_2 saturated PBS. Rotation rate: 900 RPM. Scan rate = 10 mV s^{-1}. (b) Shows the enlarged view of *i–t* response recorded before 2400 s. The inset shows the plot of linear dependence of peak current on H_2O_2 concentration.

at 10 mV s^{-1}. Fig. 6 shows set of RDE voltammogramms obtained for MWCNTs-NF-(DDAB-CAT) film at different rotating speeds from 200 to 2500 RPM. These voltammogramms increased linearly with rotation speed. If the electrocatalytic reduction of H_2O_2 occurs at RDE in a totally mass transfer controlled condition, the limiting current would linearly increase with the rotation rate [80]. Inset in Fig. 6 shows the Levich plot which shows the linear dependence of limiting current over the rotation rate. The correlation coefficient is 0.9988. Under this mass transfer controlled condition, the limiting current (I_L) is proportional to the concentration (C_0) and angular velocity $\omega^{1/2}$ (rotation rate = 200–2500 RPM). The diffusion coefficient (D) value of H_2O_2 at MWCNTs-NF-(DDAB-CAT) film is 3.4×10^{-10} cm^2 s^{-1}, which is calculated using the following Levich equation [81]:

$$I_L = 0.62nFAD^{2/3}\omega^{1/2}\upsilon^{-1/6}C_0 \quad (2)$$

where n represents the number of electrons involved in the H_2O_2 reduction reaction ($n = 1$), rotating electrode area (0.16 cm^2), the kinematic velocity υ for water ≈0.01 cm^2 s^{-1}, ω is the angular velocity, υ is the scan rate (0.01 V s^{-1}) and C_0 is the concentration of the analyte (0.21 mM).

3.9. *i–t response curve of MWCNTs-NF-(DDAB/CAT) film towards the H_2O_2 reduction*

Fig. 7 shows the typical amperometric response of MWCNTs-NF-(DDAB/CAT) film at rotating disc GCE in N_2 saturated PBS, where the electrode potential was kept constant at −0.36 V. MWCNTs-NF-CAT film has also been studied at similar conditions, however figures not shown. Initially, MWCNTs-NF-CAT and MWCNTs-NF-(DDAB/CAT) films show no significant response in the presence of 0.5 mM H_2O_2. But, a shoulder peak appeared on immediate addition of 0.7 mM H_2O_2 for MWCNTs-NF-(DDAB/CAT) film, as indicated by an arrow in (b). Similarly, for MWCNTs-NF-CAT film, a shoulder peak appears at 0.9 mM H_2O_2. Then, for every successive addition of H_2O_2, the reduction current increased linearly and progressed up to 4500 s for both films, after 4500 s they begins to level off. Both MWCNTs-NF-CAT and MWCNTs-NF-(DDAB/CAT) films show quick response to H_2O_2 with a response time of 5 s. The sensitivity, detection limit and correlation coefficient values of various electrodes are given in Table 3, which shows that MWCNTs-NF-(DDAB/CAT) is efficient than MWCNTs-NF-CAT film for H_2O_2 detection. In Table 3, other modified electrodes from literature are also shown. This comparison too reveals that the electrocatalysis of H_2O_2 is more efficient at MWCNTs-NF-(DDAB/CAT) film.

4. Conclusions

In the present study, we have reported a simple procedure to immobilize CAT with DDAB on MWCNTs-NF coated GCE. Where the direct electrochemistry of CAT is revealed through CV studies. UV–vis, EIS and pH studies reveal that CAT exhibits reversible redox peaks and CAT retains its native structure and remains more stable in the pH range 1–11. The presence of MWCNTs and DDAB in the film adds good stability to CAT. Further, MWCNTs-NF-(DDAB/CAT) film shows rapid response, with excellent catalytic activity towards the reduction of H_2O_2. This long term stability and rapid response of MWCNTs-NF-(DDAB/CAT) film remains extremely suitable for H_2O_2 sensing applications and opens a new path for the development of enzyme/surfactants based mediator less H_2O_2 sensors.

Acknowledgements

This work was supported by the National Science Council and the Ministry of Education of Taiwan (Republic of China).

References

[1] T.S. Wong, U. Schwaneberg, Curr. Opin. Biotechnol. 14 (2003) 590.
[2] T. Ikeda, K. Kano, J. Biosci. Bioeng. 92 (2001) 9.
[3] G. Gilardi, A. Fantuzzi, Trends Biotechnol. 19 (2001) 468.
[4] J.E. Frew, H.A.O. Hill, Eur. J. Biochem. 172 (1988) 261.
[5] S.D. Varfolomeev, I.N. Kurochkin, A.I. Yaropolov, Biosens. Bioelectron. 11 (1996) 863.
[6] Y. Wu, S. Hu, Microchim. Acta 159 (2007) 1.
[7] C. Leger, P. Bertrand, Chem. Rev. 108 (2008) 2379.
[8] D.H. Murgida, P. Hildebrandt, Phys. Chem. Chem. Phys. 7 (2005) 3773.
[9] M.R. Dayer, A.A.M. Movahedi, P. Norouzi, H. Ghourchian, S.J. Safarian, Biochem. Mol. Biol. 35 (2002) 364.
[10] W. Peng, X. Liu, W. Zhang, G. Li, Biophys. Chem. 106 (2003) 267.
[11] A.A.M. Movahedi, J. Chamani, H. Ghourchian, H. Shafiey, C.M. Sorenson, N. Sheibani, J. Protein Chem. 22 (2003) 23.
[12] H.Y. Chen, H.X. Ju, Y. Xun, Anal. Chem. 66 (1994) 4538.
[13] W. Zhang, H. Zhou, G. Li, H. Scheer, Biophys. Chem. 111 (2004) 229.
[14] P.C.A.G. Pinto, M.L.M.F.S. Saraiva, J.L.F.C. Lima, Anal. Sci. 24 (2008) 1231.
[15] M.E. Lai, A. Bergel, Bioelectrochemistry 55 (2002) 157.
[16] E. Horozova, Z. Jordanowa, V. Bogdanovskaya, Z. Naturforsch. 50 (1995) 499.
[17] E. Horozova, N. Dimcheva, Z. Jordanova, Z. Naturforsch. 52 (1997) 639.

[18] H. Huang, N. Hu, Y. Zeng, G. Zhoub, Anal. Biochem. 308 (2002) 141.
[19] H. Lu, Z. Li, N. Hu, Biophys. Chem. 104 (2003) 623.
[20] Y. Li, X.T. Chen, J. Li, H.H. Liu, Electrochim. Acta 49 (2004) 3195.
[21] S.F. Wang, T. Chen, Z.L. Zhang, X.C. Shen, Z.X. Lu, D.W. Pang, K.Y. Wong, Langmuir 21 (2005) 9260.
[22] M. Li, P. He, Y. Zhang, N. Hu, Biochim. Biophys. Acta 1749 (2005) 43.
[23] J. Di, M. Zhang, K. Yao, S. Bi, Biosens. Bioelectron. 22 (2006) 247.
[24] L. Shen, N. Hu, Biochim. Biophys. Acta 1608 (2004) 23.
[25] L. Shen, N. Hu, Biomacromolecules 6 (2005) 1475.
[26] P. He, M. Li, N. Hu, Biopolymers 79 (2005) 310.
[27] M.F. Yu, O. Lourie, M.J. Dyer, K. Moloni, T.F. Kelly, R.S. Ruoff, Science 287 (2000) 637.
[28] U. Yogeswaran, S. Thiagarajan, S.M. Chen, Sensors 8 (2008) 7191.
[29] U. Yogeswaran, S.M. Chen, Anal. Lett. 41 (2008) 210.
[30] R. Hobara, S. Yoshimoto, T. Ikuno, M. Katayama, N. Yamauchi, W. Wongwiriyapan, S. Honda, I. Matsuda, S. Hasegawa, K. Oura, Jpn. J. Appl. Phys. 43 (2004) 1081.
[31] Z. Xu, L. Wang, Q. Zheng, Small 4 (2008) 733.
[32] Y. Breton, G. Desarmot, J.P. Salvetat, S. Delpeux, C. Sinturel, F. Beguin, S. Bonnamy, Carbon 42 (2004) 1027.
[33] J.N. Coleman, U. Khan, W.J. Blau, Y.K. Gunko, Carbon 44 (2006) 1624.
[34] M. Musameh, J. Wang, A. Merkoci, Y. Lin, Electrochem. Commun. 4 (2002) 743.
[35] L. Deng, Y. Liu, G. Yang, L. Shang, D. Wen, F. Wang, Z. Xu, S. Dong, Biomacromolecules 8 (2007) 2063.
[36] S.G. Wang, Q. Zhang, R. Wang, S.F. Yoon, J. Ahn, D.J. Yang, J.Z. Tian, J.Q. Li, Q. Zhou, Electrochem. Commun. 5 (2003) 800.
[37] Y.M. Lee, O.Y. Kwon, Y.J. Yoon, K. Ryu, Biotechnol. Lett. 28 (2006) 39.
[38] Y. Gao, I. Kyratzis, Bioconjugate Chem. 19 (2008) 1947.
[39] K. Jiang, L.S. Schadler, R.W. Siegel, X. Zhang, H. Zhangc, M. Terrones, J. Mater. Chem. 14 (2004) 37.
[40] S. Zong, Y. Cao, H. Jua, Electroanalysis 19 (2007) 841.
[41] S. Li, P. He, J. Dong, Z. Guo, L. Dai, J. Am. Chem. Soc. 127 (2005) 14.
[42] H. Karadeniz, A. Erdem, A. Caliskan, Electroanalysis 20 (2008) 1932.
[43] J.W. Shie, U. Yogeswaran, S.M. Chen, Talanta 74 (2008) 1659.
[44] N. Li, R. Yuan, Y. Chai, S. Chen, H. An, Bioprocess. Biosyst. Eng. 31 (2008) 551.
[45] N. Li, R. Yuan, Y. Chai, S. Chen, H. An, W. Li, J. Phys. Chem. C 111 (2007) 8443.
[46] L.S. Wan, B.B. Ke, Z.K. Xu, Enzyme Microbol. Technol. 42 (2008) 332.
[47] C. Dhand, S.K. Arya, S.P. Singh, B.P. Singh, M. Dattab, B.D. Malhotra, Carbon 46 (2008) 1727.
[48] F. Yılmaz, Z. Kucukyavuz, J. Appl. Polym. Sci. 111 (2009) 680.
[49] K. Hong, S. Nam, C. Yang, S.H. Kim, D.S. Chung, W.M. Yun, C.E. Park, J. Orgel. 10 (2009) 363.
[50] K. Wu, S. Hu, Carbon 42 (2004) 3237.
[51] B.I. Kharisov, O.V. Kharissova, H.L. Gutierrez, U.O. Mendez, Ind. Eng. Chem. Res. 48 (2009) 572.
[52] M. Zhang, L. Su, L. Mao, Carbon 44 (2006) 276.
[53] R. Rastogi, R. Kaushal, S.K. Tripathi, A.L. Sharma, I. Kaur, L.M. Bharadwaj, J. Colloid Interf. Sci. 328 (2008) 421.
[54] I. Dumitrescu, N.R. Wilson, J.V. Macpherson, J. Phys. Chem. C 111 (2007) 12944.
[55] K.J. Ziegler, Z. Gu, H. Peng, E.L. Flor, R.H. Hauge, R.E. Smalley, J. Am. Chem. Soc. 127 (2005) 1541.
[56] J. Wang, M. Musameh, Y. Lin, J. Am. Chem. Soc. 125 (2003) 2408.
[57] D.R.S. Jeykumari, S.S. Narayanan, Biosens. Bioelectron. 23 (2008) 1686–1693.
[58] Y.L. Yao, K.K. Shiu, Electroanalysis 20 (2008) 2090.
[59] A.E.F. Nassar, W.S. Willis, J.F. Rusling, Anal. Chem. 67 (1995) 2386.
[60] Q. Huang, Z. Lu, J.F. Rusling, Langmuir 12 (1996) 5472.
[61] S.M. Chen, C.C. Tseng, Electrochim. Acta 49 (2004) 1903.
[62] X. Chen, H. Xie, J. Kong, J. Deng, Biosens. Bioelectron. 16 (2001) 115.
[63] Z. Lu, Q. Huang, J.F. Rusling, J. Electroanal. Chem. 423 (1997) 59.
[64] W. Liu, X. Guo, R. Guo, Int. J. Biol. Macromol. 41 (2007) 548.
[65] D. Mimica, J.H. Zagal, F. Bedioui, J. Electroanal. Chem. 497 (2001) 106.
[66] Y.C. Tsai, S.C. Li, J.M. Chen, Langmuir 21 (2005) 3653.
[67] B. Zhou, J. Wang, X. Gao, Y. Tian, Anal. Lett. 41 (2008) 1832.
[68] Y. Wu, Q. Shen, S. Hu, Anal. Chim. Acta 558 (2006) 179.
[69] J. Lu, L.T. Drzal, R.M. Worden, I. Lee, Chem. Mater. 19 (2007) 6240.
[70] J. Wang, Electroanalysis 17 (2005) 7.
[71] S. Hua, K. Wu, H. Yi, D. Cui, Anal. Chim. Acta 464 (2002) 209.
[72] H. Yi, K. Wu, S. Hu, D. Cui, Talanta 55 (2001) 1205.
[73] Y. Xu, C. Hu, S. Hu, Bioelectrochemistry 74 (2009) 254.
[74] E. Laviron, J. Electroanal. Chem. 101 (1979) 19.
[75] E. Katz, I. Willner, Electroanalysis 15 (2003) 913.
[76] H.O. Finklea, D.A. Snider, J. Fedyk, Langmuir 9 (1993) 3660.
[77] Z. Guoa, J. Chena, H. Liua, C. Cha, Anal. Chim. Acta 607 (2008) 30.
[78] C.P. Andrieux, O. Haas, J.M. Savgant, J. Am. Chem. Soc. 108 (1986) 8175.
[79] A.J. Bard, L.R. Faulkner, Electrochemical Methods Fundamentals and Applications, 2nd edn., John Wiley & Sons, Inc, 2001, p. 331.
[80] H.W. Chu, R. Thangamuthu, S.M. Chen, Electroanalysis 19 (2007) 1944.
[81] U. Yogeswaran, S.M. Chen, S.H. Li, Electroanalysis 20 (2008) 2324.
[82] A. Härtl, E. Schmich, J.A. Garrido, J. Hernando, S.C.R. Catharino, S. Walter, P. Feulner, A. Kromka, D. Steinmüller, M. Stutzmann, Nat. Mater. 3 (2004) 736.
[83] A. Salimi, E. Sharifi, A. Noorbakhsh, S. Soltanian, Biophys. Chem. 125 (2007) 540.

Talanta 78 (2009) 1280–1285

Contents lists available at ScienceDirect

Talanta

journal homepage: www.elsevier.com/locate/talanta

Alcohol vapours sensor based on thin polyaniline salt film and quartz crystal microbalance

Mohamad M. Ayad*, Nagy L. Torad

Department of Chemistry, Faculty of Science, University of Tanta, Tanta, Egypt

ARTICLE INFO

Article history:
Received 12 November 2008
Received in revised form 23 January 2009
Accepted 27 January 2009
Available online 5 February 2009

Keywords:
Quartz crystal microbalance
Sensor
Polyaniline salt
Hydrophilic character
Diffusion

ABSTRACT

A sensor based on the quartz crystal microbalance (QCM) technique was developed for detection of a number of primary aliphatic alcohols such as ethanol, methanol, 1-propanol, and 2-propanol vapours. Detection was based on a sensitive and a thin film of polyaniline, emeraldine salt (ES), coated the QCM electrode. The frequency shifts (Δf) of the QCM were increased due to the vapour absorption into the ES film. The values of Δf were found to be linearly correlated with the concentrations of alcohols vapour in mg L^{-1}. The changes in frequency are due to the hydrophilic character of the ES and the electrostatic interaction as well as the type of the alcohol. The sensor shows a good reproducibility and reversibility. The diffusion and diffusion coefficient (D) of different alcohols vapour were determined. It was found that the sensor follows Fickian kinetics.

1. Introduction

Detection of toxic odorants and air-born volatile organic compounds (VOCs) becomes the world interest in the last few decades, owing to concerns about environmental protection, human health care, industrial processing, and quality control. Alcohols such as, methanol and ethanol are volatile organic solvents that are used in many workplaces and laboratories, medicine, and food industry. The exposure to methanol vapour for a long time causes some diseases such as eyesight disturbance, nasal mucous membrane, conjunctiva inflammation, and nerve disease and even death, thus the on-line monitoring of these alcohols vapour in air is an important task. Fourier transform infrared spectrometry (FTIR), gas chromatography (GC), and mass spectrometry (MS) [1], were used for detection of methanol vapour. Also ethanol detection based on the using of metal oxides [2] was reported. Although these common methods are accurate, reliable, but are off-line analysis, need expensive instrumentations and are time-consuming [3].

The development of sensors with selectivity, rapid reliability and reproducibility for on-line monitoring and *in-situ* detection of VOCs have received great interest. For example, optical sensors involving changes of fluorescence [4] and optical absorption [5] were reported.

Recently, a number of electronic devices, chemical sensors, and sensor arrays have been developed, depend greatly on the using of different sensitive coatings to a special analyte. These sensors are mass sensitive quartz crystal microbalance (QCM), surface acoustic wave (SAW) devices, and chemical field effect transistors (ChemFETs). Amongst the various types of chemical sensors, there is a considerable interest in QCM [6] for low cost, compact volume, easy portability, and high sensitivity. Meanwhile, QCM sensor has great interest than metal-oxide semiconductor sensors, in its lower operation temperature [7,8] for detection of VOCs.

QCM is sensitive to mass change, when the surface of a quartz crystal electrode is coated with a sensitive polymeric material, capable of interacting with the analyte of interest, so it is extensively employed in gas analysis [9]. The change in mass (m') of the polymer film can be measured by the oscillating frequency of the quartz electrode. The frequency change (Δf) to the mass loaded is calculated from Sauerbrey equation [10]:

$$\Delta f = -\left(\frac{2f_o^2}{\sqrt{\rho_Q \mu_Q}}\right) m' \quad (1)$$

where f_o (Hz) is the natural frequency of the quartz crystal, ρ_Q is the quartz density (2.649 g cm^{-3}) and μ_Q is the shear modulus (2.947×10^{10} N/m^2).

Conducting polymers are used in various applications, such as in solid-state batteries, solar cells, electronic devices [11], chemical sensors [12,13], rust prevention of metals [14,15], humidity [16], and even in gas sensing [17]. Polypyrrole has been one of the first polymers used in gas sensor analysis for detection of alcohols and other organic vapours [17–19], however it shows a low sensitivity, and incomplete desorption of the gas molecules. Therefore, the researches were extended towards polyaniline (PANI) as

* Corresponding author. Tel.: +20 40 3404398; fax: +20 40 3350804.
E-mail address: mayad12000@yahoo.com (M.M. Ayad).

0039-9140/$ – see front matter © 2009 Elsevier B.V. All rights reserved.
doi:10.1016/j.talanta.2009.01.053

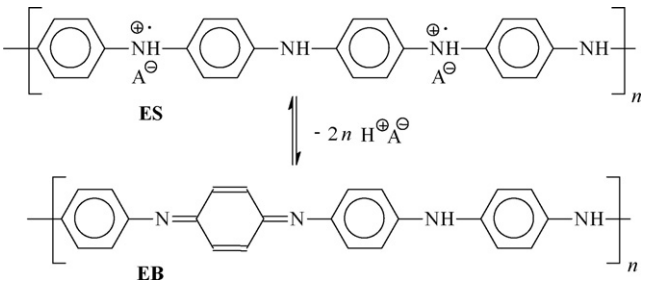

Scheme 1. Polyaniline salt, emeraldine salt (ES), is deprotonated by treatment with an alkali to polyaniline base, emeraldine base (EB).

sensing material [20–22], due to its environmental stability, high electrical conductivity, good reversibility and reproducibility, and good performance at room temperature. The deriving forces for the interaction of these gas analytes and PANI chains based on the electrostatic interaction (hydrogen-bonding, dipolar interactions, and dispersion forces). However, no reports are available for sensors based on the hydrophilic and hydrophobic character of the PANI salt, emeraldine salt (ES) and PANI base, emeraldine base (EB), forms (Scheme 1), respectively.

In previous studies [23,24], the EB coated the QCM electrode was used as sensor for the vapours of chlorinated aliphatic hydrocarbons and a number of primary aliphatic alcohols. However, an experiment was conducted, in which the ES coated the QCM electrode was used as a sensor for the primary aliphatic alcohols and concluded that the sensitivity of detection increases in comparison to the EB. This is encouraging us in the present work, to develop an on-line detection to the vapours of methanol, ethanol, 1-propanol and 2-propanol using QCM coated with thin film of ES. The strategy of the hydrophilic nature of the ES film was considered. Consequently, a sensitive and rapid sensor was obtained.

2. Experimental

2.1. Reagents and materials

Aniline (ADWIC, Egypt) was distilled twice under atmospheric pressure using zinc dust. Ammonium peroxydisulfate (APS) (WINLAB, UK) was used without purification. Sulfuric acid (ADWIC) was used as received. Ethanol and methanol were received from ADWIC, Egypt, 1-propanol was received from Aldrich, England and 2-propanol was received from BDH, England. All chemicals were used without any further purification.

2.2. Instrumentation

The design and experimental arrangement has been described in earlier studies [25–27]. A 5 MHz AT-cut quartz crystal is used. The resonance frequency of the crystal was determined by using the crystal as the frequency determining element of an electronic oscillator, the measurements being taken using a GW frequency counter, Model GFC-8055G.

2.3. Coating on the electrode of QCM with PANI film

A 0.08 mol L^{-1} solution of aniline was prepared in 50 mL of 0.1 mol L^{-1} H_2SO_4 and a solution of 0.1 mol L^{-1} APS was prepared in 50 mL of 0.1 mol L^{-1} H_2SO_4. The APS solution was added to the aniline solution. The APS/aniline molar ratio after mixing was 1.25. The solutions of the reactants were added to the polyethylene cell. As the polymerization proceeds, the *in-situ* PANI sulfate (ES) film was deposited onto the electrode of QCM. The film coated the QCM electrode at the end of the polymerization was rinsed with 0.1 mol L^{-1} H_2SO_4 and then dried in an oven at 50–60 °C for at least 30 min until the QCM attains constant frequency.

The thickness of the film, L (cm) can be determined from the density (ρ) of the ES, $\rho = 1.44$ (g/cm^3) using the relation:

$$m' = \rho L \quad (2)$$

2.4. Procedures

All measurements were carried out in a polyethylene cell with an internal volume of 140 mL. Hamilton microliter syringe (Hamilton Bonaduz AG, Switzerland) was used for alcohol injections. The concentration of injected alcohol in the cell was calculated in mg L^{-1} using its density, purity percent and volume.

The ES coated the QCM electrode after each injection and complete absorption of alcohol vapours was exposed to hot air to desorb the alcohol and recover the electrode. The backshift of the crystal frequency to its initial value was taken as an indication of full desorption. All measurements were carried out at room temperature (~25 °C).

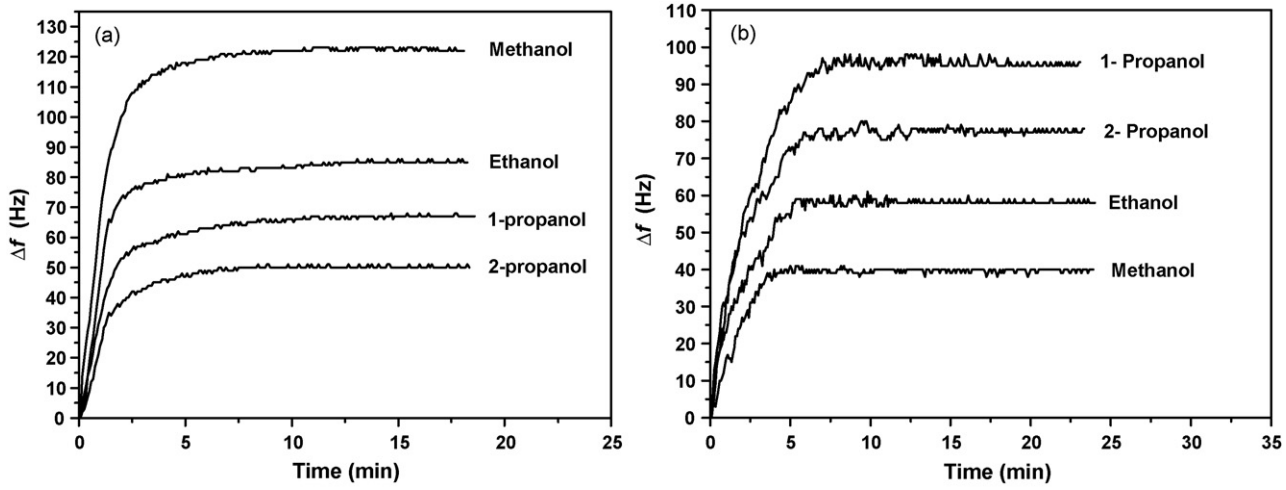

Fig. 1. Δf of QCM coated with (a) ES (120 nm) and (b) EB (191 nm) film when exposed to 5 mg L^{-1} of methanol, ethanol, 1-propanol, and 2-propanol vapours.

3. Results and discussion

3.1. The effect of the hydrophilic and hydrophobic characters of the PANI film

The polymerization of aniline and APS prepared in 0.1 mol L^{-1} H_2SO_4 ends with film (ES). This film was treated with 0.1 mol L^{-1} ammonia solution to obtain the EB form. The latter itself is relatively hydrophobic, but after protonation with the most of acids it becomes more hydrophilic [28]. Both forms coated the QCM electrodes were used to detect the alcohols under consideration. These alcohols have a hydrophilic nature, but this nature decreases with increasing the aliphatic hydrocarbon chain length attached to the hydroxyl group. Fig. 1(a) shows the sensitivity and response time of the hydrophilic ES towards a concentration of 5 mg L^{-1} of different alcohols vapour. It can be shown that, methanol records high Δf than the other alcohols and the sensitivity is in the order: methanol > ethanol > 1-propanol > 2-propanol. On the other hand, using the hydrophobic EB, 1-propanol records high Δf than the others, as shown in Fig. 1(b) and the sensitivity is in the order: 1-propanol > 2-proapnol > ethanol > methanol. It can be concluded that the hydrophilic and hydrophobic properties of the PANI film plays an important role on the sensitivity and response time, in addition to the electrostatic interaction (hydrogen-bonding, dipolar interactions, and dispersion forces). For example, we would expect that the interaction of alcohols with the imine and amine atoms in the EB chains more than its interaction with the ES form based on the electrostatic interaction [24]. The present results are in contrary with this expectation. Consequently, the interaction between the alcohols and the PANI film can be explained on basis of the hydrophilic and hydrophobic properties of the PANI forms. However, the role of the electrostatic interaction cannot be excluded. The latter conclusion can be justified in the following section.

3.2. Dopant effect on the detection sensitivity

The sensitivity and response time of different ES films doped with hydrochloric, sulfuric and phosphoric acids to ethanol vapours were studied. The polymerization of aniline and APS prepared in 0.1 mol L^{-1} hydrochloric, sulfuric and phosphoric acids were carried out and ended with *in-situ* PANI hydrochloride, sulfate and phosphate films coated the QCM electrode, respectively. Fig. 2 shows the effect of dopants on the sensitivity towards a concentration of 3 mg L^{-1} of ethanol vapour. Δf at the steady state variation with time for ES (chloride, sulfate, and phosphate) are given in Table 1. It is clear that ES doped with phosphate anions shows a high sensitivity and response time than the other dopants. This is attributed to the fact that the phosphoric acid molecule uses one proton to dope PANI, and the other two OH^- groups are free to form hydrogen bonds with PANI chains and the absorbed ethanol. In case of ES (sulfate), only OH^- group is free. Such type of group does not exist in ES (chloride). Based on this result and the results obtained from the previous section, it can be concluded that the hydrophilicity concomitant with the electrostatic interactions are responsible for the interaction between the alcohols and the ES film.

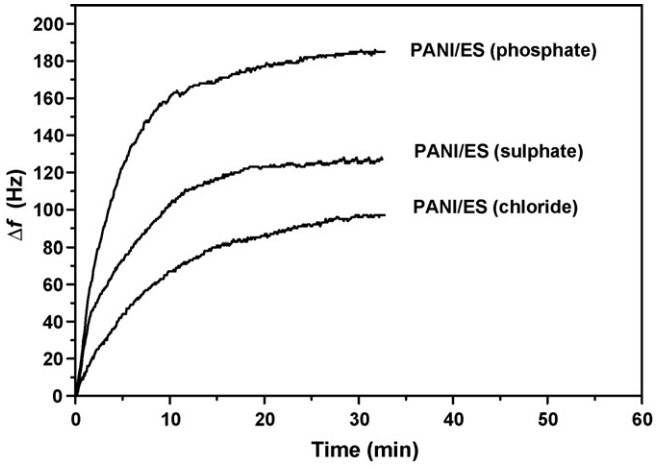

Fig. 2. Δf of QCM coated with ES (chloride, sulfate, and phosphate) when exposed to 3 mg L^{-1} ethanol vapours.

3.3. ES (sulfate) coated QCM electrode for detection of alcohols

The alcohols under consideration were detected using a thin film of ES (sulfate) coated the QCM electrode. Initially, the effect of 15 mg L^{-1} of different alcohols vapour on blank (uncoated) QCM electrode was studied. It can be shown from Fig. 3 that the frequency was constant with time upon exposure the electrode to different alcohols vapour. Therefore, it is concluded that the alcohols have no effect on the frequency of the uncoated QCM electrode. The ES film which coated the electrode was exposed to different concentrations of methanol vapours. The frequency of the quartz crystal decreases due to the absorption of methanol vapours into the film. Δf was measured and plotted against time, Fig. 3(a). It is observed that Δf increases linearly with increasing methanol vapours concentration. This is expected, since more vapour molecules in the test atmosphere, more vapour molecules would absorbed into the ES film till the equilibrium reached to the steady state. After each injection of methanol vapour and equilibrium reached, the frequency of the crystal was back shifted to its initial value by exposing the electrode to hot air, which indicates fully desorption of methanol from the electrode surface.

A calibration curve of Δf against the concentration of methanol vapours was constructed and is shown in Fig. 4(a). Linear correlation was obtained with a correlation coefficient (R) and slope equal 0.999 and 25.344, respectively.

Detections of ethanol, 1-propanol and 2-propanol vapours were also carried out. Δf versus time was plotted and is shown in Fig. 3(b–d), respectively. The same profiles were obtained like that of methanol. Calibration curves were plotted and all have linear relationships, Fig. 4(b–d). The correlation coefficients and the slopes were calculated and are depicted in Table 1.

It is expected that the film thickness would affect the response time and sensitivity of the sensor. To justify this expectation, different thicknesses of ES (sulfate) films were exposed to different concentrations of ethanol vapours and Δf was recorded. Plots of Δf with the concentrations of ethanol vapours are shown in Fig. 5. It is clear that, as the film thickness increases, the magnitude of Δf and the slope of the correlation also increase, due to the increases of the active sites of the polymer. The correlation coefficients and the slopes were calculated and are given in Table 1.

1-Propanol has the same molecular weight of 2-propanol, but exhibit higher frequency shift than its isomer. This is attributed to the steric hindrance, which prevents 2-propanol molecules from further absorption into the ES film.

3.4. Reproducibility and reversibility of the sensor

The sensor based on the ES film shows a good reproducibility and reversibility. Fig. 6 shows the Δf of the ES film of thickness 118 nm when exposed to 3 mg L^{-1} ethanol till reached to the steady state and the fully desorption of the crystal was obtained by using a hot dry air. The presence of about 2 and 3 Hz in each analyte injection is considered to be stability in the quartz crystal electrode. The exper-

Table 1
Analytical characteristic parameters for the determination of aliphatic alcohol vapours using PANI/ES coated QCM.

ES[a]	Compound	Film thickness (nm)	Δf at steady state (Hz)	Sensitivity (Hz/mg L^{-1})	R^2[b]	R.S.D[c] ($n=5$)
Sulfate	Methanol	140		25.344	0.999	8.879
	Ethanol	118		20.700	0.998	7.088
		140		22.200	0.998	6.763
		177		23.067	0.998	7.677
		160	127			
	2-Propanol	193		33.320	0.999	7.123
	1-Propanol	193		32.332	0.997	10.057
Chloride	Ethanol	158	97			
Phosphate	Ethanol	163	185			

[a] Emeraldine salt of polyaniline.
[b] Correlation coefficient.
[c] Relative standard deviation.

iment was repeated for five times to insure a complete reversibility of the sensor.

3.5. Vapours diffusion study in the ES film

The diffusion of the alcohols vapour into the ES film coated QCM electrode is expressed in terms of diffusion coefficient (D), in which an ES film of thickness 120 nm was exposed to 5 mg L^{-1} of different alcohols vapours. The experimental data was analysed using Fick's second equation, which has been reviewed by Crank [29]:

$$\frac{\Delta f_t}{\Delta f_\infty} = 4\sqrt{\frac{D}{\pi}}\frac{t^{1/2}}{L} \quad (3)$$

where Δf_t is the frequency change due to the absorption of the vapour into the ES film at any time t and Δf_∞ is the frequency change in the equilibrium state at the end of the absorption process,

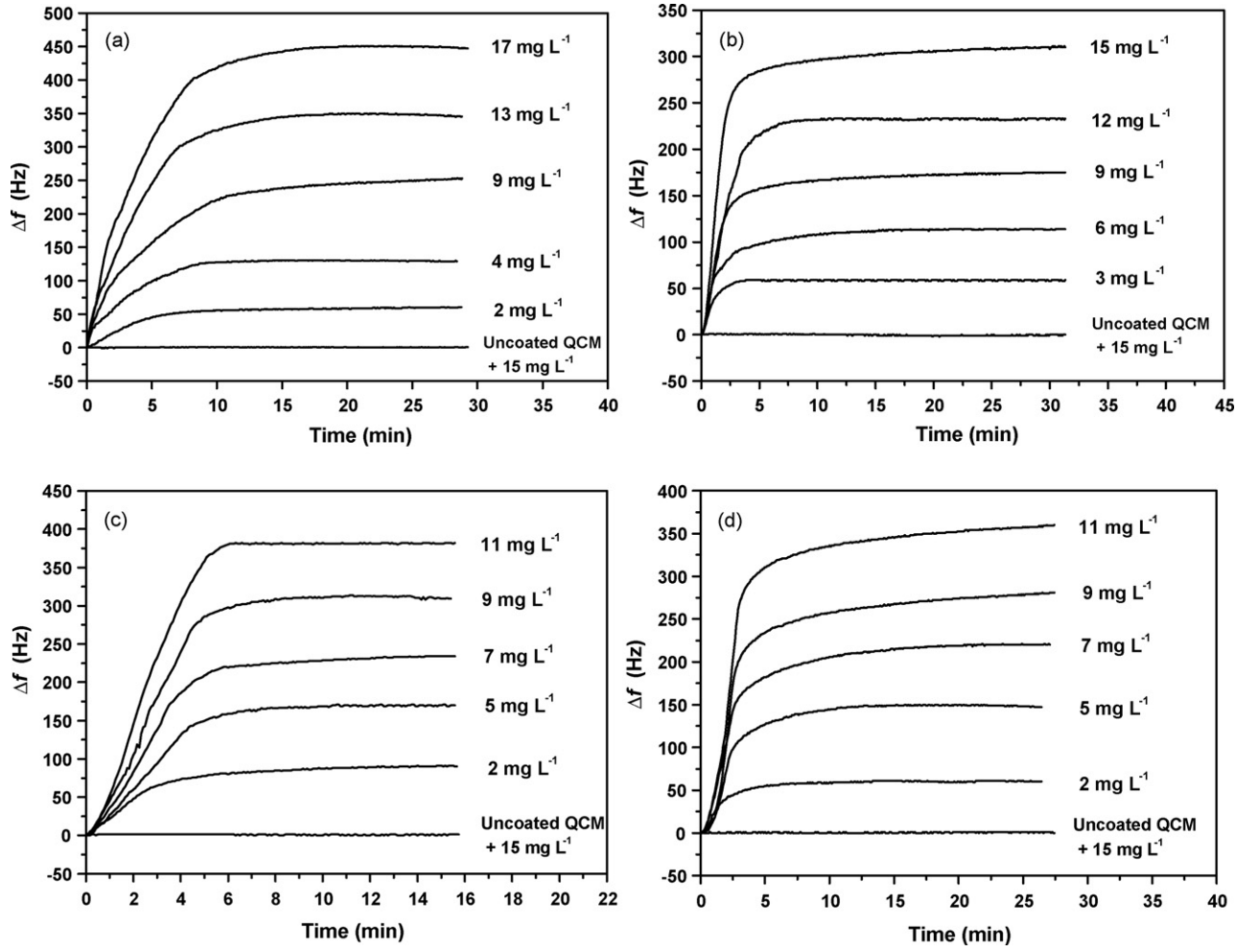

Fig. 3. Δf of QCM coated with ES film when exposed to the vapours of different concentrations of: (a) methanol (film thickness 140 nm), (b) ethanol (film thickness 118 nm), (c) 1-propanol (film thickness 193 nm), and (d) 2-propanol (film thickness 193 nm).

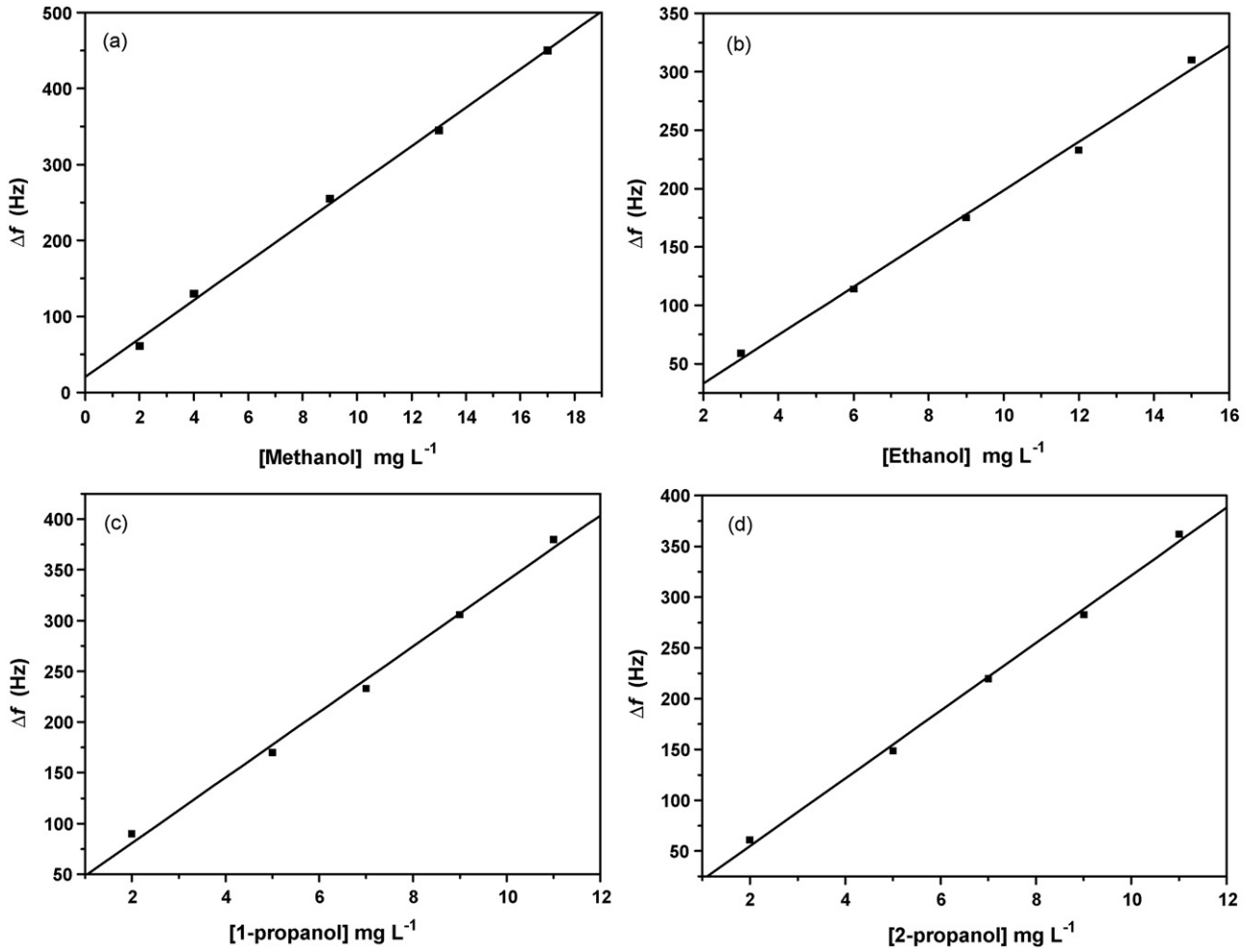

Fig. 4. Calibration curves for the determination of the alcohols vapour using the ES film coated QCM electrode: (a) methanol, (b) ethanol, (c) 1-propanol, and (d) 2-propanol.

these two parameters can be given as follows:

$\Delta f_t = f_{ES} - f_t$ and $\Delta f_\infty = f_{ES} - f_\infty$

where f_t is the frequency during the exposure process at time t, f_∞ is the frequency at the equilibrium state and f_{ES} is the frequency of the ES film.

Fig. 7 shows a plot of $\Delta f_t/\Delta f_\infty$ as a function of $t^{1/2}/L$ for methanol vapour, in which the process obeys Fickian kinetics [29]. D was calculated from Eq. (3) for methanol, ethanol, 1-propanol, and 2-propanol and equals 3.99, 2.85, 2.3, and 2.23×10^{-13} (cm^2/s), respectively. The D values are in the order: methanol > ethanol > 1-propanol > 2-propanol. This is due to the differences in hydrophilic nature and molecular structure of different alcohols.

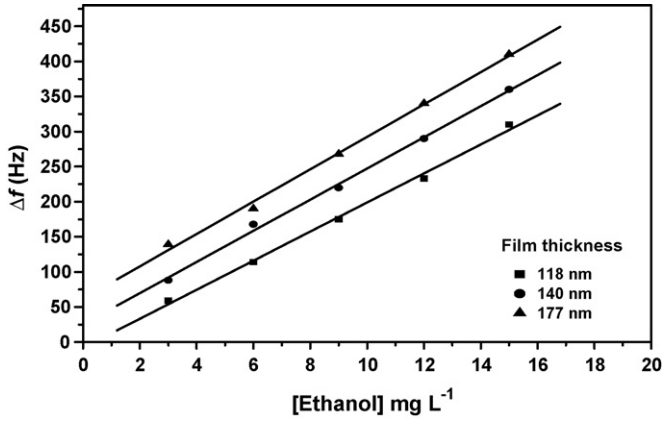

Fig. 5. The effect of film thickness on the detection of different concentrations of ethanol vapours.

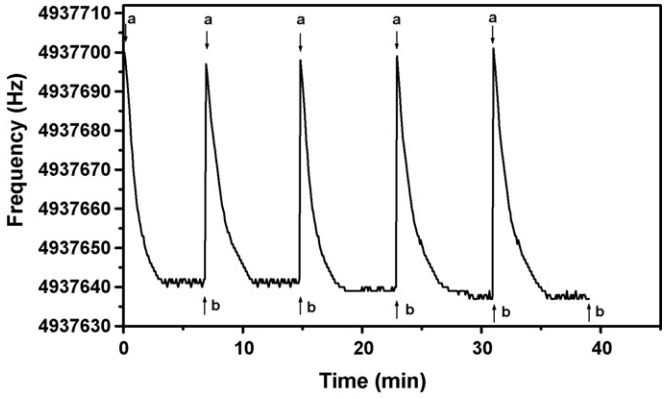

Fig. 6. . Reproducibility and reversibility of QCM electrode coated with the ES film when exposed to 3 mg L^{-1} ethanol: (a) ethanol injection and (b) ethanol desorption using hot air.

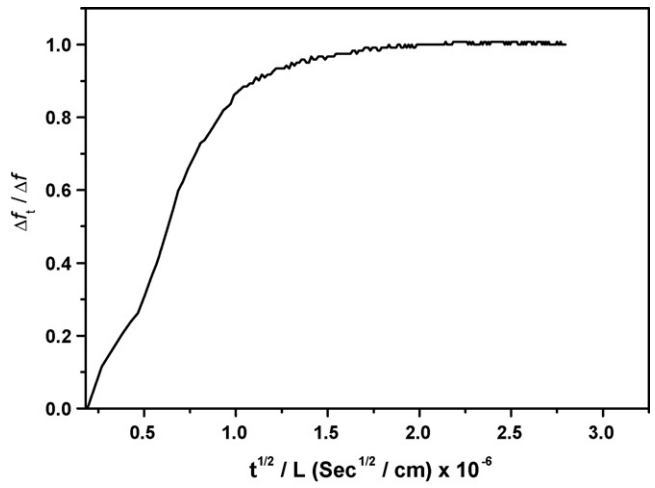

Fig. 7. $\Delta f_t/\Delta f_\infty$ as a function of $t^{1/2}/L$, when the ES film of thickness 120 nm was exposed to 5 mg L^{-1} of methanol vapours.

4. Conclusion

A sensor based on quartz crystal coated with a thin film of ES was developed for low concentrations in the range 2–17 mg L^{-1} of primary aliphatic alcohols vapour. The ES shows a high response and sensitivity towards the alcohols vapour. The hydrophilic and hydrophobic properties of the ES and EB forms of PANI film, respectively concomitant with the electrostatic interactions is responsible for the driving forces of the interaction between the alcohols and the PANI film. The hydrophilic nature of the tested alcohols has also a role on its absorption. It is concluded that, the frequency changes increased with increasing the concentrations of injected alcohol and a good linear correlations were obtained. The results indicated the reproducible and the reversible performance of the sensor. The diffusion of the alcohols vapour into the ES film was also studied and is found to obey Fickian kinetics.

References

[1] S. Bangalore, G.W. Small, R.J. Combs, R.B. Knapp, R.T. Kroutil, Anal. Chim. Acta 297 (1994) 387.
[2] P.P. Tsai, I.-C. Chen, M.H. Tzeng, Sens. Actuators B: Chem. 14 (1993) 610.
[3] M.A. Jochmann, X. Yuan, T.C. Schmidt, Anal. Bioanal. Chem. 387 (2007) 2163.
[4] K.S. Suslick, MRS Bull. 29 (2004) 720.
[5] J. Spadavecchia, G. Ciccarella, R. Rella, S. Capone, P. Siciliano, Sens. Actuators B: Chem. 96 (2003) 489.
[6] G.J. Price, A.A. Clifton, V.J. Burton, T.C. Hunter, Sens. Actuators B: Chem. 84 (2002) 208.
[7] A.K. Srivastava, Sens. Actuators B: Chem. 96 (2003) 24.
[8] S. Ampuero, J.O. Bosset, Sens. Actuators B: Chem. 94 (2003) 1.
[9] W.H. King Jr., Anal. Chem. 36 (1964) 1735.
[10] G. Sauerbrey, Z. Phys. 155 (1959) 206.
[11] H. Koezuka, A. Tsumura, T. Ando, Synth. Met. 18 (1987) 699.
[12] C.K. Tan, D.J. Blackwood, Sens. Actuators B: Chem. 71 (2000) 184.
[13] A.A. Athawale, M.V. Kulkarni, Sens. Actuators B: Chem. 67 (2000) 173.
[14] B. Wessling, Adv. Mater. 6 (1994) 226.
[15] V. Brusic, M. Angelopoulos, T. Graham, J. Electrochem. Soc. 144 (1997) 436.
[16] P.S. Barker, J.R. Chen, N.I. Agbor, A.P. Monkman, P. Mars, M.C. Petty, Sens. Actuators B: Chem. 17 (1994) 143.
[17] P.N. Bartlett, S.K. Ling-chung, Sens. Actuators B: Chem. 19 (1989) 287.
[18] P.N. Bartlett, S.K. Ling-chung, Sens. Actuators B: Chem. 19 (1989) 141.
[19] P.N. Bartlett, P.B.M. Archer, Sens. Actuators B: Chem. 19 (1989) 125.
[20] S. Sukeerthi, A.Q. Contractor, Indian J. Chem. Sect. A 33 (1994) 565.
[21] V. Hatfield, P. Neaves, P.J. Hicks, K. Persaud, P. Travers, Sens. Actuators B: Chem. 18/19 (1994) 221.
[22] M.M. Ayad, N.A. Salahuddin, M.O. Al-Ghayesh, Polym. Adv. Technol. 19 (2008) 1142.
[23] M.M. Ayad, G. El-Hefnawey, N. Torad, Sens. Actuators B: Chem. 134 (2008) 887.
[24] M.M. Ayad, G. El-Hefnawey, N. Torad, J. Hazard. Mater., in press, doi:10.1016/j.jhazmat.2009.02.003.
[25] M.M. Ayad, Polym. Int. 35 (1994) 35.
[26] M.M. Ayad, J. Appl. Polym. Sci. 53 (1994) 1331.
[27] M.M. Ayad, J. Polym. Sci. Part A: Polym. Chem. 32 (1994) 9.
[28] T.V. Shishkanova, I. Sapurina, J. Stejskal, V. Kral, R. Volf, Anal. Chim. Acta 553 (2005) 160.
[29] J. Crank, The Mathematics of Diffusion, 2nd edn., Clarendon Press, Oxford, 1975, pp. 414.

Talanta 78 (2009) 1266–1271

Contents lists available at ScienceDirect

Talanta

journal homepage: www.elsevier.com/locate/talanta

Monitoring of autoxidation in LCPUFA-enriched lipid microparticles by electronic nose and SPME-GCMS

S. Benedetti*, S. Drusch, S. Mannino

Dipartimento di Scienze e Tecnologie Alimentari e Microbiologiche, Università degli Studi di Milano, Via celoria 2, 20133 Milano, Italy

ARTICLE INFO

Article history:
Received 27 October 2008
Received in revised form 16 January 2009
Accepted 23 January 2009
Available online 4 February 2009

Keywords:
Fish oil
Stability
Analysis
Oxidation
Supplemented food

ABSTRACT

Electronic nose and SPME-GCMS were used to monitor the autoxidation in long chain polyunsaturated fatty acid (LCPUFA)-enriched lipid microparticles produced by spray congealing with ultrasonic nebulization, during storage at 20 °C up to 6 weeks with sufficient air supply and limited air supply. Conjugated dienes and peroxide value as well as secondary lipid oxidation products were analysed to follow the course of autoxidation. Principal Component Analysis evidenced that only MOS sensors but not MOSFET sensors contributed to the discrimination of the samples and facilitated the ability of the electronic nose to distinguish the LCPUFA-enriched lipid microparticles into two groups according to the different oxidative status. The selected MOS sensor responses correlated well with quantitative dominating volatile compounds (propanal and hexanal) and with volatile compounds which have been associated with fishy and rancid off flavour (1-penten-3-one, 1-penten-3-ol, 2,4-heptadienal and 2,6-nonadienal). Bread mix supplemented with the LCPUFA-enriched microparticles was analysed as an example for a LCPUFA supplemented food. Data from the present study indicate that the electronic nose can be used as a sensitive tool to evaluate the lipid oxidative status of LCPUFA-enriched microparticles. In supplemented foods like bread mix, matrix-related changes, which occur in supplemented and non-supplemented samples, make a clear distinction more difficult.

1. Introduction

In the past different reports indicated that the intake of long chain polyunsaturated fatty acids (LCPUFAs) in the Western society is far below the recommendations and supplementation of foods with LCPUFAs is generally recognized as useful and safe [1]. However, LCPUFAs are highly susceptible to oxidation and different techniques have been developed to protect the LCPUFAs from light and oxidation as well as to mask the specific flavour of LCPUFA-rich oils from marine origin. Among these techniques for protection of sensitive food ingredients are the microencapsulation by spray drying or spray chilling, complex coacervation, inclusion in microporous carbohydrates or fluidized bed coating. It is generally accepted that microencapsulation retards lipid oxidation during storage, but it has recently been shown that lipid oxidation might already occur during the encapsulation process [2,3], which in the case of microencapsulation by spray drying might affect the fish oil odour profile [4].

One possibility to monitor lipid oxidation is the direct analysis of volatile secondary lipid oxidation products using gas chromatography with static headspace technique or in a dynamic system after trapping of the volatiles using dynamic headspace sampling or solid phase microextraction (SPME). Several publications deal with the identification of volatiles in fish oil or fish oil-enriched products [5–11]. Approaches to link the presence of certain volatiles analysed by GC to the sensory profile of fish oil have been published, but these studies can only cover certain aspects of the complex sensory profile. E.g. Venkatashwarlu et al. [8,12] characterised the volatile profile of fish oil-enriched emulsions and used 1-penten-3-one, Z-4-heptenal, (E,E)-2,4-heptadienal and (E,Z)-2,6-nonadienal, as the key compounds responsible for fishy off-flavour of oxidised fish oil, to model the fishy off-flavour developing during autoxidation. An alternative method to draw conclusion from the chemical analysis on the sensory perception of fish oil is the FAST Index. The FAST index was suggested by Macfarlane et al. [13] and is based on the content of Z-4-heptenal as well as 2,6- and 3,6-nonadienal. However, it has to be emphasized that chromatogrpahic methods cannot replace sensory evaluation of fish oil and fish oil-enriched products. Since the odour threshold of the volatiles deriving from autoxidation of unsaturated fatty acids varies over a very wide range, the concentration of the individual compounds cannot be correlated with the sensory perception. Furthermore highly aroma-active compounds, which significantly contribute to the sensory profile, might be present in concentrations below the detection limit of the method [14].

* Corresponding author. Tel.: +39 02 50319215; fax: +39 02 50319061.
E-mail address: simona.benedetti@unimi.it (S. Benedetti).

0039-9140/$ – see front matter © 2009 Elsevier B.V. All rights reserved.
doi:10.1016/j.talanta.2009.01.045

In recent years, considerable efforts have been devoted to the development of innovative analytical system, so-called electronic nose, which can provide low-cost and rapid information for monitoring food quality and state of a process. The electronic nose consists of an array of gas sensors with different selectivity, a signal collecting unit and a suitable pattern recognition software. In contrast to traditional analytical methods, electronic nose sensor responses do not provide information on the individual volatile compounds under investigation or the sensory profile, but rather give a fingerprint of the food product based on the chemical species present [15]. The electronic nose technology remains an area of research that holds much potential for future development. It is a rapid means of analysis, can be easily used in conjunction with chemometrics and, as reviewed by Reid et al. [16] has had a good degree of success, e.g. in the authentication of a wide range of food types. Analysis by electronic nose has successfully been used for the characterisation of vegetable oils [17,18] and for the quality control of olive oil aroma [19]. Baranauskiene et al. [20] furthermore demonstrated that the electronic nose and SPME-GC technique could be useful for the evaluation of microencapsulated essential oils of thyme, oregano and cassia.

In the present study, LCPUFA-enriched microparticles are produced by spray congealing with ultrasonic nebulization. The volatiles released during storage are monitored using a set of solid-state gas sensors. Key volatiles are analysed and identified via SPME-GC. Aim of the present study was to elucidate whether results from the sensor-based method using an electronic nose correlate with the content of secondary lipid oxidation products as determined by gas chromatographic analysis in order to provide an easy method for standardized quality evaluation of LCPUFA-enriched microparticles and supplemented foods.

2. Experimental

Fish oil (Omevital 18/12) with approximately 33% of the long chain polyunsaturated fatty acids eicosapentanoic acid and docosahexanoic acid was provided by Cognis Deutschland GmbH & Co. KG, Germany. Hydrogenated palm oil with 44% palmitic acid and 49% stearic acid was provided by I.G.O.R., Industria Alimentare S.p.A., Italy.

2.1. Preparation of LCPUFA-enriched lipid microparticles

Lipid microparticles were prepared in cooperation with UDF System S.r.L., Bergamo, Italy. The process is based on spray congealing of a molten liquid oil or oil-based dispersion. The general principle of the method is patented [21] and the preparation of LCPUFA-enriched lipid microparticles using this method has also been described [22]. Atomization is achieved via ultrasound nebulization. The frequency was set at 20,000 Hz and the amplitude at 90 μm. Droplets were rapidly solidified in a drying chamber cooled with liquid nitrogen. The final fatty acid composition of the lipid microparticles is summarized in Table 1. Aliquots (2 g) of the microparticles were stored either in 40 mL head-space Pyrex glasses under air (sufficient air supply) or in screw-capped glass vials, tapped and filled to the very top (limited air supply) for up to 6 weeks at 20 °C. Sampling was performed every week.

Table 1
Fatty acid composition of the LCPUFA-enriched lipid microparticles.

Fatty acid	%
Palmitic acid	35.2
Stearic acid	39.2
Oleic acid	2.4
Eicosapentanoic acid	4.0
Docosahexanoic acid	2.6
Total omega-3 content	7.9

2.2. Preparation of LCPUFA-enriched bread mix

Bread mix, essentially free from LCPUFAs, was purchased from a local market. The product was supplemented with 2% of fish oil by incorporating an aliquot with 10% of the LCPUFA-enriched microparticles. The required supplementation of the bread mix is based on per capita consumption of bread and the recommended intake of LCPUFAs. Individual samples (2 g) were stored at 20 °C in 40 mL head-space Pyrex glasses (sufficient air supply) up to 24 weeks and analysed every 6 weeks by using the electronic nose and GC/MS. Non-supplemented products served as a control.

2.3. Physical analysis of the LCPUFA-enriched lipid microparticles

Particle morphology was visualized via scanning electron microscopy (CamScan 44 REM/EDX scanning electron microscope, CamScan USA Inc., Cranberry Township PA, USA). Particle size determination was performed using a laser-diffraction sensor (Helos, Sympatec GmbH, Clausthal-Zellerfeld, Germany) equipped with a cuvette. Microparticles were dispersed in water prior to analysis. Flowability of the microencapsulated fish oil was determined by determining the Carr-Index, which is calculated from the bulk density (ρ_{bulk}) and the tapped bulk density (ρ_{tapped}) of the samples according to the following formula:

$$\text{Carr index} = \frac{\rho_{tapped} - \rho_{bulk}}{\rho_{tapped}} \quad (1)$$

Analysis of bulk density and tapped bulk density was performed as described in the European pharmacopoeia [23].

2.4. Chemical analysis of lipid oxidation in LCPUFA-enriched microparticles during storage

Conjugated dienes were photometrically determined after dilution of 10 mg of the sample with 5 ml of 2-propanol at 234 nm. For calculation of the concentration, the results were expressed as millimoles of hydroperoxide per kg oil using a molar coefficient of 26,000 for methyl linoleate hydroperoxides [24]. Hydroperoxide content was determined using the IDF standard method 74A:1991 for the determination of the peroxide value in anhydrous milk fat with slight modifications [25]. 2-Propanol was used as solvent in the test protocol. After addition of the iron-II-chloride and the ammonium thiocyanate solution, samples were incubated in a water bath at 70 °C for 30 min. The extinction was measured at a wavelength of 485 nm.

Solid phase microextraction (SPME) was performed with a carboxen/polydimethylsiloxane fiber (CAR/PDMS 75-μm; Supelco, Bellefonte, PA, USA). The fiber allowed superior performance in trapping the target volatiles compared to a polydimethylsiloxane/divinylbenzene fiber, which is in agreement with the literature [11]. Prior to its use the fiber was conditioned by inserting it into the GC injector at the temperature of 280 °C according to the supplier's instructions. HS-SPME was performed by incubating 2 g of samples in a 40 ml vial with a pierceable Silicon/Teflon disks in the cap at 65 °C during 30 min. Then, the volatiles were directly desorbed in the GC injection port during 1 min. The fiber was reconditioned at 250 °C for 20 min before re-using it.

The GC–MS system consisted of a GC (CP 3800, Varian) linked to a mass selective detector (1200 Quadrupole, Varian) equipped with a SolGel Wax 60 m × 0.25 mm i.d., 0.25 μm film thickness, capillary column (SGE International S.r.L., Rome, Italy) was used. The GC oven temperature was initially held at 35 °C for 5 min, followed by an

increase of 2.5 °C/min to 90 °C, an increase of 4 °C/min to 180 °C and finally an increase of 10 °C/min to a final temperature of 200 °C held for 4 min. Helium was used as carrier gas at a flow rate of 1.3 ml/min. A GC injector was heated at 250 °C. Electron impact mass spectra were recorded at 1000 V over the range 35–300 m/z. Identification was performed both by NIST (National Bureau of Standard) library searches and by comparison with the retention time of external standards.

2.5. Analysis of LCPUFA-enriched lipid microparticles by electronic nose

A commercial electronic nose (model 3320 Applied Sensor Lab Emission Analyser, Applied Sensor Co., Linkoping, Sweden) was used in the present study. Twenty-two different sensors compose the sensor array: 10 sensors were Metal Oxide Semiconductor Field Effect Transistors (MOSFET) and 12 were Taguchi type sensors (Metal oxide Semiconductors—MOS). MOSFET sensors rely on a change of electrostatic potential. They comprise three layers, a silicon semiconductor, a silicon oxide insulator and a catalytic metal (usually palladium, platinum, iridium or rhodium), also called gate. When polar compounds interact with this metal gate, the electric field, and thus the current flowing through the sensor, are modified. The recorded response corresponds to the change of voltage necessary to keep a constant pre-set drain current. MOSFET sensors respond to gases like hydrogen, ammonia, ethanol, amines, acetone, hydrocarbons, CO and NO_2.

The MOS sensors rely on changes of conductivity induced by the adsorption of molecule in the gas phase, and on subsequent surface reactions. They consist of a ceramic substrate coated by a metal oxide semi-conducting film, and heated by a wire resistor. Due to the high-operating temperature (400–500 °C), the organic volatiles transferred to the surface of the sensors are totally combusted to carbon dioxide and water, leading to a change in the resistance. Gases detectable by MOS sensors include alcohols, ammonia, butane, carbon monoxide, chlorine, ethylene, heptane, hexane, hydrogen, hydrogen sulfide, methane, nitrogen dioxide, ozone, propane, sulfur dioxide and toluene.

In the instrument the MOSFET sensors are divided into two arrays of five sensors each, one array operating at 140 °C and the other at 170 °C, while the MOS are kept at 400–500 °C during all the process phases. The different conditions of MOSFET and MOS sensors ensure the shift of the selectivity spectrum towards different volatile compounds. The response is characteristic for each sensor and depends on the concentration and the profile of the volatile compounds.

Two grams of each sample was introduced in 40 ml vials with a pierceable silicon/Teflon disk in the cap. The samples were randomly analysed. After headspace equilibration at room temperature for 30 min, the volatile compounds were sampled by an automatic syringe and were pumped over the sensor surfaces for 60 s. During this time the sensor responses were recorded. Then, sensors were exposed to filtered air at a constant flow rate (60 ml/min) in order to keep the gas sensor signal back to the baseline. Each measurement cycle includes an internal standard as reference for the calibration method. In fact, the Senstool software implements a calibration method, Multiplicative Drift Correction (MDC), for solving problems of sensor drift and ensuring repeatability and reproducibility of sensor responses. This is a simple method in which an internal standard is used in order to correct all the subsequent readings. MDC assumes that the drift is multiplicative and that the relationship between the response of the internal standard and the response of the measured sample is linear [26,27]. The ratio between the internal standard measurement and all the following calibration measurements is calculated for each sensor:

$$\mathrm{Rc}_t = \frac{R_t}{K_t}$$

where Rc_t is the sensor response after calibration in time t, R_t is the sensor response of the sample in time t and K_t is the sensor response of the internal standard in time t.

Each sample has been evaluated in duplicate and the average of the results has been used for subsequent statistical analysis.

2.6. Statistical analysis

The data obtained from the sensor array of the electronic nose were analysed by Principal Component Analysis (PCA) performed by The Unscramble software (v. 9.2, CAMO ASA, Oslo, Norway). PCA is a procedure that permits useful information to be extracted from the data, to explore the data structure, the relationship between objects and the global correlation of the variables [28]. Linear Discriminant Analysis (LDA) was applied for sample classification. It is one of the mostly used parametric classification procedures [29]. The method maximizes the variance between categories and minimizes the variance within categories. This method renders a number of orthogonal linear discriminant functions equal to the number of categories minus one. Correlation analysis on electronic nose sensor responses and GC–MS data as well as partial least square analysis was performed using the SCAN software (MINITAB Inc., State Collage, PA).

3. Results and discussion

Spray congealing led to the formation of spherical LCPUFA-enriched microparticles with an average particle size of 185 μm. Scanning electron micrographs show, that the process did not result in a true encapsulation of the LCPUFAs but rather in the formation of LCPUFA-enriched lipid microparticles as depicted in Fig. 1. Generally, when feeding a dispersion into the spray congealing process via ultrasonic nebulisation, the dispersed phase is encapsulated in the congealed lipid phase. Ultrasonic nebulisation leads to vibrational rotation of the atomized droplets. During congealing, due to the centrifugal force the dispersed phase (with a higher density than the molten continuous fat phase) is forced to the center of the particle and surrounded by the congealing continuous phase. In contrast, when spray congealing a mixture of fish oil and molten hydrogenated palm oil, this encapsulation process does not take place. Particles are solidified prior to a possible phase separation based on differences in oil fraction densities and solidification temperature. The Carr index of 0.17 reflects the good flowability [30] and thus superior handling properties compared to spray-dried microcapsules [2].

In Table 2 the development of the hydroperoxide content and conjugated dienes content of LCPUFA-enriched lipid microparticles with limited and sufficient air supply during storage at 20 °C up to 6 weeks is reported. When stored under limited air supply the content of conjugated dienes content and hydroperoxides initially increased and levelled off after 2 weeks of storage. Within the first 2 weeks, lipid oxidation was promoted by interstitial air inclusion. In contrast, with sufficient air supply a steady increase of the hydroperoxide content conjugated dienes content was observed.

The volatile compounds leaking from LCPUFA-enriched microparticles were collected by SPME technique and analysed by GC–MS. Fig. 2 illustrates the peak area of the main volatile compounds extracted from microparticles headspace during storage at 20 °C up to 6 weeks. Among several other components, propanal, 1-penten-3-one, hexanal, 1-penten-3-ol, 2,4-heptadienal and E,Z-2,6-nonadienal were identified as the quantitatively dominating volatile compounds in the samples. Propanal is generally known to be a quantitatively important volatile deriving from autoxida-

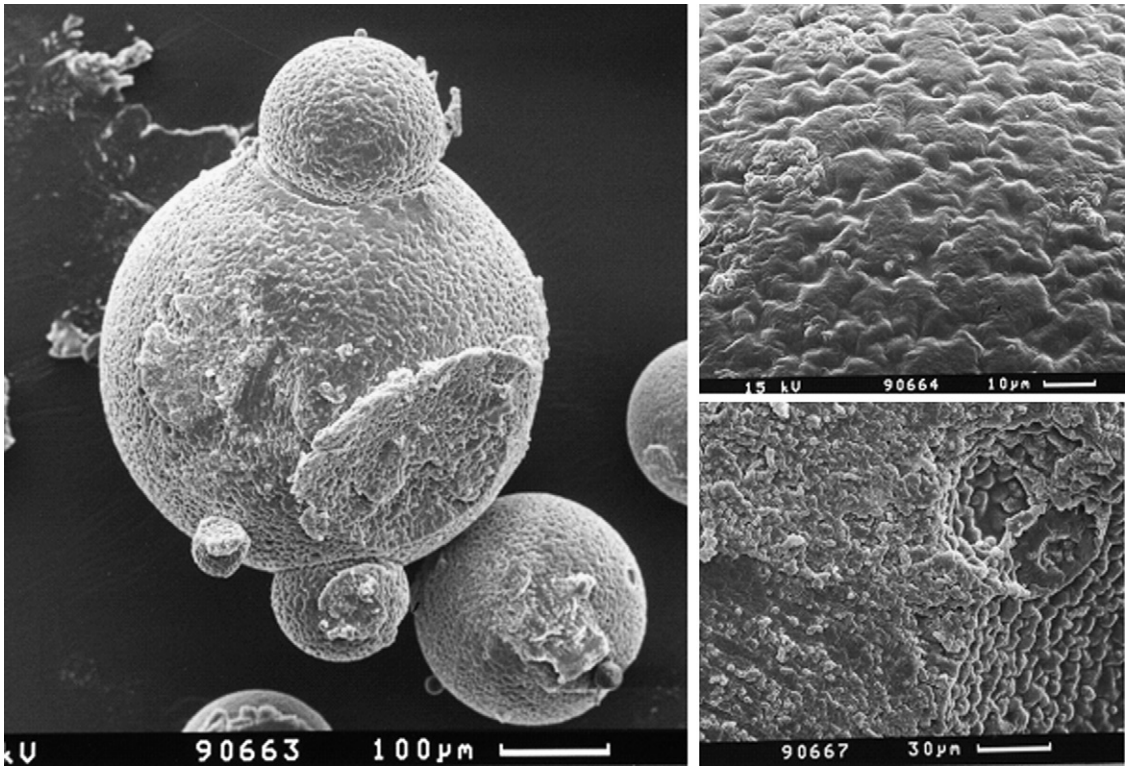

Fig. 1. Scanning electron micrograph of an LCPUFA-enriched lipid microparticle.

tion of omega-3 fatty acids [31]. 1-Penten-3-one, 1-penten-3-ol, 2,4-heptadienal and 2,6-nonadienal have been characterized as important odorants contributing to rancid-fishy off-flavour formation in fish oil and fish oil-enriched products [7,8,12,32]. In microencapsulated fish oil these compounds did not dominate the aroma profile and hexanal together with 2-nonenal and 2,4-decadienals have been suggested as quality indicators. However, in this study a PDMS/DVB fiber has been used, which is known to be less efficient in trapping certain volatiles like, e.g. propanal [11]. In the present study, the course of the formation when stored under limited or sufficient air supply differed for these six volatile compounds. Volatile secondary lipid oxidation products steadily increased over the storage period, but the pattern significantly differed depending on the two different storage conditions. Propanal, hexanal and E,Z-2,6-nonadienal content were higher in samples stored with sufficient air supply compared to the samples with limited air supply. In contrast, 1-penten-3-one and 1-penten-3-ol content were higher in samples stored with restricted air supply.

The sensor responses for MOS and MOSFET sensors were collected and elaborated by PCA performed in covariance matrix in order to provide partial visualization of the data set in a reduced dimension. The first two principal components represent 95.1% of the total variance (score plot not shown). The loading plot in Fig. 3 shows the relationship between variables and how much they influence the system. Only eight of the MOS sensors and none of the MOSFET sensors contributed to the discrimination of the samples on the first two principal components. The remaining sensors, plotted at the center, were not relevant for the discrimination.

When the PCA is only based on the MOS sensors, the first and second principal component represents 92.4% and 5.8% of the total variance, respectively. Examining the score plot a clear separation of the stored samples into two groups was found according to the different oxidative status (Fig. 4). LDA applied to the MOS sensor responses gave 100% correct classification for all samples (error rate 0%). Leave-one-out cross-validation error rate was 7.6% due to two samples not correctly classified. The relationship between the sensor responses and volatile compounds was evaluated taking into account the correlation coefficients calculated using only the MOS sensor responses. The correlation coefficients between each MOS sensor of the electronic nose and volatile compounds are listed in Table 3. Strong correlations are reported in bold and show that the MOS sensors discriminating the samples based on principal component 1 are well correlated with propanal, hexanal and E,Z-2,6-nonadienal. These are the volatiles, which strongly increase during storage with sufficient air supply. Using partial least square analysis a preliminary model was developed. The correlation coeffi-

Table 2
Development of the content of conjugated dienes and hydroperoxides in LCPUFA-enriched lipid microparticles during storage at 20 °C.

Day	Limited air supply		Sufficient air supply	
	Conjugated dienes (mmol/kg oil)	Hydroperoxide content (mmol/kg oil)	Conjugated dienes (mmol/kg oil)	Hydroperoxide content (mmol/kg oil)
0	14.2	2.5	14.2	1.7
7	15.4	13.3	15.3	17.2
14	18.1	28.8	18.2	29.2
21	18.4	27.1	20.2	37.9
28	17.5	25.4	21.9	52.1
35	17.6	26.3	22.3	56.9
42	16.8	20.1	23.3	76.5

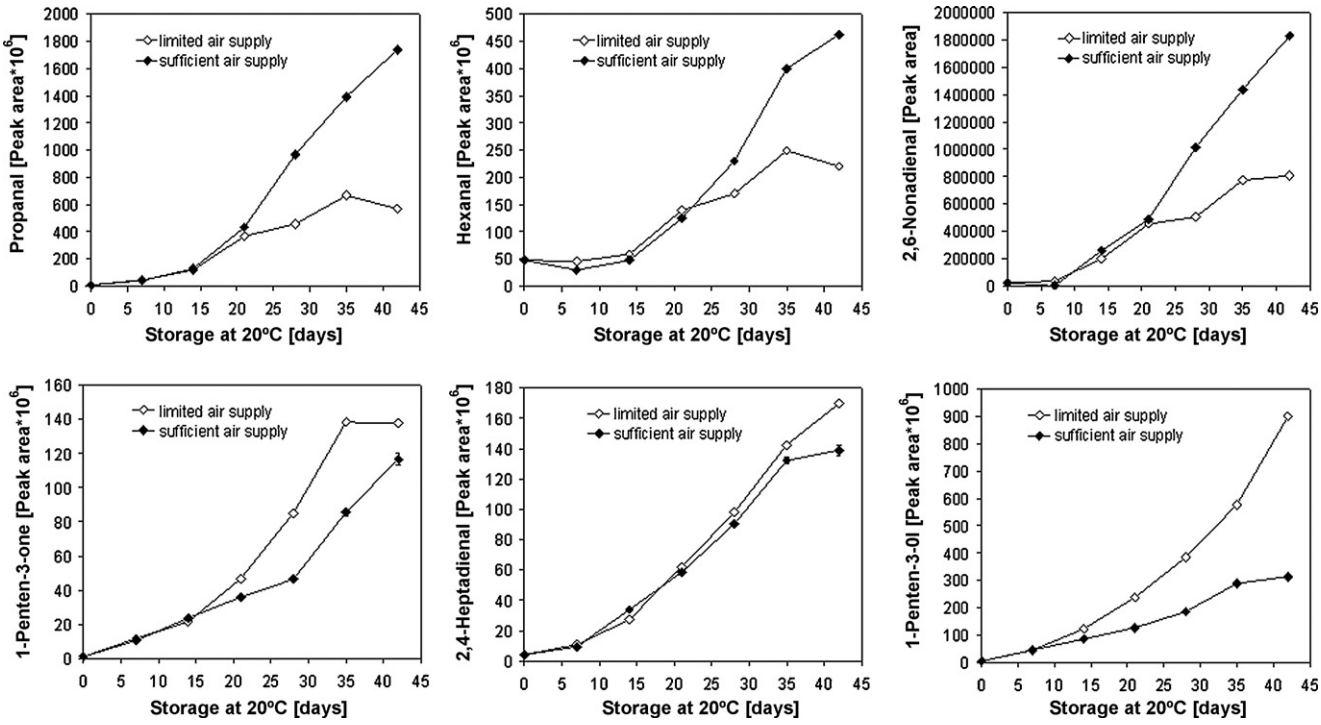

Fig. 2. Development of selected secondary volatile lipid oxidation products in LCPUFA-enriched microparticles during storage at 20 °C.

Table 3
Correlation coefficient matrix of the MOS sensor responses and selected volatile compounds detected by SPME-GC analysed during storage of LCPUFA-enriched lipid microparticles at 20 °C.

Sensor	Volatile compounds					
	Propanal	1-Penten-3-one	Hexanal	1-Penten-3-ol	2,4-Heptadienal	2,6-Nonadienal
MO101	**0.875**	0.470	**0.822**	0.217	0.585	**0.850**
MO102	**0.775**	0.487	**0.762**	0.264	0.569	**0.759**
MO104	**0.733**	0.335	**0.687**	0.098	0.433	**0.700**
MO110	0.527	0.014	0.468	−0.216	0.107	0.470
MO111	−0.273	−0.470	−0.270	−0.473	−0.464	−0.324
MO112	−0.166	−0.426	−0.178	−0.456	−0.399	−0.223
MO113	0.625	0.074	0.510	−0.079	0.263	0.581
MO114	**0.941**	0.540	**0.903**	0.271	0.657	**0.918**
MO115	0.083	0.309	0.147	0.267	0.240	0.082
MO116	**0.821**	0.641	**0.813**	0.434	0.719	**0.823**
MO117	**0.704**	0.253	**0.656**	0.009	0.351	**0.663**
MO118	**0.662**	0.197	**0.597**	−0.038	0.313	**0.618**

The highest absolute values are reported in bold.

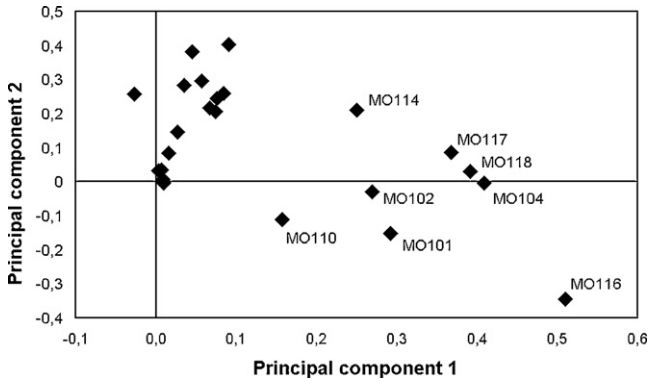

Fig. 3. Loading plot of the first two principal components for all sensor responses for LCPUFA-enriched lipid microparticles stored at 20 °C up to 6 weeks.

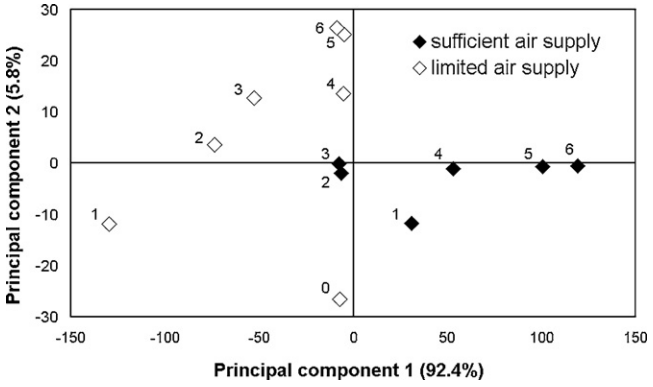

Fig. 4. Score plot of the first two principal components for selected MOS sensors for LCPUFA-enriched microparticles stored at 20 °C up to 6 weeks.

Table 4
Correlation coefficient matrix of the MOS sensor responses and selected volatile compounds detected by SPME-GC analysed during storage of bread mix at 20 °C.

Sensors	Volatile compounds				
	Propanal	1-Penten-3-one	Hexanal	1-Penten-3-ol	2,4-Heptadienal
MO101	0.804	0.719	0.988	0.665	0.680
MO102	0.800	0.703	0.971	0.650	0.667
MO104	0.771	0.674	0.970	0.617	0.634
MO110	0.729	0.626	0.971	0.566	0.582
MO111	0.572	0.465	0.865	0.396	0.420
MO112	0.611	0.503	0.923	0.434	0.453
MO113	0.742	0.661	0.990	0.602	0.615
MO114	0.771	0.680	0.989	0.623	0.637
MO115	0.640	0.577	0.792	0.536	0.546
MO116	0.858	0.767	0.959	0.721	0.739
MO117	0.731	0.628	0.972	0.568	0.584
MO118	0.772	0.675	0.973	0.619	0.636

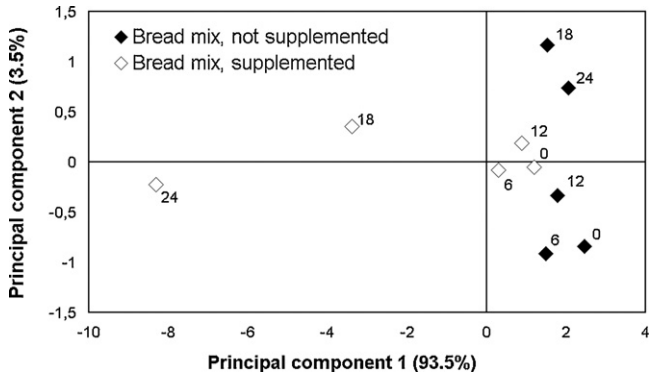

Fig. 5. Score plot of the first two principal components for selected MOS sensors for LCPUFA-enriched bread mix stored at 20 °C up to 24 weeks.

cient for the cross-validation was above $r = 0.8$ for all volatiles except for 1-penten-3-ol ($r = 0.66$).

Bread mix supplemented with the LCPUFA-enriched microparticles was analysed as an example for a LCPUFA supplemented food. Probably due to the lower content of fish oil in the supplemented food and thus a lower quantitative amount in the sample, 2,6-nonadienal could not be detected in the samples. A discrimination of the LCPUFA-supplemented bread mix after 12 weeks of storage from the non-supplemented bread mix could be achieved based on the first principal component, which accounts for 93.5% of the total variance (Fig. 5). The response of the selected eight MOS sensors correlated very clearly with the headspace content of hexanal and propanal as well as to a lower extent with 1-penten-3-ol, 1-penten-3-one and 2,4-heptadienal (Table 4). The strong correlation results from a high increase in lipid oxidation parameters in the last weeks of sample storage.

In summary, spray congealing resulted in the formation of LCPUFA-enriched microparticles with good handling properties. Since the process does not result in a true encapsulation, fast oxidation of the LCPUFAs occurs in the presence of oxygen, which limits their application to food systems, in which the food itself provides an additional oxygen barrier (e.g. cereal bars) or foods, which are packaged under protective atmosphere. Data from the present study indicate that the electronic nose can be used as a sensitive tool to evaluate the lipid oxidative status of LCPUFA-enriched microparticles. In supplemented foods like bread mix, matrix-related changes, which occur in supplemented and non-supplemented samples, make a clear distinction more difficult. Therefore, it has to be summarized that due to the low-aroma threshold of several compounds responsible for distinct notes during off-flavour formation, the electronic nose cannot replace traditional sensory evaluation. Nevertheless, since the MOS sensor response correlated with quantitative dominating volatiles, which have been associated with fishy and rancid off flavour, the electronic nose represents a useful tool for routine quality control.

References

[1] A. Bauch, O. Lindtner, G.B.M. Mensink, B. Niemann, Eur. J. Nutr. 60 (2006) 810–812.
[2] S. Drusch, Y. Serfert, K. Schwarz, Eur. J. Lip. Sci. Technol. 108 (2006) 501–512.
[3] Y. Serfert, S. Druusch, K. Schwarz, Food Chem 113 (2009) 1106–1112.
[4] W. Kolanowski, D. Jaworska, J. Weißbrodt, B. Kunz, J. Am. Oil Chem. Soc. 84 (2007).
[5] H. Lee, S.A. Kizito, S.J. Weese, M.C. Craig-Schmidt, Y. Lee, C.-I. Wei, H. An, J. Food Sci. 68 (2003).
[6] R. Jónsdóttir, M. Bragadóttir, G.Ö. Arnason, J. Food Sci. 70 (2005) C433–C440.
[7] C. Karahadian, R.C. Lindsay, J. Am. Oil Chem. Soc. 66 (1989) 953–960.
[8] G. Venkateshwarlu, M.B. Let, A.S. Meyer, C. Jacobsen, J. Agric. Food Chem. 52 (2004) 311–317.
[9] X.-Q. Pan, H. Ushio, T. Ohshima, Fish Sci. 71 (2005) 639–647.
[10] D. Jimenez-Alvarez, F. Giuffrida, P.A. Golay, C. Cotting, F. Destaillats, F. Dionisi, B. Keely, Eur. J. Lip. Sci. Technol. 110 (2008) 277–283.
[11] J. Iglesias, S. Lois, I. Medina, J. Chromatogr. A 1163 (2007) 277–287.
[12] G. Venkateshwarlu, M.B. Let, A.S. Meyer, C. Jacobsen, J. Agric. Food Chem. 52 (2004) 1635–1641.
[13] N. Macfarlane, J. Salt, R. Birkin, Int. News. Fats, Oils Relat. Mater. 12 (2001) 244–249.
[14] R.T. Marsili, in: R.T. Marsili (Ed.), Sensory-Directed Flavor Analysis, Taylor & Francis, Boca Raton, London, New York, pp. 1–22.
[15] W. Kolanowski, D. Jaworska, J. Weißbrodt, J. Sci. Food Agric. 87 (2007) 181–191.
[16] L.M. Reid, C.P. O'Donnel, G. Downey, Trends Food Sci. Technol. 17 (2006) 344–353.
[17] H.L. Gan, Y.B. CheMan, C.P. Tan, I. NorAini, S.A.H. Nazimah, Food Chem. 89 (2005) 507–518.
[18] Y.G. Martin, J.L.P. Pavon, B.M. Cardero, C.G. Pinto, Anal. Chim. Acta 384 (1999) 83–94.
[19] A. Guadarrama, M.L.R. Mendz, J.A. Saja, J.L. Ros, J.M. Olas, Sens. Actuat. B 69 (2000) 276–282.
[20] R. Baranauskiene, P.R. Venskutonis, A. Galdikas, D. Senuliené, A. Setkus, Food Chem. 92 (2005) 45–52.
[21] L. Rodrìguez, M. Cini, C. Cavallari, G. Motta, EP0726765, 1996.
[22] P. Horlacher, A. Sander, US2008/0075811, 2008.
[23] European Pharmacopeia, Schütt- und Stampfvolumen. 4.00/2.09.15.00, in (Ed.), Deutscher Apotherkerverlag, Stuttgart, pp. 254–255.
[24] H.W.S. Chan, G. Levett, Lipids 12 (1976) 99–104.
[25] International Dairy Federation, International IDF Standards, Square Vergot 41, Brussels, Belgium, 1991, sec. 74A:1991.
[26] J.E. Haugen, O. Tomic, K. Kvaal, Anal. Chim. Acta 407 (2000) 23–39.
[27] T. Artursson, T. Eklöv, I. Lundström, P. Martensson, M. Sjöström, M. Holmberg, J. Chemometr. 14 (2000) 711–723.
[28] J. Beebe, Chemometrics, A Practical Guide, John Wiley and Sons, New York NY, 1998.
[29] M. Meloun, J. Militky, M. Forina, Chemometrics for Analytical Chemistry, Horwood Publishing Ltd., New York, 1992.
[30] C. Turchiuli, M. Fuchs, M. Bohin, M.E. Cuvelier, C. Ordonnaud, M.N. Peyrat-Maillard, E. Dumoulin, Innov. Food Sci. Emerg. Technol. 6 (2005) 29–35.
[31] E.N. Frankel, Lipid Oxidation, The Oily Press, Bridgwater, England, 2005.
[32] K. Hartvigsen, P. Lund, L.F. Hansen, G. Holmer, J. Agric. Food Chem. 48 (2000) 4858–4867.

Talanta 78 (2009) 1464–1475

Contents lists available at ScienceDirect

Talanta

journal homepage: www.elsevier.com/locate/talanta

A comparison of the ion chemistry for mono-substituted toluenes and anilines by three methods of atmospheric pressure ionization with ion mobility spectrometry

H. Borsdorf[a,*], K. Neitsch[a], G.A. Eiceman[b], J.A. Stone[c]

[a] UFZ Helmholtz-Centre for Environmental Research, Department Monitoring and Exploration Technologies, Permoserstraße 15, D-04318 Leipzig, Germany
[b] New Mexico State University, Department of Chemistry and Biochemistry, Box 30001, Department 3C, Las Cruces, NM 88003-8001, USA
[c] Queen's University, Department of Chemistry, Kingston, Ontario, K7L 3N6, Canada

ARTICLE INFO

Article history:
Received 15 December 2008
Received in revised form 30 January 2009
Accepted 20 February 2009
Available online 5 March 2009

Keywords:
Ion mobility spectrometry
Atmospheric pressure ionization
Mass spectrometry
Isomeric compounds

ABSTRACT

Ion mobility spectra for a series of mono-substituted toluenes and a series of mono-substituted anilines were obtained using three different methods of atmospheric pressure ionization including photoionization, chemical ionization from a ^{63}Ni source, and chemical ionization from a corona discharge source. The product ion peak intensities were measured as functions of analyte concentration at 323 K in a purified air atmosphere. Two, and sometimes three, product ion peaks were observed in spectra from chemical ionization with the ^{63}Ni source and it is suggested that the major peak, due to the protonated molecule, arose in both series by proton transfer from $H_3O^+(H_2O)_n$. The second peak with diminished intensity and longer drift time than the protonated molecule can be seen with the toluenes and was understood to be the NO^+ adduct, formed from the reactant ion $NO^+(H_2O)_n$. Electron transfer from the anilines to the latter ion yields the molecular ions, identified by having the same reduced mobility coefficients as the molecular ions produced by photoionization. The structure of these product ions was determined by investigations using the coupling of ion mobility spectrometry with atmospheric pressure photoionization and mass spectrometry (APPI–IMS–MS). The relative abundances of both the NO^+ adducts with the toluenes and the molecular ions with the anilines are enhanced with a corona discharge source where relatively more $NO^+(H_2O)_n$ is produced than in a ^{63}Ni source. Ab initio calculations show that only the protonated anilines of all the product ions are significantly hydrated with 1 ppm_v of moisture in the supporting atmosphere of the ion mobility spectrometer.

1. Introduction

Ion mobility spectrometry (IMS) has been developed as an analytical technique for detecting and identifying volatile and semi-volatile organic compounds using fieldable and transportable devices operating at atmospheric pressure, often in a supporting atmosphere of purified air [1,2]. The IMS technique permits simple, rapid determinations of these compounds with applications in several categories including security [3], military [4], petrochemical [5], environmental analysis [6], diagnostics [7,8], process control [9] and air pollution control [10]. Ion mobility spectrometers can be used as individual units or coupled with separation techniques (GC [11] or HPLC [12]) for the analysis of complex mixtures or as a separation technique for mass spectrometry [13].

In an IMS measurement, the drift velocity is determined for an ion swarm, derived from a sample, in a weak electric field of a drift tube at atmospheric pressure. Since the measurement is made on ions, the formation of ions from neutral sample molecules is a first and controlling event in the method and the ionization of sample also occurs in air at ambient pressure. The common method for ionization in conventional IMS analyzer is through chemical reactions between sample and reactant ions arising from the emission of electrons from radioactive ^{63}Ni or a corona discharge (CD) into a supporting atmosphere. Another method of forming ions is photoionization (PI) with a gaseous discharge lamp. Regardless of reaction pathways, reactant and product ions are extracted from the source region and injected via an electronic ion shutter into a drift region moving toward a detector down a uniform voltage gradient. The speed of ion swarms for each type of ion, termed the drift velocity, v_d, is proportional to the strength of the electric field, E, the constant of proportionality being the ion mobility, K.

The value of K is dependent on mass and charge of an ion and on the collision cross-section, which is described by structural parameters (physical size and shape) and the electronic factors defining ion-neutral interaction forces. Therefore, ions with different mass and/or structure attain different drift velocities, providing a basis

* Corresponding author. Tel.: +49 3412351457; fax: +49 3412351443.
E-mail address: helko.borsdorf@ufz.de (H. Borsdorf).

0039-9140/$ – see front matter © 2009 Elsevier B.V. All rights reserved.
doi:10.1016/j.talanta.2009.02.043

for the separation of ions in IMS analyzers [14]. Both parameters are the major variables influencing the ion mobilities when parameters of drift gas, drift gas density, gas flows, humidity of drift gas and temperature are kept constant [15,16]. The influence of all these parameters on ion mobility can be described with the Mason–Schamp equation [17,18]. Mobility coefficients measured are commonly converted to reduced mobilities, K_o, in which temperature and pressure of the gas atmosphere is corrected to 273 K and 760 Torr (mm Hg).

While such corrections for temperature and pressure may normalize the physics of ion motion in a gas, there is another aspect to ion behavior which is the association of a bare positive ion, either transiently or permanently, with polar or polarizable neutrals in the drift gas. Such associations lead to increases in ion mass and in collision cross-section, though the stability of such cluster ions is dependent upon temperature and pressure. Nonetheless, water molecules that are always present in the gas atmosphere or drift gas to a greater or lesser extent will hydrate most ions particularly those with a proton core. The extent of this hydration, described by an equilibrium equation (Eq. (1)), depends on the ion structure, the moisture content of the drift gas, and temperature:

$$M^+ + nH_2O \leftrightarrows M^+(H_2O)_n \quad (1)$$

The association of water with an ion is mainly an electrostatic interaction. A more delocalized charge can cause a less degree of hydration and hence the drifting ion has a lower effective mass. Thus, Ω_D may also be dependent on the degree of charge delocalization. A relatively large ion with delocalized charge would exhibit a lower Ω_D and hence higher mobility than if the charge were localized.

Karpas has suggested that the effects of charge delocalization and structure can be seen in enhanced mobilities of cyclized protonated α,ω-diamines over those for protonated aliphatic and cyclic amines of similar mass [19]. In a further study, Karpas et al. observed two product ion peaks in the ion mobility spectra of aniline and several mono- and di-substituted anilines in air [20]. Each peak was determined using an IMS/MS (mass spectrometer) instrument as a protonated monomer with differing sites of protonation. The more mobile ion was believed to be protonated on the aromatic ring with considerable charge delocalization and diminished ion-neutral interaction with the drift gas. The second peak was thought to be protonated on the amine with high localization of charge. Consequently, enhanced interactions between the N-protonated ions could account for a greater drift time and lesser mobility than the ring-protonated ion. The quoted ratio of the intensities of the two peaks varied over more than two orders of magnitude, from 0.05 for 2-chloroaniline to 7.0 for 3,5-dimethylaniline, implying a large variation of the ring to N protonation ratio, dependent on the number, type and position of substituents.

Unlike the two product ions seen for these chemicals by Karpas et al. only a single peak was reported by Kolaitis and Lubman, who used a similar instrument equipped for both ^{63}Ni and 2-photon (λ = 266 nm) laser ionization [21]. The mobility of the product ions for each compound was independent of ionization method suggesting a common structure or identity. Expectedly, the mass spectra for many of the compounds showed molecular ion and the protonated molecule. In particular, these two ions were of almost equal intensity with aniline. It is to be noted that the mass spectrum of the air drift gas with ^{63}Ni ionization contained many more ions with NH_4^+ as the core ion than with H_3O^+. This is an unusual occurrence since, in the reactant ion spectrum, the intensity of $H_3O^+(H_2O)_n$ is usually much greater than that of $NH_4^+(H_2O)_n$. Neither Karpas nor Lubman stated the concentrations of the analytes, although from the absence of reactant ions in many of the mass spectra, Lubman appears to have saturation levels. Since vapor concentrations may influence the appearance of a mobility spectrum through cluster reactions, knowledge of these values and the effect on spectra over a range of concentrations are considered today as a necessary practice.

In this paper, the site of protonation in aniline is compared using mobility spectra with two series of compounds, mono-substituted toluenes and mono-substituted anilines. The toluenes have only the aromatic ring as the potential protonation site whereas the anilines have both the ring and the nitrogen. Since toluene and aniline differ in mass by only 1 Da, mass effects may be minimized by comparing spectra of analytes from the two series with the same substituent. Structural differences, though masses are comparable, should lead to different degrees of association with neutrals of the drift gas and this should be seen in drift velocities.

The nature of product ions formed from these compounds was investigated by comparing the ion mobility spectra obtained using three different ionization techniques. APPI–IMS–MS investigations were additionally performed for determining the structure of product ions formed. For the identification of possible interactions between product ions and neutrals, optimized structures and energies were determined using ab initio calculations. Furthermore, we calculated the enthalpies of reaction for different possible gas phase reactions.

The temperature of these studies was limited by the commercial analyzer to 323 K, well below the ~473 K used by both Karpas and Lubman. However, concentrations were controlled over a range appropriate for each ion source [22].

2. Experimental

2.1. Ion mobility measurements

Chemicals were obtained in 99% or better purity from Sigma–Aldrich (Taufkirchen, Germany), and Merck (Darmstadt, Germany). Three hundred microliter of neat sample was sealed in polyethylene permeation tubes which were positioned in a temperature-controlled glass column. Ambient air, scrubbed over charcoal and silica gel, was passed through the glass column, split, and diluted using scrubbed air to provide a range of concentrations. The moisture content of the gas streams was measured by a moisture sensor AMX1 (Panametrics, Waltham, USA) as 2.0% relative humidity (−25 °C dew point ±3 °C). A portion of flow was introduced into the ion mobility spectrometer where additional dilution occurred in the recirculated internal flow of 25 L h^{-1}. The details of the sample introduction system used for the mobility spectrometer have been described previously [23].

The mobility spectrometers were RAID 1 (Bruker, Leipzig, Germany) hand-held analyzers operating in the positive ion mode. Each of three RAID analyzers was fitted with a different ion source including a 15 mCi ^{63}Ni foil, a krypton lamp providing 10 and 10.6 eV photons, and a corona discharge. All experimental parameters, apart from ion source conditions were kept constant to ensure identical ion gating (300 μs), drift and detection, independent of the ion source. The spectrometers work with a bidirectional flow system. Spectra were obtained with the following conditions: carrier gas and drift gas: air; temperature of inlet system: 353 K; carrier gas flow rate: 25 L h^{-1}; drift gas flow rate: 25 L h^{-1}; temperature of drift tube: 323 K; and pressure: ambient ranging from 740 to 750 mm Hg. The reduced mobility values (K_o values) were calculated from drift tube parameters (length of drift tube: 5.8 cm; electric field 245 V cm^{-1}). The drift times and the reduced mobility values were controlled by measuring acetone (1.84 cm^2 V^{-1} s^{-1}) and di-iso-propylmethylphosphonate (1.53 and 1.05 cm^2 V^{-1} s^{-1}).

Each instrument was equipped with a methyl silicone membrane which discriminates against polar compounds, in particular

water, and the water concentration in the source atmosphere was equal to or less than 1 ppm_v [24]. An unwelcome consequence of the membrane inlet is that vapor sample concentrations in the source are known only at a semi-quantitative level.

2.2. Mass spectrometry

The PI mass spectra of selected isomers were examined using a mobility spectrometer coupled to a mass spectrometer. A drift tube composed of alternating stainless steel and Teflon rings was attached to a triple quadrupole mass spectrometer (API 111, PE-SCIEX, Toronto, Canada) as previously described [25]. In the IMS/MS experiments, the ion shutter was kept open to improve ion intensity in the mass spectrometer and minimize time for signal averaging. Nonetheless, the residence time for all ions in the drift tube was comparable to independent IMS measurements.

2.3. Theoretical calculations

The Connolly surfaces and volumes of the molecules were calculated on the basis of optimized molecular geometries with the CERIUS^2 software suite (Accelrys Inc., San Diego, USA). Geometry optimization was performed using the semi-empirical AM1 method integrated into the SPARTAN 5.0 suite (Wavefunction Inc., Irvine, USA).

Optimized structures and energies were calculated by the density functional three parameter hybrid model (DFT/B3LYP) with the 6-311+G(dp) basis set from the Gaussian 03W package [26].

3. Results

The analytes used in these experiments and associated physicochemical properties are shown in Table 1 and are noteworthy for the much lower ionization energies and much higher proton affinities of the anilines versus analogous toluenes. Apart from the methyanilines, the photon energies from the krypton lamp are expected to yield the molecular ions since all appearance energies for dissociative ionization are above 10.6 eV.

We investigated all compounds using ion mobility spectrometry with the different ionization techniques (PI, ^{63}Ni and CD ionization). Different degrees of association can be concluded from the comparison of reduced mobility values. While PI mainly provides molecular ions for the compounds investigated, ^{63}Ni ionization and CD ionization often form product ions which result from different interactions between polar or polarizable neutrals of the drift gas and product ions and subsequently from the formation of clustered product ions. These ions show a significant shift of reduced mobility values in comparison to those obtained for PI. Depending on the concentration, differences in the relative abundance of clustered ions formed indicate a different nature of these product ions due to differences in the composition of reactant ions formed by ^{63}Ni ionization and CD ionization.

Typical mobility spectra for the substituted toluenes, here the chlorotoluenes, obtained by the three methods of ionization, are shown in Fig. 1a. The actual sample concentration in the ion source when each spectrum was obtained is not known precisely since the samples entered the ion source via a permeable membrane and

Table 1
Physicochemical properties of compounds investigated.

	m/z	IE (eV)[a]	AE (eV)[b]	PA (kJ mol^{-1})[c]	Surface (Å^2)	Volume (Å^3)
Toluenes						
2-Methyltoluene	106	8.56	11.4 (–CH_3)	796.0	149.3	125.5
3-Methyltoluene	106	8.55	11.5 (–CH_3)	812.1	143.0	120.7
4-Methyltoluene	106	8.44	11.4 (–CH_3)	794.4	148.4	123.5
2-Ethyltoluene	120	n.a.	n.a.	n.a.	159.0	139.3
3-Ethyltoluene	120	n.a.	n.a.	n.a.	165.5	141.8
4-Ethyltoluene	120	n.a.	n.a.	n.a.	163.5	140.5
2-Chlorotoluene	126	8.72	11.5 (–Cl)	790.5	142.1	120.5
3-Chlorotoluene	126	8.76	11.4 (–Cl)	783.5	143.6	120.0
4-Chlorotoluene	126	8.69	11.4 (–Cl)	762.9	142.6	118.7
2-Fluorotoluene	110	8.91	12.3 (–H)	773.3	132.9	110.2
3-Fluorotoluene	110	8.91	11.9 (–H)	785.4	135.9	111.9
4-Fluorotoluene	110	8.79	11.9 (–H)	763.8	133.4	109.9
2-Bromotoluene	170	8.56	11.2 (–Br)	775.3	146.1	125.1
3-Bromotoluene	170	8.73	11.3 (–Br)	782.0	146.8	124.2
4-Bromotoluene	170	8.68	11.3 (–Br)	775.3	146.2	122.8
Anilines						
2-Methylaniline	107	7.47	10.5 ($C_6H_6^+$)	890.9	136.9	115.8
3-Methylaniline	107	7.54	n.a.	895.8	139.8	116.4
4-Methylaniline	107	7.61	10.8 ($C_7H_8N^+$)	896.7	143.9	118.9
2-Ethylaniline	121	7.60	n.a.	n.a.	152.0	133.0
3-Ethylaniline	121	n.a.	n.a.	897.9	156.3	135.0
4-Ethylaniline	121	7.60	n.a.	n.a.	161.7	138.1
2-Chloroaniline	127	8.20	13.1 (-Cl)	n.a.	133.4	112.2
3-Chloroaniline	127	8.10	12.3 (-Cl)	868.1	136.8	114.3
4-Chloroaniline	127	7.99	12.3 (-Cl)	873.8	138.9	115.0
2-Fluoroaniline	111	8.29	n.a.	n.a.	128.2	105.4
3-Fluoroaniline	111	8.32	n.a.	867.3	129.1	105.8
4-Fluoroaniline	111	8.09	n.a.	871.5	129.0	105.4

[a] IE: ionization energy.
[b] AE: appearance energy of fragment ions.
[c] PA: proton affinity (all values obtained from: http://webbook.nist.gov/); n.a.: not available. Surfaces and volumes of molecules were calculated using CERIUS^2 software.

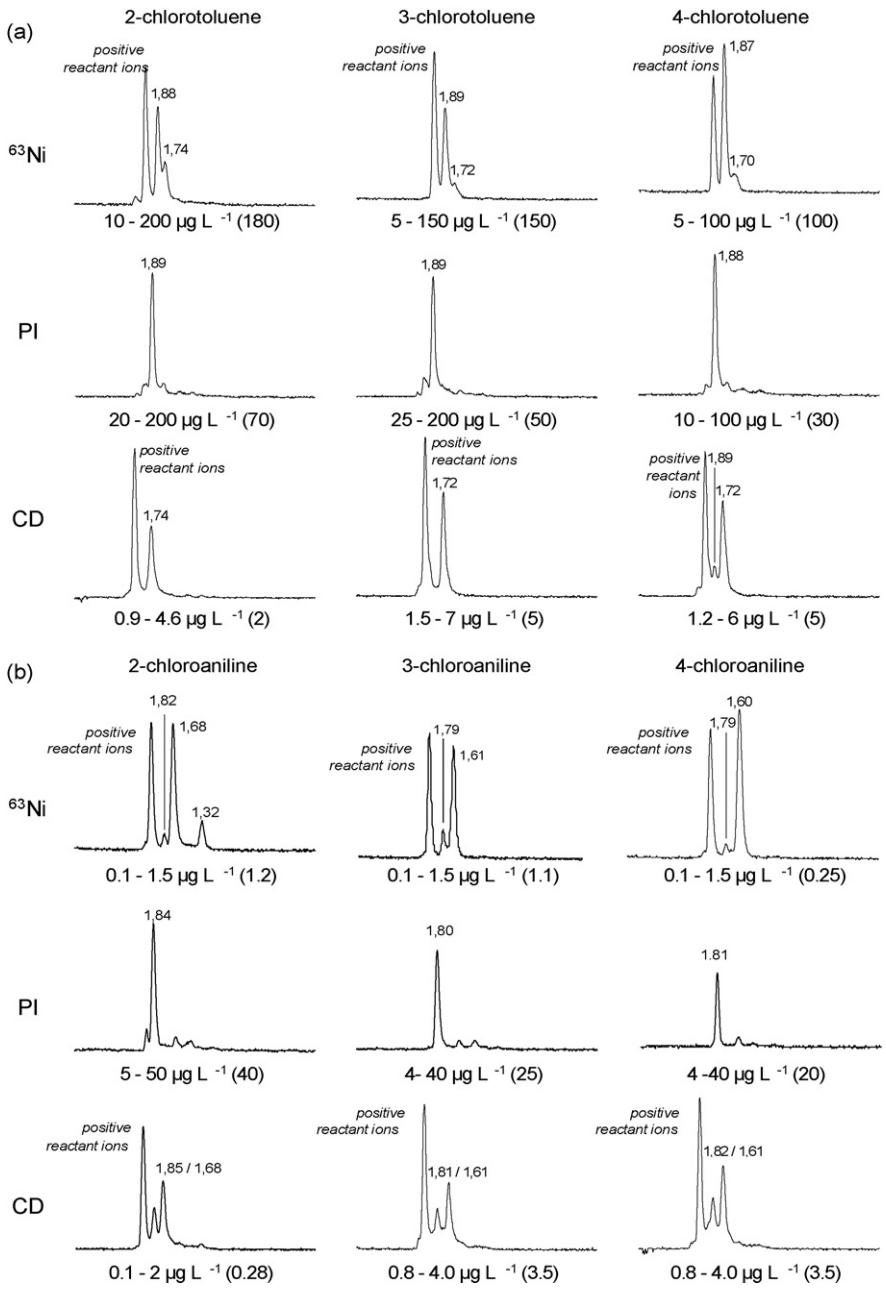

Fig. 1. Positive ion mobility spectra of the structural isomers of chlorotoluenes (a) and chloroaniline (b) with three ion sources, as labeled. The product ion peaks are shown with each value for the reduced mobility coefficient ($cm^2\ V^{-1}\ s^{-1}$).

the rate of diffusion through the membrane will be different and unknown for individual substances. However, concentration ranges in the sample flow are known and may be expected to be reproducible between measurements for a chemical on each analyzer. For ^{63}Ni and CD, the lower bound of concentration in sample flow (shown below each spectrum), is for the first appearance of product ion peak and the upper bound is when roughly 80% of the reactant ion was depleted. For PI, the upper bound is the value for intensity of a peak similar to those obtained by the other two ionization techniques. The concentration ranges employed for CD ionization are twenty times lower than for the other two ionization techniques, showing it to be the more sensitive method of analysis.

Photoionization, as expected and shown in Fig. 1, yielded one major peak and a few minor peaks for each analyte. The major peaks were identified by mass with an APPI (atmospheric pressure photoionization)–IMS–MS instrument as the molecular ion. The results of these measurements are summarized in the last column of Table 2 and are shown in Fig. 2 for selected substances. The peak for each chlorotoluene isomer is annotated with the K_o value and the values are identical for the isomers.

Each spectrum from a ^{63}Ni source shows a reactant ion peak (RIP, ~2.09 $cm^2\ V^{-1}\ s^{-1}$) and two product ion peaks with K_o values below that of the RIP. A convenient nomenclature for reduced mobility coefficiencies for the product ions are K_{on}, where $n = 1$ or 2, in order of decreasing reduced mobility. For example, the first peak for 2-chlorotoluene is K_{o1} (1.88 $cm^2\ V^{-1}\ s^{-1}$) and the second peak is K_{o2} (1.74 $cm^2\ V^{-1}\ s^{-1}$). For some spectra, there is a third product ion peak will be termed K_{o3}. The K_{o1} values for chlorotoluenes with the radioactive source were essentially identical to the single peak observed in spectra from photoionization. The values for K_{o2}, in the spectra with a radioactive source were degraded in precision due to low abundances and low resolution. Consequently, values

Table 2
Results of ion mobility measurements and mass spectrometric investigations of positive product ions formed in air at ambient pressure with three ion sources.

	Reduced mobility values ($cm^2\ V^{-1}\ s^{-1}$) obtained by			PI-IMS-MS data
	Photoionization	^{63}Ni ionization	Corona discharge	m/z; (): relative intensity of most intense peaks in mass spectra (%)
Toluenes				
2-Methyltoluene	1.93	**1.88**; 1.77 (S)	2.00; 1.79	95 (38), **106** (**100**), 109 (40), 119 (18), 122 (70)
3-Methyltoluene	1.93	**1.88**; 1.75 (S)	1.99; 1.78	
4-Methyltoluene	1.94	**1.89**; 1.76 (S)	2.01; 1.78	
2-Ethyltoluene	1.82	**1.78**; 1.69 (S)	1.80; **1.70**	95 (38), 109 (38), **120** (**100**), 123 (42), 127 (6), 133 (32), 136 (13)
3-Ethyltoluene	1.82	**1.77**; 1.68 (S)	1,80; **1.69**	
4-Ethyltoluene	1.82; 1.66; **1.19**	1.78; **1.69**; 1.19	1.80; **1.69**	
2-Fluorotoluene	1.97	**1.97**; 1.79	1.78	95 (14), **110** (**100**), 113 (17), 117 (20), 124 (19), 126 (64), 143 (10)
3-Fluorotoluene	1.97	**1.98**; 1.78	1.78	
4-Fluorotoluene	1.97	**1.98**; 1.78	1.77	
2-Chlorotoluene	1.89	**1.88**; 1.74 (S)	1.74	95 (6), 106 (4), 126 (100), 128 (35), 142 (35)
3-Chlorotoluene	1.89	**1.89**; 1.72 (S)	1.72	
4-Chlorotoluene	1.88	**1.87**; 1.70–1.66 (S)	1.89; 1.72; 1.66	
2-Bomotoluene	1.82	**1.80**; 1.67 (S)	1.68	99 (5), 107 (5), 122 (100), 126 (7), 135 (13), 170 (60), 172 (63), 186 (8), 188 (8)
3-Bromotoluene	1.81	**1.79**; 1.65 (S)	1.66	
4-Bromotoluene	1.81	**1.79**	1.80	
Anilines				
2-Methylaniline	**1.89**; 1.33	1.87; **1.72**; 1.35	1.90; 1.71	**107** (**100**), 125 (16)
3-Methylaniline	**1.88**; 1.31	1.87; **1.71**	1.89; 1.69	
4-Methylaniline	**1.89**; 1.31	1.88; **1.70**; **1.31**	1.89; 1.69	
2-Ethylaniline	**1.79**; 1.25	1.78; **1.64**; 1.27	1.80; 1.63	**121** (**100**), 124 (5), 133 (7), 139 (26)
3-Ethylaniline	**1.77**; 1.21	1.76; **1.60**; 1.23	1.89; 1.78; 1.60	
4-Ethylaniline	**1.77**; 1.21	1.76; **1.59**; 1.21	1.88; 1.79; 1.59	
2-Fluoroaniline	1.91	1.91; **1.72**	1.92; 1.72	**111** (**100**), 127 (9), 129 (79), 145 (3), 147 (3)
3-Fluoroaniline	1.89	1.88; **1.69**	1.89; 1.68	
4-Fluoroaniline	1.89	1.89; **1.69**	1.90; 1.68	
2-Chloroaniline	1.84	1.82; **1.68**; 1.32	1.85; 1.68	93 (18), 111 (10), **127** (**100**), 129 (29), 145 (24), 147 (9)
3-Chloroaniline	1.80	1.79; **1.61**	1.81; 1.61	
4-Chloroaniline	1.81	1.79; **1.60**	1.82; 1.61	

Peaks in ion mobility spectra detectable as shoulder of major peak [S], bold print: major peak.

for K_{o2}, for the chlorotoluenes were regarded as identical for the three isomers.

Spectra for the 2- and 3-chlorotoluenes with the corona discharge source showed only one significant peak, or product ion. When reduced mobilities are compared to those from the ^{63}Ni source, close or identical matches are possible with the K_{o2} peak ($1.74–1.70\ cm^2\ V^{-1}\ s^{-1}$). A minor amount of the K_{o1} peak was observed for 4-chlorotoluene; however, intensity for the K_{o2} peak was far the more intense, consistent with other CD-based mobility spectra.

The mobility spectra for chloroaniline isomers, analogs to the chlorotoluenes, are shown in Fig. 1b in scale and structure as that in Fig. 1a for chlorotoluenes. A single intense product ion was observed in spectra from a PI source and these have almost the same value for each isomer, the 2-isomer having a slightly greater K_o than the others. These matched the K_{o1} values for product ions from the ^{63}Ni source except that the K_{o2} peak has a higher intensity than the K_{o1} peak, in strong contrast to the chlorotoluenes. Additionally, 2-chloroaniline is the only isomer exhibiting a K_{o3} peak. Peaks for K_{o1} and K_{o2} were observed in with the CD source and matched those found in the ^{63}Ni source; however, intensity for K_{o1} is greater than before, though still not equal to that for K_{o2}.

Noteworthy in these findings is the difference in concentrations required for response for the chloroanilines using chemical ionization with the ^{63}Ni source. The response was about a factor of 200 smaller than that for the chlorotoluenes. A smaller difference existed between the chemicals with the CD source, though chloroanilines were again favored with response. Only a slight difference existed with the PI source, again favoring chloroanilines. Since membrane yields are reproducible and all parameters were kept stable, these differences in response were understood to be associated with mechanism of ion formation alone and were reliable measures of relative quantitative response.

Reduced mobilities for all ion peaks with each source obtained with all the mono-substituted toluenes and the mono-substituted anilines are summarized in Table 2 where peaks in all the spectra match the description given above for the two types of ions. In addition to the K_{o1} and K_{o2} peaks seen in the spectra from the ^{63}Ni source with the chloroanilines, most of the methyl- and ethyl-anilines exhibited a K_{o3} peak, as does 2-chloroaniline, with a significantly lower reduced mobility coefficient. In addition, ions observed in the APPI–IMS–MS experiments are shown in the last column where the major ion observed for each compound was the molecular ion (M^+.) except for 2-bromotoluene where the molecular ion was intense but not the most intense ion.

As known from the literature [25], molecular ions are comparatively stable during the transition from the ambient pressure region of ion mobility spectrometer to the high vacuum of the mass spectrometer. Therefore, we performed these mass spectrometric investigations using PI. In contrast, CD and ^{63}Ni often form clustered product ions which may be collisionally decomposed in the interface region. Therefore, the ions in the mass spectra obtained using CD ionization and ^{63}Ni ionization may be different to those that would be obtained under IMS conditions.

As noted above, concentration in the ion source is unknown though concentrations presented to the membrane were controlled and reproducible. A second aspect to a mobility spectrum is how the peak heights change in absolute and relative abundances with changes in sample vapor concentrations. Representative response curves are shown in Figs. 3–6. In Fig. 3, plots are given from a ^{63}Ni

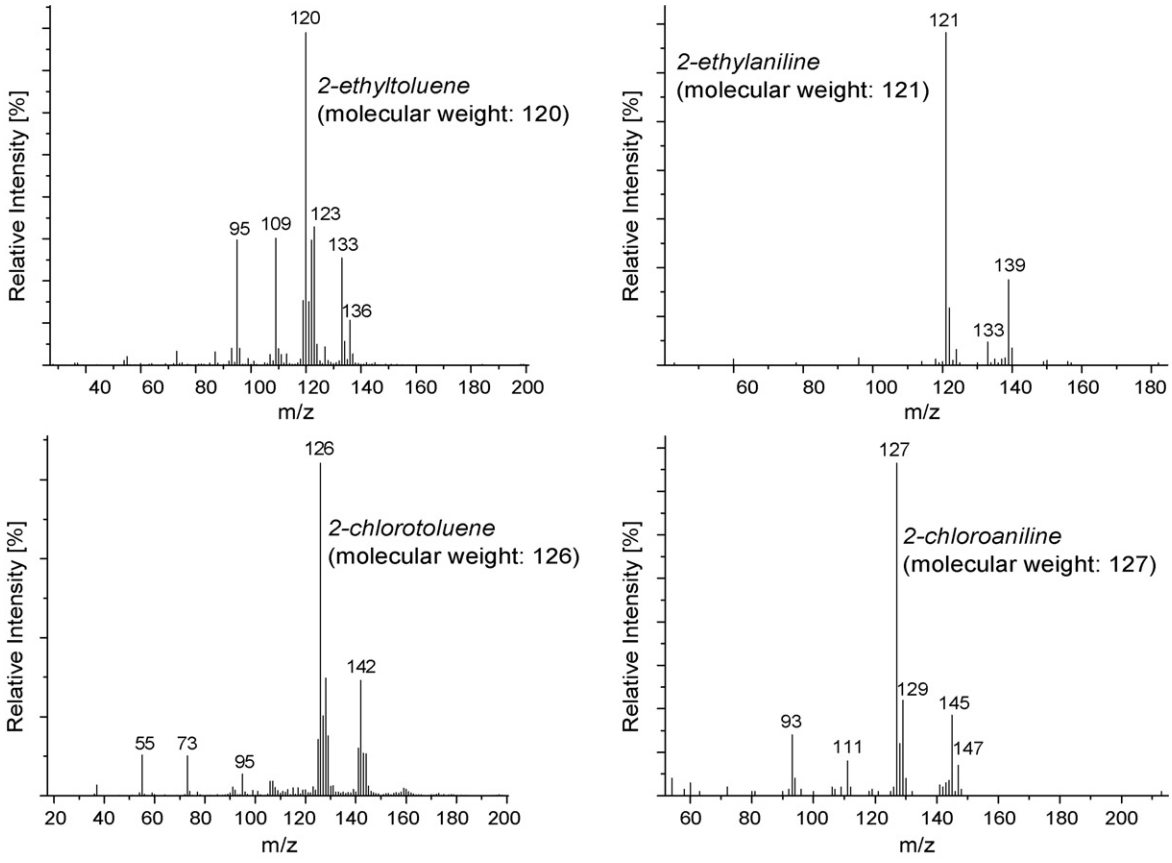

Fig. 2. Mass spectra obtained using APPI–IMS–MS.

source for 2-methyltoluene (Fig. 3a) and 2-chlorotoluene (Fig. 3b) respectively, while ionization for 2-methylaniline, 2-chloroaniline, and aniline are shown in Figs. 4–6, respectively from both ^{63}Ni and CD sources. There is an elevated baseline in all the spectra that is not subtracted in presenting the data in Figs. 3–6. The same number of scans was accumulated to obtain the peak intensities for each concentration and the contribution of the baseline to the peak intensity shown is then constant. The baseline levels are approximately 42 pA for ^{63}Ni and 37 pA for CD.

4. Discussion

Photoionization with the discharge lamp containing Krypton produce, for almost all the samples, only the molecular ion. However, ions of low intensity can be seen in the mobility spectra with a PI source and the more intense ions, other than the molecular ions, observed by mass spectrometry must be due to the further reaction of the molecular ions. Complex chemistry has been observed in the reactions of the benzene cation with air molecules [27] and can account, in part, for the complex mass spectra shown in Table 2. However, the single large peak in each mobility spectrum from photoionization in the RAID analyzer, obtained under drier and more controlled conditions than those used in the APPI–IMS–MS experiment, is due to the molecular ion.

The three reactant ions in the mobility spectrum obtained through chemical ionization with ^{63}Ni source are the hydrated forms of NH_4^+, NO^+, and H_3O^+, i.e. $NH_4^+(H_2O)_n$, $NO^+(H_2O)_n$, and $H_3O^+(H_2O)_n$ [28]. The ion mobility spectrometers used in this study cannot resolve these reactant ions, which therefore appear as a single peak in each spectrum of Fig. 1. The reactant ions are in equilibrium with water vapor in the instrument, so n represents a range of values for each ion that is also different for each ion. The distributions of the various hydrates, shown in Table 3, can be calculated from the temperature of the supporting atmosphere in the mobility spectrometer, 333 K, and 1 ppm_v of water vapor and using known enthalpies and entropies of hydration. The procedure for calculation of hydrate distributions is given in Ref. [29]. The concentration of $H_3O^+(H_2O)_n$ and the other species was calculated using the equilibrium constants for each addition of water molecules which is given by $\Delta G^0 = -RT\ln K$ and $\Delta G^0 = \Delta H^0 - T\Delta S^0$. The thermodynamic data for NH_4^+ and H_3O^+ are, as all values used in this paper unless otherwise stated, from the Chemistry Webbook (http://webbook.nist.gov/) and those for NO^+ are from Kebarle and co-workers [30]. One or more of these reactant ions is responsible for the formation, through ion–molecule reactions, of the product ions that constitute the mobility spectra. Table 3 shows $NH_4^+(H_2O)$, $NO^+(H_2O)$ and $H_3O^+(H_2O)_2$ to be the predominant forms of the reactant ions under the experimental conditions.

Ammonia has a proton affinity of 853.6 kJ mol^{-1}, much higher than those of the substituted toluenes listed in Table 1, so that proton transfer from $NH_4^+(H_2O)_n$ to these compounds is highly unlikely. Water has a much lower proton affinity (691 kJ mol^{-1}) than the toluenes but the effective proton affinities of the hydrated

Table 3
Degree of hydration of reactant ions at 333 K and 1.0 ppm_v of water.

n	$NH_4^+(H_2O)_n$[a]	$NO^+(H_2O)_n$[b]	$H_3O^+(H_2O)_n$[a]
0	0.02	0.03	3×10^{-10}
1	0.93	0.81	0.03
2	0.05	0.17	0.93
3	9×10^{-5}	6×10^{-4}	0.04
4	6×10^{-9}		3×10^{-5}

[a] Thermodynamic data from Ref. http://webbook.nist.gov/.
[b] Thermodynamic data from Ref. [30].

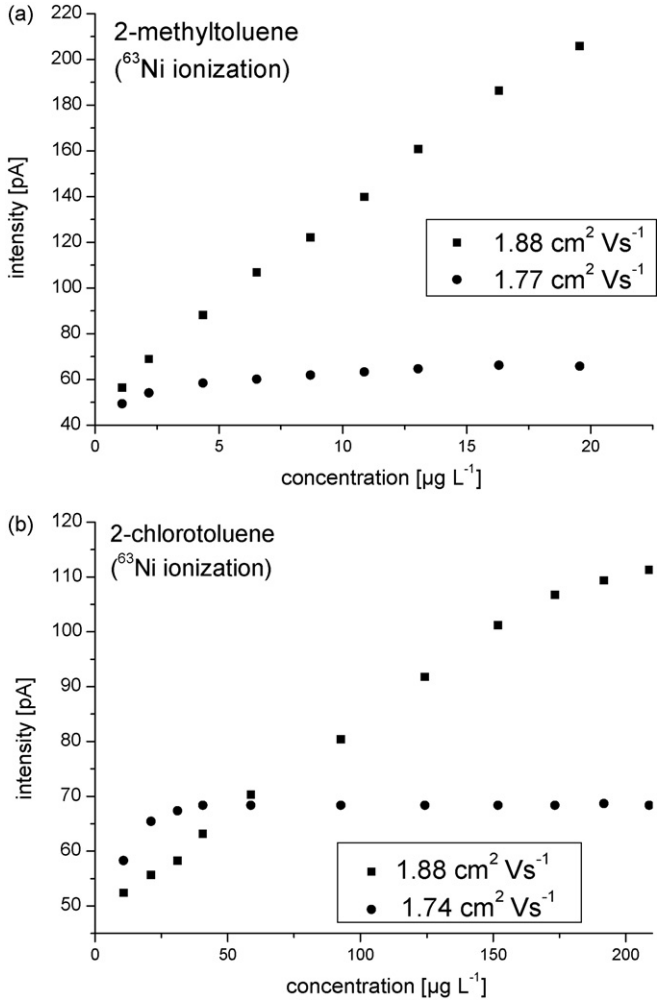

Fig. 3. Intensities of peaks for product ions versus concentration of 2-methyltoluene (a) and 2-chlorotoluene (b) from chemical ionization with a ^{63}Ni source in air at ambient pressure.

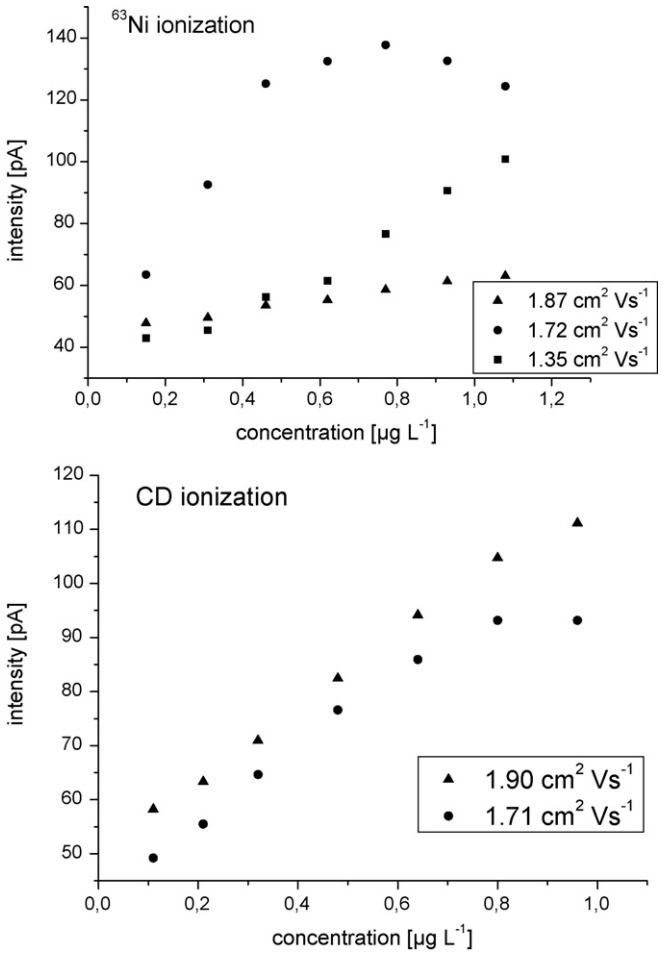

Fig. 4. Intensities of peaks for product ions versus concentration of 2-methylaniline formed by chemical ionization with a ^{63}Ni source and corona discharge source in air at ambient pressure.

forms are much higher. The value for each hydrate may be calculated by the addition of the appropriate enthalpies of association of the water molecules. The effective proton affinities for $H_3O^+(H_2O)_n$ are—$n=1$: 827 kJ mol^{-1}; $n=2$: 911 kJ mol^{-1}; $n=3$: 984 kJ mol^{-1}. Proton transfer from any of these hydrates to any of the toluenes is an endothermic reaction and would not be expected to occur. However, a selected ion flow tube study showed that even though the reaction is highly endothermic, proton transfer from $H_3O^+(H_2O)$ to toluene (PA = 784 kJ mol^{-1}) and ethyl benzene (PA = 788 kJ mol^{-1}) occurs with high efficiency [31]. In a selected ion flow tube operated with helium at 0.5 Torr, bare NO^+ was found to react at the collision rate with alkylbenzenes. The major product observed was the molecular ion, formed by electron transfer [32]. However, the association of NO^+ with substituted benzenes is well documented and tables of NO^+ affinities have been produced [33–35]. Both electron transfer and association are therefore possible in the reaction of $NO^+(H_2O)_n$ with the toluenes. In an ion mobility spectrometer operating at atmospheric pressure, the association reaction would be expected to be favored and to proceed with high efficiency.

The substituted anilines, having very high proton affinities compared with the toluenes and probably an equal or higher NO^+ affinities, would be expected to accept protons from both $NH_4^+(H_2O)_n$ and $H_3O^+(H_2O)_n$, and form an adduct with, or donate an electron to $NO^+(H_2O)_n$.

4.1. Mono-substituted toluenes

The major peak in the mobility spectra obtained in air with ^{63}Ni ionization is usually due to protonation of the analyte. Methyltoluenes are only protonated on the ring and can therefore have only one peak in the mobility spectrum for the protonated molecule. The large peak in the mobility spectrum must result from proton transfer from $H_3O^+(H_2O)_n$ according to Eq. (2):

$$CH_3C_6H_4CH_3 + H_3O^+(H_2O)_n \rightarrow CH_3C_6H_5CH_3{}^+(H_2O)_{n-x} + (x+1)H_2O \quad (2)$$

The enthalpy change for this reaction may be calculated with the reasonable assumption that the unknown enthalpy of monohydration of protonated toluene is the same as that of protonated benzene, −71 kJ mol^{-1}. For $n=2$ and $x=1$, ΔH_3^0 is +44 kJ mol^{-1}, and for $n=1$ and $x=0$, ΔH_3^0 is −40 kJ mol^{-1}. Proton transfer accompanied by one water molecule from $H_3O^+(H_2O)$ to the methyltoluenes is exothermic and therefore a feasible reaction for the formation of protonated products, whereas proton transfer from $H_3O^+(H_2O)_2$ is unlikely. Since the monohydrate constitutes only 3% of $H_3O^+(H_2O)_n$, a relatively high concentration of analyte would be required for reaction, as is observed.

K_{o1} for the major ion of each of the methyltoluenes from ^{63}Ni ionization is just slightly less than K_o of the molecular ion formed by PI, consistent with an ion that is, on average, slightly more hydrated. This near equality of reduced mobilities would be expected for ions

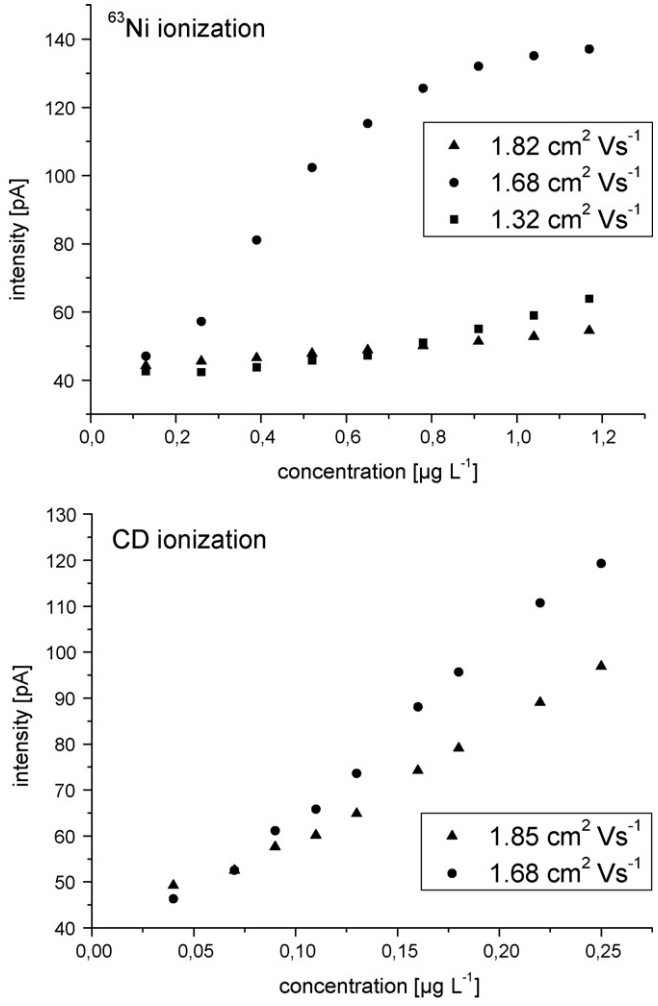

Fig. 5. Intensities of peaks for product ions versus concentration of 2-chloroaniline formed by chemical ionization with a ^{63}Ni source and corona discharge source in air at ambient pressure.

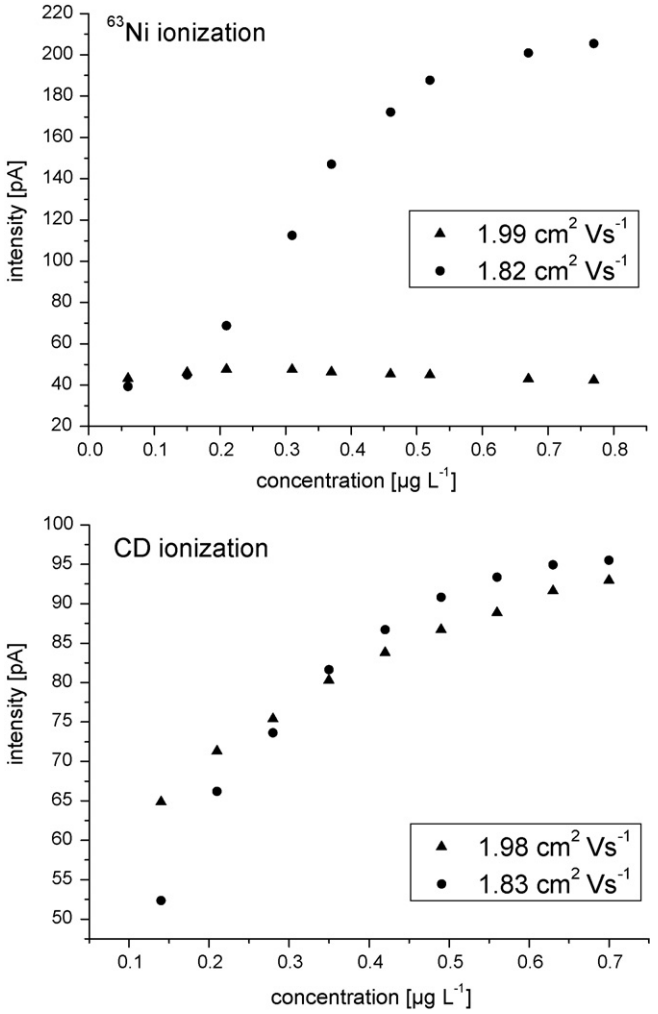

Fig. 6. Intensities of peaks for product ions versus concentration of aniline formed by chemical ionization with a ^{63}Ni source and corona discharge source in air at ambient pressure.

of almost identical mass both of which have charge delocalized around the ring. The same holds true for the ethyltoluenes, and for the halogen substituted toluenes for which K_{o1} values are closer to the PI values, and indeed for the fluoro- and chlorotoluenes the values are identical.

The concentration dependences of the ^{63}Ni signal intensities for 2-methyltoluene and 2-chlorotoluene in Fig. 3 show almost linear plots for K_{o1} and a very low yield of K_{o2}, which rapidly attains a value at very low concentration that remains constant with increasing concentration. The constant value rules out K_{o2} being a proton bound dimer or any ion related to, or resulting from, the protonated molecule since its intensity must then change as the analyte concentration increased. The ion associated with this minor product has a lower mobility than the protonated molecule, implying an ion of higher mass. If $H_3O^+(H_2O)_n$ is not the precursor of K_{o2} then either $NH_4^+(H_2O)_n$ or $NO^+(H_2O)_n$ must be. A thermodynamic argument favors $NO^+(H_2O)_n$. Calculation for unsubstituted toluene, for which some data are available, should be directly applicable to the mono-substituted toluenes.

The enthalpy of association of NO^+ with toluene is -144 kJ mol^{-1} and with benzene is -131 kJ mol^{-1} [35]. The enthalpy of association of NH_4^+ with benzene is -81 kJ mol^{-1}, and while that with toluene has not been measured a reasonable estimate is -86 kJ mol^{-1} since that with 1,3,5-trimethylbenzene is -91 kJ mol^{-1} [36]. The formation of K_{o2} is highly efficient, being complete at very low analyte concentration. Only the most abundant reactant ion hydrates will therefore be considered. Table 3 shows these to be $NH_4^+(H_2O)$ and $NO^+(H_2O)$. The pertinent ligand exchange reactions and their estimated enthalpies for the formation of the two possible adducts with toluene are shown in Eqs. (3) and (4):

$$NH_4^+(H_2O) + C_7H_8 \rightarrow NH_4^+(C_7H_8) + H_2O \Delta H^0 = 0\,\text{kJ mol}^{-1} \quad (3)$$

$$NO^+(H_2O) + C_7H_8 \rightarrow NO^+(C_7H_8) + H_2O \Delta H^0 = -67\,\text{kJ mol}^{-1} \quad (4)$$

The methyl toluenes, with the extra methyl, would form slightly more stable adducts than toluene, but the picture would remain the same; the addition of NO^+ is very exothermic while that of NH_4^+ is close to thermoneutral. A thermoneutral ligand exchange, as described by Eq. (3), should attain an equilibrium state in which both product and reactant ions are present. However, since there is only water and no analyte in the drift region the reactant ion will be favored at the detector and the apparent reaction efficiency will be low. A reaction with high exothermicity should proceed with high efficiency and the K_{o2} ion is most probably formed by the association of NO^+ with the neutral analyte.

Some evidence in favor of the formation of NO adducts is provided by the CD spectra. The CD reactant ion spectrum contains considerably more $NO^+(H_2O)_n$ relative to $H_3O^+(H_2O)_n$ than does that with ^{63}Ni ionization [37,38]. The K_{o2} peaks in the ^{63}Ni spectra of the toluenes are the same as the major peaks in the CD

spectra of the alkyl-toluenes and 4-chlorotoluene and as the lone peaks in the spectra of the other halogenated toluenes (Table 2). The ^{63}Ni spectrum of 2-chlorotoluene in Fig. 3b shows that the K_{o2} peak attains its maximum intensity at ~25 μg L^{-1} when K_{o1} has negligible intensity. With CD providing a higher concentration of $NO^+(H_2O)$, the range of concentration required for acceptable product signal is 0.9–4.6 μg L^{-1}. At this concentration, K_{o1} is not observable. 4-Chlorotoluene is the only halogenated toluene that has both a K_{o1} and a K_{o2} peak in its CD spectrum. This is consistent with the ^{63}Ni spectrum of Fig. 1a that shows that, compared with its isomers, production of K_{o1} is more efficient.

One unexplainable observation is that in the CD spectra of the methyltoluenes, K_{o1} is an ion with a slightly higher mobility than the molecular ion produced by PI. This implies a product of lower mass than the parent molecule. The ion intensity decreased after attaining a small maximum value at very low methyltoluene concentration, implying further reaction with the parent molecule.

4.2. Mono-substituted anilines

The PI-based spectra of the mono-substituted anilines, like those of the mono-substituted toluenes, have one major peak (Fig. 1 and Table 2). The mass spectral data of Table 2 show that this is the molecular ion. Again, several small peaks denote further unknown reactions with the ambient atmosphere. The ^{63}Ni-based spectra of the anilines show, as do those of the toluenes, two product ions. K_{o1} has the identical mobility value of the PI ion, however, it is only a minor product. The major product is K_{o2}, and for most of the alkyl-substituted anilines there is a small K_{o3}. A valid explanation of product formation must explain why K_{o2} is the major peak for the anilines rather than K_{o1}, as found for the toluenes.

The more mobile ion in the spectra of the anilines, $K_{o1,}$ identified above as the molecular ion, has an intensity profile in the ^{63}Ni spectra of Figs. 4 and 5 similar to, but not identical with K_{o2} for the toluenes in Fig. 3. The intensity is low but the limiting value has not been attained in the aniline spectra at the highest analyte concentration, which is understandable since the concentration is two orders of magnitude less than required for the toluenes. It is argued above that the K_{o2} peak in the toluene spectra is due to the NO^+ adduct. If that supposition is correct then, rather than forming an adduct, $NO^+(H_2O)$ must react with the anilines by electron transfer to generate the molecular ion. As shown in Table 1, all the anilines have ionization energies lower than that of NO (9.26 eV) and for each the reaction is exothermic. For example, the reaction with 2-methylaniline, which has the lowest ionization energy, has an exothermicity of 96 kJ mol^{-1} (Eq. (5)) and the reaction with 3-fluoroaniline, which has highest ionization energy, the exothermicity is 14 kJ mol^{-1} (Eq. (6)):

$$NO^+(H_2O) + CH_3C_6H_4NH_2 \rightarrow NO + H_2O + CH_3C_6H_4NH_2^+,$$
$$\Delta H^0 = -96\ \text{kJ mol}^{-1} \quad (5)$$

$$NO^+(H_2O) + FC_6H_4NH_2 \rightarrow NO + H_2O + FC_6H_4NH_2^+,$$
$$\Delta H^0 = -14\ \text{kJ mol}^{-1} \quad (6)$$

The CD spectra confirm the occurrence of the electron transfer reaction by the enhanced K_{o1} (molecular ion) peak shown in Fig. 2, which is due to the increased concentration of the reactant ion $NO^+(H_2O)_n$. Electron transfer obviously takes precedence over adduct formation in the reaction of this ion with the anilines.

The major peak in the spectra of the anilines, K_{o2}, exemplified in the spectra of the chloroanilines in Fig. 2 is that of the protonated molecule. The proton affinities of all the anilines are ~100 kJ mol^{-1} higher than those of the analogous toluenes so that proton transfer from $H_3O^+(H_2O)$ and $H_3O^+(H_2O)_2$ is possible. For example, 3-fluoroaniline has the lowest listed proton affinity in Table 2 and Eq. (7) shows an exothermicity of 40 kJ mol^{-1} for reaction with $H_3O^+(H_2O)$

$$H_3O^+(H_2O) + FC_6H_4NH_2 \rightarrow FC_6H_4NH_3^+ + 2H_2O,$$
$$\Delta H^0 = -40\ \text{kJ mol}^{-1} \quad (7)$$

The association enthalpy of one molecule of water with protonated 3-fluoroaniline is −62 kJ mol^{-1} [39] resulting in an exothermicity of 18 kJ mol^{-1} for the reaction with $H_3O^+(H_2O)_2$ (Eq. (8))

$$H_3O^+(H_2O)_2 + FC_6H_4NH_2 \rightarrow FC_6H_4NH_3^+(H_2O) + 2H_2O,$$
$$\Delta H^0 = -18\ \text{kJ mol}^{-1} \quad (8)$$

The protonation of the anilines is much more efficient than protonation of the toluenes as demonstrated by the two orders of magnitude lower analyte concentration required to obtain spectra of equivalent intensity.

Karpas et al. used an IMS/MS to obtain the spectra of aniline and a variety of mono- and di-substituted anilines [20]. There were two product peaks in each mobility spectrum for which the K_{o1} and K_{o2} values and the ratio of peak intensities were given. 2-Methylaniline and 2-chloroaniline are the only two compounds in common with our work so in order for further comparison we present data for aniline in Fig. 6. The calculated K_{o1} and K_{o2} values and the ratio K_{o1}/K_{o2} from the two studies is presented in Table 4. These data indicate that the same mobility peaks are being observed in both studies. The slight differences in drift times can result from the different temperatures or differences in drift gas composition. Karpas et al. do not state the concentration of analyte used and do not mention any concentration dependences of peak intensities. However, we note that the intensity ratio for aniline, given as 0.1, is inconsistent with the mobility spectrum shown in their Fig. 1b, for which a minimum value of 0.25 is obtained even when all of the proton bound dimer intensity is arbitrarily assigned to K_{o2}. The single ion mass spectrum, shown in the same figure, for m/z 94, protonated aniline, has contributions from both K_{o1} and K_{o2}, which leads the authors to identify K_{o1}, the more mobile product, as the charge-delocalized, ring-protonated molecule and K_{o2} as the N protonated product. High level molecular orbital calculations suggest that there is very little difference in protonation energy between the C and N sites of aniline [40]. The N site is however consistently favored, but by only a few kJ mol^{-1}. Protonation at both C and N sites is consistent with the conclusion of Karpas et al.

Reconciliation of the two different suggested identities for K_{o1}, molecular ion or protonated molecule, for the anilines is not possible at this time. In favor of our interpretation that reaction occurs to

Table 4
Reduced mobilities for the product peaks of anilines[a].

	K_{o1} (cm^2 V^{-1} s^{-1})	K_{o2} (cm^2 V^{-1} s^{-1})	K_{o1}/K_{o2}	Intensity ratio[a]
Aniline	1.99 (2.07)	1.82 (1.93)	1.09 (1.07)	0.1
2-Methylaniline	1.87 (1.95)	1.72 (1.83)	1.09 (1.07)	0.5
2-Chloroaniline	1.82 (1.91)	1.68 (1.79)	1.08 (1.07)	0.05

[a] Values in brackets and intensity ratios from Ref. [20].

give the molecular ion is: (a) the very low yield with ^{63}Ni, and the enhanced yield with CD for aniline and all its mono-substituted anilines; (b) the mobility is identical with that of the molecular ion produced by PI; and (c) the mono-substituted toluenes, whose high ionization energies precludes their participating in an electron transfer with $NO^+(H_2O)$, form a K_{o2} adduct peak whose intensity versus concentration profile is consistent with that of the K_{o1} peak of the anilines. We note that in the mobility spectrum, Fig. 1 of Ref. [20], the NO^+ reactant ion has almost completely disappeared, but there is no mention of its fate. By contrast, the NH_4^+ reactant ion is still present with what appears to be its non-depleted intensity. The experiments were carried out at 472 K when hydration of these ions would be negligible if the (non-stated) water content was unusually high. NO^+ should then only react with the anilines in an electron transfer reaction to produce the molecular ion.

4.3. Hydration of product ions

Water vapor is ubiquitous in ion mobility spectrometers and the possibility, indeed the probability, that product ions are hydrated to a greater or lesser extent, should always be considered. Unfortunately, there is a paucity of experimental or theoretical information on the hydration of the pertinent organic molecular cations. Information is available for the association of one water molecule with the benzene cation. The structure has the two lone pairs of oxygen bonding with two adjacent protons in the plane of the ring [41–44]. The experimental enthalpy and entropy of the association reaction (Eq. (9)) are −46 and −82 J K^{-1} mol^{-1} respectively [41]

$$C_6H_6^+ + H_2O \rightarrow C_6H_6^+(H_2O) \quad (9)$$

At equilibrium at 323 K with 1 ppm$_v$ of water, less than 0.01% of the benzene cations are hydrated. Hyperconjugation with the CH_3 group means that positive charge is more stabilized in the toluene cation than in the benzene cation and the association energy with a single water molecule will be slightly lower. The toluene cations are drifting as unhydrated species in the mobility experiments. Since there is only little difference between the reduced mobilities of the toluene obtained by PI (cations) and ^{63}Ni ionization (K_{o1}: protonated molecules), it follows that the latter are not hydrated to any great extent under the experimental conditions (Table 2).

By contrast, the protonated anilines (K_{o2} peak in spectra observed using ^{63}Ni ionization) have reduced mobilities that are significantly lower than those of the cations (product ions detected using PI).

The term Ω_D may be modified if the size of the ion changes or if its charge distribution changes; the attachment of one or more water molecules can lead to both. In order to determine whether differential hydration of the aniline cations and protonated molecules may be the cause of the differences in the reduced mobilities, thermodynamic data is required. The association enthalpies of one water molecule to a series of protonated mono-substituted anilines have been estimated from ΔG^0 values obtained from pulsed electron beam high pressure mass spectrometry equilibrium measurements at 433 K using an assumed entropy of −92 J K^{-1} mol^{-1} [39]. For aniline, 3-fluoroaniline and 3-chloroaniline the respective ΔH^0 values (kJ mol^{-1}) are −63.2, −61.9 and −61.9. There are no comparative values for the aniline molecular cations and we therefore resort to calculation. Because of the limit of computational capacity, calculations were carried out only for aniline itself, for both the cation and the protonated molecule. The results of DFT (density functional theory) calculations, with both optimization and energy at the B3LYP/6-311+G(d,p) level, are presented in Table 5 and Fig. 7. The structures in the figure are annotated with NBO (natural bond orbital analysis) charges and a few bond distances.

The aniline cation is planar with the positive charge distributed over all the hydrogens. An NBO analysis at the higher B3LYP/6-311++G(df,pd) level found a charge distribution almost identical to that in Fig. 7a; each of the protons on N had positive charges of +0.421e while the charges on the ring hydrogens were in the range +0.235 to +0.245e [45]. The most energetically favorable site for the attachment of a water molecule is at N–H with a hydrogen bond length of 1.785 Å, as seen in Fig. 7b. More shallow energy minima were found with water associating with ring hydrogens.

Table 5
Computed (B3LYP 6-311+G(d,p)) enthalpy and entropy changes at 323 K for the hydration reaction $M^+ + H_2O = M^+(H_2O)$.

M^+	$-\Delta H^0$ (kJ mol^{-1})	$-\Delta S^0$ (J K^{-1} mol^{-1})	$M^+(H_2O)/M^+$[a]
$C_6H_5NH_2^+$ (N)[b]	56.4	123.1	4.8×10^{-4}
$C_6H_5NH_2^+$ (C4)[c]	28.1	82.5	1.7×10^{-6}
$C_6H_5NH_3^+$ (N, N)[d]	71.7 (63.2)	113.3 (92)	0.47 (0.25)
$C_6H_5NH_3^+$ (N, C4)[e]	20.2	75.2	2.2×10^{-7}

Values in brackets from Ref. [39].
[a] Ratio of hydrated to bare ion with water vapour of 1 ppm$_v$.
[b] H_2O on N.
[c] H_2O on C4.
[d] Proton on N, H_2O on N.
[e] Proton on N, H_2O on H–C4.

The enthalpies and entropies of binding of a water molecule at the N and C4 sites of the aniline cation, shown in Table 5, allow an estimation of the equilibrium ratio of the concentrations of the mono-hydrated to the bare cation. With 1 ppm$_v$ of water present in the drift gas, the ratios at 323 K are 4.8×10^{-4} at the N site and 1.7×10^{-6} at the C4 site. Attachment of water is not significant for the cation, which should move as the bare ion under the experimental conditions. The lower mobility of the aniline cations compared with the analogous toluene cations are probably not due to a different degree of hydration but reside in differences in the interaction potential, Ω_D.

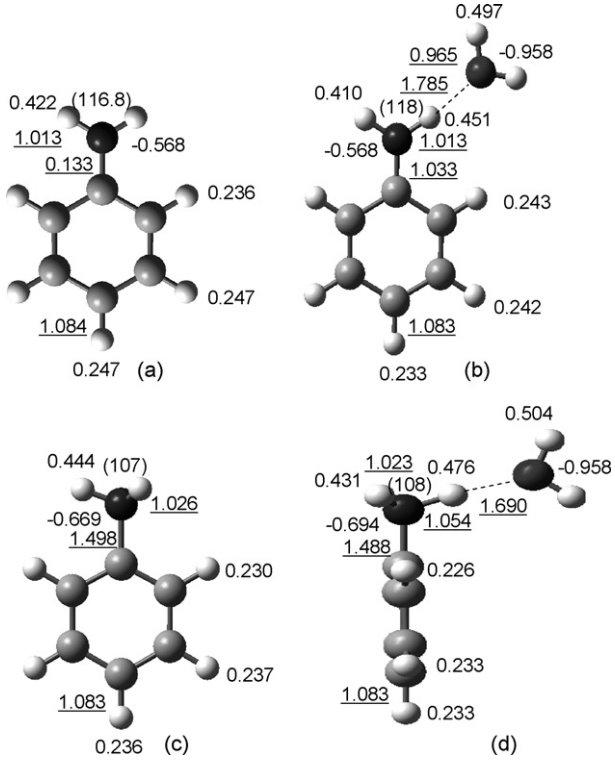

Fig. 7. NBO charges, angles in brackets, and distances underlined for aniline: (a) cation; (b) hydrated cation; (c) protonated molecule; (d) mono-hydrated protonated molecule.

Although the NBO charge on each N hydrogen is almost identical in the aniline cation and the protonated molecule, the net charge of +0.276e on the NH_2 group is much less than the +0.663e on the NH_3 group (Fig. 7a and c). A stronger association with water is therefore expected for the protonated molecule. This is borne out by computation, the results are shown in Table 5. The structures of the mono-hydrated forms in Fig. 7b and d show that the H. . .O distance is 0.1 Å shorter in the protonated molecule. The calculated enthalpy of mono-hydration of N-protonated aniline, $-71.7\,kJ\,mol^{-1}$, is in very good agreement with the experimental value of −63.2 obtained by Lau et al. [39]. The computed entropy, $-113.3\,J\,K^{-1}\,mol^{-1}$ is somewhat more negative than their estimated value of $-92\,J\,K^{-1}\,mol^{-1}$. The calculated equilibrium ratios of bare to mono-hydrated protonated aniline are shown in Table 5. Both experiment and theory agree that at 323 K with 1 ppm_v of water, N-protonated aniline is significantly hydrated: 32% theory, 20% experiment. N-protonated and ring (C4) hydrated aniline is not of significance. Protonated aniline will travel through the drift tube from 20% to 30% of the time in the hydrated form. The hydrated ion is heavier and significantly larger than the bare ion, which would lead to a smaller reduced mobility of the protonated molecule compared with the molecular cation, as is observed for all the anilines.

4.4. Comparison of reduced mobilities

The reduced mobilities, shown in Table 2, of the molecular ions produced by PI of both the toluenes and the anilines, decrease in the substituent order fluorine>methyl>chlorine>ethyl and>bromine (toluene only). Within experimental uncertainty the values are the same, independent of position, for toluene with the same substituent, but there appears to be a very small bias in favor of the ortho-substituent having a slightly higher mobility for the anilines. If this is a genuine effect then an intra-molecular interaction between the NH_2 group and the ortho-substituent is slightly decreasing the interaction potential, Ω_D.

The molecular ions (formed by PI) of the toluenes, although only 1 Da higher in mass, have a measurably higher reduced mobility than their analogous aniline counterparts. The values of alkylated compounds (methyltoluene: $1.93\,cm^2\,V^{-1}\,s^{-1}$ and methylaniline $1.89\,cm^2\,V^{-1}\,s^{-1}$; ethyltoluene: $1.82\,cm^2\,V^{-1}\,s^{-1}$ and ethylaniline $1.78\,cm^2\,V^{-1}\,s^{-1}$) show a shift of $0.04\,cm^2\,V^{-1}\,s^{-1}$. A similar behavior is observed for halogenated compounds where the differences in K_o values is $0.08\,cm^2\,V^{-1}\,s^{-1}$ (chlorotoluene $1.89\,cm^2\,V^{-1}\,s^{-1}$ and chloroaniline $1.81\,cm^2\,V^{-1}\,s^{-1}$; fluoroaniline $1.97\,cm^2\,V^{-1}\,s^{-1}$ and fluoroaniline $1.89\,cm^2\,V^{-1}\,s^{-1}$). However, there is a reasonable correlation between the K_o values of the two series as seen in Fig. 8. The equation of the line is $K_o(\text{anilines}) = 0.86K_o(\text{toluenes}) + 0.20$, with $R^2 = 0.86$. A difference in cross-sectional areas of the toluenes relative to the anilines is a possible explanation that should be considered for the differences in the mobilities.

Although differences in the sizes of the bare molecular ions can be observed (see Table 1, where surfaces and volumes of neutral sample molecules were calculated as a rough approximation), these differences (on an average of 5.6 $Å^3$ or 4.6%) do not correlate with the shift of reduced mobility values of toluenes and anilines. Toluenes are more voluminous and have more accessible surface in comparison with their analogous aniline counterparts. However, the toluenes are the more mobile ions with a shorter drift time and a higher reduced mobility although an opposite behavior can be expected from the differences in cross sectional area. Therefore, a size difference of the bare ions cannot be a satisfactory explanation for the different drift behavior of anilines and toluenes. These differences in drift velocities obviously result from different drift behavior due to different interaction potential of the molecular ions with polar or polarizable neutrals in drift gas depending on their different properties which are determined by the functional groups ($-CH_3$ or $-NH_2$).

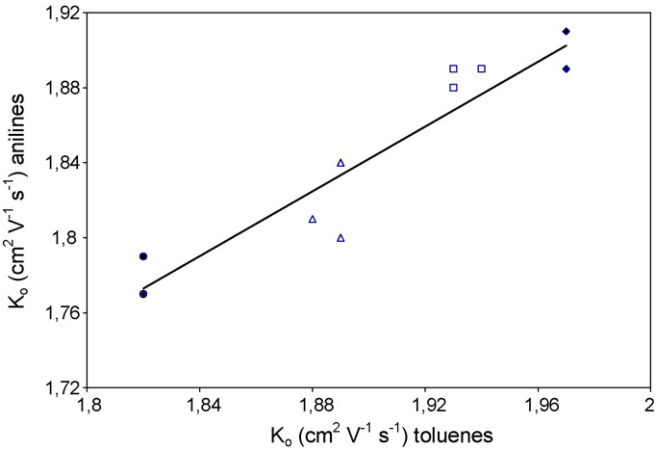

Fig. 8. Correlation of reduced mobilities of the molecular ions of mono-substituted toluenes and anilines. Substituents: ●, ethyl; △, chlorine; □, methyl; ♦, fluorine.

5. Conclusion

Although the toluenes and their analogous aniline counterparts investigated differ in mass by only 1 Da, the ion mobility spectra show considerable differences which result from different ionization pathways and a different drift behaviour. The product ions from toluenes obtained by chemical ionization using ^{63}Ni and CD ionization result from the formation of protonated molecules and NO^+ adduct. The two product ions obtained for anilines were assigned to molecular ions resulting from electron transfer to NO^+ and protonated clustered molecules. The two product ions appear in spectra of toluenes and anilines with a different relative abundance depending on the method of chemical ionization while mainly molecular ions are detectable using PI.

Acknowledgements

The authors would like to thank the Deutsche Forschungsgemeinschaft (DFG) for kindly funding this work. Furthermore, we would like to thank Prof. H.-J. Hofmann (University of Leipzig, Institute of Biochemistry) for his support in carrying out the molecular modeling.

References

[1] H. Borsdorf, G.A. Eiceman, Appl. Spectros. Rev. 41 (2006) 323.
[2] R.B. Turner, J.L. Brokenshire, Trends Anal. Chem. 13 (1994) 275.
[3] G.A. Eiceman, J.A. Stone, Anal. Chem. 76 (2004) 391A.
[4] H. Sohn, J. Steinhanses, Int. J. Ion Mobil. Spectrom. 1 (1998) 1.
[5] G.A. Eiceman, M.E. Fleischer, C.S. Leasure, Int. J. Environ. Anal. Chem. 28 (1987) 279.
[6] H. Borsdorf, A. Raemmler, D. Schulze, K.O. Boadu, B. Feist, H. Weiss, Anal. Chim. Acta 440 (2001) 63.
[7] Th. Keller, A. Schneider, E. Tutsch-Bauer, J. Jaspers, R. Aderjan, G. Skopp, Int. J. Ion Mobil. Spectrom. 2 (1999) 22.
[8] L. Elias, A.H. Lawrence, Can. J. Spectrosc. 32 (1987) 14A.
[9] J.I. Baumbach, Anal. Bioanal. Chem. 384 (2006) 1059.
[10] T. Limero, in: J.I. Baumbach, J. Stach (Eds.), Recent Developments in Ion Mobility Spectrometry, International Society for Ion Mobility Spectrometry, Dortmund, Germany, 1998, p. 317, ISBN 3-00-003676-8.
[11] Z. Xie, S. Sielmann, H. Schmidt, F. Li, J.I. Baumbach, Anal. Bioanal. Chem. 372 (2002) 606.
[12] L.M. Matz, H.M. Dion, H.H. Hill, J. Chromatogr. A 946 (2002) 59.
[13] D.C. Collins, M.L. Lee, Anal. Bioanal. Chem. 372 (2002) 66.
[14] H.C. Revercomb, E.A. Mason, Anal. Chem. 47 (1975) 970.
[15] T. Su, M.T. Bowers, J. Chem. Phys. 55 (1973) 3027.
[16] E.S. Sennhauser, D.A. Armstrong, Can. J. Chem. 58 (1980) 231.

[17] S.N. Lin, G.W. Griffin, E.C. Horning, W.E. Wentworth, J. Chem. Phys. 60 (1974) 4994.
[18] Z. Karpas, Z. Berant, O. Shahal, Int. J. Mass Spectrom. Ion Process. 96 (1990) 291.
[19] Z. Karpas, Int. J. Mass Spectrom. Ion Process. 93 (1989) 237.
[20] Z. Karpas, Z. Berant, R.M. Stimac, Struct. Chem. 1 (1990) 201.
[21] L. Kolaitis, D.M. Lubman, Anal. Chem. 58 (1986) 1993.
[22] J. Adler, G. Arnold, H.-R. Döring, V. Starrock, E. Wülfing, in: J.I. Baumbach, J. Stach (Eds.), Recent Developments in Ion Mobility Spectrometry, International Society for Ion Mobility Spectrometry, Dortmund, Germany, 1998, p. 110, ISBN 3-00-003676-8.
[23] H. Borsdorf, H. Schelhorn, J. Flachowsky, H.-R. Döring, J. Stach, Anal. Chim. Acta 403 (2000) 235.
[24] Operational Manual of Raid 1 Ion Mobility Spectrometers, Bruker Saxonia Leipzig, 1999.
[25] H. Borsdorf, E.G. Nazarov, G.A. Eiceman, J. Am. Soc. Mass Spectrom. 13 (2002) 1078.
[26] M.J. Frisch, et al. Gaussian Inc., Pittsburgh, PA, 2003.
[27] M. Tubaro, E. Marotta, R. Seraglia, P. Traldi, Rapid Commun. Mass Spectrom. 17 (2003) 2423.
[28] D.I. Carroll, I. Dzidic, R.N. Stillwell, E.C. Horning, Anal. Chem. 47 (1975) 1956.
[29] P. Kebarle, S.K. Searles, A. Zolla, J. Scarborough, M. Arshadi, J. Am. Chem. Soc. 89 (1967) 6393.
[30] M.A. French, L.P. Hills, P. Kebarle, Can. J. Chem. 51 (1973) 456.
[31] A.J. Midey, S. Williams, S.T. Arnold, A.A. Viggiano, J. Phys. Chem. A 106 (2002) 11726.
[32] S.T. Arnold, I. Dotan, S. Williams, A.A. Viggiano, R.A. Morris, J. Phys. Chem. A 104 (2000) 928.
[33] W.D. Reents, B.S. Freiser, J. Am. Chem. Soc. 103 (1981) 2791.
[34] J.A. Stone, D.E. Splinter, S.Y. Kong, Can. J. Chem. 60 (1982) 910.
[35] F. Cacace, G. de Petris, F. Pepi, Proc. Natl. Acad. Sci. U.S.A. 94 (1997) 3507.
[36] C.A. Deakyne, M. Meot-Ner, J. Am. Chem. Soc. 107 (1985) 474.
[37] M.M. Shahin, J. Chem. Phys. 45 (1966) 2600.
[38] M. Pavlik, J.D. Skalny, Rapid Commun. Mass Spectrom. 11 (1997) 1757.
[39] Y.K. Lau, K. Nishizawa, A. Tse, R.S. Brown, P. Kebarle, J. Am. Chem. Soc. 103 (1981) 6291.
[40] R. Flammang, N. Dechamps, L. Pascal, Y. van Haverbeke, P. Gerbaux, P. Nam, M.T. Nguyen, Lett. Org. Chem. 1 (2004) 23.
[41] Y.M. Ibrahim, M. Meot-Ner, E.H. Alshraeh, M.S. El-Shall, S. Scheiner, J. Am. Chem. Soc. 127 (2005) 7053.
[42] N. Solca, O. Dopfer, J. Phys. Chem. A 107 (2003) 4046.
[43] M. Miyazaki, A. Fujii, T. Ebata, N. Mikami, Chem. Phys. Lett. 349 (2001) 431.
[44] N. Solca, O. Dopfer, Chem. Phys. Lett. 347 (2001) 59.
[45] P.M. Wojciechowski, W. Zierkiewicz, D. Michalska, P. Hobza, J. Chem. Phys. 118 (2003) 10900.

Talanta 78 (2009) 1408–1413

Contents lists available at ScienceDirect

Talanta

journal homepage: www.elsevier.com/locate/talanta

Comparison of cleanup methods for fipronil and its degradation products in sediment extracts

Amanda A. Brennan [a], Jing You [b], Michael J. Lydy [a,*]

[a] Fisheries and Illinois Aquaculture Center & Department of Zoology, 171 Life Science II, Southern Illinois University, Carbondale, IL 62901, USA
[b] State Key Laboratory of Organic Geochemistry, Guangzhou Institute of Geochemistry, Chinese Academy of Sciences, Guangzhou 510640, China

ARTICLE INFO

Article history:
Received 12 December 2008
Received in revised form 16 February 2009
Accepted 17 February 2009
Available online 24 February 2009

Keywords:
Fipronil
Sediment
Accelerated solvent extraction
Solid phase extraction
Gel permeation chromatography

ABSTRACT

Gel permeation chromatography (GPC) and solid phase extraction (SPE) were compared for cleaning extracts containing fipronil, fipronil-sulfide, and fipronil-sulfone at sub-ppb concentrations in sediment. With both methods, analytes were extracted using accelerated solvent extraction, and analyzed with gas chromatography equipped with an electron capture detector. The GPC was performed with a Waters Envirogel GPC column with dichloromethane as the mobile phase, while SPE was conducted with dual-layer cartridges containing graphitized carbon black and primary and secondary amines with a mixture of acetone and hexane as the eluting solvent. Method detection limits for fipronil, fipronil-sulfide, and fipronil-sulfone from three sediments with varying organic carbon content ranged from 0.12 to 0.52 μg/kg dry weight, while percent recoveries were 72–119% from sediment aged from 0.24 to 14 d. Although both methods were effective at analyzing fipronil and its degradation products, SPE was the less expensive and less labor-intensive method.

1. Introduction

The application of the phenylpyrazole insecticide, fipronil most notably includes Frontline®, Maxforce FC®, and Icon® for the eradication of fleas and ticks, fire ants, and rice pests, respectively. In aquatic environments fipronil sorbs to sediments [1], allowing for potential exposure and toxicity to those organisms that burrow or feed upon sediment-sorbed contaminants. Fipronil is highly toxic to aquatic species, and interestingly, its degradation products, fipronil-sulfide and fipronil-sulfone are reported as having equal or greater toxicity to aquatic invertebrates than the parent fipronil [2–4]. Maul et al. [2] reported that the median lethal concentrations (LC_{50}) in sediment for fipronil, fipronil-sulfide, and fipronil-sulfone were statistically similar with values of 0.88, 1.1 and 0.89 μg/kg dry weight for the benthic invertebrate, *Chironomus dilutus* (formerly *Chironomus tentans*). Mesléard et al. [5] identified fipronil as the pesticide mainly responsible for the significant decrease in invertebrate abundance in rice fields in Camargue, France. Fipronil has been detected in sediments from rivers and lakes receiving runoff from similar rice fields and agricultural areas at concentrations ranging from 1.7 to 5.5 μg/kg [3,6]. Both fipronil-sulfide and fipronil-sulfone have been detected at concentrations ranging from 0.64 to 25 μg/kg and 1.6 to 11 μg/kg, respectively [3,6–8]. In order to connect the environmental prevalence of fipronil, fipronil-sulfide, and fipronil-sulfone to toxicity of aquatic benthic invertebrates at these sub-ppb concentrations, a sensitive analytical method is needed.

Since the introduction of fipronil to the market in the U.S. in 1996, most of the field and laboratory studies of its environmental fate and toxicity have been in water and soils, with few being reported for aquatic sediments. These analytical methods have used time-consuming extraction techniques, including sonication [9,10], Soxhlet [11], and vigorous shaking and stirring [12–17]. These methods also used silica or florisil cartridges for removal of interferences or no cleanup was used. However, techniques without cleanup of extracts have substantial co-extracted interferences for samples in which a large mass of sediment must be extracted to obtain quantifiable results. In addition to higher errors in quantification, samples without a cleanup step also can require more frequent maintenance and replacement of instrumental components. Instrumentation for detection of fipronil and its degradation products commonly includes gas chromatography (GC) with electron capture detection (ECD) or mass spectrometry.

In order to reduce the lengthy and laborious sample preparation procedure prior to quantification, while still removing interfering compounds necessary for trace analysis, accelerated solvent extraction (ASE), and solid phase extraction (SPE) and gel permeation chromatography (GPC) were investigated in the current study as extraction and cleanup techniques, respectively. The ASE is advantageous compared to the traditional extraction methods, such as Soxhlet and sonication extraction, because elevated temperature and pressure results in reduced solvent and decreased extraction

* Corresponding author. Tel.: +1 618 453 4091; fax: +1 618 453 6095.
E-mail address: mlydy@siu.edu (M.J. Lydy).

0039-9140/$ – see front matter © 2009 Elsevier B.V. All rights reserved.
doi:10.1016/j.talanta.2009.02.034

time requirements. In addition, the automation of this extraction technique produces better precision and reproducibility amongst samples as well as increased sample throughput. The objectives of the current study were to compare cleanup methods for analyzing fipronil and its degradation products in sediment at a sub-ppb level, and to investigate the influence of aging and total organic carbon on sediment extraction.

2. Experimental

2.1. Chemicals

Fipronil and its degradation products, fipronil-sulfide and fipronil-sulfone, were purchased from ChemService Inc. (West Chester, PA, USA) and Accustandard (New Haven, CT, USA), respectively. Bifenthrin was purchased from ChemService Inc. and used as a surrogate for the GPC method, while two surrogate standards 4,4′-dibromooctafluoro-biphenyl (DBOFB) and decachlorobiphenyl (DCBP) were obtained from Supelco (Bellefonte, PA, USA) and were used with the SPE method. Anhydrous Na_2SO_4 and all pesticide grade solvents were obtained from Fisher Scientific (Pittsburgh, PA, USA), while diatomaceous earth (DE) was obtained from Dionex (Sunnyvale, CA, USA). The 500 mg graphitized carbon black (GCB) and 1000 mg florisil cartridges were purchased from Restek (Bellefonte, PA, USA), while Supelco (Bellefonte, PA, USA) supplied the GCB/PSA (polymerically bonded, ethylenediamine-N-propyl phases containing primary and secondary amines) (300/600 mg) cartridges.

2.2. Sediment

Spiked sediments were prepared from three uncontaminated reference sediments collected at Touch of Nature (TON), Carbondale, IL, American River (AR), Folsom, CA, and Bearskin Lake (BS), Grand Marais, MN. The sediments had different total organic carbon (TOC) levels of 0.98 ± 0.025 (measured by Midwest Laboratories, Omaha, NE), 1.1 ± 0.07 and $7.85 \pm 0.18\%$ (measured on an EA 1110 CHN analyzer, CE Instruments, Milan, Italy) for TON, AR, and BS sediments, respectively. Prior to homogenization, TON soil was hydrated with moderately hard water [18] to achieve a sediment slurry with a dry:wet ratio of approximately 0.40, while AR and BS sediments already had a dry: wet ratio of 0.30 and 0.80, respectively. Sediments were spiked to achieve concentrations of 0.5, 1, 5 or 10 μg/kg dry weight of fipronil, fipronil-sulfide, and fipronil-sulfone to develop and validate extraction and cleanup methods. Sediments spiked with 10 μg/kg dry weight of target compounds were also analyzed with the optimized method to test the influence of aging time (0.24, 1, 4, 7 and 14 d) on recoveries. Stock solutions carried in acetone were added drop-wise to the sediment slurry to achieve the target concentrations; the slurry was stirred for 1 h using a stainless steel paddle stirrer powered by an overhead motor.

2.3. Accelerated solvent extraction

A previously established ASE method using the Dionex ASE 200 was employed using 33 ml stainless steel cells and 60 ml glass collection vials [19]. Briefly, samples were extracted by filling the cells with dichloromethane (DCM): acetone (1:1, v/v) and heating at 100 °C and 1500 pounds per square inch (psi) for two 5 min static cycles. The cells were flushed with 60% solvent for 60 s. Prior to extraction, two techniques were compared to remove water from the sediment, including the use of DE as a drying agent and freeze-drying the samples. Statistical differences in the two methods were analyzed with a *t*-test. For the drying technique using DE, 10 g sediment wet weight (ww) was centrifuged at $3300 \times g$ to initially remove excess water. After centrifugation, $5 \cdot g$ DE was added to the sample and thoroughly homogenized, and transferred to the ASE cell, where the appropriate surrogate was added. Extracts were collected in the 60 ml glass collection vials and residual water was removed with the addition of 12 g anhydrous Na_2SO_4. The Na_2SO_4 was then washed three times with 10 ml hexane, and the extracts and washes were combined and evaporated to 5 ml under nitrogen gas at 30 °C with a Zymark TurboVap II Evaporator (Hopkinton, MA, USA). The extracts were solvent exchanged with hexane and further reduced to 1 ml prior to cleanup.

The second drying technique used a FreeZone 2.5 Labconco freeze drier (Kansas City, MO, USA). Samples (10 g sediment wet weight) were dried overnight at approximately −48 °C and 0.133 psi. After homogenizing the dried sediment, it was transferred to an ASE cell, and extracted as previously discussed. The final extracts were concentrated and solvent exchanged to 1 ml of hexane. Due to the enhanced drying efficiency of the freeze-drying method, no residual water was observed in the extracts, and therefore, further drying with anhydrous Na_2SO_4 was not required.

2.4. Comparison of cleanup methods

Two cleanup methods, GPC and SPE, were developed and compared for analyzing fipronil, fipronil-sulfide, and fipronil-sulfone at sub-ppb concentrations in sediment. Optimization of the SPE method included two types of cartridge combinations, namely PSA/GCB and florisil coupled with GCB. Copper was added to samples in which SPE was applied as the cleanup technique to eliminate sulfur interference during analysis. Due to differences in size, the compounds of interest were isolated from sulfur during GPC cleanup, thereby eliminating the need for removal of sulfur with copper.

Prior to GPC, the sediment extract was filtered through a 0.2 μm Whatman GD/X filter (13 mm diameter), and then concentrated to 0.4–0.5 ml with a Pierce Model 1878 Reactivap (Rockford, IL, USA) prior to injection into the GPC. The extract was injected into the GPC with a Rheodyne 7225 injector with a 0.5 ml sample loop (Cotati, CA, USA). The GPC was performed on an Agilent 1100 high-pressure liquid chromatography (HPLC) (Agilent Technologies, Palo Alto, CA, USA) equipped with a UV detector. A Foxy Jr. fraction collector (ISCO, Inc. Lincoln, NE, USA) was used to collect the fraction that eluted between 7.5 and 8.5 min, which contained fipronil and its degradation products. The separation was completed on a Waters 300 mm × 19 mm Envirogel GPC column with a 5 mm × 19 mm precolumn (Waters, Milford, MA, USA). The mobile phase (DCM) was set at a flow rate of 5 ml/min. The fractions were evaporated to near dryness and solvent exchanged to 0.5 ml of hexane for analysis using an Agilent 6890 series GC-ECD (Agilent Technologies, Palo Alto, CA, USA).

A dual-layer cartridge containing 300 mg GCB in combination with 600 mg of PSA was evaluated as a SPE cleanup technique for fipronil and its degradation products. The PSA sorbent was used to eliminate interference from fatty acids, organic acids, polar pigments, and sugars [20,21], whereas the GCB was used to remove planar pigments and sterols [21]. Anhydrous Na_2SO_4 was added on the top of the sorbent bed to remove any residual water remaining in the extracts. After conditioning the PSA/GCB cartridge with 6 ml hexane, the extract was loaded onto the cartridge, and the tube previously containing the extract was washed twice with 0.5 ml hexane and these rinses also were transferred to the cartridge. The extract and washes were passed through the cartridge at a slow drop-wise rate of 1 drop/s. Optimization of the eluting solvent included a variety of solvent combinations and volumes ranging from 7 to 10 ml of 30% DCM in hexane, 100% DCM, 50% ether in hexane, 50% acetone in hexane and 50% acetone in DCM. The eluent was evaporated and solvent exchanged to 1 ml of hexane, and further analyzed with GC-ECD.

A second SPE cleanup approach with sorbent combinations of 1000 mg florisil and 500 mg GCB also was evaluated. The procedure was analogous to the aforementioned SPE method aside from the eluting solvent. Experimentation involved the use of the following eluting solvents with volumes ranging from 7 to 10 ml: 30, 40 and 50% ether in hexane, 100% DCM as well as 50, 60 and 75% acetone in hexane.

2.5. Instrumentation and chemical analyses

Chemical analysis of the final extracts was performed on a GC-ECD with a HP-5 column (30 m × 0.25 μm, film thickness 0.25 μm). Helium and nitrogen were employed as the carrier and make-up gas, respectively, with the flow rate of the carrier gas being 3.5 ml/min. A 2 μl sample was injected into the GC using pulsed split-less mode. The oven was set at 100 °C, heated to 180 °C at 10 °C/min increments, then to 205 °C at 3 °C/min increments and held for 4 min and then heated to 280 °C at 20 °C/min increments and held for 7 min. Seven external standards in hexane were used for linear calibration of all analytes at concentrations of 500, 250, 100, 50, 10, 5 and 1 μg/l. Qualitative identity of analytes was established using a retention window of 1%.

2.6. Lipid-like compound analysis

Analyses of lipid-like compounds were performed for sediment extracts (approximately 10 g sediment dry weight) with (i.e., GPC or SPE) and without cleanup for the TON, AR, and BS sediments to determine the removal efficiency of the lipid-like matrix by the methods following the method of van Handel [22]. An aliquot of 25 and 50 μl of sediment extracts without and with cleanup, respectively, were placed in test tubes. Chloroform: methanol (1:1, v/v) (500 μl) was added to each test tube and evaporated in a water bath. Next, 200 μl concentrated sulfuric acid was added to each test tube and heated in the water bath for 10 min. The test tubes were removed and cooled prior to the addition of 4.8 ml vanillin-phosphoric acid reagent. After 5 min of development, transmittance of the solutions was measured in a Spectronic 20 Genesys spectrophotometer (Sigma–Aldrich, St. Louis, MO) at 525 nm. A vanillin-phosphoric acid reagent blank was used for instrumental zero initially and every five samples to calibrate the reading. Calibration standards were made using 10, 50, 100, 200 and 400 μl of the 1 mg/ml vegetable oil standard and were ran on the spectrophotometer before and after the samples and averaged for the calibration curve. All standards were prepared in the same manner and at the same time as the samples.

3. Results and discussion

3.1. Optimization of the drying procedure

To remove water while minimizing the loss of analytes, the use of DE and freeze-drying were compared as drying techniques prior to extraction with ASE. Diatomaceous earth does not affect recoveries of non-polar pesticides [19,23]; however, a low DE: sediment ratio of 1:2 was used to maximize the mass of sediment extracted during ASE [19]. Therefore, 5 g of DE was used for approximately 10 g (wet weight) sediment. The use of both DE and freeze-drying produced acceptable recoveries that were not significantly different from one another for fipronil and its degradation products and ranged from 101 to 116 and 86.7 to 97.2%, respectively. While freeze-drying required up to 24 h to remove water for sediments with high moisture content, it provided higher water removal efficiency and no residual water was present in the sediment extracts, thereby eliminating the need for further drying extracts with anhydrous Na_2SO_4. In addition, less labor was needed for the drying procedure as the samples could run unattended overnight. Thus, freeze-drying was selected as the optimized drying technique prior to ASE extraction.

Table 1
Percent recoveries and corresponding relative standard deviations of seven replicates for fipronil, fipronil-sulfide, and fipronil-sulfone spiked at 0.5 and 1 μg/kg dry weight for the methods using gel permeation chromatography (GPC) and primary secondary amines/ graphitized carbon black (PSA/GCB), respectively, for Touch of Nature, IL (TON), American River, CA (AR) and Bear Skin Lake, MN (BS) sediments.

Compound	GPC	PSA/GCB		
	TON	TON	AR	BS
Fipronil	106 (8.70)	97.1 (11.3)	114 (8.84)	87.5 (18.9)
Fipronil-sulfide	114 (9.80)	98.6 (8.98)	116 (6.45)	108 (9.45)
Fipronil-sulfone	108 (8.40)	121 (3.34)	143 (9.09)	147 (9.94)

3.2. Optimization of the cleanup procedure

Gel permeation chromatography, the first cleanup technique tested, effectively removed fipronil, fipronil-sulfide, and fipronil-sulfone from co-extracted sediment interferences with analyte recoveries from 106 to 114% (Table 1). High molecular weight lipid-like compounds in the sediment extracts could deposit on the GC inlet and interfere with the GC analysis; therefore, a good cleanup method is desirable to remove those compounds from the extracts. Lipid-like compounds were analyzed before and after cleanup to verify the cleanup efficiency. The GPC procedure reduced 96% of the lipid-like compounds in TON sediment extracts; however, the sample still exhibited a yellow hue upon concentration of the collected fraction (7.5–8.5 min) to 0.5 ml. Sulfur, a potential interference in GC-ECD analysis, eluted after 14 min during GPC, and thus the use of copper to remove sulfur was not required when GPC was used as a cleanup technique. However, due to fraction collecting with manual start as well as manual injection, cleanup with GPC was time-consuming and labor-intensive. In addition, only one sample could be run at a time using GPC, and injection and run-time for the 12 samples took approximately 4 h. In addition, this technique used a large amount of solvent (over 1 l of DCM for 12 samples).

In an attempt to minimize sample cleanup time and solvent usage, while still producing satisfactory recoveries, SPE was evaluated as an alternative technique. Florisil and PSA in conjunction with GCB were tested as SPE sorbents. Various organic solvent combinations were evaluated as eluting solvents for both SPE cartridge combinations (Fig. 1). Solvent mixtures of acetone and hexane (1:1, v/v) produced the most satisfactory recoveries of the studied analytes for florisil and PSA. When florisil was used, recoveries were 96 ± 13, 88 ± 11 and 95 ± 11% for fipronil, fipronil-sulfide, and fipronil-sulfone, respectively, whereas the PSA cartridge recovered 101 ± 14, 98 ± 14, and 99 ± 13 of fipronil, fipronil-sulfide, and fipronil-sulfone, respectively. Thus, both sorbents potentially could be used to clean sediment extracts for analysis of fipronil and its degradation products. The cartridge containing PSA/GCB was chosen for two reasons, including its wide applicability for various matrices and pesticides [19–21,24], and slightly lower costs (~$5 versus $7/cartridge). Previous studies showed that PSA and other sorbents that contain amide functional groups are very effective at reducing or eliminating matrix interference compared to C-18 and strong-anion exchange (SAX) sorbents [25,26]. Elution solvents of 30% DCM in hexane have been validated for cleanup of sediment extracts containing pyrethroid, organochlorine and organophosphate insecticides [19]. However, because of the more polar nature of fipronil and its degradation products, the solvents were not adequate to elute these compounds. Therefore, solvent combinations with a higher polarity, such as ethyl ether or acetone in hexane were required for qualitative recoveries of the analytes. On the

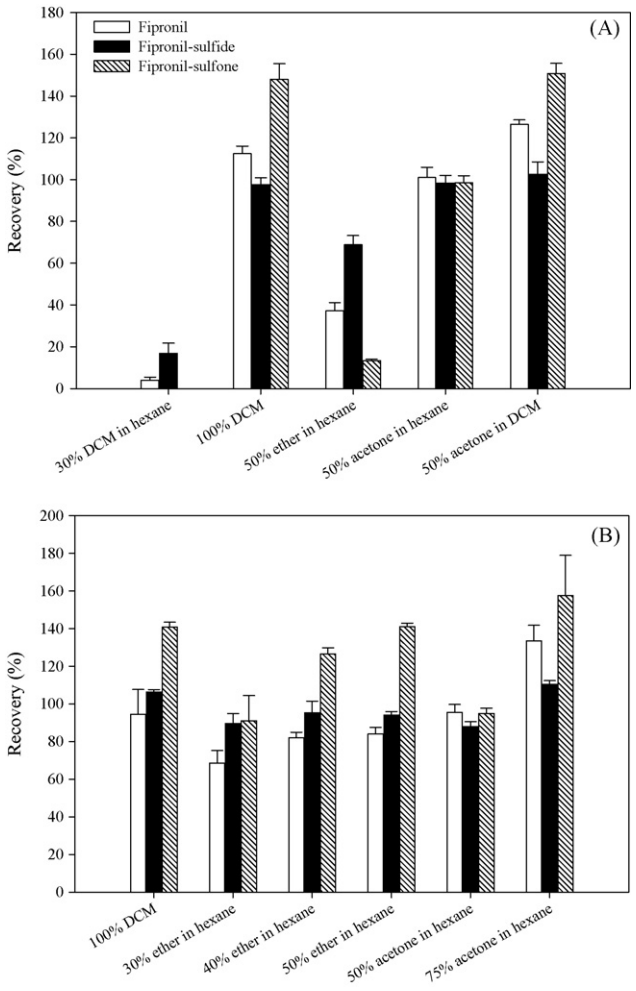

Fig. 1. Percent recoveries and corresponding relative standard deviations for fipronil, fipronil-sulfide, and fipronil-sulfone using different solvent combinations with primary and secondary amines/graphitized carbon black (A) and florisil (B) solid phase extraction absorbents. DCM = dichloromethane.

other hand, increasing the polarity of the eluting solvents increased the amount of fatty acid breakthrough from the cartridges [21,24]. Shimelis [21] stated that the use of GCB in conjunction with PSA slightly increased the retention of fatty acids in addition to removing planar pigments and sterols; however, 36% of oleic acid passed through a PSA/GCB (500 mg/500 mg) cartridge using 6 ml acetone: hexane (1:1, v/v) as the elution solvents. In the current study, 53% of the lipid-like compounds in TON sediment passed through a PSA/GCB cartridge using 10 ml of an acetone: hexane (1:1, v/v) solution. Although breakthrough of lipid-like compounds occurred, little to no interference with analytes was observed during GC-ECD analysis (Fig. 2).

3.3. Method validation

Method validation included accuracy and precision estimates, and method detection limit (MDL) determination. Accuracy and precision of SPE with PSA/GCB was determined by spiking three sediments with different total organic carbon (TOC) levels at varying analyte concentrations and aging periods. As shown in Table 2, recoveries of fipronil, fipronil-sulfide, and fipronil-sulfone ranged from 72 to 119%. Precision was determined by relative standard deviations (RSD) of three replicates, and these values ranged from 0.5 to 8.4% with most less than 5% at a spiked concentration of 10 μg/kg dry weight. The low RSD values demonstrated applicability of the established methods amongst sediments with different TOC levels and across different aging periods. Precision decreased for sediments spiked at lower concentrations of 1 μg/kg or less, with RSD values ranging from 3.3 to 19% (Table 1). In addition to increased variability, recoveries also were higher, especially for fipronil-sulfone, which ranged from 121 to 147%. The higher recoveries at lower concentrations suggested the existence of co-eluted interference and most notably the difficulty in quantifying concentrations approaching the detection limit. The presence of co-extracted interferences also can explain the variability amongst replicates. The lower sensitivity (smaller response factor) of fipronil-sulfone than those of the other analytes increased the difficulty in quantifying this compound at lower concentrations, contributing to the higher recoveries and variability. Amongst the three sediment types, the compounds spiked into the AR sediment had higher recoveries than the other two sediments at the 1 μg/kg dry weight concentration only, possibly resulting from increased interference.

The MDL is the minimum concentration of a substance that can be measured and reported with 99% confidence that the concentration is greater than zero [27]. As proposed by the U.S. EPA [27,28] the MDL was determined by multiplying the standard deviation of seven replicate samples by the Student's t value from statistical tables for a 99% confidence level and $(n-1)$ degrees of freedom. Table 3 lists the MDLs for each compound for both cleanup tech-

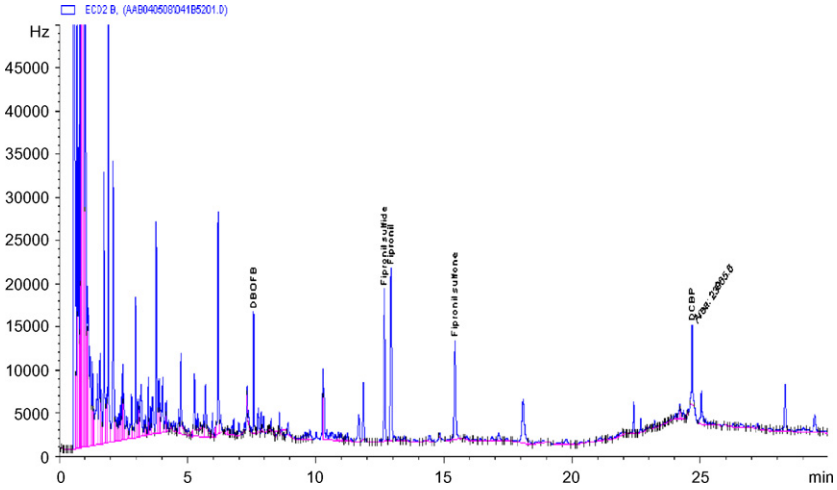

Fig. 2. Example of GC-ECD chromatogram of sample extract cleaned with primary and secondary amines/graphitized carbon black. The analytes and surrogates were spiked at 10 ng/g.

Table 2
Percent recoveries and corresponding relative standard deviations of three replicates for fipronil, fipronil-sulfide, and fipronil-sulfone at time points (0.24, 1, 4, 7, and 14 d) during sediment aging. Sediment extracts were cleaned with solid phase extraction. Sediment from Touch of Nature in IL (TON), American River, CA (AR) and Bear Skin Lake, MN (BS) was spiked at 10 μg/kg dry weight.

Sediment	Compound	Aging time (d)				
		0.24-d	1-d	4-d	7-d	14-d
TON	Fipronil	96.9 (3.20)	98.9 (6.33)	88.6 (1.25)	96.0 (4.96)	91.7 (1.29)
	Fipronil-sulfide	101 (5.54)	103 (5.71)	89.3 (2.26)	95.9 (4.43)	96.1 (1.53)
	Fipronil-sulfone	84.8 (5.58)	82.7 (8.01)	76.8 (0.510)	80.9 (5.36)	75.4 (1.45)
AR	Fipronil	83.3[a]	94.5 (6.70)	99.2 (4.71)	91.4 (8.13)	80.5 (6.82)
	Fipronil-sulfide	103.3[a]	105 (8.43)	97.1 (8.21)	89.6 (5.91)	85.0 (1.47)
	Fipronil-sulfone	94.9[a]	96.6 (6.38)	93.7 (6.21)	83.6 (6.20)	71.6 (6.63)
BS	Fipronil	94.6 (5.24)	93.7 (1.19)	109 (1.55)	102 (1.08)	119 (4.77)
	Fipronil-sulfide	99.7 (6.27)	98.9 (1.38)	101 (1.79)	97.1 (0.946)	111 (5.25)
	Fipronil-sulfone	81.7 (7.99)	84.5 (3.31)	88.6 (1.91)	85.0 (1.78)	87.8 (5.84)

[a] Unable to determine relative standard deviations since only 1 replicate was used.

niques. The MDL values for the three compounds ranged from 0.12 to 0.30, 0.22 to 0.32, and 0.32 to 0.52 μg/kg dry weight for TON, AR, and BS sediments, respectively. In comparing the MDL values for both methods in TON sediment, the SPE method had slightly lower MDL values except for fipronil, which were 0.30 and 0.17 μg/kg dry weight for SPE and GPC, respectively. For the optimized SPE method, MDLs were higher for all compounds in BS sediment, most likely due to the low mass of sediment extracted compared to the other two sediments. Since BS sediment contained 80% moisture, a total of approximately 3–4 g dry weight was extracted as opposed to approximately 10 g dry weight for TON and AR sediment. Although the spiked concentration was 1 μg/kg dry weight in all sediments, the overall extracted amount was lower for BS sediment; therefore, any loss during extraction or cleanup will be more evident. In addition, quantifying lower extract concentrations, especially those approaching detection limits, typically increases variability amongst replicates. Since the MDL calculation takes into consideration the standard deviation or variability amongst replicates, the MDL will consequently also increase with increasing variability, thus the higher MDL values for BS sediment. Again, fipronil-sulfone in BS sediment had the highest MDL value of 0.52 μg/kg dry weight, which could be a result of the lower response factor of the compounds and difficulty with quantification. The MDL values ranging from 0.12 to 0.52 μg/kg dry weight in the current study are in accord with the lower range of published MDL values for fipronil, fipronil-sulfide, and fipronil-sulfone in soils and sediments of 0.13–9.0 μg/kg dry weight [11,13–15,29].

The optimized SPE method was also used to analyze field samples from urban sites in central Texas, which potentially contain fipronil and its degradation products. Out of the 10 sediments, fipronil, fipronil-sulfide, and fipronil-sulfone were detected in all of the sediment samples. However, only half of the sediments contained fipronil, fipronil-sulfide, or fipronil-sulfone above reporting limits, with all three compounds detected in only one sediment sample (Table 4). The reporting limit was calculated as three times the MDL, which was the average of all three sediment types.

Table 3
Method detection limits (MDL) for fipronil, fipronil-sulfide, and fipronil-sulfone for the cleanup methods using gel permeation chromatography (GPC) and solid phase extraction (SPE) with primary secondary amines/ graphitized carbon black cartridge in sediment from Touch of Nature, IL (TON), American River, CA (AR) and Bear Skin Lake, MN (BS).

Compound	MDL (μg/kg dry weight)				
	GPC	SPE			
	TON	TON	AR	BS	Method[a]
Fipronil	0.17	0.3	0.32	0.44	0.44
Fipronil-sulfide	0.21	0.12	0.23	0.32	0.32
Fipronil-sulfone	0.18	0.16	0.22	0.52	0.52

[a] The MDL for the SPE cleanup method across sediments. It was the maximum MDL amongst sediments.

Table 4
Field validation of the optimized method. All values are μg/kg dry weight with reporting limits being calculated as three times the average method detection limit (of three sediment types).

Sample	Fipronil	Fipronil-sulfide	Fipronil-sulfone
1	<RL	<RL	<RL
2	<RL	<RL	<RL
3	<RL	1.78	<RL
4	<RL	1.20	1.51
5	<RL	0.824	<RL
6	1.33	3.52	0.997
7	<RL	0.903	<RL
8	<RL	<RL	<RL
9	<RL	<RL	<RL
10	<RL	<RL	<RL

<RL = below reporting limits.
Reporting limits for fipronil, fipronil-sulfone, and fipronil-sulfide are 1.05, 0.674, and 0.885 μg/kg.

4. Conclusions

Cleanup methods using GPC and SPE have been optimized and comparatively evaluated for analyzing fipronil, fipronil-sulfide, and fipronil-sulfone at sub-ppb concentrations in sediment. The MDL values ranged from 0.12 to 0.52 μg/kg dry weight. Both methods resulted in MDL values similar to the lowest reported values for fipronil and its degradation products, with decreased sample preparation times and solvent usage for the SPE cleanup. The labor-intensive cleanup and cost associated with GPC minimizes its appeal compared to SPE. Automation of GPC and fraction collecting would reduce hands-on sample cleanup, but it would still require substantial volumes of solvent that would have to be disposed of as waste. Ultimately, both cleanup techniques were shown to be effective for analyzing fipronil and its degradation products; however, preference is given to SPE.

Acknowledgment

The authors thank Rebecca Kelley for her help with sample processing.

References

[1] B.J. Konwick, A.T. Fisk, A.W. Garrison, J.K. Avants, M.C. Black, Environ. Toxicol. Chem. 24 (2005) 2350.
[2] J.D. Maul, A.A. Brennan, A.D. Harwood, M.J. Lydy, Environ. Toxicol. Chem. 27 (2008) 2582.

[3] D. Schlenk, D.B. Huggett, J. Allgood, E. Bennett, J. Rimoldi, A.B. Beeler, D. Block, A.W. Holder, R. Hovinga, P. Bedient, Arch. Environ. Contam. Toxicol. 41 (2001) 325.
[4] U.S. Environmental Protection Agency, EPA/737/F-96/005, 1996.
[5] E. Mesléard, S. Garhero, N. Beck, E. Rosecchi, C. R. Biol. 328 (2005) 955.
[6] M.T. Moore, R.E. Lizotte Jr., C.M. Cooper, S. Smith Jr., S.S. Knight, Bull. Environ. Contam. Toxicol. 72 (2004) 777.
[7] D.K. Demcheck, S.C. Skrobialowski, U.S. Geological Survey, FS-010-03, 2003.
[8] A.S. Gunasekara, T. Truong, K.S. Goh, F. Spurlock, R.S. Tjeerdema, J. Pestic. Sci. 32 (2007) 189.
[9] K. Lin, D. Haver, L. Oki, J. Gan, J. Agric. Food Chem. 56 (2008) 8594.
[10] J.L. Vílchez, A. Prieto, L. Araujo, A. Navalón, J. Chromatogr. A 919 (2001) 215.
[11] E.P. Hintzen, M.J. Lydy, J.B. Belden, Environ. Poll. 157 (2009) 110.
[12] A. Bobé, J. Cooper, C.M. Coste, M. Muller, J. Pestic. Sci. 52 (1998) 275.
[13] A. Bobé, P. Meallier, J. Copper, C.M. Coste, J. Agric. Food Chem. 46 (1998) 2834.
[14] W.J. Jones, C.S. Mazur, J.F. Kenneke, A.W. Garrison, Environ. Sci. Technol. 41 (2007) 8301.
[15] Z. Pei, L. Yitong, L. Baofeng, J.J. Gan, Chemosphere 57 (2004) 1691.
[16] G. Ying, R. Kookana, Aust. J. Soil Res. 40 (2002) 1095.
[17] M. Raveton, A. Aajoud, J. Willison, M. Cherifi, M. Tissut, P. Ravanel, Chemosphere 69 (2007) 1124.
[18] U.S. Environmental Protection Agency, EPA/600/R-99/064, 2000.
[19] J. You, D.P. Weston, M.J. Lydy, in: J. Gan, F. Spurlock, P. Hendley, D. Weston (Eds.), Synthetic Pyrethroids: Occurrence and Behavior in Aquatic Environments, American Chemical Society, Washington, DC, 2008, pp. 87–113.
[20] Y. He, Y. Liu, Chromatographia 65 (2007) 581.
[21] O. Shimelis, Y. Yang, K. Stenerson, T. Kaneko, M. Ye, J. Chromatogr. A 1165 (2007) 18.
[22] E. van Handel, J. Am. Mosq. Control Assoc. 1 (1985) 302.
[23] S.J. Lehotay, C.H. Lee, J. Chromatogr. A 785 (1997) 313.
[24] Y. Saito, S. Kodama, A. Matsunaga, J. Yamamoto, J. AOAC Int. 87 (2004) 1356.
[25] F.J. Schenck, S.J. Lehotay, J. Chromatogr. A 868 (2000) 51.
[26] F.J. Schenck, S.J. Lehotay, V. Vega, J. Sep. Sci. 25 (2002) 883.
[27] U.S. Environmental Protection Agency, EPA/620/R-96/001, 1996.
[28] U.S. Environmental Protection Agency, Federal Register 68 (2003) 11770.
[29] H. Fenet, E. Beltran, B. Gadji, J.F. Cooper, C.M. Coste, J. Agric. Food Chem. 49 (2001) 1293.

Talanta 78 (2009) 1352–1358

Contents lists available at ScienceDirect

Talanta

journal homepage: www.elsevier.com/locate/talanta

Enantioselective recognition of alanine in solution with modified gold electrodes using chiral PAMAM dendrimers G4.0

E. Bustos[a,b,*], J.E. García[a], Y. Bandala[a], Luis A. Godínez[b], E. Juaristi[a]

[a] Chemistry Department, Centro de Investigación y de Estudios Avanzados del Instituto Politécnico Nacional, P.O. Box 14-740, C.P. 07000 México, D.F., Mexico
[b] Electrochemistry Department, Centro de Investigación y Desarrollo Tecnológico en Electroquímica S.C., P.O. Box 064, C.P. 76700, Pedro Escobedo, Querétaro, Mexico

ARTICLE INFO

Article history:
Received 12 January 2009
Received in revised form 4 February 2009
Accepted 6 February 2009
Available online 20 February 2009

Keywords:
Enantioselective recognition
Chiral surfaces
Alanine
PAMAM dendrimers

ABSTRACT

Enantiomeric alanine was covalently grafted onto modified gold electrodes with mercaptopropionic acid and PAMAM dendrimers G4.0 with amine terminal groups. Cyclic voltammetric experiments in the presence of monocarboxylic ferrocene as a probe molecule proved that the alanine (Ala) was immobilized as a monolayer on the gold electrodes. Electron transfer to $Ru(NH_3)_6Cl_3$ in solutions of different pH was studied by cyclic voltammetry (CV). Changes in solution pH resulted in the variation of the charge state of the terminal group and surface p*K*a values were estimated on the basis of these results. Because of electrostatic interactions between the positive charged groups on the electrode surface and the Ala, enantioselective recognition was possible. The interaction between enantiomers can be proven with molecular simulation. The electro-oxidation peak current was linearly dependent on Ala concentration over the range 0–10 μM with slopes between 143 and 187 $\mu A\,cm^{-2}/\mu M$. The detection limit (3σ) was 0.4059 μM for PAMAM G4.0-D(+)Ala–L(−)Ala and 0.4172 μM for PAMAM G4.0-L(−)Ala–D(+)Ala.

1. Introduction

Many biomolecules are chiral in that they can exist in one of two enantiomeric forms that only differ in their structures with chiral auxiliaries of non-super-imposable mirror images of each other. Since only one enantiomer tends to be physiologically active while the other is inactive or even toxic, pharmaceutical compounds are increasingly produced in an enantiomerically pure form using chiral separations, salt resolutions, asymmetric syntheses involving solution-phase homogeneous catalysts and enzymes [1]. Chiral surfaces offer the possibility of developing heterogeneous enantioselective catalysts that can be readily separated from products and reused. In addition, such surfaces might serve as electrochemical sensors for chiral molecules. To date, chiral surfaces have been obtained by slicing single crystals so that they exhibit high-index faces or adsorbing chiral molecules, and some of these surfaces act as enantioselective heterogeneous catalysts [2–5].

For chiral electrode reactions, electrodes with an ordered atomic or molecular arrangement with chirality are expected to exhibit enantioselectivity, as reported for metal (Pt and Au) and oxide (CuO) surfaces with a chiral crystallographic orientation. As for achiral single-crystal surfaces, the modification with chiral molecules was reported to bring about an ordered molecular arrangement with two-dimensional chirality. For these surfaces, enantioselectivity is expected to appear not simply from a one-to-one interaction between the modifier and the analyte molecules but also from nanosized spaces formed by the molecular arrangement of the modifier on the surface [6].

Previous investigations have been reported on the construction and characterization of enantioselectivity of the SAM of homocysteine (Hcy), formed on a (1 1 1)-oriented gold surface and the redox behavior of 3,4-dihydroxyphenylalanine (DOPA), which is an electrochemically active chiral molecule. These investigations used cyclic voltammetry (CV) to analyze a gold electrode modified with one of the two enantiomeric forms of Hcy. The results indicate the importance of nanosized chiral spaces on the enantioselective site [6].

In addition, molecular recognition by synthetic receptors is an important area of research in the fields of supramolecular and bioorganic chemistry [7]. It is possible, by varying the molecular architecture of the kinked surface, to tailor the electrocatalytic properties of the electrode in a systematic way. However, in organic chemistry it is more common to change the stereocenter of the organic molecule and then to measure changes in reactivity and chiral discrimination to understand reaction mechanisms [8]. In this regard, dendrimers, which are highly branched, fractal-like macromolecules of defined three-dimensional size, shape and topology, can be prepared with extremely narrow molecular weight distribution [9]. Dendrimer chemistry is now occupying a unique position not only in polymer and materials chemistry, but also in various

* Corresponding author at: Centro de Investigación y de Estudios Avanzados del Instituto Politécnico Nacional, Chemistry Department, P.O. Box 14-740, 07000 México, D.F., Mexico. Tel.: +52 442 211 6059; fax: +52 442 211 6007.
E-mail addresses: ebustos@cideteq.mx, ebb2008@yahoo.com (E. Bustos).

0039-9140/$ – see front matter © 2009 Elsevier B.V. All rights reserved.
doi:10.1016/j.talanta.2009.02.010

medical and pharmaceutical areas, in particular for electrochemical interfaces [10]. The introduction of chirality into a dendritic structure will create a non-spherical, asymmetric macromolecule having a chiral surface environment with internal chiral cavities. The external functional groups residing on the chiral surface domain can act as chiral exo-receptors while the internal chiral voids may function as chiral endo-receptors. Chiral dendrimers are therefore potentially useful materials in measuring chiral recognition and enantioselective binding of guest molecules [11], their effect is better with high generations as 4.0 by their major quantity of functional groups to support the chirality effect.

In electrochemistry when there is electrochemically inactive species in the interface, it is necessary to use a probe molecule which can provide a way to detect and measure an electronic transfer. In this way, the chiral recognition can be tracked by monitoring the current change in an electrochemical system with high selectivity between two enantiomeric amino acids such as D(+) and L(−)Ala. The recognition performance can be quantitatively evaluated through the decrease of current in amperometric titrations in the presence of the probe molecule, as a result of the blocking of the electron transfer and thus providing the enantiomeric recognition at the interface.

With this precedent, our work presents the construction and characterization of a new kind of enantioselective modified gold electrodes with chiral PAMAM dendrimers. These electrodes detect enantiomers of alanine in solution.

2. Experimental

Starburst™ PAMAM® Generation 4.0 (PG4) dendrimers (bearing 64 terminal $-NH_2$ groups), enantiomeric and racemic alanine (Ala), $HS(CH_2)_2COOH$ (3-mercaptopropionic acid, MPA), 1-(3-dimethylamino)propyl)-3-ethylcarbodiimide hydrochloride (EDC), L(−)Ala-Fmoc, acetic anhydride (AA), diisopropiletanolamine (DIPEA) and pyperidine of the best commercially available quality were all obtained from Aldrich and used without further purification. Analytical grade ferrocene monocarboxylate (FcMC) and $Ru(NH_3)_6Cl_3$ were obtained from Strem Chemicals. Electrolytic solutions were prepared from analytical-grade KCl, KH_2PO_4 and Na_2HPO_4. The solvents H_2SO_4, MeOH and DMF, isopropilic alcohol (IPA) and CH_2Cl_2 (DCM), HPLC grade were obtained from J.T. Baker. All aqueous solutions were prepared with deionized water (ρ = 18 MΩ cm) and further deoxygenated by bubbling N_2 through the solution (Praxair, grade 5.0).

The electrochemical experiments reported in this work were performed using a BAS Epsilon™ potentiostat from Bioanalytical Systems, Inc. The cyclic voltammetry experiments were performed at 298 K in a 10-mL BAS cell equipped with a gold-bead working electrode, a platinum counter electrode and an Ag/AgCl (3 M NaCl) reference electrode. Before the CV experiments were carried out, the electrolytic solutions were deoxygenated by bubbling ultrapure nitrogen (PRAXAIR, grade 5.0) for at least 10 min, and during electrochemical experiments N_2 was gently blown over the solution surface.

Gold bead electrodes were prepared as previously described in the literature [12] by melting the tip of a Au wire (99.999%, 1.0 mm diameter, Premion® from Alfa) using a gas burner obtained from Flamineta to form a gold sphere (Fig. 1A). For characterization purposes, these spherical gold bead electrodes were immersed in 0.5 mM $Ru(NH_3)_6Cl_3$ solutions with a phosphate buffer pH of 7 (I = 0.1), and the geometric area was computed from the CV response of the reversible couple at different scan rates using the Randles–Sevcik equation. The geometric area thus computed (around $0.02 \pm 0.005\ cm^2$) was considered to be the actual area, since electrodes prepared in this way have been reported to have roughness factors close to unity. Electrodes which had distorted signals for the Ru redox process during the area calculation experiments were regenerated by reintroducing them into a flame and subsequently thoroughly rinsed with water until a satisfactory CV response was obtained. Electrodes that after a two cleaning cycles did not show a clean capacitive region nor a clearly reversible Ru(III)|Ru(II) electrochemical signal ($\Delta E_p \cong 60$ mV, $I_{pc}/I_{pa} \cong 1$) were discarded.

Fourier Transform Infrared with Attenuated Transmittance Reflection (FTIR-ATR) measurements were performed using a PerkinElmer FTIR System, Spectrum GX Spectrometer equipped with an ATR accessory and using the program version v3.02. All spectra consisted of an average of 250 individual scans with 6 cm^{-1} resolution and a gap of 1 cm^{-1}. All measurements were made at 298 K with a ZnSe window.

The protection of the dendrimer with L(−)Ala-Fmoc over the PG4 modified surface was made with 5 eq. L(−)Ala-Fmoc and 5 eq. EDC in DMF for 24 h. After this modification, the surfaces were washed twice with DMF, IPA and DCM. Later, to be sure of the protection, the surfaces were dipped three times for 15 min in a solution with 10% AA and 20% DIPEA in DMF and then washed with DMF, IPA and DCM (Fig. 1E). To deprotect the PG4–L(−)Ala on the surface, the electrodes were dipped two times for 10 min in 25% pypepiridine

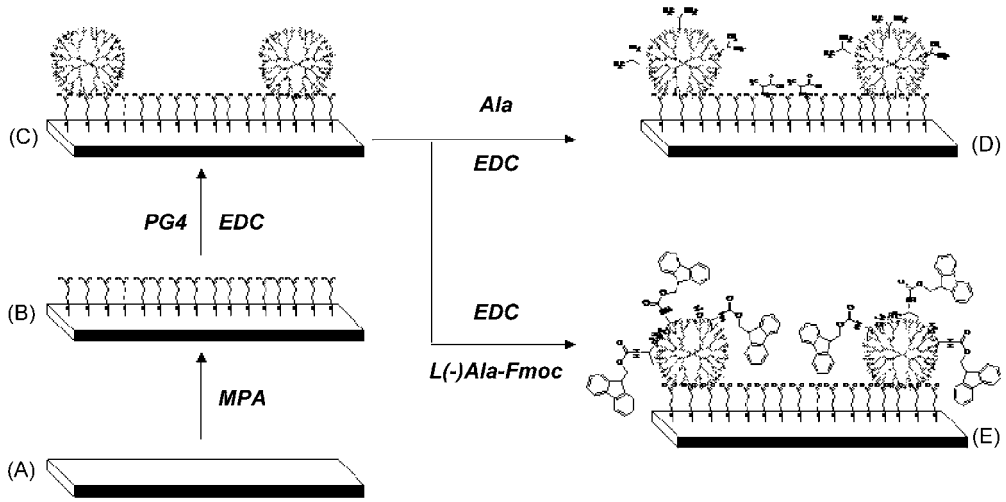

Fig. 1. Schematic representation of gold electrodes (A) modified with MPA (B), PG4 (C), Ala (D) and L(−)Ala-Fmoc (E) in MeOH.

in DMF and after each dipping were washed with DMF, IPA and DCM (Fig. 1D) [13].

The theoretical molecular modeling was carried out using a Gaussian 03 program revision C.02 [14] with the *ab initio* method of Hartree-Fock in a 3-21G level (HF 3-21G). Energy data were obtained to define the geometry of the conformers with a frequency analysis of each interaction with local minimization.

3. Results and discussion

The preparation of the modified gold bead electrodes (Fig. 1A) was made by immersing the electrodes overnight in a 1.0 mM solution of mercaptocarboxylic acid in methanol (Fig. 1B). This built $S(CH_2)_2COOH$ sub-monolayers (1.60×10^{-10} mol cm^{-2}) [12,15] with a negative charged at neutral pH due to the partial deprotonation of the exposed COOH groups.

Later, the thioled surfaces were modified with 21.06 μM PG4 in presence of 5 mM EDC in MeOH to construct the covalent modification (Fig. 1C) [12]. At a neutral pH the dendrimers presented a protonated interface by virtue of the p*K*a of the peripheral functional groups ($-NH_3^+/-NH_2$, p*K*a 9.52) [16].

To prepare the chiral surface once the PG4 was attached to the gold bead, 10 mM D(+) and L(−) were added to the dendrimer with 10 mM EDC and left standing overnight (Fig. 1D). When the alanine was added, a voltammetric titration with ferrocene monocarboxylate (FcMC) was conducted (Fig. 2). The magnitude of anodic current density increased with increasing Ala concentration and in all cases, the current density tended to be saturated at an Ala concentration higher than 1 mM. The current densities for Au (Fig. 2A) were higher than for the modified surfaces with enantiomers of alanine. Specifically in the case of Au–MPA–PG4–D(+)Ala (Fig. 2C) the densities tended to be somewhat lower than those for Au–MPA–PG4–L(−)Ala (Fig. 2B), tendency observed in the literature [6].

The fact that the system reaches a limiting current density is consistent with the voltammetric response at these low concentrations arising from FcMC units held at the electrode surface. The limiting *j* value in the plot of Fig. 2 corresponds to surface coverage values (Γ) of a monolayer of 4.99 and 5.34×10^{-10} mol cm^{-2} for the enantiomers D(+)Ala and L(−)Ala respectively. The values of Γ were obtained by integrating the current observed in the cathodic peak of each of the cyclic voltammograms at 1 mM FcMC as shown in Fig. 2 [$\Gamma = \Gamma(\int idt/fnFA) = Q/fnFA$ where Q is the charge in coulombs, f is the roughness factor (1.1), n is the number of electrons

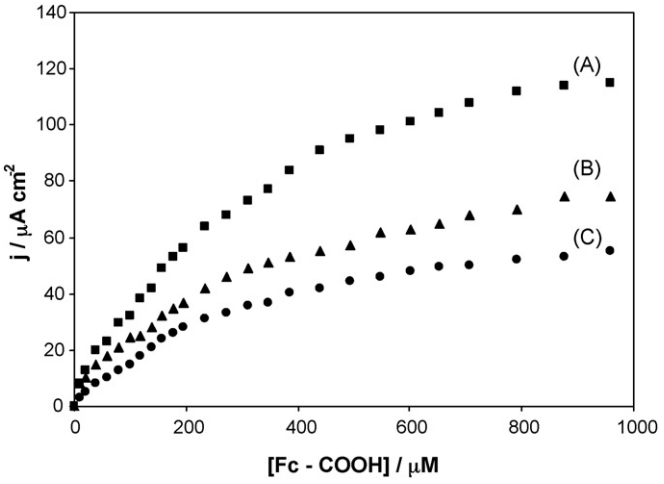

Fig. 2. Graph of the dependence of the measured ferrocene concentration on the monomeric ferrocenium subunit in the solution. The data were obtained with a Au (A), Au–MPA–PG4–L(−)Ala (B) and Au–MPA–PG4–D(+)Ala (C) electrode immersed in 0.5 M KCl solution containing variable ferrocene concentration.

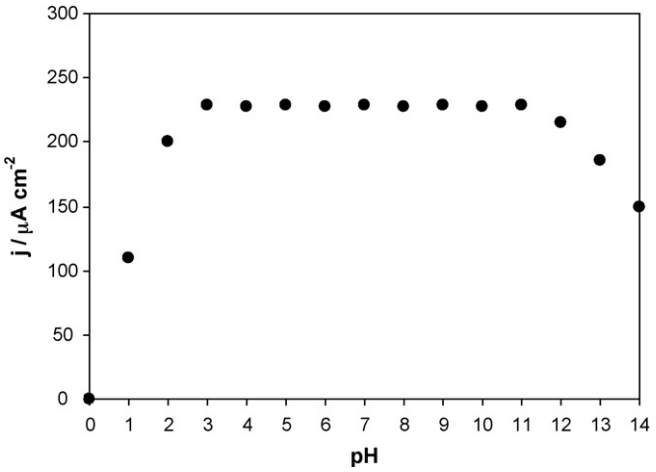

Fig. 3. Graph of the pH dependence of the cathodic peak current observed on a Au–MPA–PG4–L(−)Ala electrode immersed in a 1 mM ferrocene solution also containing 0.5 M KCl. The pH was adjusted by additions of HCl or KOH.

involved in the process ($FcMC^+ + 1e^- \rightarrow FcMC$), *F* is the Faraday constant (96,485 C mol^{-1}), and *A* is the geometric area of the working electrode in cm^{-2}] [15].

To verify the monolayer-solution interface of Au–MPA–PG4–Ala, the ferrocene was used as probe molecule which redox behavior depends on the state of protonation of the monolayer $-NH_3^+$ groups of the PG4–Ala. In this manner, the modified electrode was dipped in a solution with the limiting concentration of ferrocene (1 mM) of 0.5 M KCl with different pH values (Fig. 3), and the voltammetric reduction of the ferrocene was recorded. The shape of the graph shows two slope changes (2.26 and 11.40) which probably correspond to the p*K*a of interfacial Ala and not to the FcMC in solution

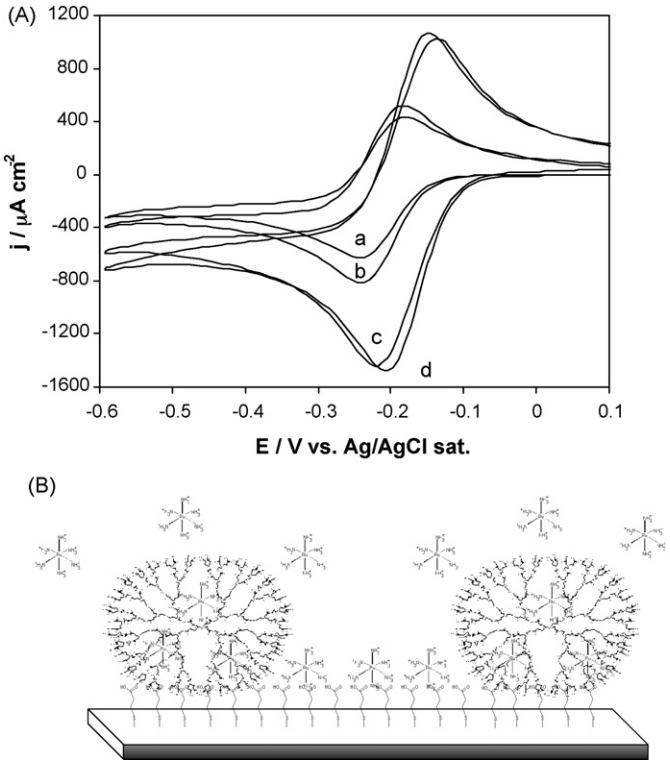

Fig. 4. (A) Comparative cyclic voltammograms of Au (a), Au–MPA (b), Au–MPA–PG4 (c) and Au–MPA–PG4–L(−)Ala (d), in 0.5 M KCl with 10 mM $Ru(NH_3)_6^{3+/2+}$, at 0.100 V s^{-1} and 278 K. (B) Representative scheme of the interaction of ruthenium over the modified covalent surface.

(p*K*a of 4.2) [17], because these values are similar those for Ala in solution (2.3 to $-COO^-|-COOH$, and 10.5 to $-NH_3^+|-NH_2$) [18–19]. This behavior indicates that at neutral conditions, some fraction of Ala in solution interacts with the surface of dendrimer across the negative charged carboxylic groups, and the rest of the Ala solution reacts with the thiols over the surface of the gold beads with the amine groups (Fig. 1D).

On other hand, using a different probe molecule, positively charged, at a relatively high concentration (10 mM) of $Ru(NH_3)_6^{3+/2+}$ in 0.5 M KCl, the gold surface (Fig. 4A-a) proved to be the interface with the lowest current density. When the thiols were used to verify the electrochemical response (Fig. 4A-b), *j* increased as a consequence of the negative charge present on the surface whose attracts the positive charge of the ruthenium in solution. The surface with dendrimers (Fig. 4A-c) showed the highest *j* because, even though the dendrimers have a positive charge in their periphery and should reject the Ru^+ ions, they concentrate the probe molecule in the interface (Fig. 4B) in their empty sites. When the covalent alanine was added to the dendrimer (Fig. 4A-d), the alanine gave a positive charge proportional to the concentration of dendrimer. For this reason the intensity of the current was similar to that without Ala (Fig. 4A-c).

To verify the mechanical resistance and stability of covalent modified surfaces with dendrimers, the surfaces were probed with constant stirring. Mechanical resistance was corroborated when the thiolated surface was modified with PG4–L(−)Ala without EDC in 0.5 M KCl (electrostatic modification, Fig. 5A-a). When this surface was examined in electrochemical experiments with $Ru(NH_3)_6^{3+/2+}$ with stirring, the voltammetry response decreased in current density and potential of peaks (Fig. 5A-b). By contrast, when the thiolated surface was modified with PG4–L(−)Ala and EDC in methanol, the electrochemical response of ruthenium before and after stirring did not change (Fig. 5B-a and B-b). This observation confirms the resistance to stirring following covalent modification.

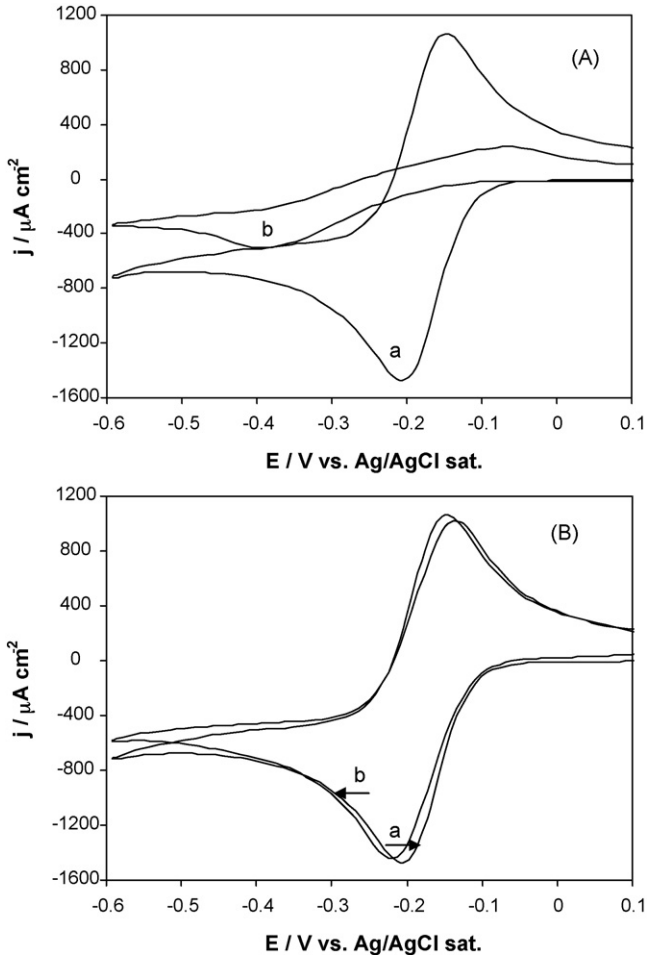

Fig. 5. Cyclic voltammetries of Au–MPA–PG4–L(−)Ala modified in electrostatic (A) or covalent (B) manner; before (a) and after (b) stirring at 900 rmp. The solution contained 0.5 M KCl with 10 mM $Ru(NH_3)_6^{3+/2+}$. Experiments developed at 0.100 V s^{-1} and 278 K.

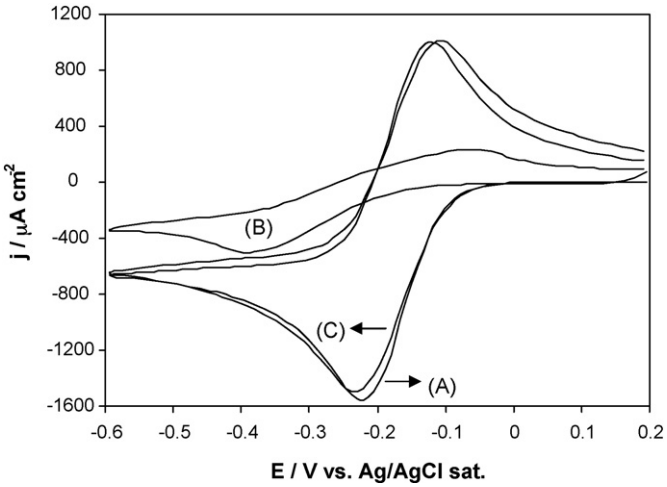

Fig. 6. Cyclic voltammetries of Au–MPAvPG4–L(−)Ala (A), protected with Fmoc (B) and deprotect (C) in 0.5 M KCl with 10 mM $Ru(NH_3)_6^{3+/2+}$ at 0.100 V s^{-1} and 278 K.

The presence of alanine on the dendrimer surface was also verified by a control experiment in which the protection consisting of L(−)Ala-Fmoc (Fig. 1E) was carried out with Fmoc. The surfaces in this case were used to obtain a CV of ruthenium (Fig. 6B), observing a decrease of the current density of the Ru signal and a change of the potential peak, providing a quasi-reversible system by the slow current transfer across the interface in the presence of the protection group Fmoc. In contrast, when the Fmoc group was removed from the interface, the voltammetry of Ru (Fig. 6C) was similar to that obtained when the dendrimer was modified with Ala without the protection group (Fig. 6A) [20]. This result confirms that there is not dendrimer blocking.

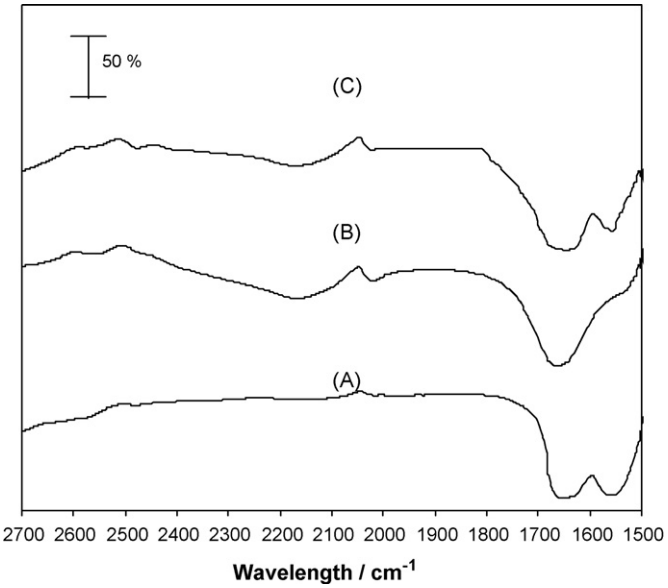

Fig. 7. Spectra of FTIR-ATR of: PG4 (A), L(−)Ala (B) and dialyzed solution of PG4–EDC–L(−)Ala (C), in MeOH. The reference was made with MeOH.

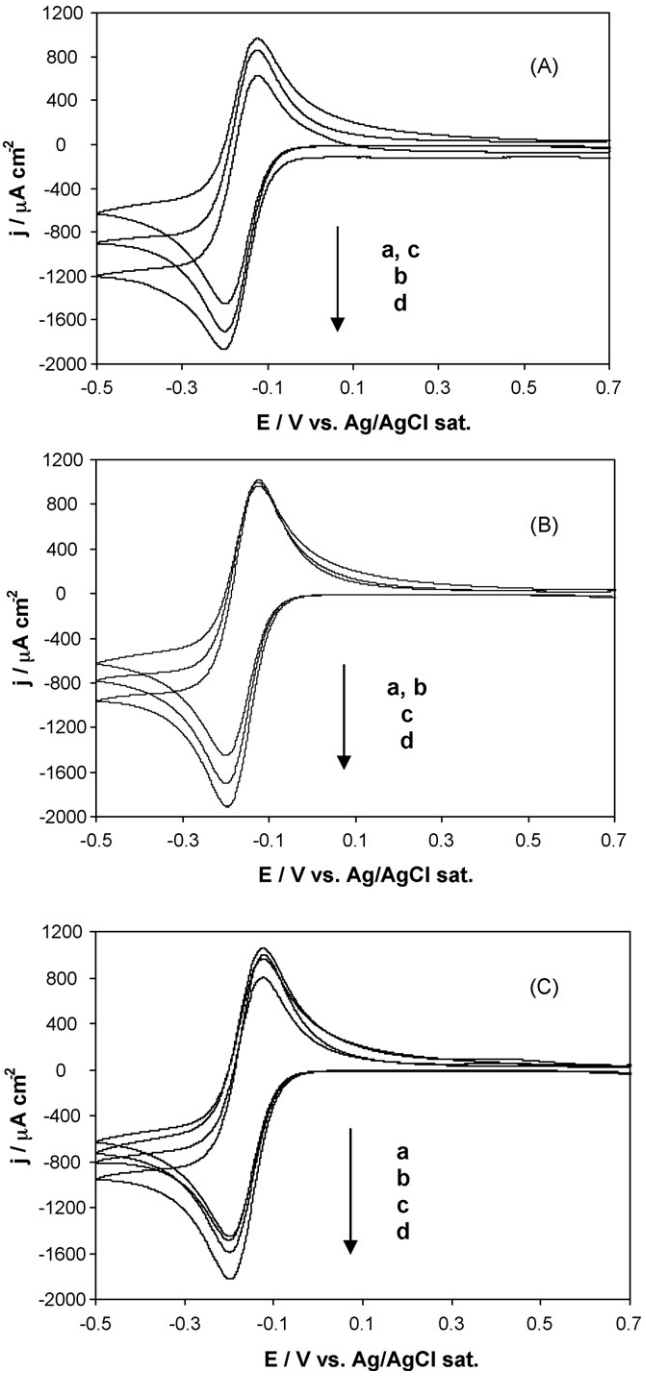

Fig. 8. Cyclic voltammetries of Au–MPA–PG4 and D(+)Ala (A), L(−)Ala (B) or DL-Ala (C), in 0.5 M KCl at 0.100 V s^{-1} and 278 K, in different solutions of 10 mM $Ru(NH_3)_6^{3+/2+}$ (a) containing 10 mM of: (b) D(+)Ala, (c) L(−)Ala or also (d) DL-Ala.

In addition, the interaction of PG4–Ala was corroborated with the technique of FTIR-ATR (Fig. 7), using a saturated solution of PG4 (A) and L(−)Ala (B). These spectra were compared with the spectrum obtained from dialyzed saturated solution of PG4–EDC–L(−)Ala (C) between 2500 and 1700 cm^{-1}, which was similar to that obtained from the solution with D(+)Ala. The spectrum of the solution of PG4–EDC–L(−)Ala (Fig. 7C) showed the characteristic bands of PG4 at 1660 and 1570 cm^{-1} which correspond to the amide I and amide II respectively [21–22]. In addition, bands at 2590, 2480, 2180 and 2030 cm^{-1} resulted from the vibration of the methylene groups of alanine [21–22]. This observation corroborated the correct covalent modification of dendrimer with alanine in the presence of the reducing agent (EDC), the excess of which was eliminated during the dialysis process.

The electrochemical technique of cyclic voltammetry is particularly sensitive to changes in the locally charged states of different surface regions. Thus, disturbance of these surface sites as a consequence of chemical reaction may readily be verified [8]. The usual way to demonstrate the enantioselective recognition is with the modification of the PG4 surface with D(+)Ala, L(−)Ala or DL-Ala. Each of these surfaces was examined by measurement of the ruthenium signal by CV in the presence of the different enantiomers of Ala and the racemic mix (Fig. 8). One way to prove the recognition of the enantiomers is by examination of the potential or current density peak changes. In all cases, there were no changes in the potential peak because there was no change in energy. Nevertheless, there were changes in current density caused by changes in interfacial concentrations of probe molecules when there is blocking by the Ala positioned at the interface by enantiomeric recognition. This situation was observed when D(+)Ala or L(−)Ala (Fig. 8A and B, respectively) were used. In the case of the DL-Ala, there was not a specific recognition (Fig. 8C).

In this way, an enantioselective recognition resulted in a current density decrease that was similar to the intensity observed by

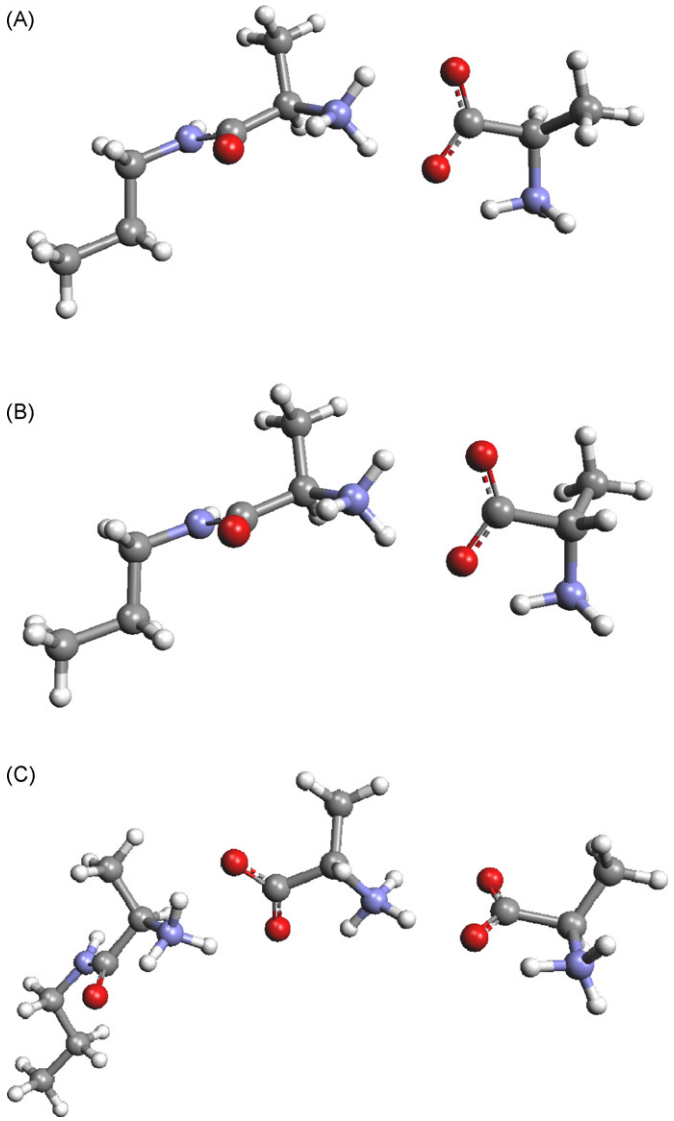

Fig. 9. Molecular representation of the interaction in linear manner between Au–MPA–PG4–D(+)Ala with D(+)Ala (A), L(−)Ala (B) and DL-Ala (C) in solution.

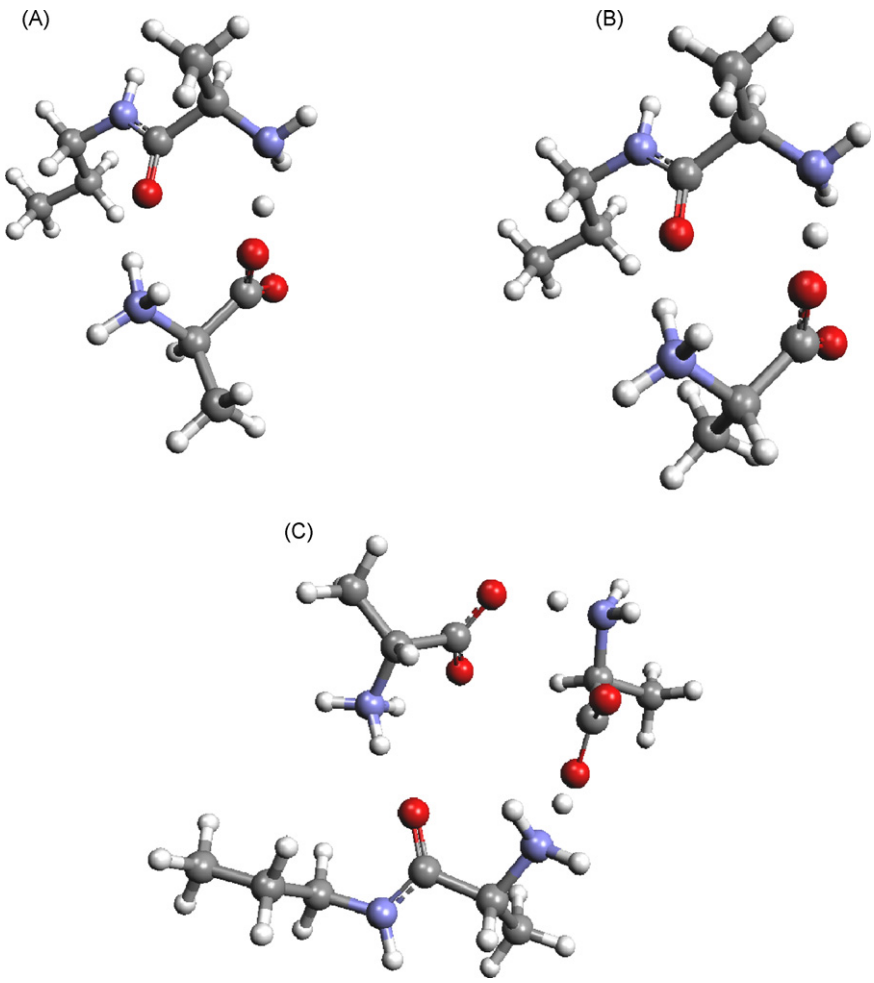

Fig. 10. Molecular representation of the interaction in non-linear manner between Au–MPA–PG4–D(+)Ala with D(+)Ala (A), L(−)Ala (B) and DL-Ala (C) in solution.

probe molecules over the Au–MPA–PG4 surface (Fig. 8a). This was the case for D(+)Ala–L(−)Ala and L(−)Ala–D(+)Ala, Fig. 8A-c and B-b respectively, as a consequence of the presence of an enantiomeric complex which allows the entrance of the same concentration of probe molecules as without the complex. Although the difference in the current density is not much, the electrochemical signals were reproducible. On the other hand, when there is no recognition, the value of *j* increased in comparison with a reference surface (with only PG4, Fig. 8a), as in the case of: D(+)Ala–D(+)Ala and L(−)Ala–L(−)Ala, Fig. 8A-b and B-c respectively. This observation suggests the lack of formation of an interfacial complex and an increase of the interfacial pre-concentration of ruthenium.

When the DL-Ala was present in solution, the value of *j* of the ruthenium signal was the highest in comparison to the signals generated with D(+)Ala and L(−)Ala (Fig. 8A-d and B-d respectively). This behavior is most likely a consequence of the interaction of the enantiomers in solution and the absence of blocking on the surface, allowing for an easier access of ruthenium to transfer charge over the surface.

The recognition effect was evaluated with a molecular simulation of a fragment of dendrimer with a covalent modification of amine acid (D- or L-Ala) and its possible interaction in a non covalent state with other fragments of amine acid in a isolated state and in a racemic mix in solution using a Gaussian 03 program [14] for the optimization process and frequencies analysis. For these models, two kinds of interactions between the surface-Ala and the Ala in solution were proposed: linear interaction (coordination by only one site, Fig. 9) and non-linear (coordination by two sites, Fig. 10), where the conformers obtained were of a minimum energy for the D(+) and L(−)Ala joined to an arm of dendrimer.

In the case of the non-linear interaction, in all cases it was necessary to elongate the N–H link (NH_3 terminal, fragment of dendrimer-Ala) to stabilize the non-linear arrangement (Fig. 10). In contrast, with the linear interaction (Fig. 9) the molecules preserved the linear arrangement. The elongation made in the case of the racemic mix (Fig. 10C) showed a significant conformational difference through the blocking of the positive charge of the amine terminal of the dendrimer-Ala fragment. Since linear conformance was not present, it was more favorable to transfer the positive charge of the ruthenium molecule across the interface, which increased the current density in the voltammetric analysis (Fig. 8A-d and B-d).

Table 1
Electroanalytical data for the enantiomeric recognition using 10 mM of $Ru(NH_3)_6^{3+/2+}$ reduction at 0.100 V s^{-1} with the different substrates considered in this study, in 0.5 M KCl at 298 K.

Substrate	Linear equation	R^2	D.L. (μM)	Q.L. (μM)
D(+)Ala–D(+)Ala	$Y = 171.84x - 28.545$	0.9955	0.3489	0.1746
D(+)Ala–L(−)Ala	$Y = 147.73x - 11.545$	0.9964	0.4059	0.2031
D(+)Ala–DL-Ala	$Y = 187.27x + 24.545$	0.9974	0.3202	0.1602
L(−)Ala–D(+)Ala	$Y = 143.73x + 24.909$	0.9980	0.4172	0.2087
L(−)Ala–L(−)Ala	$Y = 165.23x + 49.50$	0.9964	0.3629	0.1816
L(−)Ala–DL-Ala	$Y = 182.45x + 52.727$	0.9976	0.3286	0.1644

Finally, to apply the alanine to these kind of surfaces, a voltammetric titration was conducted with a constant concentration of $Ru^{3+/2+}$ (10 mM) and different concentrations of D(+)Ala and L(−)Ala. The linear behavior observed in all the curves presented suggests that passivation effects on the electrode surfaces studied are essentially absent in the Ala concentration range explored. In addition, improved detection and quantification limits (D.L. = $3\sigma/m$ and Q.L. = $10\sigma/m$, respectively, where σ is the standard deviation of the data points and m is the slope of the linear relationship) [12] can be attained using the modified surfaces. The enantioselective recognition was evident with the highest D.L. and Q.L. in the presence of D(+)Ala–L(−)Ala and vice versa. This is corroborated in Table 1 which shows that the recognition was practically the same. The use of these materials is a potentially important new source of materials for electroanalytical applications.

4. Conclusions

This work demonstrates a new kind of enantioselective surface based on dendrimers and amino acids as alanine. These were characterized by cyclic voltammetry in the presence of ferrocene monocarboxylate and hexamine ruthenium as probe molecules. From the voltammetric response the enantioselective recognition was evaluated by assessing the blocking of the charger transfer of probe molecules. The resulting decrease of current in the electrochemical signal demonstrated the importance of nanosized chiral spaces on the enantioselective site.

Although there was not a significant difference in the slope of the calibration curves, this is the first report about the modification of the dendrimer Ala to be used on enantioselective surfaces of amino acids.

Acknowledgements

The authors wish to thank the Mexican Council for Science and Technology for the financial support of this work, and Walter Meyer, Peace Corps volunteer at CIDETEQ for his English revision of this manuscript. Y.S. also would like to acknowledge CONACyT for his graduate fellowship. E.B. acknowledges CINVESTAV-IPN for their financial support of her post-doctorate position.

References

[1] E. Juaristi, Introduction to Stereochemistry and Conformational Analysis, Wiley, New York, 1991.
[2] J.A. Switzer, H.M. Kothari, P. Poizot, Sh. Nakanishi, E.W. Bohannan, Nature 425 (2003) 490.
[3] R. Raval, C.J. Baddeley, C. Muryn, M.O. Lorenzo, Nature 404 (2000) 376.
[4] A.F. Carley, M.K. Rajumon, M.W. Roberts, P.B. Wells, J. Chem. Soc., Faraday Trans. 91 (1995) 2167.
[5] A. Martins, V. Ferreira, A. Queirós, I. Aroso, F. Silva, J. Feliu, Electrochem. Commun. 5 (2003) 741.
[6] Takuya Nakanishi, Mariko Matsunaga, Makoto Nagasaka, Toru Asahi, Tetsuya Osaka, J. Am. Chem. Soc. 128 (2006) 13322.
[7] J.W. Steed, J.L. Atwood, Supramolecular Chemistry, Wiley-VCH, Chichester, U.K, 2000.
[8] G.A. Attard, J. Phys. Chem. B 105 (2001) 3158.
[9] G.R. Newkome, C.N. Moorefield, F. Vögtle, Dendritic Molecules: Concepts, Syntheses and Perspectives, VCH, New York, 1996.
[10] Y. Zhou, M.L. Bruening, D.E. Bergbreiter, R.M. Crooks, M. Wells, J. Am. Chem. Soc. 118 (1996) 3773.
[11] George R. Newkome, Advances in Dendritic Macromolecules, vol. 5, Elsevier Science, 2002, 107.
[12] E. Bustos, J. Manríquez, G. Orozco, Luis A. Godínez, Langmuir 21 (2005) 3013.
[13] P. Lloyd-Williams, F. Albericio, E. Giralt, Chemical approaches to the synthesis of peptides and proteins, CRC press, New York, USA, 1997.
[14] M.J. Frisch, G.W. Trucks, H.B. Schlegel, G.E. Scuseria, M.A. Robb, J.R. Cheeseman, J.A. Montgomery Jr., T. Vreven, K.N. Kudin, J.C. Burant, J.M. Millam, S.S. Iyengar, J. Tomasi, V. Barone, B. Mennucci, M. Cossi, G. Scalmani, N. Rega, G.A. Petersson, H. Nakatsuji, M. Hada, M. Ehara, K. Toyota, R. Fukuda, J. Hasegawa, M. Ishida, T. Nakajima, Y. Honda, O. Kitao, H. Nakai, M. Klene, X. Li, J.E. Knox, H.P. Hratchian, J.B. Cross, C. Adamo, J. Jaramillo, R. Gomperts, R.E. Stratmann, O. Yazyev, A.J. Austin, R. Cammi, C. Pomelli, J.W. Ochterski, P.Y. Ayala, K. Morokuma, G.A. Voth, P. Salvador, J.J. Dannenberg, V.G. Zakrzewski, S. Dapprich, A.D. Daniels, M.C. Strain, O. Farkas, D.K. Malick, A.D. Rabuck, K. Raghavachari, J.B. Foresman, J.V. Ortiz, Q. Cui, A.G. Baboul, S. Clifford, J. Cioslowski, B.B. Stefanov, G. Liu, A. Liashenko, P. Piskorz, I. Komaromi, R.L. Martin, D.J. Fox, T. Keith, M.A. Al-Laham, C.Y. Peng, A. Nanayakkara, M. Challacombe, P.M.W. Gill, B. Johnson, W. Chen, M.W. Wong, C. Gonzalez, J.A. Pople, Gaussian 03, Revision C.02, Gaussian, Inc., Wallingford, CT, 2004.
[15] E. Bustos, Th.W. Chapman, F. Rodríguez-Valadez, L.A. Godínez, Electroanalysis 18 (21) (2006) 2092.
[16] J. Manriquez, E. Juaristi, O. Muñoz-Muñiz, L.A. Godínez, Langmuir 19 (2003) 7315.
[17] J. Cassidy, J. O'Gorman, M. Ronane, E. Howard, Electrochem. Commun. 1 (1999) 69.
[18] A. Mayer, Chem. Rev. (2000) 3031.
[19] Zh. Chen, Y. Takei, Bh.A. Deore, T. Nagaoka, Analyst 125 (2000) 2249.
[20] R.B. Merrifield, J. Am. Chem. Soc. 85 (1963) 2149.
[21] D. Lin-Vien, N.B. Colthup, W.G. Fateley, J.G. Grasseli, Infrared and Raman Characteristic Frequencies of Organic Molecules, Academic Press, San Diego, 1991.
[22] H. Tokuhisa, M. Zhao, L.A. Baker, V.T. Phan, D.L. Dermody, M.E. García, R.F. Peez, R.M. Crooks, Th.M. Mayer, J. Am. Chem. Soc 120 (1998) 4492.

Talanta 78 (2009) 1286–1292

Contents lists available at ScienceDirect

Talanta

journal homepage: www.elsevier.com/locate/talanta

Comparative evaluation of liquid chromatography versus gas chromatography using a β-cyclodextrin stationary phase for the determination of BTEX in occupational environments

Andreu Campos-Candel, Maria Llobat-Estellés, Adela Mauri-Aucejo*

Department of Analytical Chemistry, Faculty of Chemistry, Universitat de València, Dr. Moliner 50, Burjassot, València, E-46100, Spain

ARTICLE INFO

Article history:
Received 28 November 2008
Received in revised form 21 January 2009
Accepted 28 January 2009
Available online 6 February 2009

Keywords:
BTEX
Workplace
β-Cyclodextrin
HPLC
GC–MS
Pressurized fluid extraction

ABSTRACT

An HPLC method for the determination of benzene, toluene, ethylbenzene and *o*-xylene, *m*-xylene and *p*-xylene in occupational environments was developed and compared with a GC–MS method. Chromatographic analysis using a β-cyclodextrin stationary phase was performed after active and passive air sampling by adsorption on activated charcoal and pressurized fluid extraction. The analytes were completely separated and quantified using both methods, although GC–MS provided better resolutions and lower detection limits than HPLC. The HPLC method was unsuccessfully applied to the determination of benzene in real samples because its sensitivity was too low. Both methods were applied to the analysis of certified reference materials and air samples collected in several workplaces. Statistical comparison showed that HPLC and GC–MS provided analogous accuracy.

1. Introduction

Benzene, toluene, ethylbenzene and *o*-xylene, *m*-xylene and *p*-xylene (BTEX) are aromatic hydrocarbons widely used in the chemical industry, so these compounds are usually present at occupational environments.

European legislation [1] prescribes that the exposure of individual workers to BTEX vapours shall be assessed because these can be easily inhaled and can cause adverse health effects, especially since benzene is known to be a human carcinogen.

To protect workers from toxicity, airborne BTEX concentrations are measured and then compared with the occupational exposure limit values [2,3].

On a global level, the most widely used technique for the control of BTEX in workplace air consists in active sampling with adsorption on activated charcoal followed by carbon disulfide desorption [4,5]. Several techniques have been employed as alternative to the standard method, such as the use of Tenax or multi-sorbent tubes [6], diffusive samplers [7–9] or thermal desorption tubes [10]. Diffusive sampling does not involve the use of pumping systems and can be performed with very low costs, although sampling rate can be influenced by wind speed [7,8]. Sampling and sample preparation strategies based on solid phase microextraction (SPME) have been used for many years in various applications [9]. Thermal desorption offers increased sensitivity for the analysis than solvent desorption but the analysis of a single sample cannot be replicated [10]. A cryogenic trap can be also used for preconcentrating target analytes [7,8]. In addition to these techniques, pressurized fluid extraction (PFE) can be advantageously employed to extract BTEX from activated charcoal [11] especially if the analyses are performed by reversed-phase high-performance liquid chromatography (HPLC), whose common mobile phases are incompatible with carbon disulfide. The use of acetonitrile (ACN) as the extracting solvent results in a less hazardous procedure.

Analyses of BTEX in water, soil and air are usually carried out by gas chromatography using a flame ionization detector (GC–FID) and a stationary phase of polyethylene glycol, although gas chromatography–mass spectrometry (GC–MS) is becoming increasingly common. However, the use of this stationary phase has the drawback of the impossibility of separating the *m*-xylene and *p*-xylene isomers [4,5,12–16].

A toxicokinetic model of inhalation exposure to xylene in Caucasian men suggests that there are significant isomeric differences for toxicant half-life, clearance and extrahepatic metabolism [17]. Other studies have indicated different orders of relative toxicity for the isomers and the differences in effect levels among the isomers may be small [18]. Moreover, commercial xylene usually contains

* Corresponding author. Tel.: +34 963544497; fax: +34 963544436.
E-mail address: adela.mauri@uv.es (A. Mauri-Aucejo).

0039-9140/$ – see front matter © 2009 Elsevier B.V. All rights reserved.
doi:10.1016/j.talanta.2009.01.055

about 40–65% *m*-xylene and up to 20% each of *o*-xylene and *p*-xylene and ethylbenzene [19].

Consequently, the separation of the positional isomers *m*-xylene and *p*-xylene could be interesting in order to differentiate between a worker's exposure to *m*-xylene and to *p*-xylene, and to better understand the exposure of humans in their working environments.

Literature indicates that the separation of structural isomers can be achieved by using β-cyclodextrin (β-CD) thanks to inclusion complex formation. β-CD is a torus-shaped cyclic oligosaccharide made up of glucopyranose units. This structure gives rise to a remarkable ability to form inclusion complexes which depends on size and polarity of the host molecule and its shape. BTEX are small hydrophobic aromatic hydrocarbons with great affinity for the non-polar cyclodextrin cavity, where the orientation of the analytes is selective due to the electron sharing of the aromatic methylene groups with those of the glucoside oxygens. In this way, β-CD has been used as a mobile phase component in reversed-phase HPLC [20,21] and also in stationary phases, both in liquid chromatography [22,23] and gas chromatography [24].

The principal aim of this study is to compare the performance of HPLC with fluorescence detection and GC–MS methods for the determination of benzene, toluene, ethylbenzene and *o*-xylene, *m*-xylene and *p*-xylene in occupational environments. So the results of comparisons of their resolution, sensitivity, analysis time and application to real samples are reported herein.

2. Experimental

2.1. Reagents

Benzene, toluene, ethylbenzene and *o*-xylene, *m*-xylene and *p*-xylene standards were obtained from Fluka (Buchs, Switzerland), whereas *n*-propylbenzene, used as internal standard, was purchased from Dr. Ehrenstorfer (Augsburg, Germany). All solvents used in the extraction and analysis procedures were of HPLC or GC grade quality (Merck, Darmstadt, Germany).

A BCR-562 certified reference material (Institute for Reference Materials and Measurements, Geel, Belgium) consisting of activated charcoal tubes charged with benzene, toluene, *m*-xylene and *p*-xylene, and a Radiello VOC calibration kit (Fondazione Salvatore Maugeri, Padova, Italy) composed of three blanks and nine cartridge adsorbents charged with benzene, toluene, ethylbenzene, and *m*-xylene, *o*-xylene and *p*-xylene to simulate 8 h exposures to 0.5, 1 and 2 times the exposure limit values for the mixture, were used to establish the accuracy of the HPLC and GC–MS methods.

2.2. Instrumental analysis

2.2.1. HPLC-fluorescence detection analysis

Separation of BTEX was achieved using a L-7100 liquid chromatograph from Merck-Hitachi (Darmstadt, Germany) equipped with a F-1080 fluorescence detector (Merck-Hitachi), a L-2300 column oven (Hitachi, Tokyo, Japan) and a L-7614 degasser (VWR International, Darmstadt, Germany). Excitation and emission were performed at 250 and 280 nm, respectively. Analytical column (25 cm × 4.6 mm I.D., 5 μm particle size) and guard column (2 cm × 4 mm I.D., 5 μm particle size) were β-cyclodextrin bonded phases Astec CYCLOBOND I 2000, both from Supelco (Bellefonte, PA, USA). The column and the guard column were thermostatically controlled and the oven temperature was varied from 10 to 45 °C. The flow rate was also varied between 0.6 and 1 mL/min. Sample injection volumes employed were 20, 5 and 2 μL.

Literature indicates that the separation mechanism in reverse phase mode employing a β-CD stationary phase is mainly due to inclusion complexation. Aqueous mobile phases with MeOH provide better resolution than ACN/water phases because the former is the weakest solvent to interact with the cyclodextrin cavity [25]. A binary mobile phase which comprised from 20% to 75% for methanol (MeOH) and water was applied for elution of BTEX compounds. Moreover, ACN was tested as a component of binary and ternary aqueous mobile phases, both in isocratic and gradient elution. Influence of pH on BTEX separation is minimal due to the absence of ionizable functional groups that could be affected by altering it.

2.2.2. GC–MS analysis

Determination of BTEX was performed with an Agilent (Santa Clara, CA, USA) 6890N-5973N GC–MS system equipped with a 7683 autosampler. The stationary phase was a β-cyclodextrin coated capillary column Cyclodex-B (30 m × 0.25 mm I.D., 0.25 μm) from Agilent J&W. Helium was used as carrier gas at a constant flow of 2.4 mL/min. The mass selective detector (MSD) was operated in electron impact mode with a potential ionization of 70 eV and a source temperature of 230 °C. The scan range used in SCAN mode was *m*/*z* 30–250 whereas ions *m*/*z* 78 and 91 were selected in SIM mode. The interface temperature and the injector temperature were set at 230 and 210 °C, respectively. 1 μL of the sample was injected in split mode (20:1) with a solvent delay of 2 min.

The oven temperature was optimized using a Focus gas chromatograph equipped with a flame ionization detector from ThermoFinnigan (Rodano, Italy).

2.2.3. Analytical figures of merit

Both proposed methods were evaluated in terms of resolution, linearity, sensitivity and limit of detection.

The resolution factor (R_s) was calculated using the recommended IUPAC [26] expression:

$$R_s = \frac{2(t_{r_2} - t_{r_1})}{(W_{b_1} + W_{b_2})}$$

where t_{r_1} and t_{r_2} are the retention times of two analytes and W_{b_1} and W_{b_2} are the respective widths of each adjacent peak at its base.

The detector linear range was calculated plotting detector sensitivity, *S*, against concentration or amount injected [26]. The upper limit of linearity was graphically established as the amount at which the deviation exceeds the specified value in ±5% while the lower limit of linearity was the minimum detectable amount. The limit of detection, LOD, was expressed as concentration or mass flow of the substance of interest in the mobile phase that gives a detector signal equal to twice the noise level [26]:

$$\mathrm{LOD} = \frac{2N}{S}$$

where *S* is the sensitivity and *N* is the noise, calculated as the amplitude of the envelope of the baseline which includes all random variations of the detector signal.

In the case of concentration-sensitive detectors, such as fluorescence detection, *S* is calculated per unit concentration in the mobile phase:

$$S = \frac{E_i}{C_i}$$

where E_i is the peak height and C_i is the concentration of the particular substance in the mobile phase at the detector.

In the case of mass-flow sensitive detectors, such as mass spectrometry detection, *S* is calculated per unit mass of the substance in the mobile phase:

$$S = \frac{A_i}{W_i}$$

where A_i is the integrated peak area and W_i is the mass of substance.

In both cases the limit of quantification (LOQ) was expressed as 3.04 times the LOD [26].

2.3. Sample collection

2.3.1. Active sampling

Air samples were collected from several workplaces using a portable Buck-Genie VSS-5 pump from A.P. Buck (Orlando, FL, USA), which was previously calibrated with a Multicon KS external flow calibrator (Dräger, Lübeck, Germany). Flow rate (from 100 to 150 mL/min) and sampling time (from 40 to 180 min) were programmed according to the tasks developed by each worker. The samples were collected using Dräger tubes of activated charcoal (coconut shell, 20/40 mesh) type NIOSH (100/50 mg) that were mounted in the connecting tube of the pump and attached to the worker's clothes. After collection, the tubes were closed with plastic caps, sealed in plastic bags and stored at 4 °C.

2.3.2. Passive sampling

Air samples were also collected using Radiello diffusive samplers attached to the worker's clothes. The Radiello system consists in a cylindrical adsorbing cartridge housed coaxially inside a cylindrical diffusive body. The cartridges are stainless steel net cylinders filled with 530 ± 30 mg of activated charcoal (35/50 mesh). BTEX compounds were sampled for the whole working shift of 8 h. The air volume sampled for each analyte is dependant on its sampling rate, which is provided by the manufacturer of the diffusive sampler: 68 mL/min for ethylbenzene, 70 mL/min for *m*-xylene and *p*-xylene, 65 mL/min for *o*-xylene, 74 mL/min for toluene and 80 mL/min for benzene. After collection, the cartridges were placed into their original containers, sealed in plastic bags and stored at 4 °C.

2.4. Sample preparation and extraction

2.4.1. Activated charcoal tubes

The procedure used for the sample preparation and extraction has been described previously [11] so only a brief summary follows.

The sampling tubes were broken and the front and back sorbent sections loaded in separate 1 mL extraction cells where a disposable cellulose filter had been previously installed, and then any void volume was filled with clean sand (J.T. Baker, Deventer, Holland). An ASE 200 system purchased from Dionex Corporation (SunnyVale, CA, USA) was used for the pressurized fluid extraction. The samples were extracted with ACN at 160 °C, 1500 psi, preheat time 2 min, static time 5 min, flush volume 10%, purge time 90 s and two cycles. Finally, extracts were made up to a final volume of 10 mL with ACN.

2.4.2. Activated charcoal diffusive samplers

Since Radiello diffusive samplers contain a larger amount of activated charcoal of different particle size than the tubes, the optimization of Radiello extraction was considered necessary. The extraction procedure was optimized by varying one parameter at a time, while keeping the others constant, from those optimized previously for activated charcoal tubes (ACN, 160 °C, 1500 psi, preheat time 2 min, static time 5 min, flush volume 10%, purge time 90 s and 2 cycles), although pressure and purge time were not varied because these are not considered critical experimental parameters. Neither the extracting solvent was changed because ACN had always exhibited the best results at PFE conditions.

This procedure is very similar to the one described previously. The cartridges were opened and the activated charcoal loaded in 5 mL extraction cells. The samples were extracted by PFE with ACN at 1500 psi and purge time 90 s. Temperature and preheat time were varied between 120 and 180 °C and 0 and 6 min, respectively. Static time was set at 2, 4, 6 and 8 min. The flush volume and the number of cycles ranged between 20% and 80% and 2–5 cycles, respectively. Finally, extracts were made up to a final volume of 25 mL with ACN.

2.5. Validation

The BCR-562 certified reference material and the Radiello VOC calibration kit were analysed by the HPLC and GC–MS methods using the previously optimized conditions.

The populations of values obtained by both chromatographic methods for each reference material were analysed by simple least-squares regression (experimental values = *f* (theoretical contents)). The statistical study of the intercept and the slope allows us to establish, for a determinate confidence level, the accuracy of the method and also the presence of errors [27].

2.6. Analysis of real samples

Five samples were collected at three different research laboratories using activated charcoal tubes while workers were employing some of the analytes of interest to develop their usual tasks. The concentration in the workplace air is obtained as the concentration in the solution multiplied by the extract volume (10 mL) and by the recovery [11], and divided by the volume of air collected for each sample, which is calculated as the product of flow and time.

Another six samples were collected using Radiello diffusive samplers in an organic chemistry laboratory, in a petrol station and also while a farmer was spraying the soil of a fruit trees plantation with an herbicide. The concentration in the workplace air is obtained as the concentration in the solution multiplied by the extract volume (25 mL) and by the recovery (Section 3.2.), and divided by the volume of air collected for each analyte, which is calculated as the product of sampling rate and time.

The workers' daily exposures are calculated taking into account time spent on each task and the concentration in the workplace air.

2.7. HPLC-FL versus GC–MS

The two populations of values obtained by both methods for the certified samples and for the real ones were analysed by simple least-squares regression (HPLC-FL = *f* (GC–MS)). The statistical study of the intercept and the slope allows us to establish, for a determinate confidence level, whether both methods provide analogous accuracy [27].

3. Results and discussion

3.1. Instrumental analysis

3.1.1. HPLC-fluorescence detection

The effect of the sample injection volume on the separation was studied because the resolution may be strongly dependent upon sample amount. For this, 20, 5 and 2 μL of a BTEX standard solution containing 8 ppm of *m*-xylene and *o*-xylene, 10 ppm of toluene, 2.5 ppm of *p*-xylene, 16 ppm of ethylbenzene and 100 ppm of benzene were injected. As the injected volume increases, the resolution deteriorates significantly. Therefore, 2 μL was the optimum injection volume.

Preliminary studies were carried out in isocratic conditions with binary mobile phases MeOH/water comprising from 20% to 75% for MeOH (Fig. 1). As expected, the more the MeOH content of mobile phase increases, the more the retention time decreases. Inversion of the elution order of the analytes was observed when the mobile phase contains 25%, 37%, 50% and 60% for MeOH.

To evaluate the quality of the separation of BTEX, the R_s between adjacent peaks was calculated. The resolution is highly dependent

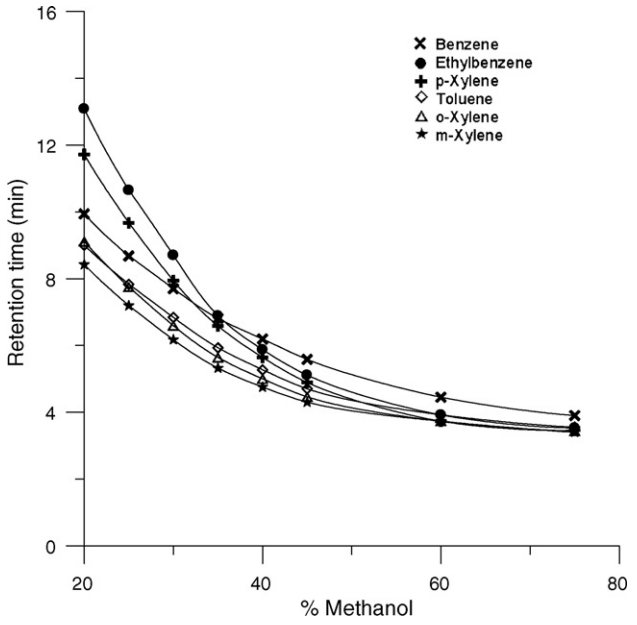

Fig. 1. Effect of methanol content of mobile phase (MeOH/water) on the retention time of benzene, toluene, ethylbenzene and *o*-xylene, *m*-xylene and *p*-xylene at 40 °C.

on the MeOH content and its values are closer to 1.0 for contents of MeOH from 40% to 45%. Neither binary (ACN/water) nor ternary (ACN/MeOH/water) mobile phases provided a more efficient separation. Gradient conditions did not supply better resolutions either. Finally, a mobile phase 45/55 MeOH/water was chosen for the following experiments.

To improve the resolution between the analytes, different column temperatures were tested (Fig. 2). Changes on temperature have a great effect on the retention of solutes because inclusion mechanism is altered. As can be seen, lower temperatures enhance the weaker bonding forces, so as the temperature decreases, the

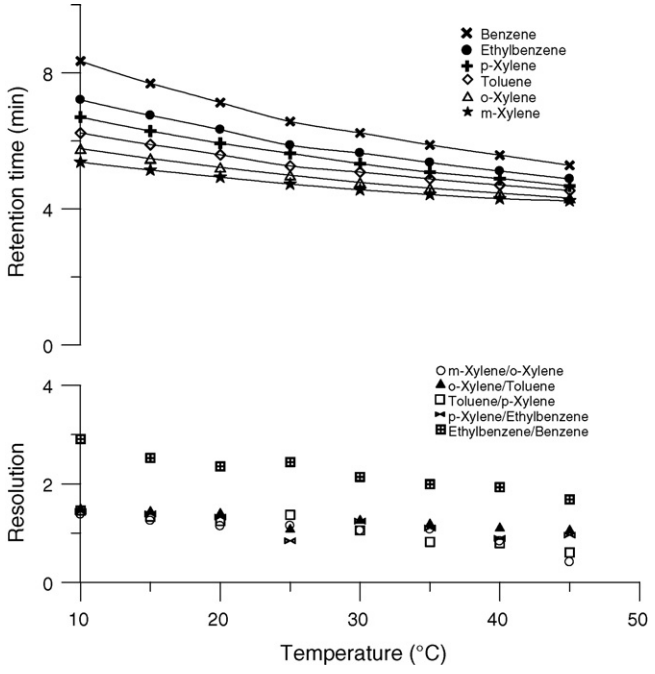

Fig. 2. Effect of temperature on the retention time and resolution of benzene, toluene, ethylbenzene and *o*-xylene, *m*-xylene and *p*-xylene.

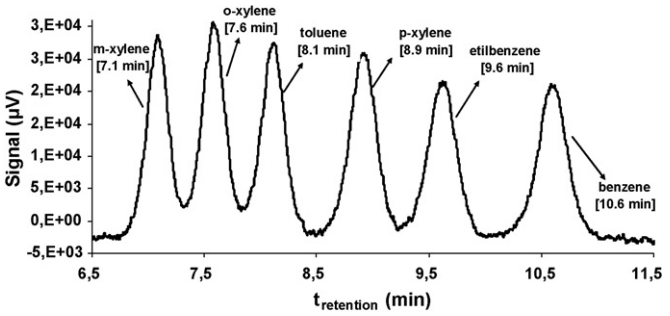

Fig. 3. Chromatogram of a standard mixture of 100 ppm of benzene, 10 ppm of toluene, 16 ppm of ethylbenzene, 8 ppm of *o*-xylene and *m*-xylene and 2.5 ppm of *p*-xylene under HPLC optimized conditions.

retention time of each analyte and the resolution between adjacent peaks go up. At 10 °C, the resolutions are closer or higher than 1.5, so 10 °C was selected as the optimum temperature.

The flow rate was varied between 0.6 and 1 mL/min. Its influence on the resolution was minimal, so 0.8 mL/min was selected as the optimum flow rate because it provides lower pressures on column than 1 mL/min and shorter analysis time than 0.6 mL/min.

Based on these results, a complete separation of all BTEX compounds under isocratic conditions (mobile phase 45/55 MeOH/water, temperature 10 °C, flow rate 0.8 mL/min and injection volume 2 μL) is possible, as it can be seen in Fig. 3.

3.1.2. GC–MS

Several programs were tested to achieve the best resolution for BTEX compounds since both the initial temperature and the ramp can be quite critical for the separation of isomers on cyclodextrin coated columns [28]. Tests were carried out by changing the initial temperature from 25 to 50 °C and the temperature gradient from 1 to 4 °C/min. Results showed that the best compromise between resolution of the analytes and analysis time was obtained when the system was ramped from 40 to 44 °C at 0.5 °C/min, following a 3 min hold, and then increased at 10 °C/min to 104 °C, kept for 5 min.

Under the chromatographic conditions described previously (injector temperature 210 °C, interface temperature 230 °C, oven temperature 40 °C – 3 min to 44 °C at 0.5 °C/min and then 10 °C/min to 104 °C – 5 min, injection volume 1 μL, split mode 20:1 and solvent delay 2 min), the resolutions are closer or higher than 1.5, so a complete separation of all BTEX compounds can be achieved, as it can be seen in Fig. 4.

3.1.3. Analytical figures of merit

Both proposed methods were evaluated in terms of resolution, linearity, sensitivity and limit of detection.

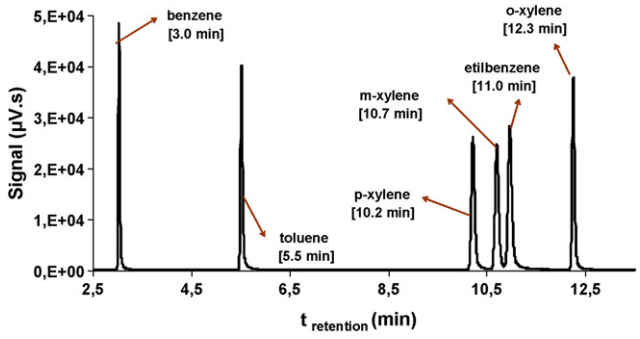

Fig. 4. Chromatograms of a standard mixture of 20 ppm of each analyte under GC–MS optimized conditions.

Table 1
Linearity range, sensitivity and detection limits for HPLC-fluorescence detection analysis and for GC–MS analysis operating in SIM mode (*m*/*z* 78 and 91).

HPLC	Linearity range (mg/L)	Sensitivity (μV L/mg)	LOD (mg/L)	LOD[a] (μg/sample)
Benzene	4–90	1600	4	40
Ethylbenzene	0.8–16	8000	0.8	8
Toluene	0.5–9	13000	0.5	5
o-Xylene	0.4–8	17000	0.4	4
m-Xylene	0.4–8	15000	0.4	4
p-Xylene	0.14–1.7	46000	0.14	1.4
GC–MS	**Linearity range (pg)**	**10^{-3} Sensitivity (μV s/μg)**	**LOD (pg/s)**	**LOD[b] (μg/sample)**
Benzene	7 to >6×10^4	52000	0.7	0.07
Ethylbenzene	9 to >6×10^4	77000	0.5	0.09
Toluene	8 to >6×10^4	61000	0.6	0.08
o-Xylene	8 to >6×10^4	65000	0.6	0.08
m-Xylene	9 to >6×10^4	62000	0.6	0.09
p-Xylene	11 to >6×10^4	63000	0.6	0.11

[a] LOD multiplied by the extract volume (10 mL).
[b] LOD multiplied by the extract volume (10 mL) and by the time that each analyte stays at the MSD, and divided by the injection volume (1 μL).

The analytes can be completely separated and quantified using both methods, although GC–MS provides a better resolution.

Table 1 displays their LOD, which are expressed as amount of analyte per air sample collected using activated charcoal tubes. As it can be seen, as the sensitivity increases, the upper limit of linearity and the LOD decrease for HPLC-fluorescence detection. The results obtained also indicate that GC–MS, in SIM mode, provides lower detection limits than reversed-phase liquid chromatography (a 1–2 order of magnitude difference). In addition, GC–MS values are slightly lower than those obtained by GC–FID using the same analytical column, whereas the LOD of benzene has significantly improved (2.0 pg/s for benzene and 1.3 pg/s for ethylbenzene, toluene and *o*-xylene, *m*-xylene and *p*-xylene).

In spite of this, only the HPLC determination of benzene is not applicable to real samples because its sensitivity is lower than that required by the European legislation [2,3]. Using a sample concentration technique, increases in sensitivity could be obtained, although the sample preparation would become more complicated. On the other hand, HPLC method provides slightly shorter analysis time (11 min against 12.5 min).

GC–MS method also provides lower LOD than the method recommended by the USA National Institute for Occupational Safety and Health [5] based on GC–FID determination (0.5 μg/sample for benzene and ethylbenzene, 0.7 μg/sample for toluene and *p*-xylene and 0.8 μg/sample for *o*-xylene and *m*-xylene).

The HPLC method requires the use of MeOH as a component of the mobile phase whereas helium is used in the GC–MS method. As a result, the amount of toxic waste generated and the risk of airborne contamination using the HPLC method may be higher.

3.2. Pressurized fluid extraction optimization for Radiello diffusive samplers

Synthetic samples were prepared by injecting 0.02–0.15 mg of benzene, 0.4–7 mg of toluene, *o*-xylene, *m*-xylene and *p*-xylene and 0.9–15 mg of ethylbenze directly onto Radiello diffusive samplers with a micropipette.

A 5 mL extraction cell was used because it most closely matches the sample size. Changing the temperature, the preheat time and the static time did not have an impact on analyte recovery, so they were set at 160 °C, 2 and 5 min, respectively, for the subsequent extractions. On the other hand, an increase in the amount of analyte extracted was found when three cycles and 40% flush volume were used. The optimized parameters for the extraction of BTEX from Radiello diffusive samplers using PFE were: ACN, 160 °C, 1500 psi, preheat time 2 min, static time 5 min, flush volume 40%, purge time 90 s and three cycles.

The optimized extraction method was applied to establish the recovery for BTEX compounds from the Radiello calibration kit. One blank and three preloaded cartridges were prepared and extracted following the previously described procedure. After the extraction, the analytes were determined using the GC–MS method. The results obtained from three independent analyses for a confidence level of 95% were 95 ± 5%, 96 ± 15%, 90 ± 7%, 88 ± 14%, 92 ± 8% and 88 ± 11% for benzene, toluene, ethylbenzene and *o*-xylene, *m*-xylene and *p*-xylene, respectively. Quantitative recoveries higher than 75% were obtained, as required by the CEN standard EN 838:1996 [29] for diffusive samplers.

3.3. Validation

The BCR-562 certified reference material and the Radiello VOC calibration kit were analysed by the HPLC and GC–MS methods using the previously optimized conditions.

The results obtained are summarized in Tables 2 and 3. Benzene could not be quantified by the HPLC method because its concentration in both certified samples was lower than the LOQ.

The population of values obtained by HPLC for the BCR-562 certified sample and for the Radiello calibration kit was analysed by simple least-squares regression (by plotting experimental values in

Table 2
Determination of BTEX compounds in BCR-562 activated charcoal tubes ($n = 3$) by GC–MS and HPLC considering the recovery (%) for each analyte.

Compound				Mean	C.V. (%)
Benzene					
μg_t		15			
μg_o^{GC-MS}	14.9	14.7	14.4	14.7	0.6
μg_o^{HPLC}	<LOQ	<LOQ	<LOQ	–	–
Toluene					
μg_t	147				
μg_o^{GC-MS}	147.9	154.2	155.2	152.4	6.5
μg_o^{HPLC}	131.3	142.7	132.3	135.4	11.6
m-Xylene					
μg_t		96			
μg_o^{GC-MS}	83.9	81.7	79.6	81.7	6.5
μg_o^{HPLC}	80.6	82.8	81.7	81.7	3.3
o-Xylene					
μg_t		93			
μg_o^{GC-MS}	79.1	74.4	70.9	74.8	13.7
μg_o^{HPLC}	72.1	74.4	64.0	70.2	19.4

μg_t: Certified value, μg_o: found value, LOQ: limit of quantification.

Table 3
Determination of BTEX compounds in the Radiello calibration kit by GC–MS and HPLC.

Benzene			
μg_t	4.69	8.97	17.9
μg_o^{GC-MS}	4.35	8.63	17.1
μg_o^{HPLC}	<LOQ	<LOQ	<LOQ
Toluene			
μg_t	711	1366	2735
μg_o^{GC-MS}	728	1252	2532
μg_o^{HPLC}	669	1266	2584
Ethylbenzene			
μg_t	416	804	1603
μg_o^{GC-MS}	385	696	1435
μg_o^{HPLC}	421	700	1512
o-Xylene			
μg_t	403	775	1545
μg_o^{GC-MS}	371	631	1396
μg_o^{HPLC}	324	540	1304
m-Xylene			
μg_t	422	813	1660
μg_o^{GC-MS}	405	727	1514
μg_o^{HPLC}	435	862	1653
p-Xylene			
μg_t	438	845	1647
μg_o^{GC-MS}	399	706	1492
μg_o^{HPLC}	410	787	1588

LOQ: limit of quantification, μg_t: certified value, μg_o: found value.

Table 4
Determination of BTEX compounds in activated charcoal tubes by GC–MS and HPLC.

Sample reference	P1	A2	A3	O4	O5
Flow (mL/min)	150	150	150	100	100
t (min)	40	55	55	180	180
V (L)	6	8.25	8.25	18	18
Benzene					
μg/mL	<LOQ	0.4	1.5	0.8	0.06
mg/m^3	<LOQ	0.5	1.8	0.4	0.03
Toluene					
μg/mL	<LOQ	0.3	1.2	0.3	0.04
mg/m^3	<LOQ	0.4	1.4	0.17	0.023
Ethylbenzene					
μg/mL	5.3 [6.0]	0.16	0.6	0.004	0.004
mg/m^3	8.9 [10.0]	0.20	0.7	0.002	0.002
o-Xylene					
μg/mL	1.6 [1.8]	0.11	0.4	<LOQ	<LOQ
mg/m^3	2.7 [3.0]	0.13	0.5	<LOQ	<LOQ
m-Xylene					
μg/mL	13.4 [14.0]	0.13	0.5	0.014	<LOQ
mg/m^3	22.4 [23.4]	0.16	0.6	0.008	<LOQ
p-Xylene					
μg/mL	2.1 [2.3]	0.14	0.5 [0.5]	<LOQ	<LOQ
mg/m^3	3.5 [3.8]	0.17	0.6 [0.6]	<LOQ	<LOQ

[HPLC values]. LOQ: limit of quantification, μg/mL: concentration in the solution, mg/m^3: concentration in the workplace air.

function of expected values of the certified materials). The application of a statistical test to the study of the slope and the intercept allows us to establish that for a 95% confidence level, HPLC method provides good accuracy and does not require correction of the blank nor does it present any constant relative errors ($y = 1.006x + 0.0018$; Student's *t*-test values: tabulated = 2.07; experimental, slope = 0.14, and intercept = 0.04). In the same way, GC–MS method also provides good accuracy and neither requires correction of the blank or presents any constant relative errors ($y = 0.9862x + 0.0007$; Student's *t*-test values: tabulated = 2.04; experimental, slope = 1.7, and intercept = 0.10).

3.4. Analysis of real samples

In order to verify the applicability of both proposed methods, the determination of BTEX in activated charcoal samplers was carried out.

Five samples were collected at three different research laboratories (P1 – parasitology lab.; A2 and A3 – analytical chemistry lab.; O4 and O5 – organic chemistry lab.) using activated charcoal tubes while workers were using some of the analytes of interest to develop their usual tasks.

The extracts of back sorbent sections and blanks did not contain any analyte of interest, so the sample collection was correctly done [30]. Table 4 displays that sample P1 shows the highest concentration of xylene and ethylbenzene. It was collected for as long as a worker was using commercial xylene to prepare several samples for their observation by microscopy and besides, there was not an air-extraction system at this laboratory. The highest content of benzene and toluene was found in the sample A3. Similar tasks were being done while the samples A2 and A3 were collected. The difference between them is probably due to the different use of collection protection equipment, on the part of the worker, because the exhaust hood was not being employed during the sample A3 collection. The same happened for the samples O4 and O5. The sample O4 was taken without air extraction whereas the sample O5 was collected when the extraction system was working.

Another six samples were collected in an organic chemistry laboratory (O1 and O2), in a petrol station (G3 and G4) and also while a farmer was spraying the soil of a fruit trees plantation with an herbicide (F1 and F2).

The extracts of blanks did not contain any analyte of interest. As it can be seen in Table 5, similar amount of benzene was found in the samples F2, O2, G3 and G4. Samples F1 and F2 were collected in two different shifts. Sample F1 was taken while the farmer was preparing the emulsion of herbicide and spraying the soil of the plantation with it whereas during the collection of sample F2 he was only spraying the soil. Benzene was not being used while the sample O1 was collected and neither the exhaust hood was being employed. The difference between O1 and O2 is probably due to this. Samples

Table 5
Determination of BTEX compounds in activated charcoal diffusive samplers by GC–MS and HPLC.

Sample reference	F1	F2	O1	O2	G3	G4
Benzene						
μg/mL	<LOQ	0.23	<LOQ	0.3	0.3	0.3
mg/m^3	<LOQ	0.20	<LOQ	0.3	0.22	0.21
Toluene						
μg/mL	0.5	0.7	0.4	0.4	2.0 [1.6]	9[9]
mg/m^3	0.4	0.5	0.3	0.3	1.2 [1.0]	5[5]
Ethylbenzene						
μg/mL	0.4	0.4	0.4	0.3	0.3	0.3
mg/m^3	0.3	0.3	0.3	0.24	0.20	0.20
o-Xylene						
μg/mL	0.3	0.3	0.3	0.3	0.3	0.3
mg/m^3	0.22	0.24	0.21	0.20	0.17	0.17
m-Xylene						
μg/mL	0.4	0.4	<LOQ	<LOQ	0.3	0.3
mg/m^3	0.3	0.3	<LOQ	<LOQ	0.20	0.20
p-Xylene						
μg/mL	0.3	0.4	<LOQ	<LOQ	0.3	0.3
mg/m^3	0.3	0.3	<LOQ	<LOQ	0.19	0.20

[HPLC values]. LOQ: limit of quantification, μg/mL: concentration in the solution, mg/m^3: concentration in the workplace air.

G3 and G4 which were collected on two different working days contained the highest amount of toluene.

Using HPLC analysis, only ethylbenzene, *o*-xylene, *m*-xylene and *p*-xylene in the P1 sample, *p*-xylene in the A3 sample and toluene in the G3 and G4 samples were quantified (Tables 4 and 5).

Taking into account time spent on each task, it can be concluded that the occupational exposures determined were always acceptable because the workers' daily exposures were lower than the tenth part of the recommended exposure limits [2,3,30].

3.5. HPLC-FL versus GC–MS

The two populations of values obtained by both methods for the certified samples and for the real ones were analysed by simple least-squares regression (by plotting the experimental values obtained with the HPLC method in function of the experimental values provided by the GC–MS method). The study of the slope and the intercept allow us to establish that for a 95% confidence level, both methods provide analogous accuracy ($y = 1.0229x + 0.0007$; Student's *t*-test values: tabulated = 2.05; experimental, slope = 0.76, and intercept = 0.03).

4. Conclusions

The GC–MS method in SIM mode provides a higher sensitivity and linearity range than the HPLC method. Moreover, the HPLC determination of benzene is not applicable to real samples because its sensitivity is lower than that required by the European legislation for the exposure limit value for an 8-h workday.

Although GC–FID is the official method and the most popular technique for the analysis of BTEX in occupational environments, GC–MS is becoming more popular due to the superior sensitivity of the mass selective detector when operated in SIM mode and its unique ability to positively identify individual compounds in real samples. Moreover, the HPLC method proposed here can be employed as an alternative for separating and determining toluene, ethylbenzene and *o*-xylene, *m*-xylene and *p*-xylene in occupational environments. Finally, the use of β-cyclodextrin stationary phase makes possible the separation and quantification of *m*-xylene and *p*-xylene structural isomers.

Acknowledgements

The authors would like to thank the Servei de Seguretat, Salut i Qualitat Ambiental (Universitat de València) for financial support, Dr. Jordi Mañes Vinuesa for instrumental support and the anonymous reviewers for their help in improving the quality of the manuscript.

References

[1] Council Directive 98/24/EC of 7 April 1998 on the protection of the health and safety of workers from the risks related to chemical agents at work.
[2] Commission Directive 2000/39/EC of 8 June 2000 establishing a first list of indicative occupational exposure limit values in implementation of Council Directive 98/24/EC on the protection of the health and safety of workers from the risks related to chemical agents at work.
[3] Spanish occupational exposure limit values (2008). Instituto Nacional de Seguridad e Higiene en el Trabajo.
[4] UNE 81581:1992, Air quality, Workplace atmospheres, Determination of aromatic hydrocarbons (benzene, toluene, ethylbenzene, *p*-xylene, 1,2,4-trimethylbenzene) in air, Charcoal tube/solvent desorption/gas chromatographic method, Spanish standard in Spanish language.
[5] National Institute of Occupational Safety and Health (NIOSH) Hydrocarbons, Aromatic: Method 1501 by S.M. Pendergrass, Issue 3, In NIOSH Manual of Analytical Methods (NMAM), 4th edition. P.C. Schlecht, P.F. O'Connor (eds.), Cincinnati, Ohio: Department of Health and Human Services, Public Health Service, Centers for Disease Control, NIOSH, 2003.
[6] W.A. McClenny, K.D. Oliver, H.H. Jacumin Jr., E.H. Daughtrey Jr., J. Environ. Monit. 4 (2002) 695.
[7] P. Bohlin, K.C. Jones, B. Strandberg, J. Environ. Monit. 9 (2007) 501.
[8] P. Aragón, J. Atienza, D. Climent, Crit. Rev. Anal. Chem. 30 (2–3) (2000) 121.
[9] J.A. Koziel, I. Novak, Trends Anal. Chem. 21 (12) (2002) 840.
[10] E.L. Atlas, K.F. Sullivan, C.S. Giam, Anal. Chem. 57 (1985) 2417.
[11] A. Campos-Candel, M. Llobat-Estellés, A.R. Mauri-Aucejo, Anal. Bioanal Chem. 387 (2007) 1517.
[12] C.M.M. Almeida, L.V. Boas, J. Environ. Monit. 6 (1) (2004) 80.
[13] H. Shin, O. Kwon, Bull. Korean Chem. Soc. 21 (2000) 1101.
[14] A. Kumar, I. Viden, Environ. Monit. Assess. 131 (2007) 301.
[15] N. Garcia, L. Nollet, in: L. Nollet (Ed.), Chromatographic Science Series 93 (Chromatographic Analysis of the Environment. 3rd ed.) 2006, p. 513.
[16] D.K.W. Wang, C.C. Austin, Anal. Bioanal. Chem. 386 (2006) 1089.
[17] J.C. Adams, R.L. Dills, M.S. Morgan, D.A. Kalman, C.H. Pierce, Reg. Tox. Pharm. 43 (2005) 203.
[18] Agency for Toxic Substances and Disease Registry (ATSDR). Toxicological profile for Xylene. Department of Health and Human Services, Public Health Service, Atlanta, GA: U.S. (2007).
[19] Xylene, Air Toxics Web Site, http://www.epa.gov/ttn/atw/hlthef/xylenes.html, U.S. Environmental Protection Agency.
[20] J. Debowski, D. Sybilska, J. Chromatogr. 353 (1986) 409.
[21] A.R. Mauri-Aucejo, M. Llobat-Estelles, M. Escarti-Carrasco, R. Marin-Saez, Anal. Lett. 39 (2006) 183.
[22] D.W. Armstrong, W. DeMond, A. Alak, Anal. Chem. 57 (1985) 234.
[23] S.K. Panda, W. Schrader, J.T. Andersson, J. Chromatogr. A 1122 (2006) 88.
[24] N. Yassaa, B.Y. Meklati, A. Cecinato, J. Chromatogr. A 846 (1999) 287.
[25] Advanced Separation Technologies, Inc. (Astec), Cyclobond Handbook: A guide to using cyclodextrin bonded phases for chiral LC separations, 6th ed., 2002.
[26] IUPAC Compendium of Chemical Terminology, 2nd ed., 1997.
[27] D.L. Massart, et al., in: B.G.M. Vandeginste, S.C. Rutan (Eds.), Handbook of Chemometrics and Qualimetrics: Part A, Elsevier, Amsterdam, 1997, pp. 379–460, chapters 13 and 14.
[28] N. Yassaa, E. Brancaleoni, M. Frattoni, P. Ciccioli, Chemosphere 63 (2006) 502.
[29] European Committee for Standardization (CEN), CEN standard EN 838 Workplace atmospheres. Diffusive samplers for the determination of gases and vapours. Requirements and test methods. European Committee for Standardization, Brusseles (1996).
[30] European Committee for Standardization (CEN), CEN standard EN 689 Workplace atmospheres. Guidance for the assessment of exposure by inhalation to chemical agents for comparison with limit values and measurement strategy. European Committee for Standardization, Brussels (1996).

Talanta 78 (2009) 1484–1488

Contents lists available at ScienceDirect

Talanta

journal homepage: www.elsevier.com/locate/talanta

Short communication

Double-armed crown ethers for calcium optical sensors

S. Capel-Cuevas [a], I. de Orbe-Payá [a], F. Santoyo-González [b], L.F. Capitán-Vallvey [a,*]

[a] Solid Phase Spectrometry Research Group, Department of Analytical Chemistry, Campus Fuentenueva, University of Granada, E-18071 Granada, Spain
[b] Department of Organic Chemistry, Faculty of Sciences, Campus Fuentenueva, University of Granada, E-18071 Granada, Spain

ARTICLE INFO

Article history:
Received 26 October 2008
Received in revised form 19 January 2009
Accepted 23 January 2009
Available online 4 February 2009

Keywords:
Double-armed diazacrown ethers
Optical sensor
Ionophore–chromoionophore chemistry
Selectivity

ABSTRACT

This paper presents the characterization of optical sensing membranes for calcium based on ionophore–chromoionophore chemistry. Six different ionophores, 18-membered crown ether derivatives, were studied, coming from 18-crown-6 ether and 4,13-diaza-18-crown-6 ether to a series of double-armed crown ethers with different type of terminal groups. The study of optical membranes containing the same transducer and plasticizer allow drawing some conclusions on the influence of lipophilicity and size of the terminal group of the side chain on calcium selectivity. We have calculated the exchange constant $K_{exch}^{II_p}$ for each equilibrium with alkaline and alkaline-earth ions and the selectivity coefficient $k_{I,J}^{Osel}$ for each ion against calcium as a way for a full characterization of sensing membranes. In all cases the ion:ionophore stability constants for calcium were the highest and the ionophore V containing an (N-adamantylcarbamoyl) acetyl moiety originated the most selective membrane for calcium. Analytical parameters for calcium determination using prepared membranes were calculated.

1. Introduction

Since Pedersen introduced them in 1967 [1], a wide variety of crown ethers have been synthesized and reported, especially during the last two decades [2–4]. The research interest focuses on their ability to form very stable molecular ensembles or complexes with alkaline, alkaline-earth metals and organic cations. Their affinity for a given cation, based on cooperative weak non-covalent interactions, depends on many factors, including the relative sizes of the cation and the macrocyclic cavity.

Double-armed crown ethers characterized by a parent macrocyclic ligand and a cation ligating sidearm [5] are suitable reagents for use as specific ionophores in areas as metal-sensing and separation processes. They form encapsulated and lipophilic complexes with stabilities intermediate between crown ethers and cryptands. Since these armed macrocycles are stronger cation binders than the crown ethers and more flexible than the cryptands, they offer great possibilities as analytical reagents.

This type of crown ethers is composed of two flexible cation-binding arms and a parent crown ring. The selectivity on the complexation is determined by the size of the crown ring and the nature and position of flexible side arms, which present a donor group that provides further coordination of a guest cation bonded in the crown ring. Consequently, it is possible to design a metal-selective reagent by choosing a combination of parent crown ring structure and functionalized side arms [6].

In this work we study the reactivity of a series of double-armed crown ethers based on an 18 atoms ring against alkaline and alkaline-earth ions. The ionophores are incorporated in optical membranes working on ion-exchange. The use of the same chromoionophore as transducer permit to extract conclusions on the influence of lipophilicity and size of the terminal group of the side chain on calcium selectivity.

2. Experimental

2.1. Reagents and materials

Calcium, magnesium, sodium and potassium stock solutions (1.000 mol L^{-1}) were prepared in water from analytical reagent grade calcium, magnesium, sodium and potassium chlorides (Panreac, Barcelona, Spain) and standardized by atomic absorption spectrometry. Solutions of lower concentration were prepared by dilution with water. pH 8.5 and 9.0 buffer solutions 0.2 M were made from diethanolamine (Probus, Barcelona, Spain), Tris (Sigma–Aldrich Química S.A., Madrid, Spain) and HCl (Panreac). All chemicals used for the ionophore synthesis were of synthesis grade and reverse-osmosis type quality water (Milli-RO 12 plus Milli-Q station from Millipore) was used throughout (conductivity 18.2 mS).

The chromoionophore 1,2-benzo-7-(diethylamino)-3-(octadecanoylimino)phenoxazine (lipophilized Nile Blue) was synthesized, purified and identified by us according to [7] and the

* Corresponding author.
E-mail address: lcapitan@ugr.es (L.F. Capitán-Vallvey).

0039-9140/$ – see front matter © 2009 Published by Elsevier B.V.
doi:10.1016/j.talanta.2009.01.046

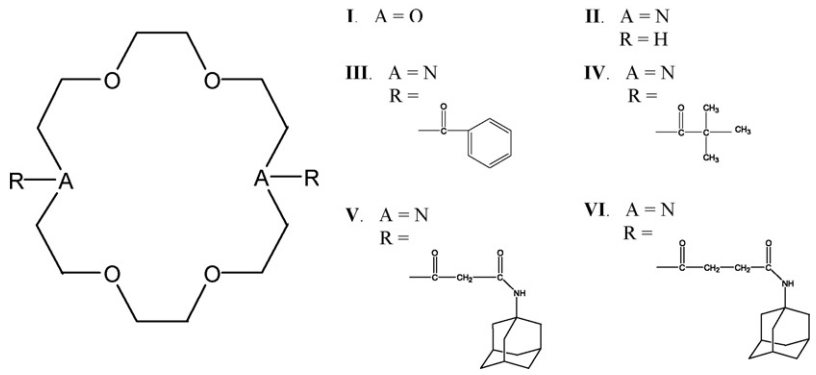

Fig. 1. Structure of ionophores studied.

ionophores 18-crown-6 ether (ionophore I) and 4,13-diaza-18-crown-6 (ionophore II) were received from Fluka (Fluka, Madrid, Spain) and Sigma–Aldrich Chemie (Aldrich, Steinheim, Germany), respectively. The rest of the ionophores were synthesized by us. Other chemical used for preparing the sensitive films, high molecular weight poly(vinyl chloride) (PVC), tributylphosphate (TBP), potassium tetrakis(4-chlorophenyl)borate (TCPB), and tetrahydrofuran (THF) as solvent, were purchased from Sigma–Aldrich. Sheets of polyester type Mylar (Goodfellow, Cambridge, UK) were used as support (Fig. 1).

2.2. Ionophore synthesis

The ionophore 7,16-[bis(N-adamantylcarbamoyl)acetyl]-1,4,10,13-tetraoxa-7,16-diazacyclooctadecane (ionophore V) was prepared according to Suzuki et al. [8]. Here, we present the synthesis of the new ionophores III, IV and VI. Characterization of the intermediate and the synthesized ionophores were made by ^{1}H-, ^{13}C-NMR, IR and HRMS (FAB^{+} and MALDI).

2.2.1. Synthesis of 7,16-dibenzoyl-1,4,10,13-tetraoxa-7,16-diazacyclooctadecane(III)

To a solution of 4,13-diaza-18-crown-6 (200 mg; 0.8 mmol) in ethyl acetate (25 mL) was added drop by drop a solution of benzoyl chloride (266 μL; 2.3 mmol) and triethylamine (638 μL; 4.6 mmol) in ethyl acetate (2 mL). The reaction mixture was stirred at room temperature for 10 min. Then, ethyl acetate (25 mL) was added and washed the solution with H_2O (2 × 30 mL) and saturated aqueous $NaHCO_3$ (2 × 30 mL), and then dried (Na_2SO_4) and concentrated. The crude product was purified by column chromatography (10:1 ethyl acetate–methanol) giving the title compound (268 mg, 74%) isolated as a solid, mp 97–99 °C. IR (KBr): 1628, 1572, 1428, 1134 and 1079 cm^{-1}. ^{1}H-NMR ($CDCl_3$, 400 MHz): δ (in ppm) 7.37 (s, 10H, Ph), 3.80 (s br, 8H, CH_2N) and 3.57 (s br, 8H, CH_2O). ^{13}C-NMR ($CDCl_3$, 300 MHz): δ (in ppm) 172.2 (CO), 136.8, 129.3, 128.5, 126.6 (aromatics C, CH), 70.6, 69.8 (CH_2O), 49.9 and 46.2 (CH_2N). HRMS (MALDI) calc. for $C_{26}H_{34}N_2O_6Na$ [M + Na]$^{+}$ 493.2314. Found 493.2305.

2.2.2. Synthesis of 7,16-dipivaloyl-1,4,10,13-tetraoxa-7,16-diazacyclooctadecane(IV)

A solution of pivaloyl chloride (72 μL; 0.6 mmol) and triethylamine (160 μL; 1.2 mmol) in ethyl acetate (2 mL) was added to a solution of 4,13-diaza-18-crown-6 (50 mg; 0.2 mmol) in ethyl acetate (10 mL). The reaction mixture was stirred at room temperature for 20 min. Next, ethyl acetate (50 mL) was added and washed the solution with H_2O (2 × 25 mL) and saturated aqueous $NaHCO_3$ (2 × 25 mL), and then dried (Na_2SO_4) and concentrated. The crude product was purified by column chromatography (10:1 ethyl acetate–methanol) giving the title compound (63 mg, 76%) isolated as a solid, mp 95–96 °C. IR (KBr): 1614, 1102 and 1137 cm^{-1}. ^{1}H-NMR ($CDCl_3$, 400 MHz): δ (in ppm) 3.67 (s, 8H, CH_2N), 3.60 (s, 8H, CH_2O) and 1.28 (s, 18H, CH_3). ^{13}C-NMR ($CDCl_3$, 300 MHz): δ (in ppm) 177.8 (CO), 70.8, 70.2 (CH_2O), 48.5, 45.8 (CH_2N), 39.1 (CH_3) and 28.7 (C). HRMS (MALDI) calc. for $C_{22}H_{42}N_2O_6Na$ [M + Na]$^{+}$ 453.2940. Found 453.2938.

2.2.3. Synthesis of 7,16-[bis(N-adamantylcarbamoyl)propionyl]-1,4,10,13-tetraoxa-7,16-diazacyclooctadecane(VI)

The synthesis of ionophore VI was made using two steps with a 37% overall yield.

2.2.3.1. Synthesis of (N-adamantylcarbamoyl)propionic acid. To a solution of succinic anhydride (0.8 g; 8 mmol) in ethyl acetate (50 mL) was added a solution of 1-adamantylamine (1.2 g; 8 mmol) and triethylamine (1110 μL; 8.8 mmol). The reaction mixture was stirred at room temperature for 30 min. After this time, the solid was separated, dissolved in water (25 mL) and acidified by addition of HCl 25 wt% (25 mL) until pH ∼2. The aqueous solution was extracted with CH_2Cl_2 (3 × 100 mL) and the combined organic phases were dried (Na_2SO_4) and concentrated giving a solid product that corresponding to the acid (957 mg, 49.5%), mp 183–185 °C.

2.2.3.2. Synthesis of 7,16-[bis(N-adamantylcarbamoyl)propionyl]-1,4,10,13-tetraoxa-7,16-diazacyclooctadecane. 0.32 g (1.26 mmol) of (N-adamantylcarbamoyl)propionic acid was dissolved in 15 mL of thionyl chloride. The reaction mixture was stirred at room temperature for 3.5 h. To remove the excess of thionyl chloride was added, and eliminated by evaporation, anhydrous toluene. To a solution of the reaction product in ethyl acetate (30 mL) was added a solution of 4,13-diaza-18-crown-6 (100 mg; 0.42 mmol) and triethylamine (351 μL; 2.52 mmol) in ethyl acetate (20 mL). After this time, the solution was washed with H_2O (2 × 35 mL), 5 wt% HCl (2 × 35 mL), saturated aqueous $NaHCO_3$ (2 × 35 mL) and next with H_2O (1 × 35 mL). The organic layer was dried (Na_2SO_4), filtered and concentrated to give a crude product that was purified by silica-gel column chromatography (10:1 methylene chloride–methanol) yielding ionophore VI (226 mg, 74%), isolated as a solid, mp 158–160 °C. IR (KBr): 3489, 1636 and 1544 cm^{-1}. ^{1}H-NMR ($CDCl_3$, 400 MHz): δ (in ppm) 3.70–3.58 (m, 24H, CH_2O and CH_2N), 2.70–2.58 (m, 8H, CH_2), 2.06 (s, 6H, CH), 2.00 (s, 12H, CH_2) and 1.68 (s, 12H, CH_2). ^{13}C-NMR ($CDCl_3$, 300 MHz): δ (in ppm) 70.9–69.8 (CH_2O), 49.5, 48.1 (CH_2N), 29.5 and 29.1 (CH). HRMS (FAB^{+}) calc. for $C_{40}H_{64}N_4O_8Na$ [M + Na]$^{+}$ 751.4610. Found 751.4622.

2.3. Optosensing manifold

The single-line flow-injection system used consist of a peristaltic pump (Gilson Minipuls-2, France) and a self-constructed

flow-through cell, of 700 μL volume and 9.9 mm ∅ quartz windows, containing the sensing membrane, mounted inside the sample compartment of a DAD spectrophotometer (HP-8453, Nortwalk, CT, USA) coupled to a computer-controlled data acquisition unit. Sample solutions were transferred to the flow system by continuous aspiration.

2.4. Preparation of sensing membranes and measurement set-up

The membranes were produced on a polyester substrate using a spin-coating technique. Mixtures for the preparation of sensing membranes were made from a batch containing ionophore, chromoionophore and lipophilic salt in 1:1:1 molar ratio (2.2×10^{-3} mmol each), next to 64.25 mg (68 wt%) of TBP and the adequate amount of PVC was added to complete the 100 wt%, all dissolved in 1 mL of freshly distilled THF. The membranes were cast by placing 20 μL of the cocktail on a 24 mm ∅ circular polyester sheet using a spin-coater and dried slowly in a dryer with saturated THF atmosphere at room temperature. The sensing area of the sensor is a transparent and red 10 mm ∅ circular film with a calculated thickness of about 25 μm.

The response of the sensors was evaluated by using standard solutions of alkaline and alkaline-earth ions under study ranging from 1×10^{-7} to 9×10^{-1} M in concentrations (50 mL volumetric flask) in pH 8.5 or pH 9.0 Tris buffer solution 2×10^{-2} M or pH 8.5 diethanolamine buffer solution 2×10^{-2} M. The membrane previously introduced in the flow-through cell was measured successively for the absorbance at 660 nm after equilibration with 10^{-2} M HCl (A_{HC^+}); 2×10^{-2} M buffer solution; buffered standard solutions to be measured (A), and 10^{-2} M NaOH solution (A_C). The membranes were not conditioned before use. All absorbance measurements were carried out at room temperature (22.0 ± 0.5 °C).

The exchange constants $K^{IL_p}_{exch}$ were calculated according to a least-squares approximation method [9] using $1-\alpha$ experimental values in the maximum slope zone of the response function obtained working at eight different concentration levels and three replicates of each one. Activities were calculated according to the Debye Hückel formalism [10].

The selectivity of these sensing membranes against Ca(II) was measured by using the selectivity coefficients $k^{Osel}_{i,J}$ [11] that were determined using the separate solutions method (SSM) by plotting the single-ion response functions $(1-\alpha)$ *vs* $\log a_{I^{z+}}$ according to Eq. (4) for all cations studied. Since the pH was constant (pH 8.5), the selectivity coefficients were given by the horizontal distance between curves of primary and interfering ions for a protonation degree $1-\alpha = 0.5$ [12].

3. Results and discussion

The sensing system is based on cation-exchange between a complete organic phase of plasticized PVC membrane and an aqueous problem containing the analyte, as was described by Bakker et al. [13]. The sensing membranes contain an ionophore L and a chromoionophore C selective for hydrogen ions, giving both the positively charged species in membrane phase, IL_p^{z+} and HC^+, where p is the stoichiometry of the complexes formed. To permit the ion-exchange equilibrium was also incorporated an alkaline salt of a highly lipophilic anion R^- to the membrane.

In contact with the aqueous solution containing alkaline or alkaline-earth ions next equilibrium occurs in sensing membrane:

$$I^{z+} + p\bar{L} + z\overline{HC^+} \leftrightarrow IL_p^{z+} + z\bar{C} + zH^+ \quad (1)$$

where the ionophore is assumed to form 1:p (M:L) complexes. Species in the organic sensing phase are barred, while all others are in the aqueous phase. This equilibrium is characterized by the exchange constant $K^{IL_p}_{exch}$ defined as:

$$K^{IL_p}_{exch} = \frac{a^z_{H^+}[C]^z[IL_p^{z+}]}{a_{I^{z+}}[HC^+][L]^p} \quad (2)$$

where concentration in membrane phase are given in molalities and in aqueous solution in activities.

The change between the protonated and deprotonated forms of the chromoionophore (Eq. (1)) depends on the activity of the ion I^{z+} in the aqueous phase. In a buffered solution, the analyte activity is determined by the degree of protonation of the chromoionophore $(1-\alpha)$; which is optically calculated using the absorbance for the fully protonated (A_{HC^+}), obtained in 10^{-2} M HCl, and deprotonated forms (A_C), obtained in 10^{-2} M NaOH, of the chromoionophore and the absorbance A for the buffered standard solution [14]:

$$1-\alpha = \frac{HC^+}{C_0} = \frac{A - A_C}{A_{HC^+} - A_C} \quad (3)$$

The ion activities ratio in aqueous phase is related to the exchange constant $K^{IL_p}_{exch}$ and the degree of protonation $1-\alpha$ through the sigmoidal response function:

$$a_{I^{z+}} = \frac{1}{K^{IL_p}_{exch}} \left(\frac{a_{H^+}\alpha}{1-\alpha}\right)^z \frac{C_R - (1-\alpha)C_C}{z(C_L - (p/z)(C_R - (1-\alpha)C_C))^p} \quad (4)$$

where C_L, C_C and C_R are the analytical concentrations of ionophore, chromoionophore and lipophilic salt, respectively.

In this paper we are interested in the study of calcium ionophores for environmental sensors that could discriminate from concomitant alkaline and alkaline-earth ions. In this way, we have studied some ionophores crown ether type coming from 18-crown-6 ether to 4,13-diaza-18-crown-6 ether and then introducing N-substituent in the diaza parent crown ring to prepare a series of double-armed crown ethers. The donor group on the functionalized flexible sidearm, that provides further coordination with the guest alkaline or alkaline-earth cation complexed in the hydrophilic crown ring, is a carbonyl group in all cases coming from an amide bonding.

We have modified the lipophilicity of ionophore molecule using different terminal units varying in lipophilicity and size at the terminal of the side chains; namely benzoyl(III), pivaloyl(IV), and N-adamantylcarbamoyl with two different size chain: acetyl(V) and propionyl(VI). With the goal to know the complexing behaviour of these ionophores and their discrimination ability of Ca(II) against Mg(II), Na(I) and K(I), we have prepared optical membranes based on ionophore–chromoionophore chemistry. Thus, plasticized PVC membranes contained lipophilized Nile Blue as chromoionophore in all cases and the corresponding ionophore were studied at pH 8.5 adjusted with Tris buffer 2×10^{-2} M. The answer of sensing membranes against alkaline and alkaline-earth ions under study was tested between 1×10^{-7} and 9×10^{-1} M using a flow-through cell according to Section 2. In each case, the experimental $1-\alpha$ values were calculated from spectroscopic data at 660 nm and were fitted to theoretical equation (Eq. (4)) in logarithm of activities. The exchange constants $K^{IL_p}_{exch}$ for all ionophores and metallic ions studied were calculated (Table 1) assuming a 1:1 stoichiometry ($p = 1$) in all the cases, except for K(I) complexes with ionophores IV, V and VI and all Na(I) complexes, with a 1:0.5 stoichiometry ($p = 0.5$).

Potassium shows the biggest changes in exchange constant $K^{IL_p}_{exch}$ with the ionophore used, coming from 1.37×10^{-7} for ionophore I to 4.5×10^{-9} for ionophore VI. The effect of the replacement of two atoms of oxygen in crown ether (ionophore I) by two atoms of nitrogen (ionophore II) is clearly demonstrated and the $K^{IL_p}_{exch}$ correspondent to ionophore I is half an order of magnitude greater than that of the unsubstituted 4,13-diaza-18-crown ether; that suppose that the complex with ionophore II is more stable. This data

Table 1
Exchange constants ($K^{IL_p}_{exch}$) of the sensing membranes based on the different ionophores studied for alkaline and alkaline-earth ions.

Ionophore	$K^{KL_p}_{exch}$	$K^{NaL_p}_{exch}$	$K^{MgL_p}_{exch}$	$K^{CaL_p}_{exch}$
I	$(1.37 \pm 0.06) \times 10^{-7}$	$(1.1 \pm 0.1) \times 10^{-8}$	$(2.63 \pm 0.04) \times 10^{-15}$	$(2.11 \pm 0.01) \times 10^{-15}$
II	$(8.7 \pm 0.4) \times 10^{-8}$	$(1.3 \pm 0.1) \times 10^{-8}$	$(1.6 \pm 0.1) \times 10^{-15}$	$(2.3 \pm 0.4) \times 10^{-15}$
III	$(1.22 \pm 0.04) \times 10^{-7}$	$(1.42 \pm 0.08) \times 10^{-8}$	$(1.6 \pm 0.1) \times 10^{-15}$	$(2.63 \pm 0.06) \times 10^{-15}$
IV	$(7.7 \pm 0.4) \times 10^{-9}$	$(1.25 \pm 0.01) \times 10^{-8}$	$(1.50 \pm 0.01) \times 10^{-15}$	$(2.48 \pm 0.01) \times 10^{-15}$
V	$(5.65 \pm 0.01) \times 10^{-9}$	$(1.18 \pm 0.06) \times 10^{-8}$	$(3.7 \pm 0.3) \times 10^{-15}$	$(4.27 \pm 0.06) \times 10^{-15}$
VI	$(4.5 \pm 0.2) \times 10^{-9}$	$(1.12 \pm 0.03) \times 10^{-8}$	$(1.50 \pm 0.07) \times 10^{-15}$	$(2.3 \pm 0.2) \times 10^{-15}$

contrast with the less stability reported for diazacrown ether complexes with alkaline ions in water respect to the parent crown ether [15].

The attachment of benzoyl-functionalized arms to the diazacrown ring (ionophore III) significantly increases the $K^{IL_p}_{exch}$ value, decreasing thus the stability constant of K(I) complex. However, the change of this group for pivaloyl (ionophore IV) or adamantyl units (ionophores V and VI) supposes a considerable increase in complex stability due to the increase in length of side chain and lipophilicity next to the new carbonyl group.

On the other hand, Na(I) shows a nearly constant behaviour, with the greatest exchange constant $K^{IL_p}_{exch}$ value for ionophore III, due probably to their smaller ionic radius. In the case of Mg(II) the influence of side arms is very small with the only exception of ionophores V and I that originate less stable complexes. The behaviour of Ca(II) is very similar to Mg(II), being the exchange constant higher than that of Mg(II). All values are very similar with the exception of the less stable complex with ionophore V. These values calculated for $K^{IL_p}_{exch}$ are similar to values previously reported by us for Ca(II) and Mg(II) complexes of ionophores V [16] and VI [17].

Selectivity, expressed as logarithmic selectivity coefficients, $\log k^{Osel}_{Ca,J}$, respect to K(I) increases with the size and the lipophilicity of the terminal group of the side chains, being the highest for ionophore VI (Table 2). The selectivity pattern is similar for Na(I), although selectivity is lower than for K(I). General speaking, the selectivity respect to Mg(II) is not very high, but there are some interesting differences. Ionophore I, 18-crown-6 ether, is more selective for Mg(II) than Ca(II), but substitution of O by N in the crown ring increases selectivity for Ca(II) and the introduction of double side arms do not suppose any variation in selectivity except for ionophores V and VI. The introduction of the N-adamantylcarbamoyl units in the diazacrown ether increases selectivity for Ca(II) respect to Mg(II). These results are surprising comparing to results given by Suzuki et al. that find ionophore V as a very selective ionophore for Mg(II) in potentiometric sensors [8] and also in optical sensors but using both a different plasticizer, NPOE, and chromoionophore [18]. Additionally, the selectivity coefficients obtained here for ionophore VI are lower than that calculated by us [17] probably due to the different composition of sensing membrane.

Fig. 2 shows the complexing behaviour of these ionophores and their discrimination ability of Ca(II) against Mg(II), Na(I) and K(I).

Table 2
Selectivity coefficients ($k^{Osel}_{Ca,J}$, I = primary ion (Ca^{2+}), J = interfering ion) for sensing membranes studied.

Selectivity coefficients, $\log k^{Osel}_{Ca,J}$			
Ionophore	K(I)	Na(I)	Mg(II)
I	−1.15	−1.20	0.10
II	−1.40	−1.18	−0.16
III	−1.31	−1.19	−0.23
IV	−1.43	−1.23	−0.22
V	−1.80	−1.49	−0.07
VI	−1.78	−1.38	−0.33

As a conclusion, the optical membrane based on the double-armed diazacrown ether possessing a malonic diamide in their side chains (ionophore V) exhibits the best Ca(II) selectivity. Additionally, it presents the highest selectivity respect to the alkaline ions K(I) and Na(I); however, it responds equally to Ca(II) and Mg(II). Consequently, the ionophore with the best Ca(II) selectivity over the rest of the cations studied is VI, since its answer to K(I) and Na(I) is similar to the corresponding to V and their differentiation from Mg(II) is the best.

In order to compare the $k^{Osel}_{I,J}$ values previously reported by us for alkaline and alkaline-earth ions for optical membranes using ionophore I [9], membranes with the same composition that the above-mentioned were prepared but the response of the sensor was evaluated using solutions buffered with pH 8.5 diethanolamine buffer solution 2×10^{-2} M instead of Tris buffer. The $k^{Osel}_{I,J}$ values obtained in these new conditions were −0.57 Mg(II); −0.63 Na(I) and −2.49 K(I) that compares favourably with selectivity coefficients values previously reported (−0.66 Mg(II); −1.58 Na(I) and −2.08 K(I)). Comparing results obtained using Tris buffer solution, the selectivity respect to Mg(II) and K(I) increases considerably, whereas it decreases respect to Na(I), which shows the significant role played by the buffer composition.

We have used ionophore V for hardness determination based on the equal response to calcium and magnesium of sensing membrane at pH 9.0 [16]. By this reason we have studied again the selectivity against alkaline and alkaline-earth ions using the same ionophore but at pH 9.0 adjusted with Tris buffer 2×10^{-2} M. The resulting $k^{Osel}_{I,J}$ values in these conditions were −0.07 Mg(II); −1.47 Na(I) and −1.76 K(I), which means that is slightly more selective for Na(I) and K(I) than the method previously reported. It is important to emphasize that the selectivity coefficients obtained at pH 8.5 (Table 2) and 9.0 were practically the same.

To compare the analytical characteristics of the different sensing membranes for Ca(II) we studied their range, detection limit and precision (Table 3). As measuring range we use the linear

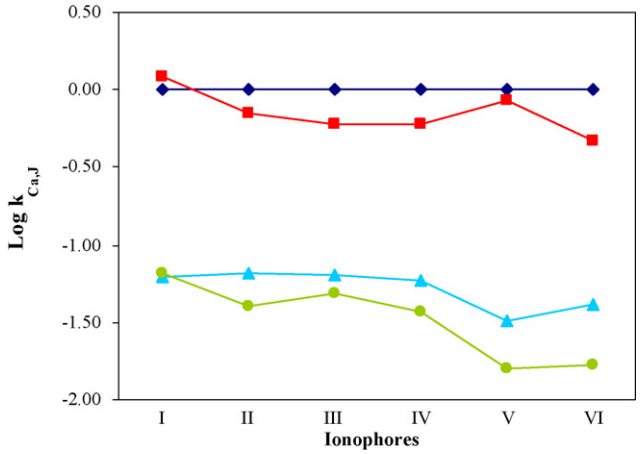

Fig. 2. Selectivity (SSM method) variation of the membranes as function of ionophore used.

Table 3
Analytical parameters for Ca(II) sensing membranes studied.

Ionophore	I	II	III	IV	V	VI
Intercept	−0.0049	−0.0207	−0.0276	−0.0354	−0.0208	−0.0354
Slope	−0.1741	−0.1902	−0.1867	−0.1921	−0.1603	−0.1921
Probability level (%) (lack-of-fit test)	53.7	69.2	50.1	87.4	49.3	87.5
Linear range (activities)	2.0×10^{-4}–0.23 M	2.3×10^{-4}–0.23 M	1.6×10^{-4}–0.23 M	1.7×10^{-4}–0.23 M	8.1×10^{-5}–0.23 M	5.9×10^{-5}–0.23 M
Detection limit (activities)	2.0×10^{-4} M	2.3×10^{-4} M	1.6×10^{-4} M	1.7×10^{-4} M	8.1×10^{-5} M	5.9×10^{-5} M
Intermembrane precision RSD (%)						
0.8 mM[a]	2.47	3.70	0.93	0.97	1.10	1.03
48 mM[a]	1.52	0.92	0.54	0.67	0.91	0.41
231 mM[a]	3.16	0.65	0.21	0.37	1.31	0.12

[a] Activities tested in mmol L^{-1}.

relationship in the middle of the sigmoidal response function defined by means a *lack-of-fit* test and as the detection limit the intersection of the linear calibration function defined above and a linear function adjusted in the minimal slope zone. As upper range we consider the highest value tested in all the cases (231 mM).

The detection limit decreases with the size and the lipophilicity of the terminal group of the side chains coming from 2.3×10^{-4} M for ionophore II to 5.9×10^{-5} M for ionophore VI according to the exchange constant values $K_{\text{exch}}^{\text{IL}_p}$ for each ionophore.

Acknowledgements

We acknowledge financial support from *Ministerio de Educación y Ciencia, Dirección General de Enseñanza Superior* (Spain) (Projects CTQ2005-09060-CO2-01 and CTQ2005-09060-CO2-02); and *Junta de Andalucia* (Proyecto de Excelencia P06-FQM-01467).

Appendix A. Supplementary data

Supplementary data associated with this article can be found, in the online version, at doi:10.1016/j.talanta.2009.01.046.

References

[1] C.J. Pedersen, J. Am. Chem. Soc. 89 (1967) 7017.
[2] G.W. Gokel, Crown ether and cryptands, 1st ed., The Royal Society of Chemistry, London, 1991.
[3] J.W. Steed, Coord. Chem. Rev. 215 (2001) 171.
[4] P.A. Gale, Philos. Trans. R. Soc. Lond. Ser. A: Math. Phys. Eng. Sci. 358 (2000) 431.
[5] H. Tsukube, Talanta 40 (1993) 1313.
[6] M. Hiraoka, Crown Ethers and Analogous Compounds, Elsevier, Amsterdam, 1992.
[7] W.E. Morf, K. Seiler, B. Rusterholz, W. Simon, Anal. Chem. 62 (1990) 738.
[8] K. Suzuki, K. Watanabe, Y. Matsumoto, M. Kobayashi, S. Sato, D. Siswanta, H. Hisamoto, Anal. Chem. 67 (1995) 324.
[9] L.F. Capitán-Vallvey, M.D. Fernandez-Ramos, P. Alvarez de Cienfuegos, Anal. Chim. Acta 451 (2002) 231.
[10] P.C. Meier, Anal. Chim. Acta 136 (1982) 363.
[11] E. Bakker, Anal. Chim. Acta 350 (1997) 329.
[12] E. Bakker, W. Simon, Anal. Chem. 64 (1992) 1805.
[13] E. Bakker, P. Bühlmann, E. Pretsch, Chem. Rev. 97 (1997) 3083.
[14] I. Tsagkatakis, S. Peper, E. Bakker, Anal. Chem. 73 (2001) 315.
[15] B.G. Cox, P. Firman, H. Horst, H. Schneider, Polyhedron 2 (1983) 343.
[16] L.F. Capitán-Vallvey, M.D. Fernandez-Ramos, P. Alvarez de Cienfuegos, F. Santoyo-Gonzalez, Anal. Chim. Acta 481 (2003) 139.
[17] L.F. Capitán-Vallvey, M.D. Fernandez-Ramos, P. Alvarez de Cienfuegos, F. Santoyo-Gonzalez, Analyst 129 (2004) 783.
[18] D. Siswanta, H. Hisamoto, S. Sato, Y. Matsumoto, Y. Koike, S. Yamamori, K. Suzuki, Anal. Sci. 13 (1997) 429.

Talanta 78 (2009) 1378–1382

Contents lists available at ScienceDirect

Talanta

journal homepage: www.elsevier.com/locate/talanta

A critical evaluation of digestion procedures for coffee samples using diluted nitric acid in closed vessels for inductively coupled plasma optical emission spectrometry

Jacira T. Castro[a,b], Elisângela C. Santos[a], Wagna P.C. Santos[a,c], Letícia M. Costa[d], Mauro Korn[e], Joaquim A. Nóbrega[f], Maria Graças A. Korn[a,*]

[a] Instituto de Quimica, Universidade Federal da Bahia, Campus Universitário de Ondina, Salvador, BA, Brazil
[b] Centro de Ciências Exatas e Tecnológicas, Universidade Federal do Recôncavo da Bahia, Cruz das Almas, BA, Brazil
[c] Centro Federal de Educação Tecnológica da Bahia, Salvador, BA, Brazil
[d] Departamento de Química, Instituto de Ciências Exatas, Universidade Federal de Minas Gerais, Belo Horizonte, MG, Brazil
[e] Departamento de Ciências Exatas e da Terra, Universidade do Estado da Bahia, Salvador, BA, Brazil
[f] Departamento de Química, Universidade Federal de São Carlos, São Carlos, SP, Brazil

ARTICLE INFO

Article history:
Received 1 December 2008
Received in revised form 9 February 2009
Accepted 11 February 2009
Available online 21 February 2009

Keywords:
Microwave-assisted heating
Conductive heating
Closed vessel
Acid decomposition
Diluted nitric acid
Liquid phase oxidizing process
Gas phase conversion

ABSTRACT

The efficiency of diluted nitric acid solutions for digesting regular coffee samples was evaluated employing two closed vessel procedures: one was based on microwave-assisted heating and the other was based on conductive heating using pressurized Parr bomb. The efficiency of digestion was evaluated by determining residual carbon content (RCC) and residual acidity. The digestion was effective using both procedures, i.e. there were no solid residues after the decomposition reactions when using up to 3.5 mol L^{-1} nitric acid solutions. It was demonstrated that the digestion procedures are critically dependent on reactions occurring in liquid and gas phase and that the formation of NO and its conversion to NO_2 by O_2 exerts a major effect in the oxidation of organic matter. These processes are more effective in closed vessels heated by microwave radiation due to the greater volume of these flasks and the temperature gradient that exists during the first step of the digestion process. The proposed model for the digestion processes in diluted nitric acid solution is corroborated by data about consumption of acid during the digestion and by measuring the pressure during the whole process.

1. Introduction

Sample pretreatment is frequently the most time consuming step of an analytical procedure and the bottleneck of the whole analytical process when elements are determined in solid samples [1]. Occasionally solid sample preparation for trace element determination can be performed by simple dilution [2,3], however, usually, chemicals and different energy sources are associated for total or partial sample decomposition [2–12]. Two procedures are generally employed for sample preparation: dry and wet decomposition. For wet decomposition, pressurized closed vessels are usually employed to avoid contamination and losses of volatile elements during acid digestion [2,3,8]. Digestion in closed systems at elevated temperatures begin to be successfully used only after the introduction of polytetrafluoroethylene (PTFE, Teflon®) as material for the reaction vessels due to the high degree of chemical and thermal resistance [10]. Digestions at elevated temperature and pressure in closed systems present advantages, such as the decrease of both decomposition time and reagent volumes required for sample digestion [11].

Most digestion procedures for biological samples employ nitric acid because it is a strong oxidizing agent at high temperatures and concentrations. Additionally, nitric acid is easily purified and diluted solutions can be used for sample preparation step in order to increase the safety and to decrease reagent volumes and residues. Diluted nitric acid solutions were successfully used for microwave-assisted plant digestion [13–18], leading to low blank values. The effect of nitric acid and hydrogen peroxide concentrations on closed vessel microwave-assisted digestion of plant materials was previously described [14] and the residual carbon did not exceed 13%. In another work, a closed vessel microwave-assisted procedure was combined with diluted nitric acid solution for digesting bovine liver and spinach leaves standard reference materials and accurate results were obtained for Al, Ca, Cu, Fe, K, Mg, Mn, P, and Zn [15]. Recently, an experimental design approach was applied to optimize the extraction of trace elements from raft mussel samples with

* Corresponding author. Tel.: +55 71 32836830; fax: +55 71 32836830.
E-mail address: korn@ufba.br (M.G.A. Korn).

0039-9140/$ – see front matter © 2009 Elsevier B.V. All rights reserved.
doi:10.1016/j.talanta.2009.02.030

Table 1
Instrumental parameters for elements determination using axial ICP OES.

Instrumental parameter	
RF generator (MHz)	40
Applied power (kW)	1.3
Plasma gas flow-rate (L min^{-1})	15.0
Auxiliary gas flow-rate (L min^{-1})	1.5
Nebulizer gas flow-rate (L min^{-1})	0.7
Integration time (s)	1.0
Stabilization time (s)	15
Reading time (s)	1
Replicates	3
Spray chamber	Cyclonic
Nebulizer	Concentric
Analytical wavelengths (nm)	
C I	193.025
Ba II	455.396
Cu II	327.395
P I	177.432

I: Atomic line. II: Ionic line.

diluted acids associated to hydrogen peroxide by exploring closed vessel short microwave irradiation cycle [16]. Major improvements in the extraction techniques have been introduced not only aiming the preparation time but also to simplify sample preparation handling for trace elements determination [18–21]. However, the behavior of closed vessel using diluted acid digestion procedures to extract trace elements from diverse matrices has not been fully explained.

Therefore, the aim of the present work was to perform a systematic investigation about the efficiency of closed vessels digestion using nitric acid solutions in different concentrations associated with hydrogen peroxide to digest organic matrices (regular powdered coffee samples) by employing heating either by microwave radiation or by conduction. Finally, a general mechanism for organic matter decomposition in both closed vessel digestion procedures were proposed based on the comparison of diverse parameters such as final acidity, residual carbon contents (RCC) as well as element concentrations.

2. Experimental

2.1. Equipments

A closed vessel microwave digestion system with control sensor pressure and temperature (ETHOS EZ, Milestone, Sorisole, Italy), and a pressurized bomb Parr (Model 4746, Parr Instrument Company, Moline, IL, USA) were used for sample digestion.

An inductively coupled plasma optical emission spectrometer with axial viewing - ICP OES (Vista Pro, Varian, Mulgrave, Australia) equipped with solid state detector, cyclonic spray chamber, and concentric nebulizer was employed for analytes and residual carbon content determinations. The operational parameters adopted are listed in Table 1. All measurements were carried out using argon as plasma gas. Total carbon concentration in powdered coffee samples was determined by elemental analyzer (ThermoQuest® Finnigan Flash EA 1112).

2.2. Reagents, solutions and samples

All solutions were prepared with analytical grade reagents (Merck, Darmstadt, Germany), and deionized water from Millipore water purification system (Milli-Q, Millipore, Bedford, MA, USA), was used for the preparation of the samples and standards. Laboratory glassware was kept overnight in 10% (v/v) nitric acid solution. Glasses were rinsed with freshly deionised water and dried in a dust free environment before use.

Table 2
Microwave heating program for digestion of powered coffee samples.

Step	Time (min)	Temperature (°C)
1	5	120
2	3	120
3	10	210
4	15	210

Reference solutions containing from 50 to 1500 mg L^{-1} C were prepared using 5.0% (w/v) C stock solution prepared from urea (Reagen, Rio de Janeiro, Brazil) as earlier reported [22].

One regular powder coffee sample purchased in a local market was manually ground and sieved to a 100–500 μm particle size range.

2.3. Digestion procedures

2.3.1. Microwave-assisted acid digestion

Masses of 250 mg of coffee samples were directly inserted into microwave closed vessels made with perfluoroalcoxi polymer (PFA) with a volume of 100 mL. Volumes of 7.0 mL of nitric acid solution were added in the following concentrations: 14.0, 10.5, 7.0, 3.5, 1.7 and 1.0 mol L^{-1}. Then, volumes of 1.0 mL of 30% (w/w) H_2O_2 were also added to each vessel. The heating program described in Table 2 was applied to six reagent vessels. The power and maximum pressure were set in 750 W and 35 bar, respectively. After sample digestion, digests were transferred to glass volumetric flasks and the volumes were made up to 20.0 mL with distilled-deionized water.

2.3.2. Pressurized bomb acid digestion

Masses of 200 mg of coffee samples were directly introduced into PTFE closed vessels with volumes of 23 mL. A volume of 2.0 mL of the previously described nitric acid solutions was added to each vessel. Then, a volume of 1.0 mL of 30% (w/w) H_2O_2 was also added to each reaction vessel. Parr bombs were sealed and put in a muffle furnace set at 120 ± 10 °C and remained at this temperature during 12 h. After cooling down at room temperature, solutions were transferred to glass volumetric flasks and volumes were made up to 15.0 mL with water.

3. Results and discussion

The use of nitric acid for organic matrices digestion is the most usual approach for wet sample pretreatment to facilitate trace elements determination. Ideally, the best digestion should led to a complete decomposition of organic material using minimal amounts of nitric acid which should be as diluted as possible to decrease residual carbon and the acid concentration in the resulting digest solution with the aim to avoid critical effects on instrument parts, such as nebulizer, nebulization chamber and torch in ICP OES [11]. The minimization of nitric acid amount for promoting decomposition processes can be performed by two different approaches: (i) by adding aliquot volumes as low as possible of concentrated nitric acid, or (ii) by using a diluted nitric acid solution. In fact it is required a minimum volume of acid solution to merge with the solid sample particles throughout the material decomposition because it may be supposed that the solid sample digestion occurs in the solid–liquid interface. In addition, a significant volume of acid solution is transferred to the gas phase when the sample digestion is carried out in pressurized closed vessels independently on the heating strategy. Therefore, the use of greater volumes of diluted nitric acid for sample decomposition have been more exploited than the minimization of the volume of concentrated solutions, in special for microwave-assisted digestion of biological samples [13–21]. Addi-

Table 3
Mean values and standard deviations ($N = 4$) for efficiency of organic matter decomposition (EOMD), residual acidity of the digests and Ba, Cu and P determinations in coffee samples applying both closed vessel digestion procedures.

Closed vessel system	HNO_3			Efficiency of organic matter decomposition (%)	Elemental concentration		
	Initial (mol L^{-1})	Final (mol L^{-1})	Consumed (%)		Ba ($\mu g\,g^{-1}$)	Cu ($\mu g\,g^{-1}$)	P ($mg\,g^{-1}$)
Parr Bomb	14	1.58 ± 0.07	88.8 ± 0.5	98.9 ± 0.2	3.4 ± 0.2	12.6 ± 0.1	1.84 ± 0.04
	10.5	1.011 ± 0.003	90.37 ± 0.03	98.60 ± 0.04	3.7 ± 0.1	12.7 ± 0.1	1.88 ± 0.02
	7	0.69 ± 0.02	90.1 ± 0.3	98.42 ± 0.05	3.8 ± 0.2	12.9 ± 0.2	1.83 ± 0.03
	3.5	0.31 ± 0.02	91.2 ± 0.6	98.16 ± 0.08	3.9 ± 0.2	12.9 ± 0.3	1.82 ± 0.04
Microwave							
	10.5	3.82 ± 0.01	63.6 ± 0.1	98.0 ± 0.2	3.7 ± 0.1	12.1 ± 0.2	1.66 ± 0.04
	7	2.50 ± 0.03	64.2 ± 0.5	97.7 ± 0.2	3.7 ± 0.1	12.0 ± 0.2	1.64 ± 0.03
	3.5	1.22 ± 0.04	65 ± 1	97.8 ± 0.5	3.6 ± 0.2	12.0 ± 0.3	1.73 ± 0.04

tionally, the use of diluted nitric acid solutions in routine analysis increases the safety of the procedure. A further advantage of the digestion using diluted nitric acid solutions is highlighted once blank values can be diminished resulting in lower limits of quantification. Despite the proper precision and accuracy when comparing diverse analytical results obtained from different digestion strategies as it can be observed in Table 3, the digestion procedure carried out with diluted nitric acid in closed vessels still needs a better understanding about the chemical processes behind organic matter decomposition. A hypothesis to explain the efficiency of closed vessel microwave-assisted organic matter digestion was recently presented and it was based on the oxygen amount and the gradient of temperature inside the digestion vessel during the beginning of the process [11].

The digestion procedures for coffee samples applied in the present work were based on the use of diluted HNO_3 solution and H_2O_2 as auxiliary reagent to take advantage of the high microwave energy absorption by water, as earlier discussed by Kingston and Haswell [23]. As a statement, the conversion of microwave energy in heat is maximized by using diluted acidic solutions.

Two different digestion alternatives for coffee sample preparation procedures with diluted nitric acid solutions were investigated for metal contents determination: microwave-assisted and pressurized bomb digestion (Table 3). A set of blanks was prepared together with each batch of samples. It is important to point out that it was not possible to perform the experiments exactly in the same experimental conditions due to safety aspects. The microwave vessel has a volume of 100 mL and it allows working safely with 250 mg of sample without any sudden increase of pressure. Taking into account vessel characteristics, the digestion was carried out using 7.0 mL nitric acid and 1.0 mL hydrogen peroxide. On the other hand, using the pressurized bombs with volumes of 23 mL it was feasible to digest only 200 mg of sample with 2.0 mL nitric acid and 1.0 mL hydrogen peroxide solutions. Solutions containing different nitric acid concentrations were employed to test their efficiency and to get a better understanding of the conductive-assisted and microwave-assisted digestion processes.

All digestion procedures were evaluated by comparing diverse parameters: residual RCC, residual acidity of the digests and the major, minor and trace element recoveries (Table 3) and no significant differences were observed for 95% confidence level by applying one-way ANOVA followed by the application of multiple comparisons Bonferroni test [24,25] for acid concentrations greater than 3.5 mol L^{-1}. As previously mentioned, it is well known that the acid concentration of digests affect pneumatic nebulization and aerosol formation whereas RCC affects plasma excitation conditions and causes spectral interferences mainly at low wavelengths. Notwithstanding, partial solid sample decomposition were obtained for experiments carried out with HNO_3 concentrations lower than 2 mol L^{-1}, some results obtained for digestion procedures using 1.75 and 1.0 mol L^{-1} nitric acid solutions in microwave and pressurized bomb systems were used to explain the processes behavior. The residual acidity of the solutions obtained after the digestion procedures performed with closed vessel microwave and in pressurized bomb systems varied from 0.31 ± 0.03 to 4.66 ± 0.02 and from 0.16 ± 0.03 to 1.58 ± 0.07 mol L^{-1}, respectively. The calculated residual acid concentrations were evidently lower starting from more diluted HNO_3 solution and the dispersions of these results (RSD, in %) were increased for microwave-assisted and conductive heating by decreasing the initial nitric acid concentration. The relative standard deviations associated to the parameter residual acid concentration for mutually independent digestions (N = 4) of the same regular coffee sample carried out with 1 mol L^{-1} and concentrated HNO_3 solutions by exploring conductive and microwave heating were 18 and 9.6% and 4.4 and 0.4%, respectively. The increases of RSD values for digestions carried out with 1 mol L^{-1} HNO_3 solution were related to the fact that only a fraction of organic matter was decomposed when using this solution.

The evaluation of the chemical mechanisms involved with microwave and pressurized digestion processes is better accomplished considering the percentage of nitric acid consumed (Table 3). Using closed vessels heated by microwave radiation, the nitric acid consumption varied in the 63.6 to 66.7% range and with pressurized bomb vessels varied in the 88.8 to 91.2% range. The greater consumption of nitric acid in pressurized bomb was a hint for understanding the processes behind the digestion. The model proposed involves conversion processes in liquid and gas phases.

The effectiveness of the digestion processes was also evaluated by the efficiency of organic matter decomposition (EOMD, expressed in %) which value is calculated by the ratio between the difference of total carbon contents (TCC) and the residual RCC determined in the digests and TCC, i.e. $(TCC - RCC/TCC) \times 100$. This proposed parameter only can be considered when a homogeneous liquid phase or only silicate solid phase residues are obtained after the digestion. The EOMD was always higher than 98% for the evaluated closed vessel digestion processes (Table 3).

It is known that the main product when employing concentrated nitric acid is NO_2 [11]. On the other hand, in diluted nitric acid solutions there is a preferential production of NO. In this case, during the oxidation of organic matter by nitric acid, NO is produced and it reacts with O_2 in gas phase generating NO_2. After, the formed NO_2 can be reabsorbed in the liquid phase leading to NO_3^- and HNO_2 production. This reaction cycle proceeds till complete consumption of the O_2 in the gas phase. These chemical processes are represented by the following equations:

$$2H_2O_2 \rightarrow 2H_2O + O_{2(g)}$$

$$2NO_{(g)} + O_{2(g)} \rightarrow 2NO_{2(g)}$$

$$2NO_{2(g)} + H_2O \rightarrow HNO_{3(aq)} + HNO_{2(aq)}$$

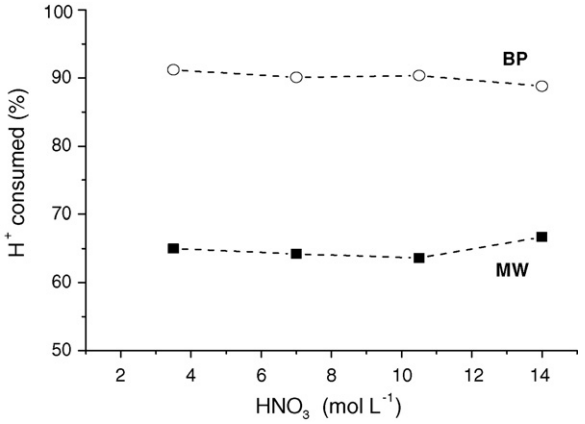

Fig. 1. Evaluation of HNO_3 consumption for digestions of coffee sample in Parr bomb (BP) and microwave oven (MW).

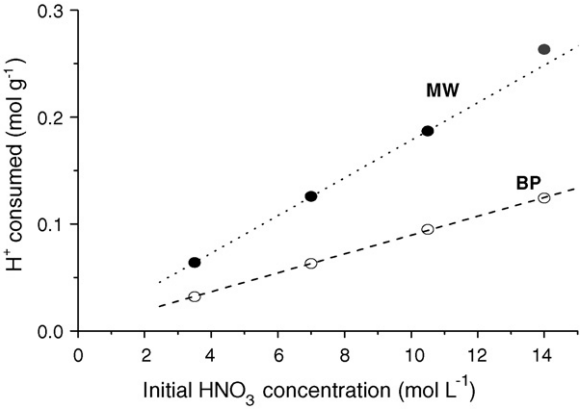

Fig. 3. Consumption of H^+ (mol) necessary to decompose 1 g of coffee sample by employing Parr bomb (BP) and microwave oven (MW) procedures.

$$2HNO_{2(aq)} \rightarrow H_2O + NO_{2(g)} + NO$$

It is clear that these processes are critically dependent on the volume of O_2 in the closed vessel. As already pointed out, the microwave vessel has a 100 mL volume and the pressurized bomb has a 23 mL volume. The greater volume of the former vessel implies that there is more O_2 available to promote oxidation processes in the gas phase despite aliquots of the same volume of H_2O_2 were added in digestion vessels.

In addition to the difference in volume, it is important to emphasize that closed vessels heated by microwave radiation present an intense temperature gradient during the first step of digestion. This

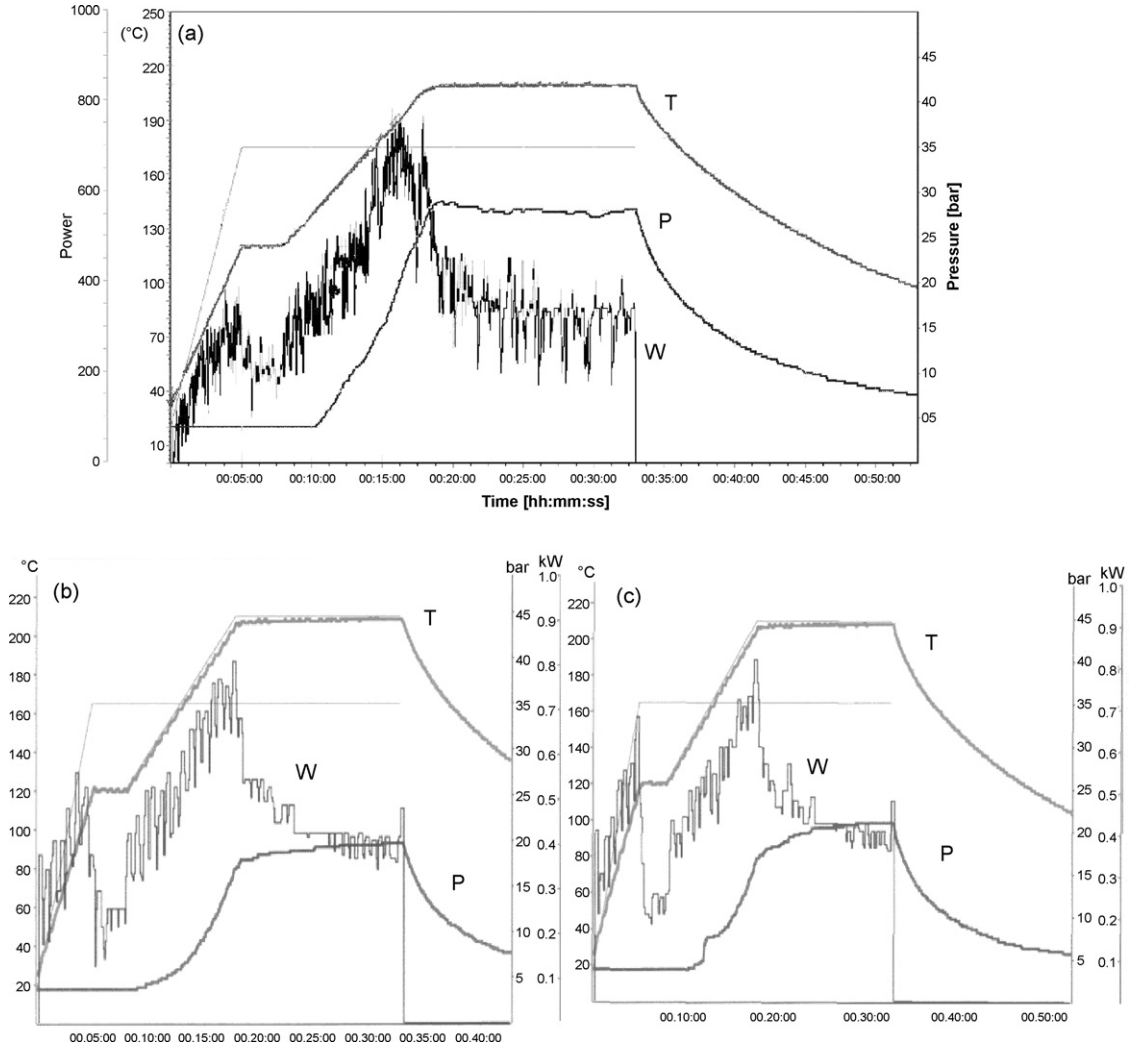

Fig. 2. Profiles of temperature and pressure during the digestion in closed vessel microwave system. *T*: Temperature; *P*: Pressure; *W*: variation of applied power to reach the set temperature. (a) HNO_3 14 mol L^{-1}; (b) HNO_3 7.0 mol L^{-1}; (c) HNO_3 3.5 mol L^{-1}.

aspect can be explained due to the transparency of the vessel to the microwave radiation and the intense absorption of it by the liquid phase but not by the gas phase. Consequently, in the first step of digestion the soluble gases as well those formed by evaporation and chemical processes are transferred to the gas phase, which remains at low temperature, and suffers condensation. This temperature gradient also acts to improve the reaction between NO, produced by the oxidation of organic matter during the digestion, and O_2 leading to NO_2 production. The formed NO_2 is reabsorbed in the acid solution and regenerates HNO_3, as discussed. The more intense occurrence of these processes in microwave-heated vessels was experimentally proved by the lowest consumption of HNO_3 during the digestion process (Fig. 1). Another evidence of the occurrence of these processes was the less intense increase of pressure observed when microwave digestion process was carried out with diluted nitric acid solution. Fig. 2 shows the variations of temperature and pressure during the digestion in closed vessel microwave system and it corroborates the proposed mechanism once the increase of pressure is slow and less pronounced only for the digestion processes with diluted nitric acid solutions (Fig. 2b and c). The pressure variation during the digestion carried out with concentrated nitric acid solution can be seen in Fig. 2a.

In other approach the quantity of matter of nitric acid consumed to decompose 1 g of coffee sample can be easily calculated for both digestion systems evaluated using diverse initial concentrations of nitric acid solutions. The aliquot volume of nitric acid solution used for digestions in Parr bomb (2 mL) was lower than that used for microwave-assisted digestions (7 mL) and thus the quantity of matter of H^+ from nitric acid consumed was higher for digestions in microwave system (Fig. 3). As it can be seen in Fig. 3, the amount consumed of H^+ per gram of sample has a linear dependence with the initial concentration of nitric acid solution and it may be supposed that the same decomposition mechanism was followed independent on the nitric acid concentration. A consistent linear relation ($r = 0.9999$) was obtained for microwave-assisted digestions carried out with diluted nitric acid solutions (Fig. 3). In theory, the quantity of matter of H^+ consumed for the decomposition of 1.0 g of coffee sample with concentrated nitric acid ($14\ mol\ L^{-1}$) by closed vessel microwave digestion process would be 0.249 ± 0.001 mol, i.e. 5% lower than that determined (0.262 mol), sustaining the hypothesis of HNO_3 regeneration.

Finally, the results obtained when these analytical methods were applied to Ba, Cu and P determination in coffee samples were summarized in Table 3 and the calculated element concentrations were similar to those obtained in other studies with Brazilian coffee samples [8,26,27]. Notwithstanding excellent agreements were obtained for Cu and Ba concentrations by comparing coffee sample digestions in pressurized Parr bomb and microwave system independent on the concentration of nitric acid. However a bias (ca. +9%) was observed by comparing phosphorous concentration after the digestion in Parr bomb and microwave system for all range of evaluated nitric acid concentrations (from 3.5 to $14\ mol\ L^{-1}$), however no significant differences were verified for 95% confidence level independently on the initial nitric acid concentration used for coffee sample decomposition with the same digestion system. Thus, the systematic error observed for phosphorous concentration determined from digests obtained by employing closed vessels conductive and microwave heated was explained by kinetic aspect.

So, taking into account important parameters such as the safety of the sample preparation procedure, operator comfort and atom economy, the use of diluted nitric acid solutions is advantageous compared to the classical microwave-assisted-acid digestion.

4. Conclusions

The use of diluted nitric acid solutions in closed vessels is a good strategy for digestion of regular coffee samples and the digestion process is critically dependent on the vessels size, availability of O_2 and temperature. Experimental data proved that the formation of NO, its conversion to NO_2 by O_2 action, and the regeneration of HNO_3 may explain the chemical processes involved with the digestion. The use of diluted nitric acid solutions for promoting digestions is promising and certainly it will open new routes for performing clean digestions compatible with trace analysis requirements.

Acknowledgements

The authors are grateful to Fundação de Amparo à Pesquisa do Estado da Bahia (FAPESB), Conselho Nacional de Desenvolvimento Científico e Tecnológico (CNPq), Coordenação de Aperfeiçoamento de Pessoal de Nível Superior (CAPES) and NQA (PRONEX, FAPESB–CNPq) for providing grants and fellowships and for the financial support. The authors also would like to express their gratitude to E.E. Silva and to EBDA (Empresa Bahiana de Desenvolvimento Agrícola S.A.) for experimental support.

References

[1] P.C. Aleixo, D. Santos Jr., A.C. Tomazelli, I.A. Rufini, H. Berndt, F.J. Krug, Anal. Chim. Acta 512 (2004) 329.
[2] J. Sneddon, C. Hardaway, K.K. Bobbadi, A.K. Reddy, Appl. Spectrosc. Rev. 41 (2006) 1.
[3] E. Oliveira, J. Braz. Chem. Soc. 14 (2003) 174.
[4] M.G.A. Korn, J.T. Castro, J.T.P. Barbosa, E.S.B. Morte, A.P. Teixeira, B. Welz, W.P.C. Santos, A.P. Fernandes, E.B.G.N. Santos, M. Korn, Appl. Spectrosc. Rev. 43 (2008) 67.
[5] P. Bermejo-Barrera, A. Moreda-Pineiro, A. Bermejo-Barrera, Talanta 57 (2001) 969.
[6] J. Moreda-Pineiro, E. Alonso-Rodrıguez, P. Lopez-Mahıa, S. Muniategui-Lorenzo, E. Fernandez-Fernandez, D. Prada-Rodrıguez, A. Moreda-Pineiro, A. Bermejo-Barrera, P. Bermejo-Barrera, Anal. Chim. Acta 572 (2006) 172.
[7] J.L. Capelo, C. Maduro, C. Vilhena, Ultrason. Sonochem. 12 (2005) 225.
[8] V.R. Amorim Filho, W.L. Polito, J.A. Gomes Neto, J. Braz. Chem. Soc. 18 (2007) 47.
[9] W.P.C. Santos, A.P. Teixeira, D.R. Gramacho, A.C.S. Costa, M.G.A. Korn, J. Braz. Chem. Soc. 19 (2008) 1.
[10] Z. Sulcek, P. Povondra, Methods of Decomposition in Inorganic Analysis, CRC Press, Inc., Boca Raton, Florida, 1992.
[11] M.A.Z. Arruda (Ed.), Trends in Sample Preparation, Nova Science Publishers, New York, 2006.
[12] N. Manutsewee, W. Aeungmaitrepirom, P. Varanusupakulle, A. Imyim, Food Chem. 101 (2007) 817.
[13] C.Y. Zhou, M.K. Wong, L.L. Koh, C.C. Woo, J. Anal. At. Spectrom. 11 (1996) 585.
[14] G.C.L. Araújo, M.H. Gonzalez, A.G. Ferreira, A.R.A. Nogueira, J.A. Nóbrega, Spectrochim. Acta B 57 (2002) 2121.
[15] P.A. Reis, C.M.R. Almeida, Food Chem. 107 (2008) 1294.
[16] E.M. Seco-Gesto, A. Moreda-Pineiro, A. Bermejo-Barrera, P. Bermejo-Barrera, Talanta 72 (2007) 1178.
[17] P. Navarro, G. Arana, N. Etxebarria, J.R. Dean, Anal. Chim. Acta 622 (2008) 126.
[18] F. Cubadda, A. Raggi, E. Coni, Anal. Bioanal. Chem. 384 (2006) 887.
[19] S. Foster, W. Maher, F. Krikowa, S. Apte, Talanta 71 (2007) 537.
[20] J.A. Nóbrega, C.C. Nascentes, G.C.L. Araújo, A.R.A. Nogueira, C. Pirola, Commun. Soil Sci. Plant Anal. 38 (2007) 2333.
[21] M.A. Augelli, R.A.A. Munoz, E.M. Richter, M.I. Cantagallo, L. Angnes, Food Chem. 101 (2007) 579.
[22] S.T. Gouveia, F.V. Silva, L.M. Costa, A.R.A. Nogueira, J.A. Nóbrega, Anal. Chim. Acta 445 (2001) 269.
[23] H.M.S. Kingston, S.J. Haswell, Microwave-Enhanced Chemistry. Fundamentals, Sample Preparation and Applications, American Chemical Society, Washington, 1997.
[24] S. Holm, Scand. J. Stat. 6 (1979) 65.
[25] R.G. Miller, Simultaneous Statistical Inference, McGraw Hill, New York, 1981.
[26] J.H. Zaidi, I. Fatima, M. Arif, I.H. Qureshi, J. Radioanal. Nucl. Chem. 267 (2006) 109.
[27] K.A. Anderson, B.W. Smith, J. Agric. Food. Chem. 50 (2002) 2068.

Talanta 78 (2009) 1259–1265

Contents lists available at ScienceDirect

Talanta

journal homepage: www.elsevier.com/locate/talanta

Potentiometric membrane sensors for polyvinylpyrrolidone determination

F.A. Chmilenko, I.V. Korobova, O.V. Gurtovaya *, T.S. Chmilenko

Dnepropetrovsk National University, av.Gagarina 72, Dnepropetrovsk 49050, Ukraine

ARTICLE INFO

Article history:
Received 11 June 2008
Received in revised form 19 January 2009
Accepted 23 January 2009
Available online 4 February 2009

Keywords:
Potentiometric sensor
Polyvinylpyrrolidone
Plasticized membranes
Dye adducts

ABSTRACT

Potentiometric sensors were developed for determining the concentration of the physiologically active polymer polyvinylpyrrolidone (PVP) with the use of its adduct with triphenylmethane and azodyes as electrode-active substances in plasticized membranes. The influences of electrolyte and pH of standard solutions on the electrode characteristics were determined. Polyvinylpyrrolidone determination in aqueous solutions of drug compounds, biological fluids and sewage was offered. The electrode selectivity factors were defined by fixed preventing ion method. The determined value of the selectivity factors varies in the $n \times 10^{-1}$ interval.

1. Introduction

Synthetic high-molecular compounds are widely applied in biochemistry, biology and medicine. One of the perspective directions of analytical chemistry is studying the polymers possessing physiological activity as they can prolong medical effects and can be of interest as macromolecular catalysts or synthetic models of biopolymers [1,2]. Research in the field of polymers for medical application has been intensified within recent years. The polymeric chain can be used as the carrier of biologically active substances. Controlling the binding force of an active chain with a macromolecule is possible via the rate of its dissociation from the complex.

Polyvinylpyrrolidone (PVP) is a physiologically active polymer. Pharmaceuticals containing PVP are used for extending the activity of biologically active substances and for decreasing organism intoxication. PVP is a water-soluble polymer that can form complexes with low- and high-molecular compounds due to hydrogen bonds, hydrophobic and other non-covalent interactions [2–4]. Currently, substantial research effort is devoted to creating and investigating medicinal dispersions and their properties on the basis of low soluble medicinal substances and PVP [5–8].

The mechanism of polymer action is determined by the macromolecule properties: the physiological activity of PVP arises at a polymeric level and depends both on the molecular weight of the polymer, and on the distribution of the molecular mass [9]. Thus, the molecular weight of the polymer is of primary importance in the mechanism of drug action:

1. PVP with low-molecular weight ($M_{r\,PVP} < 2 \times 10^4$) is used for detoxification of an organism. This is due to the ability of PVP to interact with toxins and to transport them through a renal barrier [1,4].
2. PVP with average molecular weight ($M_{r\,PVP} = (2–5) \times 10^4$) is used for drugs with prolonged effect. This is due to the ability of PVP to form complexes with pharmacologically active compounds. An increase of solubility of biologically active substances and of their action time and a decrease of toxicity is observed when injected.
3. PVP with high-molecular weight ($M_{r\,PVP} > 5 \times 10^4$) as a rule is not applied in medicinal preparations [9].

The use of physiologically active polymers in drug formulations raises the relevant question of how polymers are distributed and destroyed in an organism.

It has been established during research of PVP distribution in organism, that macromolecules with $M_r < 2.5 \times 10^4$ are removed by means of glomerular filtration through kidneys during several days. Macromolecules with M_r 2.5–11.0 $\times 10^4$ are excreted during several months via both other mechanism and through kidneys, and macromolecules with $M_r > 11.0 \times 10^4$ are removed only to a very low extent throughout several years and hence are accumulated in cells and can induce pathological processes.

Different classes of chemical substances, their associates, complexes and products of interaction can act as an exchanger at manufacturing potentiometric sensors [10–15].

* Corresponding author. Tel.: +380 56 7762049; fax: +380 56 7762049.
E-mail address: olga.gurtovaya@mail.ru (O.V. Gurtovaya).

0039-9140/$ – see front matter © 2009 Elsevier B.V. All rights reserved.
doi:10.1016/j.talanta.2009.01.049

Here, we report the production of potentiometric sensors reversibly detecting water-soluble polymers, such as polyvinylpyrrolidone with different molecular weights [16]. The widespread technical and commercial application of PVP makes such a sensor a timely task.

Polyvinylpyrrolidone is currently applied in several fields of sensor manufacturing:

- as stabilizing agent for obtaining stable colloidal solutions of nanoparticles (the electrodes from aqueous Pt colloids and glassy carbon [17], sensor with nanoparticles of Pt and Pt alloys for testing the blood alcohol content [18], PVP thin films containing barium titanate nanoparticles on electrodes [19]);
- as a modifier of electrodes (electrochemical detector having a PVP/CdS quantum dot modified electrode as working electrode for protein detection [20,21], for modifying the microstructure of the sol–gel-derived iron oxide film electrodes with embedded gold nanoparticles through the addition of PVP [22], in modified carbon paste electrode for nitrophenols in environment determination [23], for thyroxine determination [24]);
- as a compound for composite materials (chitosan/PVP hybrid composite material for the fabrication of H_2O_2 biosensor based on the immobilization of horseradish peroxidase in the chitosan/PVP hybrid film [25], the reagent in the reaction layer of the hydrophilic thin film of biosensor [26]);
- as a water-permeable matrix for sensors [27].

In our work, a novel application of PVP adducts with organic reagents as membrane-active materials for potentiometric sensor is proposed [16,28]. In this case, our sensor is useful for determining the polyvinylpyrrolidone content in environmental, medical and clinical samples.

2. Experimental

2.1. Reagents and solutions

All chemicals used were of analytical reagent grade and solutions were prepared in distilled water.

PVP with different molecular mass (8.0×10^3, 1.0×10^4, 1.2×10^4, 2.4×10^4, 4.0×10^4, 3.6×10^5) was purchased from BASF (Germany), FLUKA (Switzerland), and the Bolokhovo Chemical Plant (Russia). The monomeric unit of PVP is shown in Fig. 1. Stock PVP solution with concentration 20 g L^{-1} was prepared by dissolving a defined amount of polymer with distilled water directly prior to use. Working PVP solutions ($10.0–1.0 \times 10^{-5}$ g L^{-1}) were prepared by dilution of this stock solution. To increase ionic strength, reference solutions were prepared in 0.1 M solutions of strong electrolytes (NaCl, KCl, $NaNO_3$, KNO_3, and Na_2SO_4).

Triphenylmethane dye (bromophenol blue (BPB)) and azodyes (tropeolin 0 (Tr 0), tropeolin 00 (Tr 00), tropeolin 000 (Tr 000), diamond yellow (DY), stilbaso (SB) (Russia)) (Fig. 1) were used as a part of plasticized membranes exchanger for sensors.

For preparation of polyvinylchloride membranes purified reagents used were as follows: dibutylphthalate as a plasticizer, cyclohexanone as a solvent and high-molecular weight polyvinylchloride as a polymeric support.

2.2. Preparation of PVP adduct

PVP adducts formation with the specified dyes was determined by molecular absorption spectroscopy (Specord M40, Germany). Conditions of PVP-dye adducts formation and ratio of ingredients in adducts were found by a method of molar ratios.

Adducts for membranes were prepared by mixing the dye aqueous solutions and PVP (with different molecular weights) in the found ratio and under necessary solutions acidity (H_2SO_4 or NaOH). The adducts obtained from chloroform were prepared by mixing the fixed volumes of PVP chloroform solutions (with molecular weights 8.0×10^3, 4.0×10^4, 3.6×10^5) and BPB in the found ratio. The obtained samples were transferred to a Petri dish and left for 2–3 days for evaporation of solvent in the flue-block.

2.3. Membrane preparation and electrode construction

Sensor membranes were made as follows: 0.0050 g of an electrode-active compound (PVP-dye adduct) was mixed with 0.5 mL of dibutyl phthalate, and a solution of 0.5 g of polyvinyl chloride in 5 mL of cyclohexanone was added. The mixture was intensively stirred for 10–15 min at 50–60 °C to form a homogeneous mass. The resulting liquid was poured into a Petri dish and kept at room temperature for the evaporation of the solvent.

A membrane prepared by this technique was an elastic polymer film, from which a disk with a diameter of 10 mm was cut out and pasted to the polyvinyl chloride case of an electrode with the use of cyclohexanone. The internal reference electrode was an EM-SCN-01 silver rhodanide electrode (Russia) with a platinum lead. The inner solution of the electrode was a reference 1×10^{-2} g L^{-1} PVP solution with the addition of SCN^- ions.

In potentiometric determinations, the difference between potentials in the galvanic cell composed of a film electrode and an EVL-1M3 silver–silver-chloride electrode filled with a saturated KCl solution was used as the analytical signal. The voltage of the galvanic cell was measured with an EV-74 potentiometer.

Internal reference electrode, SCN^-, 10^{-2} g L^{-1} PVP|Electrode membrane|Investigated solution|Saturated KCl, AgCl/Ag

2.4. Analytical determinations

2.4.1. Determination of PVP concentration in pharmaceuticals

The electrode potential of the sensor in standard aqueous PVP solutions was measured within the concentration range 8.0×10^{-1} to 10^{-5} g L^{-1}. Solutions were prepared by a consistent dilution on a background solution of 0.1 mol L^{-1} KCl. Measurements were spent with internal 8.0×10^{-3} g L^{-1} PVP solution.

Determination of PVP concentration in drug "Haemodesum - H" (Ukraine, exact composition: 60 g L^{-1} PVP, 5.5 g L^{-1} NaCl, 0.42 g L^{-1} KCl, 0.5 g L^{-1} $CaCl_2$, 0.005 g L^{-1} $MgCl_2$, 0.23 g L^{-1} $NaHCO_3$). An aliquot of 0.33 mL of the drug was diluted with distilled water to 100 mL. 10.0; 1.0; and 0.1 mL of solution were transferred to volumetric flasks of 25 mL, respectively, then 2.5 mL 1.0 mol L^{-1} KCl solution was added and filled up with distilled water. Finally, an electrode potential was measured by the corresponding sensor.

Determination of PVP concentration in drug "Medichronal - Darnitsa" (Ukraine, exact composition: Package 1: 0.3 g PVP, 17.5 g glucose; Package 2: 0.2 g PVP, 7 g aminoacetic acid, 3.5 g sodium formiate). The content of a package was diluted with distilled water to 200 mL. An aliquot 1.33 mL of this drug solution then was diluted to 100 mL. 0.125; 0.625 and 1.250 mL of solution were transferred to flasks of 25 mL, respectively. Then 2.5 mL 1.0 mol L^{-1} KCl solution was added and diluted with distilled water to 25 mL. Finally, the electrode potential was measured by the corresponding sensor.

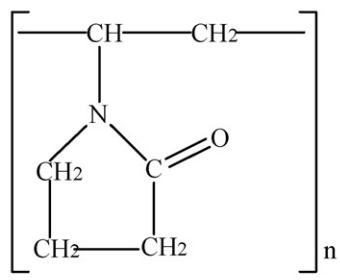

PVP

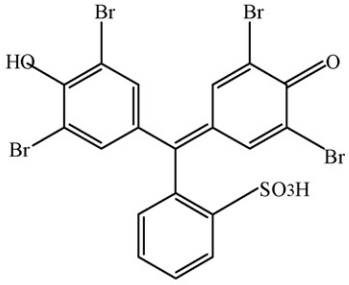

BPB

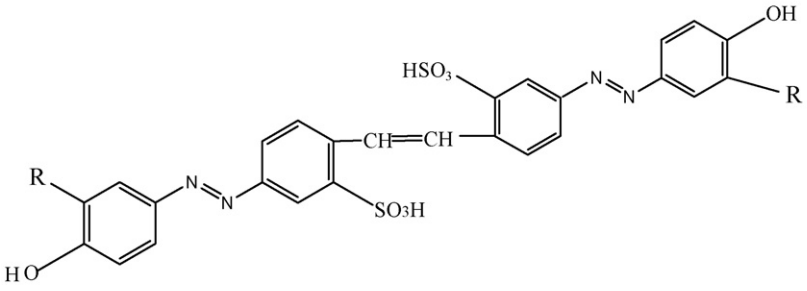

DY - R-H; **SB** – R-OH

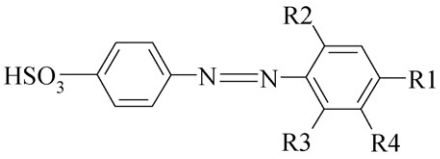

Tr 0 – $R_{1,2}$ - OH, $R_{3,4}$ - H

Tr 00 – R_1 - NH-C_6H_5, $R_{2,3,4}$ - H

Tr 000 – R_1 - OH, R_2 - H, $R_{3,4}$ – CH=CH-CH=CH-

Fig. 1. The chemical structure of polymer and dyes.

2.4.2. Determination of PVP concentration in modeling bioliquids

Urine: 1.0 mL urine was transferred to a flask of 50 mL and diluted with distilled water. Aliquots of 0.1 mL of the resulting solution were transferred to flasks of 25 mL. 0.12, 0.62 and 1.25 mL of "Haemodesum - H" with PVP content 2.0×10^{-2} g L^{-1} were added, respectively, followed by 2.5 mL 1.0 mol L^{-1} KCl solution and dilution to the notch with distilled water. The respective electrode potential was measured by the corresponding sensor.

Blood plasma: 2.0 mL blood plasmas was transferred to a flask of 50 mL, 0.12 mL 2.0×10^{-2} g L^{-1} PVP solution ($M_{r\,PVP} = 8.0 \times 10^3$) was added and the diluted with distilled water. An aliquot of 2.5 mL of the resulting solution was transferred to a flask of 25 mL, then 2.5 mL 1.0 mol L^{-1} KCl solution was added and diluted with distilled water. PVP concentration was determined by the method of standard addition. The respective electrode potential was measured by the corresponding sensor.

2.4.3. Determination of PVP concentrations in samples of urine

Patient urine samples were taken 2 and 24 h after the intake of "Medichronal–Darnitsa", respectively. 1.0 mL urine was transferred to a flask of 50 mL and diluted with distilled water. An aliquot of 0.1 mL of the resulting solution was transferred to flasks of 25 mL, and then 2.5 mL 0.1 mol L^{-1} KCl solution was added. 0.25 and 0.75 mL PVP solution with concentration 2.0×10^{-2} g L^{-1}, respectively, were added followed by dilution with distilled water and measuring the electrode potential of the corresponding sensor. PVP concentration was determined by the standard addition.

2.4.4. Determination of PVP concentration in sewage

5 mL sewage containing PVP and other contaminants were transferred to a flask of 50 mL and diluted with distilled water. 2.5 mL of the resulting solution was transferred to flasks of 25 mL and 2.5 mL 0.1 mol L^{-1} KCl solution was added. Then, 0.50 and 0.75 mL

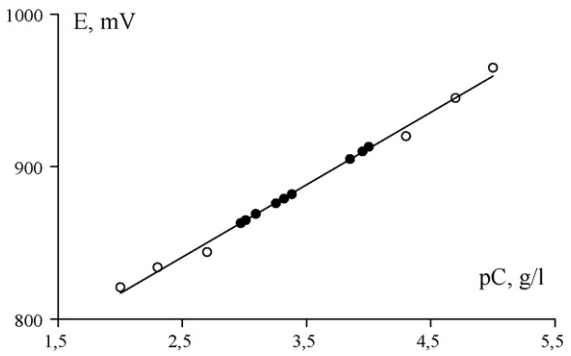

Fig. 2. The linear range of dependence for electrode potential and the logarithm of PVP concentration (PVP-sensor with diamond yellow—PVP adduct, $M_{r\,PVP} = 8.0 \times 10^3$, $pH_{DY:PVP=1:1}$ 11.0).

Table 1
Chemical–analytical characteristics of potentiometric sensors for PVP determination ($M_{r\,PVP} = 8 \times 10^3$) in aqueous solutions.

Dye of adduct (R)	Conditions of manufacturing, molar ratio in R:PVP adduct	Background electrolyte (0.1 mol L^{-1})	Dynamic range (g L^{-1})	Slope of the electrode function (mV dec^{-1})
Tropeolin 0	pH 2.5; 5:1	KNO_3	0–5	26
		$NaNO_3$	2–5	37
Tropeolin 00	pH 6.0; 5:1	–//–	–//–	26
				35
Tropeolin 000	pH 4.0; 4:1	–//–	–//–	24
				35
	pH 11.0; 1:1	–//–	–//–	22
				32
Stilbazo	pH 4.5; 5:1	KNO_3	0–5	20
	pH 10.5; 2:1	$NaNO_3$	2–5	36
Diamond yellow	pH 4.0; 4:1	KCl	0–4	22
		$NaNO_3$	(−1)–3	35
	pH 11.0; 1:1	KCl	0–4	28
		$NaNO_3$	(−1)–3	38
Bromophenol blue	Chloroform; 1:3	KCl	0–4	22
	pH 1.7; 1:1	NaCl	2–5	27
		KCl	0–4	31

PVP solution with concentration 2.0×10^{-2} g L^{-1}, respectively, were added and diluted with distilled water and the electrode potential was measured. PVP concentration was determined by the standard addition method.

3. Results and discussion

3.1. Electrode characteristics

The electrode characteristics of the sensors produced with different dyes, pH of adduct manufacturing and solvent use were investigated in the PVP concentration range of 10^1 to 10^{-5} g L^{-1} for all molecular weights of the polymer ($M_{r\,PVP} = 8.0 \times 10^3$, 4.0×10^4, 3.6×10^5). The linear range of dependence of the electrode potentials and the logarithm of PVP aqueous solution concentration is shown in Fig. 2.

The influence of exchanger composition in a membrane and pH of adducts on sensors characteristics was investigated. The content of an exchanger in an interval from 0.10 up to 2.50% in relation to mass of a membrane essentially does not influence the dynamic potential of this method, but the slope of the electrode function is increased with the decrease of exchanger content in a membrane. Such an influence is certainly connected to an exchange equilibrium time on the phase boundary "solution–membrane". The increase of pH up to 6 units in adducts manufacturing resulted in decrease of the dynamic range of the method by 1.0–1.5 decades, but the same time the slope of electrode function was increased by 5–10%. It could be found, that the increase of standard solution

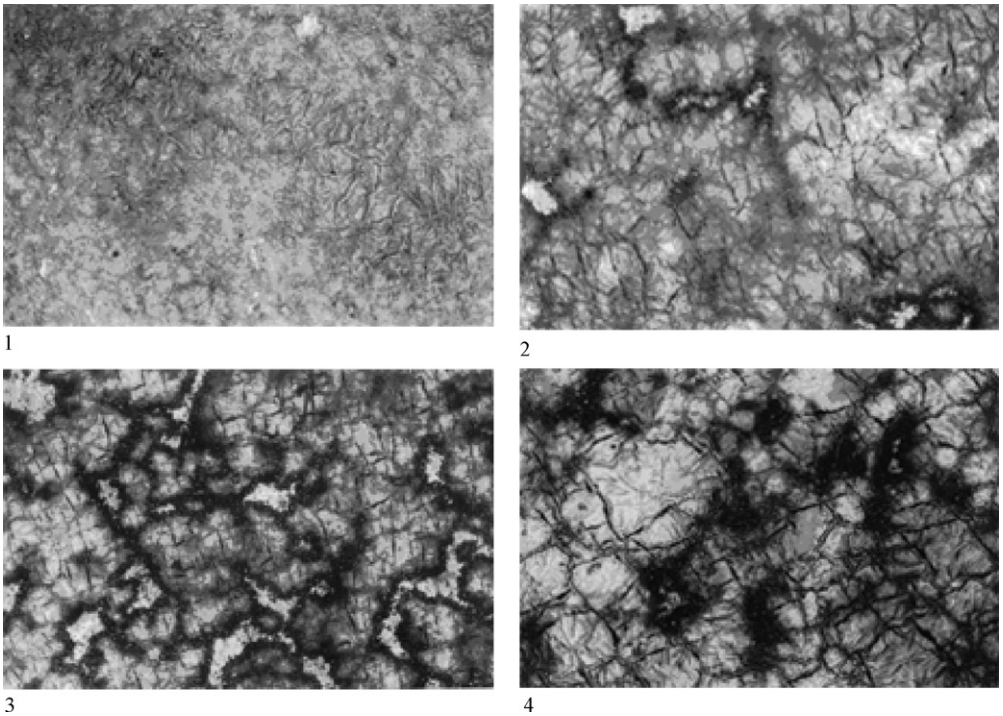

Fig. 3. Morphology of a polyvinylchloride membrane surface (200×) of the potentiometric sensors: without of an ion exchanger (1), with addition of the ion exchangers containing polymer adduct with different reagents (2) stilbazo; (3) diamond yellow; (4) bromophenol blue.

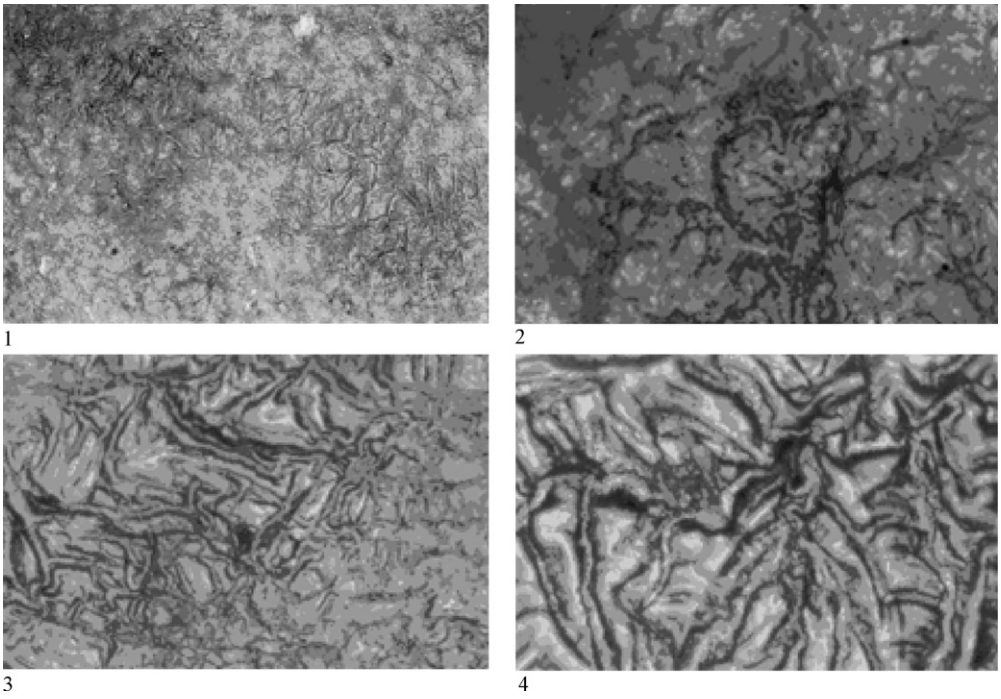

Fig. 4. Morphology of a polyvinylchloride membrane surface (200×) of the potentiometric sensors: without an ion exchanger (1), with addition of the ion exchangers containing polycation with different molecular weights (2) 8.0×10^3; (3) 40.0×10^3; (4) 360.0×10^3. Gegenion—bromophenol blue.

Table 2
Results of PVP concentration determination with the use of potentiometric sensor (exchanger—DY-PVP, pH_{adduct} 11) ($n = 3$, $P = 0.95$).

Samples	Nominal value, $C \times 10^4$ (g L^{-1})	Experimental value $(C \pm \Delta) \times 10^4$ (g L^{-1})	S_r
"Haemodesum -H"	1.0	1.1 ± 0.3	0.10
	5.0	5 ± 2	0.13
	10.0	9 ± 2	0.11
"Medichronal - Darnitsa"	1.0	1.0 ± 0.3	0.14
	5.0	5 ± 1	0.12
	10.0	11 ± 4	0.15
Urine	1.0	1.2 ± 0.4	0.13
	5.0	5 ± 1	0.11
	10.0	11 ± 3	0.11
Blood plasma	2.0	2.3 ± 0.7	0.13
	4.0	4 ± 1	0.13
	6.0	9 ± 3	0.13
Sewage	–	3 ± 1	0.15
	4.0	7 ± 3	0.14
	6.0	10 ± 2	0.09

acidity essentially decreases the slope of the electrode function.

For increasing ionic strength, the standard PVP solutions were prepared on a background of 0.1 mol L^{-1} strong electrolyte solutions. NaCl, KCl, $NaNO_3$, KNO_3, Na_2SO_4 were tested as background solutions (Table 1). The presence of NaCl in solution increases the analytical signal of the sensors: the dynamic range of the method is improved by not less than an order of magnitude and the slope of electrode function is improved by 25%.

The lifetime of the synthesized membranes is 60–90 days. Membranes used after 90 days of storage had electrode characteristics similar to just-synthesized membranes. The slope of the sensor response characteristic decreased to half the initial value after 120–130 measurements. This is apparently caused by diffusion of the exchanger from the membrane into the surrounding medium and swelling of the membrane polymeric matrix. Therefore, the sensor membranes had to be replaced after the mentioned amount of measurements.

It has been found that the linear concentration range of the method reaches 4–6 orders of magnitude, and the slope of the electrode functions of our electrodes does not exceed 15–37 mV dec^{-1}.

Table 3
Results of PVP concentration determination in urine of the patient with the use of potentiometric sensor (exchanger—DY-PVP, pH_{adduct} 11) ($n = 3$, $P = 0.95$).

Time (h)	Nominal value, $C \times 10^4$ (g L^{-1})	Experimental value $(C \pm \Delta) \times 10^4$ (g L^{-1})	S_r
2	–	1.3 ± 0.4	0.11
	2.0	3 ± 1	0.13
	6.0	7 ± 2	0.14
24	–	0.9 ± 0.3	0.13
	2.0	3 ± 1	0.13
	6.0	7 ± 2	0.13

Table 4
Conditions and results of PVP determination by spectroscopy and direct potentiometry ($n = 4$, $P = 0.95$).

Reagent	Sample	Method[a]	pH range	Linear concentration ranges, $C \times 10^4$ (g L^{-1})	Nominal value, $C \times 10^4$ (g L^{-1})	Experimental value $(C \pm \Delta) \times 10^4$ (g L^{-1})	S_r
BPB	"Haemodesum - H"	S	3.2	$(0.3–1.2) \times 10^{-1}$	0.5×10^{-1}	$(0.52 \pm 0.04) \times 10^{-1}$	0.07
		DP	3.0–10.0	1×10^{-4} to 1.0	0.5×10^{-1}	$(0.56 \pm 0.07) \times 10^{-1}$	0.11
DY	"Haemodesum - H"	S	>10.5	$(0.8–8.5) \times 10^{-4}$	5.0×10^{-4}	$(4.9 \pm 0.5) \times 10^{-4}$	0.04
		DP	3.0–10.0	1×10^{-4} to 1.0	5.0×10^{-4}	$(5 \pm 1) \times 10^{-4}$	0.11
	"Medichronal - Darnitsa"	S	>10.5	$(0.8–8.5) \times 10^{-4}$	5.0×10^{-4}	$(5 \pm 1) \times 10^{-4}$	0.05
		DP	3.0–10.0	1×10^{-4} to 1.0	5.0×10^{-4}	$(5 \pm 1) \times 10^{-4}$	0.13

[a] S: spectrophotometry; DP: direct potentiometry.

The received values of electrode function slope are linked to the process of polyelectric swelling of molecules in solutions and are defined by the shape and reactivity of the respective polycation.

An increase in the slope of the electrode functions was found for sensors based on PVPD with different average molecular masses. The slopes of electrode functions were as follows:

- for sensor with DY-PVP adduct ($M_{r\,PVP} = 8.0 \times 10^3$)—0.17 mV dec^{-1};
- for sensor with DY-PVP adduct ($M_{r\,PVP} = 49.0 \times 10^3$)—0.31 mV dec^{-1};
- for sensor with DY-PVP adduct ($M_{r\,PVP} = 360.0 \times 10^3$)—0.47 mV dec^{-1}.

Relative electrode selectivity factors were found experimentally by the method of the mixed solutions with a constant concentration of the interfering molecule [29] for checking the possibility to determine a low-molecular polymer in the presence of its high-molecular weight analogue. Magnitudes of selectivity coefficients changed from 0.62 when polymer with low-molecular weight as competing substance was used, up to 0.88 when polymer with high-molecular weight as competing was used. Resulted data allow approving an opportunity of potentiometric analysis of polymers with various molecular weights in solution.

The general principles of analytical signal formation of an electrode (i.e. a potentiometric sensor) lie in the basis of film membrane action. According to Ref. [30], PVP under some conditions can react similarly to cationic surfactant. The mobility in the membrane matrix and, correspondingly, the ability to exchange depends on the sizes and shapes of the polycations. Clearly, the exact way of polycation transport in the matrix of a membrane also determines the ability of a membrane to selectively absorb such a polycation and therefore determines the possibility of manufacturing a membrane electrode being selective to a polycation.

3.2. Morphology of a polyvinylchloride membrane film

A polyvinyl chloride sensor membrane is an elastic film with a thickness of up to 5 mm. Depending on the polymerization conditions, polyvinyl chloride, as well as other polymers, forms both amorphous and crystalline structures. Commonly, a polymer film involves crystalline portions, which are located in some order rather than chaotically and form some texture. The introduction of polyelectrolyte adducts, which are species rather large in size and complex in shape, into polyvinyl chloride at the stage of polymerization leads to a change in the structure of the polymer matrix of the membrane. In this case, its structure is affected by the amount of the ion exchanger and the size of its particles, which is governed by the size of the polycation, i.e., its molecular mass.

At exchanger contents up to 1% (m/m), it completely dissolves in a membranous solvent, and extraction processes on the phase boundary solution–membrane determine the mechanism of electrode potential formation. Classical membranes on Punghor [10] contain more then 50% (m/m) exchanger, and they can be seen as composite on the basis of the polymeric component.

In our opinion, the study of the structure of the membrane matrix can yield some information about the distribution of the ion exchanger in the membrane. The most readily available technique for estimating a change in the structure of the polymer matrix is studying the surface morphology of polyvinylchloride film membranes.

The morphology of the surface of film polyvinylchloride membranes containing adducts of polycations with inorganic and organic counterions was studied. It was found that the introduction of an ion exchanger into the polyvinylchloride matrix increases the degree of texturing of the membrane matrix at ion exchanger concentrations up to 5% (m/m) [32]. In Fig. 3, it is clearly seen that a pure polyvinyl chloride film has separate crystal-like portions with small size of "crystallites" (term used in analogy with the real crystal structure).

The introduction of an ion exchanger into a polymer matrix leads to an increase in inner stress in the polymer matrix. In addition, the larger adduct particle, i.e., the larger the molecular mass of the polycation, the larger this stress and the larger the sizes of crystallites. An increase in inner stress in a film undoubtedly must increase the number of pores in the matrix, simplify polycation adduct transport in the membrane, and, correspondingly, accelerate the solution–membrane ion exchange. According to the fixed charge theory, ion exchanger particles are aligned along areas with the largest stress [33].

It can be assumed that the larger the molecular mass of the polycation, the larger the number and sizes of pores in the membrane material and the faster the equilibrium potential of the ion-selective electrode is formed. Fig. 4 shows some increase in the size of membrane crystallites upon increasing the molecular mass of polycations in the ion exchanger.

3.3. Analytical application

The potentiometric techniques of polyvinylpyrrolidone determination in medicinal preparations, bioliquids and sewage of pharmaceutical production (Tables 2 and 3) were offered on the basis of the previous results and considerations.

Table 4 gives the conditions and the average of four measurements for PVP determination obtained by spectroscopy [34] and direct potentiometry. Results were compared and are shown.

4. Conclusions

We designed electrochemical sensors for direct potentiometric determination of polyvinylpyrrolidone concentration with different molecular weight. The received chemical–analytical characteristics of the sensors obtained have helped us to develop a complex of potentiometric techniques of PVP concentration determination in aqueous solutions of medicinal preparations, bioliquids and waste.

References

[1] N.A. Plate, A.E. Vasilev, Physiologychesky activnye polymery (Physiologic Active Polymers), Khimia, Moscow, 1986, p. 296.
[2] Synteticheskye i biolgycheskye polymery v pharmacy (Synthetic and Biological Polymers in Pharmacy), Nauka, Moscow, 1990, p. 237.
[3] F.A. Sydelkovskaya, Khimia vinylpyrrolidona i ego polymerov (Chemistry of Polyvinylpyrrolidone and it Polymers), Nauka, Moscow, 1970, p. 110.
[4] Syntez, svoistva i primenenie polymerov na osnove N-vinyllaktamov (Synthesis, Properties and Application of Polymers on the Basis of N-vinyllactams), Fantasy, Tashkent, 1990, p. 231.
[5] F. Hirayama, K. Kimura, K. Uekama, Pharm. Technol. Jpn. 18 (2002) 759–767.
[6] S. Freiberg, X.X. Zhu, Int. J. Pharm. 282 (2004) 1–18.
[7] Y. Mukai, Y. Tsutsumi, Y. Yoshioka, T. Mayumi, Pept. Protein Res. 6 (2004) 167–176.
[8] R. Chadha, V. Kapoor, A. Kumar, J. Sci. Ind. Res. 65 (2006) 459–469.
[9] Synteticheskie polymery medicinskogo naznachenia (Synthetic Polymers of Medical Purpose), Medicine, Tashkent, 1984, p. 246.
[10] R.W. Cattrall, Chemical Sensors, Oxford Univ. Press, Oxford, 1997, p. 144.
[11] G.E. Baiulescu, V.V. Cosofret, Application of Ion Selective Membrane Electrodes in Organic Analysis, Halsted, New York, 1977, p. 283.
[12] B.S. Smolyakov, V.V. Kokovkin, Izv. Akad. Nauk SSSR, Ser.: Khim. 1 2 (1983) 16–23.
[13] T.Ya. Bart, V.E. Yurinskaya, Ionnyi obmen i ionometriya. Leningradskiy Gosudarstvennuy Universitet 6 (1988) 110–132.
[14] E.G. Kulapina, O.V. Barinova, Khim. -Farm. Zh. 12 (1997) 40–44.
[15] A.I. Kulapin, R.K. Chernova, E.B. Nikolskaya, E.G. Kulapina, Zh. Anal. Khim. 3 (2003) 318–322.
[16] F.A. Chmilenko, I.V. Korobova, L.N. Danilenko, Zh. Anal. Khim. 11 (2000) 1179–1183 (J. Anal.Chem. (Engl. Transl.) 11 (2000) 1058–1062).
[17] Z. Tang, et al., J. Colloid Interf. Sci. 287 (2005) 159–166.
[18] P. He, CN Patent 1,609,607 (2005).
[19] Y. Kobayashi, A. Kosuge, T. Tanase, D. Nagao, M. Konno, Mater. Forum 29 (Adv. Mater. Process.) (2005) 268–273.
[20] Y. Kobayashi, A. Kosuge, T. Tanase, D. Nagao, M. Konno, CN Patent 1,731,174 (2006).
[21] P. Li, et al., Huaxue Xuebao 63 (12) (2005) 1075–1080.
[22] Y. Hida, H. Kozuka, Thin Solid Films 476 (2) (2005) 264–271.
[23] B. Yang, J. Mo, R. Lai, Guangdong College of Pharmacy, Guangzhou, Peop. Rep. China, Gaodeng Xuexiao Huaxue Xuebao, 26 (2) (2005) 227–230.
[24] Q. He, X. Dang, C. Hu, S. Hu, Colloids Surf. B 35 (2) (2004) 93–98.
[25] H. Wang, Q. Pan, G. Wang, Fenxi Huaxue 33 (11) (2005) 1623–1626.
[26] J. Zhang, C. Li, Z. Chen, CN Patent 1,400,466 (2003).
[27] I. Klimant, C. Krause, WO Patent 2002103334 (2002).
[28] F.A. Chmilenko, I.V. Korobova, O.V. Mikulenko, T.S. Chmilenko, Visnik Kharkivs'kogo Natsional'nogo Universitetu im, V.N. Karazina 648 (2005) 307–310.
[29] K. Cammann, Working with Ion-selective Electrodes, Springer, Berlin, 1977, p. 254.
[30] F.O. Chmilenko, M.V. Kharun, V.S. Schetinkin, T.S. Chmilenko, Voprosy khimii i technologyi (Question of chemistry and chemistry technology), Ukrainian Chemical Technological University, Dnepropetrovsk, Ukraine 2 (2001) 26–30.
[32] F.O. Chmilenko, I.V. Korobova, O.V. Mikulenko, Ukr. khim. zhurn 71 (10) (2005) 120–124.
[33] B.P. Nikolskyy, E.A. Materova, Ion-selective Electrodes, Khimia, Leningrad, 1980, p. 187.
[34] F.A. Chmilenko, Yu.S. Sapa, T.S. Chmilenko, M.V. Kharun, Visnik Kharkivs'kogo Natsional'nogo Universitetu im. V.N. Karazina. Medicine. 494 (2000) 22–24.

Talanta 78 (2009) 1383–1388

Contents lists available at ScienceDirect

Talanta

journal homepage: www.elsevier.com/locate/talanta

Novel selective kinetic spectrophotometric method for determination of norfloxacin in its pharmaceutical formulations

Ibrahim A. Darwish*, Maha A. Sultan, Hessa A. Al-Arfaj

Department of Pharmaceutical Chemistry, College of Pharmacy, King Saud University, P.O. Box 2457, Riyadh 11451, Saudi Arabia

ARTICLE INFO

Article history:
Received 2 December 2008
Received in revised form 10 February 2009
Accepted 11 February 2009
Available online 23 February 2009

Keywords:
Norfloxacin
Kinetic spectrophotometry
Initial rate method
Fixed time method
Pharmaceutical analysis

ABSTRACT

Novel selective and simple kinetic spectrophotometric method has been developed and validated for the determination of norfloxacin (NOR) in its pharmaceutical formulations. The method was based on the reaction of N-vinylpiprazine formed from the interaction of the mono-substituted piprazinyl group in NOR and acetaldehyde with 2,3,5,6-tetrachloro-1,4-benzoquinone to give colored N-vinylpiprazino-substituted benzoquinone derivative. The formation of the colored product was monitored spectrophotometrically by measuring the absorbance at 625 nm. The factors affecting the reaction was studied and optimized. The stoichiometry of the reaction was determined and the reaction pathway was postulated. The activation energy of the reaction was calculated and found to be 5.072 kJ mol^{-1}. The initial rate and fixed time (at 5 min) methods were utilized for constructing the calibration graphs. The graphs were linear in concentration ranges of 20–150 and 10–180 $\mu g\,mL^{-1}$ with limits of detection of 8.4 and 3.2 $\mu g\,mL^{-1}$ for the initial rate and fixed time methods, respectively. The analytical performance of both methods was fully validated, and the results were satisfactory. No interferences were observed from the excipients that are commonly present in the pharmaceutical formulations, as well as from tinidazole that is co-formulated with NOR in some of its formulations. The proposed methods were successfully applied to the determination of NOR in its commercial pharmaceutical formulations. The label claim percentages were 98.4–100.4 ± 0.52–1.04%. Statistical comparison of the results with those of the official method showed excellent agreement and proved that there was no significant difference in the accuracy and precision between the official and the proposed methods.

1. Introduction

Norfloxacin (NOR; 1-ethyl-6-fluoro-1,4-dihydro-4-oxo-7-(1-piprazinyl)-3-quinoline carboxylic acid (Fig. 1) is the most widely prescribed fluoroquinolone antibacterial agent. It is receiving a great interest because of to its potency and broad spectrum of activity against many Gram-positive and Gram-negative bacteria [1]. NOR and its pharmaceutical formulations are cited in the United States Pharmacopoeia [2] and European Pharmacopoeia [3]. Because of the therapeutic importance of NOR, numerous analytical methods have been developed for its determination in its bulk, pharmaceutical formulations and/or biological fluids. The USP describes a high-performance liquid chromatographic method for its determination and the European Pharmacopoeia describes a non-aqueous titrimetric method. Other techniques were a subject of many reviews [4–6].

Spectrophotometric technique is the most widely used in pharmaceutical analysis [7–9]. The widespread of spectrophotometric methods is attributed to their inherent simplicity, economic advantages, and wide availability in most quality control laboratories. Most of the spectrophotometric methods that have been described for the determination of NOR involved its common backbone structure: chelation with metal ions via the quinolone C=O and carboxylic —OH [10], charge-transfer reaction with various acceptors involving the tertiary piperazinly nitrogen [11], and formation of ion-pair associates with pairing reagent involving the carboxylic group of NOR [12]. These methods lacked the selectivity as they were unable to discriminate between NOR and the other members of the fluoroquinolones. Furthermore, many of these methods were handicapped in their applications because their procedures were tedious and time-consuming.

Kinetic spectrophotometric methods are becoming of a great interest in the pharmaceutical analysis [13–15]. The application of these methods offers some specific advantages such as improved selectivity due to the measurement of the evolution of the absorbance with the reaction time. As well, it avoids the interference of the colored and/or turbidity background of the samples, and possibility the interference of the other active ingredients present in the combined pharmaceutical formulations. Two attempts have been made for the kinetic spectrophotometric determination of

* Corresponding author. Tel.: +966 14677348; fax: +966 14676220.
E-mail address: idarwish@ksu.edu.sa (I.A. Darwish).

0039-9140/$ – see front matter © 2009 Elsevier B.V. All rights reserved.
doi:10.1016/j.talanta.2009.02.027

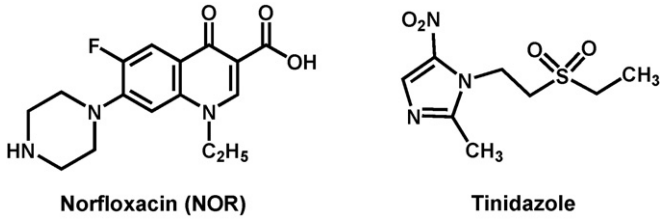

Fig. 1. Chemical structures of norfloxacin (NOR) and tinidazole (co-formulated with NOR in Conaz® tablets.

NOR based on its oxidation with potassium permanganate solution [16,17]. These methods, being based on oxidation, were non-selective and subjected to interferences by the reducing pharmaceutical excipients, and tinidazole that is co-formulated with NOR in Conaz® tablets. For these reasons, there is a need for the development of more selective and simple kinetic spectrophotometric method for determination of NOR in its pharmaceutical formulations either alone or in combination with tinidazole.

The present study describes the development and validation of a novel kinetic spectrophotometric method with enhanced selectivity and simplicity for the determination of NOR. The method is based on the reaction of NOR, via its free piperazinyl NH group, with acetaldehyde (ACD) to form the N-vinyl piperazine derivative, which is then reacted with 2,3,5,6-tetrachloro-1,4-benzoquinone (TCBQ) to give the corresponding colored N-vinylpiperazino-substituted benzoquinone derivative. The development of the color is monitored spectrophotometrically at its λ_{max}. The initial rate and fixed time methods, after their full optimization and validation, are adopted for the determination of NOR in its pharmaceutical formulations.

2. Experimental

2.1. Apparatus

Double beam V-530 (JASCO Co. Ltd., Kyoto, Japan) ultraviolet–visible spectrophotometer with matched 1-cm quartz cells was used for all the spectrophotometric measurements.

2.2. Chemicals and dosage forms

Norfloxacin (NOR; Merck & Co., Inc., Cyprus). Acetaldehyde (Sigma Chemical Co., St. Louis, USA) was 4% (v/v), prepared in methanol. 2,3,5,6-Tetrachloro-1,4-benzoquinone (TCBQ; Sigma Chemical Co., USA) was 2×10^{-2} mol L^{-1}, prepared in dioxane. All solvents and other chemicals used throughout this study were of analytical grade. The available pharmaceutical dosage forms used in the present investigation are the following: Chibroxine® eye drops (Merck & Co., Inc., Cyprus) are labeled to contain 3 mg of NOR per 1 mL solution. Noroxin® tablets (Merck & Co., Inc., Cyprus) are labeled to contain 400 mg of NOR per tablet. Conaz® tablets (Wockhardt, UK) are labeled to contain 400 mg of NOR and 600 mg of tinidazole per tablet. Uroxin® tablets (Julphar, UAE) are labeled to contain 400 mg of NOR per tablet. Laboratory-made (Lab-made) tablets were prepared to contain 400 mg of NOR hydrochloride per tablet.

2.3. Preparation of standard and sample solutions

2.3.1. Preparation of stock standard solution

Into a 50-mL calibrated flask, an accurately weighed amount (50 mg) of NOR was dissolved in 40 mL of methanol. For complete dissolution of NOR, the solution was sonicated for 5 min. The resulting solution was completed to volume with the same solvent. This stock solution (1 mg mL^{-1}) was diluted with methanol to obtain working concentrations in the range of 50–1500 μg mL^{-1}.

2.3.2. Preparation of tablets sample solution

Twenty tablets were weighed and finely powdered. A quantity of the mixed powder equivalent to 100 mg of NOR was transferred into a 50-mL calibrated flask, dissolved in 25 mL of methanol, swirled and sonicated for 5 min, completed to volume with the same solvent, shaken well for 10 min, and filtered. The first portion of the filtrate was rejected, and 25 mL of the filtrate was diluted with methanol to obtain working concentrations in the range of 50–1500 μg mL^{-1}.

For Lab-made tablets (400 mg NOR as hydrochloride salt), a quantity of the mixed powder equivalent to 100 mg of NOR was transferred into a 100-mL calibrated flask, dissolved in 40 mL water, swirled and sonicated for 5 min, completed to volume with water, shaken well for 10 min, and filtered. The first portion of the filtrate was rejected, and 50 mL of the filtrate was transferred quantitatively into a 100-mL separating funnel, then rendered alkaline with 10% NaOH solution. The liberated NOR was extracted with four 10-mL portions of chloroform. The combined extracts were passed through a small funnel containing anhydrous sodium sulphate (2 g) into a 50-mL calibrated flask. The contents of the separating funnel were washed three times with chloroform. The combined extracts and washings were then diluted to the mark with methanol to obtain a working standard solution of 1 mg mL^{-1} of NOR.

2.3.3. Preparation of eye drops sample solution

Ten milliliter of the drops (3 mg mL^{-1}) was transferred into a 10-mL tube and extracted with dichloromethane by employing the procedures described by Pauliukonis et al. [18]. The dried extract was reconstituted in 1 mL methanol and quantitatively transferred into a 10-mL volumetric flask. The volume was completed to the mark with methanol to obtain a solution of 3 mg mL^{-1}. Further dilutions were made for the extract to obtain sample solution of concentrations of 50–1500 μg mL^{-1}.

2.4. General analytical procedures and data treatment

One milliliter of the standard or sample solution (50–1500 μg mL^{-1}) was transferred into 10-mL calibrated flasks. One milliliter of the ACD solution (4%, v/v, in methanol) and 1 mL of TCBQ (2×10^{-2} mol L^{-1} in dioxane) were added. The reaction mixture was mixed and completed to volume with methanol. After dilution and mixing, the reaction mixture was immediately transferred to a spectrophotometric cell and the absorbance was recorded (at 625 nm) as a function of time against reagent blank treated similarly.

The kinetic data that has been recorded were transformed to the Slide Write Plus software, version 5.011 (Advanced Graphics Software, Inc., CA, USA) for curve fitting, regression analysis, and statistical calculations. The initial rate (K) of the reaction at different concentrations was obtained from the slope of the tangent to the absorbance-time curve. The calibration curve was constructed by plotting the logarithm of the initial rate ($\log K$) of reaction versus logarithm of the concentration ($\log C$) of NOR. Alternatively, the calibration curve was constructed by plotting the absorbance measured after a fixed time of 5 min.

2.5. Determination of molar ratio of the reactions

2.5.1. For NOR with ACD

The limiting logarithmic method [19] was employed. Two sets of experiments were carried out employing the general recommended procedures described above. The first set of experiments were carried using increasing ACD concentrations

(1.5×10^{-2} to 3.8×10^{-2} mol L^{-1}) at a fixed NOR concentration (1.9×10^{-4} mol L^{-1}). The second set of experiments were carried using increasing NOR concentrations (1.3×10^{-4} to 4.6×10^{-4} mol L^{-1}) at fixed ACD concentration (1.2×10^{-2} mol L^{-1}). The logarithms of the obtained absorbances were plotted as function of the logarithms of the ACD and NOR concentration in the first and second sets of experiments, respectively. The slopes of the fitting lines in both sets of experiments were calculated.

2.5.2. For vinylpiprazino derivative of NOR with TCBQ

The limiting logarithmic method [19] was employed. Two sets of experiments were carried out employing the general recommended procedures described above. The first set of experiments were carried using increasing TCBQ concentrations (7.5×10^{-4} to 1.5×10^{-3} mol L^{-1}) at a fixed NOR concentration (1.9×10^{-4} mol L^{-1}). The second set of experiments were carried using increasing NOR concentrations (1.3×10^{-4} to 4.6×10^{-4} mol L^{-1}) at fixed TCBQ concentration (2.0×10^{-3} mol L^{-1}). The logarithms of the obtained absorbances were plotted as function of the logarithms of the TCBQ and NOR concentration in the first and second sets of experiments, respectively. The slopes of the fitting lines in both sets of experiments were calculated.

3. Results and discussion

3.1. Involved reaction, design, and strategy for the assay development

The reaction involved in the present study is based on the interaction of the free piperazinyl NH group in NOR molecule with ACD forming N-vinylpiprazine derivative. The formed N-vinylpiprazine derivative is then allowed to react with TCBQ to give colored vinylpiperazino-substituted benzoquinone derivative which exhibits absorption maxima at 625 nm. The absorption spectrum for the reaction product is given in Fig. 2. This color reaction has not been reported yet for NOR, therefore, the present study was devoted to the investigation of this reaction for NOR and its employment in the development of a novel kinetic spectrophotometric method for the determination of NOR. Since this proposed reaction employed the piprazinyl NH of NOR, therefore, it is anticipated that tinidazole that is co-formulated with NOR in Conaz® tablets and devoid of the NH group (Fig. 1) will not interfere and ultimately a selective method will be developed. Previous studies [20] showed that free —NH groups gave more sensitive (~50 folds) assays than the corresponding hydrochloride salts. For these reasons, the reaction involved in the present study was carried out on the free NOR, rather than its HCl salts. In principal, any haloquinone reagent could be used for color development, however Darwish [20]

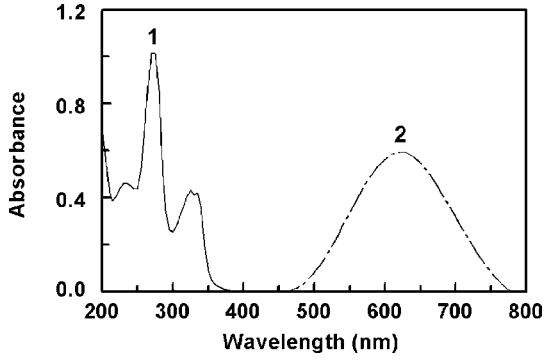

Fig. 2. Absorption spectra of NOR (1) and the reaction product (2) of NOR (60 μg mL^{-1}) with ACD (0.4%, v/v) and TCBQ (2×10^{-3} mol L^{-1}).

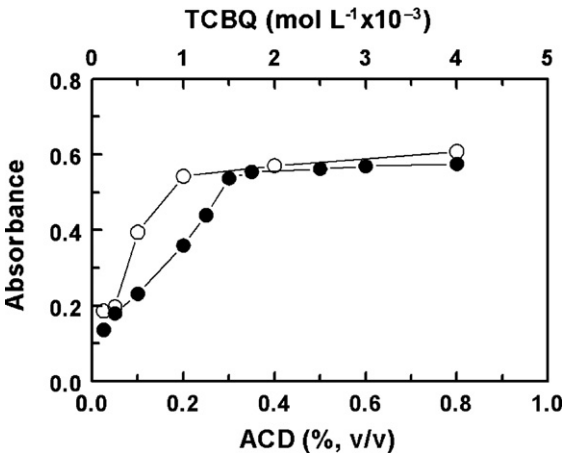

Fig. 3. Effect of ACD (○) and TCBQ (●) concentrations on the absorption intensity of their reaction with NOR (60 μg mL^{-1}).

demonstrated that TCBQ gives more sensitive assays than other haloquinone reagents (2,3,5,6-tetrabromo-1,4-benzoquinone and 2,3-dichloronaphthoquinone). Therefore, TCBQ was selected in this study.

The following sections describe the optimization of different factors affecting the reaction, kinetics, and the use of the optimized conditions in the development of the assay procedures.

3.2. Optimization of reaction conditions

The factors affecting the reaction conditions (concentrations of ACD and TCBQ reagents, temperature, and the diluting solvent) were studied by altering each variable in turn while keeping the others constant.

The color reaction was studied as a function of the concentrations of ACD and TCBQ reagent. The results indicated that the color development was dependent on the concentration of both reagents (Fig. 3). The highest color intensity was attained when the concentrations of ACD and TCBQ were 0.2–0.8% (v/v) and $1.5–4 \times 10^{-3}$ mol L^{-1} (in the final reaction solution), respectively. Considering the precision of the readings, the optimum concentrations that have been selected for further experiments were 0.4% (v/v) and 2×10^{-3} mol L^{-1} for ACD and TCBQ, respectively.

The results obtained from the optimizing of the reaction temperature indicated that the rate of color development increases significantly when the reaction temperature was raised from 20 to room temperature (25 °C). At room temperature, the maximum absorbance values (completion of the reaction) were attained after 20 min and remained constant for a further 10 min. At higher temperature (40 °C), the maximum absorbance values were attained after 15 min, however the readings decreased rapidly leading to imprecision of the results. Therefore, further experiments were carried out at room temperature (25 °C).

In order to select the most appropriate solvent for dilution, different solvents were tested: methanol, ethanol, propan-2-ol, butan-1-ol, acetonitrile, acetone, methylene chloride, 1,4-dioxane, and dimethylformamide. The highest color intensity was attained when methanol and acetone was used as diluting solvent; methanol was selected for further investigations.

3.3. Stoichiometry and kinetics of the reaction

The stoichiometry of the reaction of NOR with each of ACD and TCBQ was investigated by limiting logarithmic method [19]. Straight lines with comparable slopes (Fig. 4) were obtained indicating the 1:1 ratio for the reactions of NOR with ACD and TCBQ. Based on this

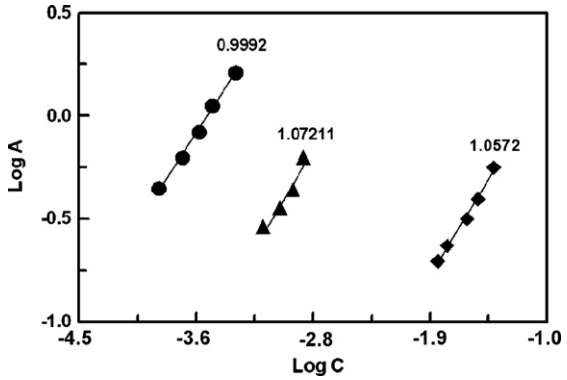

Fig. 4. Limiting logarithmic plots for molar reactivity of NOR with ACD and TCBQ. C and A are the concentration and absorbance, respectively. The first line (●): log *A* vs. log [NOR]; The second line (▲): log *A* vs. log [TCBQ]; The third line (♦): log *A* vs. [ACD]. The figures on the lines are their slopes.

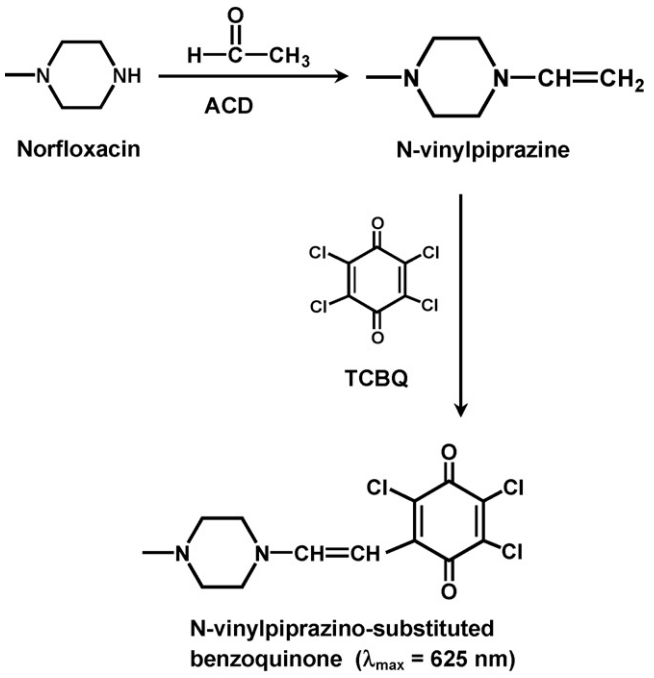

Fig. 5. Scheme for the reaction pathway of NOR with ACD and TCBQ.

ratio, the reaction pathway was postulated to proceed as shown in Fig. 5.

Under the optimum conditions, the absorbance–time curves for the reaction at varying NOR concentrations (0.63×10^{-4} to 4.70×10^{-4} mol L^{-1}) with a fixed concentration of TCBQ

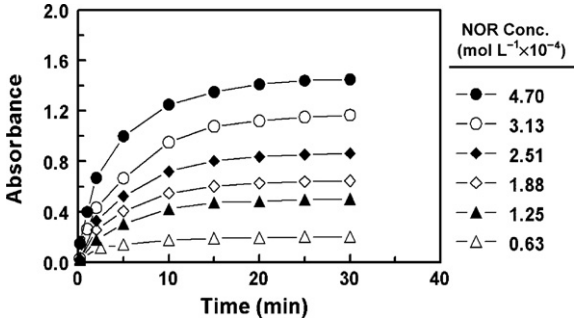

Fig. 6. Absorbance–time curves for the reaction of varying concentrations of NOR with ACD (0.4%, v/v) and TCBQ (2×10^{-3} mol L^{-1}).

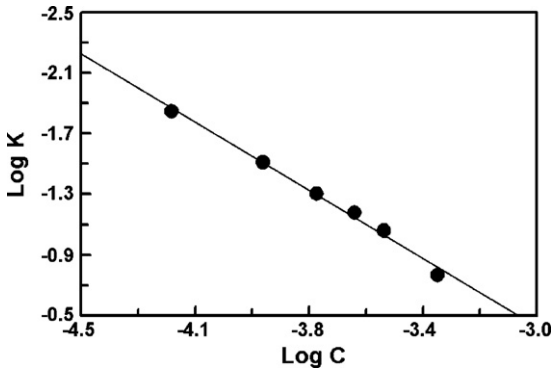

Fig. 7. Linear plot for log *C* vs. log *K* for the kinetic reaction of NOR with ACD (4%, v/v) and TCBQ (2×10^{-3} mol L^{-1}). *C* is [NOR]: (0.63×10^{-4} to 4.7×10^{-4} mol L^{-1}); *K* is the reaction rate (per s).

(2×10^{-3} mol L^{-1}) in presence of ACD (4%, v/v) were generated (Fig. 6). The initial reaction rates (k) were determined from the slopes of these curves. The logarithms of the reaction rates (log *K*) were plotted as a function of logarithms of NOR concentrations (log *C*) (Fig. 7). The regression analysis for the values was performed by fitting the data to the following equation:

$$\log K = \log k' + n \log C$$

where *K* is reaction rate, k' is the rate constant, *C* is the molar concentration of NOR, and n (slope of the regression line) is the order of the reaction. A straight line with slope values of 1.1597 ($\approx$1) was obtained confirming that the reaction was first order. However under the optimized reaction conditions, the concentrations of ACD and TCBQ were in much more excess than that of NOR in the reaction solution. Therefore, the reaction was regarded as a pseudo-first order reaction.

3.4. The apparent rate constant and activation energy

The absorbance–time curves at different temperatures (20–40 °C) were generated using fixed concentration of NOR (1.9×10^{-4} mol L^{-1}), ACD (0.4%, v/v), and TCBQ (2×10^{-3} mol L^{-1}). From these curves the apparent rate constants were calculated. The activation energy, defined as the minimum kinetic energy that a molecule possess in order to undergo a reaction, was determined using Arrhenius equation [21]:$\log k = \log F - E_a/2.303\,RT$where k is the apparent rate constant, F is the frequency factor, E_a is the activation energy, T is the absolute temperature (°C + 273), and R is the gas constant (1.987 calories degree^{-1} mol^{-1}). The values of log k were plotted as a function of $1/T$. Straight line with slope value of -338.9 ($=-E_a/2.303\,R$) was obtained. From these data, the activation energy was calculated and found to be 5.072 kJ mol^{-1}. This low activation energy explained that the proposed reaction can easily proceed under mild conditions, and ACD–TCBQ combination could be used as useful analytical reagents in the spectrophotometric determination of NOR.

3.5. Quantitation methods

3.5.1. Initial rate method

The initial rates of the NOR reactions would follow a pseudo-first order, and were found to obey the following equation:

$$K = \Delta A/\Delta t = k' C^n$$

where *K* is reaction rate, *A* is the absorbance, *t* is the measuring time, k' is the pseudo-first order rate constant, *C* is the molar concentration of NOR, and n is the order of the reaction. The logarithmic form

Table 1
Analytical parameters for the proposed fixed time spectrophotometric method for determination of NOR.

Reaction time (min)	Linear range ($\mu g\,mL^{-1}$)	Intercept	Standard deviation of intercept	Slope	Standard deviation of slope	Correlation coefficient	LOD ($\mu g\,mL^{-1}$)	LOQ ($\mu g\,mL^{-1}$)
2	40–280	0.0575	0.0420	0.0039	0.00050	0.9803	35.5	107.7
5	10–180	0.0124	0.0063	0.0064	0.00008	0.9997	3.2	9.8
10	5–140	0.0157	0.0120	0.0094	0.00014	0.9995	4.2	12.8
15	5–120	0.0307	0.0162	0.0108	0.00019	0.9994	5.0	15.0
20	5–120	0.0348	0.0163	0.0112	0.00019	0.9993	4.8	14.6
25	5–120	0.0362	0.0184	0.0115	0.00022	0.9993	5.3	16.0
30	5–120	0.0409	0.0191	0.0117	0.00023	0.9992	5.4	16.3

Table 2
Precision for the initial rate and fixed-time spectrophotometric methods for determination of NOR.

Concentration ($\mu g\,mL^{-1}$)	Recovery (±RSD)[a]			
	Initial rate method		Fixed time method	
	Intra-assay	Inter-assay	Intra-assay	Inter-assay
20	101.4 ± 1.84	101.6 ± 1.04	99.4 ± 1.66	99.6 ± 0.33
60	100.8 ± 1.15	99.6 ± 0.95	99.9 ± 1.72	99.5 ± 0.52
100	97.5 ± 1.42	101.8 ± 1.02	100.3 ± 0.27	100.3 ± 0.06

[a] Values are mean of three determinations.

of the above equation is written as follow:

$$\log K = \log \Delta A/\Delta t = \log k' + n \log C$$

Regression analysis using the method of least square was performed. The value of n (slope) was 1.1995 (≈1) in the regression equation confirmed that the reaction was first order with respect to the NOR concentration. The limit of detection (LOD) was calculated and found to be 8.4 $\mu g\,mL^{-1}$. This low value confirmed the good sensitivity of the method and consequently its capability to determine low amounts of NOR.

3.5.2. Fixed time method

In this method, the absorbance of the reaction solution containing varying amounts of NOR was measured at a pre-selected fixed time. Calibration plots of absorbance versus the concentrations of NOR were established at fixed periods of time for the reaction. The regression equations, coefficients of correlation, and detection limits are given in Table 1. The widest concentration ranges were obtained at fixed times of 2 and 5 min, however the correlation coefficient with 2 min was poor. At a fixed time of 5 min, lower LOD as well as a wide range were obtained, therefore the fixed time of 5 min was recommended for the determination [22].

3.6. Validation of the proposed methods

3.6.1. Precision

The precision of the proposed kinetic spectrophotometric method were determined at three levels of NOR concentrations (low, medium, and high of 20, 60, and 100 $\mu g\,mL^{-1}$, respectively). Five replicates of each sample were analyzed by both the initial rate and fixed time methods. The relative standard deviations (RSD) for the results did not exceed 2% (Table 2), proving the high reproducibility of the results and the precision of the method. This good level of precision was suitable for quality control analysis of NOR in its pharmaceutical dosage forms.

3.6.2. Accuracy and selectivity

The accuracy of the proposed methods was also checked by performing recovery studies. Known amounts of the pure NOR were added to preanalyzed NOR-containing pharmaceutical excipients, and then determined by the recommended procedures. The obtained mean recoveries and relative standard deviations were in the range 97.5 ± 1.42–101.8 ± 1.02% (Table 2). These results prove the accuracy of the proposed methods and absence of interferences from the common excipients. It is worth noting that all the proposed kinetic spectrophotometric methods were performed in the visible region away from the UV-absorption region of the UV-absorbing interfering excipient materials that might be co-extracted from the NOR-containing pharmaceutical formulations. The interference from the congenital tinidazole that is co-formulated with NOR in Conaz® tablets was studied. Samples were prepared by mixing NOR with tinidazole in a ratio which is normally present in the commercial tablets, and the samples were analyzed for NOR content by the proposed methods. Good percentage recovery (98.5 ± 1.46%) was obtained proving the absence of interference from tinidazole with the proposed method.

3.7. Application of the proposed methods

It is evident from the results obtained previously that the proposed initial rate and fixed time methods of the proposed

Table 3
Determination of NOR in its pharmaceutical formulations by the official and the proposed initial rate and fixed time spectrophotometric methods[a].

Pharmaceutical formulation	Official[a] (% ± RSD)	Initial rate method			Fixed time method		
		Label claim (% ± RSD)[a]	*t*-value[b]	*F*-value[b]	Label claim (% ± RSD)[a]	*t*-value	*F*-value
Chibroxine® eye drops	100.1 ± 1.05	98.7 ± 0.82	0.13	4.82	99.7 ± 0.78	0.78	1.32
Noroxin® tablets	99.9 ± 1.05	98.7 ± 0.82	0.13	4.82	98.7 ± 0.89	0.47	3.78
Conaz® tablets	100.2 ± 0.62	99.3 ± 0.94	1.32	3.42	100.4 ± 0.74	1.04	2.37
Uroxin® tablets	100.4 ± 0.62	99.9 ± 1.03	1.23	1.93	99.8 ± 0.68	0.45	1.75
Lab-made tablets	100.2 ± 0.72	98.9 ± 0.77	1.59	1.09	100.4 ± 0.52	1.41	2.84

[a] Reference [2], values are mean ± RSD of five determinations.
[b] The tabulated values of *t* and *F* at 95% confidence limit are 2.78 and 6.39, respectively.

kinetic spectrophotometric method for determination of NOR gave satisfactory results with the analysis of NOR in bulk. The methods were applied on the analysis of NOR-containing commercial pharmaceutical dosage forms. The concentration of NOR was computed from its corresponding regression equations. The results of the proposed methods (initial rate or fixed time) were statistically compared with those of the official method [2], in respect to the accuracy and precision. The obtained mean recovery values of the labeled amounts were 98.4–100.4 ± 0.52–1.04% (Table 3). In the *t*- and *F*-tests, no significant differences were found between the calculated and theoretical values of both the proposed and the reported methods at 95% confidence level. This indicated similar precision and accuracy in the analysis of NOR in its dosage forms.

4. Conclusion

The present study described a fully validated novel kinetic spectrophotometric method for the determination of NOR in its pharmaceutical formulations with enhanced selectivity. The proposed initial rate and fixed time methods can be easily applied as they do not require elaborate treatment of the samples and/or tedious procedures for extraction of the chromophore. As well, both methods are sensitive enough for analysis of lower amounts of NOR. Furthermore, the proposed methods do not require expensive instruments and/or critical analytical reagents. These advantages give the proposed methods a great value and encourage its application to the analysis of NOR in quality control laboratories.

References

[1] Martindale, in: S.C. Sweetman (Ed.), The Complete Drug Reference, 31th ed., Royal Pharmaceutical Society, London, 1966, p. 207.
[2] The United States Pharmacopoeia 31, NF 26, United States Pharmacopoeia Convention, Mack, Easton, PA, 2008, p. 2831.
[3] European Pharmacopoeia, 3rd ed., Maisonneuvc, Sainte Ruffine, France, 2005, p. 1427.
[4] G. Carlucci, J. Chromatogr. A 812 (1998) 343.
[5] F. Belal, A.A. Al-Majed, A.M. Al-Obaid, Talanta 50 (1999) 765.
[6] M.A. Marzouq, Spectrophotometric Determination of Some Fluoroquinolones, M. Sci. Thesis, Assiut University, Assiut City, Egypt, 2007.
[7] I.A. Darwish, S.A. Hussein, A.M. Mahmoud, A.I. Hassan, Spectrochim. Acta A 69 (2008) 33.
[8] I.A. Darwish, I.H. Refaat, H.F. Askal, M.A. Marzouq, Spectrochim. Acta A 69 (2008) 1287.
[9] I.A. Darwish, H.H. Abdine, S.M. Amer, L.I. Al-Rayes, Spectrochim. Acta A 72 (2009) 897.
[10] F.E.O. Suliman, S.M. Sultan, Talanta 43 (1996) 559.
[11] S. Mostafa, M. El-Sadek, E.A. Alla, J. Pharm. Biomed. Anal. 27 (2002) 133.
[12] I.A. Darwish, I.H. Refaat, H.A. Askal, M.A. El-Moez, J. AOAC Intl. 89 (2006) 334.
[13] M.A. Chamjangali, V. Keley, G. Bagherian, Anal. Sci. 22 (2006) 333.
[14] I.A. Darwish, Anal. Chim. Acta 551 (2005) 222.
[15] N. Rahman, N. Anwar, M. Kashif, Chem. Pharm. Bull. 54 (2006) 33.
[16] N. Rahman, Y. Ahmad, S. Najmul, H. Azmi, Eur. J. Pharm. Biopharm. 57 (2004) 359.
[17] Y. Ni, Y. Wang, S. Kokot, Spectrochim. Acta A 70 (2008) 1049.
[18] L.T. Pauliukonis, D.G. Musson, W.F. Bayne, J. Pharm. Sci. 73 (1984) 99.
[19] J. Rose (Ed.), Advanced Physicochemical Experiments, Pitman, London, 1964, p. 67.
[20] I.A. Darwish, J. AOAC Intl. 88 (2005) 38.
[21] A. Martin, J. Swarbric.k, A. Cammarata, A. Chun, Physical Pharmacy: Physical Chemical Principles in the Pharmaceutical Sciences, 3rd ed., Lea & Febiger, Philadelphia, p. 371 (2004).
[22] International Conference on Harmonization, ICH Harmonized Tripartite Guideline-Text on Validation of Analytical Procedures, Fed. Regist. 60, 1995, 11260.

Talanta 78 (2009) 1508

Contents lists available at ScienceDirect

Talanta

journal homepage: www.elsevier.com/locate/talanta

Retraction notice

Retraction notice to: "Simultaneous micellar electrokinetic chromatography and liquid chromatography of adriblastina and tarabine PFS: Their application to some biological fluids" [Talanta 66 (2005) 253–260]

Deia Abd El-Hady[a], Nagwa Abo El-Maali[a], Roberto Gotti[b], Vincenza Andrisano[b]

[a] *Department of Chemistry, Faculty of Science, Assiut University, 71516 Assiut, Egypt*
[b] *Dipartimento di Scienze Farmaceutiche, Via Belmeloro 6, 40126 Bologna, Italy*

Available online 18 March 2009

Reason: This article has been retracted, please see Elsevier Policy on article withdrawal: http://www.elsevier.com/locate/withdrawalpolicy.

This article has been retracted at the request of the Editors in Chief as it duplicates significant parts of a paper by the same authors, that has appeared in the Journal of Separation Science, 28 (2005) 534–542. Furthermore, the last two authors, Roberto Gotti and Vincenza Andrisano, have indicated that they were not involved in the research nor the preparation or submission of the two papers. One of the conditions of submission of a paper for publication is that authors declare explicitly that the paper is not under consideration for publication elsewhere. Re-use of any data should be appropriately cited. As such this article represents a severe abuse of the scientific publishing system. The scientific community takes a very strong view on this matter and we apologize to readers of the journal that this was not detected during the submission process.

DOI of original article:10.1016/j.talanta.2004.11.021.

0039-9140/$ – see front matter
doi:10.1016/j.talanta.2009.01.031

Talanta 78 (2009) 1476–1483

Contents lists available at ScienceDirect

Talanta

journal homepage: www.elsevier.com/locate/talanta

Optimization of experimental settings for the analysis of human neutrophils oxidative burst *in vitro*

Marisa Freitas[a], Graça Porto[b], José L.F.C. Lima[a], Eduarda Fernandes[a,*]

[a] *REQUIMTE, Departamento de Química-Física, Faculdade de Farmácia, Universidade do Porto, Rua Aníbal Cunha 164, 4099-030 Porto, Portugal*
[b] *Serviço de Hematologia Clínica, Hospital Geral de Santo António, Porto, Portugal*

ARTICLE INFO

Article history:
Received 13 December 2008
Received in revised form 12 February 2009
Accepted 23 February 2009
Available online 9 March 2009

Keywords:
Polymorphonuclear leukocytes
Reactive oxygen species
Reactive nitrogen species
Detection probes

ABSTRACT

The evaluation of reactive oxygen species (ROS) and reactive nitrogen species (RNS) production by neutrophils is currently a matter of extensive research, with scientific reports showing an enormous variability on the detection methods as well as the concentration of the detecting probes. Also the incubation media used to test neutrophils and the respective ionic concentration, as well as the glucose concentration, varies enormously from study to study. This variability often results in different sensibility and/or response of neutrophils to stimulating agents, which can be a focus of confounding and sometime contradictory results among reports. Thus, the main objective of the present study was to appraise and compare the effect of commonly described buffering media [phosphate buffer saline (PBS), Hank's balanced salt solution (HBSS) and Tris buffer], with or without glucose, on the activation of human neutrophils by phorbol myristate acetate (PMA), using different detection probes [luminol amplified chemiluminescence, dihydrorhodamine 123 fluorescence or cytochrome c reduction (UV/vis spectrometry)].

It was observed that the choice of incubation media as well as the methodology used to detect neutrophils oxidative burst has an enormous influence on posterior results. Independently of buffer, the presence of glucose is important, as a source of NADPH through pentose phosphate pathway (PPP). From the obtained results, we advise the use of HBSS, with the glucose concentration of 0.55 mM. This incubation media provided the best performance of neutrophils allowing the use of lower concentrations of the tested probes as well as of the stimulating agent, PMA.

1. Introduction

Neutrophils, also known as polymorphonuclear leukocytes (PMN), are the most common type of white blood cells, comprising about 50–70% of all white blood cells. They are the first immune cells to arrive at the site of inflammation, especially as a result of bacterial infections, through a process known as *chemotaxis*, where they recognize and phagocytise the microorganisms [1]. In the course of phagocytosis or upon contact with soluble stimulus, the killing machinery of neutrophils becomes activated for a rapid elimination of the invader. The success of that elimination depends on two concurrent events occurring in the phagolysosome of stimulated neutrophils: one oxygen-dependent, known as "oxidative burst", through the formation of reactive oxygen species (ROS) and reactive nitrogen species (RNS), and the other, oxygen-independent, consisting on the release of enzymatic or antimicrobial protein content into the granules [2]. The formation of ROS is started by the production of superoxide radical ($O_2{\cdot}^-$), via the assemblement and activation of NADPH oxidase, which transfers reducing equivalents from NADPH into molecular oxygen (O_2) [3–5]. This radical undergoes either spontaneous- or enzyme-catalyzed dismutation (through superoxide dismutase, SOD from ingested microorganisms) to hydrogen peroxide (H_2O_2) [6]. H_2O_2 may generate hydroxyl radical (HO·) via Haber Weiss cycle, which combines a Fenton reaction and the reduction of Fe(III) by $O_2{\cdot}^-$, yielding Fe(II) and oxygen. Concomitantly, myeloperoxidase (MPO), a heme protein present in azurophil granules of neutrophils is released upon cell activation into the phagolysosome or into the extracellular space. This protein contributes considerably to the bactericidal capabilities of these cells via formation of HOCl from H_2O_2 and chloride ions [2,5]. H_2O_2 can also react with HOCl, nitric oxide (·NO) or peroxynitrite ($ONOO^-$) to yield another highly reactive ROS, singlet oxygen ($^1O_2$) [7].

Likewise ROS, the production of RNS is also highly increased in the event of inflammatory processes, and contributes to the

Abbreviations: PMN, polymorphonuclear leukocytes; ROS, reactive oxygen species; RNS, reactive nitrogen species; PPP, pentose phosphate pathway; G6P, glucose-6-phosphate; G6PDH, glucose-6-phosphate dehydrogenase; PMA, phorbol myristate acetate; PBS, Dulbecco's phosphate buffer saline; HBSS, Hank's balanced salt solution; DHR, dihydrorhodamine 123; DHEA, dehydroepiandrosterone; S.E.M., standard error of the mean.

* Corresponding author. Tel.: +351 222078968; fax: +351 222004427.
E-mail address: egracas@ff.up.pt (E. Fernandes).

0039-9140/$ – see front matter © 2009 Elsevier B.V. All rights reserved.
doi:10.1016/j.talanta.2009.02.050

antimicrobial activity [8]. ·NO results from the catalysis of L-arginine by nitric oxide synthase (NOS). Three isoforms of this enzyme have been described: nNOS (neuronal), eNOS (endothelial) and iNOS (induced, inflammatory) and all of them utilize L-arginine as its substrate [9]. Activated neutrophils produce high concentrations of ·NO mainly via iNOS [10]. The rapid reaction of ·NO with $O_2{\cdot}^-$ leads to the formation of a powerful nitrative agent $ONOO^-$ [9,11].

Endogenously produced ROS and RNS are essential to life, not only for neutrophils defense system, but also for a myriad of other redox-dependent cellular signalling systems. However, the overproduction of these species or the impairment of antioxidant defenses may result to detrimental effects on the host itself, since ROS and RNS can damage or cause degradation of essential complex molecules in the cells, including lipids, proteins and DNA [12–14]. As a result of this dual effect, the evaluation of ROS and RNS production by neutrophils has become an essential constituent in numerous scientific studies, which fostered the implementation of a large number of sensitive methods for this purpose, including luminol amplified chemiluminescence [3,15], dihydrorhodamine 123 (DHR) fluorescence [16,17] or cytochrome c reduction (UV/vis spectrometry) [18]. Nevertheless, there are large variations in experimental conditions among reported studies. The concentration of each probe vary as much as 5 μM [19] to 500 μM [20] for luminol, 20 μM [21] to 150 μM [22] for cytochrome c and 2 μM [23] to 160 μM [24] for DHR. Concerning stimulating agents, the phorbol ester, phorbol myristate acetate (PMA), is commonly applied, making use of its ability to activate protein kinase C [25]. Also in this case, concentration of PMA referred on literature also varies as much as 1 nM [26] to 160 nM [20]. From this variability in the concentrations, reflected in large variations of neutrophils responses, it becomes hard to make qualitative and/or quantitative comparisons among different studies, concerning activating and/or inhibiting agents.

Above and beyond, biological relevant assay systems, such as *in vitro* cellular systems, require rigorous equilibrium of several physical and chemical parameters, like osmolarity, pH, pO_2 and temperature. These procedures will assure good cell viability and functionality conditions. Again, some of these parameters, specially the composition of incubation medium, show a high variability among scientific reports involving neutrophils. In fact, several incubation buffers are being currently used, namely phosphate buffered saline (PBS) [20,27–30], Hank's balanced salt solution (HBSS) [3,31–33] and Tris buffer [34–36]. Importantly, many authors do not reveal the complete composition and/or concentration of the incubation buffers and just report the commercial name (PBS, HBSS, Tris,. . .). For the reader who tries to reproduce such studies, it is difficult to choose the incubation media since, for example, with the name PBS there are more than five incubation media with different ionic concentrations. Considering glucose, it is not always used and its concentration has been highly variable. These are important variables, because the responsiveness of cells to exogenous stimuli may depend on extracellular environment, especially on the relative ionic and glucose concentrations. It is, therefore, essential to evaluate the influence of the commonly used incubation media with different concentrations of glucose, on the performance of neutrophils, namely on its capacity of producing reactive species upon stimulation.

Considering this rationale, the importance of the buffering media and the respective glucose concentration becomes evident and requires a comparative study among the most commonly used buffers. It is also relevant to perform that study using different detection methods, and several concentrations of activating agents and detection probes, in order to better characterize the best conditions for measuring the neutrophil's oxidative burst. Thus, the main objective of the present study was to appraise the effect of the commonly used buffering media, with or without glucose, on the activation of human neutrophils by PMA, using different detection methods. Owing to the important contribution of glucose to this activation, its influence in the energetic levels and biochemical pathways involved in the production of NADPH was also evaluated.

The singularity of this study is represented by the final suggestion of the most feasible conditions for studying neutrophil's oxidative burst *in vitro*, concerning the choice of incubation media as well as the methodology used to measure the reactive species produced, which may help to provide standardized conditions for those performing research in this area.

2. Experimental

2.1. Reagents

The following reagents were obtained from Sigma Chemical Co. (St. Louis, U.S.A.): PBS, HBSS, PMA, trypan blue solution 0.4%, luminol, DHR, cytochrome c from horse heart, potassium chloride, dehydroepiandrosterone (DHEA), and luciferin–luciferase. Sodium chloride, magnesium sulphate, perchloric acid, potassium bicarbonate and calcium chloride were obtained from Merck (Darmstadt, Germany). *Tris*(hydroxymethyl)aminomethane (Tris) was obtained from Riedel de Haën (Germany). The chemical composition of the buffering media used in this study is presented in Table 1.

2.2. Methods

All determinations were performed in a microplate reader (Synergy HT, BIO-TEK), using colorimetric, fluorimetric or chemiluminescence detection. Each study corresponds at least to five individual experiments and performed in triplicate in each experiment.

2.3. Isolation of human neutrophils

Venous blood was collected from healthy human volunteers by antecubital venipuncture, into vacuum tubes with K_3EDTA. The isolation of human neutrophils by the gradient density centrifugation method was performed as previously reported [37]. Cell viability and cell yield were evaluated by the Trypan blue exclusion method, using a neubauer chamber and an optic microscope (40×) as previously described [37].

2.4. Evaluation of the buffering media influence on PMA-induced oxidative burst in human neutrophils using luminol as detection probe

The measurement of neutrophil burst was undertaken by chemiluminescence, by monitoring the oxidation of luminol by neutrophil-generated reactive species, according to a previously described procedure [20]. Reaction mixtures contained the follow-

Table 1
Composition of incubation media used to test neutrophils.

Composition (mM)	PBS	HBSS	Tris	Tris-G
$CaCl_2{\cdot}2H_2O$	0.90	1.26	1.26	1.26
$MgCl_2{\cdot}6H_2O$	0.49	–	–	–
KCl	2.68	5.37	5.37	5.37
$MgSO_4$	–	0.81	0.81	0.81
NaCl	140	140	140	140
KH_2PO_4	1.21	0.36	–	–
Na_2HPO_4	8.10	0.34	–	–
$NaHCO_3$	–	4.17	–	–
D-Glucose	–	5.55	–	5.55
Tris	–	–	25	25
pH		7.4		

ing reagents at the indicated final concentrations (in a final volume of 200 μL): luminol (31.3–500 μM), buffers [PBS, HBSS, Tris, and Tris with glucose (Tris-G)], PMA (0.16–160 nM) and neutrophils (final suspension = 1×10^6 cells/mL). The reaction mixture was subjected to soft agitation and temperature of incubation of 37 °C during the course of the assays. Kinetic readings were initiated immediately after cell stimulation. Measurements were taken at the peak of the curve, the occurrence time of which varied depending on the buffer used. Effects are expressed as chemiluminescence arbitrary units/min.

2.4.1. Study of luminol concentrations

Reaction mixtures in the sample wells contained the following reagents at the indicated final concentrations (in a final volume of 200 μL): luminol (31.3, 62.5, 125, 250, 500 μM), buffer used to test neutrophils (PBS, HBSS, Tris or Tris-G), PMA (160 nM) and neutrophils (final suspension = 1×10^6 cells/mL).

2.4.2. Study of PMA concentrations

Reaction mixtures in the sample wells contained the following reagents at the indicated final concentrations (in a final volume of 200 μL): luminol (50 μM when HBSS was used and 500 μM with the other buffers), buffer used to test neutrophils (PBS, HBSS, Tris or Tris-G), PMA (0.16, 1.6, 16, 160 nM) and neutrophils (final suspension = 1×10^6 cells/mL).

2.4.3. Study of glucose concentrations

Reaction mixtures in the sample wells contained the following reagents at the indicated final concentrations (in a final volume of 200 μL): luminol (50 and 500 μM when HBSS and Tris was used, respectively), the buffer used to test neutrophils (HBSS or Tris) containing 0, 0.055, 0.14, 0.28, 0.55, 5.55, 55.5 mM of glucose, PMA (160 nM) and neutrophils (final suspension = 1×10^6 cells/mL). The buffer, HBSS or Tris, were prepared according to the mineral composition presented in Table 1, except glucose that was added from 0 to 55.5 mM.

2.5. Evaluation of the buffering media influence on PMA-induced oxidative burst in human neutrophils, using cytochrome c as detection probe

The reduction of cytochrome c by $O_2{\cdot}^-$ was monitored at 550 nm, according to a previously described procedure, with some modifications [38]. Reaction mixtures contained the following reagents at the indicated final concentrations (in a final volume of 200 μL): cytochrome c (12.5–100 μM), buffer used to test neutrophils (PBS, HBSS, Tris, Tris-G), PMA (0.16–160 nM) and neutrophils (final suspension = 1×10^6 cells/mL). The reactional mixture was subjected to soft agitation and incubation temperature of 37 °C during the course of the assays. Kinetic readings were initiated after a lag time of 5 min. Effects are expressed as absorbance arbitrary units/min.

2.5.1. Study of cytochrome c concentrations

Reaction mixtures in the sample wells contained the following reagents at the indicated final concentrations (in a final volume of 200 μL): cytochrome c (12.5, 25, 50 and 100 μM), buffer used to test neutrophils (PBS, HBSS, Tris or Tris-G), PMA (160 nM) and neutrophils (final suspension = 1×10^6 cells/mL).

2.5.2. Study of PMA concentrations

Reaction mixtures in the sample wells contained the following reagents at the indicated final concentrations (in a final volume of 200 μL): cytochrome c (50 μM), buffer used to test neutrophils (PBS, HBSS, Tris or Tris-G), PMA (0.16, 1.6, 16, 160 nM) and neutrophils (final suspension = 1×10^6 cells/mL).

2.5.3. Study of glucose concentrations

Reaction mixtures in the sample wells contained the following reagents at the indicated final concentrations (in a final volume of 200 μL): cytochrome c (50 μM), the buffer used to test neutrophils (HBSS or Tris) containing 0, 0.055, 0.14, 0.28, 0.55, 5.55, 55.5 mM of glucose, PMA (160 nM) and neutrophils (final suspension = 1×10^6 cells/mL). The buffer, HBSS or Tris, was prepared according to the mineral composition presented in Table 1, except glucose that was added from 0 to 55.5 mM.

2.6. Evaluation of the buffering media influence on PMA-induced oxidative burst in human neutrophils, using DHR as detection probe

The generation of reactive species by neutrophils was measured by fluorimetry, by monitoring the reactive species-induced oxidation of DHR to rhodamine 123, according to a previously described procedure, with some modifications [38]. The fluorescence signal caused by the reaction of DHR with reactive species was measured with excitation and emission wavelengths of 485 and 528 nm, respectively. Reaction mixtures contained the following reagents at the indicated final concentrations (in a final volume of 200 μL): DHR (5–40 μM), buffer used to test neutrophils (HBSS, PBS, Tris or Tris-G), PMA (1.6–160 nM) and neutrophils (final suspension = 1×10^6 cells/mL). The reactional mixture was subjected to soft agitation and incubation temperature of 37 °C during the course of the assays. Kinetic readings were initiated after a lag time of 5 min after PMA activation. Effects are expressed as fluorescence arbitrary units/min.

2.6.1. Study of DHR concentrations

Reaction mixtures in the sample wells contained the following reagents at the indicated final concentrations (in a final volume of 200 μL): DHR (5, 10, 20, 40 μM), buffer used to test neutrophils (PBS, HBSS, Tris or Tris-G), PMA (160 nM) and neutrophils (final suspension = 1×10^6 cells/mL).

2.6.2. Study of PMA concentrations

Reaction mixtures in the sample wells contained the following reagents at the indicated final concentrations (in a final volume of 200 μL): DHR (10 μM), buffer used to test neutrophils (PBS, HBSS, Tris or Tris-G), PMA (0.16, 1.6, 16, 160 nM) and neutrophils (final suspension = 1×10^6 cells/mL).

2.6.3. Study of glucose concentrations

Reaction mixtures in the sample wells contained the following reagents at the indicated final concentrations (in a final volume of 200 μL): DHR (10 μM), the buffer used to test neutrophils (HBSS or Tris) containing 0, 0.055, 0.14, 0.28, 0.55, 5.55, 55.5 mM of glucose, PMA (160 nM) and neutrophils (final suspension = 1×10^6 cells/mL). The buffer, HBSS or Tris, was prepared according to the mineral composition presented in Table 1, except glucose that was added from 0 to 55.5 mM.

2.7. Evaluation of the buffering media influence on neutrophil's ATP levels

Measurement of ATP levels in neutrophils incubated in different buffering media was performed by chemiluminescence, as previously reported [39]. Briefly, neutrophils (final suspension = 1×10^6 cells/mL) were incubated in HBSS or Tris with different concentrations of glucose (0, 0.14, 0.55, 5.55 mM), for 5 min, at 37 °C. Aliquot samples were then treated with $HClO_4$ (5% final concentration). These samples were subsequently neutralized with an equal volume of 0.76 M $KHCO_3$, and centrifuged at 16,000 × *g* for 2 min, in a refrigerated centrifuge (4 °C). Aliquots

of neutralized supernatants (100 μL) were mixed with 100 μL luciferin–luciferase assay solution (0.15 mM luciferin, 300,000 light units of luciferase) and the chemiluminescence was immediately measured. Effects are expressed as chemiluminescence arbitrary units/min.

2.8. Evaluation of glucose-6-phosphate dehydrogenase influence on PMA-induced activation of neutrophils oxidative burst

Glucose-6-phosphate dehydrogenase (G6PD) was specifically inhibited by DHEA, as described before [40], with some modifications. Reaction mixtures in the sample wells contained the following reagents at the indicated final concentrations (in a final volume of 200 μL): neutrophils (final suspension = 1×10^6 cells/mL), buffer used to test neutrophils [HBSS or Tris-G, both with (5.55 mM glucose) or without glucose], DHEA (125 μM), PMA (160 nM) and luminol (50 μM when HBSS was used and 500 μM with Tris). The reaction mixture was subjected to soft agitation and incubation temperature of 37 °C during the course of the assays. Kinetic readings were initiated immediately after cell stimulation. Measurements were taken at the peak of the curve, the occurrence time of which varied, depending on the buffer used. Effects are expressed as chemiluminescence arbitrary units/min.

2.9. Statistical analysis

Statistics were calculated using GraphPad Prism™ (version 5.0; GraphPad Software). Results are expressed as mean ± standard error of the mean (S.E.M.) (from at least five experiments, each with neutrophils from a different donor). Statistical comparison between groups was estimated using the one-way analysis of variance (ANOVA), followed by the Bonferroni's *post hoc* test. In all cases, *p*-values lower than 0.05 were considered as statistically significant.

3. Results

3.1. Influence of the buffering media in the activation of human neutrophils using luminol, cytochrome c and DHR as detecting probes

Fig. 1 shows the results obtained in the study of activation of human neutrophils, by PMA (160 nM), using HBSS, PBS, Tris and Tris-G as buffering media, and luminol, cytochrome c and DHR as detecting probes. The use of different buffers resulted in significant differences in the neutrophil's oxidative burst. HBSS provided maximal light emission in all concentrations of luminol tested ($p < 0.001$). As a representative example, for 500 μM of luminol, the activation of neutrophils tested in HBSS resulted in luminescence arbitrary values (mean ± S.E.M.) as high as 57,431 ± 6,030, while it only reached 7984 ± 839 in PBS, 19,935 ± 2,688 in Tris-G, and 4143 ± 548 in Tris. When cytochrome c was used, the results shows that the best detection of $O_2^{\cdot -}$ occurred when the cells were resuspended in HBSS and in Tris-G. The 100 μM concentration of cytochrome c provided the following mean absorbance intensity (mean ± S.E.M.) in neutrophils resuspended in HBSS, PBS, Tris-G and Tris: 43.0 ± 3.6, 21.6 ± 1.1, 46.6 ± 3.9, 18.7 ± 1.4, respectively. Using a fluorescent method based on the oxidation of DHR to rhodamine 123, the results shows that neutrophils tested in HBSS and PBS provided the higher fluorescence arbitrary units/min (mean ± S.E.M.) (366,520 ± 39,563, 318,320 ± 42,983), respectively, for 40 μM of DHR), when compared with Tris-G (116,507 ± 14,655) or Tris (133,261 ± 14,553).

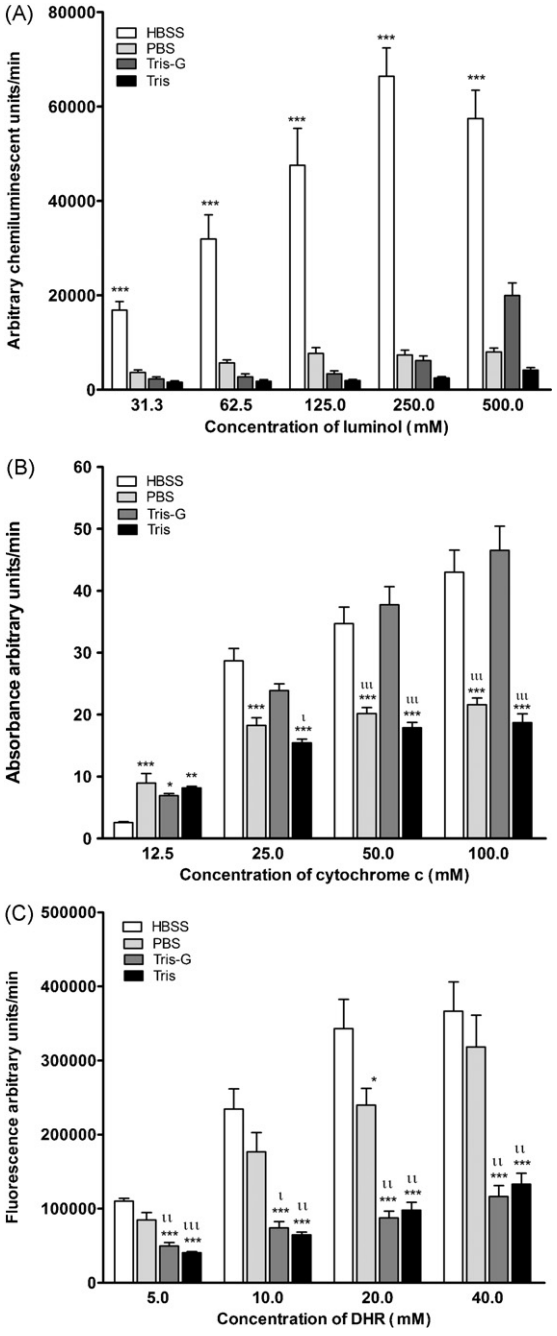

Fig. 1. Activation of human neutrophils, tested in HBSS, PBS, Tris and Tris-G, by PMA (160 nM) using different probe concentrations. (A) Luminol, ***$p < 0.001$ comparatively to both incubation media, PBS, Tris and Tris-G; (B) cytochrome c; *$p < 0.05$, **$p < 0.01$ and *$p < 0.05$ comparatively to HBSS, ι$p < 0.05$ and ιιι$p < 0.001$ comparatively to Tris-G; (C) DHR ***$p < 0.001$ comparatively to HBSS and ι$p < 0.05$, ιι$p < 0.01$ and ιιι$p < 0.001$ comparatively to PBS. Values are given as mean ± S.E.M. ($n \geq 6$).

3.2. Influence of the buffering media in the activation of human neutrophils, using various concentrations of PMA as activating agent, and luminol, cytochrome c and DHR as detecting probes

Once again, it is clearly shown that detection of human neutrophils activation was dependent on the buffer used (Fig. 2). With all the detecting probes tested, HBSS originated the highest degree of activation for all concentrations of PMA tested ($p < 0.001$), even though a lower luminol concentration was required for this buffer. By using HBSS buffer and luminol, the PMA concentration of 16 nM provided the best result (30,915 ± 2,447, 5113 ± 444,

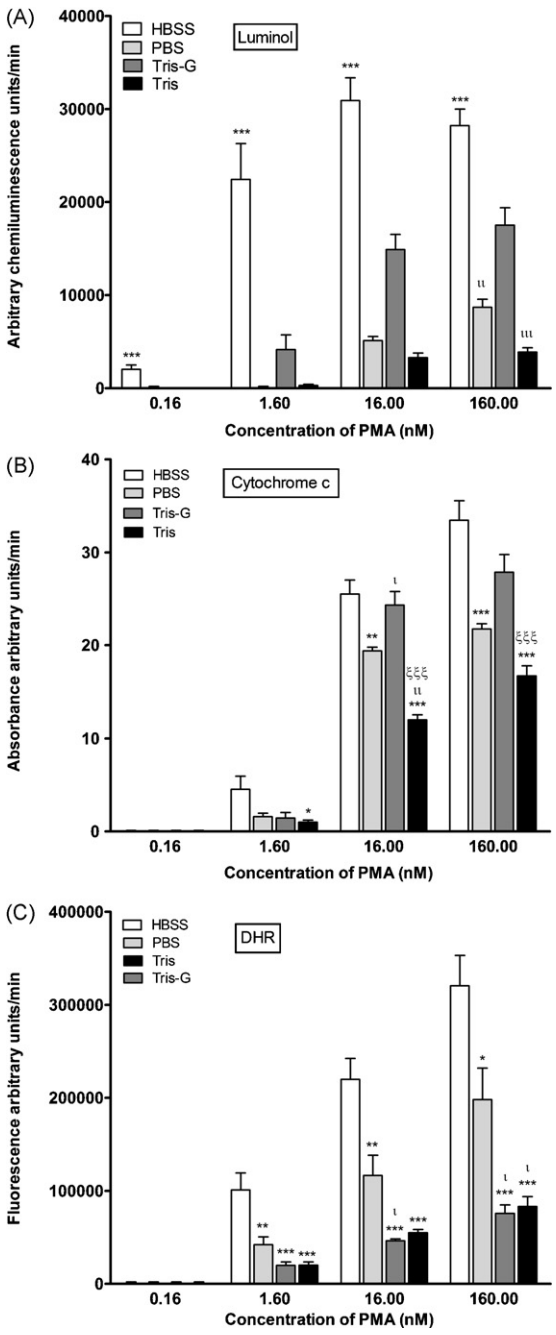

Fig. 2. Activation of human neutrophils, resuspended in HBSS, PBS, Tris-G and Tris, by PMA (0.16, 1.6, 16, 160 nM), using different detecting probes. (A) Luminol (50 μM with neutrophils resuspended in HBSS, 500 μM with neutrophils resuspended with PBS, Tris-G and Tris), $^{***}p < 0.001$ comparatively to both incubation media, PBS, Tris and Tris-G, ιι$p < 0.01$ and ιιι$p < 0.001$ comparatively to Tris-G; (B) cytochrome c (50 μM), $^{*}p < 0.05$, $^{**}p < 0.01$ and $^{***}p < 0.001$ comparatively to HBSS, ι$p < 0.05$ and ιι$p < 0.01$ comparatively to PBS, ξξξ$p < 0.001$ comparatively to Tris-G; (C) DHR (10 μM), $^{*}p < 0.05$, $^{**}p < 0.01$ and $^{***}p < 0.001$ comparatively to HBSS, ι$p < 0.05$ comparatively to PBS. Values are given as mean ± S.E.M. ($n \geq 6$).

14,898 ± 1,643, 3291 ± 491) (mean ± S.E.M.) arbitrary chemiluminescence units/min with HBSS, PBS, Tris-G and Tris, respectively. Noteworthy, the luminol chemiluminescence response of PMA-activated neutrophils was slowest when HBSS was used, that is, the peak activity was reached after 15–20 min and it remained at a steady-state maximum during 20 min, decreasing after that time. In contrast, the neutrophils tested in PBS and Tris had a faster and more short-term chemiluminescence response. The peak activity was reached after 5–10 min and remained at steady-state maximum 2–4 min.

3.3. Activation of human neutrophils tested in HBSS and Tris with different glucose concentrations, using luminol, cytochrome c and DHR as detecting probes

Fig. 3 shows the results obtained by activating human neutrophils resuspended in HBSS and Tris with different concentrations

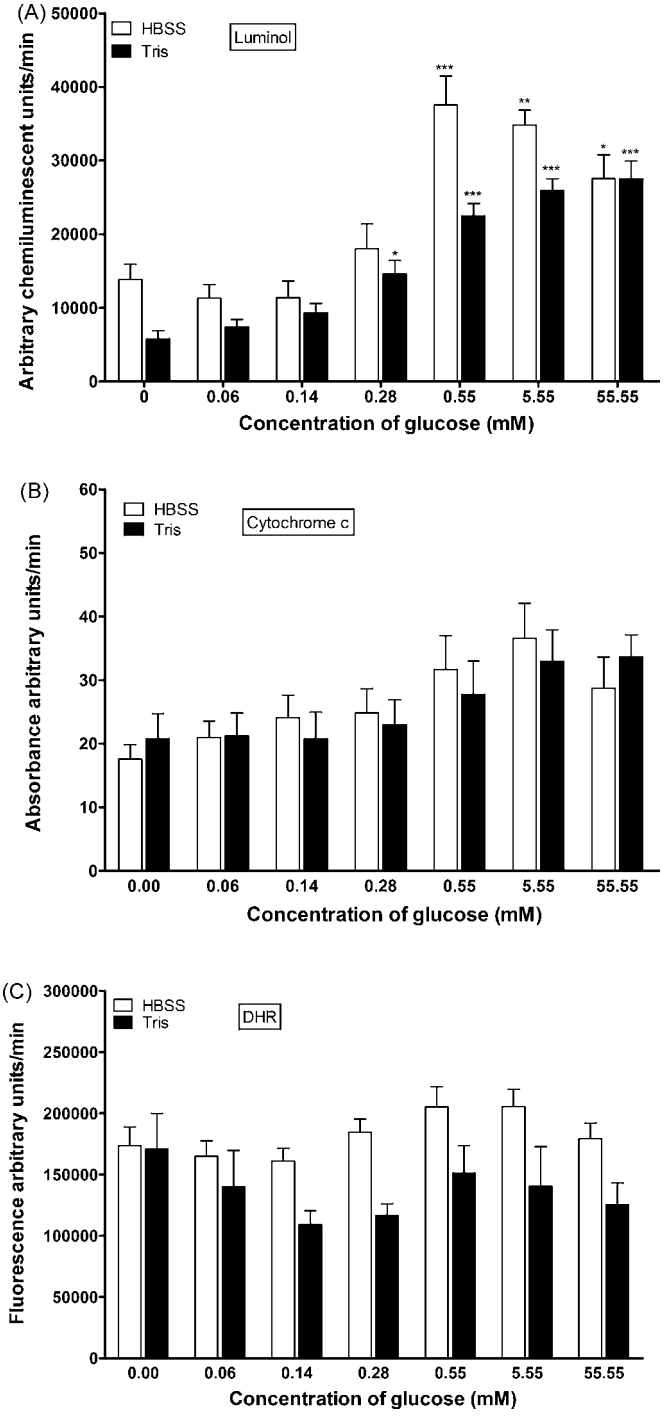

Fig. 3. Activation of human neutrophils by PMA (160 nM), tested in HBSS and Tris with different concentrations of glucose, using different detecting probes. (A) Luminol (50 μM with neutrophils tested in HBSS and 500 μM with neutrophils tested in Tris) $^{*}p < 0.05$, $^{**}p < 0.01$ and $^{***}p < 0.001$ comparatively to respective incubation media without glucose; (B) cytochrome c (50 μM); (C) DHR (10 μM). Values are given as mean ± S.E.M. ($n \geq 6$).

of glucose, by PMA (160 nM) using luminol, cytochrome c and DHR as detecting probes. The use of different concentrations of glucose results in significant differences in neutrophils activation. For all probes used to detect reactive species, it was clearly shown that 0.55 mM of glucose provides excellent results. Using the chemiluminescence method, HBSS with 0.55 mM of glucose provided the maximal light emission (37,553 ± 3,920) (mean ± S.E.M.). Also with Tris, the same concentration of glucose provided similar results, when compared to 5.55 mM (22,491 ± 1,688 *vs* 25,947 ± 1,582) (mean ± S.E.M.). The results obtained with the fluorescence method does not seem to be correlated with the levels of glucose, since in case of HBSS without glucose and with 5.55 mM of glucose the fluorescence arbitrary units/min are similar: 173,575 ± 15,397 and 205,450 ± 14,324 (mean ± S.E.M.), respectively.

3.4. ATP levels in neutrophils tested in HBSS and Tris with different concentrations of glucose

The results obtained from the measurement of ATP in neutrophils resuspended in HBSS and Tris with 0, 0.14, 0.55, 5.55 mM of glucose, showed no significant ($p > 0.05$) differences among the concentrations of glucose tested in both incubation media (Fig. 4).

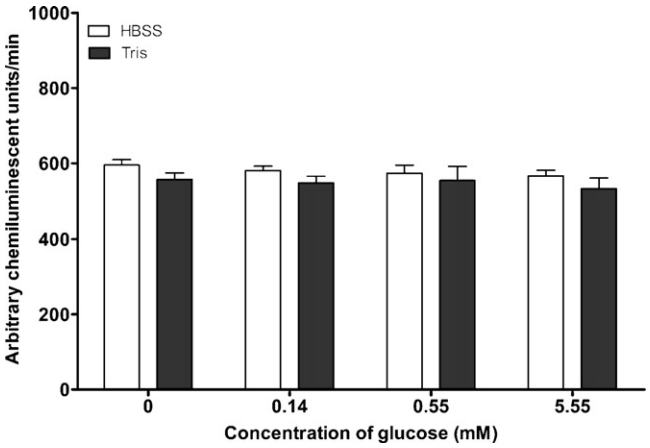

Fig. 4. Effect of different concentrations of glucose on ATP levels in human neutrophils. Values are given as mean ± S.E.M. ($n \geq 6$).

3.5. Influence of glucose-6-phosphate dehydrogenase inhibition on PMA-induced activation of neutrophils oxidative burst

The inhibition of neutrophil's glucose-6-phosphate dehydrogenase by DHEA in both incubation media, HBSS or Tris with glucose (5.55 mM), reduced the neutrophil oxidative burst to levels close to that obtained in the absence of glucose ($p < 0.001$) (Fig. 5). In the study of HBSS containing glucose, the activation by PMA results in 34,150 ± 3,737 arbitrary chemiluminescent units/min (mean ± S.E.M.) while the same activation in the presence of DHEA results in 13,208 ± 2,687 arbitrary chemiluminescent units/min (mean ± S.E.M.), which is almost the same value of neutrophils resuspended in HBSS without glucose 10,866 ± 1,716 (mean ± S.E.M.). DHEA had no effect in neutrophils oxidative burst in neutrophils resuspended in both incubation media without glucose (neutrophils resuspended in HBSS without glucose + DHEA: 8714 ± 1831).

4. Discussion

The results obtained in the present study noticeably show that the buffering media choice as well as the methodology used to detect reactive species has a strong influence on the activation and/or measurement of human neutrophils oxidative burst. It was also demonstrated that glucose potentiates PMA-induced neutrophil oxidative burst in a concentration dependent manner and that the optimal concentration of glucose, required to produce the maximal activation of neutrophils and/or measurement of oxidative burst, depends on the buffer used to test neutrophils and on the probe used to measure the formed reactive species. Glucose-mediated potentiation of PMA-induced neutrophil burst was not related to a putative increase of ATP levels, but rather on the activation the

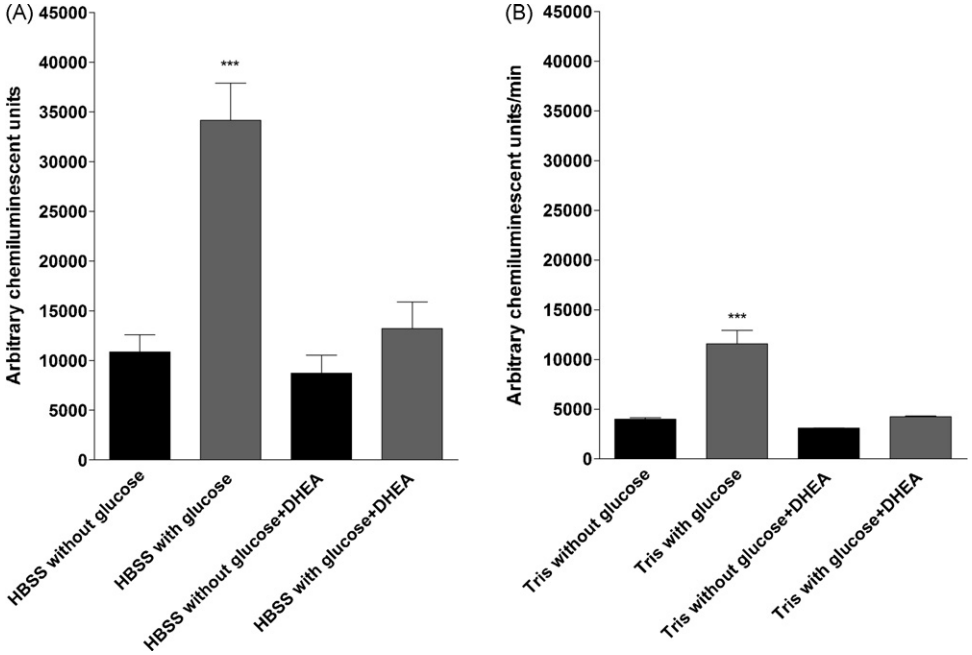

Fig. 5. Effect of dehydroepiandrosterone (DHEA) (125 μM) in the activation of human neutrophils by PMA (160 nM). (A) Cells resuspended in HBSS with (5.55 mM) or without glucose, ***$p < 0.001$; (B) cells resuspended in Tris with (5.55 mM) or without glucose, ***$p < 0.001$. Values are given as mean ± S.E.M. ($n \geq 6$).

PPP, which constitutes an essential pathway for NADPH supply, required for reactive species production through NADPH oxidase.

In the tested experimental conditions, the incubation media HBSS provided the best response for all the detection probes used (chemiluminescence, colorimetry, and fluorescence). The chemiluminescence probe luminol is thoroughly studied and used for monitoring reactive species production by neutrophils, namely $O_2\cdot^-$, H_2O_2, HO·, HOCl, $^1O_2$ [3], and $ONOO^-$ [41], due to its sensitivity, reliability and low cost [42]. By using HBSS buffer, lower concentrations of luminol and PMA can be used to achieve a maximal light emission. In line with these results, Samuni et al. [43] has previously reported that in luminol-amplified chemiluminescence, some parameters have to be carefully controlled such as pH, [O_2], temperature and media composition to hinder disturbances in the system. Also Nelson et al. [44] observed that several components of the reaction medium have influence in the chemiluminescence results. These authors demonstrated that the addition of tyrosine, tryptophan, soluble protein, or excess of nonopsonized particles on the reaction medium, increased the light production, allowing a measurement of chemiluminescence with a reduced number of human leukocytes.

There are several methods to measure the $O_2\cdot^-$ production. In the present study, it was used one of the simplest and easiest methods, which consists in following, spectrophotometrically, the reduction of cytochrome c by $O_2\cdot^-$ [45]. Various concentrations (12.5, 25, 50, 100 μM) of cytochrome c were tested and, in all of them, neutrophils resuspended in HBSS and Tris-G provided the best sensitivity. We applied 50 μM of cytochrome c to detect $O_2\cdot^-$ generated by various concentrations of PMA, and once again HBSS and Tris-G provided the best spectrophotometric signal. Nevertheless, it should be kept in mind that cytochrome c can also be reduced by HO· and ·NO, and can be re-oxidised by H_2O_2 and $ONOO^-$ [46]. Thus, care should be taken in the interpretation of results using this probe.

DHR is a cell-permeant and a non-fluorescent molecule that can undergo oxidation to the fluorophore rhodamine 123. This probe has also low specificity. Several reactive species are capable of oxidizing DHR, namely $ONOO^-$, HOCl, H_2O_2 [17,47]. In the present work, neutrophils assayed in HBSS oxidize DHR more extensively at all the tested concentrations (5, 10, 20, 40 μM), comparatively to the other buffering media used, followed by PBS. With this probe, no differences were found between oxidative burst of neutrophils tested in Tris with or without glucose.

The main difference between the buffers HBSS and PBS (Table 1) is the presence of glucose and the lower concentration of phosphates in HBSS. In turn, Tris-G has the same composition of HBSS except the phosphates that are absent in Tris-G. These differences in buffer composition dictate the results obtained in the detection of oxidative burst with the three methods tested. Our assumption is that the different results obtained following the variation of the buffers used to test neutrophils could be related to the presence or absence of glucose. We demonstrated that, using luminol amplified chemiluminescence or cytochrome c reduction, the signal is better when neutrophils were tested in HBSS or in Tris-G. The contribution of glucose for neutrophils oxidative burst has been controversial, since some authors reported that a glucose challenge induces a consistent increase in ROS [40,48–50], while others reported that high glucose concentrations impairs $O_2\cdot^-$ production [51].

To attest the effect of glucose on oxidative burst of neutrophils induced by PMA, we used HBSS and Tris as incubation media and tested different concentrations of glucose. Once again, it was clearly shown that the results and the conclusions depend on the methodology used to detect reactive species. That is, with the chemiluminescent (luminol) and colorimetric (cytochrome c) methods we observed differences on activation of neutrophils among concentrations of glucose tested. In contrast, no differences were found with DHR. We also concluded that, independently of the buffer used, 0.55 mM of glucose is sufficient to instigate an excellent response of neutrophils and that, in agreement with [51], the higher (55.55 mM) concentration of glucose tested tendencially resulted on lesser activation of neutrophils.

The neutrophil oxidative burst can be activated by a number of different soluble and particulate stimuli, including chemoattractants, certain cytokines, phorbol esters, calcium ionophores, different lectins, and opsonized as well as various unopsonized microorganisms [42]. PMA was used as neutrophil stimulator due to its capacity of activating PKC, which results in NADPH oxidase assemblement, with subsequent $O_2\cdot^-$ production [25,40]. Thus, NADPH synthesis will be determinant in the neutrophils response to PMA. It is well established that neutrophils utilize glucose essentially to generate ATP through glycolysis, and NADPH, through PPP pathway [52] (Fig. 6). The first step of PPP is mediated by G6PDH, which converts G6P into 6-phosphogluconolactone with NADPH production, which is subsequently consumed via NADPH oxidase, for biosynthesis of $O_2\cdot^-$ [40]. NADPH is also produced by 6-phosphogluconate dehydrogenase, and malic enzyme. However, G6PD is the most important regulator of NADPH levels [53]. In spite of its role in ATP and NADPH production, the contribution of glucose for neutrophils oxidative burst has been a matter of debate, as stated above. In order to increase our understanding about the mechanism associated to the better response of neutrophils to PMA with increased concentration of glucose, we performed a study to measure ATP in neutrophils tested in HBSS and Tris with 0–5.55 mM of glucose that showed no significant ($p > 0.05$) differences among the concentrations of glucose tested in both incubation media. As glucose enters in cells via facilitated diffusion, greater extracellular glucose levels lead to higher intracellular levels of its downstream products, as G6P, which is a rate-limiting step in PPP. To determine the contribution of glucose to oxidative burst depends on the PPP, we evaluated the effect of the specific inhibitor of G6PDH, DHEA. The results revealed that the addition of DHEA to neutrophils, tested in both incubation media HBSS or Tris with 5.55 mM of glucose, reduced the neutrophil oxidative burst response to levels close to those obtained without glucose ($p < 0.001$). Thus, these results show that the oxidative burst of neutrophils depends on the level of glucose, which is used on PPP for production of NADPH with subsequent release of reactive species.

Comparing the kinetic profile of cytochrome c and DHR, the results revealed that the intensity of the response with DHR, inde-

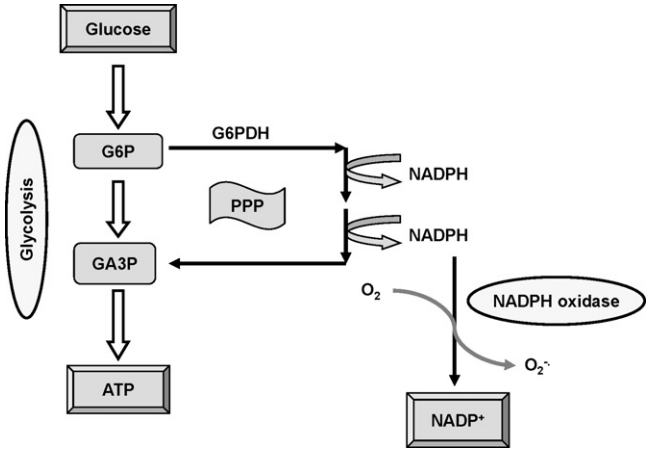

Fig. 6. Schematic representation of relationship between glycolysis, pentose phosphate pathway and formation of $O_2\cdot^-$ by NADPH oxidase. PPP, pentose phosphate pathway; G6P, glucose-6-phosphate; G6PDH, glucose-6-phosphate dehydrogenase; GA3P, glyceraldehydes-3-phosphate; ATP, adenosine triphosphate (figure adapted from [40]).

pendently of the buffer used, is higher than with cytochrome c. Two reasons for this difference could be that the reduction of cytochrome c is only extracellular, and the fact that this probe may be re-oxidised by H_2O_2 and $ONOO^-$ [46], in contrast to DHR, which detects both intracellular and extracellular reactive species, with a broader reactivity with $ONOO^-$, HOCl, H_2O_2 [17].

Taking together, our results indicate that the choice of incubation media as well as the methodology used to detect neutrophils oxidative burst has an enormously influence on the results of the assays. For that reason, before any experiment, is extremely important to test the response of neutrophils with different buffers and methodologies to avoid erroneous conclusions. Independently of buffer, the presence of glucose is important as a source of NADPH through PPP. From the obtained results, we advise the use of HBSS, with the glucose concentration of 0.55 mM. This incubation media provided the best performance of neutrophils allowing the use of lower concentrations of the tested probes as well as of the stimulating agent, PMA. Important notions are also provided for the correct use and interpretations resulting from the application of different probes for evaluating neutrophil's oxidative burst, namely luminol amplified chemiluminescence, dihydrorhodamine 123 fluorescence or cytochrome c reduction (UV/vis spectrometry).

Acknowledgements

The authors acknowledge Fundação para a Ciência e Tecnologia (FCT) and Fundo Europeu de Desenvolvimento Regional (FEDER) financial support for the Project POCI/QUI/59284/2004. Marisa Freitas acknowledges FCT and Fundo Social Europeu (FSE) her PhD grant (SFRH/BD/28502/2006).

References

[1] S.D. Kobayashi, J.M. Voyich, C. Burlak, F.R. DeLeo, Arch. Immunol. Ther. Exp. 53 (2005) 505.
[2] V. Witko-Sarsat, P. Rieu, B. Descamps-Latscha, P. Lesavre, L. Halbwachs-Mecarelli, Lab. Invest. 80 (2000) 617.
[3] H. Hasegawa, K. Suzuki, S. Nakaji, K. Sugawara, J. Immunol. Methods 210 (1997) 1.
[4] B.M. Babior, Blood 93 (1999) 1464.
[5] M.B. Hampton, A.J. Kettle, C.C. Winterbourn, Blood 92 (1998) 3007.
[6] B. Halliwell, Trends Biochem. Sci. 31 (2006) 509.
[7] S. Miyamoto, G.E. Ronsein, F.M. Prado, M. Uemi, T.C. Correa, I.N. Toma, A. Bertolucci, M.C.B. Oliveira, F.D. Motta, M.H.G. Medeiros, P. Di Mascio, IUBMB Life 59 (2007) 322.
[8] J.C. Hodgson, C.A. Watkins, C.W. Bayne, Vet. Immunol. Immunopathol. 112 (2006) 12.
[9] A. Denicola, R. Radi, Toxicology 208 (2005) 273.
[10] R.P. Patel, J. McAndrew, H. Sellak, C.R. White, H.J. Jo, B.A. Freeman, V.M. Darley-Usmar, Biochim. Biophys. Acta 1411 (1999) 385.
[11] F.L.M. Ricciardolo, A. Di Stefano, F. Sabatini, G. Folkerts, Eur. J. Pharmacol. 533 (2006) 240.
[12] D. Wu, A.I. Cederbaum, Alcohol Res. Health 27 (2003) 277.
[13] G. Folkerts, J. Kloek, R.B. Muijsers, F.P. Nijkamp, Eur. J. Pharmacol. 429 (2001) 251.
[14] W.D. Splettstoesser, P. Schuff-Werner, Microsc. Res. Tech. 57 (2002) 441.
[15] G. Briheim, O. Stendahl, C. Dahlgren, Infect. Immun. 45 (1984) 1.
[16] A. Lojek, L. Kubala, H. Cizova, M. Ciz, Luminescence 17 (2002) 1.
[17] A. Gomes, E. Fernandes, J. Lima, J. Biochem. Biophys. Methods 65 (2005) 45.
[18] M.A. Barbacanne, J.P. Souchard, B. Darblade, J.P. Iliou, F. Nepveu, B. Pipy, F. Bayard, J.F. Arnal, Free Radic. Biol. Med. 29 (2000) 388.
[19] S.D. Catz, M.C. Carreras, J.J. Poderoso, Free Radic. Biol. Med. 19 (1995) 741.
[20] D. Costa, A.P. Marques, R.L. Reis, J. Lima, E. Fernandes, Free Radic. Biol. Med. 40 (2006) 632.
[21] T. Suda, Y. Suzuki, T. Matsui, T. Inoue, O. Niide, T. Yoshimaru, H. Suzuki, C. Ra, T. Ochiai, Br. J. Dermatol. 152 (2005) 887.
[22] K. Wong, X.B. Li, N. Hunchuk, J. Biol. Chem. 270 (1995) 3056.
[23] G. Fossati, D.A. Moulding, D.G. Spiller, R.J. Moots, M.R.H. White, S.W. Edwards, J. Immunol. 170 (2003) 1964.
[24] C.F.M. Franssen, M.G. Huitema, A.C.M. Kobold, W.W. Oost-Kort, P.C. Limburg, A. Tiebosch, C.A. Stegeman, C.G.M. Kallenberg, J.W.C. Tervaert, J. Am. Soc. Nephrol. 10 (1999) 1506.
[25] J.M. Robinson, J.A. Badwey, M.L. Karnovsky, M.J. Karnovsky, J. Cell Biol. 105 (1987) 417.
[26] H.W. Lu, K. Sugahara, Y. Sagara, N. Masuoka, Y. Asaka, M. Manabe, H. Kodama, Arch. Biochem. Biophys. 393 (2001) 73.
[27] M.P. Wymann, V. Vontscharner, D.A. Deranleau, M. Baggiolini, J. Biol. Chem. 262 (1987) 12048.
[28] M.C. Perianayagam, N.E. Madias, B.J.G. Pereira, B.L. Jaber, Eur. J. Clin. Invest. 36 (2006) 353.
[29] J.L. Dou, C.Y. Tan, Y.G. Du, X.F. Bai, K.Y. Wang, X.J. Ma, Carbohydr. Polym. 69 (2007) 209.
[30] J.G. Bender, D.E. Vanepps, Infect. Immun. 41 (1983) 1062.
[31] R.A. Proctor, E. Prendergast, D.F. Mosher, Blood 59 (1982) 681.
[32] H. Faden, P. Sutyla, P.L. Ogra, Infect. Immun. 24 (1979) 673.
[33] M. Shiraishi, K. Suzuki, S. Nakaji, K. Sugawara, N. Sugita, K.J. Suzuki, S. Ohta, Luminescence 14 (1999) 239.
[34] Y. Yui, R. Hattori, K. Kosuga, H. Eizawa, K. Hiki, S. Ohkawa, K. Ohnishi, S. Terao, C. Kawai, J. Biol. Chem. 266 (1991) 3369.
[35] G.R. Tintinger, R. Anderson, Biochem. Pharmacol. 67 (2004) 2263.
[36] R. Cockeran, A.J. Theron, H.C. Steel, N.M. Matlola, T.J. Mitchell, C. Feldman, R. Anderson, J. Infect. Dis. 183 (2001) 604.
[37] M. Freitas, G. Porto, J.L. Lima, E. Fernandes, Clin. Biochem. 41 (2008) 570.
[38] M. Rinaldi, P. Moroni, M.J. Paape, D.D. Bannerman, Vet. Immunol. Immunopathol. 115 (2007) 107.
[39] H. Pontes, M. Carvalho, P.G. de Pinho, H. Carmo, F. Remiao, F. Carvalho, M.L. Bastos, Toxicol. In Vitro 22 (2008) 910.
[40] R. Oehler, G. Weingartmann, N. Manhart, U. Salzer, M. Meissner, W. Schlegel, A. Spittler, M. Bergmann, D. Kandioler, C. Oismuller, H.M. Struse, E. Roth, Blood 95 (2000) 1086.
[41] R. Radi, T.P. Cosgrove, J.S. Beckman, B.A. Freeman, Biochem. J. 290 (1993) 51.
[42] C. Dahlgren, A. Karlsson, J. Immunol. Methods 232 (1999) 3.
[43] A. Samuni, C.M. Krishna, J. Cook, C.D.V. Black, A. Russo, Free Radic. Biol. Med. 10 (1991) 305.
[44] R.D. Nelson, M.J. Herron, J.R. Schmidtke, R.L. Simmons, Infect. Immun. 17 (1977) 513.
[45] J.M. McCord, I. Fridovic, J. Biol. Chem. 244 (1969) 6049.
[46] C.L. Murrant, M.B. Reid, Microsc. Res. Tech. 55 (2001) 236.
[47] M.M. Tarpey, I. Fridovich, Circ. Res. 89 (2001) 224.
[48] P. Mohanty, W. Hamouda, R. Garg, A. Aljada, H. Ghanim, P. Dandona, J. Clin. Endocrinol. Metab. 85 (2000) 2970.
[49] A.S. Tan, N. Ahmed, M.V. Berridge, Blood 91 (1998) 649.
[50] T. Inoguchi, P. Li, F. Umeda, H.Y. Yu, M. Kakimoto, M. Imamura, T. Aoki, T. Etoh, T. Hashimoto, M. Naruse, H. Sano, H. Utsumi, H. Nawata, Diabetes 49 (2000) 1939.
[51] A. Perner, S.E. Nielsen, J. Rask-Madsen, Intensive Care Med. 29 (2003) 642.
[52] N. Borregaard, T. Herlin, J. Clin. Invest. 70 (1982) 550.
[53] Z.Q. Zhang, J. Yu, R.C. Stanton, Anal. Biochem. 285 (2000) 163.

Talanta 78 (2009) 1303–1309

Contents lists available at ScienceDirect

Talanta

journal homepage: www.elsevier.com/locate/talanta

Microorganisms recognition and quantification by lectin adsorptive affinity impedance

M. Gamella, S. Campuzano, C. Parrado, A.J. Reviejo, J.M. Pingarrón*

Dpto. Química Analítica, Facultad de CC. Químicas, Universidad Complutense de Madrid, E-28040 Madrid, Spain

ARTICLE INFO

Article history:
Received 3 December 2008
Received in revised form 22 January 2009
Accepted 30 January 2009
Available online 10 February 2009

Keywords:
Electrochemical impedance spectroscopy
Lectins
Bacteria

ABSTRACT

Lectin-based screen-printed gold electrodes are reported for the impedimetric label-free detection of bacteria. The selective interaction of lectins with carbohydrate components from microorganisms surface was used as the recognition principle for their detection and identification. Electrochemical impedance spectroscopy (EIS) was employed for the direct label-free transduction of the bacteria–lectin binding. Biotinylated Concanavalin A (Con A) and *Escherichia coli* were used for the evaluation of the lectin–bacteria complex formation. This complex was formed in solution, and then adsorbed onto the gold SPE surface. No bacteria immobilization was observed on the sensor prepared in the absence of ConA, demonstrating the absence of non-specific bacteria adsorption onto the gold SPE. On the contrary, the changes in electron transfer resistance allowed monitoring of *E. coli*–biotinylated Con A complex formation without any amplification step. Experimental variables such as the biotinylated-Con A concentration and the bacteria–lectin incubation time were optimized. The electron transfer resistance varied linearly with the logarithmic value of *E. coli* concentration over four orders of magnitude, 5.0×10^3 and 5.0×10^7 cfu mL^{-1}. The selectivity of the approach was evaluated by checking the impedimetric responses of gold SPE modified with the complexes formed between nine lectins and three different bacteria (*E. coli*, *Staphylococcus aureus* and *Mycobacterium phlei*). Different response profiles were found when the different lectins were used as recognition elements. principal component analysis (PCA) allowed classification and distinction among bacteria. Finally, electrochemical monitoring of β-galactosidase activity for the surface attached bacteria was demonstrated to be useful to distinguish between *E. coli* and *S. aureus*, which exhibit a similar affinity towards biotinylated-Con A.

1. Introduction

The early detection of low microorganisms concentrations still remains a challenge to allow immediate decisions to be taken in many important fields such as food safety, water contamination, disease diagnostics and biological terrorism threat control [1–3]. Accordingly, reliable, rapid, low cost and highly sensitive analytical methods are highly demanded. Recent alternatives to traditional bacteria detection methods (e.g. plating and culturing, biochemical tests, microscopy, flow cytometry), which are time-consuming, inconvenient and require several handling steps [3,4], are immunosensors or DNA chips. However, they have failed to gain wide acceptance due to the high user expertise required, high cost of labelling reagents and low stability of the biological recognition elements [3].

An attractive alternative detection approach is the one relying on carbohydrate recognition, which offers some potential advantages over antibody/nucleic acid detection. Most of microorganisms, proteins and viruses have carbohydrates at their surface, and therefore, the recognition of these carbohydrates can be used for their detection and identification [5]. Oligosaccharides are smaller than antibodies, thus allowing higher densities of carbohydrate-sensing elements leading to higher sensitivity and lower non-specific adsorption [3].

Lectins associate selectively and reversibly with mono- and oligosaccharide components of polysaccharide structures [6], major structural components of cells surface and secreted proteins [7,8]. Lectins are polyvalent, i.e. each lectin molecule possesses at least two carbohydrate binding sites to allow cross-linking between cells (by combining with sugars on their surfaces) [7]. Furthermore, these proteins are readily available and inexpensive, which is highly appropriate to combine with mass produced screen-printed electrodes as transducing elements [9].

Concanavalin A (Con A) is a mannose- and glucose-binding lectin. Con A can aggregate to specific terminal carbohydrates

* Corresponding author. Fax: +34 913944329.
E-mail address: pingarro@quim.ucm.es (J.M. Pingarrón).

0039-9140/$ – see front matter © 2009 Elsevier B.V. All rights reserved.
doi:10.1016/j.talanta.2009.01.059

of bacterial surface lipopolysaccharides with different binding ability [3]. Two divalent metals (Mn^{2+} and Ca^{2+}) must be present for carbohydrate binding as they are necessary for Con A to have the active conformation to interact with α-mannose [3,10].

To date, they are few reports in the literature on the use of lectins to implement biological detection systems. Ertl and Mikkelsen [6] developed lectin-based sensor arrays for qualitative discrimination of bacterial strains. Lectin-modified membranes were fixed on the surface of a Pt electrode in order to obtain electrochemical signals from respiratory cycle activity. Shen at al. [3] used lectins to form bridges between a specific carbohydrate structure and bacteria containing a complementary carbohydrate pocket to amplify the response on a quartz crystal microbalance. Recently, Serra et al. [11] proposed a method for the detection and quantification of microorganisms by immobilizing lectins on a gold-plated quartz crystal surface, with a detection limit of approximately 10^4 *Escherichia coli* cfu mL^{-1}.

Electrochemical impedance spectroscopy (EIS) is an efficient and rapid electrochemical technique suitable for characterization of biocatalytic transformations on electrode surfaces, and especially for the label-free transduction of biosensing events on electrodes [12]. In this article, the potentialities of lectin-based impedimetric Au/SPEs for the label-free detection of bacteria are investigated. Impedimetric measurements were carried out for nine biotinylated lectins with three different microorganisms, and factor based principal component analysis (PCA) was used for data analysis. Moreover, the amperometric monitoring of the metabolic activity of attached bacteria allowed discrimination between *Enterobacteriaceaes* and other bacterial families and between living and dead organisms.

2. Experimental

2.1. Apparatus and electrodes

All electrochemical measurements were performed with a Voltalab PGZ 402 potentiostat/galvanostat equipped with the VoltaMaster 4 Upgrade 4.00 electrochemical software. Gold screen printed electrodes (220BT, 4 mm diameter, Au/SPEs) were purchased from Dropsens (Oviedo, Spain). All potential values were referred to the screen printed silver pseudo-reference electrode.

2.2. Materials and solutions

Wild type *E. coli* (CECT 515), *Staphylococcus aureus* (CECT 59) and *Mycobacterium phlei* (CECT 3009) were obtained from the Spanish Collection of Type Cultures. Biotinylated lectins, supplied by Sigma, were from: *Canavalia ensiformes* (*Concanavalin A*), *Arachis hypogaea*, *Helix pomatia*, *Lens culinaris*, *Lycopersicon esculentum*, *Tetragonolobus purpureas*, *Dolichos biflorus*, *Triticum vulgaris*, *Ulex europaeus*. Buffer solutions, prepared daily, consisted of 0.1 M acetate buffer of pH 5.0 containing 1 mM of Mn^{2+} and 1 mM Ca^{2+}. This medium was chosen to obtain, according to provider instructions, optimum Concanavalin A activity in its dimmeric form. All chemicals used were of analytical-reagent grade, and water was obtained from a Millipore Milli-Q purification system.

Reagents used for the electrochemical measurements of bacterial β-galactosidase activity were: tyrosinase (from mushroom, EC 1.14.18.1, activity 6750 U mg^{-1} solid; Sigma), phenyl β-D-galactopyranoside (PG) (Fluka) as β-D-galactosidase substrate, isopropyl β-D-galactopyranoside (IPTG) (Sigma) as β-D-galactosidase inductor and polymyxin B sulfate (Sigma) as permeabilizer.

2.3. Procedures

2.3.1. Preparation of (bacteria–biotinylated-lectin) complex-modified Au/SPEs

Firstly, Au/SPEs were pre-treated by depositing 50-μL of a 0.5 M H_2SO_4 solution on the electrode active surface, and cycling the potential between 0.0 and +1.25 V at a scan rate of 100 mV s^{-1} for 10 cycles; then, the electrodes were rinsed with water and dried under a N_2 flow. Their voltammetric behavior in acidic solution was analogous to that reported in literature for gold wire electrodes [13,14]. Biotinylated-lectin–bacteria complexes were immobilized on the pre-treated Au/SPEs by successive deposition of 20 μL of a 0.06 mg mL^{-1} biotinylated-lectin solution and 20 mL of bacteria cultures with different cell numbers, and allowing the immobilization to proceed for 1 h at room temperature. Then, the modified electrodes were rinsed softly with deionised water.

2.3.2. Impedimetric and cyclic voltammetry measurements

Impedimetric and cyclic voltammetry measurements were carried out after deposition of 40 μL of a $K_3Fe(CN)_6/K_4Fe(CN)_6$, 2 mM in each component, solution in 0.1 M KCl. Impedance measurements were performed at the equilibrium potential of the $Fe(CN)_6^{4-}/Fe(CN)_6^{3-}$ pair, with a 10 mV (rms) sinusoidal excitation amplitude, and an automatic analyser integration time (0.001% S.D. of $I(jw)$ correlator output) with a 100 s cut-off time. Measurements were made at 20 steps per decade in the appropriate frequency range five times at each frequency and averaged during each run. Impedance data, were analysed by non-linear least squares (NLLS) using the EQUIVCTR.PAS (EQU) program by Boukamp [15]. The impedance Z is expressed in term of a real (Z_{re}) and an imaginary (Z_{im}) component. The changes in resistance were calculated according to:

$$\Delta R_{et} = R_{et(lectin-bacteria)} - R_{et(lectin)}$$

where R_{lectin} is the value of the resistance when the biotinylated lectin was immobilized on the electrode and $R_{lectin-bacteria}$ is the value of the resistance after lectin-bacteria complex formation. However, in some cases (see Section 3.4), we observed non-specific adsorption of bacteria (*S. aureus* and *M. phlei*) onto the activated Au/SPEs. In these cases, the latter equation should be changed for:

$$\Delta R_{et} = R_{et(lectin-bacteria)} - R_{et(lectin)} - R_{et(bacteria)}$$

in order to take into account the resistance contribution from this non-specific bacteria adsorption.

Cyclic voltammetry was used to monitor the fabrication process of the lectin based-sensor. Voltammograms were recorded from −0.2 to 0.8 V at a scan rate of 100 mV s^{-1}. All the experiments were carried out at room temperature.

2.3.3. Bacteria cultivation

All bacteria used in this work belong to the microorganism biosafety level 2 group, except *M. phlei* which belongs to level 1, and, consequently, all safety considerations concerning these groups were accomplished in the manipulation of these bacteria. *E. coli* and *S. aureus* cultures were grown overnight in Luria broth medium (LB) at 37 °C with aeration by shaking, which allowed the growing stationary phase to be reached. *M. phlei* cultures were grown during 72 h in Middlebrook broth medium at 37 °C, with aeration by shaking until the stationary phase was also reached. Then, bacterial cultures were serially diluted (10-fold steps) and 10 μL of samples were applied to LB agar or Middlebrook agar plates, respectively, and incubated for 24 h at 37 °C, for enumeration of colonies (*M. phlei* were incubated for 72 h). At the same time, the stationary-phase cultures were diluted to 10–10^8 cfu (colony forming units) mL^{-1} with deionized water for the impedimetric measurements.

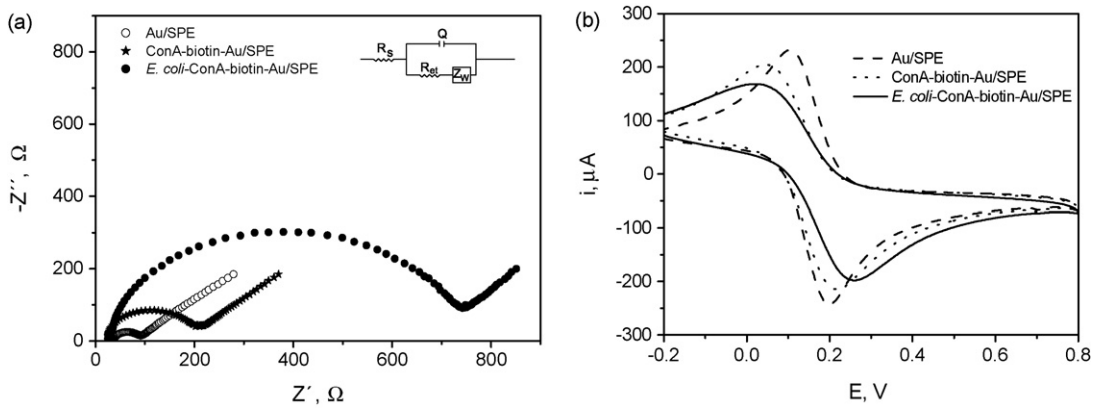

Fig. 1. (a) Complex impedance plots and (b) cyclic voltammograms for a bare Au/SPE, a biotinylated Con A-modified Au/SPE, and a (*E. coli*–biotin–Con A) complex-modified Au/SPE. 2 mM $[Fe(CN)_6]^{3-/4-}$ (1:1) in 0.1 M KCl *E. coli*, 1.0×10^6 cfu mL^{-1}. 0.1–50,000 Hz frequency range with a 10 mV rms signal for EIS measurements and $\nu = 100$ mV s^{-1} in cyclic voltammetry.

Moreover, to induce galactosidase activity during bacteria enrichment, the stationary-phase cultures were diluted to 10–10^8 cfu mL^{-1} in LB, containing 0.25 mM IPTG.

2.3.4. Data chemometric analysis

Impedimetric data obtained for three replicate runs with each cell culture were used to generate a matrix for PCA. One column in the data matrix consisted of the impedimetric responses for each of the nine biotinylated lectins assayed. Thus, three columns were generated for each microorganism. Factor analysis was performed using Statgraphics Plus (Version 5.1) and involved the generation of reduced eigenvectors to determine the optimal number of factors, examination of the resulting residuals plots for randomness, and the generation of scores for the first three principal components. These scores were obtained for each of the three replicate trials for each microorganism, and were plotted to determine whether qualitative groupings of microorganisms existed in the biotinylated-lectin-binding impedimetric responses.

2.3.5. Electrochemical measurement of bacterial β-galactosidase activity from attached bacteria

In this approach, once the bacteria were attached to the electrode surface via biotinylated-lectin interaction, the probe was rinsed with water and 50 μL of 0.1 M PBS buffer (pH 4.5, containing 10 μg mL^{-1} polymyxin B and 468 U tyrosinase) were deposited on a bacteria-biotin–ConA-Au/SPE. The electrode was then polarised to −0.10 V, which is an adequate potential value for phenol detection, and the current was allowed to stabilize. Amperometric responses were obtained after the addition of a 5-μL drop of 0.02 M PG onto the electrode surface [16].

3. Results and discussion

3.1. Formation of the lectin–bacteria complex at the Au/SPE surface

This step was evaluated by using biotinylated-Concanavalin A and *E. coli* as a model system. The lectin was adsorbed onto the pretreated Au/SPE as described in the Experimental section and EIS and cyclic voltammetry were employed to follow the stepwise assembly of the systems and the electronic transduction for the detection of *E. coli*.

Fig. 1a compares Nyquist plots obtained for bare Au/SPE and for modified electrodes with biotinylated Con A, as well as after the formation of the Con A–*E. coli* complex in the presence of equimolar $[Fe(CN)_6]^{4-/3-}$. The bare Au/SPE showed the expected fast electron transfer process with a diffusional limiting step. Formation of the adsorbed biotinylated lectin layer produced an increase in the electron transfer resistance, and the further attachment of bacterial cells to the electrode surface gave rise to an additional barrier for the access of the redox probe to the electrode, resulting in a further increase in electron-transfer resistance [17,18]. The magnitude of this increase in electron transfer resistance could be related to the number of bacterial cells immobilized through the biotinylated lectin to the electrode surface [19].

The Randles modified equivalent circuit (Fig. 1 inset) was used to fit the EIS data and to determine the electrical parameters for each step [18,19]. Table 1 summarizes the values calculated for the electrolyte resistance (R_S), the Warburg impedance resulting from ion diffusion from the electrolyte bulk (Z_W), the electron transfer resistance (R_{et}), and the constant phase element Q (instead of the double layer capacitance, C_{dl}) to take into account the frequency dispersion often related directly to electrode roughness. As can be seen, R_{et} changed from 164.75 to 663.90 Ω, i.e., increased a 403%, upon the binding of the biotin–lectin–*E. coli* complex on the activated Au/SPE surface. These results indicated that EIS is able to monitor the change in electron transfer resistance resulting from the immobilization of bacteria (through the complex formed with an appropriate lectin) on the surface of Au/SPEs without any amplification step.

Fig. 2 shows the changes in electron transfer resistance for Au/SPEs modified with biotinylated-Con A (bar 2), with the adsorbed *E. coli*–biotinylated Con A complex (bar 4), and with non-specific adsorbed *E. coli* cells (bar 3). As it can be seen, no resistance was measured in this latter case, indicating that no significant *E. coli* non-specific adsorption occurred on the electrode surface.

Cyclic voltammograms recorded at the bare and modified Au/SPEs for the $[Fe(CN)_6]^{4-/3-}$ redox pair are displayed in Fig. 1b. As expected, electrode modification with biotinylated-Con A produced a decrease in the peak current and an increase in the separation of peak potentials compared to the voltammetric behaviour of the unmodified electrode. Binding of biotinylated-lectin–bacteria complex on the electrode surface produced an increase of 59 mV in the separation of peak potentials as well as a remarkable decrease

Table 1
Calculated values of the equivalent circuit elements for a bare Au/SPE, a biotinylated Con A-modified Au/SPE and a *E. coli*–biotin–Con A-modified Au/SPE.

	Q (μF)	Z_W (Ω s$^{-1/2}$)	R_{et} (Ω)	R_s (Ω)
Au/SPE	5.81×10^{-6}	2.94×10^{-3}	50.10	34.88
Biotin–ConA–Au/SPE	3.49×10^{-6}	2.97×10^{-3}	164.75	25.26
E. coli–biotin–ConA–Au/SPE	3.63×10^{-6}	2.97×10^{-3}	663.90	30.00

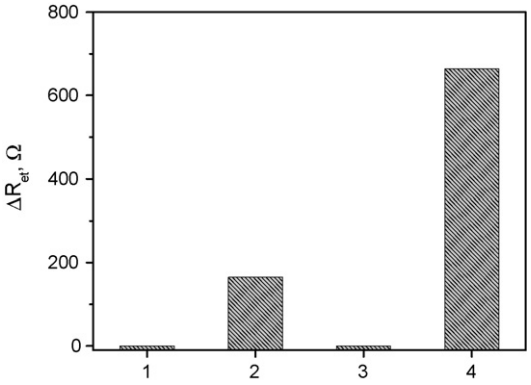

Fig. 2. Electron transfer resistance increments measured for a bare Au/SPE (bar 1), a Au/SPE on which biotinylated-Con A is adsorbed (bar 2), a Au/SPE incubated for 1 h in an 1×10^5 cfu mL^{-1} *E. coli* solution (bar 3), and a Au/SPE on which the *E. coli*–biotinylated Con A complex is adsorbed (bar 4).

in peak current. These results are consistent with the changes observed in the electron transfer resistance by EIS. However, it is important to note that the increase in electron transfer resistance upon bacteria attachment was of 403% with respect to the R_{et} found for the biotinylated-Con A-modified electrode, whereas the signal change (decrease of the anodic current) was only of 24% when cyclic voltammetry was used. This suggests that EIS measurements of electron transfer resistance were more sensitive than current voltammetric measurements for sensing the change on the electrode surface upon binding of the biotinylated-lectin–bacterial cells complex [19].

A similar set of EIS experiments was carried out using non-biotinylated Con A-modified Au/SPE. In this case no change of R_{et} was observed after modification of the Au/SPE with the lectin/bacteria mixture, which can be attributed to the fact that biotinylated-Con A is strongly adsorbed on gold, as it was demonstrated by Yam et al using combined Fourier transform infrared reflection-absorption spectroscopy (FT-IRRAS) and X-ray photoelectron spectroscopy (XPS) [20].

Another control experiment was performed by changing slightly the electrode modification process described in the Experimental section. So, an Au/SPE was modified with the 0.06 mg mL^{-1} biotinylated-Con A solution (without bacteria) allowing the immobilization to proceed for 1 h. Then the electrode was rinsed with PBS buffer to remove unbound biotinylated-Con A, and the modified Au/SPE was incubated for 1 h upon further deposition of the bacteria solution prepared in acetate buffer containing 1 mM Ca^{2+} and Mn^{2+}. This modification process produced a much lower increase in the R_{et} value, and accordingly a lower sensitivity, than that achieved by following the immobilization procedure described in the Section 2.3.1, i. e. with successive deposition of lectin and bacteria and allowing the joint immobilization to proceed for 1 h. This result suggests that it is the biotinylated-Con A in solution rather than the electrode surface-confined Con A which played a key role in the enhancement of *E. coli* cell adhesion onto the Au/SPE. This fact also suggests that Con A in solution aggregates on the *E. coli* cell walls through binding to their O-antigen structure, which produced an accumulation of Con A-*E coli* conjugates in form of multilayers at the electrode surface [3,11].

3.2. Optimization of the experimental variables

First the influence of the biotinylated-Con A concentration was checked. As expected, the electron-transfer resistance increased notably with the lectin concentration up to a value of 0.06 mg mL^{-1} (Fig. 3a). However, higher Con A concentrations provoked a decrease of the R_{et} value, which may be due to agglutination phenomena at high lectin concentrations.

Furthermore, bacteria–lectin incubation time also played and important role in the detection of *E. coli*. Fig. 3b shows that the electron-transfer resistance increased with incubation time until 1 h. Longer incubation times produced a decrease in the measured R_{et}, probably due to the instability of the biotinylated-Con A–*E. coli* complex. A similar event was already reported for an antibody-bacteria conjugate [21]. Therefore, 1 h was selected as the incubation time for further work.

3.3. Analytical characteristics

The addition of different *E. coli* concentrations gave rise to significantly different impedimetric responses, thereby suggesting the possibility of bacteria quantification. Fig. 4 shows as the electron-transfer resistance varied linearly ($r = 0.987$) with the logarithmic value of *E. coli* concentration over four orders of magnitude, between 5×10^3 and 5×10^7 cfu mL^{-1}. Signals levelled off for higher bacteria concentration indicating system saturation. Again, negative controls (without biotinylated-Con A) showed no significant R_{et} changes, demonstrating the absence of significant non-specific adsorptions even for large bacteria concentrations.

Taking the electron transfer resistance of the biotinylated lectin–Au/SPE as the signal threshold, the detection limit of this lectin-based sensor, estimated as 3 times the standard deviation of the blank signal, was 5×10^3 cfu mL^{-1}. When this value was

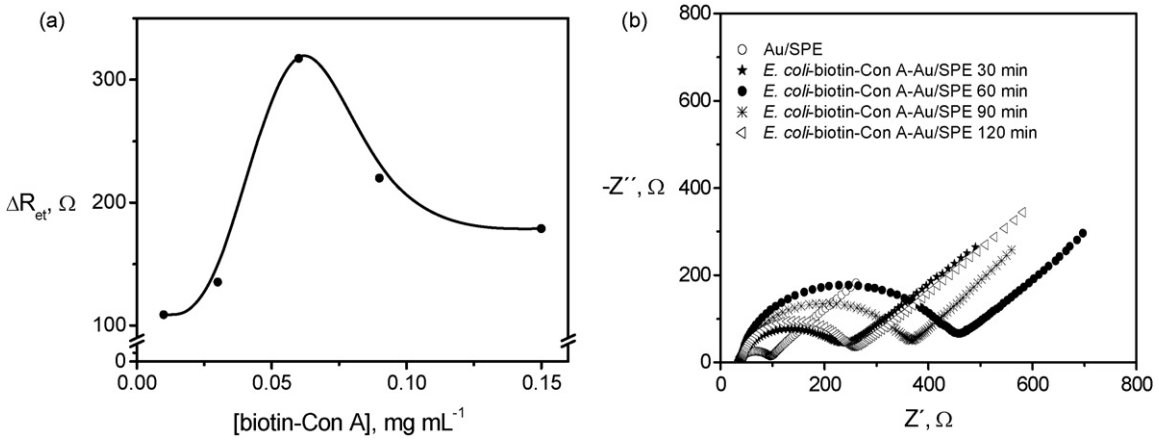

Fig. 3. Effect of the biotinylated-Con A concentration used (a), and the bacteria–lectin incubation time (b) on the electron transfer resistance obtained. 1.0×10^6 cfu mL^{-1} *E. coli*. Other conditions as in Fig. 1.

Table 2
Analytical performance of different *E. coli* impedimetric biosensors reported in the literature.

Immobilization method	L.R. (cfu mL^{-1})	LOD (cfu mL^{-1})	Time of the assay	Ref.
Covalent immobilization of antibodies using an epoxysilane monolayer on ITO substrate	6.0×10^4–6.0×10^7	6.0×10^3	~36 h: preparation of antibodies-modified chips; 1 h: antibodies-bacteria binding reaction	[17]
Covalent immobilization of antibodies onto an indium–tin oxide interdigitated array microelectrode	4.36×10^5–4.36×10^8	1.0×10^6	Overnight preparation of substrate-attached antibodies; incubation with bacteria solution until its evaporation	[18]
Covalent immobilization of antibodies using an epoxysilane monolayer on ITO substrate	–	6.0×10^5	~24 h: preparation of antibodies-modified substrates	[22]
Covalent immobilization of antibodies using an epoxysilane monolayer on ITO substrate	4.215×10^3–4.215×10^6	4.215×10^3	–	[23]
Antibody immobilization via heterobifunctional cross-linkers on a interdigitated array gold electrode	1.0×10^4–1.0×10^7	1.0×10^4	–	[24]
Biotinylated polyclonal antibody linked to a mixed SAM on a gold electrode through biotin-neutravidin interaction	1.0×10^1–1.0×10^4	10	~16 h: preparation of antibodies-modified substrates; 1 h: antibodies-bacteria binding reaction	[12]
Interdigitated array gold microelectrode coupled with magnetic nanoparticle-antibody conjugates	–	7.4×10^4	~1 h: immunomagnetic concentration of bacteria	[25]
Interdigitated array gold microelectrode coupled with magnetic nanoparticle-antibody conjugates	–	1.6×10^2	~1 h: immunomagnetic concentration of bacteria; 35 min: measurement	[26]
Covalent immobilization of antibodies through EDC and NHS on a gold electrode modified with a mercaptoacetic acid (MACA) SAM	3.0×10^3–3.0×10^7	1.0×10^3 (50 with preconcentration steps)	~38 h: preparation of antibodies-modified substrates; 1 h: antibodies-bacteria binding reaction	[21]
Interdigitated array microelectrode containing a gold layer sputtered on borosilicate glass substrate	–	8.0 (14.7 h) and 8.2×10^8 (0.8 h)	–	[27]
Biotinylated ConA–*E. coli* complex immobilization onto Au/SPE	5.0×10^3–5.0×10^7	5.0×10^3	5 min: Au/SPE pretreatment; 1 h: immobilization of the lectin–bacteria complex	This work

L.R.: linear range. LOD: limit of detection.

compared with those reported in the literature for other biosensors based on EIS techniques (Table 2), it could be deduced that we could achieve a low detection limit for *E. coli* without pre-concentration or pre-enrichment steps. Moreover, the range of linearity, covering 4 orders of magnitude, was as wide as the best ones reported for other impedimetric sensors.

In addition, the reproducibility of the responses obtained with eight different Con A–Au/SPE sensors prepared in the same manner was also tested. A RSD value of 9.8% for an *E. coli* concentration level of 1×10^5 cfu mL^{-1} was obtained, which can be considered as acceptable for this kind of disposable sensors.

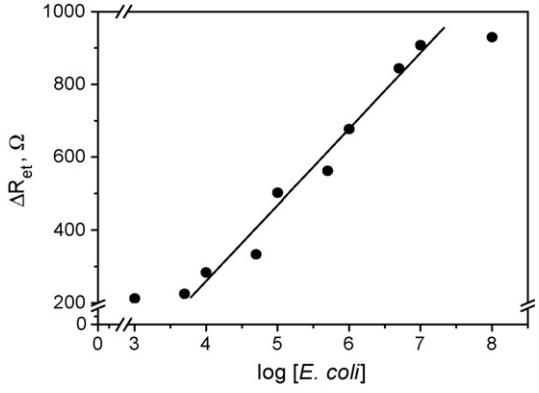

Fig. 4. Calibration plot between the logarithmic value of *E. coli* concentration and the electron-transfer resistance. Other conditions as in Fig. 1.

In summary, when the analytical performance of the biotin-Con A-based Au/SPE is compared with previous impedimetric approaches (summarized in Table 2), it can be deduced that the lectin-based approach offers significant advantages, mainly taking into account the simplicity and rapidity of the proposed methodology.

3.4. Selectivity

The selectivity of the approach was evaluated by checking the impedimetric responses of Au/SPEs modified with complexes formed between nine different lectins and three different bacteria (*E. coli*, *S. aureus* and *M. phlei*) at the same concentration level (1×10^5 cfu mL^{-1}) and under the experimental conditions selected above. Three different measurements were carried out for each case. In order to ascertain whether the impedimetric responses could be classified according to species patterns, PCA was applied to the set of results. This analysis was carried out in a semi-quantitative manner (see Table 3), in which ΔR_{et} values (corresponding to the difference in electron transfer resistance for the lectin-modified electrode in the presence and in the absence of microorganism) were classified in three ranges: R_{et} values >200 Ω were denoted as (++), R_{et} values ranging between 0 and 200 Ω (+), and (0) for those cases in which there was not increase in the R_{et} after incubation with the corresponding bacteria, i.e., the bacteria–lectin interaction was negligible. As it can be deduced from Table 3, different bacteria response profiles were found when the different lectins were used as recognition elements.

Table 3
Semi-quantitative responses for ΔR_{et} (see text for details) obtained with nine biotinylated-lectins and three different microorganisms.

Biotinylated-lectin	Microorganism		
	E. coli	*S. aureus*	*M. phlei*
Concanavalin A	+	+	0
	+	+	0
	+	+	0
Arachis hypogaea	0	+	+ +
	0	+	+ +
	0	+	+ +
Ulex europaeus	+ +	0	+
	+	0	0
	+ +	0	0
Triticum vulgaris	+ +	+ +	0
	+ +	+ +	0
	+ +	+ +	0
Helix pomatia	+ +	+	+ +
	+ +	+	+ +
	+ +	+	+ +
Tetragonolobus purpureas	+	0	0
	+	0	0
	+	0	0
Dolichos biflorus	+	0	0
	+	0	0
	+	0	0
Lens culinaris	+ +	+ +	+
	+ +	+ +	+
	+ +	+ +	+
Lycopersicon esculentum	+ +	+	+
	+ +	+	+
	+ +	+	+

PCA analysis showed that three components explained more than 95% of the total variance across the matrix: PC 1 (42%), PC 2 (35%) and PC 3 (18%). Fig. 5 shows the three-dimensional plot for the components loadings. As it can be observed, a suitable clustering for the measurements obtained from each type of microorganism was achieved with this simple approach, thus allowing classification and distinction among them.

Furthermore, semi-quantitative data in Table 3 seem to indicate that *U. europaeus*, *T. purpureas* and *D. biflorus* lectins could be more advantageous for *E. coli* detection that Con A. This point will be explored in further work.

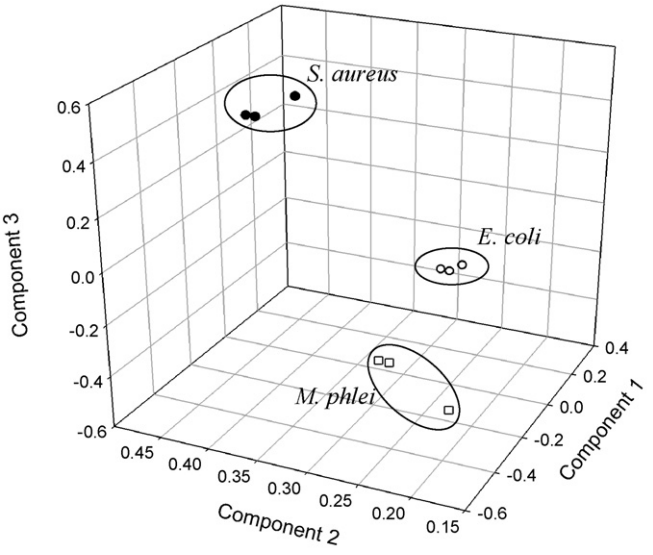

Fig. 5. Pattern recognition plot obtained using data shown in Table 3. Each point represents a column of nine individual measurements (one of each lectin assayed) with *E. coli*, *S. aureus* and *M. phlei*.

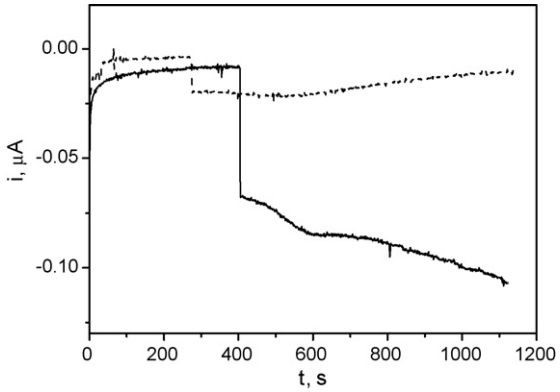

Fig. 6. Current–time recordings recorded upon addition of 2.0 mM PG after bacteria–lectin complex immobilization. Electrodes: *S. aureus*–biotinylated-ConA–Au/SPE (- - -) and *E. coli*–biotinylated-ConA–Au/SPE (—). E_{app} = −0.10 V.

3.5. β-Galactosidase activity monitoring from attached bacteria

In order to further increase the selectivity and discriminate between viable and nonviable cells, an approach involving electrochemical monitoring of β-galactosidase activity of the bacteria attached to the surface via biotinylated-lectin interaction was assayed. It has been demonstrated that β-galactosidase activity can be regarded as a good marker for *Enterobacteriaceaes* with no significant interference from other bacterial families [28,29].

Therefore, the possibility of using β-galactosidase activity monitoring to distinguish between *E. coli* and *S. aureus*, which exhibit a similar affinity towards biotinylated-Con A, was evaluated as a proof of concept. Modified electrodes with or without enzymatic induction during bacteria enrichment for both types of bacteria were prepared. Following the protocol described in 2.3.5 section, a small current change was observed for *S. aureus* with or without IPTG (Fig. 6), which is consistent with the absence of intrinsic β-galactosidase activity for non *Enterobacteriaceaes*. However, a big current increase was produced in the case of *E. coli* in the presence of the enzyme reaction inducer. As it can be deduced from Fig. 6, this approach is able to distinguish clearly between both types of bacteria. Although the methodology needs to be optimized further, these promising preliminary results suggest that the measurement of β-galactosidase activity of the surface-bound bacteria may allow an estimation of bacterial activity.

4. Conclusions

The possibility of rapid label-free detection, identification and quantification of microorganisms based on impedimetric monitoring for the specific recognition of bacteria wall cell glycocalyx components by lectins, through immobilization of (biotinylated-lectins–bacteria) complexes on gold screen-printed electrodes is demonstrated. The proposed approach can be advantageously compared with conventional bacterial plate counting methods and other electrochemical techniques, enabling the detection of 5.0×10^3 cfu mL^{-1} *E. coli* within 1 h. The use of small amounts of test solution and cheap reagents also minimizes assay costs. The selective binding of lectins to oligosaccharide residues present on the surface of the microorganisms can be exploited to generate characteristic patterns of binding to the electrodes, as it is demonstrated by the groupings obtained for three microorganisms using PCA. Moreover, this kind of information can be easily coupled with that provided by checking electrochemically the β-galactosidase

activity of the surface attached bacteria via lectin interaction, which can be used for further improvement of the selectivity and discrimination between viable and nonviable cells.

Acknowledgements

The financial support of the Spanish Ministerio de Educación y Ciencia Research Project CTQ2006-02743BQU is gratefully acknowledged. Maria Gamella acknowledges a pre-PhD fellowship of the Comunidad Autonoma de Madrid. Susana Campuzano acknowledges a "Juan de la Cierva" contract to the Spanish Ministerio de Educación y Ciencia.

References

[1] D. Ivnitski, I. Abdel-Hamid, P. Atanasov, E. Wilkins, Biosens. Bioelectron. 14 (1999) 599.
[2] A. Subramanian, J. Irudayaraj, T. Ryan, Biosens. Bioelectron. 21 (2006) 998.
[3] Z. Shen, M. Huang, C. Xiao, Y. Zhang, X. Zeng, P.G. Wang, Anal. Chem. 79 (2007) 2312.
[4] F.C. Dudak, İ.H. Boyacı, Food Res. Int. 40 (2007) 803.
[5] S.R. Haseley, Anal. Chim. Acta 457 (2002) 39.
[6] P. Ertl, S.R. Mikkelsen, Anal. Chem. 73 (2001) 4241.
[7] O.A. Sadik, F. Yan, Anal. Chim. Acta 588 (2007) 292.
[8] W. Vornholt, M. Hartmann, M. Keusgen, Biosens. Bioelectron. 22 (2007) 2983.
[9] P. Ertl, M. Wagner, E. Corton, S.R. Mikkelsen, Biosens. Bioelectron. 18 (2003) 907.
[10] M.O.J. Olson, I.E. Liener, Biochemistry 6 (1967) 105.
[11] B. Serra, M. Gamella, A.J. Reviejo, J.M. Pingarrón, Anal. Bioanal. Chem. 391 (2008) 1853.
[12] R. Maalouf, C. Fournier-Wirth, J. Coste, H. Chebib, Y. Saïkali, O. Vittori, A. Errachid, J.-P. Cloarec, C. Martelet, N. Jaffrezic-Renault, Anal. Chem. 79 (2007) 4879.
[13] E. Sabatani, I. Rubinstein, J. Phys. Chem. 91 (1987) 6663.
[14] C. Berggren, P. Stalhandske, J. Brundell, G. Johansson, Electroanalysis 11 (1999) 156.
[15] B.A. Boukamp, Equivalent Circuits. Users Manual, second ed., University of Twente, The Netherlands, 1993.
[16] B. Serra, M.D. Morales, J. Zhang, A.J. Reviejo, E.H. Hall, J.M. Pingarron, Anal. Chem. 77 (2005) 8115.
[17] A.-E. Radi, J.L. Acero Sánchez, E. Baldrich, C.K. O'Sullivan, Anal. Chem. 77 (2005) 6320.
[18] C. Ruan, L. Yang, Y. Li, Anal. Chem. 74 (2002) 4814.
[19] L. Yang, Y. Li, G.F. Erf, Anal. Chem. 76 (2004) 1107.
[20] C.-M. Yam, C.-M. Pradier, M. Salmain, P. Marcus, G. Jaouen, J. Colloid Interface Sci. 235 (2001) 183.
[21] P. Geng, X. Zhang, W. Meng, Q. Wang, W. Zhang, L. Jin, Z. Feng, Zi. Wu, Electrochim. Acta 53 (2008) 4663.
[22] L. Yang, Y. Li, Biosens. Bioelectron. 20 (2005) 1407.
[23] D. Zhang, S. Chen, L. Qin, R. Li, P. Wang, Y. Li, Conf. Proc. IEEE Eng. Med. Biol. Soc. 7 (2005) 7111.
[24] S.M. Radke, E.C. Alocilja, Biosens. Bioelectron. 20 (2005) 1662.
[25] M. Varshney, Y. Li, Biosens. Bioelectron. 22 (2007) 2408.
[26] M. Varshney, Y. Li, B. Srinivasan, S. Tung, Sens. Actuators B 128 (2007) 99.
[27] M. Varshney, Y. Li, Talanta 74 (2008) 518.
[28] İ.H. Boyacı, Z.P. Aguilar, M. Hossain, H.B. Halsall, C.J. Seliskar, W.R. Heineman, Anal. Bioanal. Chem. 382 (2005) 1234.
[29] X.T. Mo, Y.P. Zhou, H. Lei, L. Deng, Enzyme Microb. Technol. 30 (2002) 583.

Talanta 78 (2009) 1436–1439

Contents lists available at ScienceDirect

Talanta

journal homepage: www.elsevier.com/locate/talanta

Simultaneous determination of free fluoride and monofluorophosphate in toothpaste by capillary electrophoresis with capacitively coupled contactless conductivity detection

Ivanilce Cristina Guimarães, Camila Cardoso Rezende, José Alberto Fracassi da Silva, Dosil Pereira de Jesus*

Institute of Chemistry, University of Campinas – UNICAMP, 13083-970, Campinas, SP, Brazil

ARTICLE INFO

Article history:
Received 13 November 2008
Received in revised form 19 February 2009
Accepted 20 February 2009
Available online 4 March 2009

Keywords:
Capillary electrophoresis
Capacitively coupled contactless conductivity detection
Toothpaste
Free fluoride
Monofluorophosphate

ABSTRACT

Capillary electrophoresis (CE) with capacitively coupled contactless conductivity detection (C^4D) was used for rapid, accurate and simultaneous determination of free fluoride and monofluorophosphate (MFP) in six different toothpaste samples. A buffer solution containing 15 mmol L^{-1} histine, 25 mmol L^{-1} lactic acid, and 2.5 mmol L^{-1} tetradecyltrimethylammonium bromide (TTAB) was used as background electrolyte (BGE). A complete separation of the analytes and the internal standard (tartrate) could be attained in less than 2.5 min. The limits of detection (LOD) and quantification (LOQ) were, respectively, 0.17 and 0.57 mg L^{-1} for free fluoride and 0.70 and 2.33 mg L^{-1} for MFP. Recoveries ranging from 85 to 107% were obtained for samples spiked with standard solutions of free fluoride or MFP. The CE-C^4D method was compared to an ion-selective electrode (ISE) method and the results were in good agreement. More importantly, the CE-C^4D method demonstrates the advantage of being able to determine MFP without a prior hydrolysis step.

1. Introduction

Sodium fluoride and monofluorophosphate (MFP) have been used in toothpaste formulations as caries preventive agents. These compounds are sources of fluoride ions, which act in the tooth remineralization process [1] that prevents teeth against the erosion caused by caries. Fluoride ions from sodium fluoride dissociation are readily available in the toothpaste while they are gradually released from the MFP hydrolysis [1] catalyzed by phosphatases present in human saliva. MFP guarantees a low concentration of free fluoride ions in the toothpastes, minimizing the formation of insoluble fluoride compounds such as CaF_2. In most countries, public heath regulatory agencies establish the maximum allowed total fluoride concentration (free ion and MFP forms) in toothpaste as 1.50 mg g^{-1}. Total fluoride concentrations above this limit can significantly increase dental fluorosis incidence [2], caused by excessive fluoride intake, especially by children, during tooth brushing. On the other hand, total fluoride concentrations below than 0.50 mg g^{-1} are not effective for caries prevention [3]. So, the concentration determination of free fluoride and MFP in toothpaste is very important to evaluate the quality and human health risk related to this dentifrice.

Although some alternative methods are proposed in the literature [4–6] for free fluoride and MFP determinations in toothpaste, the ion-selective electrodes (ISE) [7] or ion chromatography [8] are usually the first choice. ISE methods allow detection of only free fluoride, so a MFP hydrolysis step [7] is required before analysis, making the sample treatment more laborious and time consuming. Methods based on ion chromatography can provide simultaneous determination of these analytes, however the analysis time is long. On the other hand, rapid and simultaneous determination of free fluoride and MFP is feasible by capillary electrophoresis (CE), although few papers in the literature [9–13] have reported this application. In these papers indirect photometric detection was always used and chromate buffer was the first choice as background electrolyte (BGE). However, capacitively coupled contactless conductivity detection (C^4D) [14,15] in CE (CE-C^4D) seems a suitable approach for this analysis because it is appropriate for direct detection of small ions. We have previously applied CE-C^4D for determination of cations and anions in many samples, such as ethanol fuel [16], human serum [17], rain water [18], air [19] and coconut water [20]. Other applications of CE-C^4D for several compounds and samples can be found elsewhere [21,22]. This article describes, to the best of our knowledge, the first work in which

* Corresponding author at: Grupo de Eletroforese e Microssistemas de Análise, Instituto de Química, Universidade Estadual de Campinas, P.O. Box 6154, 13083-970 Campinas, SP, Brazil. Fax: +55 19 3521 3023.
E-mail address: dosil@iqm.unicamp.br (D.P. de Jesus).

0039-9140/$ – see front matter © 2009 Elsevier B.V. All rights reserved.
doi:10.1016/j.talanta.2009.02.041

CE-C^{4}D is applied for simple, rapid, accurate and simultaneous determination of free fluoride and MFP in commercial toothpastes.

2. Experimental

2.1. Reagents and solutions

Reagents were all of analytical grade. Acetic acid, sodium acetate, sodium citrate, lactic acid (Lac), and L-histidine (His) were purchased from Labsynth (Diadema, SP, Brazil). Tetradecyltrimethylammonium bromide (TTAB), tartaric acid, NaF, and MFP were purchased from Aldrich (Milwaukee, WI, USA). Deionized water was obtained from a Milli-Q-Water-Purification-System (Millipore, Bedford, MA). A buffer solution (pH 4.0) containing 15 mmol L^{-1} His, 25 mmol L^{-1} Lac, and 2.5 mmol L^{-1} TTAB (electroosmotic flow modifier) was used as BGE throughout this work. Free fluoride and MFP solutions were prepared and stored in polypropylene flasks. Individual stock solutions of tartaric acid (1500 mg L^{-1}), NaF (420 mg L^{-1}), and MFP (1440 mg L^{-1}) were prepared by dissolving the corresponding solid reagents in deionized water. The MFP stock solution was prepared daily and stored in the refrigerator (4 °C) in order to minimize hydrolysis. Free fluoride and MFP standard solutions for CE-C^{4}D analysis were prepared by dilution of the respective stock solutions with deionized water, as required. A TISAB buffer solution (1.0 mol L^{-1} sodium chloride, 0.25 mol L^{-1} acetic acid, 0.75 mol L^{-1} sodium acetate, 0.001 mol L^{-1} sodium citrate, pH 5.2) was prepared as described in the reference cited [23] for the ISE method used in this work. TISAB buffer was used for preparation of samples and standard free fluoride solutions (0.38–2.85 mg L^{-1}) employed in the ISE method.

2.2. Sample preparation

Commercial toothpaste samples containing sodium fluoride or MFP were acquired at local markets. Polypropylene flasks were also used for preparing toothpaste samples. For CE-C^{4}D analysis, 1.25 g of toothpaste was suspended in 25 mL of deionized water under sonication by using an ultrasonic bath for 5 min. The resulting suspension was filtered with a membrane filter (pore size 0.45 μm) and diluted 20–25-fold with deionized water as required. For ISE analysis of the toothpastes containing sodium fluoride, the samples were prepared in a similar way as for CE-C^{4}D analysis, except that TISAB buffer was used for 10–25-fold dilution. According to the adopted ISE method [23] samples containing MFP require a prior acid hydrolysis step. Then 2.0 g of toothpaste was suspended in about 20 mL of deionized water (an ultrasonic bath was also used) and 4.0 mL of 6 mol L^{-1} HCl was added. The suspension was heated and stirred with a stirring hot plate at 80 °C for 30 min. After the samples were cooled to room temperature, deionized water was added to bring the volume to 50 mL. Before the potentiometric measurements, 1 mL of these hydrolyzed samples was diluted in 25 mL of TISAB buffer and finally the volume was completed to 50 mL with deionized water.

2.3. Instrumentation and procedure

A commercial Waters CE system (Milford, MA, USA), modified to contain a home-made C^{4}D, was used in the CE-C^{4}D analysis. A computer interfaced to the equipment and an in-house software, implemented in Labview 8.2 (National Instruments, Austin, TX, USA), were used for control and data acquisition. A 50 cm long (40 cm effective) bare silica capillary with internal diameter of 75 μm was used. Sample injection was performed by gravity for 30 s at a height of 100 mm. The separation voltage was 25 kV and the C^{4}D operated at 550 kHz and 2.0 V peak amplitude. Before the analysis, the capillary was flushed with 0.1 mol L^{-1} NaOH solution for 5 min, then with deionized water for 5 min, and finally with the BGE for 10 min. After each run, the capillary was flushed with BGE for 1 min.

For ISE analysis a free fluoride selective electrode Q 838-F (Quimis, São Paulo, SP, Brazil), an Ag/AgCl reference electrode (Analyser, São Paulo, SP Brazil), and a digital pH meter (Tecnal, São Paulo, SP, Brazil) were used.

3. Results and discussion

3.1. CE-C^{4}D separation

We optimized the composition of the BGE in order to attain the best peak resolution and detectability. Fig. 1 shows electropherograms obtained with the optimized BGE for a standard solution and two toothpaste samples (20-fold diluted). As one can note, separations with good peak resolution can be achieved in less than 2.5 min. Phosphate is a common component of the toothpastes and can interfere in the free fluoride determination when BGE with pH around 8.0 is used [10,11]. This occurs because at this pH condition the effective electrophoretic mobilities of the free fluoride and phosphate are very similar. However, by using a BGE with lower pH (4.0), phosphate did not interfere in the CE-C^{4}D method. Tartrate, added as tartaric acid, was a good choice as internal standard for the reason that it showed a migration time very close to that of the analytes and good peak resolution.

3.2. MFP hydrolysis

MFP hydrolyzes, producing free fluoride and phosphate ions according to the following reaction:

$$FPO_3^{2-} + H_2O \rightleftarrows F^- + H_2PO_4^-$$

The MFP hydrolysis rate is low at neutral pH but can be significantly increased in acid medium and temperatures above room temperature [24]. In order to evaluate if MFP hydrolysis could influence the accuracy of the quantitative analysis we carried out

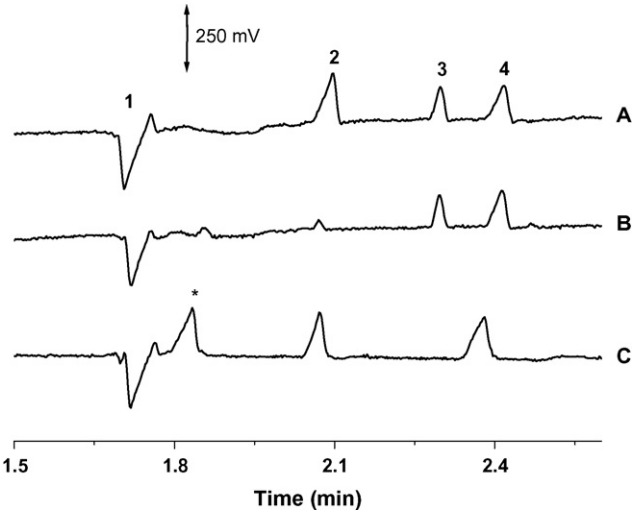

Fig. 1. Electropherograms: (A) standard solution containing 3.80 and 28.80 mg L^{-1} of free fluoride and MFP, respectively; (B) and (C) toothpaste samples with, respectively, MFP and free fluoride in their formulation. Tartrate (22.51 mg L^{-1}) was added to all solutions as internal standard. BGE: 15 mmol L^{-1} His, 25 mmol L^{-1} Lac, and 2.5 mmol L^{-1} TTAB. Separation voltage 25 kV; gravity injection for 30 s at a height of 100 mm; silica capillary with 75 μm inner diameter and 50 cm length (40 cm effective). C^{4}D operated at 550 kHz and 2.0 V peak amplitude. Peaks: (1) system peak; (2) free fluoride; (3) MFP; (4) tartrate; (*) unidentified peaks.

Table 1
Analytical characteristics of the CE-C^4D method.

Analytes	Sensitivity (V min mg^{-1} L)	LOD[a] ($mg\,L^{-1}$)	LOQ[b] ($mg\,L^{-1}$)	Concentration range ($mg\,L^{-1}$)	R^2[c]
Free fluoride	2.82×10^{-3}	0.17	0.57	0.9–15.2	0.9999
MFP	8.20×10^{-4}	0.70	2.33	4.9–78.4	0.9996

[a] Limit of detection for SNR = 3.
[b] Limit of quantification for SNR = 10.
[c] Regression coefficient.

CE-C^4D separations for a standard solution (14.40 $mg\,L^{-1}$ MFP and 22.51 $mg\,L^{-1}$ tartrate), as soon as it was prepared and after some waiting time. As can be seen in the electropherograms shown in Fig. 2, with time the MFP peak area decreases and a free fluoride peak appears. After 4 h all MFP was hydrolyzed and the free fluoride peak reaches its maximum area. Phosphate from the hydrolysis reaction was not detected because its concentration is lower than the limit of detection for this ion. Based on these results we conclude that MFP hydrolysis can affect analysis accuracy. In order to overcome this drawback, the MFP standard solutions were prepared at the moment of injection and the temperature of the stock solution was kept ca. 4 °C by storage in a refrigerator. The same procedure was adopted for the preparation of the toothpaste samples containing MFP. Moreover, we found that increasing the free fluoride concentration inhibits the MFP hydrolysis due to the equilibrium displacement towards the reagents. Thus, the analytical curves for free fluoride and MFP were simultaneously obtained with standard solutions containing both analytes.

3.3. Analytical characteristics of the CE-C^4D method

Table 1 shows some analytical characteristics of the CE-C^4D method.

Good linearity was attained for both analytes over a large range of concentrations. Limits of detection (LOD) are comparable or better than those obtained by CE methods with indirect photometric detection [10,12–13].

3.4. Toothpaste analysis

Table 2 shows the results of the recovery tests carried out by spiking the toothpaste samples with the corresponding fluoride form present in each formulation. It can be seen that only sample D exhibited a poor percent recovery, most likely due to MFP hydrolysis. We believe some component of this sample catalyzed the hydrolysis reaction, thereby releasing free fluoride and forming insoluble CaF_2, which was not detected by the CE-C^4D method.

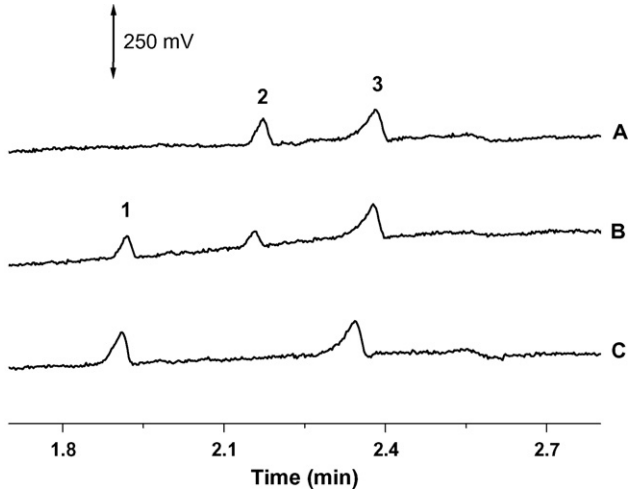

Fig. 2. Electropherograms for a standard solution containing 14.40 $mg\,L^{-1}$ of MFP and 22.51 $mg\,L^{-1}$ of tartrate (internal standard): (A) injected as soon as prepared and after (B) 2 and (C) 4 h. Separation conditions as in Fig. 1. Peaks: (1) free fluoride; (2) MFP; (3) tartrate.

Table 2
Recovery (%) for toothpaste samples spiked with free fluoride or MFP.

Samples[a]	Spiked F^- ($mg\,L^{-1}$)[b]	Spiked MFP ($mg\,L^{-1}$)[b]	Found[c] ($mg\,L^{-1}$)	Recovery (%)
A	1.90	–	1.92	101
B	1.90	–	2.03	107
C	1.90	–	1.81	95
D	–	9.80	8.33	85
E	–	9.80	9.90	101
F	–	9.80	9.51	97

[a] Samples were spiked with the corresponding fluoride form present in each formulation.
[b] Spiked concentrations in the injected samples.
[c] Concentration difference between spiked and non-spiked samples.

Table 3 summarizes the results obtained in the analysis of the toothpaste samples by the CE-C^4D and ISE methods.

The samples containing MFP showed some free fluoride concentration (see electropherogram B in Fig. 1), except sample D. This free fluoride may be provided by MFP hydrolysis or may be present as an impurity in the MFP salt added by the manufacturer. Table 3 also shows the total fluoride content, which represents the sum of the concentrations of the free fluoride and the ionizable fluoride (values in parenthesis) in the form of MFP. It is worth commenting that sample C is formulated for children, so its total fluoride content is lower than for the other samples indicated for adults. When comparing CE-C^4D and ISE methods a good agreement was observed, but sample D exhibited a lower total fluoride by the ISE method. This result may be explained by the fact that the accuracy of the ISE method is affected by incomplete MFP hydrolysis or formation of insoluble CaF_2 [7]. The extent of this calcium interference depends

Table 3
Concentrations ($mg\,g^{-1}$) of free fluoride, MFP, and total fluoride in the analyzed toothpastes.

Samples	CE-C^4D			ISE[d]
	Free fluoride	MFP	Total fluoride[c]	
A	1.33 ± 0.02	ND[a]	1.33 ± 0.02	1.35 ± 0.01
B	1.21 ± 0.06	ND[a]	1.21 ± 0.06	1.30 ± 0.03
C	0.93 ± 0.03	ND[a]	0.93 ± 0.03	0.95 ± 0.02
D	ND[a]	5.98 (1.16)[b] ± 0.05 (0.01)[b]	1.16 ± 0.01	0.75 ± 0.02
E	0.20 ± 0.06	4.8 (0.92)[b] ± 0.4 (0.07)[b]	1.12 ± 0.09	1.05 ± 0.01
F	0.14 ± 0.03	5.4 (1.05)[b] ± 0.2 (0.05)[b]	1.19 ± 0.06	1.01 ± 0.03

[a] Not detected.
[b] Values in the parenthesis represents the concentration of the ionizable fluoride in MFP form.
[c] Total fluoride concentration obtained by CE-C^4D method, calculated by summing the concentrations of the free fluoride and the ionizable fluoride (values in the parenthesis) in MFP form.
[d] Total fluoride concentration obtained by the ISE method.

on the level of insoluble calcium carbonate, added in toothpaste as abrasive agent. On the other hand, the CE-C^4D method is less prone to these errors because MFP is determined without prior hydrolysis.

4. Conclusions

The CE-C^4D method was demonstrated to be a rapid and accurate analytical technique for simultaneous determination of free fluoride and MFP in toothpaste. The total fluoride determination in this dentifrice is important for the toothpaste industry as well as for health agencies. The analysis time of the CE-C^4D method is lower than for ISE and others methods, especially for MFP, because a prior hydrolysis step or complex treatments of the samples are not necessary.

Although the CE-C^4D method was developed for toothpaste analysis, we believe it can easily be used or adapted for determination of free fluoride and MFP in other matrices, such as human saliva or cementation materials, where MFP has been added as a corrosion inhibitor of steel in concrete.

Acknowledgments

This work was supported by the Fundação de Amparo à Pesquisa do Estado de São Paulo (FAFESP), the Fundo de Apoio ao Ensino, à Pesquisa e à Extensão da Unicamp (FAEPEX-Unicamp), and the Conselho Nacional de Desenvolvimento Científico e Tecnológico (CNPq). The authors thank Dr. Carol H. Collins for the English revision of the manuscript.

References

[1] W.H. Bowen, J. Royal Soc. Med. 88 (1995) 505.
[2] D. Browne, H. Whelton, D. O'Mullane, J. Dent. 33 (2005) 177.
[3] K.G. Konig, Gesundheitswesen 64 (2002) 33.
[4] P.D. Tzanavaras, D.G. Themelis, Analyst 125 (2001) 1608.
[5] G. Wejnerowska, A. Karczmarek, J. Gaca, J. Chromatrogr. A 1150 (2007) 173.
[6] R. Pérez-Olmos, J.C. Soto, N. Zárate, I. Díez, J. Pharm. Biomed. Anal. 47 (2008) 170.
[7] M. Pavic, D. Carevic, Z. Cimerman, J. Pharm. Biomed. Anal. 20 (1999) 565.
[8] N. Yoza, S. Nakashima, T. Nakazato, N. Ueda, H. Kodama, A. Tateda, Anal. Chem. 64 (1992) 1499.
[9] S.A. Shamsi, N.D. Danielson, Anal. Chem. 67 (1995) 1845.
[10] A.H. Harakuwe, P.R. Haddad, Anal. Commun. 34 (1997) 67.
[11] A.H. Harakuwe, P.R. Haddad, J. Chromatogr. A 734 (1996) 416.
[12] P. Wang, S.F.Y. Li, H.K. Lee, J. Chromatogr. A 765 (1997) 353.
[13] T. Wang, S.F.Y. Li, J. Chromatogr. A 781 (1997) 457.
[14] J.A. Fracassi da Silva, C.L. Lago, Anal. Chem. 70 (1998) 4339.
[15] J.A. Fracassi da Silva, N. Guzman, C.L. do Lago, J. Chromatogr. A 942 (2002) 249.
[16] R.A.A. Munoz, E.M. Richter, D.P. de Jesus, C.L. do Lago, L. Angnes, J. Braz. Chem. Soc. 15 (2004) 523.
[17] J.A. Fracassi da Silva, N.L. Ricelli, A.Z. Carvalho, C.L. do Lago, J. Braz. Chem. Soc. 14 (2003) 265.
[18] F.R. Rocha, J.A. Fracassi da Silva, C.L. do Lago, A. Fornaro, I.G.R. Gutz, Atmos. Environ. 37 (2003) 105.
[19] F.R. Rocha, L.H.G. Coelho, M.L.A. Lopes, L.R.F. Carvalho, J.A. Fracassi da Silva, C.L. do Lago, I.G.R. Gutz, Talanta 76 (2008) 271.
[20] E.M. Richter, D.P. de Jesus, R.A.A. Munoz, C.L. do Lago, L. Angnes, J. Braz. Chem. Soc. 16 (2005) 1134.
[21] P. Kuban, P.C. Hauser, Electroanalysis 16 (2004) 2009.
[22] P. Kuban, P.C. Hauser, Anal. Chim. Acta 607 (2008) 15.
[23] J.L. Stuart, E.J. Duff, Analyst 105 (1980) 1098.
[24] A. Rigalli, A.M. Iglesias, R.C. Puche, Drug Dev. Ind. Pharm. 21 (1995) 517.

Talanta 78 (2009) 1332–1338

Contents lists available at ScienceDirect

Talanta

journal homepage: www.elsevier.com/locate/talanta

Gold–silver nanoclusters having dipicolinic acid imprinted nanoshell for *Bacillus cereus* spores recognition

Aytaç Gültekin[a], S. Emir Diltemiz[b], Arzu Ersöz[b], N. Yılmaz Sarıözlü[c], Adil Denizli[d], Rıdvan Say[b,e,*]

[a] Department of Chemistry, Trakya University, Edirne, Turkey
[b] Department of Chemistry, Anadolu University, Eskişehir, Turkey
[c] Department of Biology, Anadolu University, Eskişehir, Turkey
[d] Department of Chemistry, Hacettepe University, Ankara, Turkey
[e] BİBAM (Plant, Drug and Scientific Research Center) Anadolu University, Turkey

ARTICLE INFO

Article history:
Received 12 August 2008
Received in revised form 29 January 2009
Accepted 3 February 2009
Available online 13 February 2009

Keywords:
Gold–silver nanoclusters sensor
Molecularly imprinted polymers
Dipicolinic acid
Bacillus spores recognition
Photoluminesence

ABSTRACT

Molecular imprinted polymers (MIPs) as a recognition element for sensors are increasingly of interest and MIP nanoclusters have started to appear in the literature. In this study, we have proposed a novel thiol ligand-capping method with polymerizable methacryloylamidocysteine (MAC) attached to gold–silver nanoclusters, reminiscent of a self-assembled monolayer and have reconstructed surface shell by synthetic host polymers based on molecular imprinting method for recognition. In this method, methacryloyl iminodiacetic acid-chrome (MAIDA-Cr(III)) has been used as a new metal-chelating monomer via metal coordination–chelation interactions and dipicolinic acid (DPA) which is a main participant of *Bacillus* spores has been used as a template. Nanoshell sensors with templates give a cavity that is selective for DPA. The DPA can simultaneously chelate to Cr(III) metal ion and fit into the shape-selective cavity. Thus, the interaction between Cr(III) ion and free coordination spheres has an effect on the binding ability of the gold–silver nanoclusters nanosensor. The binding affinity of the DPA imprinted nanoclusters has been investigated by using the Langmuir and Scatchard methods and determined affinity constants ($K_{affinity}$) were found as 18×10^6 mol L^{-1} and 9×10^6 mol L^{-1}, respectively.

1. Introduction

The rapid identification of *Bacillus* spores is of importance because of its potential use as a biological warfare agent. Biological warfare detection equipment requires low detection limits, high specificity, portability, strong, inexpensive and the ability to simultaneously detect several broad-range potential threat agents (bacteria, viruses, spores, and toxins) within a few minutes for military and civilian use. There are many literature reported studies for the detection of *Bacillus* spores [1–8].

Dipicolinic acid (DPA) is known to be a unique and characteristic component (10%, dry weight) in all endospores [9]. DPA detection could provide good estimation of bacteria spore content. Several methods such as spectrophotometry [10], Raman spectroscopy [11], Fourier transform infrared spectroscopy [12], high-performance liquid chromatography [13], photoluminescence [14], capillary zone electrophoresis [15], fluorescence [16], potentiometric sensor based on the surface imprinting technique [17] and pyrolysis mass spectrometry [18] have been applied for DPA detection but they use large and costly instruments and require sophisticated, frequently extended analysis procedures. Also field-portable devices such as holographic sensors [2] and surface-enhanced Raman scattering (SERS) [19] have demonstrated successful spore detection.

Molecular imprinting is a technology to create recognition sites in a macromolecular matrix using molecular templates. In other words, both the shape image of the target and alignment of the functional moieties to interact with those in the target, are memorized in the macromolecular matrix for the recognition or separation of the target during formation of the polymeric materials themselves. Molecularly imprinted polymers (MIP) are easy to prepare, stable, inexpensive and capable of molecular recognition [20–23]. Therefore, MIPs can be considered as artificial affinity media. Molecular recognition-based separation techniques have received much attention in various fields because of their high selectivity for target molecules [24,20]. Three steps are involved in the ion-imprinting process: (i) complexation of template (i.e., metal ions) to a polymerizable ligand, (ii) polymerization of this complex and (iii) removal of template after polymerization [25].

In last years, interest in the preparation and characterization of nanostructured materials has increased because of their characteristic properties and potential technological applications. Nanoscale materials submit widespread possibilities for contributions to science and technology and explore the vast potential of nano-

* Corresponding author at: Fen Fakültesi, Yunus Emre Kampüsü, Anadolu Universitesi, 26470 Eskişehir, Turkey. Tel.: +90 222 335 0580; fax: +90 320 4910.
E-mail address: rsay@anadolu.edu.tr (R. Say).

0039-9140/$ – see front matter © 2009 Elsevier B.V. All rights reserved.
doi:10.1016/j.talanta.2009.02.007

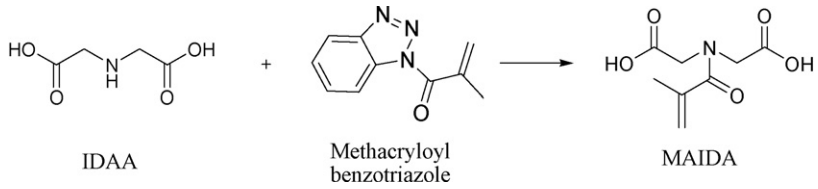

Fig. 1. Synthesis of MAIDA monomer.

materials. These equipments are designed as potential building blocks for future nanoelectronic instruments, which are expected to be smaller, faster, cheaper, and smarter [26]. Many strategies envisioned for nanotechnology require assembled nanometer-scale elements of two or more metals or semimetals to have hybrid properties [27]. The electronic conduction in such structures is varied from metallic to the insulating limit by controlling the size and the strength of the coupling. Usually, self-assembly of nanoparticles can be gained either by direct covalent attachment of different prefunctionalized building blocks or by their noncovalent interactions (electrostatic, hydrophobic, hydrogen bonding, etc.) [28,29].

In recent years, the combinations of nanoparticles and MIPs have been applied in selective sensing detection. Only a few applications of nanoclusters/MIPs have been reported [30–32]. In this work, we have proposed a novel thiol ligand-exchange method using polymerizable methacryloylamidocysteine (MAC) of gold–silver nanoclusters to cap by organic layer, reminiscent of a self-assembled monolayer and have reconstructed surface shell by synthetic host polymers based on molecular imprinting method for *Bacillus* spores recognition. MAIDA-Cr(III) was used as a new metal-chelating monomer via metal coordination–chelation interactions and DPA which is main participant of *Bacillus* spores was used as a template. We have combined nanoscale materials with MIP considering the ability of DPA to chelate of Cr(III) ion of methacryloyl iminodiacetic acid (MAIDA) monomer to create reminiscent ligand exchange (LE) assembled binding sites for *Bacillus* spores recognition, because the Cr(III) primarily interacts with the DPA which is found in *Bacillus* spores [33]. Synthesis, characterization and efficiency of the nanoclusters sensor based on DPA imprinted polymer have been reported in this work.

2. Experimental

2.1. General methods

Methacryloyl chloride was supplied by Aldrich and used as received. DPA and ethylene glycol dimethacrylate (EDMA) were obtained from Fluka A.G., distilled under reduced pressure in the presence of hydroquinone inhibitor and stored at 4 °C until use. Azobisisobutyronitrile (AIBN) and $Cr(NO_3)_3{\cdot}9H_2O$ nitrate nonahidrate were also supplied from Fluka. All other chemicals were of reagent grade and were purchased from Merck AG. All water used in the experiments was purified using a Barnstead NANOpure ultrapure water system.

Photoluminescence spectra were acquired by spectrofluorometer (Varian Cary Eclipse, Australia). ^1H and ^{13}C NMR spectra were recorded in DMSO-d6 with TMS as the internal standard using Bruker 500 MHz NMR equipment. The Transmission Emission Microscopy (TEM) images of nanocrystals were acquired on a FEI-Tecnai^{TM} G^2 Sprit transmission electron microscope (20–120 kV). Sample preparation was consisted of drop coating the nanoclusters onto carbon-coated copper grids and air dried. Raman spectra images were obtained using a Raman spectrophotometer (Bruker Senterra Dispersive Raman Microscope, Germany). Fourier Transform Infrared (FTIR) spectra images were obtained using a FTIR (Spectrum 100, Perkin Elmer, USA). The dry beads (about 0.1 g) were thoroughly mixed with KBr (0.1 g, IR Grade, Merck, Germany), pressed into a pellet and than the FTIR spectrum was recorded.

2.2. Preparation of functional and metal-chelate monomers

Methacryloylamidocysteine, monomer, was used for forming of reminiscent of self-assembled monolayer on the surface of nanocluster and was synthesized and characterized according to the previous procedure [34]. The role of ligand-exchange monomers is to assist in the creation of the specific binding cavity after the polymerization situated within the cavity in an optimal size and shape position for rebinding. MAIDA was prepared using the following literature methodology [35] (Fig. 1).

Iminodiacetic acid (IDAA) (9.52 mmol, 1 g, 1 eq) was dissolved in water. A solution of methacryloyl benzotriazole (MA-Bt) (9.52 mmol, 1 g, 1 eq) in 25 mL of 1,4-dioxane was slowly added to the IDAA solution. Reaction mixture was allowed to stir for 10–20 min at room temperature. Completion of reaction is monitored by TLC, after the reaction finished, 1,4-dioxane was evaporated under vacuum. The residue was diluted with water and extracted with ethyl acetate (3×50 mL) to remove 1*H*-benzotriazole. Collected water phases were neutralized to pH 6–7 using 10% water solution of HCl in order to prevent possible polymerization of methacryloyl group in acidic medium. Then, water was removed via rotary evaporator to give MAIDA in 85–90% yield. MAIDA monomer was characterized with FT NMR and FTIR.

Data for MAIDA: **^{1}H NMR** (DMSO-d6, 500 MHz), δ: 5.55 (s, 1H, $C\underline{H_2}$=C), 5.25 (s, 1H, $C\underline{H_2}$=C), 4.03 (s, 4H, $-C\underline{H_2}-$N(methacryloyl)$-C\underline{H_2}-$), 2.20 (s, 3H, $-C\underline{H_3}$) ppm.

^{13}C NMR (DMSO-d6, 125 MHz), δ: 168.0, 167.0, 142.0, 120.0, 49.0, 20.5 ppm.

FTIR spectrum of MAIDA has the characteristic stretching vibration amide III absorption band at 1300 cm^{-1}, carbonyl band at 1730 cm^{-1}, alken bands at 1650 cm^{-1} and 890 cm^{-1}.

MAIDA-Cr(III) was preorganized using MAIDA and $Cr(NO_3)_3{\cdot}9H_2O$. MAIDA (0.1 mmol) and $Cr(NO_3)_3{\cdot}9H_2O$ (0.1 mmol) were dissolved in 5.0 mL of ethanol and the solution was stirred for 24 h. The FTIR spectrum confirms that MAIDA-Cr(III) metal-chelate monomer structure was exactly produced (Fig. 2a). Carbonyl band at 1637 cm^{-1} shows that Cr(III) was incorporated into MAIDA. The 1700 cm^{-1} carbonyl band shifted to 1637 cm^{-1} which indicated that the metal interaction. Ligand-exchange monomer, MAIDA-Cr(III)-DPA, was preorganized using MAIDA-Cr(III) and template, DPA. MAIDA-Cr(III) (0.1 mmoL) and DPA (0.1 mmoL) were dissolved in 5.0 mL of ethanol and the solution was stirred for 4 h. MAIDA-Cr-DPA, ligand-exchange monomer, was characterized with FTIR (Fig. 2b). In FTIR spectrum of MAIDA-Cr-DPA the bands that appeared at 1384 and 1351 cm^{-1}, which indicated the pyridine vibrations. Solution color changed from green to violet after DPA ligand coordinated MAIDA-Cr complexation.

2.3. Synthesis of gold–silver nanoclusters and DPA imprinted gold–silver nanoclusters sensor

The gold–silver nanoclusters were prepared in a two-phase water/toluene system using a modified Brust method [36]. Briefly,

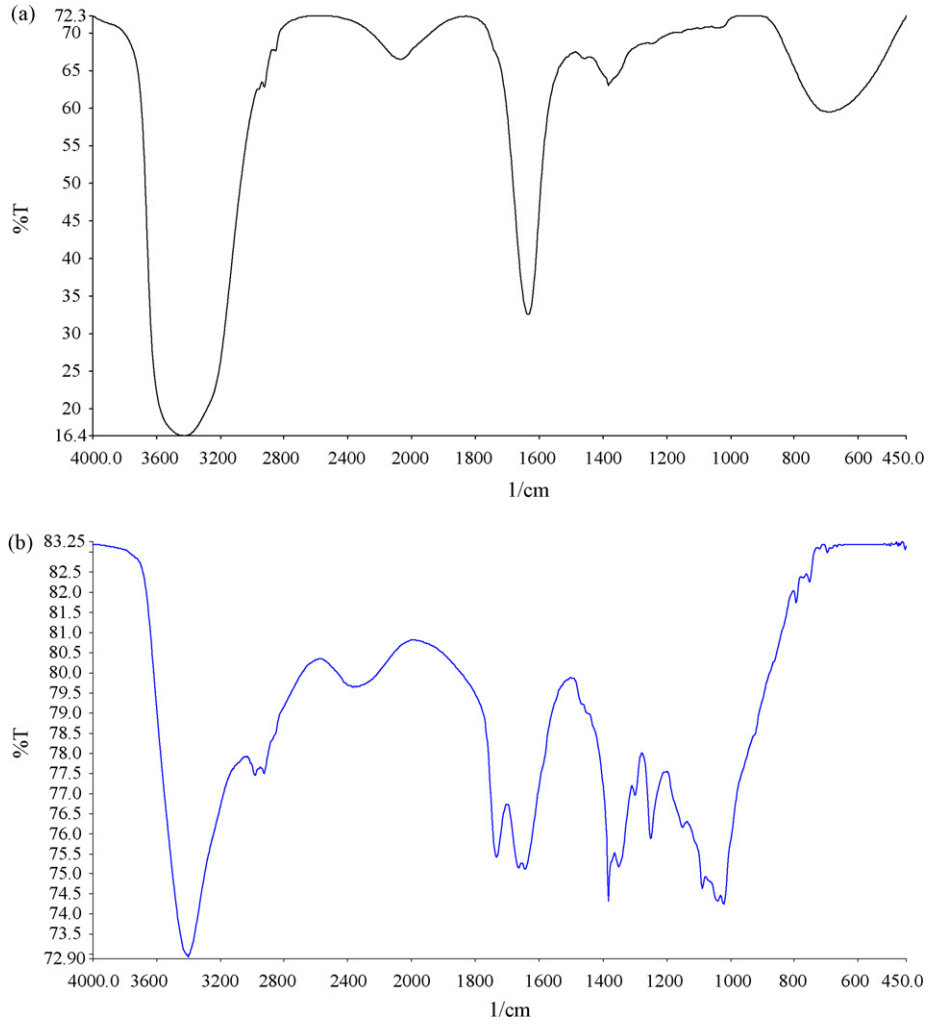

Fig. 2. FTIR spectrum of (a) MAIDA-Cr(III) and (b) MAIDA-Cr-DPA.

nanoclusters were prepared by the dropwise addition of 0.01 M aqueous $NaBH_4$ solution in an equal volume of ammonical aqueous 0.5 mM $HAuCl_4$ (pH ca. 7.8) and 1 mM MAC in ethanol under vigorous stirring. $AgNO_3$ (0.5 mM) was added to 40 mL of Au–MAC nanoclusters dispersion under continuous stirring.

Au–Ag–MAC nanoclusters were separated and washed thoroughly several times with water and toluene and dried under nitrogen, followed by redispersion in dimethyl sulfoxide (DMSO). For the synthesis of DPA recognized nanoshell/polymer Au–Ag nanoclusters, methacryloyl-activated nanoparticles were added into the reaction mixture containing the metal-chelate (MAIDA-Cr(III)/DPA) monomer (0.05 mmol) in DMSO, EDMA crosslinking monomer (0.4 mmol) and 1 mol% of the initiator (AIBN) of the radical polymerization in ethanol. This solution was transferred into the dispersion medium and stirred magnetically at a constant stirring rate of 600 rpm in a glass polymerization tube. The polymerization tube was irradiated with UV light at 365 nm for 4 h. After the polymerization, DPA nanoshells having Au–Ag nanoclusters were separated from the polymerization medium by centrifugation. The residuals (e.g., unconverted monomer and initiator) were removed by a cleaning procedure. The resulting nanocrystals were treated with 10 mL (3/1, v/v) of methanol/phosphoric acid solution for 24 h to remove the templates.

Nonimprinted (NIP) Au–Ag nanoclusters sensor, without using DPA as template, was prepared in a similar way as described above and used as a reference.

2.4. Bacterial strain and spore preparation

The type strain *Bacillus cereus* NRRL B-3711 was obtained from the ARS Culture Collection (NRRL), National Center for Agricultural Utilization Research, Peoria, Illinois.

Spores were prepared on slightly modified fortified nutrient agar (FNA) as described by [37] containing (all per liter): nutrient broth, 13 g; agar, 20 g; NaCl, 3 g; $MnSO_4{\cdot}H_2O$, 0.05 g; $CaCl_2$, 0.06 g; glucose, 0.1 g; $(NH_4)_2SO_4$, 0.08 g; $MnCl_2{\cdot}4H_2O$, 0.008 g; $CuSO_4{\cdot}5H_2O$, 0.005 g; $ZnSO_4{\cdot}7H_2O$, 0.005 g; pH 7.0. Cells were precultivated at 32 °C for 24 h in nutrient broth, and 250 μL of preculture was spread plated onto FNA. These plates were incubated at 32 °C for 5 days and cultures reached >90% spore content as determined by green malachite staining technique. Samples were stored frozen overnight and then thawed for 1–2 h at room temperature to lyse remaining vegetative cells [38]. The resulting preparation was >99% spores as determined by green malachite staining technique. The spores were harvested with a glass spatula and sterile distilled water, and then washed and concentrated four times by centrifugation (2500 × *g*, 15 min, 4 °C) with sterile distilled water [39]. Finally the spore pellet was re-suspended in sterile distilled water and stored at 4 °C.

2.4.1. Plate counting of spores

Spore concentration (CFU mL^{-1}) was determined by serially diluting washed spore stock in 0.1% buffered sterile peptone-water plus 0.05% Tween 80. Tween 80 was added to minimize clumping

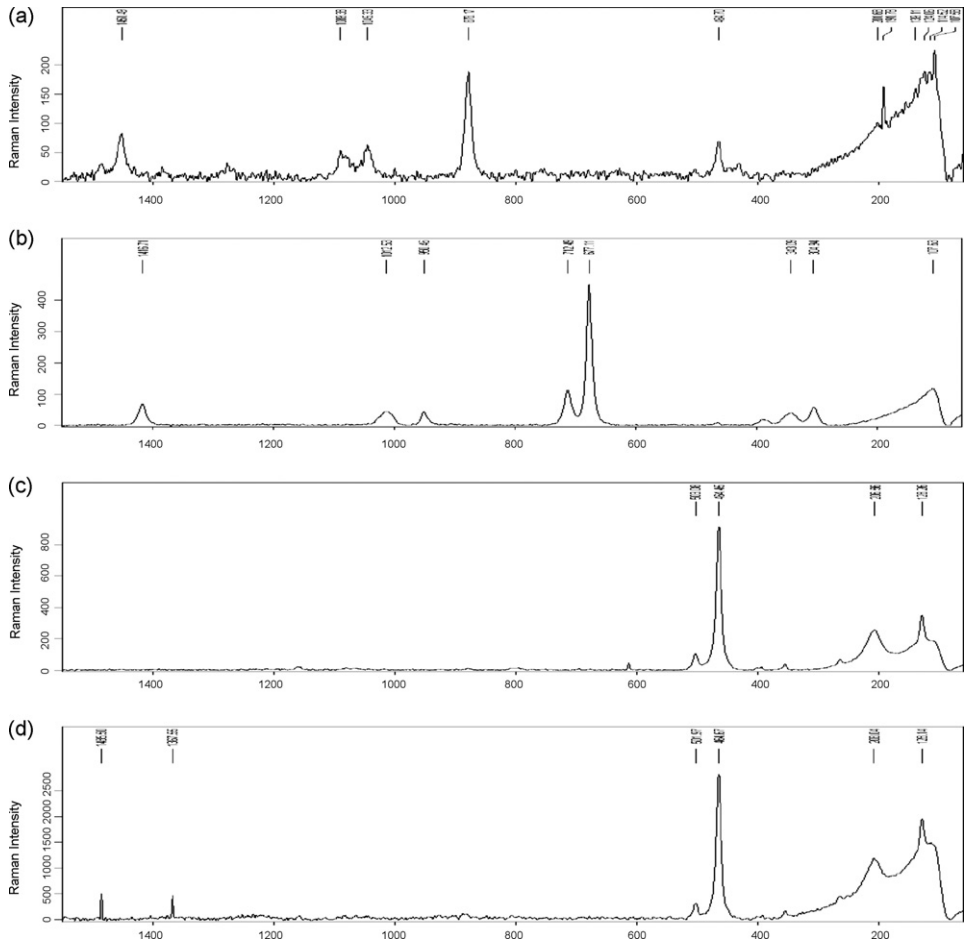

Fig. 3. Raman images of (a) DPA; (b) Au–Ag-MIP nanoclusters with DPA (unleached) and (c) Au–Ag-MIP nanoclusters with *Bacillus* spores (unleached) and (d) Au–Ag-MIP nanoclusters without DPA (leached).

of spores and consequently improve the accuracy of spore counts. 100 μL of diluted spores was plated on recovery medium (nutrient agar supplemented with 1 g L^{-1} of starch) plates in triplicate, and the number of CFU mL^{-1} was calculated following overnight incubation at 30 °C [40].

2.4.2. DPA extraction

DPA is located in the spore core. Endospores are also enriched in calcium ions, most of which are combined with DPA [41]. Due to the protection of the spore cortex, common cell lysing techniques were ineffective for DPA extraction. Techniques such as acid extraction, autoclaving at 121 °C have been utilized [9]. Autoclave treatment was applied for release of DPA in the spores. The stock suspension was diluted serially 10-fold in sterile distilled water. The dilution series were autoclaved at 121 °C for 20 min. After cooling, each dilution series were centrifuged at 10,000 × *g* for 10 min [15].

2.5. Evaluation of nanoclusters luminesence

The sensing capability and specificity of the DPA memory having Au–Ag nanoclusters sensor was further explored by introducing DPA as a template molecule. DPA adsorption studies were performed in a batch system. DPA was dissolved in water and 20 mg of MIP and NIP clusters were placed in DPA solution at different concentrations (10^{-7} to 10^{-4} mol L^{-1}) for a period of 5 min at room temperature. The interactions between DPA and MIP/NIP particles were studied observing fluorescence measurements. The DPA imprinted Au–Ag nanoclusters showed a high separation between the excitation and emission wavelengths, simplifying fluorescence measurements, recorded photoluminescence spectra using spectrofluorometer (Varian Cary Eclipse, Australia). DPA imprinted Au–Ag nanoclusters nanosensors were excited at 260 nm, and emission was recorded at 521 nm. Au–Ag nanoclusters having DPA imprinted nanoshell was tested against *B. cereus* spores. The procedure for DPA was repeated using, *B. cereus* spores suspension.

3. Results and discussion

3.1. TEM characterization of nanoshell sensors

TEM images for Au–Ag nanoclusters having MAC monolayer before and after the removal of DPA template are used for the size determination of nanoclusters. The shape of nanoclusters is close to spherical, aggregated and with average size about 42 nm. The shape of the Au–Ag-MIP nanoclusters with DPA-template (average size about 62 nm) is like spherical, more aggregated because of polymerization. Au–Ag-MIP nanoclusters without DPA template is also close to spherical and aggregated look like MAC-capped Au–Ag nanoclusters and with average size about 55 nm.

3.2. Raman characterization

DPA, Au–Ag-MIP nanoclusters with DPA, Au–Ag-MIP nanoclusters with *Bacillus* spores and Au–Ag-MIP nanoclusters without DPA template were characterized with Raman spectroscopy (Fig. 3). The Raman spectrum obtained for a solution of DPA in water (Fig. 3a)

and the following band shifts are observed 878, 1045, 1099, and 1451 cm^{-1}. Many of these bands have been previously assigned [42,43]. In Raman spectrum of Au–Ag-MIP nanoclusters with DPA has band shifts at 1417, 1012, 950, 713, and 677 cm^{-1} because of DPA itself (Fig. 3b). In Fig. 3c shows that the removal of template of the DPA imprinted nanocluster. Raman spectrum of Au–Ag-MIP nanoclusters with *Bacillus* spores has band shifts 1466 and 1368 cm^{-1} because of DPA itself (Fig. 3d).

3.3. Measurement of binding interactions of molecularly imprinted nanoshell sensor via photoluminescence

The functional metal-chelate monomer, MAIDA-Cr(III), was chosen to interact DPA, to form metal chelate and to make metal-complexing polymeric receptors for selective binding of DPA and analogues [35]. Metal-chelate monomer and DPA molecule were mixed through preorganization and this preorganization complex defines the size and direction of the chemical interactions of the DPA imprinted cavity to prepare synthetic DPA receptor of Au–Ag nanoclusters (Fig. 4).

The selective binding ability and detection of DPA imprinted Au–Ag nanoclusters MIP and NIP sensors were studied with fluorescence spectroscopy, and the results were given in Fig. 5. DPA addition caused significant decreases in fluorescence intensity because they induced photoluminescence emission from Au–Ag nanoclusters through the specific binding to the recognition sites of the crosslinked nanoshell polymer matrix.

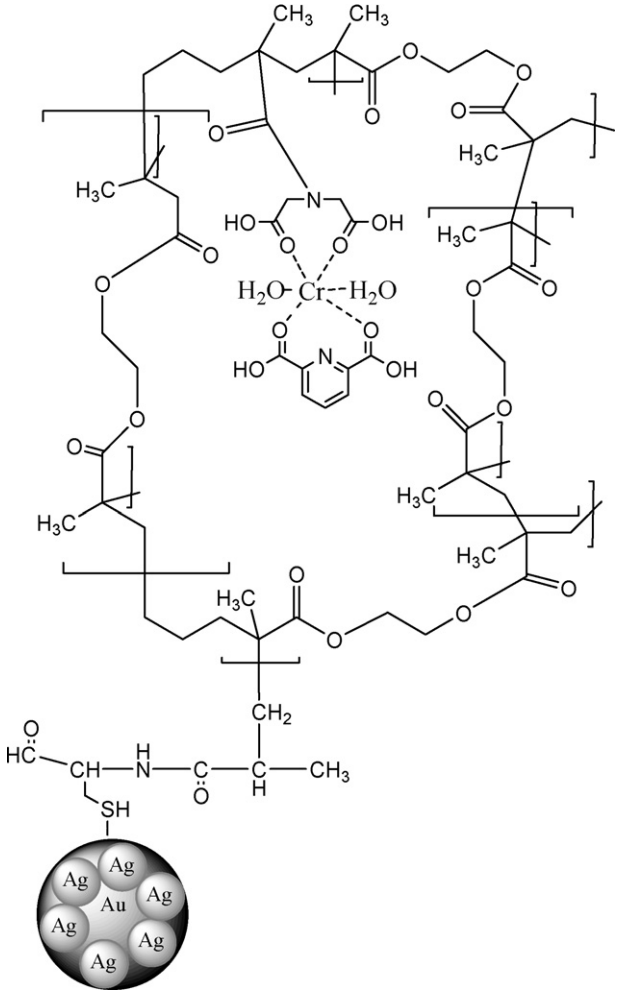

Fig. 4. Schematic representation of nanoshell based on DPA-template reconstruction on Au–Ag/nanoclusters.

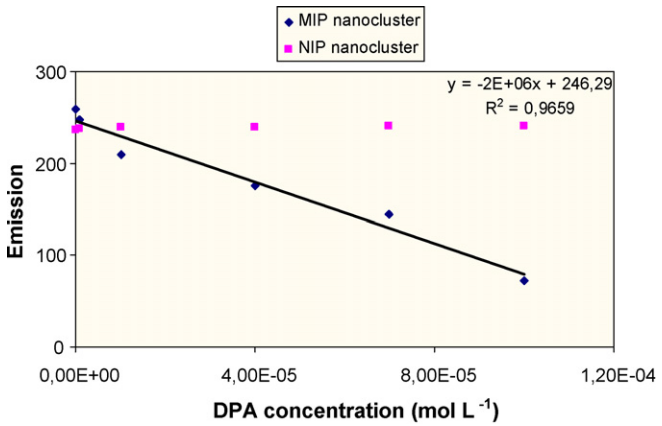

Fig. 5. The effect of concentration of DPA on the quenching of the fluorescence of the DPA imprinted Au–Ag nanosensor (sensor specificity-adsorption isotherm).

The fluorescence intensity of the DPA imprinted Au–Ag nanoclusters can be quenched by DPA. The quenching of fluorescence intensity is proportional to DPA concentration. The linearity relation between spore concentration (CFU mL^{-1}) and dipicolinate content was investigated using calibration graph (Fig. 5) and found that 85 μmol L^{-1} dipicolinate corresponds to 1.8×10^7 CFU mL^{-1}. The detection limit, defined as the concentration of analyte giving quenching of the fluorescence equivalent to three standard deviation of the blank plus the net blank quenching fluorescence, was 0,1 μmol L^{-1} corresponding to 2.1×10^4 CFU mL^{-1}. Zhou et al. [17] have been reported that the minimum detectable amount of DPA with MIP was obtained 1.5 μM and in our study the detectable amount of DPA was found to be 0.1 μM.

The experiments were performed in replicates of three and the samples were analyzed in replicates of three as well. In the literature, the lowest detection limits reported for *Bacillus* spores by a DPA assay were 1.2×10^5 CFU mL^{-1} (*Bacillus globigii*) [44], 4.4×10^5 CFU mL^{-1} (*Bacillus subtilis*) [45], 7.2×10^5 CFU mL^{-1} (*Bacillus thuringiensis*) [15]. So, this new DPA nanosensor has both low detection limit and very low cost.

The fluorescence intensity correlates to the amount of DPA analogues bounded to the nanoshell having Au–Ag nanoclusters in the cases of incubating the DPA imprinted nanoclusters sensor with the DPA aqueous solution. As can be seen in Fig. 5, fluorescence intensity decreased with increase concentration of DPA.

Au–Ag nanoclusters having DPA imprinted nanoshell was tested against *B. cereus* spores. The sensor's response as a function of both Spore concentration (CFU mL^{-1}) and DPA concentration (mol L^{-1}) is shown in Table 1.

The affinity constants of DPA can be estimated from the thermodynamic analysis of the fluorescence intensity as a function of the DPA concentration based on Scatchard analysis [46,47] and Langmuir isotherm [48].

If we consider a binding equilibrium such as:

$$\mathrm{DPA} + (\mathrm{Au\text{–}Ag})_{\mathrm{nanocluster}} \overset{k}{\rightleftharpoons} \mathrm{DPA\text{–}(Au\text{–}Ag)_{nanocluster}}$$

Table 1
The sensor's response as a function of both Spore number (CFU mL^{-1}) and DPA concentration (mol L^{-1}).

Spore number (CFU mL^{-1})	DPA concentration (μmol L^{-1})
1.8×10^7	85.3 ± 0.002
1.8×10^6	80.5 ± 0.003
1.8×10^5	75.8 ± 0.002
1.8×10^4	72.1 ± 0.004

Table 2
Comparison of Langmuir and Scatchard analysis for DPA imprinted nanoparticles.

Template molecules	Langmuir (K_a, M^{-1})	I_{max} (a.u.)	Scatchard (K_a, M^{-1})	I_{max} (a.u.)
Dipicolinic acid	18×10^6	138.9	9.0×10^6	111.1

where, DPA and $(Au–Ag)_{nanocluster}$ represent DPA in the solution and DPA imprinted polymeric nanoshell having nanocluster, respectively, and DPA–$(Au–Ag)_{nanocluster}$ is the DPA-nanocrystal bound complex. A Scatchard relationship can be obtained using the following equation.

$$\frac{I}{C_O} = \frac{I_{max}}{K_D} - \left(\frac{I}{K_D}\right) \quad (2)$$

where, K_D is the equilibrium dissociation and I is the fluorescence intensity. A plot of I versus I/C gave a straight line and the equilibrium binding constants calculated as $K_a = 1/K_D$ were given in Table 2.

The validity of the Langmuir isotherm can be tested by determining the affinity constant measuring the fluorescence intensities at equilibrium with different bulk concentrations (Fig. 5). Langmuir relationship can be obtained using the following equation;

$$\frac{C_O}{I} = \frac{1}{I_{max} \cdot b} + \frac{C_O}{I_{max}} \quad (3)$$

The results obtained from the linearized form of the Langmuir isotherm, by plotting C_O/I as a function of C_O, and the Scatchard analysis findings were compared in Table 2.

Association constant, K_a, and the apparent maximum number of recognition sites, I_{max}, values for the specific interaction between the template imprinted polymer of the nanoclusters and the template itself were determined by Langmuir isotherms and Scatchard's plots. The comparison of the K_a and I_{max} are presented in Table 2. As seen from Table 2, in general, the magnitude of K_a (18×10^6 mol L^{-1} and 9×10^6 mol L^{-1}, based on Langmuir and Scatchard analysis, respectively) is due to the accessibility of DPA template molecules. Some template cavities formed during imprinting process were stayed inside the polymer matrix of the nanoclusters.

The K_a and I_{max} values estimated from Scatchard analysis are very close to the Langmuir analysis data and DPA templated sites of nanocrystals are highly selective to the DPA recognition sites. So, the K_a based on Scatchard analysis for the binding of DPA to MIP nanosensor and I_{max} were found to be 9.0×10^6 M^{-1} and 111.1, respectively. The value of K_a suggests that affinity of the binding sites is very strong.

3.4. Recognition selectivity of DPA imprinted nanoshell sensor

Molecular imprinting process with DPA gives a cavity that is selective for DPA and its analogues. Because phtalic acid has very similar molecular structure with DPA, DPA imprinted nanocrystals were treated with phtalic acid in order to check whether the nanoshell has any effect on recognition process. The obtained results indicated that MIP nanosensor has 28 times greater selectivity for DPA than that of phtalic acid. The investigation of fluorescence intensity of NIP did not show a significant change in fluorescence intensity. The selectivity coefficient, k, of DPA and phtalic acid was found to be 28 for MIP particles and 2 for NIP particles and relative selectivity coefficient, k^1, was determined as 14. As seen that, MIP sensor was 14 times selective with respect to NIP sensor. Obtained results clearly indicated that the change of fluorescence intensity is due to specific binding between DPA and DPA memory sites having nanoclusters.

The DPA can simultaneously chelate to Cr(III) metal ion and fit into the shape-selective cavity. So, this interaction between Cr(III) ion and free coordination spheres has an effect on the binding ability of the Au–Ag nanosensor. Experimental results showed that shape-selective cavity formation was occurred for DPA.

4. Conclusion

We have developed a novel chemical preparation method for methacryloyl based self-assembled monolayer and to make up imprinting polymer via ligand exchange of DPA on Au–Ag nanoclusters. The DPA imprinted MAIDA-Cr(III)-EDMA copolymer of Au–Ag nanoshell is expected to bind DPA and its analogues for *Bacillus* spores sensing. The results showed that the change in fluorescence could be attributed to the high complexation geometric shape affinity (or DPA memory) between DPA molecules and DPA cavities occurred the on the Au–Ag nanoshells. In conclusion, the DPA imprinted nanoshell sensor has been gaining widespread recognition as a sensor for DPA because the imprinting methods create a nanoenvironment based on shape of cavity memorial, size and positions of functional groups that recognizes the imprinted molecule, DPA, based on ligand-exchange imprinting methods. Nanoshell sensors having DPA templates responses to DPA and its analogues through fluorescence intensity decrease.

References

[1] M.D. Krebs, B. Mansfield, P. Yip, S.J. Cohen, A.L. Sonenshein, B.A. Hitt, C.E. Davis, Biomol. Eng. 23 (2006) 119.
[2] D. Bhatta, G. Christie, B. Madrigal-Gonz'alez, J. Blyth, C.R. Lowe, Biosens. Bioelectron. 23 (2007) 520.
[3] J. Fichtel, J. Köster, B. Scholz-Böttcher, H. Sass, J. Rullkötter, J. Microbiol. Methods 70 (2007) 319.
[4] S. Pala, W. Yingb, E.C. Alociljaa, F.P. Downesc, Biol. Syst. Eng. 99 (2008) 461.
[5] S.B. Young, P. Setlow, J. Appl. Microbiol. 95 (2003) 54.
[6] L.R. Beuchat, C.A. Pettigrew, M.E. Tremblay, B.J. Roselle, A.J. Scouten, J. Food Prot. 67 (2004) 1702.
[7] D.E. Cortezzo, K. Koziol-Dube, B. Setlow, P. Setlow, J. Appl. Microbiol. 97 (2004) 836.
[8] P.E. Granum, in: M.P. Doyle, L.R. Beuchat, T.J. Montville (Eds.), Food Microbiology: Fundamentals and Frontiers, third ed., ASM Press, Washington, DC, 2007.
[9] L. Wang, Y.M. Lin, Bioresource Technol. 98 (2007) 3164.
[10] A.D. Warth, Anal. Biochem. 130 (1983) 502.
[11] J.D. Guingab, B. Lauly, B.W. Smith, N. Omenetto, J.D. Winefordner, Talanta 74 (2007) 271.
[12] R. Goodacre, B. Shann, R.J. Gilbert, E.M. Timmins, A.C. McGovern, B.K. Alsberg, D.B. Kell, N.A. Logan, Anal. Chem. 72 (2000) 119.
[13] J. Fichtel, H. Sass, J. Rullkötter, Food Control 19 (2008) 1006.
[14] P.M. Pellegrino, N.F. Fell Jr., J.B. Gillespie, Anal. Chim. Acta 455 (2002) 167.
[15] J. He, X. Luo, S. Chen, L. Cao, M. Sun, Z. Yu, J. Chromatogr. A 994 (2003) 207.
[16] A.A. Hindle, E.A.H. Hall, Analyst 124 (1999) 1599.
[17] Y. Zhou, B. Yu, K. Levon, Biosens. Bioelectron. 20 (2005) 1851.
[18] C.D. Havey, F. Basile, C. Mowry, K.J. Voorhees, J. Anal. Appl. Pyrolsis 72 (2004) 55.
[19] A. Kudelski, Talanta 76 (2008) 1.
[20] A.L. Hillberg, M. Tabrizian, ITBM-RBM 29 (2008) 89.
[21] F.R.R. Teles, L.P. Fonseca, Mater. Sci. Eng. C 28 (2008) 1530.
[22] C.L. Bayer, N.A. Peppas, J. Control. Rel. 132 (2008) 216.
[23] L. Ye, K. Mosbach, J. Am. Chem. Soc. 123 (2001) 2901.
[24] S.A. Piletsky, S. Alcock, A.P.F. Turner, Trends Biotechnol. 19 (2001) 9.
[25] H. Yavuz, R. Say, A. Denizli, Mater. Sci. Eng. C 25 (2005) 521.
[26] C.N.R. Rao, A.K. Cheetham, J. Mater. Chem. 11 (2001) 2887.
[27] M.P. Pileni, Supramol. Sci. 5 (1998) 321.
[28] J.F. Hicks, F.P. Zamborini, A.J. Osisek, R.W. Murray, J. Am. Chem. Soc. 123 (2001) 7048.
[29] J. Sharma, N.K. Chaki, A.B. Mandele, R. Pasricha, K. Vijayamohanan, J. Colloid Interface Sci. 272 (2004) 145.
[30] C.I. Lin, A.K. Joseph, C.K. Chang, Y.D. Lee, J. Chromatogr. A 1027 (2004) 259.
[31] A.B. Kharitonov, A.N. Shipway, I. Willner, Anal. Chem. 71 (1999) 5441.
[32] J. Matsui, K. Akamatsu, S. Nishiguchi, D. Miyoshi, H. Nawafune, K. Tamaki, N. Sugimato, Anal. Chem. 76 (2004) 1310.
[33] A.C. González-Baró, R. Pis-Diez, O.E. Piro, B.S. Parajón-Costa, Polyhedron 27 (2008) 502.

[34] S.E. Diltemiz, R. Say, S. Büyüktiryaki, D. Hür, A. Denizli, A. Ersöz, Talanta 75 (2008) 890.
[35] D. Hür, S.F. Ekti, R. Say, Lett. Org. Chem. 4 (2007) 585.
[36] M. Brust, D. Bethell, C.J. Kiely, D.J. Schiffen, Langmuir 14 (1998) 5425.
[37] A. Fernández, M.J. Ocio, P.S. Fernández, A. Martinez, Int. J. Food Microbiol. 63 (2001) 257.
[38] J. Zhang, N. Dalal, C. Gleason, M.A. Matthews, L.N. Waller, K.F. Fox, A. Fox, M.J. Drews, M. Laberge, Y.H. An, J. Supercrit. Fluids 38 (2006) 268.
[39] M. Mazas, I. González, M. López, J. González, R. Martin, Int. J. Food Sci. Technol. 30 (1995) 71.
[40] J.L. Dang, K. Heroux, J. Kearney, A. Arasteh, M. Gostomski, P.A. Emanuel, Appl. Environ. Microbiol. 67 (2001) 3665.
[41] M.T. Madigan, J.M. Martinko, Brock Biology of Microorganisms, eleventh ed., Pearson Prentice-Hall, New Jersey, 2006.
[42] A.A. Kolomenskii, H.A. Schuessler, Spectrochim. Acta Part A 61 (2005) 647.
[43] S. Farquharson, A.D. Gift, P. Maksymiuk, F.E. Inscore, Appl. Spectrosc. 58 (2004) 351.
[44] P.M. Pellegrino, N.F. Fell Jr., D.L. Rosen, J.B. Gillespie, Anal. Chem. 70 (1998) 1755.
[45] D.L. Rosen, C. Sharpless, L.B. McGown, Anal. Chem. 69 (1997) 1082.
[46] P.Y. Tsoi, J. Yang, Y.T. Sun, S.F. Sui, M.S. Yang, Langmuir 16 (2000) 6590.
[47] M. Yang, P.Y. Tsoi, C.W. Li, J. Zhao, Sens. Actuators B 115 (2006) 428.
[48] B. Persson, K. Stenhag, P. Nilsson, A. Larsson, M. Uhlen, P.A. Nygren, Anal. Biochem. 246 (1997) 34.

Talanta 78 (2009) 1272–1279

Contents lists available at ScienceDirect

Talanta

journal homepage: www.elsevier.com/locate/talanta

Equilibrium and *ab initio* computational studies on the adduct formation of 1,3-diketonato-lithium(I), -sodium(I) and -potassium(I) with 1, 10-phenanthroline and its 2,9-dimethyl derivatives

Ken-ichiro Ishimori [a,1], Seiji Mori [a,*], Yuji Ito [a], Kousaburo Ohashi [a], Hisanori Imura [b,**]

[a] *Faculty of Science, Ibaraki University, Mito 310-8512, Japan*
[b] *Division of Material Sciences, Graduate School of Natural Science & Technology, Kanazawa University, Kanazawa 920-1192, Japan*

ARTICLE INFO

Article history:
Received 11 December 2008
Received in revised form 24 January 2009
Accepted 26 January 2009
Available online 5 February 2009

Keywords:
Synergistic extraction
Lithium
Sodium
Potassium
Substituent effect
Ab initio calculations

ABSTRACT

Highly effective and selective synergistic extraction of Li^+ has been found using 2-naphthoyltrifluoroacetone (Hnta) as an acidic chelating agent and 2,9-dimethyl-1,10-phenanthroline (dmp) or 2,9-dimethyl-4,7-diphenyl-1,10-phenanthroline (dmdpp) as a neutral ligand (denoted as L) in toluene. The synergism was ascribed to the adduct formation in the organic phase, and the composition and the formation constants of the adducts for alkali metal ions (M^+) were determined by the extraction equilibrium analysis. The adducts found were M(nta)L for Li^+ and Na^+, while M(nta)L and M(nta)L_2 for K^+. To understand thermodynamics of the adduct formation with the bidentate amines, quantum chemical calculations of the 1:1 and 1:2 adduct formations with dmp and 1,10-phenanthroline (phen) were performed. The electronic and steric effects of the methyl groups at 2,9-positions of phen on the thermodynamic functions of adduct formation as well as the high lithium selectivity were quantitatively elucidated.

1. Introduction

Adduct formation of metal chelates with neutral ligands has been exclusively studied in synergistic extraction of metal ions such as bivalent alkaline earth and first transition metals and tervalent lanthanoid and actinoid metals [1]. Since these metal ions tend to form coordinately unsaturated chelates with bidentate monoprotic ligands such as β-diketones, the synergism is caused by the adduct formation of the chelates with neutral ligands, which is accompanied by the replacement of the residual water molecules coordinated to the central metal ion with the neutral ligand or further increase in the coordination number of the central metal ion.

The synergistic extraction has been also studied for univalent alkali metals. As a synergist neutral unidentate ligands such as tributyl phosphate (tbp) and trioctylphosphine oxide (topo) have been used with a combination of β-diketone such as 2-thenoyltrifluoroacetone (Htta) [2–4], dibenzoylmethane [5,6], 4-acyl-5-pyrazolones [7–9] and hydrophobic alkyl derivatives, e.g., LIX 51 and LIX 54 [10–14]. These systems showed high extractability of Li^+.

Recently, we have found a large synergistic effect of 1,10-phenanthroline (phen) [15] and 2,2′-bipyridine [16] as a neutral ligand on the extraction of Li^+ with Htta in various organic solvents. The synergism with phen provided a separation factor between Li^+ and Na^+ higher than that with topo and tbp [2]. Furthermore, in the extraction of alkali metals with Htta, 2,9-dimethyl-1,10-phenantroline showed very high selectivity for Li^+. The separation and the extraction efficiency were higher than those with several crown ether systems [17–20]. This suggests that the synergistic combination of β-diketone and heterocyclic bidentate amines gives excellent extraction system for Li^+.

In the present paper, the synergistic extraction and the adduct formation of Li^+, Na^+ and K^+ are studied with 2-naphthoyltrifluoroacetone (Hnta) as a hydrophobic β-diketone and phen, 2,9-dimethyl-1,10-phenanthroline (dmp) or 2,9-dimethyl-4,7-diphenyl-1,10-phenanthroline (dmdpp) as a bidentate amine in toluene. The extraction equilibrium of alkali metals with Hnta and the adduct formation equilibrium between the alkali metal(I)-nta chelate and the bidentate amine in the organic phase were studied in detail. The effect of the methyl groups in dmp and dmdpp on the extraction and separation efficiency was investigated by means of the equilibrium constants determined in this study. To understand thermodynamic properties of the complexation of alkali metal(I)-bidentate amines, *ab initio* and density functional calculations for

* Corresponding author. Tel.: +81 29 228 8703; fax: +81 29 228 8403.
** Corresponding author. Tel.: +81 76 264 5694; fax: +81 76 264 6060.
E-mail addresses: smori@mx.ibaraki.ac.jp (S. Mori), imura@cacheibm.s.kanazawa-u.ac.jp (H. Imura).
[1] Present address: Japan Atomic Energy Agency, Tokai-mura 319-1195, Japan.

0039-9140/$ – see front matter © 2009 Elsevier B.V. All rights reserved.
doi:10.1016/j.talanta.2009.01.052

the adduct formation of dmp were performed and compared with those of phen. The electronic and steric effects of the methyl groups at 2,9-positions of phen on the thermodynamic functions of adduct formation were discussed.

2. Experimental

2.1. Chemicals

4,4,4-Trifluoro-1-(2-naphthyl)-1,3-butanedione (Aldrich, 99% purity) was purified by vacuum sublimation. 2,9-Dimethyl-1,10-phenanthroline dihydrate (Kanto, 95% purity) was recrystallized from a benzene–hexane mixture and dried on P_4O_{10} *in vacuo* at 50 °C. The purity of dmp was checked by high performance liquid chromatography (HPLC) with an octadecyl/silica gel column (Kanto, Mightysil RP-18 GP, 4.6 mm i.d. × 150 mm) and 50% (v/v) methanol–water at pH 6.7 as a mobile phase. 2,9-Dimethyl-4,7-diphenyl-1,10-phenanthroline (ACROS, 99% purity) was used as obtained. Toluene (Kishida, 99.5% purity) was of guaranteed reagent grade.

A Li^+ stock solution was prepared by drying anhydrous lithium chloride (Kanto, high purity reagent) at 110 °C and dissolving in water. Standardization of alkali metal hydroxide solution was done by acid–base titration with a Metrohm SM Titrino E702 automatic titrator equipped with a combination glass electrode.

Other reagents and the apparatus were the same as those described previously [15]. Water was distilled, deionized, and then purified with a Milli-Q (Millipore) equipment just before use.

2.2. Extraction procedure

An aqueous solution of an alkali metal ion was shaken for 15 min with an equal volume of a toluene solution containing 3.0×10^{-5} to 1.0×10^{-2} mol dm^{-3} Hnta alone or 9.2×10^{-5} to 1.0×10^{-2} mol dm^{-3} Hnta plus 3.0×10^{-5} to 6.0×10^{-2} mol dm^{-3} bidentate amine (L) at pH 11.1–12.3 and 25 ± 0.5 °C. The initial concentrations of Li^+, Na^+ and K^+ in the aqueous phase were 2.0×10^{-6} to 3.0×10^{-2} mol dm^{-3}, 1.0×10^{-3} to 1.0×10^{-1} mol dm^{-3}, and 1.0×10^{-1} mol dm^{-3}, respectively. In the Li^+ and Na^+ cases, the ionic strength of the aqueous phase was kept constant at 1.0×10^{-1} mol dm^{-3} using potassium chloride and potassium hydroxide.

After phase separation, pH of the aqueous phase was measured with a Radiometer PHM93 REFERENCE pH meter with a combination glass electrode calibrated by the usual pH standard solutions. The H^+ concentration was calculated from the equilibrium pH and the activity coefficient at $I = 1.0 \times 10^{-1}$ mol dm^{-3}. The metal ion concentration in the aqueous phase was measured with a HITACHI 170-30 atomic absorption spectrophotometer (AAS). The metal ion extracted into the organic phase was back-extracted with 1.0×10^{-1} mol dm^{-3} hydrochloric acid or water and determined by AAS. The distribution ratio of alkali metal was calculated from the concentration in both phases. Almost all the procedures for the extraction of Na^+ and K^+ were carried out in a laminar-flow hood (class 100) to avoid the contamination of those elements from glassware as well as atmosphere.

2.3. Computational methods

All calculations were performed with the Gaussian 03 program [21]. The geometry optimizations were performed by the HF method in combination with the 6-31G(d) basis sets [22] for metal atoms, water molecules, all atoms for $HCOCHCHO^-$ ligand, all N atoms, 2- and 9-carbons and their attached hydrogens in the case of phen ligand and 2- and 9-carbons and their attached methyl groups dmp ligand, and 3-21G basis set [22] for the other atoms denoted as BI basis sets. The optimized structures were confirmed by normal coordinate analysis as minima on potential hypersurface. Enthalpies at 0 K were computed as a sum of electronic energy and zero-point vibrational energy. Gas phase Gibbs energies at 298.15 K and 1 atm were calculated based on harmonic oscillator approximation. The single point energies for HF/BI geometries were also computed with the Becke three-parameter plus Lee-Yang-Parr (B3LYP) density functional method [23] with the 6-31G(d) basis sets [22].

3. Results and discussion

3.1. Extraction equilibrium

All the equilibrium studies using Hnta and bidentate amines were carried out at pH >11. In such pH region, the extraction of alkali metal ions was little dependent on the H^+ concentration in the aqueous phase because the acidic β-diketone, Hnta, almost completely distributes into the aqueous phase and dissociates to nta^-. Since β-diketone having a trifluoromethyl group tends to decompose in alkaline solutions [24], the effect of the shaking time on the extraction of Li^+ with Hnta in the presence of dmp or phen was examined at pH 11.9. The distribution ratio of Li^+ did not depend on the shaking time during 5–90 min. Therefore, the decomposition of nta^- in the alkaline aqueous phase was negligible under the given conditions.

The extraction of Li^+, Na^+ and K^+ with Hnta alone was carried out and the distribution ratio (D_0) was measured. Fig. 1 shows the plots of $\log D_0$ as a function of the logarithmic value of the nta^- concentration in the aqueous phase, which was calculated by the

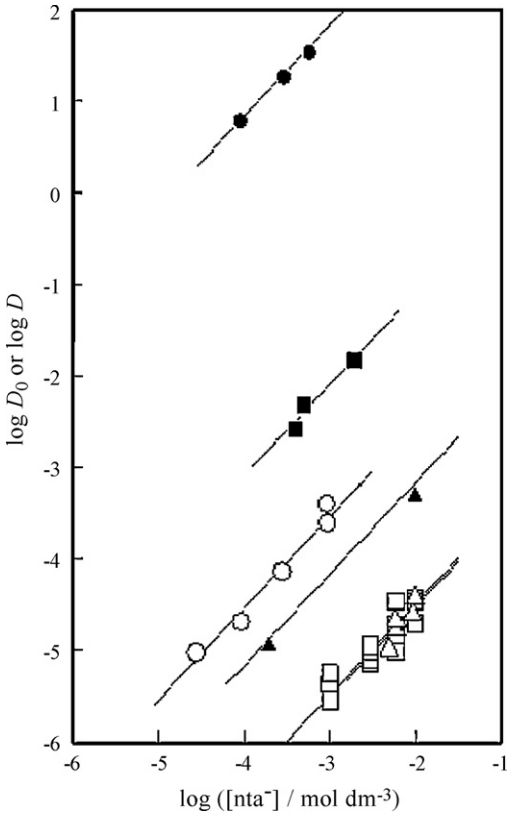

Fig. 1. Extraction of alkali metals(I) with Hnta in the presence or absence of 6.0×10^{-3} mol dm^{-3} dmp in toluene at pH 11.3–12.8. 1.0×10^{-4} to 2.0×10^{-2} mol dm^{-3} Hnta. Open symbols, Hnta alone; solid symbols, Hnta–dmp; circles, Li; squares, Na; triangles, K.

Table 1
Equilibrium constants on the synergistic extraction of alkali metals(I) with HA and L in toluene at $I = 0.1$ mol dm^{-3} and 298 K.

HA	Metal	log K'_{ex}	dmp		phen	
			log $K_{s,1}$	log $K_{s,2}$	log $K_{s,1}$	log $K_{s,2}$
Hnta	Li	−0.54 (0.05)	7.61 (0.01)	ND[a]	6.66 (0.02)[b]	ND[a,b]
	Na	−2.49 (0.04)	5.63 (0.02)	ND[a]	5.57 (0.08)	2.65 (0.07)
	K	−2.53 (0.05)	3.51 (0.05)	1.44 (0.13)	3.89 (0.07)	2.40 (0.10)
Htta	Li	−1.95[c]	7.43[c]	ND[a,c]	6.46[c]	ND[a,c]
	Na	−3.53[c]	5.19[c]	ND[a,c]	5.14[c]	2.39[c]
	K	−3.77[c]	2.71[c]	2.36[c]	3.37[c]	2.80[c]

Numerical values in parentheses show the standard errors.
[a] Not determined.
[b] Ref. [16].
[c] Ref. [26].

following equation,

$$[\mathrm{nta}^-] = \frac{C_{\mathrm{HA}} K_{\mathrm{a,HA}}}{K_{\mathrm{a,HA}} + [\mathrm{H}^+] + [\mathrm{H}^+] K_{\mathrm{d,HA}}}, \quad (1)$$

where C_{HA}, $K_{\mathrm{a,HA}}$ (=$10^{-6.28}$ [25]) and $K_{\mathrm{d,HA}}$ (=$10^{3.74}$) denote the total concentration, the acid dissociation constant, and the distribution constant of Hnta, respectively. The $K_{\mathrm{d,HA}}$ value was determined using the literature value of $K_{\mathrm{a,HA}}$ on the basis of the relationship between the distribution ratio of Hnta and pH in this work. Although the D_0 values for Na^+ and K^+ in Fig. 1 were too low to be measured across the wide nta^- concentration range, the plots for each metal ion examined give a straight line with a slope close to unity as expected from the formation of the 1:1 complex of alkali metal(I) with nta^-.

The extraction equilibrium of alkali metals(I) (M^+) and the extraction constants (K'_{ex}) in such pH region can be written by:

$$\mathrm{M}^+ + \mathrm{A}^- \rightleftharpoons \mathrm{MA}_{\mathrm{org}}, \quad (2)$$

$$K'_{\mathrm{ex}} = \frac{[\mathrm{MA}]_{\mathrm{org}}}{[\mathrm{M}^+][\mathrm{A}^-]}, \quad (3)$$

where A^- stands for nta^- and the subscript "org" denotes the species in the organic phase. Since the alkali metal chelate, MA, is present only in the organic phase, the distribution ratio is expressed as,

$$D_0 = \frac{[\mathrm{MA}]_{\mathrm{org}}}{[\mathrm{M}^+]} = K'_{\mathrm{ex}}[\mathrm{A}^-]. \quad (4)$$

The K'_{ex} values were calculated using Eq. (4) and are listed in Table 1. The logarithmic K'_{ex} values for Li^+, Na^+ and K^+ in the Hnta system are much larger than those in the Htta system. This indicates that the extractability of M^+ with Hnta is higher than that with Htta in the alkaline region. K'_{ex} is represented as follows:

$$K'_{\mathrm{ex}} = K_{\mathrm{d,MA}} \beta_1, \quad (5)$$

where $K_{\mathrm{d,MA}}$ and β_1 denote the distribution constant of MA chelate and its formation constant in the aqueous phase, respectively. In the Hnta and Htta systems, it can be assumed that the stability of M(nta) is similar to that of M(tta) since the p$K_{\mathrm{a,HA}}$ of Hnta, as a measure of the ligand basicity, is close to that of Htta. Therefore, the difference between the K'_{ex} values for Hnta and those for Htta should be mainly attributed to the difference in the $K_{\mathrm{d,MA}}$ values, which are associated with the hydrophobic property of the ligands.

3.2. Adduct formation equilibrium

Fig. 1 also shows the effect of 6.0×10^{-3} mol dm^{-3} dmp in the organic phase on the extraction of alkali metals(I). The D values increased by an order of magnitude of $10^{5.5}$ for Li^+, $10^{3.5}$ for Na^+ and $10^{1.5}$ for K^+. The largest and most selective synergism is found for Li^+. Since the slope of the log D–log[nta^-] plots for all alkali metals in Fig. 1 is almost unity, the following adduct formation reaction of MA chelate with a neutral bidentate amine (L) is expected in the organic phase.

$$\mathrm{MA}_{\mathrm{org}} + m\mathrm{L}_{\mathrm{org}} \rightleftharpoons \mathrm{MAL}_{m,\mathrm{org}}. \quad (6)$$

The overall adduct formation constant ($\beta_{s,m}$) is defined as,

$$\beta_{s,m} = \frac{[\mathrm{MAL}_m]_{\mathrm{org}}}{[\mathrm{MA}]_{\mathrm{org}}[\mathrm{L}]^m_{\mathrm{org}}}. \quad (7)$$

In the synergistic extraction of M^+ with HA and a bidentate amine, the distribution ratio of M^+ is given by,

$$D = \frac{[\mathrm{MA}]_{\mathrm{org}} + \sum [\mathrm{MAL}_m]_{\mathrm{org}}}{[\mathrm{M}^+]} = K'_{\mathrm{ex}}[\mathrm{A}^-](1 + \sum \beta_{s,m}[\mathrm{L}]^m_{\mathrm{org}}). \quad (8)$$

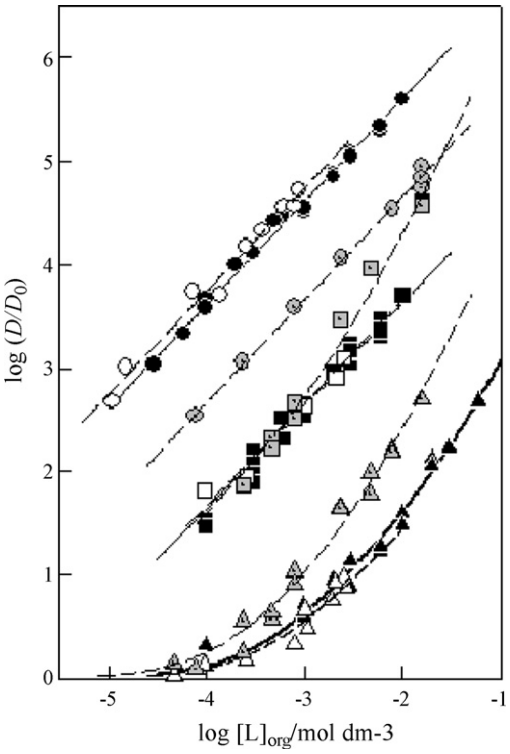

Fig. 2. Synergistic enhancement of the distribution ratio of alkali metals(I) as a function of the amine concentration in toluene at pH 11.2–12.9. 4.9×10^{-5} to 9.2×10^{-2} mol dm^{-3} Hnta. Open symbols, Hnta–dmdpp; solid symbols, Hnta–dmp; dotted symbols, Hnta–phen; circles, Li; squares, Na; triangles, K.

Table 2
Binding enthalpies (at 0 K), Gibbs energies, and entropies at 298.15 K of steps (1) and (2) in the gas phase at the HF/BI level.

L	Metal	Step (1)			Step (2)		
		ΔH (kJ mol^{-1})	ΔG (kJ mol^{-1})	ΔS (J mol^{-1} K^{-1})	ΔH (kJ mol^{-1})	ΔG (kJ mol^{-1})	ΔS (J mol^{-1} K^{-1})
phen	Li	−115.6 (−6.8)	−75.0 (−13.1)	−136 (+21.4)	−21.2	24.8	−154
	Na	−111.1 (−2.4)	−71.8 (−9.7)	−132 (+24.5)	−48.8	−3.4	−153
	K	−80.0 (+17.2)	−42.6 (+17.2)	−125 (0.0)	−56.9	−16.6	−135
dmp	Li	−122.7 (−13.8)	−83.5 (−21.6)	−131 (+25.9)	13.1	68.4	−185
	Na	−111.8 (−3.0)	−66.7 (−4.5)	−151 (+5.0)	−26.3	22.4	−163
	K	−76.4 (+20.8)	−32.5 (+27.2)	−147 (−21.5)	−46.8	0.1	−157

Numerical values in parentheses were obtained from **1a**.

Dividing Eq. (8) by Eq. (4), the following equation is derived,

$$\frac{D}{D_0} = 1 + \sum \beta_{s,m}[\mathrm{L}]_{\mathrm{org}}^{m}. \quad (9)$$

The logarithmic plots of D/D_0 as a function of the equilibrium concentration of phen, dmp or dmdpp in the organic phase are shown in Fig. 2. The equilibrium concentration of L was calculated from the total concentration (C_L) of L as follows:

$$[\mathrm{L}]_{\mathrm{org}} = \frac{C_L K_{d,L}}{K_{d,L} + 1 + [\mathrm{H}^+]/K_{a,HL}}, \quad (10)$$

where $K_{a,HL}$ and $K_{d,L}$ denote the acid dissociation constant of HL^+ and the distribution constant of L, and were cited from our previous paper [26]. In the dmdpp case, the equilibrium concentration in the organic phase was taken as the initial concentration since the distribution constant of dmdpp should be sufficiently high.

The D/D_0 values of the alkali metals increase with increase in the L concentration in the organic phase. The composition of the predominant adduct species is given from the slope of the plots. In all the extraction systems in Fig. 2, the plots for Li^+ show straight lines with a slope of unity in the wide concentration range of L in the organic phase. Therefore, the adduct of Li^+ is only MAL under the given conditions. In the Na^+ case, the dmp and the dmdpp system show the straight lines with a slope of unity, while the phen system shows the curved line trending to a straight line with a slope of two. Therefore, the dmp and dmdpp adducts are of MAL type and the phen adducts are not only MAL but also MAL_2. On the other hand, the plots for K^+ in all the systems show curved lines which give a slope of more than unity at higher concentration of L. This implies that both MAL and MAL_2 adducts are formed in the K^+–Hnta–bidentate amine systems. The compositions observed for the adducts of Li^+, Na^+ and K^+ with phen and dmp were the same as those in the Htta system reported previously [26].

The $\beta_{s,m}$ values were calculated by a nonlinear least-squares method based on Eq. (9) and the stepwise formation constant of the 1:1 ($K_{s,1}$) and the 1:2 adduct ($K_{s,2}$) are listed in Table 1 together with those of the Htta chelates. In the dmdpp case, the only log $K_{s,1}$ values could be determined as follows: 7.74 ± 0.03 for Li^+, 5.66 ± 0.05 for Na^+ and 3.42 ± 0.04 for K^+, which are very close to those for dmp. The general trend of the adduct formation constants of the Hnta chelates is similar to that of the Htta chelates.

The $\beta_{s,1}$ values in all the systems increase in the order of $K^+ < Na^+ < Li^+$, which is the decreasing order of the ionic radius of the alkali metal ions, or the increasing order of their surface charge density. In the Li^+ case, the $\beta_{s,1}$ value for dmp (also dmdpp) is larger than that for phen. This result can be explained by the difference in the basicity or $K_{a,HL}$ of the amines. Therefore, the adducts, Li(nta)(dmp) and Li(nta)(dmdpp), are expected to be free from the steric factors with two methyl groups at the 2- and 3-positions of dmp and dmdpp because of the possible tetrahedral structure of the adducts. On the other hand, in the Na^+ case, the $\beta_{s,1}$ values of dmp are nearly equal to those of phen (dmp ≈ phen), while in the K^+ case, dmp < phen. Furthermore, the $\beta_{s,2}$ values for Na^+ and K^+ are in dmp < phen. These imply the importance of the steric factor of two methyl groups of dmp and dmdpp. To understand such effect of methyl groups on the phen skeleton, quantum chemical calculations were applied.

3.3. Quantum chemical calculations

Current computational power does not allow full quantum chemical studies for the whole system. Thus, in this study nta ligand is modeled as deprotonated formylacetaldehyde $HCOCHCHO^-$ (denoted as A^-). The alkali metal complexes, MA and MAL_m, were modeled as **1** for MA, **2** for MAL and **3** for MAL_2 (M = Li, Na and K; L = phen and dmp) as shown in Scheme 1.

The difference of binding energies between **1** and L (step (1)) and binding energies between **2** and L (step (2)) were examined. Effects of explicit solvation by two H_2O molecules were also examined in step (1). The chelation process from a diaqua metal complex **1a** with a bidentate ligand to give a complex **2** and water dimer is also assumed in the present theoretical studies since the solvation of alkali metal ion is important in aqueous solution (see Eq. (11)) [27].

$$\mathrm{MA(OH_2)_2 + L \rightarrow MAL + (H_2O)_2} \quad (11)$$

Representative 3D structures of Li, Na and K complexes at the HF/BI level are shown in Figs. 3–5, respectively. In the symbols of the complexes, **L**, **N** and **K** stand for lithium, sodium and potassium complexes, respectively, and **p** and **d** for phen and dmp complexes, respectively. Binding enthalpies and Gibbs energies at the HF/BI level are shown in Table 2, and binding energies at the B3LYP/6-31G(d)//HF/BI level are shown in Table 3.

Both LiA(phen) (**2Lp**) and LiA(dmp) (**2Ld**) have tetrahedral four-coordinate Li^+ ions. Although **3Lp** and **3Ld** have six-coordinate Li^+ ions, two Li··N distances of 2.31 Å and 2.47 Å for **3Lp** are shorter than those for **3Ld** of 2.49 Å and 2.51 Å, indicating steric repulsion between the methyl groups in the two ligands. The structural arrangements of two phen and dmp ligands in the six-coordinate Li complex are different each other. An NaA(phen) (**2Np**) complex has a nearly planar four-coordinate Na ion, because of the interaction between two oxygen atoms and hydrogens at the phen ligand. An NaA(dmp) (**2Nd**) complex is a distorted four-coordinate complex since two hydrogen atoms at the phen are substituted by methyl groups. The structural arrangements of two phen and dmp ligands

Table 3
Electronic binding energies of steps (1) and (2) in kJ mol^{-1} at the HF/BI level and in bracket at the B3LYP/6-31G(d)//HF/BI level.

L	M	Step (1)	Step (2)
phen	Li	−121.4 (−127.7)	−25.8 (−29.7)
	Na	−117.5 (−127.7)	−54.9 (−60.3)
	K	−86.2 (−91.8)	−62.6 (−67.0)
dmp	Li	−128.8 (−137.6)	+9.0 (+l.7)
	Na	−118.4 (−130.3)	−31.5 (−41.7)
	K	−82.6 (−94.2)	−52.5 (−61.9)

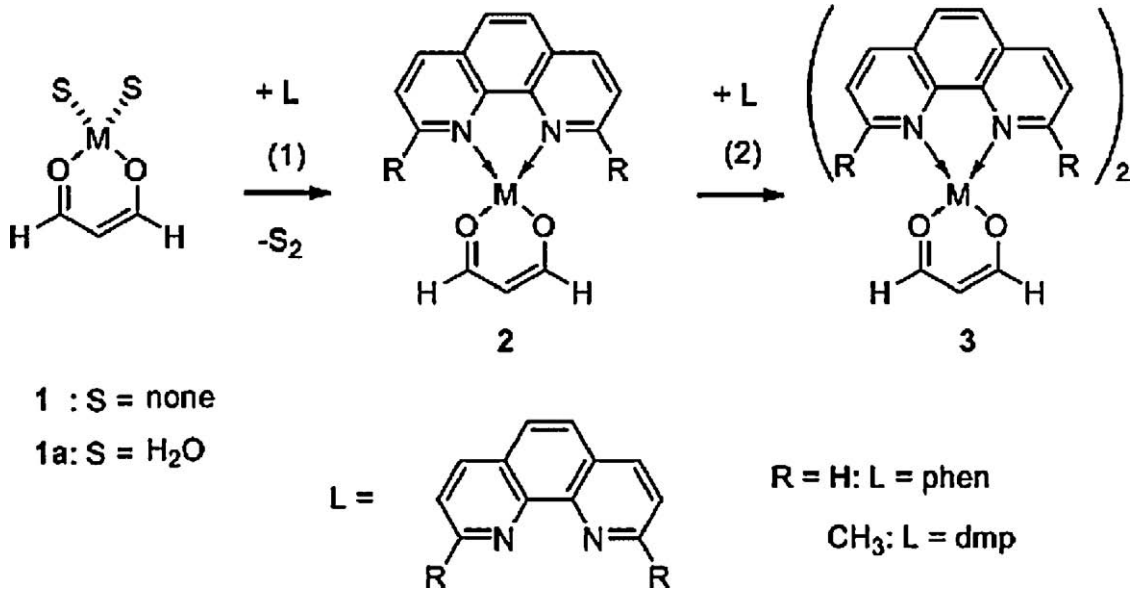

Scheme 1.

in the six-coordinate Na complexes, **3Np** and **3Nd**, are different as seen in $LiAL_2$ complexes, **3Lp** and **3Ld**. Both K complexes, **2Kp** and **2Kd**, have distorted four-coordinate K^+ ions. Complexes, **3Lp**, **3Np**, **3Kp**, **3Ld** and **3Nd**, have C_2 symmetry, whereas **3Kd** has C_1 symmetry. The K··N bond lengths of 2.94 and 3.08 Å in **3Kp** are not so shorter than those of 2.97–3.10 Å in **3Kd**, showing that the methyl groups of dmp ligands do not make the potassium ion and ligands apart.

The electronic binding energies at the B3LYP level of theory are semi-quantitatively similar to those at the simple HF level of theory as shown in Table 3. In this alkali metal system, the electron correlation is not a large factor to examine the binding energies.

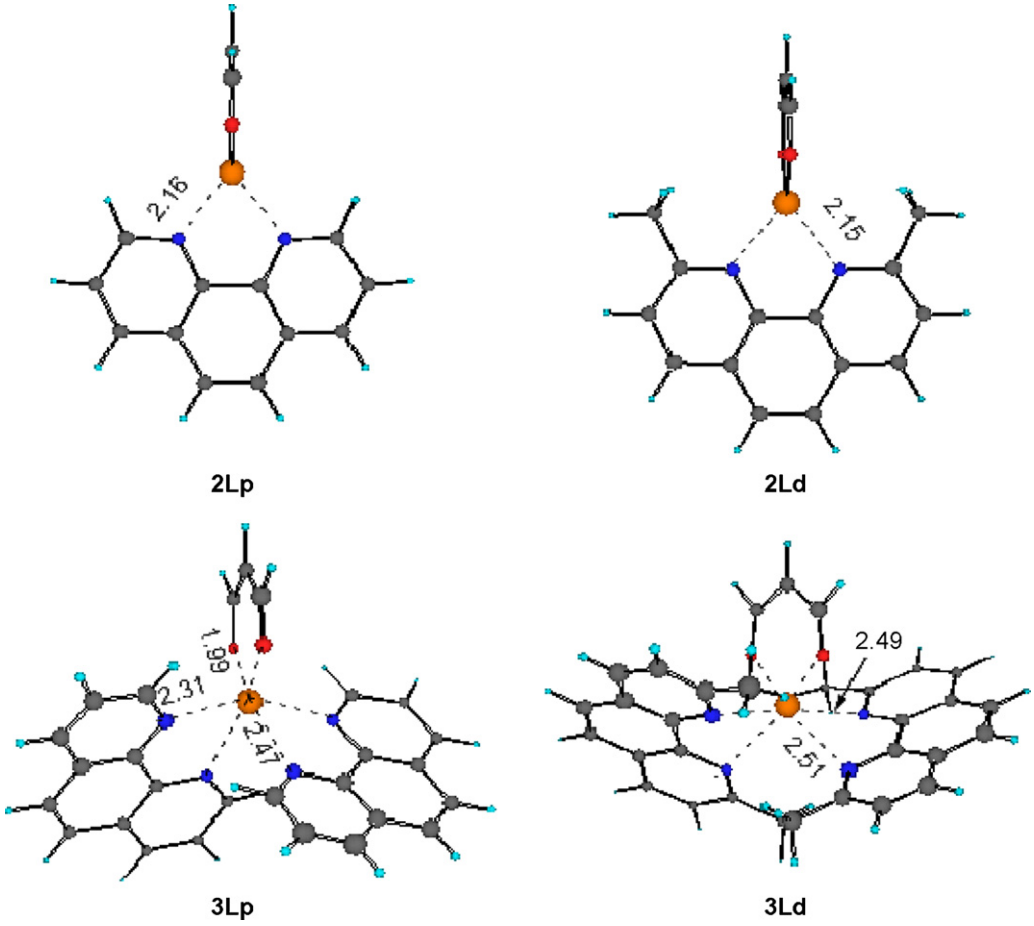

Fig. 3. Structures of LiAL and $LiAL_2$ complexes at the HF/BI level. Bond lengths are shown in angstroms.

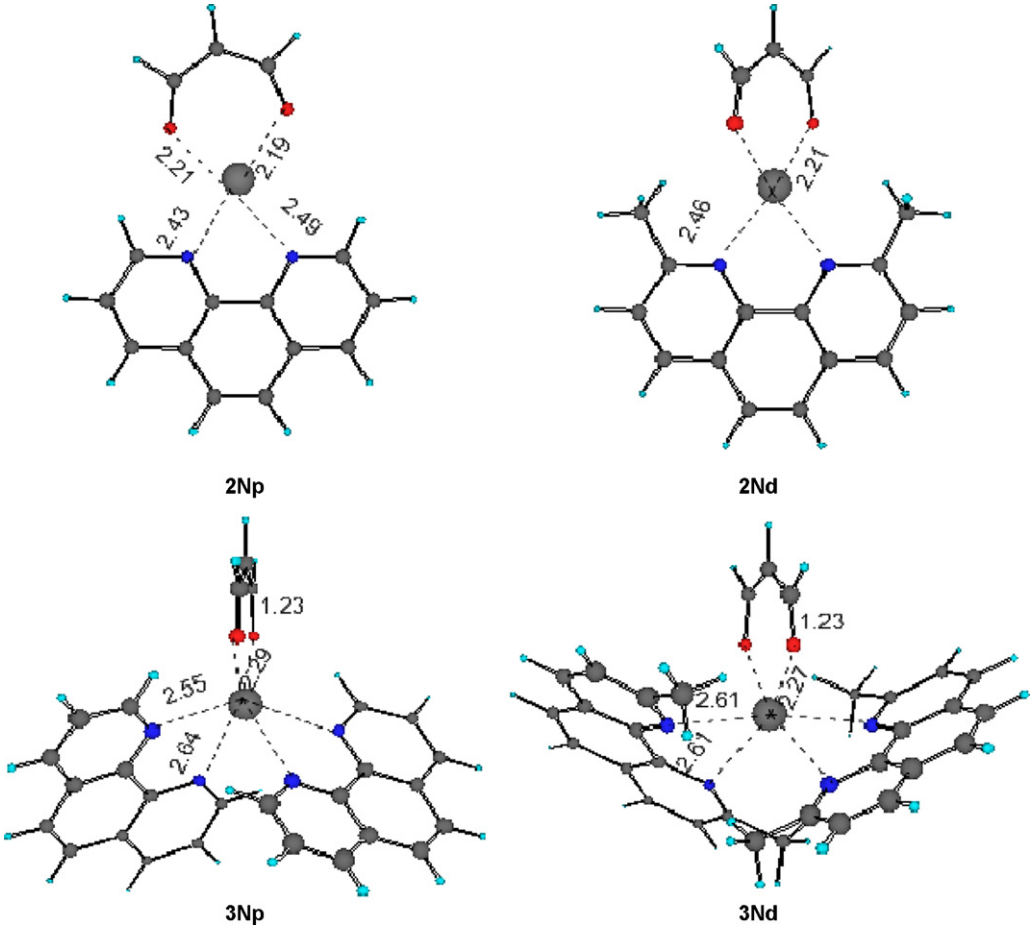

Fig. 4. Structures of NaAL and $NaAL_2$ complexes at the HF/BI level. Bond lengths are shown in angstroms.

In the order of decreasing ionic radii of $Li^+ < Na^+ < K^+$, the binding energies with any ligands (phen and dmp) for step (1) decrease but those for step (2) increase. We optimized tetra-coordinate complexes $LiA(OH_2)_2$ (**1aL**), $NaA(OH_2)_2$ (**1aN**) and $KA(OH_2)_2$ (**1aK**). The orders in the gas phase binding enthalpies and Gibbs energies at 298.15 K at the HF/BI level are the same trend as shown in Tables 2 and 3.

Actually, complexes **1** may be solvated by water molecules even in the organic phase. Hence, we investigated the effect of solvation by two water molecules in step (1). The ligand exchange reaction enthalpies, Gibbs energies and entropies at 298.15 K in Eq. (11) were shown in Table 2. The order of the enthalpies and Gibbs energies for chelate formation (ΔH and ΔG) in step (1) in the presence of water solvation, i.e., $Li^+ < Na^+ < K^+$, is the same as that in the absence of the water solvation, although the magnitudes of the energy changes are different because of the different environment dependent on water solvation. Note that the positive values of ΔH and ΔG for **1aK** (+17.2 and +17.2 kJ mol^{-1}, respectively in Table 2) are due to assumption of infinite separation between each reactant and product in the *ab initio* HF calculations in Eq. (11) and the neglect of the electron correlation. Those values will be negative if one carries out molecular dynamics simulations. Hydration numbers of alkali metals in aqueous solutions have been examined with *ab initio* MD simulation [28]. In present MD simulations, however, many efforts were needed for modeling of accurate ion hydration [29].

The 1:2 adduct formation for dmp ligand with Li^+ complex is highly endothermic and endergonic because smaller ionic radii of Li^+ makes highly compacted and distorted 1:2 Li adduct. The contribution of $-T\Delta S$ in the gas phase for Li^+ is higher than the others.

As shown in Fig. 6, there is a good correlation between the Gibbs free energies for the adduct formation, ΔG, determined by the experiment and those by *ab initio* HF calculations in the gas phase. These results show that the substituent effects in phen ligand can be explained by the models based on the quantum chemical calculations.

3.4. Selective synergistic extraction of Li^+

The separation efficiency of Li^+ from both Na^+ and K^+ was examined by means of the separation factors which were calculated from the equilibrium constants determined above. The separation factor (α) between Li and other alkali metals (M) is defined as,

$$\alpha_{Li/M} = \frac{D_{Li}}{D_M} = \frac{K'_{ex,Li}(1 + \beta_{s,1,Li}[L]_{org})}{K'_{ex,M}(1 + \sum \beta_{s,m,M}[L]^m_{org})}, \quad (12)$$

where $[L]_{org}$ is the concentration of a bidentate amine in the organic phase. Fig. 7 shows the $\alpha_{Li/M}$ values as a function of the equilibrium concentration of dmp as well as phen for comparison. As for $\alpha_{Li/Na}$, the dmp system exhibits much higher values than the phen system over a wide concentration range of dmp, and the maximum $\alpha_{Li/Na}$ value attains to $10^{3.93}$ in dmp, which enables quantitative separation between Li^+ and Na^+. The phen system shows a convex curve with a maximum of $\alpha_{Li/Na} = 10^{3.01}$ at $[phen]_{org} = 10^{-4.11}$ mol dm^{-3} because the composition of the predominant adduct species is different between Li^+ and Na^+, and dependent on the concentration of phen. Additionally, $\alpha_{Li/K}$ in the dmp system attains to a very high value, $10^{6.02}$, at $[dmp]_{org} = 10^{-2.46}$ mol dm^{-3}. From these results the quantitative separation of Li^+ from both Na^+ and K^+ can be achieved.

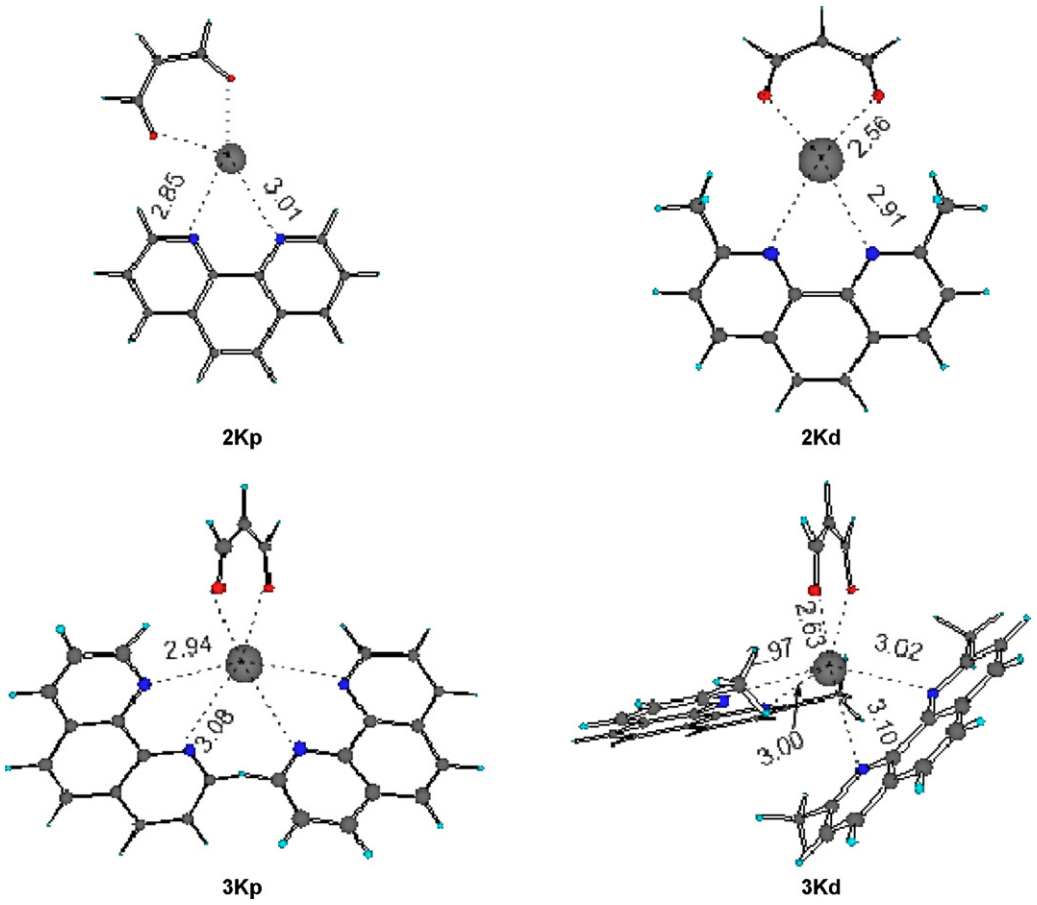

Fig. 5. Structures of KAL and KAL_2 complexes at the HF/BI level. Bond lengths are shown in angstroms.

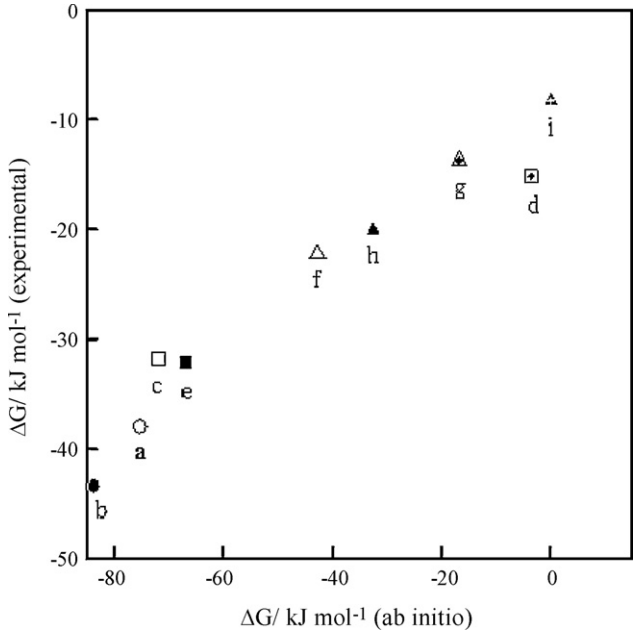

Fig. 6. Correlation between free energies of adduct formation obtained by the experiment and those calculated at the *ab initio* HF/BI level. a, Li(nta)phen; b, Li(nta)dmp; c, Na(nta)phen; d, Na(nta)$(phen)_2$; e, Na(nta)dmp; f, K(nta)phen; g, K(nta)$(phen)_2$; h, K(nta)dmp; i, K(nta)$(dmp)_2$.

The extraction and separation efficiency of alkali metals in the present Hnta–dmp system was evaluated. The extraction was performed using 1.0×10^{-3} mol dm^{-3} Hnta and dmp in toluene from aqueous solutions containing Li^+, Na^+ and K^+. The result is shown in Fig. 8 together with the theoretical *D* values calculated by the obtained equilibrium constants in both Hnta–dmp and Htta–dmp for comparison. Since the experimental plots are in good agreement with the theoretical values, the quantitative extraction separation of Li^+ from other alkaline metals can be achieved without unfavorable co-extraction. Moreover, it is found that the extraction

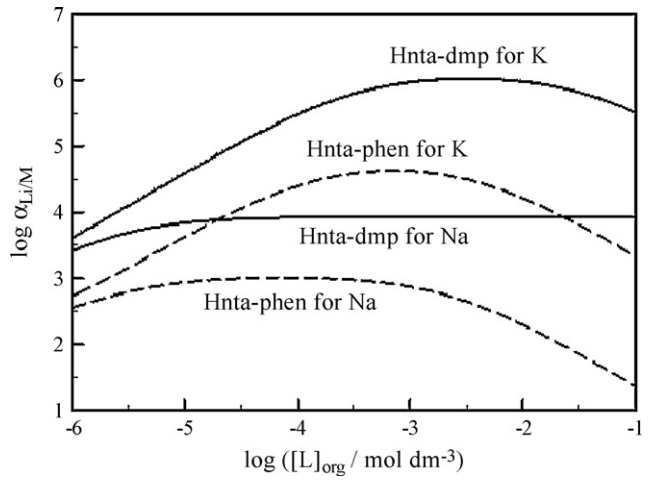

Fig. 7. Separation factors for Li^+/Na^+ and Li^+/K^+ as a function of the equilibrium concentration of bidentate amines in toluene at pH 12.1.1.0 $\times 10^{-3}$ mol dm^{-3} Hnta.

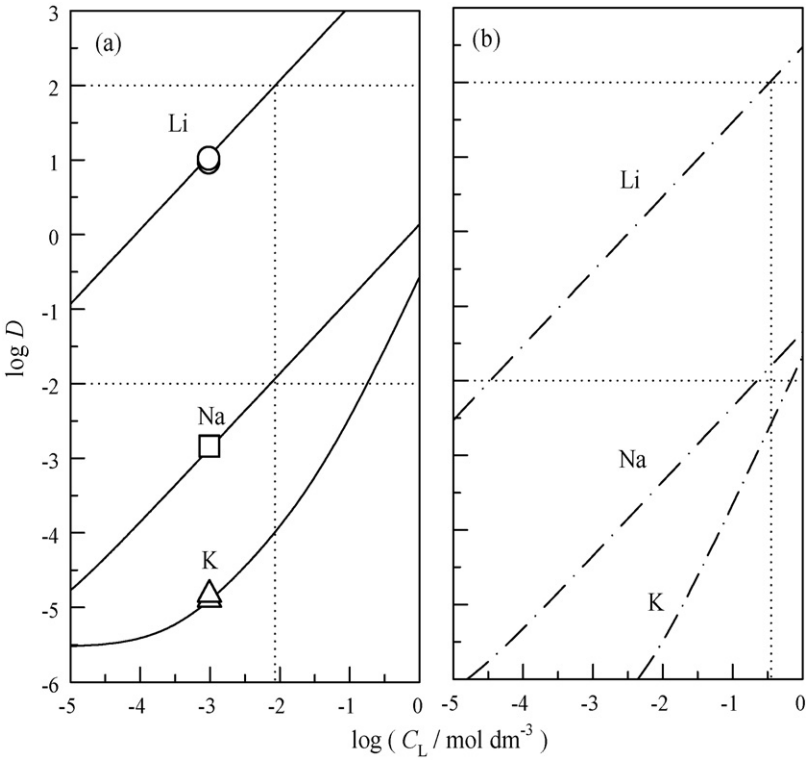

Fig. 8. Extraction efficiency of alkali metals(I) in the synergistic systems with 1.0×10^{-3} mol dm^{-3} HA and bidentate amine at pH 12.1. (a) Hnta–dmp; (b) Htta–dmp. Plots in (a) were obtained by the extraction from a mixture of Li^+, Na^+ and K^+. Theoretical values in (b) were calculated using the equilibrium constants in Ref. [26].

capability of synergistic Hnta–dmp for Li^+ is much superior to that of Htta–dmp reported previously.

4. Conclusion

The 2,9-dimethyl derivatives of 1,10-phenanthroline, dmp and dmdpp, are selective and effective synergist for the extraction of Li^+ with β-diketones. The hydrophobic β-diketone such as Hnta greatly enhances the extractability of alkali metals in higher pH region. *Ab initio* calculations for metal complexation processes are very useful for predictions of the binding ability of neutral ligands in the adduct formation.

Acknowledgements

This work was supported by Scientific Research on Priority Areas "Molecular Theory for Real Systems", no. 20038005 from MEXT. We thank Prof. Takeshi Nishikawa for granting us the permission to use TSUBAME grid cluster in the Tokyo Institute of Technology in his project supported by NEDO. The generous allotment of computational time from the Research Center for Computational Science, the National Institutes of Natural Sciences, Japan, is also gratefully acknowledged.

References

[1] J. Rydberg, M. Cox, C. Musikas, G.R. Choppin, Solvent Extraction Principles and Practices, Marcel Dekker, New York, 2004.
[2] T.V. Healy, J. Inorg. Nucl. Chem. 30 (1968) 1025.
[3] M. Munakata, S. Shiina, N. Shitaji, Bunseki Kagaku 23 (1974) 1506.
[4] H. Shibata, K. Kawabata, Y. Nishimura, Nihon Kinzoku Gakkaishi 39 (1975) 82.
[5] D.A. Lee, W.L. Taylor, W.J. McDowell, J.S. Drury, J. Inorg. Nucl. Chem. 30 (1968) 2807.
[6] T.V. Healy, J. Inorg. Nucl. Chem. 31 (1969) 499.
[7] S. Umetani, K. Sasayama, M. Matsui, Anal. Chim. Acta 134 (1982) 327.
[8] S. Umetani, K. Maeda, S. Kihara, M. Matsui, Talanta 34 (1987) 779.
[9] H. Bukowsky, E. Uhlemann, K. Gloe, P. Mühl, Anal. Chim. Acta 257 (1992) 105.
[10] E. Kunugida, J.H. Kim, I. Komasawa, Kagaku Kougaku Ronbunshu 15 (1989) 504.
[11] E. Kunugida, J.H. Kim, I. Komasawa, Kagaku Kougaku Ronbunshu 15 (1989) 857.
[12] T. Kinugasa, H. Nishibara, Y. Murao, Y. Kawamura, K. Watanabe, H. Takeuchi, J. Chem. Eng. Jpn. 27 (1994) 815.
[13] Y. Miyai, H. Kanoh, Q. Feng, K. Ooi, Nippon Kaisui Gakkaishi 49 (1995) 312.
[14] E. Zushi, A. Sakoguchi, F. Nakoshio, Kagaku Kogaku Ronbunshu 26 (2000) 511.
[15] K. Ishimori, H. Imura, K. Ohashi, Anal. Chim. Acta 454 (2002) 241.
[16] K. Ishimori, H. Imura, K. Ohashi, Anal. Sci. (17 Suppl.) (2001) a329.
[17] K. Kimura, S. Iketani, H. Sakamoto, T. Shono, Anal. Sci. 4 (1988) 221.
[18] K. Wilcox, G.E. Pacey, Anal. Chim. Acta 245 (1991) 235.
[19] C. Hamamcı, H. Hoşgören, S. Erdoğan, Talanta 47 (1998) 229.
[20] Y. Shibutani, H. Sakamoto, K. Hayano, T. Shono, Anal. Chim. Acta 375 (1998) 81.
[21] Gaussian 03, Revision E.01, M.J. Frisch, G.W. Trucks, H.B. Schlegel, G.E. Scuseria, M.A. Robb, J.R. Cheeseman, J.A. Montgomery, Jr., T. Vreven, K.N. Kudin, J.C. Burant, J.M. Millam, S.S. Iyengar, J. Tomasi, V. Barone, B. Mennucci, M. Cossi, G. Scalmani, N. Rega, G.A. Petersson, H. Nakatsuji, M. Hada, M. Ehara, K. Toyota, R. Fukuda, J. Hasegawa, M. Ishida, T. Nakajima, Y. Honda, O. Kitao, H. Nakai, M. Klene, X. Li, J.E. Knox, H.P. Hratchian, J.B. Cross, V. Bakken, C. Adamo, J. Jaramillo, R. Gomperts, R.E. Stratmann, O. Yazyev, A.J. Austin, R. Cammi, C. Pomelli, J.W. Ochterski, P.Y. Ayala, K. Morokuma, G.A. Voth, P. Salvador, J.J. Dannenberg, V.G. Zakrzewski, S. Dapprich, A.D. Daniels, M.C. Strain, O. Farkas, D.K. Malick, A.D. Rabuck, K. Raghavachari, J.B. Foresman, J.V. Ortiz, Q. Cui, A.G. Baboul, S. Clifford, J. Cioslowski, B.B. Stefanov, G. Liu, A. Liashenko, P. Piskorz, I. Komaromi, R.L. Martin, D.J. Fox, T. Keith, M.A. Al-Laham, C.Y. Peng, A. Nanayakkara, M. Challacombe, P.M. W. Gill, B. Johnson, W. Chen, M.W. Wong, C. Gonzalez, J.A. Pople, Gaussian, Inc., Wallingford CT, 2004.
[22] W.J. Hehre, L. Radom, P.V.R. Schleyer, J.A. Pople, Ab Initio Molecular Orbital Theory, John Wiley, New York, USA, 1986.
[23] (a) A.D. Becke, J. Chem. Phys. 98 (1993) 5648;
(b) C. Lee, W. Yang, R.G. Parr, Phys. Rev. B 37 (1988) 785;
(c) C.J. Cramer, Essentials of Computational Chemistry, Wiley, Chichester, UK, 2002.
[24] E.H. Cook, R.W. Taft Jr., J. Am. Chem. Soc. 74 (1952) 6103.
[25] C. Keller, H. Schreck, J. Inrog. Nucl. Chem. 31 (1969) 1121.
[26] K. Ishimori, H. Imura, Solv. Extr. Res. Devel., Jpn. 9 (2002) 13.
[27] D.T. Richens, The Chemistry of Aqua Ions, Wiley, Chichester, UK, 1997.
[28] (a) S.B. Rempe, L.R. Pratt, G. Hummer, J.D. Kress, R.L. Martin, A. Redondo, J. Am. Chem. Soc 122 (2000) 966;
(b) J. Zhou, X. Lu, Y. Wang, J. Shi, Fruid Phase Equilibria 194–197 (2002) 257.
[29] T.W. Whitfield, S. Varma, E. Harder, G. Lamoureux, S.B. Rempe, B. Roux, J. Chem. Theory Comput. 3 (2007) 2068.

Talanta 78 (2009) 1298–1302

Contents lists available at ScienceDirect

Talanta

journal homepage: www.elsevier.com/locate/talanta

Determination of ammonium and organic bound nitrogen by inductively coupled plasma emission spectroscopy

A.M.Y. Jaber[a,*], N.A. Mehanna[b], S.M. Sultan[a]

[a] King Fahd University of Petroleum & Minerals, Chemistry Department, Dhahran 31261, Saudi Arabia
[b] Industrial Support Services Laboratories, P.O. Box 11501, Dammam 31463, Saudi Arabia

ARTICLE INFO

Article history:
Received 20 November 2008
Received in revised form 30 January 2009
Accepted 30 January 2009
Available online 10 February 2009

Keywords:
Inductively coupled plasma
Hydride generation
Kjeldahl method

ABSTRACT

The continuous flow sample introduction technique with a hydride generator system in conjunction with an inductively coupled plasma emission spectrometer (ICP-AES-HG), is used in this study for quantitative determination of ammonium and organic bound nitrogen in aqueous and solid samples. Ammonia vapor released from ammonium salt after treatment with concentrated NaOH is transferred by argon to plasma for detection at 174.273 nm using axial argon plasma mode. The calibration curves were linear within a range of 25–1000 mg L^{-1} N as ammonium molybdate with correlation coefficients of better than 0.99 and limits of detection of about 10–25 mg L^{-1} N. The percent recovery of N (25–500 mg L^{-1} N) in soft (distilled) water and high salt content (1.7 mol L^{-1} NaCl) matrices was found to be in the range of about 97–102% with %RSD in the range of 4.6–0.62. The sensitivity, limit of detection, and blank contribution from the atmospheric nitrogen, were tremendously improved in this method compared with the available ICP-AES spray chamber counterpart. Furthermore, the ICP-AES-HG method gave results for real samples (soil, fertilizer, waste water) containing about 50–1800 mg L^{-1} N in good agreement with those obtained by the standard Kjeldahl method. No statistical differences at the 95% confidence level on applying the *t*-test were observed between the values obtained by the two methods. Thus, the ICP-AES-HG method is reliable and faster than the conventional tedious Kjeldahl method, superior to the ICP-AES spray chamber method, and almost free from matrix interference which is usually a critical factor in atomic emission spectroscopic techniques.

1. Introduction

Nitrogen exists at various concentration levels in water systems as dissolved inorganic species such as ammonium, nitrate and nitrite ions and organic species such as amines, amino acids, proteins and others. The sum of organic and ammonium nitrogen is usually expressed as the total Kjeldahl nitrogen. Nitrogen content in soil gives information about the agricultural status of plants, and the deficiency of nitrogen causes slow growth and diseases. Thus, nitrogen monitoring is important for treating wastewater and a variety of industrial processes for water applications. Total Kjeldahl nitrogen is also an important parameter when studying the pollution level in water systems [1].

Various methods have been used for determination of inorganic and organic bound nitrogen. These methods include the traditional Kjeldahl method, chemiluminescence detection, the Nessler method, oxidation methods using persulfate or ultraviolet or high temperature combustion and the Dumas method [1–9]. Other methods have also been reported, such as microscale Kjeldahl followed by detection using an ion-selective electrode for ammonia detection [10], microwave-assisted persulfate oxidation method followed by ion chromatographic determination of nitrate [11], microwave digestion followed by ion chromatography detection [12], ion chromatography without Kjeldahl distillation [13], HPLC and chemiluminescence detection [14], the fluorimetric method [15], the atomic emission spectral method, where the measurement was made for the cyanide band at 388.3 nm [16], and indirect determination of nitrogenated drugs by atomic absorption spectrometry [17]. Most methods were associated with problems such as limitation to high nitrogen concentrations, complication of procedures, time and reagents requirements, matrix interference and limited dynamic range.

Inductively coupled plasma emission spectroscopy, ICP-AES, has also been used for nitrogen determination [18–24]. ICP-AES with spray chamber sample introduction technique was associated with problems such as poor detection limit and severe blank contribution [20]. It has been reported that determination of nitrogen using ICP-AES is challenging due to the high nitrogen background from

* Corresponding author. Tel.: +966 3 860 2611.
E-mail address: amjaber@kfupm.edu.sa (A.M.Y. Jaber).

0039-9140/$ – see front matter © 2009 Elsevier B.V. All rights reserved.
doi:10.1016/j.talanta.2009.01.060

surrounding air, the nitrogen impurity in the plasma argon, and the nitrogen dissolved in the aqueous solutions [20]. Although the use of an extended torch could reduce the blank signal appreciably level, the detection limit prevents the technique from being applicable for low nitrogen concentrations, especially in high salt matrices. Alder et al. [21] introduced a method for the determination of low-level ammonium ion in solution by optical emission spectrometry with an inductively coupled argon plasma source. Ammonium ion was oxidized with sodium hypobromite in alkaline medium, and the nitrogen produced was introduced into the argon plasma and monitored at 336.0 nm. Some work was also reported with an extended torch for the determination of nitrogen in aqueous solution with the aid of ICP-AES [22]. The detection limit was determined and shown to be limited by high blank contributions, even in the case of an extended torch and purging of the optical path. It has been reported that this method cannot be used for low nitrogen concentration levels and it suffers from matrix interferences. The possibility of using an extended torch for successful nitrogen determination in fertilizers has been reported in a VARIAN note [23]. In this method, ICP-AES was compared with the colorimetric method for measuring nitrogen content in fertilizer samples. The extended torch was used to prevent the contact with atmospheric nitrogen and to reduce the background contribution. A high outer plasma gas flow, 22 L min^{-1}, was used successfully to reduce the background as well. Nitrogen in fertilizers was determined by a special adapter for the torch to minimize the diffusion of atmospheric nitrogen into plasma [24]. For changing a sample, the peristaltic pump of the spectrometer has to be switched off to prevent ambient air from being pumped into the plasma.

In this study, a hydride generator sample introduction system was used in conjunction with the ICP-AES technique to provide the hydride as gaseous ammonia. The sample treatment (for ammonium or organic bound nitrogen) was the same as in the Kjeldahl method, and the released ammonia vapor was transferred by argon gas directly to the ICP-AES for detection at 174.273 nm using axial the argon plasma mode. Thus, the tedious Kjeldahl distillation and titration steps were skipped. Meanwhile the sample matrix would be removed before dosing ammonia to the plasma.

2. Experimental

2.1. Chemicals and reagents

All chemicals used were of analytical reagent grade. These chemicals include: sodium hydroxide pallets (Penriac), sulfuric acid (Aldrich), Kjeldahl catalyst ($CuSO_4 \cdot 5H_2O$ and K_2SO_4), ammonium molybdate tetrahydrate (Aldrich), industrial grades of mono ammonium phosphate, urea and ammonium sulfate fertilizers (Saudi Arabian Basic Industries Corporation, SABIC). Distilled deionizer water was used to prepare all solutions.

An accurately weighed quantity of ammonium molybdate, $(NH_4)_6Mo_7O_{24} \cdot 4H_2O$, was dissolved in water and diluted to 1 L to give nitrogen concentrations of 1000 mg L^{-1}. A series of dilutions were carried out to prepare standard solutions of the required concentrations. 20% (w/v) NaOH was prepared by dissolving 200 g sodium hydroxide pellets in cold water and diluting to 1 L. Solutions of ammonium phosphate and ammonium sulfate fertilizers were prepared by dissolving accurately weighed quantities (0.5–1.5 g) in water.

The samples of organic nitrogen such as urea fertilizer, fish feed, and agriculture soil were transferred into solution after digestion with concentrated (98%) sulfuric acid for about 45 min with the Kjeldahl catalyst, and then the digested solution was neutralized by 20% NaOH and diluted by water to 500 mL. All standard solutions were stored in polyethylene bottles.

Table 1
The optimum ICP operating parameters.

Parameter	Setting
Plasma power	1400 kW
Torch	Axial, 27.12 MHz RF
Coolant flow	12.0 L min^{-1}
Auxiliary flow	1.0 L min^{-1}
Hydride generator flow	1.0 L min^{-1}
Distance from plasma interface	5.0 mm
Detector	CCD, 168–800 nm
OPI flow	0.8 L min^{-1}

2.2. Instrumentation

Spectro CIROS CCD ICP-AES was used. The sample introduction system used was the Spectro hydride generator as a two-line manifold continuous flow system. The hydride generator system, HGX 200, consists of two tubing lines. One was used for the NaOH solution, and the other for the sample solution. There was one peristaltic pump which aspirates both NaOH and the sample solution to the aeration vessel (50 mL) with inlet and outlet points for argon to carry out the generated ammonia to Plasma. The generated ammonia flow to Plasma is controlled by a manual flow meter. The Spectro Smart Analyzer Vision software was used. Water chiller was used for the interface that includes the entrance slit to be cooled down from the hot plasma.

3. Results and discussion

3.1. Preliminary instrumental settings

An axial torch mode was used with a back flow argon plasma interface, called the optical plasma interface. This technique was used to make the normal analytical zone more visible with respect to the entrance slit. The nitrogen spectral emission line, 174.273 nm was used for the signal intensity measurement. The instrument was optimized as recommended by the manufacturer. Table 1 shows the optimum operational and instrumental parameters.

The sample solution containing ammonium salts was introduced directly to the argon ICP as hydride in the ammonia vapor after reacting it with concentrated sodium hydroxide, whereas samples containing organic nitrogen were initially digested with concentrated sulfuric acid using the Kjeldahl catalyst followed by a reaction with 20% sodium hydroxide solution. Thus, ammonia vapor was released and transferred by argon to the plasma for detection at 174.273 nm using the axial argon plasma mode. Consequently, the distillation step in the conventional Kjeldahl method is replaced by the hydride generator unit where the reaction between the sample and sodium hydroxide took place. Moreover, the titration step was eliminated by the method described here. Using hydride generator technique, most of the matrix effect could be removed before dosing ammonia to the plasma, resulting in an enhancement of the detection limit.

3.2. The effect of hydride generator flow rate on the analytical and blank signals

Various hydride generator flow rates were used to study the flow rate effect on the analytical and the blank signals. The analytical signal of 1000 mg L^{-1} N as ammonium molybdate standard solution was increased with the decrease in the hydride generator flow rate. At the same time, the blank signal also showed a parallel increase in magnitude (Fig. 1). Consequently, the sensitivity and the blank contribution would increase as the hydride flow rate decreases. The significant increase in the blank contribution with the hydride flow rate might be ascribed to withdrawal of the

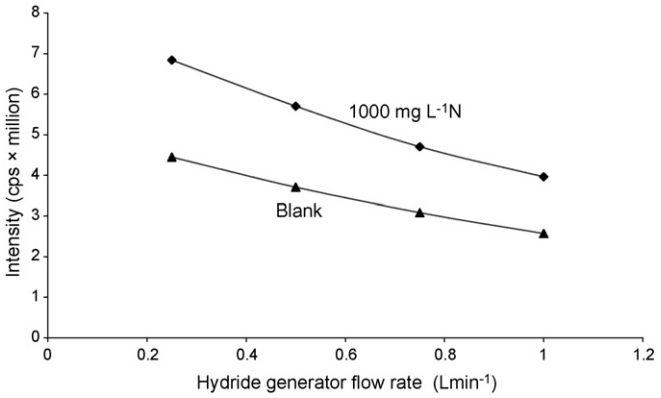

Fig. 1. The effect of hydride generator flow rate (L min^{-1}) on the analytical and blank signals.

normal analytical zone away from the entrance slit as the hydride flow rate decreases, which allows the surrounding atmospheric nitrogen to contribute much inside the plasma. The hydride generator flow rate used throughout the whole study was set at 1 L min^{-1}. Although this flow rate does not correspond to the highest sensitivity (Fig. 1), it achieves a minimal blank contribution, a property of prime importance in this study.

3.3. The optimum experimental parameters

As a result of the preliminary investigations mentioned above, the optimum procedure used in the present work can be summarized as follows: A solution of 20% (w/w) NaOH is transferred by peristaltic pump to the aeration vessel (50 mL) where ammonia gas is generated. Sodium hydroxide is aspirated continuously to the aeration vessel during the measurement process. The sample solution containing ammonium species is transferred by the same peristaltic pump and mixed with NaOH in the aeration vessel by a T-joint, confluence point, (5 cm before the vessel); and a mixing coil can be used also. Ammonia formation takes place in the aeration vessel and 30 s equilibrium time is given for each aspiration within the aeration vessel. Ammonia gas formed from the sample is transferred by argon (1 L min^{-1} flow rate) to the plasma for detection to take place at 174.25 nm line. Around 100 s was required to report one sample.

For organic nitrogen, the sample is digested in the presence of the Kjeldahl catalyst using concentrated sulfuric acid at 400 °C for 30–60 min. The digested solution is neutralized by 20% sodium hydroxide, and the liberated ammonia is introduced into the hydride generator unit.

3.4. Blank contribution in the ICP-AES-HG and ICP-AES spray chamber techniques

When a standard ammonium molybdate solution of 1000 mg L^{-1} N and a blank solution were introduced into the plasma by both techniques, the intensity of the analytical signal for the 1000 mg L^{-1} N solution introduced by ICP-AES-HG was about 3 times more than that obtained by the ICP-AES spray chamber technique (Fig. 2). Furthermore, the ratio of the analytical signal to the blank signal increased from about 1.4 times in the case of the ICP-AES spray chamber to about 2.6 times in the case of the ICP-AES-HG method. Furthermore, the signals with ICP-AES-HG became more symmetrical and the base line became more horizontal (Fig. 2). This significant increase in the signal-to-background ratio would lead to an increase in the sensitivity of the ICP-AES-HG method.

The signal-to-background ratio was also expressed using the term of background equivalent concentration (BEC) value [1]:

$$\mathrm{BEC} = \frac{C_{\max} \times S_{\mathrm{Blank}}}{S_{\max} - S_{\mathrm{Blank}}}$$

where $C_{\max}$ is the highest concentration in the calibration curve; S_{Blank} is the blank signal; and $S_{\max}$ is the highest concentration signal. The BEC values calculated for a calibration range

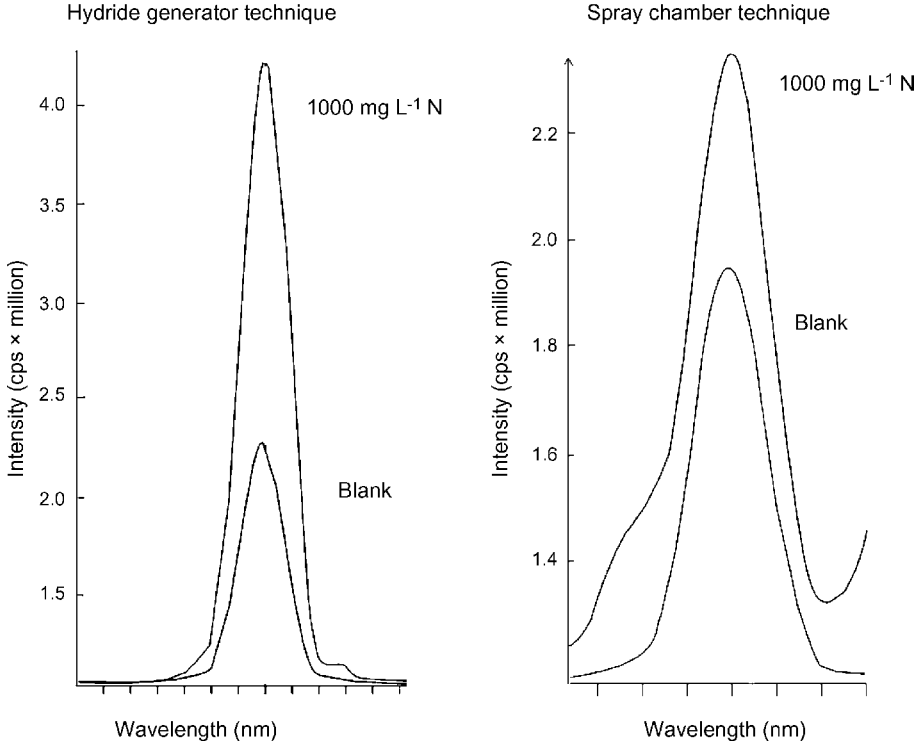

Fig. 2. Analytical and blank signals obtained for 1000 mg L^{-1} N and blank solutions using the ICP-AES-HG and ICP-AES spray chamber techniques.

Table 2
Accuracy and precision of nitrogen determination in ammonium molybdate solutions using various methods ($n = 3$).

Quantity added (mg L^{-1} N)	ICP-AES-HG		Kjeldahl method		ICP-AES spray chamber method	
	Quantity found (mg L^{-1} N)	Nitrogen recovery (%)	Quantity found (mg L^{-1} N)	Nitrogen recovery (%)	Quantity found (mg L^{-1} N)	Nitrogen recovery (%)
25.00	24.17	96.68	24.63	98.52	Not detected[b]	–
t-value		1.29		0.80		
%RSD		4.56		3.29		
25.00[b]	25.59	102.4	23.34	93.36	Not detected[b]	–
t-value		0.67		2.61		
%RSD		5.94		4.73		
50.00	50.76	101.5	49.22	98.44	Not detected[b]	–
t-value		2.94		2.19		
%RSD		0.89		1.25		
50.00[b]	50.3	100.6	50.94	101.9	Not detected[b]	–
t-value		1.19		1.38		
%RSD		0.87		2.32		
500	493	98.60	501	100.2	375	75.00
t-value		2.42		0.33		12.42
%RSD		0.95		0.96		
500[a]	507	101.4	495	99.04	Not detected[b]	–
t-value		4.16		1.48		
%RSD		0.62		1.14		

[a] The solution was prepared in 1.7 mol L^{-1} NaCl.
[b] The calibration curve had a slope of almost zero.

of 25–1000 mg L^{-1} N were found to be about 1800 mg L^{-1} N and 4000 in the case of ICP-AES-HG and ICP-AES spray chamber techniques, respectively. Thus, the blank contribution in the ICP-AES-HG method was reduced to about half of that in the case of ICP-AES spray chamber method.

3.5. Linearity, detection limit and sensitivity of calibration curves

The linearity of calibration curves was established for concentration ranges of 25–1000 mg L^{-1} N and 25–100 mg L^{-1} N using the ICP-AES-HG method. The calibration equations describing the curves for the two concentration ranges were, respectively, $I = 2.58 \times 10^6 + 1.37 \times 10^3 C$ and $I = 2.57 \times 10^6 + 1.69 \times 10^3 C$, with correlation coefficients of 0.999 and 0.995, and detection limits (estimated as 3σ according to the treatment of Miller and Miller [25]) of about 10 and 20 mg L^{-1} N, respectively, where I is the signal intensity in count per second (cps) and C is the concentration of nitrogen in mg L^{-1}.

Calibration curves were also constructed for ammonium molybdate solutions of 25–1000 mg L^{-1} N and 25–100 mg L^{-1} using the ICP-AES spray chamber method. The equation describing the calibration curve for the concentration range of 25–1000 mg L^{-1} N was $I = 1.8 \times 10^6 + 4.82 \times 10^2 C$ with a correlation coefficient of 0.992 and a detection limit of about 150 mg L^{-1} N. However, almost no variation was observed in the analytical signal for nitrogen concentrations in the range of 25–100 mg L^{-1} N (the calibration curve had an almost zero slope), and thus the nitrogen content of the samples containing 25 and 50 mg L^{-1} N was not detected (Table 2) by this method.

Comparing the slopes of the calibration equations describing the ICP-AES-HG and the ICP-AES spray chamber techniques confirms that the ICP-AES-HG technique offers better sensitivity and detection limit. Furthermore, the ICP-AES spray chamber method is not sensitive enough for the determination of low nitrogen concentrations (Table 2).

The detection limits estimated in this study for the calibration curves of the ICP-AES-HG technique were far lower than those mentioned in the previously reported techniques using ICP-AES for nitrogen determination. The detection limits reported for the ICP-AES with an extended torch [22], or that with a special torch adapter that prevents the entry of atmospheric nitrogen to the plasma [23], were found to be about 400–500 mg L^{-1} N. Another system of ICP-AES with an extended torch was used for nitrogen determination in fertilizer and the detection limit reported was about 50 mg L^{-1} N [24].

3.6. Accuracy and precision

The accuracy and precision of the ICP-AES-HG method was determined for samples of ammonium molybdate prepared in soft and high salt (100 g NaCl/L) content matrices, and the results are shown in Table 2. The *t*-values determined for three replicates of measurements (Table 2) made on each sample in the table indicate that no significant difference exists between the experimental means and the known values (no significant determinate error has been demonstrated.). The percent recoveries for 25, 50 and 500 mg L^{-1} N as ammonium molybdate in soft and high salt matrices were found to be in the range of about 97–102% with %RSDs in the range of 0.6–6 (Table 2). These results indicate that the method is accurate and precise, and they confirm the possibility of using it in matrices of high salt contents.

However, the analytical signal obtained from the ICP-AES spray chamber method could not be detected for low nitrogen concentrations (25 and 50 mg L^{-1} N) in soft or high salt content matrices (Table 2). This behavior was also reported earlier for determination of low nitrogen concentration content using the ICP-AES spray chamber method [21]. On the other hand, the percent recovery of nitrogen for samples of about 500 mg L^{-1} N in a soft matrix was found to be about 75% with %RSD of about 12. Meanwhile, no signal was detected for samples of similar concentration in a high salt (1.7 mol L^{-1} NaCl) content matrix (Table 2).

The stability of the analytical signal and consequently the precision of measurements were also tested over about 5 min for a fertilizer solution containing 670 mg L^{-1} N and ammonium molybdate solution of 50 mg L^{-1} N in a high salt (100 g L^{-1} NaCl) content matrix. The percent recoveries and %RSDs found were, respectively, 677.6 ± 7.82 mg L^{-1} N for the fertilizer and 50.26 ± 2.90 mg L^{-1} N for the high salt content sample solution. Once again, these results indicate that nitrogen determination by ICP-AES-HG is almost free of matrix interferences.

Table 3
Determination of nitrogen in various environmental samples by the ICP-AES-HG and the standard Kjeldahl methods.

Sample	Nitrogen form (units)	Quantity found		*t*-value
		Hydride generator	Standard method	
Fish feed	Organic nitrogen (%N)	46.69	47.33	1.17 ($n=3$)
%RSD		0.20	2.00	
Agriculture soil I	Total Kjeldahl nitrogen (mg L^{-1} N)	907.6	884.2	0.73 ($n=3$)
%RSD		4.90	3.74	
Agriculture soil II	Total Kjeldahl nitrogen (mg L^{-1} N)	1777	1816	1.57 ($n=3$)
%RSD		1.38	1.95	
Ammonium sulfate fertilizer	Ammonium (%N)	20.94	21.11	1.71 ($n=5$)
%RSD		0.84	0.64	
NPK fertilizer	Total nitrogen (%N)	11.86	11.74	1.01 ($n=5$)
%RSD		1.80	1.22	
Landfill monitoring well[a]	Ammonium (mgL^{-1} N)	26.33	25.10	1.40 ($n=3$)
%RSD		2.71	5.49	
Industrial wastewater[a]	Ammonium (mg L^{-1} N)	396.6	387.7	1.12 ($n=3$)
%RSD		0.83	3.54	

[a] The samples are in high salt matrices (conductivity > 6000 μs cm^{-1}).

3.7. Applications

Samples of fish food, agriculture soil, fertilizer, brine water and industrial wastewater containing about 50–1800 mg L^{-1} N were analyzed using the ICP-AES-HG and the standard Kjeldahl methods (Table 3). The two experimental means obtained by the two methods ($n=3$ or 4 for each) were compared using the unpaired *t*-test [25] and gave *t*-values always less than the tabulated values at the 95% confidence level. Thus, the results obtained by both methods did not differ significantly and the ICP-AES-HG method is in good agreement with the standard Kjeldahl method.

The ICP-AES-HG method is also useful in improving the sample-throughput, where it is much shorter than that required for the Kjeldahl method. The digested sample solutions of organic nitrogen were introduced to both the ICP-AES-HG and the Kjeldahl setups [21]. The time required was 100 s per sample for the ICP-AES-HG method and 5–10 min per sample for the Kjeldahl method.

4. Conclusion

The ICP-AES-HG technique has been developed and validated here for the determination of ammonium and organic bound nitrogen in liquid and solid samples. The blank contribution is greatly minimized compared to the previously reported ICP-AES methods. Unlike the spray chamber technique, a lower detection limit for nitrogen determination was established in soft and high salt content matrices with minimal matrix effect. The ICP-AES-HG method can be used for routine quality control work with much higher sample throughput than the Kjeldahl method.

Acknowledgments

King Fahd University of Petroleum & Minerals and Industrial Support Services Co. Ltd., Material Testing Laboratories are thanked for the support of this research project.

References

[1] A. Cerda, M.T. Oms, V. Cerda, in: Leo M.L. Nollet (Ed.), Handbook of Water Analysis, Marcel Dekker, New York, 2000, pp. 261–271.
[2] Official Methods of Analysis, vol. 1, 15th ed., AOAC Inc., 1990, pp. 17–21.
[3] Standard Methods for the Examination of Water and Wastewater, 20th ed., AWWA, APHA, 1998, pp. 4-103–4-123.
[4] G.D. Christian, Analytical Chemistry, fifth ed., John Wiley and Sons, 1994, pp. 240–241.
[5] S.E. Cornella, T.D. Jickellsa, J.N. Capeb, A.P. Rowlandc, R.A. Duced, Atmos. Environ. 37 (2003) 2173.
[6] D.A. Bronk, M.W. Lomas, P.M. Glibert, K.J. Schukert, M. Sanderson, Mar. Chem. 69 (2000) 163.
[7] S. Nozawa, H. Kasama, T. Suzuki, A. Ysui, Bunseki Kagaku 56 (2007) 179.
[8] P.G. Wiles, I.K. Gray, R.C. Kissling, J. AOAC Int. 81 (1998) 620.
[9] G. Bottom of Form Bellomonte, A. Costantini, S. Giammarioli, J. AOAC 70 (1987) 227.
[10] P. Campins-Falco, S. Meseguer-Lloret, T. Climent-Santamaria, C. Molins-Legua, Talanta 75 (2008) 1123.
[11] S. Karthikeyan, J. He, S. Palani, R. Balasubramanian, D. Burger, Talanta 15 (2009) 979.
[12] M. Colina, P.H.E. Gardiner, J. Chromatogr. A 847 (1999) 285.
[13] P. Verma, R.K. Rastogi, K.L. Ramakumar, Anal. Chim. Acta 596 (2007) 281.
[14] S.M. Lloret, C.M. Legua, P.C. Falco, Anal. Chim. Acta 536 (2005) 121.
[15] S.M. Lloret, J.V. Andres, C.M. Legua, P.C. Falco, Talanta 65 (2005) 869.
[16] I.I. Ryzhenko, S.K. Kyuregyan, T.G. Biktimirrova, L.M. Zamilova, V.I. Sokolova, Chem. Technol. Fuels Oils 25 (1990) 637.
[17] C. Nerin, A. Garnica, J. Cacho, Anal. Chem. 58 (1986) 2617.
[18] C.B. Sobel, Appl. Spectrosc. 36 (1982) 691.
[19] C.B. Boss, K.J. Fredeen, Concept Instrumentation and Techniques in Inductively Coupled Plasma Optical Emission Spectroscopy, Perkin-Elmer, 1997, pp. 3-28–3-31.
[20] G.G. Glavin, 19th Regional Phosphate Conference, Lakeland, FL, October 14–15, 2004, p. 33.
[21] J.F. Alder, A.M. Gunn, G.F. Kirkbright, Anal. Chim. Acta 92 (1977) 43.
[22] J.A.C. Broekaert, P.B. Zeeman, Spectrochim. Acta B 39 (1984) 851.
[23] S. Pethig, P. Heitland, K. Krengel-Rothensee, Spectro Application, Report No. 77, 1990.
[24] T.T. Nham, Varian Notes, ICP Note No. 14, 1993.
[25] J.C. Miller, J.N. Miller, Statistics and Chemometrics for Analytical Chemistry, fifth ed., Pearson, Harlow, 2005, pp. 121, 39.

Talanta 78 (2009) 1489–1491

Contents lists available at ScienceDirect

Talanta

journal homepage: www.elsevier.com/locate/talanta

Short communication

Encapsulation and quantification of multiple dye guests in unmodified poly(amidoamine) dendrimers as a function of generation

Katrina K. Kline, Elizabeth J. Morgan, Lisa K. Norton, Sheryl A. Tucker*

Department of Chemistry, University of Missouri, 125 Chemistry Bldg., Columbia, MO 65211, United States

ARTICLE INFO

Article history:
Received 17 December 2008
Received in revised form 25 January 2009
Accepted 26 January 2009
Available online 5 February 2009

Keywords:
Dendrimers
Encapsulation
Fluorescence

ABSTRACT

This work illustrates the remarkable ability of amine-terminated PAMAM dendrimers to entrap multiple guest molecules. While previous encapsulation studies with dendritic polymers demonstrated multi-dye uptake, the dendrimers required extensive synthetic modification. This study utilizes unmodified PAMAM dendrimers to encapsulate multiple phenol blue molecules. Quantitative data on the uptake capacity and robustness of association is presented.

Dendrimers have received considerable attention over the last 20 years due to the variety of their applications, such as molecular nanocarriers, gene transport systems, and drug delivery systems [1]. Poly(amidoamine), PAMAM, dendrimers, with tetrafunctional ethylenediamine cores, are one of the most commonly encountered dendrimer families due to their commercial availability, range of sizes (generations, G), and endgroups [2]. Fundamental, quantitative information concerning the dendrimers' host–guest properties, including loading capacity and robustness of association of the various generations, are essential to advance applications. This communication provides this insight, with supporting analytical data. While dendrimer based unimolecular encapsulation has been observed, previous studies using PAMAM dendrimers were unable to achieve multiple encapsulation without significant synthetic modification of the dendrimer [3]. This unprecedented work shows that a single, unmodified, amine-terminated PAMAM dendrimer is capable of sequestering and retaining multiple guest molecules.

The solvatochromic fluorescent reporter phenol blue (PB) was used as the guest molecule. The reported intrinsic fluorescence from the PAMAM dendrimers does not interfere in the solvatochromic region of PB [4]. Previous studies with PB indicated that this dye was fully encapsulated at or near the core of PAMAM [4]. Original studies were carried out using a 100:1 dendrimer:dye ratio [4]. Poisson statistics indicate that as the ratio of dendrimer to dye decreases, the probability of multiple dye molecules residing within a single dendrimer increases. Therefore, a dendrimer:dye ratio of 1:10, containing a 10-fold excess of dye, was utilized for these studies. Samples were prepared according to the published method using odd generation (G) dendrimers (G1–G7), as these span the association types observed in the original studies which utilized generations G0-8 [4].

Amine-terminated PAMAM dendrimers (G1–G7) with tetrafunctional ethylenediamine cores were obtained from Aldrich (Milwaukee, WI) or Dendritech, Inc. (Midland, MI), stored in the dark at −5 °C, and used as received. Samples were prepared by adding known amounts of PB and PAMAM (amine terminated), stripping off solvent using ultra high purity nitrogen, and diluting to volume with HPLC-grade water. Samples were then allowed to stir 24 h and equilibrate 24 h in the dark. Organic extractions were performed by adding 3–0.5 mL aliquots of toluene to the sample vial, shaking for 1 min and equilibrating for 10 min. The organic layer was then removed and retained for further investigations. Absorbance spectra were collected on a Hitachi U-3000 (Hitachi Instruments, Danbury, CT) double-beam spectrophotometer with a scan rate of 120 nm/min, a slit width of 1 nm, and a thermostated cell temperature of 25 °C. Fluorescence spectra and steady-state anisotropy data were collected in 1 cm^2 suprasil quartz cuvettes (Hellma) on a SLM 48000 DSCF/MHF spectrofluorometer (Jobin Yvon, Edison, NJ) at a thermostated cell temperature of 25 °C. The excitation source for fluorescence emission and anisotropy measurements was an Ion Laser Technology (Salt Lake City, UT) RPC-50-220 argon ion laser operated at 514 nm and 30 mW. Steady-state anisotropy measurements were collected in "L" format using Glan-Thompson polarizers. A 550 nm long pass filter (KV-550 Schott Glass Technologies, Duryea, PA) and a 600 nm short-pass filter (03 SWP 619 Melles Griot, Irvine, CA) were used in combination to select the wavelength range of interest for phenol blue.

* Corresponding author.
E-mail address: TuckerS@missouri.edu (S.A. Tucker).

0039-9140/$ – see front matter © 2009 Elsevier B.V. All rights reserved.
doi:10.1016/j.talanta.2009.01.051

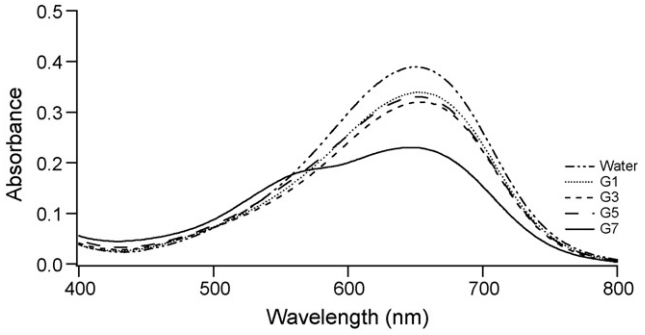

Fig. 1. Initial absorption spectra of PAMAM [10^{-6} M] with PB [10^{-5} M].

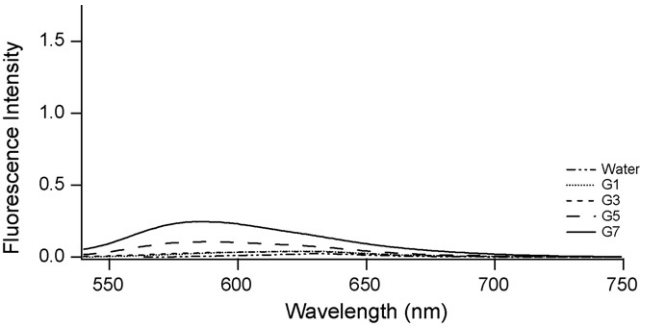

Fig. 2. Initial absorption-corrected fluorescence emission spectra of PAMAM [10^{-6} M] with [10^{-5} M] leading to excimer formation.

Initial absorbance spectra (Fig. 1) of PAMAM with PB show a large band centered around 654 nm. This band is consistent with that of aqueous PB. However, for all samples containing PAMAM dendrimers, the absorbance is less than that of aqueous PB. It can be assumed that in the presence of a large excess of dye, the spectra of dendrimer-associated PB (λ = 556 nm) is buried under the broad absorption band of aqueous PB. This was confirmed by spectral deconvolution with PeakFit™ software. The G7 PAMAM shows the lowest initial absorbance value and is also the only dendrimer-containing sample that shows a clear peak in the region of PAMAM associated PB.

The corresponding fluorescence emission data (Fig. 2), which has been absorbance and blank corrected, reveals that some amount of PB has associated with all the generations of PAMAM dendrimers investigated. The weak fluorescence emission observed for the aqueous PB is *circa* λ = 654 nm. While only a slight fluorescence emission is observed for G1 and G3 samples, G5 and G7 both show bands centered around 580 nm indicative of a significant dendrimer–dye association [4]. The broad, flat emission bands of the G1–G5 samples appear to be a mixture of dendrimer-associated dye and aqueous PB.

Anisotropy, a measure of the rotational freedom of a molecule, experiments were performed, and values range from approximately ~0.05 for aqueous PB to ~0.3 for G7 (Table 1). As seen in previous studies, the anisotropy values increase with increasing generation of dendrimer, indicating dye–dendrimer association [4]. This trend

Table 1
Anisotropy values of PAMAM with PB.

Generation	Initial *r*	Post-extraction *r*
Water	0.044 ± 0.001	0.051 ± 0.001
G1	0.105 ± 0.004	0.104 ± 0.002
G3	0.154 ± 0.001	0.100 ± 0.003
G5	0.249 ± 0.001	0.267 ± 0.002
G7	0.295 ± 0.006	0.294 ± 0.004

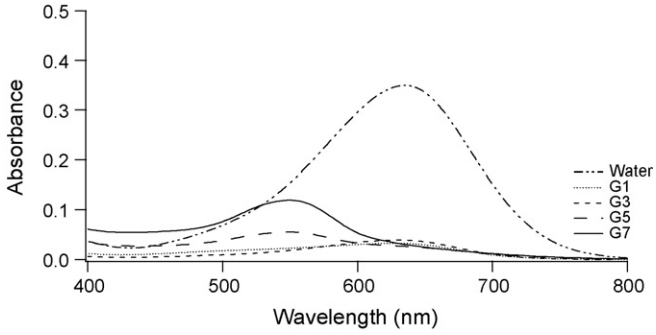

Fig. 3. Post-extraction absorption spectra of PAMAM [10^{-6} M] with PB [10^{-5} M].

Table 2
Number of PB molecules associated with a single PAMAM dendrimer.

Generation	Ratio PB:PAMAM
G1	1.58:1 ≈ 2:1
G3	1.49:1 ≈ 1:1
G5	2.66:1 ≈ 3:1
G7	6.11:1 ≈ 6:1

is attributed to the increasing molecular volume of the dendrimers containing the entrapped fluorophore.

All dendrimer-containing samples were extracted with toluene to remove excess dye. As anticipated, only loosely or unassociated PB molecules were removed. Absorption spectra of the samples post-extraction (Fig. 3) show that the broad band indicative of aqueous PB has disappeared for all the dendrimer-containing samples. This observation indicates that nearly all the aqueous PB was removed during the extraction process. There is a discernable band centered around 556 nm, the wavelength of dendrimer-associated PB, for both G5 and G7 samples. Neither of the G1 or G3 spectra initially revealed a distinct band at this wavelength. However, following deconvolution both an aqueous and dendrimer-associated band are visually evident for G3.

The concentration of dendrimer-associated PB were calculated using the Beer-Lambert Law (ε_{assoc} = 13,530 L mol^{-1} cm^{-1} at 556 nm) [4] and are presented in Table 2. Calculated dye concentrations in the larger G5 and G7 dendrimers are greater than the concentration of PAMAM, indicating that more than one dye molecule is entrapped by a single dendrimer. The larger dendrimers studied, G5 and G7, were able to entrap three and six PB molecules, respectively. As noted in earlier work, the smaller G1 and G3 samples also indicated the possibility of multiple dyes residing within a single dendrimer; however, higher-ordered species of multiple dendrimers surrounding a single dye or dendrimer–dye aggregates cannot be ruled out [4].

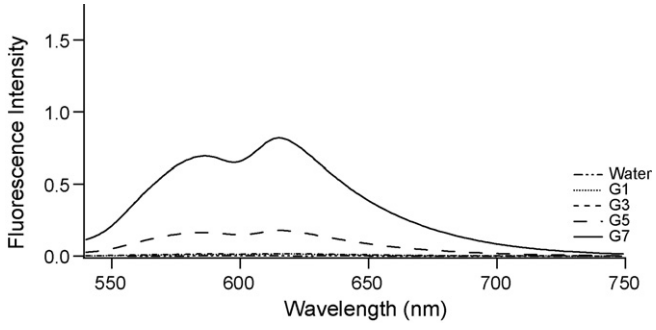

Fig. 4. Post-extraction absorption-corrected fluorescence emission of PAMAM [10^{-6} M] with PB [10^{-5} M] leading to excimer formation.

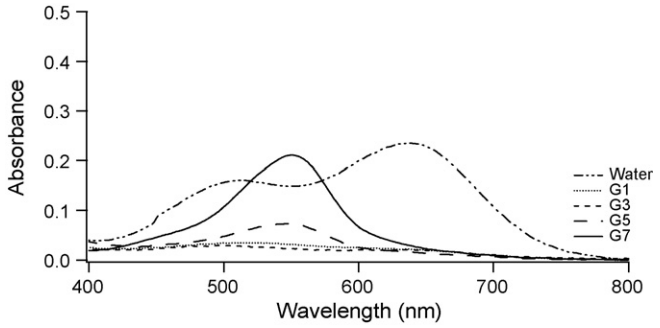

Fig. 5. Absorbance spectra of PAMAM [10^{-6} M] with PB [10^{-5} M] after extraction and titration with 50% methanol.

The post-extraction fluorescence emission spectra (Fig. 4) contain two peaks, with the longer wavelength band indicative of the formation of an excimer, an excited-state complex of two or more PB molecules. Since unassociated PB was removed by extraction, it is assumed that the excimer forms inside the PAMAM dendrimers between neighboring dye molecules. The anisotropy values are relatively unchanged, indicating that the dye–dendrimer complex, rather than the movement of the local fluorophore, remains the primary contribution to measured signal.

Absorption spectra of the toluene extraction layers (not shown) confirmed the presence of PB, and the probe concentration in these samples were also calculated using the Beer-Lambert Law ($\varepsilon_{toluene}$ = 16,960 L mol^{-1} cm^{-1} at 570 nm). The quantitative examination of the data determined a recovery of 100 ± 15% of the initial PB concentration. This higher recovery can be attributed to the increased solubility of PB in toluene, since it is hydrophobic and may adhere to the glassware in aqueous solution.

Given the hydrophobicity of PB, solvent replacement was performed to determine if changing the polarity of the bulk solution would release associated PB from the PAMAM dendrimers. Changing the solvent from water to methanol was achieved by preparing the samples in water, collecting data, evaporating off the water, rediluting the samples in methanol and repeating the measurements. These studies indicate that the dye remains encapsulated within the dendrimer even through changes to the bulk solvent. Additionally, after the aforementioned post-extraction studies, the samples were titrated with up to 50% methanol to determine if dye leaching would occur. Absorption spectra are shown in Fig. 5. In the G1–G7 samples, there is no spectral evidence of free PB, which should absorb between 610 and 650 nm in a water–methanol mixture. There is a noticeable change in the appearance of the sample containing only dye, which is a result of a reaction between PB and methanol previously observed by Richter-Egger in his studies of PAMAM with PB [4]. Titrated samples were also investigated 1 week later, and spectra continued to show no indication of dye leaching into the aqueous solution.

Previous studies of PAMAM with PB reported information on the extent of dye's association with the dendrimer family, the location of the association – near the core – and physical properties of the cavity [4]. This information was obtained using a dendrimer:dye ratio of 100:1. Absorption and fluorescence emission data at this ratio revealed that the association of PB increases with increasing dendrimer generation. The studies presented here show that association of PB with PAMAM dendrimers also increases as the PB concentration increases.

From the post-extraction data, it is shown that the maximum capacities of G5 and G7 are three and six PB molecules per dendrimer, respectively. It was also found that it is possible to remove the bulk of excess dye from the solution without disturbing the dendrimer-associated dye. Furthermore, attempts to release the bound dye by changing solvent system proved unsuccessful indicating that this dendrimer family behaves like a large-capacity dendritic box—once association has occurred, the dendrimer–dye complex is stable, and the dye remains inside the dendrimer even in the presence of external perturbation [5]. The robustness and capacity of the PAMAM 'box' continue to make this dendrimer family a desirable platform for polymeric applications.

Acknowledgment

This work was supported by a grant from the National Science Foundation.

References

[1] M. Krämer, J. Stumbé, H. Türk, S. Krause, A. Komp, S. Prokhorova, H. Kautz, R. Haag, Angew. Chem. Int. Ed. 41 (2002) 4252–4256;
C.M. Paleos, D. Tsiourvas, Z. Sideratou, Mol. Pharm. 4 (2007) 169–188;
S. Suttiruengwong, J. Rolker, I. Smirnova, W. Arlt, M. Seiler, L. Lüderitz, Y. Pérez de Diego, P. Jansens, Pharm. Dev. Technol. 11 (2006) 55–70.
[2] G.R. Newkome, et al., Dendrimers and Dendrons: Concepts, Syntheses, Applications, Wiley-VCH, Weinheim, NY, 2001;
J.M.J. Fréchet, D.A. Tomalia, Dendrimers and Other Dendritic Polymers, J. Wiley & Sons Ltd., Chichester, 2001;
D.A. Tomalia, H. Baker, J. Dewald, M. Hall, G. Kallos, S. Martin, J. Roeck, P. Smith, Polymer J. 17 (1985) 117–132;
D.A. Tomalia, H. Baker, J.R. Dewald, M. Hall, G. Kallos, S. Martin, J. Roeck, J. Ryder, P. Smith, Macromolecules 19 (1986) 2466–2468.
[3] F. Zeng, S.C. Zimmerman, Chem. Rev. 97 (1997) 1681–1712;
D.K. Smith, F. Diederich, Chem.: A Eur. J. 4 (1998) 1353–1361;
G. Pistolis, A. Malliaris, D. Tsiourvas, C.M. Paleos, Chem.: A Eur. J. 5 (1999) 1440–1444;
A.W. Bosman, H.M. Janssen, E.W. Meijer, Chem. Rev. 99 (1999) 1665–1688;
H.-B. Mekelburger, W. Jaworek, F. Vögtle, Angew. Chem. 104 (12) (1992) 1609–1614;
D.A. Tomalia, A.M. Naylor, W.A. Goddard III, Angew. Chem. 102 (2) (1990) 119–157;
D.A. Tomalia, A.M. Naylor, W.A. Goddard III, Angew. Chem. Int. Ed. 29 (2) (1990) 138–175;
D. Watkins, Y. Sayed-Sweet, J.W. Kilmash, N.J. Turro, D.A. Tomalia, Langmuir 13 (1997) 3136–3141.
[4] D.L. Richter-Egger, J.C. Landry, A. Tesfai, S.A. Tucker, J. Phys. Chem. A 105 (2001) 6826–6833;
D.L. Richter-Egger, PhD Dissertation, University of Missouri, Columbia, Missouri, 2001.;
R.D. Otte, M.S. Thesis, University of Missouri, Columbia, Missouri, 2002;
D.L. Richter-Egger, H. Li, S.A. Tucker, Appl. Spectrosc. 54 (2000) 1151–1156;
D.L. Richter-Egger, A. Tesfai, S.A. Tucker, Anal. Chem. 73 (23) (2001) 5743–5751;
C.L. Larson, S.A. Tucker, Appl. Spectrosc. 55 (2001) 679–683.
[5] J.F.G.A. Jansen, E.W. Meijer, J. Am. Chem. Soc. 117 (1995) 4417–4418.

Talanta 78 (2009) 1452–1457

Contents lists available at ScienceDirect

Talanta

journal homepage: www.elsevier.com/locate/talanta

Investigation of amine-buffered amide reagents for coulometric Karl Fischer titration

William Larsson*, Anders Cedergren

Department of Chemistry, Umeå University, SE901 87 Umeå, Sweden

ARTICLE INFO

Article history:
Received 23 October 2008
Received in revised form 15 February 2009
Accepted 20 February 2009
Available online 5 March 2009

Keywords:
Non-alcoholic KF reagent
Water determination
Amide
Amine

ABSTRACT

Formamide (FA), N-methylformamide (NMF), and dimethylformamide (DMF), were evaluated as solvents for coulometric Karl Fischer (KF) reagents in combination with several amine bases. Except for the effect of the iodine species (iodine or triiodide), the pH of the reagent and the position of the sulfur dioxide/hydrogen sulfite equilibrium were found to be the main factors explaining the large difference in the observed reaction rates between water and the KF reagent in these solvents. Acid–base titrations showed that hydrogen sulfite is the main sulfur reactant in these media. The results will be of great importance in finding suitable combinations of base and solvent with respect to stoichiometry, side reactions caused by active carbonyl compounds, and reagent stability.

1. Introduction

Surprisingly little has been reported on amide-based reagents for Karl Fischer (KF) titration, especially since formamide (FA) was used successfully to prepare some of the earliest described coulometric KF reagents [1,2] back in the 1960s. Although rapid kinetics and relatively small stoichiometric deviations have been reported [1–3], formamide has primarily found its use as a cosolvent to facilitate dissolution of proteins and sugars in foodstuffs [4]. Dimethylformamide (DMF) was early recommended for volumetric determination of moisture in carbonyl compounds [5], but problems with stoichiometric deviations were later shown [6]. More recently Cedergren and Orädd [7] managed to attain 1:1 stoichiometry in a DMF-based coulometric reagent by using an unusually high concentration of iodine to kinetically discriminate the side reaction between sulfur trioxide and water (1), in favor of the KF main reactions (2) and (3). The use of N-methylformamide (NMF) in both coulometric and volumetric reagents has been patented by Scholz [8] but is only sparsely mentioned in the literature, for example by Cedergren [3] who noted a positive effect on the KF reaction rate when added to a pyridine-based reagent:

$$SO_3 + H_2O + 2B \rightarrow SO_4^{2-} + 2BH^+ \quad (1)$$

(B denotes a suitable amine base):

$$H_2O + SO_2 + 2B \rightleftharpoons HSO_3^- + BH^+ + B \rightleftharpoons SO_3^{2-} + 2BH^+ \quad (2)$$

$$HSO_3^- + I_2 + B \rightarrow SO_3 + 2I^- + BH^+ \quad (3)$$

FA, NMF, and DMF are highly polar liquids with static relative permittivity (ε_r) of 109.5, 182.4, and 36.71 (at 25 °C) respectively, which makes them attractive as solvents for KF reagents in view of the inheritable large amount of ionic species that has to be dissolved. The relatively large differences in ε_r can be contributed to intermolecular hydrogen bonds, with DMF that lacks amido hydrogens and therefore cannot act as a hydrogen bond donor as one extreme, and NMF that associates linearly forming highly structured interlinked sheets as the other [9]. Polarity studies [10] on the other hand show the decreasing trend FA > NMF > DMF, which is also true for boiling point, density, and viscosity of the liquids. The presence of electron-donating methyl groups makes the oxygen of the substituted amides relatively more negative, which explains why DMF ($pK_a = -0.01$) and NMF ($pK_a = -0.04$) are more prone to protonation and hence more Brønsted basic than FA ($pK_a = -0.48$).

As Karl Fischer [11] developed his method for water determination he looked for a suitable base to shift the reaction to completion and concluded that the organic amines, especially aniline and pyridine, were most suitable. Cedergren [12] later showed that pyridine was not directly involved in the reaction, that it acted solely as a buffer, and that the reaction was of first order with respect to iodine, water, and sulfur dioxide with a rate constant of 1200 $M^{-2}\,s^{-1}$. Verhoef and Barendrecht [13] validated the rate expression (although with a rate constant of 2200 $M^{-2}\,s^{-1}$) and also found that the simultaneous increase in reaction rate and pH observed up to pH 5 could be explained by methyl sulfite being the reactive sulfur species in methanolic reagents. Several attempts were made to use other bases in the KF reaction, but pyridine was still the most stable

* Corresponding author.
E-mail address: william.larsson@chem.umu.se (W. Larsson).

0039-9140/$ – see front matter © 2009 Elsevier B.V. All rights reserved.
doi:10.1016/j.talanta.2009.02.047

and successful choice at the beginning of the 1980s. At that time Scholz began to systematically investigate stronger amines as replacements for pyridine. In the seventh [14] publication in a series of articles on pyridine-free reagents Scholz presented promising results using imidazole, which today is the dominating buffer base in commercial KF reagents. Orädd and Cedergren [15] made kinetic investigations on the new imidazole-buffered reagents and discovered a dramatic increase in reaction rate as the concentration of non-protonated imidazole was increased. In subsequent studies [16] it was shown that the first-order kinetics was no longer valid when using higher concentrations of imidazole, which was interpreted as a consequence of a reactive iodine species other than elemental iodine or triiodide in the KF reaction under those conditions.

In methanolic reagents it has been shown that concentrations of water up to about 1 M (after sample addition) can be allowed before the recovery begins to drop below 100% [17]. Although such high concentrations cannot be tolerated in amide-based reagents, the fact that it is still possible to maintain the 1:1 stoichiometry [1,18], under somewhat limited concentrations of water, means that the intermediate sulfur trioxide is somehow prevented from being hydrolyzed (1). Swensen and Keyworth [1] claimed that formamide was able to undergo an "addition reaction with the pyridine-sulfur trioxide compound" liberated after the oxidation step. In fact, both amine bases and amides are known to form charge-transfer (C-T) complexes with sulfur trioxide, and they are frequently mentioned as sulfonating, sulfating, or sulfamation agents for organic synthesis [19]. The reactivities of these agents are inversely proportional to the stability of the complex and hence pyridine would be expected to form a more stable adduct with sulfur trioxide than formamide. In any case, these types of charge-transfer complexes can explain the 1:1 stoichiometry in non-alcoholic reagents, but the C-T interaction is considerable weaker than the covalent bond that forms between sulfur trioxide and methanol.

The results presented in this work are part of a study of several combinations of amide solvents and amine buffers, with the aim of resolving critical factors for the kinetics and stoichiometry of the KF reaction, as well as for side reactions with active carbonyl compounds.

2. Experimental

2.1. Chemicals and reagents

For standardization of water the reagent HYDRANAL Coulomat E from Riedel dé Haën was used both as catholyte and anolyte in the Metrohm system. The sulfur dioxide content was determined coulometrically using a methanolic solution containing 1% water, ~2 mM potassium iodide and ~0.1 M of acetic acid. The reagents under investigation were prepared in 25-ml volumetric flasks by adding 0.40 M of base, 0.11–0.12 M of sulfur dioxide, and 0.10 M of iodine to the amide, followed by a careful addition of water until the iodine excess was consumed. Formamide p.a. (FA), sulfuric acid 95–97%, and aniline p.a. (An) were from Merck. N-methylformamide 99% (NMF), 3,5-lutidine 98% (3,5Lut), N-methylimidazole 99% (NMIm), 2-methylimidazole 99% (2NMIm), and 4-methylimidazole 98% (4NMIm) were from Aldrich. Piperidine 98% (Pip), 2-picoline (2Pic), 3-picoline 98% (3Pic), 2,6-lutidine 96% (2,6Lut), 2,4,6-collidine 99% (Col), 2-dimethylaminopyridine 98% (2DMAP), 1,2,2,5,5-pentamethylpiperidine 99% (PMP), dibutylamine 99% (DBA), N-benzylmethylamine 90-95% (NBMA), diethylamine 99.5% (DEyA), diethanolamine 99% (DEnA), dipropylamine 99% (DPA), and isopropylamine 99.5% (IPA) were from Fluka. Iodine r.g. and hydrochloric acid 37% were from Scharlau. Sulfur dioxide 99.9%, pyridine B.A. (Py), and imidazole B.A. (Im) were from J.T. Baker. N,N-dimethylformamide (DMF) was from Prolabo, 4-dimethylaminopyridine 99% (4DMAP) was from Reilly Industries, benzimidazole (BIm) was from Hopkin & Williams, and 4-chloroaniline (4ClAn) was from Eastman.

Attention: Several of the substances above are flammable, toxic, corrosive, and carcinogenic, even by inhalation or contact with the skin. Before use, refer to the corresponding material safety data sheets (MSDS) and take necessary precautions.

2.2. Instrumentation

Evaluation of the reagents was done using a three-compartment titration cell where the auxiliary, working, and reference compartments were separated by asbestos-filled electrolyte bridges [7]. All cells were filled with 4.5 ml of the reagent under investigation, and in addition an excess of ~50 mM iodine was added to the reference solution. The home built coulometer produced a generating current proportional to the difference between a preset voltage and the measured zero-current potential between two platinum pins in the working and reference compartments. The voltage of the zero-current indication electrode and the current between the generating electrodes were recorded using custom-made LabView software, Fluke 45 digital voltmeters and a National Instruments PCI-6052E data acquisition card (used for sampling frequencies from 4 to 20 Hz).

For calibration of water standards, and as a general reference system, a Metrohm 756 KF Coulometer with diaphragm cell was used. All results were stored and evaluated with the accompanying Vesuv database software. This system was also used for testing the performance of some of the non-alcoholic reagent mixtures. Sulfur dioxide content was determined using a LBK 16300 coulometric titrator from Jugner Instruments.

2.3. Evaluation of kinetics

The kinetics of the Fischer reaction were evaluated assuming (a) 1:1 stoichiometry between water and iodine; (b) that the KF reaction is first order with respect to each of the components water, iodine, and sulfur dioxide; (c) that the potential of the indicating electrode pair showed a perfect Nernstian response to the iodine concentration (iodide in excess). The third-order rate Eq. (4) was solved for this special case and rearranged to the straight-line Eq. (5) so that the rate constant k_3 easily could be determined from the slope by linear regression. A subscript '0' denotes starting concentrations at the time of sample injection:

$$\frac{d[I_2]}{dt} = -k_3[H_2O]^1[I_2]^1[SO_2]^1 \quad (4)$$

$$\underbrace{\frac{\ln(1+([H_2O]_0-[I_2]_0)/[I_2])}{[SO_2]_0([H_2O]_0-[I_2]_0)}}_{f(t)} = k_3 t - \frac{\ln([I_2]_0/[H_2O]_0)}{[SO_2]_0([H_2O]_0-[I_2]_0)} \quad (5)$$

The indicating system was calibrated by increasing (typically three times) the target potential of the coulometer by 5–10 mV and using the amount of generated iodine to find the Nernstian response. At iodine excess levels of 2×10^{-4} M the coulometer was turned off and the zero-current electrode potential was recorded at a suitable rate (1–20 Hz) as a 10-μL DMF sample containing about 5 μg of water (~6×10^{-5} M in 4.5 ml) was injected. Depending on the background and the rate of the reaction two to three injections were possible before all the iodine had been consumed. After transformation of the recorded potential the iodine concentration versus time profile and the linear relationship in Eq. (5) could be plotted. A simulated concentration profile (based on rate Eq. (4), the concentrations of the three reactants, and the calculated rate constant) was also superimposed on the experimental result as a visual validity check of the determined rate constant. An example of an experimentally

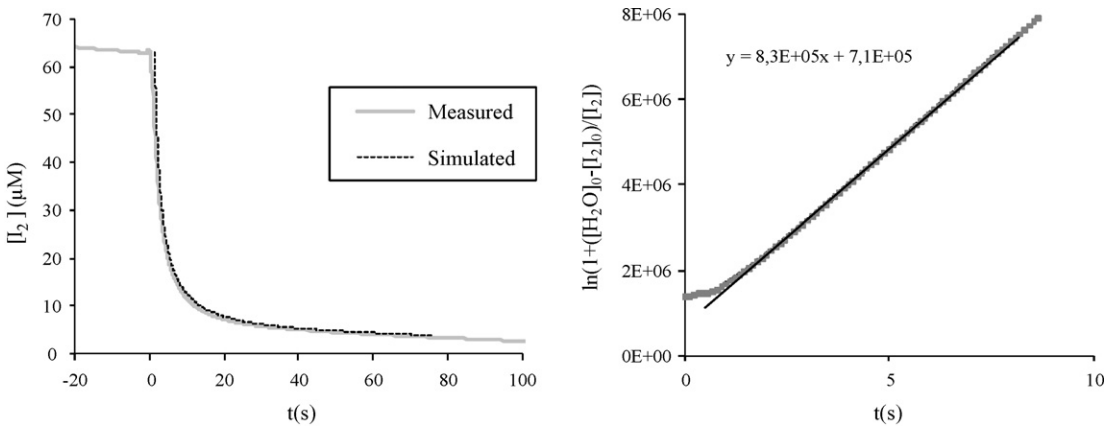

Fig. 1. Determination of the rate constant of a NMF reagent buffered with dipropylamine. The left plot shows the simulated concentration profile superimposed on experimental data and to the right is shown how the rate constant was retrieved from a least-squares fit to the linear part of $f(t)$ (Eq. (5)). The sample was injected at $t = 0$ s.

obtained potential profile is shown in Fig. 1, together with the simulated profile and the corresponding linear plot of Eq. (5).

2.4. pH titrations

pH measurement was carried out with a Mettler Toledo Inlab 412 combination electrode, filled with an aqueous reference electrolyte saturated with potassium chloride and potassium perchlorate to minimize the chloride content. Calibration was done in aqueous pH 4 and pH 7 buffers before each titration. A 10-ml sample of the amide solvent was left to stand with gentle stirring in a plastic bottle until pH was stable within 0.02 units for 10 min (typically 1.5 h). At this point 1 mmol of the base was added and after another 10 min titration was started by manually adding 5-μL portions of 37% hydrochloric acid once a minute. After the equivalence point had been reached the protonated base was titrated with 5-μL portions of piperidine, followed by a second round of titration with hydrochloric acid and piperidine. The pH at halfway to the equivalence points was plotted against the increase in ionic strength due to the additions and extrapolated to zero to estimate the apparent pK_a of the protonated base. In DMF, smaller portions were also titrated; 0.1 mmol of base was titrated once with 1-μL portions of hydrochloric acid.

The same solvent preparation was made prior to titration of sulfur dioxide with piperidine. About 1 mmol sulfur dioxide was added and the resulting small amount of hydrogen sulfite was protonated by addition of 0.5 mmol of trichloroacetic acid. In DMF, additions of 0.1 mmol of sulfur dioxide and 1 μL of hydrochloric acid were titrated as well. Before titration was started and after the equivalence point had been reached the water content of the sample was determined.

3. Results and discussion

Assuming that only the KF-main reaction takes place during preparation (see reactions (2) and (3)) the reagents were expected to contain 0.2 M base, 0.2 M protonated base, 0.2 M iodide, and 10–20 mM sulfur dioxide after decoloring with water. Relatively low concentrations of base and sulfur dioxide were chosen so that even the most rapidly reacting reagents could be followed potentiometrically. An additional reason for selecting low concentrations was to minimize expected side reactions such as bisulfite addition and reactions between amines and carbonyl compounds (aldehydes and ketones). Several bases were tested and Table 1 shows the results and conditions for base/solvent combinations giving reasonable stable and operational reagents. Owing to long conditioning times after filling the micro cell with reagent and the major effort needed to keep water standards and reference titrators (for water and sulfur dioxide determinations) confidently in order, most of the reagents were only prepared once. Also, the determination of the background shift due to addition of cyclohexanone and benzaldehyde was a one-shot test since the reagent had to be discarded afterwards. The results of the evaluation should therefore be considered as a screening and only general trends and observations covering several reagents can be regarded as confident.

As is evident from the data the major effort was devoted to the NMF-based reagents. Preparation of FA-based reagents was limited by stability, and extensive iodine consumption was observed when using stronger bases than 2,6-lutidine. Iodine dissolved quite slowly in FA and after the reagents had been used in the titration system for a while the slight iodine excess caused a gradual discoloration (usually an amber-like tone appeared within a day). Some of the stronger bases also caused a noticeable gas evolution and the explosion risk should be considered. In DMF the major problem besides low reaction rates was the poor solubility of reagent components and reaction products, often resulting in precipitation.

In the rightmost column of Table 1 are recoveries of 10-μl samples of DMF containing ~25 μg of water, or roughly 2600 ppm (w/w). For commercial titration systems that normally use 100 ml of reagent this corresponds to 550 μg of water, which can be considered as a very large amount when performing trace determinations. With the exception of 2,6-lutidine in FA close to 100% recovery was obtained in all FA and DMF reagents. NMF reagents, on the other hand, seemed to give slightly lower results, disregarding the rather low recoveries in those buffered with the weakest and some of the strongest bases. The reagents buffered with various stronger amines at the bottom of the table were examined on an earlier occasion and following a different protocol, for example using larger samples, and therefore no comparable data are given. Common to all of them, however, was a recovery close to 100%, but unfortunately with severe interference caused by cyclohexanone and benzaldehyde. The resulting background shift when adding 5 μl of the same two active carbonyl compounds in the reagents buffered with weaker bases are presented in the second rightmost column, and the only significant trend is that the interference is less in NMF than in DMF and FA. Evidently, omitting the alcohol component is not an ultimate solution to avoid interference due to reactive carbonyl compounds since the nucleophilic character of the amine bases can also cause water-forming reactions. Enamine formation can be one explanation and the strong interference between cyclohexanone and aniline may be a condensation [20] resulting in N-cyclohexylideneaniline and water.

Table 1
Results from the reagent evaluation.

Base	pK_a in water	pK_a[a] app.	Solvent	$[SO_2]$[b] (mM)	I_{max}[c] (mA)	log k	Δ_{drift}[d] (pg/min)	Recovery[e] (%)
Py	5.25	5.05	FA	6	1.4	5.4	84/56	101
3Pic	5.68	4.79	NMF	19	2.0	3.6 (3.4)	34/5	92
		5.39	FA	21		5.4	48/90	100
2Pic	5.94	5.02	NMF	22	1.8	3.8 (3.7)	0/0	99
		5.74	FA	7		5.8	50/45	100
3,5Lut	6.14	5.12	NMF	15	1.9	3.9	22/10	96
		5.79	FA	13	1.2	5.3	53/52	101
2,6Lut	6.65	5.74	NMF	16	2.0	4.4 (4.3)	5/1	100
		6.44	FA	3	1.3	6.0	39/79	96
2DMAP	7.00	5.72	NMF	21	1.9	4.4 (4.4)	4/3	98
Col	7.48	6.36	NMF	22	2.0	5.1 (5.1)	0/0	98
4DMAP	9.70	8.67	NMF	21	1.8	5.8	92/17	78
		7.92	DMF	31	1.7	4.3	47/197	101
BIm	5.40	5.47	NMF	37	1.5	4.2	8/0	99
		5.83	FA	12	1.1	5.2	127/43	100
Im	6.95	6.92	NMF	6	1.9	5.2 (5.2)	17/6	102
NMIm	6.95	6.73	NMF	11	1.8	5.7 (5.5)	20/10	100
		5.81	DMF	23	1.7	2.3		
4Mim	7.45	7.44	NMF	13	1.7	5.8 (5.8)	6/0	98
		6.85	DMF	44	1.8	3.3	33/20	100
2Mim	7.75	7.73	NMF	16	1.8	6.1 (6.1)	22/0	92
PMP	11.00		NMF	15	1.6	6.3	110/110	96
PiP	11.22		NMF	13	2.1	4.4 (4.0)	316/4805	101
4ClAn	4.15		FA	26	1.0	4.4	max	100
An	4.63		FA	8	1.3	4.6	max	101
DBA	11.25		NMF	14		5.6		
NBMA	9.58		NMF	11		5.9		
DEyA	10.98		NMF	23		5.9		
DEnA	8.88		NMF	12		6.2		
			DMF	10		3.1		
DPA	11.00		NMF	12		5.9		
IPA	10.63		NMF	60		4.1		

[a] Apparent pK_a in the solvent in question.
[b] Sulfur dioxide concentration directly after the kinetic determination.
[c] Maximum current through the cell during titration.
[d] Increase in drift (background) after addition of 5 μL cyclohexanone/benzaldehyde.
[e] Water recovery in a 10-μL DMF sample containing ~25 μg of water.

From the maximum titration currents it can be seen that in the more viscous FA the conductivity is about 30% lower than in NMF and DMF. In coulometry the conductivity of the reagent is an important factor, especially for fast reacting reagents, since it may impair the maximum possible titration rate. Rapid titrations vouch for more accurate determinations since the time with water in excess is minimized and thereby also the effect of side reactions involving water (e.g. Bunsen reaction and bisulfite addition). Background over-correction due to iodine consuming side reactions that stagnate during the titration (as the iodine concentration is lower than at the endpoint) will also be lower.

The equimolar amounts of free and protonated base in all reagents implies that pH of the reagents should have been close to the pK_a of the protonated base. An initial analysis of the reaction rates in NMF, based on pK_a values of the bases in water, indicated that imidazoles generated much higher rates at a certain pH. In order to correctly judge the effect of the Brønsted base strength on the observed rate constant k_3, estimated pK_a values (p$K_{a_{est}}$) of the protonated imidazoles and pyridines were determined with simple acid–base titrations. A rather large amount of base (100 mM) was used since initial titrations in NMF showed a disturbing presence of roughly 7 mM of an acid with an apparent pK_a around 7. The results clearly show that imidazoles in general appear to gain in base strength relative to pyridine when changing from water to NMF as solvent. A plot of log(k_3) versus p$K_{a_{est}}$ of the NMF-based reagents revealed a remarkably linear relationship (filled circles and triangles in Fig. 2) up to p$K_a \approx 8$.

This suggests that under the prevailing conditions the reaction kinetics is solely determined by the pH of the reagent and that the nucleophilic character of the base is of no importance, since both imidazoles and pyridines follow the same trend. The stronger amines (squares in Fig. 2) were not titrated in NMF but their resulting rate constants versus pK_a in water are plotted in the same figure for comparison. There is no doubt that most of those amines are also very strong bases in NMF. It is interesting that the reaction rate seems to level out at higher pH and not even the stronger amines can generate significantly higher reaction rates. Stronger amines that show unexpectedly low reaction rates have most likely reacted with other reagent components during preparation.

In Fig. 3 the results of FA and DMF-based reagents are shown together with the corresponding bases in NMF (where applicable). It is clear that the reaction rate for a reagent buffered with a certain

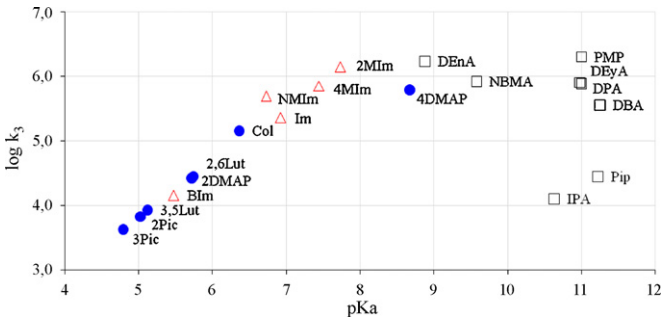

Fig. 2. Reaction rates in NMF-based reagents versus $pK_{a_{est}}$ for imidazoles and pyridines and versus pK_a in water otherwise. Triangles denote imidazoles, filled circles pyridines, and squares other kinds of amines.

base is expected to increase depending on the type of solvent in the order DMF < NMF < FA.

Although only a few FA and DMF-based reagents were evaluated it seems likely that the linear pH dependence is valid also in these solvents. In FA the bases 3,5-lutidine and benzimidazole appear to give lower reaction rates than expected in view of their base strengths and this can possibly be explained by side reactions consuming or protonating the bases. An observation that supported this conclusion was that iodine was extremely difficult to dissolve during preparation of the FA reagent buffered with 3,5-lutidine. The undissolved iodine grains stuck together in a drop-like manner at the bottom of the glass vessel and only dissolved after several hours on a shaking table. Since 3,5-lutidin has its two methyl groups opposite to the nitrogen lone electron pair it is possible that it orients with the methyl groups surrounding iodine and with the nitrogen towards the polar solvent. In that case the base would be exposed to an extreme iodine activity and it is not unlikely that iodination or some other reaction could occur.

The linear dependence in Fig. 2 was initially assumed to be linked to the sulfur dioxide/sulfite equilibrium, since a similar pH dependence in methanolic reagents was convincingly related to the sulfur dioxide/methylsulfite equilibrium by Verhoef and Barendrecht [13]. Titrations of the sulfur dioxide/sulfite system (2) were therefore carried out in order to shed some light on the equilibrium position in the three solvents.

Titration with piperidine revealed an equivalence point corresponding to an equimolar amount of protons and sulfur dioxide in all three solvents. Even titration with the stronger base ammonium hydroxide (25% ammonia in water) gave the same result in

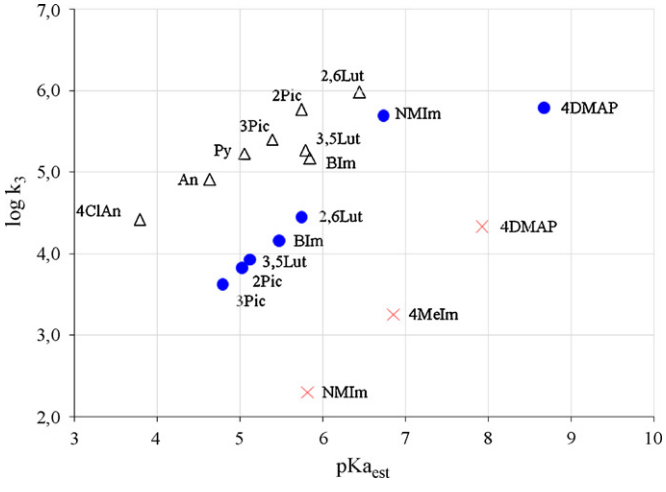

Fig. 3. Reaction rates in FA (triangles), NMF (filled circles), and DMF (crosses) versus $pK_{a_{est}}$ of the bases in the corresponding solvent.

FA and NMF, but in DMF precipitation was formed and twice the amount of protons was found, although only one equivalence point was seen. Upon standing, precipitation was also observed in the sulfur dioxide/DMF samples titrated with pyridine and pH measurements proved to be complicated by a gradual break-down of the reference electrolyte, leading to irreproducible results from one day to another. To minimize the extent of ion pairing and precipitation in DMF smaller amounts of 0.1 mmol were used and all titrations (of bases and sulfur dioxide) were performed within a few hours. Although pK_{est} of the bases in DMF was quite uncertain the relative positions of the inflection points were reproducible.

Since very strong bases are required to push equilibrium 2 all the way to sulfite in these solvents, hydrogen sulfite is likely to be the only reactive sulfur species present. This is important since hydrogen sulfite and sulfite have been shown to react at different rates [21,22]. The equilibrium constant of interest was hence:

$$K = \frac{\{HSO_3^-\}\{H^+\}}{\{SO_2\}\{H_2O\}} \quad (6)$$

At halfway to the equivalence point, i.e. when $\{HSO_3^-\} \approx \{SO_2\}$, the water concentration and measured apparent pH was used to estimate pK of the equilibrium:

$$pK \approx pK_{est} = pH_{app} + \log[H_2O] \quad (7)$$

The resulting pK_{est} values were 4.5, 5.8, and 7.7 in FA, NMF, and DMF respectively, which is in good agreement with the observed reaction rates in the three amide solvents. A high pK value means that less hydrogen sulfite will form at equilibrium at a certain pH, water activity, and sulfur dioxide activity. Since the measured apparent pH is not fixed to accurate pH scales in the three solvents the pK_{est} values should not be directly compared with each other. However, comparing $pK_{a_{est}}$ of bases titrated under similar conditions in the same solvent is reasonable. If the equilibrium is assumed to be very fast, as compared to the reaction of hydrogen sulfite in the KF reaction, a steady-state approximation can be made and the KF reaction should follow second-order kinetics with respect to hydrogen sulfite and iodine (again neglecting that activity coefficients likely deviate somewhat from unity):

$$\frac{d[I_2]}{dt} = -k_2[HSO_3^-]^1[I_2]^1 \quad (8)$$

The previously determined third-order rate constant k_3 is then related to the second-order rate constant k_2 according to Eq. (9) and taking the logarithm of both sides indicates that a plot of $\log k_3$ versus (pH − pK) would give k_2 as intercept where pH − pK = 0. If pH of the reagent is taken as the $pK_{a_{est}}$ of the protonated base and pK as pK_{est} any constant shifts between actual and apparent pH due to changes in liquid junction potential of the reference electrode will cancel out.

$$k_3 = \frac{k_2 K}{\{H^+\}} \quad (9)$$

A plot of $\log k_3$ versus $(pK_{a_{est}} - pK_{est})$ in Fig. 4 clearly shows that k_2 is smaller in DMF, which means that the unfavorable equilibrium position of the sulfur dioxide/hydrogen sulfite equilibrium is not the only explanation for the slower kinetics in this solvent. Comparing FA and NMF there is a tendency that oxidation of hydrogen sulfite is slightly faster in the former, but it cannot be confidently verified by these results. It should be mentioned that the reagents buffered with the weaker aniline bases were prepared only to extend the studied pH range downwards and the reagent with 4-chloroaniline in particular suffered from a high background drift when used in the KF titration system.

The slow kinetics of the oxidation step in DMF was, however, expected on beforehand since it has been shown that the rate of the KF reaction is markedly slower for triiodide as compared to

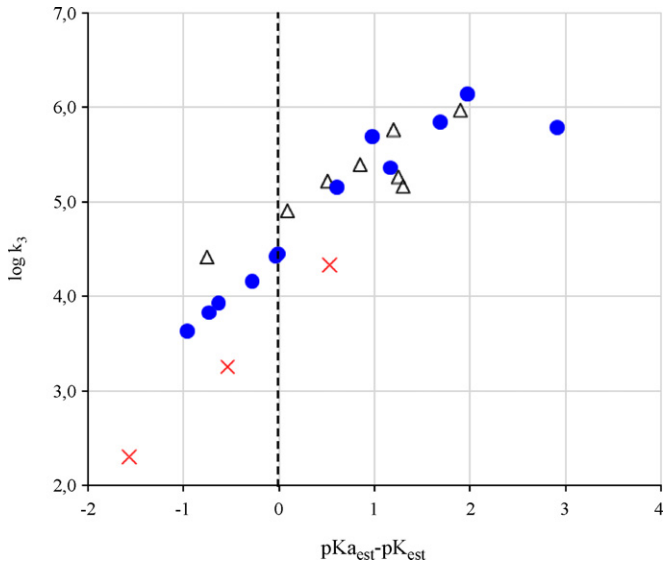

Fig. 4. Rate constants in FA (triangles), NMF (filled circles), and DMF (crosses) versus $pK_{a_{est}}$ of the base relative to pKest of the sulfur dioxide/hydrogen sulfite equilibrium.

iodine [13,22]. Triiodide is extremely stable in DMF, with a dissociation constant of $10^{-7.0}$ M compared to $10^{-3.7}$ in FA [23]. The iodide concentration of the reagent should therefore have a large influence on the reaction rate and this effect was studied in NMF. Lowering the iodide concentration from 200 to 100 mM increased the reaction rate by more than three times. This increase leveled off quite rapidly, however, and was only about 10% when going from 100 to 60 mM. Apparently both iodine and triiodide contribute to the observed reaction rate. Unfortunately the iodide concentration cannot be too low without affecting the current efficiency and therefore the concentration of triiodide will remain relatively high.

4. Conclusions

The results presented in this work provide fundamental knowledge about the possibilities and difficulties when designing amide-based reagents for coulometric KF titration. By considering the optimum pH for the sulfite equilibrium, a promising starting point for further development of rapidly reacting amide reagents has been reached.

Although DMF is the most stable solvent of the three amides studied, the KF reaction is very slow in this solvent due to the high stability of the slowly reacting triiodide ion. Further, DMF reagents suffer from limited solvation power and the need for strong bases in order to obtain reasonably high reaction rates. More promising are the results in FA because of its unique ability to dissolve sugars and proteins. NMF appears as the best compromise with respect to stability, reaction rate, conductivity, side reactions, and solvation. Surprisingly, no acceleration of the KF reaction was observed for the more nucleophilic imidazoles. It remains to be shown, however, whether higher concentrations of free base will cause such acceleration by the formation of more reactive iodine species [13,15]. In order to cope with iodine consuming side reactions, rapid kinetics of the KF reaction makes it possible to select a low iodine concentration at the end-point of a titration. This opens up the possibility to kinetically discriminate certain types of interferences. Considering side reactions caused by the reaction between amine bases and active carbonyl compounds, the described reagents are favorable due to the relatively low concentration of base required.

Acknowledgement

The authors would like to thank Dr. Michael Sharp for linguistic revision of the paper.

References

[1] R.F. Swensen, D.A. Keyworth, Anal. Chem. 35 (1963) 863–867.
[2] J. Bizot, Bull. Soc. Chim. Fr. (1967) 151–157.
[3] A. Cedergren, Talanta 25 (1978) 229–232.
[4] E. Scholz, Dtsch. Lebensm. Rundsch. 79 (1983) 302–306.
[5] V.A. Klimova, F.B. Sherman, A.M. L'vov, Bull. Acad. Sci. (USSR), Div. Chem. Sci., N.Y. (Eng Transl.) 25 (1967) 2477–2479.
[6] F.B. Sherman, Talanta 27 (1980) 1067–1072.
[7] A. Cedergren, C. Orädd, Fresenius J. Anal. Chem. 346 (1993) 539–542.
[8] E. Scholz, United States Patent 5,466,606 (1995).
[9] Y.J. Chang, E.W. Castner, J. Chem. Phys. 99 (1993) 113–125.
[10] M. Kosower, J. Am. Chem. Soc. 80 (1953) 3253–3260.
[11] K. Fischer, Angew. Chem. 48 (1935) 394–396.
[12] A. Cedergren, Talanta 21 (1974) 271–367.
[13] J.C. Verhoef, E. Barendrecht, J. Electroanal. Chem. 71 (1976) 305–315.
[14] E. Scholz, Fresenius Z. Anal. Chem. 312 (1982) 462–464.
[15] C. Orädd, A. Cedergren, Anal. Chem. 66 (1994) 2603–2607.
[16] A. Cedergren, Anal. Chem. 68 (1996) 784–791.
[17] J.C. Verhoef, E. Barendrecht, J. Electroanal. Chem. 75 (1977) 705–717.
[18] W. Larsson, J. Jalbert, R. Gilbert, A. Cedergren, Anal. Chem. 75 (2003) 1227–1232.
[19] E.E. Gilbert, Chem. Rev. 62 (1962) 549–589.
[20] V.D. Stytsenko, T.D. Hyu, V.A. Vinokurov, Kinet. Catal. 48 (2005) 292–297.
[21] J.C. Verhoef, E. Barendrecht, J. Electroanal. Chem. 86 (1978) 407–415.
[22] B.S. Yiin, D.W. Margerum, Inorg. Chem. 29 (1990) 1559–1564.
[23] R. Alexander, E.C.F. Ko, Y.C. Mac, A.J. Parker, J. Am. Chem. Soc. 89 (1967) 3703–3712.

Talanta 78 (2009) 1389–1394

Contents lists available at ScienceDirect

Talanta

journal homepage: www.elsevier.com/locate/talanta

A non-element-enriched, non-lyophilized candidate rat serum reference material prepared for once use in determination of inorganic elements by ICP-MS

Xiang-Yun Li [a], Hong-Zhen Lian [a,*], Li Mao [b,**], Yi-Jun Chen [a], Xin Hu [a], Jun-qin Qiao [a], Dong Sheng [a]

[a] Key Laboratory of Analytical Chemistry for Life Science (Ministry of Education of China), School of Chemistry and Chemical Engineering and Center of Materials Analysis, Nanjing University, 22 Hankou Road, Nanjing 210093, China
[b] School of Public Health, Nanjing Medical University, 140 Hanzhong Road, Nanjing 210029, China

ARTICLE INFO

Article history:
Received 11 October 2008
Received in revised form 10 February 2009
Accepted 12 February 2009
Available online 24 February 2009

Keywords:
Rat serum
Reference material
Candidate
Subpackage
Elements
ICP-MS

ABSTRACT

A practice about preparing a once-used native state candidate rat serum reference material has been described for inductively coupled plasma atomic emission spectrometry (ICP-MS) determination of inorganic elements in biological matrices, which is independently packed, easy to use, non-lyophilized, without element-spiking, and with stable quality. Various dispersing and storing factors influencing the serum quality have been investigated including container material, sampling volume, packing mode and storage time. The contents of twelve main elements in the rat serum have been not only evaluated by ICP-MS but also verified by other analytical techniques. The probation of this unconventional candidate serum reference material by different laboratories has given very similar contents of 12 main trace elements in the serum, and proven its applicability to support quality assurance of biological sample analyses.

1. Introduction

Various physiological functions of organism are closely linked to inorganic elements in the body, and either lack or excess of trace elements causes the occurrence of diseases, therefore, maintaining all elements in organism at the normal level is of important significance. The relationship between trace elements and health has aroused widespread concern, and biological sample analysis has become very popular. In terms of element determination, specimen including a variety of body fluids, organs, tissues and excreta, are all objects of study, among which, serum is one of the most common biological fluids [1–3].

The real biological samples always have the characteristic of small quantity with a wide element concentration range in complex matrix, therefore, the method for detecting elements in such samples should be of high sensitivity, wide dynamic range and powerful ability to overcome interference. Traditional techniques for effective determination of elements in biological samples include flame atomic absorption spectrometry (FAAS), graphite furnace atomic absorption spectrometry (GFAAS), inductively coupled plasma atomic emission spectrometry (ICP-AES). Each of these techniques possesses its strong suits, but has some drawbacks as well. FAAS and GFAAS can measure only number-limited multielements simultaneously, so that specific hollow-cathode lamps are installed and instrument parameters are individually selected to determine several different elements. Moreover, FAAS and GFAAS are of narrow dynamic range, concentration of sample solution is often adjusted because element contents in samples vary widely. ICP-AES has poor selectivity due to serious inter-element interference, so a number of man-made suppression protocols have to be tried to eliminate the matrix effect, bringing serious uncertain errors. In addition, the sensitivity of FAAS and ICP-AES does not reach as high as required for biological samples, therefore, it is necessary to put pretreatment in practice such as extraction, concentration or enrichment, which needs large amount of sample with tedious manipulation. ICP-MS has been more and more frequently applied for analysis of trace elements in biological samples because of the simple spectrum for every isotope of an element, excellent resolution, high sensitivity, good precision, wide dynamic range and small sample quantity required [3–12]. Although ICP-MS has many advantages, however, the signal intensity is significantly strengthened or weakened due to the existence of salts, such as NaCl, NH_4Cl, and the like, that is, determination results are affected

* Corresponding author. Tel.: +86 25 83686075; fax: +86 25 83325180.
** Corresponding author. Tel.: +86 25 86862938; fax: +86 25 86527613.
E-mail addresses: hzlian@nju.edu.cn (H.-Z. Lian), maoli@njmu.edu.cn (L. Mao).

0039-9140/$ – see front matter © 2009 Elsevier B.V. All rights reserved.
doi:10.1016/j.talanta.2009.02.032

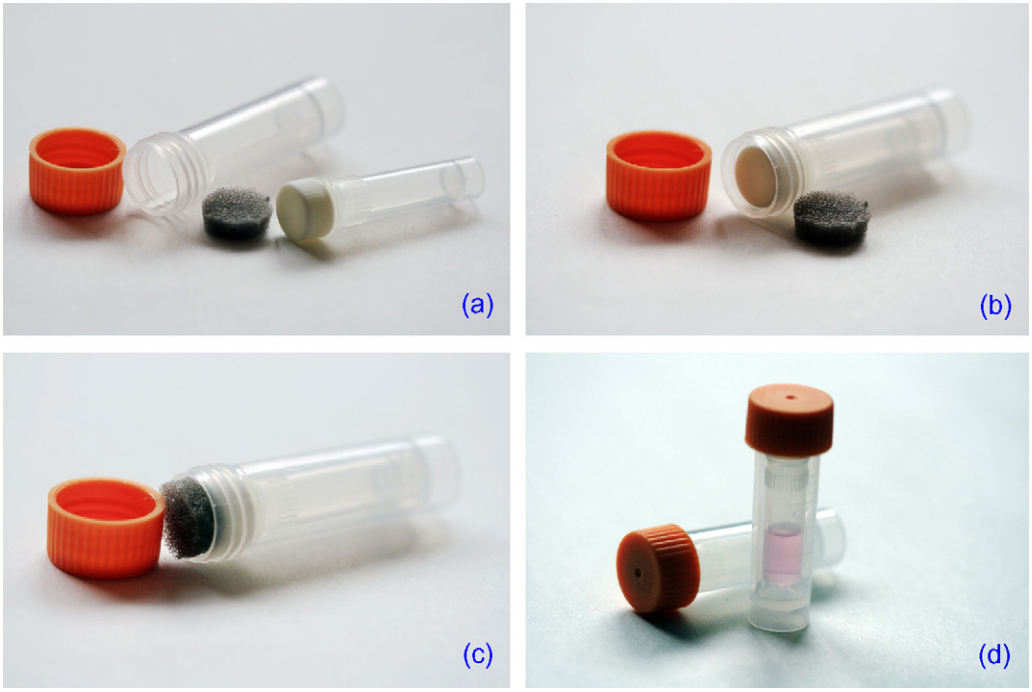

Fig. 1. The scheme of packing of serum.

seriously by the interference of complex matrices. Using standard reference substance of the similar matrix to sample analyzed is an effective strategy to evaluate the precision and reliability of an analytical procedure, and to correct determination result at different time, or between different operators or laboratories [13–18]. There are two kinds of standard reference materials commercially available in China now, Microelements Analytical Standard Human Serum (GBW 09135, first-grade) and Certificate Reference Bovine Serum (GBW (E) 090006, second-grade) [19,20]. These two standard materials are both in the form of freeze-dried powder packed in glass ampoule, with some inconvenience in the course of transport and use: (1) vitreous ampoule is friable, so there is the risk of break in long distance delivery, and the serum would be contaminated during cutting ampoule; (2) lyophilized powder is vulnerable to deliquescence at room temperature, thus it is hard to completely transfer or partially take the "serum powder" with a desired amount from the ampoule out; (3) the loads of human serum (GBW 09135) and bovine serum (GBW (E) 090006) in an ampoule are 0.2 g of freeze-dried powder and unknown weight of freeze-dried powder from 2 mL serum, respectively, which were drafted for conventional methods for elements such as FAAS and ICP-AES, obviously, are not suitable to ICP-MS any more, because relative to the high sensitivity of ICP-MS the absolute quantity is too large for one analysis. However, it is not easy to exactly weigh a small quantity of bovine serum lyophilized powder (GBW (E) 090006), matching ICP-MS analysis level, time after time. Although human serum lyophilized powder (GBW 09135) can be reversed to "original" serum by dissolving total 0.2 g in a known volume of water, matrix and volume of the recovered serum would change during repetitive frosting, thaw and aliquot sampling. If total 0.2 g lyophilized powder or 2 mL serum lyophilized is totally taken for dilution, it is a big waste of the reference materials, and the serum has to be dissolved in a huge volume of solvent or diluted by multi-step dilution to achieve the expecting concentration suitable to ICP-MS. In addition, both human serum (GBW 09135) and bovine serum (GBW (E) 090006) are enriched with elements in order that the concentration exceeds the limits of quantitation (LOQs) for other traditional analytical techniques. However, the reference material for ICP-MS capable of detecting the native contents of most elements in serum has no use for any element enrichment, which, moreover, can keep the original serum matrix constant because no foreign substances such as HCl and HNO_3 accompany the metal ions spiked. Noticeably, National Institute of Standards and Technology (NIST) has launched a 5-mL package dispensed in polypropylene tube, non-element-enriched, non-lyophilized bovine serum standard reference material (NIST SRM 1598) [21]. However, the absolute quantity in 5 mL serum was too large for ICP-MS analysis as mentioned above. Consequently, it is still essential to make serum reference materials easy to once use, with simple packing and stable quality. For this purpose, an unconventional protocol for preparing a kind of rat serum reference substance has been tried for analysis of trace elements in biological samples by ICP-MS.

2. Experimental

2.1. Preparation of candidate rat serum reference material

Screw-capped graduated polypropylene vial (also named transportation vial) was purchased from Haimen Sanhe Chenxing Experimental Equipment Factory (Nantong, China). All the vessels used in the experiment were soaked in 25% nitric acid for at least 48 h, and then rinsed by water and reserved to use after airing, ensuring no elements were detected both in water and in 1% nitric acid that were harbored within a vessel for more than 48 h.

Serum was collected on the basis of the NIST procedure [21] with some minor modifications. Briefly, rat blood was taken from healthy SD rats (supplied by Center of Experimental Animals, Nanjing Medical University, Nanjing, China) by using one-off syringes, pooled in an ion-free polypropylene vessel, and vortexed vigorously (SK-1 Votexer, Jintan Medical Equipment Work, Zhenjiang, China). Rat serum was obtained by centrifugation of the pooled rat blood for 30 min. After the element content was analyzed, 0.1 mL aliquot of this serum was dispensed into a 1.25-mL graduated polypropylene vial (inner vial) without anything added, and the screw cap was tightened. Then the inner vial containing 0.1 mL serum was put into

Table 1
Determination of elements in certificate reference materials ($n = 3$).

Element	Certificate reference tea, GBW 070605 ([mean ± U, $k = 1$], μg g^{-1})		Certificate reference bovine serum, GBW (E) 090006 ([mean ± U, $k = 1$], ng mL^{-1})		Detection limit (ng mL^{-1})
	Determined	Certificate	Determined	Certificate	
Cd	0.075 ± 0.010	0.057 ± 0.010	0.833 ± 0.184	N/A	0.003
Co	0.199 ± 0.026	0.18 ± 0.02	2.61 ± 0.30	2.8[a]	0.001
Cr	0.769 ± 0.081	0.80 ± 0.03	8.85 ± 4.36	0.21[a]	0.051
Cu	18.1 ± 1.0	17.3 ± 1.8	665 ± 22	640 ± 70	0.447
Fe	270 ± 23	264 ± 15	3465 ± 268	3620 ± 180	3.75
Mg	1627 ± 109	1700 ± 200	21,126 ± 1293	22,300 ± 1800	0.945
Mn	1330 ± 61	1240 ± 70	20.4 ± 1.9	13[a]	0.048
Mo	0.039 ± 0.004	0.038 ± 0.007	15.3 ± 1.6	14.3 ± 5.6	0.018
P	3243 ± 178	2840 ± 60	125,856 ± 6290	129,000 ± 8000	4.47
Pb	5.01 ± 0.50	4.4 ± 0.3	13.0 ± 0.9	15.4[a]	0.063
Sr	14.6 ± 1.3	15.2 ± 0.7	137 ± 11	134 ± 19	0.005
Zn	27.8 ± 1.6	26.3 ± 2.0	828 ± 38	880 ± 70	0.759

[a] Reported-but-not-certified values.

a 5-mL graduated polypropylene vial (outer vial), a sponge pad was put above the lid of inner vial and underneath the lid of outer vial, and the cap was screwed on the outer vial (as shown in Fig. 1a–d). Finally, the independently packed serum reference was stored at −20 °C until use. All operations were performed under strict protocols designed to preserve the original composition and to minimize contamination.

2.2. Determination of elements in rat serum by ICP-MS

Nitric acid (ultra-pure grade) and perchloric acid (70–72%, ultra-pure grade) were purchased from Suzhou Crystal Clear Chemical Co., Ltd. (Suzhou, China) and Tianjin Xingyuan Chemical Factory (Tianjing, China), respectively. Water (18.2 MΩ cm) was lab-made from Millipore Milli-Q Advantage A10 Water Purification System (Billerica, MA, USA). Working solutions for calibration and internal standard were prepared by dilution with 1% nitric acid (v/v) from 1.0 mg mL^{-1} inorganic element standard stock solutions made up from spectro-grade metal simple substances, oxides or salts. For all the elements the concentrations in the calibration solutions were 0, 1, 10, 50 and 100 ng/mL.

The independently packed 0.1 mL rat serum was thawed at room temperature, and transferred into a 10-mL beaker with a cover after vortexing. The inner vial was washed three times with 0.1 mL water, and the water was also placed into the beaker for transferring the serum completely. 0.5 mL nitric acid and 0.25 mL perchloric acid were added, and the serum was digested mildly on a hot plate at low temperature (about 50 °C) for 3 h and then heated to near dryness at 150–200 °C. The residue was subsequently dissolved in 3 mL of 1% nitric acid and the content of elements was measured by ICP-MS in triplicate against a corresponding reagent blank. The determination throughout the experiment was carried out in a SCIEX ELAN 9000 ICP-MS (PerkinElmer, Norwalk, CT, USA) under the operating conditions as follows, radio frequency power: 1100 W; outer Ar gas: 16.0 L min^{-1}; intermediate Ar gas: 1.0 L min^{-1}; carrier Ar gas: 0.95 L min^{-1}; sample lifting speed: 1.1 mL min^{-1}; ion lens voltage: 5.6 V; analog voltage: 1600 V; pulsed voltage: 950 V; scanning mode: skip; residence time: 50 ms; scanning times: 3; integral time: 1000 ms. High-abundance-ratio isotopes of the elements of interest were employed for quantitation except for magnesium which detection isotope was ^{26}Mg other than ^{24}Mg, the strongest isotope, owing to too large magnesium content in the serum. Additionally, in order to correct for changes in instrument hardware response or for sample-to-sample variations in sensitivity, as well as quantify and correct matrix effect if it exist, three isotopes ^{45}Sc, ^{103}Rh and ^{187}Re were selected as the internal standards for close mass of elements measured respectively [22], that is, ^{45}Sc for ^{59}Co, ^{52}Cr, ^{65}Cu, ^{57}Fe, ^{26}Mg, ^{55}Mn, ^{31}P, and ^{66}Zn; ^{103}Rh for ^{114}Cd, ^{98}Mo and ^{88}Sr; and ^{187}Re for ^{208}Pb.

Limit of detection (LOD) of element by the proposed ICP-MS method was determined from the three times of standard deviation (S.D.) of the background intensity of 10 measurements of reagent blank. The LODs of elements (ng mL^{-1}) were listed in Table 1.

In order to validate the method, certificate references tea (GBW 070605, first-grade) and bovine serum (GBW (E) 090006, second-grade) were employed for determination of trace elements. Appropriate amount of certificate reference was weighed, digested and analyzed as described in Section 2.2. The analysis results of most elements in two certificate reference materials were in agreement with their certificate values (Table 1).

All the results given were expressed as mean ± expanded uncertainty (the expanded factor $k = 2$ was taken, 95% confidence levels, except for the results in Table 1 where $k = 1$ was taken, 98% confidence levels, in order to match the format of certificate data) [23–26], and the combined standard uncertainty was estimated by considering the contribution of the uncertainties of standard solution preparation, sample solution preparation, standard curve fitting, measured repeatability and recovery.

2.3. Statistical analysis

Statistical analyses were performed using SPSS version 11.5 (SPSS Inc., Chicago, IL) software. Paired-samples t-test was used to analyze the differences between the ICP-MS results in element contents and those by other individual methods. After equal variances were assessed using Levene's test, one-way ANOVA and Kruskal–Wallis (K–W) tests were used to analyze the differences between different experimental conditions, respectively, for homogeneous and inhomogeneous variances. A statistically significant difference was considered when $p < 0.05$.

3. Results and discussion

3.1. Contents of trace elements in the candidate rat serum reference material

The dispensed rat serum reference material was determined by ICP-MS under the proposed experimental conditions. The contents of 12 main trace elements in the serum, within-day and between-day vial-to-vial differences, obtained from triplicate determinations of independent vials, are shown in Table 2. The results were in accordance with those obtained from GFAAS, FAAS or ICP-AES. No statistically significant differences were observed between the results by ICP-MS and those by other individual meth-

Table 2
Comparison of element contents between dispersed and undispersed rat serum ($n = 3$).

Element	Dispersed (content [mean ± U, $k = 2$], ng mL^{-1})			Undispersed (content [mean ± U, $k = 2$], ng mL^{-1})		T-test p values (2-tailed)[d]	One-way ANOVA test p values[e]
	Within-day	Between-day	Other methods	Within-day	Between-day		
Cd	3.16 ± 0.83	3.45 ± 1.39	3.28 ± 0.73[a]	2.89 ± 0.71	3.18 ± 1.18	0.271	0.465
Co	3.90 ± 1.05	4.16 ± 1.25	3.89 ± 0.79[a]	3.67 ± 1.00	3.85 ± 1.22	0.850	0.578
Cr	46.2 ± 10.4	42.1 ± 15.9	45.6 ± 10.9[a]	44.5 ± 10.6	45.5 ± 12.9	0.824	0.694
Cu	1547 ± 161	1518 ± 108	1522 ± 175[b]	1534 ± 123	1537 ± 168	0.607	0.942
			1533 ± 93[c]			0.843	
Fe	4650 ± 676	4818 ± 893	4751 ± 726[b]	4649 ± 727	4884 ± 874	0.422	0.493
			4684 ± 740[c]			0.764	
Mg	25,680 ± 3337	25,259 ± 3069	25,777 ± 3427[b]	25736 ± 3178	25386 ± 3126	0.832	0.341
			25,530 ± 3155[c]			0.819	
Mn	30.2 ± 5.8	30.9 ± 5.1	29.6 ± 2.8[a]	28.9 ± 6.2	31.5 ± 4.4	0.849	0.582
Mo	24.4 ± 2.5	23.3 ± 7.2	22.8 ± 4.4[a]	24.1 ± 2.3	24.2 ± 5.4	0.133	0.922
P	162,756 ± 20,011	163,916 ± 21,368	163,002 ± 27,227[c]	164,656 ± 20,243	161111 ± 19501	0.958	0.840
Pb	81.9 ± 15.6	89.5 ± 16.8	88.0 ± 9.0[a]	83.2 ± 18.7	86.6 ± 12.6	0.321	0.552
Sr	67.2 ± 11.8	68.4 ± 12.2	66.6 ± 14[a]	65.3 ± 11.8	68.4 ± 12.5	0.650	0.257
Zn	1569 ± 142	1595 ± 198	1568 ± 126[b]	1546 ± 165	1545 ± 324	0.942	0.891
			1586 ± 128[c]			0.595	

[a] GFAAS.
[b] FAAS.
[c] ICP-AES.
[d] Between within-day result by ICP-MS and that by other method for dispersed serum.
[e] Among within- and between-day results for dispersed and undispersed sera by ICP-MS.

Table 3
Recoveries of elements in candidate rat serum reference material ($n = 3$).

Element	Original (ng mL^{-1})	Added (ng mL^{-1})	Found (ng mL^{-1})	R.S.D. (%)	Recovery (%)
Cd	3.16	4.50	8.18	9.6	111.6
Co	3.90	4.50	8.52	8.0	102.7
Cr	46.2	60.0	104	4.8	95.5
Cu	1547	1500	3150	0.7	106.9
Fe	4650	4500	8432	6.0	84.0
Mg	25,680	24,000	48,284	3.4	94.2
Mn	30.2	30.0	50.6	1.9	90.4
Mo	24.4	15.0	41.5	3.4	114.5
P	162,756	210,000	387,729	4.7	107.1
Pb	81.9	60.0	139	2.2	95.4
Sr	67.2	60.0	121	2.6	89.2
Zn	1569	1500	2832	2.3	94.4

ods via paired-samples t-test ($p > 0.05$). The recovery was evaluated by respectively spiking a known amount of element standard to an independent vial and analyzing according to the same experiment procedure. It can be seen from Table 3 that the recoveries were between 84.0% and 111.6%.

3.2. Correlative factors on serum quality

Graduated polypropylene vials were used as the serum vials. The screw caps feature a molded-in sealing ring to prevent leakage. They are suitable as primary containers for lodging, shipping and delivering sera. The vials were filled with ultra-pure water and then 1% nitric acid after cleaned carefully. The elements in any extracts were measured after they were stocked in the vials for 48 h. The results showed that the contents of every element in the water or 1% nitric acid were all far lower than the LODs. Therefore, storing rat serum in the vials would not make significant influence on determination of elements.

Generally, the minimum sampling quantity of final solution is 3 mL for continuous infusion during an effective ICP-MS measure-

Table 4
Comparison of element contents in rat serum among different sampling volume and dilution rate ($n = 3$).

Element	Content (mean ± U, $k = 2$) (ng mL^{-1})				One-way ANOVA test p values
	0.1 mL serum, 30 times	0.5 mL serum, 6 times	0.5 mL serum, 30 times	2.0 mL serum, 1.5 times	
Cd	2.89 ± 0.71	2.95 ± 0.71	2.87 ± 0.68	3.04 ± 0.69	0.485
Co	3.67 ± 0.82	3.91 ± 0.95	3.98 ± 1.09	3.63 ± 0.93	0.528
Cr	44.5 ± 10.2	47.0 ± 10.5	44.6 ± 10.7	43.4 ± 9.36	0.366
Cu	1534 ± 122	1611 ± 154	1605 ± 141	1526 ± 93	0.139
Fe	4649 ± 766	4892 ± 778	4906 ± 713	4745 ± 690	0.156
Mg	25,736 ± 3178	25,557 ± 3147	25,424 ± 3237	25,374 ± 3110	0.563
Mn	28.9 ± 6.2	30.6 ± 5.5	31.5 ± 6.0	29.8 ± 4.7	0.620
Mo	24.1 ± 2.3	24.4 ± 3.0	23.4 ± 2.7	23.6 ± 2.9	0.437
P	164,656 ± 20,243	161,220 ± 18,462	165,769 ± 20,220	163,737 ± 18,004	0.558
Pb	83.2 ± 18.7	80.4 ± 14.3	75.5 ± 15.2	79.6 ± 9.0	0.540
Sr	65.3 ± 11.8	70.1 ± 14.0	70.8 ± 13.3	70.8 ± 12.8	0.146
Zn	1546 ± 165	1574 ± 158	1483 ± 137	1500 ± 135	0.261

Table 5
Comparison of element contents between dispersed and undispersed rat serum ($n = 3$).

Element	Content (mean ± U, $k = 2$) (ng mL^{-1})			One-way ANOVA test p values
	1st month	2nd month	4th month	
Cd	3.16 ± 0.83	3.26 ± 0.90	2.80 ± 0.73	0.111
Co	3.90 ± 1.05	3.67 ± 0.78	3.64 ± 0.94	0.512
Cr	46.2 ± 10.4	44.5 ± 10.8	44.4 ± 9.43	0.604
Cu	1547 ± 162	1594 ± 88	1557 ± 123	0.496
Fe	4650 ± 676	4649 ± 661	4665 ± 673	0.966
Mg	25,680 ± 3336	25,267 ± 3130	25,440 ± 3148	0.485
Mn	30.2 ± 5.86	30.2 ± 4.6	29.1 ± 4.3	0.760
Mo	24.4 ± 2.5	22.3 ± 3.6	24.5 ± 3.5	0.110
P	162,756 ± 20,009	166,784 ± 18,049	164,567 ± 18,260	0.358
Pb	81.9 ± 15.8	83.2 ± 10.8	80.0 ± 13.0	0.756
Sr	67.2 ± 11.8	64.6 ± 17.0	67.6 ± 11.1	0.733[a]
Zn	1569 ± 143	1587 ± 197	1561 ± 123	0.808

[a] Kruskal–Wallis test was used to analyze the differences, for inhomogeneous variances by Levene's test.

ment, but some element concentrations in diluted solutions would be near or even below the LOD, which makes results suspect. So, 0.5 mL rat serum was used to examine the effects of dilution rate. Six aliquots of 0.5 mL undispersed rat serum were taken, placed into six 10-mL beakers respectively. After 1.5 mL nitric acid and 0.25 mL perchloric acid were added, they were digested to nearly dryness as described in 2.2. Three of the residues were diluted 6 times to 5 mL with 1% nitric acid, and the rest were diluted 30 times to 15 mL with 1% nitric acid. The element contents in the serum were measured against the relevant reagent blanks. The results from different dilution rates were listed in Table 4, displaying that dilution did not make obvious impact on determination.

0.1 mL, 0.5 mL and 2 mL undispensed rat serum were transferred into three 10-mL beakers, then 0.5 mL, 1.5 mL and 5 mL nitric acid were added in terms of the serum amount, and all were added 0.25 mL perchloric acid. The residues were dissolved in 3 mL of 1% nitric acid after digestion respectively, and the relevant blanks were made accordingly. Serum with different sampling volume was analyzed in triplicate, respectively. The comparison of results in Table 4 showed that the contents of the same element from different sampling volumes were very close too, proving that 0.1 mL serum is enough for quantitation by ICP-MS and that various subpackage volume can be optioned for different purpose. Finally, after verifying the homogeneity of variances by Levene's test, one-way ANOVA analysis ($p > 0.05$) revealed that no significant differences were observed between sampling volume and dilution rate groups.

0.1 mL rat serum was taken out from undispersed rat serum and put into a 10-mL beaker. The serum was digested and analyzed under the proposed procedure. The results for element contents in comparison with those obtained from 0.1 mL dispersed rat serum packed in vials was exhibited in Table 2. There were no significant differences between dispersed and undispersed sera by one-way ANOVA analysis based on the homogeneous variances by Levene's test. In addition, for the determination of 12 main trace elements in undispersed serum, the uncertainties were at the same level as those for 0.1 mL dispensed rat serum listed in Table 2, which indicated that subpackaging serum did not affect element measurement and did not bring any contamination either.

Keeping the quality constant during a certain storage period is essential for a reference material. To examine the stability of the self-made candidate rat serum reference material stored at −20 °C, the contents of 12 main trace elements in the serum of 0.1 mL packaging were measured in successive 4 months. Apparently, no significant differences were observed from Table 5 by using one-way ANOVA and K–W tests according to the homogeneous and inhomogeneous variances, respectively.

0.1 mL independently packed rat serum candidate reference materials of the same batch freshly prepared were distributed to three laboratories for comparison purpose. The vials were transported for as long as 24 h in a common flask containing ice for medical use before they were parked in the refrigerator of other laboratory. The comparison of results for element content in three joined laboratories evaluated by ICP-MS are shown in Table 6. It is found that the all the uncertainties for the results form different laboratories were rather low, fundamentally meeting the requirement of detection of trace element in serum in different existing level. In fact, because the rat serum loaded in the vial was fixed, the amount of elements of interest was changeless during the once-use of the whole candidate rat serum even after frosting and thaw. Moreover, one-way ANOVA or K–W test indicated that the results did not vary significantly ($p > 0.05$) according to the homogeneity of variances.

Table 6
Inter-laboratory difference of elements contents in candidate rat serum reference material ($n = 3$).

Element	Content (mean ± U, $k = 2$) (ng mL^{-1})			One-way ANOVA test p values
	Lab 1	Lab 2	Lab 3	
Cd	2.46 ± 0.66	2.32 ± 0.56	2.51 ± 0.63	0.293
Co	3.19 ± 0.73	3.45 ± 0.74	3.27 ± 0.75	0.171
Cr	34.7 ± 8.5	33.7 ± 10.4	36.8 ± 8.9	0.193[a]
Cu	1295 ± 86	1246 ± 71	1242 ± 115	0.150
Fe	5407 ± 780	5217 ± 850	5507 ± 798	0.139
Mg	24,386 ± 3003	25,639 ± 3154	25,066 ± 3674	0.148[a]
Mn	13.5 ± 2.7	12.3 ± 3.4	13.7 ± 2.7	0.188
Mo	20.7 ± 3.5	20.4 ± 3.3	18.8 ± 2.0	0.170
P	154,247 ± 22,409	154,172 ± 16,887	147,899 ± 17,386	0.193[a]
Pb	33.0 ± 7.7	30.6 ± 7.2	29.5 ± 6.7	0.219
Sr	76.9 ± 17.0	76.8 ± 12.3	71.6 ± 13.7	0.148[a]
Zn	1454 ± 134	1411 ± 165	1363 ± 134	0.133

[a] Kruskal–Wallis test was used to analyze the differences, for inhomogeneous variances by Levene's test.

It is most noticeable that the rat serum reference material was prepared without anything spiking and without lyophilization, so that its composition is identical to sera to be analyzed and the matrix effect is avoided, which is a key factor to guarantee the reliability of determination. On the other hand, because the contents of main trace elements in native serum are generally higher than LOQs of ultra-sensitive ICP-MS, the element enhancement is dispensable.

No significant differences were found between the results under different conditions including sampling volume, dispersing or not, dilution rate, storage time, inter-laboratories, respectively. The overall analysis merits implied that this candidate reference material based on unaltered rat serum matrix with stable and credible quality could be potentially adopted as the reference substance for ICP-MS analysis of trace elements in serum and other similar biological samples.

4. Conclusions

A novel candidate rat serum reference material for trace element determination has been developed aiming at the feature of ICP-MS. In spite that uniform values of elements labeled are unavailable for the rat sera of all batches, this reference substance can be expediently prepared and delivered, and directly used, because it is not freeze-dried, not element-spiked, independently packed, and the element content of a certain batch serum is certificated and stable during at least 4 months. This is the first attempt to prepare such a simple and convenient rat serum reference material of inorganic elements. This used-once rat serum with simple packing, well-defined levels of the analytes of interest and stable quality can in fact be reliably produced in the future.

Acknowledgments

This work was supported by National Natural Science Foundation of China (no. 20575027), National Basic Research Program of China (973 program, no. 2009CB421601), National Science Funds for Creative Research Groups (no. 20821063), and Analysis and Test Fund of Nanjing University.

References

[1] W. Kaim, B. Schwederski, Bioinorganic Chemistry: Inorganic Elements in the Chemistry of Life, Wiley, Chichester, 1994.
[2] D.M. Taylor, D.R. Williams, Trace Element Medicine and Chelation Therapy, Royal Society of Chemistry, Cambridge, 1995.
[3] P.J. Parsons, F. Barbosa, Spectrochim. Acta B 62 (2007) 992.
[4] C.S. Muniz, J.M. Larchante-Gayon, J.I.G. Alonso, A. Sanz-Medel, J. Anal. Atom. Spectrom. 14 (1999) 193.
[5] J.A.C. Broekaert, Spectrochim. Acta B 55 (2000) 739.
[6] A. Sanz-Medel, Analyst 125 (2000) 35.
[7] H.T. Chen, S.Q. Cao, X.J. Zeng, Chin. J. Anal. Chem. 29 (2001) 592.
[8] E. Hoffmann, C. Ludke, J. Skole, H. Stephanowitz, J. Wollbrandt, W. Becker, Spectrochim. Acta B 57 (2002) 1535.
[9] L.H. Reyes, J.M.M. Gayon, J.I.G. Alonso, A. Sanz-Medel, J. Anal. Atom. Spectrom. 18 (2003) 11.
[10] D. Schaumlöffel, P. Giusti, M.V. Zoriy, C. Pickhardt, J. Szpunar, R. Łobiński, J.S. Becker, J. Anal. Atom. Spectrom. 20 (2005) 17.
[11] R. Łobiński, D. Schaumlöffel, J. Szpunar, Mass Spectrom. Rev. 25 (2006) 255.
[12] J.A. Nóbrega, M.C. Santos, R.A. de Sousa, S. Cadore, R.M. Barnes, M. Tatro, Spectrochim. Acta B 61 (2006) 465.
[13] L.L. Petrov, E.A. Anchutina, Y.N. Kornakov, L.A. Persikova, Spectrochim. Acta B 58 (2003) 265.
[14] H. Ihara, N. Hashizume, T. Matsubayashi, K. Futaki, M. Yoshida, N. Sagawa, M. Fujisaki, K. Mita, A. Kadota, J. Clin. Lab. Anal. 18 (2004) 240.
[15] R.D. Josephs, R. Krska, S. MacDonald, P. Wilson, H. Pettersson, Anal. Bioanal. Chem. 378 (2004) 1182.
[16] R.E. Sturgeon, S.N. Willie, L. Yang, R. Greenberg, R.O. Spatz, Z. Chen, C. Scriver, V. Clancy, J.W. Lam, S. Thorrold, J. Anal. Atom. Spectrom. 20 (2005) 1067.
[17] R. Krska, E. Welzig, E. Drs, R.D. Josephs, R.C. Schothorst, H.P. van Egmond, H. Pettersson, D. Chan, S. MacDonald, J. AOAC Int. 89 (2006) 1573.
[18] B.C. Reynolds, J. Aggarwal, L. Andre, D. Baxter, C. Beucher, M.A. Brzezinski, E. Engstrom, R.B. Georg, M. Land, M.J. Leng, S. Opfergelt, I. Rodushkin, H.J. Sloane, S.H.J.M. van den Boorn, P.Z. Vroon, D. Cardinal, J. Anal. Atom. Spectrom. 22 (2007) 561.
[19] National Standard Substance Research Center, http://www.gbw114.com/class_content.asp?id=1907.
[20] National Standard Substance Research Center, http://www.gbw114.com/class_content.asp?id=1889.
[21] NIST SRM 1598, NIST renews benchmark SRMs for accurate determinations of trace elements in serum and liver, http://www.cstl.nist.gov/projects/fy06/health0683904.pdf.
[22] X.L. Cai, Y.J. Chen, L.M. Dai, H.Z. Lian, Spectrosc. Spect. Anal. 26 (2006) 2125.
[23] M.S. Levenson, D.L. Banks, K.R. Eberhardt, L.M. Gill, W.F. Guthrie, H.K. Liu, M.G. Vangel, J.H. Yen, N.F. Zhang, J. Res. Natl. Inst. Stand. Technol. 105 (2000) 571.
[24] R. Kellner, J.-M. Mermet, M. Otto, M. Valcárcel, H.M. Widmer (Eds.), Analytical Chemistry, second ed., Wiley–VCH, Weinheim, 2004.
[25] T. Watanabe, K. Kato, N. Matsumoto, T. Maeda, Talanta 72 (2007) 1655.
[26] J. Caro, M. Gallego, Talanta 76 (2008) 847.

Talanta 78 (2009) 1497–1502

Contents lists available at ScienceDirect

Talanta

journal homepage: www.elsevier.com/locate/talanta

Short communication

Coupling poly-(methacrylic acid-co-ethylene glycol dimethacrylate) monolith microextraction to capillary electrophoresis for the determination of phenols in water samples

Tingting Li[a], Qiong Jia[a,*], Lihua Song[a], Riyan Su[a], Yin Lei[a], Weihong Zhou[a], Hongfei Li[b]

[a] College of Chemistry, Jilin University, Changchun 130022, China
[b] State Key Laboratory of Rare Earth Resources and Application, Changchun Institute of Applied Chemistry, Chinese Academy of Sciences, Changchun 130022, China

ARTICLE INFO

Article history:
Received 11 November 2008
Received in revised form 7 February 2009
Accepted 9 February 2009
Available online 20 February 2009

Keywords:
Poly-(methacrylic acid-co-ethylene glycol dimethacrylate) monolith microextraction
Capillary electrophoresis
Catechol
Resorcinol
2,6-Dimethylphenol
2,4,6-Trinitrophenol

ABSTRACT

In the present work, a simple, selective, and sensitive method has been proposed for the determination of four phenols (catechol, resorcinol, 2,6-dimethylphenol, and 2,4,6-trinitrophenol) in water samples. The method is based on poly-(methacrylic acid-co-ethylene glycol dimethacrylate) monolith microextraction (PMME) and capillary electrophoresis–ultraviolet (CE–UV) analysis. The operation parameters including sample pH, sample flow rate, sample volume, and eluent flow rate have been studied and optimized. Under the optimal experimental conditions the limits of detection for catechol, resorcinol, 2,6-dimethylphenol, and 2,4,6-trinitrophenol based three times of standard deviations of blank by seven replicates are 0.085, 0.030, 0.159 and 0.006 μg/mL, respectively. The intra-day and inter-day relative standard deviations are less than 5.6% and 5.9%. The proposed method has been successfully applied to the determination of the four phenols in water samples and the accuracy is assessed through recovery experiments.

1. Introduction

As a class of organic pollutants in aquatic media, phenols and their substitutes are of great environmental concern owing to their high toxicity. The decomposition of phenols is difficult due to, principally, their stability and their solubility in water. Because of their high toxicity, as well as their unpleasant organoleptic properties, some phenols have been included in the priority pollution list of the European Union (EU) and US Environmental Protection Agency (EPA). Therefore, the determination of trace phenols is very important for evaluating the total toxicity of an environmental water sample. Various methods, such as spectrophotometry [1,2], electrochemical methods [3–7], gas chromatography (GC) [8,9], GC–mass spectrometry (GC–MS) [10–13], liquid chromatography (LC) [14–20], LC–MS [21], and capillary electrophoresis (CE) [22–38] have been described in the literatures for the detection of phenolic compounds in water samples. Some authors have even reviewed the determination of phenols [39,40].

Among the various methods, GC and HPLC have been commonly used for the determination of individual phenols. As a powerful complementary new technique to GC and HPLC, CE has been shown to be a rapid, powerful and efficient technique for separating phenols due to its major merit of high separation efficiency, no need of organic solvent for separation, extremely low solvent consumption, small sample volume requirement, ease of automation, and low running cost. This technique avoids the derivatization procedure and allows the accomplishment of well-resolved separations in less time than that usually taken by chromatographic methods [22,26,34,37]. In Table 1, various reported CE procedures for the determination of phenols are summarized. Many authors have reported the determination of catechol [21,23,25,28–30,35,36,40], resorcinol [22–26,28–32,35,36], 2,6-dimethylphenol [27,30,33–35], and 2,4,6-trinitrophenol [37,38] with CE. For instance, Xie et al. [23] developed a capillary zone electrophoresis method coupling square wave amperometric detection for the determination of catechol and resorcinol. The efficacy of the boric acid and ascorbic acid in the running buffer was discussed. The limits of detection of the method were in the range of 0.5–1.5 μmol/L. Kaniansky et al. [38] investigated the use of β-CD and polyvinylpyrrolidone as complexing agents to capillary zone electrophoretic separations of a group of 10 nitrophenols. Rain, drinking and process water samples were employed as matrices to assess the practical applicability of the procedure. The limit of detection of 2,4,6-trinitrophenol was determined as 0.046 μg/mL.

Nevertheless, CE techniques usually suffer from poor detection sensitivity, especially in the conventional UV absorbance detection

* Corresponding author. Tel.: +86 431 85095622; fax: +86 431 85095622.
E-mail address: jiaqiong@jlu.edu.cn (Q. Jia).

0039-9140/$ – see front matter © 2009 Elsevier B.V. All rights reserved.
doi:10.1016/j.talanta.2009.02.021

Table 1
Application of capillary electrophoresis to the determination of phenols.

Phenols	Buffer	Mode	Detection method	Limit of detection	Application	Ref.
Catechol	$Na_2B_4O_7$ and Na_2HPO_4	CZE	Chemiluminescence	8.4×10^{-8} mol/L	Hair dye	[22]
	Ammonium borate and ascorbic acid	CZE	Square wave amperometry	1.5 μmol/L	Environmental wastewater	[23]
	Borax and Na_2CO_3	CZE	DAD	6.70×10^{-6} mol/L	Wastewater from river	[25]
	Borax	CZE	UV	2.4 μg/mL		[28]
	Na_2HPO_4	CE	Electrochemistry	0.80 μmol/L	–	[29]
	Phosphate and borate/phosphate buffer containing SDS	CZE/MEKC	UV	–	Oil shale	[30]
	NaH_2PO_4, Na_2HPO_4, MES	EKC	UV	–	–	[35]
	Sodium phosphate and *p*-sulfonic calix[4]arene	CE	UV	37.8 pg	–	[36]
	Borax and SDS	CE	UV	0.085 μg/mL	Environmental water	Present work
Resorcinol	$Na_2B_4O_7$ and Na_2HPO_4	CZE	Chemiluminescence	3.7×10^{-7} mol/L	Hair dye	[22]
	Ammonium borate and ascorbic acid	CZE	Square wave amperometry	1.0 μmol/L	Environmental wastewater	[23]
	Disodium tetraborate	CZE	UV	–	Tincture piyanning	[24]
	Borax and Na_2CO_3	CZE	DAD	5.13×10^{-6} mol/L	Wastewater from river	[25]
	Benzyltriethylammonium chloride, tetrabutylammonium acetate, 1-butyl-3-methyl imidazolium trifluoroacetate, and 1-butyl-3-methyl imidazolium heptafluorobutanoate	CE	UV	–	–	[26]
	Borax	CZE	UV	1.6 μg/mL	–	[28]
	Na_2HPO_4	CE	Electrochemistry	4.12 μmol/L	–	[29]
	Phosphate and borate/phosphate containing SDS	CZE/MEKC	UV	–	Oil shale	[30]
	NaAc + TMA, TEA, DMP, and PDADMA	CEKC	UV	–	–	[31]
	MES, PEI, and methanol (or acetonitrile)	CEKC	UV	–	–	[32]
	NaH_2PO_4, Na_2HPO_4, and MES	EKC	UV	–	–	[35]
	Sodium phosphate and *p*-sulfonic calix[4]arene	CE	UV	33.2 pg	–	[36]
	Borax and SDS	CE	UV	0.030 μg/mL	Environmental water	Present work
2,6-Dimethylphenol	TBABr, TBACl, TBAP, TBAAc, TBAOH	CE	UV	–	–	[27]
	Phosphate and borate/phosphate containing SDS	CZE/MEKC	UV	–	Oil shale	[30]
	Sodium tetraborate decahydrate, KH_2PO_4, and SDS	EKC	UV	–	–	[33]
	HCl and Brij-S	CE	UV	–	–	[34]
	NaH_2PO_4, Na_2HPO_4, and MES	EKC	UV	–	–	[35]
	Borax and SDS	CE	UV	0.159 μg/mL	Environmental water	Present work
2,4,6-Trinitrophenol	Glycine, BTP, *m*-HEC, and PVP/glycine, BTP, *m*-HEC, and Cl^-	CZE/ITP-CZE	UV	46/2.9 μg/L	Rain, process, drinking water	[37]
	β-CD, PVP, and *m*-HEC	CZE	UV	0.046 μg/mL	Rain, drinking, process water	[38]
	Borax and SDS	CE	UV	0.006 μg/mL	Environmental water	Present work

–, not mentioned

because the system has the intrinsic drawbacks of short optical path length and low volume load ability [23,37]. In order to improve the limited sensitivity in CE, coupling of CE to sample preconcentration techniques such as extraction, evaporation, and dialysis is an effective approach to determine analytes present at low levels in environmental samples.

Conventional extraction methods, such as liquid–liquid extraction (LLE) and solid-phase extraction (SPE) are the most commonly used techniques for preconcentration and cleanup of phenols [8,10,14–16,18–21,39,40]. However, these methods involving multistep procedures are complex, laborious and time-consuming. Besides, LLE requires large volumes of organic solvent, making it environmentally unfriendly and a potential danger to human health. With respect to sample preconcentration, miniaturization of the pretreatment system has become the recent trend in consideration of the environmental compatibility and the high capability of the analytical systems. Recently, solid-phase microextraction (SPME), stir bar sorptive extraction (SBSE) and liquid-phase microextraction (LPME) have been applied to the extraction of phenols from water samples [9,11–13,17]. SPME is a solvent-free extraction technique that incorporates sample pretreatment, concentration and sample introduction into a single procedure. But SPME fiber is fragile and has limited lifetime, and the sample carryover is also a problem. SBSE is based on the same principles as those of SPME but has much higher recoveries and higher sample capacity than the latter. To date, PDMS is the only commercialized coating for SBSE, which restricts the application of SBSE to the extraction of polar compounds [17]. LPME has also been successfully applied to the extraction of organic compounds from aqueous matrices. However, the major problem of conventional LPME is that the volume of extractant is too small, which leads to relatively less precision and low sensitivity [13].

As an alternative to SPME, a methodology for polymer monolith microextraction (PMME) based on the use of a capillary monolithic column was introduced in 2006 [41]. Compared with conventional SPME methods, the monolithic structure has a larger surface area and emerges as a more popular alternative to packed columns due to the simplicity of its preparation. The in-tube configuration is better at protecting the extraction material from physical damage. In addition, the convective mass transfer procedure and low pressure-drop offered by the porous structure can facilitate the extraction process. So far, poly-(methacrylic acid-ethylene glycol dimethacrylate) (MAA-EGDMA) and poly-(acrylamide-vinylpyridine-*N*,*N*′-methylene bisacrylamide) (AA-VP-Bis) have been employed for the preparation of PMME monolithic column [41–50]. Poly-(MAA-EGDMA) monolith microextraction is widely applied to the determination of angiotensin II receptor antagonists [41], ephedrine and pseudoephedrine [42], opiates [43] and sulfonamides [44] when coupled with CE. The combination of poly-(MAA-EGDMA) monolith extraction of chloramphenicol [45], hexanal and heptanal [46], and nitric oxide [47–49] with HPLC has also been investigated. PMME can not only enrich the analytes, but also purify the sample and thus reduce the effect of the sample matrix. It is proved to be inexpensive and applicable for a common laboratory to achieve comparable sensitivity.

The work presented here is to study the combination of poly-(MAA-EGDMA) monolith microextraction with CE for the determination of phenols. Catechol, resorcinol, 2,6-dimethylphenol, and 2,4,6-trinitrophenol are chosen as respensitives. The objective of this study is to extend the potential use of the PMME technique to determine phenolic compounds in water samples. Parameters affecting the extraction efficiency have been investigated. Under the experimental conditions, the proposed method is validated for the quantitative analysis and applications to tap water, lake water, rain water, and industrial wastewater samples have been illustrated.

2. Experimental

2.1. Instrumentation and electrophoretic conditions

The poly-(MAA-EGDMA) monolithic capillary tube was kindly supplied by Prof. Feng of Wuhan University. The synthesizing method has been described previously [41–49]. The PMME apparatus consists of a regular plastic syringe (1 mL), the poly-(MAA-EDGMA) monolithic capillary tube (50 μm i.d. × 3 cm) and a plastic pinhead (one part of the whole syringe). The syringe barrel was coupled seamlessly to one end of the pinhead, while on the other end of the pinhead, the metallic needles were removed and replaced by a 3 cm monolithic capillary tube (cut from the prepared monolithic capillary) with adhesive.

For the CE analysis, a 1229-HPCE Analyser (Binta Instrument Technology Co., Ltd., Beijing, China) equipped with a UV detector (214 or 254 nm) was employed, which comprised a ±30 kV high voltage power supply, and an uncoated fused-silica capillary (Yongnian Fiber Plant, Hebei, China) of 50 μm i.d. and an effective length of 51 cm (total length 60 cm). The UV absorbance detection was performed at 254 nm.

A mixing solution containing 0.05 mol/L borax and 0.02 mol/L sodium dodecyl sulfate (SDS) was chosen as the separation buffer. Before use, the electrolyte solutions were filtered through a 0.45 μm microfilter and degassed in an ultrasonic bath for 5 min. The capillary was conditioned every day with 0.1 mol/L NaOH for 20 min and then with deionized water for 10 min in order to obtain a stable baseline and to improve the reproducibility of the migration time. Before each injection the capillary was flushed with 0.1 mol/L NaOH, deionized water and running buffer for 5 min each, successively. At the end of day, the capillary was flushed with 0.1 mol/L NaOH for 10 min and finally rinsed with water overnight. Electrophoretic separations were carried out at positive power supply of 18 kV, maintaining the capillary temperature at 25 °C.

For pH measurements, a pHS-3C digital pH meter (Shanghai Rex Instruments Factory, China) was used.

The Milli-Q SP system (Millipore, Milford, MA, USA) was employed to prepare deionized water.

2.2. Reagents and materials

Catechol, resorcinol, 2,6-dimethylphenol, and 2,4,6-trinitrophenol were purchased from Guangzhou Chemical Reagent Industries (Guangzhou, China). The stock solutions of catechol and resorcinol were prepared in water while those of 2,6-dimethylphenol and 2,4,6-trinitrophenol were prepared in an ethanol–water (1:1) mixture. All the stock solutions were stored at 4 °C protected against daylight. Working solutions were prepared by appropriate dilution from the individual stocks. Borax, SDS, Na_2HPO_4, H_3PO_4, NaOH, methanol, and ethanol were all of analytical reagent grade.

Tap water was collected from our lab, and lake water was obtained from a lake nearby. Rain water sample was collected from Changchun (Jilin province, China) on September 22nd, 2008. Industrial wastewater samples were collected from urban wastewater treatment plants. Acid-cleaned polyethylene bottles were used for water sampling. All the samples were analyzed after simple filtering with a 0.45 μm micropore membrane, and stored at the temperature of 4 °C after collection.

2.3. PMME procedure

The whole PMME procedure was composed of precondition, sample loading, washing, and desorption. A TS2-60 programmable syringe pump (Baoding Longer Precision Pump Co., Ltd, Hebei, China) was employed for delivery by providing smooth and regular

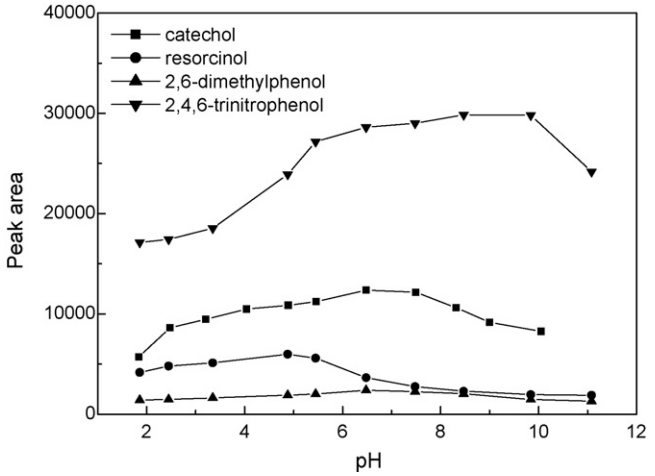

Fig. 1. Effect of sample pH on the PMME. Phenols concentration = 6.50 μg/mL, sample flow rate = 0.075 mL/min, sample volume = 1.0 mL, eluent flow rate = 0.10 mL/min, extraction conditions and CE conditions are outlined in Section 2.

movement of the syringe plunger in a high reproducible manner, automatically. In the precondition step, the syringe was filled with 0.2 mL methanol, which was then ejected via the monolithic capillary tube at 0.05 mL/min by the syringe pump, and then 0.5 mL Na_2HPO_4 (pH 6.50) was ejected at a flow rate of 0.15 mL/min. Then the sample solution was passed through the monolithic capillary by the pump. In the washing step, 0.2 mL Na_2HPO_4 (pH 6.50) was kept to flow through the monolithic capillary tube at a flow rate of 0.15 mL/min in order to eliminate the residual sample solution and the adsorbed sample matrix. Then residual solution in the pinhead and monolithic capillary tube was pushed out with an empty and clean syringe to avoid polluting the eluate. In the desorption step, the desorption solution (0.1 mL ethanol) was injected via the monolithic capillary tube and the eluate was collected for the analysis by CE. In order to avoid contamination, special syringes were used for injecting sample, buffer, and desorption solution, respectively.

3. Results and discussion

3.1. Optimization of PMME conditions

3.1.1. Effect of sample pH values

Sample pH is an important parameter in achieving quantitative adsorption and recovery of analytes. It not only influences the molecule form of the analytes but also relates closely to the interactions between analytes and the extraction material. In order to evaluate the effect of sample pH, the standard solutions containing 6.50 μg/mL catechol, resorcinol, 2,6-dimethylphenol, and 2,4,6-trinitrophenol have been loaded onto the poly-(MAA-EDGMA) monolithic capillary after pH adjustment using H_3PO_4 or NaOH solutions. The effect of sample pH within the range of 2.0–11.0 is shown in Fig. 1. It is obvious that the peak area increases firstly but decreases at higher pH values for all the four phenols. This may be because the interaction between the analytes and the monolithic column is mainly based on the hydrophobic interactions and the ion-exchange sites, which arise from the polymer bone structure and its acidic pendant groups [42]. When pH is too low, the ion-exchange interaction decreases because the carboxyls on the monolithic column are difficult to be ionized. The decrease of the peak area at higher pH could be attributed to the deprotonation of the analytes and the resulted electrostatic repulsion between the analytes and the monolithic column. A pH of 6.50 is selected in subsequent experiments.

3.1.2. Effect of sample flow rate

The effect of sample flow rate (0.05–0.30 mL/min) on the sorption of phenols (6.50 μg/mL) has been investigated. The peak area does not change much at a flow rate greater than 0.20 mL/min for catechol, resorcinol, and 2,6-dimethylphenol in the tested range. However, for 2,4,6-trinitrophenol, the peak area reaches a maximum value at 0.075 mL/min and then decreases with an increasing sample flow rate. Too low flow rate is not employed in order to avoid long extraction time while too fast flow rate may cause less contact time between the analytes and the sorbents. In this work, a sample flow rate of 0.20 mL/min is chosen in the experiments due to the shorter extraction time and the acceptable back-pressure of the monolith capillary.

3.1.3. Effect of sample volume

The effect of the sample volume on the peak has been studied in the range of 0.5–3.0 mL at a constant flow rate of 0.20 mL/min in extracting 6.50 μg/mL standard sample solutions. The peak area increases with increasing 2,4,6-trinitrophenol sample volume but changes little for the other three phenols. This result is different from previous work [42–45]. When poly-(MAA-EGDMA) monolithic capillary column is employed for the extraction of opiates from 0.5 to 3 mL, the signals increases with increasing sample volume up to 2 mL. However, when the sample volume is higher than 2 mL, the signals of some analytes reach equilibrium while those of the others keep increasing [43]. The sample volume should be chosen according to the sensitivity required and the time acceptable for a whole analysis. The increase of the sample volume is not desirable because the total time needed for an analysis will be prolonged. In the present study, a sample volume of 1.0 mL is chosen for subsequent analysis.

3.1.4. Optimization of desorption conditions

The poly-(MAA-EGDMA) monolithic microextraction is off-line combined with CE, the desorption procedure after extraction has been investigated to achieve an accurate quantitative analysis of the phenols. In the present work, ethanol is employed as the eluent. The less is the eluent volume, the higher is the detection sensitivity. After a desorption process with 0.1 mL ethanol, no peak has been found in the following blank analysis. Therefore, 0.1 mL ethanol is chosen as the eluent to desorb the analytes from the sorbent. The effects of eluent flow rate on the peak area have also

Table 2
Calibration curves, LOD, LOQ, intra-day and inter-day precision of peak areas for PMME of phenols.[a]

Phenols	Linear range (μg/mL)	Calibration curves			LOD (μg/mL)	LOQ (μg/mL)	Precision (%R.S.D.)	
		Slope	Intercept	r			Intra-day (n = 7)	Inter-day (n = 7)
Catechol	0.4–26	1015.7	4554.2	0.9997	0.085	0.284	2.9	2.5
Resorcinol	0.1–26	688.5	357.2	0.9993	0.030	0.098	4.5	5.9
2,6-Dimethylphenol	0.4–26	263.2	129.1	0.9991	0.159	0.530	5.6	5.0
2,4,6-Trinitrophenol	0.03–26	5762.6	1095.0	0.9991	0.006	0.021	2.0	1.2

[a] %R.S.D. are for phenols at a concentration of 6.50 μg/mL.

Table 3
Extraction recoveries (%) of phenols in water samples ($n = 3$).[a].

	Catechol	Resorcinol	2,6-Dimethylphenol	2,4,6-Trinitrophenol
Tap water sample				
Found (μg/mL)	–	–	–	–
Recovery (%)				
Level1	93.8	102.5	82.5	97.0
Level2	84.2	100.8	91.5	96.3
Level3	87.4	91.3	96.5	98.6
Lake water sample				
Found (μg/mL)	–	–	–	–
Recovery (%)				
Level1	82.5	88.0	88.1	80.2
Level2	89.9	90.0	82.7	81.3
Level3	85.2	88.7	87.6	84.3
Rain water sample				
Found (μg/mL)	–	–	–	–
Recovery (%)				
Level1	81.0	100.3	84.0	93.0
Level2	86.4	88.9	92.5	97.3
Level3	83.9	97.8	83.5	95.0
Industrial wastewater sample 1				
Found (μg/mL)	–	0.90	0.19	–
Recovery (%)				
Level1	82.3	80.7	90.9	86.9
Level2	91.0	82.5	95.0	90.7
Level3	92.2	88.3	86.0	80.8
Industrial wastewater sample 2				
Found (μg/mL)	4.12	0.33	0.43	0.10
Recovery (%)				
Level1	93.2	84.5	92.4	88.7
Level2	81.5	85.0	86.2	82.3
Level3	90.7	89.5	89.3	86.5

–, not detected. The concentrations of catechol, resorcinol, 2,6-dimethylphenol, and 2,4,6-trinitrophenol spiked to the water samples are 1.0, 1.0, 1.0, 0.5 μg/mL (Level1); 5.0, 5.0, 5.0, 0.5 μg/mL (Level2); and 15.0, 15.0, 15.0, 1.0 μg/mL (Level3), respectively.

[a] Extraction conditions and CE conditions are outlined in Section 2.

been investigated in the range of 0.025–0.175 mL/min. A flow rate of 0.10 mL/min is chosen in the experiments to obtain fast desorption and satisfactory desorption efficiency.

3.2. Analytical figures of merit

Under the optimized experimental conditions, a summary of the time required for the PMME procedure can be obtained. 16 min is enough for the PMME procedure. The whole analysis of phenols including the PMME and CE procedures can be achieved within 20 min, indicating that the proposed method is a rapid one for the determination of phenols.

In order to evaluate the efficiency of the proposed method, calibration curves have been constructed with a series of standard samples under the optimal experimental conditions. Results are listed in Table 2. It can be seen that the regression coefficients (r) are always greater than 0.9991.

The limits of detection (LOD), calculated using the IUPAC recommendation (based on three times the standard deviation of the peak area), have been obtained for the phenols. The limits of quantitation (LOQ), calculated as ten times its standard deviation, have also been calculated. Results are also shown in Table 2, showing that the proposed method has low LOD and LOQ values.

The reproducibility of the developed method is determined by the intra-day and inter-day precisions. The intra-day relative standard deviations (R.S.D.) are determined at a known concentration of catechol, resorcinol, 2,6-dimethylphenol, and 2,4,6-trinitrophenol in seven replicates. The inter-day precision is similarly evaluated on several days up to 3 successive days. Every day, a new calibration graph is constructed. The intra-day and inter-day precisions of the peak areas are lower than 5.6% and 5.9%, respectively, indicating

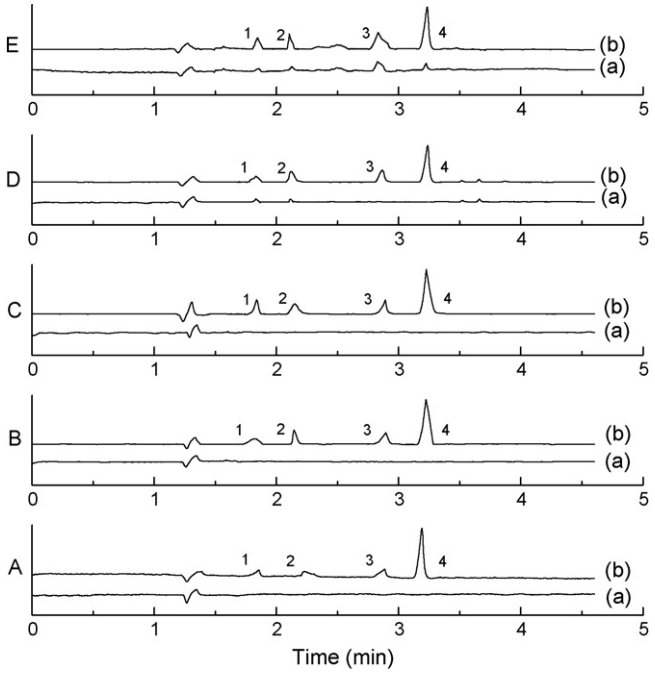

Fig. 2. Electropherograms obtained by PMME-CE of tap water (A), lake water (B), rain water (C), industrial wastewater 1 (D), and industrial wastewater 2 (E). (a) Blank water sample, (b) water sample spiked with Level2. Peaks: (1) resorcinol, (2) 2,6-dimethylphenol, (3) catechol, and (4) 2,4,6-trinitrophenol. Level2 is as shown in Table 3; extraction conditions and CE conditions are outlined in Section 2.

high precision of the proposed method. Both intra-day and inter-day precisions are calculated as R.S.D.s for seven measurements.

In order to examine the stability of the poly-(MAA-EDGMA) monolithic capillary under the experimental conditions, the reusability of the capillary has been investigated. It is observed that no significant changes in the back-pressure and extraction efficiency of the capillary column are verified after 3 months of operation. Therefore, multiple use of the monolithic capillary is feasible.

3.3. Analysis of water samples

Under the optimized conditions, the method has been applied to the simultaneous determination of phenols in tap water, lake water, rain water, and industrial wastewater samples. The utility of this method is examined using recovery studies by adding phenols in blank water samples at different concentration levels. Triplicate injections of the sample are carried out for the determination. Results are shown in Table 3 and Fig. 2. The recoveries are in the range of 80.2–102.5%, indicating that the proposed method is effective for the determination of phenols in water samples.

4. Conclusions

A method combining poly-(methacrylic acid-co-ethylene glycol dimethacrylate) monolith microextraction with capillary electrophoresis has been developed and validated for the determination of four phenols, catechol, resorcinol, 2,6-dimethylphenol, and 2,4,6-trinitrophenol in environmental water samples. Variable parameters including sample pH, sample flow rate, sample volume, and eluent flow rate are studied. The stability, precision, linearity and accuracy have been investigated. Based on the results, the method is proved to be simple, fast, sensitive, selective, and suitable for the purpose for the determination of phenols in water samples.

Acknowledgements

The authors wish to thank the valuable discussion and experimental assistance from Prof. Yuqi FENG of Wuhan University, Prof. Yumei TIAN of Jilin University, and Prof. Jianbo JIA of Changchun Institute of Applied Chemistry, Chinese Academy of Sciences. This project was partly supported by the National Basic Research Program of China (2006CB403302).

References

[1] K.O. Lupetti, F.R.P. Rocha, O. Fatibello-Filho, Talanta 62 (2004) 463.
[2] G. Norwitz, N. Nataro, P.N. Keliher, Anal. Chem. 58 (1986) 639.
[3] J. Kochana, A. Gala, A. Parczewski, J. Adamski, Anal. Bioanal. Chem. 391 (2008) 1275.
[4] A.S. Santos, A.C. Pereira, M.D.P.T. Sotomayor, C.R.T. Tarley, N. Duran, L.T. Kubota, Electroanalysis 19 (2007) 549.
[5] J.G. Sun, G.F. Wang, S.F. Jiao, Y. Wei, B. Fang, Chin. J. Anal. Chem. 35 (2007) 335.
[6] M.A. Kim, W.Y. Lee, Anal. Chim. Acta 479 (2003) 143.
[7] C.D. Garcia, P.I. Ortiz, Anal. Sci. 15 (1999) 461.
[8] P. Bartak, P. Frnkova, L. Cap, J. Chromatogr. A 867 (2000) 281.
[9] H. van Doorn, C.B. Grabanski, D.J. Miller, S.B. Hawthorne, J. Chromatogr. A 829 (1998) 223.
[10] A. Kovacs, A. Kende, M. Mortl, G. Volk, T. Rikker, K. Torkos, J. Chromatogr. A 1194 (2008) 139.
[11] M. Llompart, M. Lourido, P. Landin, C. Garcia-Jares, R. Cela, J. Chromatogr. A 963 (2002) 137.
[12] V. Pino, J.H. Ayala, V. Gonzalez, A.M. Afonso, Talanta 73 (2007) 505.
[13] L.W. Chung, M.R. Lee, Talanta 76 (2008) 154.
[14] N. Masque, M. Galia, R.M. Marce, F. Borrull, J. Chromatogr. A 771 (1997) 55.
[15] D. Puig, D. Barcelo, J. Chromatogr. A 778 (1997) 313.
[16] D. Puig, D. Barcelo, J. Chromatogr. A 733 (1996) 371.
[17] X.J. Huang, N.N. Qiu, D.X. Yuan, B.L. Huang, Talanta 78 (2009) 101.
[18] E. Pocurull, M. Calull, R.M. Marce, F. Borrull, J. Chromatogr. A 719 (1996) 105.
[19] E. Pocurull, R.M. Marce, F. Borrull, Chromatographia 41 (1995) 521.
[20] O. Busto, J.C. Olucha, F. Borrull, Chromatographia 32 (1991) 566.
[21] C. Nistor, A. Rose, M. Farre, L. Stoica, U. Wollenberger, T. Ruzgas, D. Pfeiffer, D. Barcelo, L. Gorton, J. Emneus, Anal. Chim. Acta 456 (2002) 3.
[22] X.D. Xu, Y.G. Hu, X.X. Li, Chin. J. Anal. Chem. 34 (2006) S151.
[23] T.Y. Xie, Q.W. Liu, Y.R. Shi, Q.Y. Liu, J. Chromatogr. A 1109 (2006) 317.
[24] H.X. Liu, A.M. Yu, J. Wu, X.Y. Mi, H.Q. Zhang, Chin. J. Pharm. Anal. 25 (2005) 838.
[25] X.F. Guo, Z.H. Wang, S.P. Zhou, Chin. J. Anal. Chem. 32 (2004) 489.
[26] R. Kuldvee, M. Vaher, M. Koel, M. Kaljurand, Electrophoresis 24 (2003) 1627.
[27] S.P. Porras, R. Kuldvee, S. Palonen, M.L. Riekkola, J. Chromatogr. A 990 (2003) 35.
[28] R.M. Liu, F.Y. He, J. Liaocheng Teachers Univ. (Nat. Sci.) 15 (2002) 39.
[29] W.C. Yang, X.D. Yu, A.M. Yu, H.Y. Chen, J. Chromatogr. A 910 (2001) 311.
[30] A. Ebber, Chromatographia 53 (Suppl.) (2001) S307.
[31] B. Maichel, K. Gogova, B. Gas, E. Kenndler, J. Chromatogr. A 894 (2000) 25.
[32] B. Maichel, B. Potocek, B. Gas, E. Kenndler, J. Chromatogr. A 853 (1999) 121.
[33] A.L. Gray, J.T. Hsu, J. Chromatogr. A 824 (1998) 119.
[34] W.L. Ding, J.S. Fritz, Anal. Chem. 70 (1998) 1859.
[35] B. Maichel, B. Potocek, B. Gas, M. Chiari, E. Kenndler, Electrophoresis 19 (1998) 2124.
[36] T. Zhao, X. Hu, J. Cheng, X. Lu, Anal. Chim. Acta 358 (1998) 263.
[37] D. Kaniansky, E. Krcmova, V. Madajova, M. Masar, Electrophoresis 18 (1997) 260.
[38] D. Kaniansky, E. Krcmova, V. Madajova, M. Masar, J. Marak, F.I. Onuska, J. Chromatogr. A 772 (1997) 327.
[39] I. Rodriguez, M.P. Llompart, R. Cela, J. Chromatogr. A 885 (2000) 291.
[40] D. Puig, D. Barcelo, Trends Anal. Chem. 15 (1996) 362.
[41] M. Zhang, F. Wei, Y.F. Zhang, J. Nie, Y.Q. Feng, J. Chromatogr. A 1102 (2006) 294.
[42] F. Wei, M. Zhang, Y.Q. Feng, J. Chromatogr. B 850 (2007) 38.
[43] F. Wei, M. Zhang, Y.Q. Feng, Electrophoresis 27 (2006) 1939.
[44] T. Li, Z.G. Shi, M.M. Zheng, Y.Q. Feng, J. Chromatogr. A 1205 (2008) 163.
[45] J.F. Huang, H.J. Zhang, Y.Q. Feng, J. Agric. Food Chem. 54 (2006) 9279.
[46] H.J. Zhang, J.F. Huang, B. Lin, Y.Q. Feng, J. Chromatogr. A 1160 (2007) 114.
[47] K.J. Huang, M. Zhang, W.Z. Xie, H.S. Zhang, Y.Q. Feng, H. Wang, J. Chromatogr. B 854 (2007) 135.
[48] K.J. Huang, M. Zhang, W.Z. Xie, H.S. Zhang, Y.Q. Feng, H. Wang, Anal. Chim. Acta 591 (2007) 116.
[49] K.J. Huang, M. Zhang, W.Z. Xie, H.S. Zhang, Y.Q. Feng, H. Wang, Anal. Bioanal. Chem. 388 (2007) 939.
[50] H.J. Zhang, J.S. Li, H. Wang, Y.Q. Feng, Anal. Bioanal. Chem. 386 (2006) 2035.

Talanta 78 (2009) 1429–1435

Contents lists available at ScienceDirect

Talanta

journal homepage: www.elsevier.com/locate/talanta

Determination of brominated flame retardants in electrical and electronic equipments with microwave-assisted extraction and gas chromatography–mass spectrometry

Ying Li[a], Tianran Wang[a], Yuki Hashi[a], Haifang Li[b], Jin-Ming Lin[a,b,*]

[a] State Key Laboratory of Environmental Chemistry and Ecotoxicology, Research Center for Eco-Environmental Sciences, Chinese Academy of Sciences, Beijing, China
[b] The Key Laboratory of Bioorganic Phosphorus Chemistry & Chemical Biology, Department of Chemistry, Tsinghua University, Beijing 100084, China

ARTICLE INFO

Article history:
Received 29 October 2008
Received in revised form 16 February 2009
Accepted 19 February 2009
Available online 5 March 2009

Keywords:
Brominated flame retardant
Polybrominated biphenyl
Polybrominated diphenyl ether
Microwave-assisted extraction
Electrical and electronic equipment
Gas chromatography–mass spectrometry

ABSTRACT

Determination of brominated flame retardants in electrical and electronic equipments (EEE) was achieved through microwave-assisted extraction (MAE) and gas chromatography–mass spectrometry. Polybrominated biphenyls (PBBs) and polybrominated diphenyl ethers (PBDEs) including mono-brominated through deca-brominated congeners were qualified and quantified with good linearity (0.9963–0.9998) and repeatability (RSD, 1.1–8.1%). Multivariable orthogonal experimental design was used to optimize the MAE parameters. Extraction temperature and time were the most significant factors for extraction process. The extractants were cleaned up with SPE method after extraction. Recoveries of spiked blank samples ranged from 72.4% to 108.4% for most of the analytes. The method was applied to the determination of PBBs and PBDEs in several kinds of real EEE samples. It was found that no detectable level of PBBs was detected among them. Different contents of PBDEs were tested in the tested samples and the total contents ranged from 25.0 ng g^{-1} to 194.0 ng g^{-1}. The proposed approach demonstrated an environmentally friendly and convenient alternative, which only consumed 10 mL hexane to microwave extraction for 10 min at 100 °C.

1. Introduction

Polybrominated biphenyls (PBBs) and polybrominated diphenyl ethers (PBDEs) represent an important group of brominated flame retardants (BFRs) [1]. They have the potential to diffuse out of the material into the environment because they are physically combined with the polymeric material being treated. Moreover, there have been some reports on their toxic effects [2,3] and accumulation in environmental biota and human tissues [4–6] due to their similar structure to polychlorinated biphenyls. Therefore, increasing attentions have been paid on these new emerging persistent organic pollutants. PBBs and PBDEs were forbidden in the production and usage by the European Union (EU) as well as other regions. Some legislations and regulations, such as "Directive 2002/95/EC on the Restriction of the Use of certain Hazardous Substances in Electrical and Electronic Equipment (RoHS)" and "Directive 2002/96/EC on Waste Electrical and Electronic Equipment (WEEE)" of EU, and "Testing methods for hazardous substances in electronic information products (SJ/T 11365—2006)" of China, and so on, were proposed to monitor and control the contents of PBBs and PBDEs in the EEE samples. However, procedures of most legislations and regulations are ambiguous and need large consumption of organic solvents and tedious manual operation. Thus a convenient, rapid and accurate method for the determination of PBBs and PBDEs in electrical and electronic equipments is a requisite for the applicable operation.

The classical extraction technique used in the determination of PBBs and PBDEs in solid samples is the solid–liquid partitioning with organic solvents, followed sometimes by subsequent clean-up of extracts before their gas chromatographic determination. The traditional Soxhlet extraction has been widely employed using non-polar solvents such as toluene, hexane or solvent mixtures like hexane–acetone [7,8]. Sinkkonen et al. [9] screened the occurrence of persistent halogenated aromatic compounds including PBDEs of waste samples for an aluminum recycling plant, and the samples were Soxhlet extracted with toluene for 48 h. The drawbacks of Soxhlet extraction are the large consumption of solvents and glassware and the time-consuming process. These drawbacks can be reduced by using other extraction techniques developed lately, such as the ultrasonic-assisted extraction (UAE), selective pressurized liquid extraction (PLE) and microwave-assisted extraction (MAE) which reduce the consumed time and amount of organic solvent. de la Cal et al. applied PLE method

* Corresponding author at: Department of Chemistry, Tsinghua University, Beijing 100084, China. Tel.: +86 10 62792343; fax: +86 10 62792343.
E-mail address: jmlin@mail.tsinghua.edu.cn (J.-M. Lin).

0039-9140/$ – see front matter © 2009 Elsevier B.V. All rights reserved.
doi:10.1016/j.talanta.2009.02.046

to extract 39 PBDE congeners in sediment samples with the reduction of the sample preparation time from days to 30 min [10]. UAE method was used to extract PBDEs from soil samples with a low volume of 5 mL ethyl acetate and 2×15 min [11].

MAE, also a newly developed method for pretreatment of persistent organic pollutants from solid samples, has been reported to extract polycyclic aromatic hydrocarbons, polychlorinated biphenyls and organochlorine pesticides in airborne particulates and sediments samples [12,13]. Yusá et al. evaluated the extraction efficiency of PBDEs and polychlorinated naphthalenes with MAE method and applied it to a sewage treatment plant [14], as well as for domestic dust and marine biological tissues samples [15,16]. Vilaplana et al. applied three kinds of extraction methods, PLE, UAE and MAE to extract BFRs from styrenic polymer samples [17]. The excellent performance of MAE methods guaranteed the efficient extraction of target analytes from complex matrixes.

In this work, the proposed method was an environmentally friendly alternative for determining PBBs and PBDEs in electrical and electronic equipment samples. The solvent hexane (10 mL) with 4 mL ultrapure water to absorb microwave energy was adopted to extract analytes instead of toxic toluene. The whole extraction process can be finished within 10 min microwave irradiation at the temperature of 100 °C with the recoveries of 72.4–108.4% for most of the targets. The LODs of analytes ranged from 0.17 ng g^{-1} to 68.2 ng g^{-1} with gas chromatography–mass spectrometry under selected ion monitoring mode. The MAE method was firstly applied to the determination of BFRs in EEE samples of people's daily life, such as electrical wire, DVD player, computer and mobile phone, and so on, and was proved to be a convenient and rapid procedure for the determination of BFRs in EEE samples.

2. Experimental

2.1. Chemicals

PBB and PBDE standards were purchased from Accustandard (New Haven, CT, USA) and consisted of 2-bromobiphenyl (B-001), 2,5-dibromobipheny (B-009), 2,4,6-tribromobiphenyl (B-030), 2,2′,5,5′-tetrabromobiphenyl (B-052), 2,2′,4,4′,6,6′-hexabromobiphenyl (B-155), 2,4,4′-tribromodiphenyl ether (BDE-028), 2,2′,4,4′-tetrabromodiphenyl ether (BDE-047), 2,2′,4,4′,5-pentabromodiphenyl ether (BDE-099), 2,2′,4,4′,6-pentabromodiphenyl ether (BDE-100), 2,2′,4,4′,5,6′-hexabromodiphenyl ether (BDE-154), 2,2′,4,4′,5,5′-hexabromodiphenyl ether (BDE-153), 2,2′,3,4,4′,5′,6-heptabromodiphenyl ether (BDE-183) and 2,2′,3,3′,4,4′,5,5′,6,6′-decabromodiphenyl ether (BDE-209) as individual standard solutions of 50 μg mL^{-1}. 2,4,5,6-Tetrachloro-m-xylene (TCMX) of 100 μg mL^{-1} in hexane and 2,2′,3,3′,4,4′,5,5′,6,6′-decachlorobiphenyl (CB-209) of 35 μg mL^{-1} in isooctane were used as internal standards (I.S.). 4,4′-dibromoctafluoronated biphenyl (DBOFB) was used as surrogate standard for recovery test. Stock solutions were prepared in isooctane and working solutions were prepared by subsequent dilutions in isooctane and hexane. Stock and working solutions were stored at −20 °C. When not being used, the stock solutions were placed at a mark on the vial at the level of the solution so that solvent loss by evaporation can be detected. Replace the solution if solvent loss has occurred. Hexane, isooctane, toluene and acetone were the pesticide residual grades from J.T. Baker (Phillipsburg, NJ, USA). LC-Si SPE column and absorbent were purchased from Supelco (Bellefenote, PA, USA). Prior to use, the absorbent was conditioned overnight at 160 °C.

2.2. Sample preparation

The real electrical and electronic equipment samples were collected from recycle bins of waste electrical and electronic equipments of Beijing, China and cut into small pieces and ground to powder by a high-speed disintegrator after they were embrittled with liquid nitrogen. The powder was sieved to obtain the homogenous fraction through a 1 mm sieve. This fraction was stored at 4 °C until it was analyzed. Besides, a polypropylene (PP) powder sample without any additives was obtained from factory as blank sample used for determining targets recovery. The sample was fortified with the targets PBBs and PBDEs solution. To favor the homogeneous distribution of the analytes into the whole solid sample, a small volume of clean hexane was also added. Spiked sample vessels were maintained open at room temperature until the organic solvent was completely evaporated (approximately 2–3 h). Through this spiking procedure, the sample appeared to be more similar to real samples than those obtained with the common technique of spiking the sample just before the analysis.

2.3. Microwave-assisted extraction

Microwave-assisted extraction (MAE) was performed on 0.3 g of dried sample in closed vessels with pressure and temperature control. Prior to extraction, DBOFB was added to each sample as recovery standard. 60 ng g^{-1} DBOFB was added to each sample as recovery standard when MAE parameters were optimized. For the recovery test of the proposed method, the 50 ng g^{-1} and 200 ng g^{-1} DBOFB was added, respectively. The samples were in equilibrium for 2 h. The extraction solvent of mixture of 10 mL hexane and 4 mL H_2O was added to three microwave vessels and the vessels were closed and introduced into the microwave cavity. The extraction was carried out as the preset temperature and hold time. After extraction, the vessels were allowed to cool at room temperature before they were opened. The co-extracted polymer matrices can be removed through adequately shaking the extracted solution twice with same volume concentrated sulfonated acid. After centrifugation, the organic solvents were collected and evaporated to approximately 1 mL using rotary evaporator. The 6 mL LC-Si SPE column was prewashed and conditioned by 10 mL hexane, then the extracted solution was transferred to the column, and the targets were eluted using 20 mL hexane. Next the elution was additionally concentrated to 0.2 mL under the gentle stream of nitrogen. Final extracts were stored at −20 °C until analysis. The internal standards TCMX and CB-209 were added before determination with GC–MS.

2.4. Soxhlet extraction

Approximately 1.0 g of spiked sample was directly weighed in the cellulose thimble and then introduced into the Soxhlet extraction chamber. Toluene was chosen as the solvent on the basis of previous studies [18]. 60 mL toluene was added and refluxed for 5 h. The extract was cooled to room temperature and condensed to dry under the gentle blow of nitrogen. The residue was resolved with hexane and cleaned up with silica column chromatography. The elute was evaporated to 1 mL and stored at 4 °C till GC–MS analysis.

2.5. GC–MS analysis

GC–MS analysis was carried out by a Shimadzu GCMS-QP2010 gas chromatograph with an automatic split–splitless injector Model AOC-20i and an AOC-20s auto sampler, which was equipped with a quadrupole mass spectrometric detector (Shimadzu, Kyoto, Japan). A capillary column (DB-5ms, 5% phenylmethylpolysiloxane, 15 m × 0.25 mm i.d. and 0.1 μm film thickness, Agilent, USA), was employed. Operating conditions were as follows: injector port tem-

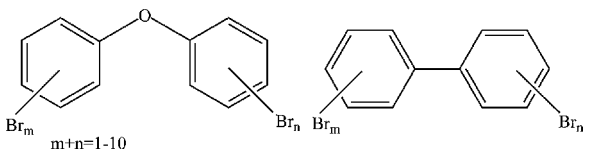

Fig. 1. General structures of PBBs and PBDEs.

perature 300 °C; Helium (99.999%) as carrier gas at a flow-rate of 1.2 mL min^{-1}; pulsed splitless mode (pulsed pressure 250 kPa for 1.0 min). The column temperature was maintained at 100 °C for 2 min, programmed at 8 °C min^{-1} to 200 °C; then ramped at 10 °C min^{-1} to 300 °C held for 2 min and at the rate of 40 °C min^{-1} to 325 °C held for 5 min. The total analysis time was 32.13 min and the equilibration time 1 min. 1 μL sample was injected in a splitless mode, with the split valve closed for 2 min. The mass spectrometric detector was operated in electron impact ionization mode with an ionizing energy of 70 eV, scanning from *m*/*z* 100–1000. The detector was tuned with the standard of perfluorotributylamine prior to analysis periodically. The ion source temperature was 250 °C and the interface temperature 300 °C. The electron multiplier voltage (EM voltage) was maintained 0.1 kV above auto tune and a solvent cut of 5 min was employed. Analysis was performed with selected ion monitoring (SIM) mode. The target ion and qualifier ions abundances were determined by injection of standard solutions under the same chromatographic conditions using full-scan with the mass/charge ratio ranging from *m*/*z* 100 to 1000.

3. Results and discussion

3.1. Performance of GC–MS-SIM method

13 different PBBs and PBDEs congeners ranging from B-001 to BDE-209 were determined by gas chromatography–mass spectrometry with selected ion monitoring (GC–MS-SIM) method. The general structures were illustrated in Fig. 1. To improve the resolution and accuracy, the chromatography conditions were optimized to get the satisfactory qualitative and quantitative results. For PBBs, the most abundant ions were the $[M]^+$ and other minor signals of $[M–n\mathrm{Br}]^+$ during ionization by EI mode, while the EI spectra of PBDEs were dominated by $[M–2\mathrm{Br}]^+$ showing losses of two bromine atoms. Therefore, *m*/*z* of $[M]^+$ ion and $[M–2\mathrm{Br}]^+$ were respectively selected as target ions for PBBs and PBDEs, the identification ions of each PBB and PBDE were listed in Table 1.

Linearity was tested in the concentration range from 1 ng mL^{-1} to 100 ng mL^{-1} by injection standard solutions for at least 3 times at five different concentration levels except the concentration range of deca-BDE was from 200 ng mL^{-1} to 1000 ng mL^{-1}. Correlation coefficients (R^2) between 0.9963 and 0.9998 were obtained.

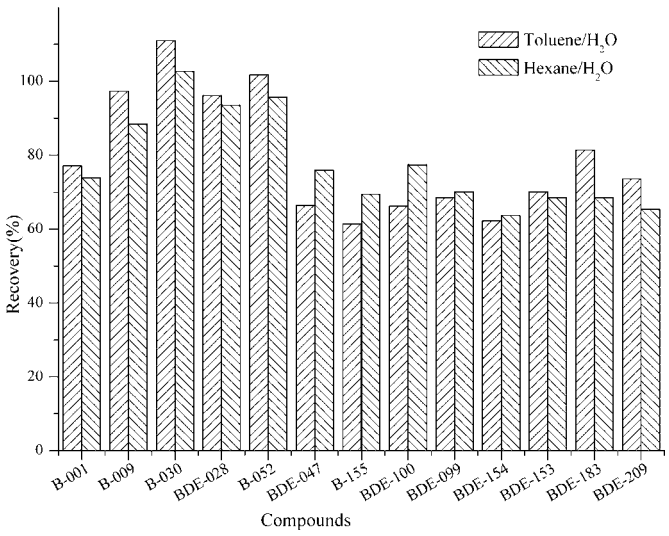

Fig. 2. Effect of solvent on recovery of PBBs and PBDEs of the spiked sample. MAE conditions: temperature: 100 °C; time: 10 min; solvent: toluene/H_2O (5:2, v/v), hexane/H_2O (5:2, v/v).

3.2. Preliminary experiments

Toluene is the most commonly adopted solvent to extract PBBs and PBDEs from solid samples when using traditional Soxhlet extraction, while hexane, as a usual solvent with the lower toxicity, has good solubility to PBBs and PBDEs [7]. So, hexane and toluene were initially chosen as extractant for the targets from the spiked samples. However, both of them have little permittivity which is unfavorable to absorb microwave energy and promote the extraction process. As proposed by Fidalgo-Used et al. [19], a binary solvent mixture was commonly selected to perform MAE in which a polar solvent was used to absorb microwave energy, such as methanol [20] or water [16]. Herein, ultrapure water was added to the vessels as an aqueous phase to absorb the microwave energy and facilitate the production of high temperature and pressure, then subsequently transfer the targets from the solid matrix into the organic phase. The two kinds of binary mixture solvents were compared according to the extraction efficiency. There was no significant difference in the recoveries of all the analytes between two kinds of mixture solvents, as shown in Fig. 2. Moreover, a clearer organic solution was obtained as well as less matrix interference was observed from the GCMS chromatogram with hexane/H_2O mixture when comparing with toluene/H_2O mixture. Fig. 3 showed the typical GC–MS-SIM chromatograms of extraction solution obtained from the spiked sample when hexane/H_2O mixture solvent was used. 13 PBBs and PBDEs were detected clearly. The

Table 1
Retention time (Rt), molecular weight, qualitative ions and quantitative ions of the targets.

Homologue group	IUPAC name	Rt (min)	Molecular weight	Identification ions (*m*/*z*)	Target ion (*m*/*z*)
Mono-BB	B-001	5.1	233	152, 232	234
Di-BB	B-009	9.3	312	310, 152	312
Tri-BB	B-030	11.5	391	392, 230	390
Tri-BDE	BDE-028	14.0	407	246, 406	246
Tetra-BB	B-52	14.7	470	389, 391	470
Tetra-BDE	BDE-47	16.4	486	486, 488	326
Hexa-BB	B-155	17.9	628	626, 630	628
Penta-BDE	BDE-100	18.0	564	564, 566	404
Penta-BDE	BDE-99	18.5	564	564, 566	404
Hexa-BDE	BDE-154	19.7	644	644, 642	484
Hexa-BDE	BDE-153	20.3	644	644, 642	484
Hepta-BDE	BDE-183	21.9	722	564, 722	562
Deca-BDE	BDE-209	28.3	960	801, 959	799

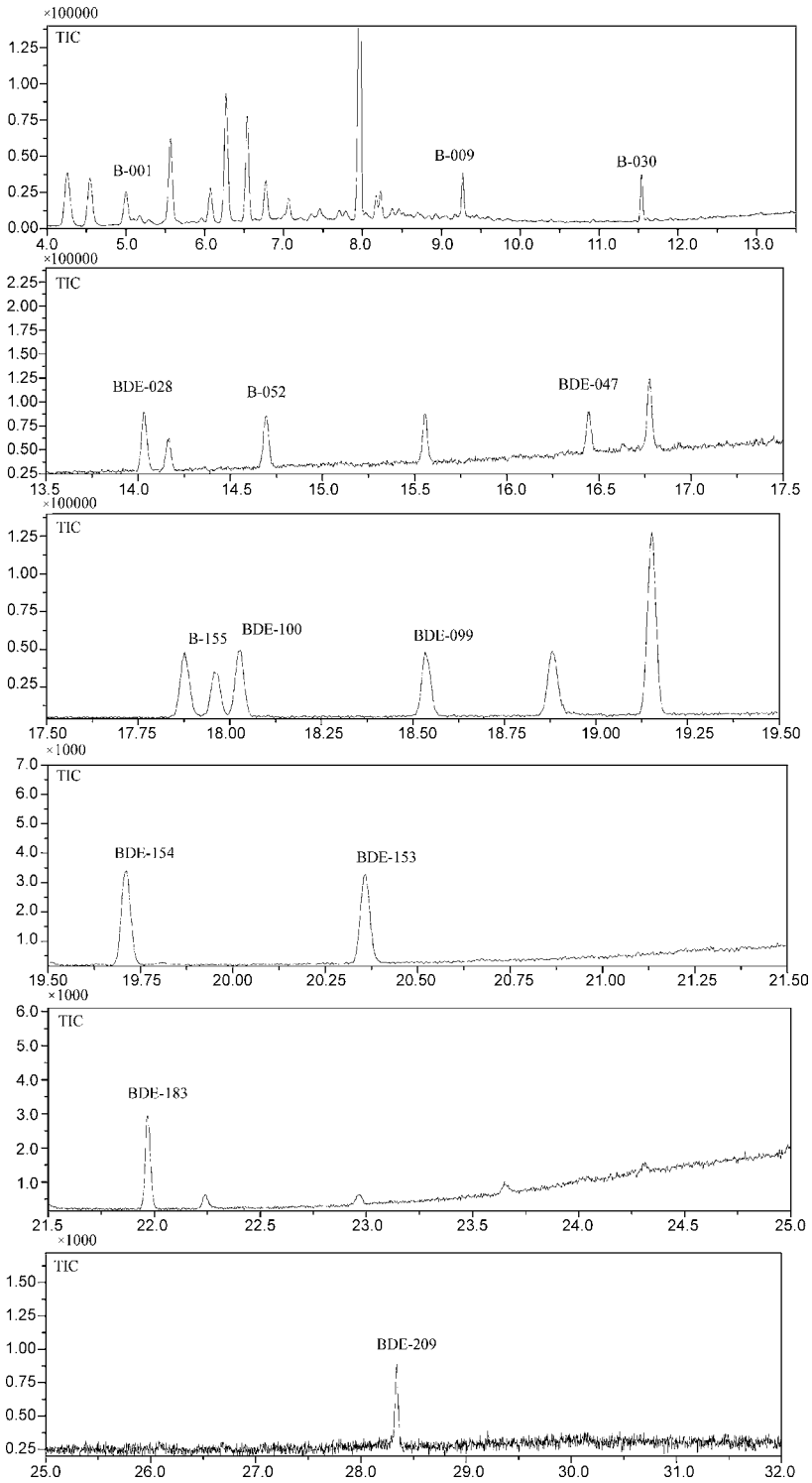

Fig. 3. Typical GC–MS-SIM chromatograms of extraction solution with hexane/ultrapure water as solvent for the spiked sample (GC–MS conditions as described in the text).

Table 2
Factors and levels selected for the orthogonal design.

Factor	Low level	High level	Optimized values	Selected level
pH	0	14	0, 7, 14	7
Organic phase volume (mL)	5	13	5, 8, 10, 13	10
Aqueous phase volume (mL)	2	6	2, 4, 6	4
Extraction time (min)	5	15	5, 8, 10, 15	10
Temperature (°C)	80	110	80, 90, 100, 110	100

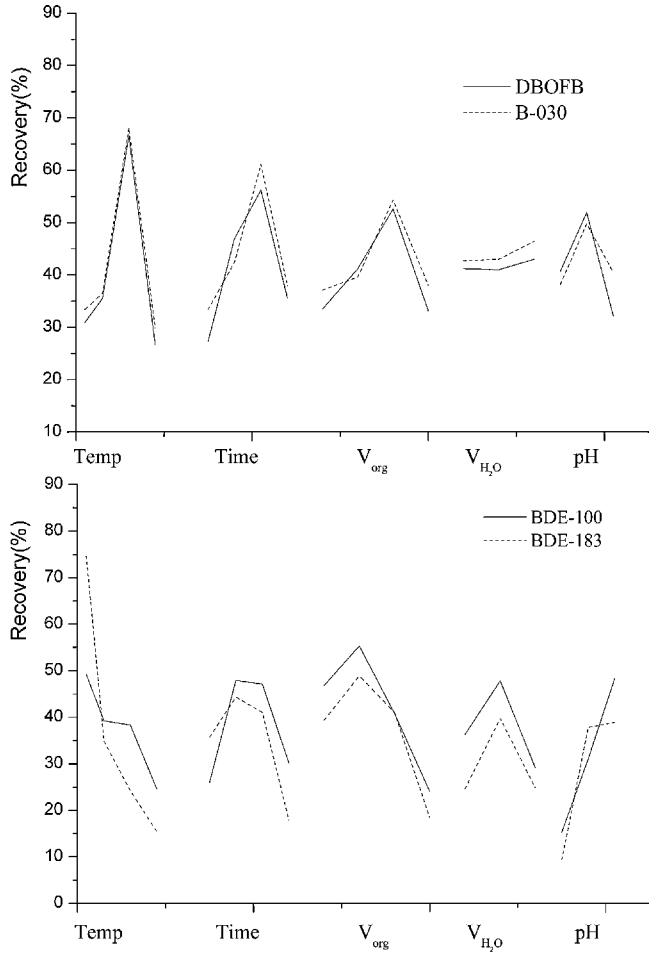

Fig. 4. Plots showing the influence of MAE parameters on the extraction of four targets.

extra peaks might come from the co-extracted compounds of polymer matrix or degradation compounds of higher brominated BDEs, such as deca-BDE. However, these peaks did not interfere with the detection of target compounds. Besides, toluene was not welcomed because of its toxicity and environmental impact.

3.3. Optimization of microwave-assisted solvent extraction

Parameters influencing MAE process were extraction temperature, extraction time, organic solvent volume, aqueous phase volume and pH. A screening study of main variables affecting the microwave extraction process was performed by means of a mixed level orthogonal factorial design $L_{16}(2^4)$ involving 16 randomized runs. Temperature was a crucial parameter for MAE as lower temperature could lead to the incomplete extraction while higher temperature led to degradation of analytes [15,19]. So, the temperatures of 80 °C, 90 °C, 100 °C and 110 °C were tested for the optimization. The second parameter considered was the extraction time at the preset temperature and the changed range of extraction time was from 5 min to 15 min. Owing to the volume of extraction solvent must not exceed one third of the volume of microwave vessel, so the total volume of hexane and ultrapure water should be less than 20 mL. The influence of volume of hexane and aqueous solution was studied at different ratio. The optimized composition of organic solvent and aqueous solution could ensure the efficient extraction and good selectivity. Three levels of aqueous solution with different pH value (pH 0 (1 mol L^{-1} sulfuric acid solution), pH 7 (ultrapure water) and pH 14 (1 mol L^{-1} NaOH solution)) were tested for the optimization of MAE conditions according to the reported results [16]. The studied range and the selected level of each parameter were shown in Table 2.

The blank PP samples were spiked with standard solution to get the concentration of 60 ng g^{-1} for each analyte except that the spiked value of BDE-209 was 600 ng g^{-1}. Recoveries were calculated by dividing the measured concentrations of the spiked samples by the spiked concentrations. Fig. 4 showed the main effect plot for the selected BFRs and DBOFB. As can be seen, the most important factors to the extraction process were the extraction temperature and extraction time. However, their influences had different effect on each compound. For DBOFB and B-30 which had relatively lower boiling point and good volatile property, extraction temperature of 100 °C and short extraction time can fulfill the extraction. While for the higher brominated analytes such as BDE-183, extraction efficiency decreased with the increasing temperature and long extraction time. The descents of extraction efficiencies observed could be attributed to the thermal degradation due to the fact that higher brominated BDEs were easy to degrade when exposed to higher temperature [21]. So, the temperature of 100 °C was used for the maximum extraction and maintained for 10 min. The volume of aqueous solution had similar trend to extraction temperature. As mentioned above, the existence of aqueous solution in the microwave system was favorable to the absorbance of microwave energy, and then promoted the transfer of the analytes towards the organic phase. Nevertheless, the greater the volume of ultrapure water was, the higher temperature was achieved in the vessels and the heavier degradation would happen, e.g. recoveries of BDE-100 and BDE-183 at 80 °C was higher than that at 110 °C, which was consistent with the results of ref. [21]. Hence, 4 mL ultrapure water

Table 3
Linearity, repeatability and reproducibility of the proposed method.

Compound	Linearity (R^2)	Repeatability (%, $n=5$)		Reproducibility (%, $n=3$)	
		5 ng mL^{-1}	100 ng mL^{-1}	5 ng mL^{-1}	100 ng mL^{-1}
B-001	0.9996	3.2	0.9	2.9	2.0
B-009	0.9998	1.6	1.4	2.8	2.2
B-030	0.9997	2.8	1.2	4.3	1.8
BDE-028	0.9998	3.4	1.5	5.2	2.9
B-052	0.9996	2.3	1.5	2.5	2.9
BDE-047	0.9992	2.0	1.8	2.0	4.7
B-155	0.9965	2.5	3.6	3.0	5.3
BDE-100	0.9989	1.2	1.9	3.5	4.1
BDE-99	0.9989	1.5	1.1	2.0	3.7
BDE-154	0.9968	1.7	3.3	4.5	3.2
BDE-153	0.9963	3.4	3.7	4.2	3.8
BDE-183	0.9970	2.2	2.8	5.3	3.2
BDE-209	0.9976	5.4	7.5	8.8	9.1

Table 4
Recovery and LOD of MAE and SE method.

Compounds	MAE recovery (%)		LOD of MAE (ng g^{-1})	SE recovery (%)
	50 ng g^{-1}	200 ng g^{-1}		50 ng g^{-1}
B-001	85.0	73.0	5.17	95.6
DBOFB	79.0	78.1	6.70	89.1
B-009	98.3	105.6	0.23	92.8
B-030	108.4	86.6	4.80	97.0
BDE-028	102.2	79.8	0.18	77.2
B-052	101.4	101.0	0.35	73.2
BDE-047	89.4	81.3	1.05	77.2
B-155	83.9	72.4	4.41	77.6
BDE-100	83.1	105.3	0.69	76.3
BDE-99	94.3	97.8	8.33	81.8
BDE-154	75.7	81.0	0.17	73.1
BDE-153	77.2	79.3	8.3	78.2
BDE-183	83.4	72.8	1.55	78.0
BDE-209	82.2[a]	52.1[a]	68.2	80.1[a]

[a] The spiked levels were 10 times of that noted.

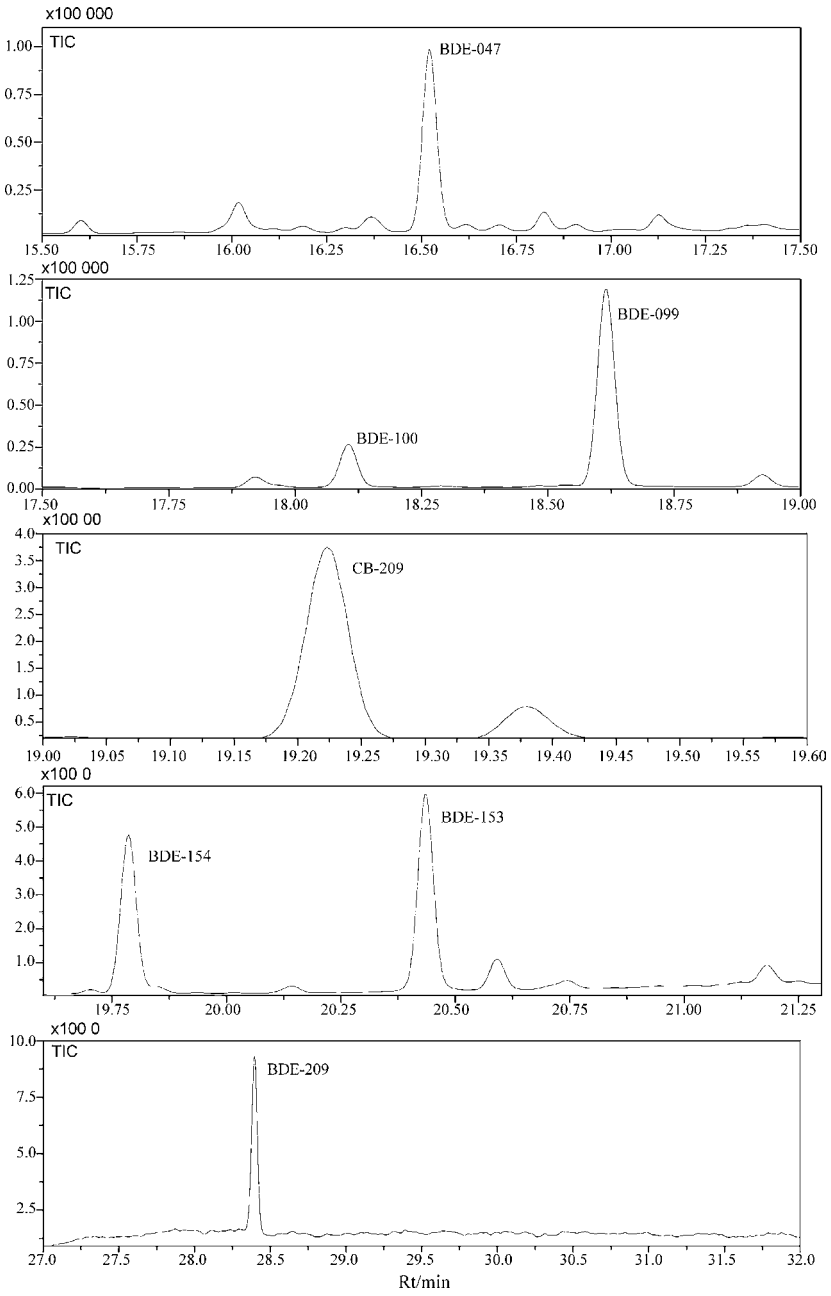

Fig. 5. GC–MS-SIM chromatograms of a real EEE sample (sample 2 in Table 5, GC–MS conditions as described in the text).

was preferred for the MAE process. The influence of the aqueous solution pH was not significant for the extraction of BFRs from EEE samples as that from domestic dust samples [16]. A possible explanation for this might be attributed to the special components of the samples which mainly were polymer and difficult to be affected by the acid or basic solution.

As known, electrolyte solutions interacted strongly with microwave radiation, the enhancement of ion strength could strongly speed microwave absorption and transformation [16]. Therefore, the ultrapure water with 5%, 10% and 20% sodium chloride solution was used to compare the extraction efficiency with the solution containing no salt. It was found that the salt addition

Table 5
PBDEs contents detected in several real EEE samples.

Sample	Concentration (ng g^{-1} EEE)								
	BDE-028	BDE-047	BDE-100	BDE-99	BDE-154	BDE-153	BDE-183	BDE-209	Total
1	n.d.	10.1	n.d.	8.3	3.1	3.5	n.d.	n.d.	25.0
2	n.d.	28.0	8.2	32.2	4.4	5.4	n.d.	86.7	165.1
3	n.d.	n.d.	n.d.	n.d.	n.d.	n.d.	n.d.	194.0	194.0
4	9.9	21.1	6.0	6.0	n.d.	n.d.	n.d.	n.d.	43.0

n.d.: Not detected (below LOD).

had no significant effect on the extraction. Taking all these results into account, the optimal conditions performed for the MAE of PBBs and PBDEs from EEE samples were chosen to be: an extraction temperature of 100 °C with the mixture solution of 10 mL hexane and 4 mL ultrapure water for 10 min. The proposed MAE method for EEE samples needs less organic solvent consumption (10 mL versus 70–100 mL required by Soxhlet method) and largely saves the pretreatment time (10 min versus 5 h).

3.4. Analytical performance

In order to evaluate the repeatability of the proposed method, five consecutive independent analyses were performed at two different concentration levels in the same day. The run-to-run variation, expressed as relative standard deviation (RSD), ranged from 1.2% to 5.4% for 5 ng mL^{-1} level and from 0.9% to 7.5% for 100 ng mL^{-1} level. Besides repeatability evaluation, the same levels were analyzed by duplicate in three different days to establish the method day-to-day variation. Obtained results were in the range from 2.0% to 8.8% for 5 ng mL^{-1} and from 1.8% to 9.1% for 100 ng mL^{-1} respectively, and the detailed results were summarized in Table 3.

In order to assess the performance of the proposed methods, analytical quality parameters were tested. Method recoveries were evaluated using spiked blank samples. The target analytes were added at two different concentration levels corresponding to 50 ng g^{-1} and 200 ng g^{-1} of BFRs mixture for compounds from B-001 to BDE-183, while the spiked level of BDE-209 were 500 ng g^{-1} and 2000 ng g^{-1}, respectively. Recovery values were calculated by dividing the measured concentrations of the spiked samples by the added concentrations. Results ranged from 72.4% to 108.4% for most of the target compounds, except that recovery of BDE-209 at the higher spiked level of 2000 ng g^{-1} (Table 4). The low recoveries of BDE-209 in higher concentration samples might be attributed to thermal degradation during MAE process. The moderate extraction temperature could avoid or reduce the degradation of deca-BDE, just as indicated by ref. [20], extraction temperature was identified as statistically significant factors for the MAE extraction.

Limits of detection for the overall methods, defined for a signal-to-noise of 3, were estimated employing spiked samples. Under these conditions, the LODs of the developed method ranged between 0.17 ng g^{-1} and 8.33 ng g^{-1} for compounds including mono-BB through hepta-BDE, and 68.2 ng g^{-1} for BDE-209, respectively. The obtained values were shown in Table 4.

To check the accuracy of the complete analytical procedure, results of the proposed analytical method for the spiked sample were compared with that of conventional Soxhlet extraction. The obtained recoveries ranged from 73.2% to 95.6% as shown in Table 4, demonstrated the MAE method showed the same performance with traditional Soxhlet extraction method.

3.5. Application to real EEE samples

To examine the applicability of the proposed method, several real EEE samples were analyzed with MAE method for the first time. These samples were the most ordinary products among people's daily life, including electrical wires, plastic part of DVD player, computer and mobile phone. The ground powder of each sample was tested separately. No detectable levels of PBBs were found in all the samples. Different contents of PBDEs were detected from four samples respectively. A representative chromatogram was depicted in Fig. 5. In fact, it was found that there was great difference in the content of PBDEs among the detected samples. In samples 1 and 4, PBDEs levels were relatively low (Table 5) and the sum of PBDEs in both samples were lower than the threshold of 0.1 μg g^{-1} proposed by EU. Therefore, both kinds of sample could meet the requirement. In samples 2 and 3, the total concentration of PBDEs were 165.1 ng g^{-1} and 194.0 ng g^{-1}, respectively, in which the most dominant congener was BDE-209 with the contents of 86.7 ng g^{-1} and 194.0 ng g^{-1}. The fact indicated that BDE-209 was still adopted as most ordinary BFRs in EEE samples up to now.

4. Conclusion

A large amount of waste electrical and electronic equipments were produced as one of the byproducts of advanced developed industry and science technology, and had been the source of kinds of pollution to the environmental and biological media, including PBBs and PBDEs. In the present work, a rapid and convenient approach to identify and quantify PBBs and PBDEs in EEE sample was proposed with MAE and GC–MS-SIM method. More environmentally friendly extraction solvent hexane/water substituted for the hazardous and toxic solvents, e.g. toluene or dichloromethane [7]. Sufficient extraction of analytes from polymer samples could be achieved within shorter time and less solvent consumption compared with the published works [17]. Though, it was difficult to clarify which kind of polymers were contained in real EEE samples due to their versatile complexity, several kinds of real EEE samples were detected and the results showed the good applicability of the proposed method. However, more attention should be paid to the extraction and determination of BDE-209 and more suitable procedures should be adopted.

Acknowledgement

This work was supported by the National Natural Science Foundation of China (Nos. 20621703, 20728505).

References

[1] J. de Boer, P.G. Wester, H.J. Klamer, W.E. Lewis, J.P. Boon, Nature 394 (1998) 28.
[2] P.O. Darnerud, Environ. Int. 29 (2003) 841.
[3] G.C. Balch, L.A. Vèlez-Espino, C. Sweet, M. Alaee, C.D. Metcalfe, Chemosphere 64 (2006) 328.
[4] R.C. Hale, M.J. La Guardia, E. Harvey, M.O. Gaylor, T.M. Mainor, Chemosphere 64 (2006) 181.
[5] W. Song, J.C. Ford, A. Li, W.J. Mills, D. Buckley, K.J. Rockne, Environ. Sci. Technol. 38 (2004) 3286.
[6] M.F. Fernandez, P. Araque, H. Kiviranta, J.M. Molina-Molina, P. Rantakokko, O. Laine, T. Vartiainen, N. Olea, Chemosphere 66 (2007) 377.
[7] T. Hyootylaoinen, K. Hartonen, Trends Anal. Chem. 21 (2002) 13.
[8] A. Covaci, S. Voorspoels, J. de Boer, Environ. Int. 29 (2003) 735.
[9] S. Sinkkonena, J. Paasivirta, M. Lahtiperä, A. Vattulainen, Environ. Int. 30 (2004) 363.
[10] A. de la Cal, E. Eljarrat, D. Barceló, J. Chromatogr. A 1021 (2003) 165.
[11] C. Sánchez-Brunete, E. Miguel, J.L. Tadeo, Talanta 70 (2006) 1051.
[12] L.B. Liu, Y. Liu, J.-M. Lin, N. Tang, K. Hayakawa, T. Maeda, J. Environ. Sci. 19 (2007) 1.
[13] M. Numata, T. Yarita, Y. Aoyagi, A. Takatsu, Anal. Chem. 75 (2003) 1450.
[14] V. Yusá, A. Pastor, M. de la Guardia, Anal. Chim. Acta 565 (2006) 103.
[15] S. Bayen, H.K. Lee, J.P. Obbard, J. Chromatogr. A 1035 (2004) 291.
[16] J. Regueiro, M. Llompart, C. García-Jares, R. Cela, J. Chromatogr. A 1137 (2006) 1.
[17] F. Vilaplana, P. Karlsson, A. Ribes-Greus, P. Ivarsson, S. Karlsson, J. Chromatogr. A 1196–1197 (2008) 139.
[18] E. Eljarrat, D. Barceló, Trends Anal. Chem. 23 (2004) 10.
[19] N. Fidalgo-Used, E. Blanco-González, A. Sanz-Medel, Anal. Chim. Acta 590 (2007) 1.
[20] A. Ranz, E. Maier, C. Trampitsch, E. Lankmayr, Talanta 76 (2008) 102.
[21] J. Björklund, P. Tollbäck, C. Hiärne, E. Dyremark, C. Östman, J. Chromatogr. A 1041 (2004) 201.

Talanta 78 (2009) 1364–1370

Contents lists available at ScienceDirect

Talanta

journal homepage: www.elsevier.com/locate/talanta

Extraction of polyunsaturated fatty acid methyl esters by imidazolium-based ionic liquids containing silver tetrafluoroborate—Extraction equilibrium studies

Min Li, Charles U. Pittman Jr., Tingyu Li*

Department of Chemistry, Box 9573, Mississippi State University, Mississippi State, MS 39762, USA

ARTICLE INFO

Article history:
Received 11 January 2009
Received in revised form 8 February 2009
Accepted 9 February 2009
Available online 20 February 2009

Keywords:
Liquid phase extraction
Ionic liquids
Polyunsaturated fatty acid methyl ester
Distribution ratio
Extraction isotherm
Separation

ABSTRACT

The extraction/enrichment of omega − 3 polyunsaturated fatty acid methyl esters (PUFAMEs) by hydrophobic ionic liquids (ILs) containing silver salts as the extraction phase has been extended to include equilibrium studies. The extraction time, organic solvents, IL structures, and $AgBF_4$ concentrations all influence the organic/ionic liquid biphasic extraction equilibrium. Each of these parameters was studied. The PUFAME distribution ratios, partition coefficients and the PUFAME–Ag^+ complex stability constants were determined from gas chromatography (GC) analyses. When $AgBF_4$ dissolved in [hmim][PF_6] was used as the extraction phase, both the distribution ratios of PUFAMEs and the stability constants of PUFAME–Ag^+ complexes increased significantly with an increase in the degree of unsaturation of the PUFAMEs. Investigation of the IL structures indicated that larger PUFAME distribution ratios were obtained when $AgBF_4$ was dissolved in hydrophobic ILs than in hydrophilic ILs. Higher PUFAME distribution ratios occurred using shorter chain alkanes as the organic solvents. The extraction isotherms for PUFAME uptake were obtained from which saturated extraction capacities were determined. Compared with previous aqueous $AgNO_3$ extractions, a more efficient extraction of PUFAMEs was obtained by using a hydrophobic IL containing $AgBF_4$. Much higher extraction capacities and significant shorter operation times were also achieved.

1. Introduction

Polyunsaturated fatty acids, especially the omega-3 fatty acids such as docosahexaenoic acid, eicosapentaenoic acid and α-linolenic acid, are used to lower the level of low-density lipoprotein in the blood and treat heart disease, circulatory disorders, and cancer [1,2]. OMACOR, a concentrated form of omega-3 fatty acids (as ethyl esters), is approved by the Food and Drug Administration (FDA) for treating patients with high triglycerides. Unfortunately, humans cannot biosynthesize omega-3 fatty acids, due to the absence of Δ-15 and Δ-12 desaturase enzymes [3]. Consequently, omega-3 fatty acids have to be obtained from external sources. Omega-3 fatty acids are known to exist in fish, microalgae, krill, and flax [4]. For example, fish oils are frequently used as omega-3 fatty acid supplements. However, more concentrated forms of omega-3 fatty acids are desirable, as the amount of fish oil required to achieve the desired biological effects carries the risk of vitamin A and D overdose and increases intake of saturated fatty acids [5]. Therefore, efficient methods to enrich sources of omega-3 fatty acids are needed. Efficient enrichment methods could also enable the preparation of omega-3 fatty acids economically [6] from other natural sources. An efficient separation method requires the separation of omega-3 fatty acids from saturated fatty acids which exist in large quantities and have undesirable health effects. Due to the similarity of molecular size, polarity, and structure, separation of omega-3 fatty acid from their saturated analogues is challenging.

Toward this goal, several separation methods have been investigated, including urea inclusion complexation [7], low temperature fractional crystallization [8], liquid–liquid extraction by aqueous silver nitrate solutions [9], solid phase extractions [10], $AgNO_3$-modified benzenesulfonic acid silica gel column separations [11], high performance liquid chromatography [12], and supercritical fluid extraction [13,14]. Among them, liquid–liquid extraction is a favored process owing to its high separation capacity and simple manipulations. However, in traditional solvent extractions, toxic, flammable, volatile and sometimes expensive organic solvents are required and they may not work well for certain compounds due to their low solubilizing ability.

Room temperature ionic liquids (RTILs) are salts with a melting point close to or below room temperature. RTILs have recently been noted as "green" solvents mainly due to their extremely low vapor pressure. The application of RTILs as replacement solvents for various catalytic reactions [15] and in separation process [16–18] is being extensively explored. Unlike conventional volatile organic extraction solvents, RTILs are nonflammable, chemically tunable, and have no detectable vapor pressure [19]. Therefore, different

* Corresponding author. Tel.: +1 703 292 4949; fax: +1 703 292 9037.
E-mail address: li1640@gmail.com (T. Li).

0039-9140/$ – see front matter © 2009 Elsevier B.V. All rights reserved.
doi:10.1016/j.talanta.2009.02.011

kinds of RTILs have been used to extract and separate various compounds from organic or aqueous solutions [20,21]. Moreover, a large number of papers have reported the distribution ratios (or distribution coefficients) of organic compounds between RTIL and organic phases. For example, Meindersma et al. [22] reported the distribution ratios of toluene between IL and heptane phases in liquid phase extraction of aromatics from paraffins. Other work investigated the distribution coefficients of metal ions between aqueous and IL phases [23,24]. Studies on distribution ratio, extraction equilibrium or extraction isotherm kinetics may provide insightful understandings of separation processes and ultimately help optimize separation efficiencies. However, the distribution ratios and extraction isotherms of PUFAMEs between organic phase and IL phase have not been reported so far. It is worth noting that Teramoto et al. [9] have reported the distribution ratios of polyunsaturated fatty acid ethyl esters between aqueous $AgNO_3$ extraction phase and organic heptane phase. The distribution ratios were found to increase drastically as temperature was lowered. The extractions were effective for the separation of polyunsaturated fatty acid ethyl esters with degrees of high unsaturation, can be operated under mild conditions, and are suitable for mass production. However, this separation method requires large amounts of expensive $AgNO_3$ and prolonged operation time, probably due to the hydration of $AgNO_3$ and the low solubility of polyunsaturated fatty acid ethyl esters in aqueous solution.

We have been interested in developing IL-based solvent extraction for separating and enriching omega-3 PUFAMEs from fish oil or soy-derived biodiesel [25]. An efficient extraction method based on π-complexing interactions between silver ions and double bonds of polyunsaturated fatty acid methyl esters (PUFAMEs) was established using ILs containing $AgBF_4$ as extraction phases. The reusability of the $AgBF_4$–ionic liquid extraction phase was confirmed [25]. The recovery of the extracted PUFAMEs from IL phase was achieved by back-extraction using 1-hexene as the stripping solvent [25]. A successful and practical application of this extraction method to real samples such as cod liver oil was also demonstrated [25]. The omega-3 PUFAMEs such as methyl ester of all-*cis*-5,8,11,14,17-eicosapentaenoic acid (20:5 or EPA) and methyl ester of all-*cis*-4,7,10,13,16,19-docosahexaenoic acid (22:6 or DHA) were significantly enriched from 18% (total concentration of 20:5 and 22:6, wt.%) in the original cod liver oil to greater than 80% in the 1-hexene stripping solvent. In addition, much lower amounts of silver salts and shorter extraction times were realized using the novel IL-based extraction phases compared with previous water-based extraction phase [25]. As mentioned before, the extraction and concentration of omega-3 PUFAMEs from cod liver oil confirmed the feasibility of our new separation method. However, it is of both practical and mechanistic importance to further investigate the extraction equilibrium parameters and the extraction mechanisms. Moreover, it is well established that thermodynamic data generated by gas chromatography (GC) are fairly accurate and reliable [26]. Therefore, in this current paper, we wish to present a further detailed study of the extraction equilibrium parameters including the distribution ratios, partition coefficients of PUFAMEs. The stability constants of PUFAME–Ag^+ complexes and the liquid phase extraction isotherms of PUFAMEs are also investigated.

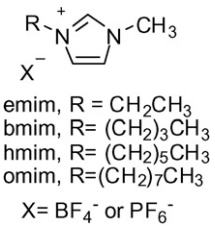

Scheme 1. Structures of the two series of ionic liquids used.

2. Experimental

2.1. Materials and reagents

$AgBF_4$ (98%), 1-methylimidazole, ethyl bromide, 1-butyl chloride, 1-hexyl chloride, 1-octylbromide, ethyl acetate, $NaBF_4$, from Aldrich (Milwaukee, WI, USA), octane, decane, dodecane, HPF_6 from Alfa Aesar (Ward Hill, MA, USA), hexane, chloroform, dichloromethlyene from Fisher Scientific (Pittsburgh, PA, USA, all HPLC grade) were used without further purification. The fatty acid methyl esters (FAMEs, Table 1), DHA (22:6), methyl all-*cis*-4,7,10,13,16,19-docosahexaenoic acid; EPA (20:5), methyl all-*cis*-5,8,11,14,17-docosahexaenoic acid; (18:3), methyl all-*cis*-9,12,15-octadecatrienoic acid; (18:2), methyl all-*cis*-9,12-octadecadienoic acid; (18:1), methyl *cis*-9-octadecaenoic acid; (18:0), methyl octadecanoate; and (19:0), methyl nonadecanoate were obtained from Aldrich (Milwaukee, WI, USA). In the abbreviations of FAMEs shown above in parentheses, the first number represents the number of carbons in the fatty acid; the second number represents the number of double bonds in that fatty acid's alkyl chain (Table 1). More detailed information about the FAMEs is provided in Table 1.

Imidazolium-based ionic liquids were synthesized according to the general methods [27]. The ionic liquid cations (Scheme 1) are referred to using the following abbreviations: [emim]: 1-ethyl-3-methylimidazolium, [bmim]: 1-butyl-3-methylimidazolium, [hmim]:1-hexyl-3-methylimidazolium, and [omim]: 1-octyl-3-methylimidazolium. Two different kinds of anions were use in this work, BF_4^- and PF_6^-.

2.2. Analyses of fatty acid methyl esters by GC-FID

Gas chromatography analyses of fatty acid methyl esters were performed using an HP 5890 series II gas chromatograph (Hewlett Packard, Palo Alto, CA) equipped with an autoinjector (model HP6890) and a flame ionization detector (FID). A Supelco Omegawax 320 (30 m × 0.32 mm, d_f 0.25 μm) fused silica capillary column with a bonded poly(ethylene glycol) phase was employed.

Table 1
Typical fatty acid methyl esters[a].

Shorthand designation	Systematic name	Trivial name	Formula
22:6	All-*cis*-4,7,10,13,16,19-docosahexaenoic acid methyl ester	DHA	$CH_3(CH_2CH{=}CH)_6(CH_2)_2CO_2CH_3$
20:5	All-*cis*-5,8,11,14,17-eicosapentaenoic acid methyl ester	EPA	$CH_3(CH_2CH{=}CH)_5(CH_2)_3CO_2CH_3$
18:3	All-*cis*-9,12,15-octadecatrienoic acid methyl ester	Methyl α-linolenate	$CH_3(CH_2CH{=}CH)_3(CH_2)_7CO_2CH_3$
18:2	All-*cis*-9,12-octadecadienoic acid methyl ester	Methyl linoleate	$CH_3(CH_2)_3(CH_2CH{=}CH)_2(CH_2)_7CO_2CH_3$
18:1	*cis*-9-Octadecenoic acid methyl ester	Methyl oleate	$CH_3(CH_2)_7CH{=}CH(CH_2)_7CO_2CH_3$
18:0	Octadecanoic acid methyl ester	Methyl stearate	$CH_3(CH_2)_{16}CO_2CH_3$
19:0[b]	Nonadecanoic acid methyl ester	N/A	$CH_3(CH_2)_{17}CO_2CH_3$

[a] 20:5, 22:6 and 18:3 are $\omega-3$ polyunsaturated fatty acid methyl esters.
[b] Used as the internal standard in the GC-FID quantification analyses.

The Omegawax™ column provides highly reproducible analyses of fatty acid methyl esters, specifically the omega-3 and omega-6 fatty acids. GC analyses of fatty acid methyl esters exhibited high reproducibilities. The oven temperature was programmed as follows: held constant at 190 °C for 10 min; and then increased at 3 °C/min to 230 °C; and finally kept constant for 20 min. The internal standard (IS) (nonadecanoic acid methyl ester, 19:0) method was used for quantifying FAME compositions via the equation $C_i = R_f C_s(A_i/A_s)$, where R_f is the response factor of the individual fatty acid methyl ester, C_i is the amount of any methyl ester I, C_s is the amount of 19:0, A_i is the area under the chromatographic peak of I, and A_s is the peak area of internal standard 19:0. Nonadecanoic acid methyl ester, 19:0, with an odd number of carbons in the carboxylic acid alkyl chain is widely used as an internal standard in the GC quantification of FAMEs because it does not interfere with the natural FAMEs. The response factors of each FAMEs were determined according to the reported method [28,29]. All the GC analyses were run in triplicate and the average values were reported in this study.

2.3. Batch extraction operations and determination of PUFAME distribution ratios

The detailed extraction procedures were reported in our previous work [25]. Briefly, fatty acid methyl esters (dissolved in hexane or other alkanes, 1 mL) were extracted by an ionic liquid (1 mL) containing $AgBF_4$. ILs were used as the solvents to dissolve and immobilize π-complexing reagent $AgBF_4$. ILs also form two immiscible phases with alkanes. It is worthy of note that an anion-exchange reaction could possibly take place when $AgBF_4$ is dissolved in ILs with PF_6^- as anions, for example, [hmim][PF_6]. However, the apparent or the total concentration of Ag^+ is not affected by the anion-exchange reaction. The apparent concentrations of $AgBF_4$ in ILs (mg/mL or mmol/mL) were used in this work. The extractions (shaken on a Mistral Multi-Mixer) were performed in capped amber-colored vials (4 mL) for various times at 25 °C. The vials were wrapped with aluminum foil to avert daylight. After standing and centrifuging, 0.5 mL of the upper hexane phase was pipetted out and transferred to a small vial (2 mL) containing a known amount of the internal standard (19:0). Then the amount of PUFAMEs in hexane solution was determined by GC-FID. The amount of PUFAMEs left in IL phase after extraction was calculated by the mass balance. The distribution ratios of PUFAMEs between IL phase and alkane phase were calculated by the following equation:

$$D_{FAME} = \left\{\frac{C_I - 2C_D}{2C_D}\right\}\left\{\frac{\text{volume of alkane solution}}{\text{volume of IL}}\right\}$$

where C_I represents the initial PUFAME concentration in hexane (or other alkanes). C_I was known according to the preparation of feedstock solution; C_D represents the PUFAME concentration in the transferred hexane solution (0.5 mL) (or other alkane solutions). C_D is determined by GC using the internal standard method. Because only 0.5 mL of hexane solution was transferred and analyzed from the total 1 mL of the upper hexane phase used in the extraction, the coefficient 2 was employed in this equation. The volumes of IL and hexane phases were omitted because they were both 1 mL in this study.

2.4. Determination of the extraction capacities of PUFAMEs from extraction isotherms

To determine the saturated extraction capacities for PUFAME uptake, 1 mL of hexane solution containing PUFAME (18:3, 20:5, or 22:6, respectively) with a concentration range between 0.3 and 4.0 mg/mL was extracted by $AgBF_4$ (5.5 mg) dissolved in [hmim][PF_6] (1 mL). The PUFAME extraction isotherms were obtained by plotting the PUFAME concentrations in hexane (mg/mL) as the *X*-axis and the amount of PUFAME extracted (mg/g $AgBF_4$) as the *Y*-axis.

2.5. Determination of water content in IL [hmim][PF_6] by Karl Fishers titration method

[Hmim][PF_6] was selected for water content analysis because it was the IL used in the majority of the experiments conducted. After it was freeze-dried on a lyophilizer overnight, an exact amount of [hmim][PF_6] was weighed and dissolved in dry dichloromethane. The water content in IL [hmim][PF_6] was determined by a Mettler Toledo DL 32 coulometer using the Karl Fishers method [30].

3. Results and discussion

3.1. Effect of extraction time

Long chain fatty acid methyl esters are generally more readily soluble in hexane than in polar ILs. However, the π-complexing interaction between silver ions and double bonds of PUFAMEs enables the highly selective extraction of unsaturated fatty acid methyl esters from hexane into the IL phase. This specific and reversible π-complexing interaction has already been widely utilized to separate olefins from saturated paraffins including an example using functionalized ionic liquids [31–33]. However, mass transfer of PUFAMEs between the two phases needs to overcome the phase barrier energy. This transport process takes time to occur. Therefore, the effect of extraction time on the distribution ratios of PUFAMEs was studied (Fig. 1). The distribution ratios of the di-unsaturated FAME 18:2 increased from 0.2 (1 min) to 18.3 (30 min). The distribution ratios of tri-unsaturated FAME 18:3 significantly went up to 42.0 after a 30-min extraction from only 0.3 (1 min). The distribution ratios of the penta-unsaturated FAME 20:5 increased mostly significantly from 1.0 (1 min) to 329.1 (30 min). At short extraction time (1 min), the distribution ratios of all the three

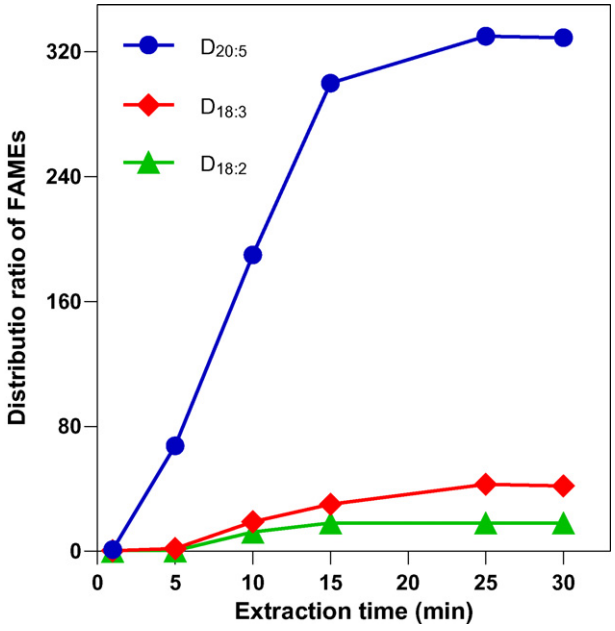

Fig. 1. Effect of extraction time on PUFAME distribution ratios. Individual 18:2, 18:3 or 20:5 (2 mg) dissolved in hexane (1 mL) was extracted by $AgBF_4$ (5.5 mg) dissolved in [hmim][PF_6] (1 mL), respectively.

PUFAMEs showed lower values. Thus, the transport of PUFAMEs from hexane phase into IL phase needs a suitable period of time even in the presence of $AgBF_4$. The increase in distribution ratios gradually leveled off after 30-min of extractions, indicating that distribution equilibrium was reached. Extraction times greater than 30 min were not used because longer extractions at room temperature and exposures to daylight might lead to oxidation, polymerization, isomerization or degradation of the thermally and photochemically liable PUFAMEs [34]. Silver salts are also known as light-sensitive compounds. Therefore, a 30-min vibration in the dark was selected as the standard extraction time.

3.2. Effect of alkane solvents as organic phases

Because of an ample availability and suitable stability, 18:3 was selected as a representative PUFAME to investigate the influence of alkane solvents as organic phases on the distribution ratios (Fig. 2). Since alkylimidazolium tertrafluoroborate or hexafluorophosphate ILs are highly miscible with polar solvents such as acetone, methanol, acetonitrile, and chloroform, these polar solvents could not be used in this liquid–liquid biphasic extraction. Nonpolar toluene or benzene shows low miscibility with ILs. However, because of their aromatic π-bond structures, toluene and benzene may impair the extraction capability of $AgBF_4$ by coordinating with Ag^+. Therefore, neither toluene nor benzene could be used. In contrast, alkanes show no ability to coordinate silver ions and are immiscible with ILs. Moreover, PUFAMEs show high solubilities in alkanes. Therefore, an alkane was finally selected as the organic phase to dissolve PUFAME. To investigate the effect of alkanes on the distribution ratios, 18:3 dissolved in alkanes possessing different alkyl chain lengths was extracted by $AgBF_4$ (5.5 mg) dissolved in [hmim][PF_6] (1 mL) (Fig. 2). According to Teramoto's work [9], the distribution ratio was proportional to the activity coefficient of eicosapentaenoate's ethyl ester in the organic phase. The distribution ratios of 20:5 increased with an increase in carbon number of the alkane employed [9]. However, our results showed a reversed trend. As seen in Fig. 2, the distribution ratios of PUFAME 18:3 gradually decreased with an increase in the alkyl chain length of the alkane. The distribution ratio of PUFAME 18:3 in hexane showed the highest value of 6.7. It was only 1.6 when n-dodecane was used as organic solvent. This discrepancy between Teramoto's work and ours could be possibly due to the different extraction phases used in the two studies. Aqueous $AgNO_3$ solution was used as the extraction phase in Teramoto's work, while $AgBF_4$–ionic liquid [hmim][PF_6] was used in our work.

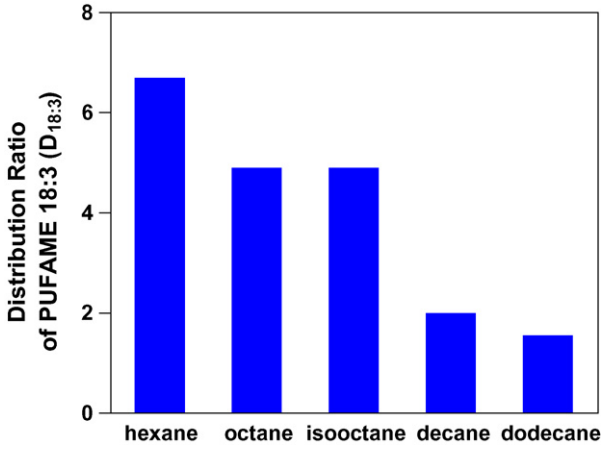

Fig. 2. Effect of alkane solvents on the PUFAME 18:3 distribution ratios. 18:3 (2 mg) dissolved in different alkanes (1 mL) was extracted by $AgBF_4$ (5.5 mg) dissolved in [hmim][PF_6] (1 mL).

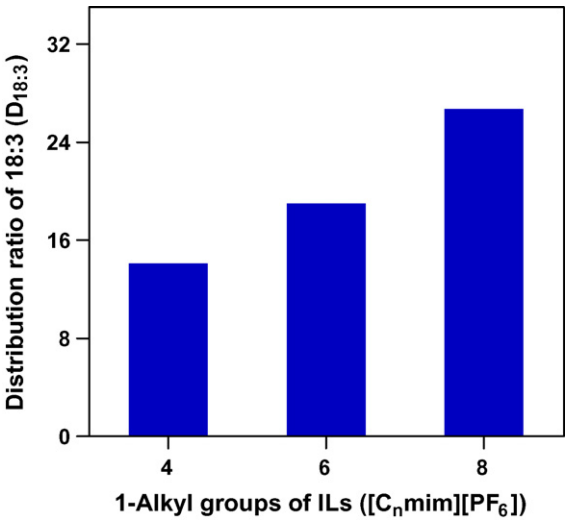

Fig. 3. Effect of ionic liquid structures, [$C_n$mim][PF_6] (n = 4, 6 and 8), on the PUFAME 18:3 distribution ratios. 18:3 (2 mg) dissolved in hexane (1 mL) was extracted by $AgBF_4$ (5.5 mg) dissolved in various ionic liquids (1 mL).

3.3. Effect of the ionic liquid structures

To investigate the effect of the IL structures on the distribution ratios of PUFAME 18:3, two series of different ILs with dissolved $AgBF_4$ were used as extraction phases. Particularly, the influence of the hydrophobicity of different ILs was considered using 18:3 as the representative PUFAME. Both the cation and anion structures could influence the IL hydrophobicities. Generally, ILs with PF_6^- as anions are more hydrophobic than those containing BF_4^- when their cations are identical [35]. When the anions are identical, IL hydrophobicities increase when the imidazolium cation's alkyl chain length is increased. Extraction results clearly indicated that $AgBF_4$ dissolved in the more hydrophobic [$C_n$mim][PF_6] series ILs exhibited significantly higher extraction capabilities than in the more hydrophilic [$C_n$mim][BF_4] ILs (Figs. 3 and 4). For instance, the

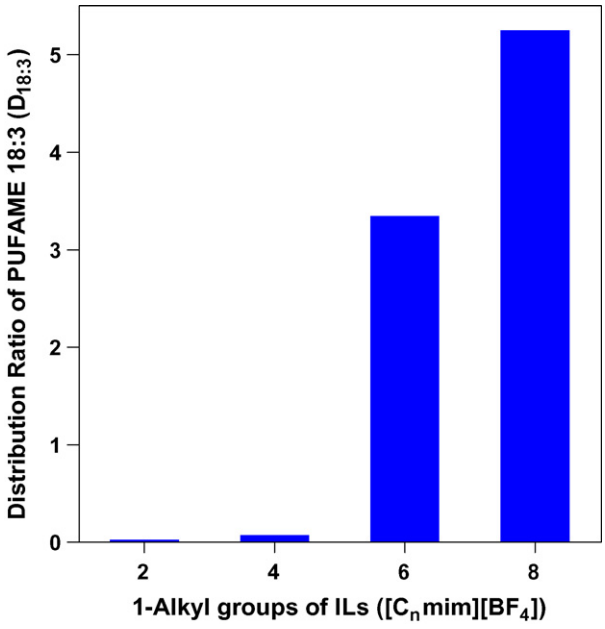

Fig. 4. Effect of ionic liquid structures, [$C_n$mim][BF_4] (n = 2, 4, 6, and 8), on the PUFAME 18:3 distribution ratios. 18:3 (2 mg) in hexane (1 mL) was extracted by $AgBF_4$ (5.5 mg) dissolved in various ionic liquids (1 mL).

two ILs ([hmim][PF_6] and [hmim][BF_4]) share the same cation (1-hexyl-3-methylimidazolium) but possess different anions (PF_6 or BF_4). The distribution ratio of 18:3 is 19.0 with $AgBF_4$–[hmim][PF_6] as extraction phase (Fig. 3), but only 3.4 with $AgBF_4$–[hmim][BF_4] (Fig. 4). When ILs share the same anion, the distribution ratios of PUFAME 18:3 also increased with an increase in the IL hydrophobicity. For example, the distribution ratio of 18:3 increased from 0.03 using $AgBF_4$–[emim][BF_4] to 5.3 using $AgBF_4$–[omim][BF_4] (Fig. 4). In another series of ILs, the 18:3 distribution ratios were 14.1 and 26.7 when $AgBF_4$–[bmim][PF_6] and $AgBF_4$–[omim][PF_6] were used as extraction phases, respectively. This result again demonstrated that $AgBF_4$ dissolved in hydrophobic ILs had higher extraction capabilities than when dissolved in hydrophilic ILs. The higher extraction capabilities of $AgBF_4$ in hydrophobic ILs could possibly be ascribed to the fact that hydrophobic ILs can more readily solubilize the highly hydrophobic omega-3 fatty acid methyl esters. In addition, the lower solvation or hydration of $AgBF_4$ in hydrophobic ILs could also be an explaination.

3.4. *Effect of $AgBF_4$ concentration in ILs on the extraction equilibrium parameters*

The preferential extraction of polyunsaturated fatty acid methyl esters (PUFAMEs) fundamentally stems from the π-complexing interaction between Ag^+ and the PUFAMEs' double bonds. ILs without silver salt only gave minimal extraction of PUFAMEs [25]. In this work, the effect of $AgBF_4$ concentrations on PUFAME distribution ratios was further studied. A profile of the various PUFAME (18:2, 18:3, or 20:5) distribution ratios versus $AgBF_4$ concentrations in [hmim][PF_6] is shown in Fig. 5. The PUFAMEs were dissolved in hexane. The distribution ratios for all three PUFAMEs increased with an increase in $AgBF_4$ concentrations. When $AgBF_4$ concentrations were near 0.01 mmol/mL, the distribution ratios for all the PUFAMEs were very low. The distribution ratios of PUFAME 20:5 went up significantly with increasing $AgBF_4$ concentration, climbing to 331.1 when the $AgBF_4$ concentration was 0.042 mmol/mL. The distribution ratios of PUFAMEs 18:3 and 18:2, however, increased rather slowly compared with that of 20:5, reaching only 42.0 and 18.4, respectively, at a $AgBF_4$ concentration of 0.042 mmol/mL.

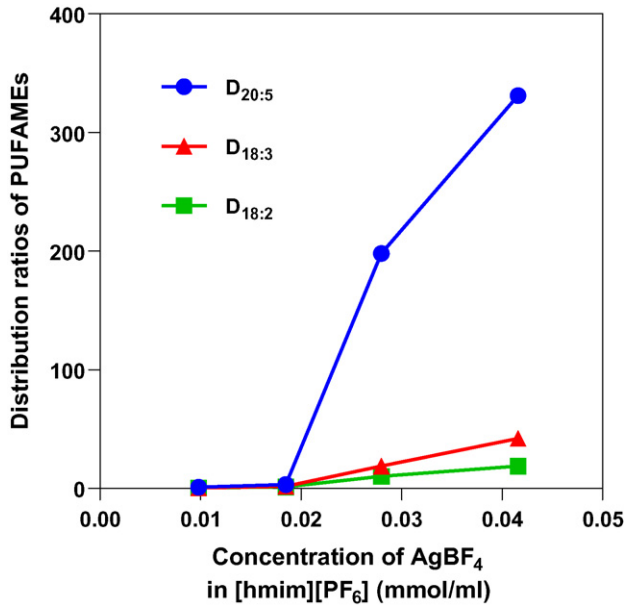

Fig. 5. Effect of $AgBF_4$ concentration on PUFAME distribution ratios. Individual 18:2, 18:3 or 20:5 (2 mg) dissolved in hexane (1 mL) was extracted by $AgBF_4$ dissolved in [hmim][PF_6] (1 mL), respectively.

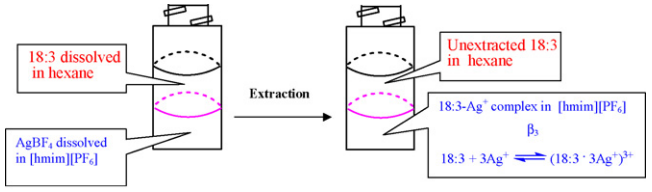

Scheme 2. Proposed extraction process of PUFAME 18:3 using $AgBF_4$–[hmim][PF_6] as the extraction phase. PUFAME18:3 dissolved in hexane is extracted by $AgBF_4$ dissolved in [hmim][PF_6]. β_3 is the stability constant of the complex formed between 18:3 and $AgBF_4$.

Teratomo [9] deduced that one Ag^+ coordinates, on average, with one PUFAME double bond. Assuming this is correct, a possible mechanism for organic/silver-IL biphasic liquid extraction of PUFAMEs is postulated in Scheme 2. In addition, the apparent equilibrium parameters such as partition coefficient and Ag^+–PUFAME complex stability constant were also calculated as follows.

First, the PUFAME physically dissolves in the IL phase or physically distributes between organic hexane and ionic liquid [hmim][PF_6] phases:

$$(\text{PUFAME})_\text{O} \rightleftharpoons (\text{PUFAME})_\text{IL}, \qquad K_\text{D} = \frac{(\text{PUFAME})_\text{IL}}{(\text{PUFAME})_\text{O}} \tag{1}$$

where K_D is the partition coefficient and subscripts O and IL denote the organic and IL phases, respectively.

Subsequently, the dissolved PUFAME coordinates with n moles of Ag^+ in the IL phase to form a $(\text{PUFAME}{\cdot}n\text{Ag})^{n+}$ complex, where n is the number of double bonds of PUFAME.

$$(\text{PUFAME})_\text{IL} + n(\text{Ag}^+)_\text{IL} \rightleftharpoons \langle \text{PUFAME} \cdot n\text{Ag} \rangle_\text{IL}^{n+},$$

$$\beta_n = \frac{[\langle \text{PUFAME} \cdot n\text{Ag} \rangle^{n+}]_\text{IL}}{[(\text{PUFAME})_\text{IL} \cdot (\text{Ag}^+)_\text{IL}^n]} \tag{2}$$

Here β_n is the stability constant for the formation of $(\text{PUFAME}\ n\text{Ag})^{n+}$ complex in IL phase. The distribution ratio, D, is defined as the ratio of total PUFAME concentration (free + complexed form) in IL phase to the total concentration in organic alkane phase. Thus, D can be derived from Eqs. (1) and (2) and expressed as:

$$\text{Distribution ratio, } D = \frac{[\text{PUFAME}]_\text{IL} + [(\text{PUFAME} \cdot n\text{Ag})^{n+}]_\text{IL}}{[\text{PUFAME}]_\text{O}}$$

$$= K_\text{D} + K_\text{D}\beta_n([\text{Ag}^+]_\text{IL})^n \tag{3}$$

The following Eq. (4) was derived from Eq. (3), when the extractions of PUFAMEs, 20:5, 18:3, or 18:2 (n = 5, 3, or 2), were performed, respectively. The distribution ratios D were obtained when extractions were performed using $AgBF_4$ dissolved in [hmim][PF_6] as extraction phase, whereas the partition coefficients K_D were obtained using the pure IL [hmim][PF_6] without $AgBF_4$ as the extraction phase. The stability constants β_n of the $(\text{PUFAME}{\cdot}n\text{Ag})^{n+}$ complexes were then obtained by substituting these values into Eq. (4).

$$\beta_n = \frac{D - K_\text{D}}{K_D[\text{Ag}^+]^n} \tag{4}$$

Here $[Ag^+]$ represents the free Ag^+ concentration in IL phase which can be estimated using Eq. (5):

$$[\text{Ag}^+] = [\text{Ag}^+]_I - n[(\text{PUFAME} \cdot n\text{Ag})]^{n+} \tag{5}$$

where the subscript I denotes the initial $AgBF_4$ concentration in [hmim][PF_6]. From the values of D, K_D, and $[Ag^+]$, β_n was calculated by Eq. (4). All of these values are listed in Table 2.

The distribution ratio of PUFAME 20:5, $D_{20:5}$, was about 2 orders of magnitude higher than $D_{18:2}$ using $AgBF_4$–[hmim][PF_6] as extraction phases (Table 2). However, the physical partition coefficients

Table 2
Values of PUFAME partition coefficients (K_D), distribution ratios (D_{PUFAME}), and PUFAME–Ag^+ complex stability constants (β_n).

PUFAME	K_D [a]	D_{PUFAME} [b]	β_n (mL/mmol)
20:5	0.09	198	7.03×10^{19}
18:3	0.05	19	3.44×10^{8}
18:2	0.04	2.1	1.27×10^{5}

[a] Partition coefficient (K_D) was obtained by extracting PUFAME (2 mg) dissolved in hexane (1 mL) using [hmim][PF_6] (1 mL) without adding $AgBF_4$ as the extraction phase for 30 min.

[b] Distribution ratio (D_{PUFAME}) was obtained using the experimental procedures described in Section 2. The initial concentration of $AgBF_4$ dissolved in [hmim][PF_6] was 5.5 mg/mL.

(K_D) of the three PUFAMEs (20:5, 18:3 and 18:2) between the hexane and the [hmim][PF_6] phases had similar values. This confirmed that the selective extraction of PUFAMEs resulted almost entirely from the differences in PUFAME–Ag^+ complex formation rather than from physical partition of the PUFAME in the IL phase. The stability constants (β_n) of PUFAME–Ag^+ complexes also increased as the degree of FAME unsaturation rose. This demonstrated that PUFAME–Ag^+ complexes become increasingly stable in ILs as the number of double bonds of the PUFAMEs increases.

3.5. Extraction isotherms and extraction capacities

The extraction isotherms of PUFAMEs (22:6, 20:5, and 18:3) were investigated by extracting each individual PUFAME hexane solution (0.3–4.0 mg/mL) with $AgBF_4$–[hmim][PF_6] (5.5 mg/mL) for 30 min at 25 °C. The amount of each PUFAME extracted into [hmim][PF_6] phase was determined by GC-FID using the material balance method. The extracted amounts of PUFAMEs were plotted versus the PUFAME concentrations in hexane in Fig. 6. The maxim extraction capacities from the extraction isotherms for PUFAMEs 18:3, 20:5 and 22:6 were 420.5, 540.7 and 650.3 mg/g $AgBF_4$, respectively. The extraction capacities increased as the degree of unsaturation increased. In a control test, the extraction isotherm of PUFAME 20:5 between aqueous methanol (water:methanol = 4:1, v/v) and hexane phases was also determined in order to compare the [hmim][PF_6] with aqueous methanol that used to dissolve $AgBF_4$. The extraction capacity was only 15.9 mg/g $AgBF_4$ using $AgBF_4$/aqueous methanol as extraction phase. Therefore, it is clear that $AgBF_4$ in the IL [hmim][PF_6] showed a much higher extraction capacity (540.7 mg/g $AgBF_4$) than in aqueous methanol solution (15.9 mg/g $AgBF_4$). Moreover, in another control test, the extraction capacity of PUFAME 20:5 was only 1.0 mg/g $AgBF_4$ when $AgBF_4$–pure water was tested as the extraction phase. Therefore, the extraction capability of $AgBF_4$ in pure water without organic co-solvent such as methanol was even lower than that in aqueous methanol solution. This may be because water strongly hydrates Ag^+ making π-coordination by PUFAMEs more difficult or because water could not solubilize the Ag^+–PUFAMEs complex well. Under our experimental conditions, a very low water content (38.2 ppm) as determined by Karl Fishers method existed in the hydrophobic IL [hmim][PF_6]. This suggests that silver ion could be less strongly or unhydrated in the hydrophobic ionic liquid. These extraction capacity tests using various extraction phases clearly confirmed and illustrated the unique and exceedingly high extraction capacity of $AgBF_4$ when dissolved in hydrophobic ILs. Although the production cost of ILs is higher than that of water or methanol, the much higher extraction capacities of $AgBF_4$ in ILs and the ability to reuse the ILs would compensate for the IL production cost. In this circumstance, higher extraction capacities allow for using less $AgBF_4$ to extract the same amount of PUFAMEs. Teramoto et al. [9] extracted only 0.76 mg of 20:6's ethyl ester that dissolved in heptane (1 mL) using a highly concentrated aqueous $AgNO_3$ (1.02 g/mL) solution as the extraction phase. However, in our work, only 0.0041 g of $AgBF_4$ dissolved in [hmim][PF_6] (1 mL) was used to completely extract 0.9 mg of 20:6's methyl ester in hexane (1 mL). This comparison clearly established the unique and remarkably high extraction efficiency of silver salts when dissolved in hydrophobic ILs.

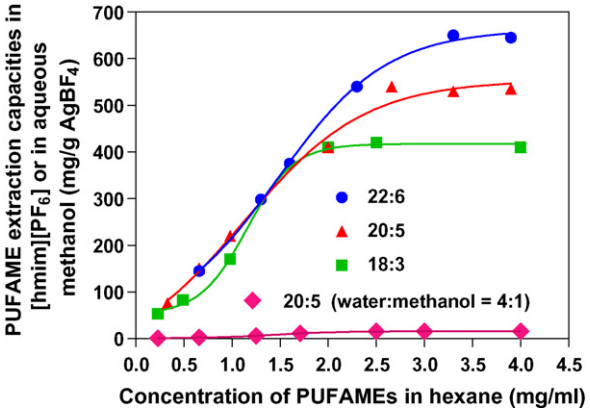

Fig. 6. Extraction isotherms of PUFAME. $AgBF_4$ (5.5 mg) dissolved in [hmim][PF_6] (1 mL) or water:methanol = 4:1 (v/v) were used as extraction phases. PUFAMEs (18:3, 20:5, or 22:6) with a concentration range between 0.3 and 4.0 mg/mL were extracted.

4. Conclusion

In summary, a novel and efficient method to extract and enrich polyunsaturated fatty acid methyl esters (PUFAMEs) has been described. The excellent separation power of ILs containing silver salts has also been established. The extraction equilibrium parameters were investigated using GC-FID and an extraction mechanism was tentatively proposed. The PUFAME extraction isotherms and extraction capacities were determined using the novel $AgBF_4$–IL extraction phase. These values clearly demonstrated that $AgBF_4$–[hmim][PF_6] has a much higher extraction capability than the traditional water–silver salt system. The higher extraction capabilities of $AgBF_4$ in hydrophobic ILs result from lower Ag^+ hydration in ILs than in aqueous solution. This allows silver ions to efficiently coordinate with the PUFAME double bonds. This coordination strength increases as the degree of unsaturation increases. Water, in contrast, strongly coordinates with silver ions (hydration), thereby competing with PUFAME coordination. In addition, ILs may also solubilize the Ag^+–PUFAMEs complex well, due to their ionic character. These examples clearly demonstrate the synergy between silver compounds and ionic liquids for PUFAME extraction.

Acknowledgement

Partial support of this work by the Department of Energy, DE-FG36-06G086025 is gratefully acknowledged.

References

[1] M. Penny, E.S. William, J. Harris, A. Lawrence, Circulation 106 (2002) 2747.
[2] C.E. Roynette, P.C. Calder, Y.M. Dupertuis, C. Pichard, Clin. Nutr. 23 (2004) 139.
[3] H. Sprecher, D.L. Luthria, B.S. Mohammed, S.P. Baykoushewa, J. Lipid Res. 36 (1995) 2471.
[4] Y. Özogul, F. Özogul, Food Chem. 100 (2007) 1634.
[5] M.H. Davidson, J.H. Burns, P.V. Subbaiah, M.E. Conn, K.B. Drennan, Arch. Intern. Med. 151 (1991) 1732.
[6] T. Okada, M.T. Morrissey, Food Chem. 103 (2007) 1411.
[7] A.M. Abu-Nasr, R.T. Holman, J. Am. Oil Chem. Soc. 31 (1954) 16.
[8] T.C. Chen, H.Y. Ju, Ind. Eng. Chem. Res. 40 (2001) 3781.
[9] M. Teramoto, H. Matsuyama, N. Ohnishi, S. Uwagawa, K. Nakai, Ind. Eng. Chem. Res. 33 (1994) 341.
[10] M. Arai, H. Fukuda, US Patent 4,721,584 (1988).
[11] W.W. Christie, J. Lipid Res. 30 (1989) 1471.

[12] M.P. Mansour, J. Chromatogr A. 1097 (2005) 54.
[13] H.J. Kim, S.B. Lee, K.A. Park, I.K. Hong, Sep. Purif. Technol. 15 (1999) 1.
[14] J.Z. Yin, A.Q. Wang, W. Wei, Y. Liu, W.H. Shi, Sep. Purif. Technol. 43 (2005) 163.
[15] J.S. Wilkes, J. Mol. Catal. A: Chem. 214 (2004) 11.
[16] G. Absalan, M. Akhond, L. Sheikhian, Talanta 77 (2008) 407.
[17] R. Vijayaraghavan, N. Vedaraman, M. Surianarayanan, D.R. MacFarlane, Talanta 69 (2006) 1059.
[18] N. Hirayama, M. Deguchi, H. Kawasumi, T. Honjo, Talanta 65 (2005) 255.
[19] T. Welton, Chem. Rev. 99 (1999) 2071.
[20] Y. Mochizuki, K. Sugawara, Energy Fuels 22 (2008) 3303.
[21] M.L. Dietz, D.C. Stepinski, Talanta 75 (2008) 598.
[22] G.W. Meindersma, A. Podt, A.B. Haan, Fuel Process. Technol. 87 (2005) 59.
[23] K. Nakashima, F. Kubota, T. Maruyama, M. Goto, Anal. Sci. 19 (2003) 1097.
[24] S. Dai, Y.H. Ju, C.E. Barnes, J. Chem. Soc., Dalton Trans. (1999) 1201.
[25] M. Li, T. Li, Sep. Sci. Technol. 43 (2008) 2072.
[26] J.R. Conder, C.L. Young, Physicochemical Measurement by Gas Chromatography, 2nd ed., John Wiley & Sons, New York, 1979, pp. 31, 146.
[27] P. Wasserscheid, T. Welton, Ionic Liquids in Synthesis, 1st ed., Wiley-VCH, Weinheim, Germany, 2003.
[28] C.D. Bannon, J.D. Craske, A.E. Hilliker, J. Am. Oil Chem. Soc. 63 (1986) 105.
[29] J.L. Beare-Rogers, A. Dieffenbacher, Pure Appl. Chem. 62 (1990) 795.
[30] C.A. De Caro, A. Aichert, C.M. Walter, Food Control 12 (2001) 431.
[31] J. Padin, R.T. Yang, C.L. Munson, Ind. Eng. Chem. Res. 38 (1999) 3614.
[32] D.J. Safarik, R.B. Eldridge, Ind. Eng. Chem. Res. 37 (1998) 2571.
[33] D. Jiang, S. Dai, J. Phys. Chem. B 112 (2008) 10202.
[34] R.C. Wijesundara, W.M.N. Ratnayake, R.G. Ackman, J. Am. Oil Chem. Soc. 66 (1989) 1822.
[35] C. Chiappe, D. Pieraccini, J. Phys. Org. Chem. 18 (2005) 275.

Talanta 78 (2009) 1246–1252

Contents lists available at ScienceDirect

Talanta

journal homepage: www.elsevier.com/locate/talanta

Simultaneous determination of sixteen metabolites related to neural tube defects in maternal serum by liquid chromatography coupling with electrospray tandem mass spectrometry

Xiao-Ping Liang[a], Qiong-Lin Liang[b,*], Jian-Fei Xia[a], Yong Wang[a], Ping Hu[c,**], Yi-Ming Wang[b], Xiao-Ying Zheng[d,**], Ting Zhang[e], Guo-An Luo[a,b,*]

[a] School of Pharmaceutics, East-China University of Science & Technology, PR China
[b] Key Laboratory of Bioorganic Phosphorus Chemistry & Chemical Biology (Ministry of Education), Department of Chemistry, Tsinghua University, PR China
[c] College of Chemical and Molecular Engineering, East-China University of Science & Technology, PR China
[d] WHO Collaborating Center for Research, in Reproductive Health and Population Science, Institute of Population Research, Peking University, PR China
[e] Capital Institute of Pediatrics, Beijing, PR China

ARTICLE INFO

Article history:
Received 5 November 2008
Received in revised form 16 January 2009
Accepted 18 January 2009
Available online 24 February 2009

Keywords:
LC/MS/MS
Folate
Homocysteine
Glutathione
Neural tube defects

ABSTRACT

Disturbances in maternal folate, homocysteine, and glutathione metabolism have been reported to be associated with neural tube defects (NTDs). However, the role played by specific components in the metabolic pathways leading to NTDs remains unclear. Thus an analytical method for simultaneous measurement of sixteen compounds involved in such three metabolic pathways by high performance liquid chromatography–tandem mass spectrometry was developed. The use of hydrophilic chromatography column improved the separation of polar analytes and the detection mode of multiple-reaction monitoring (MRM) enhanced the specificity and sensitivity so as to achieve simultaneous determination of three class of metabolites which have much variance in polarity and contents. The influence of parameters such as temperature, pH, flow rate on the performance of the analytes were studied to get an optimal condition. The method was validated for its linearity, accuracy, and precision, and also used for the analysis of serum samples of NTDs-affected pregnancies and normal women. The result showed that the present method is sensitive and reliable for simultaneous determination of as many as sixteen interesting metabolites which may provide a new means to study the underlying mechanism of NTDs as well as to discover new potential biomarkers.

1. Introduction

Neural tube defects (NTDs) are among the most common human congenital malformations that occur as a result of failure of the neural tube to close during the fourth week of human embryogenesis with defects occurring at any point along the formation of the spinal cord. Although the diagnosis is easy, NTDs etiology is quite complex and multifactorial, involving environmental [1], nutritional [2,3] and genetic [4–6] components. In addition, NTDs' prevalence varied according to geographical area, ethnic group and socioeconomic level [7–9]. In Europe 10/10,000 new-born children present with NTDs [10], whereas in China these defects occur in 10/10,000 births in southern areas, 50–60/10,000 in northern areas [11], and 160–180/10,000 in the area of our study [12,13]. Despite the great majority of prenatal losses, NTDs can lead to lifelong disability and cause tremendous social costs annually.

There is now ample evidence that low blood folate status is closely associated with the risk of NTDs [14–17]. In folate metabolism, 5-methyltetrahydrofolate (5-MT), 5-formyltetrahydrofolate (5-FT), tetrahydrofolate (THF) and unmetabolized dietary folic acid (FA) are the main folate vitamers. In our previous publication [18], serum concentrations of 5-MT, 5-FT and FA were found significantly reduced in pregnancies affected by NTDs. Therefore, the accurate characterization of folate metabolism

Abbreviations: NTDs, neural tube defects; HPLC/MS/MS, high-performance liquid chromatography-electrospray tandem mass spectrometry; FA, folic acid; THF, tetrahydrofolate; 5-FT, 5-formyltetrahydrofolate; 5-MT, 5-methyltetrahydrofolate; Met, methionine; Hcy, homocysteine; His, histidine; Ser, serine; Cysta, cystathionine; SAH, S-adenosyl-homocysteine; SAM, S-adenosyl-methionine; GSH, reduced glutathione; GSSG, oxidized glutathione; CysGly, cysteinylglycine; GluCys, glutamylcysteine; Cys, cysteine; Ade, adenosine; DTT, dithiothreitol; QC, quality control; MRM, multiple-reaction monitoring; 5,10-MT, 5,10-methylenetetrahydrofolate; MS, methionine synthase; MTHFD, methylenetetrahydrofolate dehydrogenase; MTHFR, 5,10-methylenetetrahydrofolate reductase; MT, methyltransferases; CBS, cystathionine β-synthase; SAHH, S-adenosyl-homocysteine hydrolase; GCL, glutamate-cysteine ligase; GS, glutathione synthase; GR, glutathione reductase.

* Corresponding authors at: Department of Chemistry, Tsinghua University, Beijing 100084, PR China. Tel.: +86 1062781688 fax: +86 1062781688.
** Corresponding authors.
E-mail address: luoga@mail.tsinghua.edu.cn (G.-A. Luo).

0039-9140/$ – see front matter © 2009 Elsevier B.V. All rights reserved.
doi:10.1016/j.talanta.2009.01.063

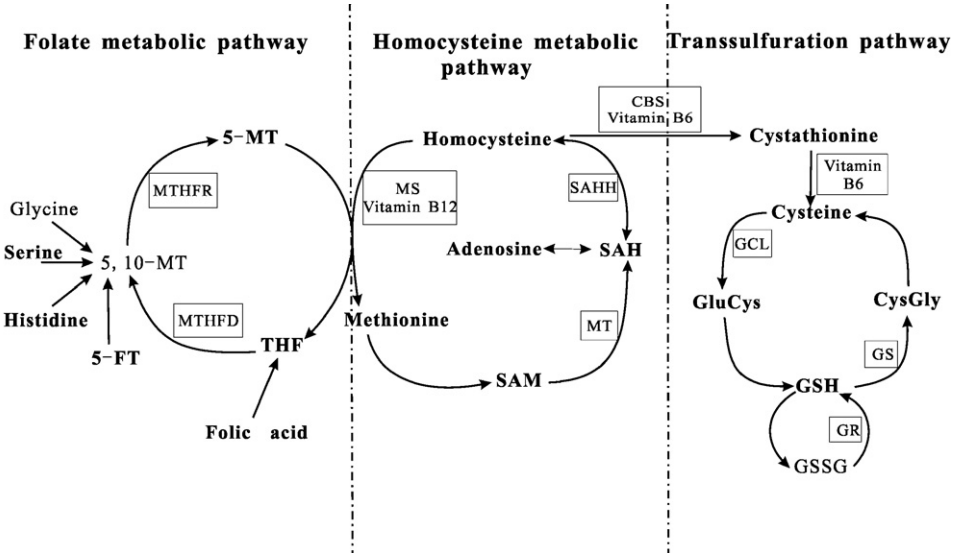

Fig. 1. The folate, homocyseine and glutathione related metabolic pathways.

will make us better understand the potential mechanisms of NTDs. Furthermore, folate is involved in the methylation of homocysteine (Hcy) into methionine (Met), and a low-folate status can result in the accumulation of Hcy [19]. Accumulated Hcy results in the secondary accumulation of S-adenosyl-homocysteine (SAH). Elevated SAH concentrations will reduce the methylation index and thus depress the process of transmethylathion [20]. Additionally, the significant decrease in the ratio of S-adenosyl-methionine (SAM):SAH, also called "methylation index", is an indicator of hypomethylation [21]. Therefore, the disturbances of Hcy metabolism as well as folate metabolism could both impact the formation of NTDs.

Additionally, the metabolic pathway from Hcy to glutathione is referred to as the transsulfuration pathway. Elevated Hcy is associated with alterations in the transsulfuration pathway that lead to greater oxidative stress [22]. Some experimental models have suggested that, in addition to evidence of a direct teratogenic effect, elevated Hcy may have an indirect embryo toxic effect by increasing oxidative stress through excessive production of reactive oxygen species and by decreasing the glutathione-dependent antioxidant-defense mechanisms [22,23]. To sum up, the underlying alterations in folate, Hcy and glutathione metabolism are well associated with NTDs.

Pathways involved in folate, Hcy and glutathione metabolism are depicted in Fig. 1 (the compounds investigated in our study were signed in bold type). To better understand the underlying mechanism of NTDs, sixteen pivotal metabolites in the three pathways were quantified simultaneously, namely FA, THF, 5-MT, 5-FT, histidine (His) and serine (Ser) in folate metabolic pathway; Hcy, Met, SAM, SAH and adenosine (Ade) in Hcy metabolic pathway; and cystathionine (Cysta), reduced glutathione (GSH), cysteine (Cys), cysteinylglycine (CysGly) and glutamylcysteine (GluCys) in transsulfuration pathway.

Various analytical tools based on gas or liquid chromatography have been developed for the determination of folates, amino acids, glutathiones and other aforementioned metabolites in biological samples [24–28]. Although gas chromatography/electron impact-mass spectrometry (GC/EI-MS) allows sensitive detection of amino acids [25], this technique requires chemical derivation procedures in order to enhance the volatility of compounds. Alternatively, liquid chromatographic analysis generally relies on derivatization followed by ultraviolet [28,29], fluorometric [30–32] detection. However, because of the prior derivatization of sulfydryl groups, these methods are limited to free thiol-containing compounds bearing a blocked thiol function such as Met or GSH. These drawbacks can be overcome by the use of liquid chromatography coupled to electrospray tandem mass spectrometric (LC/MS/MS) detection, due to its high sensitivity and specificity. Based on these considerations, a LC/MS/MS method for simultaneous quantification of sixteen metabolites of the three pathways in human serum was developed in our research.

Table 1
Mean retention times and compound-dependent MS parameters for each analyte.

Measured compound	Mean retention time (min ± S.D.)	Precursor ion	Fragment ion	DP	FP	EP	CE	CXP
FA	31.91 ± 0.05	442.2	295.1	45	150	9	18	10
THF	29.03 ± 0.03	446.1	299.0	45	150	8	18	10
5-MT	30.14 ± 0.04	460.2	313.1	40	150	9	24	15
5-FT	31.68 ± 0.02	474.2	327.2	45	150	10	25	15
Hcy	7.05 ± 0.03	136.0	90.0	27	110	6	16	8
Met	12.66 ± 0.02	150.0	104.0	30	110	6	15	9
SAH	19.83 ± 0.04	385.2	136.2	40	140	8	25	12
SAM	8.07 ± 0.03	399.2	250.1	40	150	8	20	10
Cysta	6.51 ± 0.02	223.0	134.1	35	130	8	20	11
His	6.13 ± 0.03	156.0	110.1	30	115	8	19	10
Ser	11.50 ± 0.03	106.1	60.0	30	110	7	15	11
Cys	12.12 ± 0.03	122.1	76.1	32	110	6	18	15
GluCys	14.08 ± 0.02	251.2	122.1	33	120	7	16	10
CysGly	13.45 ± 0.03	179.2	76.1	30	120	5	20	13
Ade	22.03 ± 0.03	268.2	136.1	40	150	9	22	10
GSH	14.61 ± 0.04	308.2	179.2	35	130	8	16	15

Table 2
Precisions and recoveries of spiked QC serum samples.

Compound	Intra-day ($n=6$)						Inter-day ($n=9$)	Spiked concentration		
	Low[a]		Medium[a]		High[a]		Medium[a]	Low[a]	Medium[a]	High[a]
	Recovery (%)	CV (%)	Recovery (%)	CV (%)	Recovery (%)	CV (%)	CV (%)	(ng mL^{-1})	(ng mL^{-1})	(ng mL^{-1})
FA	97.1	4.99	90.9	7.31	86.7	7.91	7.84	1	2	4
THF	76.5	9.75	83.4	6.29	91.8	8.23	8.83	5	10	20
5-MT	113.1	7.27	102.0	5.04	99.1	2.43	8.64	5	10	20
5-FT	86.8	9.77	109.4	4.15	93.5	3.63	6.94	5	10	20
Hcy	100.4	5.43	103.6	3.71	93.2	4.89	7.09	400	800	1200
Met	89.3	6.75	106.3	5.68	111.2	4.67	6.78	1000	2000	4000
SAH	88.4	5.38	108.8	7.44	92.0	4.25	5.89	5	10	20
SAM	85.2	3.66	93.1	4.12	108.6	5.25	6.67	10	20	40
Cysta	75.6	5.84	93.5	4.42	93.2	1.27	4.98	5	10	20
His	84.5	2.46	114.8	2.38	94.7	4.37	5.37	1500	3000	6000
Ser	78.9	8.16	105.5	7.52	94.5	10.1	3.04	50	100	200
Cys	98.5	3.85	105.3	2.17	97.3	5.12	4.65	1500	3000	6000
GluCys	94.4	6.63	95.6	3.29	95.7	4.88	6.20	300	600	1200
CysGly	85.2	4.47	90.9	5.01	94.7	3.52	4.67	1000	2000	4000
Ade	83.5	3.76	98.4	4.78	89.4	2.45	7.23	80	160	320
GSH	100.4	6.69	106.2	8.44	119.0	10.5	5.79	500	1000	2000

[a] Serum samples spiked with low, medium, or high concentrations.

To our knowledge, owing to the instabilities, wide concentration ranges and strong polarities of the analytes, the simultaneous quantification of relevant components that cover the three metabolic pathways has not been reported. The established method is a multi-class metabolites analysis and will be helpful to the study of the underlying mechanism of NTDs.

2. Experimental

2.1. Apparatus

An Applied Biosystems (Toronto, Canada) API 3000 triple-quadrupole tandem mass spectrometer, equipped with a Turbo Ionspray interface and an Agilent 1100 binary HPLC system (Palo Alto, CA, USA), was used for LC–MS/MS analysis. Separation was performed on an Ultimate^{TM} AQ-C_{18} analytical column (250 mm × 4.6 mm I.D., 5 μm, Welch Materials, MD, USA) connected to an Alltech guard column (7.5 mm × 4.6 mm, 5 μm particles). For pH measurement, a microprocessor pH meter was used (HANNA, Italia). Ultrapure water (18.2 MΩ) was prepared with a Milli-Q water purification system (Millipore, France).

2.2. Chemicals and reagents

The following compounds were obtained from Sigma–Aldrich (St. Louis, MO, USA): FA, THF 5-MT, 5-FT, Hcy, Met, Cysta, SAM, SAH, His, Ser, Ade, GSH, Cys, CysGly, GluCys, dithiothreitol (DTT). HPLC-grade methanol, acetonitrile were purchased from Honeywell Burdick & Jackson (Muskegon, MI, USA); analytical-grade ammonium formate, formic acid, ascorbic acid and citric acid monohydrate were purchased from Beijing Chemical Company (Beijing, China).

2.3. Methods

2.3.1. Preparation of samples

Before analysis, 100 μL of aqueous DTT (15 mg/mL) were added to 200 μL aliquots of serum, vortexed for 2 min, and then treated with 800 μL of methanol containing ascorbic acid and citric acid (both 100 μg/mL). The mixture was vortexed for 2 min and then centrifuged at 10,000 rpm for 15 min at 4 °C. The clear supernatant was transferred to a 1.5 mL polypropylene tube, and dried under a gentle stream of nitrogen at room temperature. The residue was reconstituted with 100 μL of water containing 10 μg/mL of ascorbic acid, citric acid, and DTT, and stored at −20 °C before analysis.

2.3.2. LC–MS/MS methods

HPLC analysis was performed with an Agilent 1100 Series system. Separation was carried out with an analytical reversed-phase column Ultimate^{TM} AQ-C_{18}, 250 × 4.6 mm I.D. packed with 5 μm particles (Welch Materials, MD, USA). The mobile phases were set as follows: 5 mM ammonium formate, adjust to pH **3.2** with 0.15% (v/v) formic acid (eluent A), and 0.15% (v/v) formic acid in acetonitrile (eluent B). The following linear elution gradient was used (flow rate, 500 μL/min): 0–25 min, 100% A to 20% A; 25–28 min, 20% A to 5% A; 28–30 min, 5% A to 100% A. The equilibration time was 10 min. And the flow was reduced to 200 μL/min prior to MS detection using a T-split. Column temperature was set to 30 °C. The total analysis time was 40 min and the injection volume was 20 μL in each run.

The MS/MS operating parameters were obtained and optimized under positive-ion (ESI+) mode. Multiple-reaction monitoring (MRM) transitions for each analyte were individually optimized and summarized in Table 1. To ensure the sensitivity of detection, MRM experiments were divided into two periods to monitor the transitions of particular analytes separately. The ionspray voltage of 5000 V and source temperature of 400 °C were adopted. The collision gas (nitrogen) was set at 6 mTorr. The flow rates of the nebulizer gas (air), curtain gas (nitrogen), and drying gas (nitrogen) were 8, 9, 1.2 L/min, respectively. The choice of ionization conditions for each analyte was made with the aim of maximizing the sensitivity under the experimental conditions.

2.3.3. Preparation of calibration standards and quality control samples

Stocked solutions for each standard were prepared at a concentration of 100 μg/mL in 50:50 (v/v) methanol/water and stored at −20 °C. For folates, the standard solutions were containing 100 μg/mL each of ascorbic acid, citric acid and DTT to inhibit oxidation. And the DTT of 100 μg/mL was added to the standard solutions of Hcy, GSH, and Cys to keep their reduced forms. Calibrants were prepared by diluting the stocked solutions with water (containing assembled antioxidants as above), resulting in concentrations of 0.5, 1, 2, 5, 10, 50 ng/mL for FA, 5-MT, 5-FT, Cysta, and SAH, 2, 5, 10,50, 100, 200 ng/mL for THF and SAM, 0.02, 0.05, 0.1, 0.2, 0.5, 1 and 2 μg/mL for Hcy, Ser, and Ade, 0.1, 0.2, 0.5, 1, 2, 5, 10 μg/mL for Met and His, and 0.05, 0.1, 0.2, 0.5, 1, 2, 4, 8 μg/mL for Cys, GluCys, CysGly, and GSH. Quality control (QC) samples were prepared by

spiking 200 μL aliquots of blank serum with low, medium, and high concentrations of standards to obtain a serum spiking solution, respectively (see Table 2 for individual standard enrichments). All the stock solutions, working solutions and QC samples were stored at −20 °C and brought to room temperature before use.

2.3.4. Calibration curve

External calibration method was used for the quantitative analysis. Calibration curves were obtained by the plots of the peak-area versus the concentration of the standards and analyzed for three runs. The concentrations of the metabolites in serum samples were determined by using the equations of linear regression obtained from the calibration curves.

2.3.5. Method validation

The precision and accuracy studies were performed by calculating the CVs (coefficient of variations) and recoveries obtained from the QC samples. Intra-day precision (each $n = 6$) was evaluated by analysis of QC samples at different times on the same day. Inter-day precision ($n = 9$) were determined by repeated analysis of QC samples spiked with standards of medium concentration thrice per day over three consecutive days. The calibration curves were calibrated everyday by analyzing two working solution samples before analyzing the serum samples to ensure the precision of the results.

The extraction recoveries were determined by analysis of the blank serum spiked with an equivalent concentration of exogenous replications. Three concentrations were studied: the center was the endogenous level, the low and high were 50% and 200% of the center, respectively.

The compound stability for 0, 2, 4, 8, 16 and 24 h at −20 °C in serum was evaluated by repeated analysis at the medium concentration of QC samples.

2.3.6. Date analysis

The mass spectrometry data were processed using Analyst software (Applied Biosystems, Foster City, CA, USA) in the API3000 LC/MS/MS system. Linear regression analysis (Excel) was used to verify the linearity of the calibration curves.

3. Results and discussion

3.1. Optimization of sample preparation

3.1.1. Optimization of sample extraction

Unless the analyte species were extracted from the serum samples prior to LC/MS/MS, co-eluting serum components either suppressed ionization or interfered with analytes detection. Therefore, preliminary sample extraction would be necessary to LC/MS/MS analysis in order to eliminate interference from the serum matrix, although MS/MS can provide high specificity because of its ability to monitor selected mass ions. Preliminary sample extraction was usually carried out by protein precipitation with acids (including sulfosalicylic acid, perchloric acid, trichloroacetic acid, meta-phosphoric acid), methanol, acetonitrile, solvent to solvent extraction, solidphase extraction (SPE), or combinations thereof. However, the use of acid solutions was prevented by the need to obtain a pH compatible with the column specifications. And the SPE was excluded due to its time-consuming procedure and the analytes' thermal instability. To simplify and increase the speed of sample preparation, serum samples were deproteined with methanol and acetonitrile respectively. Owing to poor solubilities in acetonitrile, some of the analytes were separated from the supernatant and resulted in low recoveries. Finally, the methanol was chosen as protein precipitation agent for its good intermiscibility with analytes and protein precipitation ability.

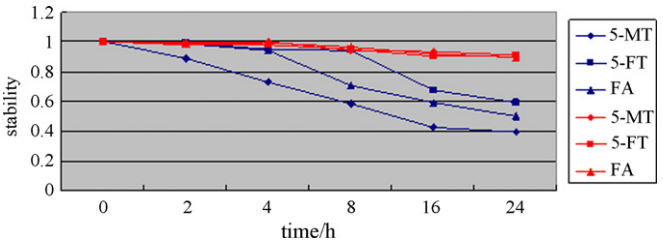

Fig. 2. The stability of folates in the absence and presence of the antioxidants at room temperature.

3.1.2. Application of the dithiothreitol

In biological systems, low-molecular-mass aminothiols such as homocysteine, cysteine, and reduced glutathione contain thiols, were easily oxidized to various disulfides. In serum, aminothiols exist in different forms, including the protein-bound fraction, free oxidized fraction such as cycteine–homocysteine or other mixed disulfides, and aminothiol dimers. To determine total aminothiols, it is necessary to cleave disulfide bounds in order to form the free sulfydryl group. As described in our previous work [33], the DTT was effective at reducing amino disulfides to its monomers and stabilizing the monomers once they are formed [30,31,34]. Besides, as a reducer, DTT also has protective and reductive effects on folates.

3.1.3. Optimization of antioxidants system

Folates are susceptible to light, heat, and other oxygen conditions. Because of the instability of folates, it was necessary to add antioxidants to the system to prevent degradation. Based on literature review [35–37], it was found that ascorbic acid and 2-mercaptoethanol were frequently used antioxidants, while citric acid was a good synergist of them. In order to achieve the best protective effect, we evaluated different combinations of ascorbic acid, citric acid, 2-mercaptoethanol and DTT of varying concentrations. And the optimal combinations and concentrations of antioxidants were the combination of ascorbic acid (100 μg/mL), citric acid (100 μg/mL) and DTT (15 mg/mL). The protective effect of the optimal antioxidants system for folates in 24 h was evaluated. Fig. 2 shows that stabilities of folates were obviously increased with the presence of the antioxidants, especially after 4 h.

3.2. Optimization of chromatography and mass spectrometry conditions

3.2.1. Optimization of chromatography condition

Standard reversed-phase chromatography yields little retention for amino acids because of their hydrophilic and ionic character. They were eluted close to the solvent front, which made the separation difficult. In order to minimize ion suppression from both matrix effects and interferences from co-eluted compounds in the system, it was essential to increase chromatographic separation. Derivatization methods are conventionally used for hydrophilic amino acid separation and determination, but these methods were not suitable for this thermally unstable system. Therefore, the hydrophilic column was chosen over standard reverse-phase columns due to its better adsorption capacity of polarity compounds, which can help overcoming the minimal retention of hydrophilic compounds in reversed-phase HPLC. In this study, based upon "hydrophilic interaction liquid chromatography", we evaluated four different hydrophilic chromatography columns, including Alltima HP HILIC (250 mm × 4.6 mm, 5 μm particles, Alltech Associates, Deerfield, IL, USA), Ultimate AQ-C18 (150 mm × 2.1 mm, 5 μm particles,

Welch Materials, MD, USA), Ultimate AQ-C18 (250 mm × 2.1 mm, 3 μm particles, Welch Materials, MD, USA), and Ultimate AQ-C18 (250 mm × 4.6 mm, 5 μm particles, Welch Materials, MD, USA). Finally, the Ultimate AQ-C18 column (5 μm, 4.6 × 250 mm, Welch Materials Inc.) was chosen for its better retention and separation of the analytes than the other three columns.

The mobile phases included organic solvents and volatile aqueous buffers at various pH values and ionic strengths. Considering the compatibility with electrospray mass spectrometry, only the volatile buffers include ammonium formate, ammonium acetate, formic acid, and acetic acid were investigated over the concentration range of 2–20 mM. Besides, the influences of pH, temperature, mobile phase flow rate on retention were also studied. The final chromatography conditions were determined as described in Section 2.3.2.

3.2.2. Optimization of mass spectrometry condition

In order to identify the major species formed in the collisional sequential fragmentation of MS/MS analysis, a mass characterization study was firstly performed for direct infusion (flow rate 10.0 μL/min) of solutions of each compound (10.0 mg/L in methanol). Parameters such as collision energy, capillary voltage, cone voltage, and nitrogen pressure in the collision cell were optimized in both positive and negative ion mode. Most analytes provided better results in positive-ion mode.

However, individual optimization of liquid and mass spectrometry conditions may not obtain the optimum conditions when the liquid chromatography is connected to mass spectrometry. In order to obtain the highest selectivity and lowest limit of quantification, the ion source temperature (TEM), ionspray voltage (IS), collision gas (CAD), curtain gas (CUR), and nebulizer gas (NEB) were optimized in turn by the manual sample injector and HPLC pump directly connected to ion source without column. The flow rate and injection volume were the same as sample analysis for each analyte. In addition, many ion source parameters interact with each other, which require repeated modulation. The final MS parameters were determined as described in Section 2.3.2. The representative chromatograms of the sixteen analytes in the blank sample fortified with stock solution are shown in Fig. 3.

3.3. Validation

The developed analytical method was then validated by evaluating linearity, intra-day ($n = 6$) and inter-day ($n = 9$) precision, recovery, stability and by determining the limits of detection and quantification.

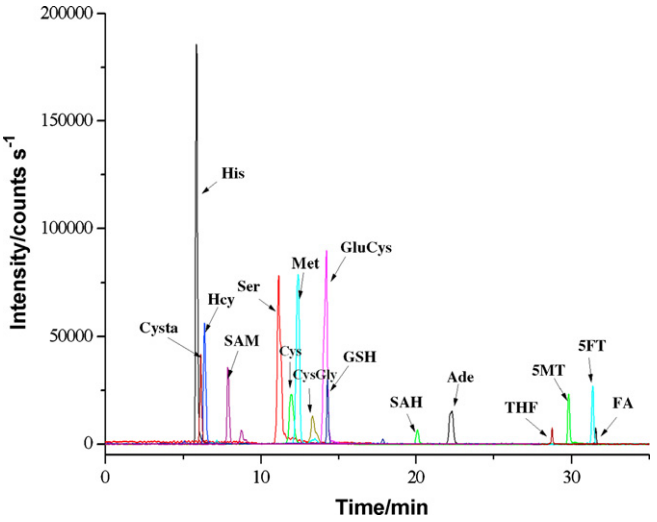

Fig. 3. Multiple extracted ion chromatograms of each analyte in blank sample fortified with stock solution.

3.3.1. Calibration curves and linearity

Under the optimized conditions, the calibration curves were obtained. The correlation between analyte concentration and detector was linear. The regression equation of calibration curves and their correlation coefficients (r) were shown in Table 3. All the calibration curves were suitable for the analysis of maternal serum except that of THF for its low concentration in serum.

3.3.2. Detection and quantitation limits

The limit of detection (LOD) is the concentration of analyte giving a signal/noise ratio of 3:1, whereas the limit of quantification (LOQ) refers to the lowest concentration of the standard curve that can be measured with acceptable accuracy and precision. The LOQs for all the metabolites were established by calculating the CVs at lowest concentration point of three different calibration curves. The LOQ of each compound was fixed at the lowest concentration exhibiting a CV inferior to 10%. Table 3 displays the values of these two parameters for all the investigated metabolites.

3.3.3. Precision, extraction recovery and stability

The data from QC samples were calculated to estimate the intra-day precision, inter-day precision, and extraction recoveries. The results were displayed in Table 2.

The CVs (%) of the QC samples in 24 h at room temperature were all below 9.5% and no significant degradation was observed.

Table 3
The regression equations and limits of detection and quantitation of sixteen compounds.

Measured compound	Regression equation	Linear range (ng mL^{-1})	r^2	LOQ (ng mL^{-1})	LOD (ng mL^{-1})
FA	$y = 26.217x + 3.803$	0.5–50	0.9986	0.5	0.1
THF	$y = 12.195x + 0.318$	2–200	0.9989	2	1
5-MT	$y = 32.358x - 3.317$	0.5–50	0.9991	0.5	0.1
5-FT	$y = 52.609x - 1.384$	0.5–50	0.9994	0.5	0.1
Hcy	$y = 316.184x + 15.658$	20–2000	0.9992	20	0.1
Met	$y = 416.503x + 18.566$	100–10,000	0.9981	100	0.05
SAH	$y = 32.358x - 3.317$	0.5–50	0.9987	0.2	0.1
SAM	$y = 163.198x + 4.162$	2–200	0.9986	2	0.25
Cysta	$y = 235.711x + 5.022$	0.5–50	0.9995	0.5	0.1
His	$y = 870.313x + 157.228$	100–10,000	0.9983	100	0.05
Ser	$y = 222.039x + 27.759$	20–-2000	0.9991	20	0.1
Cys	$y = 108.478x + 1.731$	50–8000	0.9991	50	0.5
GluCys	$y = 249.388x - 2.498$	50–8000	0.9986	50	0.25
CysGly	$y = 203.499x - 2.873$	50–8000	0.9999	50	0.25
Ade	$y = 1000x + 80.040$	20–2000	0.9986	20	0.1
GSH	$y = 177.621x - 0.048$	50–8000	0.9993	50	0.25

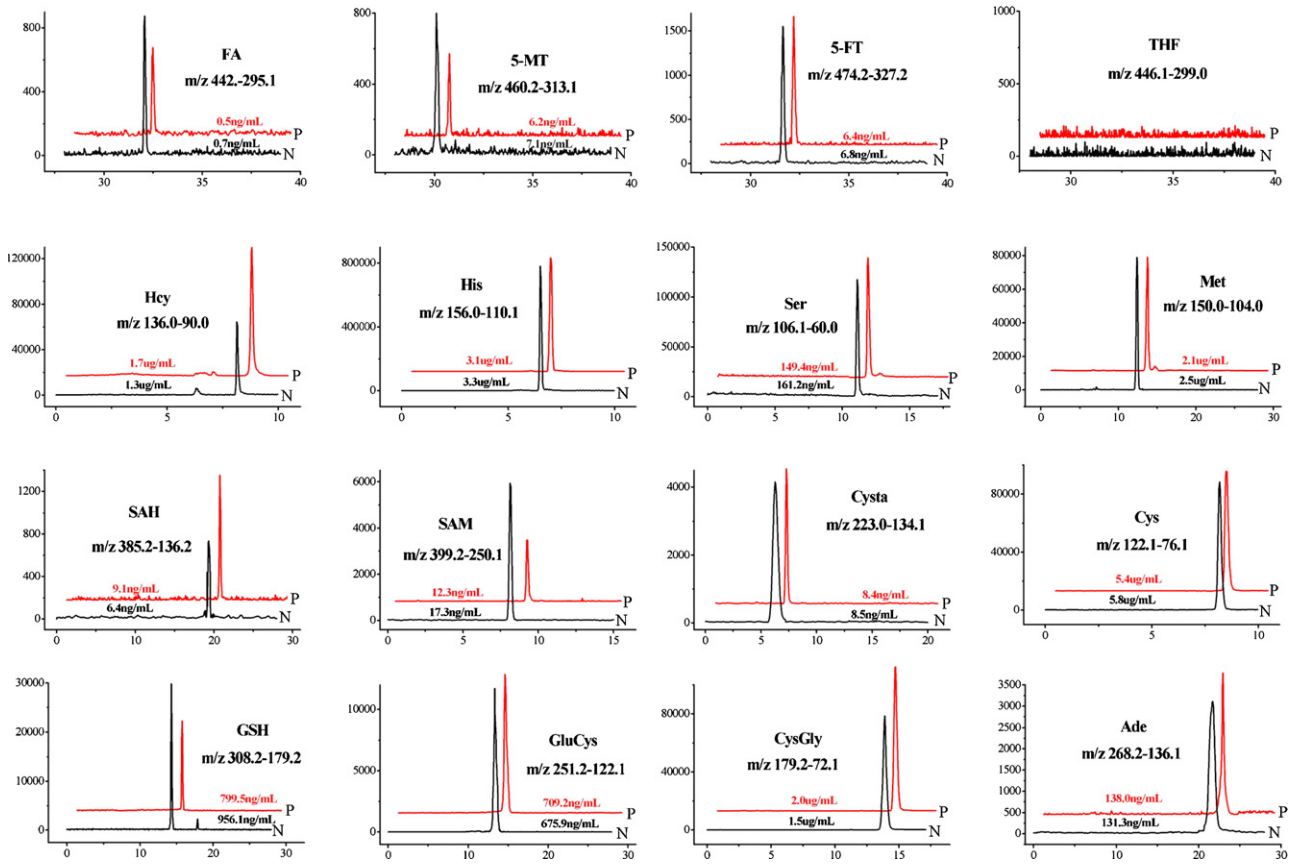

Fig. 4. Extracted ion chromatograms of sixteen components in the serum of case and control (P: patient, N: normal).

Therefore, the result showed good stability of the analytes during processing and storage.

3.4. Application of the method

The method was validated by determining the linearity ($r^2 > 0.998$), sensitivity (limit of detection range from 0.25 to 1.0 ng/mL), intra- and inter-day precision (both CVs < 10.5%). The mean recovery for each analyte was 75.6% or higher. No significant degradation was observed by performing the stability test (CVs < 9.5%) when stored at 4 °C for 24 h. Therefore, the values for the methods validation suggested that the method fulfilled the criteria for bio-analytical analysis. The validated method has been successfully applied to the analysis of serum samples of cases and controls.

The clinical sample collection for this study was sponsored by the Capital Institute of Pediatrics (Beijing, China). Serum samples of 2 NTDs-affected pregnant women (age 20–35 years) in Lvliang of Shanxi Province, China were collected as cases and 2 serum samples of healthy pregnant women (age 20–35 years) in the same area, China as controls. All blood samples were centrifuged to obtain serum in the hospital and sent to our laboratory, where they were stored at −80 °C until sample preparation. All study participants were given informed consents.

The validated method was used to analyze serum samples of cases and controls. Fifteen serum compounds, including FA, 5-MT, 5-FT, Hcy, Met, Cysta, SAM, SAH, His, Ser, Ade, GSH, Cys, CysGly, GluCys, could be separated and detected simultaneously using the established LC/MS/MS method. The analyte THF was not observed in any of the serum samples at the detection limit of this assay. The representative LC/MS/MS chromatograms and metabolites concentration of NTDs-affected and not affected pregnant woman serum for each component are shown in Fig. 4.

To better understand the role of one-carbon metabolism in the occurrence of NTDs, we measured serum concentrations of metabolites of the folate and homocysteine pathways in women who had pregnancies that were affected by NTD and in controls. We found that women with NTD-affected pregnancies had lower 5-MT, and 5-FT and high SAH concentrations than did women with unaffected pregnancies [18]. We postulated that the periconceptional supplemented folic acid prevented neural tube defects by normalizing the disordered states of one-carbon metabolism and concluded that SAH was an risk factor for NTDs. The purpose of this study was to develop a method to investigate the relationship between disturbed maternal folate, homocysteine and glutathione metabolism with the risk of having pregnancies affected by NTDs.

The clinical sample collection in Lvliang of Shanxi Province is still in progress. The method developed will be then applied to the analysis of serum samples of cases and controls, thus providing results complementary to those obtained in a previous analysis [18].

4. Conclusion

A sensitive, specific, accurate and repeatable method was developed for the simultaneous determination of sixteen compounds of the folate, Hcy and glutathione metabolic pathways in human serum for the first time. This methodology has been applied to the analysis of the serum of NTDs-affected pregnant women, and fifteen metabolites were quantified. This established method may help us to understand the pathogenesis of NTDs and to provide scientific support for current nutritional intervention strategies. In conclusion, the presented method will provide a solid foundation

for prenatal diagnosis and prevention of NTDs, as well as some other disease related to disturbed folate, Hcy or glutathione metabolism such as congenital heart defects.

Acknowledgements

This study was supported by the National Basic Research Program (973 Program) of China (No. 2007CB511903) and the National Natural Science Foundations of China (No. 20805026). We thank the staff and all participants who joined in and contributed to the laborious fieldwork and also appreciate to the volunteer women for their participation in this study.

References

[1] L. Suarez, M. Felkner, J.D. Brender, M. Canfield, K. Hendricks, Matern. Child Health J. 12 (2008) 394.
[2] A.R. Sayed, D. Bourne, R. Pattinson, J. Nixon, B. Henderson, Birth Defects Res. Part. A: Clin. Mol. Teratol. 82 (2008) 211.
[3] B.Y. Zhang, T. Zhang, L.M. Lin, F. Wang, R.L. Xin, X. Gu, Y.N. He, D.M. Yu, P.Z. Li, Q.S. Zhang, J. Zhao, Y.F. Qin, X.F. Yang, G. Chen, J.F. Liu, X.M. Song, X.Y. Zheng, Biomed. Environ. Sci. 21 (2008) 37.
[4] R. Brouns, N. Ursem, J. Lindemans, W. Hop, S. Pluijm, E. Steegers, R. Steegers-Theunissen, Prenatal Diagn. 28 (2008) 485.
[5] A.L.A. Cunha, M. Hirata, C.A. Kim, E.M. Guerra-Shinohara, K. Nonoyama, R.D. Hirata, Clin. Chim. Acta 318 (2002) 139.
[6] A.S. Whitehead, P. Gallagher, J.L. Mills, P.N. Kirke, H. Burke, A.M. Molloy, D.G. Weir, D.C. Shields, J.M. Scott, Q. J. Med. 88 (1995) 763.
[7] A.K. Njamnshi, V. de, P. Djientcheu, A. Lekoubon, M. Guemse, M.T. Obama, R. Mbu, S. Takongmo, I. Kago, J. Neurol. Sci. 270 (2008) 13.
[8] R.M. Pitkin, Am. J. Clin. Nutr. 85 (2007) 285.
[9] L.D. Botto, C.A. Moore, M.J. Khoury, J.D. Erickson, N. Eng. J. Med. 341 (2006) 1509.
[10] A. Busby, L. Abramsky, H. Dolk, B. Armstrong, A Eurocat Folic Acid Working Group, BMJ 330 (2005) 574.
[11] R.J. Berry, Z. Li, J.D. Erickson, S. Li, N. Engl. J. Med. 341 (1999) 1485.
[12] Z.W. Li, A.G. Ren, L. Zhang, R.W. Ye, S. Li, J.C. Zheng, S.X. Hong, T.M. Wang, Z. Li, Birth Defects Res. Part. A: Clin. Mol. Teratol. 76 (2006) 237.
[13] Z.W. Li, A.G. Ren, L. Zhang, S.Y. Guo, S. Si, R.W. Ye, Chin. J. Epidemiol. 26 (2003) 252.
[14] N.J. Wald, N. Engl. J. Med. 350 (2004) 101.
[15] S. Hernandez-Diaz, M.M. Werler, A.M. Walker, A.A. Mitchell, N. Engl. J. Med. 343 (2000) 1608.
[16] M.A. Honein, L.J. Paulozzi, T.J. Mathews, J.D. Erickson, L.Y.C. Wong, J. Am. Med. Assoc. 285 (2001) 2981.
[17] Q.H. Yang, H.K. Carter, J. Mulinare, R.J. Berry, J.M. Friedman, J.D. Erickson, Am. J. Clin. Nutr. 85 (2007) 1409.
[18] H.Y. Zhang, G.A. Luo, Q.L. Liang, Y. Wang, H.H. Yang, Y.M. Wang, X.Y. Zheng, X.M. Song, G. Chen, T. Zhang, J.X. Wu, Exp. Neurol. 212 (2008) 515.
[19] S.S. Kang, P.W. Wong, M. Norusis, Metabolism 36 (1987) 458.
[20] R. Castro, I. Rivera, E.A. Struys, E.E.W. Jansen, P. Ravasco, M.E. Camilo, H.J. Blom, C. Jakobs, I.T.D. Almeida, Clin. Chem. 49 (2003) 1292.
[21] F.M.T. Loehrer, M. Tschopl, C.P. Angst, P. Litynski, K. Jager, B. Fowler, W.E. Haefeli, Atherosclerosis 154 (2001) 147.
[22] R.F. Huang, Y.C. Hsu, H.L. Lin, F.L. Yang, J. Nutr. 131 (2001) 33.
[23] E. Menegola, M.L. Broccia, M. Prati, R. Ricolfi, E. Giavini, Biol. Neonate 69 (1996) 293.
[24] E.W. Gunter, B.A. Bowman, S.P. Caudill, D.B. Twite, M.J. Adams, E.J. Sampson, Clin. Chem. 42 (1996) 1689.
[25] Y.M. Lin, S.R. Dueker, A.D. Jones, A.J. Clifford, Anal. Biochem. 301 (2002) 14.
[26] R.J. Pawlosky, V.P. Flanagan, C.M. Pfeiffer, Anal. Biochem. 298 (2001) 299.
[27] A.R. Ivanov, I.V. Nazimov, L. Baratova, J. Chromatogr. A 895 (2000) 157.
[28] A.R.T.S. Araujo, M.L.M.F.S. Saraiva, J.L.F.C. Lima, Talanta 74 (2008) 1511.
[29] E. Bald, E. Kaniowska, G. Chwatko, R. Glowacki, Talanta 50 (2000) 1233.
[30] S.T. Chou, L.E. Ko, C.S. Yang, Anal. Chim. Acta 429 (2001) 331.
[31] C. Chassaing, J. Gonin, C.S. Wilcox, I.W. Wainer, J. Chromatrogr. B 735 (1999) 219.
[32] R. Rossi, A. Milzani, I. Dalle-Donne, D. Giustarini, L. Lusini, R. Colombo, P.D. Simplicio, Clin. Chem. 48 (2002) 742.
[33] Y. Wang, H.Y. Zhang, Q.L. Liang, H.H. Yang, Y.M. Wang, Q.F. Liu, P. Hu, X.Y. Zheng, X.M. Song, G. Chen, T. Zhang, J.X. Wu, G.A. Luo, J. Chromatogr. B 863 (2008) 94.
[34] V. Ducros, D. Schmitt, G. Pernod, H. Faure, B. Polack, A. Favier, J. Chromatrogr. B 729 (1999) 333.
[35] S.D. Garbis, A. Melse-Boonstra, C.E. West, R.B.V. Breemen, Anal. Chem. 73 (2001) 5358.
[36] R.M. Kok, D.E.C. Smith, J.R. Dainty, J.T. van den Akker, P.M. Finglas, Y.M. Smulders, C. Jakobs, K. de Meer, Anal. Biochem. 326 (2004) 129.
[37] B.C. Nelson, C.M. Pfeiffer, S.A. Margolis, C.P. Nelson, Anal. Biochem. 313 (2003) 117.

Talanta 78 (2009) 1492–1496

Contents lists available at ScienceDirect

Talanta

journal homepage: www.elsevier.com/locate/talanta

Short communication

Identification of amino acid substitutions in mutated peptides of nucleoprotein from avian influenza virus

Ning Liu [a], Kim-Chung Lee [a], Wenjun Song [b], Pui Wang [b], Zongwei Cai [a,*], Honglin Chen [b,**]

[a] Department of Chemistry, Hong Kong Baptist University, Kowloon Tong, Hong Kong, SAR, China
[b] State Key Laboratory for Emerging Infectious Diseases, Department of Microbiology, The University of Hong Kong, Hong Kong, SAR, China

ARTICLE INFO

Article history:
Received 15 December 2008
Received in revised form 27 January 2009
Accepted 30 January 2009
Available online 10 February 2009

Keywords:
Amino acid substitution
Mutated peptide
Nucleoprotein
H5N1 virus
Nanospray-MS/MS

ABSTRACT

Nucleoprotein (NP), the structural component of ribonucleoprotein complex of avian influenza virus, performs multiple essential functions in the regulation of viral RNA synthesis and in the control of nuclear traffic of viral proteins. Mutations have often been found in NP, some of which are relevant to viral survival strategies. In this study, we used nanospray-MS/MS to analyze tryptic digestion of nucleoprotein of avian influenza virus (H5N1) and to identify three mutated peptides. The MS/MS analyses allowed the confident determination of the three mutated amino acid residues F313Y, I194V and V408I/L in the mutated peptides of LLQNSQV**Y**SLIRPNENPAHK, GVGTMVMEL**V**R and ASAGQ**I/L**SVQPTFSVQR, respectively.

1. Introduction

The influenza A virus, especially the avian flu virus (H5N1), continues to be a global health threat. The avian influenza virus can mutate to acquire the ability for the transmission to humans and to facilitate the generation of pandemic and epidemic strains [1]. Nucleoprotein (NP), a polypeptide of 498 amino acids in length, is encoded by influenza A virus RNA segment 5. As the structural component of the virus transcription machinery, NP performs multiple essential functions throughout the virus life cycle, by regulating viral RNA synthesis through the interaction with other viral components [2,3] and by controlling the nuclear traffic of viral proteins and ribonucleoprotein complexes [4]. NP has been found to exhibit some mutations at several sites [5]. Some of the mutations often result in amino acids (AA) substitutions and thus may be relevant to viral survival strategies [6,7]. Thus, identification of the mutations may be important in the prevention and control of influenza pandemics.

Mass spectrometry with soft ionization techniques such as ESI and MALDI has been successfully applied to analyze peptides, proteins, and other large bio-molecules. Characterization of the mutations at the protein level by using mass spectrometry has been reported [8–11]. Previously, we reported the use of nanospray-MS and MS/MS to analyze the matrix protein 1 (M1) isolated and purified from the viral particles, in which AA substitutions were identified [12]. In this study, nanospray-MS/MS was applied to investigate another structural protein (NP) in H5N1 virus after the protein was isolated from SDS-PAGE. Three AA substitutions were identified through the *de novo* sequencing.

2. Experimental

2.1. Chemicals and materials

Avian influenza virus A/Chicken/Hong Kong/YU22/2002 (H5N1) [13] was kept and propagated in a biosafety level 3 (BL-3) containment facility. HPLC grade ACN and methanol were from Fisher (Fairlawn, NY, USA). Sequencing grade trypsin was obtained from Promega (Madison, WI, USA). All other chemicals were purchased from Sigma–Aldrich (St. Louis, MO, USA).

2.2. Virus cultivation

After passaged several times, avian influenza virus strain A/Chicken/Hong Kong/YU22/2002 (H5N1) was harvested from allantoic fluid of chick embryos inoculated as 10-day old embryos. The allantoic fluid was inactivated with 0.03% Formalin at 4 °C for 72 h to eliminate the highly pathogenicity the virus possessed before it was transferred to further experiments. All the

Abbreviations: AA, amino acid; NP, nucleoprotein.

* Corresponding author. Fax: +852 34117348.
** Corresponding author.
E-mail addresses: zwcai@hkbu.edu.hk (Z. Cai), hlchen@hkucc.hku.hk (H. Chen).

0039-9140/$ – see front matter © 2009 Elsevier B.V. All rights reserved.
doi:10.1016/j.talanta.2009.01.057

experiments using the active virus were carried out in a bio-safety level three laboratory.

2.3. Isolation of virus by ultracentrifugation

The inactivated allantoic fluid was cleared from large debris by low-speed centrifugation. The virus was isolated and purified from the supernatant by ultracentrifugation in gradient sucrose cushion as described [12]. The virus band was carefully collected and stored at −80 °C until use.

2.4. SDS-PAGE

The purified virus particles were lysed with equal volume of reducing sample loading buffer (2% SDS, 20% glycerol, 10% 2-mercaptoethanol, 20 mM Tris–Cl and 0.001% Bromophenol Blue, pH 6.8) and kept at 95 °C for 5 min. The protein concentration was determined by using the Micro BCA (bicinchoninic acid) protein assay kit (Pierce, Rockford, IL, USA) with BSA as a standard protein. The sample (approximate 1.0 μg protein) was then diluted with appropriate amount of reducing sample loading buffer just before SDS-PAGE analysis. Electrophoretic analyses were made in a Mini-Cell system (Bio-Rad, Hercules, CA, USA), and run in 12% Tris–glycine–SDS polyacrylamide gels with a 5% stacking gel at a constant voltage setting of 200 V. After electrophoretic separation, the gels were stained with colloidal Coomassie G250 and scanned with a calibrated densitometer (GS800, Bio-Rad).

2.5. In-gel digestion

The gel bands of interest were cut off and transferred into 0.6 ml Eppendorf vials. After being washed with Milli-Q water several times, the gel bands were cut into pieces of about 1.0 mm^3. The gel pieces were destained, reduced, alkylated and then in-gel digested as described [14]. The resulting tryptic peptides were extracted by a solution of 5% TFA in 50% ACN. The extract was dried in a vacuum centrifuge and then re-dissolved in 0.5% TFA and 5% ACN prior to the mass spectrometric analysis.

2.6. Mass spectrometric analysis

Samples were loaded into a PicoTip emitter (New Objective, USA) and analyzed on a quadrupole orthogonal acceleration time-of-flight mass spectrometer (QSTAR, Applied Biosystems, CA) equipped with an external nanospray ion source (Protana A/S, Odense, Denmark) as described previously [15]. After the full-scan mass spectra of tryptic peptides were obtained in TOFMS mode, the parent ions of interest were subject to sequence analysis in product ion mode where the resolution of Q1 was typically set at unit mass as long as the fragment ion intensity was high enough. For database searching in MS/MS mode, Mascot generic files were created by using a script embedded in the Analyst QS 1.1 software (MDS Sciex). The obtained peak lists were searched against the SwissProt database in the entry of *other viruses* on an in-house Mascot server (Matrix Science, London, UK) with the following parameters: peptide tolerance, 0.2 Da; MS/MS tolerance, 0.2 Da; one missed cleavage; fixed cysteine carbamidomethylation and variable modifications such as asparagine/glutamine deamidation and methionine oxidation. Manual *de novo* sequencing of peptide tandem mass spectra was performed with the aid of Pepsea (1.1) in Analyst QS 1.1 software (MDS Sciex). For the use of sequence tags for database searching in the sequence query mode, the obtained sequence tags were searched against the SwissProt database in the entry of *other viruses* with the parameters similar to those used in MS/MS search mode. The peptide charge was set as the charge state of the individual peptide being analyzed.

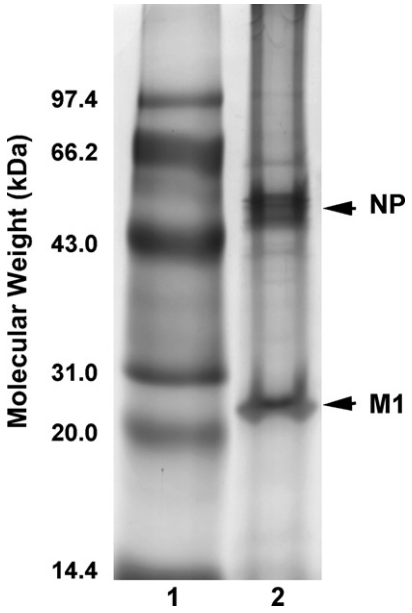

Fig. 1. SDS-PAGE separation of viral proteins from virus lysate. After being purified by ultracentrifugation in sucrose cushion, the virus particles were lysed and the viral proteins were separated on a 12% SDS-PAGE, followed by colloidal Coomassie G250 staining (Lane 1: marker, lane 2: virus lysate).

3. Results and discussion

3.1. Analysis of nucleoprotein

The virus particles were purified from allantoic fluid by using ultracentrifugation in discontinuous sucrose cushion. The purified virus was lysed and separated on SDS-PAGE (Fig. 1). The protein bands (around 56 kDa) were cut off and subject to in-gel digestion. While the successful separation of viral proteins was performed by using 1-D SDS-PAGE, it should be noted that multidimensional separations such as 2-D electrophoresis and 2-D chromatography might significantly improve the analytical capability for more complicated protein mixtures [16]. However, in our efforts to separate the major antigens from influenza virus, the full-length nucleoprotein was difficult to be detected on 2D gels, even with pH range of 3–11.

The tryptic digests were analyzed by using nanospray-MS/MS. A Mascot score of 345 which was the sum of the unique ion scores was obtained for the identification of the nucleoprotein from avian influenza H5N1 virus (A/Chicken/Hong Kong/YU22/2002) after the database searching in the MS/MS search mode. The Mascot searches identified ten expected sequences in the nucleoprotein. The *de novo* sequencing of the MS/MS data allowed the identification of three mutated peptides. Accordingly, a total of 13 tryptic sequences (T1–T13) were identified, which allowed the assignment of 11 unique peptide sequences (Table 1).

3.2. Identification of F313Y substitution

With the interpretation of obtained MS/MS spectrum of the T8 peak and the aid of Pepsea software, the peak with the triply charged ion at *m/z* 774.41 was identified as LLQNSQV**Y**SLIRPNENPAHK (Fig. 2). The mutated peptide could be easily located with the native NP peptide sequence in the residues from 306 to 325 or LLQNSQVFSLIRPNENPAHK from the comparison with the expected peptide sequence in NP. Compared to the theoretical *m/z* value of 769.09 for the triply charged ion of the native peptide, a difference of nominal mass of 16 Da was observed for T8. The mass

Table 1
Summary of proteolytic peptides identified in nucleoprotein of avian influenza H5N1 virus (A/Chicken/Hong Kong/YU22/2002).

Peak ID	Peptide sequence	Charge status	Calculated *m/z*	Measured *m/z*	Residues
T1	GVFELSDEK	2	512.25	512.26	462–470
T2	LIQNSITIER	2	593.84	593.85	56–65
T3	MVLSAFDER	2	534.26	534.27	66–74
T4	M*VLSAFDER	2	542.26	542.27	66–74
T5	EGYSLVGIDPFR	2	676.85	676.84	294–305
T6	MM*ESARPEDVSFQGR	3	585.93	585.94	447–461
T7	M*M*ESARPEDVSFQGR	3	591.26	591.27	447–461
T8	LLQNSQV**Y**SLIRPNENPAHK	3	774.42	774.41	306–325
T9	GVGTM*VM*EL**V**R	2	612.31	612.31	185–195
T10	TTIM*AAFN*GNTEGR	2	750.34	750.35	423–436
T11	NPGN*AEFEDLTFLAR	2	847.90	847.91	247–261
T12	GVQIASNENM*EAM*DSNTLELR	3	785.36	785.37	362–382
T13	ASAGQIS**I/L**QPTFSVQR	2	845.45	845.44	401–416

M*: mono-oxidized methionine; N*: deamidated asparagine; the identified mutated amino acid residues were labeled with bold.

difference of 16 Da was identified as the substitution of $F_{313} \rightarrow Y$ through the following sequence analyses and illustrations. Theoretically, four other AA substitutions with the nominal mass shift of 16 Da, namely $V_{312} \rightarrow D$, $S_{310} \rightarrow C$, $A_{323} \rightarrow S$, $P_{318,322} \rightarrow L$, could exist in the expected peptide sequence of LLQNSQVFSLIRPNENPAHK. The possibility for AA substitution of $S_{310} \rightarrow C$ was first eliminated because the C residue, if existed, should have been alkylated by iodoacetamide in the sample preparation process. The possibilities of $V_{312} \rightarrow D$, $A_{323} \rightarrow S$ and $P_{318,322} \rightarrow L$ were removed because the corresponding characteristic fragment ions were not detected in the MS/MS spectrum of the mutated peptide. For example, the AA substitution of $V_{312} \rightarrow D$ should have produced the y_{13}^{+2} ion at *m/z* 761.91, which, however, was not observed (Fig. 2). For the possibility of $A_{323} \rightarrow S$, y_3 ion at *m/z* 371.20, y_4 ion at *m/z* 468.26 and y_5 ion at *m/z* 582.30 should have been produced. The AA substitution of $P_{318} \rightarrow L$ should have produced y_8 ion at *m/z* 922.47, y_8^{+2} ion at *m/z* 461.74, y_{10} ion at *m/z* 1191.66 and y_{10}^{+2} ion at *m/z* 596.33, etc., from MS/MS analysis of the mutated peptide. Similarly, the $P_{322} \rightarrow L$ should have produced y series ions from y_4 to y_8 at *m/z* 468.29, 582.34, 711.34, 825.42 and 922.4, respectively. Therefore, the elimination of other impossible AA substitutions suggested the possible mutation at F_{313} residue ($F \rightarrow Y$). The clearly detected both y and b ion series confirmed the identification of the mutation position (Fig. 2).

3.3. Identification of I194V substitution

The obtained product ion spectrum of the doubly charged ion peak T9 at *m/z* 612.31 showed a characteristic fragment ion at *m/z* 175, indicating that the corresponding peptide might possibly be ended with an R at C terminus (Fig. 3). Prominent y ion series of *m/z* 1166.59, 1067.44, 1010.56, 909.45 at the high end of the spectrum were observed for the R-terminated tryptic peptide. Thus, the *de novo* sequencing of this spectrum suggested GVGT as its N-terminal sequence of the corresponding peptide. It was easy to locate GVGT in an expected tryptic sequence GVGTMVMELIR

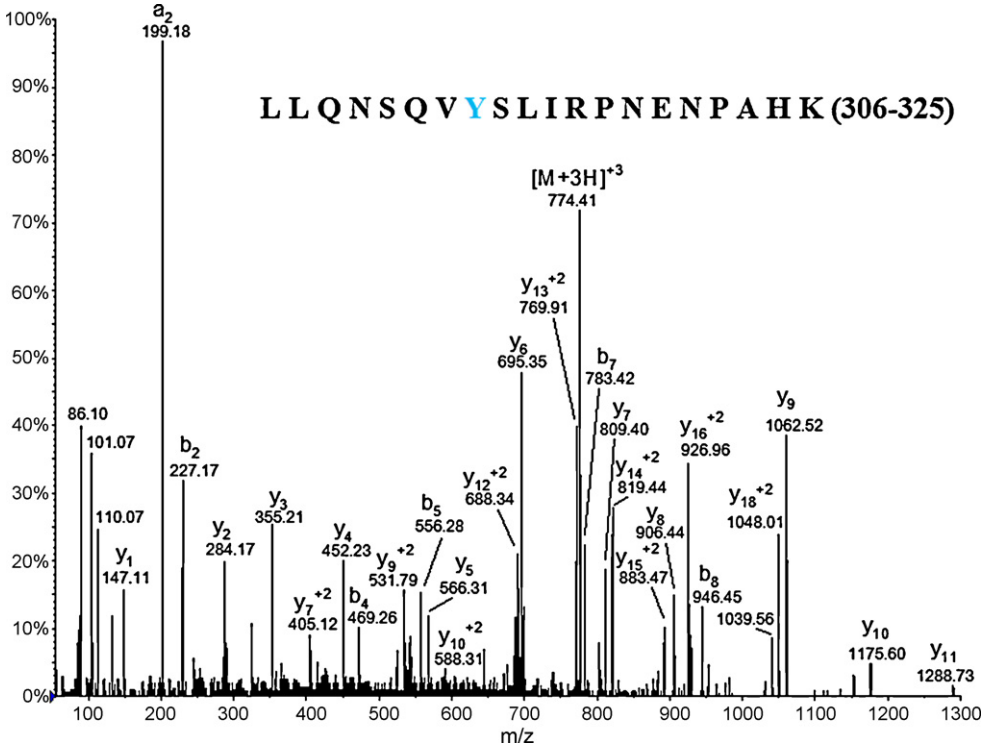

Fig. 2. ESI-MS/MS spectrum of triply charged T8 peak at *m/z* 774.41 that was identified as the mutated peptide LLQNSQV**Y**SLIRPNENPAHK with the sequence of residues 306–325 from tryptic digestion of nucleoprotein.

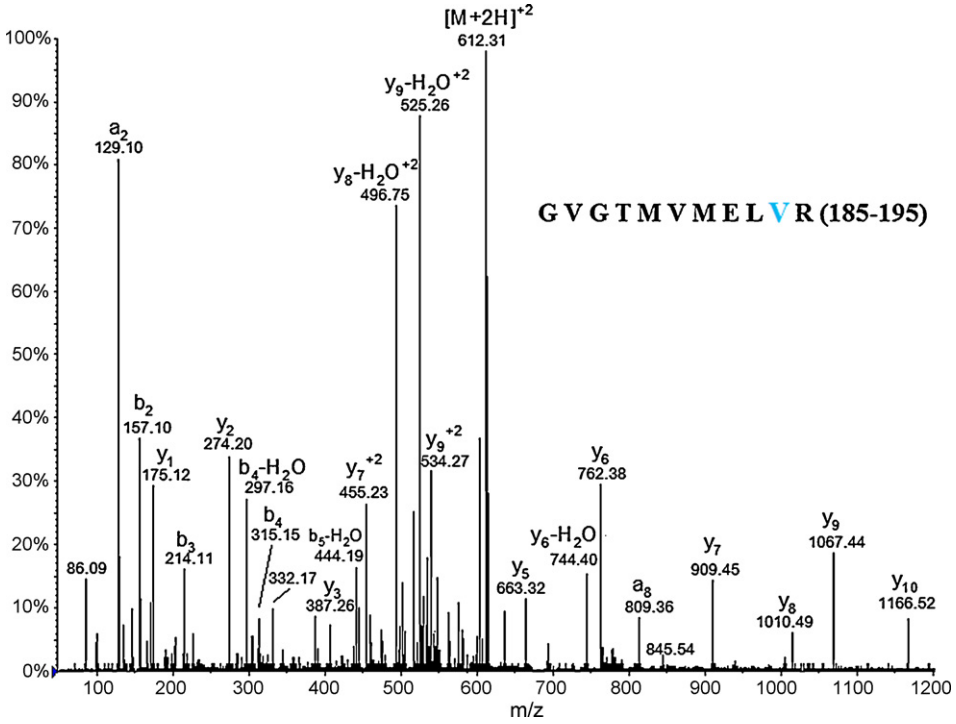

Fig. 3. ESI-MS/MS spectrum of doubly charged T9 peak at *m/z* 612.31 that was identified as the mutated peptide GVGTM**V**MELVR with the sequence of residues 185–194 from tryptic digestion of nucleoprotein.

(185–195) in NP with the theoretical *m/z* value of 619.32 for the doubly charged ion, considering that two methionines were oxidized (Table 1). However, a mass difference of 14 Da was observed for the detected doubly charged ion of T9 when compared to the corresponding theoretical value of the sequence of GVGTMVMELIR (185-195) in NP. Four possible AA substitutions, namely $E_{192} \rightarrow D$, $T_{188} \rightarrow S$, $L_{193} \rightarrow V$ and $I_{194} \rightarrow V$ in the peptide, might have a nominal mass shift of −14 Da. Because the four AA substitutions had the same exact value of mass shift, they could not be distinguished from each other without the MS/MS analysis. The interpretation of the MS/MS spectrum of T9 was therefore performed to illustrate possibility of the AA substitution and the site of peptide mutation. The detection of y_2 ion at *m/z* 274 suggested that the tryptic peptide likely contained a V residue next to the C-terminus. Additionally, the absence of ions at *m/z* 288 and *m/z* 401 eliminated the possibilities of $E_{192} \rightarrow D$, $T_{188} \rightarrow S$ and $L_{193} \rightarrow V$. In addition to the y_2 ion, other y series ions as well as the b series ions such as b_2, b_3, b_4-H_2O and b_4, were also readily assigned, confirming the identification of the mutation site at I_{194} ($I \rightarrow V$) in the mutated peptide GVGTMVMEL**V**R.

The partial sequence VGT was deduced from the initial interpretation of the mass spectrum shown in Fig. 3, which could be included into a qualifier in an alternative database searching algorithm in Mascot called sequence query. The Mascot result layout containing the parameters and conditions in database searching was provided in supplementary materials (Fig. S1). The use of the sequence tag qualifier [612.31 etag(1166.52, VGT, 909.45)] in the database searching against SwissProt in the entry of *other virus* in the sequence query mode of Mascot software had identified the GVGTMVMELIR (185–195) in the nucleoprotein of avian influenza virus (A/Chicken/Hong Kong/YU22/2002), but with M_{191} oxidized and the unsuspected M_{189} modification with a mass shift of 1.98 Da. However, the fragmentation pattern of the ions in the MS/MS spectrum of the peak T9 did not support the sequence query result regarding the unsuspected modification on M_{189}. Careful interpretation of the MS/MS data indicated that the M_{189} was oxidized (with a mass shift of +16 Da) and the I_{194} was substituted by V residue (with a mass shift of −14 Da). The unsuspected modification (with a mass shift of 1.98 Da) obtained from the sequence query database searching resulted from the combination of oxidation at M_{189} and substitution at I_{194}.

3.4. Identification of V408I/L substitution

Similar to the interpretation of the product ion spectrum of peak T9, a fragment ion at *m/z* 175 from the MS/MS analysis of peak T13 with the doubly charged ion at *m/z* 845.44 suggested that the corresponding peptide might end with an R at C terminus (Fig. 4). An internal sequence tag GQIS was deduced from the detected ion series at *m/z* 1460.80, 1403.77, 1275.70, 1162.62 and 1075.58. The possible tryptic peptide including this sequence tag (GQIS) in NP was ASAGQISVQPTFSVQR (401–416) with the theoretical *m/z* value of 838.44 for the doubly charged ion. The observed mass difference of 14 Da for T13 might be resulted from AA substitution at one of six possible sites, namely $G_{404} \rightarrow A$, $V_{408} \rightarrow I/L$, $V_{414} \rightarrow I/L$, $S_{402} \rightarrow T$, $S_{407} \rightarrow T$ and $S_{413} \rightarrow T$. Given the fact that the sequence tag GQIS has already been deduced from the detected high-end y ion series, possibilities for $G_{404} \rightarrow A$ and $S_{407} \rightarrow T$ were eliminated. Similar to the interpretation of the product ion spectrum of peak T8, evaluation on the fragment ions of peak T13 indicated that the residue V_{408} ($V \rightarrow I/L$) was the site of the AA substitution in ASAGQIS**I/L**QPTFSVQR. The clearly assigned y and b ion series eliminated the mutation possibilities at other residues in this peptide.

The sequence qualifier [845.44 etag(1460.80, GQIS, 1075.58)] was searched against the SwissProt database in sequence query mode of Mascot software. The corresponding Mascot result layout was provided in supplementary materials (Fig. S2). As a result, the sequence ASAGQISVQPTFSVQR (401–416) in nucleoprotein was identified, but with a mass shift of 14 Da which occurred at V_{408}. Therefore, the substitution of V408I/L was readily determined without the need of interpreting other fragment ions such as y and b series ions at the low-end of the spectrum.

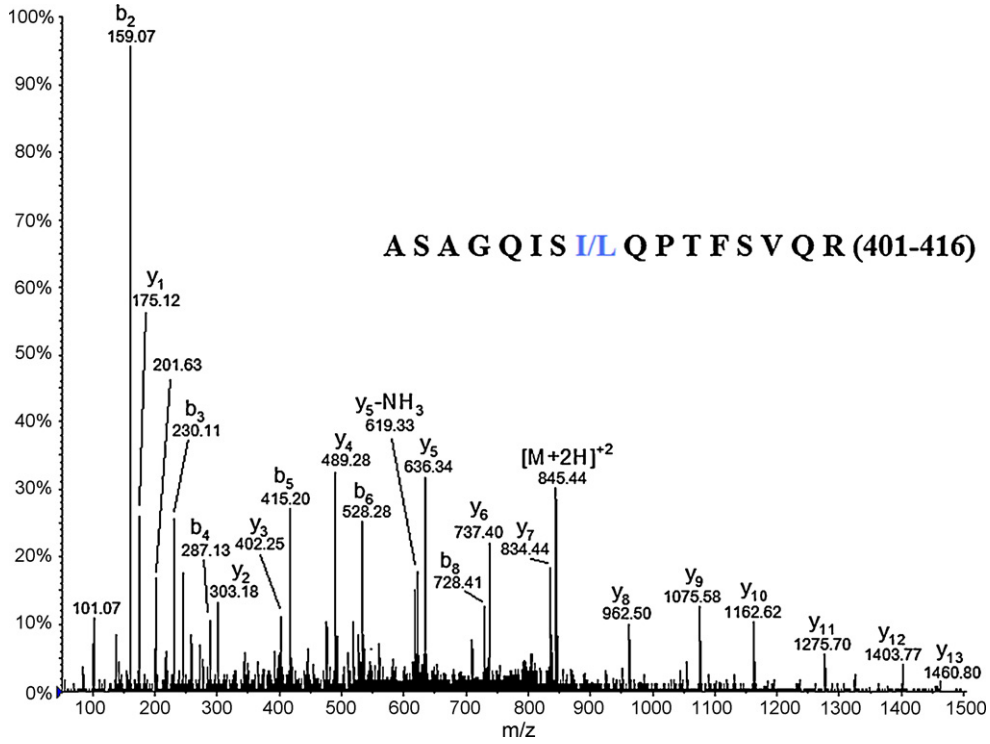

Fig. 4. ESI-MS/MS spectrum of triple-charged T13 peak at *m/z* 845.44 that was identified as the mutated peptide ASAGQIS**I/L**QPTFSVQR with the sequence of residues 401–416 from tryptic digestion of nucleoprotein.

4. Conclusion

Three AA substitutions, namely F313Y, I194V and V408I/L, were identified from the nanospray-MS/MS analysis of mutated peptides in nucleoprotein of avian influenza H5N1 virus. With the interpretation of the obtained MS/MS data, the database searching on a local Mascot server with MS/MS ion search option allowed the identification of ten expected sequences in nucleoprotein from avian influenza H5N1 virus (A/Chicken/Hong Kong/YU22/2002). Three mutated peptides were identified by *de novo* interpretation of the available data. An alternative database searching algorithm [17] called sequence query search option in Mascot was then used to confirm the results of the mutated peptides, whose specific sequence tags were readily obtained from the interpretation of MS/MS data. The results indicated that the sequence tag search algorithm was effective to directly identify mutated peptides when the sequence tags could be accurately deduced. This approach might serve as complementary to *de novo* sequencing in interpretation of MS/MS data from mutated peptides and provided useful sequence information that would facilitate *de novo* sequencing of mutated peptides. The determination of the mutated residues in peptides involved in NP provided an actual example of *de novo* sequencing of the mutated peptides, which might be useful for better understanding the mutability and structure–function relationship of the key protein in influenza virus.

Acknowledgement

The authors would like to acknowledge financial support from the Faculty Research Grant (FRG/07-08/11-21) from Hong Kong Baptist University.

Appendix A. Supplementary data

Supplementary data associated with this article can be found, in the online version, at doi:10.1016/j.talanta.2009.01.057.

References

[1] G. Brankston, L. Gitterman, Z. Hirji, C. Lemieux, M. Gardam, Lancet Infect. Dis. 7 (2007) 257.
[2] M.A. Rameix-Welti, A. Tomoiu, E. Dos Santos Afonso, S. van der Werf, N. Naffakh, J. Virol. 83 (2008) 1320.
[3] S.L. Noton, E. Medcalf, D. Fisher, A.E. Mullin, D. Elton, P. Digard, J. Gen. Virol. 88 (2007) 2280.
[4] S. Boulo, H. Akarsu, R.W. Ruigrok, F. Baudin, Virus Res. 124 (2007) 12.
[5] K. Bragstad, L.P. Nielsen, A. Fomsgaard, Virol. J. 5 (2008) 40.
[6] K. Ohba, S. Yoshida, M. Zahidunnabi Dewan, H. Shimura, N. Sakamaki, F. Takeshita, N. Yamamoto, K. Okuda, Vaccine 25 (2007) 4291.
[7] G.F. Rimmelzwaan, A.C. Boon, J.T. Voeten, E.G. Berkhoff, R.A. Fouchier, A.D. Osterhaus, Virus Res. 103 (2004) 97.
[8] K. Tanaka, S. Takenaka, S. Tsuyama, Y. Wada, J. Am. Soc. Mass Spectrom. 17 (2006) 508.
[9] A.K. Mandal, S. Bisht, V.S. Bhat, P.R. Krishnaswamy, P. Balaram, Clin. Biochem. 41 (2008) 75.
[10] A.I. Nepomuceno, C.J. Mason, D.C. Muddiman, H.R. Bergen 3rd, S.R. Zeldenrust, Clin. Chem. 50 (2004) 1535.
[11] V. Cunsolo, S. Foti, R. Saletti, S. Gilbert, A.S. Tatham, P.R. Shewry, J. Mass Spectrom. 39 (2004) 66.
[12] N. Liu, W. Song, K.C. Lee, P. Wang, H. Chen, Z. Cai, J. Am. Soc. Mass Spectrom. 20 (2009) 312.
[13] K.S. Li, Y. Guan, J. Wang, G.J. Smith, K.M. Xu, L. Duan, A.P. Rahardjo, P. Puthavathana, C. Buranathai, T.D. Nguyen, A.T. Estoepangestie, A. Chaisingh, P. Auewarakul, H.T. Long, N.T. Hanh, R.J. Webby, L.L. Poon, H. Chen, K.F. Shortridge, K.Y. Yuen, R.G. Webster, J.S. Peiris, Nature 430 (2004) 209.
[14] W. Song, Q. Lin, S.B. Joshi, T.K. Lim, C.L. Hew, Mol. Cell. Proteom. 5 (2006) 256.
[15] N. Liu, W. Song, P. Wang, K. Lee, W. Chan, H. Chen, Z. Cai, Proteomics 8 (2008) 1851.
[16] D.A. Lubman, M.T. Kachman, H.X. Wang, S.Y. Gong, F. Yan, R.L. Hamler, K.A. O'Neil, K. Zhu, N.S. Buchanan, T.J. Barder, J. Chromatogr. B 782 (2002) 183.
[17] M. Mann, M. Wilm, Anal. Chem. 66 (1994) 4390.

Talanta 78 (2009) 1458–1463

Contents lists available at ScienceDirect

Talanta

journal homepage: www.elsevier.com/locate/talanta

Ion-exchange preconcentration and determination of vanadium in milk samples by electrothermal atomic absorption spectrometry

Ignacio López-García, Pilar Viñas, Rafael Romero-Romero, Manuel Hernández-Córdoba*

Department of Analytical Chemistry, Faculty of Chemistry, University of Murcia, E-30071 Murcia, Spain

ARTICLE INFO

Article history:
Received 7 November 2008
Received in revised form 2 February 2009
Accepted 20 February 2009
Available online 5 March 2009

Keywords:
Electrothermal atomic absorption spectrometry
Ion exchange preconcentration
Vanadium
Milk
Infant formula

ABSTRACT

A new method for the electrothermal atomic absorption spectrometric determination of vanadium in milk and infant formulas using suspensions to avoid the need for previous dissolution of samples is described. Sensitivity is improved by a procedure based on preconcentration and removal of the matrix, using ion-exchange (Dowex 1X8-100). Suspensions of 15% (m/v) infant formula samples were prepared in a medium containing 0.05 M sodium citrate (pH 7.2) and passed through the ion exchange column. Vanadium was eluted from the column using 1 M hydrochloric acid and injected in the graphite furnace using a mixture of hydrofluoric acid plus magnesium nitrate as chemical modifiers. Calibration was carried out using multiple injection and aqueous standards prepared in the same medium. Detection limits were 0.2 ng g^{-1} for infant formulas and 0.02 μg L^{-1} for cow milk samples. The reliability of the procedure was checked by comparing the results obtained with those found using a previous mineralization stage and by analyzing five certified reference materials.

1. Introduction

Vanadium is an essential element which is extracted from soil and assimilated by vegetables and animals, thus entering the food chain. The daily intake for humans, through feeding, is 100 μg and most of this amount is excreted without being absorbed. The element is associated with glucose metabolism regulation and improves insulin receptivity. However, the element is toxic at high concentrations. The insulin mimetic properties [1] in human have stimulated interest in the element, which is also found in the environment in seaweed, vegetables, invertebrates, fish and other species. Very variable concentrations are found in foods. In breast milk, the content [2] is between 0.1 and 0.2 μg kg^{-1}, equivalent to an intake of 0.1–0.2 μg/day [3]. Levels in drinks, fat, oil, fruit juices and vegetables are in the range 1 to 5 μg kg^{-1}. Cereals, fish, meat and milk derived products have concentrations of 5–30 μg kg^{-1}. Dill leaves and black pepper contains higher levels (between 431 and 987 μg kg^{-1}), while the mean content of cow milk is variable, different studies finding between 0.2 μg kg^{-1} and 10 μg kg^{-1}.

The analytical methods for vanadium preconcentration and determination have been reviewed [4,5]. The most common for food samples are inductively coupled plasma atomic emission or mass spectrometry (ICP-AES or ICP-MS) and atomic absorption spectrometry (AAS) with flame (FAAS) or electrothermal atomization (ETAAS). FAAS is only useful for samples containing μg mL^{-1} levels [6] and using a nitrous oxide-acetylene flame and an ionization buffer. When ETAAS is used, the element forms refractary carbides which are very difficult to atomize, meaning that very high temperatures are needed for both calcination and atomization steps [7]. Although sensitivity is improved in this way, the characteristic mass of vanadium is not enough for it to be determined in cow milk. Consequently, most procedures using ETAAS include a preconcentration step after sample mineralization. Preconcentration can be carried out with ion-exchange resins [8], coprecipitation with iron hydroxide [9] or complexation with ammonium pyrrolidin dithiocarbamate and extraction with methyl isobutyl ketone (MIBK) [10], cupferron and MIBK [11], 8-hydroxiquinoline and MIBK [12], among others. Alternatively, a procedure has been proposed [13] using multiple heat injection (3 × 30 μL) without sample mineralization which has permitted detection limits of 0.5 μg L^{-1}.

Generally, analysis includes prior mineralization of the sample, which involves long and tedious dissolution processes, with the risk of analyte losses or sample contamination. Because the importance of developing clean chemistry procedures, emerging methods for food matrices are based on reducing sample treatment and the use of solvents. In this study, a transversal heating ETAAS procedure is proposed for vanadium determination in infant formula and milk samples. The direct introduction of the sample as a suspension, in addition to saving time, avoids the use of toxic solvents and minimizes the risk of contamination. To achieve good sensitivity, the procedure includes a previous separation and preconcentration step using ion exchange and multiple injections.

* Corresponding author. Fax: +34 968364148.
E-mail address: hcordoba@um.es (M. Hernández-Córdoba).

0039-9140/$ – see front matter © 2009 Elsevier B.V. All rights reserved.
doi:10.1016/j.talanta.2009.02.045

2. Experimental

2.1. Instrumentation

A model 800 atomic absorption spectrometer (Perkin-Elmer, Shelton, USA) equipped with both a deuterium-arc background corrector and a Zeeman correction device, a THGA (Perkin-Elmer) graphite furnace atomizer and an AS-800 autosampler (Perkin-Elmer) were used. Pyrolytic graphite platforms (Part number B050-4033) inserted into the pyrolytically coated graphite tubes were obtained from Perkin-Elmer. Argon was used as the inert gas, the flow rate being 250 mL min^{-1} in all the stages, except during atomization when the flow was stopped. Measurements were performed using a vanadium hollow cathode lamp (Perkin-Elmer) operated at 30 mA and 318.4 nm. The instrumental parameters selected are shown in Table 1.

For the ion-exchange preconcentration step, a Gilson Minipuls 3 (Villiers, France) peristaltic pump and Omnifit glass columns (Cambridge, UK) with Teflon cap pieces (10 and 5 cm length × 5 mm internal diameter, working at middle and low pressure) and filled with Dowex1X8-100 (Fluka, Buchs SG, Switzerland) were used. To decrease the risk of vanadium contamination, the use of glassware was avoided and plastic (polypropylene) vessels were used for preparing and storing the solutions or suspensions. Pipette tips were also of polypropylene. All plasticware was nitric acid-washed and rinsed with ultrapure water.

Mineralization of the samples for comparison purposes was carried out in closed Teflon cups using an MLS-1200 MEGA microwave oven (Milestone) and MDR-1000/6 Rotor (Radiometer).

2.2. Reagents

High quality water, obtained using a Milli-Q system (Millipore, Bedford, MA, USA), was used exclusively. Vanadium standard solution (1000 μg mL^{-1}) was obtained from Panreac (Barcelona, Spain) and diluted as necessary to obtain working standards. Concentrated (65%, m/v) nitric acid, concentrated (40%, m/v) hydrofluoric acid, 30% (m/v) hydrogen peroxide, concentrated (29%, m/v) ammonium hydroxide, sodium hydroxide and citric acid (Fluka, Buchs SG, Switzerland) were also used. Magnesium nitrate (Fluka) was used as matrix modifier.

Table 1
Instrumental parameters.[a].

Lamp current (mA)	30
Wavelength (nm)	318.4
Bandwidth (nm)	0.7
Atomizer type	Platform with end caps
Sample injected volume (μL)	90 (30 + 30 + 30)
Background correction	Zeeman
Chemical modifier	80% (v/v) HF + 0.1% (m/v) $Mg(NO_3)_2 \cdot 6H_2O$
Modifier injected volume (μL)	15
Analytical characteristics[a]	
Analytical range (μg L^{-1})	0–2
Characteristic mass (pg)	0.95
Detection limit (μg L^{-1})	0.02
RSD, % (n = 10)	3.2

Furnace heating programme[a]

Step	Temperature (°C)	Ramp (s)	Hold (s)
1. Dry	110	1	20
2. Dry	130	1	15
3. Calcination	1700	10	20
4. Atomization[b,c]	2600	0	5
5. Clean	2600	1	3

Sequence for the procedure with preconcentration

i	Sample injection
ii	Run steps 1 to 2 of the heating programme (for several injections, repeat this stage until three times)
iii	Injection of the chemical modifier and run the rest of the heating programme

[a] Values correspond to the procedure with preconcentration.
[b] Flow of argon stopped.
[c] Reading step.

2.3. Reference materials and samples

The samples of different types of milk (cow milk and infant formulas: starting, follow-on, prebiotic and lactum) were obtained commercially or supplied by local manufacturers (Hero España, S.A.). The reliability of the procedure was checked using five reference materials, wheat flour 1567a, rice flour 1568a, bovine liver 1577b, apple leaves 1515 and spinach leaves 1570a, supplied by the National Institute of Standards and Technology, NIST (USA).

2.4. Preconcentration procedure

For liquid cow milk samples, aliquots of 50 mL were mixed with 5 mL of a 0.5 M citric acid solution previously adjusted to pH 7.2 with sodium hydroxide solution. For powder infant formulas, 15% (m/v) samples were prepared and aliquots of 50 mL were heated in a water bath at 90 °C for 15 min and, before cooling, 5 mL of the 0.5 M citric acid solution (pH 7.2) were added. Both solutions from liquid or powder milk, were submitted to the preconcentration procedure by passing through the anionic exchange column at a flow-rate of 2 mL min^{-1} and then air was passed at 2 mL min^{-1} for 2 min. Vanadium was eluted from the column using a 1 M hydrochloric acid solution at 1 mL min^{-1} and the fraction corresponding to the fourth milliliter was collected. Then, three 30 μL aliquots of this fraction were injected into the ETAAS and separated by a drying step, according to the conditions summarized in Table 1. Calibration was performed by the same procedure and the graph was linear between 0.1 and 2 μg L^{-1} of vanadium using corrected peak area as the analytical signal. Certified reference samples were treated in the same way with previous mineralization of the samples as indicated.

2.5. Procedure for mineralization of the certified reference materials

To assess the reliability of the procedure, several reference materials were mineralized and analyzed for comparison purposes. Fractions of 3 g were weighed in a porcelain capsule and calcined in a furnace at 450 °C for 8 h. The ashes were treated with 2 mL of concentrated HNO_3, 2 mL of 30% (m/v) H_2O_2 and, again, 2 mL of concentrated HNO_3 and the mixture was evaporated to almost dryness. Finally, it was diluted to 10 mL using a volumetric flask. From this solution, aliquots of different volumes were taken, according to the vanadium content, and diluted to 50 mL. The recommended procedure was then applied.

3. Results and discussion

3.1. Direct determination

Vanadium forms refractory carbides with the graphite coating before atomization [14,15], which considerably reduce sensitivity and reproducibility. A heterogeneous distribution of compounds through the tube appeared, which depended of temperature [16]. For example, VO was principally found on the inside upper wall of atomizer, VC, VO and V_2O_3 in the sample deposition site, and VC in the cold ends of the tube. To avoid these problems, the use of pyrolytic graphite tubes [17] and graphite tubes coated with

elements forming stable carbides as tungsten [18,19], molybdenum [20] and nickel + boron [21] has been proposed. Another way to avoid the formation of vanadium carbide is to use suitable matrix modifiers, such as palladium nitrate [22,23], magnesium nitrate [24,25], magnesium nitrate with Rh or Pt [26], chromium nitrate [27], sodium seleniate + calcium chloride [28], ascorbic acid + magnesium nitrate + 8-hydroxiquinoline [20] and barium fluoride [13,29].

Depending on the modifier, the graphite coating and the technique used (wall or platform atomization, longitudinal or transversal heating systems, with Zeeman or deuterium corrector), the characteristic mass (c.m.) varies considerably. Thus, a c.m. of 30 pg has been reported for longitudinal heating systems with wall atomization and 40 pg for transversal heating systems, Zeeman correction and STPF conditions [30]. A c.m. of 15 pg was found using magnesium nitrate + Pt [26] and 80 pg with barium fluoride [13] as modifiers, with longitudinal heating systems, deuterium correction and pyrolytic graphite tubes. These c.m. values increased to 120 pg with tungsten coated tubes [18] and 298 pg with molybdenum coated tubes [20]. When using transversal heating systems and Zeeman correction, c.m. values in the range 40–50 pg with modifiers and 80 pg in their absence have been reported [31].

In this study, several preliminary experiments were carried out using STPF conditions and in the absence of chemical modifier, leading to a c.m. of 65 pg. When using a solution containing 200 μg mL^{-1} palladium in 1% (v/v) nitric acid as modifier, the c.m. decreased to 55 pg. These experiments were carried out using open ended atomizers. With end cap atomizers, the c.m. was 42 pg. Consequently, the end cap atomizer was selected, as it avoided analyte losses during atomization, increasing the residence time [32].

The optimal conditions for the chemical modifier and the suspension medium were then studied. When palladium nitrate was used as the modifier, the vanadium was retained in the tube. To avoid this effect, caused by the formation of vanadium carbides, the use of barium fluoride has been proposed [13]. The use of hydrofluoric acid, which has been seen to provide good results for several analytes [33,34], was tried for the same purpose, and appropriate peaks with maximal signals were obtained in the presence of 10% (v/v) concentrated HF, avoiding the retention of vanadium in the atomizer and obviating the need for cleaning injections. To improve sensitivity, the use of different modifiers along side HF were assayed and best results were obtained by using 0.1% (m/v) magnesium nitrate and 10% (v/v) HF, which decreased the c.m. value to 47 pg. The introduction of milk samples into the atomizer led to the appearance of carbonaceous residues due to incomplete pyrolysis of the organic matter. Hydrogen peroxide [35] added for microdigestion of the sample during the pyrolysis step minimised this problem, but its combination with HF decreased sensitivity.

The possibility of performing multiple injections of the sample to decrease detection limits was also assayed. The results showed that linearity between peak area and the number of injections was obtained up to three consecutive 30 μL injections. However, the injection of such an amount of milk sample produced a high amount of carbonaceous residue, which affected sensitivity and led to the need for frequent manual cleaning. Because of the experiments clearly showed that the direct procedure is not sufficiently sensitive for both infant formula and milk samples, and that sensitivity cannot be increased by increasing the amount of sample used, a procedure based in ion exchange separation was developed to preconcentrate the sample and eliminate most of the matrix.

3.2. Preconcentration of vanadium by ion-exchange

3.2.1. Selection of the stationary phase

For selecting the stationary phase, several anionic (Dowex 1X8-100, AG1-X8 and Amberlite IRA-743) and cationic (Dowex 50WX2-100 and AG50W-X8) resins were tested filling 50 cm length × 10 mm i.d. glass columns for low pressure liquid chromatography. The best results were obtained using the strong anionic resin Dowex 1X8-100, which had particles of 200–400 mesh (37–74 μm) containing trimethylammonium functional groups on a macro-reticular structure of estirene-divinylbenzene.

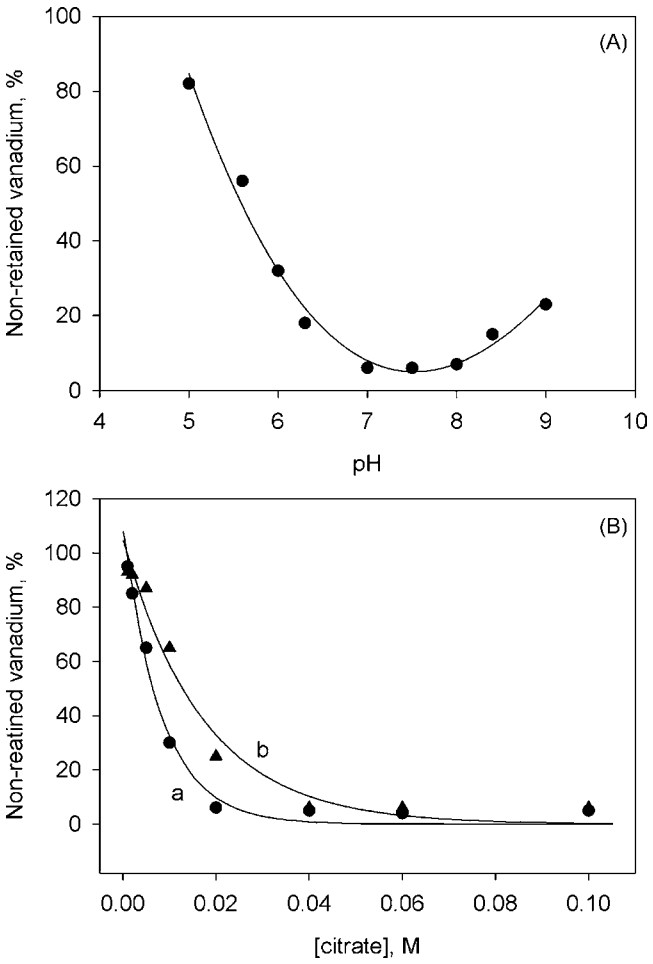

Fig. 1. (A) Influence of pH on vanadium retention using the anionic resin Dowex 1X8. (B) Effect of the sodium citrate concentration on vanadium retention for an aqueous standard solution (curve a) and an infant formula fortified with vanadium (curve b). The graphs show the percentages of non-retained vanadium.

3.2.2. Optimization of the experimental variables

Several acidic and basic media were assayed to achieve the quantitative retention of vanadium in the column and its subsequent elution. Best results were obtained using sodium citrate. Quantitative retentions for both aqueous standards and spiked milk samples were achieved in the pH range 6.8 to 8 (Fig. 1A), using a 0.05 M sodium citrate concentration. A 7.2 pH value was selected. Fig. 1B shows the effect of the sodium citrate concentration on the efficiency of vanadium retention in the column. As can be seen, concentrations above 0.02 M led to quantitative retention for aqueous standards, while infant formulas fortified with 5 μg L^{-1} vanadium required citrate concentrations above 0.04 M. Consequently, a 0.05 M concentration was selected.

To totally release the vanadium retained in the column, different acidic (hydrochloric or nitric acid) and alkaline (sodium or ammonium hydroxide) media were assayed. The elution profiles obtained when using hydrochloric acid solutions as the eluent are shown in Fig. 2. When a 1 M HCl solution was used, the sensitivity for vanadium was similar to that found in the optimal conditions for the

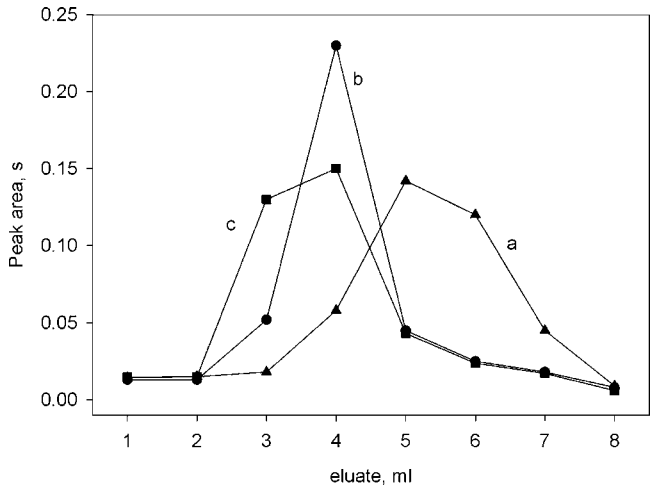

Fig. 2. Effect of the hydrochloric acid concentration on the elution of vanadium retained in the column from a 0.5 μg L^{-1} standard solution. Profiles a–c correspond to 0.1, 1 and 3 M HCl, respectively.

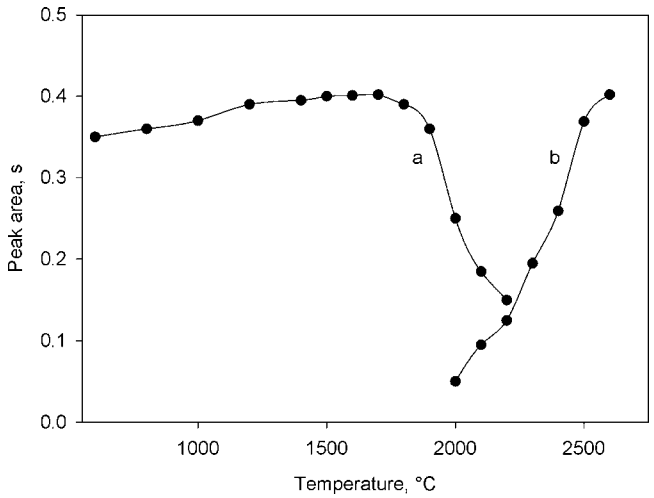

Fig. 3. Effect of calcination (curve a) and atomization (curve b) temperatures for a vanadium standard solution in a 1 M HCl medium using 80% (v/v) HF and 0.1% (m/v) magnesium nitrate as chemical modifiers.

direct introduction of the milk samples into the atomizer, and this is the concentration recommended. Using a HF-magnesium nitrate mixture as chemical modifier, the slope of the calibration graph was 0.0072 ± 0.0002 s L μg^{-1}, while a value of 0.0069 ± 0.0003 s L μg^{-1} was obtained for the direct procedure, with no noticeable changes in the atomization profiles.

The flow-rates to be used for the retention and elution of vanadium were optimized. Total retention was found for flow-rates of the sample through the column up to 2 mL min^{-1} using 100 mm length columns. A washing step was necessary to eliminate the matrix residues, prior to elution of vanadium from the column. For this purpose, the column was washed with air for 2 min at a flow of 2 mL min^{-1} using the peristaltic pump. This cleaning step with air eliminated a large amount of the milk matrix, avoiding analyte losses, as reported elsewhere [33]. Following the air washing step, vanadium was eluted with 1 M HCl. Using these conditions, most analyte eluted in the fourth mililiter. After each determination, the column was washed by flushing 1 M HCl for 10 min at 0.5 mL min^{-1}, then water for 5 min at 5 mL min^{-1}, finally, air at 2 mL min^{-1} for 2 min. In this way the column could be used up to 50 times without deterioration or decrease in vanadium recovery.

3.2.3. Optimization of the heating programme

When using the preconcentration procedure, the composition of the solution introduced into the atomizer was very different from the suspension medium in the direct procedure and, consequently, it was necessary to re-consider the optimal heating programme. Fig. 3 shows the ash-atomize graph for an aqueous standard solution of vanadium in 1 M HCl, the eluent used for releasing the analyte from the chromatographic column. As can be seen, calcination temperatures higher than 1800 °C produced a gradual decrease in the signal and so a temperature of 1700 °C was selected. A study of the influence of the atomization temperature showed that maximal signal was achieved at 2600 °C, the maximum temperature applied by the transversal atomizer. The introduction of a cooling step prior to atomization did not produce any improvement and was discarded. Table 1 summarizes the optimal conditions for the furnace heating programme.

3.2.4. Optimization of the injection volume

Since the solution eluted from the column was practically matrix-free, in an attempt to increase sensitivity, the maximum volume to be injected and the possible use of multiple injections were studied. Fig. 4A shows the effect of the injected sample volume, linearity being evident up to 45 μL. Fig. 4B shows the study corresponding to multiple 30 μL injections of the 1 M HCl eluate obtained from a milk sample submitted to the preconcentration procedure. The dotted line corresponds to the background signal. As can be seen, linearity was obtained up to four consecutive injections. However, a sequence of three injections was selected as a compromise between sensitivity and short analysis times. These injections were programmed as follows: injection of 30 μL of sam-

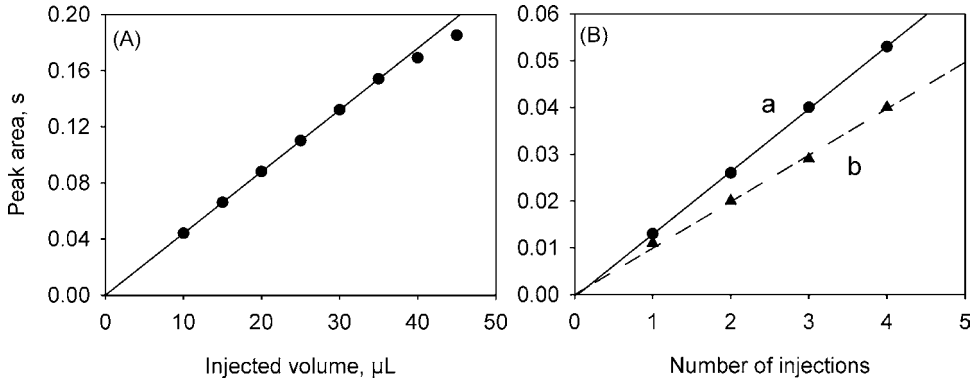

Fig. 4. (A) Effect of the sample volume for a single injection of the eluate corresponding to the fourth mililiter of a 1 μg L^{-1} vanadium standard. (B) Effect of the number of injections (30 μL each injection) on the signal of the fourth mililiter of the eluate of a milk sample containing 0.1 μg L^{-1} vanadium. Curve a corresponds to the variation of the atomic signal and curve b to the background signal.

Table 2
Characteristics of some procedures for vanadium determination.

Technique	Remarks	Sample	DL ($\mu g\,L^{-1}$)	Ref.
ETV-ICP-MS	Simple dilution	Honey	0.3[a]	[36]
ETAAS	Sample mineralization	Honey	87[a]	[37]
ETAAS	Hot injection and preconcentration	Milk	0.5	[13]
ICP-MS	Lyophilisation and microwave digestion	Milk	0.016	[38]
ICP-MS	Room temperature acid sonication	Milk	0.07	[39]
ETAAS	Ion-exchange preconcentration	Milk	0.02	This work

[a] $ng\,g^{-1}$.

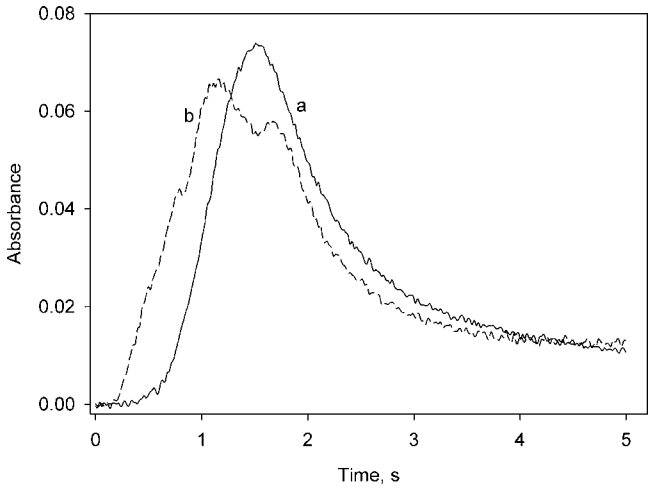

Fig. 5. Atomization profiles obtained from a cow milk sample submitted to the preconcentration procedure. Lines a and b correspond to the corrected analytical signal and background signal, respectively.

ple followed by the drying step; this sequence was repeated three times; after the drying step of the last injection, the modifier containing solution was injected and the programme completed. As can be seen in Fig. 5, the background signal was low.

3.2.5. Calibration and validation of the preconcentration procedure

When using the preconcentration procedure, elution of vanadium with 1 M HCl for both aqueous standards and milk samples was mainly obtained in the fourth mililiter (Fig. 6). Consequently, to improve sensitivity, quantitation was carried out using this fraction.

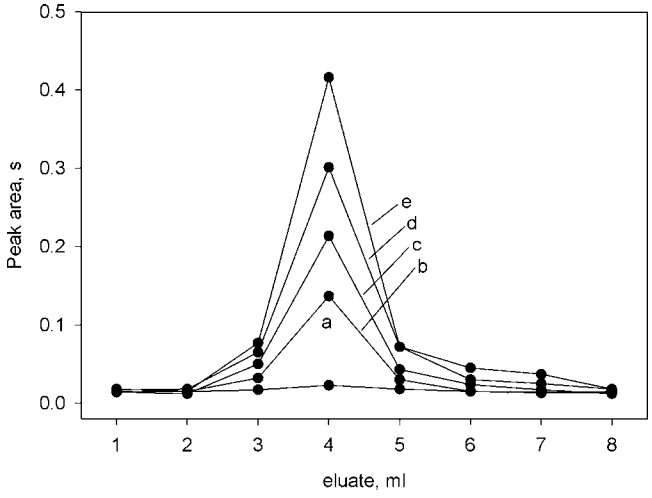

Fig. 6. Elution profiles for vanadium standard solutions. Curves a–e correspond to 0, 0.25, 0.5, 0.75 and 1 $\mu g\,L^{-1}$ vanadium, respectively.

In this way, the calibration graph was linear up to 2 $\mu g\,L^{-1}$ vanadium, using the conditions recommended in Experimental. The slope was 0.413 ± 0.005 s L μg^{-1}, which led to a preconcentration factor of approximately 60 times with respect to the direct procedure. For a calibration graph obtained with aqueous standards of vanadium of 0.25, 0.5, 1, 1.5 and 2 $\mu g\,L^{-1}$, a regression coefficient of 0.9972 and a standard error of the estimate ($s_{y/x}$) of 0.0031 were obtained. The detection limit (DL) calculated on the basis of three times the standard error of the estimate of the regression line was 0.02 $\mu g\,L^{-1}$ of vanadium in the cow milk samples. Table 2 shows DLs reported in the literature for other similar procedures.

The preconcentration procedure was applied to the determination of the vanadium content in different milk samples and infant formulas. To check the accuracy of the proposed procedure, a standard additions method was carried out by fortifying the different cow milk and infant formulas. The samples were also analyzed by direct calibration with aqueous standards. Table 3 shows that the contents of vanadium found using both calibration procedures were very similar, and so the simplest direct calibration with aqueous standards is recommended. The analysis of cow milk samples showed that similar vanadium levels were found for both whole and skimmed milk, thus confirming that the element was found in the soluble fraction of milk.

Since milk samples with certified vanadium content were not available, several standard reference materials (wheat flour (SRM 1567a), rice flour (SRM 1568a), cow liver (SRM 1577b), apple leaves (SRM 1515) and spinach leaves (SRM 1570a)) were used to check the reliability of the results. For this purpose the samples were first mineralized in order to be submitted to the preconcentration procedure. Table 4 shows the results in this way obtained together with those found for infant formula samples when submitted to the same treatment (mineralization followed by preconcentration) and using direct calibration as well as the standard addition method. As expected, similar vanadium contents were obtained for milk

Table 3
Vanadium content found in milk and infant formula using the preconcentration procedure.

Sample	Vanadium content		
	Direct calibration	Standard additions	Slope ratio[c]
Cow milk[a]			
Whole milk 1	0.23 ± 0.04	0.25 ± 0.04	0.96
Whole milk 2	0.35 ± 0.05	0.31 ± 0.05	1.02
Semiskimmed milk 1	0.32 ± 0.04	0.36 ± 0.04	0.97
Semiskimmed milk 2	0.16 ± 0.03	0.19 ± 0.03	1.01
Skimmed milk 1	0.18 ± 0.02	0.16 ± 0.02	0.99
Skimmed milk 2	0.25 ± 0.04	0.27 ± 0.04	0.98
Infant formula[b]			
Infant formula (starting)	4.5 ± 0.2	4.4 ± 0.3	1.03
Infant formula (follow-on)	3.9 ± 0.3	3.7 ± 0.3	1.01
Infant formula (prebiotic)	6.2 ± 0.4	6.5 ± 0.3	0.99
Infant formula (lactum)	5.7 ± 0.5	5.9 ± 0.4	1.03

[a] Mean value ± standard deviation for 5 determinations, $\mu g\,L^{-1}$.
[b] Mean value ± standard deviation for 5 determinations, $ng\,g^{-1}$.
[c] Slope aqueous calibration to slope standard additions method ratio.

Table 4
Vanadium content found in infant formula and certified reference materials using previous mineralization followed by the preconcentration procedure.

Sample	Vanadium[a] ($ng\,g^{-1}$)	
	Direct calibration	Standard additions
Infant formula (starting)	4.3 ± 0.4	4.7 ± 0.5
Infant formula (follow-on)	4.1 ± 0.5	3.9 ± 0.5
Infant formula (prebiotic)	6.1 ± 0.6	6.5 ± 0.4
Infant formula (lactum)	5.9 ± 0.6	5.5 ± 0.5
Certified reference materials	**Direct calibration**	**Reference value**
SRM NBS 1567a (wheat flour)	13 ± 0.9	11[b]
SRM NBS 1568a (rice flour)	6 ± 0.5	7[b]
SRM NBS 1577b (cow liver)	120 ± 2	123[b]
SRM NBS 1515 (apple leaves)	198 ± 3	206 ± 30[c]
SRM NBS 1570a (spinach leaves)	582 ± 5	570 ± 30[c]

[a] Mean ± standard deviation ($n = 3$).
[b] Informative value.
[c] Certified value.

powder samples in Tables 3 and 4 confirming the reliability of the direct procedure against aqueous standards. The application of the Wilcoxon test revealed no significant differences between the values found by the proposed procedure and those certified at the 95% confidence level. A statistical study of the standard addition calibration graphs for different cow milk and infant formula samples and calibration graphs obtained from vanadium solutions concluded that there were no significant differences in the slopes at the 95% confidence level ($p = 0.7856$).

Acknowledgments

The authors are grateful to Comunidad Autónoma de la Región de Murcia (CARM, Fundación Séneca, Project 02993/PI/05) and to the Spanish MEC (Project CTQ2006-08037/BQU) for financial support. R. Romero acknowledges a fellowship from Fundación Séneca, CARM. The authors also acknowledge Hero España, S.A. for the kind gift of some infant formula samples.

References

[1] Y. Shechter, S.J.D. Karlish, Nature 284 (1980) 556.
[2] D.R. Myron, T.J. Zimmerman, T.R. Shuler, L.M. Klevay, D.E. Lee, F.H. Nielsen, Am. J. Clin. Nutr. 31 (1978) 527.
[3] D.J.A. Davies, B.G. Bennett, Exposure Commitment Assessments of Environmental Pollutants, Vol. 30. Summary Exposure Assessments for Copper, Vanadium, Antimony, Monitoring and Assessment Research Centre, Chelsea College, University of London, London, 1983.
[4] Z.L. Chen, G. Owens, Anal. Chim. Acta 607 (2008) 1.
[5] K. Pyrzynska, T. Wierzbicki, Talanta 64 (2004) 823.
[6] H.G. Seiler, in: H. Sigel, A. Sigel (Eds.), Metal Ions in Biological Systems, Vanadium and its Role in Life, 31, Marcel Dekker, New York, 1995, pp. 671–688, Chapter 20.
[7] D. Tsalev, Atomic Absorption Spectrometry in Occupational and Environmental Health Practice, II, CRC Press, Boca Raton, 1984.
[8] S. Hirata, Y. Umezaki, M. Ikeda, Anal. Chem. 58 (1986) 2602.
[9] C.P. Weisel, R.A. Duce, J.L. Fasching, Anal. Chem. 56 (1984) 1050.
[10] L. Pyy, E. Hakala, Anal. Chim. Acta 158 (1984) 297.
[11] J.P. Buchet, E. Knepper, R. Lauwerys, Anal. Chim. Acta 136 (1982) 243.
[12] P. Bermejo-Barrera, E. Beceiro-González, A. Bermejo-Barrera, F. Bermejo-Martínez, Analyst 115 (1990) 545.
[13] P. Bermejo-Barrera, T. Pardinas-Alvite, M.C. Barciela-Alonso, A. Bermejo-Barrera, J.A. Cocho de Juan, J.M. Fraga-Bermudez, J. Anal. At. Spectrom. 15 (2000) 435.
[14] J.P. Matousek, H.K.J. Powell, Spectrochim. Acta 41B (1986) 1347.
[15] D. Littlejohn, I. Duncan, J. Marshall, J.M. Ottaway, Anal. Chim. Acta 157 (1984) 291.
[16] J.P. Matousek, H.K.J. Powell, Appl. Spectrosc. 42 (1988) 166.
[17] J.P. Matousek, H.K.J. Powell, Spectrochim. Acta 43B (1988) 167.
[18] Z. Benzo, C. Cecarelli, N. Carrion, M.A. Alvarez, C. Rojas, M. Rosso, J. Anal. At. Spectrom. 7 (1992) 1273.
[19] Y. Nakamoto, T. Ishimaru, N. Endo, K. Matsusaki, Anal. Sci. 20 (4) (2004) 739.
[20] P. Pantano, J. Sneddon, Appl. Spectrosc. 43 (1989) 504.
[21] K. Matsusak, M. Nomi, M. Higa, T. Sata, Anal. Sci. 15 (1999) 145.
[22] A. Lechotycki, J. Anal. At. Spectrom. 5 (1990) 25.
[23] G. Heinemann, W. Vogt, Clin. Chem. 42 (8) (1996) 1275.
[24] D.C. Manning, W. Slavin, Spectrochim. Acta 40B (1985) 461.
[25] P. Bermejo-Barrera, E. Becerro-Gonzalez, A. Bermejo-Barrera, Anal. Chim. Acta 236 (1990) 475.
[26] N.S. Thomaidis, E.A. Piperaki, Analyst 121 (1996) 111.
[27] R. Chakraborty, A.K. Das, Fresenius' J. Anal. Chem. 349 (1994) 774.
[28] K. Hiraki, Y. Nakaguchi, Y. Morita, H. Kitamaki, Anal. Sci. 2 (1986) 561.
[29] K.G. Fernandes, A.R.A. Nogueira, J.A.G. Neto, J.A. Nóbrega, J. Braz. Chem. Soc. 15 (2004) 676.
[30] B. Welz, M. Sperling, Atomic Absorption Spectrometry, third ed., Wiley-VCH, Weinheim (FRG), 1999, p. 569.
[31] K.G. Fernandes, A.R.A. Nogueira, J.A. Gomes Neto, J.A. Nóbrega, Talanta 71 (2007) 1118.
[32] L. Benes, O. Szakács, N. Szoboszlai, Z. Ajtony, G. Bozsai, J. Anal. At. Spectrom. 18 (2003) 105.
[33] P. Viñas, I. López-García, R. Romero-Romero, M. Hernández-Córdoba, Anal. Chim. Acta 597 (2007) 187.
[34] I. López-García, N. Campillo, I. Arnau-Jerez, Hernández-Córdoba, Anal. Chim. Acta 531 (2006) 125.
[35] P. Viñas, N. Aguinaga, I. López-García, M. Hernández-Córdoba, J. Assoc. Off. Anal. Chem. Int. 85 (2002) 736.
[36] M. Bettinelli, U. Baroni, S. Spezia, C. Terni, Atom. Spectrosc. 12 (2000) 195.
[37] M. Taddia, A. Musiani, S. Schiavi, Ann. Chim. 94 (2004) 107.
[38] A. Ataro, R.I. McCrindle, B.M. Botha, C.M.E. McCrindle, P.P. Ndibewu, Food Chem. 111 (2008) 243.
[39] P. Cava-Montesinos, M.L. Cervera, A. Pastor, M. de la Guardia, Anal. Chim. Acta 531 (2005) 111.

Talanta 78 (2009) 1219–1226

Contents lists available at ScienceDirect

Talanta

journal homepage: www.elsevier.com/locate/talanta

Review

Automatic flow injection based methodologies for determination of scavenging capacity against biologically relevant reactive species of oxygen and nitrogen

Luís M. Magalhães, Marlene Lúcio, Marcela A. Segundo*, Salette Reis, José L.F.C. Lima

REQUIMTE, Serviço de Química-Física, Faculdade de Farmácia, Universidade do Porto, Rua Aníbal Cunha 164, 4099-030 Porto, Portugal

ARTICLE INFO

Article history:
Received 31 July 2008
Received in revised form 31 January 2009
Accepted 3 February 2009
Available online 13 February 2009

Keywords:
Antioxidants
Reactive oxygen species
Reactive nitrogen species
Flow injection analysis

ABSTRACT

Redox reactions are the heart of numerous biochemical pathways found in cellular chemistry, generating reactive oxygen species (ROS) and reactive nitrogen species (RNS), that includes superoxide anion radical ($O_2^{\bullet -}$), hydrogen peroxide (H_2O_2), hydroxyl radical ($HO^{\bullet}$), singlet oxygen ($^1O_2$), hypochlorite anion (OCl^-), peroxynitrite anion ($ONOO^-$) and nitric oxide radical ($NO^{\bullet}$). The measurement of scavenging capacity against these reactive species presents new challenges, which can be met by flow injection analysis (FIA). In the present review several methods based on FIA and also on its predecessors computer-controlled techniques (sequential injection analysis, multisyringe flow injection analysis, multicommutated and multipumping flow systems) are critically discussed. The selectivity and applicability of the methodology, the generation and detection of the target reactive species, the benefits and limitations of automation when compared to batch methods are some of the issues addressed.

Contents

1. Introduction

Redox reactions are the heart of numerous biochemical pathways found in cellular chemistry, including biosynthesis and regulation [1]. They are also important for understanding the oxidative stress phenomena and radical/antioxidant effects. In a biological context, the chemical terms “oxidant” and “reductant” are usually replaced by pro-oxidant and antioxidant, respectively [2]. Therefore, pro-oxidant is a substance that can induce oxidative damage to various biological targets (oxidizable substrates) such as nucleic acids (e.g. base modification, single and double-strand breaks), lipids (e.g. peroxidation, fatty acid loss), and proteins (e.g. oxidation of specific amino acid residues, formation of carbonyls). On the other hand, an antioxidant is a substance that, when present at low concentrations compared with those of an oxidizable substrate, significantly delays or prevents oxidation of that substrate [3].

In general these pro-oxidants are referred to as reactive oxygen species (ROS) and reactive nitrogen species (RNS) that can have

* Corresponding author. Tel.: +351 222078994; fax: +351 222078961.
E-mail address: msegundo@mail.ff.up.pt (M.A. Segundo).

0039-9140/$ – see front matter © 2009 Elsevier B.V. All rights reserved.
doi:10.1016/j.talanta.2009.02.006

(or not) one or more unpaired electrons (radical species). Depending on the site and the concentration generated, these species are well recognized for playing a dual role, as both beneficial and deleterious effects have been established [4]. These reactive species are formed from exogenous and endogenous sources [1]. The exogenous sources include exposure of biological systems to γ- or UV-irradiation that results in the production of hydrogen peroxide (H_2O_2), hydroxyl radical ($HO^{\bullet}$), and superoxide anion radical ($O_2^{\bullet-}$). Additionally, a large variety of xenobiotics (e.g. drugs, pollutants, toxins, pesticides, and herbicides) produce ROS/RNS as a by-product of their in vivo metabolism. Despite the contribution of exogenous sources, the exposure to endogenous sources is much more important and extensive because it is a continuous process. The main endogenous sources are related with the mitochondrial electron-transport chain, and also with the activity of some enzymes, such as nitric oxide synthases (NOSs) and xanthine oxidase (XOD) that catalyzes the production of nitric oxide radical ($NO^{\bullet}$) and $O_2^{\bullet-}$, respectively. These two species may react with each other, originating peroxynitrite ion ($ONOO^-$). Moreover, activated phagocytes produce a variety of reactive oxygen, halogen (e.g. HOCl, which production is catalyzed by myeloperoxidase) and nitrogen species that play an important role in the mechanism of defense against infectious agents [5].

In a normal biological system, there is an appropriate pro-oxidant/antioxidant balance. However, this balance can be shifted towards the pro-oxidant agents when there is an overproduction of ROS/RNS and/or when levels of antioxidant protection are diminished. This state is called 'oxidative stress', and it can be triggered by several factors such as diseases, diet, lifestyle, and environmental conditions [6]. As mentioned before, the excess of ROS/RNS can oxidize cellular lipids, proteins, or nucleic acids, inhibiting their normal function. Because of this, oxidative stress has been implicated in the pathogenesis of several human diseases, including atherosclerosis, cancer, cardiovascular diseases, diabetes mellitus, inflammatory diseases, ischemia/reperfusion injury, and neurodegenerative disorders (Alzheimer's and Parkinson's diseases) as well as in the ageing process [3,4]. Oxidation can also affect food, where it is one of the major causes of chemical spoilage, resulting in rancidity and/or deterioration of the nutritional quality, color, flavor, texture and safety of food [7].

Considering the protective effects of antioxidants against these deleterious oxidative-induced reactions, interest in antioxidant research has become a topic of increasing attention in the last few years. This situation demands the existence of simple, convenient, and reliable in vitro analytical methodologies for the fast determination of antioxidant capacity of pure compounds or in complex matrices, such as foods and biological samples [8–11]. In this context, flow injection techniques are an excellent tool to automate these analyses [12].

Flow Injection Analysis (FIA) was proposed in 1975 by Ruzicka and Hansen [13] as an automation tool for chemical analysis. After 33 years, this technique is well known and accepted by the scientific community, and it also allows the performance of assays that are not feasible when carried out manually, by taking advantage of the reproducible timing attained in these systems. The implementation of methods based on transient light formation, generated by bio- and chemiluminescence [14] is only one example that illustrates the advantages of FIA features. During the 1990's the increased availability of computers in the chemical lab fostered the development of sequential injection analysis (SIA) [15] and of flow systems relying on the flow network concept [16,17]. More recently, multipumping flow systems have been proposed [18]. Although based on the same principles of FIA, this new generation of computer-controlled flow systems offers more flexibility concerning the method development and operation [19]. Any changes (sample volume, reagent selection, sample dilution and reagent to analyte ratio) are accomplished via flow programming rather than by physical reconfiguration of the flow path.

In the present review, the specific features of existing flow injection based systems for determination of scavenging capacity against biologically relevant reactive species of oxygen and nitrogen will be critically discussed, considering the target reactive species and its generation, the type of flow system chosen and the application to real samples (Tables 1–3). The benefits of performing antioxidant assays using this type of automatic systems will also be highlighted.

2. Flow-based methods for determination of scavenging capacity against specific ROS

2.1. Superoxide anion radical ($O_2^{\bullet-}$)

A versatile and simple FIA system based on chemiluminescence (CL) detection was developed by Sariahmetoglu et al. for the determination of scavenging capacity against superoxide anion radical ($O_2^{\bullet-}$) [20]. A three-channel manifold (Fig. 1a) was designed to accommodate the chemiluminogenic reagent (luminol), the reactive species ($O_2^{\bullet-}$ in this case), and the carrier stream, which transported the injected sample with putative antioxidant properties. Using this manifold configuration, the $O_2^{\bullet-}$ produced off-line in a solution containing xanthine and xanthine oxidase (XOD) was firstly mixed with the injected sample. After a residence time of about 5 s in the reaction coil, this mixture was subsequently merged with luminol, just before entering in the CL-flow cell (reaction time estimated to be 1.8 s). Thus, the FIA-design exploits the consumption of $O_2^{\bullet-}$ by antioxidant(s), which results in the appearance of negative CL signal proportional to the scavenging ability of the com-

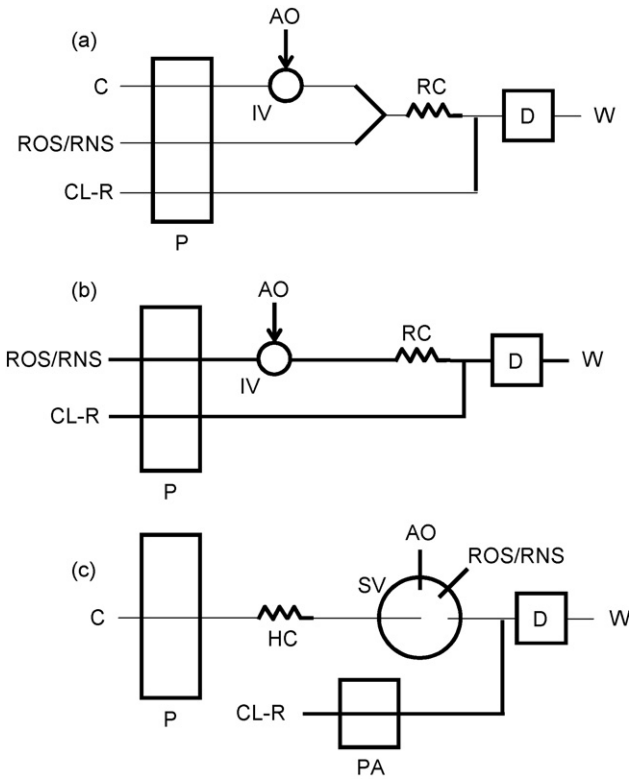

Fig. 1. Schematic representation of flow systems where the reaction between ROS/RNS and antioxidants from sample takes place before addition of a chemiluminescence detection probe. (a) FIA system adapted from Ref. [20,21]; (b) FIA system adapted from Ref. [18,27]; (c) SIA system adapted from Ref. [23,32,33]. AO, antioxidant sample; C, carrier; CL-R, chemiluminescence reagent; D, detector; HC, holding coil; IV, injection valve; P, pump; PA, auxiliary pump; RC, reaction coil; ROS/RNS; reactive species of oxygen or nitrogen; SV, selection valve; W, waste.

Table 1
Flow-based methods for determination of scavenging capacity against reactive oxygen species.

Reactive species	Flow method	Detection probe	Source of reactive species	pH value	Detection system	Application to samples	Det. rate (h^{-1})	RSD (%)	Reference
$O_2^{\bullet -}$	FIA	Luminol	XOD + xanthine	10.0	CL	Indolamines	n.g.	n.g.	[20,21]
	FIA	2-(2-pyridil)-benzothiazoline	Alkaline $Na_2S_2O_4$	9.2	Fluorimetry	Food extracts (Garlic, onion and scallion)	55	<0.3	[24]
	SIA	Luminol	XOD + hypoxanthine	8.2	CL	Multivitamin supplements	30	<3.8	[23]
H_2O_2	FIA	Luminol	Commercial solution	10.0	CL	Indolamines	n.g.	n.g.	[20,21]
	SIA	HVA	Commercial solution	7.5	Fluorimetry	Wines	15	<1.8	[29]
	MPFS	Lucigenin	Commercial solution	7.4	CL	Pharmaceutical formulations and tea	70	<2.0	[28]
	MPFS	Luminol	Commercial solution	Alkaline	CL	Pharmaceutical formulations and tea	160	<2.0	[28]
	FIA-microfluidic	CCPO + BPEA	Commercial solution	n. g.	CL	–	14	<2	[18]
	FIA	Luminol	Commercial solution	7.4	CL	Plant extracts	n.g.	n.g.	[27]
HO•	FIA	Luminol	O_2 + $FeSO_4$ + buffer	10.0	CL	Indolamines	n.g.	n.g.	[20,21]
	FIA	Terephthalate	H_2O_2 + Co(II)	7.4	Fluorimetry	Food extracts and maize pollen polysaccharide	16	<0.6	[30]
	FIA	Ninhydrin	H_2O_2 + Co(II)	7.27	Fluorimetry	Food extracts	22	<1.0	[31]
$^1O_2$	SIA	Luminol	Lactoperoxidase + H_2O_2 + bromide ion	4.5	CL	Multivitamin supplements	40	<1.6	[32]
HOCl	FIA	Luminol	Commercial solution	10.0	CL	Indolamines	n.g.	n.g.	[20,21]
	FIA	Luminol	Commercial solution	7.4	CL	Plant extracts	n.g.	n.g.	[27]
	SIA	Luminol	Commercial solution	9.5	CL	–	45	<3.7	[33]
	MSFIA	Luminol	Commercial solution	7.4 and 10.0	CL	NSAIDs	92	<2.3	[35]

BPEA, 9,10-bis-(phenylethynyl)anthracene; CCPO, 2-carbopentyloxy-3,5,6-trichlorophenyl oxalate; CL, chemiluminescence; FIA, flow injection analysis; HO•, hydroxyl radical; H_2O_2, hydrogen peroxide; HOCl, hypochlorous acid; HVA, homovanillic acid; MPFS, multipumping flow system; MSFIA, multisyringe flow injection analysis; n.g., not given; NSAIDs, non-steroidal anti-inflammatory drugs; $O_2^{\bullet -}$, superoxide radical anion; $^1O_2$, singlet oxygen; SIA, sequential injection analysis; XOD, xanthine oxidase.

Table 2
Flow-based methods for determination of scavenging capacity against reactive nitrogen species.

Reactive species	Flow method	Detection probe	Source of reactive species	pH value	Detection system	Application to samples	Det. rate (h^{-1})	RSD (%)	Reference
NO•	SIA	Luminol	NOR1	8.2	CL	Multivitamin supplements	30	<1.2	[23]
$ONOO^-$	FIA	Luminol	$NaNO_2 + H_2O_2$	10.0	CL	Indolamines	n.g.	n.g.	[20,21]
	MPFS	Luminol	H_2O_2 + nitrite	Alkaline	CL	–	200	2.0	[36]

CL, chemiluminescence; FIA, flow injection analysis; MPFS, multipumping flow system; n.g., not given; NO•, nitric oxide radical; NOR1, (±)-(*E*)-4-methyl-2-[(*E*)hydroxyimino]-5-nitro-6-methoxy-3-hexenamide; $ONOO^-$, peroxynitrite anion; SIA, sequential injection analysis.

Table 3
Flow-based methods for simultaneous determination of scavenging capacity against several reactive species.

Reactive species	Flow method	Detection probe	Source of reactive species	pH value	Detection system	Application to samples	Det. rate (h^{-1})	RSD (%)	Reference
H_2O_2, $O_2^{\bullet-}$ and HO•	FIA	Luminol	Cytochrome c + H_2O_2	7.4	CL	Plant extracts	144	<1.9	[43,44]
	FIA	Luminol	Co(II) + EDTA + H_2O_2	9	CL	Uric acid, ascorbic acid, glutathione	<120	<3.1	[45]
TAC (several)	FIA	Lucigenin	Not controlled, in vivo	11	CL	Rat blood dialysate	n.g.	n.g.	[40,46]

CL, chemiluminescence; EDTA, ethylenediaminetetraacetic acid; FIA, flow injection analysis; HO•, hydroxyl radical; H_2O_2, hydrogen peroxide; n.g., not given; $O_2^{\bullet-}$, superoxide radical anion; TAC, total antioxidant capacity.

pound(s) (Fig. 2a). This manifold was also applied to determination against other reactive species by changing the solution fed to one of the flow channels, as discussed in more detail in the following sections.

For this ROS in particular, the flow system was applied to estimation of the scavenging capacity of superoxide dimutase (SOD) and ascorbic acid, for which the IC_{50} value (Fig. 2b) was calculated. It was also applied for assessing the antioxidant effects of indolamines, namely melatonin, DL-tryptophan and serotonin [21]. Nevertheless, two aspects that may be a source of error in this methodology should be cleared. First, the IC_{50} values obtained are probably overestimated because they are calculated from the initial concentration of sample, without regarding the dilution due to dispersion along its transportation inside the flow conduits. Second, the inhibition of chemiluminescence is partly due to the reaction between the antioxidant and $O_2^{\bullet-}$ and partly due to reaction between the antioxidant and luminol-derived radicals and it will reflect the rates of both these reactions [22]. The strategy adopted by the authors minimizes this problem by allowing more time to the first reaction (5 s) than for the two simultaneously (1.8 s).

A chemiluminescence SIA system has also been proposed for assessing the scavenging capacity against superoxide anion radical [23] using a strategy similar to that described above (Fig. 1c). In this case, sample, XOD, and xanthine solutions were aspirated into the holding coil sequentially. After flow reversal, the zones overlapped while they were directed towards the detector. During this step, the $O_2^{\bullet-}$ formed from XOD/xanthine system was scavenged by antioxidants present in the sample. Subsequently, the remaining $O_2^{\bullet-}$ was measured after addition of luminol from a T connector just before the detector. The system was applied to compounds/enzyme with known activity against this radical, such as ascorbic acid, α-tocopherol, trolox and SOD. It was also applied to commercial vitamin supplements.

Compared to the FIA system proposed before [20], the SIA system allows a more efficient utilization of reagents. In opposition to the continuous flow of solutions found in FIA systems, only the volume of reagent necessary to the determination is aspirated into the flow system. On the other hand, as this system relies in the same chemical principles for detection of $O_2^{\bullet-}$ as described before [20], it also suffers from the interferences mentioned before. Furthermore, as the $O_2^{\bullet-}$ is produced in-line, when the segments of XOD and xanthine overlap in the holding coil of the SIA system, it is also possible that the decrease in CL intensity may be due to inhibition of XOD activity by sample components. In this case, the production of $O_2^{\bullet-}$ is decreased, resulting in a lower CL signal.

The problems of selectivity related to the chemiluminescence detection were circumvented by Tang et al., who proposed a fluorimetric FIA system for determination of $O_2^{\bullet-}$ scavenging capacity [24]. A novel, selective fluorescent probe (2-(2-pyridil)-benzothiazoline) was synthesized and applied, yielding the strong

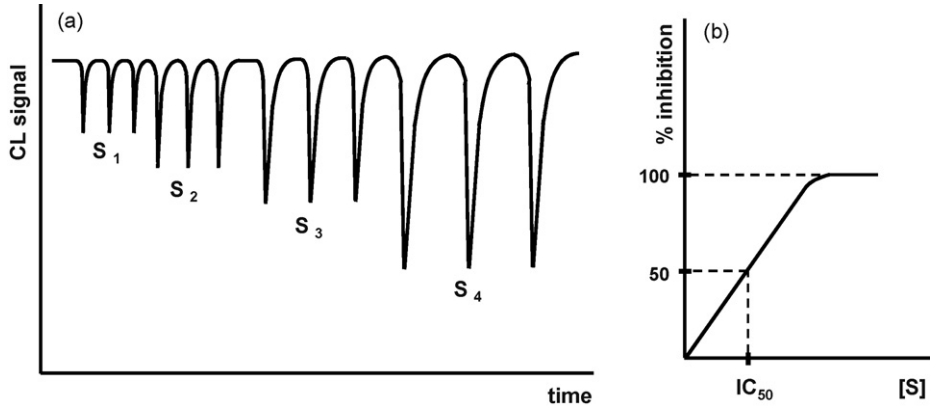

Fig. 2. Schematic representation of (a) inhibition signal profile for increasing concentrations (S_1–S_4) of antioxidant and (b) graphical representation of IC_{50} determination.

fluorescent compound 2-(2-pyridil)-benzothiazol (λ_{ex} = 377 nm, λ_{em} = 528 nm) upon oxidation by $O_2^{\bullet-}$. This reagent was regarded as a selective probe for $O_2^{\bullet-}$ as it was not oxidized by other ROS (H_2O_2 or $HO^{\bullet}$) when tested at the same concentration levels employed for $O_2^{\bullet-}$. In order to save the fluorescent reagent, it was injected into a carrier-buffer stream while the sample was continuously introduced into the system through the peristaltic pump. The $O_2^{\bullet-}$ was also introduced continuously from an alkaline $Na_2S_2O_4$ solution. Hence, the fluorescent probe was injected into the carrier stream and then mixed with alkaline $Na_2S_2O_4$ (generator of $O_2^{\bullet-}$) and sample. The scavenger compounds present in the sample compete with 2-(2-pyridil)-benzothiazoline for $O_2^{\bullet-}$, and the inhibition of fluorescence signal was proportional to the scavenging capacity. The system was applied to vegetable extracts. A major shortcoming of this method is the utilization of alkaline $Na_2S_2O_4$ solution as source of $O_2^{\bullet-}$ because it is unstable and has to be replaced every 2 h.

2.2. Hydrogen peroxide (H_2O_2)

The flow system proposed by Sariahmetoglu et al. [20] was also applied to the CL determination of scavenging capacity against H_2O_2 (Fig. 1a). Using a diluted commercial solution as source of the reactive species, the system was applied for assessing the scavenging capacity of indolamine compounds [21]. In both systems, the luminol solution also contained Co(II). The presence of Co(II) causes the concomitant generation of other oxygen reactive species ($HO^{\bullet}$ and $O_2^{\bullet-}$, for instance), derived from a Fenton-like reaction [25,26]. Although luminol was added to the mixture sample + H_2O_2 just before detection, this system may not be considered selective to this ROS.

A similar flow injection system was applied for determination of scavenging capacity against H_2O_2 of plant extracts from the Lamiaceae family [27]. In this case, the sample was injected directly in the H_2O_2 stream (Fig. 1b). The mixture between the reactive species and antioxidants in the plant extracts were attained through dispersion of the sample in the carrier stream, which may constitute a drawback as a concentration gradient of H_2O_2 is formed along the sample plug. Compared to the systems described before, a pH value closer to that found in vivo (7.4 instead of 10.0) is applied, which is more adequate to study in vivo putative effects. A phosphate-buffered saline (PBS) solution was used and it also contained luminol, Co(II) and hexadecyltrimethylammonium bromide to avoid luminol precipitation. As mentioned before, the presence of Co(II) leads to the generation of other ROS, which makes this methodology not selective towards scavenging of H_2O_2.

A multipumping flow system (MPFS), also based in CL detection, was developed by Meneses et al. to determine "total antioxidant capacity" [28]. In this flow system, the active components are solenoid micropumps that enabled the insertion and efficient mixing of sample and reagents (H_2O_2 and chemiluminogenic reagent) as well as the transportation of the reaction zone toward the CL-flow cell. Two chemiluminogenic reagents were tested: luminol and lucigenin. It was observed that the procedure involving luminol was more sensitive than that using lucigenin, providing IC_{50} values for ascorbic acid and trolox that were ten times lower than those obtained using lucigenin. As the detection takes place before endpoint conditions, this difference may be due to the highest reaction rate observed for luminol- H_2O_2 elicited CL than for lucigenin-H_2O_2 elicited CL. A high sample throughput was attained: 70 or 160 determinations per hour for lucigenin or luminol based system, respectively. Both strategies were applied for the determination in pharmaceutical formulations and tea extracts.

Recently, Amatatongchai et al. developed a microfluidic-based flow method for estimating the H_2O_2 scavenging capacity based on a modified peroxyoxalate chemiluminescence assay [18]. Chemiluminescence was generated from the reaction of 2-carbopentyloxy-3,5,6-trichlorophenyl oxalate (CCPO) with H_2O_2 in the presence of the fluorophore 9,10-bis-(phenylethynyl)anthracene (BPEA) and sodium salicylate used as a catalyst. Thus, when an antioxidant (β-carotene, quercetin or α-tocopherol) was present in the assay mixture, it scavenged the H_2O_2 and quenched the production of light. In the 2-inlet microfluidic system devised, the antioxidant plugs were injected into the hydrogen peroxide stream, which afterwards was merged with the flow stream containing CCPO + BPEA + sodium salicylate (Fig. 1b). Although performed in a microchip, this assay has features of FIA, since the sample plug was injected into a flowing reagent stream followed by controlled and reproducible dispersion and detection after a fixed time. However, unlike most FIA-based methods that use capillaries or tubing, these microchips use planar microchannels, enabling potentially faster mixing and also facilitating planar integration of optical detectors to devise portable, point-of-care measurement devices. It should be highlighted that this system is suitable for compounds with poor solubility in aqueous media as the reaction takes place in a 3:7 mixture of ethyl acetate:acetonitrile that was used for preparation of all solutions.

A SIA fluorimetric procedure has also been proposed for the assessment of H_2O_2 scavenging capacity of wines [29]. In this assay, the homovanillic acid (HVA) was oxidized to its fluorescent dimer (λ_{ex} = 325 nm, λ_{em} = 425 nm) in the presence of H_2O_2 and peroxidase enzyme. Hence, H_2O_2, sample, peroxidase and HVA solutions were sequentially aspirated into the holding coil of the SIA system. After flow reversal, the solutions were mixed and direct to the fluorimeter. Therefore, antioxidant(s) inhibit the oxidation of HVA by a competitive reaction scheme and the reduction in the intensity of the fluorescence signal is proportional to the scavenging capacity. However, this methodology is prone to both positive and negative systematic errors. Besides scavenging H_2O_2, the putative antioxidant(s) may react with intermediates formed from the action of peroxidase enzyme upon H_2O_2, depleting the scavenging capacity of the sample. Otherwise, the compounds present in the sample may inhibit the activity of the peroxidase enzyme, generating less fluorescent dimer and overestimating the scavenging capacity.

2.3. Hydroxyl radical ($HO^{\bullet}$)

Considering the short-life and high reactivity of the hydroxyl radical ($HO^{\bullet}$), the automation using flow-based methods for determining the scavenging capacity against this ROS is advantageous. In fact, $HO^{\bullet}$ radicals are the strongest known oxidant present in vivo [3], therefore the possibility of evaluating the scavenging effects of putative antioxidants against $HO^{\bullet}$ radical immediately after its generation represents a considerable improvement when compared to batch procedures. Moreover, the introduction of flow-based techniques led to the $HO^{\bullet}$ generation and capture took place in controlled environment, reducing the contact of higher reactive $HO^{\bullet}$ with oxygen and other substances present in the lab environment.

In this context, Tang et al. [30] developed a FIA spectrofluorimetric method for detecting scavenging activity against $HO^{\bullet}$ using sodium terephthalate as the fluorogenic probe. In the proposed FIA manifold, H_2O_2 was injected in a buffer carrier stream (pH 7.4) and consecutively merged with the sodium terephthalate solution and with Co(II), yielding $HO^{\bullet}$. This ROS reacted with terephthalate, with formation of highly fluorescent 2-hydroxyterephtalate (λ_{ex} = 313 nm, λ_{em} = 431 nm) by aromatic hydroxylation (a stop-flow period of 3 min was required for reaction development). The relative fluorescence intensity was proportional to the amount of $HO^{\bullet}$ generated. Scavenger compounds/samples were added to the previous mixture in-line by a merging stream placed before the flow-through reactor and they compete with the fluorogenic probe for $HO^{\bullet}$. Therefore, the inhibited fluorescence signal was directly related to $HO^{\bullet}$ scavenging capacity. The method was successfully

applied to pure compounds (mannitol, thiourea), food extracts (walnut, sesame, garlic, ginger, peanut, chili, and soybean) and maize pollen polysaccharide. Although the authors had referred that Fe(II) and Cu(II) had little interference in the determination (tolerance ratio in mol = 2 or 5, respectively), the presence of these species in food products may cause an overproduction of hydroxyl radical through the Fenton reaction, providing higher fluorescence signals.

Later, the same research group presented a similar FIA spectrofluorimetric method using ninhydrin as fluorogenic probe [31]. Ninhydrin is not fluorescent but, when attacked by $HO^{\bullet}$, a strong fluorescent product resulting from aromatic hydroxylation was obtained (λ_{ex} = 300 nm, λ_{em} = 406 nm). The flow manifold is similar to that described before [30], but the $HO^{\bullet}$ is mixed first with sample and subsequently with the fluorogenic probe. It was applied to the determination of scavenging effects of thiourea and vitamin C as well as to aqueous extracts of some food products (walnut, sunflower seed, black and white sesame, garlic, ginger, peanut, and soybean). Compared to the previous flow method, this method was less susceptible to interference from Fe(II) (tolerance ration in mol = 50). In addition, this method had higher sampling rate (Table 1). Nevertheless, in both methodologies, the antioxidant compounds may interfere with the generation system of $HO^{\bullet}$, by reacting directly with H_2O_2 and/or by chelating Co(II).

The flow system proposed by Sariahmetoglu et al. [20] was also applied to the CL determination of scavenging capacity against $HO^{\bullet}$. In this case, $HO^{\bullet}$ was produced off-line through reduction of dissolved oxygen in carbonate buffer by iron(II). The exact concentration of $HO^{\bullet}$ is not known, but repeatable conditions were attained by controlling the concentration of iron(II) and carbonate present in the stock solution. The system was applied for assessing the scavenging capacity of indolamine compounds [21].

2.4. Singlet oxygen ($^1O_2$)

Singlet oxygen ($^1O_2$) may be formed from the reaction of OCl^- or OBr^- with H_2O_2. In this regard, Miyamoto et al. developed a SIA system with CL detection for the screening of compounds possessing scavenging capacity against $^1O_2$ [32]. Hence, lactoperoxidase (LPO) enzyme was used to catalyze the reaction between bromide ion and H_2O_2 to generate $^1O_2$, through the formation of an intermediate species (OBr^-). A manifold configuration similar to that used for superoxide and nitric oxide was applied (Fig. 1c). Thus, after assessing the intensity of the CL signal when varying the order by which the reagents were aspirated, sample, H_2O_2, LPO and NaBr were sequentially placed into the holding coil. After flow reversal, the four segments overlapped, taking place the formation of $^1O_2$ with simultaneous scavenging by compounds present in the sample. The chemiluminogenic reagent (luminol), used as an indicator for $^1O_2$, was introduced to the main stream through an extra peristaltic pump just before the CL detector and the attenuation of luminol CL due to scavenging of $^1O_2$ by antioxidant compounds was assessed. By using this SIA-CL method, the scavenging capacity of well known antioxidants such as vitamins C and E, trolox and sodium azide as well as multivitamin supplements was determined. However, some considerations about the accuracy of this methodology should be discussed. Besides scavenging $^1O_2$, the antioxidant compounds may react directly with H_2O_2 and/or inhibit the activity of LPO enzyme. The formation of OBr^- as an intermediate species may also be a drawback as this powerful oxidizing agent may react itself with antioxidants present in the sample [5].

2.5. Hypochlorite anion (OCl^-)

The automation of hypochlorous acid scavenging capacity has been reported by different groups, using in all cases luminol based chemiluminescence. The flow systems proposed by Sariahmetoglu et al. [20,21] (Fig. 1a) and by Erdemoglu et al. [27] (Fig. 1b) for the determination of scavenging capacity against H_2O_2 were also applied to the assessment of this property against HOCl. A diluted commercial solution was used as source of this reactive species and the decrease of the CL signal by the presence of scavenging compounds was assessed. Excluding the remarks about the presence of other reactive species, the comments presented in the section dedicated to H_2O_2 are also applicable here.

The same chemistry was implemented in a SIA system by Nakamura et al. [33]. In this automatic analytical procedure, the stacked zones of OCl^- (20 μL) and sample (5 μL) were mixed by flow reversal. Luminol solution was just added prior to detection through a merging stream propelled by an auxiliary pump (Fig. 1c). The feasibility of this assay was shown by application to antioxidant compounds (ascorbic acid, α-tocopherol, and trolox). The reagent consumption and the analysis time were considerably lower than those attained in the batch method. However, dimethyl sulfoxide (DMSO) was used to dissolve the standard antioxidants as well as for acquiring the blank signal. Considering that recent literature [34] reports the scavenging capacity of DMSO toward HOCl, the choice of this solvent may not be appropriate, under penalty of decreasing the sensitivity. Finally, the scavenging reaction was carried out at pH 9.5, which does not correspond to physiological conditions (pH value 7.4).

In this regard, Magalhães et al. proposed an automatic flow methodology for the in vitro determination of hypochlorous acid scavenging capacity, under pH and oxidant concentration conditions similar to those found in vivo [35]. For this, a manifold based on multisyringe flow injection analysis (MSFIA) was developed to perform in-line the reaction of HOCl and the putative scavenger molecule at physiological pH (or at pH 10 of CL detection, for comparison purposes) prior to the reaction of remaining HOCl with luminol at alkaline conditions. The HOCl scavenging capacity was evaluated through the decrease in the CL emission. In this MSFIA method, the time taken between the contact of HOCl and putative scavenger compounds plus CL detection was about 3 s. Compared to batch methods, this is an advantage because the scavenger compounds that react fast, closer to the time frame of generation of HOCl in vivo, are determined. Moreover, the interference of antioxidant compounds in the CL-reaction is minimized, since the previous mixture HOCl/antioxidant was added to luminol solution just before CL measurement. The proposed MSFIA method was applied to non-steroidal anti-inflammatory drugs representative of various chemical families and to well-known HOCl scavenger compounds (cysteine, gallic acid, and lipoic acid). A high determination throughput was also attained (Table 1). The results showed that the pH of scavenging reaction affects the ability of some compounds to react with HOCl, indicating that the conditions of in vitro testing should be as close as possible to those found in vivo.

3. Flow-based methods for determination of scavenging capacity against specific RNS

3.1. Peroxynitrite anion ($ONOO^-$)

The FIA manifold proposed by Sariahmetoglu et al. [20] was also applied to the CL determination of scavenging capacity against $ONOO^-$ (Fig. 1a). In this case, $ONOO^-$ was produced off-line through the reaction between $NaNO_2$ and H_2O_2. The exact concentration of $ONOO^-$ was determined by spectrophotometry (λ = 302 nm). The system was applied for assessing the scavenging capacity of indolamine compounds [21].

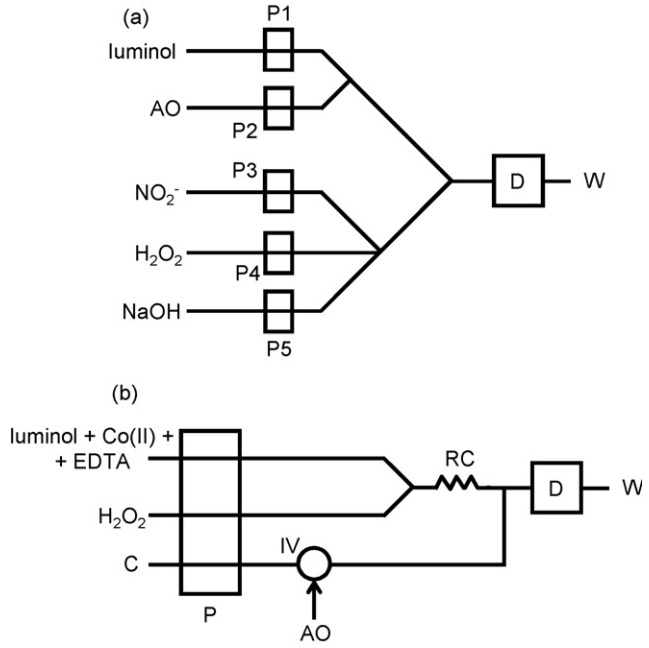

Fig. 3. Schematic representation of flow systems where the generation of ROS/RNS is performed in-line prior to mixing with antioxidants from sample. (a) Multipumping flow system adapted from Ref. [36]; (b) FIA system adapted from Ref. [45]. AO, antioxidant sample; C, carrier; D, detector; IV, injection valve; P, pump; P*i*, micropumps; RC, reaction coil; W, waste.

Recently, a multipumping flow system (MPFS) was proposed for the same determination. It was also based on the inhibition of luminol/$ONOO^-$ elicited CL [36]. In this case, $ONOO^-$ was generated by on-line reaction of acidified H_2O_2 and NO_2^-, which was rapidly quenched by the addition of NaOH (Fig. 3a). Next, the sample and luminol streams were merged with the $ONOO^-$ source. By taking advantage of the pulsed flow and the time synchronized insertion of sample and reagent solutions provided by the MPFS, the complete reaction zone was established only inside the flow cell, thus allowing maximum CL emission detection. The proposed system was successfully applied to several compounds, namely lipoic acid, dihydrolipoic acid, cysteine, glutathione, sulindac and sulindac sulfone. Nevertheless, although the sample solutions were prepared in buffer with pH 7.4, all reactions took place at alkaline conditions, far from those found at physiological conditions. Furthermore, it is very likely to still exist H_2O_2 in the reaction media because the reported yield for the reaction of peroxynitrite formation is <90%, even using cold solutions [37]. Therefore, the CL signal may also be affected by this species, which may react with putative antioxidants present in the sample.

3.2. Nitric oxide radical ($NO^\bullet$)

There are FIA systems described in the literature for $NO^\bullet$ detection [38] or in vivo measurement in blood or brain tissues [39] for investigation concerning physiological $NO^\bullet$ concentrations at different conditions (body temperature, presence of $NO^\bullet$ donors or $NO^\bullet$ activators, etc) or for studies concerning acute myocardial infarction mediated damages [40]. A flow based manifold, comprising a microdialysis probe and on-line CL detection of $NO^\bullet$ have also been described for studying the release of this reactive species (and its inhibition) in rat brain following traumatic injury [41]. However, none of these systems were applied to the direct study of scavenging properties of a compound or extract.

In fact, a FIA system for nitrite determination based on the Griess reaction and equipped with a cadmium–copper reduction column was applied to study the scavenging activity of melatonin and its precursors against $NO^\bullet$ [42]. After batch pre-incubation of a source of $NO^\bullet$ (NOC-7, hydroxyl-2-oxo-3-(N-methyl-3-aminopropyl)-3-methyl-1-triazene) with the compound under study, an aliquot of the reaction media was taken and processed in the flow system for the determination of the stable end products of $NO^\bullet$ oxidation. In this case, the potential of automation were underexploited, as both scavenging and detection of remaining reactive species could have been accommodated in the automatic flow system.

Recently, Miyamoto et al. proposed a SIA system for CL determination of $NO^\bullet$ (and also of $O_2^{\bullet-}$) that accommodates both reactions [23]. In this system, sample and NOR1 ((±)-(*E*)-4-methyl-2-[(*E*)hydroxyimino]-5-nitro-6-methoxy-3-hexenamide), a $NO^\bullet$ donor, were sequentially aspirated into the holding coil (Fig. 1c). After flow reversal, the two overlapped zones were directed towards the detector while $NO^\bullet$ was scavenged by antioxidants present in the sample. Subsequently, the remaining $NO^\bullet$ was measured after addition of luminol from a T connector just before the detector. The system was applied to compounds/enzyme with known activity against this radical, and also to commercial vitamin supplements (Table 2).

4. Several species simultaneously

In 1998, Choi et al. proposed a single line FIA-CL system for the measurement of radical scavenging capacity ($O_2^{\bullet-}$ and $HO^\bullet$) [43]. In this work, the carrier stream was a phosphate buffer (pH 7.4) solution containing 50% methanol, cytochrome c, and luminol. The authors suggested that the CL generation was based on the oxidation of luminol mediated by free radicals, probably $O_2^{\bullet-}$ and $HO^\bullet$, generated from the reaction of H_2O_2 and cytochrome c. Hence, a standard solution of H_2O_2 was injected into the carrier stream for generation of reactive species (control), while a mixture of H_2O_2 and sample was injected for measuring the radical scavenging capacity. Compounds such as gallic acid were reported to scavenge the free radicals generated, and the decrease of CL intensity was proportional to the concentration of the scavengers. Nevertheless, taking into consideration that the mixture between H_2O_2 and scavenger sample was performed off-line, the possibility of scavenging H_2O_2 should not be discarded. Later, the same research group applied this FIA-CL method to elucidate the relation between radical scavenging effect and the structure of flavonoids and also to assess the radical scavenging capacities of various Chinese herbal ingredients [44] (Table 3).

Recently, Giokas et al. introduced an analytical FIA-CL procedure that minimizes the antioxidant-oxidant (H_2O_2) interactions while favours the inhibition effects of antioxidants on the free radicals generated in situ [45]. In this way, the H_2O_2 was previously mixed with luminol/Co(II)/EDTA solution for the generation of a steady flux of free radicals (mostly $HO^\bullet$ and $O_2^{\bullet-}$), while sample was added just before the inlet of the CL-flow cell (Fig. 3b). In the presence of a metal chelator (EDTA), there is an equilibrium regime between the Co^{2+} and the [$Co(EDTA)_2$] complex, which allowed a constant source of $HO^\bullet$ radicals by catalytic oxidation of H_2O_2. Hence, a prolonged CL-signal was produced which was stable for about 30 s. In the present flow conditions, the low H_2O_2 concentrations and the excess of Co^{2+} and EDTA ensures the consumption of the oxidant before it enters in contact with the sample. Furthermore, because of the very high reactivity of the free radicals generated and the reduced time of exposition of sample, the direct reaction between antioxidants and H_2O_2 was minimized. In this way, the interference of H_2O_2 is ignored and the CL inhibition reflects the scavenging capacity of antioxidants toward the free radicals,

improving the sensitivity and the reproducibility. The application of the proposed method was restricted to pure compounds (ascorbic acid, glutathione, and uric acid).

Finally, a FIA method for in vivo, real time monitoring of total antioxidant capacity (TAC) was proposed by Yao et al. [46]. In this work a microdialysis system is used for sampling the components of blood through the jugular veins of rats, and TAC-equivalent is detected by lucigenin based sensitive CL emission since in the presence of reductants, lucigenin can generate CL emission under alkaline conditions. This system was used for monitoring in vivo the levels and changes of TAC upon administration of known biological reductants, such as ascorbic acid, uric acid, glucose, glutathione, cysteine and dopamine. Later, the same system was applied to the study of pathophysiological variance in acute myocardial infarction using in vivo monitoring of TAC in rabbits, among other parameters [40].

5. Conclusions

Considering all the methods reported in the previous sections, it is clear that CL detection was applied in more than 80% of the methods. This is due to the enhanced sensitivity of this type of detection and also due to the benefits of its association to flow based techniques. These features include the reproducible control of mixing conditions and time events, making possible the application of reactions that will provide intense but short-living analytical signals. Furthermore, high determination throughputs are attained.

Nevertheless, it should be emphasized that CL methodologies may not be selective against a specific reactive species, depending upon the generation system chosen. In most cases, several reactive species are present in the reaction media. Furthermore, as discussed previously, free radical species generated from luminol oxidation may also deplete the antioxidant pool present in the sample, providing lower results for its scavenging capacity. This low specificity towards a single reactive species is the Achilles' heel of most flow injection methodologies discussed here. Other aspect that should be careful considered on future work in this field is the reaction pH. As reported here, in most of the flow systems presented until now, reaction pH was chosen upon the detection strategy applied, and it was often different from physiological pH. For attaining biologically relevant results, it is essential to devise a methodology where the interaction between antioxidant and ROS/RNS occurs at physiological pH.

Considering also that all methods discussed here were designed to assess antioxidant interactions with biologically relevant species, its application to pharmaceutical formulations, plant and food extracts is limited. Novel methods should also target biological samples (e.g. plasma, serum, urine, and synovial fluid), aiming the measurement of antioxidant status for diagnostic and treatment monitoring. Flow injection systems would be an excellent tool in this field of application as they generally require only a few microliters of sample per analysis. Finally, miniaturization using flow-based concepts [47,48] may also provide enhanced tools or point-of-care devices to achieve these goals.

Acknowledgements

L.M. Magalhães thanks FCT and FSE (III Quadro Comunitário de Apoio) for the PhD grant SFRH/BD/12539/2003. This work was financially supported by FCT through project PTDC/SAU-FCF/67718/2006. The authors would also like to thank the helpful suggestions from reviewers of this paper.

References

[1] R. Kohen, A. Nyska, Toxicol. Pathol. 30 (2002) 620.
[2] G.H. Cao, R.L. Prior, Clin. Chem. 44 (1998) 1309.
[3] B. Halliwell, J.M.C. Gutteridge, Free Radicals in Biology and Medicine, Fourth ed., Oxford University Press, Oxford, 2007.
[4] M. Valko, D. Leibfritz, J. Moncol, M.T.D. Cronin, M. Mazur, J. Telser, Int. J. Biochem. Cell Biol. 39 (2007) 44.
[5] B. Halliwell, Trends Biochem. Sci. 31 (2006) 509.
[6] B. Halliwell, M. Whiteman, Br. J. Pharmacol. 142 (2004) 231.
[7] E.N. Frankel, A.S. Meyer, J. Sci. Food Agric. 80 (2000) 1925.
[8] R.L. Prior, X.L. Wu, K. Schaich, J. Agric. Food Chem. 53 (2005) 4290.
[9] A. Somogyi, K. Rosta, P. Pusztai, Z. Tulassay, G. Nagy, Physiol. Meas. 28 (2007) R41.
[10] H.E. Seifried, D.E. Anderson, E.I. Fisher, J.A. Milner, J. Nutr. Biochem. 18 (2007) 567.
[11] L.M. Magalhães, M.A. Segundo, S. Reis, J.L.F.C. Lima, Anal. Chim. Acta 613 (2008) 1.
[12] L.M. Magalhães, M. Santos, M.A. Segundo, S. Reis, J.L.F.C. Lima, Talanta 77 (2009) 1559.
[13] J. Ruzicka, E.H. Hansen, Anal. Chim. Acta 78 (1975) 145.
[14] E.H. Hansen, L. Norgaard, M. Pedersen, Talanta 38 (1991) 275.
[15] J. Ruzicka, G.D. Marshall, Anal. Chim. Acta 237 (1990) 329.
[16] B.F. Reis, M.F. Gine, E.A.G. Zagatto, J.L.F.C. Lima, R.A. Lapa, Anal. Chim. Acta 293 (1994) 129.
[17] V. Cerda, J.M. Estela, R. Forteza, A. Cladera, E. Becerra, P. Altimira, P. Sitjar, Talanta 50 (1999) 695.
[18] M. Amatatongchai, O. Hofmann, D. Nacapricha, O. Chailapakul, A.J. De Mello, Anal. Bioanal. Chem. 387 (2007) 277.
[19] M.A. Segundo, L.M. Magalhães, Anal. Sci. 22 (2006) 3.
[20] M. Sariahmetoglu, R.A. Wheatley, I. Cakici, I. Kanzik, A. Townshend, Anal. Lett. 36 (2003) 749.
[21] M. Sariahmetoglu, R.A. Wheatley, Y. Cakycy, Y. Kanzyk, A. Townshend, Pharmacol. Res. 48 (2003) 361.
[22] C. Lu, G. Song, J.M. Lin, Trac-Trends Anal. Chem. 25 (2006) 985.
[23] A. Miyamoto, K. Nakamura, N. Kishikawa, Y. Ohba, K. Nakashima, N. Kuroda, Anal. Bioanal. Chem. 388 (2007) 1809.
[24] B. Tang, L. Zhang, L.I. Zhang, Anal. Biochem. 326 (2004) 176.
[25] I. Parejo, C. Petrakis, P. Kefalas, J. Pharmacol. Toxicol. Methods 43 (2000) 183.
[26] G. Yildiz, A.T. Demiryurek, J. Pharmacol. Toxicol. Methods 39 (1998) 179.
[27] N. Erdemoglu, N.N. Turan, I. Cakici, B. Sener, A. Aydin, Phytother. Res. 20 (2006) 9.
[28] S.R.P. Meneses, K.L. Marques, C.K. Pires, J.L.M. Santos, E. Fernandes, J.L.F.C. Lima, E.A.G. Zagatto, Anal. Biochem. 345 (2005) 90.
[29] P.C.A.G. Pinto, M.L.M.F.S. Saraiva, S. Reis, J.L.F.C. Lima, Anal. Chim. Acta 531 (2005) 25.
[30] B. Tang, L. Zhang, Y. Geng, Talanta 65 (2005) 769.
[31] J.J. Gao, K.H. Xu, J.X. Hu, H. Huang, B. Tang, J. Agric. Food Chem. 54 (2006) 7968.
[32] A. Miyamoto, K. Nakamura, Y. Ohba, N. Kishikawa, K. Nakashima, N. Kuroda, Anal. Sci. 22 (2006) 73.
[33] K. Nakamura, Y. Ohba, N. Kishikawa, N. Kuroda, Bunseki Kagaku 53 (2004) 925.
[34] E. Floriano-Sanchez, C. Villanueva, O.N. Medina-Campos, D. Rocha, D.J. Sanchez-Gonzalez, N. Cardenas-Rodriguez, J. Pedraza-Chaverri, Free Radic. Res. 40 (2006) 523.
[35] L.M. Magalhães, M.A. Segundo, S. Reis, J.L.F.C. Lima, J.M. Estela, V. Cerdà, Anal. Chem. 79 (2007) 3933.
[36] M.F.T. Ribeiro, A.C.B. Dias, J.L.M. Santos, E. Fernandes, J.L.F.C. Lima, E.A.G. Zagatto, J. Biomol. Screen. 12 (2007) 875.
[37] W.H. Koppenol, R. Kissner, J.S. Beckman, Methods Enzymol. 269 (1996) 296.
[38] D.C. Yao, A.G. Vlessidis, N.P. Evmiridis, Anal. Chim. Acta 435 (2001) 273.
[39] D.C. Yao, A.G. Vlessidis, N.P. Evmiridis, A. Evangelou, S. Karkabounas, S. Tsampalas, Anal. Chim. Acta 458 (2002) 281.
[40] D.C. Yao, A.G. Vlessidis, N.P. Evmiridis, S. Siminelakis, M. Dimitra, Anal. Chim. Acta 505 (2004) 115.
[41] J.N. Wang, M.Q. Lu, F.Z. Yang, X.R. Zhang, W.R.G. Baeyens, A.M.G. Campaña, Anal. Chim. Acta 428 (2001) 173.
[42] Y. Noda, A. Mori, R. Liburdy, L. Packer, J. Pineal Res. 27 (1999) 159.
[43] H.Y. Choi, J.H. Song, D.K. Park, Anal. Biochem. 264 (1998) 291.
[44] H.Y. Choi, E.J. Jhun, B.O. Lim, I.M. Chung, S.H. Kyung, D.K. Park, Phytother. Res. 14 (2000) 250.
[45] D.L. Giokas, A.G. Vlessidis, N.P. Evmiridis, Anal. Chim. Acta 589 (2007) 59.
[46] D.C. Yao, A.G. Vlessidis, N.P. Evmiridis, Anal. Chim. Acta 467 (2002) 133.
[47] N. Baker, G.M. Greenway, R.A. Wheatley, C. Wiles, Analyst 132 (2007) 104.
[48] A.V. Krylov, R. Sczech, F. Lisdat, Analyst 132 (2007) 135.

Talanta 78 (2009) 1440–1445

Contents lists available at ScienceDirect

Talanta

journal homepage: www.elsevier.com/locate/talanta

Voltammetric determination of some anti-malarial drugs using a carbon paste electrode modified with $Cu(OH)_2$ nano-wire

Mohammad Hossein Mashhadizadeh*, Mitra Akbarian

Faculty of Chemistry, Tarbiat Moallem University, Tehran, Iran

ARTICLE INFO

Article history:
Received 28 January 2009
Received in revised form 19 February 2009
Accepted 20 February 2009
Available online 4 March 2009

Keywords:
Chloroquine
Primaquine
Differential pulse voltammetry
$Cu(OH)_2$ nano-wire
Modified carbon paste electrode

ABSTRACT

A sensitive electroanalytical methodology for the determination of chloroquine and primaquine using differential pulse voltammetry (DPV) at a $Cu(OH)_2$ nano-wire-modified carbon paste electrode is presented. The cyclic voltammetric and DPV pulse voltammetric techniques are compared. The effects of scan rate and pH on current were investigated and an optimal scan rate of 50 mV s^{-1} and a pH 5.5, 0.1 mol L^{-1} phosphate buffer solution (PBS), were used. Additions of chloroquine and primaquine using DPV show linear ranges from 0.068 to 6.88 μg mL^{-1} with a detection limit of 0.01 μg mL^{-1} for chloroquine and 0.58–5.89 μg mL^{-1} with a detection limit of 0.25 μg mL^{-1} for primaquine. The method was then successfully utilized for the determination of chloroquine and primaquine in a real sample of their tablets and a recovery of 95% was obtained without interference from tablet matrix.

1. Introduction

Chloroquine, 4-(7-chloro-4-quinolylamino) pentyldiethylamine (Fig. 1), has been used extensively for several decades as a suppressant in the prophylaxis and the treatment of clinical attacks of malaria, which is probably the most widespread disease to afflict mankind. It is also used in the treatment of rheumatoid arthritis and similar collagen diseases, as well as for amoebic hepatitis [1]. After the malaria parasite *Plasmodium falciparum* started to develop widespread resistance to chloroquine, new potential utilizations of this cheap and widely available drug have been investigated. For example, chloroquine is in clinical trials as an investigational antiretroviral in humans with HIV-1/AIDS and as a potential antiviral agent against chikungunya fever. Moreover, the radio-sensitizing and chemo-sensitizing properties of chloroquine are beginning to be exploited in anticancer strategies in humans [2].

Primaquine (Fig. 1) is the only anti-malarial drug used as tissue schizonticide and in relapsing malaria. It acts on latent or hipnozoite forms of *Plasmodium ovule* and *Plasmodium vivax*, in the liver of the host, and its combination with blood schizonticide can be completely curative [3].

Determination of these drugs concentrations in different body fluids is important for prophylaxis and the treatment of malaria cases. Investigation of pharmacokinetics helps to decide true resistance of malaria parasites to different anti-malarial. The drugs have been determined in biological fluids with methods such as colorimetric tests [4,5], spectrophotometry [6], spectrofluorometry [7,8], high-performance liquid chromatography with fluorescence detection [9–12], thin-layer chromatography [13,14], gas chromatographic methods [15,16], and capillary zone electrophoresis [17].

However, most of the above methods require several time-consuming manipulation steps, sophisticated instruments and special training. For these reasons, the rapid, simple and accurate method with high sensitivity is expected to be established. Recently, materials in the nanometer range have shown superior or advantageous functional properties for a wide range of technological applications, including catalysis, optics, microelectronics, and chemical/biological sensors. Metals in the nanometer range provide three important functions for electroanalysis: the roughening of the conductive sensing interface, catalytic properties, and conductivity properties [18]. Typical nano-wires exhibit aspect ratios (length-to-width ratio) of 1000 or more. As such they are often referred to as one-dimensional materials. Nano-wires have many interesting properties that are not seen in bulk or 3D materials. This is because electrons in nano-wires are quantum confined laterally and thus occupy energy levels that are different from the traditional continuum of energy levels or bands found in bulk materials [2].

Peculiar features of this quantum confinement exhibited by certain nano-wires such as carbon nano-tubes manifest themselves in discrete values of the electrical conductance. Such discrete values arise from a quantum mechanical restraint on the number of electrons that can travel through the wire at the nanometer scale. The magnetic properties of $Cu(OH)_2$ are remarkably sensitive to

* Corresponding author. Tel.: +98 21 88848949; fax: +98 21 88820993.
E-mail address: mashhadizadeh@tmu.ac.ir (M.H. Mashhadizadeh).

0039-9140/$ – see front matter © 2009 Elsevier B.V. All rights reserved.
doi:10.1016/j.talanta.2009.02.040

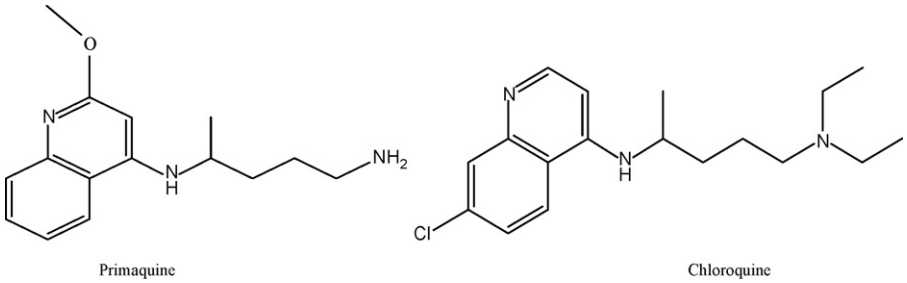

Fig. 1. Chemical structure of chloroquine and primaquine.

the intercalation of molecular anions [19,20], making the material a candidate for sensor applications.

Carbon pastes are well known as useful materials for the fabrication of various electrometric sensors for analytical propose. The operation mechanism of such chemically modified carbon paste electrodes (CMCPEs) depends on the properties of the modifier used to important selectivity towards the target species. Each measurement was performed on a new surface, obtained by a simple/polishing procedure [21].

Carbon paste electrode (CPE) has been widely used in determination of drugs, biomolecule, and other organic species because of their easy preparation and wider potential window of −1.4 to +1.3 V (versus SCE) according to experimental conditions [22,23]. Their residual currents are 10 times lower than those of the glassy carbon electrodes or noble metallic electrodes [24]. So far, few electrochemical techniques have been attempted for the purpose of the study of chloroquine and/or primaquine [25–27]. Arguelho et al. [25] determined hydroxychloroquine in plaquenil using DPV and achieved a LOD of 11.2 $\mu g\,mL^{-1}$ with a relative standard deviation of 0.46%. Radi [26] performed the accumulation and measurement of chloroquine drug at DNA-modified carbon paste electrode by DPV and obtained a LOD of 3.0×10^{-8} mol L^{-1} in the range 1.0×10^{-7}–1.0×10^{-5} mol L^{-1}. In this work, an electrochemical analysis for chloroquine and primaquine was proposed by differential pulse voltammetry (DPV) at a CPE-modified by $Cu(OH)_2$ nano-wire (Cu-NW-CPE). A sensitive anodic oxidative peak of chloroquine and primaquine was used for quantitative determination. A good linear relationship was realized between the anodic peak currents and chloroquine or primaquine concentrations in the range of 0.068–6.88 and 0.58–5.89 $\mu g\,mL^{-1}$, respectively with a good reproducibility. The validation parameters of the method were evaluated. The detection limits of this method for chloroquine and primaquine were 0.01 and 0.25 $\mu g\,mL^{-1}$, respectively.

2. Experimental

2.1. Apparatus

Voltammetric experiments were performed with an EN 50081-2 electrochemical workstation (Declaration of company, Netherlands). A conventional three-electrode system was used with a carbon-paste working electrode (unmodified or modified), a saturated Ag/AgCl reference electrode and a Pt wire as the counter electrode. During the measurement, the solution in the cell was not stirred and the phosphate buffer solution (PBS) was used without unaeration. A pH meter (Crison model GLP 22) was applied for the preparing the buffer solutions, which in turn were used as the supporting electrolyte in voltammetric experiments.

2.2. Reagents and solutions

Paraffin oil and graphite powder were obtained from Merck Company and used as received. All other chemicals were of analytical grade and used without further purification. Chloroquine

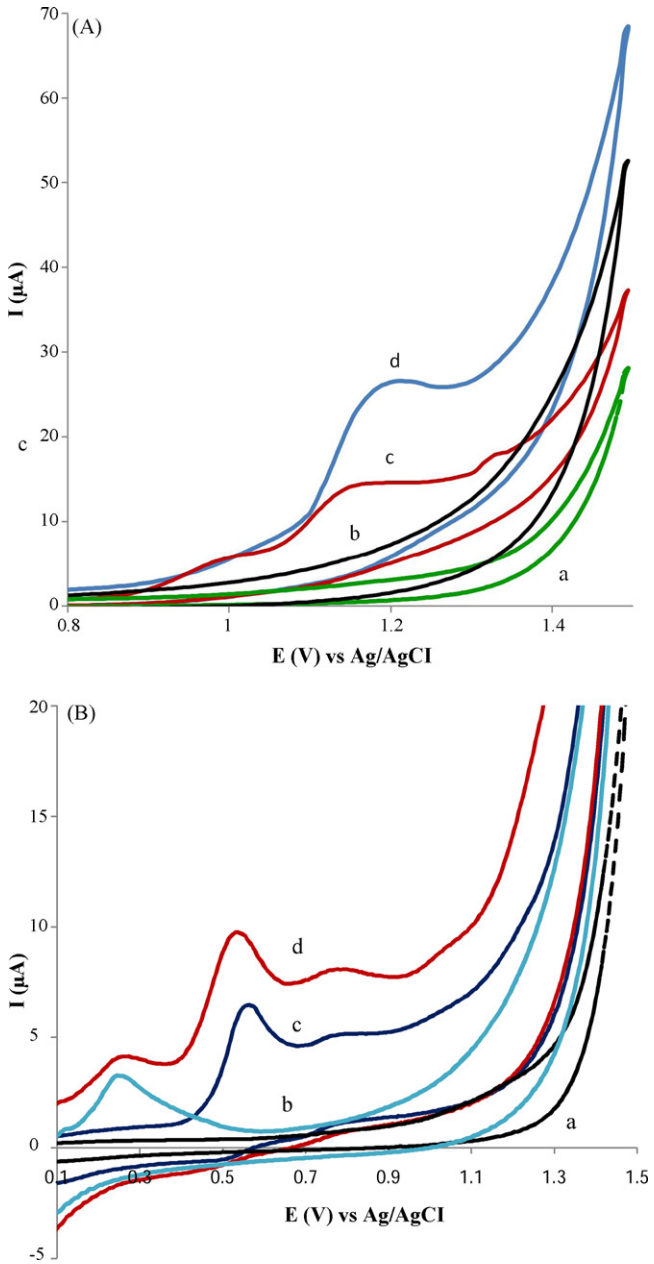

Fig. 2. Cyclic voltammograms of chloroquine (A) and primaquine (B). (a) Blank solution at bared CPE. (b) Blank solution at Cu-NW-CPE, (c) and (d) 6.6×10^{-5} mol L^{-1} of chloroquine or primaquine at bared CPE and Cu-NW-CPE, respectively. Conditions: 0.1 mol L^{-1} phosphate buffer solution with pH 5.5 and sweep rate was 50 mV s^{-1}.

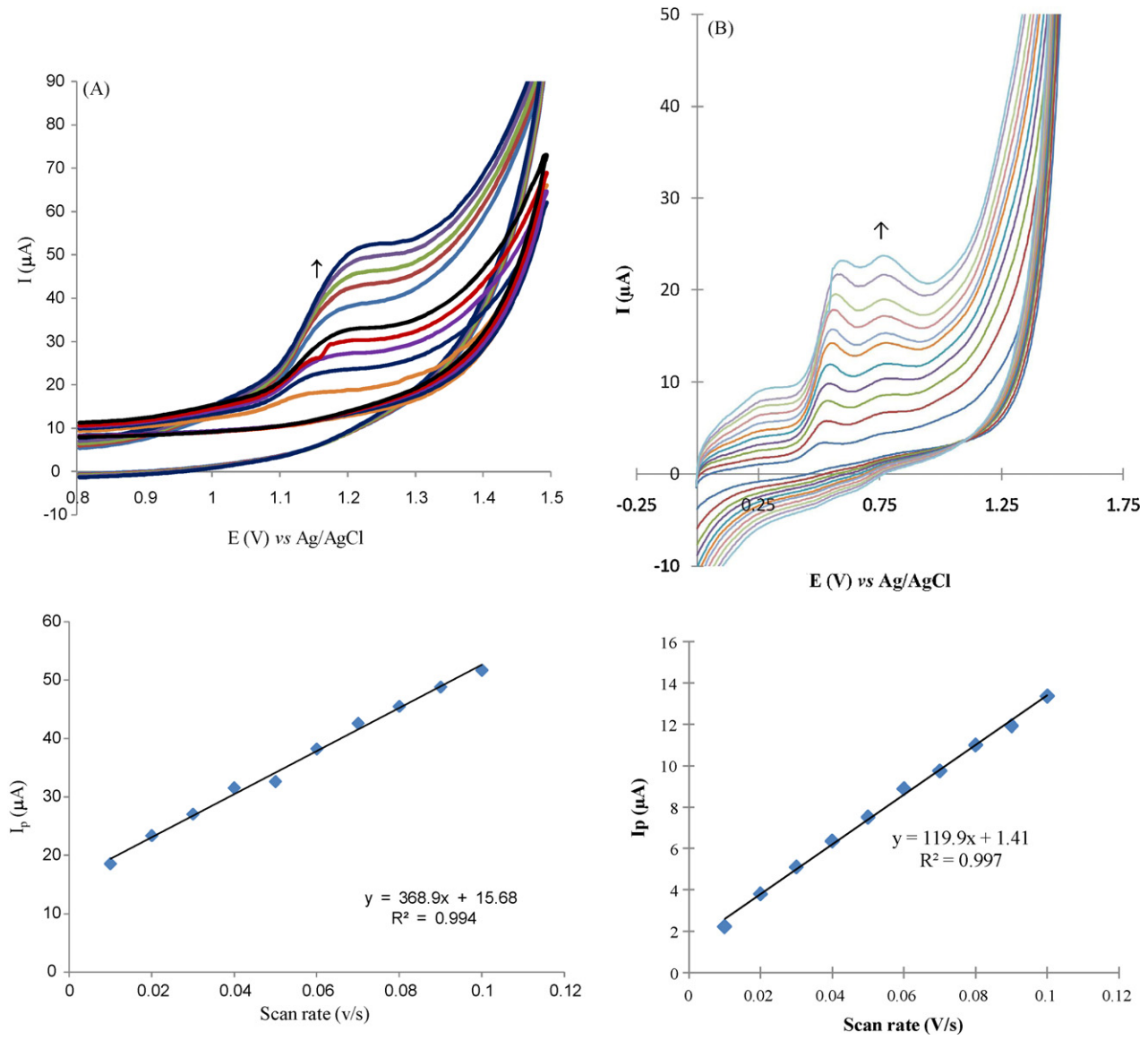

Fig. 3. Cyclic voltammograms at various scan rates and Ip_a versus scan rate of chloroquine (A) and primaquine (B) used a Cu-NW-CPE as working electrode. Solution contains 6.6×10^{-5} mol L^{-1} of chloroquine or primaquine in 0.1 mol L^{-1} phosphate buffer solution with pH 5.5.

and primaquine in analytical grade were prepared from Pars pharmaceutical Company (Tehran, Iran). 1.0×10^{-2} mol L^{-1} chloroquine and primaquine stock standard solutions were prepared. Working standard solutions were prepared by appropriate dilution of the stock standard solution with buffer.

A $Cu(OH)_2$ nano-wire was prepared by chemical method according to the literature [28].

2.3. Procedure for pharmaceutical analysis

The contents of 10 tablets of each of chloroquine and primaquine (Pars Co., Tehran, Iran) were weighed for obtaining the average mass of each tablet, then powdered, and an amount of one tablet of each drug were transferred to a 50 mL beaker and dissolved in distilled water, shaken well for 10 min, then the solution filtered and diluted in a 50 mL volumetric flask to the mark with distilled water. Appropriate aliquots from the working solutions were taken for the voltammetric determination of them by DPV techniques in the standard addition mode, and diluted with buffer to obtain final concentrations in the range of calibration graph. Then solutions assayed as described under optimized proposed procedure.

2.4. Preparation of modified electrode

The unmodified carbon-paste electrode was prepared by mixing graphite powder with appropriate amount of mineral oil (paraffin) and thorough hand mixing in a mortar and pestle (60:25, w/w), and a portion of the composite mixture was packed into the end of a polyethylene syringe (2.5 mm diameter). Electrical contact was made by forcing a thin copper wire down into the syringe and into the back of the composite. The modified electrode was prepared by mixing unmodified composite with $Cu(OH)_2$ nano-wire (%15, w/w). Then, the modified composite was packed into the end of a polyethylene syringe.

3. Results and discussion

3.1. Electrochemical behaviors of chloroquine and primaquine on CPE modified with $Cu(OH)_2$ nano-wire

Results of previous works showed that the CPEs modified with various types of nano-wires and nano-particles have catalytic effects in the electro-oxidation of biologically important drugs com-

pounds. The catalytic rule of the modifier causes lowering the anodic over potential and enhancement of the anodic peak current in the electrode process. Fig. 2 shows the cyclic voltammograms of chloroquine (A) and primaquine (B) for the following cases: (a) the blank solution (only supporting electrolyte) at bared CPE, (b) the blank solution at Cu-NW-CPE, (c) and (d) 6.6×10^{-5} mol L^{-1} of chloroquine or primaquine at bared CPE and Cu-NW-CPE, respectively, in 0.1 mol L^{-1} phosphate buffer solution with pH 5.5. In all cases the sweep rate was 50 mV s^{-1}. As seen, a relatively broad and weak anodic wave for the electro-oxidation of chloroquine and primaquine on the unmodified electrode reveals that the electrode process is very sluggish. When the CPE modified with $Cu(OH)_2$ nano-wire, on the other hand, a well-defined and sharp anodic wave with a peak potential of 1.21 (±0.02) V and 0.56 (±0.01) V are obtained for chloroquine and primaquine, respectively. However, in blank solution no peak is seeing with Cu-NW-CPE-modified electrode. On the basis of these observations, it can be postulated that the addition of $Cu(OH)_2$ nano-wire to the matrix of CPE exhibits an effective catalytic fashion in the electrochemical oxidation of chloroquine and primaquine, leading to a remarkable enhancement of the anodic peak current. The results showed that for both chloroquine and primaquine, in the potential range of 0.0–1.5 (versus Ag/AgCl) and all potential scan rates (from 10 to 100 mV s^{-1}), no cathodic peak was observed on the reverse sweep. This confirms an irreversible process for its oxidation on the Cu-NW-CPE.

The cyclic voltammetric investigations at various scan rates for chloroquine and primaquine were performed on the Cu-NW-CPE (Fig. 3). In these studies, a linear relationship with a correlation coefficient of $R^2 = 0.9942$ and $R^2 = 0.9971$ are observed between the anodic peak current and the scan rate for chloroquine and primaquine, respectively, which reveals that the oxidation of chloroquine and primaquine are an adsorption-controlled process.

3.2. Effect of carbon paste composition

It is well known that the electrochemical characteristics of the CPE electrodes depend significantly on the paste composition. Thus, the influence of the amounts of modifier ($Cu(OH)_2$ nano-wire), oil, and graphite powder on the response of the electrode to concentration of chloroquine and primaquine were investigated by cyclic voltammetry. Electrodes with different percents of modifier (0, 5, 10, 15, and 20%), graphite powder (69, 66, 63, 60, and 57%), and paraffin oil (31, 29, 27, 25, and 23%) were prepared and examined for their voltammetric signals under identical conditions. The results showed that, in the absence of modifier ($Cu(OH)_2$ nano-wire) the electrode had low response towards drugs. However, the maximum peak current was obtained for 15% of $Cu(OH)_2$ nano-wire in the paste. According to these results, a carbon-paste composition of 15% modifier $Cu(OH)_2$ nano-wire, 60% graphite and 25% paraffin oil was the optimum composition with higher peak currents and used in further studies.

3.3. The pH effect

The effect of pH of the supporting electrolyte was also studied by varying the pH in the range 3–6. Cyclic voltammetric studies on the electro-oxidation of chloroquine and primaquine at various pHs were performed at the Cu-NW-CPE. The peak current as a function of pH is shown in Fig. 4. Both chloroquine and primaquine shows a maximum anodic peak current at pH 5.5, this was agreed with previous reports [24,25].

3.4. Differential pulse voltammetry, analytical performance characteristics

The DPV using the Cu-NW-CPE was used as a very sensitive method with a low detection limit for determination of chloroquine and primaquine. The differential pulse voltammetry was immediately performed from 0.5 to 1.5 V and 0.3 to 1.0 V for chloroquine and primaquine, respectively. In order to establish the optimum conditions by means of DPV technique, various instrumental variables were studied, and the optimum conditions were as follows: scan rate: 50 mV s^{-1}, pulse amplitude: 25 mV, and pulse period: 0.07 s. DPV waves for various concentrations of chloroquine and primaquine in 0.1 mol L^{-1} phosphate buffer (pH 5.5) are shown in Fig. 5. The i_p versus concentration curve of chloroquine and primaquine, which is shown in Fig. 5, has a linear range between 0.068 and 6.88 μg mL^{-1} with a detection limit of 0.010 (±0.002) μg mL^{-1} for chloroquine. The linear range for primaquine was found between 0.58 and 5.89 μg mL^{-1} with a detection limit of 0.25 (±0.01) μg mL^{-1}. For chloroquine the slope and the correlation coefficient (R^2) of the calibration curve were found 1.325 (±0.028) μA/μg mL^{-1} and 0.9938, respectively. These data for primaquine were found 0.388 (±0.009) μA/μg mL^{-1} and 0.9966, respectively.

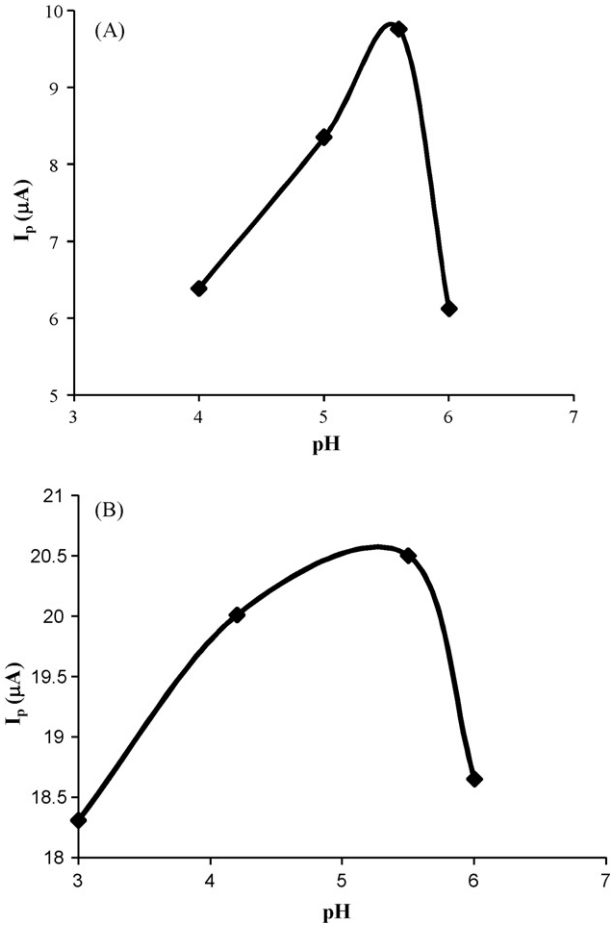

Fig. 4. Effect of pH of (A) chloroquine and (B) primaquine solutions on the cyclic voltammetric peak current. Experimental conditions are the same as in Fig. 3 and sweep rate was 50 mV s^{-1}.

3.5. Reproducibility, repeatability, and stability

The main attraction of using the carbon paste modified electrode is that the electrode surface can be renewed after every use. Indeed, seven successive renewing of a modified Cu-NW-CPE electrode were used for determination of 6.6×10^{-5} mol L^{-1} of chloroquine or primaquine repeatedly. The average peak current for chloroquine and primaquine were found 6.25 and 1.57 μA with R.S.D.s 1.9 and 2.1%, respectively. Then the precision of peak

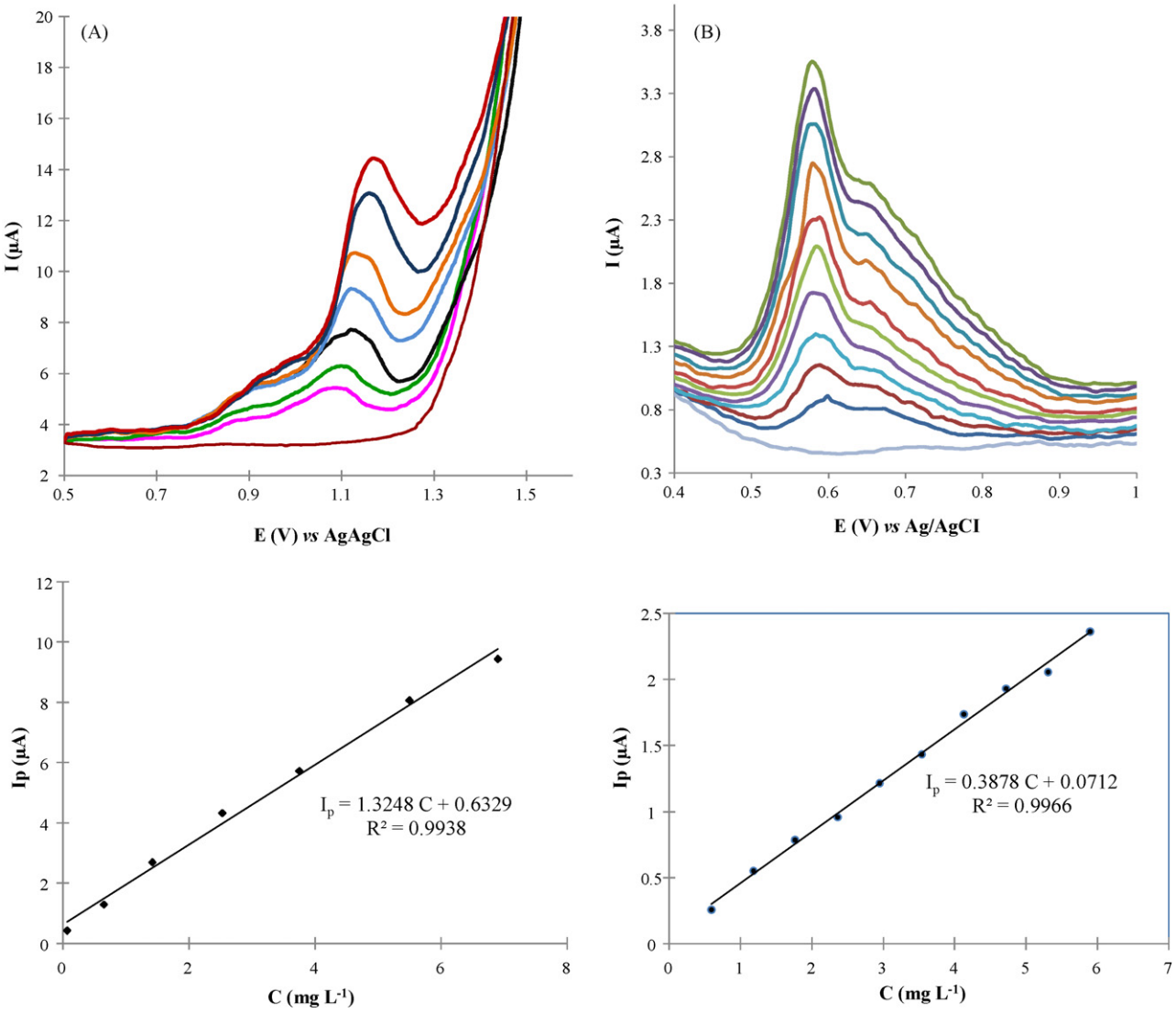

Fig. 5. Differential pulse voltammograms of solutions containing various concentrations and calibration curve of peak current versus concentration of (A) chloroquine and (B) primaquine at a Cu-NW-CPE. Supporting electrolyte in all measurements was 0.1 mol L^{-1} phosphate buffer with pH 5.5 and pulse amplitude was 50 mV.

current values with five Cu-NW-CPE electrodes (with the same paste composition) were also measured. The average peak current of 6.6×10^{-5} mol L^{-1} of chloroquine was 6.18 μA with the R.S.D. of 2.7%. For 6.6×10^{-5} mol L^{-1} of primaquine solution the average peak current and R.S.D. were found 1.60 μA and 2.6%, respectively. With the same electrode, the measurement results were in good agreement in 2 months indicating that the stability of the electrode was remarkable.

3.6. Interference studies

The interference of a few common interferes was investigated in the presence of 6.6×10^{-5} mol L^{-1} chloroquine and primaquine. Sorbitol, lactose, Na^+, and K^+ in 200-fold of the chloroquine and primaquine concentration did not change the signal of DPV.

3.7. Determination of chloroquine and primaquine in a pharmaceutical product

Chloroquine and primaquine were determined by DPV at the Cu-NW-CPE in the tablets containing these compounds. Following the procedure described in Section 2.3, a DPV for chloroquine and primaquine were obtained. No signals appeared from other compounds of the sample, since their concentrations in the analytical solutions were low enough to prevent any interfering effect. The determination of chloroquine and primaquine were performed by using the standard addition method in order to minimize the matrix effect. The results collected in Table 1 show a mean chloroquine and primaquine of 111.6 (±2.1) mg and 89.4 (±1.1) mg in each tablet, respectively, which agrees very well with the labeled value (114 and 90 mg/tablet, respectively). The R.S.D. obtained for these determinations, 3.4 and 2.6% for chloroquine and primaquine, respectively, indicated a good precision. The HPLC method was employed as a comparison to evaluate the validity of the developed method. The average amount of chloroquine and primaquine in each tablet obtained from three replicate measurements were 108.9 (±1.1) and 90.5 (±0.8), respectively. As seen, there was no significant difference between methods and a good agreement was achieved. The results obtained from this study show that proposed method would be recommended for the determination of primaquine and chloroquine in tablets.

Table 1
Determination and recovery of chloroquine and primaquine in pharmaceutical of these drugs.

Sample	Labeled claim (mg/tablet)	Added (mg)	Found	Recovery (%)
Chloroquine tablet	150	–	146.8 ± 2.1[a]	97.9
Chloroquine tablet	–	103	250.2 ± 3.5	98.9
Chloroquine tablet	–	206	350.5 ± 3.7	98.4
Chloroquine tablet	–	298	444.5 ± 3.0	99.2
Primaquine tablet	15	–	14.9 ± 2.3	99.3
Primaquine tablet	–	70	82.3 ± 2.2	96.8
Primaquine tablet	–	140	153.8 ± 2.4	99.2
Primaquine tablet	–	245	260.9 ± 0.4	100.3

[a] Average of five determination.

4. Conclusions

The results described in this paper demonstrate fairly well that Cu-NW-CPE constitute excellent electrode materials for the voltammetric determination of chloroquine and primaquine. The electroanalytical measurements performed with this electrode exhibit a good reproducibility, both with the same electrode and different Cu-NW-CPE prepared under the same conditions, and it has advantages over similar measurements carried out at bare CPE electrode. Finally, the suitability of Cu-NW-CPE for the analysis of chloroquine and primaquine in real samples has been proved.

References

[1] P.E. Thompson, L.M. Werbel, Antimalarial Agents: Chemistry and Pharmacology, Academic Press, New York, 1972, p. 100.
[2] http://en.wikipedia.org/.
[3] A. Korolkovas, Essentials of Medicinal Chemistry, 2nd Ed., John Wiley & Sons, 1988, p. 579.
[4] Y. Bergqvist, C. Hed, L. Funding, A. Suther, Bull. WHO 63 (1985) 893.
[5] D.L. Mount, L.C. Patchen, S.B. Williams, F.C. Churchill, Bull. WHO 65 (1987) 615.
[6] V. Singh, J.S. Mahanwal, S.K. Shukla, Ind. J. Forensic Sci. 4 (1990) 183.
[7] S.A. Adelusi, L.A. Salako, J. Pharm. Pharmacol. 32 (1980) 711.
[8] M. Tsuchiya, J.J. Aaron, E. Torres, J.D. Winefordner, Anal. Lett. 18 (1985) 1647.
[9] J. Ducharme, R. Farinotti, J. Chromatogr. B 698 (1997) 243.
[10] K. Croes, P.T. McCarthy, R.J. Flanagan, J. Anal. Toxicol. 18 (1994) 255.
[11] D.R. Brocks, F.M. Pasutto, F. Jamali, J. Chromatogr. Biomed. Appl. 119 (1992) 581.
[12] Y. Bergqvist, B. Domeij-Nyberg, J. Chromatogr. Biomed. Appl. 23 (1983) 137.
[13] B. Betschart, A. Sublet, S. Steiger, J. Planar Chromatogr. Mod. TLC 4 (1991) 111.
[14] D.L. Mount, B.L. Nahlen, L.C. Patchen, F.C. Churchill, J. Chromatogr. 423 (1987) 261.
[15] F.C. Churchill, D.L. Mount, I.K. Schwartz, J. Chromatogr, Biomed. Appl. 25 (1983) 111.
[16] A. Viala, E. Deturmeny, M. Estadieu, A. Durand, J.P. Cano, J. Chromatogr. Biomed. Appl. 13 (1981) 503.
[17] R.B. Taylor, R.G. Reid, J. Pharm. Biomed. Anal. 13 (1995) 21.
[18] A. Cavicchioli, M.A. La-Scalea, I.G.R. Gutz, Electroanalysis 16 (2004) 697.
[19] W. Fujita, K. Awaga, Inorg. Chem. 35 (1996) 1915.
[20] W. Fujita, K. Awaga, J. Am. Chem. Soc. 119 (1997) 4563.
[21] M. Aslanoglu, N. Peker, J. Pharm. Biomed. Anal. 33 (2003) 1143.
[22] C.A. Grimes, E.C. Dickey, M.V. Pishko, Encyclopedia of Sensors, vol. 4, American Scientific Publishers, Stevenson Ranch, California, 2006, pp. 283–430.
[23] M.H. Mashhadizadeh, A. Mostafavi, H. Allah-Abadi, I. Sheikhshoai, Sens. Actuator B 113 (2006) 930.
[24] K. Kalcher, J.-M. Kauffmann, J. Wang, I. Svancara, K. Vytras, C. Neuhold, Z. Yang, Electroanalysis 7 (1995) 5.
[25] M.L.P.M. Arguelho, M.V.B. Zanoni, N.R. Stradiotto, Anal. Lett. 38 (2005) 1415.
[26] A. Radi, Talanta 65 (2005) 271.
[27] M.A. La-Scalea, C.M.S. Menezes, G.C. Matsutami, M.C. Polli, S.H.P. Serrano, E.I. Ferreira, Electrochim. Acta 51 (2006) 5103.
[28] W. Wang, C. Lan, Y. Li, K. Hong, G. Wang, Chem. Phys. Lett. 366 (2002) 220.

Talanta 78 (2009) 1235–1239

Contents lists available at ScienceDirect

Talanta

journal homepage: www.elsevier.com/locate/talanta

Enrichment with air-sandwiched method of on-line collection/concentration using chelating resin and simultaneous determination of trace elements by inductively coupled plasma atomic emission spectrometry

Osamu Noguchi [a,b,*], Mitsuko Oshima [a], Shoji Motomizu [a]

[a] Graduate School of Natural Science and Technology, Okayama University, 3-1-1, Tsushimanaka, Okayama 700-8530, Japan
[b] Criminal Investigation Laboratory, Okayama Prefectural Police H.Q., 1-3-2, Tonda, Okayama 700-0816, Japan

ARTICLE INFO

Article history:
Received 11 December 2008
Received in revised form 15 January 2009
Accepted 15 January 2009
Available online 5 February 2009

Keywords:
On-line collection/concentration
ICP-AES
Chelating resin
Concrete

ABSTRACT

The application of inductively coupled plasma atomic emission spectrometry (ICP-AES) to the forensic sample was studied. On-line collection/concentration method of the sample with chelating resin column (TE-05) and air-sandwiched method to isolate the analyte zone at the highest concentration of an eluent was coupled with ICP-AES. The limits of detection (LODs) were much improved to 35 fold (Co): from Sc, 0.15 ng ml^{-1} to Ni, 1.99 ng ml^{-1}, and the concentration efficiency was 7–14 times. This method was applied to the concrete with about 10 mg of samples. Major elements (Al, Fe, Mg) measured by conventional/ICP-AES and trace elements measured by this method, such as Cd, Co, Ni, and Pb were determined without matrices interference. Four concrete samples can be discriminated by comparing the content profiles of the trace elements and the major elements.

1. Introduction

In the field of the forensic chemistry, the identification of a target substance in complex/matrix-enriched samples, such as medicine, glass and paint, sometimes is very important and must be performed reliably [1–3]. One of the ways for such identification is a technique to compare the distribution of inorganic elements: an inorganic elements profiling method. For determining inorganic elements, neutron activation analysis (NAA) [4–5], and atomic absorption spectrometry (AAS) [6] have been widely used. Recently, synchrotron radiation X-ray fluorescence spectrometry (SR-XRF) [7–8] was used for small volume samples. However, SR-XRF needs a specific operator with a license and a large-scale special facility. Inductively coupled plasma mass spectrometry (ICP-MS) is one of the most sensitive analytical tools at the laboratory level, and can be applied to the analysis of glass and so on [9–10]. However, ICP-MS has several problems in measuring samples, which contain high concentration elements as matrices. As forensic samples are usually gathered on the criminal scene, the volumes of the samples obtained are often scarcely low, and the concentrations of the elements contained in the samples are much diluted when the samples are dissolved in solutions for the measurement; sometimes their concentrations are much lower than LODs by ICP-MS. For such forensic samples, we developed a sensitive method to measure using a small sample size by ICP-MS [11].

In this work, we developed a sensitive analysis method by inductively coupled plasma atomic emission spectrometry (ICP-AES). The sensitivity of ICP-AES is usually worse than ICP-MS. However, ICP-AES is much more convenient and more widely used than ICP-MS [12–13]. In ICP-AES, for overcoming its weak point, low sensitivity, it has been improved by coupling the on-line method for the collection/concentration of analytes with a solid phase column with ICP-AES [14]: the detection was carried out by using an analyte zone at the highest concentration of an eluent, which was sandwiched by air. One of commercially available solid phases, TE-05, was used: it is a silica-based chelating resin and can collect various kinds of elements for simultaneous determination of trace elements. Usually, TE-05 cannot adsorb alkali and alkaline earth elements in aqueous sample solutions, and is very stable and can be used repeatedly for column procedures. The pretreatment procedure with a column packed with a solid phase can be performed by a laboratory-made computer-controlled system (Auto-Pret system) [15–17]. The method with the auto-Pret system was applied to a concrete sample, which is very difficult to discriminate in the forensic chemistry [18].

* Corresponding author at: Criminal Investigation Laboratory, Okayama Prefectural Police H. Q., Tonda, Okayama 700-0816, Japan. Tel.: +81 86 234 0110; fax: +81 86 234 0110.
E-mail address: op-euaec907@pref.okayama.jp (O. Noguchi).

0039-9140/$ – see front matter © 2009 Elsevier B.V. All rights reserved.
doi:10.1016/j.talanta.2009.01.050

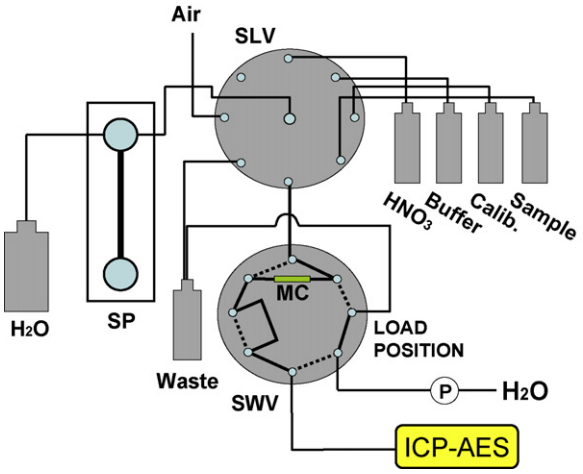

Fig. 1. Laboratory-assembled auto-pretreatment system for on-line collection/concentration. SP, syringe pump; SLV, eight-port selection valve; SWV, eight-way switching valve; MC, mini-column; P, peristaltic pump.

2. Experimental

2.1. Instrumentation

A modular digital syringe pump (Hamilton: Reno, NV, USA), a selection valve and a switching valve (Hamilton: Reno, NV, USA) were used to assemble an Auto-Pret system, which is computer-controlled by a laboratory-written VISUAL BASIC program. Flow lines were constructed with PTFE tubing (0.5 mm i.d.). The laboratory-made mini-column was prepared with the volume of about 0.13 ml (2 mm i.d. × 40 mm length). The Auto-Pret system was coupled with ICP-AES (Vista-Pro: Seiko Instruments, Chiba, Japan). The manifold of the Auto-Pret System coupled with ICP-AES used in this work was shown in Fig. 1. The operating condition of ICP-AES is shown in Table 1.

Table 1
Operating conditions of ICP-AES.

Spectrometer	ICP-AES (Vista-Pro)
RF generator	Frequency 40 MHz, power of 1.2 kW
Plasma gas flow	Ar 15.0 l min^{-1}
Auxiliary gas flow	Ar 1.50 l min^{-1}
Nebulizer gas flow	Ar 0.75 l min^{-1}
Spray chamber	Glass cyclonic spray chamber
Nebulizer	K-style concentric glass nebulizer
Torch	One-piece low flow extended torch in the axial view mode

2.2. Reagents and materials

Multi-element standard solutions were prepared by diluting several kinds of a single-element standard solution for atomic absorption spectrometry (1000 μg ml^{-1}, Wako Pure Chemicals, Osaka, Japan) and a multi-element standard solution for ICP-MS

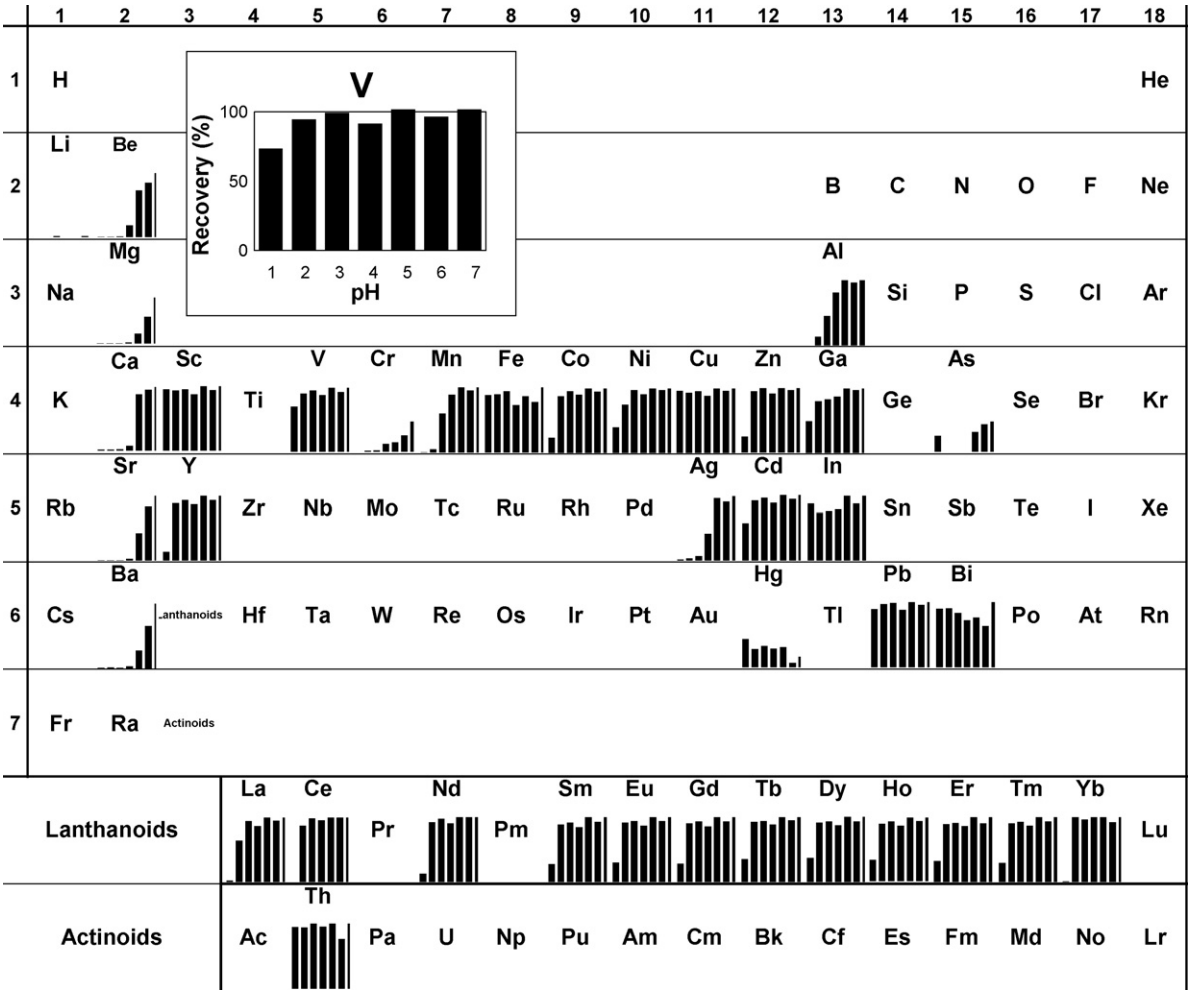

Fig. 2. Adsorption behavior of trace elements at various pHs with TE-05 resin. Samples, 4 ml of solution containing 250 ng g^{-1} various elements; eluent, 4 ml of 3 M HNO_3.

($10\,\mu g\,ml^{-1}$, Spex CertiPrep Inc., NJ, USA); XSTC-13 (31 elements) and XSTC-1 (16 rare earth elements) by using a weight method. Ultrapure water ($18.2\,M\Omega\,cm^{-1}$ resistivity) prepared by an Elix 3/Milli-Q Element system (Nihon Millipore, Tokyo, Japan) was used throughout. Ultrapure grade nitric acid (60%, Kanto Chemicals, Tokyo, Japan) was diluted with the ultrapure water to give adequate acid concentrations. Acetic acid (minimum 96%) and ammonia water (29%) used for the preparation of ammonium acetate solution were of an electronic industrial reagent grade (Kanto Chemicals, Tokyo, Japan). A chelating resin, MetaSEP AnaLig® TE-05 (100–200 mesh: supplied by GL Science Inc., Tokyo, Japan) was used for collection/concentration of trace elements. Four kinds of concrete block samples were purchased from different companies.

3. Result and discussion

3.1. Collection behavior by batch-wise procedure with mini-column

A resin, TE-05 (45 mg), was packed in the mini-column. The column packed with the resin was washed by passing 10 ml of 3 M HNO_3 through it, followed by passing 10 ml of ultrapure water. The column was then conditioned at an appropriate pH by passing 5 ml of buffer solutions (pH 1–7, adjusted with HNO_3 and 0.2 M ammonium acetate solution). A multi-element sample solution containing $250\,ng\,g^{-1}$ of each element (4 ml), whose pH was adjusted at the same pH as the column conditioning, was passed through the column, and then 5 ml of buffer solution was passed through the column. The buffers remaining in the column were washed out by passing 5 ml of the ultrapure water. Finally, 4 ml of 3 M HNO_3 was passed through the column for recovering metal ions, which were adsorbed on the resin. The flow rate of the eluent was $0.9\,ml\,min^{-1}$; the eluents were adjusted to 10 g with ultrapure water, and then measured by a conventional method with ICP-AES. The results obtained were shown in Fig. 2. Twenty-nine elements were collected by almost 100% at around pH 6. By changing the collection pH from 6 to 3, alkaline and alkaline-earth metals were not collected on the resin. From such collection behavior, trace levels of elements Cd, Co, Cu, Fe, Ga, In, Ni, Pb, Th, V, Zn, and 14 rare earth elements in samples could be collected quantitatively at pH 3, even though Ca, Na, K, and Ba were contained in the samples as matrices.

3.2. Air-sandwiched method for peak sharpness

For measuring with a very small volume of a sample solution by ICP-MS, we proposed the method by sandwiching a sample zone with air (air-segmented sample injection technique) [19–20] in order to prevent the dispersion of the sample zone into a carrier solution. This method was applied to the improvement of the sensitivity. However, when the column pretreatment method with a solid phase was incorporated for on-line collection/concentration of trace elements, the sandwiched method must be reformed. When a conventional flow line is used, air bubbles must pass through the column; these are often divided irregularly in the column, and therefore the reproducibility of measurements becomes worse. In the present study, a new program for using the sandwiched zone and overcoming the disadvantage was developed and examined as is shown in Table 2. Air -sandwiched zone was prepared at the step "Elution with 3 M HNO_3 sandwiched with air" in Table 2 by changing the flow direction alternatively through the column. Though the flow exchange steps were increased, air did not pass through the column; such an operation can be carried out automatically. The most concentrated eluent zone was isolated from the back and forward dispersed eluent zone.

Table 2
Flow program of this Auto-Pret system.

	SWV[a] position	Flow rate ($ml\,min^{-1}$)	Flow volume (ml)
Washing with ultrapure water	Inject	6	2
Conditioning with 0.2 M CH_3COONH_4	Inject	6	1
Collection of elements	Inject	0.9	2
Washing with 0.2 M CH_3COONH_4	Inject	6	0.5
Washing with ultrapure water	Inject	6	1
Elution with 3 M HNO_3	Load	0.9	0.17
sandwiched with air	Inject	0.6	0.06
	Load	0.12	0.10
	Inject	0.6	0.05
	Load	0.9	0.88

[a] Switching valve.

3.3. Optimal conditions for on-line collection/concentration

The dispersion of an element in an effluent was investigated. One ml of the eluent (2 M HNO_3) was passed through the column, followed by passing 2 ml of $10\,ng\,g^{-1}$ Co solution through the column, and at the same time, the 100 μl portion of the Co solution flowed out of the column was sandwiched with air bubbles and measured by ICP-AES. Then, the zone sandwiched with air was shifted stepwise: the results were shown in Fig. 3 with a flowing zone image. From these results, the highest concentrated zone could be sandwiched with air bubbles as is shown in Fig. 3(b); the sandwiched zone was somewhat dispersed.

The optimal volume of the effluent sandwiched with air was investigated using the Co solution ($10\,ng\,g^{-1}$) as a sample. When the volume of the effluent sandwiched with air was varied from 50, 75, 100 to 125 μl; using the volumes of 50 μl and 75 μl, the highest portion of the cobalt concentration could not be recovered. When 100 μl of the effluent was used, almost all of the peak area can be recovered. Though the highest portion of the cobalt concentration can be recovered using 125 μl, the peak height was lower than that of 100 μl. This is due to the dispersion of the analyte zone in the sandwiched effluent zone. As a result, the volume of the effluent sandwiched with air was selected to be 100 μl.

The concentration of HNO_3 used as an eluent was examined. The results, which were obtained by using 2, 3, and 6 M HNO_3 as an eluent, were compared with one another. When 2 M HNO_3

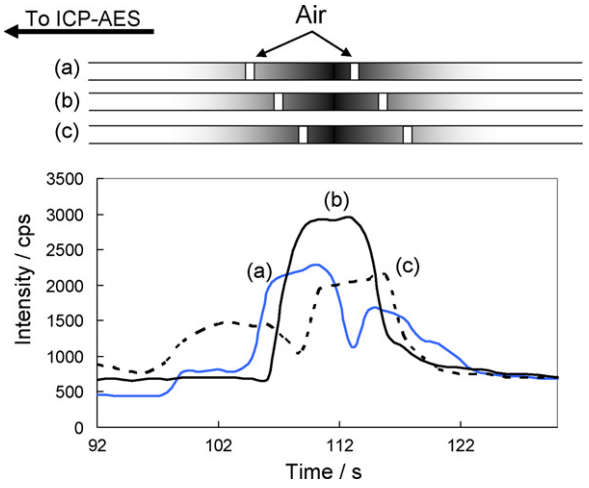

Fig. 3. The distribution profile of the collected zone in the eluent with its images. (a), top portion of the eluent; (b), middle portion of the eluent; (c), bottom portion of the eluent; sample, 2 ml of Co, $10\,ng\,g^{-1}$; flow rate, $0.9\,ml\,min^{-1}$; volume of eluent sandwiched with air, 100 μl of 3 M HNO_3.

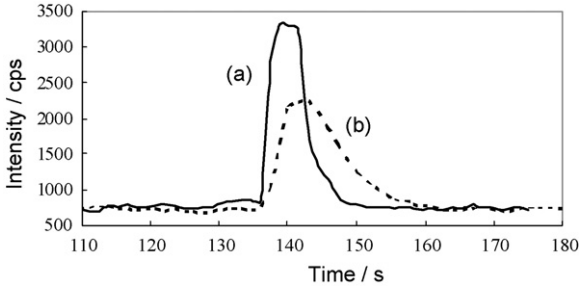

Fig. 4. Effect of air-segmentation on the peak profile. (a), Proposed air-sandwiched method; (b), conventional on-line elution method without air; sample, 2 ml of Co, 10 ng g^{-1}; flow rate, 0.9 ml min^{-1}; eluent, 3 M HNO_3.

was used, the elution was not enough, while 3 M HNO_3 was used, the peak shape was improved to be sharper. However, remarkable improvement was not achieved with 6 M HNO_3. As a result, the concentration of the eluent (HNO_3) was selected to be 3 M.

3.4. Effect of air-segmentation on the peak profile

The proposed air-sandwiched method was compared with the conventional on-line elution method without air sandwich technique. The effect of air-segmentation was shown in Fig. 4. The peak profile (a) is air sandwich one and (b) is without air sandwich one: (a) is clearly sharper than (b) and 100 μl was enough for the determination (for 7 s as the eluent flow rate was 0.9 ml min^{-1}). The peak height of the collected zone in the eluent could be increased twice to avoid dispersion by air-segmentation.

3.5. Analytical characteristics and validation

Under the optimized conditions, calibration graphs could be prepared for 11 elements at pH 3 of the collection step. The detection wavelengths, the concentration efficiency, the limits of the detection (LOD, 3σ of the reagent blank) were summarized in Table 3, together with LOD of the conventional/ICP-AES. The LODs were much improved by 35 fold for the maximum effective element, Co. The concentration efficiency was 7–14 times calculated with the peak height of the proposed method to those of the system without a column. The concentration efficiency was somewhat lower than the calculated values with a ratio of the sample volume (2 ml) to the eluent volume (100 μl), which is due to lowering by the dispersion of the zone and the collection efficiency of TE-05. However, the proposed method could eliminate the spectrum interferences caused from matrices, because the resin in this work, TE-05, did not collect major elements, such as Na, K and Ca.

Table 3
Concentration efficiency and limit of detection (LOD).

Element	Anal. line (nm)	Concentration efficiency	LOD (ng g^{-1})	
			This method	Conventional[a]
Cd	228.802	13.3	0.22	4.88
Co	228.615	13.0	0.23	8.13
Cu	327.395	9.6	0.85	1.36
La	379.477	10.2	0.81	0.86
Mn	257.610	7.2	0.18	0.49
Ni	231.604	8.9	1.99	10.58
Pb	220.353	14.3	1.85	36.96
Sc	335.372	13.0	0.15	0.51
V	311.837	11.0	0.80	1.63
Y	371.029	12.0	0.20	0.29
Zn	206.200	12.3	0.83	10.93

[a] LOD of conventional/ICP-AES.

Table 4
Analytical results of artificial concrete sample.

Element	Anal. line nm	Found (ng g^{-1})	
		Artificial blank solution[a]	Artificial solution[b]
Cd	228.802	−0.05 ± 0.07[c]	4.80 ± 0.10
Co	228.615	−0.01 ± 0.11[c]	4.73 ± 0.17
Cu	327.395	0.55 ± 0.33[c]	4.72 ± 0.24
Ni	231.604	0.49 ± 0.18[c]	4.84 ± 0.53
Pb	220.353	1.76 ± 0.19[c]	6.46 ± 0.12
V	311.837	0.36 ± 0.26[c]	4.99 ± 0.21
Zn	206.200	−0.96 ± 0.17[c]	4.32 ± 0.40

n = 3.
[a] Prepared with 10 μg g^{-1} of Ca and each 2 μg g^{-1} of Fe and Al as concrete matrices.
[b] Five ng g^{-1} of each element was added to the artificial blank solution. One ng g^{-1} of 16 kinds of rare earth elements was also added, but the reproducibility was not good. Therefore the results were deleted in this Table.
[c] These values were under LOD.

The validation of the proposed method was evaluated by using an artificial concrete sample solution, because the standard concrete sample could not be obtained. To examine the interferences from matrices, the blank solution for the artificial concrete solution was prepared by dissolving 10 μg g^{-1} of Ca and each 2 μg g^{-1} of Fe and Al. The artificial concrete sample solution was prepared by adding 5 ng g^{-1} of 31 kinds of transition elements and 1 ng g^{-1} of 16 kinds of rare earth elements to the artificial concrete blank solution. Such artificial solutions were measured; the results obtained were shown in Table 4. Rare earth elements could not be determined in good reproducibility by this system. From Table 4, major elements in concrete samples did not interfere with the determination and Cd, Co, Cu, Ni, Pb, V, and Zn could be measured with sufficient accuracy and reproducibility.

3.6. Application to real concrete samples

The proposed method was applied to the determination of HNO_3 soluble trace elements in concrete samples, and the discrimination from other samples was discussed. Without hydrofluoric acid (HF), silicate does not affect the determination of HNO_3 soluble trace elements [21]. High concentration elements (Al, Fe, Mg) were measured by a conventional ICP-AES method. Sample solutions were prepared by the following procedure. Conc. nitric acid, 0.75 ml (1.02 g), was added to about 10 mg of concrete samples, and the mixture was sonificated for a few minutes. After standing 15 h at room temperature, the sample solution was centrifuged at 3000 rpm for 10 min, and 0.5 ml (0.68 g) of supernatant was pipetted out. Then, the supernatant solution was adjusted to pH 3 by adding 2 ml of 2 M ammonium acetate and 1 ml of 29% ammonia water. Finally it was made up to 20 g with ultrapure water. The results obtained for three major elements and four trace elements (V, Co, Ni, Pb) were shown in Table 5. The samples, A1, A2, and A3, were prepared with three sites of a concrete block A: A1 at edge, A2 at corner and A3 at inner hole site, and the samples, B, C, and D were sampled at each inner hole site. The samples, A, B, C, and D were made in different companies. From the comparison of the analytical values in Table 5, each sample could not be discriminated. This is because the concrete block composed mainly of two constituents, a HNO_3 soluble component and an HNO_3 insoluble component, and the mixing of these components were not homogeneous, especially in a small amount of sample (about 10 mg). However, the abundance ratio of the HNO_3 soluble elements suggested to be the same. Therefore, the abundance ratio (%) of each Co, Ni, Pb, and V (μg g^{-1}) to sum of these four elements (μg g^{-1}) in samples were calculated. The results were shown in Fig. 5(b). The same calculation was performed for major elements, Al, Fe, and Mg as is shown in Fig. 5(a). The patterns of Samples A1, A2, and A3 obtained by using the same concrete block A, resembled closely, though the lines were deleted due to over-

Table 5
Analytical results of concrete samples.

Element	Anal. line (nm)	Found ($\mu g\,g^{-1}$)					
		Sample A1 11 mg[a]	Sample A2 13 mg[a]	Sample A3 12 mg[a]	Sample B 10 mg[a]	Sample C 14 mg[a]	Sample D 10 mg[a]
Al[b]	237.312	8009 ± 96	9091 ± 113	14625 ± 109	49980 ± 529	3723 ± 95	13354 ± 95
Co[c]	228.615	4.61 ± 0.42	4.69 ± 0.39	7.83 ± 0.93	3.16 ± 0.40	1.98 ± 0.06	4.63 ± 0.28
Fe[b]	259.940	7087 ± 91	6925 ± 18	11737 ± 109	3771 ± 30	4499 ± 57	7594 ± 71
Mg[b]	279.553	2537 ± 21	2506 ± 36	3735 ± 25	18294 ± 222	804 ± 14	3366 ± 26
Ni[c]	231.604	7.99 ± 0.25	8.06 ± 0.44	15.85 ± 0.17	3.31 ± 0.58	3.08 ± 0.69	5.34 ± 0.97
Pb[c]	220.353	18.02 ± 0.19	17.61 ± 0.48	29.27 ± 1.56	14.71 ± 2.25	5.98 ± 1.08	11.86 ± 0.63
V[c]	311.837	13.76 ± 0.41	11.70 ± 0.38	14.45 ± 1.00	36.22 ± 1.74	8.64 ± 0.43	23.53 ± 0.84

$n = 3$.
[a] The weight of concrete sample.
[b] Measured by conventional/ICP-AES.
[c] Measured by this method.

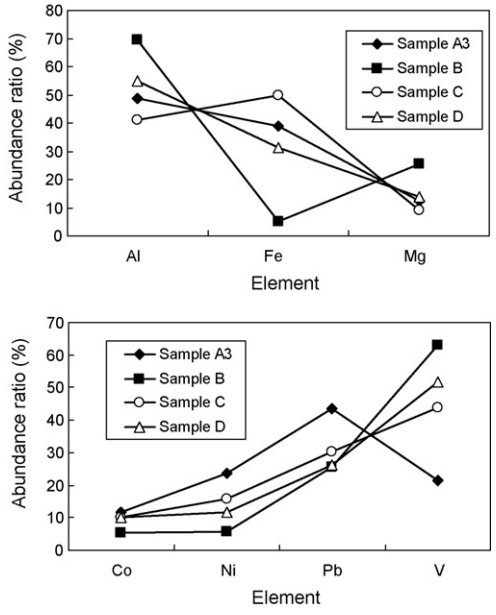

Fig. 5. Major and trace elements distribution patterns for concrete samples. The samples were the same as shown in Table 4; (a), major elements obtained by conventional/ICP-AES; (b), trace elements obtained by this method.

lapping. From the results of major elements, only Samples B and C could be discriminated. With the results of the trace elements patterns, Samples A and B could be discriminated. To consider the results of both patterns, four samples can be discriminated.

4. Conclusion

The sensitive on-line ICP-AES analysis method could be developed. The aim of this method was the determination with small amounts of concrete samples (about 10 mg), simultaneous multi-elements determination and automatic procedures for discrimination of forensic samples. For concrete samples, the comparison of the HNO_3 soluble trace elements, which were determined by coupling the column procedure with the chelating resin to ICP-AES, was enough for the discrimination. The consumption of the sample solution for a measurement was 2 ml. To sandwich the concentrated parts of the effluent with air, the concentration efficiency was improved twice. In this case with 2 ml of sample solutions, rare earth elements could not be detected, because of its low concentration. They are expected to be determined by coupling the proposed pretreatment method to ICP-MS.

References

[1] J.I. Thornton, J. Forensic Sci. 34 (1989) 1323.
[2] L.C. Haag, J. Forensic Sci. Soc. 16 (1977) 255.
[3] T. Inoue, K. Tanaka, T. Ohmori, Y. Togawa, S. Seta, J. Forensic Sci. Int. 69 (1994) 97.
[4] T. Kishi, T. Inoue, S. Suzuki, T. Yasuda, T. Oikawa, T. Niwaguchi, Eisei Kagaku 29 (1983) 400.
[5] S. Suzuki, S. Hirai, T. Mitsugashira, Bunseki Kagaku 43 (1994) 845.
[6] Y. Suzuki, Y. Marumo, Bunseki Kagaku 42 (1993) 417.
[7] S. Muratsu, T. Ninomiya, Y. Kagoshima, J. Matsui, J. Forensic Sci. 47 (2002) 944.
[8] S. Suzuki, Y. Suzuki, H. Ohta, M. Kasamatsu, T. Nakanishi, Anal. Sci. 21 (2005) 775.
[9] S. Suzuki, H. Tsuchihashi, K. Nakajima, A. Matsushita, T. Nagao, J. Chromatogr. 437 (1988) 322.
[10] Y. Marumo, T. Inoue, S. Seta, Forensic Sci. Int. 69 (1994) 89.
[11] O. Noguchi, M. Oshima, S. Motomizu, Anal. Sci. 24 (2008) 631.
[12] Y. Suzuki, M. Kasamatsu, S. Suzuki, K. Ohashi, A. Kawase, Bunseki Kagaku 50 (2001) 335.
[13] H. Ohsaki, M. Kasamatsu, Y. Suzuki, S. Suzuki, Bunseki Kagaku 56 (2007) 1191.
[14] S. Hirata, T. Kajiya, M. Aihara, K. Honda, O. Shikino, Bunseki Kagaku 52 (2003) 1091.
[15] L. Hakim, A. Sabarudin, M. Oshima, S. Motomizu, Anal. Chim. Acta 588 (2007) 73.
[16] A. Sabarudin, N. Lenghor, M. Oshima, L. Hakim, T. Takayanagi, Y.-H. Gaob, S. Motomizu, Talanta 72 (2007) 1609.
[17] L. Hakim, A. Sabarudin, M. Oshima, S. Motomizu, Talanta 76 (2008) 1256.
[18] K. Yamaguchi, S. Kurata, Jpn. J. Forensic Sci. Technol. 13 (2008) 187.
[19] K.-H. Lee, M. Oshima, S. Motomizu, Bunseki Kagaku 49 (2000) 529.
[20] K.-H. Lee, M. Oshima, T. Takayanagi, S. Motomizu, J. Flow Injection Anal. 16 (1999) 225.
[21] K. Saito, N. Tachiiri, S. Sasaoka, K. Usui, S. Ito, T. Yoshida, K. Miura, Abstract of 11th Annual Meeting of Japanese Association of Forensic Science and Technology, 2005, 106.

Talanta 78 (2009) 1321–1326

Contents lists available at ScienceDirect

Talanta

journal homepage: www.elsevier.com/locate/talanta

A method for benzoyl chloride derivatization of biogenic amines for high performance liquid chromatography

Özgül Özdestan*, Ali Üren

Ege University, Faculty of Engineering, Food Engineering Department, 35100 Bornova İzmir, Turkey

ARTICLE INFO

Article history:
Received 7 November 2008
Received in revised form 26 January 2009
Accepted 2 February 2009
Available online 10 February 2009

Keywords:
Biogenic amines
Benzoyl derivatization
RP-HPLC-UV
Polyvinylpyrrolidone

ABSTRACT

A new benzoylation procedure was developed which was more reliable than the most common benzoylation procedures in terms of reaction time, peak resolution, detector response and repeatability. Methylamine, putrescine, cadaverine, tryptamine, β-phenylethylamine, spermidine, spermine, histamine, tyramine and agmatine were studied. Linearity for each biogenic amine was observed with a good regression coefficient. Limits of detection were found between 0.2 mg/l and 2.5 mg/l. Recovery rates varied from 72.8% to 103.4%. Temperature and pH of mobile phase were studied and found that 20 °C of column temperature with a pH of 8 was preferable. It was established that polyvinylpyrrolidone adsorbed biogenic amines and caused interference in HPLC determination of biogenic amines that had been used by some authors to eliminate interfering phenolic compounds in wine samples.

1. Introduction

Biogenic amines are basic nitrogenous organic compounds and are synthesized by microbial, vegetable and animal metabolisms. Biogenic amines in fermented or spoiled foods are generated by microbial decarboxylation of amino acids during fermentation or are formed by the enzymes of raw material. Biogenic amines are present in a wide range of food products including fish and fish products, meat and meat products, dairy products, fermented soybean products, wine, beer, vegetables and fermented vegetable products. Histamine, tyramine, putrescine, cadaverine, tryptamine, β-phenylethylamine, spermine, spermidine, agmatine, methylamine, ethylamine and ethanolamine are the most important biogenic amines occurring in foods. Biogenic amines have important metabolic roles in living cells. Polyamines and putrescine are essential for growth and other amines like histamine, tyramine and serotonin are involved in nervous system functions and the control of blood pressure [1].

Biogenic amines are of importance because of their potential toxicity and they have been responsible for many cases of food poisoning. Low levels of biogenic amines in food are not considered as a serious risk. However, if amount consumed is high enough or normal routes of amine catabolism are inhibited or genetically deficient, they may induce headache, respiratory distress, heart palpitation, hypotension (in the case of histamine, putrescine and cadaverine), hypertension (as in the case of tyramine), nausea, rash, dizziness, emesis and even intracerebral hemorrhage, anaphylactic shock syndrome and death, in very severe cases [1–3]. The estimation of biogenic amines is important not only from the toxicological point of view, but also they can be used as indicators of degree of freshness or spoilage of food [4]. Yamanaka et al. [5] reported that cadaverine seemed to be the most useful index for decomposition of fish. Agmatine could be a quality marker specific for common squid [6], histamine, putrescine, cadaverine and agmatine for Atlantic herring [7], cadaverine and tyramine for red meat, cadaverine for white meat [8], agmatine for Korean fermented soybean paste [9] and tryptamine for tomato and tomato products [10].

Several methods have been reported for the analyses of biogenic amines. Most of them have been chromatographic and capillary electrophoresis techniques. Among these, high performance liquid chromatography (HPLC) has been the mostly used one. It is difficult to determine biogenic amines in foods due to the matrix effect. Therefore, extraction and purification steps must be undertaken prior to chromatographic analysis. These steps are most critical in terms of obtaining an adequate recovery for each amine. The aim of the extraction and purification steps is to remove interfering compounds from the matrix, but during these steps losses of biogenic amines must be as little as possible. Most of the times extraction of biogenic amines from a food matrix can be carried out by hydrochloric acid, perchloric acid or trichloroacetic acid (TCA). After extraction of biogenic amines from the complex food matrix, purification is necessary to remove inter-

* Corresponding author. Tel.: +90 232 3884000/1315; fax: +90 232 3427592.
E-mail address: ozgul.ozdestan@ege.edu.tr (Ö. Özdestan).

0039-9140/$ – see front matter © 2009 Elsevier B.V. All rights reserved.
doi:10.1016/j.talanta.2009.02.001

fering compounds including amino acids. It can be performed by liquid–liquid extraction or solid phase extraction by using C_{18} cartridges [3,11–14]. Several organic solvents such as diethyl ether, n-butanol, chloroform or mixtures of these solvents have been applied to extract biogenic amines in a quantitative way. Most of the methods for biogenic amine determinations apply only extraction. Thus biogenic amine losses can be reduced and time of analysis is shortened by omitting the purification step. But this technique has some disadvantages especially in the case of complex food matrices such as cheese. Interfering substances may remain in the medium and cause a decrease in recovery rates for some biogenic amines, and formation of additional peaks at the same retention times as biogenic amines. There is no need for extraction and purification steps while studying with non-complex samples like wine, beer and fermented vegetable brine. After filtering and centrifugation steps derivatization can be realized.

After extraction and purification steps, biogenic amines are converted to their derivatives, since the majority of the biogenic amines do not possess chromophoric or fluorogenic moieties. Biogenic amines are determined by pre-column or post-column derivatization using mainly benzoyl chloride, orto-phthaldialdehyde (OPA) or dansyl chloride. Among these reagents, benzoyl chloride has some advantages, including short elution time, stability, being relatively inexpensive and easily accessible. Benzoyl chloride reacts with both primary and secondary amines and forms stable derivatives. It can derivatize most of the naturally occurring amines including spermidine, spermine and agmatine [2,7,9,15]. Benzoyl derivatives of biogenic amines are not sensitive to light [16]. The most important advantage of OPA is that it reacts quickly with biogenic amines. However it has the drawbacks that it only reacts with primary amines and gives unstable derivatives. Spermidine and spermine are not detectable using pre-column derivatization with OPA [4,17–19]. Dansyl chloride was used as derivatization reagent in most studies. Dansyl chloride is light sensitive and has limited stability [16]. It is not possible to determine agmatine by this reagent [8,10,19–21]. Redmond and Tseng [22] were the first to use benzoyl chloride for derivatization of biogenic amines. They realised the derivatization at room temperature in 20 min. Asotra et al. [23] described the application of benzoyl chloride dissolved in methanol thereby enhancing the reaction with biogenic amines. 2% benzoyl chloride in methanol was applied at 37 °C for 18–20 min. Hwang et al. [24] investigated the roles of derivatization temperature and time and reported that derivatization of biogenic amines with benzoyl chloride at 30 °C for 40 min was the optimum condition to eliminate interfering peaks. The method of Hornero-Méndez and Garrido-Fernández [2] consisted basically of treating a sample with benzoyl chloride at room temperature for 45 min. Křížek and Pelikánová [25] modified the method of Redmond and Tseng [22] by shaking the solution for 2.5 min following the benzoyl chloride addition. Then the reaction mixture was allowed to stand in the water bath of a ultrasound cleaner for 15–20 min. Özoğul et al. [7] reported a method by dissolving benzoyl chloride in acetonitrile. This was compared with benzoyl chloride dissolved in methanol and with only benzoyl chloride to find the optimum derivatization conditions. Optimum times of derivatization at room temperature were 15 min, 20 min and 40 min for 2% benzoyl chloride in acetonitrile, 2% benzoyl chloride in methanol and only benzoyl chloride, respectively.

Due to the inconsistent or incorrect results in the literature relative to the extraction, purification and derivatization of biogenic amines, it was necessary to improve the biogenic amines analysis. First of all benzoylation procedure of biogenic amines was investigated in more detail, and a rapid, accurate, precise and reliable benzoylation procedure was developed.

2. Experimental

2.1. Materials

2.1.1. Wine samples

Two red wines and 2 white wines, produced in Aegean region of Turkey in the year 2006 were purchased from local markets.

2.1.2. Chemicals

Cadaverine dihydrochloride, tryptamine, β-phenylethylamine, spermidine trihydrochloride, spermine, histamine dihydrochloride, tyramine and agmatine sulphate were obtained from Sigma (Steinheim, Germany). Methylamine hydrochloride, butylamine, 1,7-diaminoheptane (internal standard, IS) and ethanolamine were obtained from Merck (Schuchardt, Germany). Putrescine dihydrochloride was obtained from Fluka (Steinheim, Germany) and ethylamine hydrochloride from Acros Organics (Geel, Belgium). The other reagents: sodium hydroxide, ammonium chloride, benzoyl chloride, sodium chloride, anhydrous sodium sulphate, n-butanol, chloroform, OPA, 2-mercaptoethanol and distilled water were supplied from Merck (Darmstadt, Germany), tetrahydrofuran and hydrochloric acid from J.T. Baker (Deventer, Holland), methanol, acetonitrile and diethyl ether (all of them HPLC grade) from Lab-Scan (Dublin, Ireland), boric acid and sodium acetate trihydrate from Riedel (Germany), PVP from ISP England. Standard solutions of biogenic amines were prepared by dissolving each of them in 0.1 M HCl separately. These standard solutions were stored in glass containers at 4 °C and contained 1 mg of free base form of biogenic amine in 1 ml. Internal standard solution contained 2 mg of 1,7-diaminoheptane in 1 ml. To prepare mixture of standard biogenic amines, suitable volumes of standard solutions were mixed and diluted to 25 ml with distilled water just before used.

2.2. Methods

2.2.1. Derivatization with benzoyl chloride

To 0.5 ml aliquot of the mixture of standard biogenic amines in a glass tube were added 2 ml of distilled water, 0.1 ml of internal standard solution, 2 ml of 2 M NaOH solution and 30 μl of benzoyl chloride. The mixture was shaken for 5 min using a vortex mixer and after the addition of 1.5 ml of acetonitrile, allowed to stand for 10 min at 25 °C. Total volume of the solution in the derivatization tube was approximately 6.1 ml. Following the addition of 1.5 g of solid sodium chloride and vortexing for 1 min resulting derivatives were extracted 3 times with 4 ml aliquots of diethyl ether in a separator funnel. The upper organic phases were combined and dried with anhydrous sodium sulphate, decanted and evaporated under a current of nitrogen. The solid residue was dissolved in 1 ml of methanol, filtered through a 0.5 μm pore size filter and 10 μl of the solution was injected into HPLC. When determining the recovery rates, 1 ml of wine sample was derivatized with the addition of 1.5 ml of distilled water, 0.1 ml of internal standard solution, 2 ml of 2 M NaOH solution and 50 μl of benzoyl chloride, and then 1 ml of wine sample was derivatized by adding 0.5 ml aliquot of the mixture of standard biogenic amines, 1 ml of distilled water, 0.1 ml of internal standard solution, 2 ml of 2 M NaOH solution and 50 μl of benzoyl chloride. The volume of benzoyl chloride might be increased up to 80 μl depending on the nature and amount of food sample to be analysed. Throughout the present study chromatograms were obtained for three aliquots of the same solution that underwent the whole analytical procedure.

To compare the new derivatization procedure with those in literature, 0.5 ml aliquot of the same mixture of standard biogenic amines was derivatized following the methods of Hornero-Méndez and Garrido-Fernández [2], Křížek and Pelikánová [25] and Özoğul et al. [7]. Thirty microliters of benzoyl chloride was used when

applying the methods of Hornero-Méndez and Garrido-Fernández [2] and Křížek and Pelikánová [25], and 1.5 ml of 2% benzoyl chloride in acetonitrile was used for Özoğul et al. [7]. Total volume of the derivatization medium was also 6.1 ml. The derivatization procedure of Hornero-Méndez and Garrido-Fernández [2] was realised at 20 °C, 25 °C and 30 °C, and the other two methods were achieved at 25 °C.

2.2.2. OPA derivatization

In the determination of biogenic amines in wine samples by benzoyl or dansyl derivatization, phenolic compounds from wine samples react with benzoyl chloride and dansyl chloride, thus reduce concentration of derivatization reagent. Consequently signals of biogenic amine derivatives become less. Some authors used PVP to eliminate interfering phenolic compounds [26,27]. PVP adsorbs phenolic compounds mainly by forming hydrogen bonding [28]. However, PVP may adsorb not only phenolic compounds but also biogenic amines and causes a decrease in detector responses for biogenic amine derivatives. To examine this possibility, in the present study biogenic amines of wine samples were determined by pre-column OPA derivatization, since OPA does not react with phenolic compounds. OPA derivatization was achieved following the method of Yıldırım et al. [29]. Wine samples were derivatized with and without PVP treatment. In PVP treatment 0.2 g of PVP was added into 5 ml of wine sample. The resulting mixture was then stirred for 15 min and filtered through a Whatman (41) filter paper. Filtrate was made up to the initial volume of 5 ml with distilled water and derivatized by OPA reagent. Quantifications were performed by the standard addition method. As spermine and spermidine were not detectable by pre-column OPA derivatization, ethylamine and ethanolamine, widespread biogenic amines occurring in wine samples were added into these experiments to acquire better statistical results.

2.2.3. Chromatographic conditions

Chromatographic separations of benzoyl derivatives were realized following the method of Yeğin and Üren [30] using a binary gradient elution consisting of methanol and acetate buffer. Mobile phase was prepared as follows. Solvent A, 0.05 M acetate buffer: methanol 60:40; solvent B, methanol. The pH of solvent A was adjusted to pH 6, 7 or 8. The chromatographic column was thermostated at 20 °C, 25 °C or 30 °C and detection was performed at 254 nm. HPLC separation of OPA derivatives was carried out following the method of Yıldırım et al. [29]. Mobile phase was prepared as follows. Solvent A [0.05 M acetate buffer–tetrahydrofuran (96–4)]:methanol, 60:40; solvent B, methanol. Detector response was measured using a fluorescence detector operating at 340 nm and 420 nm as excitation and emission wavelengths, respectively.

2.3. Apparatus

Chromatographic separations were performed by using Hewlett-Packard 1050 liquid chromatograph (Agilent, Santa Clara, CA) equipped with a Waters 486 variable wavelength UV–vis detector, a Waters 470 scanning fluorescence detector (Waters Corporation, Milford, MN), a gradient elution pump and a Rheodyne 7125 injection loop of 20 μl (Rheodyne LLC., Rohnert Park, CA). The chromatographic column was Hichrom C_{18} (10 μm particle size, 300 mm × 3.9 mm ID, Hichrom Ltd., Theale, UK).

2.4. Statistical analysis

Significant differences between experimental means were calculated by *t*-test. Paired *t*-test was used for comparison of wine samples in terms of biogenic amine contents. Evaluation of linearity was achieved by applying Microsoft Excel.

3. Results and discussion

3.1. The effect of derivatization temperature

Due to the inconsistent results in the literature, benzoylation procedure of biogenic amines was investigated in terms of reaction temperature in the present study. Mixture of standard biogenic amines including methylamine, putrescine, cadaverine, tryptamine, β-phenylethylamine, spermidine, spermine, histamine, tyramine and agmatine was treated with benzoyl chloride following the method of Hornero-Méndez and Garrido-Fernández [2], at 20 °C, 25 °C and 30 °C separately. Areas of biogenic amine derivatives obtained at different temperatures were compared and derivatization at 25 °C was found to be optimum. The area of histamine derivative at 25 °C was significantly greater than those at 20 °C and 30 °C ($P < 0.05$). Histamine derivative decomposed to ammonia derivative especially at 20 °C and 30 °C. Agmatine area at 25 °C was greater significantly than the other two temperatures ($P < 0.05$). Agmatine derivative partially decomposed, especially at 20 °C and 30 °C and produced ammonia derivative, putrescine derivative and a new peak which had the same retention time as butylamine derivative. Order of spermine responses was 25 °C > 30 °C > 20 °C and there was a significant difference between areas for 25 °C and 20 °C ($P < 0.05$). The remaining biogenic amines did not show any significant differences in terms of derivatization temperature. These results were different from that of Hwang et al. [24] who reported that derivatization of biogenic amines with benzoyl chloride at 30 °C for 40 min was the optimum condition to eliminate interfering peaks.

3.2. The effects of pH of mobile phase and column temperature on resolution of biogenic amines

To find the effect of mobile phase pH on resolution of biogenic amines, mixture of standard biogenic amines derivatized at 25 °C was separated on C_{18} column thermostated at 20 °C. Separations were achieved using three different mobile phases with the pH values of 6, 7 and 8. Then for the examination of the effect of column temperature on separation of biogenic amines, chromatographic analyses were carried out at three different column temperatures of 20 °C, 25 °C and 30 °C with the mobile phase of pH 8. In these experiments 2 split peaks were established in the chromatograms, one of them after histamine and the other following tyramine. Both split peaks moved to the left hand side with increasing pH and decreasing column temperature and combined with histamine and tyramine. As a result, these split peaks disappeared when separations were realised at 20 °C of column temperature with the mobile phase of pH 8.

3.3. Comparison of the new derivatization procedure with those in literature

To compare the new derivatization procedure with those in literature, the same volume of the mixture of standard biogenic amines was derivatized following the new procedure and the methods of Hornero-Méndez and Garrido-Fernández [2], Křížek and Pelikánová [25] and Özoğul et al. [7]. Fig. 1 illustrates HPLC traces obtained for these methods. Detector responses of 10 biogenic amines were given for these 4 procedures in Fig. 2. From the examination of Figs. 1 and 2 it can be observed that the new method is much more reliable than the others in terms of peak resolution, detector response, repeatability and reaction time. As it is seen from Fig. 1, these 4 chromatograms have several additional peaks.

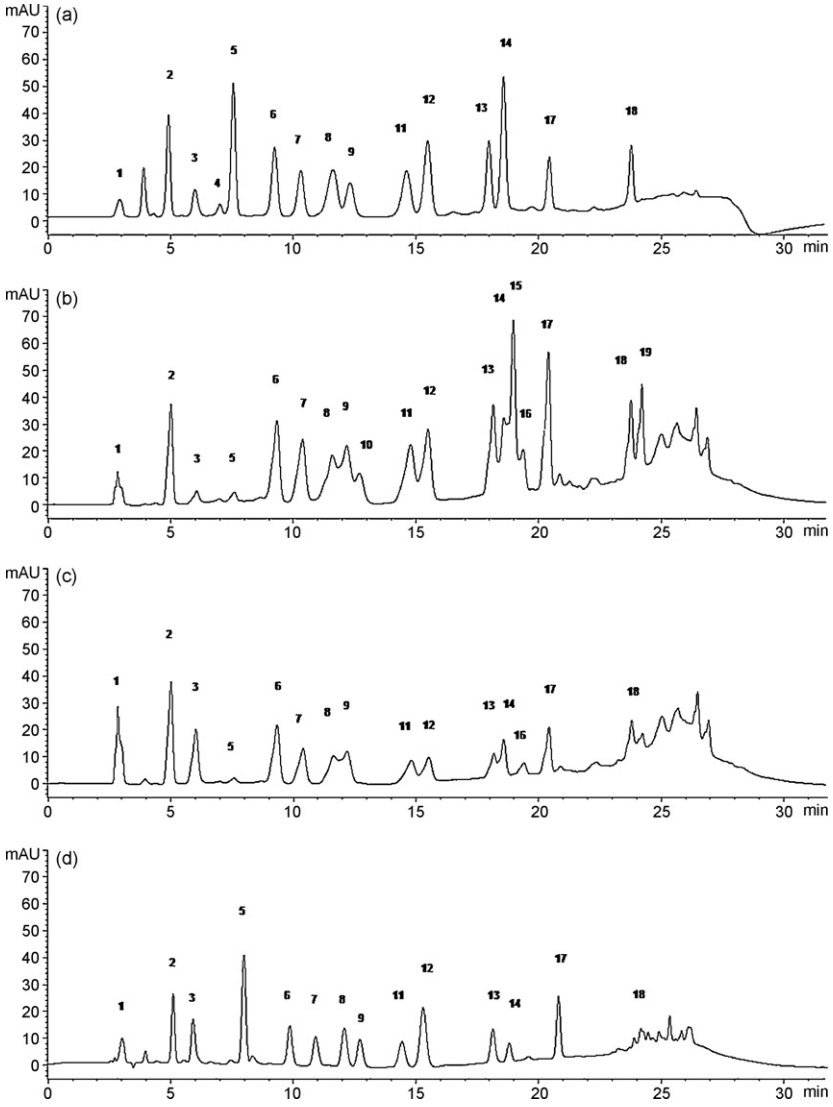

Fig. 1. HPLC chromatograms of mixture of standard biogenic amines derivatized according to the new method (a), Hornero-Méndez et al. [2] (b), Křížek et al. [25] (c) and Özoğul et al. [7] (d). Peak identification: 1, ammonia; 2, methylamine; 3, ethylamine (from decomposition of histamine); 4, ammonia; 5, ammonia; 6, putrescine; 7, cadaverine; 8, tryptamine; 9, β-phenylethylamine; 10, decomposition product of histamine derivative; 11, spermidine; 12, 1,7-diaminoheptane (IS); 13, spermine; 14, histamine; 15, ammonia; 16, ammonia; 17, tyramine; 18, agmatine; 19, dibenzoylated histamine.

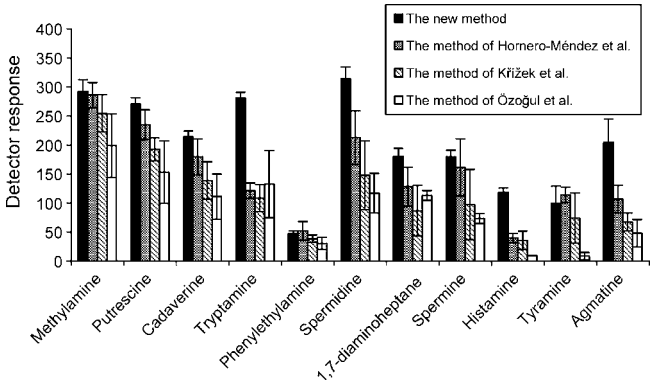

Fig. 2. Detector responses (peak areas), with standard deviations of 10 biogenic amines and internal standard for the new method and the methods of Hornero-Méndez et al. [2], Křížek et al. [25] and Özoğul et al. [7]. Detector responses were obtained for 0.25 μg of each of biogenic amines in injected volume.

Peaks with the numbers 1, 4, 5, 15 and 16 arose from derivatization of ammonia, peaks 3, 10 and 19 from histamine. Peaks 3 and 10 must be decomposition products of histamine derivative. Peak 3 has the same retention time as benzoyl derivative of ethylamine. Peak 19 is possibly dibenzoylated histamine. Consequently peak 14 is mono-benzoylated histamine. Peak 15 is one of the disadvantages of the procedure of Hornero-Méndez and Garrido-Fernández [2], which co elutes with histamine. Most food products containing biogenic amines contain also ammonia. Peaks 10, 15 and 16 appear in some applications of the method of Hornero-Méndez and Garrido-Fernández [2], but sometimes do not appear. Moreover, in the reports of Hornero-Méndez and Garrido-Fernández [2] and García-García et al. [31] retention time of spermine was smaller than that for spermidine, but all of the remaining studies reported spermidine peak before spermine peak [15,22–24]. Corrected order was used in Fig. 1(b). In the study of Özoğul et al. [7], the order of biogenic amines on HPLC chromatogram was considerably different than those in Fig. 1(d) and the other methods. Spermidine and spermine were reported much before the expected retention times in the study of Özoğul et al. [7]. Results of our study are different from that of Hwang et al. [24], since they defined

Table 1
Method performances.

Biogenic amine	*r*	LR (up to mg/l)	DL (mg/l)	*R* (%)
Methylamine	0.9991	133.6	0.2	93.1
Putrescine	0.9988	185.7	0.2	84.0
Cadaverine	0.9995	186.0	0.3	94.0
Tryptamine	0.9977	265.0	0.2	81.8
β-Phenylethylamine	0.9995	272.0	0.5	103.4
Spermidine	0.9991	268.4	0.2	72.8
Spermine	0.9881	226.6	0.5	103.4
Histamine	0.9924	995.3	0.4	86.1
Tyramine	0.9940	1433	2.5	101.9
Agmatine	0.9949	95.32	NQ	NQ

r, correlation coefficient; LR, linear range in food extract derivatized; DL, detection limit in wine sample; *R*, recovery in wine sample; NQ, not quantified due to the interfering compounds in wine sample.

Table 2
Peak areas for benzoyl derivatives of biogenic amines dissolved in methanol and stored at 4 °C (numbers in parentheses are standard deviations).

	Storage time (days)	
	0	3
Methylamine	113.6 (4.3)	115.0 (4.1)
Putrescine	149.5 (12.7)	158.5 (6.8)
Cadaverine	118.2 (6.8)	117.8 (4.5)
Tryptamine	132.2 (10.7)	133.2 (15.0)
β-Phenylethylamine	483.7 (21.6)	487.9 (12.5)
Spermidine	128.8 (4.2)	130.3 (4.1)
Spermine	117.3 (3.1)	120.4 (28.6)
Histamine	150.1 (15.8)	145.9 (23.4)
Tyramine	125.9 (10.7)	130.1 (8.8)
Agmatine	99.8 (20.4)	106.4 (12.1)

the ammonia peak (peak 15) as a peak of excess benzoyl chloride and used this incorrect datum in determining optimum derivatization conditions. In accordance with our study, diacyl derivatives of histamine were reported in the literature. Kirschbaum et al. [32] studied liquid chromatographic determination of biogenic amines after derivatization with 3,5-dinitrobenzoyl chloride (DNBZ-Cl) and reported the presence of $(DNBZ)_2$histamine derivative. Loukou and Zotou [27] determined the biogenic amines as dansyl (Dns) derivatives in alcoholic beverages, characterized dansylated amines and found that histamine produced $(Dns)_2$histamine. However, further research on the characterization of dibenzoylated histamine by liquid chromatography-mass spectrometry may be useful.

3.4. Performance characteristics of the method

Table 1 shows performance characteristics of the method. Calibration graphs were constructed by plotting the amine to internal standard peak areas ratios against the amine concentrations as mg/l in food extract derivatized. Data for calibration curves were collected, using triplicate responses for 4 concentrations. Linearity was observed in the tabulated concentration range for each biogenic amine with a good regression coefficient. The limits of detection were calculated to give a signal-to-noise ratio of 3 and found between 0.2 mg/l and 2.5 mg/l in wine sample, biogenic amines of which were removed completely by extracting with excess volume of n-butanol–chloroform mixture (1/1, v/v) at pH 11.7. Recovery rate was calculated for each biogenic amine in a wine sample. Fig. 3 illustrates HPLC chromatogram of a red wine sample. As seen from Table 1 recoveries varied from 72.8% to 103.4%. We obtained better recovery rates for other fermented foods.

3.5. Stabilities of the benzoyl derivatives

Subsequent to evaporation of diethyl ether, derivatives of biogenic amines were dissolved in methanol containing 3×10^{-4} M benzoyl chloride. Benzoyl chloride was added into methanol to prevent decomposition of benzoyl derivatives. Part of this methanolic solution was analysed immediately. The remaining part was stored at 4 °C and analysed after 3 days (Table 2). Comparison of initial responses with those after 3 days indicated that there were not any significant differences for methylamine, putrescine, cadaverine, tryptamine, β-phenylethylamine, spermidine, spermine, histamine, tyramine and agmatine ($P < 0.05$). For further testing of the stability, derivatives were stored at 4 °C for 1 month without dissolving in methanol. Then biogenic amines were determined and results were compared with initial values. It was established that there were not any significant differences for cadaverine, β-phenylethylamine, spermidine, spermine, histamine, tyramine and agmatine ($P < 0.05$). Peak areas of methylamine, putrescine and tryptamine decreased during the storage period as 11.6%, 10.8% and 13.9%, respectively. These results were in accordance with literature data. Asotra et al. [23] studied with putrescine, cadaverine, spermidine and spermine and found that benzoylated amines dissolved in methanol could be stored up to 3 weeks at −20 °C. If samples were not dissolved in methanol, they could be stored for more than a month at −70 °C. Hornero-Méndez and Garrido-Fernández [2] reported that derivatives of putrescine, cadaverine, tryptamine, β-phenylethylamine, spermidine, spermine, histamine, tyramine and agmatine could be stored at room temperature for at least 48 h without appreciable decomposition.

3.6. Adsorption of biogenic amines by PVP

To examine the possibility of adsorption of biogenic amines by PVP, biogenic amines of wine samples were determined by pre-column OPA derivatization. Biogenic amine contents of two red wines and two white wines with and without PVP treatment were reported in Table 3. As seen from Table 3, PVP treatment caused a considerable decrease in biogenic amine levels, especially in red wines. PVP application caused 21.9%, 26.3%, 2.3% and 9.0% decreases for red wine 1, red wine 2, white wine 1 and white wine 2, respectively. The decrease for red wine 1 was found to be statistically significant ($P < 0.10$). Our results are different than those of Busto et

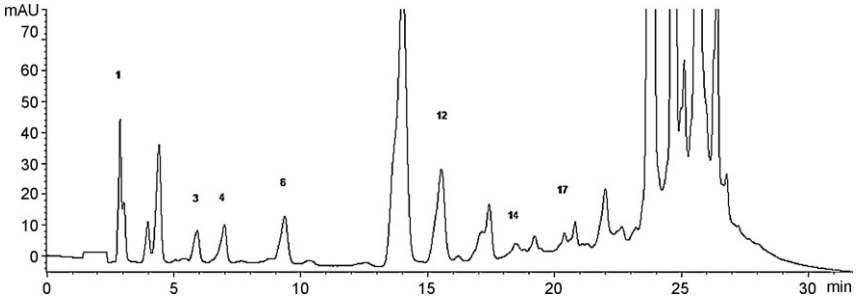

Fig. 3. HPLC chromatogram of a red wine. Peak identification: 1, ammonia; 3, ethylamine; 4, ammonia; 6, putrescine; 12, 1,7-diaminoheptane (IS); 14, histamine; 17, tyramine.

Table 3
Biogenic amine contents of red wines and white wines (mg/l) with and without PVP treatment.

	Red wine 1		Red wine 2		White wine 1		White wine 2	
	Without PVP	With PVP	Without PVP	With PVP	Without PVP	With PVP	Without PVP	With PVP
Methylamine	1.02	0.56	0.78	0.65	0.95	0.76	0.58	0.57
Ethylamine	3.46	2.49	2.33	1.30	3.13	2.92	0.50	0.55
Putrescine	7.42	6.70	9.25	6.98	2.10	2.91	1.21	1.09
Cadaverine	0.47	0.29	0.51	0.24	ND	0.49	0.39	0.23
Tryptamine	ND	ND	ND	ND	ND	ND	0.93	0.61
β-Phenylethylamine	ND	ND	ND	ND	ND	ND	0.31	ND
Histamine	6.67	5.07	2.39	2.04	ND	ND	0.46	0.45
Tyramine	15.71	10.57	20.77	13.34	4.93	4.74	2.18	2.38
Agmatine	ND	ND	ND	ND	ND	ND	ND	ND
Ethanolamine	12.29	11.06	10.44	9.68	12.64	11.38	7.45	6.87
Total concentration	47.04	36.74	46.47	34.23	23.75	23.20	14.01	12.75

ND, not detected.

al. [26] who calculated percentage recoveries of biogenic amines in a red wine after PVP treatment and reported that PVP application had caused a 7% decrease or less.

4. Conclusions

Benzoyl chloride derivatization is one of the most common derivatization methods for HPLC determination of biogenic amines. It can derivatize most of the naturally occurring amines including spermidine, spermine and agmatine. Agmatine is a useful biogenic amine as a potential index for freshness or spoilage of various food products. Spermidine is a major biogenic amine in various foods of vegetable origin.

A new rapid and reliable benzoylation procedure was developed which takes only 15 min. Repeatability, linearity, recovery rates and detection limits were estimated for the most common biogenic amines including methylamine, putrescine, cadaverine, tryptamine, β-phenylethylamine, spermidine, spermine, histamine, tyramine and agmatine. Linearity for each biogenic amine was observed with a good regression coefficient. The limits of detection were found between 0.2 mg/l and 2.5 mg/l for various biogenic amines in a wine sample. Recovery rates of biogenic amines were calculated in a wine sample, and varied from 72.8% to 103.4%. When compared with the most common benzoylation procedures encountered in the literature, the new method is much more reliable than the others in terms of reaction time, peak resolution, sensitivity and repeatability. Temperature and pH of mobile phase were studied and found to be critical in terms of repression of split peaks. Application of 20 °C as a column temperature with a mobile phase pH of 8 is preferable.

Stabilities of benzoyl derivatives were studied. Benzoyl derivatives of biogenic amines dissolved in methanol containing benzoyl chloride could be stored for 3 days at 4 °C without appreciable decomposition. It was established that PVP adsorbed biogenic amines. When applying the proposed method it is not necessary to use PVP, since it is possible to increase the amount of benzoyl chloride. The effective mixing of derivatization medium prevents appearance of interfering peaks or split peaks that might arise from the excess benzoyl chloride.

References

[1] A. Lonvaud-Funel, FEMS Microbiol. Lett. 199 (2001) 9.
[2] D. Hornero-Méndez, A. Garrido-Fernández, J. Food Protect. 60 (1997) 414.
[3] J. Lange, K. Thomas, C. Wittmann, J. Chromatogr. B 779 (2002) 229.
[4] M.R. Alberto, M.E. Arena, M.C. Manca De Nadra, Food Control 13 (2002) 125.
[5] H. Yamanaka, K. Shimakura, K. Shiomi, T. Kikuchi, Bull. Jpn. Soc. Sci. Fish. 52 (1986) 127.
[6] H. Yamanaka, K. Shiomi, T. Kikuchi, J. Food Sci. 52 (1987) 936.
[7] F. Özoğul, K.D.A. Taylor, P. Quantick, Y. Özoğul, Int. J. Food Sci. Technol. 37 (2002) 515.
[8] G. Vinci, M.L. Antonelli, Food Control 13 (2002) 519.
[9] J.H. Kim, H.S. Ahn, D.H. Kim, C. Jo, H.S. Yook, H.J. Park, M.W. Byun, J. Food Sci. 68 (2003) 80.
[10] E. Chiacchierini, D. Restuccia, G. Vinci, Talanta 69 (2006) 548.
[11] D. Hornero-Méndez, A. Garrido-Fernández, Analyst 119 (1994) 2037.
[12] A.R. Shalaby, Food Chem. 52 (1995) 367.
[13] S. Moret, L.S. Conte, J. Chromatogr. A 729 (1996) 363.
[14] S.R. Vale, M.B.A. Glória, J. AOAC Int. 80 (1997) 1006.
[15] G. Yen, C. Hsieh, J. Food Sci. 56 (1991) 158.
[16] J. Karovičová, Z. Kohajdová, Chem. Pap. 59 (2005) 70.
[17] I. Mafra, P. Herbert, L. Santos, P. Barros, A. Alves, Am. J. Enol. Viticult. 50 (1999) 128.
[18] G.J. Soleas, M. Carey, D.M. Goldberg, Food Chem. 64 (1999) 49.
[19] S. Moret, D. Smela, T. Populin, L.S. Conte, Food Chem. 89 (2005) 355.
[20] R. Jeya Shakila, T.S. Vasundhara, K.V. Kumudavally, Food Chem. 75 (2001) 255.
[21] N. Innocente, M. Biasutti, M. Padovese, S. Moret, Food Chem. 101 (2007) 1285.
[22] J.W. Redmond, A. Tseng, J. Chromatogr. 170 (1979) 479.
[23] S. Asotra, P.V. Mladenov, R.D. Burke, J. Chromatogr. 408 (1987) 227.
[24] D.F. Hwang, S.H. Chang, C.Y. Shiua, T.J. Chai, J. Chromatogr. B 693 (1997) 23.
[25] M. Křížek, T. Pelikánová, J. Chromatogr. A 815 (1998) 243.
[26] O. Busto, Y. Valero, J. Guasch, F. Borrull, Chromatographia 38 (1994) 571.
[27] Z. Loukou, A. Zotou, J. Chromatogr. A 996 (2003) 103.
[28] K.J. Siebert, P.Y. Lynn, J. Am. Soc. Brew. Chem. 66 (2008) 48.
[29] H.K. Yıldırım, A. Üren, U. Yücel, Food Technol. Biotechnol. 45 (2007) 62.
[30] S. Yeğin, A. Üren, Food Chem. 111 (2008) 983.
[31] P. García-García, M. Brenes-Balbuena, D. Hornero-Méndez, A. García-Borrego, A. Garrido-Fernández, J. Food Protect. 63 (2000) 111.
[32] J. Kirschbaum, K. Rebscher, H. Brückner, J. Chromatogr. A 881 (2000) 517.

Talanta 78 (2009) 1327–1331

Contents lists available at ScienceDirect

Talanta

journal homepage: www.elsevier.com/locate/talanta

Estrogens and their conjugates: Determination in water samples by solid-phase extraction and liquid chromatography–tandem mass spectrometry

Marta Pedrouzo, Francesc Borrull, Eva Pocurull*, Rosa Maria Marcé

Department of Analytical Chemistry and Organic Chemistry, Universitat Rovira i Virgili, Marcel·lí Domingo s/n, Sescelades Campus, Tarragona 43007, Spain

ARTICLE INFO

Article history:
Received 17 July 2008
Received in revised form 30 January 2009
Accepted 3 February 2009
Available online 12 February 2009

Keywords:
Estrogens
LC–MS–MS
SPE
Wastewaters

ABSTRACT

A sensitive method for simultaneously determining eleven free and conjugated steroid estrogens has been developed using liquid chromatography–(electrospray)triple quadrupole–mass spectrometry (LC–(ESI)MS–MS) in negative mode with application to environmental aqueous matrices. Two selected reaction monitoring (SRM) transitions per compound were used, one of which was used for quantification and the second one for confirmation. The procedure includes a solid-phase extraction with an Oasis HLB solid-phase cartridge. Recoveries in 500 mL of river water spiked at 50 ng/L for sulfate estrogens and 100 ng/L for the rest of the compounds were 46–87%, except for E2, which had lower values (32%). Recoveries in wastewater were higher than 49% and 30% for all the compounds, except E2-17A and E2-17G (lower than 26% and 28%, respectively), in effluent (250 mL) and influent (100 mL), respectively. Ion suppression is a well-known phenomenon when using ESI; thus its impact on method recovery made us consider this effect when quantifying our samples. Limits of detection varied from 2 to 30 ng/L in river water and 10 to 100 ng/L in sewage water. The method was used to determine the target compounds in the Ebro river water where none of the analytes were found. In effluent and influent water samples, EE2, E1-3S and E2-3S were determined at concentration levels ranging from 35 to 160 ng/L.

1. Introduction

Recently, evidence has emerged that endocrine disrupting compounds (EDCs) can have harmful effects on aquatic organisms. Recent publications suggest that steroids may be the main source of estrogenicity in many municipal sewage treatment plants (STPs) [1]. Since the sources of natural estrogens cannot be eliminated, a number of specific treatment processes in STPs have been optimized and discussed with regard to estrogens removal [2,3]. Thus, it is also important to determine the fate and distribution of steroid conjugates in the environment since they are potential sources of active estrogens as a result of dissociation in sewage treatment plants or the input of treated wastewater directly into surface waters [4,5]. Estrogens are largely excreted from humans as conjugates, mainly glucoronides [3]. Occasionally, these conjugates can breakdown into other molecules in sewage treatment plants, resulting in the release of the active parent compound [6]. Several studies have identified the natural steroids E2 and E1 and the synthetic estrogen EE2 as the most potent estrogenic compounds in treated municipal sewage [6,7]. In a survey of effluents from German STPs, EE2 was detected above the quantification level of 1 ng/L [8] in all 20 STPs investigated. Kuch and Ballschmiter [9] reported levels of estrone between 3 and 13 ng/L in several effluent samples in Germany.

Studies of estrogens in river waters revealed a lower concentration than in sewage waters. Research into 15 German rivers and streams showed that only estrone was present at a maximum concentration of 1.6 ng/L [10]. In various Catalan studies, estrone and estrone-3-sulfate were detected in the Llobregat river (0.68 and 0.33 ng/L, respectively) [11], and maximum levels of 0.13 μg/L of EE2 were found in the Ebro river [12].

Highly sensitive techniques are needed to detect the low contents of estrogenic compounds in the environmental samples. The most commonly used analytical technique for estrogens in the past has been gas chromatography coupled to mass spectrometry (GC–MS) [5,13,14] and tandem mass spectrometry (GC–MS–MS) [7,15], preceding by derivatization steps. However, in recent years, separation and determination with liquid chromatography coupled to mass spectrometry (LC–MS) [14,16,17] and tandem mass spectrometry (LC–MS–MS) [4,5,18–20] has become a widely used tool for determining estrogens in environmental samples because of its sensitivity and specificity and the fact that it does not need the derivatization step. For example, when Brossa et al. [12] used LC–MS for determining free steroids in river waters they found limits of detection (LODs) between 0.002 and 0.06 μg/L per 500 mL sample. Nowadays, a triple quadrupole with multiple reaction monitoring

* Corresponding author. Tel.: +34 977558492; fax: +34 977558446.
E-mail address: eva.pocurull@urv.cat (E. Pocurull).

0039-9140/$ – see front matter © 2009 Elsevier B.V. All rights reserved.
doi:10.1016/j.talanta.2009.02.005

(MRM) and selected reaction monitoring (SRM) is the most suitable tool for target analysis of high sensitivity. This is demonstrated in several papers, such as Reddy et al. [4], who used tandem MS–MS to detect steroid conjugates in an MRM method in STP waters. They reported minimum detection limits (MDL) lower than 0.16 ng/L in 100 mL of influent waters.

The most extensively used method of sample preconcentration is solid-phase extraction (SPE), and the selection of the sorbent depends basically on the nature of the matrix and the properties of the analytes. For example, Kuch and Ballschmiter [9] studied two types of sorbent (Amberlite XAD 2 and a mixture of LiChrolut EN/Bondesil C-18) to determine estrogens in effluent STP waters. However, in several papers [4,21,22] Oasis HLB is the most commonly used sorbent for this kind of analytes. SPE is one of the most common techniques for preconcentrating estrogens in waters, but some authors have also used SPME as well [23,24]. For example, Mitani et al. [24] used an on-line in tube SPME-LC–MS–MS system. They found recoveries of 86% (E3) in river water and levels of 35.7 pg/mL (E3) in the effluent sewage water.

The aim of this work was to develop a method to determine free estrogens and their conjugates which can be applied to a variety of water matrices and to determine the occurrence of these compounds in wastewater samples.

2. Experimental

2.1. Reagents and standards

The standards of estrone (E1), estrone 3-sulfate (E1-3S), estrone 3-glucoronide (E1-3G), 17β-estradiol (E2), estradiol 3-sulfate (E2-3S), 17β-estradiol 17-acetate (E2-17A), estradiol 17-glucuronide (E2-17G), 17α-ethinylestradiol (EE2), 17α-estradiol (α-E2), estriol (E3) and diethylstilbestrol (DSB) were from Sigma (St. Louis, USA). Stock solutions of individual standards were prepared by dissolving each compound in methanol at a concentration of 1000 mg/L and storing it at −5 °C. Fresh stock solutions were prepared each six months. A mix of all compounds in methanol at a concentration of 50 mg/L was prepared weekly. Working solutions were prepared daily by diluting the previous solution with water.

Ultra-pure water was obtained with a Milli-Q water purification system (Millipore, Bedford, MA, EEUU), acetonitrile and methanol were HPLC grade from SDS (Peypin, France), and nitrogen was from Carburos Metálicos (Tarragona, Spain). Chlorhydric acid (HCl), sodium hydroxide (NaOH) and acetic acid from Prolabo (Bois, France) were used to adjust the pH of the sample and the mobile phase.

2.2. Sample collection

The river water samples were collected near to the mouth of the river Ebro. The wastewater samples were collected from the influent and effluent of two Catalan domestic sewage treatment plants (STPs) with an activated sludge system. They are located in two cities, Reus and Tarragona, with populations of about 120,000 habitants. All samples were collected using pre-cleaned amber glass bottles, acidified to pH 2 (HCl) and stored at 4 °C until analysis.

2.3. Sample extraction

Before the extraction, the sample was adjusted to pH 7 with NaOH and filtered using a 0.45-μm nylon filter (Whatman, Maidstone, UK). For each sample, a 12 mL, 500 mg Oasis HLB SPE cartridge was preconditioned by washing with 5 mL of MeOH followed by 5 mL of Milli-Q water. Sample volumes of 100 and 250 mL were extracted for the influent and effluent of the STP, respectively, and 500 mL for river water samples. The samples were passed through the cartridge at a flow rate of 10–15 mL/min. The analytes retained were eluted using 5 mL of MeOH (with 5% ACN). Extracts were reduced to dryness under a gentle flow of N_2 gas, using an evaporation system and final extracts were redissolved with 1 mL of MeOH:H_2O (80:20). After being filtered through 0.45 μm syringe filters (Scharlab, Barcelona, Spain), 50 μL of this solution was injected into the chromatographic system.

2.4. LC–(ESI)MS–MS

The target compounds were separated and identified using liquid chromatography–(electrospray ionization)–tandem mass spectrometry in negative mode. The chromatographic instrument was an HP1200 series LC–triple quadrupole mass spectrometer from Agilent Technologies (Waldbronn, Germany) with an ESI interface, an automatic injector, a degasser, a quaternary pump and a column oven. The chromatographic column was a Kromasil 100 C_{18} (25.0 cm × 0.46 cm) with a 5 μm particle size (Teknokroma, Barcelona, Spain), and the volume injected was 50 μL. The mobile phase flow-rate was 1 mL/min and the column temperature was kept at 35 °C.

A binary mobile phase with a gradient elution was used to optimize the extraction conditions. Solvent A was Milli-Q water with acetic acid (pH 2.8) and solvent B was acetonitrile. The gradient was performed as follows: 10% B, constant for 10 min, increased to 40%B for 5 min, to 60%B for 10 min, to 100%B for 5 min, and then decreased to 10%B for 2 min. The system was re-equilibrated for 3 min between runs.

In order to sensitively and selectively determine the analytes, the optimization of the MS–MS parameters was carried out by flow injection analysis (FIA) for each estrogen. Experiments were performed in triplicate to be sure the observed phenomena were valid and not influenced by previous tests. Analysis was performed in the negative ionization mode with an optimized spray potential of 3000 V, a nebulizer of 45 psi and a source temperature of 350 °C and 12 L/min of drying gas flow. Nitrogen was used as the collision, nebulizing and desolvation gas. Selected reaction monitoring (SRM) experiments in the negative ionization mode were performed to detect ion transitions (Table 1). Product ions used for monitoring were selected on the basis of their significance in the MS–MS spectra.

3. Results and discussion

3.1. LC–MS–MS analysis

For the mobile phase we evaluated methanol and acetonitrile since they are the most relevant organic solvents in reversed-phase chromatography. We used the mobile phase with acetonitrile as an organic modifier because it gave the best peak shape for the estrogens, as it was also reported by Benijts et al. [25]. The effect of the pH of the mobile phase was investigated by injecting a working solution at various pH (3, 7 and 9). From the chromatographic point of view, we saw that acidified mobile phase (pH 3) gave the best peak shapes. Also, when pH was increased with ammonium hydroxide no significant difference was observed in the signal intensities. The SRM transitions, cone voltage and collision energy, were determined for each compound with direct injection of the standards in the MS–MS. Upon ionization, all the compounds produced negative precursor ions that were fragmented into one or more product ions. The cone voltage was 60 V for E2, αE2 and EE2, 100 V for E2-17A and 150 V for the rest of the compounds. Collision energy between 5 and 55 V was optimized for each analyte and the best values are shown in Table 1. For each compound, two characteristic fragmentations of the deprotonated molecular ion $[M-H]^-$ were

Table 1
SRM settings for the studied compounds.

Compound (abbreviation)	SRM ions	Collision energy (V)
Diethylstilbestrol (DSB)	**267 > 222**	30
	267 > 237	55
Estrone (E1)	**269 > 145**	45
	269 > 143	45
17β-estradiol (E2)	**271 > 145**	30
	271 > 183	45
17α-Estradiol (α E2)	**271 > 145**	30
	271 > 183	45
Estriol (E3)	**287 > 171**	45
	287 > 145	45
17α-Ethynilestradiol (EE2)	**295 > 145**	45
	295 > 159	30
Estradiol 17-acetate (E2-17A)	**313 > 253**	30
	313 > 145	55
Estrone 3-sulphate (E1-3S)	**349 > 269**	30
	349 > 113	55
Estradiol 3-sulphate (E2-3S)	**351 > 271**	30
	351 > 145	55
Estrone 3-glucoronide (E1-3G)	**445 > 269**	45
	445 > 113	20
Estradiol 17-glucoronide (E2-17G)	447 > 271	30
	447 > 113	20

In bold the SRM transition for quantification.

monitored, the first and most abundant one being used for quantification, while the second one was used as a qualifier (Table 1). During the optimization experiments, eight of the eleven estrogens investigated (E1, E2, β-E2, E3, EE2, E2-17A, E1-3S and E2-3S) gave intense fragments at m/z 145 corresponded to $[C_{10}H_9O]^-$, as reported in previous studies [13,15]. In the case of steroid sulfates, product ion spectra were characterized by base peaks $[M-H-80]^-$ corresponding to the loss of SO_3. The glucoronides showed a loss of glucoronide moiety $[M-H-176]^-$.

Since the signal intensity of individual ions generally decreases as the number of ions being simultaneous scanned increases, we used time segment monitoring so that only a few of the ions were monitored within specific small time windows based on chromatographic separation. Three time windows were used: 0–17 min (E2-17G, E1-3G, E2-3S and E3), 17–22 min (E1-3S, EE, α-E2 and β-E2) and 22–36 min (E2-17A, E1 and DSB).

The compounds showed the following linear range by direct injection: 0.01–1000 μg/L for E1-3S and E2-3S, 0.05–1000 μg/L for E1-3G and E2-17G, 0.75–250 μg/L for E1 and DSB, 3–1000 μg/L for E3, 10–250 μg/L for α-E2 and E2-17 and 10–500 μg/L for E2 and EE2.

3.2. Optimization of the extraction procedure

Oasis HLB cartridges were selected because of their excellent capture capabilities for acidic and neutral analytes across a wide polarity range [26]. The effect of the sample pH on extraction efficiency was investigated using enrichment tests between pH 3 and pH 7 in 100 mL Milli-Q samples spiked at 200 ng/L. This revealed that the recoveries did not show any differences, except for E1-3S and E2-3S which were not recovered at pH 3, meaning that a neutral pH was needed. Moreover, it is reported that under neutral pH conditions, humic acids are not so well retained in the SPE sorbent,

Table 2
Recoveries and relative standard deviations (%RSD, $n = 4$) of selected compounds in different kinds of water.

Compound	Influent STP		Effluent STP		River water	
	%R[a]	%RSD	%R[b]	%RSD	%R[c]	%RSD
DSB	58	4	76	5	67	7
E1	60	2	51	6	49	5
E2	53	11	61	16	32	13
α E2	30	9	49	15	76	11
E3	56	15	59	12	49	5
EE2	37	11	52	9	68	14
E2-17A	–	–	26	15	46	17
E1-3S	57	6	74	8	84	2
E2-3S	57	9	78	4	87	3
E1-3G	66	7	65	2	67	2
E2-17G	23	5	28	2	59	5

[a] 100 mL spiked at 1000 ng/L.
[b] 250 mL spiked at 300 ng/L.
[c] 500 mL spiked at 50 ng/L (E1-3S and E2-3S) and 100 ng/L.

which means there are fewer interferences [11]. Another important parameter to optimize is the elution solvent. Different solvents have been used to elute these compounds such as ACN [12] or MeOH [4,15]. We studied the recoveries when estrogens were eluted with MeOH and acidified MeOH (with 5% acetic acid) from 100 mL of milli-Q water. The results showed that acidified MeOH could not effectively elute the sulfate estrogens. As the aim of this work was to extract all target analytes in one single step and because the recoveries obtained were good, 5 mL of MeOH were selected to elute all the compounds from the cartridge. However, from the experiments, we added 5% of ACN to MeOH to improve the recoveries in the real samples. We found that the recovery of E2-17A increased from 12% to 26% when ACN was added to the eluent in the extraction with the same volume of effluent samples.

When the volume of Milli-Q water was increased to 1000 mL the recoveries were between 79% and 101%. Not only was the elution solvent modified when real samples were analysed, but also the sample volume decreased so that the recoveries were acceptable. When 500 mL of river water was extracted, without evaporating the elution solvent, the recoveries were 70–108%, except for E3 and E2-17G, which had recoveries lower than 55%. These recoveries were slightly lower when the extract was evaporated to dryness. Thus, when we analysed 500 mL of river water spiked at 50 ng/L for the sulfate estrogens, and 100 ng/L for the rest of the compounds, recoveries decreased to 32–87% because of the concentration of the interferences in the matrix. The sample matrix strongly affected the recoveries in sewage water samples. As Table 2 shows, when 100 mL of influent water was spiked at 1000 ng/L, the recoveries of the compounds were between 23% and 66%, except for E2-17A, whose recovery was very low. When 250 mL of effluent samples was spiked at 300 ng/L, the recoveries were between 28% and 76%. These recoveries agree with the results in the bibliography for most of the compounds [18,27]. For example, Gomes et al. [27] found recoveries between 63% and 72% for E1, E2, E3 and E1-3G in 100 mL of influent waters. As can be seen in Table 2, these recoveries were similar to our results (53–66%) for the same compounds in 100 mL of influent waters.

Ionization suppression can be a substantial drawback with ESI [26,28] and this was evaluated when the method was developed. The differences observed in MS–MS response could be attributed to the effect of the sample matrix on the ionization efficiency. We observed a reduction in the response in the range of 10–35% when a standard of Milli-Q water was compared with the same standard in an extract of river water, and a reduction of 10–43%, when the extract was from influent sewage water. In other studies, deuterated estrogens have been added as surrogate standard to minimise the effect of the ionization suppression [13,22,29,30]. Unfortunately, it

Table 3
Concentrations (ng/L) found in sewage samples from STP_1 and STP_2 ($n = 3$, RSD < 15%).

Compound	STP_2 March 07		STP_2 May 07		STP_1 Nov 07	
	Influent	Effluent	Influent	Effluent	Influent	Effluent
E1	–	–	–	–	<LOQ	–
E3	<LOQ	–	<LOQ	–	–	–
EE2	154	–	–	–	–	–
E1-3S	160	35	64	<LOQ	52	<LOQ
E2-3S	76	<LOQ	–	–	<LOQ	<LOQ
E2-17G	–	–	<LOQ	–	–	–

is not easy to find the most suitable surrogate and they are generally very cost prohibitive. Thus, in order to select the best approach for quantifying the real samples, different calibration curves were prepared using three extracts (river, effluent sewage water and influent sewage water).

3.3. Method validation

The entire method was validated for river water and influent and effluent sewage water. In a blank of river water none of the analytes was found. Linear range was tested following the procedure developed in the negative SIM mode and the range studied with river water was 15–1500 ng/L for sulfate estrogens and 75–1500 ng/L for the rest. All the compounds showed $r^2 > 0.992$ when this type of water was used as the matrix. The repeatability and reproducibility between days were determined by spiking 500 mL of river water at 50 and 100 ng/L. The results, expressed as relative standard deviations (%RSD), were lower than 17% for repeatability ($n = 3$), and 21% for reproducibility between days ($n = 4$). The limits of detection, calculated as a signal-to-noise ratio of 3, were 1 ng/L for E1-3S and E2-3S, 15 ng/L for DSB, E1, E1-3G, E2-17G and 30 ng/L for the rest of the compounds. The LOQs were calculated as the concentration of the lowest point of the calibration.

To quantify the sewage samples (both effluent and influent) two calibration curves with both kinds of samples were constructed. A blank of effluent sample did not show any of the estrogens studied. However, the chosen influent sample showed the presence of E1-3S, and the signal was subtracted to the rest of the calibration samples. The linear range for sulfate estrogens in the effluent samples was between 30 and 1500 ng/L while the rest of the compounds gave linear ranges from 100 to 1500 ng/L. The limits of detection, calculated as a signal-to-noise ratio of 3, were 10 ng/L for E1-3S and E2-3S, between 10 and 35 ng/L for DSB, E1, E1-3G, E2-17G, E3 and 70 ng/L for other compounds.

Sulfate estrogens showed linear range between 50 and 1000 ng/L in 100 mL influent samples. The rest of the estrogens were tested from 150 to 1000 ng/L. The LOD and LOQ values were higher than those in pure and river water due to the complex matrices and the

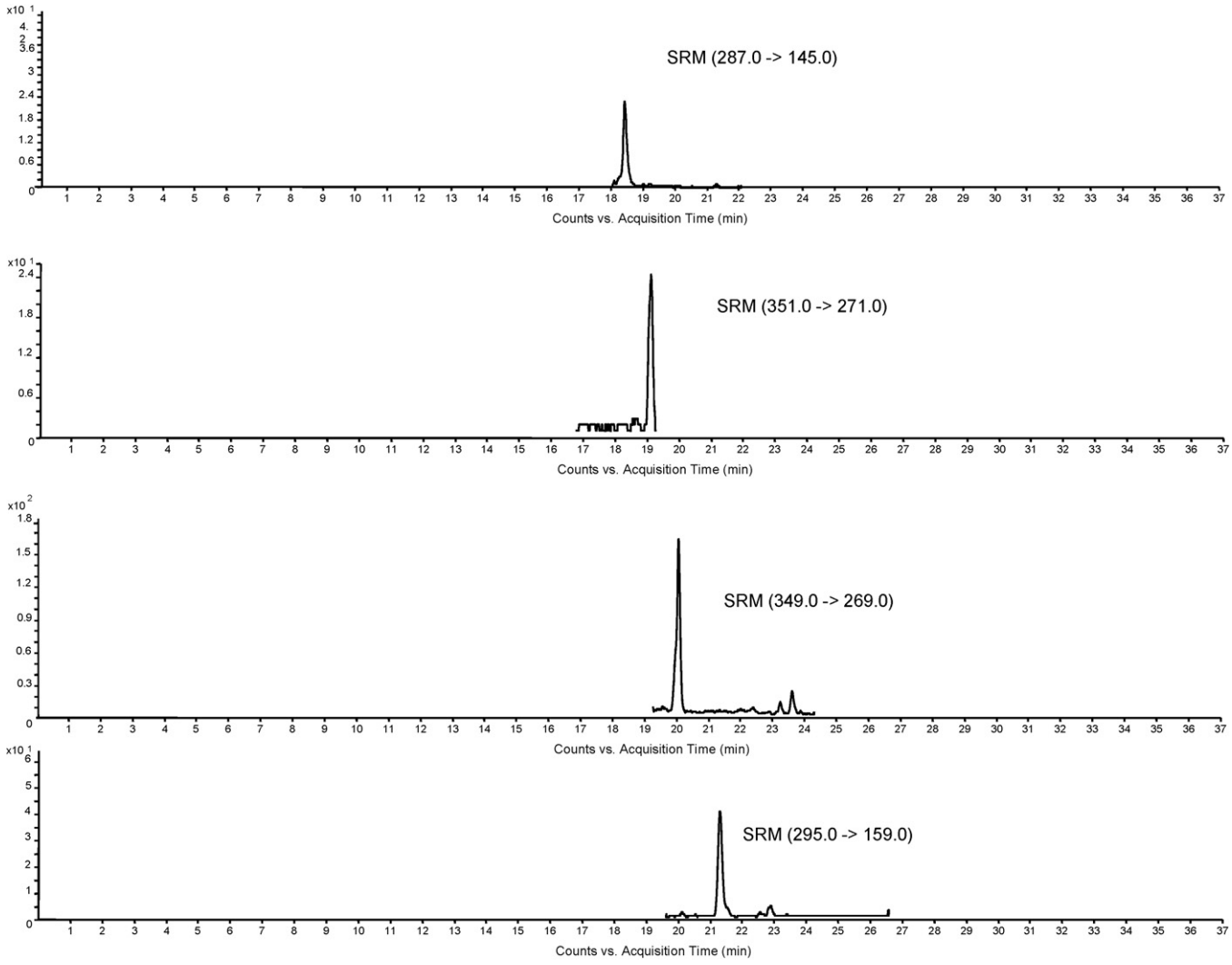

Fig. 1. SRM chromatograms of the compounds found in a sample from an STP influent.

low sample volume stated above. The LODs were 15 ng/L (E1-3S and E2-3S), 35 ng/L (DSB, E1-3G and E2-17G), 50 ng/L (E1 and E3), and 100 ng/L for the rest of the compounds.

3.4. Application to environmental samples

Although Brossa et al. [12] reported finding levels of 0.10 μg/L of EE2 in one sample of the Ebro river, in the present study no estrogens were detected in the same river. Other studies in different Catalan rivers found some estrogens (E1, E2, E3 and EE2) below limit of detection (<3 ng/L) [31].

The method described was applied to wastewater samples to investigate the occurrence of the estrogens in samples from two municipal STPs in Catalonia. In STP influents, DSB, E2-17A and E1-3G were never detected. As Table 3 shows, concentrations of E1, E2-17G and E3 were found below LOQ. However, EE2, E1-3S and E2-3S showed the highest concentrations in influents, with values between 52 and 160 ng/L. In effluent waters only E1-3S showed the highest value (35 ng/L). The SRM chromatogram obtained for the influent sample from STP2 (March 07) is shown in Fig. 1. Free estrogens have been reported to have removal efficiencies of 95% (E3), 87% (E2), and 61% (E1) [19,32]. Chen et al. [33] agreed with these high values of removal at 100 ng/L, but they concluded that the removal rate was lower at higher concentrations of E3. Although we only found values <LOQ of E3 in our samples, higher levels (470 ng/L) were detected in influents, which were reduced to 99 ng/L in effluents [18]. Servos et al. [32] showed maximum values of 78 and 96 ng/L of E1 in influent and effluent samples, respectively, from Canadian municipal STPs.

EE2 is used in oral contraceptives and has been reported to have a high estrogenic potency [20]. Concentrations of EE2 in STPs have varied significantly in reported investigations. The maximum value for EE2 in the influents in our investigation was 154 ng/L. This is comparable with the results found by Kolpin et al. [34], who published a mean concentration of 73 ng/L. However, some authors have stated lower values, with Ternes et al. [35], for example, finding 3.3 ng/L of EE2 in influent sewage water with a removal of 67%.

In our study of influents, the conjugate of the steroid hormones E1-3S and E2-3S were found at maximal concentrations of 160 and 76 ng/L respectively. Similar results were obtained by Schlüsener and Bester [18] and Reddy et al. [4] who found 37 ng/L of E2-3S and 34.1 ng/L of E1-3S, respectively. No glucoronides were detected when the STP wastewaters were analyzed. This is consistent with the well-known pathway of the deconjugation of glucoronides during the wastewater treatment process and the consequent generation of the free compounds [20]. This study has demonstrated the importance of simultaneously determining free and conjugated estrogens in very complex matrices like STP waters.

4. Conclusions

The analytical method based on LC–(ESI)MS–MS allows the simultaneous extraction, identification and quantification of eleven estrogens and their conjugates in water samples at low levels. Different complex matrices have been studied (influent and effluent STP waters and river water). They were enriched by SPE (Oasis HLB) in volumes of 500, 250 and 100 mL, for river, effluent and influent water, respectively. To solve the problem of matrix effect, different calibration curves were made according to each kind of sample. The applicability of the method has been demonstrated in real samples from river water and wastewater STPs. None of these compounds were found in river water, however, in the STPs, E1-3S was the most commonly found compound, with a maximum value of 160 ng/L in an influent sample. EE2 was found at 154 ng/L and E1 and E3 were found at values <LOQ in influent samples. Some compounds such as DSB, E2, αE2 and E2-17G were not detected in any of the samples studied.

Acknowledgement

This study was funded by the Dirección General de Investigación of the Ministry of Science and Technology, project CTM2005-01774.

References

[1] I. Robinson, G. Junqua, R.V. Coillie, O. Thomas, Anal. Bioanal. Chem. 387 (2007) 1143.
[2] M. Auriol, Y. Filali-Meknassi, R.D. Tyagi, C.D. Adams, R.Y. Surampalli, Process Biochem. 41 (2006) 525.
[3] H. Andersen, H. Siegrist, B. Halling-Sorensen, T. Ternes, Environ. Sci. Technol. 37 (2003) 4021.
[4] S. Reddy, C.R. Iden, B.J. Brownawell, Anal. Chem. 77 (2005) 7032.
[5] R.A. Trenholm, B.J. Vanderford, J.C. Holady, D.J. Rexing, S.A. Snyder, Chemosphere 65 (2006) 1990.
[6] F.D.L. Leusch, H.F. Chapman, W. Korner, S.R. Gooneratne, L.A. Tremblay, Environ. Sci. Technol. 39 (2005) 5781.
[7] M.D. Hernando, M. Mezcua, M.J. Gómez, O. Malato, A. Aguera, A.R. Fernández-Alba, J. Chromatogr. A 1047 (2004) 129.
[8] A.C. Belfroid, A. Van der Horst, A.D. Vethaak, A.J. Schafer, G.B.J. Rijs, J. Wegener, W.P. Cofino, Sci. Total Environ. 225 (1999) 101.
[9] H.M. Kuch, K. Ballschmiter, Fresenius J. Anal. Chem. 366 (2000) 392.
[10] T.A. Ternes, P. Kreckel, J. Mueller, Sci. Total Environ. 225 (1999) 91.
[11] S. Rodríguez-Mozaz, M.J.L. de Alda, D. Barceló, Anal. Chem. 76 (2004) 6998.
[12] L. Brossa, R.A. Marcé, F. Borrull, E. Pocurull, Environ. Toxicol. Chem. 24 (2005) 261.
[13] F. Gosetti, V. Gianotti, S. Polati, M.C. Gennaro, J. Chromatogr. A 1090 (2005) 107.
[14] H.B. Lee, T.E. Peart, M.L. Svoboda, J. Chromatogr. A 1094 (2005) 122.
[15] T.R. Croley, R.J. Hughes, B.G. Koenig, C.D. Metcalfe, R.E. March, Rapid Commun. Mass Spectrom. 14 (2000) 1087.
[16] D. Matejicek, V. Kuban, Anal. Chim. Acta 588 (2007) 304.
[17] Y. Filali-Meknassi, M. Auriol, C.D. Adams, R.Y. Surampalli, Water Environ. Res. 79 (2007) 687.
[18] M.P. Schlüsener, K. Bester, Rapid Commun. Mass Spectrom. 19 (2005) 3269.
[19] G. D'Ascenzo, A. Di Corcia, A. Gentili, R. Mancini, R. Mastropasqua, M. Nazzari, R. Samperi, Sci. Total Environ. 302 (2003) 199.
[20] T. Isobe, H. Shiraishi, M. Yasuda, A. Shinoda, H. Suzuki, M. Morita, J. Chromatogr. A 984 (2003) 195.
[21] V. Gabet, C. Miège, P. Bados, M. Coquery, Trends Anal. Chem. 26 (2007) 1113.
[22] P. Labadie, H. Budzinski, Anal. Bioanal. Chem. 381 (2005) 1199.
[23] L.H. Yang, T.G. Luan, C.Y. Lan, J. Chromatogr. A 1104 (2006) 23.
[24] K. Mitani, M. Fujioka, H. Kataoka, J. Chromatogr. A 1081 (2005) 218.
[25] T. Benijts, R. Dams, W. Günther, W. Lambert, A.D. Leenheer, Rapid Commun. Mass Spectrom. 16 (2002) 1358.
[26] M. Pedrouzo, F. Borrull, R.M. Marcé, E. Pocurull, J. Sep. Sci. 31 (2008) 2182.
[27] R.L. Gomes, J.W. Birkett, M.D. Scrimshaw, J.N. Lester, Int. J. Environ. Anal. Chem. 1 (2005) 1.
[28] C. Hao, R. Clement, P. Yang, Anal. Bioanal. Chem. 287 (2007) 1247.
[29] X. Xu, J.M. Roman, T.D. Veenstra, J. Van Anda, R.G. Ziegler, H.J. Issaq, Anal. Chem. 78 (2006) 1553.
[30] A. Salvador, C. Moretton, A. Piram, R. Faure, J. Chromatogr. A 1145 (2007) 102.
[31] M. Farré, R. Brix, M. Kuster, F. Rubio, Y. Goda, M.J.L. de Alda, D. Barcelo, Anal. Bioanal. Chem. 385 (2006) 1001.
[32] M.R. Servos, D.T. Bennie, B.K. Burnison, A. Jurkovic, R. McInnis, T. Neheli, A. Schnell, P. Seto, S.A. Smyth, T.A. Ternes, Sci. Total Environ. 336 (2005) 155.
[33] C.-Y. Chen, T.-Y. Wen, G.-S. Wang, H.-W. Cheng, Y.-H. Lin, G.-W. Lien, Sci. Total Environ. 378 (2007) 352.
[34] D. Kolpin, E.T. Furlog, M.Y. Meyer, E.M. Thurman, S.D. Zaugg, L.B. Barber, H.T. Buxton, Environ. Sci. Technol. 36 (2002) 1202.
[35] T.A. Ternes, M. Bonerz, N. Herrmann, B. Teiser, H.R. Andersen, Chemosphere 66 (2007) 894.

Talanta 78 (2009) 1293–1297

Contents lists available at ScienceDirect

Talanta

journal homepage: www.elsevier.com/locate/talanta

Solid phase extraction of mercury on sulfur loaded with N-(2-chloro benzoyl)-N′-phenylthiourea as a new adsorbent and determination by cold vapor atomic absorption spectrometry

N. Pourreza*, H. Parham, A.R. Kiasat, K. Ghanemi, N. Abdollahi

Department of Chemistry, College of Science, Shahid Chamran University, Ahvaz, Iran

ARTICLE INFO

Article history:
Received 4 November 2008
Received in revised form 27 January 2009
Accepted 29 January 2009
Available online 7 February 2009

Keywords:
Mercury
Sulfur
N-(2-chloro benzoyl)-N′-Phenylthiourea
Marine samples
Cold vapor atomic absorption spectrometry (CV-AAS)

ABSTRACT

This paper reports sulfur powder loaded with N-(2-chloro benzoyl)-N′-phenylthiourea as a new solid phase extractor for determination of ultra trace amounts of mercury. The mercury ions were retained on a mini-column filled with the solid phase at a flow rate of 16 mL min^{-1}. The retained Hg(II) ions were eluted with 3 mol L^{-1} solution of HCl and measured by cold vapor atomic absorption spectrometry (CV-AAS). The mercury vapors were generated by a homemade Reaction Cell-Gas Liquid Separator (RC-GLS). The effect of different variables such as pH, sample flow rate, amounts of ligand loaded on sulfur and $SnCl_2$ concentration was investigated. Calibration curve was linear in the range of 0.02–1.20 μg L^{-1} with $r = 0.9991$ ($n = 8$). The limit of detection (LOD) based on three times the standard deviation of the blank was 0.012 and 0.003 μg L^{-1} when 250 and 1000 mL sample volumes were used, respectively. The relative standard deviation (R.S.D.) for determination of 0.04 and 1.00 μg L^{-1} of Hg(II) was 3.9 and 1.2% ($n = 8$), respectively. The method was successfully applied to determine Hg(II) in water and marine samples.

1. Introduction

Mercury is one of the most toxic elements for plants and animals. This metal is so volatile that it could be easily exposed to human environment. Industrial wastes and mineral deposits are the major sources for mercury contaminations. Mercury hazards to living organisms such as marine samples are due to the accumulation and biomagnification character of this toxic element that can influence the entire food chain and humans who consume marine food [1]. In waters, inorganic mercury is converted by bacteria to methyl mercury, which is known to bioaccumulate in the fish tissue. This process, additionally, increases the danger of mercury exposure even at ultra-trace levels of concentration because organo-mercury species shows a larger potential threat to human life and exhibit more toxic effects than inorganic mercury species. Therefore, concentrations of mercury in natural water, sediments, soil, vegetation, fish and human hair need to be measured in order to monitor the pollution level of mercury in the environment.

There are several analytical techniques for mercury determination at sub-ppb levels such as electroanalytical [2], inductively coupled plasma atomic emission spectrometry (ICP-AES) [3], inductively coupled plasma mass spectrometry (ICP-MS) [4], atomic fluorescence spectrometry [5] and neutron activation analysis [6]. Cold vapor atomic absorption spectrometry is a very efficient, simple, low cost and widely used technique for accurate determination of sub-micrograms per milliliters of mercury [7]. However, due to its low concentrations in numerous samples and high levels of non-toxic components that usually accompany analytes (especially marine samples), a clean up and preconcentration step is often necessary prior to its measurement [8].

Among many preconcentration techniques used in the process of trace metal analysis, solid phase extraction (SPE) is one of the versatile techniques that can be used for different samples. It has several advantages over other techniques, including minimal waste generation, reduction of sample matrix effects, less time consuming, achievement of high enrichment factors and sorption of the target species on the solid surface in a more stable chemical form [8,9].

The selective solid phase extractors are derived from chemically or physically immobilization of sulfur containing organic compounds such as Dithizone [10], dithiocarbamate derivatives [11], diphenylthiocarbazone [12], hexathio-18-Crown-6-tetraone [13] and methylthymol Blue [14] on solid supports. Different solid phases such as alumina [15], activated carbon [16], silica-C_{18} [17], silica gel [18], naphthalene [19], chemically modified chloromthylated polystyrene-PAN [20] and sol–gel sorbent doped with Cyanex-301 [21] have been applied to the determination of mercury.

* Corresponding author. Fax: +98 611 333 7009.
E-mail address: npourreza@yahoo.com (N. Pourreza).

0039-9140/$ – see front matter © 2009 Elsevier B.V. All rights reserved.
doi:10.1016/j.talanta.2009.01.056

Sulfur is a multivalent non-metal, abundant, tasteless, odorless and non-toxic element. In nature, it occurs as the pure element or as sulfide and sulfate minerals. We have recently reported the use of sulfur as a solid phase extractor for preconcentration and determination of lead and cadmium flame atomic absorption spectrometry [22].

At the present work, we applied sulfur as a new solid support for column preparation used in solid phase extraction and preconcentration of mercury ions. For improvement of the recovery, selectivity and sensitivity of the solid phase extraction and preconcentration of mercury ions, a synthesized ligand, N-(2-chloro benzoyl)-N′-phenylthiourea was loaded on sulfur and used as an adsorbent for mercury ions. Moreover, for transformation of mercury ions to elemental mercury and determination of produced mercury cold vapor by atomic absorption spectrometry a homemade RC-GLS [23].

2. Experimental

2.1. Instrumentation

A Philips PU9100X (England) atomic absorption spectrometer fitted with a mercury hollow cathode lamp (Unicam, Franklin, MA) was used to perform atomic absorption measurements. The wavelength of 253.7 nm and spectral bandpass of 0.5 nm were used throughout. A T-cell quartz tube (120 mm length and 5 mm i.d.) was placed directly on the nitrous oxide/acetylene burner equipped with T-cell tube holder. The nitrous oxide/acetylene flame was turned off throughout the process. All measurements were recorded on the height mode of atomic signal.

The characteristics of homemade RC-GLS were as follows: length 150 mm, internal diameter 10 mm, an inlet for N_2 gas and the outlet for N_2 and Hg gas mixture. In each experiment, Hg(II) sample solution and reductant were introduced to the RC-GLS from the removable cap and placed directly on the frit glass that was fitted to this glassware.

pH adjustments were carried out by model 632 pH-meter (Metrohm, Herisau, Switzerland). A Shimadzu rotary oil vacuum pump type SA18 (Kyoto, Japan) was used for sample elutions.

2.2. Reagents

All solutions were prepared with distilled deionized water and all chemicals were of analytical reagent grade.

The Hg(II) stock solution (1000 $\mu g\,mL^{-1}$) was prepared by dissolving 0.1349 g of $HgCl_2$ (Merck, Darmstadt, Germany) in 1 mL of concentrated HNO_3 (Merck, $d = 1.4$, 70%) and diluting to 100 mL with water. The working solutions of Hg(II) were prepared daily by appropriate dilution of the 10 $\mu g\,mL^{-1}$ mercury solutions which was prepared weekly by water. A 2%, w/v, $SnCl_2{\cdot}2H_2O$ (Merck) used as reducing agent was prepared daily by dissolving appropriate amounts of $SnCl_2{\cdot}2H_2O$ in HCl (Merck, $d = 1.18$, 37%) and diluting with water.

Sulfur (Merck) of mesh 60 size was used as solid phase support. All containers were soaked in 20% of HCl and HNO_3 and then cleaned thoroughly with water. A citrate–citric acid buffer solution was prepared by adding 0.2 mol L^{-1} of NaOH to 50 mL of 0.2 mol L^{-1} citric acid solution and adjusting the pH to 2.5 using a pH meter.

2.3. Synthesis of N-(2-chloro benzoyl)-N′-phenylthiourea

N-(2-chloro benzoyl)-N′-phenylthiourea reagent was synthesized according to previously reported procedures [24,25]. Ammonium thiocyanate (3.75 mmol, 0.285 g), 2-chloro benzoyl chloride (2.5 mmol, 0.437 g), PEG-400 (0.25 mmol), DMF (2 drops) and $CHCl_3$ (20 mL) were placed in a dried round-bottom flask and stirred at room temperature for 1 h. Then a mixture of aniline (2.5 mmol, 0.232 g) and $CHCl_3$ (5 mL) was added dropwise and the mixture was stirred for 2 h. After cooling to room temperature, water (15 mL) was added to the mixture. The organic layer was separated and the aqueous phase was washed with $CHCl_3$ (2 mL × 5 mL). The combined $CHCl_3$ layer was dried over anhydrous $MgSO_4$. The solvent was removed by evaporation under reduced pressure to afford N-(2-chloro benzoyl)-N′-phenylthiourea. The product was washed with water to remove inorganic salts. The resulting solid was recrystallized from DMF-H_2O to give product in 85% isolated yield. The product was characterized by FT-IR and NMR spectra.

2.4. Preparation of the adsorbent

150 mg of N-(2-chloro benzoyl)-N′-phenylthiourea was dissolved in 50 mL of acetone (Merck) in a 100 mL beaker and heated up to 45 °C. Then 40 g of sulfur powder was added gently to the solution and mixed thoroughly. The mixture was placed at 40–45 °C for 20–30 min to evaporate the acetone and dry the adsorbent. 2.0 g of this dried adsorbent was packed in a mini-column (7 mm i.d. and 80 mm length) for preconcentration procedure. The dried adsorbent can be stored and used for several months after preparation.

2.5. Sample pre-treatment

Persian Gulf water sample was collected in a 1 L glass bottle, acidified by 5 mL of nitric acid, kept in a refrigerator and filtered through a filter paper (Whatman No. 40) before use. 200 mL of water sample was transferred to a round-bottom flask, 7.5 mL of H_2SO_4 (98%), 2.5 mL of HNO_3 (70%), 8.0 mL of $K_2S_2O_8$ (5%) and 15 mL of $KMnO_4$ (5%) were added and refluxed at 80 °C for 2 h [26]. This solution was cooled, neutralized with sodium hydroxide and diluted to 1000 mL in a volumetric flask. 200 mL of this solution was treated under recommended procedure.

1.0 g of dried fish or oyster sample was placed in a round-bottom flask and 10 mL of HNO_3 (70%), 10 mL of H_2SO_4 (98%), 10 mL of $K_2S_2O_8$ (5%) and 8 mL of $KMnO_4$ (5%) were added and refluxed at 250 °C for about 2 h. The digested fish sample was cooled to room temperature [26]. Appropriate amounts of 2 mol L^{-1} of NaOH solution was added to neutralize the excess of HNO_3 and diluted to 1000 mL in a volumetric flask. An aliquot of the solution was treated under recommended procedure.

200 mg of certified reference material (DORM-3) was refluxed with 10 mL of H_2SO_4 (98%) and 10 mL of HNO_3 (70%) at 250 °C for 2 h. Then 10 mL of $K_2S_2O_8$ (5%) and 10 mL of $KMnO_4$ (5%) was added and refluxed for 2 h. It was cooled, filtered, neutralized with sodium hydroxide and diluted to 500 mL in a volumetric flask [26]. 50 mL of this solution was treated under the general procedure.

2.6. Recommended procedure

250 mL solutions containing mercury in the range of 0.02–1.20 $\mu g\,L^{-1}$ and 3.5 ml of citrate buffer (pH 2.5) was passed through a mini-column packed with 2.0 g of the adsorbent at a flow rate of 16 mL min^{-1}. The mercury ions were eluted from the mini-column by 3.0 mL of 3 mol L^{-1} of HCl at a flow rate of 6 mL min^{-1}. The eluted mercury solution was placed in the RC-GLS and 4 mL of 2% (w/v) of $SnCl_2$ solution was added. After 1 min, nitrogen gas at a flow rate of 350 mL min^{-1} was passed through the RC-GLS to take the mercury vapors to the T-cell quartz tube. The measurements were performed on the height mode of atomic signal.

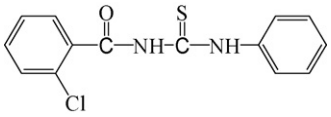

Fig. 1. Structure of N-(2-chloro benzoyl)-N′-phenylthiourea.

3. Results and discussion

N-(2-chloro benzoyl)-N′-phenylthiourea (Fig. 1) was synthesized and used as a new reagent for solid phase extraction of Hg(II). It was loaded on solid sulfur as a new solid support material and packed in a mini-column. The effect of various parameters such as pH, the amount of ligand loaded, amount of adsorbent in the column, sample flow rate, sample volume and the effect of diverse ions on the preconcentration of 250 mL solution containing 1.0 $\mu g\,L^{-1}$ of Hg(II) was studied in detail.

3.1. Effect of pH

The influence of pH on the preconcentration of Hg(II) was investigated. Fig. 2 shows that the recovery of Hg(II) ions increased with increasing the pH of the solution up to 2 and remained constant in the range of 2–3. Thus, the pH 2.5 was selected as the optimum value for the sorption of Hg(II) ions and 3.5 mL of citric acid–citrate buffer solution with pH 2.5 was used to maintain this pH.

3.2. Optimization of vapor generation conditions

Important parameters of the cold vapor generation that should be optimized included the flow rate of the nitrogen carrier and concentration of the $SnCl_2$ solution used as the reducing agent. It was found that a nitrogen flow rate of 350 mL min^{-1} was suitable for this system.

The effect of the $SnCl_2$ concentration on the cold-vapor generation was also evaluated within the range of 1.0–5.0% (w/v). The results showed that the maximum absorbance is obtained at concentrations between 2.0 and 3.5% (w/v). Thus, a concentration of 2.0% (w/v) of $SnCl_2$ was selected as optimum.

3.3. Effect of ligand quantity

The quantity of ligand immobilized on the adsorbent is an important chemical variable affecting the preconcentration of the examined analyte. Therefore, the effect of quantity of N-(2-chloro benzoyl)-N′-phenylthiourea on the retention of Hg(II) was examined. Various amounts of N-(2-chloro benzoyl)-N′-phenylthiourea (10.0–250.0 mg) were added to 40 g of sulfur powder and the procedure for preparation of the adsorbent was followed. 2.0 g of the adsorbent was used in the mini-column for preconcentration of the analyte. The results presented in Fig. 3 show that highest recoveries are obtained when the amount of N-(2-chloro benzoyl)-N′-phenylthiourea was in the range of 3.75–5.00 mg g^{-1} of solid support.

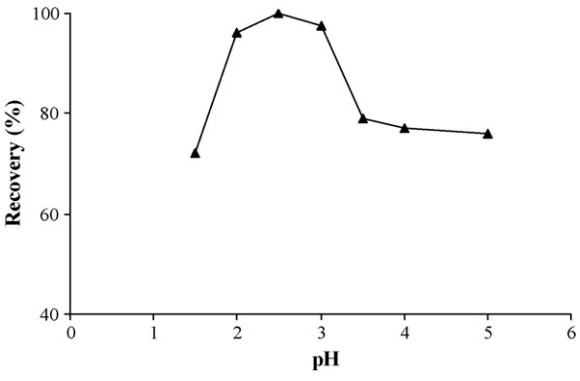

Fig. 2. Effect of pH on the recovery of 1.0 $\mu g\,L^{-1}$ of Hg (II); 2.0 g of sulfur adsorbent; flow rate 16 mL min^{-1}; sample volume 250 mL.

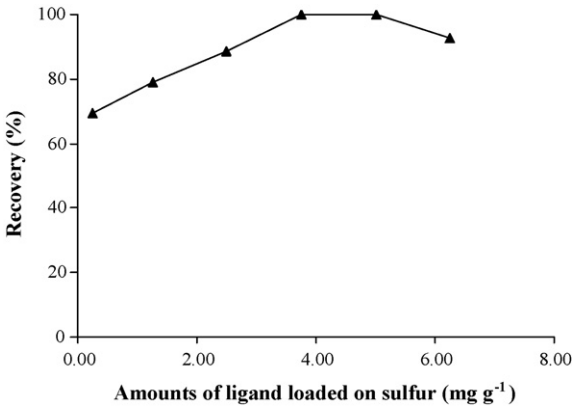

Fig. 3. Effect of amounts of ligand loaded on sulfur powder on the retention of 1.0 $\mu g\,L^{-1}$ Hg(II), pH 2.5; flow rate 16 mL min^{-1}; sample volume 250 mL.

A considerable increase in the recovery and therefore the retention of Hg(II) by changing of N-(2-chloro benzoyl)-N′-phenylthiourea concentration indicates that the use of N-(2-chloro benzoyl)-N′-phenylthiourea is necessary for quantitative retention of the analyte. Very low recoveries are obtained without adding the ligand. Thus, 2.0 g of the adsorbent containing 3.75 mg g^{-1} of the ligand was used for further investigations.

3.4. Effect of the adsorbent amount

The amount of adsorbent is another important parameter to obtain quantitative recovery. In order to estimate the optimum adsorbent quantity, the recoveries of Hg(II) were examined by using the adsorbent quantities between 0.5 and 3.0 g. Quantitative recoveries were achieved when adsorbent amount was greater than 2.0 g. Accordingly, 2.0 g of sulfur loaded with N-(2-chloro benzoyl)-N′-phenylthiourea was used in all experiments.

3.5. Effect of eluent type, concentration and volume

In order to choose a proper eluent for the retained mercury ions after preconcentration, various acids and organic solvents were tested and the percentage recovery for each eluent type was determined. Among the eluents studied, hydrochloric acid provided higher recoveries in comparison to the others (Table 1).

Then the experiments were carried out for selecting the concentration of hydrochloric acid solution. The hydrochloric acid concentrations in the range of 0.5–4.0 mol L^{-1} were studied for this purpose. The recovery values were almost quantitative above 2.0 mol L^{-1} concentrations. Therefore, acid concentration of 3.0 mol L^{-1} was chosen as optimum in the subsequent experiments.

Table 1
Effect of different eluting solutions on the absorbance of 1 $\mu g\,L^{-1}$ Hg(II).

Eluting solution	Absorbance[a]
H_2SO_4 (3 mol L^{-1})	0.211
HNO_3 (3 mol L^{-1})	0.379
HCl (3 mol L^{-1})	0.463
HCl (3 mol L^{-1}) + Thiourea	0.050
HCl (3 mol L^{-1}) + Ethanol	0.450

[a] Average of three determinations.

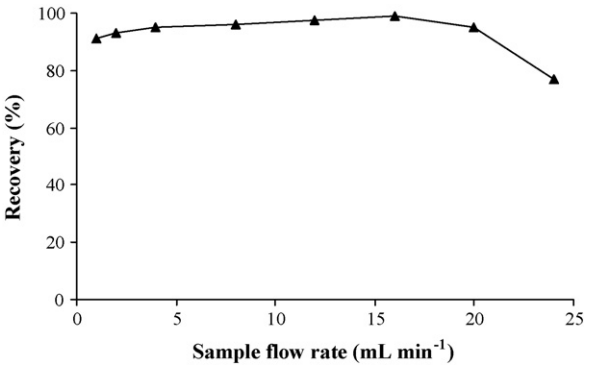

Fig. 4. Effect of sample flow rate on the recovery of 1.0 μg L^{-1} of Hg(II), pH 2.5; 2.0 g of sulfur adsorbent; sample volume 250 mL.

The effect of the volume of 3.0 mol L^{-1} hydrochloric acid solution on the recovery was also investigated. The quantitative recoveries were found when 3.0 mL of eluent was used. Thus 3.0 mL of the eluent was selected as optimum in the subsequent experiments.

3.6. The effect of flow rate

The flow rate of the Hg(II) solution through the column is a very important parameter for the time controls of adsorption and analysis. Using the column procedure, the effect of flow rate on sorption of 1.0 μg L^{-1} of Hg(II) in the range of 1–24 mL min^{-1} was investigated. The results presented in Fig. 4 show that Hg(II) can be retained on the column quantitatively (>95%) with flow rates in the range of 8–20 mL min^{-1}. Therefore, to achieve higher speed of operation, a sample rate of 16 mL min^{-1} was selected as optimum value. The effect of the flow rate of eluent solution was also studied in the range of 1–10 mL min^{-1} and it was found that up to flow rates of 6 mL min^{-1} the recovery remained constant. Therefore, a flow rate of 6 mL min^{-1} was selected for eluting the retained mercury ions from the column.

3.7. Effect of sample volume

The sample volume is also an important parameter to reach high preconcentration factors. Therefore, the effect of sample volume on the recoveries of the Hg(II) was investigated by using different volumes of solutions in the volume range of 50–2000 mL containing the same amount of Hg(II). These solutions were passed through the column under optimum conditions. The recoveries were found to be quantitative and constant up to 1000 mL. Therefore, 1000 mL was chosen as the largest applicable sample volume.

3.8. Analytical figures of merit

The analytical parameters were evaluated using the optimum experimental conditions. The calibration graph was linear in the range of 0.02–1.20 μg L^{-1} of Hg (II) in the initial solution and obeyed the equation $A = 0.4344C + 0.0135$ ($r = 0.9991$, $n = 8$), where A is the absorbance and C is the concentration of mercury in micrograms per liter. The limit of detection (LOD) calculated from three times the standard deviation of ten blank signal measurements [27] was 0.012 and 0.003 μg L^{-1} when using 250 and 1000 mL sample volumes, respectively. The relative standard deviation (R.S.D.) for determinations of 0.040 and 1.0 μg L^{-1} of Hg(II) were 3.9 and 1.2% ($n = 8$), respectively. A preconcentration factor of 333 is achieved if 1000 mL solutions are used and the retained ions are eluted by 3.0 mL of the eluent.

Table 2
Effect of foreign species in the determination of 1 μg L^{-1} of Hg(II).

Species	Tolerance limit (mg L^{-1})
Na^+, K^+, NO_3^-	400
Cu^{2+}, Pb^{2+}, Ni^{2+}, NH_4^+, Ca^{2+}, Fe^{3+}, Mg^{2+}, Zn^{2+}, Co^{2+}, Cd^{2+}, Al^{3+}, Cr^{3+}, Bi^{3+}, Mn^{2+}, SO_4^{2-}, CO_3^{2-},, HCO_3^-, Cl^-, F^-, I^- Br^-, $C_2O_4^{2-}$	80
Tartarate, EDTA, urea, Fe^{2+}	40

3.9. Interference studies

The selectivity of the proposed method was studied by determination of 1.0 μg L^{-1} Hg(II) in the presence of various species. Each ion or organic substance was considered to be an interferent when it caused an error greater than ±5% in the determination of mercury. The relevant data is presented in Table 2. The result shows that most common ions do not interfere in the determination and the method is highly selective in the presence of different species.

4. Application

The validity of the proposed method was tested by applying it to fish, oyster and seawater samples. Additionally, the method was also applied for the analysis of mercury content in the certified reference material (DORM-3). It was found that there is no significant difference between results obtained by the proposed method and the certified value (Table 3).

4.1. Analysis of marine samples

The proposed method was applied to the determination of total mercury in two fish samples, Otolithes and Platicephalus and oyster (*Macta aequisulcata*) were purchased from local fish market. 1.0 g of each dried sample was initially digested as stated in the sample pre-treatment (Section 2.5) and then subjected to the proposed procedure. The recovery of the spiked standard solutions as shown in Table 4 was in the range of 95–103% which demonstrates that good recoveries are obtained by the method.

Table 3
Determination of mercury in a certified reference material.

Certified reference material	Certified[a] (μg g^{-1})	Found[a] (μg g^{-1})	Relative error (%)
DORM-3	0.409 (±0.027)	0.396 (±0.076)	3.18

[a] Values in parentheses are S.D. based on five replications.

Table 4
Determination of Hg(II) in Persian Gulf water and marine samples.

Sample	Added (μg L^{-1})	Found (μg L^{-1})[a]	Recovery (%)
Persian Gulf water	–	0.99 (±0.03)	
	0.04	1.04 (±0.01)	100.9
	0.60	1.59 (±0.01)	100.0
Otolithes[b]	–	0.35 (±0.01)	
	0.04	0.39 (±0.01)	100.0
	0.60	0.92 (±0.02)	96.8
Platicephalus[c]	–	0.05 (±0.01)	
	0.04	0.09 (±0.02)	100.0
	0.60	0.64 (±0.01)	98.4
Oyster[d]	–	0.35 (±0.05)	
	0.04	0.39 (±0.01)	100.0
	0.60	0.93 (±0.01)	97.9

[a] Values in parentheses are S.D. based on five replications.
[b] Amount of mercury in Otolithes was 1.75 μg g^{-1}.
[c] Amount of mercury in Platicephalus was 0.25 μg g^{-1}.
[d] Amount of mercury in oyster was 87.50 μg g^{-1}.

4.2. Analysis of Persian Gulf water

The water sample was passed through the mini-column at optimum conditions, after the appropriate treatment described earlier. The recovery test was also conducted to evaluate the feasibility of the method. The water sample was spiked with two standard solutions. The results are listed in Table 4.

5. Conclusion

N-(2-chloro benzoyl)-N′-phenylthiourea immobilized on sulfur powder was used as a new solid phase for preconcentraion and determination of mercury ions. To the best of our knowledge, this is the first application of modified sulfur as a solid phase extractor. The limit of detection of the method was comparable to or better than some of the previously reported methods [7,12,15,19,21,24]. The selectivity of the method in terms of co-existing ions was quite high and most of the ions did not interfere at high concentrations as seen in Table 2. The RC-GLS system used in this procedure is faster and provides higher sensitivity than commercially available continuous flow vapor system. The preconcentration factor of this method is 333 for 1000 mL sample volumes, which is superior to some of the similar procedures. The proposed method can successfully be applied for separation and preconcentration of Hg(II) ions from water and marine samples.

Acknowledgement

The authors are grateful to Shahid Chamran University for financial support of this project (Grant No. 259–1386).

References

[1] M. Plessi1, D. Bertelli, A. Monzani, J. Food Compos. Anal. 14 (2001) 461.
[2] U. Tamer, T. Oymak, N. Ertas, Electroanalysis 19 (2007) 2565.
[3] X. Zhu, S.D. Alexandratos, Microchem. J. 86 (2007) 37.
[4] L. Jian, W. Goessler, K.J. Irgolic, Freseniu's J. Anal. Chem. 86 (2000) 43.
[5] Y.W. Chen, J. Tong, A. D'Uliv, N. Belzile, Analyst 127 (2002) 1541.
[6] N.V. Suc, M.M. Hung, N.V. Hung, J. Radioanal. Nucl. Chem. 213 (1996) 65.
[7] S. Gil, I. Lavilla, C. Bendicho, Spectrochim. Acta Part B 62 (2007) 69.
[8] V. Camel, Spectrochim. Acta Part B 58 (2003) 1177.
[9] K. Roberts, P.R. Haddad, P.E. Jackson, Principles and Practice of Modern Chromatographic Methods, Academic Press, London, 1994, p. 445.
[10] M.E. Mahmouda, M.M. Osmana, M.E. Amer, Anal. Chim. Acta 415 (2000) 33.
[11] M.E. Mahmoud, Anal. Chim. Acta 398 (1999) 297.
[12] N. Rajesh, M.S. Hari, Spectrochim. Acta Part A 70 (2008) 1104.
[13] Y. Yamini, N. Alizadeh, M. Shamsipur, Anal. Chim. Acta 355 (1997) 69.
[14] J.C.A. De Wuilloud, R.G. Wuilloud, R.A. Olsina, L.D.J. Martinez, J. Anal. Atom. Spectrom. 17 (2002) 389.
[15] N. Rajesh, G. Gurulakshmanan, Spectrochim. Acta Part A 69 (2008) 391.
[16] A.M. Starvin, T. Prasada Rao, J. Hazard. Mater. B 113 (2004) 75.
[17] S.R. Segede, J.F. Tyson, Talanta 71 (2007) 1696.
[18] J. Fan, C. Wu, Y. Wei, C. Peng, P. Peng, J. Hazard. Mater. 145 (2007) 323.
[19] N. Pourreza, M. Behpour, Anal. Chim. Acta 341 (2003) 23.
[20] M.A.H. Hafez, I.M.M. Kenawy, M.A. Akl, R.R. Lashein, Talanta 53 (2001) 749.
[21] F. Mercader-Trejo, E. Rodriguez de San Miguel, J. de Gyves, J. Anal. Atom. Spectrom. 20 (2005) 1212.
[22] H. Parham, N. Pourreza, N. Rahbar, J. Hazard. Mater. (2008), doi:10.1016/j.jhazmat.2008.07.007.
[23] N. Pourreza, K. Ghanemi, J. Hazard. Mater. 161 (2009) 982.
[24] Y.M. Zhang, T.B. Wei, L.M. Gao, Synth. Commun. 31 (2001) 3099.
[25] L. Bai, S. Li, J.X. Wang, M. Chen, Synth. Commun. 32 (2002) 127.
[26] K. Helrich, Official Methods of Analysis, vol. 1, 15th ed., Association of Official Analytical Chemists (AOAC), Inc, Arlington, Virginia, USA, 1990.
[27] J.D. Ingle, S.R. Crouch, Spectrochemical Analysis, Prentice-Hall, Inc., USA, 1988, pp. 172–173.

Talanta 78 (2009) 1359–1363

Contents lists available at ScienceDirect

Talanta

journal homepage: www.elsevier.com/locate/talanta

Luminescence switching of CdTe quantum dots in presence of *p*-sulfonatocalix[4]arene to detect pesticides in aqueous solution

Fengge Qu[a], Xiufen Zhou[a], Jing Xu[a], Haibing Li[a,*], Guangyong Xie[b]

[a] *Key Laboratory of Pesticide and Chemical Biology (CCNU), Ministry of Education, College of Chemistry, Central China Normal University, Wuhan 430079, PR China*
[b] *Key Laboratory of Catalysis and Materials Science of the State Ethnic Affairs Commission & Ministry of Education, Hubei Province, South-Central University for Nationalities, Wuhan 430074, PR China*

ARTICLE INFO

Article history:
Received 11 December 2008
Received in revised form 5 February 2009
Accepted 9 February 2009
Available online 20 February 2009

Keywords:
Quantum dots
Calixarene
Pesticides
Fenamithion
Acetamiprid

ABSTRACT

A simple, rapid, and sensitive identification method of fenamithion and acetamiprid is developed using supramolecular nano-sensitizers combining of CdTe quantum dots (QDs) and *p*-sulfonatocalix[4]arene as additive by fluorescent spectroscopic technique in water. Depending on *p*-sulfonatocalix[4]arene, the selectivity of CdTe QDs is tuned between fenamithion and acetamiprid. The luminescence of free CdTe QDs is quenched selectively to fenamithion. While in the presence of *p*-sulfonatocalix[4]arene, it shows that the fluorescence intensity of QDs is enhanced selectively to acetamiprid due to the cooperation of QDs and *p*-sulfonatocalix[4]arene. Based on the response characteristics of the QDs, a fluorescent method is performed for tuning selective determination of the pesticides. Under optimum conditions described, it is found that the pesticides effect on the luminescence of the CdTe QDs in concentrations dependence are described by a Stern–Volmer-type equation or a Langmuir binding isotherm equation in the range of 0–10^{-4} M (fenamithion) and 0–10^{-3} M (acetamiprid), with the corresponding detection limits (3σ) of 1.2×10^{-8} M (fenamithion) and 3.4×10^{-8} M (acetamiprid), respectively. The possible mechanism is discussed.

1. Introduction

Pesticides are used widely for agriculture, vector control, and domestic purposes. Despite the apparent benefits of these uses acute, pesticide poisoning is an increasing worldwide problem, particularly in rural areas. Pesticides are the most important cause of severe toxicity and death from acute poisoning worldwide [1–3]. Thus, analytical techniques with high sensitivity and selectivity are developed to monitor pesticide poisoning. Now, pesticide detecting techniques mostly focus on chromatographic separation, such as high performance liquid chromatography (HPLC) [4], gas chromatography (GC) [5], solid phase microextraction-HPLC [6], immunoaffinity chromatography (coupled column liquid chromatography/mass spectrophotometry) [7], and thin layer chromatography [8]. However, these methods are relatively time consuming and require a tedious sample pretreatment. Thus, the development of a simple and rapid pesticides detecting technique still presents a challenge.

Luminescent semiconductor quantum dots (QDs), which have unique electronic and optical properties such as high quantum yields (QY), narrow emission bands, continuous broad absorption bands, and high resistance to photobleaching, receive more and more attention in recent years [9–10]. QDs modified with macrocyclic host molecules, show excellent selective recognition abilities. A number of papers about chemical sensing of neutral molecules [11] and ions [12–15], with QDs via analyte-induced changes in photoluminescence have been reported. Calixarenes have been demonstrated outstanding complex ability towards ions, organic molecules, etc., and are considered as the third host molecules after crowns and cyclodextrin [16–20]. Of particular relevance are the studies performed in water, where most of the biological processes take place. Therefore, water soluble calixarenes [21] have been well established and general procedures are available for the selective preparation. As far as we know, calixarenes have also been used to modify semiconductor QDs, recently. For example, Jin and co-workers have found that the surface of CdSe/ZnS QDs could be modified with amphiphilic calixarene derivatives to give water soluble QDs [22–23]. We reported sulfur calix[4]arene modified QDs as mercuric ions probes [24]. These reports stimulate us to establish a simple and rapid detection system combining *p*-sulfonatocalix[4]arene as the specific detecting switch and CdTe QDs as signal reporter.

Herein we develop a new strategy for the efficient recognition and determination of fenamithion and acetamiprid in aqueous solution using a cooperation of *p*-sulfonatocalix[4]arene via the fluorescence (FL) response of CdTe QDs. In our proposed approach,

* Corresponding author. Tel.: +86 27 67866423.
E-mail address: lhbing@mail.ccnu.edu.cn (H. Li).

0039-9140/$ – see front matter © 2009 Elsevier B.V. All rights reserved.
doi:10.1016/j.talanta.2009.02.013

the free CdTe QDs respond selectively to fenamithion. While in the presence of *p*-sulfonatocalix[4]arene, CdTe QDs show remarkably selective and sensitive to acetamiprid.

2. Materials and methods

2.1. Materials

All chemicals used were of analytical grade or of the highest purity available. All solutions were prepared with double-distilled, deionized water. Tellurium (reagentpowder, 99.999%, about 200 mesh), thioglycolic acid (TGA, 99%), $CdCl_2{\cdot}2.5H_2O$ (99%), NaBH4 (96%) were purchased from Aldrich (Milwaukee, WI). *p*-sulfonatocalix[4]arene (Scheme S1 in the supporting information) was synthesized according to the reported method [25]. Pesticide standards (parathion–methyl, fenamithion, methomyl, optunal, and acetamiprid) studied were provided by the Key Laboratory of Pesticide and Chemical Biology (CCNU), Ministry of Education, China. All pesticides tested were of 98–99% purity. Parathion–methyl and optunal were dissolved in the mixture of water and ethanol, and others were dissolved in water and stored at room temperature. The garlic samples were prepared according the standard extraction procedure (detailed extraction experiments were seen in supporting information).

2.2. Apparatus

The UV–vis absorption spectra were acquired on a TU-1901 UV–vis spectrometer (Beijing Purkinje General Instrument Co. Ltd.). Fluorescence spectra were taken on a Fluoromax-P luminescence spectrometer (HORIBA JOBIN YVON INC.). The transmission electron micrograph (TEM) was recorded with a JEOL-JEM 2010 electron microscope operating at 200 kV.

2.3. Synthesis of CdTe QDs

CdTe QDs were prepared using the reaction between Cd^{2+} and NaHTe solution following the method described elsewhere [26]. The molar ratio of Cd^{2+}:TGA:HTe was fixed at 1:2.5:0.5. Briefly, 0.095 g of $CdCl_2{\cdot}2.5H_2O$ was dissolved in 5 mL of Mill-Q water and 0.092 g of TGA was added. Then the solution was adjusted to pH 11 with 1 M NaOH and deaerated with N_2 for 30 min. Next, oxygen-free NaHTe solution, which was freshly prepared from tellurium powder and $NaBH_4$ in water, was injected into the above solution under vigorous stirring. The solution was then heated at 95 °C and further refluxed for 2 h. Finally, the stock solution of 10^{-5} M CdTe QDs was prepared at pH 6 and kept at room temperature without light irradiation.

2.4. Preparation of pesticides/p-sulfonatocalix[4]arene mixed solution

The 1 mM stock solution of *p*-sulfonatocalix[4]arene was prepared by dissolving the material in doubly distilled water. Stock solutions of 10^{-3} M pesticides were prepared by dissolving the appropriate amount of each compound in doubly distilled water. Working solutions were prepared by successively diluting the stock solutions with doubly distilled water. The mixed solution of pesticides/*p*-sulfonatocalix[4]arene was prepared by adding 2 mL of the stock solution of pesticides at a concentration of 10^{-5} M added to 1 mL of *p*-sulfonatocalix[4]arene at a concentration of $5\,M \times 10^{-4}$ M. Blank solution of pesticides/*p*-sulfonatocalix[4]arene were prepared under the same conditions but used 1 mL of water to instead *p*-sulfonatocalix[4]arene solution.

2.5. Determination of pesticides.

The fluorescence measurements were carried out in a quartz cell (1.0 cm × 1.0 cm cross-section). Before detection, added 1 mL of CdTe QDs at a concentration of 10^{-5} M to the pesticides/*p*-sulfonatocalix[4]arene mixed solution. And the mixed solution was allowed to stand for a few minutes to allow complete formation of stable solution.

3. Results and discussion

3.1. UV–vis spectra and TEM images.

Fig. S1 shows the UV–vis spectra of CdTe QDs (Fig. S1a) and CdTe QDs solution after adding *p*-sulfonatocalix[4]arene (Fig. S1b). It is found no distinct difference in the positions and peak widths of them, which suggests that the *p*-sulfonatocalix[4]arene does not change the optical property of original CdTe QDs. Fig. S2 shows the TEM image of CdTe QDs used in the experiment, which indicates that CdTe QDs are monodisperse and uniform.

3.2. Effect of the concentration of p-sulfonatocalix[4]arene on the fluorescence intensity of CdTe QDs.

As shown in Fig. S3, the effects of *p*-sulfonatocalix[4]arene on the fluorescent intensity of CdTe QDs were carried in the aqueous system. The concentrations of *p*-sulfonatocalix[4]arene from 10^{-6} M to 10^{-3} M were studied in the experiment. When the concentration of *p*-sulfonatocalix[4]arene is 5×10^{-4} M, the fluorescence intensity reaches to maximum. Here, *p*-sulfonatocalix[4]arene indeed plays an important role in the fluorescence intensity of water soluble CdTe QDs. When the amount of *p*-sulfonatocalix[4]arene is small, the surface defects and dangling bonds on the surface of QDs can not be passivated well. Thus, the CdTe QDs become unstable, showing a lower FL intensity. The FL intensity is increased with the concentration increase of *p*-sulfonatocalix[4]arene when less than 5×10^{-4} M. If the amount of *p*-sulfonatocalix[4]arene is higher than 5×10^{-4} M, the excessive *p*-sulfonatocalix[4]arene generates an additional trap state, which is the center of nonradiative recombination. The CdTe QDs trend the aggregation and the FL intensity of quantum dots decreases, which may be attributed to the self-quenching or re-absorption. In other words, once these defect sites are saturated, the additional *p*-sulfonatocalix[4]arene plays a role of hole traps, resulting in a lower FL emission [27,28]. According to the above experiments, the concentration of *p*-sulfonatocalix[4]arene at 5×10^{-4} M was selected for the following experiment.

3.3. Effect of the pesticides on the photochemical properties of CdTe QDs in the presence/absence of p-sulfonatocalix[4]arene.

The effects of 10^{-5} M relevant pesticides on the photochemical properties of CdTe QDs in the absence or presence *p*-sulfonatocalix[4]arene were studied and the results were shown as in Fig. 1. The structures of relevant pesticides are shown in Fig. 2, including parathion–methyl, fenamithion, methomyl, optunal, and acetamiprid. Fig. 1(A) and (B) showed the effects of pesticides on the fluorescent intensity of CdTe QDs without and with *p*-sulfonatocalix[4]arene, respectively. As can be seen from Fig. 1(A), the FL intensity was quenched by fenamithion, which demonstrated that CdTe QDs turned out to be sensitive to fenamithion in water. However, when the same amounts of pesticide were added to the CdTe QDs and *p*-sulfonatocalix[4]arene mixed solution, the FL intensity of the CdTe QDs was increased gradually with acetamiprid. These results demonstrated that the luminescent response of CdTe

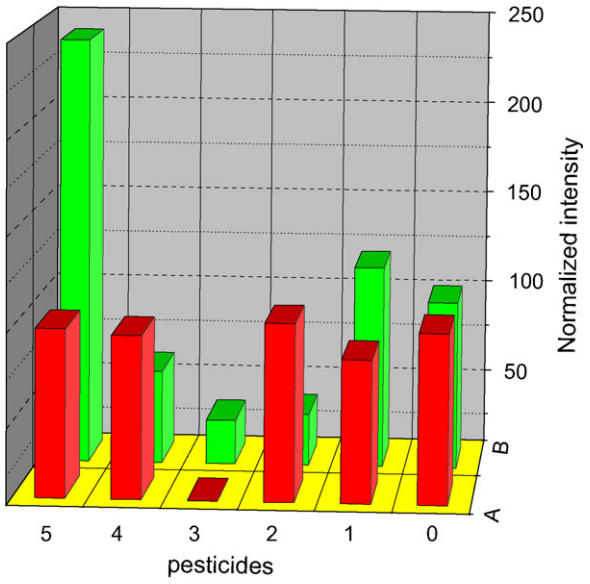

Fig. 1. Effects of 10^{-5} M relevant pesticides on the fluorescence of CdTe QDs (A), CdTe QDs + *p*-sulfonatocalix[4]arene (B) (from 0 to 5: control, parathion–methyl, methomyl, fenamithion, optunal and acetamiprid).

QDs towards fenamithion and acetamiprid were highly dependent on *p*-sulfonatocalix[4]arene, which could tune the fluorescent recognition of CdTe QDs between two pesticides.

3.4. Fluorescence response and calibration curve.

Fig. S4 showed the fluorescence responses of CdTe QDs toward different concentration of pesticides in the presence/absence of *p*-sulfonatocalix[4]arene. As shown in Fig.S4, the FL intensity of CdTe QDs was progressively decreased with an increase in fenamithion. However, with an increase in acetamiprid, the FL intensity of CdTe QDs in the presence of *p*-sulfonatocalix[4]arene was progressively increased. It was clear that *p*-sulfonatocalix[4]arene has played an important role for the selective recognition of acetamiprid. Furthermore, it was found that the quenching effect of fenamithion on the FL intensity of CdTe QDs could be used to develop a method for the determination of the fenamithion in concentration dependence. A good linear relationship was observed up to fenamithion concentration when to use a Stern–Volmer-type equation [12]:

$$\frac{I_{max}}{I} = 1 + K_{sv}[Q]$$

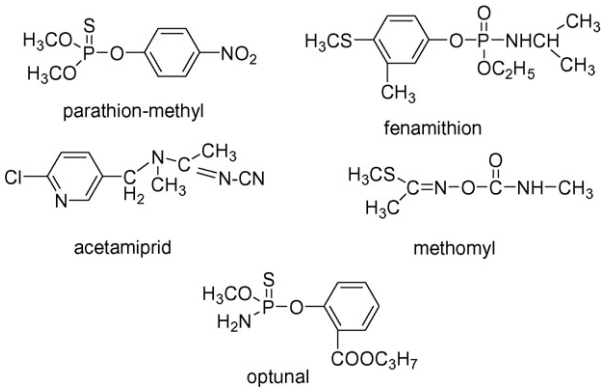

Fig. 2. The chemical structures of pesticides investigated.

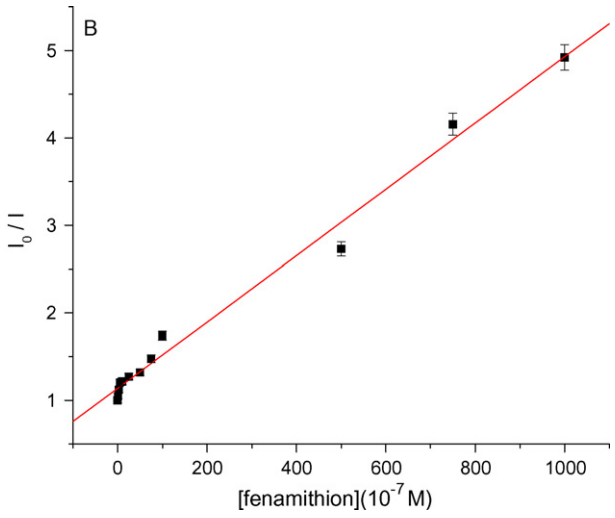

Fig. 3. Stern–Volmer-type description of the fluorescence of CdTe QDs showing a linear fit throughout the fenamithion concentration range, with a correlation coefficient = 0.994.

where I and I_{max} are the FL intensity of the CdTe QD at a given fenamithion concentration and fenamithion free solution, respectively. [Q] is the given fenamithion concentration and K_{sv} is Stern–Volmer quenching constant. Fig. 3 shows the Stern–Volmer quenching curve describing the I_{max}/I as a function of fenamithion concentration, the coefficient of the linear fit is 0.994, and K_{sv} is found to be 4.6×10^5 M and. The detection limit of 1.2×10^{-8} M is calculated following the 3σ IUPAC criteria.

For the observed luminescence emission quenching by fenamithion, we supposed that after adding fenamithion, the mixed solution may result from the generation of a new and efficient nonradiative path and/or from the suppression of a radiative process. Accordingly to the typical Stern–Volmer quenching behavior, when collisions is occurring between quencher and luminescent molecules, a part of the energy is lost, which results in the fluorescence intensity quenching.

On the other hand, the enhanced FL intensity of CdTe QDs towards acetamiprid in the presence of *p*-sulfonatocalix[4]arene was effectively described by a Langmuir-type binding isotherm

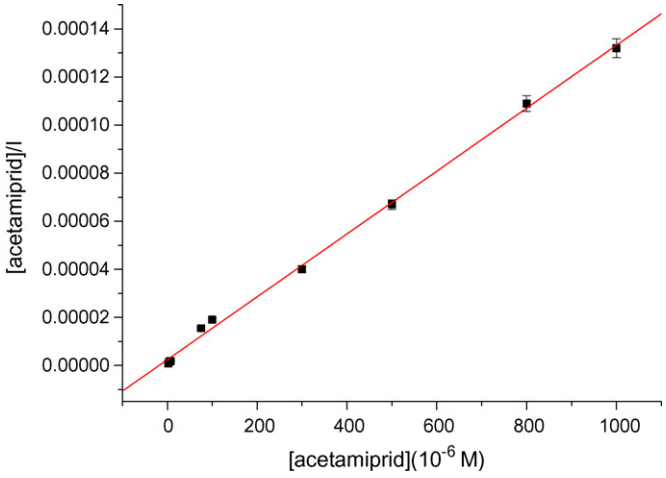

Fig. 4. Langmuir binding isotherm description of the FL intensity of CdTe QDs in the presence of *p*-sulfonatocalix[4]arene showing a linear fit throughout the acetamiprid concentration range, with a correlation coefficient >0.998.

Table 1
Results of the analysis of garlic samples.

Pesticides	Amount in sample (ng mL^{-1})	This method			Amount found by HPLC (ng mL^{-1})
		Amount found (ng mL^{-1})	Average recovery (n = 5) (%)	R.S.D. (%)	
Fenamithion	20	19.2	96	3.4	19.5
	30	29.2	97.3	4.6	30.3
Acetamiprid	75	76.5	102	3.9	77.3
	120	117.6	98	4.5	124.2

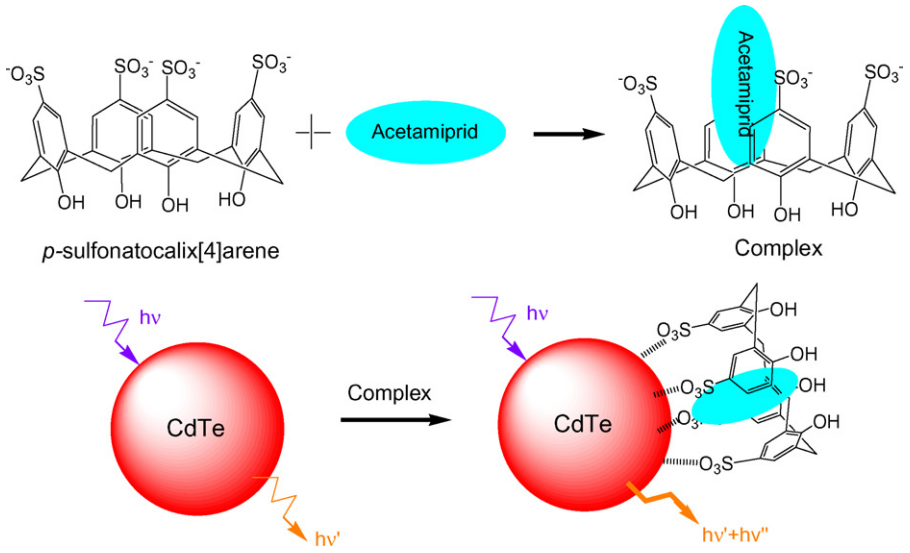

Fig. 5. acetamiprid enhances the fluorescence of CdTe QDs in the presence of *p*-sulfonatocalix[4]arene.

[29]. The equation could be linearized to take the form:

$$\frac{C}{I} = \left(\frac{I}{BI_{\max}}\right) + \left(\frac{1}{I_{\max}}\right) C$$

where I and $I_{\max}$ are the FL intensity of the CdTe QD at a given acetamiprid concentration and the maximum intensity. [C] is the given acetamiprid concentration and B is Langmuir type binding constant. Accordingly, if the Langmuir description of the acetamiprid-binding on the surface of the CdTe QDs was correct, a plot of C/I as a function of C should be linear, as shown in Fig. 4. A relative linearity was observed throughout the entire range of acetamiprid concentration. The coefficient of the linear fit was higher than 0.998. And the detection limit of 3.4×10^{-8} M was calculated following the 3σ IUPAC criteria. The detection limit of the method is sufficient for real food and environmental analysis. To further demonstrate the practicality of the proposed nanosensor, the recovery test was studied by adding different amounts of some substances into garlic samples of 0.1 M PBS (pH 7.0). As can be seen in Table 1, the results are very close to those detected by HPLC. The recoveries were from 96.0% to 102.0%. The results indicated that the proposed method was highly accurate, precise and reproducible. It can be used for direct analysis of relevant samples.

Concerning the explanation for acetamiprid enhancement, the possible reasons was given. For the above experiment, it was reasonable to believe that *p*-sulfonatocalix[4]arene plays an important role for CdTe QDs in selective luminescence response to acetamiprid. It was known that the well-defined structure of the *p*-sulfonatocalixarene cavities can be exploited for the inclusion of positive charged ammonium group [21,30]. As shown in Fig. 5, under the experimental conditions (pH 6), acetamiprid could be ionized as positive charged ammonium salts, which could be embedded into *p*-sulfonatocalix[4]arene cavity to form supramolecular complex [31,32]. According to literatures [33,34], water soluble *p*-sulfonatocalixarene can be modified on the surface of quantum dots in aqueous solution via SO_3^- group coupling. Therefore, it is reasonable to believe that an inclusion complex *p*-sulfonatocalix[4]arene/acetamiprid can be gradually adsorbed on the surface of QDs, which resulted in restricting the disordered orientation and so inducing a uniform arrangement. Such ordered orientation may suppress the quenching path to the medium by effective core protection and thus increase the luminescence intensity [35].

It was also found that CdTe QDs exhibited fluorescence emission blue shifts after adding acetamiprid in the present of *p*-sulfonatocalix[4]arene. The possible reason of the blue shift may be due to environmental factors such as differences in hydrophobicity, hydrophilicity, electric charge, etc. The blue shift might also be due to physical deformation of the QDs when they were near the acetamiprid/*p*-sulfonatocalix[4]arene inclusion complex. Since QDs are quantum confined "boxes" for electrons, the confined wavelength and emission wavelength can also change when the size or shape of the "box" changes. Thus, if a spherical QD became compressed (ovoid) near the acetamiprid/*p*-sulfonatocalix[4]arene complex by even a nanometer or less, it could dramatically influence the emission wavelength. The similar phenomenon might be observed in the reported case [36].

4. Conclusion

In conclusion, we have proposed a new method that allows simple and efficient recognition and quantification of fenamithion and acetamiprid in aqueous solution via fluorescence response of CdTe QDs by adding *p*-sulfonatocalix[4]arene as additive. The selectivity of luminescent QDs is switched between fenamithion and acetamiprid, depending on *p*-sulfonatocalix[4]arene.

Acknowledgements

This work was financially supported by the National Natural Science Foundation of China (20602015,20772038), Program for Distinguish Young Scientist of Hubei Province (2007ABB017), Program for Chenguang Young Scientist for Wuhan (200750731283) and Open Fund of Hubei Key Laboratory of Catalysis and Materials Science (CHCL0805).

Appendix A. Supplementary data

Supplementary data associated with this article can be found, in the online version, at doi:10.1016/j.talanta.2009.02.013.

References

[1] G. Istamboulie, D. Fournier, J.-L. Marty, T. Noguer, Talanta 77 (2009) 1627.
[2] C. Lourencetti, M.R. Rodrigues de Marchi, M.L. Ribeiro, Talanta 77 (2008) 701.
[3] A. Coly, J.J. Aaron, Talanta 46 (1998) 815.
[4] J.W.B. Braga, C.B.G. Bottoli, I.C.S.F. Jardim, et al., J. Chromatogr. A 1148 (2007) 200.
[5] U. Tamrakar, A.K. Pillai, V.K. Gupta, J. Braz. Chem. Soc. 18 (2007) 337.
[6] J.S. Aulakh, A.K. Malik, V. Kaur, Crit. Rev. Anal. Chem. 35 (2005) 71.
[7] H. Sucsse, H.J. Mücller, J. Chromatogr. A 730 (1996) 337.
[8] M.D.C. Quintero, M. Silva, D. Perez, Analyst 114 (1989) 497.
[9] M. Siswana, K.I. Ozoemena, T. Nyokong, Talanta 69 (2006) 1136.
[10] W. Vastarella, R. Nicastri, Talanta 66 (2005) 627.
[11] H.B. Li, F.G. Qu, Chem. Mater. 19 (2007) 4148.
[12] Y.F. Chen, Z. Rosenzweig, Anal. Chem. 74 (2002) 5132.
[13] K.M. Gattás-Asfura, R.M. Leblanc, Chem. Commun. (2003) 2684.
[14] H.B. Li, Y. Zhang, X.Q. Wang, Sens. Actuators B. 127 (2007) 593.
[15] H.B. Li, C.P. Han, L. Zhang, J. Mater. Chem. 18 (2008) 4543.
[16] C.D. Gutsche, Calixarenes Revisited, Royal Society of Chemistry, London, 1998.
[17] H.B. Li, Y.Y. Chen, D.M. Tian, Z.N. Gao, J. Membr. Sci. 310 (2008) 431.
[18] H.B. Li, J.Y. Zhan, J. Incl. Phenom. Macrocycl. Chem. 60 (2008) 379.
[19] H.B. Li, Y.Y. Chen, React. Funct. Polym. 55 (2003) 171.
[20] H.B. Li, Y.Y. Chen, S.L. Liu, J. Appl. Polym. Sci. 89 (2003) 1139.
[21] S. Shinkai, K. Araki, T. Matsuda, J. Am. Chem. Soc. 112 (1990) 9053.
[22] T. Jin, F. Fujii, H. Sakata, M. Tamura, M. Kinjo, Chem. Commun. (2005) 2829.
[23] T. Jin, F. Fujii, H. Sakata, M. Tamura, M. Kinjo, Chem. Commun. (2005) 4300.
[24] H.B. Li, Y. Zhang, X.Q. Wang, D.J. Xiong, Y.Q. Bai, Mater. Lett. 61 (2007) 1474.
[25] S. Shinkai, S. Mori, H. Koreishi, J. Am. Chem. Soc. 108 (1986) 2409.
[26] M.Y. Gao, S. Kirstein, H. Möhwald, J. Phys. Chem. B 102 (1998) 8360.
[27] Q. Wang, Y.C. Kuo, Y.W. Wang, G. Shin, C. Ruengruglikit, Q.R. Huang, J. Phys. Chem. B 110 (2006) 16860.
[28] S. Jeong, M. Achermann, J. Nanda, S. Ivanov, V.I. Klimov, J.A. Hollingsworth, J. Am. Chem. Soc. 127 (2005) 10126.
[29] W. Brey, Physical Chemistry and its Biological Applications, Academic Press, New York, 1978.
[30] A. Pochini, R. Ungaro, F. Vögtle, Comprehensive Supramolecular Chemistry. vol 2, Pergamon Press, 1996, p. 135.
[31] C.D. Gutsche, I. Alam, Tetrahedron 44 (1988) 4689.
[32] X.J. Li, Z.R. Zeng, S.Z. Gao, H.B. Li, J. Chromatogr. A 1023 (2004) 15.
[33] M.L. Ben-Ishay, A. Gedanken, Langmuir 23 (2007) 5238.
[34] X.Q. Wang, J.F. Wu, F.Y. Li, H.B. Li, Nanotechnlology 19 (2008) 205501.
[35] K. Konishi, T. Hiratani, Angew Chem. Int. Ed. 45 (2006) 5191.
[36] S. Dwarakanatha, J.G. Brunob, A. Shastrya, T. Phillips, A. Johnc, A. Kumarc, L.D. Stephensonc, Biochemical Biophysical Research Communications 325 (2004) 739.

Talanta 78 (2009) 1371–1377

Contents lists available at ScienceDirect

Talanta

journal homepage: www.elsevier.com/locate/talanta

Pt/Au bimetallic hierarchical structure with micro/nano-array via photolithography and electrochemical synthesis: From design to GOT and GPT biosensors

Hong-Xuan Ren [a], Xing-Jiu Huang [b,*], Ju-Hyun Kim [b], Yang-Kyu Choi [b], Ning Gu [a]

[a] Department of Chemistry, Southeast University, Nanjing, 210098, China
[b] Nano-Oriented Bio-electronic Lab, School of Electrical and Computer Science, KAIST, Daejeon, 305-701, South Korea

ARTICLE INFO

Article history:
Received 20 December 2008
Received in revised form 9 February 2009
Accepted 10 February 2009
Available online 20 February 2009

Keywords:
Pt/Au
Bimetallic hierarchical structure
GOT and GPT biosensors

ABSTRACT

A novel matrix for enzyme immobilization was successfully developed by using Pt/Au bimetallic hierarchical structure with micro/nano-array to generate highly sensitive biosensors for glutamic oxaloacetic transaminase (GOT, EC 2.6.1.1) and glutamic pyruvic transaminase (GPT, EC 2.6.1.2) determination. The structures of the Pt/Au particles were confirmed with a dual-beam FIB image, transmission electron microscopy (TEM), selected area electron diffraction (SAED) pattern, and X-ray diffraction (XRD) pattern. The morphologies of the Pt/Au bimetallic hierarchical structure before and after enzyme modification were checked using scanning electron microscopy (SEM). The effects of Nafion membrane and enzyme loading were established. Both GOT and GPT activities have been investigated singly and sequentially. The sensing performances were recorded by employing cyclic voltammetric and chronoamperometry (concentration variations of GOT and GPT) techniques. The interference of ascorbic acid and uric acid was also included. We believe that this study will provide a good inspiration in the development of new generation amperometric biosensors.

1. Introduction

The effect of electrode surface structure on electroanalytical performance has been widely recognised. Researchers have since attempted to capture these properties in constructing a roughened surface, which can provide more catalytic sites or accommodate much more biomolecules in a given region [1]. Significant advances have been made over the past few years through chemical self-assembly techniques or electrochemical deposition to introduce nanoparticles on the electrode surface [2,3]. Especially, recent experimental results reveal that nanoparticles having flower-like morphology have significantly higher electrocatalytic activity than the spherically shaped nanoparticle [4]. And the high electrocatalytic activity is ascribed to the flower-like morphology of the nanoparticles. However, some electrochemical difficulties were also encountered: nanoparticles might be dissociated from the electrode surface due to the nature of the contact, leading to an unstable signal, etc.

Glutamic oxaloacetic transaminase (GOT, EC 2.6.1.1) and glutamic pyruvic transaminase (GPT, EC 2.6.1.2) are enzymes found mainly in the liver but are also found in red blood cells, heart cells, muscle tissue, and other organs, such as the pancreas and kidneys. When body tissue or an organ such as the liver or heart is diseased or damaged, additional GOT and GPT are released into the bloodstream, causing levels of the enzyme to rise, as the amount of GOT and GPT in the blood is directly related to the extent of tissue damage [5–7]. Therefore, it is significant to determine GOT and GPT amounts due to the clinical importance of GOT and GPT in monitoring patients with liver diseases. The assay of GOT and GPT activity all based on the following enzyme reactions:

$$L\text{-aspartate} + \alpha\text{-ketoglutarate} \xrightarrow{\text{GOT}} \text{oxalacetate} + L\text{-glutamate} \quad (1)$$

$$L\text{-alanine} + \alpha\text{-ketoglutarate} \xrightarrow{\text{GPT}} \text{pyruvate} + L\text{-glutamate} \quad (2)$$

$$L\text{-glutamate} + O_2 \xrightarrow{\text{GLOX}} \alpha\text{-oxogluatrate} + NH_3 + H_2O_2 \quad (3)$$

As can be seen from Eqs. (1) and (2), L-glutamate was produced by GOT and GPT, so the electrochemistry was set to measure the formation of hydrogen peroxide from the oxidation of L-glutamate (Eq. (3)).

Bimetallic Pt based catalysts are widely used in industry and for proton exchange membrane fuel cells. Reactivity studies show that the catalytic behavior of Pt/Au bimetallic nanoparticles is signifi-

* Corresponding author. Current address: Department of Chemistry, Physical and Theoretical Chemistry Laboratory, Oxford University, South Parks Road, Oxford OX1 3QZ, UK. Tel.: +44 1865 275413/82 42 869 8077; fax: +82 505 869 8077.
E-mail addresses: xingjiuhuang@hotmail.com, xing-jiu.huang@chem.ox.ac.uk (X.-J. Huang).

0039-9140/$ – see front matter © 2009 Elsevier B.V. All rights reserved.
doi:10.1016/j.talanta.2009.02.024

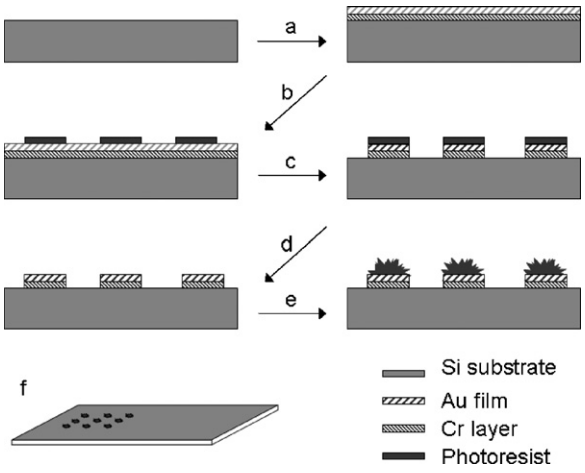

Fig. 1. (a–e) Schematic diagrams outlining the fabrication process for creating Pt/Au bimetallic hierarchical structure with micro/nano-array electrode using photolithography and electrodeposition. (a) Cr layer and Au film deposition; (b) positive photoresist pattern by optical photolithography; (c) Au etching by KCN and Cr layer etching using a CR-7 Cr etchant; (d) photoresist patterns were removed using acetone and AZ400T; (e) directed electrodeposition of Pt/Au bimetallic structure; (f) the design of Pt/Au bimetallic hierarchical structure array electrode with dimension of 1 cm × 2 cm (wide × length).

cant enhanced in comparison with the pure Au and Pt nanoparticle system [8]. Therefore, Pt/Au bimetallic nanoparticles have been extensively synthesized and studied for a variety of catalytic application [8–17]. Unfortunately, in electrochemistry, the preparations of the electrode are often limited in terms of 'bottom-up' methods and no flowerlike micro-arrayed electrodes have been addressed thus far. The signal from the arrays of sensors can be amplified many times compared to that seen from a single electrode on the one hand. On the other hand, it is well-known that immobilization of biomolecules in designer-made nano/microscale structures can significantly improve the performance of biocatalytic processes [18], but the candidates of nano/microstructure materials should be with a high loading, high active surface area, and long-term stability, as well as high electron transfer [1]. Here, we construct Pt/Au bimetallic hierarchical structure with micro/nano-array and immobilize enzymes at these predefined positions to detect GOT and GPT activity. The enzymes could be immobilized and stabilized onto the rough surface. We show that the regular array of biofunctionalized templates provides a useful tool for elucidating recognition events, with the result of enhanced biosensor performance through the use of these hierarchical structures with micro/nano-array.

2. Experimental

2.1. Fabrication of Pt/Au bimetallic hierarchical structure with micro/nano-array electrode

The Au pattern was first prepared using a photolithography technique [11]. Fig. 1 shows the flow process diagram of the preparation. As a starting substrate, a p-type 4 in. silicon wafer with a thickness of 525 μm was used. After a standard cleaning of the silicon wafer for 30 s using a 100:1 diluted HF solution, a 10 nm Cr layer and a 100 nm Au layer were deposited onto the silicon wafer by thermal evaporation. The role of the Cr layer is to improve the adhesion of the gold to the silicon. Following the formation of the Cr/Au layers, dot-shaped mask patterns were made on the Au surface using optical photolithography with a positive photoresist. This lithography step provided designed mask patterns with various sizes and densities of a dot pattern array. Through the use of G-line lithography with a wavelength of 436 nm, an AZ6612KE positive photoresist was patterned. The photoresist patterns served as a mask for a subsequent Au/Cr wet etching. A 100:1 diluted KCN solution transferred the photoresist patterns to the Au layer. This wet etching process was performed at 25 °C for 60 s. After Au etching, the remaining Cr layer was etched by a Cr etchant (CR-7) at 25 °C for 30 s. All photoresist patterns were then removed using acetone and a photoresist remover (AZ400T) at 50 °C for 1 h. Finally, the Au-patterned silicon wafer was washed using deionized water (DIW) and dried in nitrogen gas.

The Pt/Au bimetallic hierarchical structure with micro/nano-array was then synthesized onto an Au patterned silicon wafer in an aqueous solution containing H_2PtCl_6 ($H_2PtCl_6{\cdot}6H_2O$, Sigma–Aldrich), $HAuCl_4$ ($HAuCl_4{\cdot}3H_2O$, Sigma–Aldrich), and 20 g l^{-1} polyvinylpyrrolidone (K30, Fluka) using a two-electrode system. The cleaned Au pattern was employed as a working electrode and a clean graphite sheet served as counter electrode. The applied potential was controlled using a Triple Output DC power supply (Agilent, E3631A).

2.2. Enzyme electrode preparation

The Pt/Au bimetallic hierarchical structure array electrode was modified by L-glutamate oxidase (GLOX, 1.4.3.11, Sigma–Aldrich) according to procedures available in the literature [19,20]. Prior to enzyme immobilization, the Nafion (Fluka) membrane was placed on the electrode by covering the working area with 2.0, 3.5, 5, and 7.5 μl (this is for controlled experiments) of ethanolic solution containing 5 wt.% of Nafion and dried for 8 h at room temperature, respectively. To immobilize the enzyme, 12 μl of the enzyme solution (2.5 mg ml^{-1}) was mixed with 2 μl of a 10 wt.% bovine serum albumin (Fluka) solution. Then, 2 μl of a 10 wt.% glutaraldehyde solution (Sigma–Aldrich) was mixed for cross-linking. With a micropipette, 1, 2.5, 3.5, 4.5 μl of the mixed solution was dropped onto the working electrode to form the electrodes (coded as 1#, 2#, 3#, and 4#) with different enzyme contents, respectively. After the reaction was allowed to proceed, the sensitive area was rinsed with distilled-deionized water and was immersed in a 0.1 M glycine solution.

2.3. Cyclic voltammetry (CV) measurements

CV measurements were performed with a CHI 600B electrochemical analyzer (CH Instruments, Inc.) in a phosphate-buffered saline solution (PBS, pH 7.4) in a conventional three-electrode cell at room temperature. Ag/AgCl was used as a reference and Pt wire as a counter electrode (CH Instruments, Inc.). For the sequential determination of GOT and GPT, The solution was prepared with 100 mM PBS, 1 mM α-ketoglutarate (Sigma–Aldrich), 25 mM L-aspartate (Sigma), 100 U l^{-1} GOT (Sigma), and 100 U l^{-1} GPT (Sigma). After the measurement of GOT activity was recorded, 100 mM L-alanine was added into the system. All experiments were carried out at 35 °C after consideration of normal body temperature and the activity of the electrode at this temperature.

2.4. Materials characterization

Sample morphologies were analyzed using a Philips XL 30 AFEG field-emission scanning electron microscope (FESEM, Eindhoven, Netherlands) and a FEI NOVA 2000 dual-beam focused ion beam (FIB, Netherlands). TEM images were obtained from FEI Tecnai F20. The samples for TEM examination were prepared by focused ion beam (FIB) etching and then transferred to Cu grids coated with thin carbon film. The X-ray diffraction (XRD) spectrum analysis was carried out with a diffractometer (Philips X'pert PRO with Cu Kα radiation).

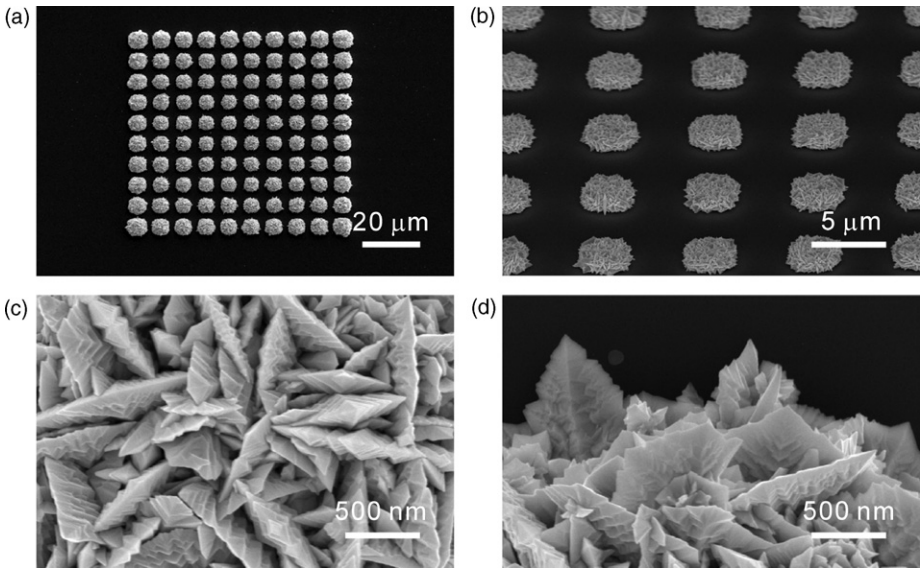

Fig. 2. Typical SEM images of Pt/Au bimetallic hierarchical structure with micro/nano-array. (a) Low magnification top view SEM image of Pt/Au bimetallic array. (b) A 40° view of synthesized Pt/Au bimetallic array in high magnification; (c) and (d) shows the corresponding enlarged SEM images of the Pt/Au bimetallic hierarchical structure at the edge and in the central part, respectively.

3. Results and discussion

Electron microscopy images of the Pt/Au bimetallic hierarchical structure with micro/nano-array electrode directly grown onto the gold patterned silicon substrate are shown in Fig. 2. Fig. 2a shows the status of the electrode containing a 10×10 Pt/Au bimetallic array, which clearly shows that Pt/Au bimetallic particles grew onto the silicon substrate. A side view of synthesized Pt/Au bimetallic array in high magnification is shown in Fig. 2b, indicating that the synthesized Pt/Au bimetallic particles in the array exhibit hierarchical structure. From the high resolution SEM images shown in Fig. 2c and d, we observed that each Pt/Au particle in the array presents a natural flowerlike structure, and the physical attributes of the Pt/Au flower carries many nanoscaled leaflike flakes with sharp edges

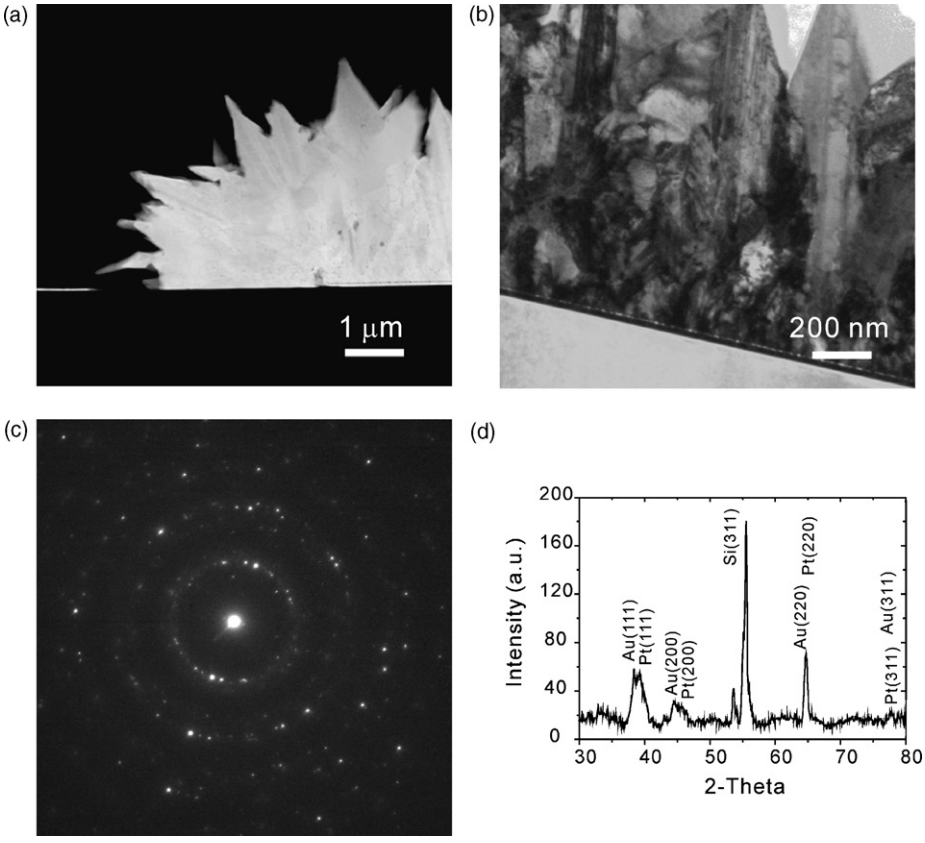

Fig. 3. Characterization of Pt/Au bimetallic hierarchical structures. (a) A dual-beam FIB image of the cross-section. (b) Corresponding TEM image. (c) SEAD pattern corresponding to panel (b); (d) XRD analysis data.

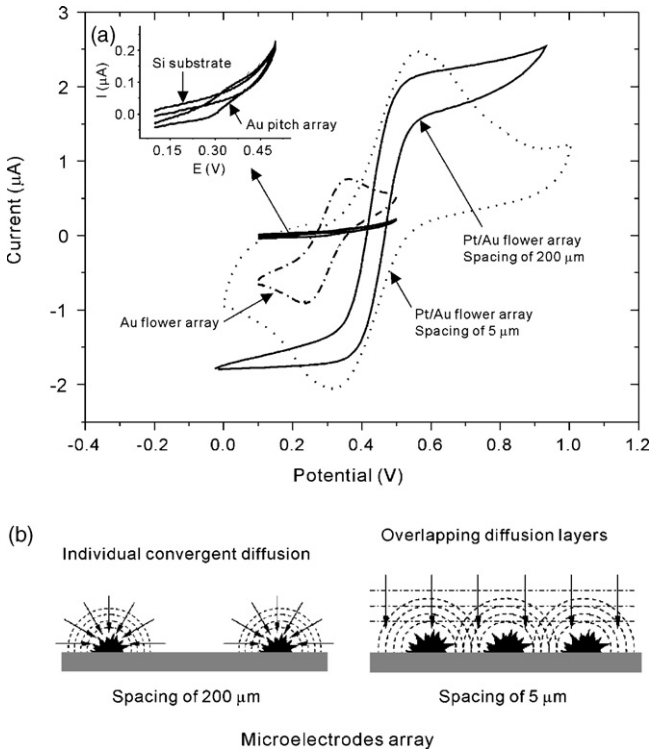

Fig. 4. Enhanced voltammetric responses of Pt/Au bimetallic hierarchical structure array electrode. (a) Cyclic voltammograms of the Si substrate, a 10×10 Au pitch array, Au microflower array (10×10), and Pt/Au bimetallic hierarchical structure array (10×10, with spacing of 200 and 5 μm) electrodes in 0.125 mM $Fe(CN)_6^{3-}$. Scan rate: 0.005 V s^{-1}. The inset shows the cyclic voltammograms of the Si substrate and a pure Au pitch array in high-resolution; (b) illustration of diffusion domain of Pt/Au bimetallic hierarchical structure array electrode with different spacing.

and corrugated surface. Some leaflike flakes are interdigitatedly arranged around the flower and form a multilayer structure, which emanates from the cores to the outside. Numerous gaps between the interdigitated flakes can be observed. It is expected that each hierarchical structure provides a higher surface area, which can accommodate much more enzymes or other biomolecules in a given region. Furthermore, the signal from the arrays of sensors can be amplified many times compared to that seen from a single electrode. Consequently, we can expect an enhanced voltammetric response for biosensing.

The structures of the Pt/Au particles were confirmed with a dual-beam FIB image, transmission electron microscopy (TEM), selected area electron diffraction (SAED) pattern, and X-ray diffraction (XRD) pattern. Fig. 3a shows a dual-beam FIB image of the Pt/Au bimetallic particle. The image suggests that the particle is polycrystal. TEM image (Fig. 3b) and SAED (Fig. 3c) pattern shows that the Pt/Au structure includes many small grains that have independent orientations, further demonstrating its polycrystalline structure. Fig. 3d presents an XRD pattern of the sample shown in Fig. 2. Broad diffraction peaks corresponding to metallic Pt and Au are observed which are indicative of the presence of nanosized Pt/Au particles [21].

The fabricated Pt/Au arrayed-electrode was firstly characterised voltammetrically using redox couples, $Fe(CN)_6^{4-}/Fe(CN)_6^{3-}$, a well-defined and known metal complex that undergoes a fast, reversible one-electron reduction in the following sections. Fig. 4a shows the comparison results of cyclic voltammograms for the Si substrate, a 10×10 Au pitch array, Au microflower array (10×10), and Pt/Au bimetallic array (10×10, with different spacing) electrodes in 0.125 mM $Fe(CN)_6^{3-}$. The electrochemical responses of Si substrate and a 10×10 Au pitch array are extremely weak and could be ignored in comparison with that of Au and Pt/Au bimetallic hierarchical structure array. Therefore, it is realistic to consider that the signals at the latter two electrodes can be attributed to the Au and Pt/Au bimetallic array. Considering that the sharp edges or tips on the nano/micro-metal particles have been theoretically demonstrated to increase electric-field enhancement [22], the voltammetric features of the Au microflower array electrode are obviously due to the presence of a large surface area as well as nanoscaled sharp edges or tips on the flower surface. The large surface area can be confirmed by the high capacitance (C) which was calculated from the cyclic voltammogram [23] with $C = i/v$, where i is the current and v is the scan rate (V s^{-1}). At a potential of 0.2 V, as an example, the effective capacitance is over 20 times larger than that of the Au pitch array electrode. Directly, the surface area can be calculated by Randles–Sevcik equation as 4.25×10^{-4} cm^2. However, at Pt/Au bimetallic microflower array electrode, it is interesting that not only the response currents extremely increase but also the potential window becomes wide. Meanwhile, the arrayed electrode with spacing of 5 μm exhibits a similar macroelectrode cyclic voltammetry, and the arrayed electrode with spacing of 200 μm shows a microelectrode voltammetric behavior. We suggest that the addition of metal Pt has noticeable influence on the electrochemical reactions.

What should be the reasons of the Pt/Au bimetallic hierarchical structure array electrode be for it to result in a similar macroelectrode and microelectrode cyclic voltammetry? To answer this, we analyzed the influence of non-linear diffusion on the cyclic voltammetric response of Pt/Au bimetallic microflower array electrode, as illustrated in Fig. 4b. Compton et al has demonstrated the effect of different domain radius of the plane electrodes on the cyclic voltammograms by simulation [24]. For single plane microelectrode, the sigmoidal shape characteristic voltammetric responses can be ascribed to the convergent diffusion. Based on these results, we suggest the diffusion at an individual Pt/Au bimetallic array electrode will be spherically convergent diffusion due to the high roughened surface. As increasing the flower number to an array, two modes should be considered here, one is that if the spacing between the flowers (each flower can be considered as individual microelectrode) is narrow, the diffusion layers of adjacent microelectrodes may start to overlap resulting in a situation where solution on the "overlapping region" is similar to a macroelectrode [24]. The extreme of this diffusion layer overlap is complete diffusion over the whole surface, resulting in near linear concentration profiles and therefore, the voltammetric response will no longer resemble that of individual microelectrodes but rather display characteristics similar to macroelectrode cyclic voltammetry. The array's peak current is therefore given below [25]:

$$|I_p| = 2.69 \times 10^5 \pi n^{3/2} D^{1/2} c v^{1/2} N(\overline{r_d}^2 + \sigma^2)$$

where $\overline{r_d}^2$ is the mean electrode radius, σ the standard deviation of electrode radius, N the number of electrons transferred, v the potential scan rate, D the diffusion coefficient, n the electron number, and c is the concentration. The other is that if the spacing between the microflower is so wide that each with their own undisturbed diffusion layer, the arrayed electrode still presents the behavior of microelectrode. The total array current is the sum of the limiting currents from each constituent electrode [25]:

$$|I_{\lim}| = N \int_0^\infty |i_{\lim}| f(r_d) \mathrm{d}r_d,$$

where N is the total number of microelectrode present, r_d the electrode radius, and $i_{\lim}$ is the limiting current of each microelectrode.

Fig. 5 displays the result after the immobilization of L-glutamate oxidase on Pt/Au bimetallic hierarchical surface. As can be seen, L-glutamate oxidase was uniformly immobilized onto the surface. After immobilization, hierarchical structure is still seen clearly.

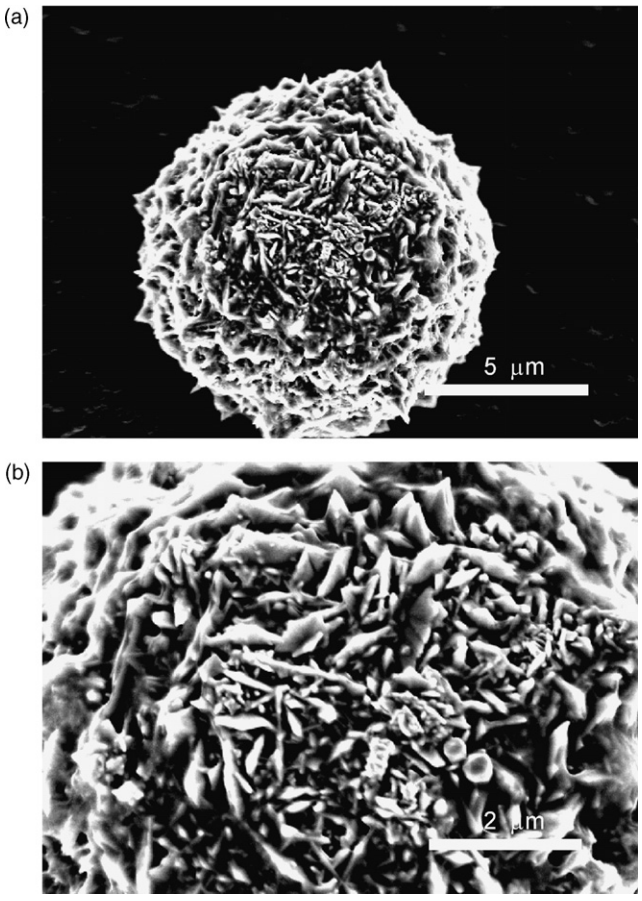

Fig. 5. Typical SEM images of Nafion and L-glutamate oxidase immobilized Pt/Au bimetallic hierarchical structure. (a) Low magnification. (b) High magnification.

This highly roughened structure with enzyme immobilization provides a higher surface area, which can accommodate much more biomolecules in a given region. Consequently, we can expect a higher level of sensitivity, as will be further discussed by the responses of single and sequential determination of GOT and GPT activity (Figs. 7 and 8).

To reduce the interfering response of some easily oxidized species, such as ascorbic acid and uric acid, Nafion membrane was used in this study. Fig. 6 shows the effect of Nafion membranes with 2.0, 3.5, 5, and 7.5 μl of ethanolic solution containing 5 wt.% of Nafion together with enzyme modification (4.5 μl of the mixed enzyme solution, see Section 2 for the details). As can be seen, in comparison with the case of 2.0 μl of Nafion solution modification, the currents decrease 77.2% and 95.2%, respectively, when 3.5 and 5 μl of Nafion solution was used. For 7 μl of Nafion solution modification, the low response can be ignored. These observations are excellent in agreement with the previously reported [19,20], suggesting that the Nafion membrane would result in an additional diffusion barrier or mass and electron transportation. 2.0 μl Nafion solution was therefore used for the sensors fabrication in the following experiment.

To investigate the biosensor performance of the Pt/Au bimetallic hierarchical structure array, we immobilized L-glutamate oxidase onto the hierarchical surfaces. We prepared a set of different L-glutamate oxidase content electrodes coded as 1#, 2#, 3#, and 4# for GOT and GPT single determinations. Fig. 7 shows the calibration curves for GOT and GPT at different loading of L-glutamate oxidase. The rates of the reaction (μA/min) were plotted against the GOT and GPT activity, respectively, over the range of 20–180 U l^{-1} (GOT,

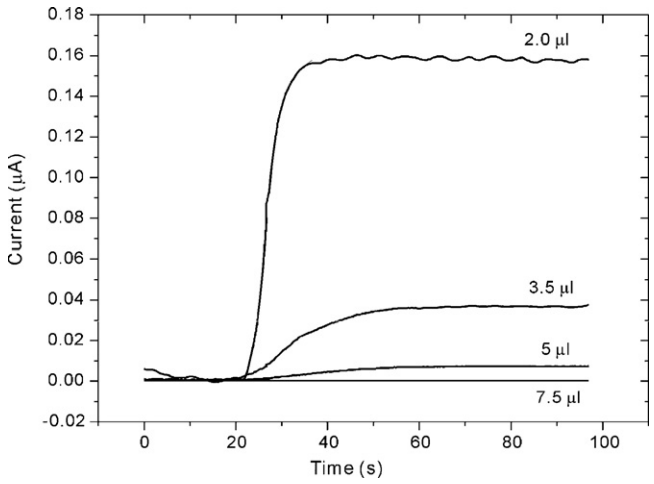

Fig. 6. Effect of Nafion film (different Nafion/ethanol volumes) immobilized on the surface of Pt/Au bimetallic hierarchical structure. Measurements were carried out with 1 mM α-ketoglutarate, 25 mM L-aspartate, and 80 U l^{-1} GOT.

Fig. 7a) and 20–140 U l^{-1} (GPT, Fig. 7b). And thus suggests that the Pt/Au bimetallic arrayed electrode may function as a biosensor.

Fig. 8 shows the studies of the sequential determination of GOT and GPT activity (4# electrode) by adding L-alanine into the reac-

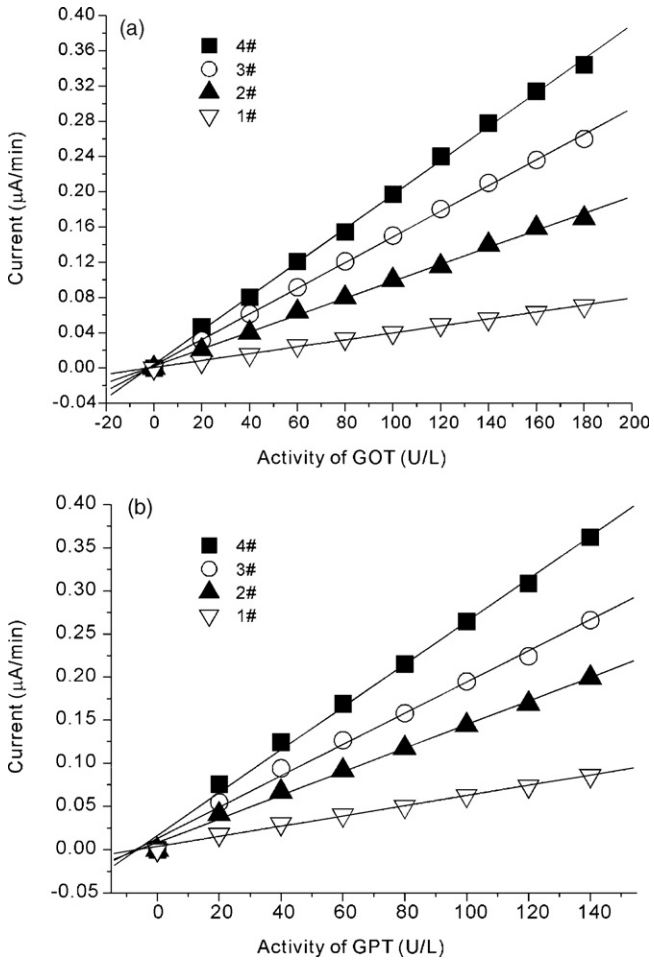

Fig. 7. Activity of (a) GOT and (b) GPT measured with different L-glutamate oxidase contents. The initial potential was 0.3 V. GOT: 100 mM pH 7.0 PBS buffer containing 1 mM ketoglutarate and 25 mM L-aspartate. GPT: 100 mM PBS buffer (pH 7.0) containing 1 mM ketoglutarate and 100 mM L-alanine as substrates.

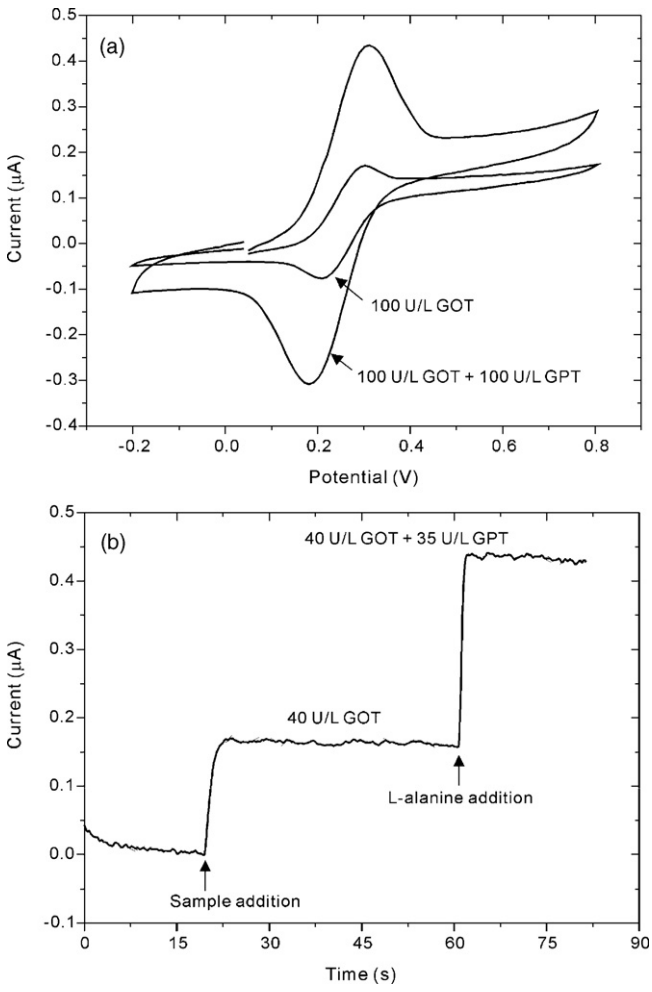

Fig. 8. Electrochemical responses of Pt/Au bimetallic hierarchical structure array electrode (4# electrode) with spacing of 200 μm to GOT and GPT activity in PBS (pH 7.0) containing 1 mM α-ketoglutarate, 25 mM L-aspartate, 100 U l^{-1} GOT, and 100 U l^{-1} GPT before (GOT activity) and after (GPT activity) L-alanine addition. Scan rate was 0.1 V s^{-1}. (a) Cyclic voltammograms of the sequential determination of GOT and GPT activity; (b) response curve for the sequential determination of GOT and GPT activity as a function of time. The initial potential was 0.3 V.

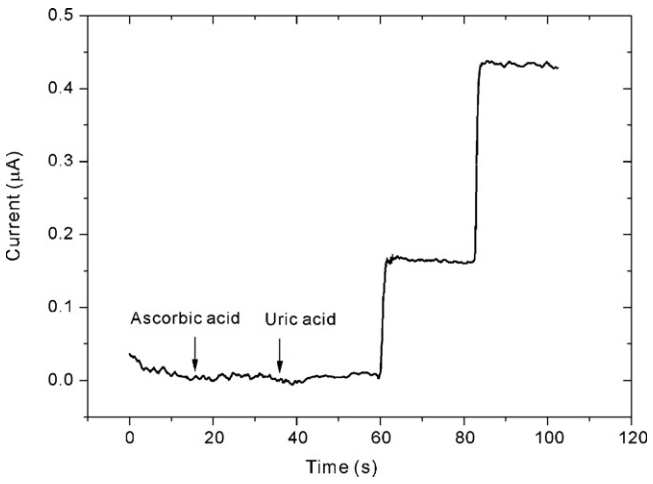

Fig. 9. Measurements of the L-glutamate electrode exposed to 0.2 mM ascorbic acid and 0.2 mM uric acid followed by the determination of 40 U l^{-1} GOT and 35 U l^{-1} GPT activity. 2.0 μl of Nafion solution was used in this measurement.

tion cell before and after the addition of L-alanine. Fig. 8a reveals the cyclic voltammograms of 100 U l^{-1} GOT and 100 U l^{-1} GPT activities. Before L-alanine addition, a significant increased current is observed. This implies that the reaction between ketoglutarate and L-aspartate was specifically catalyzed by GOT. As the addition of L-alanine was carried out, the current increased substantially, indicating that the reaction between ketoglutarate and L-alanine was catalyzed by GPT. The responses were 0.15 and 0.42 μA, respectively. This value is higher than those of biosensors employing a gold film matrix [26]. To continue to probe the high sensitivity of Pt/Au matrix biosensor, we investigated the real-time current behavior at a constant electrode potential of 0.3 V where the oxidation current peak appears shown in Fig. 8a. The result is presented in Fig. 8b. The response is very fast in reaching a dynamic equilibrium upon the addition of the sample solution and L-alanine, generating a steady-state current signal within several seconds. The current reaches 0.08 μA at 40 U l^{-1} GOT and 0.22 μA after the addition of 35 U l^{-1} GPT. This fast and high response can be explained by the fact that the unique hierarchical structure and array lead to the effective electron transfer from the substrate to products through the Pt/Au matrixes that contain enzymes.

The above studied shown in Figs. 7 and 8 demonstrate that Pt/Au bimetallic arrayed biosensors are capable of highly sensitive to real-time detection of GOT and GPT, although other interferences such as ascorbic acid and uric acid should be considered. To explore this issue, we studied the performance of the presented biosensor by the addition of ascorbic acid and uric acid before sequential determination of GOT and GPT activity. Time-dependent current measurements are presented in Fig. 9. Obviously, when 2.0 μl of Nafion solution was used, Pt/Au bimetallic arrayed biosensors do not exhibit a current change after adding ascorbic acid. Also, addition of uric acid does not result in a change in current, whereas subsequent addition of α-ketoglutarate, L-aspartate, GOT, GPT, and L-alanine addition produces a current increase. These controls show that there is little influence of ascorbic acid and uric acid on the L-glutamate biosensing, suggesting that the biosensors also exhibit highly selective real-time detection of GOT and GPT activity.

Finally, we should point out that the reproducibility and stability of the present biosensors are excellent. We ultrasonicated the substrate covered by Pt/Au bimetallic structure before enzyme modification, no changes can be observed. This is because of the use of photolithographic techniques. The Pt/Au bimetallic particles tightly attach Au pitches.

4. Conclusions

A novel matrix for enzyme immobilization was successfully developed by using Pt/Au bimetallic hierarchical structure with micro/nano-array to generate highly sensitive biosensors for GOT and GPT determination. The amount of Nafion membrane affects the mass and electron transfer of the biosensors. The response is dependent on the enzyme content. As increasing enzyme loading, the current increases. The optimized Pt/Au bimetallic biosensors are constituted by 2.0 μl of Nafion solution, 4.5 μl of enzyme solution. The biosensors exhibit high sensitivity. The linear range of the sensor was 20–180 U l^{-1} GOT activity and 20–140 U l^{-1} GPT activity, respectively. The current reaches 0.08 μA at 40 U l^{-1} GOT and 0.22 μA after the addition of 35 U l^{-1} GPT. Also, the biosensors exhibit high selectivity, there is little influence of ascorbic acid and uric acid on the responses when real-time detecting GOT and GPT activity. This Pt/Au bimetallic array based biosensor is capable of generating enhanced responses an order of magnitude higher than that reported in the recent literature [19,20,26] by accounting for the "plugging into enzymes" effect [27] of hierarchical structures, the prefect arrays, and Pt addition, even though more work will have to be done to confirm their effects, such as Pt:Au ratios in the structure and the size of the hierarchical structures. Therefore,

we believe that this study will provide a good inspiration in the development of new generation amperometric biosensors.

Acknowledgements

This work was supported by the National Research and Development Program (NRDP, 2005-01274) for biomedical function monitoring biosensor development sponsored by the Korea Ministry of Science and Technology (MOST), as well as by the NRL program under a Korea Science and Engineering Foundation grant funded by the Korean government (MOST) (No. R0A-2007-000-20028-0).

References

[1] X.J. Huang, C.C. Li, B. Gu, J.H. Kim, S.O. Cho, Y.K. Choi, J. Phys. Chem. C 112 (2008) 3605.
[2] X.A. Dai, R.G. Compton, Anal. Sci. 22 (2006) 567.
[3] X.J. Huang, H.S. Im, D.H. Lee, H.S. Kim, Y.K. Choi, J. Phys. Chem. C 111 (2007) 1200.
[4] B.K. Jena, C.R. Raj, Langmuir 23 (2007) 4064.
[5] J.C.M. Hafkenscheid, C.C.M. Dijt, Clin. Chem. 25 (1979) 55.
[6] G.V. Purcell, D.B. Behenna, P.R. Walsh, Clin. Chem. 25 (1979) 780.
[7] E.J. Sampson, V.S. Whitner, C.A. Burtis, S.S. McKneally, D.M. Fast, D.D. Bayse, Clin. Chem. 26 (1980) 1156.
[8] H.G. Lang, S. Maldonado, K.J. Stevenson, B.D. Chandler, J. Am. Chem. Soc. 126 (2004) 12949.
[9] C.W. Chen, T. Serizawa, M. Akashi, Chem. Mater. 14 (2002) 2232.
[10] D.I. Garcia-Gutierrez, C.E. Gutierrez-Wing, L. Giovanetti, J.M. Ramallo-Lopez, F.G. Requejo, M. Jose-Yacaman, J. Phys. Chem. B 109 (2005) 3813.
[11] X.J. Huang, J.H. Kim, Y.K. Choi, Gold Bull. 41 (2008) 58.
[12] Y.B. Lou, M.M. Maye, L. Han, J. Luo, C.J. Zhong, Chem. Commun. 5 (2001) 473.
[13] M.M. Maye, N.N. Kariuki, J. Luo, L. Han, P. Njoki, L.Y. Wang, Y. Lin, H.R. Naslund, C.J. Zhong, Gold Bull. 37 (2004) 217.
[14] L. Qian, X.R. Yang, J. Phys. Chem. B 110 (2006) 16672.
[15] M.L. Wu, D.H. Chen, T.C. Huang, Chem. Mater. 13 (2001) 599.
[16] S.G. Zhou, K. McIlwrath, G. Jackson, B. Eichhorn, J. Am. Chem. Soc. 128 (2006) 1780.
[17] D. Garcia-Gutierrez, C. Gutierrez-Wing, M. Miki-Yoshida, M. Jose-Yacaman, Appl. Phys. A: Mater. Sci. Proc. 79 (2004) 481.
[18] D. Lee, J. Lee, J. Kim, J. Kim, H.B. Na, B. Kim, C.H. Shin, J.H. Kwak, A. Dohnalkova, J.W. Grate, T. Hyeon, H.S. Kim, Adv. Mater. 17 (2005) 2828.
[19] K.S. Chang, C.K. Chang, S.F. Chou, C.Y. Chen, Biosens. Bioelectron. 22 (2007) 29140.
[20] S.T. Pan, M.A. Arnold, Talanta 43 (1996) 1157.
[21] L.H. Lu, R. Capek, A. Kornowski, N. Gaponik, A. Eychmuller, Angew. Chem. Int. Ed. 44 (2005) 5997.
[22] K.L. Kelly, E. Coronado, L.L. Zhao, G.C. Schatz, J. Phys. Chem. B 107 (2003) 668.
[23] C.Y. Liu, A.J. Bard, F. Wudl, I. Weitz, J.R. Heath, Electrochem. Solid State Lett. 2 (1999) 577.
[24] C.E. Banks, T.J. Davies, G.G. Wildgoose, R.G. Compton, Chem. Commun. 7 (2005) 829.
[25] I. Streeter, R.G. Compton, Sens. Actuators B: Chem. 130 (2008) 620.
[26] H.Q. Li, Z.H. Guo, H. Wang, D.F. Cui, X.X. Cai, Sens. Actuators B: Chem. 119 (2006) 419.
[27] Y. Xiao, F. Patolsky, E. Katz, J.F. Hainfeld, I. Willner, Science 299 (2003) 1877.

Talanta 78 (2009) 1339–1344

Contents lists available at ScienceDirect

Talanta

journal homepage: www.elsevier.com/locate/talanta

Simultaneous fluorimetric determination of the biodegradation processes of dissolved multi-component PAHs

Ling Zi Sang [a], Xing Yuan Wei [b], Jia Ning Chen [b], Ya Xian Zhu [a], Yong Zhang [b,*]

[a] Department of Chemistry, Xiamen University, Xiamen 361005, PR China
[b] State Key Lab of Marine Environmental Science (Xiamen University), Environmental Science Research Center, Xiamen University, Xiamen 361005, Fujian Province, PR China

ARTICLE INFO

Article history:
Received 12 December 2008
Received in revised form 1 February 2009
Accepted 3 February 2009
Available online 13 February 2009

Keywords:
Fluorimetry
Dissolved
Multi-component polycyclic aromatic hydrocarbons
Biodegradation

ABSTRACT

A fluorimetric method for simultaneous determination of dissolved acenaphthylene (Ace) phenanthrene (Ph) and pyrene (Py), mixed in an aqueous mineral salts medium (MSM), was developed. The linear ranges for determination of Ace, Ph and Py dissolved in the mixture were 4.00×10^{-6} to 3.00×10^{-3} g/L, 2.00×10^{-6} to 1.00×10^{-3} g/L and 7.00×10^{-7} to 1.00×10^{-4} g/L. The limits of detection for Ace, Ph and Py were 8.53×10^{-7}, 4.98×10^{-7} and 6.01×10^{-8} g/L and the relative standard deviations 1.05%, 1.62% and 1.16% ($n = 8$), respectively. Satisfactory results were obtained when this method was used to simultaneously study the biodegradation processes of mixtures of dissolved Ace, Ph and Py in an MSM aqueous solution.

1. Introduction

Polycyclic aromatic hydrocarbons (PAHs) are organic contaminants of significant environmental concern, since they are well known teratogenic, carcinogenic and mutagenic agents [1]. The persistence of PAHs in the environment poses a potential threat to human health through bioaccumulation and biomagnification via food chains [2]. Therefore, removal of PAHs from contaminated environments is of significant concern.

At present, microbial degradation is believed to be one of the principal and environmentally friendly means of successfully removing PAHs from contaminated environments [3–5]. In the last decades, PAH biodegradation processes and their mechanisms have been extensively studied using high performance liquid chromatography (HPLC), gas chromatography (GC) and GC with mass spectrometric detection (GC–MS) [6–12]. However, the initial concentration of PAHs, used to carry out the biodegradation processes in the laboratory, were usually as high as several milligrams per liter, and sometimes even hundreds or thousands of milligrams per liter, so as to meet the requirement of sample pretreatment processes and the detection limits of these HPLC, GC or GC/MS methods [5,12]. The results obtained using these methods usually lead inevitably to a misunderstanding of PAH biodegradation processes in the environment, due to the fact that concentrations of PAHs in the environment are much lower than those used in laboratory experiments. On the other hand, traditional research methods for the determination of PAHs are time-consuming, arduous, and need a large amount of organic solvent, with separation and extraction procedures which might cause secondary pollution problems [11,12]. In addition, utilization of entirely destructive chemical extraction techniques during sample pretreatment for traditional methods can destroy the originally existing forms and eliminate the originally existing state of the PAHs in environmental samples. Thus, the results derived from these traditional methods only reflect the total concentration of PAHs in the samples and are difficult to use in order to comprehensively understand the biodegradation processes of the bioavailable fractions of PAHs in environmental samples. It is known that the fraction of PAHs dissolved in the environment has a crucial relationship with their bioavailability and toxicity, and the biodegradation rate of PAHs is directly related to their solubility and mass transfer rates in the aquatic environment [13,14]. Since we need to comprehensively understand the environmental behavior of PAHs, it was necessary for us to first study the biodegradation processes of dissolved PAHs in the aquatic environment. The most important step was to develop a rapid, accurate and user friendly method to quantify the variation of dissolved PAHs, especially of multi-component PAHs in a mixture, during their biodegradation in aqueous solutions.

It is well known that PAHs are suitable for study using luminescence because of their high native fluorescence quantum yield. Synchronous fluorimetry (SF) is already widely used for multi-component PAH analysis, because of its high sensitivity and

* Corresponding author. Tel.: +86 592 2188685; fax: +86 592 2184977.
E-mail address: yzhang@xmu.edu.cn (Y. Zhang).

0039-9140/$ – see front matter © 2009 Elsevier B.V. All rights reserved.
doi:10.1016/j.talanta.2009.02.009

acceptable selectivity [15]. In 2004, a fluorimetric method for studying the biodegradation process of dissolved pyrene (Py) in MSM solution was proposed [5]. A method for simultaneous determination of 2-component PAHs by SF is also reported [16]. However, approaches to the simultaneous determination of three or more multi-component PAHs in aqueous solutions have rarely been published, even though PAHs are not encountered alone in the environment. To the best of our knowledge, the greatest difficulty involves selecting a suitable synchronous wavelength interval ($\Delta\lambda$) for all of the target components in mixtures, for one SF scan. This is because a non-optimized $\Delta\lambda$ will possibly lead to a weakening of the fluorescent signal of some components and damage the sensitivity of the method. Moreover, PAHs with high molecular weight structures often have a stronger toxicity and so their biodegradation in aqueous solution is rarely studied [1]. Therefore, researches on the biodegradation of these PAHs make practical sense.

In this work, acenaphthylene (Ace), phenanthrene (Ph) and Py, with 3, 3 and 4 rings in their molecular structure, were selected as model PAH compounds. Based on the many advantages of 3-dimensional fluorimetry, and using the conventional excitation and emission spectra of each target component in aqueous solution, optimized wavelengths were selected and a fluorescence method for simultaneous determination of Ace, Ph and Py mixed in an aqueous mineral salts medium (MSM) was developed. Satisfactory results were obtained when this type of fluorimetry was used for the simultaneous study of the biodegradation processes of these three PAHs dissolved in MSM solution.

2. Materials and methods

2.1. Apparatus

All spectra were obtained using a Cary Eclipse fluorescence spectrophotometer (Varian, USA) equipped with a 150W Xenon flash lamp. The spectrofluorimeter was controlled by Cary Eclipse software for acquiring and processing the spectral data. With such software, each fluorescence intensity of multi-component PAHs could be obtained in one scan, since optimized wavelengths for each of them were set up before scanning. Fluorescence measurements were performed using a standard 1 cm × 1 cm quartz cell.

The fluorescence signals of the three PAHs were obtained simultaneously using the following instrumental parameters: excitation and emission slits were both set at 5 nm, the scan speed was 600 nm/min, and the PMT voltage set at 600 V.

2.2. Chemicals and media

Stock solutions of Ace (Aldrich, USA, purity >99%), Ph (Aldrich, USA, purity >99.5%) and Py (Aldrich, USA, purity >99%) were prepared by dissolving the solutes in dichloromethane. They were stored at 4 °C in brown volumetric flasks to avoid possible photolysis. The concentration of the Ace, Ph and Py standard solutions were all 0.20 g/L.

Mineral salt solution was used as the MSM [$(NH4)_2SO_4$, 1000 mg; Na_2HPO_4, 800 mg; K_2HPO_4, 200 mg; $MgSO_4{\cdot}7H_2O$, 200 mg; $CaCl_2{\cdot}2H_2O$, 100 mg; $FeCl_3{\cdot}H_2O$, 5 mg; $(NH_4)_6Mo_7O_{24}{\cdot}H_2O$, 1 mg; 1000 mL of Milli-Q water; pH 7.0]. Milli-Q water was used throughout the experiment.

Individual aqueous solutions of Ace, Ph and Py, together with a mixture of the three, were prepared by transferring small aliquots of each stock solution into several colorimetric tubes. After allowing evaporation of the solvent by a gentle flow of high-purity nitrogen gas (≥99.99%), the MSM solution was added to the mark in all the colorimetric tubes in order to obtain their calibration curves. To study the biodegradation processes, colorimetric tubes were replaced by conical flasks. Working MSM solutions of the individual Ace, Ph and Py, and the three of them in a mixture, were prepared. All conical flasks were ultrasonicated in an ultrasonic water bath (Model KQ-3200, power 150W) for 20 min at room temperature, kept in the dark for 8 h to ensure that the target PAHs were sufficiently dissolved, as well as to avoid possible photolysis. The concentration of each individual PAH, and the concentrations of the PAHs in the mixture in the MSM aqueous solutions were within their solubility to ensure that all of them were "truly dissolved".

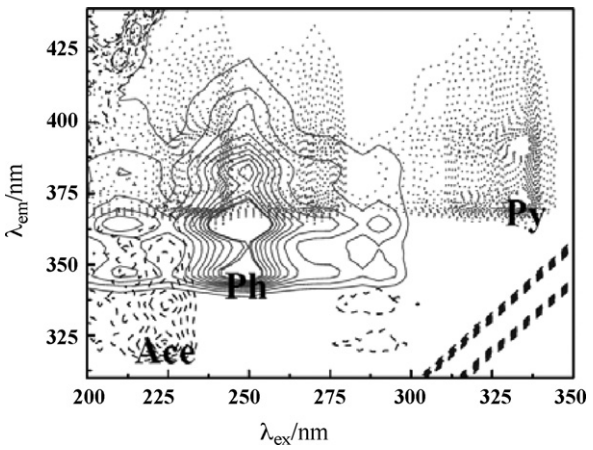

Fig. 1. Theoretical contour map of Ace, Ph and Py and their measurement points. Concentrations of Ace, Ph and Py were 3.0, 1.0 and 0.1 mg/L respectively.

2.3. Microorganisms

The bacterial strains MEBIC5138 (*Mycobacterium duvalii*) and MEBIC5139 (*Mycobacterium flavescens*) were used as degraders. The culture medium (50 mL) for each bacterial strain, each bacterial stain became turbid after 72 h incubation in two 150 mL conical flasks, shaken at 150 rpm at 25 °C. Then the solution of the microorganisms was equally divided and transferred into six centrifuge tubes. After 15 min centrifugation, the liquid was discarded. This procedure was repeated three times for each bacterial strain just before use to ensure that all of the culture medium was clean.

3. Results and discussion

3.1. Theoretical contour map and fluorescence spectra of Ace, Ph and Py

In developing a fluorescence method, one of the important objects was to select optimized excitation and emission wavelengths for each target component in the mixture. Three-dimensional spectra of Ace, Ph and Py individually in MSM solution were scanned. The data obtained were analyzed and processed using Origin software and the theoretical contour map for each component was superposed [17] as shown in Fig. 1. As can be seen from Fig. 1, three "measurement points", without fluorescence interference each other for Ace, Ph and Py can be picked out respectively. Based on the experimental results obtained by conventional fluorimetry, as shown in Fig. 2, the accurate excitation and emission wavelengths for Ace, Ph and Py, with which three of the PAHs in a mixture in MSM solution can be simultaneously determined in one scan using Cary Eclipse, were 225.00/321.07 nm, 249.06/347.07 nm and 333.07/372.00 nm, respectively.

Considering these optimized excitation and emission wavelengths, excitation and emission spectra of each individual component and the MSM solution mixture were scanned. The fluorescence signal for the measured points of each component

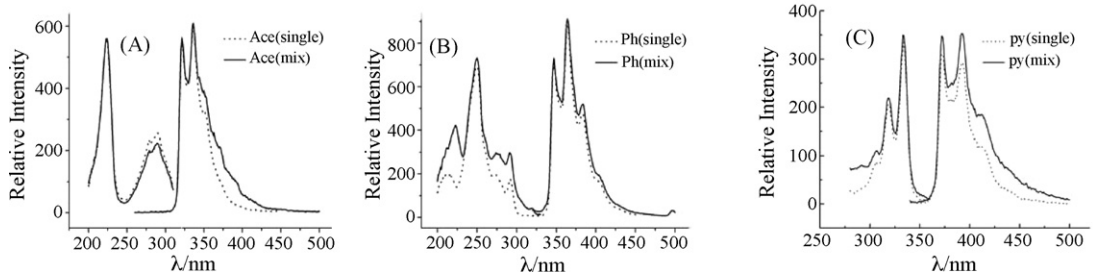

Fig. 2. Fluorescence excitation and emission spectra as individual component (dashed line) and in a mixture (solid line). (A) Ace (3.0 mg/L, λ_{ex} = 260.93 nm, λ_{em} = 304.00 nm). (B) Ph (1.0 mg/L, λ_{ex} = 249.06 nm, λ_{em} = 347.07 nm). (C) Py (0.1 mg/L, λ_{ex} = 333.07 nm, λ_{em} = 372.00 nm).

Table 1
Calibration curves and their correlation coefficients.

Analytes	Calibration equation[a]	Linear range (g/L)	Correlation coefficient (r)	LOD (g/L)	Apparent solubility in MSM solution (g/L)
Ace	$I = 223488C + 4.570$	4.0×10^{-6} to 3.0×10^{-3}	0.9975	8.53×10^{-7}	3.50×10^{-3}
Ph	$I = 1332520C + 6.225$	2.0×10^{-6} to 1.0×10^{-3}	0.9898	4.98×10^{-7}	3.00×10^{-3}
Py	$I = 3771870C + 3.206$	7.0×10^{-7} to 1.0×10^{-4}	0.9974	6.01×10^{-8}	1.50×10^{-4}

[a] The calibration equation relates the fluorescence intensity (I) and the concentration of analyte (C g/L).

individually and in the mixture (such as the excitation and emission spectra presented in Fig. 2) showed little difference. The fluorescence intensity of the mixture of the three components was same or a little less than that for the individual components.

3.2. The apparent solubility of Ace, Ph and Py and analytical figures of note

It has been reported that co-existing organic and inorganic compounds may alter the apparent solubility of PAHs in aqueous solutions [18–20]. Furthermore, as an important factor that controls the biodegradation kinetics of PAHs and their mobilization rates, the apparent solubility of Ace, Ph and Py must be determined before carrying out a study of their biodegradation processes in an MSM aqueous solution mixture [14].

Three series of standard solutions were prepared for the mixture of PAHs. In each series, the concentration of one component was variable and the others were fixed. The fluorescence intensity of each of the PAHs was determined using the developed method. Results showed that a good linear relationship existed between the fluorophore concentration and the fluorescence intensity, and the apparent solubility of Ace, Ph and Py in the MSM solution mixture was determined using the reported method [5,21], and the results are shown in Table 1.

Similarly, the reproducibility of the proposed method was examined by measuring eight replicates with concentrations of 1.50×10^{-3} g/L for Ace, 5.00×10^{-4} g/L for Ph and 5.00×10^{-5} g/L for Py. The fluorescence intensity of the samples was measured and the concentrations of Ace, Ph and Py were calculated together with their calibration equations. The mean values of Ace, Ph and Py were 1.51×10^{-3}, 5.06×10^{-4} and 4.96×10^{-5} g/L with relative standard deviations (RSDs) of 1.05%, 1.62%, and 1.16%, respectively. Meanwhile, using MSM aqueous solution as a blank, the limits of detection (LOD) values for Ace, Ph and Py, which were calculated as the concentration corresponding to the signal multiplied by three times the standard deviation of the blank measurements [16], were obtained as 8.87×10^{-7}, 4.98×10^{-7} and 6.01×10^{-8} g/L.

Table 2
Results of interference experiments.

No.		1	2	3	4	5	6	7	8	9
Ace	Added	2.00	5.00	10.0	2.00	5.00	10.0	2.00	5.00	10.0
($\times 10^{-4}$ g/L)	Found	1.98	5.04	9.88	2.01	4.97	9.94	2.16	5.10	10.2
Ph	Added	5.00	5.00	5.00	10.0	10.0	10.0	20.0	20.0	20.0
($\times 10^{-5}$ g/L)	Found	5.05	5.13	4.99	10.1	10.2	9.93	20.3	19.8	20.0
Py	Added	40.0	40.0	40.0	40.0	40.0	40.0	40.0	40.0	40.0
($\times 10^{-6}$ g/L)	Found	40.2	40.0	40.0	41.2	40.9	40.4	41.5	41.8	40.2

No.		10	101	12	13	14	15	16	17	18
Ace	Added	5.00	5.00	5.00	5.00	5.00	5.00	5.00	5.00	5.00
($\times 10^{-4}$ g/L)	Found	5.09	5.02	5.15	4.90	4.99	5.16	5.05	5.01	5.14
Ph	Added	5.00	5.00	5.00	10.0	10.0	10.0	20.0	20.0	20.0
($\times 10^{-5}$ g/L)	Found	5.11	5.00	5.01	10.0	10.2	9.94	19.9	20.1	19.9
Py	Added	5.00	40.0	80.0	5.00	40.0	80.0	5.00	40.0	80.0
($\times 10^{-6}$ g/L)	Found	4.93	41.7	79.8	4.99	41.7	79.3	4.93	40.4	80.4

No.		19	20	21	22	23	24	25	26	27
Ace	Added	2.00	5.00	10.0	2.00	5.00	10.0	2.00	5.00	10.0
($\times 10^{-4}$ g/L)	Found	1.95	4.93	10.1	2.02	5.05	10.5	1.88	5.13	10.6
Ph	Added	10.0	10.0	10.0	10.0	10.0	10.0	10.0	10.0	10.0
($\times 10^{-5}$ g/L)	Found	9.98	9.88	10.1	10.1	10.2	9.70	10.2	10.0	10.0
Py	Added	5.00	5.00	5.00	40.0	40.0	40.0	80.0	80.0	80.0
($\times 10^{-6}$ g/L)	Found	4.93	5.09	4.86	40.8	39.5	41.0	79.3	80.5	80.2

Table 3
Results of recovery experiments.

No.	Ace			Ph			Py		
	Added ($\times 10^{-4}$ g/L)	Found ($\times 10^{-4}$ g/L)	Recovery (%)	Added ($\times 10^{-5}$ g/L)	Found ($\times 10^{-5}$ g/L)	Recovery (%)	Added ($\times 10^{-6}$ g/L)	Found ($\times 10^{-6}$ g/L)	Recovery (%)
1	5.00	5.11	102.2	9.00	9.60	106.7	9.00	9.29	103.2
2	4.50	4.76	105.8	7.00	6.76	96.50	7.00	6.65	95.00
3	4.00	3.93	98.30	5.00	4.97	99.30	5.00	5.21	104.2
4	3.50	3.37	96.20	3.00	3.11	103.8	3.00	2.83	94.20
5	3.00	2.93	97.80	1.00	0.96	95.70	1.00	0.99	98.80

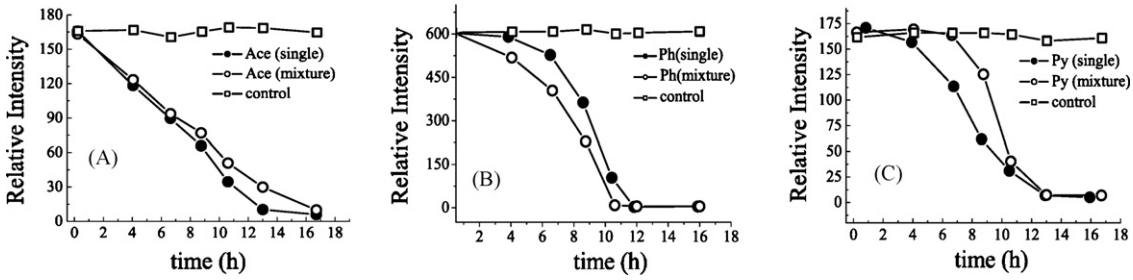

Fig. 3. Biodegradation processes of the three PAHs by MEBIC5138. (A) Concentration of Ace is 3.0 mg/L. (B) Concentration of Ph is 1.0 mg/L. (C) Concentration of Py is 0.1 mg/L.

From Table 1, it can be seen that the determined apparent solubilities of 3.50×10^{-3}, 3.00×10^{-3} and 1.50×10^{-4} g/L for Ace, Ph and Py respectively in mixtures in MSM solution were slightly higher than those of their individual component in the aqueous solution, which were reported as 3.42×10^{-3}, 4.35×10^{-4} and 1.33×10^{-4} g/L, respectively [21]. The determined apparent solubility of 3.50×10^{-3}, 2.50×10^{-3} and 2.50×10^{-4} g/L for Ace, Ph and Py individually in MSM solution showed slightly different from that of the three PAHs in mixtures in MSM solution. The reasons for this phenomenon will be explored elsewhere. Here, we focused mainly on the biodegradation processes in a mixture of PAHs dissolved in MSM solution. On the other hand, fluorescence intensity is a relative value, and it is sensible to ignoring small changes in apparent solubility caused by different co-existing compounds.

3.3. Interference experiments

In order to ensure the tolerance of one target compound to the other two co-existing components, interference experiments were performed. Three series of standard solutions were prepared, in each of which the concentration of Ace, Ph and Py were fixed as low, middle and high concentrations, and the interference caused by the co-existing components was determined (Table 2). As can be seen from this table, when the concentration of Py was fixed at the middle level (labeled as samples No. 1–9) with increasing Ace and Ph concentrations, there was no significant influence on the fluorescence signal of Py caused by the two co-existing components. The RSD for determination of the Py concentration from samples No. 1 to 9 was calculated as 1.71%. Similar conclusions can be drawn from the results from samples No. 10 to 18 for Ace and from samples No. 19 to 27 for Ph; and their RSD values were 1.61% and 1.50%, respectively.

3.4. Recovery experiments

Recovery experiments were performed using the standard addition method. Five samples were prepared, each of them containing the three PAHs in a mixture in the MSM solution. The concentrations of Ace, Ph and Py were 1.50×10^{-3}, 5.00×10^{-4} and 5.00×10^{-5} g/L. Different amount of the three PAHs were added into each sample, and the fluorescence intensity of all three PAHs was simultaneously measured using the developed method. The concentrations of the added Ace, Ph and Py were calculated according to their corresponding calibration equation. Results of the recovery experiments are shown in Table 3, which shows that the recovery for Ace, Ph and Py varied from 94.2% to 106.7%. This illustrated that the accuracy of the method developed was satisfactory.

3.5. Biodegradation of the three PAHs in a mixture in MSM solution

Ace, Ph and Py stock solutions were transferred into a series of erlenmeyer flasks and working solutions of Ace, Ph and Py individually and also in a mixture in MSM aqueous solution were prepared with initial concentrations of 3.00×10^{-3}, 1.00×10^{-3} and 1.00×10^{-4} g/L respectively. After sterilization, MEBIC5138 and

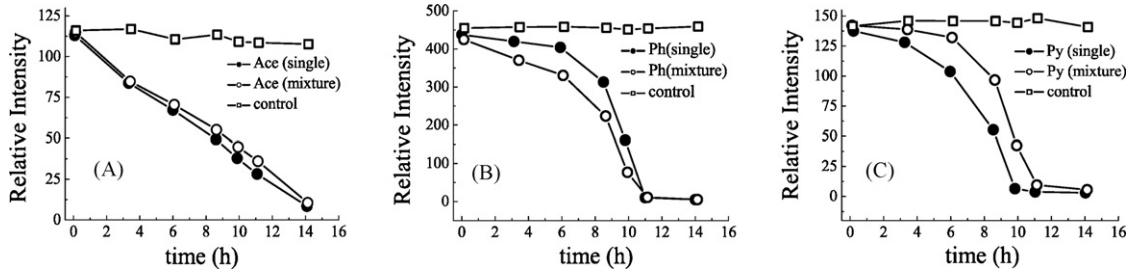

Fig. 4. Biodegradation processes of the three PAHs by MEBIC5139. (A) Concentration of Ace is 3.0 mg/L. (B) Concentration of Ph is 1.0 mg/L. (C) Concentration of Py is 0.1 mg/L.

Table 4
Biodegradation results of the three PAHs by MEBIC 5138 and MEBIC 5139.

	Biodegradation rate (%)								
	Ace			Ph			Py		
	Time (h)	Single	Mixture	Time (h)	Single	Mixture	Time (h)	Single	Mixture
MEBIC 5138	4.08	29.2	26.1	4.05	2.90	14.8	6.67	31.6	1.20
	8.80	60.2	53.5	6.50	13.3	33.5	8.60	62.7	14.4
	10.6	79.6	69.9	8.60	41.0	62.8	10.6	80.0	75.5
	13.0	93.9	82.3	10.4	82.7	84.9	13.0	95.6	95.3
MEBIC 5139	3.38	25.9	26.3	3.28	4.02	12.8	3.34	6.85	2.42
	6.04	40.5	38.8	6.00	7.61	22.2	5.97	24.5	7.15
	8.62	56.4	52.1	8.56	8.48	47.4	8.53	59.8	32.0
	9.90	66.5	61.1	9.86	63.2	81.9	9.83	95.2	70.2
	11.1	75.1	68.6	11.1	97.7	97.4	11.0	97.2	93.3
	14.1	92.5	90.9	14.1	98.8	98.7	14.0	97.7	96.0

MEBIC5139 were incubated with both the individual PAHs and the mixture solution. The initial biomass of MEBIC5138 and MEBIC5139, represented by their OD values, were 0.009 and 0.013. Blank samples without the microbes were also prepared; and all the solutions were incubated at 25 °C and 150 rpm, in the dark. During the biodegradation processes, the variation of Ace, Ph and Py concentration with time in all of the samples was directly measured using the developed method, and the results are shown in Figs. 3 and 4. The biodegradation processes of Ace, Ph and Py, both individually and as a mixture in MSM solution were successfully monitored using the developed method.

It is evident that it took about 10–16 h for both the MEBIC5138 and the MEBIC5139 to completely biodegrade the three PAHs either individually or in the MSM solution mixtures. The total time which the biodegradation processes took was slightly different for MEBIC5138 and MEBIC5139. The total time for Ace and Py to be degraded by MEBIC5139 was 2–2.5 h shorter than that by MEBIC5138. On the other hand, the time taken by MEBIC5139 to degrade Ph was almost 2 h longer than that by MEBIC5138. Furthermore, the biodegradation processes of Ace, Ph and Py showed obvious differences. A relatively longer time was taken at the beginning for MEBIC5138 and MEBIC5139 to degrade Ph and Py. On the contrary, almost no time was taken for MEBIC5138 and MEBIC5139 to start degrading Ace. The fluorescence intensity of the blank samples remained almost at the same level during the whole biodegradation period.

From the results shown in Fig. 3, for MEBIC5138, the biodegradation rate of Ace individually was a little higher than that of in a mixture in MSM solution (Fig. 3A). The biodegradation processes of Ph individually in MSM solution had a nearly 4 h lag phase, which was longer than that of in mixtures (Fig. 3B). However, the lag phase of the biodegradation process of individual Py was shortened by nearly 3 h than that of in a mixture (Fig. 3C). A common phenomenon observed was that the biodegradation rate was obviously expedited in both individual PAH and in the mixture after the lag phases finished. A comparison of the biodegradation rates of the PAHs either individually or in a mixture is shown in Table 4.

From Fig. 4, it can be seen that the biodegradation processes of the three PAHs by MEBIC5139 for each component, or for their mixture, showed a similar tendency to that of the MEBIC5138. This result indicated that their biodegradation processes might be related to the decomposition path or the biodegradation intermediates produced in the processes. As reported in previous work, variation of apparent solubility [14] and co-metabolic degradation [22] are considered to be the main factors that affect the biodegradation rate of PAHs, since the biodegradation processes of PAHs individually or in a mixture each have their own different mechanism [23,24]. Further studies to detect the intermediates produced in the biodegradation processes should be carried out.

4. Conclusions

The results presented in this paper showed that the developed fluorescence method could not only be used successfully for the simultaneous analysis of dissolved Ace, Ph and Py in mixtures in MSM aqueous solution, but also can be conveniently used to simultaneously investigate biodegradation processes of individual dissolved PAHs or a mixture of these in MSM solution, as well as to investigate the capacity difference between the strains used. Compared with the conventional methods, such as HPLC, GC and GC/MS, the method developed was simple, rapid and easy to operate, and no organic solvents were needed for complicated pretreatment. Furthermore, originally existing states of dissolved PAHs both individually or as mixtures in MSM aqueous solution were successfully determined, and their biodegradation processes directly investigated. This, therefore, provides us with a potentially powerful tool for in situ analysis, and to study the environmental behavior of dissolved multi-component PAHs in the lab, especially for real sample analysis and study in the aqueous environment [9–14].

However, only the residual quantities of the target compounds during the biodegradation processes were determined using this method and an analysis of the intermediates (which is also required and even more important for the understanding of into the mechanisms of biodegradation processes) was not achieved in this work. Thus, further studies combining this fluorescence method with other possible methods are needed in the future.

Acknowledgements

The authors wish to acknowledge financial support provided by the NSFC (20577037, 20777062 and 405210003), SRFDP (200803840015) and the NFFTBS (No. J0630429). We would like to express our thanks to Dr. Sang-Jin Kim (Microbiological Laboratory, Korea Ocean Research and Development Institute) for providing us with the bacterial strains and Professor John Hodgkiss for his assistance with English.

References

[1] M. He, Ph.D. Thesis, Tsinghua University, Beijing, China, 2006.
[2] P. Wang, K.Z. Du, Y.X. Zhu, Y. Zhang, Talanta 76 (2008) 1177–1182.
[3] S.Y. Yuan, S.H. Wei, B.V. Chang, Chemosphere 41 (2000) 1463–1468.
[4] Y. Tian, T.L. Zheng, Z. Hu, Chin. J. Appl. Environ. Biol. 9 (2003) 439–443.
[5] Y. Zhang, Y.X. Zhu, K.K. Kwon, J.H. Park, S.J. Kim, Chemosphere 55 (2004) 389–394.
[6] E. Rodríguez, O. Nuero, F. Guillén, A.T. Martínez, M.J. Martínez, Soil Biol. Biochem. 36 (2004) 909–916.
[7] S.Y. Zang, P.J. Li, W.X. Li, D. Zhang, A. Hamilton, Chemosphere 67 (2007) 1368–1374.
[8] D. Garon, S. Krivobok, D. Wouessidjewe, F. Seigle-Murandi, Chemosphere 47 (2002) 303–309.
[9] N. Fuchedzhieva, D. Karakashev, I. Angelidaki, J. Hazard. Mater. 153 (2008) 123–127.

[10] E.C. Santos, R.J.S. Jacques, F.M. Bento, M. do C.R. Peralba, P.A. Selbach, E.L.S. Sa, F.A.O. Camargo, Bioresour. Technol. 99 (2008) 2644–2649.
[11] J.L. Chen, M.H. Wong, Y.S. Wong, N.F.Y. Tam, Mar. Pollut. Bull. 57 (2008) 695–702.
[12] O. Geffard, A. Geffard, E. His, H. Budzinski, Mar. Pollut. Bull. 46 (2003) 481–490.
[13] J.T. Oris, A.J. Hall, J.D. Tylka, Environ. Toxicol. Chem. 9 (1990) 575–583.
[14] S. Viamajala, B.M. Peyton, L.A. Richards, J.N. Petersen, Chemosphere 66 (2007) 1094–1106.
[15] W. Zhang, D.L. Lin, Z.X. Zhou, Y.Q. Li, Talanta 71 (2007) 1481–1486.
[16] Z.Q. Cai, Y.X. Zhu, Y. Zhang, Spectrochim. Acta Part A 69 (2008) 130–133.
[17] J.N. Chen, Z.Q. Cai, Y.X. Zhu, Y. Zhang, Chin. J. Anal. Chem. 3 (2008) 301–305.
[18] J.F. Dong, B.Z. Chowdhry, S.A. Leharne, Colloids Surf. A: Physicochem. Eng. Aspects 246 (2004) 91–98.
[19] Y.J. An, E.R. Carraway, M.A. Schlautman, Water Res. 36 (2002) 300–308.
[20] S. Tanaka, K. Oba, M. Fukushima, K. Nakayasu, K. Hasebe, Anal. Chim. Acta 337 (1997) 351–357.
[21] J. Zhang, Ph.D. Thesis, Graduate School of the Chinese Academy of Sciences, Beijing, China, 2003.
[22] Y. Zhong, T.G. Luan, X.W. Wang, C.Y. Lan, N.F.Y. Tam, Appl. Microbiol. Biotechnol. 75 (2007) 175–186.
[23] H. René van, P. Wattiau, L. Bastiaens, Res. Microbiol. 154 (2003) 199–206.
[24] Y.S. Keum, J.S. Seo, Y. Hu, Q.X. Li, Appl. Microbiol. Biotechnol. 71 (2006) 935–941.

Talanta 78 (2009) 1503–1507

Contents lists available at ScienceDirect

Talanta

journal homepage: www.elsevier.com/locate/talanta

Short communication

Quantification of fullerene nanoparticles suspensions in water based on optical scattering

Juliana A. Sene[a,b], Maurício V.B. Pinheiro[b], Klaus Krambrock[b], Paulo J.S. Barbeira[a,*]

[a] Departamento de Química, ICEx, UFMG, Av. Antônio Carlos 6627, 31270-901 Belo Horizonte, MG, Brazil
[b] Departamento de Física, ICEx, UFMG, Av. Antônio Carlos 6627, 31270-901 Belo Horizonte, MG, Brazil

ARTICLE INFO

Article history:
Received 26 November 2008
Received in revised form 9 February 2009
Accepted 11 February 2009
Available online 21 February 2009

Keywords:
Fullerene
Nanoparticles
Nephelometry
Spectrophotometry

ABSTRACT

Fullerenes, and in particular the C_{60}, have been intensively investigated in the last decades mainly because of their vast range of potential applications in biomedicine and materials science. These molecules are inherently hydrophobic, tending thus to form clusters and aggregates in polar solvents resulting in colloidal suspensions. In this work was developed a quantification method for C_{60} nanoparticles (nano-C_{60}) in colloidal aqueous suspensions based on optical light scattering (nephelometry). This method can be done in a conventional spectrofluorimeter either on the excitation wavelengths or on the second-order satellite lines that arise from the diffraction gratings. The detection limit of the proposed method was about $(0.0090 \pm 0.0008)\,mg\,L^{-1}$, in a linear concentration range from 0.007 to 0.360 $mg\,L^{-1}$. A comparison of this scattering technique with spectrophotometry based on molecular absorption shows that for the former, even at the second-order lines, the threshold concentrations detected are about 20 times lower that the latter.

1. Introduction

Fullerenes are three-dimensional cage-like molecules shaped as closed polyhedra with pentagonal and hexagonal faces. They are essentially composed of a large number of carbon atoms, from 42 up to about 1000. The most common fullerenes, the C_{60} and the C_{70} were discovered in 1985 [1]. The C_{60} in particular, known as 'Buckyminsterfullerene' is the most abundant, and it has a structure that resembles a soccer ball, a truncated icosahedra of I_h symmetry with 12 pentagons and 20 hexagons.

Due to its unique electronic and structural properties [2], the fullerenes have several potential applications in materials science, electronics and biomedicine. Since their synthesis in macroscopic quantities [3], they have been intensively investigated in different forms: in solutions and colloidal suspensions, as nano-crystals (known as fullerites) or thin-films, bonded or immersed in polymers, incorporated in an inorganic phase, or modified with a vast range of functional groups. This of course, depends on the specific application intended.

In biomedicine, the fullerenes can be used in several ways [4]: as enzymatic inhibitors, for DNA photo-cleaving, as radio-isotope carriers for radio-diagnostics and radio-therapy, as photosensitizers in photodynamic therapy, as radical sponges against free-radicals and as drug carrier, for example, for osteoporosis. When modified with functional groups for specific applications the fullerenes tend to conserve their physical and chemical properties, therefore, for most of their applications in biomedicine, fullerene derivatives are investigated, instead of pristine C_{60}.

The major drawback for biomedical applications of C_{60} is their negligible solubility in water [5,6]. Several works have attempted to overcome this difficulty, from attaching polar groups like–OH on the carbon cage as in the case of fullerols [7,8] or micelleating with hydrophilic polymers [9]. In their pure C_{60} phase, fullerene form aggregates in water yielding naturally nanoparticles in suspension.

Such suspensions can also be prepared in different controlled ways for obtaining a monodispersion of different particle sizes [10–12], known as nano-C_{60}. One way to prepare them is by stirring a solution of C_{60} in tetrahydrofurane and water, under argon atmosphere at room temperature for 24 h [12]. In other method, the C_{60} solution with a mixture of organic solvent (toluene or benzene) and water undergoes an ultrasonic treatment. The organic phase evaporates while the C_{60} is incorporated in the aqueous phase [10,11].

The detection and quantification of fullerene traces in water is another problem when dealing with biological applications. It has also impact in environmental sciences, since the effects of fullerene nanoparticles for human health are still controversial [13]. With the drastic enhancement in the production of fullerenes because of their applications, novel analytic methods are required for their quantification with high sensitivity, and although the fullerenes are not water-soluble, colloidal suspensions of stable C_{60} nanoparticles can be formed in high concentrations and transported in water

* Corresponding author. Tel.: +55 3134095767; fax: +55 3134096650.
E-mail address: barbeira@ufmg.br (P.J.S. Barbeira).

0039-9140/$ – see front matter © 2009 Elsevier B.V. All rights reserved.
doi:10.1016/j.talanta.2009.02.029

between biological networks [10]. The high chemical stability of C_{60}, even in the presence of acids or bases [14], indicates that its biodegradation is difficult in biological and environmental systems, though their functional groups, in case of fullerene derivatives, may be lost.

Most methods of fullerene analysis described in the literature involve extraction of fullerenes by organic solvents combined with ultraviolet–visible (UV–vis) spectrophotometry [15] and other techniques, which are highly expensive, like high-performance liquid chromatography (HPLC) [16–20] and high-performance thin layer chromatography [21], both using either mass spectrometer (MS) or UV–vis spectrometer as detectors.

For biological samples, the quantitative extraction of fullerenes is arduous involving several stages and accumulating great losses which reduce the efficiency in small concentration [17]. Direct extraction of C_{60} nanoparticles from water, to organic solvents, is also difficult since the particles are negatively charged. Using toluene as organic solvent such extraction, for 1 h, results in a small efficiency of 1.1% [19]. Moussa et al. [17] developed an analytical method for quantification of C_{60} in blood and tissues of male Swiss mice by HPLC–MS and HPLC–UV–vis using carefully prepared suspensions of C_{60} nanoparticles in water and using C_{70} as internal standard. RP-18 (5 μm) was used as stationary phase and a mixture of acetonitrile and toluene (40:60, v/v) as mobile phase. Linear analytical curves of 0.05 up to 5% of C_{60} per tissue mass, and 0.05 up to 200 mg L^{-1} for blood samples were obtained. The detection limit was about 0.1 ng per injection. With a simplified extraction method Xia et al. [19] obtained a detection limit of 0.34 mg L^{-1}.

For the quantification by UV–vis spectrophotometry, the direct absorbance of the C_{60} in solution (or C_{60} nanoparticles in suspension) is measured at the peak of the molecular absorption bands, followed by the calculation, using the Beer–Lambert Law and the molar absorptivity (ε) for the specific solvent [17]. The C_{60} presents HOMO–LUMO absorption bands when in *n*-hexane at 208, 252 and 380 nm, the latter with ε = 51,000 L mol^{-1} cm^{-1} [11]. In toluene, bands are observed at 332, 399, 515 and 507 nm with ε values of 52,443, 2578, 866 and 774 L mol^{-1} cm^{-1} respectively. A superposition of the C_{60} lines with the toluene UV bands for lower wavelengths occurs [22].

The optical absorption spectrum of C_{60} nanoparticles in water is very similar to the one of the C_{60} in *n*-hexane. In this case the bands are broadened and slightly red-shifted. The strongest bands are observed at 217, 260, 340 nm (with ε = 68,000 L mol^{-1} cm^{-1}), with a weaker one at 450 nm (ε = 21,000 L mol^{-1} cm^{-1}) [11,23]. The direct quantification of fullerene in water by spectrophotometry is however limited for higher concentrations of nanoparticles in suspension. A natural alternative for direct quantification of C_{60} in water would be scattering techniques like nephelometry or turbidimetry, extensively used for quantification of solids in suspension [24], or spectrofluorimetry, which unfortunately is limited by the lack of strong fluorescence bands from the C_{60} molecules and its nanoparticles [2].

In nephelometry, scattered radiation is measured at an angle of 90° to the radiation source while in turbidimetry is measured the decrease in the radiation transmitted power. When the concentration of the scattering particles in the solution is small, the intensity of the transmitted radiation is very similar to the intensity of the radiation source. Thus, nephelometry is a more appropriated choice for samples containing few scattering particles while turbidimetry is more appropriated for samples with high scattering particle concentration. Another important factor in choosing between turbidimetry and nephelometry is the size of scattering particle. For nephelometry the intensity of the scattered radiation is greatest if the particles are small enough that Rayleigh scattering occurs. For larger particles the scattering intensity decreases at 90° so turbidimetry is more suitable [24].

Nephelometry is widely used to determine the turbidity of water samples, drinks and foodstuffs. The turbidity of water can be determined by comparison to the scattered light by the suspended particles in sample and standard formazin solutions in nephelometric turbidity units (NTU). In similar form, the turbidity of samples of orange juice, beer and syrups can be analysed [24].

Several cations and anions also can be determined by nephelometry, after reacting with a specific reagent in appropriate conditions to maintain the solids formed in suspension. Besides the applications in environmental and food areas, the light scattering technique has become an interesting method for determination of micro-amounts of biomacromolecules as immunoglobulins, nucleic acids, specific proteins, coagulation factors and therapeutic drugs [25].

Light scattering techniques have been used for the characterization of nanoparticles, giving information on particle structure or aggregation behavior [26,27] and nephelometry, specifically, was used as particle concentration detector in chromatographic analysis [28]. Although light scattering has been used before, for studying the aggregation dynamics and other properties of C_{60} in solutions [29–32], but no work on the quantification of such particles by using these techniques has been published yet.

The purpose of this work was to develop a simple analytical methodology for quantification of C_{60} in aqueous solutions with high sensitivity. The proposed method uses a standard nephelometric experimental setup and is based on optical incoherent light scattering, which depends linearly on the concentration of the scatter centers, if they are sufficiently spaced from each other [33]. In this case, the scatter centers are the C_{60} nanoparticles in water.

2. Experimental

2.1. Materials and techniques

Fullerene C_{60} from MER Corporation with 99.5% purity was used without further purification. Toluene (F. Maia), with 99.5% purity, was previously distilled. Deionized water (DI water) was obtained from a Simplicity 185 system (Millipore).

For the preparation of the C_{60} colloidal suspensions a Maxiclean 1450 ultrasound, a rota-evaporator Fisatom 802 and a Millipore WP 6111560 vacuum pump were used.

For the characterization of the C_{60} nanoparticles the following equipments were employed: an Atomic Force Microscope (AFM) Nanoscopy® IV from Veeco Metrology Group for imaging the nanoparticles in the tapping mode, and a BI 9000AT Photon Correlation System from Brookhaven Instruments Corporation.

The spectrophotometric experiments were done with a HP 8451A diode array UV–vis spectrophotometer with 1 cm thick quartz cuvette. For the nephelometric experiments we used a Shimadzu RF-5301PC spectrofluorimeter and an appropriate 1 cm thick quartz cuvette. No low-pass or high-pass optical filters were used to suppress second order satellite lines from the diffraction gratings of the spectrofluorimeter.

2.2. Sample preparation

The first solution prepared was a standard C_{60}/toluene solution (FTS) with 10.94 mg of C_{60} (99.5%) in 50.00 mL of toluene, resulting in a concentration of 217.71 mg L^{-1}. For the preparation of C_{60} nanoparticle aqueous suspension (FAS), 2.00 mL of the FTS solution was transferred to a 100 mL round flask adapted for the rota-evaporator, with a size compatible to the ultrasound bath.

About 30 mL of deionized water were then added to the flask and it was gently rotated by the rota-evaporator, without vacuum, inside the ultrasound bath for 1 h. After that, 30 mL of water was

added and the process continued for one more hour. An emulsion was then formed. More 20 mL of water were added to the flask and the mixture was left turning in the ultrasound bath for more 28 h until the emulsion turbidity disappeared.

In order to remove all residual toluene, the solution was left in the ultrasound bath for more 5 h under vacuum. In the sonification process the temperature did not exceed 50 °C and the pressure at the flask was reduced by a mechanical vacuum pump adapted at the vapor output of the rota-evaporator. The obtained suspensions were transparent with a slightly pink hue. They were transferred then to a 100 mL volumetric flask and deionized water was added to complete the volume. A blank solution without C_{60} (FBS) was prepared in the same way.

Four FAS and FBS were prepared to evaluate the reproducibility of the process and the influence of toluene residues on the spectrophotometric and nephelometric measurements.

2.3. Analytical curves

For the construction of the spectrophotometric analytical curves, both the C_{60} nanoparticle suspensions (FAS) and blank solutions (FBS) were diluted in various concentrations. The optical absorption spectra of the four FAS suspensions in different concentration ranges, as well as the respective blank solutions, were done in quintuplicate in the spectral range between 190 and 800 nm using deionized water as reference.

The nephelometric quantification of the C_{60} nanoparticles in the water suspensions were done, as mentioned above, in a spectrofluorimeter by fixing the excitation wavelength and scanning the scattered light spectrum at 90° from the excitation beam in intervals of 10 nm, from 220 up to 900 nm. The excitation was also incremented in 10 nm steps from 220 up to 700 nm. The four FAS with different concentrations and FBS were also measured in quintuplicate.

2.4. Statistical analysis

The absorbance and the intensity of the scattered light as a function of the C_{60} concentration were averaged for the determination of the linear range (LR) and, the detection (DL) and quantification (QL) limits. The detection limits of both methods were calculated by the following equation [34]:

$$\mathrm{DL} = \bar{X} + t_{(n-1,1-\infty)}s$$

where $\bar{X}$ denotes the average value for the control samples (without C_{60}), t the value of the Student parameter for $n-1$ degrees of freedom within an interval of 95% confidence, and s the standard deviation for the five replicates. The quantification limits, on the other hand, were determined from the following equation [34]:

$$\mathrm{QL} = \bar{X} + 10s$$

where $\bar{X}$ is the average value for the control samples and s the standard deviation for the five replicates. These two values were interpolated in the analytical curves in order to obtain the values in terms of C_{60} concentration (mg L^{-1}).

3. Results and discussion

3.1. Characterization of the nanoparticles suspensions

After synthesis, the C_{60} nanoparticle size was characterized by AFM and dynamic light scattering (photon-correlation). The AFM images of a suspension deposited on SiO_2 substrate showed dots with nanometer sizes indicating the presence of C_{60} nanoparticles, as can be seen in Fig. 1. For the same sample, photon-correlation

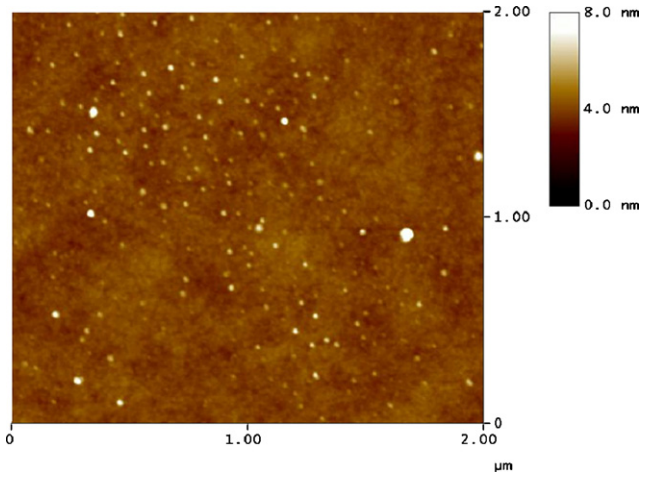

Fig. 1. AFM image obtained for C_{60} aqueous suspension deposited on SiO_2 substrate.

using He-Ne LASER (632.8 nm) has allowed to determine the average size of the nanoparticles in water, 17 ± 2 nm, which is in accordance with the AFM results and other data previously published by other groups (10–50 nm) [10,11].

3.2. Quantification by optical absorption

Optical absorption in the UV–vis range confirmed the presence of fullerene nanoparticles in water as it can be seen in Fig. 2, for the mother solutions as well as their dilutions, after subtraction of the spectra of the blank. The spectra are typical for C_{60} suspensions [10–12,22], and clearly show a decrease of the absorbance at the main bands at 264 and 340 nm with the dilution. The fullerene concentration of the four FAS was calculated by using the molar absorptivity at 344 nm, given by Andrievsky et al. [11] (ε = 68,000 L mol^{-1} cm^{-1}), and the average of the absorbance at this wavelength. This calculation yielded solutions with 2.30–2.95 mg L^{-1} instead of 4.35 mg L^{-1} as expected from the initial fullerene mass.

The analytical curves were built for the bands at 264 and 340 nm (insert in Fig. 2), because of the enhanced sensitivity at these wavelengths and also because these bands were not strongly influenced by the UV bands due to traces of solvent. A slight influence of the solvent was however observed in the 264 nm band. The molar absorptivity, the detection and quantification limits are shown in

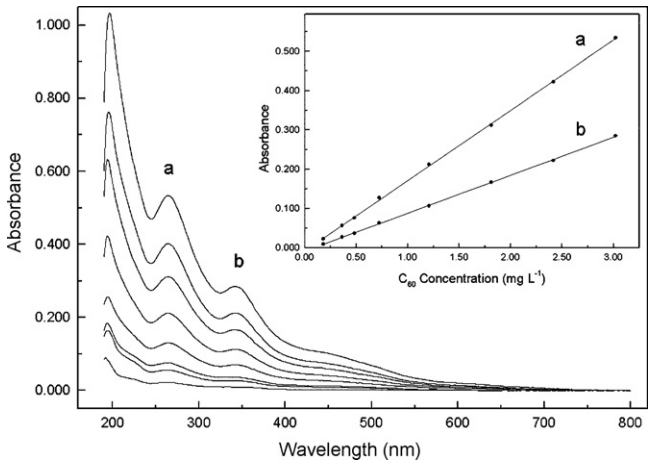

Fig. 2. Optical absorption spectra for different concentrations of C_{60} aqueous suspensions (FAS). The insert shows the two analytical curves, absorbance as function of C_{60} concentration, obtained for 264 and 340 nm.

Table 1
Detection (DL) and quantification (QL) limits, linear range (LR), linear determination coefficient (R^2) and molar absorptivity (ε), obtained from the two analytical curves (at 264 and 340 nm) for the C_{60} aqueous suspension measured by optical absorption.

Parameter	Values	
	264 nm	340 nm
DL (mg L^{-1})	0.184	0.259
QL (mg L^{-1})	0.283	0.371
LR (mg L^{-1})	0.180–3.000	0.180–3.000
R^2	>0.9996	
ε (L mol^{-1} cm^{-1})	128,079 ± 125	69,489 ± 80

the Table 1, as well as the linear range (LR) as calculated from the two analytical curves at 264 and 340 nm.

It can be noted from Table 1 that both wavelengths have similar linear quantification ranges, between 0.180 and 3.000 mg L^{-1}. This concentration range was slightly lower than that obtained by Moussa et al. [17] for HPLC quantification of C_{60} in blood after an extraction process, i.e. 0.05 to 200 mg L^{-1}. The obtained linear determination coefficient (R^2) was high for both curves indicating an improved linearity. The non-zero intercept lines are due to the direct influence of the C_{60} nanoparticles on the transmittance beam.

The detection limit was even lower than previous values from literature like, for example, the value of 0.34 mg L^{-1} obtained by Xia et al. [19] for a HPLC method. Even though the DL and QL values for the analytical curve measured at 264 nm (0.280 and 0.370 mg L^{-1}, respectively) are still lower than for 340 nm. However, the quantification of C_{60} at this wavelength may not be error-free, depending on the solvent residuals in the samples. In addition the obtained ε for the 340 nm curve is very similar to the one obtained by Andrievsky et al. [11].

Finally, the absorbance results combined to already published data show that although the spectrophotometric method is simple and precise, it has a low sensitivity. It can only be applied in suspensions with concentrations higher than 0.370 mg L^{-1} at 340 nm.

3.3. Quantification by light scattering

For this method, a spectrofluorimeter was used to monitor the spectrum of the light scattered by the C_{60} nanoparticles. The incident illumination was selected by the excitation diffraction grating. As usual, without optical spectral filters, the second-order satellite lines of the diffraction grating, at wavelengths which are double and half of the excitation light, also incidence on the sample together with the original excitation beam. All these excitation wavelengths are scattered by the nanoparticles and pass through the second grating, at 90° from the first, known as the detector grating, which is used commonly for scanning the fluorescence spectra.

For the measurements, the excitation wavelengths were incremented each by 10 nm, from about 220 up to 700 nm, and for all excitation wavelengths was measured the intensity of the scattered spectrum. With that the contour plot shown in the Fig. 3 was built. The more intense peaks indicate high intensity in the scattered light. It is clear from the Fig. 3, the unambiguous identification of the scattered light due to the more intense excitation beam as well as the second order satellite peaks.

Fig. 4 shows the maximum intensity of the scattered light as a function of wavelengths for the first order peak (curve *a*), together with the second order (curve *b*) at the higher wavelength (curves *a* and *b* of Fig. 3). Although these two curves carry information about the light source and detector spectral properties, they also show, at least qualitatively, the nephelometric behavior of the nanoparticles in water [33], since the scattering is more noticed for lower wavelengths (290 and 350 nm) than for higher wavelengths (480 and 550 nm). For this explanation, it is assumed that both the light-

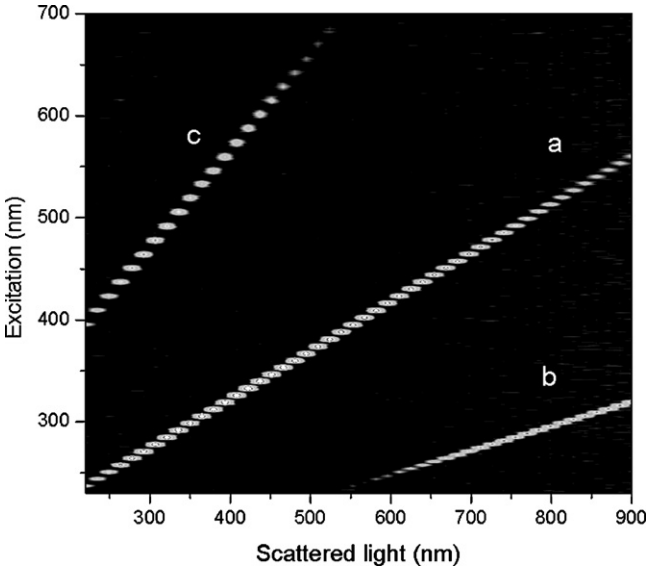

Fig. 3. Contour plot showing the scattered light intensity for several excitations. The lighter the color, the more intense is the scattering. The central line is the original excitation beam, the two other side-lines are the scattered light at the wavelengths of the second-order beams. The quantification of the C_{60} in water suspensions can be done in each spot showed in this contour plot. Lines (a) and (c) are scattered light at the wavelengths of the second-order lines of the excitation diffraction grating. Line (b) is the scattered light at the excitation wavelength (first-order).

source as well as the detector spectral bands vary monotonously in the range between the near UV to the near IR range. The scattered light intensity at the second-order wavelengths is by far, weaker than the first-order, as expected. Despite this, as it can be seen below, it was still possible to quantify the C_{60} nanoparticles using also the light scattered at the second-order wavelengths.

The analytical curves for the scattered light were calculated for several pairs of excitation/scattered light wavelengths in the first and second order scattered light peaks. All curves were linear for the four C_{60} suspensions in the different used concentrations. One typical example of how these analytical curves were built is shown in the Fig. 5.

Fig. 5 shows the intensity of the second-order scattered light peaks at 580 nm (excitation at 290 nm) as a function of the C_{60} concentrations in the suspensions diluted from a FAS, after subtracting the spectra of the control samples (FBS and its respective dilutions). The analytical curve from these data is shown in the insert. Note the linearity of the points indicating that the assumption of non-coherent optical light scattering is true [33]. Therefore, this linear

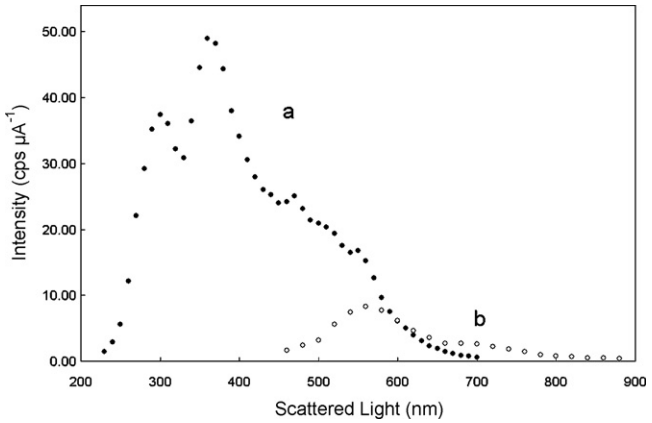

Fig. 4. Scattering intensities for different incident wavelength beams obtained for a C_{60} aqueous suspensions (FAS): (a) 1st order (290 nm) and (b) 2nd order (580 nm).

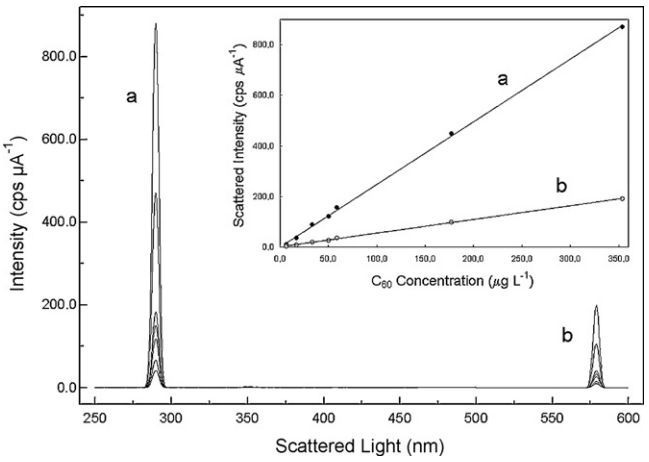

Fig. 5. Scattering spectra for different concentrations of C_{60} aqueous suspensions (FAS). The insert shows the two analytical curves, scattering intensity as function of C_{60} concentration, obtained for 290 and 580 nm.

Table 2
Mean values for detection (DL) and quantification (QL) limits, linear range (LR) and linear determination coefficient (R^2), obtained from the analytical curves built by the scattered light intensity, for 1st and 2nd orders, as function of the C_{60} aqueous suspension concentration.

Parameter	Values
LR ($mg\,L^{-1}$)	0.007–0.360
DL ($mg\,L^{-1}$)	0.0090 ± 0.0008
QL ($mg\,L^{-1}$)	0.017 ± 0.004
R^2	>0.9995

range can be used to determine C_{60} nanoparticle concentrations in water. Table 2 shows LR, DL, QL and R^2 values obtained from the analytical curve shown in Fig. 5.

The linear range obtained by this method, as seen in Table 2, demonstrated concentration values lower than the optical absorption method and also the results by Moussa et al. [17]. The DL and QL were also lower, even though the scattered light was measured in the second order excitation wavelengths. The linearity was very high $R^2 > 0.999$. These results show clearly an improved sensitivity compared to the optical absorption method. The sensitivity gain is about 20 times higher than the quantification method based on optical absorption spectrophotometry.

4. Conclusions

C_{60} nanoparticles with diameters of (17 ± 2) nm in water were prepared by a modified ultrasonification and solvent evaporation route. Different dilutions were quantified by optical absorption spectrophotometry. The linear range obtained was between 0.180 and 0.300 $mg\,L^{-1}$ whereas the detection and quantification limits were 0.184 and 0.283 $mg\,L^{-1}$, respectively.

A simple quantification method for C_{60} in water was developed by measuring the intensity of the light scattered by the C_{60} nanoparticles using a standard spectrofluorimeter without optical filters. This method works well at first and second-order excitation wavelengths, with a linear range from 0.007 to 0.360 $mg\,L^{-1}$, and a quantification limit of about 0.017 $mg\,L^{-1}$. These results show that the quantification by light scattering can be at least 20 times more sensitive than standard optical absorption.

Acknowledgments

We would like to acknowledge the following people: Prof. Pedro Licínio for photo correlation experiments and useful comments on light scattering, Prof. Bernardo Ruegger e Elizângela Silva for the AFM images and finally to CNPq, FAPEMIG and the Instituto do Milênio de Nanotecnologia for financial support.

References

[1] H.W. Kroto, J.R. Heath, S.C. O'Brien, R.F. Curl, R.E. Smalley, Nature 318 (1985) 162.
[2] M.S. Dresselhaus, G. Dresselhaus, P.C. Eklund, Science of Fullerenes and Carbon Nanotubes, Academic Press, San Diego, 1996.
[3] W. Kratschmer, K. Fostiropoulos, D.R. Huffman, Chem. Phys. Lett. 170 (1990) 167.
[4] S. Bosi, T. Da Ros, G. Spalluto, J. Balzarini, M. Prato, Bioorg. Med. Chem. Lett. 13 (2003) 4437.
[5] R.S. Ruoff, D.S. Tes, R. Malhotra, D.C. Lorents, J. Phys. Chem. 97 (1993) 3379.
[6] M.T. Beck, Pure Appl. Chem. 70 (1998) 1881.
[7] G.C. Alves, L.O. Ladeira, A. Righi, K. Krambrock, H.D. Calado, R. Gil, M.V.B. Pinheiro, J. Braz. Chem. Soc. 17 (2006) 1186.
[8] L.Y. Chiang, J.B. Bhonsle, L. Wang, S.F. Shu, T.M. Chang, J.R. Hwu, Tetrahedron 52 (1996) 4963.
[9] M.L. Sushko, H. Tenhu, S.I. Klenin, Polymer 43 (2002) 2769.
[10] V.P. Belousov, I.M. Belousova, A.V. Kris'ko, T.K. Kris'ko, T.D. Murav'eva, A.K. Sirotkin, Russ. J. Gen. Chem. 76 (2006) 251.
[11] G.V. Andrievsky, V.K. Klochkov, A.B. Bordyuh, G.I. Dovbeshko, Chem. Phys. Lett. 364 (2002) 8.
[12] S. Deguchi, R.G. Alargova, K. Tsujii, Langmuir 17 (2001) 6013.
[13] M.N. Moore, Environ. Int. 32 (2006) 967.
[14] K. Balasubramanian, M. Burghard, Small 1 (2005) 180.
[15] C.D. Tran, V.I. Grishko, S. Challa, Spectrochim. Acta 62 (2005) 38.
[16] D. Heymann, L.P.F. Chibante, R.E. Smalley, J. Chromatogr. 689 (1995) 157.
[17] F. Moussa, M. Pressac, E. Genin, S. Roux, F. Trivin, A. Rassat, R. Céolin, H. Szwarc, J. Chromatogr. 696 (1997) 153.
[18] M. James, J. Treubig, R.B. Phyllis, J. Chromatogr. 960 (2002) 135.
[19] X.R. Xia, N.A. Monteiro-Riviere, J.E. Riviere, J. Chromatogr. 1129 (2006) 216.
[20] C.W. Isaacson, C.Y. Usenko, R.L. Tanguay, J.A. Field, Anal. Chem. 79 (2007) 9091.
[21] P.K. Zarzycki, H. Ohta, F.B. Harasimiuk, K. Jinno, Anal. Sci. 23 (2007) 1391.
[22] T. Tomiyama, S. Uchiyama, H. Shinohara, Chem. Phys. Lett. 264 (1997) 143.
[23] P. Scharff, K. Risch, L. Carta-Abelmann, I.M. Dmytruck, M.M. Bilyi, O.A. Golub, A.V. Khavryuchenko, E.V. Buzaneva, V.L. Aksenov, M.V. Avdeev, Y.I. Prylutskyy, S.S. Durov, Carbon 42 (2004) 1203.
[24] D. Harvey, Modern Analytical Chemistry, Mc Graw Hill, New York, 2000.
[25] I.P. Morais, I.V. Toth, A.O. Rangel, Spectrosc. Lett. 39 (2006) 547.
[26] M. Hassellov, J.W. Readman, J.F. Ranville, K. Tiede, Ecotoxicology 17 (2008) 344.
[27] K. Tiede, A.B.A. Boxallae, S.P. Tearb, J. Lewisa, H. Davidc, M. Hassellov, Food Addit. Contam. 25 (2008) 795.
[28] F. Von der Kammer, M. Baborowski, K. Friese, J. Chromatogr. A 1100 (2005) 81.
[29] S. Nath, H. Pal, D.K. Palit, A.V. Sapre, J.P. Mittal, J. Phys. Chem. B 102 (1998) 10158.
[30] T. Rudalevige, A.H.F. Zand, J. Phys. Chem. A 102 (1998) 9797.
[31] K.L. Chen, M. Elimelech, Langmuir 22 (2006) 10994.
[32] S. Nath, H. Pal, A.V. Sapre, Chem. Phys. Lett. 360 (2002) 422.
[33] H.C. Hulst, Light Scattering by Small Particles, Courier Dover Publications, New York, 1981.
[34] D.C. Harris, Análise Química Quantitativa, 5ª ed., LTC Editora, Rio de Janeiro (2001).

Talanta 78 (2009) 1310–1314

Contents lists available at ScienceDirect

Talanta

journal homepage: www.elsevier.com/locate/talanta

High performance liquid chromatography method for the pharmacokinetic study of bicalutamide SMEDDS and suspension formulations after oral administration to rats

Ajeet Kumar Singh[a,*], Akash Chaurasiya[b], Gaurav K. Jain[b], Anshumali Awasthi[a], Dinesh Asati[c], Gautam Mishra[a], Roop K. Khar[b], Rama Mukherjee[d]

[a] Dabur Research Foundation, Plot No. 22 Site IV, Sahibabad, Ghaziabad, 201010, U.P., India
[b] Department of Pharmaceutics, Faculty of Pharmacy, Jamia Hamdard (Hamdard University), 110062, New Delhi, India
[c] Department of Dermatology, All India Institute of Medical Sciences, 110029, New Delhi, India
[d] ARA healthcare Pvt. Ltd., Plot No. 10, Electronic City, Sector 18, Gurgaon, 122015, Haryana, India

ARTICLE INFO

Article history:
Received 10 December 2008
Received in revised form 28 January 2009
Accepted 30 January 2009
Available online 10 February 2009

Keywords:
Column liquid chromatography
Bicalutamide
Pharmacokinetic study
Self micro-emulsifying drug delivery (SMEDDS)

ABSTRACT

Bicalutamide is a non-steroidal antiandrogen and is an oral medication that is used for treating prostate cancer. To evaluate the bioavailability of bicalutamide from bicalutamide self-microemulsifying drug delivery systems (SMEDDS) and bicalutamide suspension formulations, a sensitive, specific reversed-phase high performance liquid chromatographic (HPLC) method using ultraviolet detection was developed and validated for the analysis of bicalutamide (BCT) in rat blood plasma.

Letrozole (LZ) was used as the internal standard. The chromatographic separation was achieved on C18 column at 35 °C, with a mobile phase consisting of water: acetonitrile (adjusted to pH 3.0 with 20% *o*-phosphoric acid) (60:40), at a flow rate of 1.0 mL min^{-1}. Bicalutamide and letrozole were well separated with retention times of 10.9 ± 0.2 and 5.7 ± 0.2 min, respectively. The method was successfully used to determine pharmacokinetics of bicalutamide, following oral administration of bicalutamide suspension and bicalutamide SMEDDS to wistar rats.

Significant difference was observed in main pharmacokinetic parameters of t_{max}, C_{max} and $AUC_{0\rightarrow\infty}$ between SMEDDS and suspension, and a two fold increase in the relative bioavailability of bicalutamide was observed with the SMEDDS compared with suspension formulation. It was concluded that the absorption of bicalutamide from SMEDDS was enhanced.

1. Introduction

Bicalutamide (BCT), *N*-[4-cyano-3-(trifluoromethyl) phenyl]-3-[(4-fluorophenyl) sulfonyl]-2-hydroxy-2-methyl-propanamide, is an orally active, non-steroidal anti-androgens used for the treatment of prostate cancer [1,2]. BCT (Fig. 1a) is used as mono-therapy for the treatment of earlier stages of the disease by competitively blocking the growth-stimulating effects of androgens (testosterone and 5α-dihydrotestosterone) on prostate and other androgen-sensitive tissues. It binds preferentially to receptors located outside the central nervous system and causes little increase in testosterone levels with little agonist activity [3–5]. BCT is well tolerated and has high in vitro potency, however, its absolute bioavailability and pharmacokinetics after oral administration are markedly variable due to poor absorption, which is related to the high lipophilicity (log *P*: 2.92) and poor aqueous solubility (5 mg L^{-1}) [6–8]. As a result, there is a need to develop strategies to enhance the oral bioavailability of BCT. To evaluate the efficacy of the novel formulations of BCT, in vivo pharmacokinetic studies are the prime requirement. Such pre-clinical pharmacokinetic investigations require the support of a fast and reliable bio-analytical methodology for the measurement of the drug involved. A review of literature reveals limited reports since the drug is not yet official in any pharmacopoeia. To best of our knowledge, no validated analytical method for the quantification of BCT in biological fluids, has been published in the literature, although methods for the enantiomeric separation of BCT and its related compounds has been published [9]. Methods reported for determination of enantiomers of BCT are mainly based on chiral HPLC [10–13]. A stability indicating HPLC methods and isolation of process related impurities and degradation products of BCT have

* Corresponding author. Tel.: +91 9899200511; fax: +91 120 4378400.
E-mail addresses: ajeetrj@rediffmail.com (A.K. Singh), akashchaurasiya@rediffmail.com (A. Chaurasiya), gaurav.jain@gmail.com (G.K. Jain), awasthi.anshumali@dabur.com (A. Awasthi), dineshasati@rediffmail.com (D. Asati), mishra.gautam@dabur.com (G. Mishra), roopkhar@hotmail.com (R.K. Khar), rama.mukherjee@gmail.com (R. Mukherjee).

0039-9140/$ – see front matter © 2009 Elsevier B.V. All rights reserved.
doi:10.1016/j.talanta.2009.01.058

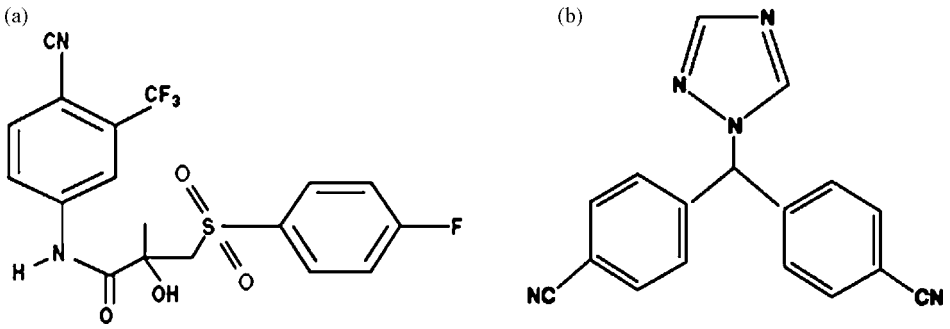

Fig. 1. (a) Molecular structure of bicalutamide (BCT). (b) Molecular structure of letrozole (LZ).

been described in the literature in recent years [14,15]. The present work comes up from the lack of analytical methods that permit to determine BCT in plasma, which is an essential tool in pre-clinical and clinical studies. A non-time consuming, simple and sensitive, isocratic reversed-phase high performance liquid chromatographic method has been developed and validated for determination of BCT in rat plasma with a quantification limit sufficiently low to support pharmacokinetic studies. The proposed method is also applied to monitor pharmacokinetic profile following oral administration of BCT suspension and BCT SMEDDS formulations to wistar rats.

2. Experimental

2.1. Chemical and reagents

BCT and Letrozole (LZ, internal standard) were obtained from Dabur Research Foundation (Ghaziabad, India). Purity analysis suggested that their purities were all above 99% by HPLC method. HPLC-grade acetonitrile was purchased from Qualigens fine chemicals (Mumbai, India) and HPLC-grade water was produced in the laboratory by a Milli-Q purification system (Millipore, Billerica, MA, USA). All other chemicals and reagents used were of analytical grade and were purchased from Merck Ltd. (Worli, Mumbai, India).

2.2. Chromatography

Chromatography was performed using a Shimadzu LC-2010CHT series chromatographic system (Shimadzu, Nakagyo-ku, Kyoto, Japan) with a Model LC-10 AT*VP* binary pump and a SPD-10 A*VP* UV–vis detection system. The injector was a Rheodyne manual injection valve Model 7725, fitted with a 50 μL sample loop. The chromatographic system operation and recording of data were performed with the use of LC solutions software version 1.21 SP1. Chromatographic separations were achieved on Gemini C-18 column (250 mm × 4.6 mm I.D.; particle size 5 μm) using the mobile phase formed by water: acetonitrile (60:40) (adjusted to pH 3.0 with 20% *o*-phosphoric acid). Before delivering the mobile phase into the system, it was degassed for 15 min by sonication and filtered through 0.45 μm filter (Sartorius, Germany) using vacuum. The HPLC system was operated isocratically at a flow rate of 1.0 mL min^{-1} and elution was performed at a controlled temperature of 35 °C. The samples of 50 μL were injected into HPLC system and the UV detection was performed at 270 nm. Letrozole (LZ) (Fig. 1b) was used as an internal standard.

2.3. Standard solutions and spiked samples

Standard solutions of BCT and LZ were prepared with mobile phase at concentrations of 1000 μg mL^{-1}. Working solutions of BCT and LZ were prepared daily from the standard solution by diluting the appropriate aliquot with mobile phase. All solutions were stored at 4 °C and were identified as being stable for at least 1 month.

Plasma standards were prepared by spiking blank rat plasma with an adequate aliquot of stock standard solutions of BCT and LZ. Calibration standards from 0.1 to 20 μg mL^{-1} in plasma samples were prepared by spiking blank rat plasma with 10 μL of working stock solutions of BCT. Quality control (QC) samples at three different levels were independently prepared at concentrations of 0.3 μg mL^{-1} (LQC, low QC), 7.5 μg mL^{-1} (MQC, medium QC) and 15.0 μg mL^{-1} (HQC, high QC) of BCT in the same manner. The spiked samples were then treated following the sample preparation procedure as indicated in Section 2.4.

2.4. Plasma sample preparation

10 μL of internal standard (LZ concentration; 100 μg mL^{-1}) solution was added to 100 μL plasma standard or sample followed by 1000 μL of dichloromethane: diethyl ether (7:3) (extraction solvent). The sample was vortexed for 5 min followed by 5 min centrifugation at 10,000 rpm. The supernatant was collected and evaporated to dryness in DNA speed oven (Sawant DNA speedvac, NJ, USA) at 40 °C under vacuum. The dried residue was reconstituted with 150 μL of diluent (mobile phase) and vortexed for 2 min. The supernatant was sonicated for 5 min and a volume of 50 μL was injected into the HPLC system.

2.5. Preparation of SMEDDS formulation of BCT

Capryol PGMC (55%), Polyethylene glycol 300 (7.5%) and Cremophore RH 40 (37.5%) were accurately weighted into screw-capped glass vials. BCT was added into the mixture and heated at 40 °C in a water bath to facilitate solubilization and then vortex mixed. The formulation was equilibrated at 37 °C for 24 h and then stored at room temperature.

2.6. Validation procedures

The chromatographic method was further validated for linearity, specificity, sensitivity, precision and accuracy according to ICH guidelines [16].

2.6.1. Linearity

The linearity of an analytical method is its ability within a definite range to obtain results directly proportional to the concentrations of the analyte in the sample. The linearity of the detector response for the test compounds was evaluated by injecting a total of eight calibration (working) standard solutions (0.1–20 μg mL^{-1}) covering the working range of the assay. The calibration curves were constructed by plotting peak area ratios of BCT to LZ against corresponding concentrations. The linearity of the calibration curve was tested and evaluated using linear regression model of internal standard calibration curve.

2.6.2. Specificity and sensitivity

Specificity of the method was determined by analyzing six different batches of blank plasma obtained from healthy rats.

2.6.3. Precision and accuracy

The reproducibility of the analytical procedure was determined by calculating intra- and inter-day precision and accuracy. Precision and accuracy was performed by six replicate analysis of spiked plasma quality control samples at the concentration ranges of LQC (0.3 μg mL^{-1}), MQC (7.5 μg mL^{-1}) and HQC (15.0 μg mL^{-1}) followed by their comparison with the calibration curves prepared on the same day and on three different days. Precision was expressed as the percentage coefficient variation (CV) (%), of measured concentrations for each calibration level whereas, accuracy was calculated as the percentage difference between the mean concentration of drug measured from calibration curve and the concentration of drug added to the blank plasma.

2.6.4. Extraction efficiency

The mean recovery of BCT and LZ from spiked rat plasma was evaluated to test the efficiency and reproducibility of the extraction procedure. The determination of the extraction efficiency in plasma was made by injecting replicates at the concentration ranges of LQC, MQC and HQC. The extraction was conducted as described in Section 2.4, after addition of 10 μL of LZ working solution. The responses of these standards, taken by means of the extraction procedures, have been compared with those of standard solution at the same concentration injected directly into the liquid chromatographic apparatus. The peak area ratios were compared to the ratio of the standard aqueous samples without extraction.

2.7. Stability studies

The stability of the BCT in plasma at room temperature (25 °C) and at −20 °C was assessed by analyzing 500 μL stability sample at a concentrations of 7.5 μg mL^{-1}. Three repeated determinations were made in each case and at each stipulated time period. The concentration of BCT measured in the stability samples were compared to the theoretical spiked concentration.

2.8. Pharmacokinetic study

Eight healthy female wistar rats (supplied by the Animal Facility, Dabur Research Foundation, Sahibabad, Ghaziabad, India) weighing 200 ± 10 g were used in the study. The rats were housed under standard conditions. All rats were dosed following an overnight fast; food was returned after 4 h after dosing. Rats were divided in two groups at random. First group was administered exemestane suspension (0.25% CMC Na) because bicalutamide was virtually insoluble in water and the second group was administered bicalutamide SMEDDS formulation. The amount of bicalutamide in each one of these formulations was adjusted to contain 25 mg/kg body weights.

Blood samples (approx. 0.5 mL) was collected from retro-orbital plexus of rat in tube containing saturated solution of di-sodium EDTA at pre-dose, and 0.5, 1.0, 2.0, 4.0, 6.0, 8.0, 10.0, 12.0, 24.0, 32.0, 48.0, 56.0, 72.0, 80.0 and 144.0 h, respectively post dose. During collection, blood sample has been mixed thoroughly with di-sodium EDTA solution in order to prevent blood clotting. Samples were centrifuged at 5000 rpm for 5 mins at room temperature. Separated plasma sample was transferred into pre-labeled tubes and stored at −20 °C until the completion of analysis. The experimental procedures were approved by the intuitional animal ethical committee and were in compliance with the National Institutes of health Guide for Care and Use of Laboratory Animals.

Pharmacokinetic parameters (PK) were calculated by noncompartmental analysis also called as model independent analysis using WinNonLin version 4.0 (Pharsight Corp., Mountain View, CA). Peak plasma concentration (C_{max}) and time of its occurrence (t_{max}) were read directly from the individual plasma concentration–time profiles. Area under concentration time curve $AUC_{\rightarrow t}$ was calculated according to linear trapezoidal method whereas mean residence time (MRT) was calculated by dividing the $AUMC_{\rightarrow t}$ by $AUC_{0\rightarrow t}$.

2.9. Statistical analysis

Data of in vivo analysis was expressed as mean ± SD (n = 8). The data was compared for statistical significance by the one-way analysis of variance (ANOVA) followed by Tukey–Kramer multiple comparisons test using GraphPad Instat software (GraphPad Software Inc., CA, USA).

3. Results and discussion

3.1. Method development

The HPLC method proposed provides a simple procedure for the determination of BCT in biological samples. A straightforward and accurate HPLC method to determine BCT in rat plasma was initially developed. Chromatographic condition, based on the isocratic separation, gave a good profile in plasma using a reverse phase C18 column. Different ratios of the mobile phase were studied in order to shorten retention times of the analyte and to improve peak symmetry. Best results in terms of peak symmetry and retention time were obtained using water: acetonitrile (60:40), as mobile phase. The pH of the mobile phase was adjusted with 20% *o*-phosphoric acid to pH 3.0, due to stability problems of BCT at basic conditions, as reported earlier [14,15]. The BCT detection was carried out at 270 nm, since at this wavelength maximum response is achieved along with the absence of endogenous interfering peaks occurring from blank matrix. The samples of BCT were successfully extracted from interfering plasma using dichloromethane: diethyl ether (7:3) (extraction solvent) with excellent recoveries. In the present study, LZ was selected as internal standard because of its similar physico-chemical characteristics as that of BCT. Both drugs possess poor aqueous solubility, nearly similar log P values and a cyanophenyl moiety in their structure. Furthermore, with proposed HPLC method, LZ demonstrated high recovery, less retention time and good validation results.

3.2. Linearity

The calibration curve was obtained by plotting the area ratios *ABCT−/−ALZ* against the concentration of BCT. The equation for the calibration curve is $Ar = 0.3214C - 0.0009$ (n = 6) where, C is the concentration of bicalutamide in plasma, and Ar is the ratio of peak area of BCT to that of LZ. The linearity of the calibration graphs and adherence of the system to Beer's law was validated by high value of correlation coefficient ($r^2 \pm SD = 0.9999 \pm 0.0003$) over a concentration range of 0.1–20 μg mL^{-1}.

3.3. Specificity and sensitivity

Specificity was demonstrated by the absence of any endogenous interference at retention times of peaks of interest as evaluated by chromatograms of blank rat plasma (Fig. 2a) against those spiked with LZ alone (Fig. 2b) and with LZ and BCT (Fig. 2c). Compounds LZ and BCT were well separated and were identified by their relative retention time i.e. 5.7 ± 0.2 and 10.9 ± 0.2 min, respectively. Limit of quantification (LOQ) of the method is 0.1 μg mL^{-1}.

Table 1
Precision and accuracy of HPLC method for BCT in plasma ($n = 6$).

Concentration spiked ($\mu g\,mL^{-1}$)	Mean concentration found ($\mu g\,mL^{-1}$)	Precision[a]		Accuracy[b] (%)
		SD.	CV (%)	
Intra-day				
0.3 (LOQ)	0.294	0.002	2.04	98.00
7.5 (MOQ)	7.430	0.270	3.64	99.06
15.0 (HOQ)	15.131	0.241	1.61	100.87
Inter-day				
0.3 (LOQ)	0.288	0.003	3.32	96.00
7.5 (MOQ)	7.390	0.304	4.11	98.53
15.0 (HOQ)	14.484	0.331	2.29	96.56

[a] Precision as coefficient of variation (CV, %) = standard deviation divided by mean concentration found × 100.
[b] Accuracy = mean concentration found/concentration spiked × 100.

3.4. Precision and accuracy

Table 1 summarizes the intra- and inter-day precision and accuracy of the BCT assay in plasma. Quality control (QC) samples for BCT were prepared in replicates ($n = 6$) at three different concentrations viz. low (LQC), medium (MQC) and high (HQC). The intra-day and inter-day precisions determined as coefficient of variation (CV) ranged between 1.61–3.64 and 2.29–4.11%, respectively. Intra- and inter-day accuracy calculated as percent recovery was in the range of 96.0–100.87 %. Both precision and accuracy was found to be suitable and do not depend on the concentration assayed or on the day of the assay.

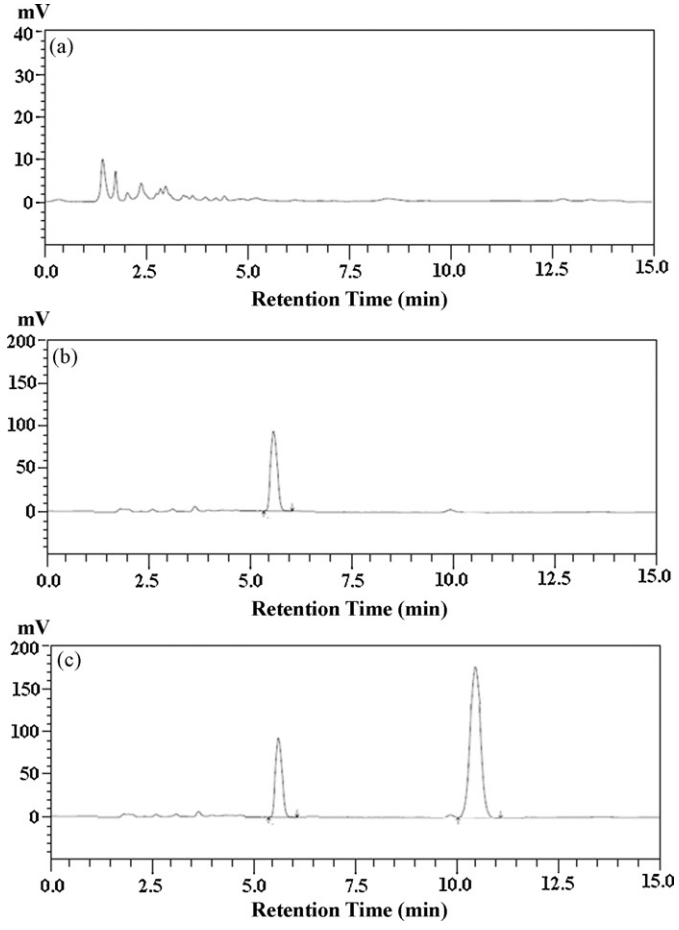

Fig. 2. (a) Chromatogram of extracted blank rat plasma at 270 nm. (b) Chromatogram of extracted rat plasma spiked with LZ (internal standard) at 270 nm. (c) Chromatogram of extracted rat plasma spiked with BCT (retention time, 10.9 min) and LZ (retention time, 5.7 min) at 270 nm.

3.5. Extraction efficiency

Various extraction procedures including protein precipitation methods and liquid–liquid extraction was investigated. Direct protein precipitation with acetonitrile gave low recovery with high background noise. For liquid–liquid extraction procedure selection of suitable solvent is a critical parameter. Ideally, the selected solvent should be compatible, immiscible with water, stable enough over the extraction time and have high solubility for the target analyte. A series of organic solvents and their mixtures of varying polarity (viz. ethyl acetate, dichloromethane, *tert*-butyl methyl ether, diethyl ether, *n*-hexane) were evaluated for extraction of BCT from plasma. Finally, a combination of dichloromethane and diethyl ether (7:3) effectively eliminates the interfering material and gave the best recovery for BCT. The extraction efficiency (CV), expressed as mean recovery of BCT from rat plasma, was determined at LOQ, MOQ and HOQ and was found to be 98.0% (1.8%), 99.2% (1.4%) and 97.8% (1.1%), respectively (Table 2).

3.6. Stability

Fig. 3 demonstrates the effect of time of storage on stability of BCT in plasma stored at room temperature and at −20 °C. The studied compound was shown to be stable in plasma at room temperature for up to 24 h, and for up to 60 days at −20 °C. The percentage recovery of drug in plasma samples ranged from 94.30% to 99.32 %. Date of percentage recovery of BCT is presented in the Fig. 3.

3.7. Pharmacokinetic analysis

BCT suspension and BCT SMEDDS (BCT dose; 25 mg kg^{-1} body weight) were administered orally to wistar rats and the developed HPLC method is applied to determine their in vivo pharmacoki-

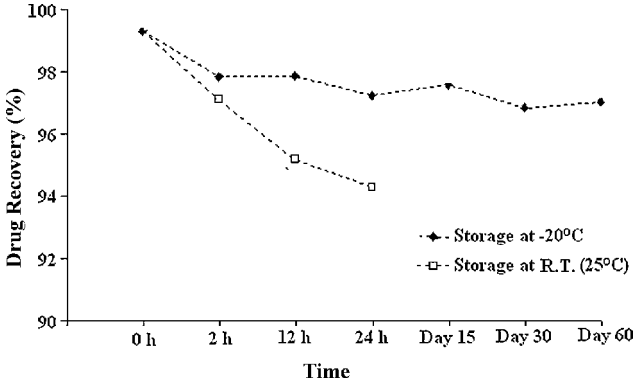

Fig. 3. Stability profile of BCT in rat plasma.

Table 2
Extraction efficiency of BCT from plasma at different concentration levels ($n = 6$).

Concentration spiked ($\mu g\,mL^{-1}$)	Mean concentration found ($\mu g\,mL^{-1}$)	Extraction efficiency (%)	Coefficient of variation (%)
Bicalutamide			
0.3 (LOQ)	0.294	98.0	1.8
7.5 (MOQ)	7.440	99.2	1.4
15.0 (HOQ)	14.670	97.8	1.1
Letrozole (internal standard)			
1.0 (HOQ)	0.998	99.8	0.8

Table 3
Mean pharmacokinetic parameters of bicalutamide SMEDDS and suspension formulation after single dose administration ($25\,mg\,kg^{-1}$; $n = 8$).

Pharmacokinetic parameters	Bicalutamide suspension	BCTME2	Ratio (SMEDDS/suspension)
AUC (0 to t) $\mu g\,h\,mL^{-1}$	221.74 ± 26.10	$462.04 \pm 68.09^{**}$	2.08
AUC (0 to ∞) $\mu g\,h\,mL^{-1}$	229.33 ± 27.03	$464.62 \pm 69.22^{**}$	2.03
MRT (h)	38.23	37.4811^{**}	–
C_{max} ($\mu g\,mL^{-1}$)	4.21 ± 2.09	$12.04 \pm 1.57^{**}$	2.86
T_{max} (h)	8	10	NA
Relative bioavailability (%)	–	–	208.37

** $P < 0.001$ when compared with suspension formulation using one-way ANOVA followed by Tukey–Kramer multiple comparison test.

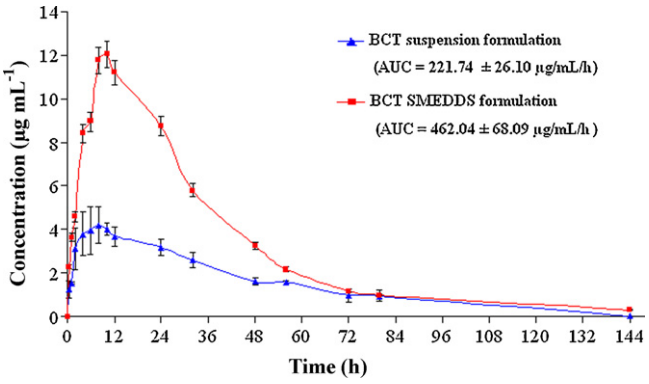

Fig. 4. Mean Pharmacokinetic parameters of bicalutamide SMEDDS and suspension formulation after single dose administration ($25\,mg\,kg^{-1}$; $n = 8$) BCT suspension (▲) and BCT SMEDDS (■-)

netics. Plasma profiles of BCT in rats following oral administration of the BCT suspension and BCT SMEDDS are shown in Fig. 4, whereas, pharmacokinetic parameters in plasma obtained from the pooled concentration–time data are listed in Table 3. As determined by HPLC method, the $AUC_{0\to t}$ of BCT SMEDDS was $462.04 \pm 68.09\,\mu g\,h\,mL^{-1}$, while $AUC_{0\to t}$ of orally administered BCT suspension was $221.74 \pm 26.10\,\mu g\,h\,mL^{-1}$. The $AUC_{0\to\infty}$ of BCT SMEDDS was $464.62 \pm 69.22\,\mu g\,h\,mL^{-1}$, while $AUC_{0\to\infty}$ of orally administered BCT suspension was $229.33 \pm 27.03\,\mu g\,h\,mL^{-1}$ This resulted into 2.03 fold increased relative bioavailability (Fig. 4). Results (Table 3) also demonstrated that C_{max} values of BCT SMEDDS ($12.04 \pm 1.57\,\mu g\,mL^{-1}$) are about 2.9 times higher as compared to BCT suspension ($4.21 \pm 2.09\,\mu g\,mL^{-1}$). The evidence (as determined through HPLC) suggests the protective role of SMEDDS as a carrier system to deliver BCT to the systemic circulation in the body. The results were in accordance with previous findings, where drugs administered through SMEDDS showed higher plasma concentration [17–19]. Accordingly, through the developed HPLC method, it can be identified that the bioavailability of the BCT SMEDDS formulation is significantly higher ($P < 0.001$) compared to BCT suspension.

4. Conclusion

A simple, rapid and sensitive HPLC method was developed and validated for the determination of BCT in rat plasma. The sensitivity of the method allowed the pharmacokinetic study of BCT in plasma after oral administration of BCT SMEDDS and BCT suspension formulations to wistar rats. BCT formulated in SMEDDS formulation significantly improved the pharmacokinetic profile of the drug administered to rats. Furthermore, the sensitivity of the established method provides a reliable bio-analytical methodology to carry out tissue-distribution and pharmacokinetics of BCT.

References

[1] Y. Fradet, Expert Rev. Anticancer Ther. 4 (2004) 37.
[2] I.D. Cockshott, S.D. Oliver, J.J. Young, K.J. Cooper, D.C. Jones, Biopharm. Drug Dispos. 18 (1997) 499.
[3] S.M. Singh, S. Gauthier, F. Labrie, Curr. Med. Chem. 7 (2000) 211.
[4] B.J. Furr, B. Valcaccia, B. Curry, J.R. Woodbum, G. Chesterson, H. Tucker, J. Endocrinol. 113 (1987) R7.
[5] R.K. Chandolia, G.F. Weinbauer, H.M. Behre, E.J. Steroid, Biochem. Mol. Biol. 38 (1991) 367.
[6] P.F. Schellhammer, J.W. Davis, Clin. Prostate Canc. 2 (2004) 213.
[7] A.S. Zidan, O.A. Sammour, M.A. Hammad, N.A. Megrab, M.J. Habib, M.A. Khan, J. Pharm. Sci. 96 (2007) 2409.
[8] D.R. Vega, G. Polla, A. Martinez, E. Mendioroz, M. Reinoso, Int. Pharm. J. 328 (2007) 112.
[9] British National Formulary, 50th ed., British Medical Association and Royal Pharmaceutical Society of Great Britain, September 2005.
[10] D.K. James, N.N. Ekwuribe, Tetrahedron 58 (2002) 5905.
[11] N. Bargmann-Leyder, A. Tambuté, M. Caude, Chirality 7 (1995) 311.
[12] H. Tucker, G.J. Chesterson, J. Med. Chem. 31 (1988) 885.
[13] R.N. Rao, A.N. Raju, D. Nagaraju, J. Pharm. Bio. Med. Anal. 42 (2006) 347.
[14] R.N. Rao, A.N. Raju, R. Narsimha, J. Pharm. Bio. Med. Anal. 46 (2008) 505.
[15] G. Saravanan, B.M. Rao, M. Ravikumar, M.V. Suryanarayana, N. Someswararao, P.V.R. Acharyulu, Chromatographia 66 (2007) 219.
[16] Topic Q2B: validation of analytical procedures: Methodology, in: International Conference on Harmonisation (ICH), 1996.
[17] J.S. Woo, Y.K. Song, J.Y. Hong, S.J. Lim, C.K. Kim, Eur. J. Pharm. Sci. 33 (2008) 159.
[18] D. Patel, K.K. Sawant, Drug Dev. Ind. Pharm. 33 (2007) 1318.
[19] D.K. Wang, Z.H. Shi, L. Liu, X.Y. Wang, C.X. Zhang, P. Zhao, PDA J. Pharm Sci. Technol. 60 (2006) 343.

Talanta 78 (2009) 1401–1407

Contents lists available at ScienceDirect

Talanta

journal homepage: www.elsevier.com/locate/talanta

An amperometric urea biosensor based on covalently immobilized urease on an electrode made of hyperbranched polyester functionalized gold nanoparticles

Ashutosh Tiwari [a], Santosh Aryal [a], Srikanth Pilla [a], Shaoqin Gong [a,b,*]

[a] Department of Mechanical Engineering, University of Wisconsin-Milwaukee, 3200 North Cramer Street, Milwaukee, WI 53211, USA
[b] Department of Materials, University of Wisconsin-Milwaukee, 3200 North Cramer Street, Milwaukee, WI 53211, USA

ARTICLE INFO

Article history:
Received 17 January 2009
Received in revised form 12 February 2009
Accepted 13 February 2009
Available online 26 February 2009

Keywords:
Urea biosensor
Amperometric detection
Covalent immobilization
Boltron® H40
Gold nanoparticles

ABSTRACT

An amperometric biosensor was fabricated for the quantitative determination of urea in aqueous medium using hematein, a pH-sensitive natural dye. The urease (Urs) was covalently immobilized onto an electrode made of gold nanoparticles functionalized with hyperbranched polyester-Boltron® H40 (H40–Au) coated onto an indium–tin oxide (ITO) covered glass substrate. The covalent linkage between the Urs enzyme and H40–Au nanoparticles provided the resulting enzyme electrode (Urs/H40–Au/ITO) with a high level of enzyme immobilization and excellent lifetime stability. The response studies were carried out as a function of urea concentration with amperometric and photometric measurements. The biosensor based on Urs/H40–Au/ITO as the working electrode showed a linear current response to the urea concentration ranging from 0.01 to 35 mM. The urea biosensor exhibited a sensitivity of 7.48 nA/mM with a response time of 3 s. The Michaelis–Menten constant for the Urs/H40–Au/ITO biosensor was calculated to be 0.96 mM, indicating the Urs enzyme immobilized on the electrode surface had a high affinity to urea.

1. Introduction

Kidneys perform key roles in various body functions, including excreting metabolic waste products such as urea from the bloodstream, regulating the hydrolytic balance of the body, and maintaining the pH of body fluids [1]. The level of urea in blood serum is the best measurement of kidney function and staging of kidney diseases [2]. The normal urea level in serum ranges from 15 to 40 mg/dL (i.e., 2.5–7.5 mM). An increase in urea concentration causes renal failure such as acute or chronic urinary tract obstruction with shock, burns, dehydration, and gastrointestinal bleeding, whereas a decrease in urea concentration causes hepatic failure, nephritic syndrome, and cachexia [3]. Therefore, there is an urgent need to develop a device that rapidly monitors urea concentration in the body.

Most existing urea biosensors utilize urease (Urs) as the sensing element. The available Urs on the electrode surface hydrolyzes urea into NH_4^+ and HCO_3^- ions [4]. The concentration of urea is measured by monitoring the librated ions using a transducer such as amperometric, potentiometric, optical, thermal, or piezoelectric [5–11]. Although various urea biosensors that use a range of transducers have been studied extensively, the Urs-based amperometric urea biosensor is considered one of the most promising approaches because it offers fast, simple, and low-cost detection. The response time of such a biosensor is directly associated with the hydrolysis rate of urea on the electrode surface; therefore, rapid production of NH_4^+ ions on the electrode will lead to a highly sensitive biosensor.

It is well established that the performance of biosensors greatly depends on the physicochemical properties of the electrode materials, enzyme immobilization procedure, and enzyme concentration on the electrode surface [12]. Many electrode materials have been used to fabricate urea biosensors such as bovine serum albumin embedded polypyrrole [13]; polyvinyl alcohol–polyacrylamide composite [14]; amine functionalized glassy carbon [15]; polyvinylferrocenium [16]; poly(*N*-3-aminopropylpyrrole)-*co*-pyrrole [17]; polyaniline–Nafion®/Au composite [18]; polyethylenimine [19]; poly(*N*-vinyl carbazole)/stearic acid [20]; polyaniline–poly(n-butyl methacrylate) composites [21]; chitosan [22]; and polyaniline–perfluorosulfonated ionomer composite [5]. However, there is an ongoing demand for new types of electrode materials that can provide the Urs enzyme with better stability and performance for *in vitro* urea measurement.

In this context, the use of nanomaterials to fabricate biosensors is one of the most exciting approaches because nanomaterials have a unique structure and high surface-to-volume ratio [23]. The surfaces of nanomaterials can also be tailored in the molecular scale in order to achieve various desirable properties [24]. Many

* Corresponding author at: Department of Mechanical Engineering, University of Wisconsin-Milwaukee, 3200 North Cramer Street, Milwaukee, WI 53211, USA. Tel.: +1 414 229 5946; fax: +1 414 229 6958.
E-mail address: sgong@uwm.edu (S. Gong).

0039-9140/$ – see front matter © 2009 Elsevier B.V. All rights reserved.
doi:10.1016/j.talanta.2009.02.038

attempts have been made to fabricate a third-generation biosensor with self-assembly technology [25–31]; however, these approaches were based on planar self-assembly that may only offer limited available surface area on the electrode, which can compromise the performance of the biosensor.

Meanwhile, gold nanoparticles have played an increasingly important role for biosensor applications over the last decade [29,30]. Gold nanoparticles can (1) provide a stable surface for the immobilization of biomolecules without compromising their biological activities and (2) permit direct electron transfer from the redox biomolecules to the bulk electrode materials, thereby enhancing the electrochemical sensing ability [29]. For example, Shipway et al. systematically studied the new electronic, photoelectronic, and sensoring systems that used gold nanoparticle superstructures on the electrode surface [30]. In addition, previous studies indicated that biological macromolecules such as enzymes can generally retain their enzymatic and electrochemical activity after being immobilized onto the gold nanoparticles [32,33].

This study investigates the feasibility of using gold nanoparticles functionalized with hyperbranched polyester, Boltorn® H40 (H40–Au), for a potential urea biosensing application. H40–Au nanoparticles are particularly attractive for biosensor fabrication because they can be prepared under ambient conditions and they exhibit tunable porosity, high thermal stability and chemical inertness while experiencing negligible swelling in aqueous solution. In this work, successful attempts have been made toward the fabrication of an efficient urea biosensor using H40–Au nanoparticles. This novel urea biosensor offers a relatively long shelf life, a broad detection range, a high sensitivity, and a short response time.

2. Experimental

2.1. Materials

Boltorn® H40 (64 hydroxyl groups per molecule and M_n of 2833) was provided by Perstorp Polyols, Inc. and used after purification. The following materials were used without further purification: 3-mercaptopropionic acid (Aldrich, 99%), sodium borohydride (Aldrich, 99%), hydrogen tetrachloroaurate (III) hydrate (Aldrich, 99.99%), 1-ethyl-3-(3-dimethylaminopropyl) carbodiimide hydrochloride (Aldrich, 99%), *N*,*N*′-dicyclohexylcarbodiimide (Aldrich, 99%), *N*-hydroxysuccinimide (Aldrich, 99%), hematein (Fluka, 98%), L-serine (Acros, 99%), L-threonine (Acros, 98%), α-ketoglutaric acid (Fluka, 98%), L-alanine (Acros, 99%), L-phenylalanine (Acros, 98.5%), uric acid (Acros, 99%), L-cystine (Acros, 99%), L (+)-glutamic acid (Acros, 99%) sodium pyruvate (Fisher, 99%), L-glutamine (Fisher, 98.5%), L-ascorbic acid (Fisher, 99.8%), urea (Acros, 99%) and urease (Aldrich, from *Canavalia ensiformis*). All supplementary chemicals were of analytical grades and solutions were prepared with 18.2 MΩ deionized water. Indium–tin oxide (ITO) coated glass sheets (Balzers) with a resistance of 15 Ω/cm^2 were used as substrates for the deposition of electrodes.

2.2. Functionalization of gold nanoparticles with hyperbranched polyester

Functionalization of gold nanoparticles with hyperbranched polyester was conducted via a two-step procedure. First, the gold nanoparticle was functionalized with mercapto propionic acid (Au–COOH). Next, amine functionalized hyperbranched Boltorn® H40 (H40–NH_2) was covalently grafted onto Au–COOH nanoparticles using *N*,*N*′-dicyclohexylcarbodiimide (DCC) and *N*-hydroxysuccinimide (NHS) mediated reaction [34].

2.2.1. Preparation of carboxyl functionalized gold (Au–COOH) nanoparticles

To prepare the Au–COOH nanoparticles, concentrated solutions of tetrachloroauric acid ($HAuCl_4$) and 3-mercaptopropionic acid (MPA) were first prepared in ethanolic acetic acid, 0.001 M. Next, 10 mL of a solution containing 6 mM $HAuCl_4$ and 12 mM MPA was prepared by diluting the concentrated stock solutions with ethanol. All solutions were prepared fresh prior to reduction. Reduction was carried out by adding 65 μL of a 1.4 M aqueous solution of sodium borohydride ($NaBH_4$) in 5 μL portions under constant stirring. To form stable thiol monolayers on the gold nanoparticles, the suspension was allowed to stir slowly overnight in a dark at room temperature for 24 h. After that, the gold suspension was placed into an eppendorf tube and washed three times (centrifugation at 5000 rpm for 25 min) with ethanol to remove excess alkanethiol from the suspension.

2.2.2. Preparation of amine functionalized Boltorn® H40 (H40–NH_2)

First, 1.5 mL hydrazoic acid (1 M) was added into 20 mL Boltorn® H40 solution (5%, w/v in THF) and then mixed at room temperature. In this mixture, 0.3 mL diisopropyl azodicarboxylate (1.5 mM) and 5 mL triphenylphosphine (3.0 mM) were added under continuous stirring. After 1 h, the reaction mixture was heated to 50 °C and kept for 3 h; after which 1 mL HCl (1N) was added drop wise. The reaction then continued for additional 3 h. Finally, the reaction products were cooled to room temperature, filtered, and dried under vacuum.

2.2.3. Grafting H40–NH_2 onto the Au–COOH nanoparticles

H40–NH_2 was grafted onto Au–COOH using DCC and NHS as the condensing agents at room temperature (Fig. 1A). In a typical experiment, 50 mg of Au–COOH was dissolved in 10 mL DMSO and activated with 0.3 mM of DCC and NHS at room temperature. Next, 1 g of H40–NH_2 dissolved in 40 mL THF was added to the solution and the resulting solution mixture was stirred for 24 h. After that, the solution mixture was filtered to remove any insoluble byproducts, residual impurities, and aggregates. The final product was recovered by precipitation with cold diethylether and dried under vacuum.

2.3. Preparation of the Au–H40/ITO electrode

Ten microlitres of 2% (w/v) H40–Au nanoparticle solution in $CHCl_3$ was uniformly spread on the ITO substrate by drop coating technique at room temperature (Fig. 1B). The H40–Au/ITO electrode was dried under vacuum.

2.4. Fabrication of the urea bioactive electrode

The urea bioactive electrode was prepared by covalent immobilization of the urea-specific enzyme, urease, over the H40–Au/ITO electrode. In order to immobilize Urs, the H40–Au/ITO electrode was immersed in a phosphate buffer solution (1 M, pH 7.0) containing previously activated Urs enzyme (50 mg/mL) with 0.02 M 1-ethyl-3-(3-dimethylaminopropyl) carbodiimide (EDC) and 0.02 M NHS for 3 h. The enzyme immobilized electrode was rinsed with phosphate buffer solution (pH 7.0) to remove the excess unbound enzyme (Fig. 1B). All experiments were carried out at room temperature. The enzyme immobilized electrode was stored under dry conditions at 4 °C in a refrigerator.

2.5. Characterization

Electrochemical measurements of the electrodes were carried out on a Potentiostat/Glavanostat (Princeton Applied Research, Versa Stat3) unit with three electrodes in a 50 mM phosphate buffer

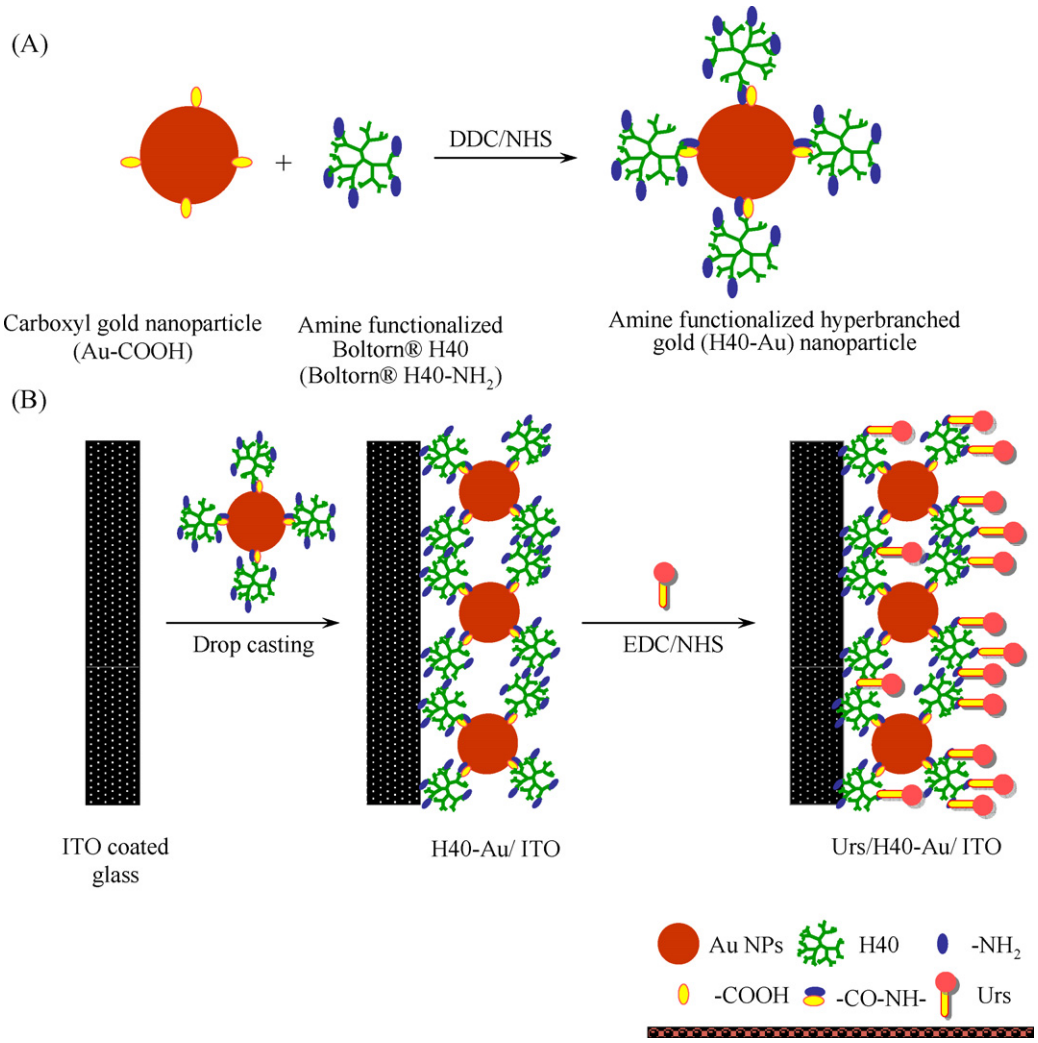

Fig. 1. Schematic presentation of the [A] preparation of hyperbranched gold (H40–Au) nanoparticles and [B] fabrication of H40–Au/ITO and Urs/H40–Au/ITO electrodes.

solution (pH 7.0, 0.9% NaCl) containing 0.5 mM hematein. The working electrode was either H40–Au/ITO or Urs/H40–Au/ITO. Platinum foil and Ag/AgCl were used as the counter and reference electrodes, respectively.

Photometric study was performed using a Varian Cary 100 Bio UV-visible spectrophotometer. For photometric measurements, a Urs/H40–Au/ITO electrode was dipped in a 5 mL phosphate buffer solution (50 mM, pH 7.0), which contained 200 μL of Nessler's solution and 1 mL of urea solution with varying concentrations. After 2 min of Urs/H40–Au/ITO electrode incubation, the absorbance of the colored product (i.e., $NH_2Hg_2I_3$, a complex formed between the Nessler's reagent and ammonia produced by the enzymatic hydrolysis of urea) in the solution at λ_{max} 385 nm, was measured to monitor the Urs enzyme kinetics.

FTIR spectra were recorded on a Perkin Elmer, Spectrum BX-II spectrophotometer. The surface morphology of the electrodes was examined with a Hitachi S-4800 field emission scanning electron microscope (SEM) operated at 5 kV. The specimens were sputter-coated with a thin layer of iridium (~5 nm) prior to examination. The morphology of H40–Au nanoparticles was further studied by transmission electron microscopy (TEM, Hitachi H-600) operated at 75 kV. A TEM sample was prepared by depositing 6 μL solution of H40–Au (ultrasonically dispersed in THF) on a copper grid coated with formbar and a carbon film using phosphotungstic acid (PTA) as a negative staining agent. All measurements were carried out at 20 °C.

3. Results and discussion

3.1. Electrode fabrication and characterization

The H40–NH_2 grafted Au–COOH nanoparticles were prepared via the formation of amide bonds between the amine groups of H40–NH_2 and the carboxylic acid group of Au–COOH. The resulting H40–Au nanoparticles were deposited onto an ITO coated glass substrate to form a uniform film. The free amino groups still present in the H40–Au nanoparticles were further used for covalent immobilization of Urs using NHS and EDC as the coupling agents during the bioelectrode preparation process [9]. Fig. 1 shows the overall steps for preparing H40–Au nanoparticles and fabricating the H40–Au/ITO and Urs/H40–Au/ITO electrodes.

The resultant enzyme immobilized electrode was characterized by FTIR spectroscopy. Fig. 2 shows the FTIR spectra of the H40–Au/ITO and Urs/H40–Au/ITO electrodes. The FTIR spectrum of the H40–Au/ITO electrode (Fig. 2A) showed the characteristic peaks at: (1) 3117–3281 cm^{-1} (O–H and N–H stretching); (2) 2946 and 2881 cm^{-1} (C–H stretching of $-CH_2$ groups); (3) 1731 cm^{-1} (C=O stretching of ester group); and (4) 1639 cm^{-1} (C=O stretching of amide group). The C=O characteristic peaks at 1639 cm^{-1} confirms the formation of amide bonds between H40–NH_2 and Au–COOH nanoparticles. In addition, the absorption band at 3117–3281 cm^{-1} indicates the presence of residual amino groups on the H40–Au nanoparticles that are used to immobilize the Urs.

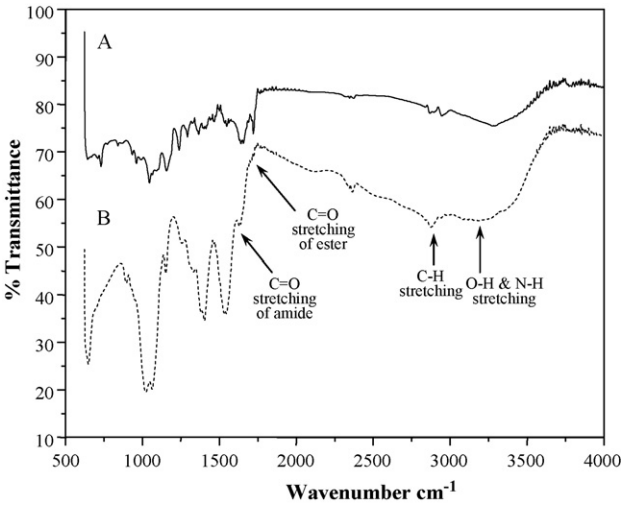

Fig. 2. FTIR spectra of the [A] H40–Au/ITO and [B] Urs/H40–Au/ITO electrodes.

The FTIR spectrum of the Urs/H40–Au/ITO electrode (Fig. 2B) showed peaks broadening at (1) 3067–3330 cm^{-1} (N–H stretching vibration); (2) 2930–2872 cm^{-1} (C–H stretching of $–CH_2$ groups); and (3) 1633 cm^{-1} (C=O stretching of amide group) due to the attachment of Urs enzyme through the peptide linkage on the electrode. Hence, FTIR spectra confirm the covalent immobilization of Urs onto the H40–Au/ITO electrode.

A typical SEM picture of H40–Au/ITO (Fig. 3A) exhibited tiny H40–Au particles with a porous surface. The nanoporous surface of the H40–Au/ITO electrode provided a very high surface-to-volume ratio, which can enhance the interaction between Urs and the H40–Au film of the electrode. Consequently, this will lead to a much higher level of enzyme stability and much better enzyme reproducibility for the Urs/H40–Au/ITO electrode. Immobilization of the Urs enzyme over the H40–Au/ITO electrode surface produced a homogeneous dentritic surface morphology (Fig. 3B). The uniform dentritic-like enzyme electrode surface may be formed due to the covalent binding of Urs molecules over the gold nanoparticles functionalized with hyperbranched polyester, i.e., the H40–Au nanoparticles.

To further understand the morphology of the H40–Au nanoparticles, TEM analysis was conducted using PTA as a staining agent (Fig. 3C). As demonstrated in Fig. 1A, multiple hyperbranched H40–NH_2 polyester molecules may be grafted onto one Au–COOH nanoparticle by amide bonds. The average size of the resulting H40–Au nanoparticles was 16 nm according to the TEM analysis. The PTA stain clearly showed the light contrast of hyperbranched H40–NH_2 molecules/nanoparticles and the dark contrast of Au–COOH nanoparticles with an average size of 3 and 12 nm, respectively. The size of the H40–NH_2 molecules/nanoparticles detected here is consistent with the average size of Boltron® H40 molecules/nanoparticles (i.e., 3 nm) reported in the literature [35]. The TEM image of the H40–Au nanoparticles clearly showed the formation of hyperbranched H40–NH_2 functionalized gold nanoparticles.

3.2. Amperometric measurements

Fig. 4 shows the CVs of the electrochemical cells using either H40–Au/ITO or Urs/H40–Au/ITO electrode at a constant 50 mV s^{-1} scan rate in 50 mM phosphate buffer solution (pH 7.0, 0.9% NaCl) containing 0.5 mM hematein. The current of the electrochemical cell using the Urs/H40–Au/ITO electrode (2.1×10^{-4} A) was about one-half of that using the H40–Au/ITO electrode (3.9×10^{-4} A). Thus, immobilizing Urs onto the electrode reduced the current. A decrease in current after the immobilization of Urs may be attributed to a slower redox behavior when compared with the bare H40–Au/ITO electrode. The covalent binding of Urs on the H40–Au/ITO electrode controls the moment of the supporting electrolytes [36]. Also, the non-conducting nature of the Urs molecules might have contributed to the decrease in current when using the Urs/H40–Au/ITO electrode.

Amperometric measurements were carried out with the Urs/H40–Au/ITO electrode for quantitative determination of urea in an aqueous medium using hematein, a pH-sensitive natural dye

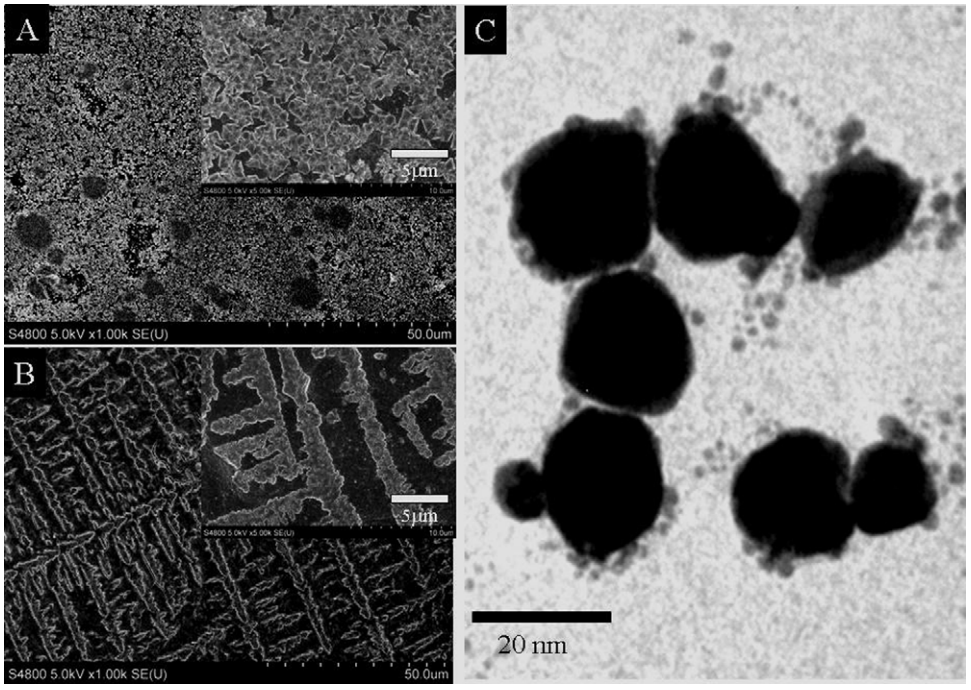

Fig. 3. Electron microscopic study of the [A] H40–Au/ITO using SEM, [B] Urs/H40–Au/ITO using SEM, and [C] hyperbranched H40–Au nanoparticles using TEM.

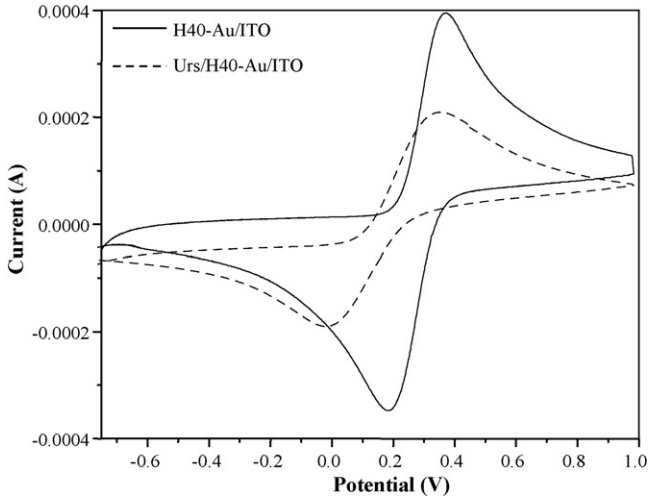

Fig. 4. Cyclic voltammograms of the [A] H40–Au/ITO and [B] Urs/H40–Au/ITO electrodes in 50 mM phosphate buffer solution at pH 7.0 containing 0.9% NaCl and 0.5 mM hematein.

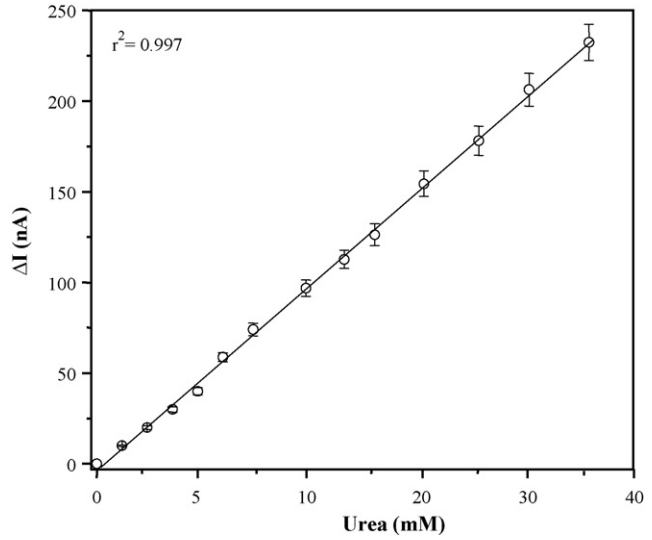

Fig. 5. Amperometric response of Urs/H40–Au/ITO bioelectrode with the urea concentration ranging from 0.01 to 35 mM at working potential of 0 mV vs. Ag/AgCl using 50 mM phosphate buffer solution containing 0.9% NaCl and 0.5 mM hematein.

[37]. Cyclic voltammetric studies were carried out in 50 mM phosphate buffer solution containing 0.5 mM hematein and 0.9% NaCl. It was observed that the cathodic peak shifted to a more positive potential as the pH value decreased. The shift in the cathodic peak potential was approximately 29 mV per pH unit. Previous studies indicated the stability of hematein in electrochemical cells using Pt and graphite composite electrodes depended on both pH and the applied voltage [37,38]. Thus, to avoid electrochemical interference on the stability of hematein, an amperometric measurement of urea should be conducted at a working potential of 0 mV [37].

Fig. 5 shows the steady-state current dependence calibration curve for the urea concentration ranging from 0.01 to 35 mM. An amperometric linear response (r^2 = 0.997) was observed with the successive addition of urea to the phosphate buffer solution containing 0.9% NaCl as the electrolyte and 0.5 mM hematein as the redox indicator under a constant stirring of 100 rpm at 2-min intervals. The electrode responded within 3 s to the change of urea concentration. The current sensitivity of the enzyme electrode toward urea concentrations was 7.48 nA/mM. This new type of urea

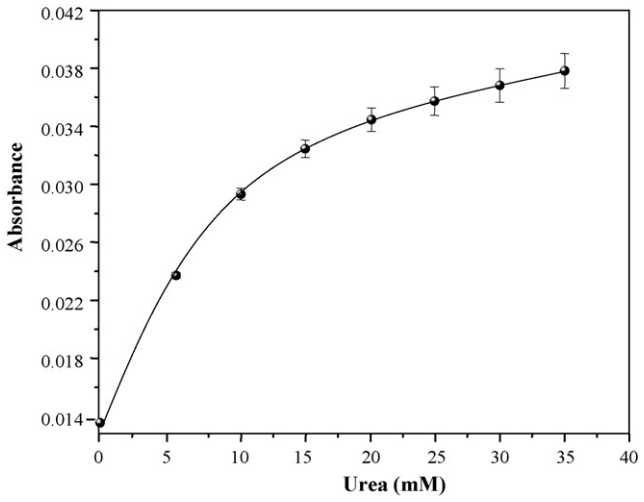

Fig. 6. Photometric response as a function of urea concentration ranging from 0.01 to 35 mM using a Urs/H40–Au/ITO electrode exposed with an equal amount of Nessler's reagent.

biosensor demonstrated a shorter response time and a broader detection range compared with those reported previously, as shown in Table 1. Table 1 provides the comparison of the performance of this new type of urea biosensor with those reported previously and will be further discussed later.

The affinity of Urs to the urea was estimated using the Hanes plot [39]. The Michaelis–Menten kinetic parameter (K_m^{app}) was calculated to be 0.96 mM for the Urs/H40–Au/ITO electrode. K_m^{app} usually depends on the electrode material as well as the enzyme immobilization process [40]. The K_m^{app} of the biosensor using Urs/H40–Au/ITO as the electrode is much less than that of these previously reported biosensors (typically 2–7 mM) [41,6]. The small K_m^{app} value indicates a high affinity of Urs to the urea over the Urs/H40–Au/ITO electrode surface, which may be attributed to (1) the advantageous nanoporous surface of the H40–Au/ITO electrode for the enzyme immobilization that can favor conformational changes of the enzyme and (2) the high surface-to-volume ratio, which can help to effectively immobilize Urs onto the H40–Au/ITO electrode. In addition, functionalized H40–Au nanoparticles can provide efficient electron transfer between the active site of the enzyme and the electrode, thereby enhancing the urea sensing activity.

3.3. Photometric study

A photometric response study was performed to calculate the apparent enzyme activity of the Urs/H40–Au/ITO electrode. Urs catalyzes the hydrolysis of urea to produce ammonia, which in turn reacts with the Nessler's reagent to form a colored product, $NH_2Hg_2I_3$ [42]. By following the absorbance of $NH_2Hg_2I_3$ at 385 nm, urea can be quantified and the analytical performance of the biosensor can be determined. The difference between the initial and final absorbance value at 385 nm were plotted as a function of urea concentration, as shown in Fig. 6. The enzyme electrode responded to the urea concentration within the range of 0.01–35 mM. The apparent enzyme activity ($^{enz}a_{app}$) was calculated using equation $^{enz}a_{app} = AV/\varepsilon ts$, where A is the difference in absorbance before and after incubation, V is the total volume of the solution, ε is the millimolar extinction coefficient, t is the reaction time and s is the surface area of the electrode. The apparent enzyme activity was calculated to be 71.59 mg/cm^2, indicating 71.59 mg of Urs was actively working per unit area of electrode surface.

Table 1
Assessment of the Urs/H40–Au/ITO biosensor characteristics with other previously reported amperometric urea biosensors.

Sl. No.	Electrode material	Immobilization method	Stability	Linear range	Detection limit	Response time	Reference
1.	Nylon net	Encapsulation	4 days	$0.1–3 \times 10^{-4}$ M	10^{-5} M	–	[44]
2.	Graphite and platinum composite	Physical adsorption	90 days	$1–25 \times 10^{-5}$ M	1×10^{-5} M	120 s	[37]
3.	Polyaniline-Nafion/Au/ceramic composite	Covalent	–	6–60 mg/dL	0.3 mg/dL	–	[18]
4.	Poly(*N*-3-aminopropyl pyrrole-*co*-pyrrole)	Covalent	60 days	$0.16–5.02 \times 10^{-5}$ M	0.16×10^{-5} M	40 s	[17]
5.	Poly(vinylferrocium)	Ionic binding	29 days	$1–25 \times 10^{-5}$ M	1×10^{-6} M	60 s	[45]
6.	Functionalized H40–Au nanoparticles	Covalent	126 days	$1–3500 \times 10^{-5}$ M	1×10^{-5} M	3 s	Present work

Table 2
Evaluation of the present method with the spectrophotometric method for the determination of urea from human blood serum and urine.

Sample no.	Urea concentration		% Error
	Present method	Standard spectrophotometric method	
Blood serum sample-1	2.8 ± 0.01 mM	2.6 ± 0.015 mM	7.14
Blood serum sample-2	3.4 ± 0.01 mM	3.1 ± 0.015 mM	8.82
Urine sample-1	316.2 ± 0.01 mM	309.4 ± 0.015 mM	2.19
Urine sample-2	274.9 ± 0.01 mM	262.7 ± 0.015 mM	4.64

3.4. Reproducibility and accuracy

The lowest detection limit of the urea electrode was 0.01 mM. The reproducibility of the response of the enzyme electrode was investigated at a 5 mM urea concentration. No significant decrease in current response was observed after at least 10 uses in testing; thus, the enzyme electrode displayed good reproducibility. The relative standard deviation was found to be about 8% determined by five successive measurements of a 5 mM urea standard using a single biosensor with the same Urs/H40–Au/ITO electrode. In a series of 10 biosensors using 10 different Urs/H40–Au/ITO electrodes, a relative standard deviation of about 6% was obtained for the individual current response of the same sample (5 mM urea). The good reproducibility observed with the biosensor may be attributed to the efficient bonding of the enzyme with the functionalized H40–Au nanoparticles.

3.5. Thermal stability

The thermal stability of the Urs/H40–Au/ITO electrode was studied by measuring the current at different temperatures ranging from 20 to 45 °C in the presence of 5 mM urea. It was observed that the reaction rate increased with the temperature up to 30 °C and the optimum temperature range was between 28 and 30 °C due to the increased kinetic energy of the reacting molecules. The storage stability of the Urs/H40–Au/ITO electrode was amperometrically measured and a similar current response was found after storing for 18 weeks at 4 °C.

3.6. Interference study

The effect of interferents was studied on the amperometric responses of the biosensor employing the Urs/H40–Au/ITO electrode in the presence of 5 mM urea. The interference effects of L-serine, L-threonine, α-ketoglutaric acid, L-alanine, L-phenylalanine, uric acid, L-cystine, L (+)-glutamic acid, sodium pyruvate, L-glutamine, and L-ascorbic acid was investigated by measuring the amperometric response of the Urs/H40–Au/ITO electrode. These substances were added into the reaction mixture at their normal physical concentration, i.e., 0.2 mM. It was found that the presence of interferents had a relative error of less than 4% in the current measured by the amperometric method; therefore, this bioelectrode can detect urea with negligible interference.

3.7. Performance of biosensor with biological samples

To demonstrate the feasibility of the Urs/H40–Au/ITO biosensor for urea analysis, samples of fresh blood serum and urine from a healthy person were analyzed. The analyses were performed without any sample pretreatment and results were compared with those obtained from the standard spectrophotometric method [43]. As shown in Table 2, the value of urea concentration in blood serum and urine obtained with Urs/H40–Au/ITO biosensor was ~2–9% higher than those obtained from the standard method [43], most

likely due to the interferences of the electroactive species present in blood plasma and urine. Overall, a good agreement of the urea concentration in both cases was observed.

Table 1 compares the characteristics of the new amperometric urea biosensor based on the Urs/H40–Au/ITO electrode with those reported in the literature. It is apparent that the Urs/H40–Au/ITO based urea biosensor exhibited a longer shelf life, higher sensitivity, wider range of detection limit, and shorter response time.

4. Conclusion

A new type of urea biosensor based on a Urs/H40–Au/ITO bioelectrode was successfully fabricated and evaluated. Urs was covalently immobilized onto the nanoporous film formed by gold nanoparticles functionalized with hyperbranched Boltron® H40 polyester on the ITO coated glass (H40–Au/ITO). The H40–Au/ITO electrode surface offered a high level of enzyme immobilization leading to a highly stable Urs/H40–Au/ITO bioelectrode. The urea biosensor showed a linear current response to the urea concentration ranging from 0.01 to 35 mM and it exhibited a sensitivity of 7.48 nA/mM with a response time of 3 s. The relatively low Michaelis–Menten constant of 0.96 mM indicates that the H40–Au/ITO electrode surface had a high affinity for the Urs enzyme. This new type of urea biosensor has demonstrated superior performance compared with those reported previously, including a longer shelf life, higher sensitivity, wider range of detection limit, and shorter response time.

Acknowledgement

The authors would like to acknowledge the financial support to carry out this work from National Science Foundation (NSF), USA under the project CMMI-0734881.

References

[1] A.C. Guyton, Science 252 (1991) 1813.
[2] D. Aronson, Am. J. Med. 116 (2004) 466.
[3] C. Ronco, R. Bellomo, P. Homel, A. Brendolan, M. Dan, P. Piccinni, G.L. Greca, Lancet 355 (2000) 26.
[4] D.H. Yun, M.J. Song, S.I. Hong, J. Korean Phys. Soc. 47 (2005) S445.
[5] W.J. Cho, H.J. Huang, Anal. Chem. 70 (1998) 3946.
[6] C. Eggenstein, M. Borchardt, C. Diekmann, B. Grundig, C. Dumschat, K. Cammann, E.M.I.M. Ekanayake, D.M.G. Preethichandra, K. Kaneto, Biosens. Bioelectron. 23 (2007) 107.
[7] A.Q. Contractor, T.N. Sureshkumar, R. Narayanan, S. Sukeerthi, R. Lal, R.S. Srinavasa, Electrochim. Acta 39 (1994) 1321.
[8] A. Ramsing, J. Ruzicka, E.H. Hansen, Anal. Chim. Acta 114 (1980) 165.
[9] A. Riklin, E. Katz, I. Willner, A. Stocker, A.F. Buckmann, Nature 376 (1995) 672.
[10] B. Xie, U. Harborn, M. Mecklenburg, B. Danielsson, Clin. Chem. 40 (1994) 2282.
[11] Z. Yang, S. Si, H. Dai, C. Zhang, Biosens. Bioelectron. 22 (2007) 3283.
[12] A. Tiwari, S. Gong, Electroanalysis 20 (2008) 2119.
[13] S.B. Adeloju, S.J. Shaw, G.G. Wallace, Anal. Chim. Acta 341 (1997) 155.
[14] S.K. Jha, A. Topkar, S.F. D'Souza, J. Biochem. Biophys. Methods 70 (2008) 1145.
[15] X. Wang, H. Watanabe, N. Sekioka, H. Hamana, S. Uchiyama, Electroanalysis 19 (2007) 1300.
[16] F. Kuralay, H. Ozyoruk, A. Yıldız, Sens. Actuators B: Chem. 109 (2005) 194.
[17] Rajesh V. Bisht, W. Takashima, K. Kaneto, Biomaterials 26 (2005) 3683.
[18] Y.C. Luo, J.S. Do, Biosens. Bioelectron. 20 (2004) 15.
[19] B. Lakard, G. Herlem, S. Lakard, A. Antoniou, B. Fahys, Biosens. Bioelectron. 19 (2004) 1641.
[20] R. Singhal, A. Gambhir, M.K. Pandey, S. Annapoorni, B.D. Malhotra, Biosens. Bioelectron. 17 (2002) 697.
[21] M.M.C. Ortega, D.E. Rodriguez, J.C. Encinas, M. Plascencia, F.A.M. Velarde, R. Olayo, Sens. Actuators B: Chem. 85 (2002) 19.
[22] J.M.C.S. Magalhaes, A.A.S.C. Machado, Talanta 47 (1998) 183.
[23] A. Tiwari, S. Gong, Electroanalysis 20 (2008) 1775.
[24] J.D. Swalen, D.L. Allara, J.D. Andrade, E.A. Chandross, S. Graoff, J. Israelachvili, T.J. McCarthy, R. Murray, R.F. Pease, J.F. Rabolt, K.J. Wynne, H. Yu, Langmuir 3 (1987) 932.
[25] T. Wink, S.J. van Zuilen, A. Bult, W.P. Bennekom, Analyst 122 (1997) 43R.
[26] K. Habermuller, M. Mosbach, W. Schuhmann, Fresenius' J. Anal. Chem. 366 (2000) 560.
[27] Y. Xiao, H.X. Ju, H.Y. Chen, Anal. Biochem. 278 (2000) 22.
[28] Z. Cao, X. Jiang, Q. Xie, S. Yao, Biosens. Bioelectron. 24 (2008) 222.
[29] J.F. Hicks, F.P. Zamborini, A.J. Osisek, R.W. Murray, J. Am. Chem. Soc. 123 (2001) 7048.
[30] A.N. Shipway, M. Lahav, I. Willner, Adv. Mater. 12 (2000) 993.
[31] R. Polsky, R. Gill, L. Kaganovsky, I. Willner, Anal. Chem. 78 (2006) 2268.
[32] K.R. Brown, A.P. Fox, M.J. Natan, J. Am. Chem. Soc. 118 (1996) 1154.
[33] Y. Xiao, H.X. Ju, H.Y. Chen, Anal. Chim. Acta 391 (1999) 73.
[34] M. Prabaharan, J.J. Grailer, D.A. Steeber, S. Gong, Macromol. Biosci. 8 (2008) 843.
[35] E. Zagar, M. Zigon, J. Chromatogr. A 1034 (2004) 77.
[36] A. Tiwari, S. Gong, Talanta 77 (2009) 1217.
[37] A. Pizzariello, M. Stredansky, S. Stredanka, S. Miertus, Talanta 54 (2001) 763.
[38] M. Stredansky, A. Pizzariello, S. Stredanka, S. Miertus, Anal. Chim. Acta 415 (2000) 151.
[39] J.M. Walker, Principles, Techniques of Practical Biochemistry, 5th ed., Cambridge University Press, UK, 2000.
[40] G.K. Kouassi, J. Irudayaraj, G. McCarty, J. Nanobiotechnol. 3 (2005) 1.
[41] J.X. Wang, X.W. Sun, A. Wei, Y. Lei, X.P. Cai, C.M. Li, Z.L. Dong, Appl. Phys. Lett. 88 (2006) 233106.
[42] Rajesh V. Bisht, W. Takashima, K. Kaneto, Surf. Coat. Technol. 198 (2005) 231.
[43] F.K. Fawcett, J.E. Scott, J. Clin. Pathol. 13 (1960) 156.
[44] P. Bertocchi, D. Compagnone, G. Palleschi, Biosens. Bioelectron. 11 (1996) 1.
[45] F. Kuralay, H. Ozyoruk, A. Yildiz, Sens. Actuators B: Chem. 114 (2006) 500.

Talanta 78 (2009) 1345–1351

Contents lists available at ScienceDirect

Talanta

journal homepage: www.elsevier.com/locate/talanta

Method development for the analysis of organophosphate and pyrethroid insecticides at low parts per trillion levels in water

Dongli Wang [a], Donald P. Weston [b], Michael J. Lydy [a,*]

[a] Fisheries and Illinois Aquaculture Center & Department of Zoology, 171 Life Science II, Southern Illinois University, Carbondale, IL 62901, USA
[b] Department of Integrative Biology, University of California, 3060 Valley Life Sciences Building, Berkeley, California 94720-3140, USA

ARTICLE INFO

Article history:
Received 22 December 2008
Received in revised form 4 February 2009
Accepted 6 February 2009
Available online 20 February 2009

Keywords:
Pyrethroid insecticides
Organophosphate insecticides
Liquid–liquid extraction
Solid-phase extraction

ABSTRACT

In the current study, organophosphate and pyrethroid insecticides including diazinon, chlorpyrifos, bifenthrin, fenpropathrin, permethrin, λ-cyhalothrin, cyfluthrin, cypermethrin, esfenvalerate and deltamethrin were analyzed in laboratory and field-collected water samples. Water samples were extracted and analyzed by gas chromatography/electron capture detector (GC/ECD) and gas chromatography/nitrogen–phosphorous detector (GC/NPD). Comparison of results from liquid–liquid extraction and subsequent normal phase solid-phase extraction cleanup (LLE–NPSPE), and reversed phase solid-phase extraction (RPSPE) showed that LLE–NPSPE was the better choice to extract trace amounts of pesticides from water. Pesticide recoveries from four spiked water samples using LLE–NPSPE ranged from 63.2 to 148.8% at four spiking concentrations. Method detection limits were 0.72–1.69 ng/L using four different water sources. The stability of the target pesticides in lake water was investigated at 4 °C for 1 h, 1 d, 4 d, and 7 d under three conditions: (1) water samples only; (2) with 20 mL hexane used as a keeper solvent; and (3) with acidification to pH 2 with HCl. Results showed that water storage without treatment resulted in slow degradation of some pesticides with storage time, storage using water acidification led to significant degradation and loss of diazinon and chlorpyrifos, while water storage with hexane as a keeper solvent showed good stability for all of the target pesticides over the 7 d storage period.

1. Introduction

Some of the most widely used organophosphate pesticides (OPs) were recently withdrawn from residential use by both professional pest control applicators and homeowners. The relatively high water solubility of OPs has led to their detection in urban-dominated waters following rain events, frequently at concentrations toxic to aquatic life [1,2]. Chlorpyrifos has often been detected in surface waters and appears to be rather persistent [3,4]. The potential toxicity of OPs to aquatic life and humans, especially children, has led to their replacement with pyrethroid insecticides, which have assumed many roles formerly held by organophosphates. Pyrethroids are synthetic derivatives of pyrethrins, which are natural insecticides that are produced from chrysanthemum plants [5], and act as neurotoxins [6]. Pyrethroids are extensively used by professional pest control applicators, with about 325,000 kg used for nonagricultural purposes in California in 2005, primarily for structural pest control and landscape maintenance (http://www.cdpr.ca.gov/docs/pur/purmain.htm). They also dominate retail insecticide sales to homeowners, although the amounts used are not publicly reported. Pyrethroids are transported into surface waters by agricultural and urban runoff from rainstorms [7,8], drift from aerial or ground-based spraying [9], urban landscape irrigation [10], and release of agricultural tailwaters [11]. Once in receiving waters, these insecticides can potentially induce toxicity in aquatic organisms [12,13].

Pyrethroids are strongly adsorbed onto soil and sediment, which leads to the relatively low concentrations of these pesticides in surface water. In addition, toxicological studies performed in water-only systems have found that these pesticides cause lethal and sublethal effects at extremely low concentrations, with LC50s being generally less than 1 ng/mL [14]. For example, cypermethrin has LC50 values of 1.2, 0.9 and 0.5 ng/mL for brown trout, carp and rainbow trout, respectively [15]. When mosquito and midge larvae were tested, 24 h LC50 values for deltamethrin, cypermethrin, fenvalerate and permethrin ranged from 0.02 to 13 ng/mL [16]. Deltamethrin and cypermethrin have 96 h LC50s of about 0.01 ng/mL in lobster (*Homarus americanus*) and shrimp (*Crangon septemspinosa*) [17,18]. Toxicity to the amphipod *Hyalella azteca* occurs at concentrations as low as 0.002 and 0.005 ng/mL for λ-cyhalothrin and cypermethrin, respectively [19,20]. Therefore, there is a need to employ sensitive trace analysis methods for the measurement and positive identification of these pesticides at the low nanogram per liter level. Solid-phase extraction

* Corresponding author.
E-mail address: mlydy@siu.edu (M.J. Lydy).

0039-9140/$ – see front matter © 2009 Elsevier B.V. All rights reserved.
doi:10.1016/j.talanta.2009.02.012

(SPE) [21–27], solid-phase micro-extraction (SPME) [24,28,29], stir bar sorption extraction (SBSE) [30–32] and liquid-phase micro-extraction (LPME) [33,34] have attracted increasing attention as novel sample pretreatment techniques. The need for strict experimental control and long equilibrium times, however limits the application of SPME, SBSE and LPME in large-scale analysis of field-collected water samples. Moreover, the strong tendency of pyrethroids to adsorb to glass containers can cause decreased SPE recoveries and substantial underestimation of pyrethroid concentrations [27] and can significantly affect the observed outcome in toxicological testing [35]. Thus, liquid–liquid extraction (LLE) still ranks as one of the most conventional and effective isolation techniques, which is particularly suitable for direct extraction of field-collected water samples to exclude possible analyte loss during sample collection, shipment, and storage [27].

Instrumental analysis of pesticides in water samples tends to be performed on high-resolution gas chromatography/high-resolution mass spectrometry (HRGC/HRMS) [36] and liquid chromatography/electrospray ionization mass spectroscopy [26]. These instruments provide high selectivity and mass resolution to reduce potential interference and enable the method to routinely achieve low levels of chemical detection, but higher costs of instrumental maintenance have limited their application in most environmental laboratories. A less expensive alternative is the use of gas chromatography/electron capture detection (GC-ECD) and gas chromatography/nitrogen–phosphorous detection (GC-NPD) with a dual column system which could provide the necessary sensitivity and selectivity for pesticides analysis [37,38].

In the current study, three extraction methods were tested to optimize extraction efficiencies of the pesticides from water. These methods included liquid–liquid extraction with normal phase solid-phase extraction (LLE–NPSPE) cleanup, and the use of two different C_{18} reversed phase solid-phase extraction (RPSPE) cartridges. Additional method development was then conducted on the best of the extraction efficiency techniques. The stability of the pesticides during storage was also examined in lake water using different stabilization agents including hexane and acidification. Finally, the optimized method was tested using field-collected water samples.

2. Materials and method

2.1. Chemicals and reagents

Two type-I pyrethroids, bifenthrin and permethrin, six type-II pyrethroids, λ-cyhalothrin, cyfluthrin, cypermethrin, deltamethrin, esfenvalerate and fenpropathrin, and two organophosphate pesticides, diazinon and chlorpyrifos, were purchased from ChemService Inc. (West Chester, PA, USA). All of the insecticides had certified purities >95%. A working standard solution was prepared with a concentration of 2000 ng/mL in hexane and stored in the freezer. The surrogates 4,4′-dibromooctafluoro-biphenyl (DBOFB) and decachlorobiphenyl (DCBP) were purchased from Supelco (Bellefonte, PA, USA).

Acetone, hexane, dichloromethane (DCM), and methanol were purchased from Fisher Scientific (Pittsburgh, PA, USA). Hydrochloric acid (1 M HCl) was obtained from Supelco. Anhydrous Na_2SO_4 was baked in a muffle furnace at 450 °C for 4 h prior to use. Solid-phase extraction cartridges included dual layer Supelclean ENVI™-Carb II (GCB)/Supelclean™ primary/secondary amine (PSA) (3.0 mg/600 mg, 6.0 mL, ResPrep, Bellefonte, PA, USA) and bonded-phase silica C_{18} cartridges (1000 mg, 8.0 mL, Alltech Associates Inc, Deerfield, IL; or Agilent Technologies, Palo Alto, CA).

2.2. Sample collection and storage

Deionized water was obtained from our research laboratory, while lake water was collected from Campus Lake at Southern Illinois University in Carbondale, Illinois. A sample from a publicly owned treatment works (POTW) facility was obtained from the final treated effluent of the Sacramento Regional County Sanitation District, Sacramento, California. A sample of runoff from the city of Vacaville and surrounding farmlands was obtained from Alamo Creek (Vacaville, California) following heavy rains. Finally, an additional 14 field-collected water samples were taken from Roseville, CA, north of Sacramento to test the newly developed analytical methods. Water samples were taken either by immersing a 2-L solvent-cleaned glass bottle just below the water surface, or when depths were too shallow to allow this, then by dipping a stainless steel container into the water repeatedly and transferring its contents to the glass bottle. The water sample bottles were held on ice until return to the laboratory where they were refrigerated at 4 °C.

2.3. Method development

Three extraction methods were tested to optimize extraction efficiencies of the pesticides from water. These methods included LLE–NPSPE cleanup, and the use of two different C_{18} RPSPE cartridges, one from Alltech and one from Agilent. This initial comparison study was conducted using four replicate lake water samples spiked with the target pesticides at 20 ng/L.

After the water samples were shipped to the laboratory, they were stored at 4 °C in the dark. A 500 mL water sample was measured using a graduated cylinder and transferred to a 1-L glass separatory funnel after the original sample container was vigorously shaken to reduce the container adsorption of the analytes [27]. Each sample was spiked with 50 ng of the DBOFB and DCBP surrogates. Liquid–liquid extraction was performed using a slightly modified version of EPA Method 3510 [39]. Samples were allowed to sit for 1 h prior to LLE when spiked with the target analytes. Fifty millilitres of DCM was used to rinse the graduated cylinder and then added to the separatory funnel, and shaken for 2.0 min. The DCM layer was drained into a 200 mL Turbovap vial after the solution separated into two defined layers. This procedure was repeated two additional times. The combined extracts were concentrated to 1.0 mL in hexane and then added to a GCB/PSA cartridge, which was preconditioned using 3.0 mL of hexane. The GCB/PSA cartridge was used to effectively remove plant pigments such as chlorophyll, and plant sterols from the final extracts without the loss of planar compounds [40]. Analytes were eluted from the cartridges with 7.0 mL of a 30% DCM in hexane solution. Eluates were concentrated to 0.5 mL in a 0.1% acetic acid in hexane solution for subsequent GC analysis. Analyte recoveries ranged from 95 to 110% using the clean-up step with this cartridge.

The RPSPE method was performed using 500 mL water samples, which were spiked with 50 ng of the two surrogates DBOFB and DCBP. Two commercially available C_{18} SPE cartridges were tested (one from Alltech and one from Agilent) and each was conditioned with 3.0 mL of a solution of hexane and acetone (1:1, v/v), 3.0 mL methanol, and 6.0 mL distilled water with a flow rate of one drop per second. The water sample was introduced into the cartridge using the same flow rate, and then the cartridge was vacuum-dried for 10 min to remove any excess water. The beaker that contained the original sample was rinsed twice with 4.0 mL of a mixture of hexane and acetone (1:1, v/v), and the solvent pumped through the cartridge. The solvent elution (8.0 mL) was collected and concentrated to 0.5 mL in 0.1% acetic acid in hexane under a gentle stream of nitrogen prior to GC analysis. Excess water was removed by adding baked anhydrous Na_2SO_4.

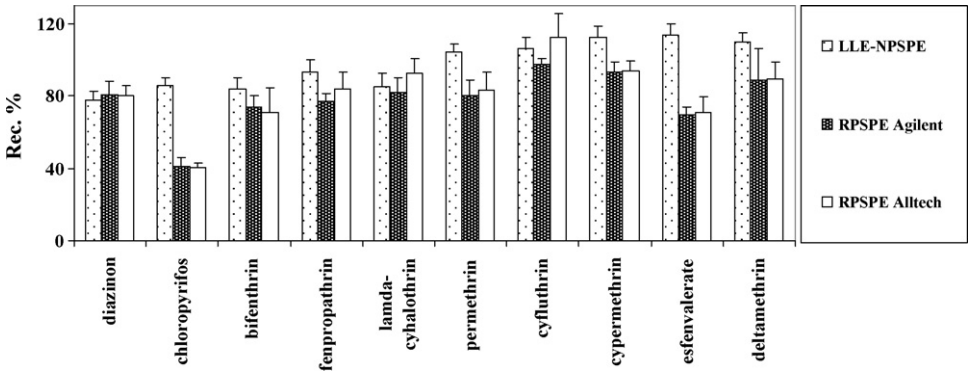

Fig. 1. Percent recoveries and standard deviations from four replicate analyses of lake water spiked at 20 ng/L with the target pesticides. LLE–NPSPE refers to the liquid–liquid extraction normal phase solid-phase extraction method, and RPSPE refers to the two different commercial reversed phase solid-phase extraction cartridges.

The stability study was initiated by spiking the target pesticides at a concentration of 20 ng/L into 500 mL of lake water, and storing the sample at 4 °C in the dark for 1 h, 1 d, 4 d and 7 d. A separate batch of water samples was spiked at the same concentration and was treated with 1N HCl to adjust the pH of the water to 2.0, while 20 mL of hexane was added to a third batch of water samples to act as a keeper solvent. These treated water samples were also stored at 4 °C in the dark for 1 h, 1 d, 4 d and 7 d to compare results with those without acidification or hexane addition.

The best storage method for the water samples was selected and applied to the field-collected samples. After the field-collected water samples (at least 2 L) were shipped to the analytical laboratory, 500 mL aliquots were filled into separate bottles prior to analysis, and stored at 4 °C with the addition of 20 mL of hexane as a keeper solvent.

2.4. Instrumental analysis

The final extracts were analyzed on two Agilent 6890 series gas chromatographs (GC), both equipped with an Agilent 7683 autosampler, a micro-electron capture detector (GC-μECD), and a nitrogen–phosphorous detector (GC/NPD) (Agilent Technologies, Palo Alto, CA). Diazinon was quantified by GC/NPD, and the remaining compounds were quantified by GC/ECD. The ECD temperature was set at 320 °C, and the NPD temperature was set at 290 °C. Two columns, a HP-5 ms (30 m × 0.25 mm × 0.25 μm film thickness) and a DB-608 (30 m × 0.32 mm × 0.50 μm film thickness) (Agilent Technologies, Palo Alto, CA) were used to confirm the analytical results. Helium and nitrogen were employed as the carrier and makeup gas, respectively. The flow rates of carrier gas were 3.5 and 1.8 mL/min for the HP-5 ms and DB-608 columns, respectively. A 2.0 μL sample was injected into the GC using a pulsed split-less mode. For the HP-5 ms column, the oven was set at 100 °C, heated to 180 °C at 10 °C/min, then to 205 °C at 3 °C/min, and held at 205 °C for 4 min, then heated to 280 °C at 20 °C/min and held at this temperature for 10 min. For the DB-608 column, the oven was set at 100 °C, heated to 250 °C at 10 °C/min, then to 280 °C at 3 °C/min, and held at 280 °C for 15 min. Instrumental calibration was performed using the external standard method with seven sets of the calibration standard solutions with 2.5, 5, 10, 50, 100, 250, 500 ng/mL of each pesticide and surrogates in hexane. Qualitative identity was established using a retention window of 0.5% with confirmation on a second column. Data analysis was performed using Microsoft Office Excel 2003, and SAS 9.1.3 service pack 4 (SAS Institute Inc., Cary, NC, USA).

2.5. Quality assurance–quality control

A method blank was included with each batch of spiked, aged, and field-collected water samples by analyzing 500 mL of deionized water only. A matrix spike and matrix spike duplicate were performed with every batch. Surrogates were added to each sample prior to extraction to check method performance. Method detection limits (MDLs) were evaluated using three times the standard deviation of seven replicates of extractions of spiked water at a concentration of 1.0 ng/L. The GC was calibrated on a daily basis, and the calibration curve had good linearity (R^2, 0.995). A mid standard (50 ng/mL) was run every 10 samples to assure less than 20% variation from the calibration standards.

3. Results and discussion

3.1. Comparison of LLE–NPSPE and RPSPE

The LLE–NPSPE method effectively extracted the target pesticides spiked into campus lake water at a concentration of 20 ng/L; however, other interfering compounds (such as pigments and sterols) were also extracted. Therefore, the extracts required subsequent NPSPE cleanup to remove the interfering compounds prior to the final GC analysis and a dual layer Superclean GCB/PSA cartridge was used. Recoveries of the target pesticides from the lake water samples were very good for the LLE–NPSPE method and ranged from 77.7 to 114.1% (Fig. 1). In addition, good chromatographic separation was achieved for the target analytes spiked in lake water samples using both GC columns (Fig. 2, only GC/ECD signals were shown). Extraction efficiencies of the pesticides were also determined using two different C_{18} RPSPE cartridges for comparison with the LLE–NPSPE method. Initial experiments conducted with the pyrethroids found that they strongly bound to the glass beakers in the spiked water samples with an almost complete loss of these analytes. Lee et al. [27] also found strong container absorption of pyrethroids. Therefore, a mixture of hexane and acetone (8 mL) was used to rinse the beakers and the rinsing solvent was pumped through the cartridge (termed "back extraction" in the current study). Although back extraction significantly enhanced the extraction recoveries of the analytes, results from the two commercial C_{18} cartridges showed that RPSPE produced lower recoveries (40.5–112.3%) for the target pesticides than the LLE–NPSPE method (Fig. 1). The lower recoveries noted for the RPSPE cartridges might be due to an inability to effectively trap or adsorb the analytes from the water samples, and this resulted in analyte loss. Therefore, the LLE–NPSPE was chosen as the technique for further method development.

3.2. Testing of the LLE–NPSPE method

Method detection limits for the LLE–NPSPE method ranged from 0.12 to 1.70 ng/L for the four water matrices tested (Table 1) and were chosen as the maximum value among the four matrices

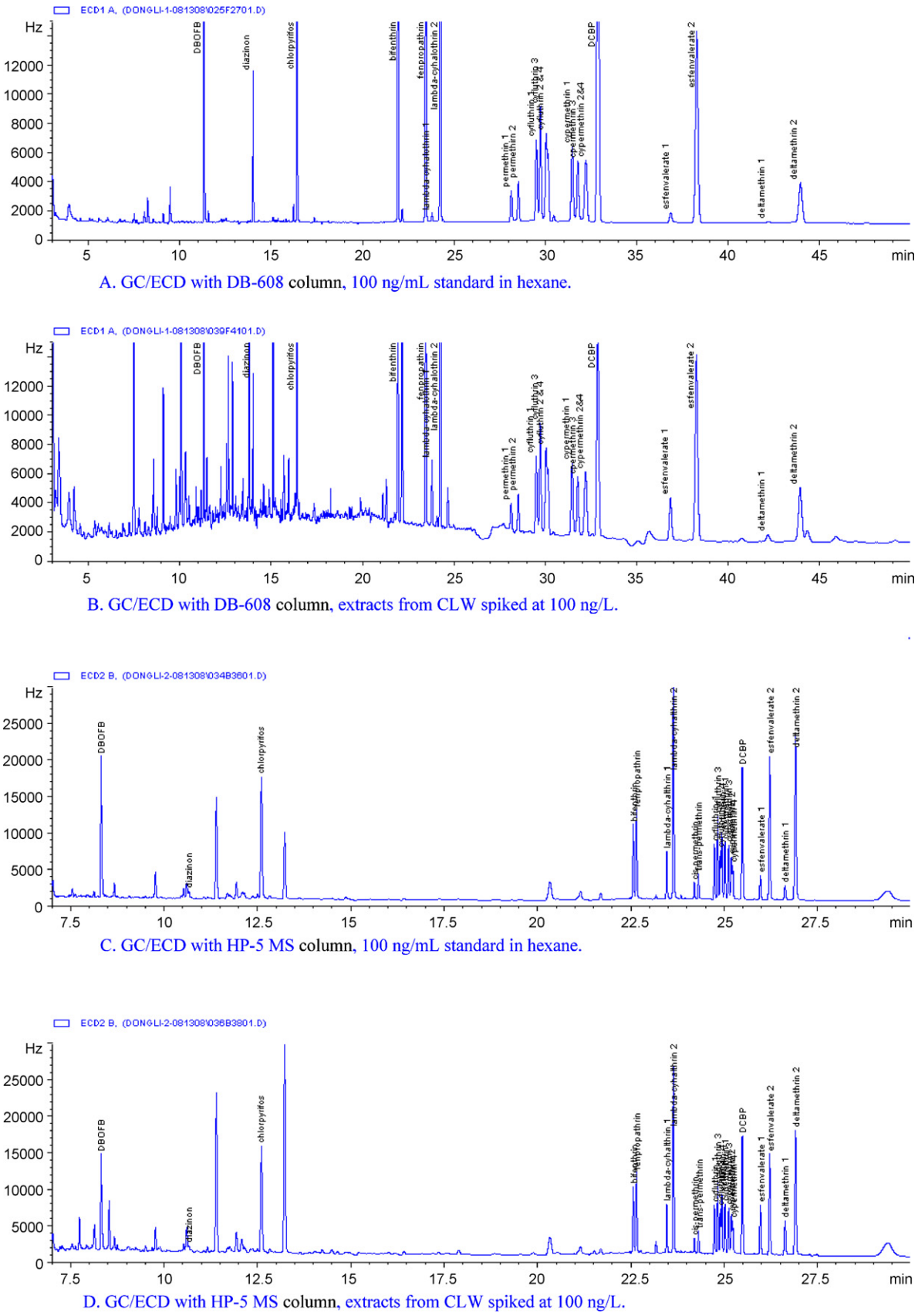

Fig. 2. Chromatograms for GC/ECD analysis of extracts of campus lake water (CLW) spiked at 100 ng/L and a 100 ng/L calibration standard. Data are shown for both the HP-5 ms and DB-608 columns.

Table 1
Method detection limits (MDL, ng/L) in deionized water (DIW), Campus lake water (CLW), runoff water and publicly owned treatment works water spiked with the target analytes at 1 ng/L. The MDLs were chosen based on the highest value for the four water matrices.

Pesticides	DIW	CLW	Runoff	POTW	Method MDL
Diazinon	0.55	0.99	1.69	0.81	1.69
Chlorpyrifos	0.12	0.42	1.59	0.30	1.59
Bifenthrin	0.31	0.37	1.12	1.24	1.24
Fenpropathrin	0.45	0.45	1.65	1.24	1.65
λ-Cyhalothrin	0.73	0.43	0.59	1.27	1.27
Permethrin	0.73	0.63	1.00	1.59	1.59
Cyfluthrin	0.50	0.69	0.65	1.09	1.09
Cypermethrin	0.51	1.70	0.59	1.13	1.70
Esfenvalerate	0.30	0.52	0.41	0.75	0.75
Deltamethrin	0.36	0.72	0.64	0.41	0.72

tested. The MDLs determined in the current study were comparable with those determined using a stir bar sorptive extraction-capillary gas chromatographic-mass spectrometric method (1.0–2.5 ng/L) [30] and for ground water (0.2–0.5 ng/L) and seawater samples (0.3–0.7 ng/L) using liquid chromatography/electrospray ionization mass spectrometry [26]. Much higher MDLs were reported in the literature for OPs in water using a single drop microextraction-gas chromatography mass spectrometry method (49–810 ng/L) [33] and for pyrethroids determined using a temperature-controlled ionic liquid dispersive liquid-phase micro-extraction method (280–600 ng/L) [34].

The LLE–NPSPE method was initially tested by spiking four different water sources including deionized water, lake water, runoff water and final effluent from a POTW with the target pesticides at 1, 3, 20 and 100 ng/L. Mean pesticide recoveries using the LLE–NPSPE method were 66.5–129.4% with relative standard deviations (RSDs) of 1.0–24.2% in deionized water and 63.2–148.8% with RSDs of 1.3–26.6% in lake water (Table 2). Pesticide recoveries from runoff water were 70.9–125.8% with RSDs of 4.9–37.9% and 70.8–148.1% with RSD of 1.5–33.4% in POTW effluent (Table 2). Higher recoveries and RSDs tended to occur in runoff and POTW effluent when these matrices were spiked at 1 ng/L (Table 2), since matrix effects become more problematic at MDL levels.

3.3. Storage stability of the pesticides

Campus lake water samples were spiked with 20 ng/L of the analytes and then stored at 4 °C for 1 h, 1 d, 4 d and 7 d to study the stability of the analytes under three holding conditions: (I) water samples only; (II) with acidification to pH 2 with HCl; (III) with 20 mL hexane which was used as a keeper solvent. Triplicate experiments were performed under all three conditions at each time point. The results are shown in Fig. 3.

Under storage condition I, recoveries of bifenthrin (from 83.6% in 1 h to 67.8% in 7 d) and fenpropathrin (from 92.2% in 1 h to 59.9% in 7 d) in lake water significantly decreased with increased storage time ($p \leq 0.05$). Recoveries of λ-cyhalothrin (from 79.9% in 1 h to 61.4% in 4 d to 74.9% in 7 d) and permethrin (from 105.1% in 1 h to 81.1% in 7 d) also slightly decreased in lake water with increasing storage time, even if no significant difference was observed for the recoveries of each compound with various storage times. For bifenthrin, fenpropathrin, λ-cyhalothrin, permethrin, cyfluthrin, cypermethrin, esfenvalerate and deltamethrin, lower or slightly lower recoveries were found with storage times up to 4 d, but no significant difference was observed from 1 h to 7 d.

Under storage condition II, water acidification resulted in the rapid degradation of diazinon in lake water over increasing storage time ($p \leq 0.05$), but no significant degradation was observed for other compounds in lake water with the storage times up to 7 d (Fig. 3, $p > 0.05$). These results suggested that water acidification led to the hydrolytic decomposition of diazinon and chlorpyrifos, to a certain degree [41], and the hydrolytic decomposition rates might depend on water matrix, pH value, and pesticides chemical structure, which is beyond the scope of this study to further investigate.

Under storage condition III, no significant difference was found in target analyte recoveries in lake water with increasing storage time (Fig. 3). However, hexane addition did improve the recoveries of chlorpyrifos, bifenthrin, fenpropathrin, λ-cyhalothrin, permethrin, cyfluthrin, cypermethrin, esfenvalerate and deltamethrin in lake water stored for 4 d and this is the time frame where we start to

Table 2
Mean percent pesticide recoveries and relative standard deviations (RSD) in deionized water (DIW), Campus lake water (CLW), runoff water and publicly owned treatment works water samples spiked at 1.0, 3.0, 20 and 100 ng/L.

	DIW								CLW							
	1.0 (ng/L)[a]		3.0 (ng/L)[a]		20 (ng/L)[a]		100 (ng/L)[a]		1.0 (ng/L)[a]		3.0 (ng/L)[a]		20 (ng/L)[a]		100 (ng/L)[a]	
	Mean	RSD	Mean	RSD	Mean	RSD	Mean	RSD	Mean	RSD	Mean	RSD	Mean	RSD	Mean	RSD
n	7		3		3		3		7		3		3		3	
Diazinon	92.4	19.1	94.1	21.5	95.9	3.7	81.1	3.8	103.9	22.0	104.5	12.1	92.8	15.0	79.8	14.2
Chlorpyrifos	67.2	5.2	93.2	11.9	80.9	6.4	72.1	7.3	100.3	12.4	89.8	22.3	81.1	2.3	63.2	8.2
Bifenthrin	98.1	10.2	76.4	3.1	77.2	1.6	88.7	7.0	87.8	12.5	79.3	13.0	83.6	4.3	76.2	7.0
Fenpropathrin	125.6	11.4	78.0	20.6	86.1	1.0	91.5	5.1	98.7	13.6	97.1	16.8	86.7	1.3	79.0	4.2
λ-Cyhalothrin	96.4	24.2	71.6	15.5	66.5	7.1	86.4	12.0	103.9	12.3	89.7	14.4	79.9	3.2	87.1	11.2
Permethrin	129.4	18.1	79.8	11.5	91.4	1.3	98.0	9.8	133.0	14.0	98.9	17.9	105.2	9.9	110.5	8.5
Cyfluthrin	119.0	13.4	109.8	4.3	78.6	1.3	98.5	6.1	119.9	17.3	86.7	14.9	83.6	10.1	99.4	10.1
Cypermethrin	116.5	14.1	100.7	9.4	80.6	1.9	97.0	7.7	148.8	26.6	87.2	8.4	96.3	12.9	100.1	11.9
Esfenvalerate	110.1	8.6	80.9	1.5	77.6	2.3	109.8	7.3	86.7	18.0	90.1	24.8	84.9	7.0	107.0	13.2
Deltamethrin	109.7	10.5	96.5	4.7	78.3	3.9	110.9	11.6	115.0	18.7	101.7	22.6	82.9	5.6	107.5	10.7
	Runoff								POTW							
Diazinon	121.5	28.9	91.4	19.3	88.0	6.6	93.8	6.6	103.8	18.7	90.2	13.0	100.2	9.7	78.5	13.2
Chlorpyrifos	91.6	37.9	70.9	5.7	82.2	4.9	72.0	8.0	102.5	8.9	113.7	20.6	101.9	1.5	77.9	6.1
Bifenthrin	80.2	32.5	75.0	5.9	93.3	7.9	89.2	7.1	117.2	28.2	116.6	24.7	77.9	8.6	87.7	6.0
Fenpropathrin	103.0	36.4	97.9	6.3	92.9	8.8	91.2	13.6	117.8	30.2	86.6	17.4	95.1	11.0	92.3	6.3
λ-Cyhalothrin	90.0	20.8	81.1	12.9	87.5	15.3	99.5	18.1	109.5	28.7	119.1	16.7	96.4	8.0	93.7	7.2
Permethrin	119.0	26.7	125.8	16.5	103.4	6.6	102.9	16.6	137.3	25.8	148.1	12.1	103.9	8.6	113.6	8.6
Cyfluthrin	114.8	18.0	116.7	5.7	96.5	6.8	90.1	9.7	119.6	29.0	145.3	8.5	110.2	5.9	97.0	7.3
Cypermethrin	108.7	17.2	107.6	9.4	92.1	5.7	89.1	11.5	70.8	33.4	145.1	11.8	101.7	8.0	95.5	9.1
Esfenvalerate	76.7	16.9	77.6	12.4	91.0	5.9	88.2	12.9	84.8	27.0	93.3	9.7	83.7	11.4	102.4	7.6
Deltamethrin	102.7	19.9	110.4	19.9	83.0	8.5	99.5	14.9	102.8	10.9	96.7	4.1	81.9	5.5	108.3	8.0

[a] Spiking concentration.

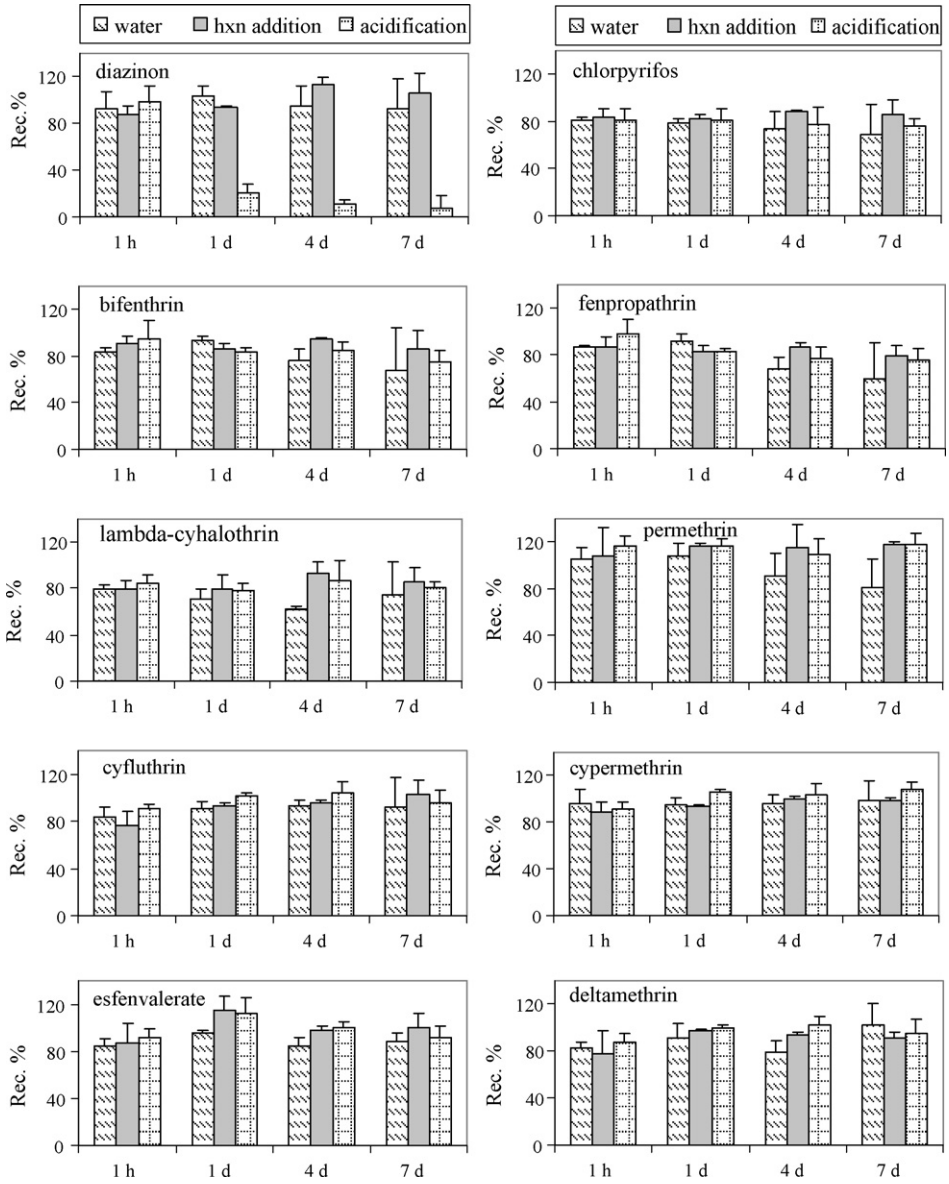

Fig. 3. The stability of the target pesticides (spiked at 20 ng/L) in campus lake water when stored at 4 °C for 1 h, 1 d, 4 d and 7 d under different storage conditions. Bars represent the mean of three replicates ±standard deviation. hxn = hexane.

find that these pesticides have lower recoveries in lake water under storage conditions I and II (Fig. 3).

In summary, the best choice for pesticide water storage is to extract the target analytes from the water within 4 days if applying no protection, or extract them within 7 days if applying hexane as a keeper solvent.

3.4. Validation of the LLE–NPSPE method using field-collected water samples

The newly developed LLE–NPSPE method was further tested using a series of 14 field-collected water samples and the data are presented in Table 3. The water samples were run as a single batch

Table 3
Mean pesticide concentrations and concentration ranges in 14 field-collected water samples taken from Roseville, CA.

Pesticide	Samples analyzed	Samples where pesticides were detected	Mean concentration (ng/L)	Concentration range (ng/L)	
Diazinon	14	0	<1.69	<1.69	<1.69
Chloropyrifos	14	3	3.45	2.89	4.23
Bifenthrin	14	14	14.0	2.55	29.7
Fenpropathrin	14	0	<1.65	<1.65	<1.65
λ-Cyhalothrin	14	2	4.89	2.84	6.95
Permethrin	14	9	21.7	7.43	66.1
Cyfluthrin	14	11	8.20	2.24	22.6
Cypermethrin	14	11	9.94	5.51	25.9
Esfenvalerate	14	0	<0.75	<0.75	<0.75
Deltamethrin	14	2	2.94	2.34	3.53

<: less than MDL in Table 1.

and were taken from a residential area in northern California. A matrix spike and matrix spike duplicate spiked at 20 ng/L was performed with this batch of samples. Mean recoveries of the target analytes from the matrix-spiked samples were 63.3–112.1% with relative percent differences (RPDs) of 3.7–17.2%. A replicate field-collected water sample was also conducted and it had lower RPDs of 0.38–13.2%. Surrogate recoveries ranged from 49.0 to 101.8% for DBOFB and from 44.2 to 116.8% for DCBP in the 14 water samples. The most often detected pesticides were bifenthrin, followed by cypermethrin, cyfluthrin, permethrin, and chloropyrifos (Table 3). The concentrations of individual pesticides ranged from 2.2 to 66.1 ng/L.

4. Conclusion

This study showed that LLE–NPSPE was the best choice for the trace extraction, cleanup and analysis of organophosphate and pyrethroid insecticides in laboratory and field-collected water samples. The developed method was well validated with four different water matrices, and provided satisfactory pesticide recoveries with method detection limits comparable to those from GC/MS and LC/MS. The storage stability of the target pesticides in water showed that the collected water samples should be extracted and analyzed within 4 days after they are shipped to the laboratory, or, the samples could be kept up to 7 days if they are held at 4 °C with hexane as a keeper solvent. The developed method has been successfully used for the analysis of field-collected waters with good results.

Acknowledgement

This research was funded in part by the Surface Water Ambient Monitoring Program of the California State Water Resources Control Board.

References

[1] H. Bailey, L. Deanovic, E. Reyes, T. Kimball, K. Larson, K. Cortright, V. Conner, D.E. Hinton, Environ. Toxicol. Chem. 19 (2000) 82.
[2] K. Schiff, M. Sutula, Environ. Toxicol. Chem. 23 (2004) 1815.
[3] B. Liu, L.L. McConnell, A. Torrents, Chemosphere 44 (2001) 1315.
[4] J.A. Harman-Fetcho, L.L. McConnell, J.E. Baker, J. Environ. Qual. 28 (1999) 928.
[5] D.M. Soderlund, J.M. Clark, L.P. Sheets, L.S. Mullin, V.J. Piccirillo, D. Sargent, J.T. Stevens, M.L. Weiner, Toxicology 171 (2002) 3.
[6] T. Narahashi, K.S. Ginsburg, K. Nagata, J.H. Song, H. Tatebayashi, Neurotoxicology 19 (1998) 581.
[7] J. Bacey, F. Spurlock, K. Starner, J. Feng, J. Hsu, J. White, D.M. Tran, Bull. Environ. Contam. Toxicol. 74 (2005) 864.
[8] H. Lutnicka, T. Bogacka, L. Wolska, Water Res. 33 (1999) 3441.
[9] D.K. Tanner, M.L. Knuth, Arch. Environ. Contam. Toxicol. 31 (1996) 244.
[10] D.P. Weston, R.W. Holmes, M.J. Lydy, Environ. Pollut. 157 (2009) 287.
[11] D.P. Weston, J. You, M.J. Lydy, Environ. Sci. Technol. 38 (2004) 2752.
[12] S. Rebach, Bull. Environ. Contam. Toxicol. 62 (1999) 448.
[13] E.L. Amweg, D.P. Weston, N.M. Ureda, Toxicol. Chem. 24 (2005) 1300.
[14] J.R. Goats, D.M. Symonik, S.P. Bradbury, S.D. Dyer, L.K. Timson, G.J. Atchison, Environ. Toxicol. Chem. 8 (1989) 671.
[15] R.R. Stephenson, Aquat. Toxicol. 2 (1982) 175–185.
[16] National Research Council of Canada, Pyrethroids: Their effect on aquatic and terrestrial ecosystems, Publication 14376, Ottawa, Ontario, 1986.
[17] V. Zitko, D.W. Mcleese, C.D. Metcalfe, W.C. Carson, Bull. Environ. Contam. Toxicol. 21 (1979) 338.
[18] D.W. Mclease, C.D. Metcalf, V. Zitko, Bull. Environ. Contam. Toxicol. 25 (1980) 950.
[19] S.J. Maund, M.J. Hamer, J.S. Warinton, T.J. Kedwards, Pest. Sci. 54 (1998) 408.
[20] S.J. Maund, M.J. Hamer, M.C.G. Lane, E. Farrelly, J.H. Rapley, U.M. Goggin, W.E. Gentle, Environ. Toxicol. Chem. 21 (2002) 9.
[21] A. Hildebrandt, S. Lacorte, D. Barceló, Anal. Bioanal. Chem. 387 (2007) 1459.
[22] G.R. van der Hoff, S.M. Gort, R.A. Baumann, P. van Zoonen, U.A.Th. Brinkman, J. High Res. Chromatogr. 7 (1991) 465.
[23] G.R. van der Hoff, F. Pelusio, U.A.Th. Brinkman, R.A. Baumann, P. van Zoonen, J. Chromatogr. A 719 (1996) 59.
[24] W.R. Barrionuevo, F.M. Lanças, Bull. Environ. Contam. Toxicol. 69 (2002) 123.
[25] N. Xue, X. Xu, Z. Jin, Chemosphere 61 (2005) 1594.
[26] M.D. Gil-García, D. Barranco-Martínez, M. Martínez-Galera, P. Parrilla-Vázquez, Rapid Commun. Mass Spectrom. 20 (2006) 2395.
[27] S. Lee, J. Gan, J. Kabashima, J. Agric. Food Chem. 50 (2002) 7194.
[28] V. Casas, M. Llompart, C. García-Jares, R. Cela, T. Dagnac, J. Chromatogr. A 1124 (2006) 148.
[29] A. Boyd-Boland, S. Magdic, J. Pawliszyn, Analyst 121 (1996) 929.
[30] P. Serodio, J.M.F. Nogueira, Anal. Bioanal. Chem. 382 (2005) 1141.
[31] N. Ochiai, K. Sasamoto, H. Kanda, S. Nakamura, J. Chromatogr. A 1130 (2006) 83.
[32] E.V. Hoeck, F. David, P. Sandra, J. Chromatogr. A 1157 (2007) 1.
[33] C.B.M. Rahul, P. Roy, Res. J. Chem. Environ. 10 (2006) 5.
[34] Q. Zhou, H. Bai, G. Xie, J. Xiao, J. Chromatogr. A 1177 (2008) 43.
[35] C.E. Wheelock, J.L. Miller, M.J. Miller, B.M. Phillips, S.J. Gee, R.S. Tjeerdema, B.D. Hammock, Aquat. Toxicol. 74 (2005) 47.
[36] M.B. Woudneh, D.R. Oros, J. Agric. Food Chem. 54 (2006) 6957.
[37] S.M. Pyle, A.B. Marcus, G.L. Robertson, Environ. Sci. Technol. 32 (1998) 3213.
[38] J. You, D.P. Weston, M.J. Lydy, Arch. Environ. Contam. Toxicol. 47 (2004) 141.
[39] EPA Method 3510C, Revision 3. December 1996.
[40] O. Shimelis, Y. Yang, K. Stenerson, T. Kaneko, M. Ye, J. Chromatogr. A 1165 (2007) 18.
[41] Y. Ku, J.-L. Chang, S.-C. Cheng, Water Air Soil Pollut. 108 (1998) 445.

Talanta 78 (2009) 1227–1234

Contents lists available at ScienceDirect

Talanta

journal homepage: www.elsevier.com/locate/talanta

An electrochemical biosensor for detection of PML/RARA fusion gene using capture probe covalently immobilized onto poly-calcon carboxylic acid modified glassy carbon electrode

Na Wei[a], Jinghua Chen[a], Jing Zhang[b], Kun Wang[a], Xiongwei Xu[a], Jianhua Lin[a], Guangwen Li[a], Xinhua Lin[a,*], Yuanzhong Chen[a,c,**]

[a] Department of Pharmaceutical Analysis, Faculty of Pharmacy, Fujian Medical University, 88 Jiaotong Road, Fuzhou 350004, China
[b] Pharmaceutical Department of Fujian College of Medical Occupation and Technology, Fuzhou 350101, China
[c] Fujian Institute of Hematology, The Affiliated Union Hospital of Fujian Medical University, Fuzhou 350001, China

ARTICLE INFO

Article history:
Received 2 September 2008
Received in revised form
23 December 2008
Accepted 23 December 2008
Available online 15 January 2009

Keywords:
Calcon carboxylic acid
PML/RARA fusion gene
Electrochemical biosensor

ABSTRACT

In this article, the poly-calcon carboxylic acid (poly-CCA) film modified electrode was prepared by cyclic voltammetry (CV). Then, an electrochemical DNA biosensor was developed for detection of PML/RARA fusion gene in acute promyelocytic leukemia (APL) by using 18-mer single-stranded deoxyribonucleic acid as the capture probe. The capture probe was covalently attached through free amines on the DNA bases using 1-ethyl-3-(3-dimethylaminopropyl) carbodiimide (EDC) and *N*-hydrosulfosuccinimide (NHS) cross-linking reaction on a carboxylate-terminated poly-CCA monolayer modified glassy carbon electrode (GCE). The covalent immobilized capture probe could selectively hybridize with its target DNA to form double-stranded DNA (dsDNA) on GCE surface. The aim of this work is to provide a well-defined recognition interface for the detection of DNA. Differential pulse voltammetry (DPV) was used to monitor the hybridization reaction on the capture probe electrode. The decrease of the peak current of methylene blue (MB), an electroactive indicator, was observed upon hybridization of the probe with the target DNA. The results indicated that in pH 7.0 phosphate buffer solution (PBS), the oxidation peak current was linear with the concentration of complementary strand in the range of 1.0×10^{-12} to 1.0×10^{-11} M with a detection limit of 6.7×10^{-13} M. This new method demonstrates its excellent specificity for single-base mismatch and complementary sequence (dsDNA) after hybridization, and it would be proposed to use in real sample.

1. Introduction

Acute promyelocytic leukemia (APL) is a kind of acute leukemia which often goes with bleeding severely. The bleeding mechanism of the APL patient is very complex. Almost all of the APL patients are characterized by chromosome reciprocal translocation, t(15;17) (q22;q12), resulting in the generation of fusion gene between promyelocytic leukemia (PML) and retinoic acid receptor alpha (RARA), which forms PML/RARA fusion gene. It would have crucial meanings of APL [1]. The reported methods for the detection of PML/RARA fusion gene were chromosome analysis [2], fluorescence in situ hybridization (FISH) [3], flow cytometry (FCM) [4], real-time quantitative reverse transcription polymerase chain reaction (RT-PCR) [5], etc. Despite the chromosome analysis would analyze the abnormality of the single cellular chromosome in structure and number, it spends long time and much energies. At the same time, it has low sensitivity. FISH has high sensitivity, but it has poor precision in immobilization. Although FCM would detect 5000–10,000 cells, it identifies the cellular shape, size and fluorescence feature only in single cellular level. The result of RT-PCR detection is sensitive and accurate, but often appears the false positive and false negative. Besides, it is difficult to quantitate. Thus, it is important to develop a new effective method to detect PML/RARA fusion gene.

In recent years, it has been considerable interested in developing DNA electrochemical biosensors for the rapid and inexpensive diagnosis of genetic diseases and other applications [6–8]. Such biosensors show both high selectivity and sensitivity in detecting a specific sequence, since a specific oligonucleotide can be immobilized on the surface of electrode. The immobilization step of the capture probe could lead to a well-defined probe orientation,

* Corresponding author. Tel.: +86 591 22862016; fax: +86 591 22862016.
** Corresponding author at: Department of Pharmaceutical Analysis, Faculty of Pharmacy, Fujian Medical University, 88 Jiaotong Road, Fuzhou 350004, China. Tel.: +86 591 3357896/8376; fax: +86 591 3357896/8376.
E-mail addresses: xinhua63@126.com (X. Lin), chenyz@pub3.fz.fj.cn (Y. Chen).

0039-9140/$ – see front matter © 2009 Elsevier B.V. All rights reserved.
doi:10.1016/j.talanta.2008.12.053

which allows for ready accessibility of the target. Thus, specific DNA probe–target interactions and charge transfer reactions give an electrical signal which can be directly monitored. In addition, electrochemical devices offer certain advantages over the optical devices. They are easy to miniaturize, simple, rapid and inexpensive because electrochemical transduction is independent in solution turbidity or optical pathway. The immobilization of DNA onto the transducer surface plays an important role in the overall performance of the DNA biosensors. The effective immobilization of the probe not only improves the sensitivity and selectivity of biosensor, but also eliminates the non-specifically adsorption. It is of importance to effectively control the coverage of the probe on the electrode, the direction of the immobilization and the stability as to the successful detection of hybridization. However, traditional methods in immobilization of DNA onto electrode surfaces have poor hybridization efficiency [9,10]. Such as self-assembly monolayer (SAM)/Au-orientated system has been widely reported for the fabrication of biosensors [11], but gold–thiol bond can only withstand reasonably mild potentials and the alkanethiols. Moreover, the potential window of a gold electrode is limited to a relatively positive range due to its low overpotential for hydrogen evolution. Thus, it is important to develop a new effective process of immobilization.

Recently, application of chemical modified electrode in biology and chemistry has been paid more and more attention. Especially, the conducting polymers are very effective substrates for biomaterial immobilization. Some conducting polymers are doped and/or covalently or physically modified by bionanomaterials, especially proteins and nucleic acids, which exhibit unique catalysis [12] or affinity properties that can be easily employed in the design of biosensors [13]. Otherwise, polymer film modified electrodes [14–17] can form function groups of high concentration on the surface of the electrode, at the same time, they can increase the stability of fix function groups and selectivity of reactions. Therefore, the polymer film modified electrodes have found broadly studied and applied. Thus, the immobilized DNA by conducting polymeric materials have the properties of mechanical flexibilities, high surface areas, chemical specificities, tunable conductivities and easy processing, which make the conducting polymer the promising sensing materials for ultrasensitive, trace-level biological and chemical sensors [18–20].

In this paper, we describe the use of an electrochemical deposition procedure, to fabricate the poly-calcon carboxylic acid (poly-CCA) film (Fig. 1, Part A (A)) modified electrode using the GCE as the working electrode. In the presence of *N*-hydrosulfosuccinimide (NHS) and 1-ethyl-3-(3-

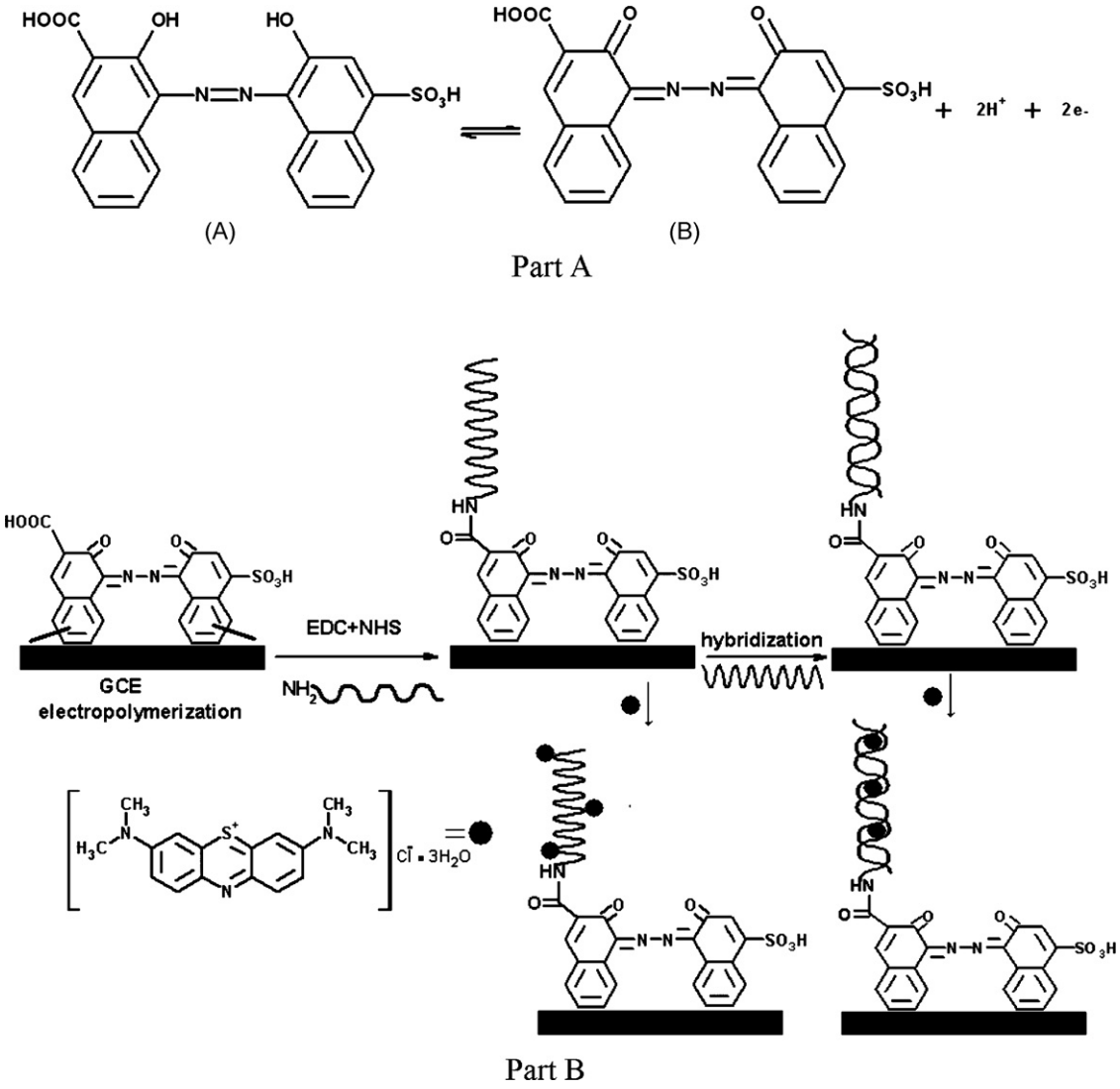

Fig. 1. (Part A) Mechanism of the poly-CCA electrode reaction: (A) the structure of CCA; (B) the benzoquinone diimine structure of CCA. (Part B) Diagram of the procedure for the fabrication of DNA biosensor for APL.

dimethylaminopropyl) carbodiimide (EDC), amines groups of oligonucleotides probe at the 5′end were covalently immobilized onto the carboxyl groups of poly-CCA film on the electrode. Hybridization was conducted by immersing the electrode immobilized DNA probe into the buffer solution containing its complementary sequence. Then DPV measurement was performed using electroactive methylene blue (MB) as an indicator. The method can effectively discriminate complementary DNA sequence from non-complementary and single mismatched sequence. The performance of the DNA biosensors with respect to the sensitivity and linear range was discussed. To our knowledge, this is the first time poly-CCA has been used for DNA detection. This method foreshows that the new immobilization of film modified electrode to detect DNA would be the basis of detecting diseases such as leukemia in early diagnosis and prognostic monitoring.

2. Experimental

2.1. Reagents and apparatus

The 18-base synthetic oligonucleotides were purchased from Shanghai Sheng gong Bioengineering Ltd. Company (Shanghai, China). Their base sequences were: immobilized probe (18-base sequence, S1)-5′-NH_2-TCT CAA TGG CTG CCT CCC-3′; target (S2)-5′-GGG AGG CAG CCA TTG AGA-3′; non-complementary (S3)-5′-ACT TCA TCC TTC GCT CTC-3′; single-base mismatch (S4)-5′-GGG AGG CAG CCA TTG AAA-3′. Stock solutions (100 μM) of all oligonucleotides were prepared with TE solution (10 mM Tris–HCl, 1.0 mM EDTA, pH 8.00) and kept frozen. More dilute solutions were prepared with 20 mM acetate buffer (pH 4.80). MB was purchased from Aldrich. Stock solutions of MB (1.0 mM) were prepared with deionized water. CCA was purchased from Sigma. EDC and NHS from Sigma were used without further purification. Other all chemicals were of analytical reagent grade. Phosphate buffer solution (PBS) was prepared by mixing the stock solutions of NaCl and NaH_2PO_4–Na_2HPO_4, and then adjusting the pH with H_3PO_4 or NaOH. All the buffer solutions contained 50 mM NaCl. Sterilized and deionized water was used in all solutions.

Electrochemical impedence spectroscopy (EIS), cyclic voltammetry (CV) and DPV measurements were performed by using CHI 660C Electrochemical Workstation (CH Instrument, USA). The electrochemical system consisted of GCE (3 mm diameter) as the working electrode, a platinum wire as the auxiliary electrode, and the reference electrode (Ag/AgCl, 3 mol L^{-1} KCl). All potentials mentioned in this paper referred to this reference electrode.

2.2. The preparation of surface of biosensor and its modification with DNA

The diagram for preparation of the electrochemical DNA biosensor is illustrated in Fig. 1.

2.2.1. GCE modification to form poly-CCA/GCE

We had ever reported the method that a novel poly-CCA modified GCE was fabricated by electropolymerization. Then the characterization of electrochemically synthesized poly-CCA film was investigated by atomic force microscopy (AFM), EIS and voltammetric methods [21]. So, GCE modification to form poly-CCA/GCE was done according to the procedure previously described by the method [21]. Before surface modification, the GCE was polished in sequential order with 1.0, 0.3 and 0.05 μm alumina (AlfaAesar, USA). The electrode was thoroughly washed with water, sonicated in ethanol, and finally dried thoroughly under N_2 flow. The surface modification of the GCE was performed by procedure reported in Ref. [21]. Briefly, GCE was polarized in 0.1 M H_2SO_4 by cyclic scanning between −0.40 and +1.60 V for 5 min at scan rate of 100 mV s^{-1}. Then the polarized electrode was carried out in 0.05 M NaOH containing 0.3 mM CCA solution by cyclic scanning between −0.40 and +1.80 V for 40 cyclic times at scan rate of 100 mV s^{-1}.

2.2.2. Immobilization of single-stranded DNA (ssDNA, S1) on poly-CCA/GCE

A versatile method for covalently attaching S1 to the poly-CCA/GCE was by using EDC and NHS linking reaction. The terminal carboxylic acid groups of the poly-CCA/GCE were activated by immersion in the 50 mM PBS (pH 7.40) containing 2 mM EDC and 5 mM NHS for 1 h. The linker/poly-CCA/GCE was rinsed with 50 mM PBS (pH 7.40) to wash off the redundant EDC and NHS. Then, S1 immobilization onto the surface was performed by the following procedure: 10 μl of 1.0×10^{-12} M S1 was pipetted onto the chemically modified GCE. The S1 droplet was left to dry. Thus, a S1-modified GCE was obtained. This electrode S1/poly-CCA/GCE was designated as probe electrode. Then the electrode was washed with 0.1% SDS phosphate buffer (pH 7.30) for 5 min to remove the unbound DNA probes.

2.2.3. Hybridization with synthetic oligonucleotides

The hybridization was performed by immersing the S1/poly-CCA/GCE into 0.1 M PBS (pH 7.00) containing 5 μl of different concentrations of S2. This hybridization process was left for 30 min at 45 °C [22]. Thus, a hybrid-modified GCE was obtained. The electrode surface was then washed with ultra-pure water and 0.1% SDS phosphate buffer (pH 7.30) for 5 min to remove the unbound oligonucleotides. The same protocol as above was applied at S1-modified GCEs for hybridization reactions of S1 with S3 and also with S4.

2.2.4. MB accumulation and voltammetric transduction

MB for DNA hybridization detection is illustrated in Fig. 1. MB was accumulated onto the surface of hybrid-modified GCE by immersing the electrode into stirred 0.1 M PBS (pH 7.00) containing 20 μM MB with 50 mM NaCl for 5 min without applying any potential. In the optimal condition, the concentration of MB was chosen as 20 μM and the accumulation time of MB was chosen as 5 min for optimum analytical performance. After accumulation of MB, the electrode was rinsed with 0.1 M PBS (pH 7.00) in ultrasonic bath for 10 s to remove the non-specific MB. MB was intercalated into the DNA to form DNA/MB system on the probe electrode after hybridization. Then, CVs were collected between −0.50 and +0.40 V with scan rate of 100 mV s^{-1}; differential pulse voltammetries were collected from −0.50 V to 0.40 V with amplitude of 5 mV.

2.2.5. Regeneration of modified electrode surface

The probe modified GCE surface denaturation/regeneration cycles were investigated. Both hybridization and detection involve reversible-binding processes, so that the biosensor could be reusable for five cycles of hybridization and regeneration. Surface denaturation/regeneration cycles using MB as indicator were carried out as follows. A probe modified GCE electrode was first characterized by DPV in a stirred 0.1 M PBS (pH 7.00) containing 20 μM MB with 50 mM NaCl for 5 min without applying any potential. The reduction signal of MB was measured as in Section 2.2.2. Then, hybridization of the complementary was performed as in Section 2.2.3 and intercalation of MB was performed as in Section 2.2.4. Subsequently, the reduction signal of MB was measured as in Section 2.2.4. After this measurement, the surface-immobilized dsDNA was then denatured in ultra-pure water at 95 °C for 1 min, thus, this gave rise to the probe modified GC electrode. Then a new cycle of denaturation/regeneration would start again.

3. Results and discussion

3.1. Covalent modification of GCE with CCA

The potential scan range, especially the positive potential, affects considerably the formation of polymerization film. It is found that it is difficult to initiate the polymerization reaction by the electrochemical method when the positive limited potential was less than +1.3 V [21]. It is clear that the anodic peak at about 0.4 V corresponding to the oxidation of CCA monomer decreased sharply for the first two cycles (figure not shown). Upon further potential cycling, it decreased gradually. This phenomenon implies the formation of poly-CCA membrane on GCE [21]. The electro-deposited behavior of CCA at the GCE is similar to some reports [23,24] referring to the electrochemical responses of a few azo compounds at solid electrode. The reaction mechanism could be explained as follows (Fig. 1): CCA (A) was first deposited at the surface of GCE and oxidized to form a benzoquinone diimine structure (B); and then the benzoquinone diimine structure (B) was reduced to CCA (A) at the surface of GCE. After electropolymerization, the modified electrode was carefully rinsed with doubly distilled water and then kept in pH 7.00 PBS. This modified electrode was used within 4 weeks.

3.2. Electrochemical behavior of $Fe(CN)_6^{3-/4-}$ on different modified GCE

Prior to hybridization of the target DNA on the surface of the S1-modified electrodes, we examined the surface coverage of S1 on the electrode by CV in the presence of $Fe(CN)_6^{3-}$ marker ion in solution, according to the reported procedure [25,26]. The bare GCE, poly-CCA/GCE, S1/poly-CCA/GCE, were used as the working electrodes, respectively (figure not shown). The result showed that a symmetric, reversible voltammogram was obtained for a bare GCE, whereas the poly-CCA modified electrode showed an asymmetric, irreversible wave. Both the anodic and cathodic currents are severely reduced for the poly-CCA modified electrode, due to the electrostatic repulsion between $Fe(CN)_6^{3-}$ anion and negatively charged poly-CCA film on the electrode surface. When the probe DNA immobilized on the modified electrode, compared with bare GCE and poly-CCA/GCE, the peak current decreased further and the potential deviation increased. That is, the probe DNA had negative charge, the negative charge on the surface would further increase, so hampered $Fe(CN)_6^{3-}$ to participate the electrode reaction on the surface [27]. These results suggest that the electrode surface is well covered with the probe DNA under the modification conditions.

The EIS was also used to identify the immobilization of S1 on the GCE. In the Nyquist diagram the semicircle diameter of the electrochemical impedance spectra equaled to the electron transfer resistance R Nyquist diagrams of $[Fe(CN)_6]^{3-/4-}$ at different modified electrodes were illustrated in Fig. 2. After the poly-CCA film modified on the GCE, the interfacial Ret increased greatly (curve b) compared with that of the bare GCE (curve a); this was attributed to the large quantity of negative charges from $-COO^-$ groups or $-SO_3^-$ groups that perturbed the rates of interfacial electron transfer between the electrode and the electrolyte solution. After the probe DNA S1 was immobilized on the electrode surface, R_{et} increased because of the strong electrostatic repulsion between the negatively charged $[Fe(CN)_6]^{3-/4-}$ molecules and the negative charges on the DNA phosphate backbone [28]. This phenomenon was further enhanced after hybridization was completed on the electrode surface, and an obvious increase in R_{et} was observed (as shown in curve c and curve d). The surface coverage (θ) of poly-CCA film on a bare GCE can be calculated from the EIS in terms of the

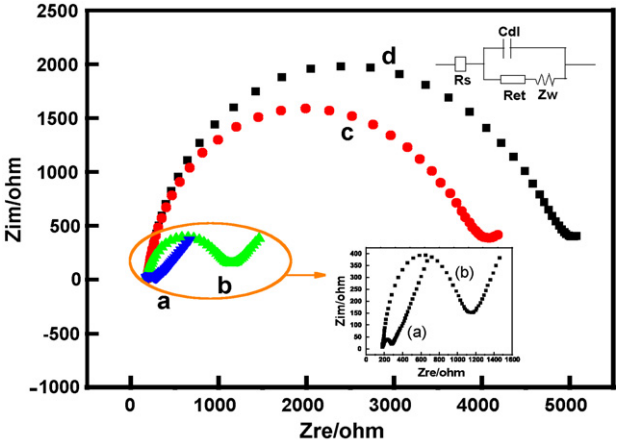

Fig. 2. Impedance plots of 10 mM $Fe(CN)_6^{3-/4-}$ in 1.0 M KCl on different modified electrode: (a) bare GCE; (b) poly-CCA/GCE; (c) S1/poly-CCA/GCE; (d) S1–S2/poly-CCA/GCE.

equation [21,29–33]:

$$\theta = 1 - \frac{R_{ct}^{Bare}}{R_{ct}^{poly\text{-}CCA}} \quad (1)$$

where R_{ct}^{Bare} denotes the charge transfer resistance of the bare GCE, and $R_{ct}^{poly\text{-}CCA}$ is the corresponding resistance of the poly-CCA/GCE with different electropolymerization cyclic times. It is evident that a saturated monolayer of poly-CCA film on the bare GCE surface was formed after electropolymerization for 40 cyclic times; in 0.1 M KCl solution with 5 mM $Fe(CN)_6^{3-/4-}$ (pH 7.0), R_{ct}^{Bare} is 65 Ω. Under the same conditions, $R_{ct}^{poly\text{-}CCA}$ is about 9000 Ω. Using Eq. (1), the coverage was calculated to be 99.3%. The EIS results indicated that modification and hybridization were successfully accomplished on the electrode surface.

3.3. The electrochemical behavior of MB on different electrodes

Fig. 3 shows that bare GCE, poly-CCA/GCE, S1/poly-CCA/GCE and S1–S2/poly-CCA/GCE interacted with pH 7.00 PBS containing 20 μM MB, respectively. There is a rather low signal of MB on bare GCE obtained as shown in Fig. 3A (curve a). The oxidoreduction peak potential for non-specifically adsorbed MB peak was at −100 mV versus Ag/AgCl. This is due to the relatively low quantity of MB adsorbed on the GCE surface [25,34]. When the poly-CCA modified on the electrode, the peak current increased (Fig. 3A, curve b). As CCA was a kind of chelometric titration indicator, and the whole name was 1-(2-hydroxy-4-sulfo-1-naphthylazo)-2-hydroxy-3-naphthoic acid, which containing a sulfonic group($-SO_3H$) in the structure. As it was known, the pK_a value of $R-SO_3H$ was usually between 3.00 and 4.00 [35,36]. When the solution pH was equal to 7.00, the $-SO_3H$ group of poly-CCA film could dissociate favorably into a negative charge group $-SO_3^-$. Under this condition, the MB in the solution would interact with proton (H^+) and form the positive ion of MBH^+ (pK_a: 5.18–6.03) [37]. Therefore, the negative charge group $-SO_3^-$ on the surface of poly-CCA modified electrode had a well affinity to the MBH^+ positive ions and could catalyze and promote the oxidation of MB in the pH 7.00 PBS (mechanism shown in Fig. 3C). The highest MB oxidoreduction signal was observed with capture probe on the electrode because the electronegative phosphate skeletons of capture probe immobilized on the electrode had a powerful attracting force to MB cation. At the same time, many more free guanine bases of DNA molecules were exposed out and had a strong affinity with MB, and hence the greatest amount of MB accumulation occurs at this sur-

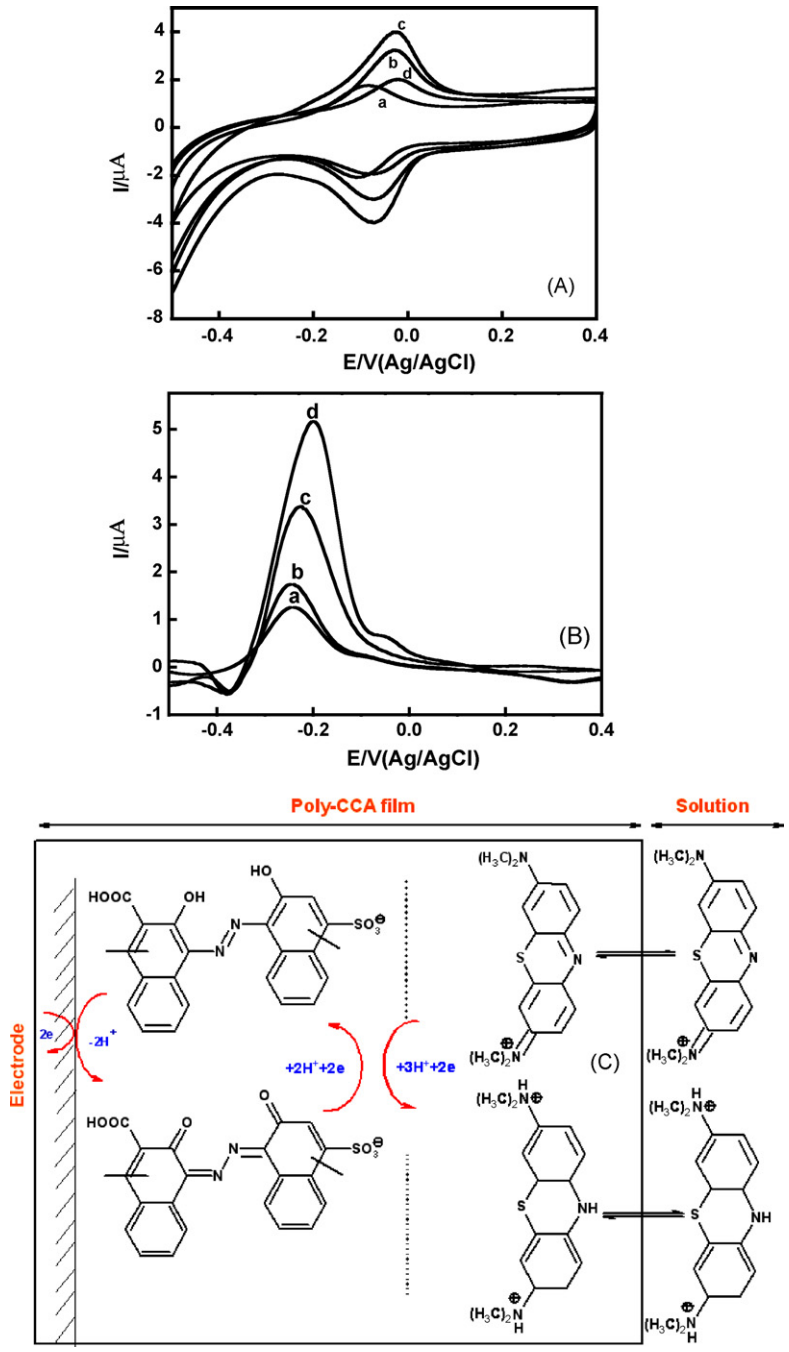

Fig. 3. (A) Cyclic voltammetries of 20 μM MB interacted on bare GCE (a), poly-CCA/GCE (b), 1.0×10^{-12} M S1/poly-CCA/GCE (c), and 1.0×10^{-12} M S1–S2/poly-CCA/GCE (d). (B) Differential pulse voltammetries of 20 μM MB on bare GCE (a), poly-CCA/GCE (b), 1.0×10^{-12} M S1/poly-CCA/GCE (c), and 1.0×10^{-12} M S1–S2/poly-CCA/GCE (d). Pulse amplitude, pulse width and pulse period were 0.05 V, 0.05 s, and 0.2 s, respectively. (C) Mechanism of MB reaction at the poly-CCA/GCE. Cyclic voltammetries were collected between −0.50 and +0.40 V with scan rate of 50 mV s^{-1}; differential pulse voltammetries were collected from −0.50 V to 0.40 V with amplitude of 5 mV.

face [22,38–45] (Fig. 3A, curve c). However, a significant decrease in the voltammetric peak current of MB was observed after complementary target sequence S2 was allowed to hybridize with the capture probe electrode (Fig. 3A, curve d). After hybridization, the current signal of MB decreased due to less MB binding to dsDNA, caused by the inaccessibility of MB to the guanine bases [38,46–49]. This decrease is attributed to the steric inhibition of the reducible groups of MB packed between the bulky double helix of the hybrid. Another interaction may be related to majority of the MB molecules starting intercalating between the double helix of dsDNA at high ionic strength conditions, because the ionic shielding of the negative charges on the DNA was established. It showed that less MB was associated with dsDNA in a high ionic strength solution. The result indicated that less charge was being passed through dsDNA and upon intercalation the reduction potential became less cathodic [47].

Fig. 3B displays DPV of the bare, poly-CCA-modified, S1-modified and S1–S2-modified GCE previously accumulated with MB in blank buffer solution. The results were in good agreement with those obtained from CV. The decrease in the magnitude of the voltammetric peak current of MB intercalator thus reflects the extent of the hybridization at the electrode surface [50].

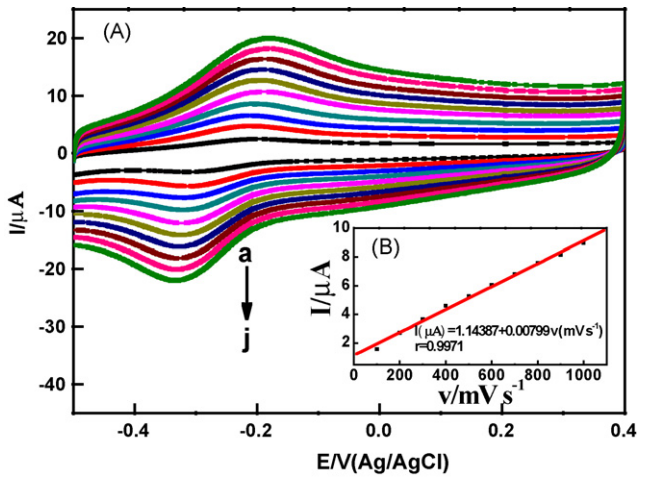

Fig. 4. (A) Cyclic voltammetries of 2.0 μM MB (PBS pH 7.00) on probe modified electrode at various scan rates (mV s^{-1}): (a) 100; (b) 200; (c) 300; (d) 400; (f) 500; (g) 600; (h) 700; (i) 800; (j) 900. (B) The relationship of peak current I (μA) and scan rate v (mV s^{-1}).

3.4. The CV study of MB interacted with the probe modified electrode along with change of scan rate

The probe modified electrode immersed in pH 7.00 PBS containing 20 μM MB and CV were collected with the scan rate of 0.1, 0.2, 0.3, 0.4, 0.5, 0.6, 0.7, 0.8, 0.9, and 1.0 V s^{-1}. As shown in Fig. 4A, a pair of evident oxidoreduction peak appeared, and the peak current increased along with the increasing of the scan rate. Fig. 4B shows that the reduction peak current was linear with the scan rate. The regression equation was I (μA) = 1.14387 + 0.00799v (mV s^{-1}), and the coefficient correlation r = 0.9971. It also indicated that MB strongly bound to the probe modified electrode [27].

3.5. Hybridization specificity of probe-DNA/poly-CCA/GCE

The selectivity of this assay was investigated by using the DNA/poly-CCA/GCE as the capture probe (S1) to hybridize with various DNA sequences complementary oligonucleotide (S2), non-complementary oligonucleotide (S3), and one base mismatch oligonucleotide (S4). Fig. 5 shows the DPV signal of MB at S1 before hybridization (Fig. 5, curve a), and after hybridization with the same amount of S2 (Fig. 5, curve d), S3 (see Fig. 5, curve b) and S4 (see Fig. 5, curve c). As can be seen, the largest DPV peak current of MB was observed when exposed the S1/poly-CCA/GCE to the S3 (Fig. 5, curve b), which was similar to that of the blank measurement (Fig. 5, curve c) (a blank measurement means the response of MB at the S1/poly-CCA/GCE, indicating that no change occurred at the electrode surface, and the greatest amount of MB accumulated on the electrode because of the strong affinity of MB with the free guanines; an obviously decreased peak current of MB was obtained when incubating with the S2 (Fig. 5, curve d), suggesting that hybrids (dsDNA) formed at the electrode surface, and the interaction of MB and guanine residues of the probe was prevented by duplex formation on the electrode surface; after S1 hybridized with S4, the peak current of MB was significantly increased and approached to that of S1/poly-CCA/GCE (Fig. 5, curve c), indicating the complete hybridization was not accomplished due to the base mismatch). Thus, response of MB on the probe electrode can be considered as an efficient intercalator to distinguish between hybrids, non-complementary and single-base mismatch oligonucleotides.

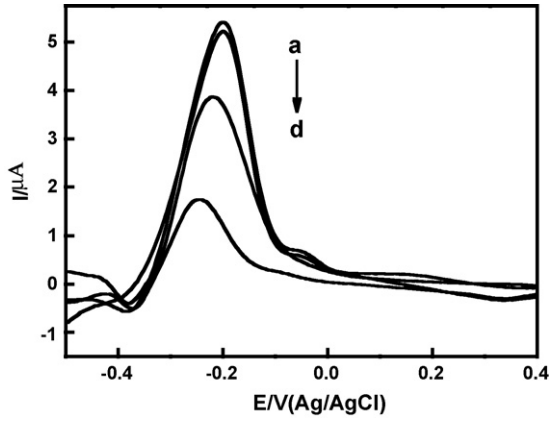

Fig. 5. Differential pulse voltammetries of 20 μM MB accumulated on the 1.0×10^{-12} M S1/GCE (a), 1.0×10^{-12} M S1–S3/GCE (b), 1.0×10^{-12} M S1–S4/GCE (c) and 1.0×10^{-12} M S1–S2/GCE (d) in 0.10 M PBS (pH 7.00) with 50 mM NaCl. Differential pulse voltammetries were collected from −0.50 V to 0.40 V with amplitude of 5 mV.

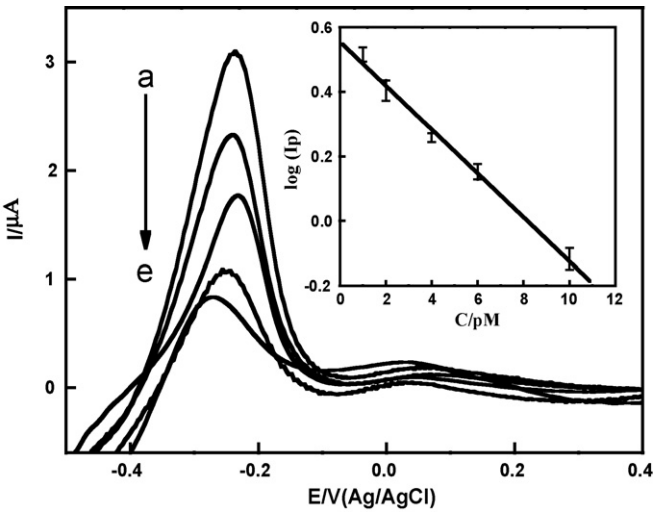

Fig. 6. Differential pulse voltammetries of 20 μM MB accumulated on the probe -1.0×10^{-12} M S1 after its hybridization with different concentration of the S2 in 0.10 M pH 7.00 PBS buffer solution. Target concentration ($\times 10^{-12}$ M): (a) 1.0, (b) 2.0, (c) 4.0, (d) 6.0 and (e) 10. Inset shows the plot of the peak current of MB as a function of the target concentration. Error bars = ±relative standard deviation.

The sensitivity of this electrochemical biosensor for the target DNA was investigated by varying the target oligonucleotide concentration according to the procedure described in Section 2. The different current value obtained in the DPV response of MB after hybridization of probe with target was recorded with three repetitive measurements. The current response at about −0.24 V decreased in proportion to the amount of the target sequence used. The average logarithmic current response shows excellent correlation with the amount of the complementary oligonucleotides in the range of 1.0×10^{-12} to 1.0×10^{-11} M (shown in Fig. 6). The regression equation is $\log I_p$ (μA) = 0.068C (pM) + 0.555 (r = 0.9963). A detection limit of 6.7×10^{-13} M for the target DNA can be estimated using 3σ (where σ is the standard deviation of the blank solution, n = 8). The reproducibility of the biosensor for detection of 1.0×10^{-12} M target DNA is 7.32% (n = 8). Compared with the other method which our laboratory had been established [51], the novel covalently modification method can get a lower detection limit and has higher sensitivity.

3.6. Optimization of conditions

3.6.1. The selectivity of hybridization time and hybridization temperature

The co-influence of hybridization time and hybridization temperature were studied in these experiments. The result indicated that hybridization time decreased with the increasing of hybridization temperature due to the fact that higher temperature sped the movement of DNA molecules. On the other hand, higher hybridization temperature accelerated the denaturation of dsDNA [52], resulting in the decreasing of the absolute hybridization number. Taking consideration of the above two factors, the probe modified electrode reacted with target DNA in solution was chosen at 45 °C for 30 min, which was the optimal hybridization condition.

3.6.2. The selectivity of the concentration about MB

The indicator of DNA electrochemical sensor was a kind of electroactive compound which would be interacted with probe and dsDNA in different ways. The conjugation way of indicator and DNA had three kinds of fundamental modes [46,53]. The good functional indicator would be the different selectivity in the binding ability of the probe and dsDNA. So the indicator in the dsDNA and probe-DNA modified electrode would be the different level of accumulation and different current response. MB was selected as indicator, that's because MB was of good specificity to recognize the different modified electrode [50]. The concentration about MB would be the great influence on the electrochemical signal. Therefore, the concentration of MB was examined.

In order to examine the effect of MB concentration on the enhanced DPV signal (ΔI_p), DNA modified electrode was prepared, and selected different concentrations of MB to detect DPV signal, respectively. The result showed that ΔI_p was increased with the increasing of concentration of MB after hybridization. When MB concentration was 2.0×10^{-5} M, the peak current reached the maximum. When the concentration of MB was increased more, the ΔI_p kept constant, which indicated that the concentration of MB reached saturation, thus 2.0×10^{-5} M was selected as experimental concentration.

3.6.3. The selectivity of MB accumulation time

The effect of accumulation time of MB on ΔI_p was examined, and the results showed that ΔI_p increased exponentially with the accumulation time of MB in the first 5 min. Beyond this accumulation time, ΔI_p tended to constant, which indicated that intercalation of MB into DNA reached a saturation value. Thus, accumulation time of 5 min was chosen as the optimal accumulation time.

3.6.4. The effect of pH

CVs for the electro-oxidation of MB were performed at the DNA modified GCE in various pHs of PBS, and the results showed that the peak potential shifted to negative value with increasing of pH. The peak current of MB showed a maximum at pH 7.00, so the electro-oxidation of MB was preformed better in pH 7.00 PBS.

3.6.5. The selectivity of the concentration about NaCl in the hybridization solution

The monovalent cation such as NaCl would increase the speed of the generation about the heterogenous heteroduplexes [54]. In the hybridization solution, since changing of the concentration of NaCl would greatly affect the hybridization signal, the effect of NaCl concentration on the hybridization of 1.0×10^{-12} M complementary strand was examined, when the concentration of NaCl was lower than 0.05 M, the oxidation peak current of MB increased along with the increasing of the NaCl concentration. On the contrary, when the concentration of NaCl was higher than 0.1 M, the oxidation peak current of MB decreased with increasing of NaCl. While the peak current reached maximum and constant when Na^+ was between 0.05 and 0.1 M. Therefore, 0.05 M of NaCl was selected for subsequent experiments.

4. Conclusion

In this article, through using poly-CCA films, the new immobilization was studied to modify covalently on the carbon surface in order to detect APL PML/RARA fusion gene. The results of new covalent bond manifested that the probe would show the specificity of the signal compared with that of hybridization. Conferred to the same kind of immobilization method, it provided a simple, stable detection and might have a promising future in the electrochemical DNA biosensors. Along with the deep study of immobilization, it would play the potential predominance in diagnosis of diseases and the new APL DNA biosensor would be proposed to use in real sample.

Acknowledgements

The authors gratefully acknowledge the financial support of the National High Technology and Development of China (863 Project: 2006AA02Z4Z1 and 2008AA02Z433); the National Natural Science Foundation of China (20675015, the Foundation of Fujian Provincial Technology International Cooperation (2006I0016) and the Foundation of Fujian Education Department (2005K051) and the Foundation of Fujian Health Department (2005123).

References

[1] M.S. Tallman, C. Nabhan, J.H. Feusner, J.M. Rowe, Blood 99 (2002) 759.
[2] S.J. Yoo, E.J. Seo, J.H. Lee, Y.H. Seo, P.W. Park, J.Y. Ahn, Cancer Genet. Cytogenet. 167 (2006) 168.
[3] P.S. Amare, C. Baisane, T. Saikia, R. Nair, H. Gawade, S. Advani, Cancer Genet. Cytogenet. 131 (2001) 125.
[4] C.A. Tirado, V. Golembiewski-Ruiz, J. Horvatinovich, J.O. Moore, P.J. Buckley, T.T. Stenzel, B.K. Goodman, Cancer Genet. Cytogenet. 145 (2003) 31.
[5] J. Han, K. Kim, K. Kim, J. Park, J. Kim, Leukemia Res. 31 (2007) 239.
[6] E. Palecek, F. Jelen, Crit. Rev. Anal. Chem. 3 (2002) 261.
[7] P. De-los-Santos-Alvarez, M.J. Lobo-Castanon, A.J. Miransa-Ordieres, P. Tunon-Blanco, Anal. Bioanal. Chem. 378 (2004) 104.
[8] F. Lucarelli, G. Marrazza, A.P.F. Turner, M. Mascini, Biosens. Bioelectron. 19 (2004) 515.
[9] R. Levicky, T.M. Herne, M.J. Tarlov, S.K. Satija, J. Am. Chem. Soc. 120 (1998) 9787.
[10] M.I. Pividori, A. Merkoci, S. Alegret, Biosens. Bioelectron. 15 (2000) 291.
[11] H. Koji, I. Keiko, I. Yoshio, Anal. Chem. 66 (1994) 3830.
[12] A. Malinauskas, Synthetic Met. 107 (1999) 75.
[13] A. Ramanaviciene, A. Ramanavicius, Biosens. Bioelectron. 20 (2004) 1076.
[14] A.A. Karyakin, A.D. Strakhova, S.D. Varfolomeye, Bioelectrochem. Bioenerg. 32 (1993) 35.
[15] S.J. Dong, Q.H. Chu, Electroanalysis 5 (1993) 135.
[16] H. Zhao, Y.Z. Zhang, Z.B. Yuan, Anal. Chim. Acta 454 (2002) 75.
[17] H.X. Ju, C. Shen, Electroanalysis 13 (2001) 789.
[18] B.W. Maynor, S.F. Filocamo, M.W. Grinstaff, J. Liu, J. Am. Chem. Soc. 124 (2002) 522.
[19] C.G. Wu, T. Bein, Science 264 (1994) 1757.
[20] J.D. Noll, M.A. Nicholson, P.G. Van Patten, C.W. Chung, M.L. Myrick, J. Electrochem. Soc. 145 (1998) 3320.
[21] A.L. Liu, S.B. Zhang, W. Chen, X.H. Lin, X.H. Xia, Biosens. Bioelectron. 23 (2008) 1488.
[22] X.H. Lin, P. Wu, W. Chen, Y.F. Zhang, X.H. Xia, Talanta 72 (2007) 468.
[23] A. Eriksson, L. Nyholm, Electrochim. Acta 44 (1999) 4029.
[24] A. Eriksson, L. Nyholm, Electrochim. Acta 496 (2001) 1113.
[25] S.Y. Niu, S.S. Zhang, L. Wang, X.M. Li, Electroanal. Chem. 597 (2006) 111.
[26] C. Hao, L. Ding, H.X. Ju, Anal. Chem. 79 (2007) 4442.
[27] Y. Jin, X. Yao, Q. Liu, J.H. Li, Biosens. Bioelectron. 22 (2007) 1126.
[28] Y. Xu, L. Yang, X.Y. Ye, P.G. He, Y.Z. Fang, Electroanalysis 18 (2006) 873.
[29] E. Sabatani, J. Cohen-Boulakia, M. Bruening, I. Rubinstein, Langmuir 9 (1993) 2974.
[30] C. Henke, C. Steinem, A. Janshoff, G. Steffan, H. Luftmann, M. Sieber, H.J. Galla, Anal. Chem. 68 (1996) 3158.
[31] C.H. Wang, C. Yang, Y.Y. Song, W. Gao, X.H. Xia, Adv. Funct. Mater. 15 (2005) 1267.
[32] K. Wang, J.J. Xu, X.H. Xia, Biosens. Bioelectron. 20 (2005) 1366.
[33] Y.Y. Song, D. Zhang, W. Gao, X.H. Xia, Chem. Eur. J. 17 (2005) 2177.
[34] M.F. Sistare, R.C. Holmberg, H.H. Thorp, J. Phys. Chem. B 103 (1999) 10718.
[35] H. Yao, Y.Y. Sun, X.H. Lin, Y.H. Tang, L.Y. Huang, Electrochim. Acta 52 (2007) 6165.

[36] H. Yao, Y.Y. Sun, X.H. Lin, Y.H. Tang, A.L. Liu, G.W. Li, W. Li, S.B. Zhang, Anal. Sci. 23 (2007) 677.
[37] X.L. Wang, L.G. Song, G.B. Li, Y.F. Tang, Z.K. Xi, Acta Phys. Chim. Sin. 9 (1993) 89.
[38] A. Erdem, K. Kerman, B. Meric, M. Ozsoz, Electroanalysis 13 (2001) 219.
[39] K. Kerman, D. Ozsoz, P. Kara, B. Meric, J.J. Gooding, M. Ozsoz, Anal. Chim. Acta 462 (2002) 39.
[40] J. Yang, T. Yang, Y.Y. Feng, K. Jiao, Anal. Biochem. 365 (2007) 24.
[41] N.N. Zhu, Z. Chang, P.G. He, Y.Z. Fang, Electrochim. Acta 51 (2006) 3758.
[42] W.R. Yang, M. Ozsoz, D.B. Hibbert, J. Gooding, J. Electroanal. 14 (2002) 1299.
[43] R. Rohs, H. Sklenar, R. Lavery, B. Roder, J. Am. Chem. Soc. 122 (2000) 2860.
[44] M. Enescu, B. Levy, V. Gheorghe, J. Phys. Chem. B 104 (2000) 1073.
[45] S.O. Kelley, E.M. Boon, J.K. Barton, N.M. Jackson, M.G. Hill, Nucleic Acids Res. 27 (1999) 4830.
[46] A. Erdem, K. Kerman, B. Meric, U.S. Akarca, M. Ozsoz, Anal. Chim. Acta 422 (2000) 139.
[47] P. Kara, K. Kerman, D. Ozkan, B. Meric, A. Erdem, Z. Ozkan, M.I. Ozsoz, Electrochem. Commun. 4 (2002) 705.
[48] W. Yang, M. Ozsoz, D.B. Hibbert, J.J. Gooding, Electroanalysis 14 (2002) 1299.
[49] H.F. Teh, H.Q. Gong, X.D. Dong, X.T. Zeng, A.L.K. Tan, X.H. Yang, S.N. Tan, Anal. Chim. Acta 551 (2005) 23.
[50] A. Tani, A.J. Thomson, J.N. Butt, Analyst 126 (2001) 1756.
[51] X.H. Lin, H.Y. Wan, Y.F. Zhang, J.H. Chen, Talanta 74 (2008) 944.
[52] S. Iijima, Nature 354 (1991) 56.
[53] K. Kerman, D. Ozkan, P. Kara, B. Meric, J.J. Gooding, M. Ozsoz, Anal. Chim. Acta 462 (2002) 39.
[54] M. Tsuruoka, K. Yano, K. Ikebukuro, H. Nakayama, Y. Masuda, I. Karube, J. Biotechnol. 48 (1996) 201.

Talanta 78 (2009) 1395–1400

Contents lists available at ScienceDirect

Talanta

journal homepage: www.elsevier.com/locate/talanta

Investigation of voltammetric enzyme-linked immunoassay system based on *N*-heterocyclic substrate of 2,3-diaminopyridine

Fengli Yu, Ping Du, Xi Lei, Shusheng Zhang*

Key Laboratory of Eco-chemical Engineering, Ministry of Education, College of Chemistry and Molecular Engineering, Qingdao University of Science and Technology, Qingdao 266042, China

ARTICLE INFO

Article history:
Received 29 October 2008
Received in revised form 10 February 2009
Accepted 12 February 2009
Available online 24 February 2009

Keywords:
Electrochemical immunoassay (ECIA)
Horseradish peroxidase (HRP)
2,3-Diaminopyridine (DAP)
Prostate specific antigen (PSA)

ABSTRACT

A new voltammetric enzyme-linked immunoassay system using the electrochemical substrate 2,3-diaminopyridine (DAP) and horseradish peroxidase (HRP) system has been developed. DAP is oxidized with H_2O_2 catalyzed by HRP, and the resulting electroactive product produces a sensitive voltammetric peak at potential of −0.72 V (*vs.* saturated calomel electrode (SCE)) in Britton–Robinson (BR) buffer solutions. The enzyme-catalyzed reaction conditions and voltammetric detection conditions have been investigated in detail. Under the selected optimum conditions, the linear range for detection of free HRP is from 6.0×10^{-11} to 1.0×10^{-8} g mL^{-1} with a detection limit of 1.0×10^{-12} g mL^{-1}. The new voltammetric detection system has been successfully applied for the assay of prostate specific antigen (PSA) in human serum ranging from 0.4 to 100 ng mL^{-1} with a detection limit of 0.1 ng mL^{-1}, which is five times lower than that of traditional *o*-phenylenediamine (OPD) spectrophotometric enzyme-linked immunosorbent assay (ELISA) method. The proposed *N*-heterocyclic electrochemical detection system of DAP–H_2O_2–HRP has provided a new and much improved immunoassay method.

1. Introduction

Approximately 100 million immunoassays are processed every year world-wide in a variety of analytical areas including clinical, medical, biotechnology and environmental fields. The development of immunoassay techniques is one of the greatest achievements in bioanalytical sciences. The highly advanced immunoassay techniques which have been introduced to many application areas include radioimmunoassay (RIA) [1,2], enzyme-linked immunosorbent assay (ELISA) [3–6], chemiluminescence immunoassay (CLIA) [7,8], fluorescence immunoassay (FIA) [9,10] and electrochemical immunoassay (ECIA) [11,12].

Electrochemical immunoassay has been applied for the assay of a number of antigens and antibodies with satisfactory results [13–16]. The method not only has the advantages of high detection sensitivity, but it also like other substrate-based end point detection methods, couples well with the high selectivity of antibody-based techniques [17–22]. In addition, the electrochemical immunoassay methods, combined with modern separation techniques such as flow-injection [23–25] and capillary electrophoresis (CE) [26–28] are powerful analytical tools for determination of low levels of analytes and application in multianalyte immunoassays. A CE-based electrochemical immunoassay system, with *o*-aminophenol–H_2O_2–horseradish peroxidase (HRP) system, for simultaneous detection of three important tumor markers was developed by our group [29].

Up to now, there has been only one example of electrochemical immunoassay system based on *N*-heterocyclic substrate, 3-hydroxyl-2-aminopyridine–H_2O_2–HRP system, reported by our group [30]. The study has showed that *N*-heterocyclic substrate-based immunoassay system is superior to not only traditional spectrophotometric ELISA method but also traditional benzenecyclic substrate-based immunoassay system [31]. The introduction of *N*-heteroatom to benzene cycle may reduce the molecular conjugation, while improve the reactivity of substitute groups. This provides a probability for much active hydrogen donors. So, the introduction of *N*-heterocyclic substrate to electrochemical immunoassay has broken the conventionality of benzenecyclic substrate, and exploited a new field of electrochemical substrates for seeking more superior electrochemical immunoassay system. In addition, the investigation on the redox process of *N*-heterocyclic compounds may facilitate to understand the process and mechanism of biological activity in life science, since the structures of many biologically active molecules in organism body contain pyridine ring or other *N*-heterocycles. In a word, the investigation on *N*-heterocyclic electrochemical immunoassay is of much significance.

It is all known that *o*-phenylenediamine (OPD) is the most common substrate used in not only traditional spec-

* Corresponding author. Tel.: +86 532 84022750; fax: +86 532 84022750.
E-mail address: shushzhang@126.com (S. Zhang).

0039-9140/$ – see front matter © 2009 Elsevier B.V. All rights reserved.
doi:10.1016/j.talanta.2009.02.031

trophotometric ELISA method but also traditional benzenecyclic substrate-based electrochemical immunoassay. For comparison, 2,3-diaminopyridine (DAP) as a substrate has been introduced to electrochemical immunoassay. The results of the study have showed that DAP is a novel electrochemical oxidisable *N*-heterocyclic compound, and DAP-based immunoassay system has exhibited much improved analysis performance. The study has showed that DAP is oxidized with H_2O_2 catalyzed by HRP, and the resulting electroactive product produces a sensitive voltammetric peak at potential of −0.72 V (*vs.* saturated calomel electrode (SCE)) in Britton–Robinson (BR) buffer solutions. By using this voltammetric peak, free HRP and labeled HRP can be measured. Under the selected optimum conditions, the linear range for detection of free HRP was from 6.0×10^{-11} to 1.0×10^{-8} g mL^{-1} with a detection limit of 1.0×10^{-12} g mL^{-1}.

Sensitive and specific detection of prostate specific antigen (PSA) has been proved to be the most reliable clinical tool for preparative diagnosing and monitoring prostate cancer. Besides traditional spectrophotometric ELISA method, some techniques have been applied for the assay of PSA with satisfactory results. Sarker et al. have developed amperometric biosensors for detection of PSA with the detection limit of 0.25 ng mL^{-1} [32]. Xu and co-workers have reported a rapid enzyme immunoassay for serum PSA at low concentrations by flow-injection electrochemical detection, which offers a much lower detection limit of 0.008 ng mL^{-1} [33]. Recently, our group have applied 3,4-diaminobenzoic acid–H_2O_2–HRP electrochemical immunoassay system for the assay of PSA with the linear range of 0.20–16.0 ng mL^{-1} and the detection limit of 0.10 ng mL^{-1} [34].

In this paper, sensitive and specific detection of PSA in human serum using DAP–H_2O_2–HRP voltammetric enzyme-linked immunoassay new system based on *N*-heterocyclic substrate of DAP and HRP-labeled enzyme is presented. The detection limit of PSA is 0.10 ng mL^{-1}, which is five times lower than that of traditional OPD spectrophotometric ELISA method. In addition, the linear range for PSA detection is from 0.4 to 100 ng mL^{-1}, which is much wider than that of not only traditional OPD spectrophotometric ELISA method but also benzenecyclic substrate-based electrochemical immunoassay system developed in our previous work. The proposed sensitive, specific, simple, inexpensive and rapid method for the detection of PSA in human serum has been proved to be a reliable clinical tool for preparative diagnosing and monitoring prostate cancer.

2. Experimental

2.1. Apparatus

The electrochemical measurement was carried out by using a MP-2 voltammetric analyzer (Shandong No. 7 Electric Communication Factory, China) with a three-electrode system composed of a dropping mercury electrode or a hanging mercury drop electrode as working electrode, a platinum wire electrode as auxiliary electrode and a saturated calomel electrode as reference electrode. Model PHS-25 pH meter was purchased from Shanghai Leici Apparatus Factory. Model OG3022A enzyme labeled meter was produced by Huadong Electronal Group Medical Treatment Instrument Ltd. in China. Incubation for the immune reaction was carried out in a Model HH.W21.420 incubator (Guangdong Shantou Instrument Factory, China).

2.2. Reagents

2,3-Diaminopyridine (ACROS) solution: 1.0×10^{-2} mol L^{-1}, prepared by dissolving 0.1100 g DAP in water and diluted to 100 mL. HRP (Shanghai Xueman Biochemical Technique Company, 250 units mg^{-1} enzyme) stock solution: 1.0×10^{-3} g mL^{-1}, prepared by dissolving 0.0100 g HRP in 10 mL water, and stored in a refrigerator at 4 °C. H_2O_2 solution: 1.0×10^{-3} mol L^{-1}, prepared before use. Britton–Robinson (BR) buffer solutions: 0.2 mol L^{-1}, pH 5.0 and pH 10.0. The substrate solution in the electrochemical enzyme immunoassay system was prepared as follows: 4.0 mL of 1.0×10^{-2} mol L^{-1} DAP solution, 3.0 mL of 1.0×10^{-3} mol L^{-1} H_2O_2 solution and 1.5 mL of 0.2 mol L^{-1} pH 5.0 BR buffer solution were added to a colorimetric tube of 10 mL in sequence, then diluted to the scale and shaken to uniformity. The PSA ELISA Kit was purchased from Zhengzhou Bosai Biotechnique Academe. The kit included 48-well immunoplates precoated by anti-PSA serum, HRP-conjugated anti-PSA (anti-PSA-HRP), 0–100 ng mL^{-1} of PSA quality control serum, rinsing solution. All other reagents were of analytical grade and doubly deionized water was used throughout.

2.3. Electrochemical measurement of free and labeled HRP

The 4.0 mL of 1.0×10^{-2} mol L^{-1} DAP solution, 3.0 mL of 1.0×10^{-3} mol L^{-1} H_2O_2 solution, 1.5 mL of 0.2 mol L^{-1} pH 5.0 BR buffer solution and 1.0 mL of a certain concentration of HRP solution were added to a 10 mL colorimetric tube in sequence. The mixture was diluted to the scale and shaken to uniformity. Then, let the solution react for 50 min at 37 °C. 5.0 mL of above reaction solution was transferred into another 10 mL colorimetric tube and 1.0 mL of 0.2 mol L^{-1} pH 10.0 BR buffer solution was subsequently added. The mixture was diluted to the scale and shaken to uniformity. Then, the solution was transferred to an electrochemical cell of 10 mL. The second-order derivative linear-sweep voltammogram was recorded with the MP-2 voltammetric analyzer. The instrumental conditions were as follows: initial potential, −0.20 V; final potential, −1.20 V; mercury drop standing time, 7 s; potential scanning rate, 400 mV s^{-1}.

2.4. Determination of PSA

The commercial PSA Kit was directly used. All regents were equilibrated at room temperature before use. The wells of polystyrene immunoplates precoated by PSA serum were written numbers. 100 μL of different concentrations of the PSA quality control sera or the serum samples were added to each well and incubated at 37 °C for 30 min. After the wells were rinsed five times with doubly deionized water, 100 μL of anti-PSA-HRP was added to each well and incubated at 37 °C for 30 min. The wells were rinsed with the rinsing solution of PBS-Tween 20, then with double deionized water. After that, 350 μL of DAP substrate solutions were added to each well, and the enzymatic reaction was allowed to proceed for 40 min at 37 °C. The reaction solution was transferred into a cell of 1 mL. 70 μL of 0.2 mol L^{-1} pH 10.0 BR buffer solution and 280 μL doubly deionized water were added into the cell. The second-order derivative linear-sweep voltammogram was recorded as above.

For comparison, spectrophotometric detection of ELISA was also preformed in parallel using OG3022A enzyme labeled meter.

3. Results and discussion

3.1. Second-order derivative linear-sweep voltammograms

HRP can efficiently catalyze the oxidation reaction of DAP with H_2O_2, yielding the electroactive product that produces a sensitive voltammetric reduction peak at potential of −0.72 V (*vs.* SCE) in BR buffer solutions. Fig. 1 shows the results of the second-order derivative linear-sweep voltammograms in different conditions. Curve 1 represented the voltammogram of sole BR buffer solutions, in which no voltammetric peak was observed. Curve 2 represented

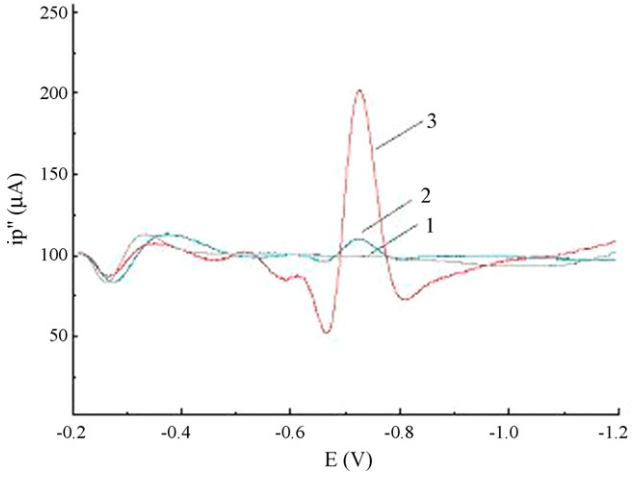

Fig. 1. Second-order derivative linear-sweep voltammograms: (1) BR buffer; (2) BR + DAP + H_2O_2; (3) BR + DAP + H_2O_2 + HRP.

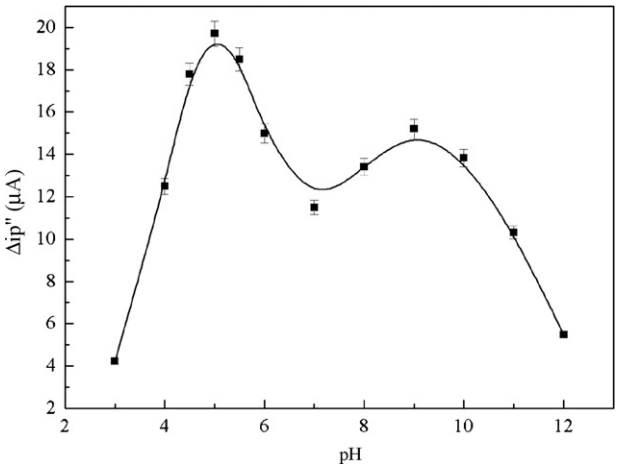

Fig. 3. Effect of pH of BR buffer solutions on the HRP-catalyzed oxidation reaction.

the voltammogram of BR buffer solutions containing DAP and H_2O_2, in which a small voltammetric peak at −0.72 V was found. Such a small peak was due to slow oxidation of DAP with H_2O_2 which generated a small number of electroactive products. Whereas, curve 3 gave a very high and well-defined voltammetric peak at −0.72 V. Since curve 3 represented the voltammogram of enzyme-catalyzed reaction of DAP, the results showed that the addition of HRP much quickened the oxidation of DAP with H_2O_2, which generated a large number of electroactive products. In addition, the voltammetric peak current increased with the increase of HRP concentration. By using this voltammetric peak, free HRP and labeled HRP can be measured. Therefore, with HRP being the labeling enzyme, DAP as the electrochemical substrate can be used in voltammetric enzyme-linked immunoassay.

3.2. Optimization of enzyme-catalyzed reaction conditions

DAP was oxidized with H_2O_2 catalyzed by HRP, and the enzymatic product was electroactive. Referring to the oxidation reaction of *o*-phenylenediamine with H_2O_2 affording the product of 2,3-diaminophenazine in voltammetric enzyme-linked immunoassay system [35], the process of the enzyme-catalyzed oxidation reaction of DAP could be expressed as Fig. 2.

The effect of reaction conditions on the enzyme-catalyzed oxidation reaction of DAP has been investigated in detail. The activity of HRP was greatly influenced by the surroundings. According to the electrochemical respond of the enzymatic product in different conditions, the effect of the pH of the BR buffer solutions from 2.0 to 12.0 on enzyme-catalyzed reaction was studied. The results are shown in Fig. 3. When pH was 5.0, the strongest voltammetric peak current was observed, indicating that the enzyme-catalyzed reaction adapted to undergo in weak acidic solutions. Therefore, pH 5.0 of BR buffer solution was chosen for enzyme-catalyzed reaction. The effect of the concentration of H_2O_2 was also studied by the same method. The result showed the voltammetric peak current increased with the increase of the concentration of H_2O_2, but much higher concentration of H_2O_2 could prevent the activity of HRP. The optimized concentration of H_2O_2 was

Fig. 2. The process of the enzyme-catalyzed oxidation reaction of DAP.

1.0×10^{-3} mol L^{-1}. Additionally, the concentration of substrate DAP and the amount of each component in reaction solutions including BR buffer, H_2O_2 and DAP were also optimized. The selected optimum reaction conditions were that the 10 mL reaction solution consisted of 1.5 mL of 0.2 mol L^{-1} pH 5.0 BR buffer solution, 4.0 mL of 1.0×10^{-2} mol L^{-1} DAP solution and 3.0 mL of 1.0×10^{-3} mol L^{-1} H_2O_2 solution. Under such enzyme-catalyzed reaction conditions, the equilibrium was achieved within 50 min at 37 °C. So, 50 min was selected as the time for the enzyme-catalyzed reaction at 37 °C.

3.3. Optimization of voltammetric detection conditions

The enzymatic product of DAP with H_2O_2 proceeded a reduction process at the dropping mercury electrode affording a sensitive voltammetric peak in a certain buffer solution. The optimization of voltammetric detection conditions was investigated. Among experimental buffer solutions of BR, HAc–NaAc and Na_2HPO_4–KH_2PO_4, BR buffer solutions as the supporting electrolyte for the polarographic measurement afforded the finest second-order derivative linear-sweep voltammetric peak of the product, and pH 10.0 BR buffer solution gave the strongest peak current. Additionally, the optimum amount of pH 10.0 BR buffer solution as the supporting electrolyte was 1.0 mL for 10 mL of the overall detection solution containing 5 mL of reaction solution. The optimum instrumental conditions for the detection were chosen as follows: the initial potential, −0.20 V; the final potential, −1.20 V; the mercury drop standing time, 7 s; the potential scanning rate, 400 mV s^{-1}.

3.4. The electrode procedure of the enzymatic product

After enzyme-catalyzed reaction in pH 5.0 BR buffer solution, the cyclic voltammetric experiments were performed in different pH BR buffer solutions from 4.0 to 13.0 using the hanging mercury drop electrode. The results are shown in Fig. 4. There appeared both anodic peak and cathodic peak in all the experiments. The height of these two peaks was almost equal when pH was between 6.0 and 10.0, indicating that the enzymatic product processed a reversible redox at the mercury electrode. When pH was 10.0, it gave the highest and finest redox peaks. When pH <6 or pH ≥11.0, the anodic peak height was lower than the cathodic height, indicating one pair of irreversible redox peaks. Another pair of very weak redox peaks in all cyclic voltammograms resulted from the adsorption of product on the mercury electrode.

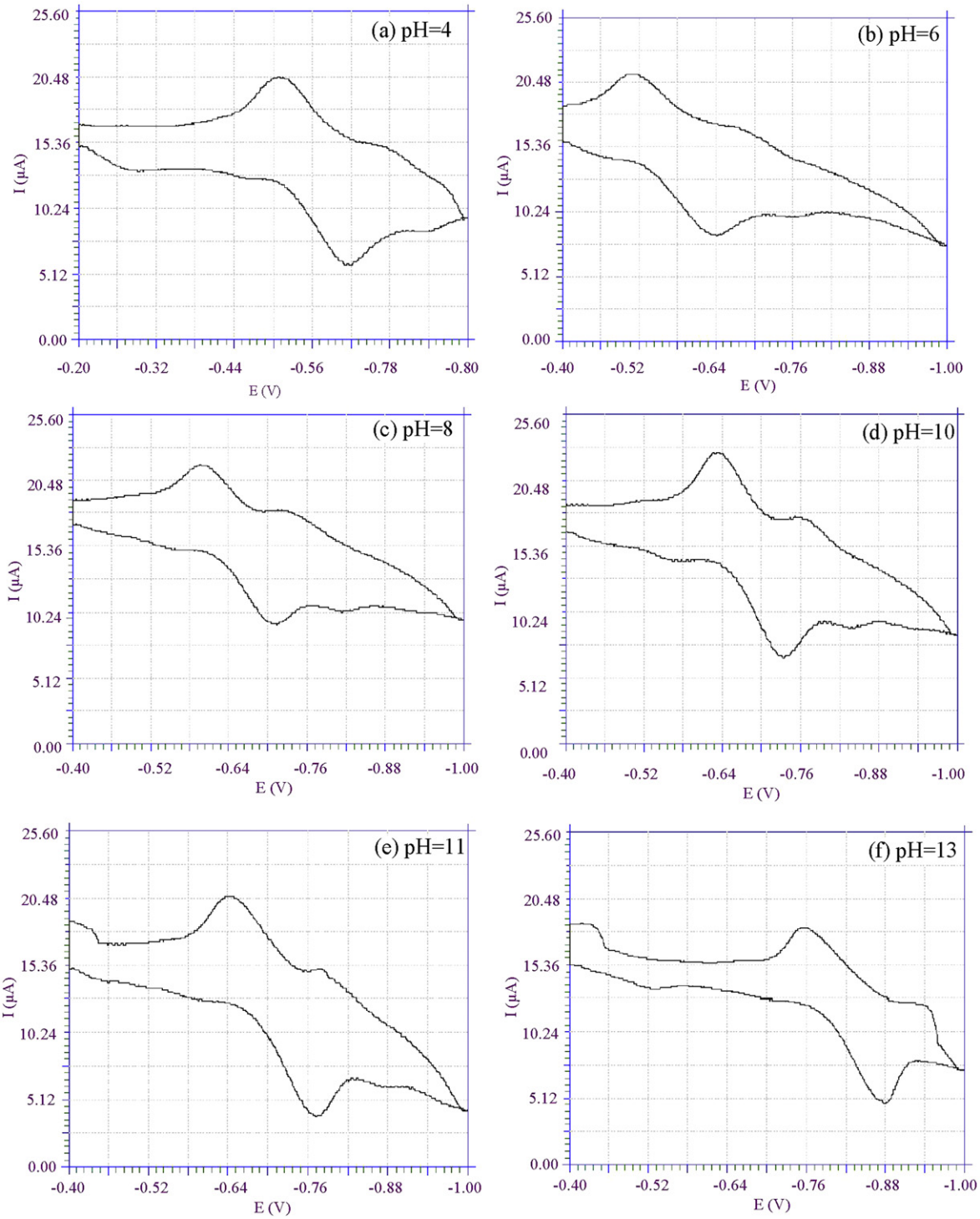

Fig. 4. The cyclic voltammograms in different pH BR buffer solutions. The enzymatic product was generated by oxidation reaction of DAP in BR buffer solution at pH 5.0.

The influence of pH value on the peak potential was investigated in detail. The reduction peak potential shifted to more negative values with the increase of pH value of BR buffer solutions from 2.0 to 13.0. The peak potential value had a good linear relation with the pH value of detection solutions in the range of 6.0–10.0 referring to Fig. 5. The equation of linear regression was $Ep = -0.2410 - 0.0617\text{pH}$ (Ep was the peak potential, $n = 9$, $\gamma = 0.9978$) with a slope of −0.0617. According to the formula [36], $-0.059x/n = -0.0617$, where n was the number of the electron transfer, and x was the hydrogen ion number participating the reaction, $x \approx n = 2$.

The multiple sweep cyclic voltammogram was recorded well. The result is shown in Fig. 6. There were good cathodic and anodic peaks, and these two peaks were similar in height. Moreover, the height of both peaks kept stable with the increase of scanning cycle. The results indicated that the product of the enzymatic reaction processed a reversible adsorption on the mercury electrode. From above experimental results, the enzymatic product appeared

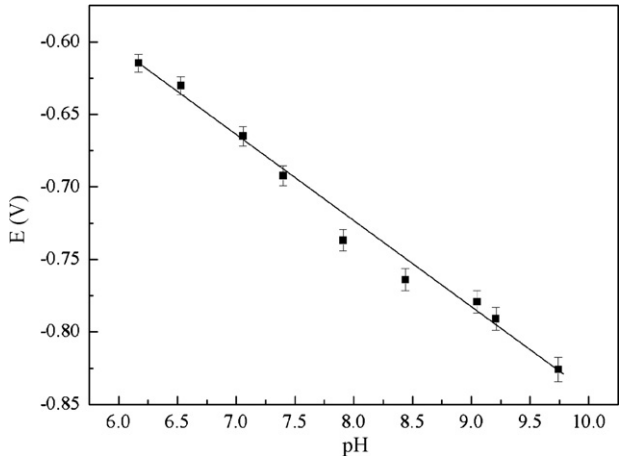

Fig. 5. Effect of pH of detection solution on the peak potential.

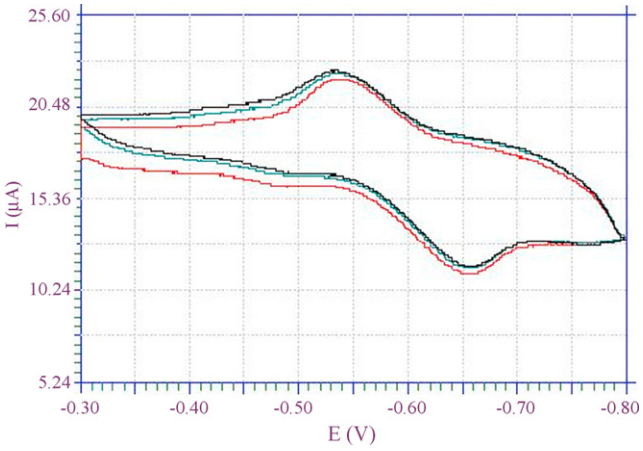

Fig. 6. Multiple sweep cyclic voltammograms of the BR + DAP + H_2O_2 + HRP.

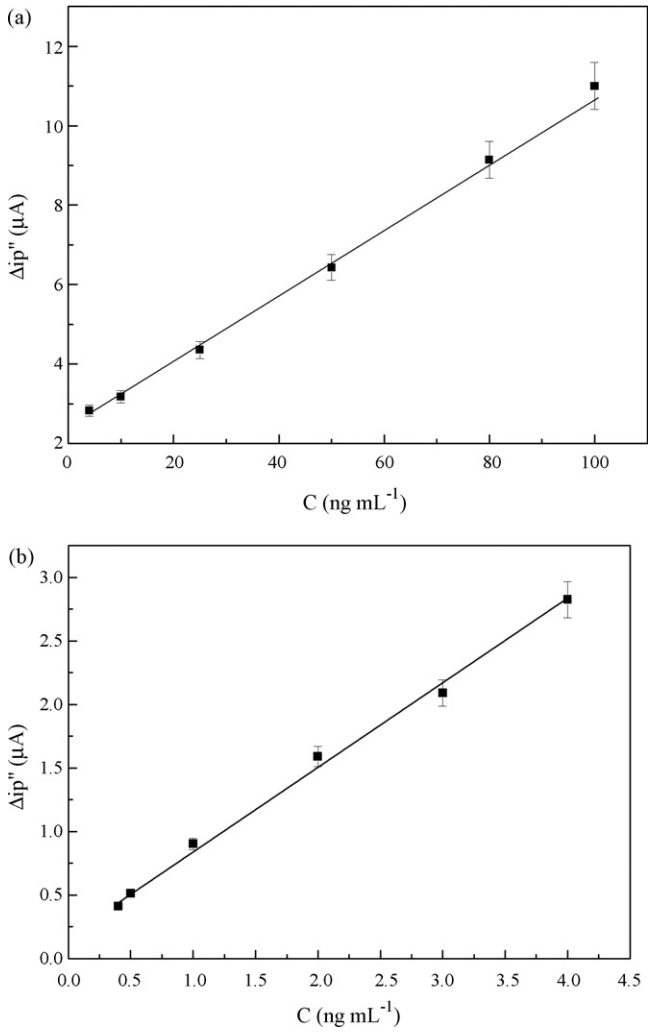

Fig. 8. Working curves of PSA detection: (a) PSA concentration, 4.0–100 ng mL^{-1}. (b) PSA concentration, 0.4–4.0 ng mL^{-1}.

a two-electron adsorptive reversible redox process in pH 6.0–10.0 BR buffer solutions. The process is expressed as Fig. 7.

3.5. Determination of free HRP

Under the selected enzyme-catalyzed reaction conditions and the detection conditions, different concentrations of HRP were used to catalyze the oxidation reaction of DAP with H_2O_2 and the second-order derivative linear-sweep voltammograms were recorded. The results showed the peak height exhibited a good linear relation with free HRP concentration from 6.0×10^{-11} to 1.0×10^{-8} g mL^{-1}. The relative standard deviation was 3.6% for seven parallel determinations with 6.0×10^{-11} g mL^{-1} HRP. The detection limit of free HRP was 1.0×10^{-12} g mL^{-1}.

3.6. Determination of labeled HRP

For the purpose of applying DAP–H_2O_2–HRP system for immunoassay, labeled HRP was determined through the similar electrochemical method with free HRP. HRP-conjugated antibodies of prostate specific antigen (anti-PSA-HRP) were determined under the optimum experimental conditions. For comparison, OPD spectrophotometric detection of ELISA was also preformed. The electrochemical method based on DAP–H_2O_2–HRP system showed higher sensitivity for the detection of labeled HRP. The highest dilution ratios detected by our electrochemical method and OPD spectrophotometric ELISA method were $1{:}1 \times 10^6$ and $1{:}6 \times 10^4$, respectively.

3.7. Working curve of PSA determination

DAP–H_2O_2–HRP voltammetric enzyme-linked immunoassay new system was used for the determination of PSA carried out with double-antibody-sandwich immunoassay method. Under the optimum conditions, the working curves of PSA determination are exhibited in Fig. 8. The peak current had a good linear relation with the concentration of PSA in the range of 0.4–100 ng mL^{-1}. The equations of linear regression were $y = 2.0982 + 0.1049x$ (y represented

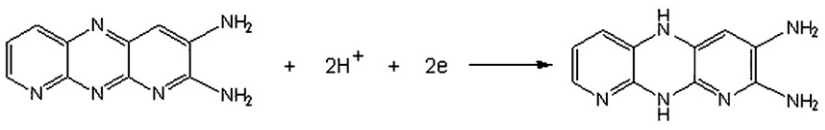

Fig. 7. The enzymatic product appeared a two-electron adsorptive reversible redox process in BR solution.

Table 1
Comparison of results of the electrochemical method with the spectrophotometric ELISA method for the detection of PSA in human serum.

Sample	Electrochemical method (ng mL^{-1})	R.S.D. (%)	Spectrophotometric method (ng mL^{-1})	R.S.D. (%)
1	0.53	4.2	–	–
2	0.68	3.8	–	–
3	1.57	3.7	1.78	3.4
4	3.05	2.5	3.12	3.0
5	10.32	2.8	10.15	1.9
6	14.30	3.1	14.67	2.6
7	23.56	3.3	25.12	3.5
8	56.52	2.3	57.94	3.2
9	68.63	2.1	70.35	3.8

the peak current, x was the concentration of PSA, 4.0–100 ng mL^{-1}, $n = 6$, $\gamma = 0.9988$) and $y = 0.2135 + 0.8096x$ (y represented the peak current, x was the concentration of PSA, 0.4–4.0 ng mL^{-1}, $n = 6$, $\gamma = 0.9961$). The repeatability of the assay was studied by running seven replicate assays on 5.0 ng mL^{-1} of PSA, and the relative standard deviation was 4.1%. The detection limit of new method for PSA was 0.1 ng mL^{-1}. For OPD spectrophotometric ELISA method, the linear range of the PSA quality control serum was 1.0–32 ng mL^{-1} with the linear regression equation of $A = 0.0823 + 0.0467C$ (A was the absorbance, C was the concentration of PSA) and the detection limit was 0.5 ng mL^{-1}. Therefore, the detection limit of new electrochemical enzyme-linked immunoassay method was five times lower than that of the traditional OPD spectrophotometric ELISA method.

3.8. Determination of PSA in human serum samples

According to the above working curves, DAP–H_2O_2–HRP voltammetric enzyme-linked immunoassay new system was practically applied for the determination of PSA content in human serum samples. The compared results with OPD spectrophotometric ELISA method are listed in Table 1. The results corresponded well to each other. The results of electrochemical method based on DAP–H_2O_2–HRP system were linearly proportional to those of OPD spectrophotometric ELISA method, and the equation of linear regression was $y = 0.1435 + 1.0312x$ (x was the result of electrochemical method; y was the result of spectrophotometric method; $n = 7$, $\gamma = 0.9997$).

4. Conclusions

A new electrochemical enzyme-linked immunoassay system based on a novel electrochemical oxidisable *N*-heterocyclic compound, 2,3-diaminopyridine has been developed. The developed DAP–H_2O_2–HRP new system has exhibited much higher sensitivity for detection of free HRP and labeled HRP. With HRP being the labeling enzyme, the sensitive and specific detection of prostate specific antigen in human serum based on DAP–H_2O_2–HRP system has been successfully accomplished. In comparison with the traditional *o*-phenylenediamine spectrophotometric ELISA method, the sensitivity of PSA detection is much improved for five times. What is more, the linear range of PSA detection of the new system is much wider than that of not only traditional OPD spectrophotometric ELISA method but also traditional benzenecyclic substrate-based electrochemical immunoassay system. The work curves of PSA detection of the new system have been obtained. The proposed *N*-heterocyclic electrochemical enzyme-linked immunoassay system of DAP–H_2O_2–HRP can be broaden to assays of other antigens or antibodies. The study has provided a new and much improved immunoassay method, and proved that *N*-heterocyclic compound is a promising electrochemical immunoassay substrate.

Acknowledgements

This work was supported by the National Natural Science Foundation of China (No. 20775038), the Natural Science Foundation of Shandong Province (No. JQ200805), and the University Doctoral Foundation of the Ministry of Education (No. 200804260001).

References

[1] M. Cioffi, M.T. Vietri, P. Gazzerro, R. Magneta, Lung Cancer 33 (2001) 163.
[2] D.M. Crow, L. Williams, D. Colcher, J.Y.C. Wong, Bioconjug. Chem. 16 (2005) 1117.
[3] H. Nakajima, M. Yagi, Y. Kudo, T. Nakagama, T. Shimosaka, K. Uchiyama, Talanta 70 (2006) 122.
[4] S. Kurosawa, J. Park, H. Aizawa, S. Wakida, H. Tao, K. Ishihara, Biosens. Bioelectron. 22 (2006) 473.
[5] M.J. Donohue, M.B. SatterWeld, J.J. Dalluge, M.J. Welch, Anal. Biochem. 339 (2005) 318.
[6] S. Rodriguez-Mozaz, M.J.L. de Alda, M.P. Marco, D. Barcelo, Talanta 65 (2005) 291.
[7] L.X. Zhao, J.M. Lin, Z.J. Li, X.T. Ying, Anal. Chim. Acta 558 (2006) 290.
[8] Z.F. Fu, F. Yan, H. Liu, J.H. Lin, H.X. Ju, Biosens. Bioelectron. 23 (2008) 1422.
[9] T. Matsuya, S. Tashiro, N. Hoshino, N. Shibata, Y. Nagasaki, K. Kataoka, Anal. Chem. 75 (2003) 6124.
[10] F. Yan, J.N. Zhou, J.H. Lin, H.X. Ju, X.Y. Hu, J. Immunol. Methods 305 (2005) 120.
[11] N.R. Stradiotto, H. Yamanaka, M.V.B. Zanoni, J. Braz. Chem. Soc. 14 (2003) 159.
[12] D. Ivnitski, R. Sitdykov, N. Ivnitski, Anal. Chim. Acta 504 (2004) 265.
[13] S.S. Zhang, J. Yang, J.H. Lin, Bioelectrochemistry 72 (2008) 47.
[14] K. Jiao, W. Sun, S.S. Zhang, Fresen. J. Anal. Chem. 367 (2000) 667.
[15] W. Sun, K. Jiao, S.S. Zhang, Anal. Lett. 33 (2000) 2653.
[16] K. Jiao, W. Sun, S.S. Zhang, G. Sun, Anal. Chim. Acta 413 (2000) 71.
[17] Y. Zhang, A. Heller, Anal. Chem. 77 (2005) 7758.
[18] M.S. Wilson, W. Nie, Anal. Chem. 78 (2006) 2507.
[19] S.H. Alarcon, G. Palleschi, D. Compagnone, M. Pascale, A. Visconti, I. Barna-Vetro, Talanta 69 (2006) 1031.
[20] H.S. Jung, J.M. Kim, J.W. Park, H.Y. Lee, T. Kawai, Langmuir 21 (2005) 6025.
[21] D.-G. Maria, M.B. Gonzalez-Garci, A. Costa-Garcia, Electroanalysis 17 (2005) 1901.
[22] W. Vastarella, R. Nicastri, Talanta 66 (2005) 627.
[23] S. Zhang, C. Cardona, L. Echegoyer, Chem. Commun. 43 (2006) 4461.
[24] B. Pejcic, R. De Marco, Electrochim. Acta 51 (2006) 6217.
[25] J. Pan, Q. Yang, Anal. Bioanal. Chem. 388 (2007) 279.
[26] Z. He, W. Jin, Anal. Biochem. 313 (2003) 34.
[27] Z. He, N. Gao, W. Jin, Anal. Chim. Acta 497 (2003) 75.
[28] Z. He, N. Gao, W. Jin, J Chromatogr. B 784 (2003) 343.
[29] S.S. Zhang, X.M. Li, F. Zhang, Electrophoresis 28 (2007) 4427.
[30] S.S. Zhang, J. Zou, F.L. Yu, Talanta 76 (2008) 122.
[31] S.S. Zhang, K. Jiao, H.Y. Chen, Anal. Lett. 32 (1999) 1761.
[32] P. Sarker, P.S. Pal, D. Ghosh, S.J. Steford, I.E. Tothill, Int. J. Pharm. 238 (2002) 1.
[33] S.F. Chen, Y. Xu, M.P.C. Ip, Clin. Chem. 43 (1997) 1459.
[34] S.S. Zhang, P. Du, F. Li, Talanta 72 (2007) 1487.
[35] J.T. Peter, P.C. Victor, W. Dave, Anal. Biochem. 165 (1987) 230.
[36] R.S. Nicholson, Anal. Chem. 37 (1965) 1351.

Talanta 78 (2009) 1240–1245

Contents lists available at ScienceDirect

Talanta

journal homepage: www.elsevier.com/locate/talanta

A sensitive impedimetric thrombin aptasensor based on polyamidoamine dendrimer

Zhanxia Zhang[a,b], Wen Yang[a,b], Juan Wang[a,b], Cheng Yang[a,b], Fan Yang[a], Xiurong Yang[a,*]

[a] State Key Laboratory of Electroanalytical Chemistry, Changchun Institute of Applied Chemistry, Chinese Academy of Sciences, Renmin Street 5625, Changchun, Jilin 130022, China
[b] Graduate School of the Chinese Academy of Sciences, Beijing 100039, China

ARTICLE INFO

Article history:
Received 28 October 2008
Received in revised form 14 January 2009
Accepted 18 January 2009
Available online 24 January 2009

Keywords:
Aptamer
Thrombin
Polyamidoamine dendrimer
Electrochemical impedance spectroscopy

ABSTRACT

A label-free and highly sensitive impedimetric aptasensor based on a polyamidoamine dendrimer modified gold electrode was developed for the determination of thrombin. Amino-terminated polyamidoamine dendrimer was firstly covalently attached to the cysteine functionalized gold electrode through glutaraldehyde coupling. Subsequently, the dendrimer was activated with glutaraldehyde, and amino-modified thrombin aptamer probe was immobilized onto the activated dendrimer monolayer film. The layer-by-layer assembly process was traced by surface plasmon resonance and electrochemical impedance spectroscopy. After electrode preparation, the detection of thrombin was investigated in the presence of the reversible $[Fe(CN)_6]^{3-/4-}$ redox couple using impedance technique. The results showed that the charge-transfer resistance (R_{ct}) value had a linear relationship with the concentrations of thrombin in the range of 1–50 nM, and the detection limit (S/N = 3) as low as 0.01 nM was obtained. The covalent immobilization of dendrimer on the electrode surface not only improved the immobilization capacity of probe molecules but also magnified the response signal. The aptasensor exhibited favorable regeneration ability, selectivity and stability. It also showed the detectability in biological fluid.

1. Introduction

Aptamers are a kind of single-stranded DNA or RNA sequences generated by *in vitro* selection techniques from a pool of DNA or RNA by repetitive binding of the target molecules. They possess high recognition ability towards specific molecular targets ranging from small inorganic and organic substances to proteins and even cells [1,2]. Aptamers have numerous advantageous characteristics over traditional recognition elements such as antibodies, including ease of synthesis, thermal stability and lack of immunogenicity [3]. Based on their biomolecular recognition ability, a number of aptamer biosensors (aptasensors) have been developed over the past decade [4].

Up to now, aptasensors mainly include optical aptasensors [5–8] and electrochemical aptasensors [9–12]. The field of electrochemical aptasensors has developed rapidly in recent years because they can provide fast, simple and inexpensive detection capabilities for biological binding events [13,14]. In order to amplify signals, many electrochemical aptasensors have been constructed mainly based on the aptamers labeled with electroactive materials, such as ferrocene and methylene blue [15–18]. Such labeling bears the disadvantages that the labeling process not only makes the experiment comparatively complicated and expensive but also affects the binding affinity between the targets and their aptamers to a certain degree [19]. Therefore, it is very necessary to develop a kind of label-free and highly sensitive electrochemical aptasensors. Electrochemical impedance spectroscopy (EIS) has been proved as one of the most sensitive tools for the analysis of interfacial properties because of its unique properties of high sensitivity, low cost, convenience and being label-free [20–23]. Recently, Zhang's group has reported an EIS thrombin aptasensor with the detection limit of 0.06 nM by using the signal enhancement of gold nanoparticles, which were electrodeposited onto a glassy carbon electrode [24]. In the paper, a label-free impedimetric aptasensor for the determination of thrombin based on a dendrimer-functionalized gold electrode was constructed, and the dendrimer employed here was expected to improve the response signals.

Dendrimers are a new class of synthetic macromolecules. They possess regularly branched treelike spherical morphologies and monodisperse sizes depending on the number of generations. The unique structural properties of dendrimers, such as structural homogeneity, integrity, controlled composition and biocompatibility, extend their use in biosensing applications [25,26]. Many approaches adopting dendrimers as biosensor materials have been reported [27,28]. A DNA biosensor using a polyamidoamine (PAMAM) dendrimer modified electrode had been previously

* Corresponding author. Tel.: +86 431 85262056; fax: +86 431 85689278.
E-mail address: xryang@ciac.jl.cn (X. Yang).

0039-9140/$ – see front matter © 2009 Elsevier B.V. All rights reserved.
doi:10.1016/j.talanta.2009.01.034

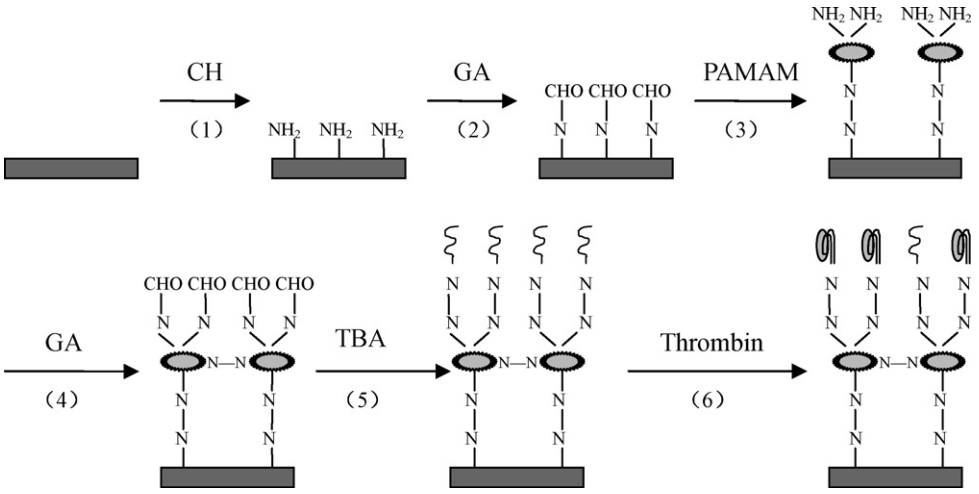

Scheme 1. The schematic illustration for the fabrication procedure on a gold surface. (1) 10 mM CH, 10 h; (2) 5% GA in 0.01 M PBS (pH 7.4), 4 h; (3) 5% PAMAM dendrimer methanolic solution (16 h) and 5 mM $NaBH_4$ (30 min); (4) 5% GA in 0.01 M PBS (pH 7.4), 4 h; (5) 10 μM probe TBA in 0.01 M PBS (pH 7.4) (16 h) and 5 mM $NaBH_4$ (30 min); (6) interaction with target thrombin, 1 h. CH, cysteamine hydrochloride; GA, glutaraldehyde; PAMAM, G_4-NH_2 PAMAM dendrimer; TBA, thrombin-binding-aptamer.

developed by our group [29]. The sensor exhibited good assembly capacity for probe DNA with favorable sensitivity and stability.

Thrombin was selected as target molecules for this study because it is a major stimulus of both procoagulant and anticoagulant reactions, and thus is a key element in various pathogenesis, including leukemia, arterial thrombosis and liver disease, etc. [30,31]. The most extensively investigated prototype thrombin-binding-aptamer (TBA) is a 15-mer single-stranded DNA. When binding to thrombin, TBA forms an intermolecular quadruplex structure and restricts the activity of thrombin [32]. So the study of thrombin and its aptamer interaction plays essential roles in fundamental research and clinical application, such as detection and quantification of thrombin in plasma, regulation of blood clotting in surgery, etc. [33].

In this paper, amino-terminated PAMAM dendrimer was firstly covalently attached to the cysteine self-assembly gold electrode surface through glutaraldehyde coupling. Then the dendrimer was activated with glutaraldehyde, and amino-modified TBA probe was immobilized onto the activated dendrimer monolayer film. The whole assembly process was characterized by SPR and EIS, and recognition events of the aptasensor for thrombin were monitored by impedance technique.

2. Experimental

2.1. Chemical and reagents

Cysteamine hydrochloride (CH) was purchased from Fluka. Glutaraldehyde (GA, 25% aqueous solution) was supplied by Acros. G_4-NH_2 polyamidoamine dendrimer (MW 14,215, 10% methanol solution) was obtained from Aldrich. α-Thrombin from bovine plasma (1000 μ) was provided by Sigma. Bovine serum albumin (BSA) was obtained from Beijing Like biochemical technology and trade Co., Ltd. Guanidine hydrochloride and bovine serum was purchased from Beijing Dingguo biotechnology Co., Ltd. 15-mer amino-terminal TBA was provided by Shanghai Sangon biological engineering technology and services Co., Ltd. 15-mer TBA: 5′-NH_2-$(CH_2)_6$-GGTTGGTGTGGTTGG-3′.

The immobilization buffer was 0.01 M phosphate-buffered saline (PBS, pH 7.4). The redox couple solution was 5 mM equimolar mixture of $K_3[Fe(CN)_6]$ and $K_4[Fe(CN)_6]$ in 0.01 M PBS (pH 7.4) containing 0.1 M KCl. And 20 mM Tris–HCl buffer (pH 7.4) containing 140 mM NaCl, 5 mM KCl and 5 mM $MgCl_2$ was used as thrombin-binding buffer. All other chemicals were of analytical grade and used without further purification. Doubly distilled water was used throughout.

2.2. Apparatus

2.2.1. SPR system

SPR was used to characterize the fabrication procedure of the aptasensor because of its gold reaction surface. Angle-resolved SPR measurements were carried out with a cuvette-based Autolab SPR instrument (Eco Chemie BV, Netherlands). A cleaned gold disk was attached to the half-cylinder prism with a refractive-index-matching oil, and then the SPR cuvette was mounted on the gold substrate. Before sample injection, the cuvette cell was balanced with 0.01 M PBS (pH 7.4) for at least 30 min. The cell and the disk were washed three times with water after each reaction process and the SPR data were recorded in 0.01 M PBS (pH 7.4). For this instrument, the measured $\Delta\theta$ values correspond to the amount of adsorbed substances with a mass sensitivity coefficient of 120 millidegree per 100 ng/cm^2.

2.2.2. EIS system

EIS experiments were carried out using a conventional three-electrode system with an Autolab PGSTAT30 electrochemical analyzer system (Eco Chemie BV, Netherlands), controlled by frequency response analyzer (FRA) 4.9 software. The modified gold electrode was used as working electrode, a platinum wire as counter electrode and an Ag/AgCl electrode with saturated KCl solution as reference electrode. All impedance measurements were performed with a 0.23 V alternating current potential and a 5 mV voltage amplitude in a frequency range from 100 kHz to 0.1 Hz. And the supporting electrolyte was 5 mM $[Fe(CN)_6]^{3-/4-}$ in 0.01 M PBS (pH 7.4) containing 0.1 M KCl. The frequency interval was divided into 61 logarithmically equidistant measuring points (10 points pre decade). The electrochemical cell was housed in a specially shielded cage to reduce stray electrical noise during measurements.

2.3. Modification procedure

A gold electrode (A = 6.4 mm^2) was polished carefully with 1, 0.3, 0.05 μm alumina slurries and washed ultrasonically with water. Then it was electrochemically cleaned in 0.1 M H_2SO_4 by cyclic potential scanning between −0.2 and 1.55 V until a standard cyclic voltammogram of gold electrode was obtained. Subsequently, the

gold electrode was washed ultrasonically with water and absolute ethanol, respectively, and dried in a nitrogen stream.

Scheme 1 provides an overview of the modification procedure of the aptasensor. Firstly, the cleaned gold electrode was immersed into a 10 mM cysteamine hydrochloride aqueous solution for about 10 h. Then the CH modified electrode was placed in 5% glutaraldehyde (GA) in 0.01 M PBS (pH 7.4) for 4 h. Secondly, the gold electrode was incubated in a 5% G_4-NH_2 PAMAM dendrimer methanolic solution for about 16 h, washed with methanol and dried under flowing nitrogen gas. The covalent immobilization of G_4-NH_2 PAMAM dendrimer is based on the fact that each aldehyde group of GA allows the introduction of one amino group, either from the cysteamine or from the dendrimer to form Schiff base configuration. The double bond in Schiff base was reduced by 5 mM $NaBH_4$ for 30 min and formed a more stable single bond structure. Finally, for the immobilization of probe TBA, the dendrimer modified electrode was activated with 5% GA for 4 h. Then the electrode was immersed in 0.01 M PBS (pH 7.4) containing 10 μM TBA for about 16 h at ambient temperature, and reduced by 5 mM $NaBH_4$ for 30 min.

The interaction time of thrombin and its aptamer ranged from less than 20 min to about 1 h according to the previous articles [16,29,34]. In order to make the reaction completely, 1 h was adopted in our experiments. The detection of thrombin was carried out by immersing the probe TBA functionalized gold electrode into thrombin-binding buffer containing a certain concentration of target thrombin for 1 h at room temperature. Before characterizing with EIS, the electrode was rinsed separately with thrombin-binding buffer and water, dried with nitrogen gas. The thrombin-binding electrode was regenerated with 6 M guanidine hydrochloride for 5 min after each thrombin measurement.

3. Results and discussion

3.1. SPR measurements of assembly process

SPR experiments were carried out to track the assembly process of various organic layers on the surface of gold substrate. Fig. 1 showed the superimposed angle-resolved SPR curves for the modification process. After formation of the CH monolayer film on the bare gold surface, the SPR angle shift ($\Delta\theta$) was about 150 millidegree. When the GA layer and the dendrimer layer were linked to the CH modified electrode, the $\Delta\theta$ values were approximately 150 and 400 millidegree, respectively. The $\Delta\theta$ values for the sequential deposition of the second GA layer and the TBA layer were about 200 and 300 millidegree, respectively. Because the mass sensitivity coefficient of the measured $\Delta\theta$ value is 120 millidegree per 100 ng/cm^2. Therefore 300 millidegree corresponds to 250 ng/cm^2. The molecular weight of TBA is 4726.03 μg/μmol. So the surface coverage of TBA molecules was calculated to be about 3.2×10^{13} molecules/cm^2, this value is higher than related literature [19]. It is likely that TBA is a 15-mer short-chain DNA molecule and this method improves the assembly capacity of probe molecule greatly.

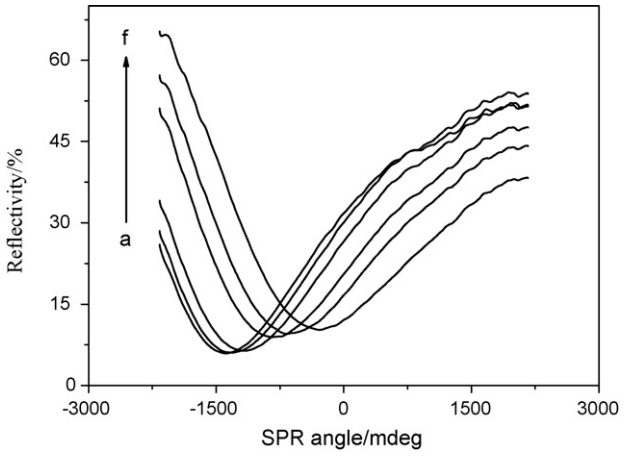

Fig. 1. Angle-resolved SPR curves for the layer-by-layer assembly procedure on a gold substrate. (a) Bare Au disk; (b) CH; (c) GA; (d) den + $NaBH_4$; (e) GA; (f) TBA + $NaBH_4$. den, G_4-NH_2 PAMAM dendrimer.

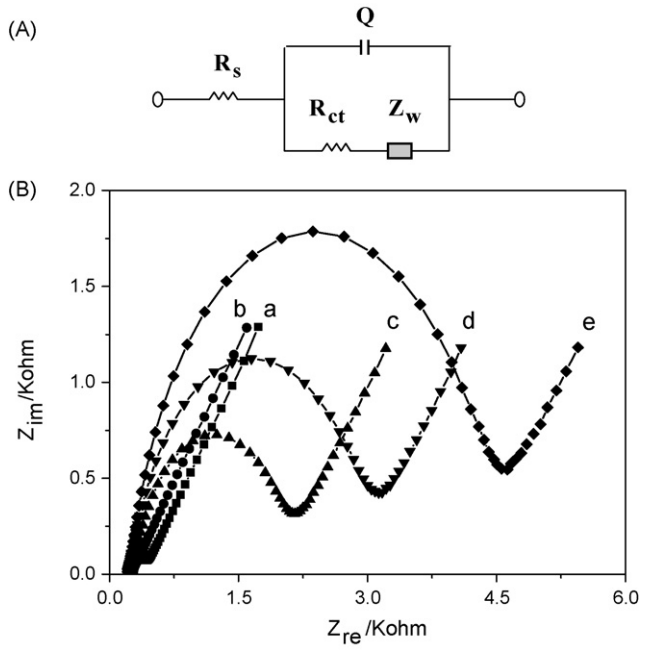

Fig. 2. (A) The Randle modified equivalent circuit model for the impedance spectra. (B) The Nyquist impedance spectra for the modification procedure on a gold electrode in the presence of 5 mM $[Fe(CN)_6]^{3-/4-}$ in 0.01 M PBS (pH 7.4) containing 0.1 M KCl. (a) Bare Au electrode; (b) CH; (c) GA + den + $NaBH_4$ + GA; (d) TBA + $NaBH_4$; (e) after incubation in 20 nM thrombin. AC potential, 0.23 V; frequency range, 100 kHz to 0.1 Hz; voltage amplitude, 5 mV.

3.2. EIS characterization of modified electrode

As shown in Fig. 2A, Randle modified equivalent circuit model [3] was used to fit impedance data. The parameters in the equivalent circuit included the solution resistance (R_s), the Warburg impedance (Z_w) resulting from the diffusion of the redox-probe, the double layer capacitance (C_d) is substituted by the constant phase element (Q) when taking into account electrode roughness, and the charge-transfer resistance (R_{ct}). The latter two components (Q and R_{ct}) represent interfacial properties of the electrode, which are highly sensitive to the surface modification.

Impedance responses of the functionalized gold electrode accompanying the stepwise modification process were depicted in Fig. 2B. The bare gold electrode exhibited a very small semicircle domain, corresponding to the R_{ct} value of approximately 250 Ω. The CH deposited electrode resulted in an almost straight line, which is characteristic of a diffusional limiting step due to the extremely fast charge-transfer process. This is attributed to the electrostatic attraction between the positive charges of CH molecules and the negatively charged $[Fe(CN)_6]^{3-/4-}$ redox couple. When the GA layer, the dendrimer layer, and the second GA layer were further grafted onto the CH modified electrode, the R_{ct} value increased to about 2 kΩ, due to the compact structure of fabricated multilayer films and the neutral property of GA molecules. The assembly of the TBA monolayer film onto the electrode surface led to a further increase in the R_{ct} value by approximately 0.8 kΩ, because there are a lot of negative charges on the TBA sugar-phosphate back-

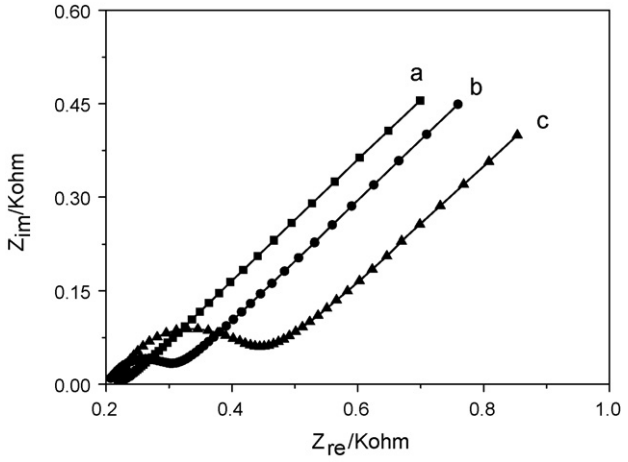

Fig. 3. The impedance spectra of a non-dendrimer modified gold electrode. (a) Au/CH; (b) Au/CH/GA/TBA + $NaBH_4$; (c) the modified electrode (b) after being immersed in 20 nM thrombin. Other conditions as in Fig. 2.

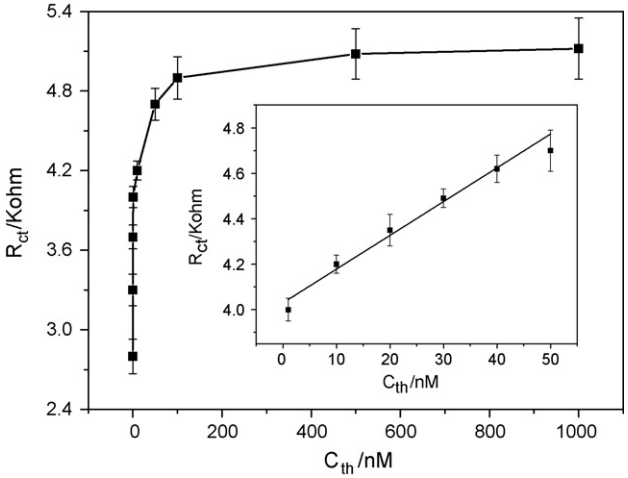

Fig. 5. EIS responses of the dendrimer modified electrode to different concentrations of thrombin, $n = 3$. Inset: the calibration curve of the aptasensor between the R_{ct} values and the concentrations of thrombin in the range of 1–50 nM; $n = 5$.

bone. After incubation in 20 nM thrombin, the formation of the TBA–thrombin complex on the electrode surface contributed to a significant increase in the R_{ct} value to about 4.4 kΩ. This is consistent with the fact that thrombin and its aptamer complex insulates the electron transfer between the electrode surface and the electrolyte solution [20,24,34]. Both the SPR and the EIS data indicated that various organic layers were successfully immobilized onto the gold substrate.

To investigate whether the application of the dendrimer improved the immobilization capacity of probe molecules and magnified the response signals of the aptasensor, a non-dendrimer modified electrode was fabricated as control. As depicted in Fig. 3, when both GA and TBA molecules were immobilized on the CH functionalized gold electrode surface, the R_{ct} value changed from about 20–110 Ω. After the non-dendrimer modified electrode was immersed in 20 nM thrombin, the R_{ct} value increased to about 260 Ω. Fig. 4 showed the changes of R_{ct} (ΔR_{ct}) value for the probe-binding capacity and the response signals of the two methods. It was observed that the ΔR_{ct} values of the immobilization capacity of TBA molecules and the response signals of 20 nM thrombin of the dendrimer modified electrode were approximately 8-fold and at least 10 times higher than those of the non-dendrimer modified electrode. This may be due to the fact that each molecular CH can only combine with one TBA molecule, while an individual dendrimer molecule can bind several TBA molecules due to 64 amino groups on its surface. Therefore, the dendrimer layer is not only able to remarkably improve the immobilization capacity of probe molecules but also to magnify the response signals greatly.

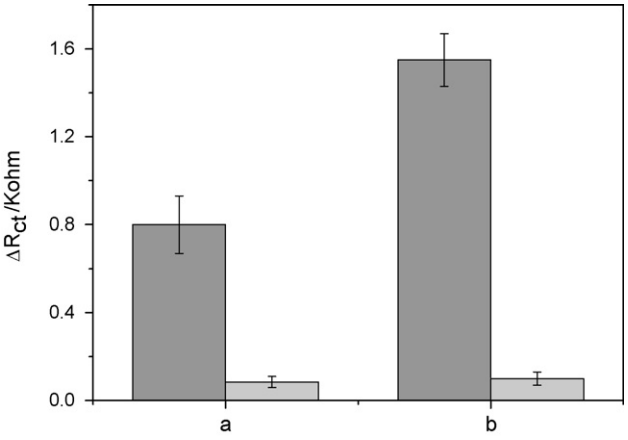

Fig. 4. The histogram of the change of R_{ct} value ($\Delta R_{ct} = R_{ct(2)} - R_{ct(1)}$) for different methods of electrode preparation. The dark gray part corresponds to the Au/CH/GA/den/GA/TBA-modified electrode, while the light gray part represents the Au/CH/GA/TBA prepared electrode. (a) the ΔR_{ct} value of TBA immobilization; (b) the ΔR_{ct} value of the detection of 20 nM thrombin; $n = 3$.

3.3. Aptasensor responses to target thrombin

For thrombin detection, the Au/CH/den/TBA-modified electrode was incubated in the thrombin solution with different concentrations for 1 h, and washed with thrombin-binding buffer and water, respectively. Fig. 5 indicated that the R_{ct} value increased with increasing the concentration of thrombin from 0.01 to 1000 nM. When the concentration of thrombin exceeded 500 nM, the change of the R_{ct} value could be neglected as a result of the saturated adsorption of target molecules. As also seen in Fig. 5, the R_{ct} value had a positive linear relationship with the concentration of thrombin in the range of 1–50 nM. The regression equation was $Y = 4.029 + 0.015X$ (Y: the R_{ct} value, kΩ; X: the concentration of thrombin, nM), and the correlation coefficient (R) was 0.978. The detection limit (S/N = 3) for thrombin as low as 0.01 nM was obtained, which was more sensitive than most available impedimetric thrombin aptasensors [20,34].

It was reported that thrombin has two positively charged sites termed Exosite I (the fibrinogenrecognition exosite) and II (the heparin-binding exosite) on the opposite sides of the protein [24]. The 15-mer TBA used has specificity to the Exosite I, while a 29-mer TBA is easy to bind with the Exosite II [35]. So the affinity of the 15-mer TBA to the fibrinogenrecognition exosite should be higher than to the heparin-binding exosite of thrombin.

3.4. Aptasensor regeneration

After target detection, the sensing interface could be regenerated with acid, alkali or salt to remove adsorptive target molecules for the second measurement [17,29]. And the regeneration of sensing interface is still a challenge for most existing biosensors [19]. In this paper, a mild regeneration reagent guanidine hydrochloride was used to renew the sensing interface. As shown in Fig. 6, when the thrombin-binding electrode was immersed in 6 M guanidine hydrochloride for 5 min, the R_{ct} value was almost recovered to the original value of newly prepared electrode, suggesting that the treated electrode was reusable. When this electrode was incubated

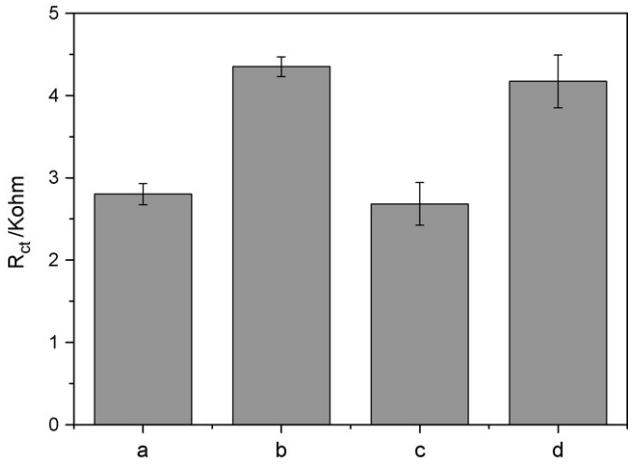

Fig. 6. Thrombin detection and regeneration of the sensing interface: (a) newly prepared electrode; (b) after being immersed in 20 nM thrombin; (c) regeneration with 6 M guanidine hydrochloride for 5 min; (d) detection of 20 nM thrombin for the second time; $n = 3$.

in 20 nM thrombin for the second time, the R_{ct} value was approximately the same value of the first detection of 20 nM thrombin. After being challenged with 20 nM thrombin and regenerated for at least six cycles, the electrode still possessed 85% sensing activity. This may be because the stable covalent immobilization strategy and the insusceptible TBA molecules are used in this aptasensor.

3.5. Aptasensor selectivity and stability

To investigate the specificity of the aptasensor, bovine serum albumin was adopted in the control experiments. BSA normally constitutes about 60% of plasma protein and is the most abundant protein in blood plasma [36]. As depicted in Fig. 7, when the Au/CH/den/TBA-functionalized electrode was exposed to 100 nM BSA for 1.5 h, the ΔR_{ct} value increased to about 280 Ω. However, after the electrode was incubated in 20 nM thrombin for 1 h, the ΔR_{ct} value increased to approximately 1.6 kΩ, which was 5–6-fold higher than that of 100 nM BSA. The results indicated that the aptasensor had considerable selectivity to its target thrombin.

As for the reproducibility of the electrode modification procedure, using the same electrode, after five processes of electrode construction under identical experimental conditions, the measured R_{ct} value of 20 nM thrombin was 4.35 ± 0.16 kΩ and the relative standard deviation (R.S.D.) was 2.7%. The life stability of

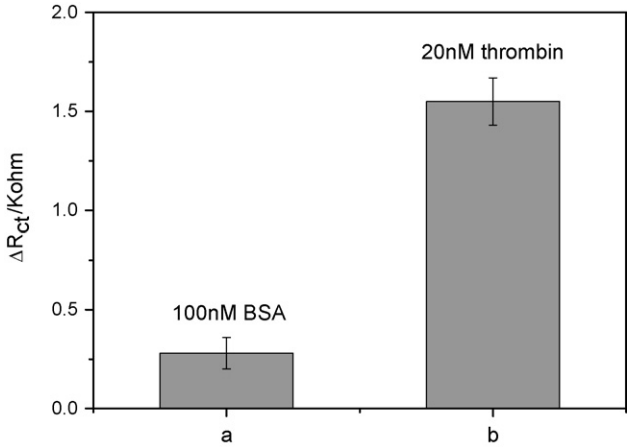

Fig. 7. Control experiments of the aptasensor. (a) 100 nM BSA, 1.5 h; (b) 20 nM thrombin, 1 h; $n = 3$.

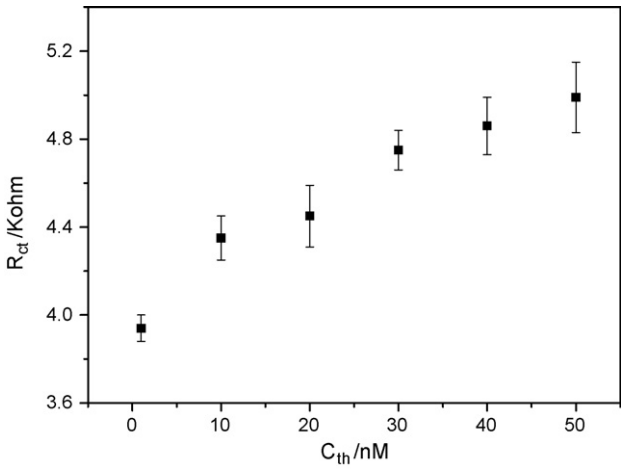

Fig. 8. EIS responses of the aptasensor to thrombin at different concentrations (1–50 nM) in 1% bovine plasma; $n = 3$.

the aptasensor was also studied. A newly prepared Au/CH/den/TBA-modified electrode was dried in a nitrogen stream and covered with a plastic cap to protect the gold surface. The modified electrode was stored at 4 °C and measured at intervals of one week. It remained about 85% of its original response after one month, indicating that the modified electrode was very stable.

3.6. Application of the aptasensor in biological assay

For further study the potential application of the modified electrode, the determinations of thrombin in real samples were performed. As shown in Fig. 8, the EIS responses at the sensing interface to the different concentrations of thrombin in 1% bovine plasma exhibited the same phenomena to those in blank buffer but were less sensitive. The R_{ct} value increased with increasing the concentrations of thrombin in the range of 1–50 nM. The results definitely illuminate the potential application of this aptasensor in real samples.

4. Conclusions

We have described a reusable aptasensor based on the Au/CH/den/TBA-modified electrode. The dendrimer immobilization on the electrode surface not only improved the probe-binding capacity but also magnified the response signals of the aptasensor. The immobilization process of the aptasensor and recognition events changed the charge-transfer kinetics of $[Fe(CN)_6]^{3-/4-}$ redox couple at the electrode interface, which had been characterized by EIS. The dendrimer-functionalized aptasensor exhibited high sensitivity, favorable specificity and stability in the detection of thrombin. Although the preparation process of this aptasensor is a bit complex, the sensitivity is satisfactory. In a word, this work establishes a methodology for the developing of biosensors with good analytical properties.

Acknowledgements

This work was supported by the National Natural Science Foundation of China (No. 90713022), the National Key Basic Research Development Project of China (No. 2007CB714500) and the Project of Chinese Academy of Sciences (No. KJCX2-YW-H11).

References

[1] A.D. Ellington, J.W. Szostak, Nature 346 (1990) 818.
[2] C. Tuerk, L. Gold, Science 249 (1990) 505.

[3] J.A. Lee, S. Hwang, J. Kwak, S.I. Park, S.S. Lee, K.C. Lee, Sens. Actuators B: Chem. 129 (2008) 372.
[4] C.K. O'Sullivan, Anal. Bioanal. Chem. 372 (2002) 44.
[5] V. Pavlov, B. Shlyahovsky, I. Willner, J. Am. Chem. Soc. 127 (2005) 6522.
[6] X.H. Fang, Z.H. Cao, T. Beck, W.H. Tan, Anal. Chem. 73 (2001) 5752.
[7] H. Wei, B.L. Li, J. Li, E.K. Wang, S.J. Dong, Chem. Commun. (2007) 3735.
[8] Y. Li, H.J. Lee, R.M. Corn, Nucleic Acids Res. 34 (2006) 6416.
[9] R. Polsky, R. Gill, L. Kaganovsky, I. Willner, Anal. Chem. 78 (2006) 2268.
[10] Y. Xiao, B.D. Piorek, K.W. Plaxco, A.J. Heeger, J. Am. Chem. Soc. 127 (2005) 17990.
[11] K. Ikebukuro, C. Kiyohara, K. Sode, Biosens. Bioelectron. 20 (2005) 2168.
[12] F.L. Floch, H.A. Ho, M. Leclerc, Anal. Chem. 78 (2006) 4727.
[13] E. Bakker, Y. Qin, Anal. Chem. 78 (2006) 3965.
[14] M. Zayats, Y. Huang, R. Gill, C.A. Ma, I. Willner, J. Am. Chem. Soc. 128 (2006) 13666.
[15] Y. Xiao, A.A. Lubin, A.J. Heeger, K.W. Plaxco, Angew. Chem. 117 (2005) 5592.
[16] Y. Lu, X.C. Li, L.M. Zhang, L.Q. Mao, Anal. Chem. 80 (2008) 1883.
[17] A.E. Radi, J.L.A. Sánchez, E. Baldrich, C.K. O'sullivan, J. Am. Chem. Soc. 128 (2006) 117.
[18] G.S. Bang, S. Cho, B.G. Kim, Biosens. Bioelectron. 21 (2005) 863.
[19] Y. Du, B.L. Li, H. Wei, Y.L. Wang, E.K. Wang, Anal. Chem. 80 (2008) 5110.
[20] A.E. Radi, J.L.A. Sánchez, E. Baldrich, C.K. O'Sullivan, Anal. Chem. 77 (2005) 6320.
[21] D.K. Xu, D.W. Xu, X.B. Yu, Z.H. Liu, W. He, Z.Q. Ma, Anal. Chem. 77 (2005) 5107.
[22] M.C. Rodriguez, A.-N. Kawde, J. Wang, Chem. Commun. (2005) 4267.
[23] C.Z. Li, Y.L. Liu, J.H.T. Luong, Anal. Chem. 77 (2005) 478.
[24] X.X. Li, L.H. Shen, D.D. Zhang, C.X. Zhang, Biosens. Bioelectron. 23 (2008) 1624.
[25] H.C. Yoon, H.S. Kim, Anal. Chem. 72 (2000) 922.
[26] H.C. Yoon, M.Y. Hong, H.-S. Kim, Anal. Biochem. 282 (2000) 121.
[27] Z.M. Liu, Y. Yang, H. Wang, Y.L. Liu, G.L. Shen, R.Q. Yu, Sens. Actuators B: Chem. 106 (2005) 394.
[28] L. Shen, N.F. Hu, Biomacromolecules 6 (2005) 1475.
[29] A.X. Li, F. Yang, Y. Ma, X.R. Yang, Biosens. Bioelectron. 22 (2007) 1716.
[30] R. Kita, A. Takahashi, M. Kaibara, K. Kubota, Biomacromolecules 3 (2002) 1013.
[31] J.A. Páramo, J. Rifón, J. Fernández, B. Cuesta, E. Rocha, Blood Coagul. Fibrin. 2 (1991) 227.
[32] T. Hermann, D.J. Patel, Science 287 (2000) 820.
[33] A. Joachimi, G. Mayer, J.S. Hartig, J. Am. Chem. Soc. 129 (2007) 3036.
[34] H. Cai, T.M.H. Lee, I.M. Hsing, Sens. Actuator B: Chem. 114 (2006) 433.
[35] Z.H. Cao, W.H. Tan, Chem. Eur. J. 11 (2005) 4502.
[36] K.A. Mahmoud, S. Hrapovic, J.H.T. Luong, ACS Nano 2 (2008) 1051.

Talanta 78 (2009) 1253–1258

Contents lists available at ScienceDirect

Talanta

journal homepage: www.elsevier.com/locate/talanta

Rapid and sensitive detection of point mutation by DNA ligase-based electrochemiluminescence assay

Huijuan Zhou, Da Xing*, Debin Zhu, Xiaoming Zhou

MOE Key Laboratory of Laser Life Science & Institute of Laser Life Science, South China Normal University, Guangzhou 510631, China

ARTICLE INFO

Article history:
Received 8 November 2008
Received in revised form 16 January 2009
Accepted 18 January 2009
Available online 24 January 2009

Keywords:
Point mutation
Electrochemiluminescence
Oligonucleotide ligation assay

ABSTRACT

The identification of single-base mutations in particular genes plays an increasingly important role in medical diagnosis and prognosis of genetic-based diseases. Here we report a new method for the analysis of point mutations in genomic DNA through the integration of allele-specific oligonucleotide ligation assay (OLA) with magnetic beads-based electrochemiluminescence (ECL) detection scheme. In this assay, the tris(bipyridine) ruthenium (TBR) labeled probe and the biotinylated probe are designed to perfectly complementary to the mutant target; thus a ligation can be generated between those two probes by Taq DNA Ligase in the presence of mutant target. If there is an allele mismatch, the ligation does not take place. The ligation products are then captured onto streptavidin-coated paramagnetic beads, and detected by measuring the ECL signal of the TBR label. Results showed that the new method held a low detection limit down to 10 fmol and was successfully applied in the identification of point mutations from ASTC-α-1 cell line, PANC-1 cell line and blood cell in codon 273 of *TP53* oncogene. In summary, this method provides a sensitive, cost-effective and easy operation approach for point mutation detection.

1. Introduction

The analysis of genomic mutations in disease-related gene fragments is playing an increasingly important role in fields of genetic-based diseases diagnosis and drug reaction prediction. Since large numbers of mutations must be evaluated in order to obtain an accurate diagnosis/prognosis of that disease, a sensitive, rapid and cost-effective DNA identification method is in need. A variety of technologies based on allele discrimination strategies have been applied in the identification of point mutations, such as primer extension [1–4], allele-specific hybridization [5–8], enzymatic cleavage [9,10], and oligouncleotide ligation [11–13]. Among these allele-discrimination strategies, DNA enzyme-based assay is popular because it is highly specific, cost effective, and easy to operate and fast to implement. In these enzyme-based assays, DNA ligase is an enzyme which is used frequently in the discrimination of point mutations [14–17], insertions and deletions [18]. Several conventional detection methods, such as denaturing gradient gel-electrophoresis [19,20], mass spectrometry [21,22] and fluorescence signal-based detection [23,24] have been used to the ligase based strategy. These technologies provide accurate or highly sensitive approaches for point mutation detection. However, each of them still has its disadvantages. For example, some of them are time consuming, complicated, or requiring special instruments and the use of expensive fluorescent substances. Recently, methods based on chemiluminescence [25,26] and electrochemistry [27,28] have also been used to facilitate single-base mutation identification for the advantages of rapidness and cost efficiency.

In recent years, electrochemiluminescence (ECL) has attracted considerable attention due to its feature of high-sensitivity, low-cost, simple instrumentation, and time efficiency. The most common ECL luminophore is tris(2,2-bipyridine)ruthenium(II) (TBR), and tripropylamine (TPA) is the most efficient known coreactant. In this ECL reaction, TBR and TPA are first oxidized at the surface of an anode forming the strong oxidant $Ru(bpy)_3^{3+}$ and the cation radical $TPA^{\bullet+}$, respectively. The resulted $TPA^{\bullet+}$ immediately loses a proton and becomes a powerful reducer, $TPA^{\bullet}$. Then $Ru(bpy)_3^{3+}$, a strong oxidant, and $TPA^{\bullet}$, a strong reductant, react to form the excited state of the ruthenium complex, $Ru(bpy)_3^{2+*}$, as well as other inactive products. Relaxation of the excited-state $Ru(bpy)_3^{2+*}$ to the ground state results in a light emission, at 620 nm [29,30]. It should be noticed that $Ru(bpy)_3^{2+}$ is not consumed during the reaction, and may be oxidized and excited repeatedly when there is excessive TPA in the buffer. Since Kenten et al. [31] firstly used ECL in DNA probe assays, the technology has been widely applied in the areas of DNA analysis [32], immunoassay, food and water testing and biowarfare agent detection [33].

In this paper, we describe a specific and sensitive method for point mutations assay which is accomplished by incorporating OLA into magnetic beads-based ECL detection scheme. Taq DNA ligase is applied for single-base mutation discrimination through catalyzing the joint of the common probe and the discriminating probe

* Corresponding author. Tel.: +86 20 85210089; fax: +86 20 85216052.
E-mail address: xingda@scnu.edu.cn (D. Xing).

0039-9140/$ – see front matter © 2009 Elsevier B.V. All rights reserved.
doi:10.1016/j.talanta.2009.01.032

Table 1
Oligonucleotides used in this assay.

Oligonucleotide	Sequence (5′–3′)
TP53 exon 8 forward	5′-CTGATTTCCTTACTGCCTCTTG-3′
TP53 exon 8 reverse	5′-TACCTCGCTTAGTGCTCCCT-3′
TBR-labeled probe	5′-TBR-$(CH_2)_6$-TGGGACGGAACAGCTTTGAGGTGCA-3′
Biotin-labeled probe	5′-Phosphate-TGTTTGTGCCTGTCCTGGGAGAGAC-Biotin-3′
Target 1 (MI)	5′-CCAGGACAGGCACAAACATGC ACCTCAAAGCTGTT-3′
Target 2 (WI)	5′-CCAGGACAGGCACAAACACGCACCTCAAAGCTGTT-3′

The location of the allele-specific recognition site in TBR-labeled probe and the polymorphism sites in target is underlined.

to form a single oligonucleotide in the presence of perfect match target DNA. Ligation products are then captured onto streptavidin-coated paramagnetic beads through biotin-streptavidin interaction, and then the luminescence signal will be detected by ECL system. According to the signal we can determine whether the sample is mutant type or wild type. This method is proven to be effective in analyzing the point mutation in codon 273 of *TP53* oncogene target from PANC-1 human pancreatic cancer cell line, ASTC-α-1 lung cancer cell line, and blood cells.

2. Experimental

2.1. Oligonucleotides and reagents

The primers (Table 1) for PCR amplification were designed using Primer Premier 5 software and the two probes (Table 1) used in DNA ligase reaction were designed with the help of DNA probe design software (Zucker folding program, www.bioinfo.rpi.edu/applications/mfold/dna/form1.cgi). The mutant target (M1, Target 1), wild-type target (W1, Target 2) and the primers, the 5′-amino modified probe (TBR labeled probe) and the other probe which is labeled with biotin at 3′ and phosphate at 5′ probe (Table 1) were synthesized by Shanghai Sangon Biological Engineering & Technology Services Co. Ltd. (SSBE), China. All probes were HPLC purified. TPA, and the chemicals to synthesize the $Ru(bpy)_3^{2+}$ N-hydroxysuccinimide ester (TBR-NHS ester) were products of Sigma (Louis, MO, USA). TBR-NHS ester was synthesized by our laboratory according to Terpetschnig's paper [34]. Streptavidin microbeads (2.8 μm diameter) were purchased from Dynal Biotech (Lake Success, NY, USA). Taq DNA ligase was purchased from New England BioLabs, Inc. (Beverly, MA). Taq DNA polymerase, dNTP, 2000 bp DNA Marker and the UNIQ-10 column genome DNA extraction kit were all purchased from SSBE. All other reagents were of analytical grade.

2.2. Extraction of DNA from cell lines

Genomic DNA was extracted from PANC-1 human pancreatic cancer cell line, ASTC-α-1 lung cancer cell line and blood cells. The PANC-1, ASTC-α-1 cell lines were cultured as described in our recent papers [35,36].

The blood samples were obtained from healthy donors. 1 mL of ACD decoagulant (0.48% citric acid, 1.32% sodium citrate, 1.47% glucose) was added to each 6 mL blood. 500 μL of blood was diluted by adding 1 mL sterile distilled water, and then was centrifuged at 5000 rpm for 2 min at 25 °C. The sediment was resuspended with 200 μL Tris–EDTA (TE) buffer (pH 8.0) for DNA extraction.

DNA was extracted according to the protocol of the UNIQ-10 column genome DNA extraction kit.

2.3. PCR amplification of genomic DNA

The extracted genomic DNA was amplified using the primers (Table 1) specific for exon 8 of *TP53* gene in a total volume of 50 μL. Each reaction contained 5 μL of 10 × buffer, 1 μL of 10 μM each amplification primers, 1 μL of 10 mM dNTP mixture, 1 U of Taq DNA polymerase, and 1 μL of extracted DNA. After a 5 min denaturation step, the application was achieved by thermal cycling for 35 cycles at 95 °C for 1 min, 60 °C for 30 s, 72 °C for 1 min and a final extension at 72 °C for 10 min.

2.4. Oligonucleotide ligation assay

For oligonucleotide ligation assay, a 20 μL reaction mixture containing template (synthetic oligonucleotide targets or PCR products) in different concentrations, 1 μM biotin-labeled probes, 1 μM TBR-labeled probes and Taq ligation buffer [20 mM Tris–HCl (pH 7.6), 25 mM potassium acetate, 10 mM magnesium acetate, 10 mM DTT, 1 mM NAD^+, 0.1% Triton X-100] was prepared. The mixture was denatured for 5 min at 95 °C, hybridized for 60 min at 55 °C, followed by adding of 2 U of Taq DNA ligase, and then the ligase reaction took place at 45 °C for 30 min.

2.5. ECL detection

A custom-made ECL detection system was described in detail in our previous research [29]. For the sample analysis, 10 μL OLA products and 10 μL streptavidin coated beads were added to 80 μL bind buffer (10 mM TE, 500 mM NaCl, pH 7.4), and then incubated in an Effendorf thermomixer for 30 min at 30 °C. The reaction products were separated by using magnetic racks (Dynal, mpc-s), and washed first with 50 mM NaOH and then with bind buffer to remove the unbound probes labeled with TBR. Then the magnetic-ligation products were resuspended in 100 μL ECL assay buffer (0.2 M NaH_2PO_4, 50 μM NaCl, 7 mM NaN_3, 0.8 μM Tirton X-100, 0.4 mM Tween 20, 0.1 M TPA, pH 8.0) and was sequentially used for ECL detection. 50 mM NaOH solution was used to denature the duplex and dissociate the DNA template, retaining the DNA fragments contained biotin on the streptavidin coated magnetic beads. 50 mM NaOH can denature DNA duplexes with 1 min whereas biotin-streptavidin bind is essentially undisturbed under this condition [37,38]. The applied potential of the ECL reaction was fixed at 1.25 V and the ECL system was controlled by Labview software.

3. Results and discussion

3.1. Assay principle

The detection principle is illustrated in Fig. 1. In the design, common probes modified with biotin at 3′ end and discriminating probes modified with TBR at 5′ end. Both probes hybridize with the target DNA at adjoining positions. Since the probes we designed are only perfectly complementary to the mutant template DNA, Taq DNA ligase can specially catalyze the formation of a phosphodiester bond between the juxtaposed 5′-phosphate and 3′-hydroxyl groups of above noticed probes to form a single oligonucleotide in the presence of mutant target DNA, but no ligation occurs for probes associated with the wild-type template. After ligation reaction, the products are concentrated by streptavidin-coated magnetic beads through the highly selective biotin-streptavidin reaction. The unlinked DNA fragments are washed away, thus, only the products labeled with both biotin and TBR can be detected in the detection cell.

3.2. Optimization of assay conditions

The hybridization temperature between the probes (biotin-labeled probe and TBR-labeled probe) and target DNA in analysis of targets is an important factor. As we know, there will be a melting temperature (T_m) which means half of the hybridized DNA duplex

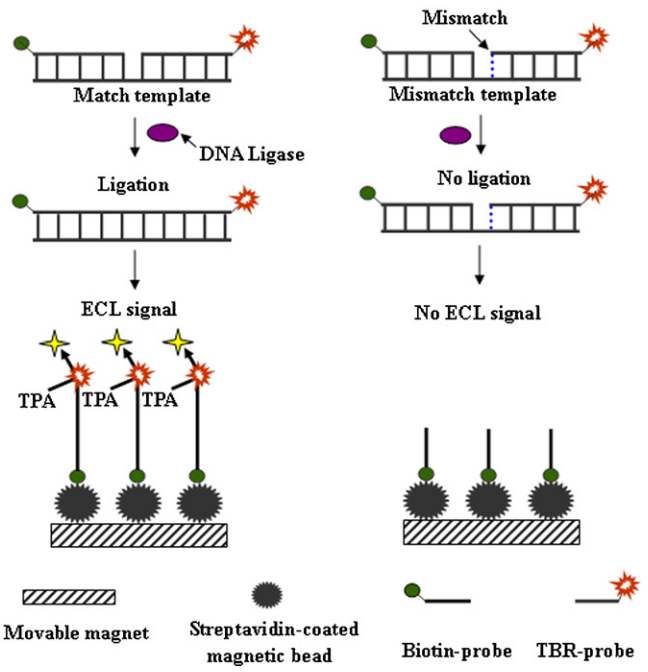

Fig. 1. Schematic for point mutation detection based on OLA and magnetic beads-based ECL detection scheme. Biotin-probe: biotin labeled probe. TBR-probe: TBR labeled probe.

melted at this temperature. The T_m between two designed probes (biotin-labeled probe TBR-labeled probe) and the target DNA is 65 and 68 °C respectively, according to DNA probe design software (Zucker folding program) and the theoretical calculation [39]. In common practice, the temperature approximately 10 °C lower than the melting temperature is chosen as the optimal Hybridization temperature. So, the hybridization temperature was fixed at 55 °C in the detection system. At the relatively higher temperature, the formed duplex DNA will melt. However, if oligonucleotides hybridize at relatively lower temperature, there will be nonspecific hybridization.

The effect of hybridization time on the ECL intensity was also investigated, to ensure the method timesaving. A mixture containing each probes and 10 nM target incubated at 55 °C for various hybridization times. As shown in Fig. 2, the ECL intensity response increased rapidly with the hybridization time up to 1 h. After 1 h, the ECL intensity could not be further improved, indicating that the hybridization equilibrium was reached at 1 h. Therefore, a

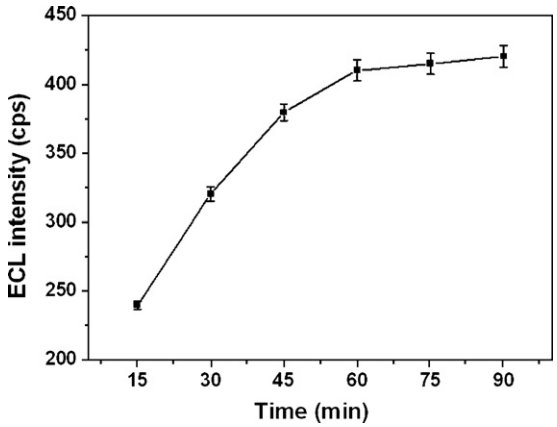

Fig. 2. The effect of hybridization time on the ECL intensity. The ECL intensity was plotted vs. hybridization time.

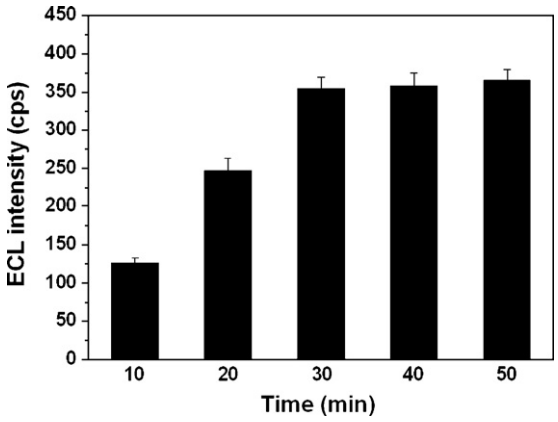

Fig. 3. The effect of ligase deposition time on the ECL intensity. The response represents the ECL intensity change induced by the deposition time changed from 10 min to 50 min for the ligation reaction. The concentrations of synthetic mutant template is 10 nM.

hybridization time of 1 h was selected as the optimum in the following experiments.

We also investigated the effect of ligase reaction time on the ECL intensity. After hybridized at 55 °C for 1 h, the Taq DNA ligase was added to the reaction solution and incubated at 45 °C for different times varying from 10 to 50 min. As shown in Fig. 3, the ECL intensity increased rapidly until 30 min. After 30 min, ECL intensity increased slowly. That phenomenon is mostly probably because Taq DNA ligase lost its activity with the increase in the reaction time. So the reaction time was fixed at 30 min throughout the experiment.

In the ECL detection, the quantity of magnetic beads is a vital factor [40]. Since the appropriate amount of beads can capture the entire special ligation products, thus improving the sensitivity. But excessive beads would be absorbed on the surface of electrode, and influence the reaction of TPA and $Ru(bpy)_3^{2+}$ on the surface of electrode. In the experiments, the ligation products were linked on to the surface of streptavidin-coupled beads by the biotin modified on the common probe at the 3′ end through the highly selective biotin-streptavidin linkage. The unlinked DNA fragments were washed away. As shown in Fig. 4, the quantity of magnetic beads from 4 to 14 μL gave the different ECL responses, and it is observed that the ECL response is maximized at a beads quantity of 10 μL. Therefore, 10 μL beads were added to each 10 μL ligation product throughout the experiment.

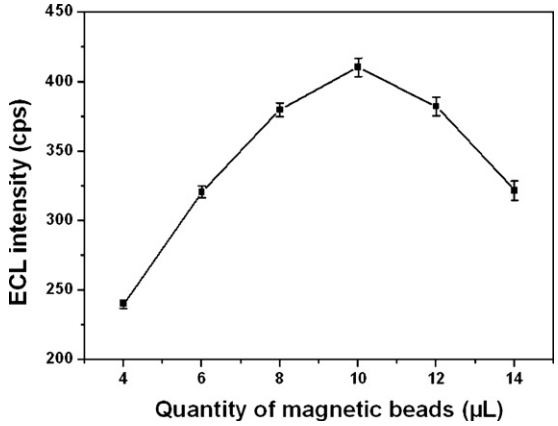

Fig. 4. The effect of the quantity of streptavidin-coupled magnetic beads on the ECL intensity. The concentration of the mutant target is 10 nM, hybridization time is 1 h and ligase deposition time is 30 min.

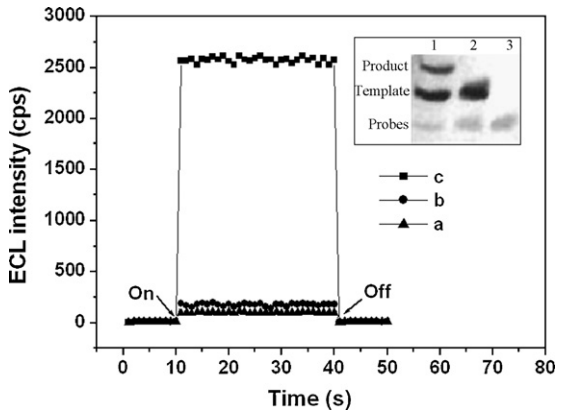

Fig. 5. Specificity evaluation of OLA-ECL method. ECL intensity corresponding to (a) template free control, (b) 1 μM wild-type template, (c) 1 μM mutant template. 1 μM ligation products were separated by 10% ployacrylamide gel electrophoresis containing 8 M urea, and DNA was screened with a standard silver-staining method. (1) Mutant ligation products, (2) Wild-type liagtion products, (3) Template free ligation products control. On: potentiostat on. Off: potentiostat off.

3.3. Analysis of single-base variations in synthetic oligonucleotide targets

In order to evaluate the feasibility of the method, we firstly analyzed single-base mutation in synthetic oligonucleotide templates (Table 1), to avoid the effects of variability between real DNA samples on the evaluation results. Wild-type template (W1) and mutant template (M1) were derived from variants of human *TP53* gene sequence. Fig. 5 displays the results obtained from template free control (a), 1 μM wild-type template (b), 1 μM mutant template (c). It was observed that the ECL signal obtained from analysis of perfectly matched mutant target (2568 cps) was significantly higher than that of wild-type target (177 cps) with a single-base mismatch. As a result, the signal-to-noise ratio in discriminating point mutation reaches 14.5 in the proposed method, demonstrating that the proposed method based on Taq DNA ligase reaction can be used to distinguish mutant target DNA and the wild target DNA efficiently. The incorporation of OLA not only provides high specificity but also is easy to operate. The application of DNA ligase reaction for single base mismatch identification substantially improved the capacity of point mutation discrimination without tight control of the assay conditions. In contrast, the application of specific DNA sequence based on DNA hybridization assay for point mutation detection requires stringent temperature control in hybridization reaction [5–8]. In mutation detection, specificity and operational ease are of the most significance. To further validate the accuracy of the current method, the ligation products were analyzed by 10% polyacrylamide gel electrophoresis. As shown in Fig. 5, there is an obvious product band appeared in mutant ligation products, but without product band was found for the wild-type ligation products. Thereby, the results of gel electrophoresis are consistent with the results of ECL detection.

Under the optimal experimental conditions, the sensitivity of the reported system was evaluated through analysis of various quantities of the perfectly matched and mismatched targets (quantity banding from 10 pmol to 1 fmol). In order to avoid cumulated background, this assay started from low quantity to high quantity. As depicted in Fig. 6A. The proposed method offers well-defined concentration dependence. It was found that when the quantity of target was down to 10 fmol, the wild-type target and mutant target can be distinguished easily. The detection limit is 10 times higher than that shown previously [36]. Furthermore, the technique is much simpler than conventional DNA detection methods. This is attributed to the application of streptavidin-coated paramagnetic

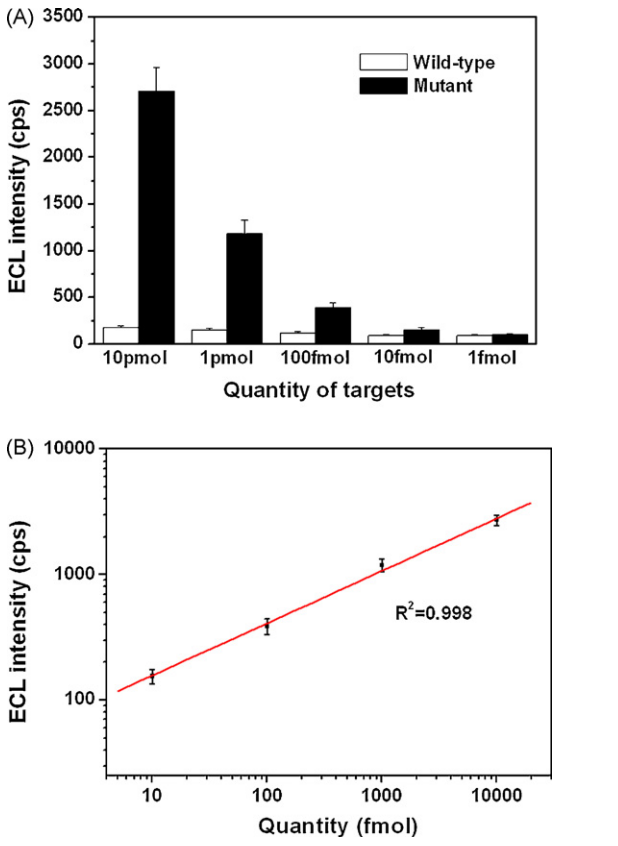

Fig. 6. Sensitivity and linearity of OLA-ECL method. (A) ECL intensity as a function of the sensitivity for detecting perfectly matched and mismatched templates of various concentrations varying from 10 pmol to 1 fmol. (B) Linearity of ECL intensity was observed in different quantities of mutant template DNA with OLA-ECL.

beads. In the reported method, streptavidin-coated paramagnetic beads were specifically chosen for selective capture of biotinylated ligation products. The binding interaction of streptavidin and biotin is quick, reliable and strong ($Kd = 10^{-15}$), and dramatically reduces the time of sample preparation. Otherwise, in ECL detection, the magnetic beads-ligation products complex can readily be collected on the electrode surface only by using a magnet without any modification on electrode surface. This ensures that the electrode can be reused by simply washing out the beads from the surface, resulting in a rapid detection process and a reduce detection cost. Moreover, the method can be easily extended to high-throughput and automatic screening format with the use of the magnetic beads. The calibration plot depicted in Fig. 6B shows that the ECL intensity exhibit an excellent linear relationship to the quantity of mutant target DNA in the range from 10 pmol to 10 fmol and the correlation coefficient is 0.998. It is noteworthy that our detection method covers a dynamic range of at least two orders of magnitude.

3.4. Analysis of TP53 point mutation

In order to further validate the OLA-ECL method, we applied the method to detect point mutations in PCR products from cell lines. *TP53* point mutation at codon 273 was chosen as the target. *TP53* gene is one of the most studied genes in cancer research and the role of *TP53* as an important early diagnostic marker of tumours has been suggested [41]. As shown in Fig. 7A, the ECL signals obtained from PCR products of PANC-1 human pancreatic cell lines, ASTC-α-1 lung cancer cell lines and blood cells are 262.2 ± 13.4 cps, 24.3 ± 2.9 cps, 26.4 ± 3.6 cps, respectively. PCR

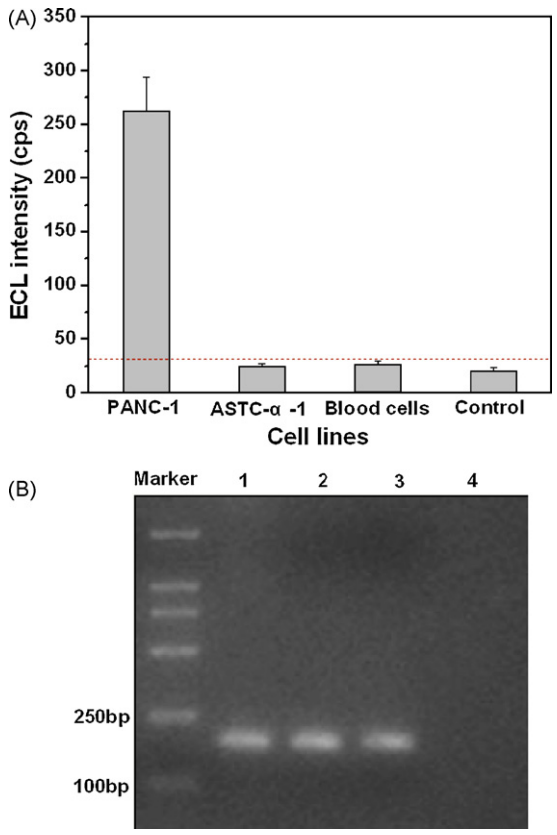

Fig. 7. Detection of real cell line samples. (A) ECL intensities obtained by analysis of single-base mutation at codon 273 of *TP53* gene in PCR products (186 bp) from PANC-1, ASTC-α-1, normal blood cells, and without template control. All ECL signal value were subtracted the blank control signal (ECL assay buffer). The red dash line represents the cut-off value for mutation positive samples. (B) Gel electrophoresis analysis the PCR products of PANC-1 cells (1), ASTC-α-1 cells (2), normal blood cells (3), and template free control (4).

reaction solution without template was as the control, the signal of which is 20.1 ± 3.5 cps. To define if a sample is mutation-positive, a cut-off value was calculated based on the average ($V_{control}$) and standard deviation ($V_{stdev(con)}$) of the ECL reading from the control sample, shown as in the following formula:

$$V_{cutoff} = V_{control} + 3V_{stdev(con)} \quad (1)$$

According to this formula, the cut-off level for mutation-positive samples was set at 31 cps. ECL signal less than 31 cps should not be indicated as mutation-positive under our conditions. According to the data, only PANC-1 is mutation-positive sample, and there is no G→A point mutation at codon 273 of *TP53* gene in ASTC-α-1 cell lines and blood cells. It was implied that the PCR template only from PANC-1 could perfect match with the probes at the mutation site then the two adjacent probes were integrated to form a single-stand oligonucleotide. That is to say, the codon 273 of *TP53* gene is mutant from CGT to CAT in PANC-1 cell lines. To validate if the difference of ECL intensity comes from the effect of concentration of real DNA samples and the PCR efficiency, 1% agarose gel electrophoresis analysis for PCR products was performed in the experiment. Fig. 7B shows the concentrations of the PCR products (186 bp) from PANC-1 cell line (line 1), ASTC-α-1 cell line (line 2) and blood cells (line 3) are almost the same. Without strap was observed in the PCR control (line 4) indicated the PCR process was fairly specific. Therefore the proposed approach could potentially serve as robust assay for mutation detection.

4. Conclusions

We reported a novel simple and sensitive approach for DNA point mutation detection. The approach bases on the high-fidelity perfect-match ligation by OLA and magnetic beads-based ECL detection scheme. Taq DNA ligase was used to offer very high fidelity in identification of template gene containing single-base mutation, which was proved to be efficient and specific. The magnetic beads-based ECL detection scheme provides the assay system with simple operation, cost-efficiency and significantly sensitivity. Thereby the proposed OLA-ECL approach could be potentially applied in the field of genetic-based diseases clinic early diagnosis and drug response prediction as well as point mutation detection in cancer studies.

Acknowledgements

This research is supported by the National Natural Science Foundation of China (30600128, 30870676, 30800261), the Natural Science Foundation of Guangdong Province (7005825), and the National High Technology Research and Development Program of China (863 Program) (2007AA10Z204).

References

[1] B.P. Sokolov, Nucleic Acids Res. 18 (1990) 3671.
[2] R.A. Gibbs, P.N. Nguyen, C.T. Caskey, Nucleic Acids Res. 17 (1989) 2437.
[3] S. Sauer, I.G. Gut, Rapid Commun. Mass Spectrom. 17 (2003) 1265.
[4] S. Bortolin, M. Black, H. Modi, I. Boszko, D. Kobler, Clin. Chem. 50 (2004) 2028.
[5] J.G. Hacia, B. Sun, N. Hunt, K. Edgemon, D. Mosbrook, C. Robbins, S.P. Fodor, D.A. Tagle, F.S. Collins, Genome Res. 8 (1998) 1245.
[6] S. Tyagi, D.P. Bratu, F.R. Kramer, Nat. Biotechnol. 16 (1998) 49.
[7] G.C. Kennedy, H. Matsuzaki, S. Dong, W.M. Liu, J. Huang, Nat. Biotechnol. 21 (2003) 1233.
[8] S. Haasl Russom, A.J. Brookes, H. Andersson, G. Stemme, Anal. Chem. 78 (2006) 2220.
[9] D. Botstein, R.L. White, M. Skolnick, R.W. Davis, Am. J. Hum. Genet. 32 (1980) 314.
[10] V. Lyamichev, A.L. Mast, J.G. Hall, J.R. Prudent, M.W. Kaiser, Nat. Biotechnol. 17 (1999) 292.
[11] U. Landegren, R. Kaiser, J. Sanders, L. Hood, Science 241 (1988) 1077.
[12] F. Barany, Proc. Natl. Acad. Sci. U.S.A. 88 (1991) 189.
[13] P. Hardenbol, F. Yu, J. Belmont, J. Mackenzie, C. Bruckner, et al., Genome Res. 15 (2005) 269.
[14] N.P. Gerry, N.E. Witowskl, J. Day, R.P. Hammer, G. Barany, F. Barany, J. Mol. Biol. 292 (1999) 251.
[15] X.X. Meng, H.M. Li, K.M. Wang, W.H. Tan, J. Li, Q.P. Guo, X.H. Yang, Q.H. Mo, X.M. Xu, Talanta 73 (2007) 23.
[16] H.X. Tang, X.H. Yang, K.M. Wang, W.H. Tan, H.M. Li, L.F. He, B. Liu, Talanta 75 (2008) 1388.
[17] P. Zhang, X. Chu, X.M. Xu, G.L. Shen, R.Q. Yu, Biosens. Bioelectron. 23 (2008) 1435.
[18] R. Favis, J.P. Day, N.P. Gerry, C. Phelan, S. Narod, F. Barany, Nat. Biotechnol. 18 (2000) 561.
[19] S. Dieter, B. Alexei, A.N. Mark, Nucleic Acids Res. 28 (2000) e43.
[20] S.A. Brazill, W.G. Kuhr, Anal. Chem. 74 (2002) 3421.
[21] J. Tost, I.G. Gut, Mass Spectrom. Rev. 21 (2002) 388.
[22] K. Tang, D.J. Fu, D. Julien, A. Braun, C.R. Cantor, H. Köster, Proc. Natl. Acad. Sci. U.S.A. 96 (1999) 10016.
[23] X. Chen, L. Levine, P.Y. Kwok, Genome Res. 9 (1999) 492.
[24] P.Y. Kwok, Hum. Mutat. 19 (2002) 315.
[25] M. Ronaghi, S. Karamohamed, B. Pettersson, M. Uhlen, P. Nyren, Anal. Biochem. 242 (1996) 84.
[26] T. Langaee, M. Ronaghi, Mutat. Res. 573 (2005) 96.
[27] F. Patolsky, A. Lichtenstein, I. Willner, J. Am. Chem. Soc. 123 (2001) 5194.
[28] M. Cho, S. Lee, S.-Y. Han, J.-Y. Park, M.A. Rahman, Y.-B. Shim, C. Ban, Nucleic Acids Res. 34 (2006) e75.
[29] J.F. Liu, D. Xing, X.Y. Shen, D.B. Zhu, Biosens. Bioelectron. 20 (2004) 436.
[30] D.B. Zhu, D. Xing, X.Y. Shen, J.F. Liu, Biochem. Biophys. Res. Commun. 324 (2004) 964.
[31] J.H. Kenten, J. Casadei, J. Link, S. Lupold, J. Willey, M. Powell, Clin. Chem. 37 (1991) 1626.
[32] X.M. Zhou, D. Xing, D.B. Zhu, L. Jia, Electrochem. Commun. 10 (2008) 564.
[33] W.J. Miao, Chem. Rev. 108 (2008) 2506.
[34] E. Terpetschnig, H. Szmacinski, H. Malak, J.R. Lakowicz, Biophys. J. 68 (1995) 342.
[35] Y.H. Pei, D. Xing, X.J. Gao, L. Liu, T.S. Chen, Apoptosis 12 (2007) 1681.
[36] D.B. Zhu, D. Xing, X.Y. Shen, J.F. Liu, Q. Chen, Biosens. Bioelectron. 20 (2004) 448.

[37] P. Nilsson, B. Persson, M. Uhlen, P.-A. Nygren, Anal. Biochem. 224 (1995) 400.
[38] H. Xu, H.P. Wu, F. Huang, S.P. Song, W.X. Li, Y. Cao, C.H. Fan, Nucleic Acids Res. 33 (2005) e83.
[39] N.R. Markham, M. Zuker, Nucleic Acids Res. 33 (2005) 577.
[40] S. Gudibande, J.H. Kenten, J. Link, Mol. Cell Probes 6 (1992) 495.
[41] C.V. de Moura Gallo, E.S. Azevedo, G. Mendonca, E. de Moraes, M. Olivier, P. Hainaut, Mutat. Res. 589 (2005) 192.